



Ulrich Weidmann
Uwe Kirsch
Michael Schreckenberg
Editors

Pedestrian and Evacuation Dynamics 2012

 Springer

Pedestrian and Evacuation Dynamics 2012

Ulrich Weidmann • Uwe Kirsch
Michael Schreckenberg
Editors

Pedestrian and Evacuation Dynamics 2012

 Springer

Editors

Ulrich Weidmann
Institut für Verkehrsplanung
und Transportsysteme (IVT)
ETH Zürich
Zürich, Switzerland

Uwe Kirsch
Pestalozzi & Stäheli
Ingenieurbüro Umwelt Mobilität Verkehr
Basel, Switzerland

Michael Schreckenber
Physik von Transport und Verkehr
Universität Duisburg-Essen
Duisburg, Germany

ISBN 978-3-319-02446-2 ISBN 978-3-319-02447-9 (eBook)
DOI 10.1007/978-3-319-02447-9
Springer Cham Heidelberg New York Dordrecht London

Library of Congress Control Number: 2014933212

© Springer International Publishing Switzerland 2014

This work is subject to copyright. All rights are reserved by the Publisher, whether the whole or part of the material is concerned, specifically the rights of translation, reprinting, reuse of illustrations, recitation, broadcasting, reproduction on microfilms or in any other physical way, and transmission or information storage and retrieval, electronic adaptation, computer software, or by similar or dissimilar methodology now known or hereafter developed. Exempted from this legal reservation are brief excerpts in connection with reviews or scholarly analysis or material supplied specifically for the purpose of being entered and executed on a computer system, for exclusive use by the purchaser of the work. Duplication of this publication or parts thereof is permitted only under the provisions of the Copyright Law of the Publisher's location, in its current version, and permission for use must always be obtained from Springer. Permissions for use may be obtained through RightsLink at the Copyright Clearance Center. Violations are liable to prosecution under the respective Copyright Law.

The use of general descriptive names, registered names, trademarks, service marks, etc. in this publication does not imply, even in the absence of a specific statement, that such names are exempt from the relevant protective laws and regulations and therefore free for general use.

While the advice and information in this book are believed to be true and accurate at the date of publication, neither the authors nor the editors nor the publisher can accept any legal responsibility for any errors or omissions that may be made. The publisher makes no warranty, express or implied, with respect to the material contained herein.

Cover illustration: By courtesy of Uwe Kirsch

Printed on acid-free paper

Springer is part of Springer Science+Business Media (www.springer.com)

Preface

6th International Conference on Pedestrian and Evacuation Dynamics

Editorial

Why Is Pedestrian Research Important?

People have been walking for millions of years. Humans walked out of Africa on their journey to settle the whole world. Yet, in spite of how long and how far we have walked, there is still a great deal we do not know about walking. And, more importantly, in spite of our advanced transport technologies, the demand for walking is growing since it provides the foundation for sustainable and practical transport solutions. In summary, as the following challenges show, pedestrian research is more important than ever.

First, the density of human settlement is increasing. The world population is approximately seven billion and by 2050 it will be over nine billion. Today, over 50 % of people live in cities; by 2050 it will be over 70 %. Many of these cities will be megacities with settlement densities hard for us to imagine today. Even in places with stagnant population growth, such as Europe, forecasts show that the number of people living in major cities will increase as a result of better economic opportunities and efforts to protect rural landscapes. These population increases pose a major challenge for urban infrastructure and transport systems everywhere. Not only must more people be served, but crowded transport systems pose additional risks during technical breakdowns or emergency situations. Managing these risks is becoming more complex and important to society. In short, our cities will have more pedestrians, so we need to better understand their behaviour and needs.

Second, the number of older and disabled persons is rapidly increasing. We need to design fully accessible infrastructure and transport systems to meet the needs of older and disabled people, but also recognize that they move more slowly than younger people. So we also need to reduce distances, simplify paths and reduce detours. Understanding the physical requirements of walking will be fundamental to achieving these important goals.

In addition to becoming more crowded, new social media are enabling people to quickly organize spontaneous gatherings. Whether for a celebration or a revolution, social media can bring together thousands of people in hours. Once the process has

started, there is little time to evaluate a location's physical safety conditions or to establish necessary pedestrian control systems. New pedestrian assessment methods and applications are needed to help quickly evaluate and plan for these types of events.

Third, increasing land use intensity encourages the construction of underground infrastructure, especially for transport. Many cities will build or extend underground metro systems. Many existing and new railway lines will be placed underground to serve as a backbone for regional transport networks. For example, in Zurich a new underground railway line is being built between the main station and the northern part of the city. But underground transport will not be confined to cities; long distance rail lines – especially high speed lines – will include many tunnels and underground structures to both maximize speed and reduce environmental impacts. Examples include Switzerland's 35-km Loetschberg railway tunnel (operating since 2007) and 57-km Gotthard tunnel (opening in 2016). Designing underground transport systems and facilities that can efficiently and safely accommodate large numbers of people in regular operations and, especially in emergency conditions, requires a very detailed understanding of pedestrian behaviour and needs. Government authorities have very stringent requirements that must be fulfilled in order to obtain approval for these types of projects.

Fourth, walking is a fundamental element of public transport and therefore must be carefully considered as operators seek ways of reducing costs and improving productivity. One example: today it costs Zurich's public transport operator 1 million CHF annually to operate a tram and 0.5 million CHF to operate a bus! The faster the service, the fewer the vehicles needed to run the same schedule. So, a powerful means for reducing costs is accelerating service – only fast public transport can be efficient. A good way of achieving this is to reduce dwell times at stops, but doing this successfully requires careful analysis of pedestrian movements.

Similarly, a growing number of railways are adopting the principle of cyclic timetables (“Integrierter Taktfahrplan”). Achieving the required node-to-node running times needed to meet these timetables can mean spending many millions of CHF on infrastructure improvements per minute of travel time saved. The alternative, reducing station dwell times through better design of pedestrian transfer facilities, can be much less expensive and make service more attractive to passengers.

But even in a continuously changing world, there are constants: The Swiss distance measure “Schweizerstunde” (“Swiss hour”) used in the nineteenth century was equal to $4.8 \text{ km} = 1.33 \text{ m/s}$ or exactly the average of today's pedestrian speed!

Answering these challenges requires new knowledge, new methods and new tools. We must understand pedestrian behaviour under different conditions as well as be able to predict and simulate these behaviours in advance. We must develop accurate simulation for use in designing pedestrian facilities, helping us avoid dangerous situations, plan adequately for emergencies, and, last but not least, to make walking more attractive and enjoyable in general. The PED 2012 conference was an excellent opportunity to showcase research focused on these important topics.

At PED 2012, over 170 people enjoyed 70 presentations and keynotes as well as 70 poster presentations. The conference included presentations on new mathematical models and improvements to existing models. Many presentations described new insights on pedestrian behaviour in normal situations and emergency cases. Exciting new fields of research based on new technologies such as sensors and advanced means of observation were opened. In short, PED 2012 highlighted the transportation research community's commitment to meeting the challenges inherent in creating the pedestrian society of the future and has served as a starting point for innovative new research ideas, building a strong foundation for future research and the next conference.

Zürich, Switzerland

Ulrich Weidmann

Contents

Part I Keynotes

Automatic Detection and Tracking of Pedestrians in Videos with Various Crowd Densities	3
Afshin Dehghan, Haroon Idrees, Amir Roshan Zamir, and Mubarak Shah	
London Bridge: The Role Pedestrian Modelling Played in Designing the New Station	21
Nicolas Le Glatin, Isabelle Milford, and Andrew Hutton	
Mass Psychology Revisited: Insights from Social Psychology, Neuroscience and Simulation	39
Thomas Brudermann	
Shaping the Space: Turning Function into Inspiration	55
Peter Jenkins	
Simple Heuristics and the Modelling of Crowd Behaviours	75
Mehdi Moussaïd and Jonathan D. Nelson	
The Characteristics and Needs of Pedestrians with Mobility Impairments	91
Marjolein de Jong	

Part II Experiment and Evacuation

An Evacuation Validation Data Set for Large Passenger Ships	109
Edwin Richard Galea, Steven Deere, Robert Brown, and Lazaros Filippidis	
An Information Processing Based Model of Pre-evacuation Behavior for Agent Based Egress Simulation	125
Vaisagh Viswanathan and Michael Lees	

An Innovative Evacuation System for Multiplex Cinemas	135
Athanasios Kosmopoulos and Stavros Katsoulis	
An Innovative Scenario for Pedestrian Data Collection: The Observation of an Admission Test at the University of Milano-Bicocca	143
Mizar Luca Federici, Andrea Gorrini, Lorenza Manenti, and Giuseppe Vizzari	
Trajectory Analysis of Pedestrian Crowd Movements at a Dutch Music Festival	151
Dorine C. Duives, Winnie Daamen, and Serge Hoogendoorn	
An Experimental Study on the Correlation Between “Attachment to Belongings” “Pre-movement” Time	167
Marco D’Orazio and Gabriele Bernardini	
Bottlenecks in Evacuation Design Considering Both Structural and Human Behavioural Aspects: An Experimental Study	179
Tuomo Rinne, Timo Korhonen, and Peter Grönberg	
Comparison of Evacuation Simulation Models	189
Burkhard Forell, Hubert Klüpfel, Volker Schneider, and Sören Schelter	
Crowd Guidance in Building Emergencies: Using Virtual Reality Experiments to Confirm Macroscopic Mathematical Modeling of Psychological Variables	197
Kerry L. Marsh, Christian T. Wilkie, Peter B. Luh, Zhenxiang Zhang, Timothy Gifford, and Neal Olderman	
Development of Smoke Control System Ensuring Safe Evacuation Through Stairwell for High-Rise Building in Korea	213
Jung-Yup Kim, Hyun-Joon Shin, and Ji-Seok Kim	
Early-Stage Egress Simulation for Process-Driven Buildings	223
Gabriel Wurzer	
Effect of Guidance Information and Human Relations Among Agents on Crowd Evacuation Behavior	231
Masaru Okaya and Tomochi Takahashi	
Empirical Fundamental Diagrams for Bidirectional Pedestrian Streams in a Corridor	245
J. Zhang, A. Schadschneider, and A. Seyfried	
Empirical Study and Modelling of Pedestrians’ Route Choice in a Complex Facility	251
Armel Ulrich Kemloh Wagoum, Armin Seyfried, Frank Fiedrich, and Ralph Majer	

Evacuation Analyses for Venues	267
Sven Hebben, Patrick Gessler, and Hubert Klüpfel	
Influence of Spreading Hazardous Material in Macroscopic Evacuation Dynamics: A Proof of Concept	275
Simone Göttlich, Sebastian Kühn, Jan Peter Ohst, and Stefan Ruzika	
Evacuation Exercises in a TV Studio	283
Patrick Gessler and Sven Hebben	
Experimental Study and Modelling of Pedestrian Space Occupation and Motion Pattern in a Real World Environment	289
F. Zanlungo, Y. Chigodo, T. Ikeda, and T. Kanda	
Experimental Study of the Following Dynamics of Pedestrians	305
C. Appert-Rolland, A. Jelic, P. Degond, J. Fehrenbach, J. Hua, A. Cretual, R. Kulpa, A. Marin, A.-H. Olivier, S. Lemercier, and J. Pettre	
FDS+Evac Model Validation for Seated Row Arrangements: Aircraft and Cinema Theatre	317
K. Naveesh Reddy, A.K. Babbar, and Timo Korhonen	
Fundamental Diagram of Stairs: Critical Review and Topographical Measurements	329
Sebastian Burghardt, Armin Seyfried, and Wolfram Klingsch	
Hermes: An Evacuation Assistant for Large Arenas	345
Stefan Holl, Andreas Schadschneider, and Armin Seyfried	
Influence of Emissions on Pedestrian Evacuation	351
Hermann Mayer, Dirk Hartmann, Wolfram Klein, and Oliver Zechlin	
Large-Scale Multi-modal Evacuation Analysis with an Application to Hamburg	361
Dirk Durst, Gregor Lämmel, and Hubert Klüpfel	
Measuring Individual’s Egress Preference in Wayfinding Through Virtual Navigation Experiments	371
Jan Dijkstra, Qunli Chen, Bauke de Vries, and Joran Jessurun	
Modelling Evacuation Using Escalators: A London Underground Dataset	385
Michael J. Kinsey, Edwin R. Galea, and Peter J. Lawrence	
Observations from Student Exercises to Collect Human Behavior and Movement Data	401
Majed Almejmaj and Brian J. Meacham	

On Measuring Pedestrian Density and Flow Fields in Dense as well as Sparse Crowds	411
Matthias Plaue, Günter Bärwolff, and Hartmut Schwandt	
On the Simulation for Rail Tunnel Evacuation with Cross-Passageways	425
S.B. Liu, S.M. Lo, and J. Ma	
Pedestrian-Vehicles Interaction During Evacuation: Agent-Based Hybrid Evacuation Modelling of Southeast Asian Cities	435
Manuela Di Mauro, Michael Lees, Kusnowidjaja Megawati, and Zhenhua Huang	
PedGo Guardian: Evacuation Decision Support System for Events	445
H. Klüpfel and T. Meyer-König	
RiMEA: A Way to Define a Standard for Evacuation Calculations	455
Christian Rogsch, Hubert Klüpfel, Rainer Könnecke, and Andreas Winkens	
Simulation Model of Evacuation Behavior Following a Large-Scale Earthquake that Takes into Account Various Attributes of Residents and Transient Occupants	469
Toshihiro Osaragi, Takayuki Morisawa, and Takuya Oki	
Simulation of City Evacuation Coupled to Flood Dynamics	485
A.S. Mordvintsev, V.V. Krzhizhanovskaya, M.H. Lees, and P.M.A. Sloot	
Large Scale Outdoor Events	501
Hubert Klüpfel and Sven Hebben	
The Study on the Effects of the Counter-Flow on the Evacuation of People from Tall Buildings	509
Piotr Tofilo, Marcin Cisek, and Krzysztof Lacki	
Study of Human Behavior Before Evacuation	521
Tao Chen, Lili Pan, and Guoquan Zhang	
Tracking People in Crowded Scenes	533
Maik Boltes and Armin Seyfried	
Validation and Calibration of the EXIT89 Evacuation Model for Road Tunnel Evacuation Applications	543
Enrico Ronchi, Rita Fahy, Pasquale Colonna, and Nicola Berloco	
Waiting Zones for Real Life Scenarios: A Case Study Using a German Railway Station as an Example	551
Maria Davidich, Florian Wilhelm Geiss, Hermann Mayer, Alexander Pfaffinger, and Christian Royer	

Part III Simulation and Modeling

A Data-Driven Model of Pedestrian Following and Emergent Crowd Behavior 561
 Kevin Rio and William H. Warren

A Macroscopic Model for Bidirectional Pedestrian Flow 575
 Cécile Appert-Rolland, Pierre Degond, and Sébastien Motsch

A Macroscopic Multiple Species Pedestrian Flow Model Based on Heuristics Implemented with Finite Volumes 585
 Frank Huth, Günter Bärwolff, and Hartmut Schwandt

Quantitative Validation of the Generalized Centrifugal Force Model ... 603
 Mohcine Chraïbi, Armin Seyfried, and Andreas Schadschneider

An Econometric-based Model of Pedestrian Walking Behavior Implicitly Considering Strategic or Tactical Decisions 615
 Daisuke Fukuda, Toru Seo, Kaoru Yamada, Hideki Yaginuma, and Nobuhiro Matsuyama

An Empirically-Grounded Emergent Approach to Modeling Pedestrian Behavior 625
 Stephane Bonneaud and William H. Warren

Calibrating a General Pedestrian Stream Simulation Model According to a Specific Real Life Scenario of a German Railway Station 639
 M. Davidich and G. Köster

Cognition-oriented Simulation of Pedestrian Dynamics 647
 Wassim Abu Abed and Volker Berkhahn

Comparison of Different Calibration Techniques on Simulated Data ... 657
 Christian Rudloff, Thomas Matyus, and Stefan Seer

Evacuation Agent Simulation in an Underground Shopping Street Adding a Floor Field Approach and Its Three Dimensional Expression 673
 Yoshiyuki Kobayashi, Toshiyuki Kaneda, Masaki Tamada, Taichi Shimura, and Keisuke Hata

Frozen Shuffle Update in Simple Geometries: A First Step to Simulate Pedestrians 683
 J. Cividini, C. Appert-Rolland, and H.J. Hilhorst

Fundamental Diagram as a Model Input: Direct Movement Equation of Pedestrian Dynamics 691
 E. Kirik, A. Malyshev, and E. Popel

Improving Flexibility of Agent’s Path Selection in Cellular Pedestrian Flow Model	703
Juha-Matti Kuusinen and Sergey Kitov	
Including Route Choice Models into Pedestrian Movement Simulation Models	713
D. Bauer and J. Gantner	
Integrating Lateral Swaying of Pedestrians into Simulations	729
Barbara Krausz and Christian Bauckhage	
Integration of a Multi-modal Simulation Module into a Framework for Large-Scale Transport Systems Simulation	739
Christoph Dobler and Gregor Lämmel	
Merging Processes of Pedestrian Queues	755
Daniel Weber, Florian Knorr, and Michael Schreckenberg	
Methodology for Pedestrian Analysis in Public Spaces Based on Probabilistic Approach	761
Ignacio Martínez and Ana Olmeda	
Methods for Modeling and Simulation of Multi-destination Pedestrian Crowds	775
Günter Bärwolff, Minjie Chen, Frank Huth, Gregor Lämmel, Kai Nagel, Matthias Plaue, and Hartmut Schwandt	
Modeling Pedestrian Route Choice During Large Public Gatherings ...	789
Lei Feng and Elise Miller-Hooks	
Pedestrian Group Behavior in a Cellular Automaton	807
Michael Seitz, Gerta Köster, and Alexander Pfaffinger	
Modeling Time Duration of Planned and Unplanned Store Visits in a Multi-Agent Simulation of Pedestrian Activity in City Centers	815
Jan Dijkstra, Harry Timmermans, Joran Jessurun, and Bauke de Vries	
Motions Effect for Crowd Modeling Aboard Ships	825
K.V. Kostas, A.-A.I. Ginnis, C.G. Politis, and P.D. Kaklis	
On Modeling Groups in Crowds: Empirical Evidence and Simulation Results Including Large Groups	835
Verena Reuter, Benjamin S. Bergner, Gerta Köster, Michael Seitz, Franz Treml, and Dirk Hartmann	
Pedestrian Agent Based Model Suited to Heterogeneous Interactions Overseen by Perception	847
L. Bourgois and J.-M. Auberlet	

Pedestrian Gap Acceptance in Micro-Simulation Modelling	861
Paul Simon Townsend	
Pedestrian Simulation Using Geometric Reasoning in Velocity Space ...	875
Sean Curtis and Dinesh Manocha	
Quantitative and Qualitative Validation Procedure for General Use of Pedestrian Models	891
Mario Campanella, Serge Hoogendoorn, and Winnie Daamen	
Shared Space Modeling Based on Social Forces and Distance Potential Field	907
Bani Anvari, Winnie Daamen, Victor L. Knoop, Serge P. Hoogendoorn, and Michael G.H. Bell	
Simulation Model for Vehicle and Pedestrian Interaction Considering Road Crossing Activities	917
Bruno R. Werberich, Carlos O. Pretto, and Helena B.B. Cybis	
Simulation Models of Merging Priorities in Staircases	925
Henri Hakonen and Marja-Liisa Siikonen	
Simulation of Handicapped People Finding Their Way Through Transport Infrastructures	935
Helmut Schrom-Feiertag, Thomas Matyus, and Martin Brunnhuber	
Simulation of Pedestrian Dynamics with Density Control on a Regular Grid	949
Minjie Chen, Günter Bärwolff, and Hartmut Schwandt	
Evacuation of Day Care Centres for Children 0–6 Years: Simulations Using Simulex	959
L. Ulriksen and A.S. Dederichs	
Stochastic Transition Model for Pedestrian Dynamics	971
Michael Schultz	
Toward Simulation-Based Egress Optimization in Smart Buildings Using Symbiotic Simulation	987
Heiko Aydt, Michael H. Lees, Stephen J. Turner, and Wentong Cai	
The Development and Calibration of an Agent-Based Microsimulation Model for Vehicle-Pedestrian Interaction	1001
Rahul Jobanputra and Marianne Vanderschuren	
The Effect of Integrating Travel Time	1013
Tobias Kretz	
Using a Multi-Scale Model for Simulating Pedestrian Behavior	1029
Angelika Kneidl, Dirk Hartmann, and André Borrmann	

Using the Social Force Model to Represent the Behavior of Pedestrians at Chaotic Intersections of Developing Countries: The Case of Peru 1039
 Felix Cabrera Vega and Juan Carlos Dextre

Validation of Crowd Models Including Social Groups 1051
 Gerta Köster, Franz Treml, Michael Seitz, and Wolfram Klein

Velocity-Based Models for Crowd Simulation 1065
 Julien Pettré, David Wolinski, and Anne-Hélène Olivier

Part IV Psychology

Fuzzy Prediction of Pedestrian Steering Behavior with Local Environmental Effects 1081
 Mojdeh Nasir, Matthew Glenn Watson, Vu Le, Saeid Nahavandi, and Douglas Creighton

Group Dynamic Behavior and Psychometric Profiles as Substantial Driver for Pedestrian Dynamics 1097
 Michael Schultz, Lars Rößger, Hartmut Fricke, and Bernhard Schlag

Investigating Human Factors in Fire Evacuation: A Serious-Gaming Approach 1113
 K. Schatz, J. Schlittenlacher, D. Ullrich, U. Rüppel, and W. Ellermeier

Occupants Emergency Behaviour in Turkey 1123
 Nese Çakici Alp and Gülen Çağdaş

Psychological Aspects of German Signal Words in Evacuation Warnings 1135
 Laura Künzer, Gesine Hofinger, and Tina Zink

Psychological Aspects of Human Dynamics in Underground Evacuation: Field Experiments 1149
 Robert Zinke, Gesine Hofinger, and Laura Künzer

The Effects of the Design Factors of the Train-Platform Interface on Pedestrian Flow Rates 1163
 Taku Fujiyama, Roselle Thoreau, and Nick Tyler

Understanding Crowd Panic at Turning and Intersection Through Model Organisms 1175
 Nirajan Shiwakoti, Majid Sarvi, Charitha Dias, and Martin Burd

Part V Miscellaneous

A Study for Estimation of Ventilation Capacity of Large Enclosure Considering Real Fire Load 1187
 Chan-sol Ahn and Jung-yup Kim

Multi-agent Transport Simulation for Regional Evacuation Processes 1197
 Mohamed Bakillah, Hubert Klüpfel, Gregor Lämmel, and Georg Walenciak

Agent-Based Simulations of Pedestrian Movement for Site Security: U. S. Secret Service’s Current Capabilities and Next Steps.... 1207
 Douglas A. Samuelson

Ant Colony Based Evacuation Route Optimization Model for Mixed Pedestrian-Vehicle Flows..... 1213
 Qiuping Li, Zhixiang Fang, and Qingquan Li

Collecte of Data Stemming from the Fine Trajectory of the Pedestrians 1225
 Adiaviakoye Ladji, Plainchault Patrick, Bourcerie Marc, and Auberlet Jean Michel

Dynamic Medium Scale Navigation Using Dynamic Floor Fields 1237
 Dirk Hartmann, Jana Mille, Alexander Pfaffinger, and Christian Royer

Effect of Social Groups on Crowd Dynamics: Empirical Findings and Numerical Simulations 1251
 Dirk Oberhagemann, Rainer Könnecke, and V. Schneider

Estimating PCE-Type Factors for Heterogeneous Pedestrian Traffic Using Simulation 1259
 Ronald John Galiza, Luis Ferreira, and Phil Charles

Getting Out of the Way: Collision-Avoiding Pedestrian Models Compared to the Real World 1275
 Gregor Lämmel and Matthias Plaue

Influence of Rhythm and Velocity Variance on Pedestrian Flow 1291
 Daichi Yanagisawa, Akiyasu Tomoeda, and Katsuhiro Nishinari

Interaction Behavior Between Individual Pedestrians 1305
 Winnie Daamen, Serge Hoogendoorn, Mario Campanella, and Dirk Versluis

New Wayfinding Techniques in Pathfinder and Supporting Research... 1315
 Charles Thornton, Richard O’Konski, Bryan Klein, Brian Hardeman, and Daniel Swenson

OpenPedSim: A Framework for Pedestrian Flow Analysis 1323
Armel Ulrich Kemloh Wagoum, Mohcine Chraïbi,
Christian Eilhardt, Stefan Nowak, Igor Kulkov, Daniel Weber,
Kathrin Sauer, Hubert Klüpfel, and Andreas Schadschneider

Optimizing Pedestrian Environments with Evolutionary Strategies 1331
Marijn Swenne and Thomas Bäck

**Estimating Pedestrian Destinations Using Traces from WiFi
Infrastructures** 1341
Antonin Danalet, Michel Bierlaire, and Bilal Farooq

**Pedestrian Conflicts, Pedestrian Comfort Levels, and Current
Pedestrian Levels of Service**..... 1353
Jaisung Choi, Sangyoup Kim, Sunggyu Kim, Minsu Jin,
Yongseok Kim, and Jinkug Kim

**Scalable Evacuation Simulation and Visualization Using GPU
Computing** 1365
Kensuke Yasufuku

Starting-wave and Optimal Density in a Queue 1375
Akiyasu Tomoeda, Daichi Yanagisawa, Takashi Imamura,
and Katsuhiro Nishinari

The Love Parade Disaster 1385
Hubert Klüpfel

Utilizing Crowd Insights to Refine Disease-Spreading Models 1395
Anders Johansson and Lara Goscè

**Venue Suitability for Large-Scale Events from the Viewpoint
of Safety Measures** 1405
Masatoshi Kaitsuji and Akihiko Hokugo

WALK: A Modular Testbed for Crowd Evacuation Simulation 1417
Stefan Münchow, Ia Enukidze, Stefan Sarstedt,
and Thomas Thiel-Clemen

List of Participants

Wassim Abu Abed Leibniz Universität Hannover, Germany

Tomoeda Akiyasu Meiji University/Japan Science and Technology Agency, Core Research for Evolutional Science and Technology, Japan

Bani Anvari Imperial College London, UK

Cecile Appert-Rolland Centre national de la recherche scientifique/University Paris-Sud, France

Jean-Michel Auberlet Institut français des sciences et technologies des transports, de l'aménagement et des réseaux, France

Rebekka Axthelm Zürcher Hochschule für Angewandte Wissenschaften, Switzerland

Günter Bärwolff Technische Universität Berlin, Germany

Dietmar Bauer Austrian Institute of Technology, Austria

Olivier Benz Analysis Simulation Engineering GmbH, Switzerland

Gabriele Bernardini Università Politecnica delle Marche, Italy

Christian Blättler Schweizerische Bundesbahnen, Switzerland

Maik Boltes Forschungszentrum Jülich GmbH, Germany

Stephane Bonneaud Brown University, USA

André Borrmann Technische Universität München, Germany

Thomas Bruderermann University of Graz, Austria

Sebastian Burghardt Bergische Universität Wuppertal, Germany

Alain Bützberger Swisstraffic AG, Switzerland

Felix Israel Cabrera Pontificia Universidad Católica del Perú, Peru

Nese Çakici Alp Kocaeli University, Turkey
Mario Campanella Delft University of Technology, Netherlands
Ahn Chan-Sol Korea Institute of Construction Technology, South Korea
Tao Chen Technische Universität Berlin, Germany
Jaisung Choi University of Seoul, South Korea
Mohcine Chraïbi Forschungszentrum Jülich GmbH, Germany
Marcin Cisek Main School of Fire Service, Poland
Julien Cividini Université Paris-Sud 11, France
Sean Curtis University of North Carolina at Chapel Hill, USA
Helena Cybis Universidade Federal do Rio Grande do Sul, Brazil
Antonin Danalet École Polytechnique Fédérale de Lausanne, Switzerland
Maria Davidich Siemens AG, Germany
Marjolein de Jong Hasselt University, Belgium
Manuela Di Mauro Nanyang Technological University, Singapore
Jan Dijkstra Eindhoven University of Technology, Netherlands
Christoph Dobler Eidgenössische Technische Hochschule Zürich, Switzerland
Kristen Dorcey-Joyce Quadstone Paramics, UK
Dorine C. Duives Delft University of Technology, Netherlands
Dirk Durst Federal Office of Civil Protection and Disaster Assistance, Germany
Bilal Farooq École Polytechnique Fédérale de Lausanne, Switzerland
Lei Feng University of Maryland, USA
Ralf Frisch Planung Transport Verkehr AG, Germany
Taku Fujiyama University College London, UK
Ed Galea University of Greenwich, UK
Ronald John Galiza The University of Queensland, Australia
Patrick Gessler TraffGo HT GmbH, Germany
Henri Hakonen KONE Corporation, Finland
Uwe D. Hanebeck Karlsruher Institut für Technologie, Germany
Flurin Hänseler École Polytechnique Fédérale de Lausanne, Switzerland
Dirk Hartmann Siemens AG, Germany

- Sven Hebben** TraffGo HT GmbH, Germany
- Gesine Hofinger** Schutzkommission beim Bundesministerium d. Inneren, Germany
- Akihiko Hokugo** Kobe University, Japan
- Beat Hürzeler** Schweizerische Bundesbahnen, Switzerland
- Frank Huth** Technische Universität Berlin, Germany
- Andrew Hutton** Network Rail, UK
- Ulrike Huwer** Basler & Hofmann AG, Switzerland
- Gregor Jäger** BFT Cognos GmbH, Germany
- Peter Jenkins** Building Design Partnership, UK
- Anders Johansson** University of Bristol, UK
- Susan Johnson** Johnson Engineered Solutions Limited, Canada
- Masatoshi Kaitsuji** Kobe University Graduate School, Japan
- Toshiyuki Kaneda** Nagoya institute of Technology, Japan
- Stavros Katsoulis** DEMCO SA, Greece
- Erich von Känel** Bundesamt für Verkehr, Switzerland
- Armel Ulrich Kemloh Wagoum** Forschungszentrum Jülich GmbH, Germany
- Chris Kemp** Bucks New University, UK
- Nicolas Keusen** Bundesamt für Verkehr, Switzerland
- Junkug Kim** Korea Institute of Construction Technology, South Korea
- Yongseok Kim** Korea Institute of Construction Technology, South Korea
- Jung Yup Kim** Korea Institute of Construction Technology, South Korea
- Michael Kinsey** University of Greenwich, UK
- Ekaterina Kirik** Institute of Computational Modeling of Siberian Branch of Russian Academy of Sciences, Russia
- Uwe Kirsch** Eidgenössische Technische Hochschule Zürich, Switzerland
- Sergey Kitov** KONE, Finland
- Bryan Klein** Thunderhead Engineering Consultants, Inc., USA
- Wolfram Klein** Siemens AG, Germany
- Hubert Klüpfel** TraffGo HT GmbH, Germany
- Angelika Kneidl** Technische Universität München, Germany

- Yoshiyuki Kobayashi** Nagoya Institute of Tecnology, Japan
- Rainer Könnecke** IST GmbH, Germany
- Timo Korhonen** VTT Technical Research Centre of Finland, Finland
- Athan Kosmopoulos** Village Roadshow Group of Companies, Greece
- Konstantinos Kostas** Technological Educational Institute of Athens, Greece
- Gerta Köster** Hochschule München, Germany
- Barbara Krausz** Fraunhofer Institut für Intelligente Analyse- und Informationssysteme, Germany
- Tobias Kretz** Planung Transport Verkehr AG, Germany
- Sebastian Kühn** Technische Universität Kaiserslautern, Germany
- Laura Künzer** Friedrich-Schiller-Universität Jena, Germany
- Gregor Lämmel** Technische Universität Berlin, Germany
- Peter Lawrence** University of Greenwich, UK
- Qiuping Li** Wuhan University, China
- S.B. Liu** City University of Hong Kong, Hong Kong
- Peter Luh** University of Connecticut, USA
- Lorenza Manenti** University of Milano-Bicocca, Italy
- Dinesh Manocha** University of North Carolina at Chapel Hill, USA
- Kerry Marsh** University of Connecticut, USA
- Ignacio Martínez** NECO Ingeniería y Economía del Transporte, Spain
- Okaya Masaru** Meijo University, Japan
- Thomas Matyus** Austrian Institute of Technology, Austria
- Hermann Mayer** Siemens AG, Germany
- Brian Meacham** Worcester Polytechnic Institute, UK
- Elise Miller-Hooks** University of Maryland, USA
- Michael Moos** Analysis Simulation Engineering GmbH, Switzerland
- Mehdi Moussaïd** Max Planck Institute for Human Development, Germany
- Stefan Münchow** Hamburg University of Applied Sciences, Germany
- Mojdeh Nasir** Deakin University, Australia
- Kai Nagel** Technische Universität Berlin, Institut für Land- und Seeverkehr, Verkehrssystemplanung und Verkehrstelematik, Germany

Takuya Oki Tokyo Institute of Technology, Japan
Ana Olmeda INECO Ingeniería y Economía del Transporte, Spain
Toshihiro Osaragi Tokyo Institute of Technology, Japan
Christine Palmer WSP, UK
Wieger Pasma NPC – DHV, Netherlands
Thomas Pestell WSP, UK
Julien Pettré INRIA, France
Matthias Plaue Technische Universität Berlin, Germany
Carlos Pretto Universidade Federal do Rio Grande do Sul, Brazil
Verena Reuter Technische Universität Kaiserslautern, Germany
Kevin Rio Brown University, USA
Christian Rogsch RiMEA e.V., Executive Committee, Germany
Enrico Ronchi Lund University, Sweden
Marai Marlène Ruffieux Bundesamt für Verkehr, Switzerland
Daniel Sauter Urban Mobility Research, Switzerland
Michael Schreckenberg Universität Duisburg-Essen, Germany
Michael Schultz Technische Universität Dresden, Germany
Stefan Seer Austrian Institute of Technology, Austria
Michael Seitz Hochschule München, Germany
Armin Seyfried Forschungszentrum Jülich GmbH, Germany
Mubarak Shah University of Central Florida, USA
Nirajan Shiwakoti Monash University, Australia
Swen Stemmer Hochschule München, Germany
Marijn Swenne Leiden University, Netherlands
Daniel Swenson Thunderhead Engineering, USA
Tomoichi Takahashi Meijo University, Japan
Thomas Thiel-Clemen Hamburg University of Applied Sciences, Germany
Paul Townsend Crowd Dynamics International Limited, UK
Franz Treml Hochschule München, Germany
Lene Ulriksen COWI A/S, Denmark

- Vaisagh Viswanathan** Nanyang Technological University, Singapore
- Vladimir Vukadinovic** Disney Research Zurich, Switzerland
- Nathalie Waldau-Drexler** Ingenieurbüro WALDAU, Austria
- Urs Walter** City of Zürich, Switzerland
- Ulrich Weidmann** Eidgenössische Technische Hochschule Zürich, Switzerland
- Ilan Paul Weinmann** ICTS Europe, France
- Marian Weltevreden** NPC – DHV, Netherlands
- Bruni Werberich** Universidade Federal do Rio Grande do Sul, Brazil
- Roland Wiederkehr** Pöyry Infra AG, Switzerland
- Markus Wiersch** Consorcium, Germany
- Andreas Winkens** BPK Brandschutz Planung Klingsch GmbH, Germany
- Gabriel Wurzer** Technische Universität Wien, Austria
- Isami Yahiro** MT Security Company, Japan
- Kaoru Yamada** Tokyo Institute of Technology, Japan
- Daichi Yanagisawa** Ibaraki University, Japan
- Kensuke Yasufuku** Osaka University, Japan
- Francesco Zanlungo** Advanced Telecommunications Research Institute International, Japan
- Oliver Zechlin** Siemens Switzerland AG, Switzerland
- Jun Zhang** Bergische Universität Wuppertal, Germany
- Robert Zinke** Friedrich-Schiller-Universität Jena, Germany

Part I
Keynotes

Automatic Detection and Tracking of Pedestrians in Videos with Various Crowd Densities

Afshin Dehghan, Haroon Idrees, Amir Roshan Zamir, and Mubarak Shah

Abstract Manual analysis of pedestrians and crowds is often impractical for massive datasets of surveillance videos. Automatic tracking of humans is one of the essential abilities for computerized analysis of such videos. In this keynote paper, we present two state of the art methods for automatic pedestrian tracking in videos with low and high crowd density. For videos with low density, first we detect each person using a part-based human detector. Then, we employ a global data association method based on Generalized Graphs for tracking each individual in the whole video. In videos with high crowd-density, we track individuals using a scene structured force model and crowd flow modeling. Additionally, we present an alternative approach which utilizes contextual information without the need to learn the structure of the scene. Performed evaluations show the presented methods outperform the currently available algorithms on several benchmarks.

Keywords Human detection • Tracking • Data association • Crowd density • Crowd analysis • Automatic surveillance

1 Introduction

The number of surveillance cameras in urban area is increasing at a significant rate which results in massive amounts of videos to be analyzed. Observing crowds and pedestrians manually in such large amount of data is cumbersome and often impractical which makes automated methods extremely favorable for this purpose.

A. Dehghan • H. Idrees • A.R. Zamir • M. Shah (✉)
Computer Vision Lab, University of Central Florida, Orlando, USA
e-mail: adehghan@cs.ucf.edu; haroon@cs.ucf.edu; aroshan@cs.ucf.edu; shah@cs.ucf.edu

Automatic tracking of pedestrians is one of the required abilities for computerized analysis of such videos.

The density of pedestrians significantly impacts their appearance in a video. For instance, in the videos with high density of crowds, people often occlude each other and usually few parts of the body of each individual are visible. On the other hand, the full body or a significant portion of the body of each pedestrian is visible in videos with low crowd-density. These different appearance characteristics require tracking methods which suite the density of the crowd. In this paper, we present two state of the art methods for tracking pedestrians in videos with low and high density of crowds.

For videos with low density of pedestrians (Sect. 2), first we detect individuals in each video frame using a part-based human detector which efficiently handles occlusion (Sect. 2.1). Later, we employ a global data association method based on Generalized Minimum Clique Graphs for tracking each person over the course of the whole video (Sect. 2.2).

We present two approaches to tracking for videos with high density of crowds. In the first one, the scene layout constraint which is captured by learning Dynamic Floor Field, Static Floor Field and Boundary Floor Field along with crowd flow is leveraged to track individuals in the crowd. In the second approach, no learning or crowd flow is used to track targets. Instead, the tracking is performed utilizing salient and contextual information.

2 Pedestrian Tracking in Videos with Low Crowd Density

Our framework for tracking pedestrians in videos with low density of crowds consists of two main steps: Human Detection (Sect. 2.1) and Data Association (Sect. 2.2):

2.1 *Part-based Human Detection*

Human detection is a fundamental problem in video surveillance. Robust human tracking is highly dependent on reliable detection in each frame. Although human detection has been well studied in computer vision, most of the existing approaches are unsuitable for detecting targets with large variance in appearance. Therefore, robust human detection remains a challenge due to the highly articulated body postures, occlusion, background clutter and viewpoint changes.

Many approaches have been proposed for human detection over the last decade. In most of them, the problem is formulated as a binary sliding window classification, i.e. an image pyramid is constructed and a fixed size window is scanned over all of its levels to localize humans using a non-maximum suppression procedure.



Fig. 1 (a) A sample positive image and its HOG descriptor. (b) *Left*: detections obtained using part-based human detector in [6]. *Right*: a model for root and parts and a spatial model for the location of each part relative to the root

Dalal and Triggs [5] use HOG as low a level feature which is shown to outperform other competitive features, such as wavelets, for human detection. HOG provides a robust feature set that allows the human body to be distinguished discriminatively even in cluttered background. The descriptor proposed by Dalal and Triggs computes an edge oriented histogram on a dense grid of uniformly spaced cells. Then, they use overlapping local contrast normalizations in order to improve the overall performance. A linear SVM classifier is used to learn a model for the human body using positive and negative samples. The detector is then applied to the image to localize human bodies, i.e. the detector takes an image, a position within that image and a scale as the inputs and determines if there is a person in that particular location and scale. Figure 1a shows a sample positive image and its HOG descriptor.

Using local features to learn body parts is another approach to human detection. Part-based approaches which model an object as a rigid or deformable configuration of parts are shown to be very effective for occlusion handling. Felzenszwalb et al. [6] simultaneously learn parts and an object model. Their model is an enriched version of Dalal and Triggs' which uses a star structured part-based model defined by a root filter plus a set of parts associated using a deformation model. The score associated to each star model is the summation of the scores of the root filter and parts at a given location and scale minus a deformation cost which measures the deviation of parts from their ideal location relative to the root. The scores of both parts and root are defined as the dot product of a learnt filter which belongs to that part and a set of extracted features for that specific location. The same set of features as [5], i.e. HOG, is used in [6] with the difference that principle component analysis has been applied to HOG features in order to reduce the dimensionality.

2.1.1 Human Detection with Occlusion Handling

While the deformable part-based model has recently shown excellent performance in object detection, it achieves limited success when the human is occluded. In particular, the final score in [6] is computed using the score of all the parts



Fig. 2 *Left*: human detection results using [6]. *Right*: human detection results using our approach where *red boxes* show the human detected as full bodies, *green boxes* show the humans detected as upper bodies, and *yellow boxes* show the humans detected as heads only. It is clear that [6] failed to detect occluded humans since it does not have an explicit occlusion model, while our approach detects the occluded parts and excludes them from the total detection scores, thus achieving significant improvements especially in crowded scenes

without considering that some of them can be occluded by other pedestrians or static objects in the scene. The occlusion happens especially in crowded scenes such as the example shown in Fig. 2 which signifies the drawback of this method. Considering the score of the occluded parts in the final decision score may cause the algorithm to ignore most of the partially occluded humans in the final detection results. Therefore, some methods such as [7] or [8] rely on head detection only and disregard the rest of the body.

To address this problem, we purpose in [9] to infer occlusion information from the score of the parts and utilize only the ones with high confidence in their emergence. By looking at the score of each part, we find the most reliable set of parts that maximizes the probability of detection. Let H denote the HOG feature of the image, and $p = (x, y)$ represent the location of a part. The detection score at location (x_0, y_0) defined in [6] is:

$$score(x_0, y_0) = b + \sum_{i=1}^{i=n} s(p_i),$$

where b is the bias term, n is the number of parts, and $s(p_i)$ is the score of part i which is computed as:

$$s(p_i) = F_{p_i} \cdot \mathcal{O}(H, p_i) - d_{p_i} \cdot \mathcal{O}_d(d_x, d_y),$$

where F_{p_i} is the part filter, and $\mathcal{O}(H, p_i)$ denotes the vector obtained by concatenating the feature vectors from H at the sub window of the part p_i (d_x, d_y) denotes the displacement of the parts with respect to the anchor position. To address the discussed issue, instead of aggregating the score of all the parts, we select the subset of parts which maximize the detection score:

$$score(x_0, y_0) = b + \underset{S_m}{\operatorname{argmax}} \frac{1}{|S_m|} \times \sum_{i \in S_m} \frac{1}{1 + \exp(A(p_i) \cdot s(p_i) + B(p_i))}.$$

The sigmoid function is introduced to normalize the score of the parts. The parameters A and B are learned by the sigmoid fitting approach and $|S_m|$ is the set cardinality. This equation corresponds to the average score of the parts in a subset which makes the comparison between different subsets easy.

If there is an occluded part in a subset $|S_m|$, its average score will be lower than a case which doesn't have any occluded parts. Therefore, by maximizing the above equation, we obtain the most reliable set of parts and its corresponding detection score. In our experiments we consider only three subsets of parts (full body, upper body and head only). We found these three subsets to be representative enough for most scenarios. That way, we do not need to search for all the 2^n parts. Figure 2 demonstrates the qualitative comparison between [6] and our approach.

2.2 Data Association Using Generalized Graphs

The method explained in Sect. 2.1 detects humans in each video frame. However, it does not specify which detections belong to one identity. We need to determine the detections which correspond to one particular pedestrian in order to form a trajectory. We employ a data association method based on Generalized Minimum Clique Problem (GMCP) for this purpose. The input to the data association method is the detections obtained using the human detector of Sect. 2.1, and the output is the trajectory of each pedestrian in the video. Figure 3 shows the block diagram of this process. First a video is divided into smaller segments and the human detector is applied to each video frame. Then, the GMCP-based data association method is utilized in order to form the tracklets of pedestrians in each segment. Later, we perform another data association using GMCP to merge the tracklets of one person found in different video segments into a full trajectory spanning over the course of the whole video.

2.2.1 Finding Tracklets of Pedestrians in One Video Segment

In order to determine if a group of detections from different video frames belong to one person, we utilize two features for each detection: Appearance and Spatial Location. If the visual appearances of a group of detections are similar and the tracklet they form is smooth, we conclude that they belong to one identity. On the other hand, if the appearances of some of the detections are not similar to the rest or if the trajectory they form includes abrupt jumps, we infer that some of the detections must belong to other pedestrians. In order to perform this task, we formulate the input to our data association problem as the graph $G = (V, E, W)$ where V , E and W denote the set of nodes, edges and edge weight respectively. Each node represents one human detection. The nodes in V are divided into a number of disjoint clusters. Each cluster represents one video frame and the nodes therein represent the detections in that particular frame. An edge weight is defined as the difference between the color histograms of two detections. Therefore, if two human

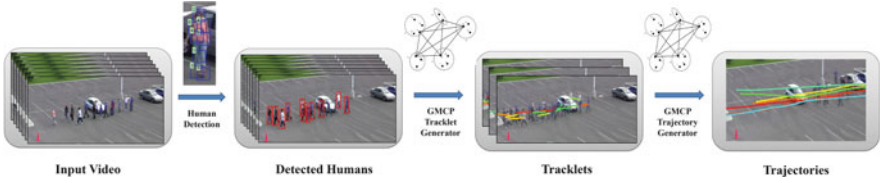


Fig. 3 Block diagram of the data association method. A video is divided into smaller segments, and the GMCP-based method is employed to find pedestrian tracklets and trajectories

detections are visually similar, the weight of the edge between their representing nodes is expected to be low and vice versa.

The solution to our data association problem is found by identifying one detection from each frame in a way that all the selected detections belong to one person. In other words, a feasible solution can be represented by a subset of the nodes of G which we call V_s . We define the appearance cost of a feasible solution, $\gamma_{appearance}(V_s)$ as the summation of all the edge weights between its nodes. Therefore, by solving the optimization problem $\arg \min_{V_s} (\gamma_{appearance}(V_s))$, the feasible solution with the most consistent appearance features is found.

Generalized Minimum Clique Problem (GMCP) [11] is defined as selecting a subset of nodes from a superset in a way that the summation of edges weights between the selected nodes is minimized. The nodes in the superset are divided into a number of disjoint clusters. Exactly one node from each cluster should be included in the subset of selected nodes. As can be understood from the definition of GMCP, solving GMCP for the graph G is equivalent to solving our data association problem of $\arg \min_{V_s} (\gamma_{appearance}(V_s))$. Therefore, we find the generalized minimum clique of G in order to find the feasible solution V_s which has the minimum cost.

However, we add a term based on motion to our optimization function in order to incorporate the smoothness of trajectory in identifying the best feasible solution. Therefore, the optimal feasible solution, \hat{V}_s , is found by solving:

$$\hat{V}_s = \underset{V_s}{\operatorname{argmin}} (\gamma_{appearance}(V_s) + \gamma_{motion}(V_s)).$$

The motion cost, $\gamma_{motion}(V_s)$, is based on the fact that humans tend to move smoothly and avoid unnecessary abrupt changes in direction and speed. Since a video segment usually covers a short temporal span of a few seconds, the motion of pedestrians therein can be assumed to be near constant velocity. We utilize a global motion model proposed in [10] in order to assign a cost to a feasible solution based on motion. The employed motion model assigns a low cost to V_s if the corresponding tracklet follows constant velocity model and vice versa.

\hat{V}_s found by solving the aforementioned optimization problem identifies the detections in different video frames which belong to one person. Therefore, by finding \hat{V}_s the tracklet of one pedestrian in one video segment is found. Then, we exclude the nodes included in \hat{V}_s from the graph G and solve the optimization

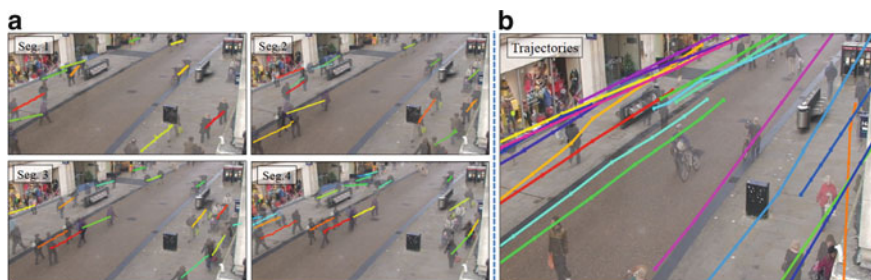


Fig. 4 (a) Tracklets found in four segments of a sample video sequence. (b) Tracklets are merged into full trajectories for all the pedestrians

problem again in order to compute the tracklet for the next pedestrian in the segment. This process continues until the time no or few nodes are left in graph G which implies all the pedestrians are tracked.

The human detector may fail to detect a pedestrian in one frame. This may happen due to several reasons such as occlusion, articulated pose or noise. Since GMCP selects one detection from each frame, it will choose an incorrect node for the frames where a particular person does not have a detection. Therefore, we add hypothetical nodes to each cluster which are supposed to represent virtual detections for the cases where human detector failed. The appearance features and spatial locations of hypothetical nodes are calculated based on the other detections included in V_s as explained in [10].

The tracklets found in four segments of a sample video sequence are shown in Fig. 4a.

2.2.2 Merging Tracklets into Trajectories

The explained process forms the tracklets of pedestrians in each video segment. In order to form the full trajectory of one person over the course of the whole video, we need to identify the tracklets which belong to one identity and merge them into a trajectory. This task in fact requires solving another data association problem. We employ a method similar to the one explained earlier in order to perform the association between tracklets. For this purpose, each tracklet in one segment is represented by one node. The appearance feature of each node is the average of color histograms of the detections in the corresponding tracklet. The spatial location of a node is defined as the middle point of the corresponding tracklet. We form an input graph similar to G and solve the optimization problem explained earlier [11]. Doing that, the tracklets which include visually similar detections and form a smooth trajectory are associated together. Therefore, the trajectories of all pedestrians in the whole video are found. Sample result of the merging process

Table 1 Tracking results on town center data set

	MOTA	MOTP	MODP	MODA
Benfold et al. [13]	64.9	80.4	80.5	64.8
Zhang et al. [14]	65.7	71.5	71.5	66.1
Pellegrini et al. [15]	63.4	70.7	70.8	64.1
Yamaguchi et al. [16]	63.3	70.9	71.1	64.0
Leal-Taixe et al. [17]	67.3	71.5	71.6	67.6
Ours/GMCP	75.59	71.93	72.01	75.71

Table 2 Tracking results on TUD and PETS 09 sequence

Dataset	MOTA	MOTP	Prec	Rec	IDsw
TUD-Crossing [18]	84.3	71.0	85.1	98.6	2
TUD-Crossing [19]	85.9	73.0	89.2	98.8	2
TUD-Crossing-Ours	91.63	75.6	98.6	92.83	0
TUD-Stadtmitte [20]	60.5	65.8	–	–	7
TUD-Stadtmitte-Ours	77.7	63.4	95.6	81.4	0
PET2009-View 1 [21]	80.00	58.00	81.00	60.00	28
PET2009-View 1 [22]	81.46	58.38	90.66	90.81	19
PET2009-View 1 [20]	81.84	73.93	96.28	85.13	15
PET2009-View 1 [23]	84.77	68.742	92.40	94.03	10
PET2009-View 1-Ours	90.3	69.02	93.64	96.45	8

is shown in Fig. 4b. The tracklets shown in Fig. 4a are merged to form the full trajectories shown in Fig. 4b.

2.2.3 Experimental Results

We evaluated the described data association method on four standard sequences. Town Center is a sequence of 4,500 frames which shows a semi-crowded scene. TUD-Crossing and TUD-Stadtmitte are two sequences with 201 and 170 frames respectively. PETS2009-S2L1 includes 800 frames with a challenging scenario because of frequent changes in the directions of the pedestrians.

Table 1 shows the tracking results for town center sequence along with comparison to the state of the art. MOTA and MOTP represent the accuracy and precision of tracking based on CLEAR MOT metrics [12]. Prec. and Rec. denote precision and recall value of assigning detections to their appropriate trajectories respectively. IDsw denotes number of ID-switches which represents the number of times a trajectory incorrectly switches between two different identities. Table 2 shows the evaluation results for TUD-Crossing, TUD-Stadtmitte and PET2009-S2L1 sequences. As can be seen, the presented data association method outperforms the state of the art on all the sequences.

The average time of performing data association is 4.4 s per frame using non-optimized Matlab code. The time complexity can be significantly improved upon availability of a parallel and optimized implementation in C.

3 Pedestrian Tracking in Videos with High Crowd Density

High density crowded scenes are characterized by a large number of individuals per unit area. With high density comes a new set of challenges that are not present in non-crowded scenes. These include a large number of individuals and their complex interactions, small target size, and difficulty in establishing correspondences due to proximity among individuals as well as occlusions caused by inter-object interactions. Furthermore, these challenges are dependent on density, the higher the crowd density, the more difficult it is to detect and track individuals. Figure 5 provides some examples of dense crowds.

3.1 Tracking in Dense Crowds Using Floor Fields

The first approach [25] we present for tracking high-density crowds leverages on the observation that the behavior of one individual in a crowded scene is dependent on its interactions with other individuals as well as structure of the scene. A model that captures these interactions in space-time can serve as an auxiliary source of information, thereby constraining the likely movement of individuals in the scene. Since movement of individuals in a crowd is restricted by other individuals and scene structure, we can treat the crowd as a collection of mutually interacting particles. At each point in the scene, we build a matrix of preferences that captures the likelihood of transition of a particle from one point in the scene to another point in its spatial neighborhood. Each transition is associated with a probability, where higher probability higher likelihood for a transition to occur. With inspiration from evacuation dynamics, where floor fields are manually specified for simulation purposes, in this approach, we automatically learn and model the interactions among individuals of a crowd through floor fields and use them for generating better predictions when establishing correspondences across frames (Fig. 6).

Static Floor Field (SFF) SFF captures the general movement of crowd in the scene, for instance, the dominant path taken by the crowd towards the preferred exit location. People tend to form crowds when they share the same goal and this goal-directed and rational behavior of crowds provides an important cue to the movement of individuals in the crowd. The process to compute SFF follows: First, optical flow is computed at each location for the initial N_s frames. The flow vectors are then averaged over N_s frames providing smoothed-out average flow at each location in the scene. Next, sink seeking process is performed to discover the sinks – attractive



Fig. 5 Examples of high-density crowded scenes

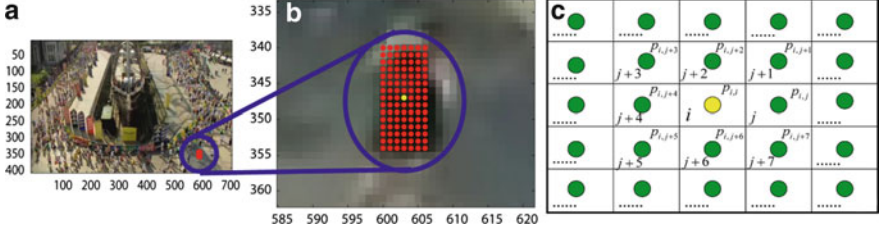


Fig. 6 In (a, b), the *red dots* are the particles on an individual while (c) shows the transition matrix that is obtained from the floor fields

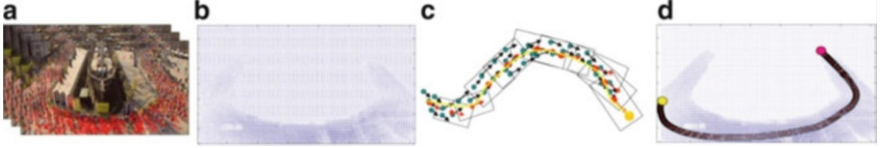


Fig. 7 Computation of Static Floor Field. (a) Shows the dense optical flow whereas (b) is the smoothed out flow. (c) Describes the sink-seeking process where *red dots* are velocity vectors from (b) for one particle, *cyan dots* are the neighbors, *orange dot* is the sink, whereas *rectangles* are the sliding windows. (d) Shows the path for one particle originating at *yellow* and ending at *red* (the sink)

regions towards which the individuals in the crowd move. For this, we initialize a grid of particles over computed flow field. Each particle moves under the influence of the flow field taking into account the influence from neighboring flow vectors (Fig. 7).

$$X_{i,t+1} = X_{i,t} + V_{i,t}, V_{i,t} = \frac{\sum_{j \in neighbors} V_{j,t} W_{i,j,t}}{\sum_{j \in neighbors} W_{i,j,t}}, W_{i,j,t} = \exp\left(-\|V_{i,t-1} - V_{j,t}\|^2\right)$$

where X is the location, V is the velocity, i denotes the individual and j is its neighbor. After performing sink seeking for each point in the scene, each point in a path is replaced by the number of steps required to reach the sink. Repeating this for all paths gives the SFF (shown in Fig. 8d).

Boundary Floor Field (BFF) BFF captures the influence from barriers and boundaries of the scene. Walls and boundaries tend to repel the individuals away from them. BFF is computed on NB frames from the future. First, crowd flow is

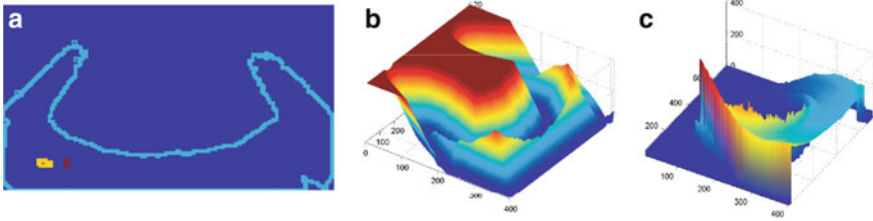


Fig. 8 (a) Is the FTLE field computed using [24] and (b) shows the boundaries computed as the derivative of (a). (c) Is BFF using distance transform on (b). (d) Is SFF obtained after sink-seeking process

segmented using the segmentation algorithm proposed in [24] where the boundaries in the flow field are computed as ridges in Finite Time Lyapunov Exponent (FTLE) field. The segmentation map is then used compute an edge map retaining only the boundary pixels. Next, for each point in the scene, its distance to the nearest barrier/boundary is computed using a distance transform thus, giving BFF. The larger the distance of a point from the boundary, the smaller its influence on an individual near that point. Figure 8a–c show the computation of BFF.

Dynamic Floor Field (DFF) DFF captures the instantaneous flow around point, using the ND frames in the future. The idea is similar to SFF but DFF is temporally localized compared to SFF. Stacking optical flow for ND frames into a 3D volume, a grid of particles is then overlaid and numerically advected while keeping counts of how many times a particle jumps from one point to another during advection. This gives a measure of dynamic interaction between points at each time instant, or DFF.

Tracking The probability for an individual at cell i transitioning to cell j is given by:

$$p_{ij} = C e^{k_D D_{ij}} e^{k_S S_{ij}} e^{k_B B_{ij}} R_{ij}$$

where D_{ij} , S_{ij} and B_{ij} are the transition probabilities based on the three floor fields and k_D , k_S and k_B are the corresponding coefficients while R_{ij} is probability based on appearance calculated using Normalized Cross Correlation.

Experiments We performed experiments on three marathon sequences for this approach. Sequence 1 has 492 frames and 199 individuals were selected for tracking, sequence 2 has 333 frames with 120 individuals, and 50 individuals were selected for tracking in sequence 3 which has 453 frames. Figure 9a–c shown the tracks obtained through the proposed approach. We compared this approach against MeanShift and the ground truth. Figure 9d shows a significant difference in tracking error between the proposed approach (green) and MeanShift (yellow). Figure 9e shows the comparison with the ground truth for selected individuals. The y-axis is the track length from proposed approach (black) and ground truth (green). As evident from the graph, for the 100 individuals compared, track length is very close to that of ground truth.

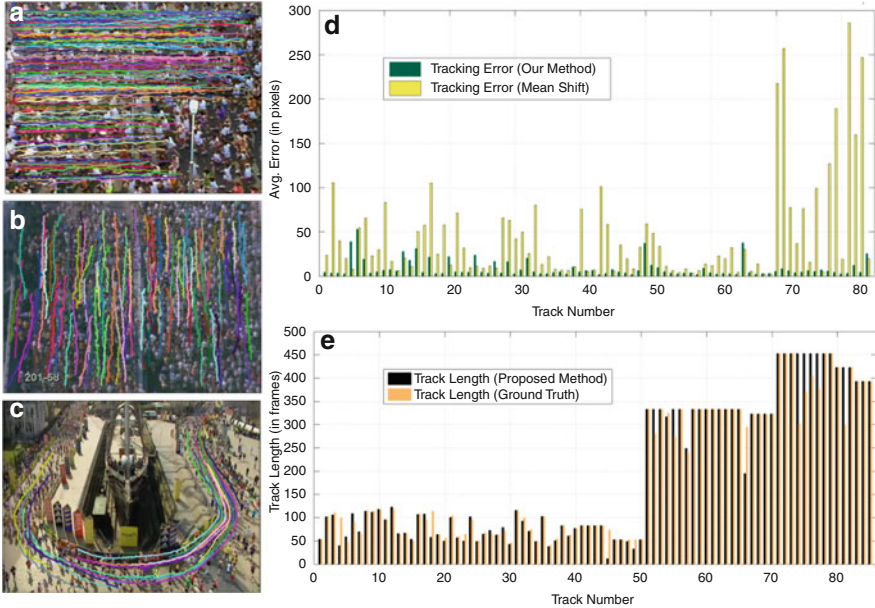


Fig. 9 (a–c) Tracked individuals in the three sequences. (d) Comparison with Meanshift. (e) Comparison with ground truth

3.2 Tracking in Dense Crowds Using Prominence and Neighborhood Motion Concurrence

The approach presented in previous section depends on learning the crowd flow, both averaged over time (SFF) as well as dynamic flow (DFF). The floor fields serve as a strong prior on the motion of individuals at each point in the scene. The assumption that an individual always behaves in a manner consistent with global crowd behavior does not always hold. The restriction on the motion of individuals from time-invariant priors may cause the tracker to fail when the crowd flow is dynamic, the crowd flow explores new region in the scene not previously learned, or when there is camera motion which may introduce errors in learning. In this section, we introduce the second approach [26] to the problem of tracking dense crowds in an online fashion without using any learning or crowd flow modeling.

Similar to the previous approach, we use Normalized Cross Correlation to obtain confidence for appearance. Owing to the challenges introduced by the high density crowds, the simplicity of template based tracker demands more than just appearance to perform well in crowded scenes. For that, we supplement the tracker with salient and contextual sources of information that significantly reduce the confusion in establishing correspondence across frames.

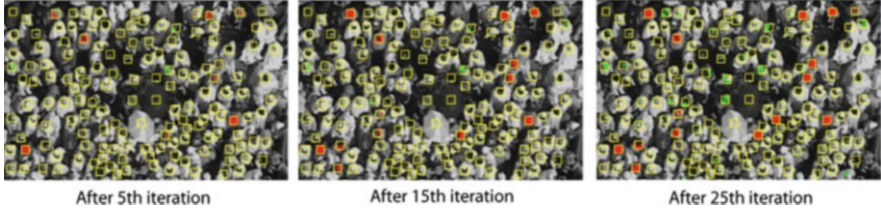


Fig. 10 Intermediate steps for the method of selecting prominent individuals. *Red* are the ground truth (manually selected) prominent individuals whereas *green* are the rest of the individuals. As evident, during back assignment, templates belonging to prominent individuals get filled first and therefore selected

Prominence The first idea in this approach is the prominence of individuals in terms of appearance. In any crowded scene, appearance of certain individuals will be different from the rest, that is, such prominent individuals can be tracked with high confidence.

In order to select prominent individuals, we generate features from the templates by extracting RGB values at each pixel. Then, we cluster all the features into k clusters using mixture of Gaussians. The clusters are sorted w.r.t density, where mass equals the number of points in that cluster and volume is given by $(2\pi)^{3/2} |\Sigma|^{1/2}$. Next, all the points in each cluster are assigned back to individual templates starting from the least dense cluster. This process of back assignment is stopped once $T\%$ of the templates are filled by at least two-thirds. Figure 10 shows the intermediate results of this procedure.

Neighborhood Motion Concurrence (NMC) The motion of an individual in dense crowd is similar to its neighbors. This information can be captured through a motion model that incorporates influence from neighbors. Let $x_i^t = [x \ \dot{x}]^T$ (position, velocity), Σ_i^t represent the state and covariance of an individual i at time t , A be the 2×4 matrix that captures state transition, and $\mathfrak{N}(\mu, \Sigma)$ a 2d Gaussian distribution. NMC for individual i with neighbors j has two components, self and neighbor. The two components are given by:

$$p_S = p\left(z_i^{t-1} \mid \hat{x}_i^{t-1}\right) \cdot \mathfrak{N}\left(Ax_i^{t-1}, A\Sigma_i^{t-1}A^T\right),$$

$$p_N = \sum_j w_j \cdot \mathfrak{N}\left(Ax_{ij}^{t-1}, A\Sigma_j^{t-1}A^T\right),$$

$$w_j = \frac{\exp\left(-\|x_j - x_i\|\right)}{\sum_{k \in \text{Neighbors}} \exp\left(-\|x_k - x_i\|\right)}.$$

Figure 11b, c is an illustration depicting NMC. Black Gaussian in Fig. 11 © corresponds to self-component of the individual under consideration (black square in Fig. 11b) while the colored Gaussians show the neighbor component of NMC.

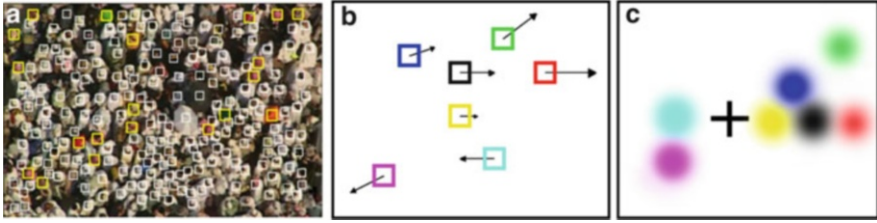


Fig. 11 Final output of the procedure to detect prominent individuals. (b) *Black square* is the individual under consideration while *colored squares* are its neighbors. *Black arrows* show the velocities with which the individuals are moving. (c) *Cross hair* marks the position of individual with *black square* in (b). *Colored Gaussians* are the corresponding contributions to NMC of individual under consideration

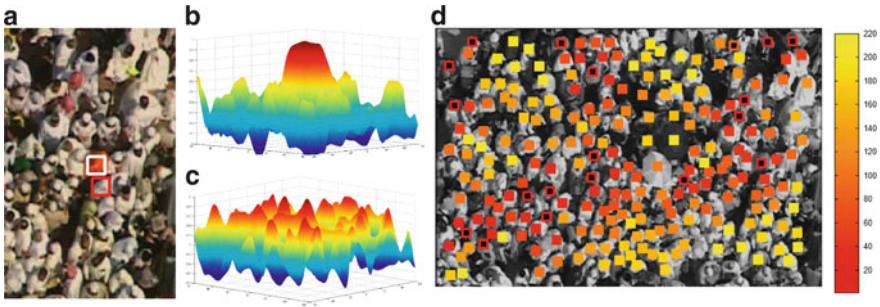


Fig. 12 Hierarchical update. (a) *White square* marks a prominent individual whereas *red square* marks its non-prominent neighbor. (b, c) Are their appearance surfaces which shows that prominent individuals with their unique appearance are less likely to be confused with the neighbors and therefore should be places at the top of tracking hierarchy. (d) Shows the order in which individuals in this scene were updated (*red to yellow*)

Hierarchical Update After having defined the notions of prominence and NMC, the final aspect of this approach is the order in which individuals in a crowded scene are updated. In Fig. 12, the prominent individual (white square in Fig. 12a) has appearance surface given in Fig. 12b, whereas its neighbor (red square in Fig. 12a) has the appearance surface given in Fig. 8c. It is evident that prominent individuals have less confusion with their neighbors and they should be placed on top of the tracking hierarchy. The algorithm, therefore, starts by updating prominent individuals, followed by their neighbors and continues till all the position of all individuals is updated. The position of non-prominent individuals is updated using NMC.

Results We compared approach presented in this section with MeanShift, Normalized Cross Correlation tracker, MeanShift Belief Propagation as well as the approach based on floor fields presented in previous section. The experiments were performed on nine sequences of medium to high density. In Table 3, various characteristics of the nine sequences such as number of frames, number individuals

Table 3 Quantitative comparison for the two approaches against Normalized Cross Correlation, MeanShift and MeanShift Belief Propagation for nine crowded sequences of medium to high density

	Seq 1	Seq 2	Seq 3	Seq 4	Seq 5	Seq 6	Seq 7	Seq 8	Seq 9
# Frames	840	134	144	492	464	333	494	126	249
# People	152	235	175	747	171	600	73	58	57
Template size	14	16	14	16	8	10	10	10	14
NCC	49 %	85 %	57 %	52 %	33 %	52 %	50 %	86 %	35 %
MeanShift	19 %	67 %	17 %	8 %	7 %	36 %	28 %	43 %	11 %
MSBP	57 %	97 %	80 %	69 %	62 %	81 %	68 %	94 %	45 %
Floor fields	75 %	99 %	85 %	84 %	66 %	92 %	67 %	97 %	57 %
Prominence/NMC	80 %	100 %	93 %	94 %	72 %	94 %	67 %	92 %	63 %

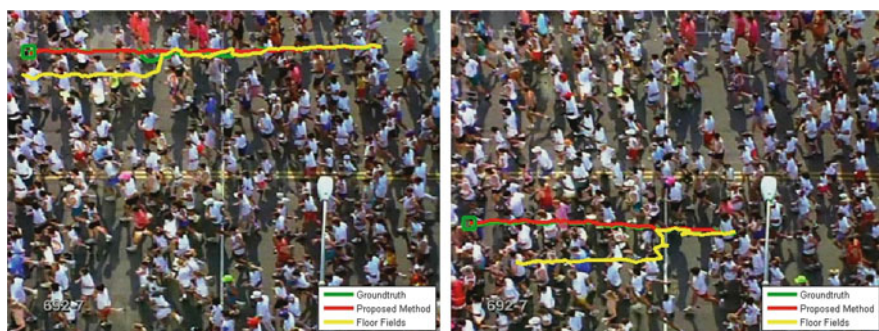


Fig. 13 This figure provides the comparison between the two approaches presented. *Green* is the ground truth trajectory, *yellow* is from first approach and *red* is from the second approach

and template size used for tracking are given in first three rows. Tracking accuracy is reported for the five methods and nine sequences as a percentage of number of points (in all trajectories) that lie within 15 pixel threshold.

Qualitative comparison between the two approaches is given in Fig. 13. The three cases are presented where the second approach (red) performs better than floor fields (yellow). Ground truth trajectory is drawn in green.

4 Conclusion

Automatic tracking of pedestrians is essential for computerized analysis of surveillance videos. In this keynote paper, we present two state of the art tracking methods for videos with low and high density of crowds. The method for low density scenarios first detects pedestrians in each video frame using a part-based human detector. Then, a data association method based on Generalized Graphs is employed for tracking each individual in the whole video. For videos with high crowd density, two approaches are presented. The first one is based on using the scene structure

based force model, while the second approach utilizes contextual information. Our Experiments show the presented frameworks outperform the currently available methods on several benchmarks.

References

1. E. Osuna, R. Freund, and F. Girosi, "Training Support Vector Machines: An Application to Face Detection," *Proc. IEEE Conf. Computer Vision and Pattern Recognition*, pp. 130–136, 1997.
2. C. Papageorgiou, T. Evgeniou, and T. Poggio, "A Trainable Pedestrian Detection System," *Proc. Symp. Intelligent Vehicles*, pp. 241–246, 1998.
3. P. Viola and M. Jones, "Rapid Object Detection Using a Boosted Cascade of Simple Features," *Proc. IEEE Conf. Computer Vision and Pattern Recognition*, vol. 1, pp. 511–518, 2001.
4. Y. Wu, T. Yu, and G. Hua, "A Statistical Field Model for Pedestrian Detection," *Proc. IEEE Conf. Computer Vision and Pattern Recognition*, vol. 1, pp. 1023–1030, 2005.
5. N. Dalal and B. Triggs, "Histograms of Oriented Gradients for Human Detection," *Proc. IEEE Conf. Computer Vision and Pattern Recognition*, vol. 1, pp. 886–893, 2005.
6. P. Felzenszwalb, R. Girshick, D. McAllester, and D. Ramanan. Object detection with discriminatively trained part based models. In *PAMI*, 2010.
7. B. Benfold and I. Reid. Stable multi-target tracking in realtime surveillance video. In *CVPR*, 2011.
8. M. Rodriguez, I. Laptev, J. Sivic, and J.-Y. Audibert. Density-aware person detection and tracking in crowds. In *ICCV*, 2011.
9. G. Shu, A. Dehghan, O. Oreifej, E. Hand, M. Shah. Part-based Multiple-Person Tracking with Partial Occlusion Handling. In *CVPR*, 2012.
10. Amir Roshan Zamir, Afshin Dehghan, and M. Shah. GMCP-Tracker: Global Multi-object Tracking Using Generalized Minimum Clique Graphs. In *ECCV*, 2012.
11. Feremans, C., Labbe, M., Laporte, G.. Generalized network design problems. In: *EJOR*, 2003.
12. Kasturi, R., et al.: Framework for performance evaluation of face, text, and vehicle detection and tracking in video: Data, metrics, and protocol. In: *PAMI*. (2009).
13. Benfold, B., Reid, I.: Stable multi-target tracking in real time surveillance video. In: *CVPR*.(2011)
14. Zhang, L., Li, Y., Nevatia, R.: Global data association for multi-object tracking using networkflows. In: *CVPR*. (2008)
15. Pellegrini, S., Ess, A., Van Gool, L.: Improving data association by joint modeling of pedestrian trajectories and groupings. In: *ECCV*. (2010)
16. Yamaguchi, K., Berg, A., Ortiz, L., Berg, T.: who are you with and where are you going? In: *CVPR*. (2011)
17. Leal-Taixe, L., Pons-Moll, G., Rosenhahn, B.: Everybody needs somebody: Modeling social and grouping behavior on a linear programming multiple people tracker. In: *ICCV Workshops*. (2011)
18. Breitenstein, M.D., Reichlin, F., Leibe, B., Koller-Meier, E., Gool, L.V.: Robust tracking-by-detection using a detector confidence particle filter. In: *ICCV*. (2009)
19. Brendel, W., Amer, M., Todorovic, S.: Multiobject tracking as maximum weight independent set. In: *CVPR*. (2011)
20. Andriyenko, A., Schindler, K.: Multi-target tracking by continuous energy minimization. In: *CVPR*. (2011)
21. Berclaz, J., Fleuret, F., Turetken, E., Fua, P.: Multiple object tracking using k-shortest paths optimization. In: *PAMI*. (2011)

22. Shitrit, H.B., Berclaz, J., Fleuret, F., Fua, P.: Tracking multiple people under global appearance constraints. In: ICCV. (2011)
23. Henriques, J.F., Caseiro, R., Batista, J.: Globally optimal solution to multi-object tracking with merged measurements. In: ICCV. (2011)
24. S. Ali and M. Shah, A Lagrangian Particle Dynamics Approach for Crowd Flow Segmentation and Stability Analysis, IEEE CVPR, 2007.
25. S. Ali and M. Shah, Floor Fields for Tracking in High Density Crowded Scenes, ECCV 2008.
26. H.Idrees, N. Warner and M.Shah, Tracking in Dense Crowds using Prominence and Neighborhood Motion Concurrence, Submitted to CVIU Journal, 2012.

London Bridge: The Role Pedestrian Modelling Played in Designing the New Station

Nicolas Le Glatin, Isabelle Milford, and Andrew Hutton

Abstract This paper presents an overview of the redevelopment of the London Bridge national railway station as part of the delivery of the Thameslink Programme. The Programme's objective is to significantly improve the capacity of the existing rail services and experience for passengers. The paper illustrates how the design solution has been informed by a rigorous process of assessment, evaluation and validation using a combination of static and dynamic station capacity assessments. This approach has enabled Network Rail to make the design process as efficient and cost effective as possible, and ensuring that passenger flow and experience is at the centre of the design process.

Keywords Railway station design • Pedestrian flow • Station capacity • Static analysis • Dynamic modelling

1 Introduction

The Thameslink rail services run north–south through London and link major transport hubs including Luton and Gatwick airports and St Pancras International. The Thameslink Programme, when completed in 2018, is intended to deliver major public benefits. Not only will there be more and longer trains but there will also be a larger catchment area with more stations across the South East served by Thameslink services, providing direct access to more destinations. The

N. Le Glatin (✉)

NG Space Engineering Ltd, Milton Keynes, United Kingdom

e-mail: Nicolas.leglatin@gmail.com

I. Milford • A. Hutton

Network Rail Ltd, London, United Kingdom

e-mail: Isabelle.Milford@networkrail.co.uk; Andrew.hutton@networkrail.co.uk

improvements to London Bridge station are the last major part of the Thameslink Programme to be delivered. The London Bridge station redevelopment proposal outlined in this paper was driven by the need to increase the number of through trains serving the station and meet the anticipated growth in passenger numbers.

In addition to the delivery of a world-class transport interchange the redevelopment will allow the creation of a new street level concourse providing new entrances directly onto Tooley Street and Thomas Street. This will give the station a civic scale and a street presence appropriate for its importance, both within the Borough of Southwark, and London. It will provide a truly legible layout, allowing the station to feel like a single station for the first time.

This paper illustrates how the proposed design solution has been informed by a rigorous process of assessment, evaluation and validation including in the discipline of pedestrian flow analysis. The design has been supported at an early stage by the use of both pedestrian flow static and dynamic modelling analysis. This approach has allowed the design team to optimise the station layout, plan for future passenger growth and size the station facilities appropriately. It also demonstrates the station is safe, comfortable to use and easy to navigate with a minimum of operational management.

The four key stages of the design process influenced by pedestrian flow analysis are as follows and form the basis of the discussion in this paper.

- (a) *Site and Context* – Understanding the limitations and opportunities presented by the existing site.
- (b) *Meeting Future Demand and Design Principles* – Defining the design principles in terms of layout, amount, scale and usage to meet anticipated passenger growth.
- (c) *Design Development* – Testing and validating the design principles through the use of pedestrian dynamic simulation.
- (d) *Construction Strategy* – A key project restriction is to enable a construction strategy that keeps the station in operation during the construction period and provides a train service throughput equivalent to today. Pedestrian flow analysis has played a significant role in demonstrating to the construction engineers and project stakeholders that the sequencing of the works provides a safe environment for passengers.

2 Thameslink Programme

The Thameslink Programme, when completed, will deliver major public benefits. It will significantly increase the capacity of the existing rail services by providing up to 24 train paths per hour in each direction through Central London in peak hours (Fig. 1) and further increase capacity through the use of 12 car trains. The new Thameslink rail services are intended to operate as a ‘metro’ style service with very frequent trains stopping only for a short period of time. It will also reduce crowding

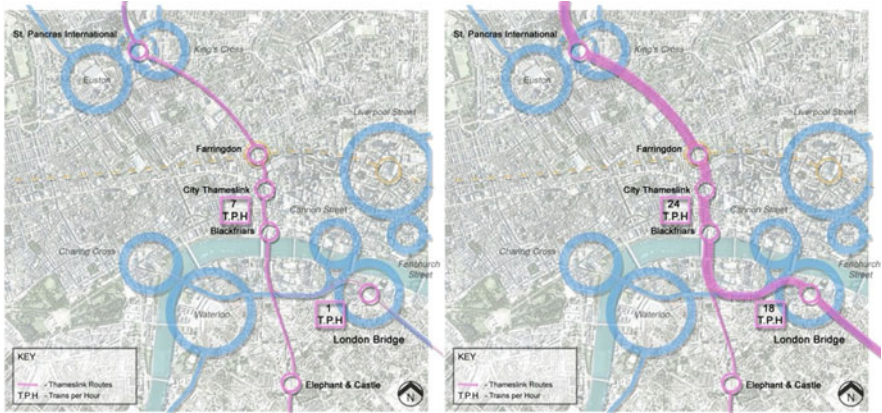


Fig. 1 Train service capacity without and with London Bridge’s station redevelopment

on London Underground by allowing passengers to travel straight through without changing onto the tube and is intended to bring about a significant modal shift by encouraging travel by train rather than by car.

The improvements to London Bridge station are the last major part of the Thameslink Programme to be delivered. Improvements to the other Thameslink stations in Central London are either completed, or are already under construction. A new Thameslink station has been provided at St Pancras International. The station at Blackfriars has been rebuilt, now spanning the river Thames. The redeveloped Farringdon station has now opened and in 2018 the station will be the only one where Crossrail, Thameslink and London Underground meet.

2.1 London Bridge Station

London Bridge station is the cornerstone of the Thameslink Programme. The station is currently a major bottleneck for the delivery of additional Thameslink services and without the reconfiguration of the track and platform layout at London Bridge, up to 80 % of the Thameslink Programme benefits cannot be delivered.

The existing concourse at London Bridge is at the bus station level (Fig. 2) and this is essentially designed to serve the nine terminating platforms. The six through platforms really have no concourse area at all, just a long, low ceiling, narrow corridor which links the platforms. The existing station is one of the most confusing in London, particularly for visitors to the city unfamiliar with its layout. The station has no real street presence, with only the narrow Joiner Street entrance.

The track and platform re-alignments required to deliver the Thameslink services will reduce the number of terminating platforms and increase the number of through platforms, cutting across the existing concourse on a new viaduct. The site is

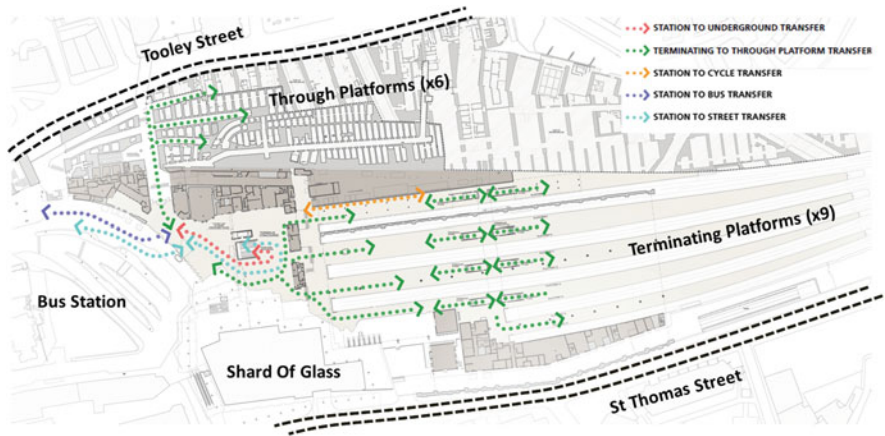


Fig. 2 London Bridge concourse layout to date (2012)

bounded to the north by Tooley Street and to the south by St Thomas Street, constrained by sheer viaduct walls. The pavements and road widths on both sides of the station are relatively narrow and there is therefore no scope to increase the width of the station viaduct or station footprint overall.

3 Site and Context

3.1 Station Usage

To inform the pedestrian flow analysis supporting the redevelopment of London Bridge station, a number of passenger count surveys were carried out to establish the volume of passengers using the station to date. Each year the station brings around 55 million passengers into the city of London, making it one of the busiest railway station in the country. The surveys have not only provided a dataset of the magnitude of passengers using the station in both morning (Table 1) and evening peak periods but also assisted in identifying the key interchange patterns with other modes of transports.

In addition to surveying the station internal flows of passengers, a comprehensive passenger survey of the local street movements has also been completed to map out the connectivity of the station with its wider street landscape (Fig. 3). The survey help develop a thorough understanding of the station interaction within its environment. This in turn has helped inform the design process, delivering a better design solution for London Bridge redevelopment.

Table 1 Origin-destinations AM peak survey matrice (2010)

2010 – Preliminary survey data
 AM peak – (7.00–10.00)

Origins/ destinations	Terminating platforms	Through platforms	LUL	Bus	Streets	Total
Terminating platforms	0	8,000	13,300	3,600	15,900	40,800
Through platforms	1,900	8,500	10,800	1,600	18,300	41,100
LUL	3,200	2,500	–	100	17,700	23,500
Bus	100	400	0	–	–	500
Streets	600	1,500	4,400	–	–	6,500
Total	5,800	20,900	28,500	5,300	51,900	112,400

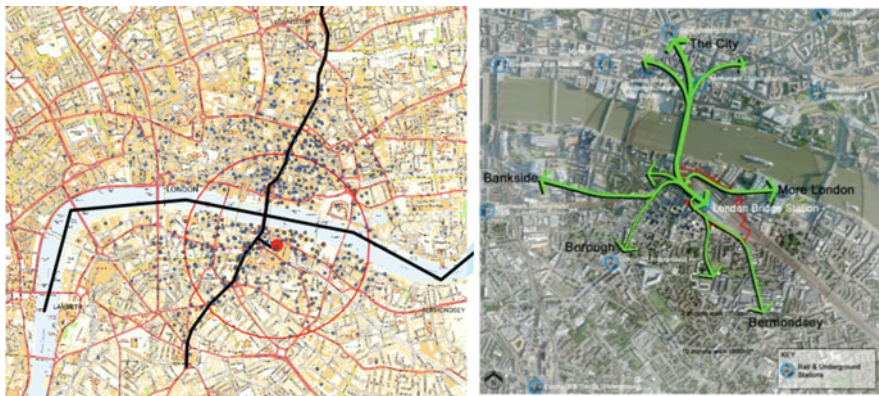


Fig. 3 Passenger destinations and key routes within the street network at London Bridge

3.2 Station Current Limitations

To review the ability of London Bridge station to accommodate additional passenger growth in the future, a baseline pedestrian dynamic model of the current station was developed by the design team. The station layout and operational configurations have been assessed using the LEGION dynamic software for both normal and degraded station operations. The LEGION software [3] was used as it provides a wide-range of functionalities allowing the development of realistic station models.

A key aspect of the model development was to work in collaboration with the station management team to fully capture the day to day operational conditions at the station. The performance of the model was also reviewed and subsequently approved by all key project stakeholders. Involving project partners in the development of the dynamic modelling has contributed in increasing confidence in the use of such analysis technique and also provided a powerful tool to communicate any future changes to the layout and operational conditions.

The results of the dynamic modelling demonstrate that the existing station has a number of constraints which limit its ability to accommodate future growth. This is

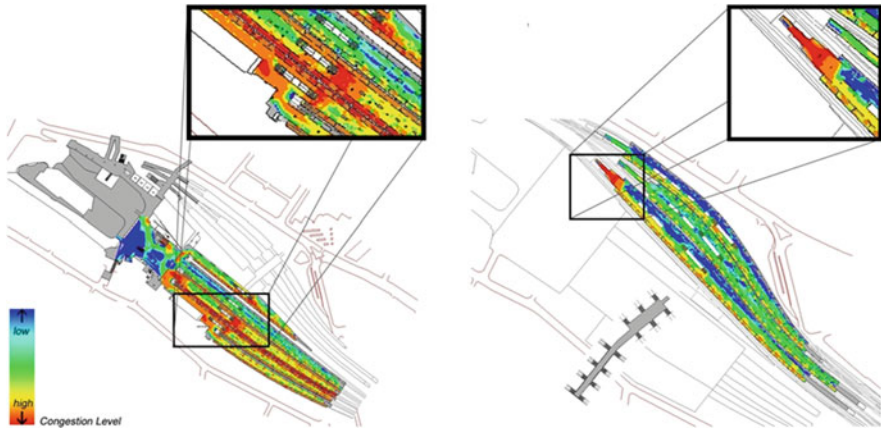


Fig. 4 Existing layout constraints at London Bridge station

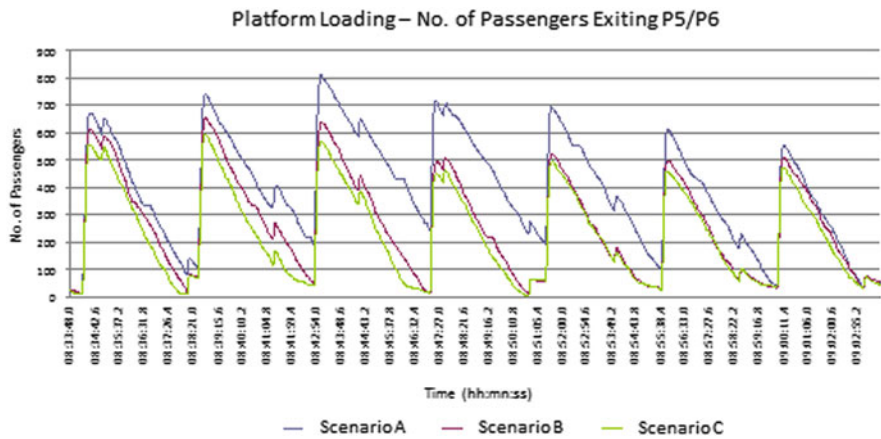


Fig. 5 Through platforms clearance time as result of passenger growths

most apparent at the through platform-end ramps (Fig. 4), the terminating platform adjacent to the footbridge stairs and the platform widths on the through platforms during the evening peak.

It is anticipated that this situation will continue to deteriorate and will soon reach a point where trains will need to be held outside the station while the previous train passengers exit the platform and other congested areas. The analysis shows that the passenger demand growth will result in extended platform clearance time. This is particularly concerning for platform P5/P6 (Fig. 5) where passenger growth results in significant residual platform populations preventing the arrival of the following trains. A situation where the platform is occupied on arrival of the following train is a potential safety risk and a major operational and performance concern.

4 Meeting Future Passenger Demand

The purpose of this section is to present the main passenger and station operation design requirements and aspirations identified as part of the redevelopment of the station. Furthermore, it discusses the key design constraints the design team had to accommodate to deliver the new station design.

4.1 Design Requirements

Train services specifications – To deliver the Thameslink services, the station track layout has to be converted to six terminating platforms and nine through platforms (Fig. 8). In its final configuration the following train service pattern (train per hour – tph) will serve London Bridge station:

- Terminating services (20 tph)
- Cannon Street services (20 tph)
- Thameslink services (18 tph)
- Charing Cross services (28 tph)

All trains will be 12-car trains in the through platforms and a combination of 10-car train platforms and 12-car trains for the terminating station.

Passenger capacity – The most significant factor driving the size and layout of the new station is the need to increase its capacity to meet the anticipated growth in passenger numbers. The passenger forecast requirement was developed in collaboration with the Department for Transport and agreed with all key project stakeholders (Network Rail, LUL, Bus station, TfL Interchange and the Train Operating Companies). The future passenger flows predicted within the interchange hub in shown in Fig. 6. In summary, the station capacity is designed to accommodate an increase in passengers up to 65 % above the current station usage.

Design an Efficient Transport Hub – The Network Rail station at London Bridge is part of a much wider transport hub. The London Underground station and bus station are both located immediately next to the rail station and it is important that there are direct, efficient connections to these. The provision of adequate facilities for cycles and taxis is also vital to deliver an integrated transport interchange.

Optimise Horizontal Connectivity – The Thameslink Programme provides extra capacity on the rail system. Part of the way in which this is achieved is by providing longer platforms to allow for longer 12 car trains. The new Thameslink rail services are intended to operate as a ‘metro’ style service with very frequent trains stopping only for a short period of time. In order to maintain a reliable train service performance it is important that passengers are spread along the length of the platform to optimise boarding and alighting time.

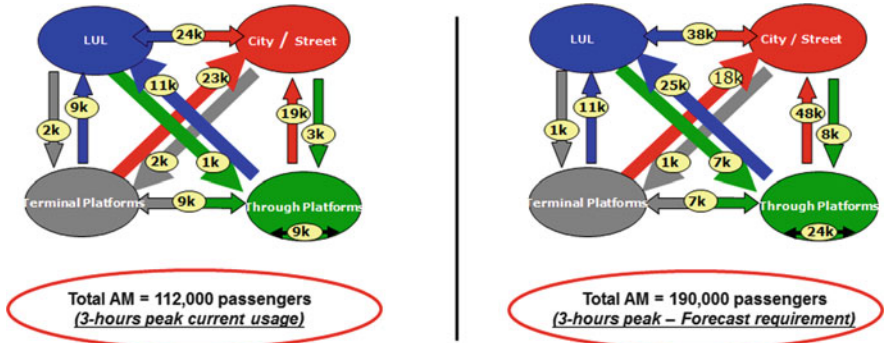


Fig. 6 London Bridge passenger volume today versus the passenger forecast requirement

Optimise Vertical Connectivity – The existing station is not easily accessible from street level and the split concourses and platform arrangements do not assist passenger movements. It is therefore an important design objective to have easy vertical access to the platforms and trains to minimize the journey times of passengers within the station and provide an efficient connectivity with the street level.

Improve Urban Connectivity – Network Rail is also keen to support the London Borough of Southwark plan to see the areas to the north and south of the station connected in a more pedestrian friendly way. The railway viaduct is currently a physical barrier and this has not assisted the regeneration of the area to the south.

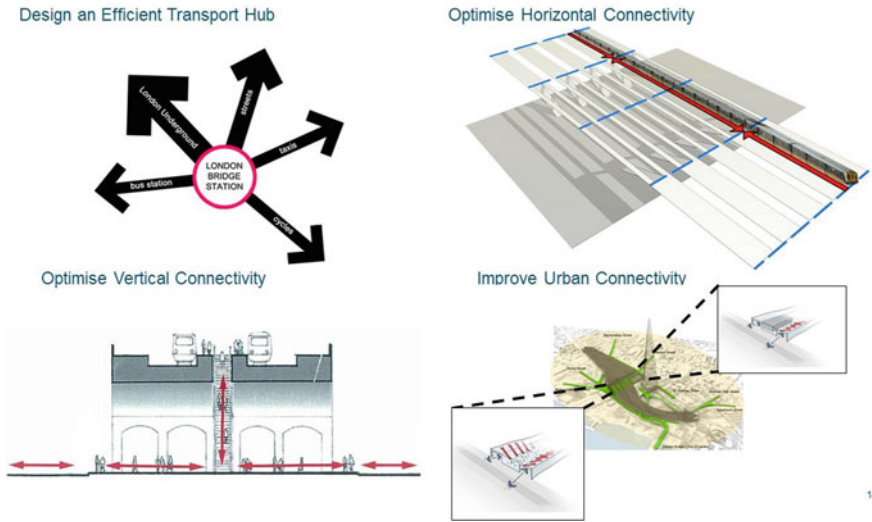
Concourse Size – This is driven by pedestrian flow and capacity issues as well as the fixed dimensions of the escalators, lifts, stairs and associated circulation zones which need to be accommodated within the space.

Concourse Location – This is defined by the need to get people to and from platforms quickly and easily. It is also determined by the existing streetscape, and the need to relate to other major public spaces and routes around the station (Fig. 7).

4.2 Design Constraints

A number of design constraints to accommodate future passenger growth at London Bridge were identified during the design development. The key constraints are introduced below and represented in (Fig. 8)

- (a) **Engineering constraints:** The existing viaduct walls along Tooley St limit expansion of the station footprint to the north and south. There is inadequate space to add new platforms, so all the track realignment has to occur within the current station footprint. The station has also to remain in operation during construction, resulting in a highly complex phasing and construction strategy.



14

Fig. 7 Station design development – key requirements and aspiration

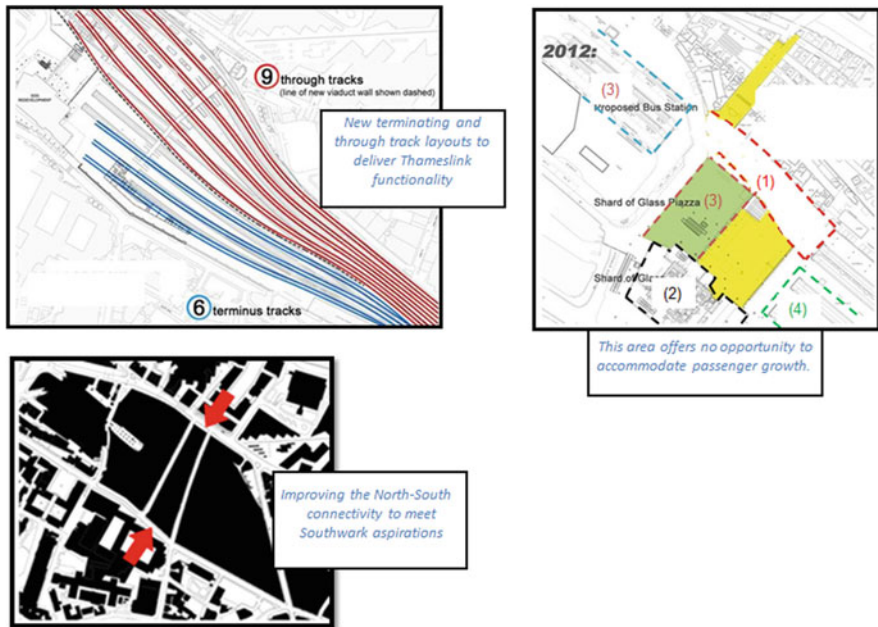


Fig. 8 Station design constraints at London Bridge

(b) **Physical site constraints:** The existing station concourse is not large enough to accommodate the anticipated passenger numbers for the whole station. The expansion of the existing terminating concourse is constrained (Fig. 8) by the

introduction of (1) a viaduct (to the North), (2) the Shard of Glass (to the South), (3) a new bus station and piazza (to the West) and (4) the new revised terminating track layout (to the East).

- (c) **Planning constraints:** Improving the North–south connectivity to meet London Borough of Southwark’s aspirations

5 Concept Development

Informed by the design requirements and constraints discussed in the section above, a concept design was developed following the set station capacity guidelines available in the Network Rail Station Capacity Assessment Guidance [1]. The document provides practical guidance to station capacity requirements to the planning and design of railway station. Station capacity can be described as the ability of the station and its associated spaces and facilities to safely, comfortably and conveniently accommodate and circulate the numbers of passengers expected to use the station.

The Station Capacity Assessment Guidance promotes a consistent “best practice” approach to capacity assessments in planning and designing railways stations, including elements such as platforms, concourses and interchanges routes. It helps achieve the optimum sizing and relative arrangement of waiting areas, decision making points, circulation spaces. It also ensures that the station design is provided with:

- Appropriately sized public spaces and facilities
- Safe, effective and convenient access to train services
- Safe, effective and convenient operation and management of the station
- Clear circulation routes with minimum travel distances
- Adequate revenue protection facilities (gateline and ticketing)
- Circulation spaces free from unnecessary obstructions
- Good line of sight and efficient routes to all modes of transport
- A predictable plan for growth (active versus passive provisions at the station)

Below are two illustrations of how Network Rail guidelines have been applied and contributed to the definition of the station final layout overall dimension and location.

5.1 Concourse Location

The escalators up from the street level concourse were first positioned as evenly as possible along the platforms to ensure even distribution of passengers along each platform and to enable passenger egress down to concourse level as efficiently as possible. The ideal position for the head of each escalator is at approximately

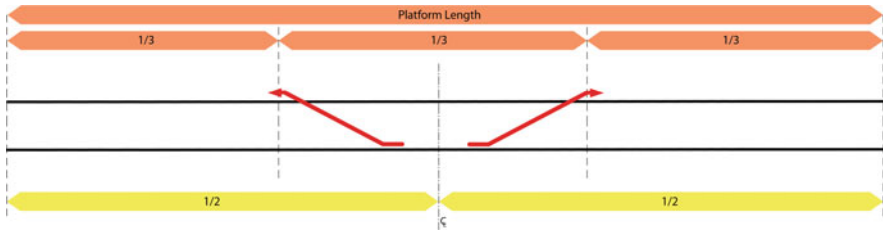


Fig. 9 Concourse location principles

third points along each platform which means that no matter where a passenger alights, they never have to walk more than a third of the platforms length to reach an escalator. This layout results in the concourse being positioned centrally in relation to the platform lengths above as shown in Fig. 9.

In addition to the operational constraints, the concourse should also be positioned appropriately in relation to the major approaches and surrounding public spaces. Because the platforms at London Bridge are staggered it is impractical to position the concourse centrally on all platforms. The concourse has therefore been positioned as centrally as possible on the through platforms which constitute the majority of the station. This allows the concourse to face onto More London's central axis (Fig. 11), a major pedestrian route, without being too far east, to link conveniently to the underground, bus station, and terminating concourse.

5.2 Concourse Footprint

The diagram below shows how the concourse width is informed by the functional and operational requirements. In addition to the escalator length required to accommodate the level difference between concourse and through platform level, the minimum concourse width is determined by the “run-off” zones [1] required at the end of each escalator to reduce the risk of congestion at the potential pinch points between the escalators and central lift core (Fig. 10).

The resulting concourse layout (Fig. 11) is a sizeable area, which is able not only to achieve passenger comfort during normal operations and accommodate commercial retail, but also provides significant resilience for the station to operate safely during degraded conditions and train services perturbations.

At this stage in the design process, a number of new layout constraints, such as the number of escalators, the minimum stairs and corridor width, locations of the entrances to the station were fixed on plans. These constraints were then passed onto the architects and structural design team to develop a detailed station layout. These detailed plans were subsequently assessed using a more detailed level of analysis through the use of pedestrian dynamic modelling technique.

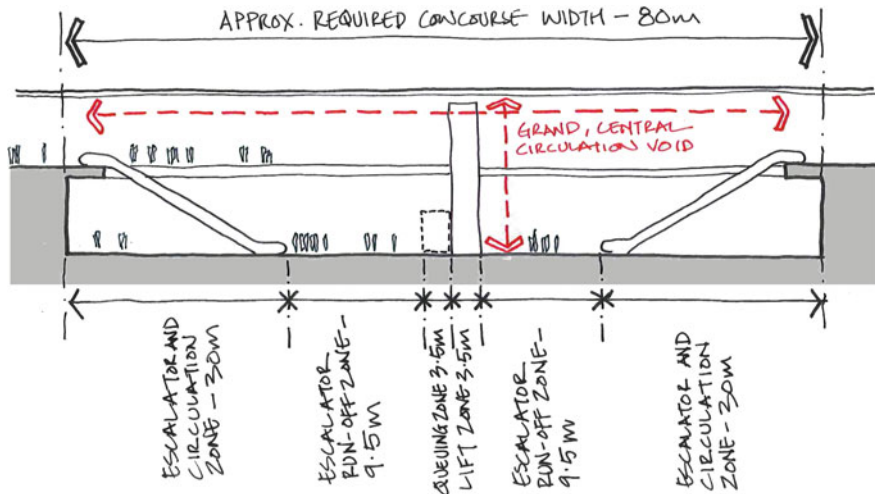


Fig. 10 Concourse scale principles

6 Design Validation

6.1 Pedestrian Dynamic Modelling

Based on the design layout progressed by the project's architect [2] and design team, a LEGION dynamic model was developed to evaluate the final design and provide an assessment of key performance targets against Network Rail Station Capacity Assessment Guidance. This design stage has involved a number of design iterations between the pedestrian modelling team and designers to refine the station layout and passenger experiences through the station.

The LEGION model captures the dynamics of the complete London Bridge interchange hub (Fig. 13), including the Underground and bus stations and adjacent street landscape. The model has been used to confirm the compliance of the design with Network Rail Guidelines and test the station layout under normal, degraded and perturbed scenarios during both morning and evening peak periods.

Additional sensitivity studies were also completed to assess the requirements of the design against future passenger growth. This allows for the inclusion of passive provisions within the layout for the future installation of additional gatelines, escalators and ticketing facilities. The provision of retail facilities has also been reviewed in light of future passenger demand as more retail can be provided in the first years of the station life cycle.

The dynamic modelling confirmed that the station design operates within Network Rail design requirements. The key features of the design from a passenger flow perspective are summarised below:

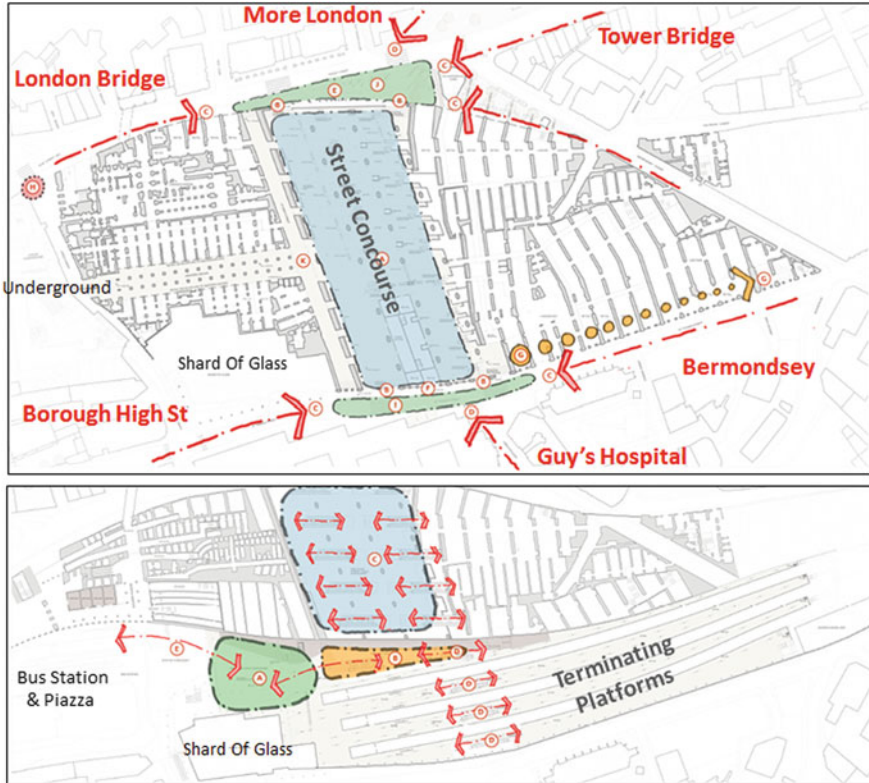


Fig. 11 Proposed new London Bridge station layout at both street and bus station levels

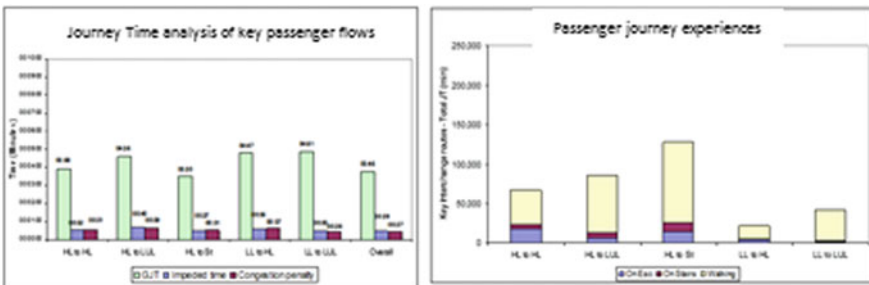


Fig. 12 Average passenger journey times and passenger journey experience analysis

- (a) London Bridge station provides a legible design with direct/shortest routes for the major interchange flows. Figure 12 shows an analysis of the average passenger journey times and journey experience for some key interchange flows within the station.

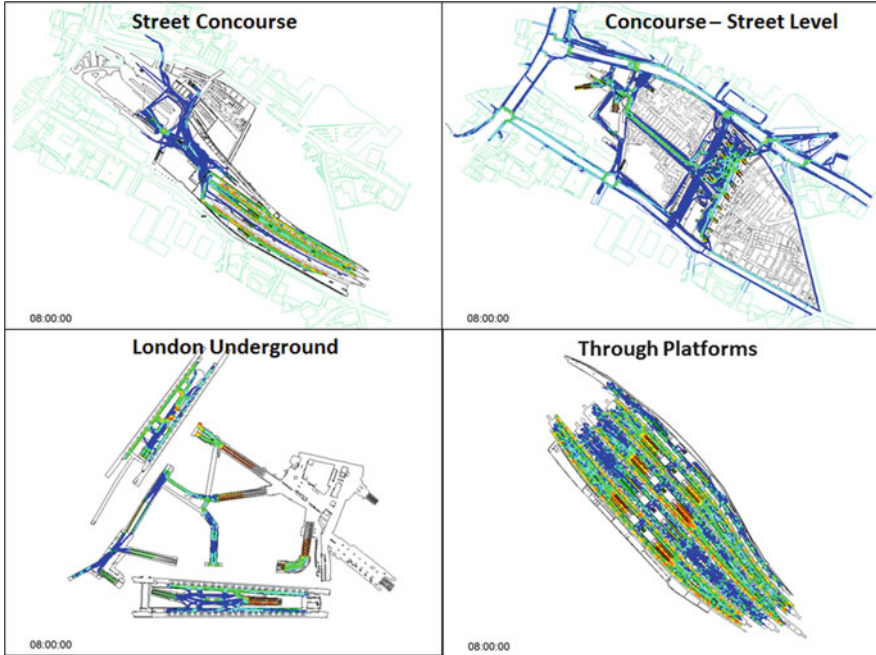


Fig. 13 London Bridge interchange LEGION model – AM peak analysis

- (b) Most commuters move through the new concourse at street level. This in turn has moved the “centre of gravity” of the station and alters the pedestrian dynamic in the London Bridge wider area. It also provides a much improved north–south connectivity through the station.
- (c) The configuration of the design intrinsically limits the number of passengers using the terminating concourse, resulting in greater flexibility for the provision of station facilities and retail opportunities at this level.
- (d) The through platforms provide direct access to the concourse at street level via two banks of stairs/escalators located at the western and eastern ends. The banks of escalators/stairs optimise the distribution of passenger on the through platforms and help compliance with Network Rail platform egress times and train service performances.
- (e) The retail value at street level is optimised – both in terms of space available for retail and numbers of passengers passing through.
- (f) The dynamic modelling also confirms that design provides sufficient resilience during degraded conditions at the station (Fig. 13).

In addition to assessing the design layout under normal, degraded and perturbed operational conditions, the performance of the proposed solution was also reviewed in the terms of fire safety evacuation. A number of evacuation scenarios were agreed with Network Rail Fire Safety engineers and the London Fire and Emergency

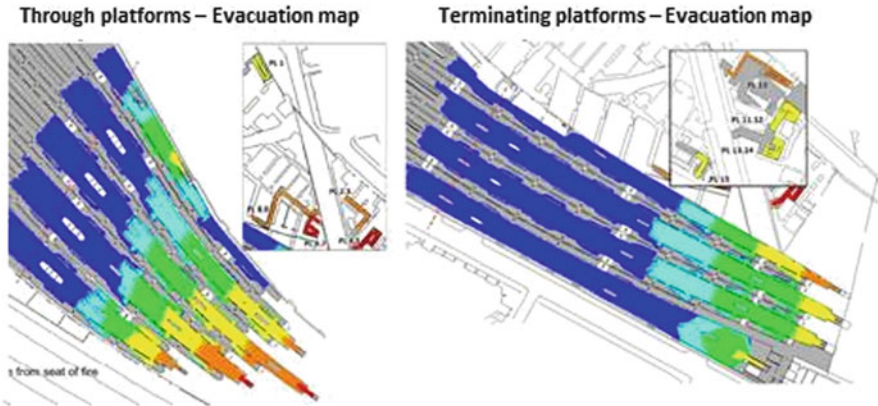


Fig. 14 Fire evacuation performance

Planning Authority (LFEPA) with a view to capturing a range of worst case scenarios.

The initial review of the platform evacuation times indicated that the platform layout did not all provide sufficient evacuation stairs width to meet Network Rail guidance of clearing platforms in 8-min. The key constraints preventing the meeting of the guidelines were identified as a combination of (1) the overall site footprint, (2) the tracks convergence and (3) the railway clearances for maintenance purpose. Unfortunately, these are constraints that cannot be changed without major impacts (both in terms of engineering solutions and costs) on the programme delivery.

At this stage, the fire evacuation static analysis was complemented by a dynamic modelling exercise to demonstrate (Fig. 14) that all passengers can reach a place of relative safety within 8-min. This supplementary exercise has been critical in providing the project team with the reassurance that the solution was safe. Informed by these results both Network Rail Fire Safety officers and LFEPA have confirmed that the evacuation performance of the proposed design satisfies their requirements.

7 Construction Strategy

The existing station will be completely demolished and rebuilt over a 5 year periods. However, the station has to remain open during the reconstruction period to minimise the disruption to passengers. This has brought significant challenges for the design team, one of those being to provide a safe environment for passengers during major building work. While the station will see a minor reduction in the number of train services over the construction period, the trains stopping at London Bridge will be busier than at present and the ‘working’ station footprint reduced.

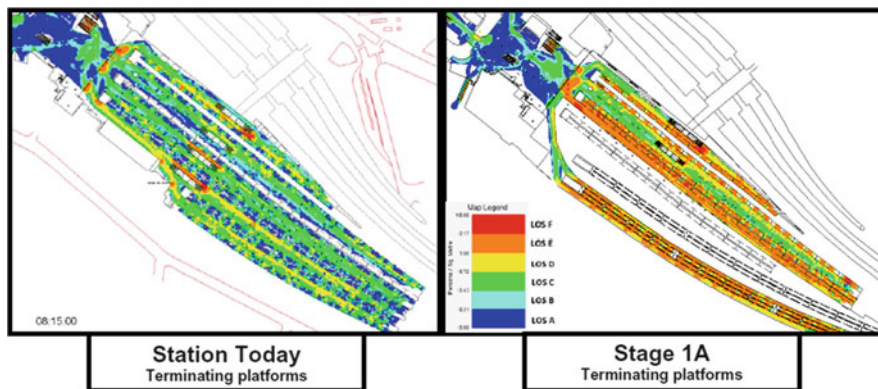


Fig. 15 Construction phasing Stage 1A comparative assessment

To support the construction strategy, the project team used LEGION dynamic models to assess the sequence of the works at the station, developing a nine phase strategy. The current station performance was used as a starting point for reviewing each of the nine phases to the assess changes to the layout and operations over the coming years (Fig. 15). This work is on-going and provides a mechanism for ordering the construction works alongside other disciplines.

8 Discussion

By applying Network Rail Station Capacity Assessment Guidelines in combination with the use of the dynamic modelling simulation, the design team has been able at an early stage to optimise the station layout and provide a safe and comfortable environment for passengers to navigate. This approach enables Network Rail to make the design process as efficient and cost effective as possible. For new station design an early appraisal and design intervention provides much better value than retro-fixes. During the conceptual development stage, there is still flexibility to test and balance cost and performance, and the proposed station layout value can be thoroughly tested to quantify its performance under a multitude of operational scenarios. At later design stages, the design is mostly fixed and the impact pedestrian planning can have is limited.

To fully capture the benefits of pedestrian planning, it is important that pedestrian flows specialists are involved right at the beginning of the design process to define the critical geometrical and operational constraints. This approach also provides the design team with the confidence that at the end of the design process the station will be able to accommodate future passenger growth and that the minimum station operation requirements are embedded within the design. The application of pedestrian dynamic modelling can be a powerful tool to analyse, explain and

effectively communicate the results within the design team and with the project stakeholders.

It is important to stress that it is necessary to correctly interpret the results of any capacity analysis and that it is essential for any modeller to have a good understanding of human behaviours, crowd dynamics and the principles and limitations of technical capacity assessment before establishing any set interpretations or recommendations. The creation of a simulation model is not the end in itself. It is the interpretation of the results, by looking beyond the limitations of static and dynamic modelling analysis technique that counts.

References

1. Network Rail Station Capacity Assessment Guidance. <http://www.networkrail.co.uk>
2. Grimshaw. <http://www.info@grimshaw-architects.com>
3. Legion Limited. <http://www.legion.com>

Mass Psychology Revisited: Insights from Social Psychology, Neuroscience and Simulation

Thomas Brudermann

Abstract Mass psychology plays a role in many different phenomena like human stampedes, financial bubbles, fashion trends or political movements. Although of different nature, phenomena driven by mass psychology have a common ground: Individual decision making is replaced by psychological contagion, and facts are replaced by opinions about facts. The aim of the paper is to illustrate how technological and methodological progresses in recent years advance the understanding for mass dynamics. Neurosciences allow for a better understanding of human behavior on the individual level; studies inter alia indicate that human brains are not well-equipped for independent decision making. Moreover, agent-based simulations close the analytic gap between individual decisions and collective outcomes. Simple simulation models for example reveal that the susceptibility of people to certain messages, opinions or emotions is the key factor for large-scale propagation of social phenomena. Results from both fields hence contribute to a better understanding of mass dynamics.

Keywords Mass psychology • Crowd psychology • Collective behavior • Collective dynamics • Social influence • Neuroscience • Agent-based modeling • Simulation

1 Introduction

Behavior of crowds as well as behavior of individuals in crowds increasingly gained attention in recent years, not least because of large-scale disasters like the stampedes in Duisburg 2010 and in Mekka 2006. Crowd behavior can also be observed in many

T. Brudermann (✉)

ISIS/Institute for Systems Science, Innovation and Sustainability Research, University of Graz,
Merangasse 18/I, A-8010 Graz, AUSTRIA
e-mail: Thomas.Brudermann@uni-graz.at

other and completely different situations. Crowd dynamics hence are highly relevant for, but not restricted to applications related to pedestrian dynamics, evacuation or transport.

The broad field of mass psychology, also referred to as “crowd psychology”, extends beyond “physical” crowds – situations in which many people physically come together at the same place. It rather deals with “psychological” crowds – situations, in which individual reasoning and individual decision making are substituted by collective dynamics and other-directedness. The involvement of many people is a prerequisite, but is not sufficient for the emergence of mass psychology. As a matter of fact, behavior of “psychological” crowds often is supposed to be unpredictable and irrational. A variety of phenomena are at least partly driven by mass psychology: Political movements, riots, fashion trends, collective manias like the bird flu hysteria in 2006, or even stock market bubbles and crashes. Although these phenomena are definitely different in their nature, they have in common basic mechanisms, which will be discussed throughout this paper.

The overall aim of the paper is to give an overview on the broad field of mass psychology on the one hand, and to discuss relevant insights from social psychology, neurosciences and agent-based simulation on the other hand. Although it is written from the perspective of an economic psychologist, the psychological mechanisms addressed here should be as well relevant for pedestrian and evacuation dynamics.

The structure of the paper is as follows: Sect. 2 summarizes how insights from social psychology inform the study of mass psychology. Subsequently, Sect. 3 discusses relevant results from neurosciences, followed by lessons from basic agent-based simulations in Sect. 4. Concluding remarks complete the paper.

2 Insights from Social Psychology

Classical studies on mass psychology already appeared in the nineteenth century [1–3] and became especially relevant in the first half of the twentieth century, when fascist regimes learned to utilize respective insights. As a consequence, research in this field became a taboo after World War II and the psychology of crowds only rarely has been addressed by social scientists. Additionally, methodological problems made it and still make it difficult to study mass dynamics directly.

2.1 *Other-Directedness*

David Riesmann [4] coined the term “other-directedness”, which encompasses the observation that human attitudes, decisions and behaviors are heavily influenced by attitudes, decisions and behaviors of other people in the social environment: What others are doing has a strong effect on our own behavior. Although this might not be a very popular statement in western individualistic societies, where

people usually consider themselves as independent and rational beings, a large body of evidence supports this claim. Human sociality involves different aspects of other-directedness, e.g. imitation, alignment of attitudes, norm compliance, social competition and reciprocity. Behavior often results from interplay of several of these factors: Human desire to belong to a collective, to be in line with “others” is well-marked, but at the same time people also strive for surpassing “others” and to be special.¹ Apart from that, humans have strong aspirations for reciprocity [5, 6]. People act cooperatively, if their counterparts act cooperatively, and people obey to social norms, if a majority of other people does so. On the other hand, a minority of non-compliers might induce wide-spread defection from prevailing norms [7]. Hence, humans usually display “contingent behavior”, as Nobel laureate Thomas Schelling [8] puts it – behavior that is heavily dependent on the behaviors of others.

2.2 *Psychological Contagion*

For practical and methodological reasons, psychological studies on social influence usually were conducted with groups of people rather than with large crowds. Important findings include: Group pressure seems to suppress independent thinking [9]; decision making in groups easily gets flawed by groupthink [10]; and high degree of anxiety and fear lead to the desire to affiliate with others [11]. Other-directedness becomes especially strong under two prerequisites: First, emotional arousal makes people more susceptible to psychological suggestion [12]. The second factor is uncertainty. In unfamiliar situations, for which experience is lacking, people tend to orientate themselves to others. If we do not know what is going on and if we have no experience to rely on, we use other people as the primary source of information [13]. A combination of uncertainty and emotional arousal hence provides the ground for psychological contagion, which can be considered as a particular strong and sometimes maladaptive form of social influence. Given appropriate circumstances, an idea, opinion or emotion may spread like a virus. Psychological contagion serves as the underlying mechanism for mass phenomena: Orientation to others replaces orientation to facts, and opinions replace knowledge.

Approaching mass psychology from a macro level perspective, we to a certain degree observe synchronization of thoughts and alignment of behavior [1, 13]; a tendency also referred to as “mass sentiment,” respectively to as “investor sentiment”, when applied to financial markets [14], or as “social mood” on a societal level [15]. The process of synchronization usually is accompanied by strong

¹Conspicuous consumption, which is an important driver in saturated markets, heavily relies on these two behavioral traits and many marketing campaigns hence utilize them as a lever for advertising.

emotions, e.g. euphoria or fear, and often culminates in “irrational exuberance”.² Political mass movements usually are characterized by thoroughgoingness and a strong focus on one single goal, e.g. the removal of the head of state, the stop of immigration or the prevention of a certain law. Psychological crowds are furthermore not responsive to reasoning or compromises [16]. Decoupling of individual motives and collective outcomes [8] can be seen as another frequently occurring property: Consider a bank run, where a rumor about financial difficulties of a bank causes widespread withdrawals of money. The individual desire of savers to rescue their money eventually leads to a bank default and losses for the clients – an outcome that is not intended by the single savers, who solely aim at rescuing themselves and do not intend the ultimate consequence of their collective behavior.

2.3 *Basic Crowd Properties*

Although pedestrian and evacuation dynamics in many regards are different from political mass movements, fashion trends, collective hysteria or financial bubbles and crashes, the common basic mechanism are sometimes similar and hence relevant for many kinds of mass phenomena:

- Independent reasoning steps back: Opinions and behaviors are aligned to behaviors and opinions of others.
- Others are the main source of information. This might lead to information cascades with incorrect information spreading out, e.g. in evacuation situations.
- Psychological crowds are not very responsive to logical reasoning. Consequently, explicitly provided information might be ignored or not perceived in an emergency situation. Subtle visual and architectural cues hence are more promising than pure information provision.
- Decoupling of motives and outcomes: The individual desires to get closer to the stage during a concert might entail shock waves and crushes of people, resulting in causalities which of course nobody intended.
- Nonetheless it has to be noted that not every emergency situation is dominated by mass psychology and irrationality. Rational and cooperative behavior might occur as well.

When investigating mass phenomena and collective dynamics, researchers face a series of methodological problems. Traditional research methods are limited; mass psychology cannot be analyzed in the lab or through surveys, since decisions in crowds are often instinct-driven and only rationalized post-hoc. Field observations

²In a 1996 speech, FED chairman Alan Greenspan coined the term “irrational exuberance” for describing the new economy boom in the 1990s, which like many previous financial bubbles was driven by expectations and opinions and was largely decoupled from economic facts. The “new economy” boom ended with a crash in 2000.

are difficult as well. Hence alternative methods are needed in order to enhance the understanding of mass dynamics. In this paper the further focus lies on lessons from two different approaches, namely the emergent field of neuroscience and agent-based simulations.

3 Insights from Neuroscience

With technical and methodological progress in recent years, brain research becomes an essential line of investigation in the overall aim of better understanding human behaviors in various situations. The most relevant lesson we can draw from neuroscience with regards to mass psychology is that our brains are not well equipped for independent decision making. As soon as we are exposed to behaviors, attitudes and preferences of others, our own behaviors, attitudes and preferences are biased.

The human brain represents a network of multiple functional modules that are highly interconnected. Decision making is not the result of a single process but always involves neural circuits or collaborative systems of specialized brain regions. Hence there is no 1:1 mapping from a certain brain region to a certain kind of action [17]. The brain region that has evolved most in course of human evolution is the pre-frontal cortex (PFC). The PFC represents a collection of interconnected neocortical areas and is highly connected with many other brain systems such as sensory systems, motor systems as well as memory, affect and reward systems. While the pre-frontal cortex is not essential for automated activities, it is central for cognitive planning and deliberate decision making [18, 19].

3.1 Energy Efficiency

Of all human organs, the human brain has the highest energy demand. Although it constitutes only two percent of the body mass, its metabolism accounts for 50 % of total body glucose utilization [20]. Neurons consume 94 % of the brain's oxygen, although they only make up 40 % of the brain [21]. Since the brain is characterized by limited processing capacity, it constantly strives for energy-efficient operation and automated activities in order to save cognitive resources [22]. It does so via different means: Firstly, it must limit the sensory inflow to the pre-frontal cortex by ignoring a substantial portion of incoming sensory data. Otherwise the deliberative system would be overwhelmed by huge amounts of signals. Before sensory information is sent to the slower deliberate system for analysis, it is initially processed and judged by the faster affective system [23, 24]. Although slower, the deliberative system has the potential to "over-write" impulses initially suggested by the affective system. This "primacy of affect" also is relevant for decision heuristics and gut feelings. Secondly, the brain tries to automate many processes. If a certain

behavior becomes habituated due to repetition and the respective neural circuits consequently become well honed, less energy is required to operate them. Habits hence fulfill the purpose of saving cognitive resources for possibly more important tasks [24]. Thirdly, mimicking decisions of others also comes with less cognitive effort. From an evolutionary point of view, imitating others enhances survival fitness (i.e. “flee, when others flee – they probably have a reason”). We here have to consider that human brains developed under circumstances radically different from today and that some mechanism might be mal-adaptive in modern, complex environments.³

3.2 *Mirroring*

Mirror neurons are multimodal association neurons and supposed to be one important basis for mimicking. They increase their activity not only during the execution of certain actions but also while corresponding actions are observed [25]. They have first been detected in the cerebrum of the macaque brain by Rizzolatti et al. [26] and have been confirmed in the human brain just recently by a first piece of direct evidence [27]. Since several different brain areas are supposed to have mirror properties [25], most researchers hypothesize a human mirror system rather than single mirror neurons, but its actual purpose remains disputed [28]. Supposed tasks include: (i) Sharing actions in the premotor and parietal cortex. Mirroring seems to occur primarily at the level of motor goals, e.g. observing somebody crossing red pedestrian lights might evoke a mirroring impulse. (ii) Sharing sensations in the somatosensory cortex, e.g. we contort our face while seeing somebody else getting hurt. (iii) Affective sharing of emotions, e.g. we feel disgusted when we see somebody else being disgusted, or we start laughing if people around us laugh. It is important to note that sharing emotions of others may not be limited to sharing their affective states; motor and somatosensory aspects of emotions may be shared as well [29]. Alternative explanations limit the purpose of mirror neurons to quick processing of some form of automatic reaction, similar to Pavlovian learning [28]. The automatic reaction induced by the mirror neuron system hence might involve imitation, but also different automated behaviors.

Apart from that, the human mirror system fits well to the principle of a highly efficiently operating human brain and comes along with several benefits: Mirroring does not require cognitive effort and therefore saves resources; mirroring happens quickly; and finally, mirroring is likely to result in a fairly good choice: If others are crossing the red pedestrian lights, it is probably safe. Thus, by mirroring what others are doing, our brain operates in a highly efficient way. However, impulses offered by

³Two examples shall be named here: (1) human tendency to herd is not beneficial in many situations; (2) human preferences for fat and sugary nutrition often cause health problems.

the mirror neuron system might be overwritten by the deliberative system, causing pedestrians to stand still despite others are crossing the red lights. Conversely, deliberation might step in only afterwards as “post-hoc-rationalizing”: Pedestrians might conclude that it is alright to cross the red lights, since the others are doing it as well and they are in a hurry anyway.

3.3 The Power of Social Influence

Human social behavior evidently extends beyond mirroring the behaviors of others and also involves social and moral norms as well as alignment of perceptions, attitudes and preferences. Preferences are neither stable nor independent from others’ preferences: Indeed it has been shown that exposure to preferences of others alters individual preferences and related neural activity [30].

Interestingly, social influence does not only affect our preferences; social influence may even alter our perceptions. Thus social conformity is not only associated with emotional, but also with perceptual processes. As known from the classical Asch [9] studies, participants in group experiments tend to give wrong answers on cognitive tasks due to conformity pressure, if other group members give wrong answers, too. A brain imaging study by Berns et al. [31] revealed that participants in such a setting are not merely conforming to the wrong confederates’ answers due to conformity pressure, but are experiencing a change in perception: Erroneous answers by others indeed evoke functional changes in brain circuits associated with cognitive tasks. Additionally, and as expected, emotional processes play a role. Non-conformity with others correlates with integrated activity in reward-related and fear-related brain regions, which might represent interplay of two behavioral traits: The unpleasantness of standing alone, versus the pleasantness of being special.

With regards to the understanding of mass psychology, these neuroscience insights are vital. Studies clearly prove that human brains are not well equipped for independent decision making, and that rational deliberation only is involved in a minority of decisions. Still, we have to keep in mind methodological and technological constraints. Experiments are so far necessarily embedded in artificial brain scanning environments and therefore not very social in a common sense. But we also should consider the enormous future potential, e.g. portable live-scanning environments with good temporal and spatial resolution. Nonetheless, neuroscience enhances our understanding of how decisions are made in various situations already by now. Consequently, some existing decision making models like utility maximization have to be rejected in light of neuroscience insights, while others can be at least partly supported. A simple model which is in line with neuroscience insights will be the basis of the simulations discussed in the next section.

4 Insights from Agent-Based Simulation Models

The third pillar for understanding mass psychology is provided by agent-based modeling (ABM). This section highlights how simple agent-based simulations contribute to the understanding of mass phenomena. The most important lesson is: Susceptibility matters. Whether psychological contagion leads to a wide-spread propagation of a certain phenomenon is heavily reliant on how susceptible a population is to a certain message, attitude or opinion. The popular concept of critical mass however is too vague to serve as an explanation model and must be questioned in light of simulation results.

The main contribution of agent-based simulation models with regards to the understanding of mass dynamics seems obvious. Simulation has the potential to close the analytic gap between individual behavior and collective outcome: Individuals and their interactions with each other and with their environment are modeled, and the emergent collective behavior is revealed by simulation. This concept is across scientific disciplines implemented in a growing number of models. Models can be sophisticated and detailed, for example if they aim at simulating movements of large crowds at a certain location, or if evacuation situations are simulated for a particular building. On the other hand there are also rather simple interaction models aiming at the investigation of basic relations. In this section, results from a simple generic contagion model [32, 33] will be discussed. It addresses basic mass psychological mechanisms and is in line with the insights summarized in the preceding sections.

4.1 *Psychological Contagion Modeled with ABM*

Psychological contagion is the main underlying mechanism of mass phenomena. Whether an individual succumbs to psychological contagion (and consequently “joins” a mass phenomenon) depends on various factors. Every person is different and thus differently susceptible to psychological contagion. Some will never succumb, some will always succumb, but most people will succumb if and only if “enough” others in their environment will succumb as well. How much is “enough” varies and depends on personal factors, situational factors, environmental factors as well as general circumstances. In an economic psychology scenario such general circumstances could involve difficult economic conditions or ongoing media reports which for example make people more sensitive to rumors about a possible bank default and in further consequence to a possible bank run; regarding pedestrian dynamics general circumstances could for example involve a recently issued terror alert which makes people more sensitive to unusual observations and events. Note

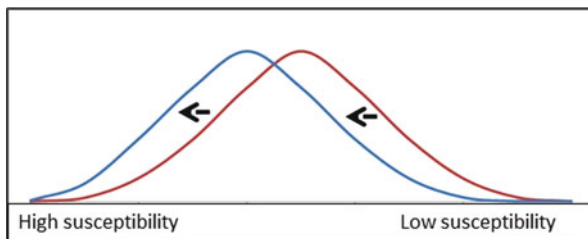
that a change in the general circumstances affects the susceptibility of many people, while changes in personal and situational factors only affect single individuals and to a certain degree their closer environment [32]. Thus two variables are involved on the micro level: The strength of the signal on the one hand (how many others do a certain thing), and the individual threshold on the other hand (how easily can the person be influenced). The epidemic threshold model approach [34] chosen here is, although simple, supported by neuroscience insights, since it models the interplay of signal strength and the cerebral control system, as illustrated by the red pedestrian lights example mentioned earlier. Each agent is differently susceptible, represented by a different individual threshold in the model. Some succumb to contagion very quickly and others very slowly or not at all, depending on how many others in their environment already succumbed. The communication neighborhood (i.e. “peers”) of each individual agent is assigned randomly. In the model each agent interacts with 5–50 other agents; this means that each agent is influenced by and influences 5–50 agents.

A threshold of 0.5 indicates average susceptibility: An agent will succumb to psychological contagion if at least 50 % of his communication neighborhood already succumbed. The thresholds are assigned to the agents in the model according to a probability distribution. The model discussed here operated with normal distribution, having a varying mean value and an arbitrarily fixed standard deviation of 0.25. The agent population comprised 8,000 agents. Hence, there are many agents with average susceptibility, and a few agents with very high, respectively very low susceptibility. However, it turned out that the type of probability distribution does not seem to be very relevant: Simulations carried out with uniform distribution or with normal distributions with different standard deviations brought forth very similar outcomes.

Of course in reality the threshold parameter should not be regarded just quantitative. Influence is asymmetric, and people are differently influential. However, these details are left out in the model, since they are not essential for understanding the basic mass psychological mechanisms. The focus of the simulations is on the propagation of psychological contagion. For this purpose, a small number of agents in the model are marked as so called “initial agents” in the beginning of the simulation run. These “initial agents” represent the starting points from where the psychological contagion process might spread out (or not) via the interactions of the agents.

As usual in agent-based modeling, the simulations are carried out as Monte Carlo simulations, meaning that some degree of randomness is involved – in this case the within a probability distribution randomly assigned thresholds, the randomly assigned communication neighborhood for each agent as well as the semi-random placement of the initial agents within the communication structure. For each parameter setting 100 simulation runs are carried out.

Fig. 1 Increasing susceptibility



4.2 Lessons Learned from a Simple Contagion Model

Already such a simple contagion model entails important lessons and helps to identify the main factors that enable mass propagation and decide whether an emotion, opinion or attitude spreads across large parts of a population.⁴

It turns out that interplay of several factors decides whether mass propagation occurs or not. These factors are (i) the number and the influence of the “initial agents” (ii) the density and closeness of these initial agents, (iii) the communication structures within the population, (iv) the average individual thresholds in the overall population, respectively the susceptibility of people as well as, needless to say, (v) a certain degree of randomness. The most important of these factors is the average susceptibility of the population. Here already small changes in the parameters may entail large effects.

The first question thus is: What happens, if the average susceptibility of agents towards contagion is slightly increased (Fig. 1)? The answer is ambiguous: Usually a slight change entails only marginal effects. However, in a very small corridor propagation rate jumps from low to high (Fig. 2). The exact characteristics of this corridor depend on various model settings like communication structure, number, influence and placement of initial agents. However, the jump from low to high propagation rate usually occurs if the mean individual thresholds are set to around 0.41–0.43. Given a sufficiently large agent population, this result is remarkably stable across conditions (different probability distributions, varying communication structures, different number and occurrence of initial agents), with only minor deviations.

It is not surprising that mass propagation gets more likely the higher the susceptibility is in the population. However surprising is the small corridor of average thresholds where the propagation rate jumps from low to high. Small changes on the micro level here might have dramatic effects on the macro level. If the thresholds are low and susceptibility high, already a small number of initial agents are sufficient to make mass propagation probable. Higher thresholds respectively lower susceptibility requires a larger group of initial agents and/or initial agents with

⁴“Population” here refers to the agent population in an agent-based model.

Fig. 2 Correlation between susceptibility and propagation rate

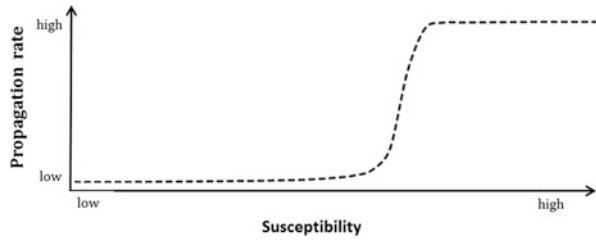
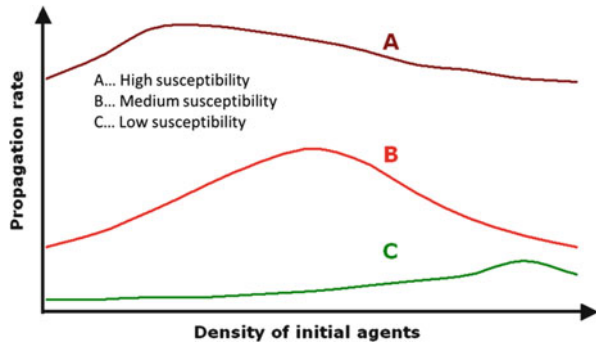


Fig. 3 Schematic representation of the relationship between susceptibility, density of initial agents and expected propagation rate [33]



stronger influence. This relationship is also non-linear. If thresholds are too high, even a relatively large number of initial agents will not evoke mass propagation.

Remember that the individual susceptibility is not only influenced by personal and situational factors, but also by general circumstances on the macro level. General circumstances influence the susceptibility of the overall population. A slight change in this parameter might slightly increase the mean susceptibility in a population, and, as indicated by the simulations, this slight change might already provide the ground for mass propagation.

Density and closeness of initial agents play a role as well: If initial agents are scattered among the entire population, they can only affect agents with high susceptibility. Indeed propagation may remain locally limited because agents with higher thresholds, respectively lower susceptibility, will not be affected by scattered agents. If the initial agents are however pooled and close together, they reach more agents in their environment than only a few individuals or any single individual agent could do. This however involves the risk that the initial agents remain a closed group of outsiders. It therefore depends on the average thresholds of actors, whether concentrated or scattered initial agents are more successful. A schematic representation of this relationship is shown in Fig. 3. If mean thresholds are low and susceptibility high, rather scattered agents will have more success: Propagation takes place faster and reaches a higher degree (curve A). If individual thresholds are high and susceptibility low, the probability of wide-spread propagation is generally lower and even will approach zero if initial agents are scattered. In this case mass propagation is hardly possible. However, a more concentrated occurrence of initial

agents will increase the probability, that at least some parts of the population become affected (curve C). Curve B indicates medium susceptibility in the population: Here medium density of initial agents promises the highest propagation rates [33].

4.3 Critical Mass: Popular, But Inapplicable

Critical mass is a popular and widely applied concept in social sciences. Critical mass models reduce the question, whether it comes to wide-spread propagation of a certain phenomenon or not, basically to one single factor, namely to the factor of critical mass. This concept from nuclear physics postulates some kind of self-sustaining activity which cannot be stopped from the outside as soon as a certain level of propagation has been reached [8]. Examples include: If a critical mass of investors on financial markets panic, stock markets will crash. If a critical mass of consumers obey to a certain fashion trend, it will become a great success. If a critical mass of citizens initiate a riot, a large scale revolution will emerge. If a critical mass of pedestrians panic, a stampede will be the result – and so on.

However, while the concept of critical mass is well proven in nuclear physics, there is no proof for its applicability in social sciences. The simulations discussed in this paper cannot find support for the existence of a critical mass either. When observing the variables visible on the macro level such as the propagation rate in previous simulation steps we cannot predict the further development of the propagation, even in the relatively simply arranged simulations. If one has no accurate knowledge of all micro- and macro level parameters and their interdependence in the simulation model, it is impossible to determine a critical mass which must be achieved at least in order to guarantee mass propagation.

Experience shows that similarly social scientists cannot determine critical mass for a concrete real-world phenomenon. The variety of variables and influences makes it incalculable and unpredictable. Therefore there is no clear and mathematically feasible definition for critical mass in the social sciences. Critical mass is a vague concept, which can neither be supported by empiricism nor by simulation. This finding is in accordance with a statement supposedly made by Isaac Newton in the course of a financial bubble in the early eighteenth century: “I can calculate the motions of the heavenly bodies, but not the madness of people.” Newton’s words might serve as a warning for both social scientists and physicists. Transferring concepts from one domain to the other might work out for certain applications – but we should not forget that human beings behave differently from atoms.

For enhancing the understanding of mass psychology and crowd dynamics, agent-based models are essential. Already very simple and generic simulation models can contribute significantly, as they provide vital insights on contagion processes and their critical variables. Most importantly, they indicate that even minor changes on the micro level, for example induced by an external factor, might provide the ground for mass propagation and therefore entail large effects on the macro level.

5 Concluding Remarks

For economic psychologists and for researchers in pedestrian and evacuation dynamics the same principle applies: If one aims at understanding crowd dynamics, a single-method approach is insufficient. Mass psychology and crowd behavior are difficult to comprehend and each methodological approach has substantial limits. Thus a methodological triangulation undoubtedly is required. In order to overcome these limits this paper attempted to combine insights and methods from three different fields, namely social psychology, neuroscience and simulation. Such an approach seems to be promising, and even though not perfect, it offers vital insights: From the micro-level perspective we can state that human brains are not well equipped for independent decisions; other-directedness is a strongly pronounced human behavioral tendency and this tendency becomes especially strong under uncertainty and emotional arousal. Appropriate circumstances which foster these two factors at the same time facilitate psychological contagion. The discussed simulation results furthermore suggest that even minor changes in these circumstances, accompanied by a change in people's susceptibility to certain messages, emotions or opinions, have the potential to evoke a mass psychological phenomenon.

Of course it has to be considered that researchers in pedestrian and evacuation dynamics have a different perspective on mass phenomena when compared to researchers in social psychology or economic psychology. However, and as argued throughout this paper, there are many similarities regarding the underlying psychological mechanisms. An integration of mass psychological insights into architecture, city planning or crowd management to a larger degree hence seems reasonable. In particular the rapid progresses in neuroscience methods and simulation techniques make this integration worthwhile and might serve as a strong incentive for cooperation with social and cognitive psychologists as well as neuroscientists in the foreseeable future.

Acknowledgments I thank Linda Pelzmann, Thomas Fenzl, Karin Dobernic and Nina Braschel for their comments. Furthermore I thank several participants of the PED 2012 conference for remarks and discussions which notably improved this paper.

References

1. Le Bon, G.: *La Psychologie des Foules* (French Edition). Alcan, Paris (1895).
2. MacKay, C.: *Extraordinary Popular Delusions and the Madness of Crowds*. Harmony Books, New York (1841).
3. Veblen, T.: *The Theory of the Leisure Class*. Penguin Books, New York, N.Y. (1899).
4. Riesman, D.: *The Lonely Crowd. A study of the changing American character*. Yale Nota Bene, New Haven (1952).
5. Axelrod, R.: *The evolution of cooperation*. Basic Books, New York (1984).
6. Fehr, E., Fischbacher, U., Gächter, S.: Strong Reciprocity, Human Cooperation and the Enforcement of Social Norms. *Human Nature*. 13, 1–25 (2002).

7. Spitzer, M., Fischbacher, U., Herrnberger, B., Grön, G., Fehr, E.: The Neural Signature of Social Norm Compliance. *Neuron*. 56, 185–196 (2007).
8. Schelling, T.C.: *Micromotives and Macrobehavior*. W.W. Norton & Company, New York/London (1978).
9. Asch, S.E.: Effects of group pressure upon the modification and distortion of judgements. In: Guetzkow, H. (ed.) *Groups, Leadership and Men Research in Human Relations*. pp. 177–190. Carnegie Press, Pittsburgh (1951).
10. Janis, I.L.: *Victims of groupthink; a psychological study of foreign-policy decisions and fiascoes*. Houghton, Mifflin, Boston (1972).
11. Schachter, S.: *The Psychology of Affiliation: Experimental Studies of the Sources of Gregariousness*. Stanford University Press, Stanford, CA (1959).
12. Schachter, S., Singer, J.: Cognitive, social and physiological determinants of emotional states. *Psychological Review*. 69, 379–399 (1962).
13. Pelzmann, L.: *The Triumph of Mass Manufactured Will – Circumstances and Rules*. *Malik on Management*. 10, 188–204 (2002).
14. Prechter, R.R.: *The Wave Principle of Human Social Behavior and The New Science of Socionomics*. New Classics Library, Gainesville (1999).
15. Casti, J.L.: *MOOD MATTERS: From Rising Skirt Lengths to the Collapse of World Powers*. Copernicus Books, New York, N.Y. (2010).
16. Drucker, P.: *Die Chance des Unternehmers. Signale für das Management von morgen*. Econ Verlag, Düsseldorf/Wien/New York (1987).
17. Camerer, C., Loewenstein, G., Prelec, D.: Neuroeconomics: Why Economics Needs Brains. *Scandinavian Journal of Economics*. 106, 555–579 (2004).
18. Miller, E.K., Cohen, J.: An Integrative Theory of Prefrontal Cortex Function. *Annual Review of Neuroscience*. 24, 167–200 (2001).
19. Bechara, A., Damasio, H., Damasio, A.: Emotion, Decision Making and the Orbitofrontal Cortex. *Cerebral Cortex*. 10, 295–307 (2000).
20. Fehm, H.L., Kern, W., Peters, A.: The selfish brain: competition for energy resources. In: A. Kalsbeek, Fliers, E., Hofman, M.A., Swaab, D.F., Someren, E.J.W. van, and Buijs, R.M. (eds.) *Progress in Brain Research*, Vol. 153, pp. 129–40. Elsevier (2006).
21. Zak, P.J.: Neuroeconomics. *Phil. Trans. R. Soc. Lond. B*. 359, 1737–1748 (2004).
22. Camerer, C., Loewenstein, G., Prelec, D.: Neuroeconomics: How Neuroscience Can Inform Economics. *Journal of Economic Literature*. 43, 9–64 (2005).
23. Sanfey, A.G.: Social Decision-Making: Insights from Game Theory and Neuroscience. *Science*. 318, 598–602 (2007).
24. McKenzie, R.B., Zak, P., Turner, J.: The Neuroeconomics of Rational Decision Making. In: McKenzie, R.B. (ed.) *Predictably Rational?* Springer Verlag, Berlin-Heidelberg (2010).
25. Keysers, C.: Mirror neurons. *Current Biology*. 19, 971–973 (2009).
26. Rizzolatti, G., Fadiga, L., Gallese, V., Fogassi, L.: Premotor cortex and the recognition of motor actions. *Cogn. Brain Res.* 3, 131–141 (1996).
27. Mukamel, R., Ekstrom, A.D., Kaplan, J., Jacoboni, M., Fried, I.: Single-Neuron Responses in Humans during Execution and Observation of Actions. *Current Biology*. 20, 750–756 (2010).
28. Hickok, G.: Eight Problems for the Mirror Neuron Theory of Action Understanding in Monkeys and Humans. *Journal of Cognitive Neuroscience*. 21, 1229–1243 (2008).
29. Bastiaansen, J.A.C.J., Thioux, M., Keysers, C.: Evidence for mirror systems in emotions. *Phil. Trans. R. Soc. B*. 364, 2391–2404 (2009).
30. Mason, M.F., Dyer, R., Norton, M.I.: Neural mechanisms of social influence. *Organizational Behavior and Human Decision Processes*. 110, 152–159 (2009).
31. Berns, G.S., Chappelow, J., Zink, C.F., Pagnoni, G., Martin-Skurski, M.E., Richards, J.: Neurobiological Correlates of Social Conformity and Independence During Mental Rotation. *Biological Psychiatry*. 58, 245–253 (2005).
32. Brudermann, T.: *Massenpsychologie. Psychologische Ansteckung, kollektive Dynamiken, Simulationsmodelle* (German Edition). Springer, Wien/New York (2010).

33. Brudermann, T., Fenzl, T.: Agent-based Modelling: A new approach in viral marketing research. In: Terlutter, R., Diehl, S., and Okazaki, S. (eds.) *Advances in Advertising Research* (Vol. 1): Cutting Edge International Research. pp. 397–412. Gabler Verlag, Wiesbaden (2010).
34. Granovetter, M.: Threshold Models of Collective Behavior. *The American Journal of Sociology*. 83, 1420–1443 (1978).

Shaping the Space: Turning Function into Inspiration

Peter Jenkins

Abstract At BDP our station design process is focused on creating ‘Places For People’. This results in a design process which aims to integrate the following issues:

1. Providing access for all
2. Ensuring clarity of wayfinding and information provision
3. The intelligent use of light (both natural and artificial)
4. Making secure, easily managed spaces
5. Developing sustainable, loose-fit environmental control strategies
6. Creating site responsive design solutions
7. Reflecting the civic role of a rail gateway
8. Respecting heritage constraints
9. Considering how the station can be a destination in its own right
10. Considering permeability and regeneration

Many aspects of the design process influence (and are influenced by) the movement and activities of passengers. This presentation/paper therefore covers various themes, but ultimately it presents an explanation of the importance of understanding pedestrian movement and wayfinding to our work.

Keywords Railway heritage • Urban development • Station design • Passenger environment

1 The Development of Cities and Their Transport Networks

The historic development of our urban centres defines, and in turn is defined by, its transport opportunities and connections. The process of city development can be seen as a series of concentric circles, or ‘onion rings’ which can be peeled back

P. Jenkins (✉)

BDP, 11 Ducie Street, Piccadilly Basin, PO Box 85, Manchester M60 3JA, United Kingdom

e-mail: peter.jenkins@bdp.com

U. Weidmann et al. (eds.), *Pedestrian and Evacuation Dynamics 2012*,

DOI 10.1007/978-3-319-02447-9_4,

© Springer International Publishing Switzerland 2014

to explain how and why the transport networks interface with a city. They also define where people live and work, and hence define the nature of our transport interchanges. This is common across countries around the world, but for the purposes of this paper the focus will Manchester, where BDP have developed, and are developing, rail projects that encircle the city centre.

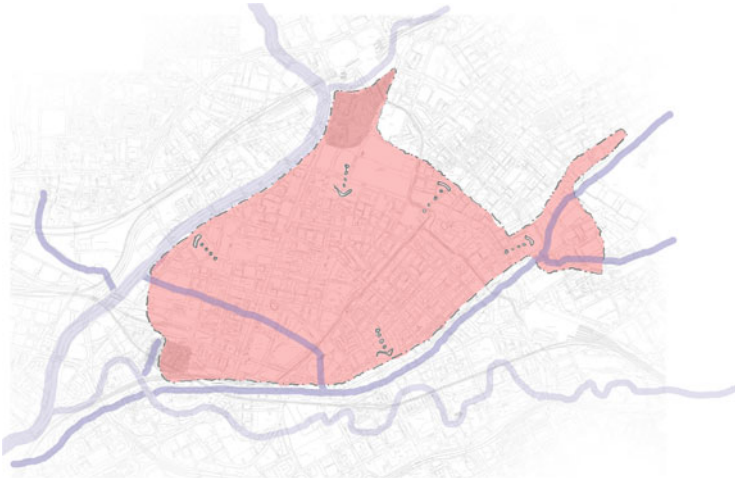
2 Case Study: Manchester

The earliest settlements around the city were defined by their proximity to water, the first of which was a Roman fort situated close to the confluence of the Irwell and Medlock rivers. Subsequent to this was the development of the medieval city to the north, at the confluence of the Irwell with the River Irk.



The city then grew to the south, across relatively dry, level ground. Canals, and the canalization of rivers, provided connections for the emerging city in all directions as the city became a trading and then industrial focal point for the region. The canals skirted the edges of the then city core, feeding a series of buildings and wharves developed on the free, cheap land beyond established buildings.

The growth of the successful city subsequently expanded the boundaries, and the development of the next transport mode formed the next ring around the city edge. The development of passenger railways began in Manchester, with the link to Liverpool to the west. Manchester was becoming one of the most important cities in the industrial world, and this new transport mode soon ringed the city. As with the preceding development, the railways took readily available land with viaducts and



buildings specifically for the purpose of railway uses. This ring of railway lines was studded with station interchanges, from Victoria in the north and tracking round in and anticlockwise direction through Exchange, Salford, Liverpool Road, Deansgate, Central, Oxford Road, Piccadilly and Mayfield Stations.



The twentieth century saw the rise of the car, creating the next encirclement of the city, again on the on the peripheries of the active (and valuable) urban core as it stood at the time. This took the form of an urban motorway, elevated in stretches. As with

previous rings, this leaves a legacy today of urban disconnection, with pedestrian and vehicular routes adversely affected (and a consequently detrimental impact on land values and urban quality).

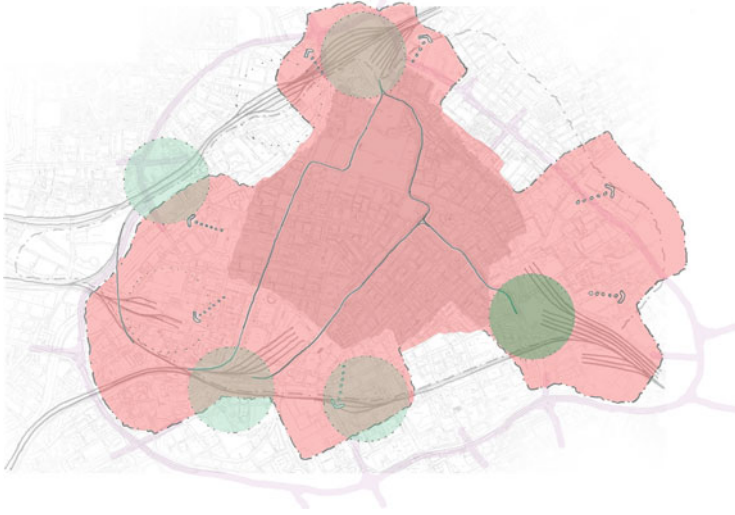


The post-industrial decline of the city saw the urban core shrink back beyond the rings as defined. This left the rail stations in peripheral locations, resulting in a negative character to the station buildings and their immediate context. Land uses evaporated or declined leaving a sequence of unpleasant streets, vacant buildings and open sites. The late-twentieth and early-twenty-first century regeneration of the city began to reverse this decline, shining a light on neglecting buildings and areas, including each of the primary railway stations. This has in turn led to a series of redevelopment projects for the stations and the infrastructure, of which BDP has played a prominent role.

3 Manchester Piccadilly Station

Piccadilly has become one of the most significant station developments of recent times in Britain, topping nationwide passenger surveys in 2008 with a 92 % approval score. It has raised the ambitions for a number of similar regional cities for the transport hubs and the positive influence they can have on the regeneration and image of the city.

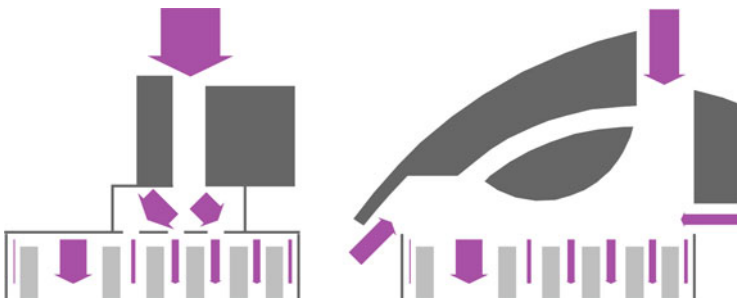
The brief was to give the station a twenty-first century image, improve visibility and links with the city and to improve circulation for passengers and access for



pedestrians and vehicles. To achieve this, a new larger passenger concourse was constructed on two levels, giving clarity of location and function for the passenger. The scheme also includes a new 500 space multi-storey car park with links to the station and new service area. The building integrates with existing 1960s and Victorian listed structures. Diverse activities and concerns are combined; these begin with the creation of a bright, logical and safe concourse which provides ticketing and retail facilities, information and way finding, security and rail operational issues.

There were numerous problems with station which presented themselves to the client and consultant team. The station environment had responded to the post-industrial decline through the progressive reduction of permeability into and through the station; the surrounding streets became barriers, spaces of a negative character. A key design response was to reverse this gradual sealing-up of the station complex, opening up new entrances to make the station easier to use for all passengers and also provide a subsequent catalytic effect on the regeneration of surrounding sites. Separating the different users of the station complex was critical (passengers arriving by foot, bicycle from neighbouring areas; road uses including taxi and private cars; intermodal transfer from, bus and tram; servicing and station management).

The existing station was entirely accessed from a single direction, crushing all users through a single entrance. The spaces of the station were inadequately sized for the capacity required, regardless of forecast increases in passenger numbers. This led into a dark and dingy concourse with limited commercial aspects which if correctly designed can provide retail income but probably more importantly provide passenger amenity, animation and activity.



Despite the tightly constrained urban site, the reassessment of external circulation patterns went in hand with the widening of internal spaces and the rearrangement of routes in both horizontal and vertical directions. Functions are dispersed and sized according to logical movement patterns and an ongoing passenger modeling process.

The opening up of the station in terms of transport connections around the station was matched by architectural form-making which opened the station up to natural light and ventilation. This creates a positive passenger environment and encouraged views through the station complex, physically as well as metaphorically connecting the city to the railway.

Architectural elements and forms are used to promote natural way-finding and induce movement. Way-finding can be immensely improved via a strategy of providing visual linkage to your destination; a sign providing direction to the platforms is unnecessary if the trains are already visible. Architectural cues such as curved elements and forms naturally lead the eye around corners, based on the intrigue of what is beyond.

A visually open and well-lit space provides significant amounts of passenger reassurance and comfort; knowing the location of your train and its punctuality (or otherwise) can relax station users to enjoy other facilities and the spaces of

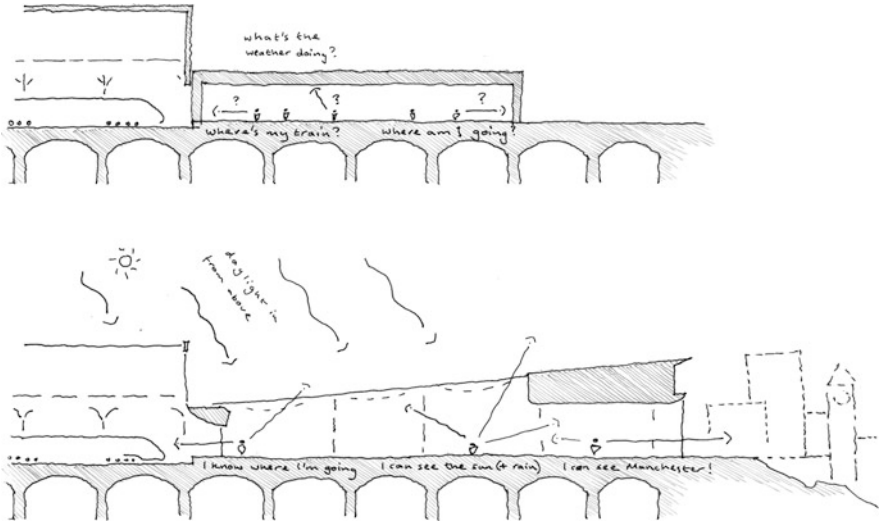


the interchange The separation of vehicles and pedestrians produces entrances of a scale and character which befit the needs of each. The uplift to the image of the station has been reflected in significantly increased patronage and the regeneration of surrounding sites.

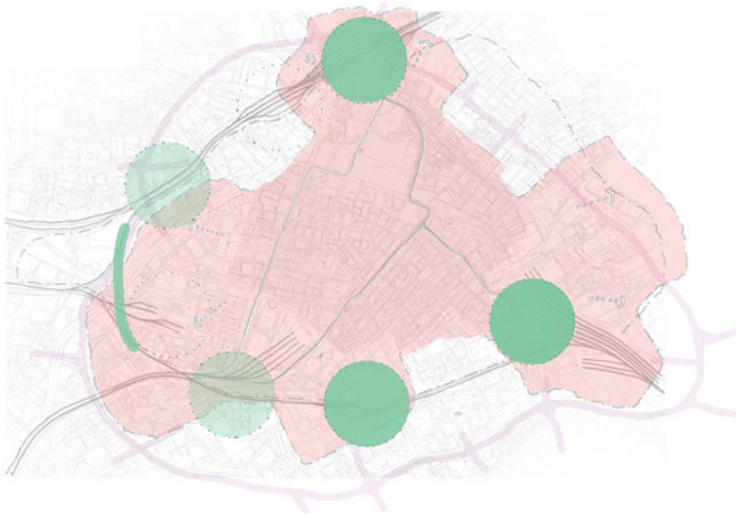
4 The Northern Hub

This project is passenger flow management on a massive scale, rebalancing railway circulation from coast to coast across the north of England. It combines station extensions, new infrastructure and timetabling improvements to massively increase passenger capacity. This will relieve an already over-stressed network and provide for significant expansion. The station expansion projects are being developed, with proposals for sites that encircle Manchester city centre. These consist of four stations (Piccadilly, Victoria, Oxford Road, Manchester Airport) and a series of bridges (known as the Ordsall Chord).

The success of **Piccadilly** has been reflected in a 60 % increase in footfall since the completion of the project 10 years ago. This increase exceeds rises in passenger numbers elsewhere, due to other intermodal transfers and the use of the station as a destination in its own right for non-travelling people using the

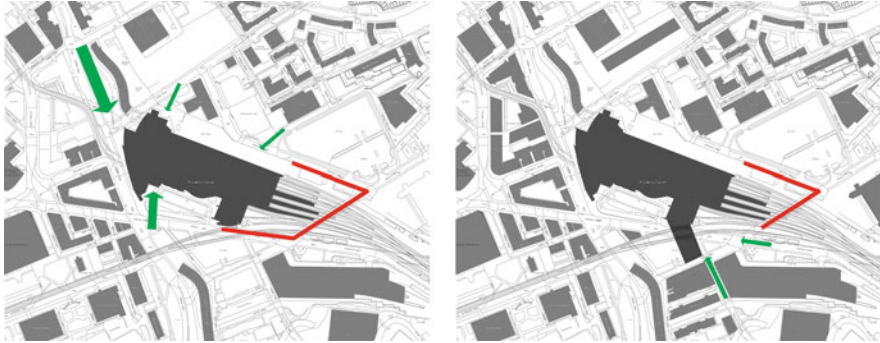


commercial and information facilities. The new proposals will extend the station complex to the south, with the addition of two new platforms, connected to the rest of the station by a new elevated concourse space. In addition to new passenger facilities and waiting areas, this concourse will connect back down to street level



to form a new station entrance. This will further develop the previous strategy to improve permeability into the station, altering pedestrian movement patterns around and inside the station. These new circulation routes will provide impetus to the continuation of regeneration sites around the rest of the station perimeter.

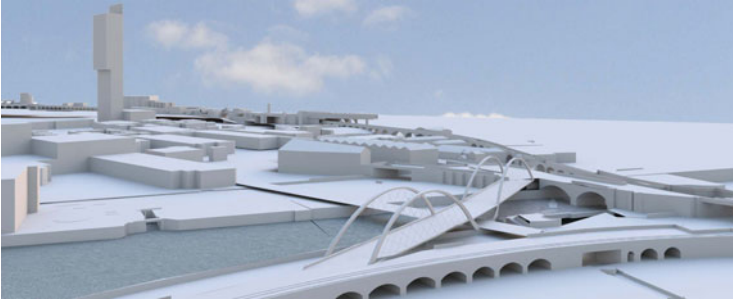
Oxford Road Station shares many services with the through platforms of Piccadilly, albeit on a much tighter site. Whilst the major inter-city connections of Piccadilly cater for the whole range of passengers (from occasional tourists to



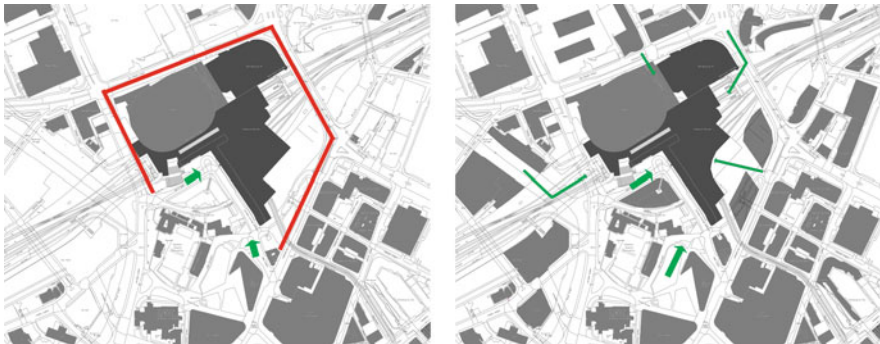
regular daily trips), Oxford Road is focused around two particular user categories: commuters (from the business quarter to the north) and students (from the University to the south). This creates a different dynamic for the station to its bigger neighbour, with passengers moving on well-known routes through to their specific train (and sometimes a specific seat). It is important to understand the different needs of these focused individuals against those casual, occasional users. The existing concourse spaces are tight and overcrowded, and constrained by the heritage-listed building fabric around. This presents a major challenge when designing for the users described above. At the next scale up, the station expansion (doubling the length of the platforms) must be shoe-horned into the densely-packed urban context around. This consequently affects passenger movements, as unconventionally arranged footbridge structures stretch between available spaces, creating landing points on asymmetrically arranged platforms.

Elsewhere in the city centre, a new rail link known as the **Ordsall Chord** is to be provided between divergent rail lines, connecting Victoria and Piccadilly Station for the first time. This project has significant historic issues to incorporate, with a series of viaducts and bridges arcing around past Liverpool Road Station, the first passenger railway station in the world, and a contemporaneous bridge by pioneering rail engineer George Stephenson. Whilst this rail connection has no passenger movement impact, it does have consequences for pedestrian and cyclist circulation on the ground plane, situated at the focal point of local desire lines, in this manner, this piece of railway infrastructure retains a role to play in the smaller scale city realm of pathways and cycle routes.

Whilst the rail bridges of the Ordsall Chord aren't directly to do with passengers the connections they form will redistribute passengers alighting from trains to arrive into the city centres. This will re-balance the two main stations (Piccadilly and Victoria) and hence influence the development of the city centre and surrounding neighbourhoods. At the closest scale, it will affect pedestrian movement patterns into and around the stations, as rail users re-calibrate their mental maps of the city and the stations.

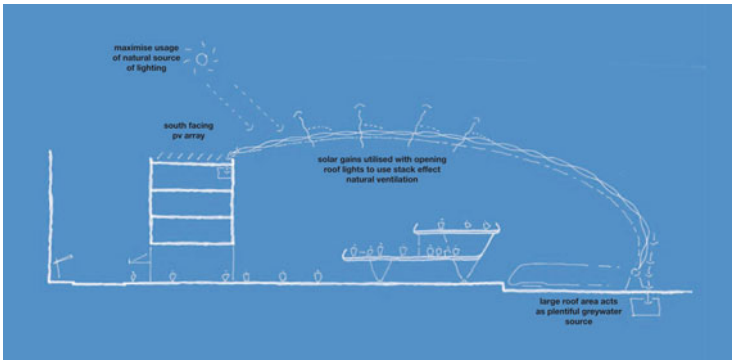


As a consequence of this situation we are following our work at Piccadilly with the redevelopment of **Victoria Station** on the opposite side of the city centre. The transport complex is to be updated and with new structures to replace derelict, deteriorating buildings. The station complex covers a variety of functions, including a 19,000 multi-sport arena and a 1,500 space multi-storey car park. This unique combination of uses requires careful consideration of how to mix and separate the disparate users, considering times of peak flow (and the quieter times in-between). A multi-modal interchange, it integrates both heavy and light rail, regional and shuttle buses, taxis, private cars and bicycles. The location of the station makes it a key regeneration connection between the city centre (to the south) and development projects to the northern boundaries of the site; as a result of this it will be not only a gateway to the city but also a destination in its own right.



What is currently a relatively impenetrable piece of the city, the project aims to dissolve the station into its context by way of a variety of means; to the west, existing voids through viaducts are exploited to provide vertical circulation up to the station; to the north a new footbridge spans through a narrow division between two buildings; to the east a route is punctured through a new roof skin. The disparate

functions of the site are to be drawn together into a single iconic space, defined by this landmark 10,000 m² roof. New concourse facilities are to be constructed inside this space, with high level connections through the space feeding out to the surrounding sites.

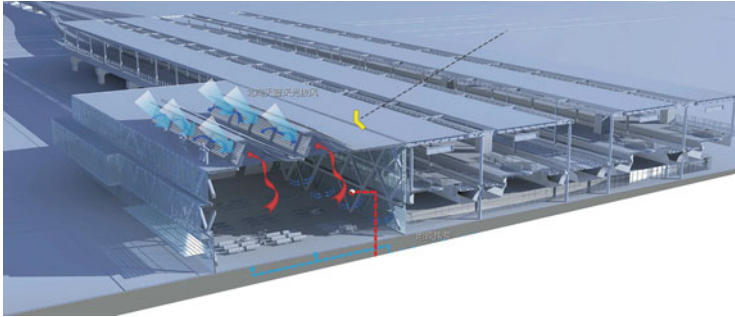


In addition to pedestrian links, the station will be physically plugged into its surroundings as it will be a green energy facility feeding new developments around. Easily gathered benefits created by the very nature of a station building (the substantial roof area) will be used to feed the needs of others. These will be a photovoltaic array to the roof of the existing buildings, and rainwater collection from the new roof which will be utilized for grey-water uses. In turn, the neighbouring office buildings will feed back into the station via CHP plant. As with Piccadilly the concourse space will exploit the opportunities of beneficial solar gain. The transparent ETFE roof will make maximum use of daylight (when available) and solar gain will induce stack effect ventilation to draw air through the space during summer.

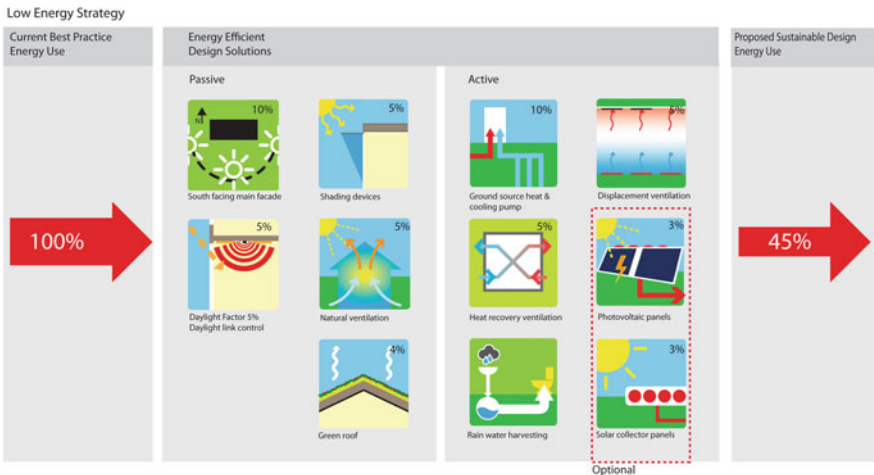
5 Further Consideration of Key Themes

The case studies of projects in Manchester introduce key themes that underpin much of our work. Transferring our experience to other locations has to be carefully handled to ensure that the proposals integrate effectively with their context.

In the **Hunan Region of China** we're developing nine high-speed railway stations, part of the Shanghai – Kunming line. The design philosophy for all stations is derived from sustainability strategies appropriate for the location, function and aspiration of the individual projects. BDP have developed a sustainability strategy toolkit for application to all nine stations, five of which BDP are the architect for and four are being developed by our partner local design institute. The stations



range from 2 to 8 platforms, with individual context varying from existing towns to proposed masterplans.



The development of significant high-speed rail networks in China reflects the growing appreciation of the need for sustainable transport systems. Different modes of transport vary in their respective levels of environmental benefits. For example air travel continues to struggle with emission levels and efficiency through reliance on fuel intensive aeroplanes and the heavily serviced nature of airport buildings while rail transport offers more opportunities for ‘loose-fit’ sustainability strategies. But even with this flexibility and the better fuel efficiencies trains offer compared to flight, rail needs to press home its advantage as a low-carbon, highly sustainable mode of public transport through innovative design and construction. The modular toolkit of technologies developed for Hunan aims to provide flexibility

in procurement and construction but also sustainable, future-proofed buildings that can be readily modified and not require substantial modifications the future.

At **Northampton Station** we have prepared designs for a major new station complex surrounded by regeneration sites creating a new gateway and transport interchange. At the hub of the site is a new concourse building to expand rail and retail facilities, acting as a new gateway to the town with excellent local connections for both commuter traffic and high-speed connections to London.



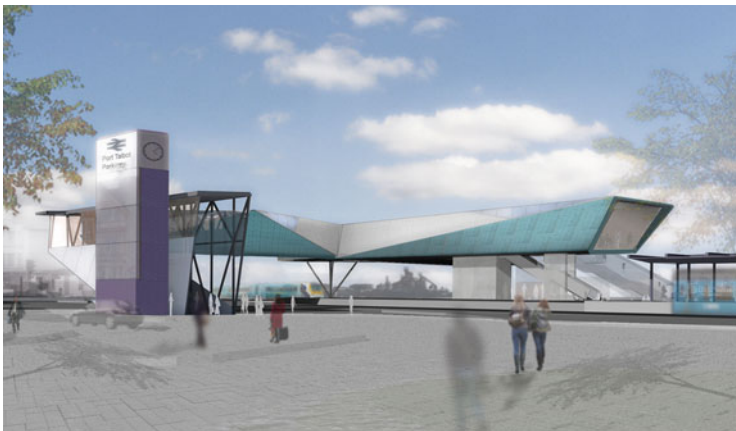
A series of tight constraints have been analysed through dynamic pedestrian modeling to guide the design process for footfall and pedestrian movement. As with Piccadilly a key tenet is the redistribution of routes around the building and on different levels. To accompany and support improvements in passenger circulation, a rationalisation of existing parking into a safe and secure 1,250 space multi-storey creates a major mixed-use redevelopment scheme in a key urban location. At present the station does not provide an adequate transport interchange and is a poor gateway for visitors to Northampton.

The vision is to establish Northampton Station as a business and communications hub for the town centre, to create a true transport interchange, a major new business address to increase employment in the town, and to regenerate the surrounding areas, including deprived residential neighbourhoods. As with other locations the station can become a destination in its own right, independent of transport functions. It can provide a neighbourhood with a meeting point, catering facilities and perhaps most importantly a unique identity.

Our scheme for **Port Talbot Parkway Station** is intended to act as a catalyst for proposals that will reverse the post-industrial decline of the town, which developed rapidly in the nineteenth century around the steel industry and maritime trade. The Victorian station was replaced in the 1970s by a structure of its time, which



is showing signs of its age and damage from vandalism. Our project proposes the removal of all existing structures with a new crossing over the railway and a high-level station suspended over the high-speed lines below. A new 400 space car park is proposed to improve the commuter use of the station. The buildings are to become a local beacon, a focus for transport connections and a civic landmark. At an immediate scale, the scheme provides exemplary access for all and on a wider range the long-distance use of the route with enhanced and expanded car parking. The intention is for the station to act as a catalyst for further regeneration in the surrounding area, and the design caters for the future doubling of infrastructure capacity.



Whilst station projects such as Port Talbot are founded on ambitions for increases in passenger numbers, designs must bear in mind the intermediate times of lower demands, and the effects on the station environment of quieter, later times during the day. At these times the consideration of pedestrian movement is not related to capacity consideration but instead to focus on the safety and security. It is important to provide passengers with the reassurance that they can be seen; providing areas which are easily overlooked by staff. This provides benefits in reverse; malicious behavior can be deterred by the sensation that one is 'on show'. Both wide-angle and axial views through the station are utilized to connect local landmarks and provide orientation. From outside structural elements such as the lift enclosures are exploited as clock towers, a traditional civic landmark for buildings such as a station. To supplement these 'natural' techniques the use of linear artificial lighting elements (to provide orientation during the night) and technological systems such as REACT (for the visually impaired) are integrated into the design.

As noted above, constraints produced by existing structures must be accommodated within designs for modern passengers. At **Chester Station**, a highly significant heritage asset was adapted into a transport interchange which integrates sleek contemporary design into the attractive character of the original buildings. The Station was built in 1848 before being extended in 1889; the development of the station during this initial period displayed disciplined and clear diagrammatic relationships, with respect to both to the function of the station and between individual elements. Whilst aesthetic styles varied, the references to underlying grids remained, and appropriate choice of materiality and robustness was a consistent approach. Additions made during the twentieth century did not follow this discipline and were assembled on an ad-hoc basis, with no reference to the original forms. Their materiality and detailing was inconsistent, ranging from ignorant functionality to inappropriate pastiche. Both approaches can be said to diminish and disguise the importance of the original fabric and passenger circulation routes were compromised. The new concourse introduced contemporary forms with an organising order for additions (both now and into the future) whilst respecting the original station principles. This new approach removes or wraps the previous amendments, producing a diagram with clarity which is complementary to, but distinct from, the original forms. The intention is to create additions which are in a clearly modern idiom, articulated from the historic fabric.

To support this geometric approach, pre-patinated copper is to be used, with the rich and evocative quality of the surface chosen to sit well against the existing masonry. The reasons for this material choice are historic, commercial and pragmatic. The historical references result from the traditional qualities of the material; copper is perceived as having character associated with civic or religious buildings (something that the use of a modern, standardised monolithic panel would not achieve). The distinctive colour of pre-patinated copper articulates a clear difference between the new and old. The colour is also used as a subtle reference to the corporate colours of the client. For pragmatic purposes, the surface finish and colour of the material are ideal for the robust environment which the buildings sit



within; wear and tear can be absorbed by the material without it looking tired or dirty. The priorities of the client were to expand and improve the facilities of the station, and to create a distinctive identity for this important station which acts as a gateway to the town and the county. The local authorities are concerned with the overall public transport infrastructure, and intend the building to act as a catalyst for an urban renaissance in this area, improving the area in terms of retail trade, the value of commercial property rentals and the number of visitors.

The success of Chester has led to a suite of further projects for the same client across Wales. Basic design concepts are shared across many of the schemes including clarity of identity, natural daylight penetration and ventilation, passive security methods and way-finding, and utilising similar material surfaces and textures.

At **Nottingham Station** we are undertaking the redevelopment of heritage-listed station complex, including refurbishment and new-build works to create a modern, multi modal transport interchange facility (incorporating tram station, pedestrian concourses, retail space, staff accommodation and 1,000-space multi-storey car park). The primary purposes of the proposals are to improve the function and perception of the station for users and operators alike.

The scheme intends to incorporate the extension of the existing tram network, and proposes the removal of all vehicular traffic from currently congested and confused spaces to the front of the station, with a pedestrian atrium created inside an existing space to connect all the different facilities. These include the Booking Hall and a new South Concourse, which links various levels and activities across the site.

The end result of the station redevelopment which meets the need to have appropriate gateway which reflects the values and ambitions of the city. A railway



station forms the vital first impression of a place to arriving passengers and will form the lasting memory of those departing the city.

Our proposals for the **Abu Dhabi International Airport Midfield Terminal Complex Intermodal Transit Centre** encompass the major interface between other modes of transport, including high speed, regional and light rail services; these connect to the airport and the other transport modes in the building, including a 3,000 space car park, limosine parking, private car and taxi pick-up and drop-off. The building acts as the connecting element between the new terminal building and Airport City, a major new business quarter. This landmark building is focussed around a 300 m long concourse space, which steps up from the rail platforms to the

airport via a series of terraced levels. A soaring roof floats above and glass walls enable visual connections to aeroplanes landing and taking off from the airport.



As with other stations described above, a key element in the design strategy is the encouragement of natural way-finding strategies. Rail passengers arriving in the sub-surface platforms rise through an expansive canyon with views through the side walls of the concourse to aeroplanes taking off and landing at the runways which align themselves parallel to the main concourse. In the opposite direction, arrivals landing at Abu Dhabi are provided with views down the terraces to the railway station below. In both directions there is a key identifier of ‘I can see the planes/trains’.



6 Conclusions

The improvement of stations internally provides an enhanced passenger experience and encourages the continuing increase in passenger numbers while the external gateway aspect of a station has a major impact on the regeneration of the surrounding areas, with benefits for the local authority and private developers.

Critical to this development of modern, exemplary transport interchanges is an understanding of the needs, requirements and movement patterns of passengers. The preceding text aims to outline the many aspects of station that affect the perception and function of passengers which must be incorporated into the design process.

And while these different priorities will continue to shape the future of passenger interchange design, companies like BDP will continue to respond accordingly – appreciating nuanced priorities and understanding the sensitivities involved in partnership working. We will also strive to strike the right balance each time, and ensure that civic leaders, rail operators and passengers alike all get the high quality transport environment they want and deserve.

Simple Heuristics and the Modelling of Crowd Behaviours

Mehdi Moussaïd and Jonathan D. Nelson

Abstract A crowd of pedestrians is a complex system that exhibits a rich variety of self-organized collective behaviors, such as lane formation, stop-and-go waves, or crowd turbulence. Understanding the mechanisms of crowd dynamics requires establishing a link between the *local* behavior of pedestrians during interactions, and the *global* dynamics of the crowd at high density. For this, the elaboration of a model is necessary.

In this contribution, we will make a distinction between two kinds of modelling methods: outcome models that are often based on analogies with Newtonian mechanics, and process models based on concepts of cognitive science. While outcome models describe directly the movements of a pedestrian by means of repulsive forces or probabilities to move from one place to another, process models generate the movement from the bottom-up by describing the underlying cognitive process used by the pedestrian during navigation.

Here, we will describe and compare two representatives of outcome and process models, namely the social force model on the one hand, and the heuristic model on the other hand. In particular, we will describe the strength and the limitations of each approach, and discuss possible future improvements for process models.

Keywords Outcome models • Process models • Pedestrian behaviour • Crowd dynamics • Complex systems • Social forces • Simple heuristics

M. Moussaïd (✉) • J.D. Nelson
Center for Adaptive Behavior and Cognition, Max Planck Institute for Human Development,
Lentzeallee 94, 14195 Berlin, Germany
e-mail: moussaïd@mpib-berlin.mpg.de

1 Introduction

Human crowds display a rich variety of collective behaviors that support an efficient motion under everyday conditions [1]. For example, when two flows of people are moving in opposite directions in a crowded street, pedestrians spontaneously share the available space by forming lanes of uniform walking directions [2–4]. This apparent “highway of pedestrians” is a decentralized collective organization that enhances the traffic efficiency by reducing the need for avoidance maneuvers among individuals. As another example, when two opposite flows meet at a narrow bottleneck, each flow temporarily “captures” the doorway during a short time period, resulting in alternating bursts of pedestrians passing first in one direction and then in the other. Again, this spontaneous group coordination allows for efficient usage of congested areas [5].

The combination of local interactions among pedestrians, however, does not always generate efficient traffic solutions at the group level. For example, it has been shown recently that above a critical density level the collective coordination may suddenly break down, giving way to a dangerous phenomenon called crowd turbulence, in which the flow of pedestrians becomes chaotic [6]. This particular regime is often observed during crowd disasters and is characterized by random and unintended displacements of people in all possible directions. The emergence of stop-and-go waves is another example of collective traffic perturbation that emerges spontaneously out of local interactions among pedestrians [6].

The key element for understanding the wide variety of collective behaviours observed in crowds lies in the different *natures* of local interactions among individuals [7]. A local interaction is any kind of social influence that motivates an individual to change or adapt his or her behaviour based on social cues originating from neighbouring individuals. In pedestrian crowds, one may distinguish at least five different types of interactions:

- **Collision avoidance** is the basic and most common interaction among pedestrians. It describes the strategic adaptation of walking speed and direction to avoid an upcoming collision with another person. Collision avoidance is at the origin of the lane formation phenomenon in bidirectional flows, and also gives rise to stop-and-go waves in unidirectional flows at intermediate density.
- **Physical interaction** takes place when people are in physical contact with one another, at high density levels. Unlike collision avoidance that is based on *intentional* navigation strategies driven by visual information, physical interaction results in *unintentional* movements based on pushing and physical pressures exerted among densely packed people. Physical interaction is typically involved in the emergence of crowd turbulence.
- **Social interaction** drives the behaviour of social groups of pedestrians, such as friends going together to the same place. In social interaction, group members not only try to avoid collisions with one another, but also try to stay together, and often to converse with other group members. Social interactions are at the origin

of the walking patterns observed in small groups of pedestrians and may reduce overall traffic efficiency [8].

- **Imitation** is another kind of interaction that takes place when people modify their walking destination to move in the same direction as other surrounding individuals. Imitation is assumed to have a major role during escape panics and to give rise to herding behaviour and unbalanced exit usage [9].
- Finally, we may also mention **indirect interaction**, wherein people adapt their walking behaviour not directly based on their neighbours' behaviour, but on the traces left in the environment by other pedestrians who are not present any more. This is the case, for example, when people walk over the trails left by others over green places or snowy areas [10].

Understanding the link between local interactions and emerging collective patterns is among today's most interesting challenges in the study of crowd behavior. For this, it is necessary to find a proper description of how pedestrians adapt their walking behaviour during each kind of interaction, and to explore the resulting collective patterns through computer simulations.

Nevertheless, finding a realistic description of pedestrians' behaviour is surprisingly challenging. Collision avoidance, for example, is a seemingly very complex cognitive task that requires collecting information about the location, the movements and the expected behaviours of other people, processing this information in real time, and planning a new trajectory every time the environment changes. Despite its apparent cognitive complexity, people easily perform this task in everyday life, even without being fully focused on the problem. We wish to distinguish two possible approaches to describe the pedestrian behaviour:

1. Elaborate an *outcome model* that directly describes the movements of the pedestrian based on complete information available in the environment. The social force model, for example, is an illustration of such an approach, in which the movements of people are described by means of repulsive and attractive forces.
2. Elaborate a *process model* that describes the underlying cognitive process that give rise to the movement. Process models typically aim at reproducing how the pedestrian processes a large amount of visual information to adapt his or her movement in real time. The heuristic model that we discuss below is an example of such an approach.

In this article, we will first describe an outcome model and discuss its strengths and limitations. Then, we will define more precisely the distinction between outcome models and process models. Finally, we will describe a process model of pedestrian behaviour, compare both approaches, and discuss its possible future improvements. Throughout the paper, we will focus mainly on two kinds of interaction, because these are responsible for the major part of collective crowd behaviours: collision avoidance and physical interaction.

2 Modelling

The process of modeling consists of finding a good description of the behavior of a pedestrian in his social and physical environment. A great deal of current research is devoted to the modeling of crowd behavior. In particular, a relevant model should be able to predict the emergence of observed crowd behavior during computer simulations. The necessity of elaborating a good and reliable model is twofold:

- First, the model constitutes an essential *research tool* to understand the precise mechanisms underlying the emergence of collective patterns. For instance, a model can be used to grasp why a particular pattern emerges, under which conditions, and which behavioral variables affect its features.
- Second, the model is also an important *planning tool* from an applied perspective. It can be used by urban planners to anticipate the behavior of crowds in a given environment, and help them manage events with large groups of people, the planning of evacuation strategies, or the assessment of urban layouts.

Many current models of pedestrian behavior are outcome models based on analogies with physical systems. The main idea of this family of models is to suppose that the movements of a pedestrian in the crowd could be described by means of mathematical tools and theoretical concepts previously elaborated to describe the movements of a particle in a gas. Force-based models inspired from Newtonian mechanics are probably the most dominant in the scientific literature, and the most commonly used for the development of commercial modeling software.

In the following section, we will first focus specifically on force-based models, describe their basic underlying principles and discuss the strengths and limitations of this approach.

2.1 Force-Based Modeling Framework

The so-called social force model was probably the first individual pedestrian-based model that was capable of predicting the emergence of collective, self-organized crowd patterns out of local interactions among individuals [11, 12]. Since its first publication in 1995, there has been important development of this model and new models based on similar concepts [13, 14]. Therefore, the original social force model can be seen today as a general framework commonly used in the community of crowd modelers.

The basic ingredients of the social force framework describe the motion of a pedestrian i at place $\vec{x}_i(t)$ by means of a vector \vec{F}_i , reflecting his or her movement in a particular direction. Accordingly, the velocity $\vec{v}_i(t) = d\vec{x}_i/dt$ of pedestrian i is given by the acceleration equation $d\vec{v}_i(t)/dt = \vec{F}_i(t) + \vec{\varepsilon}(t)$, where $\vec{\varepsilon}(t)$ is a fluctuation term that takes into account random variations of behavior. The acceleration force \vec{F}_i is the core element of this modeling approach. It is defined

as the sum of several terms denoting different attractive and repulsive effects, such as moving toward a destination point, avoiding static obstacles and other pedestrians, or staying close to other group members. In its simplest specification, the acceleration force includes three components:

- A driving force, \vec{D}_i , which lets the pedestrian i move in his or her desired direction \vec{e}_i at the desired speed v_i^o . The driving force is set such that the pedestrian adjusts the current velocity \vec{v}_i to the desired one $v_i^o \vec{e}_i$, within a certain relaxation time τ_i . This implies $\vec{D}_i = (v_i^o \vec{e}_i - \vec{v}_i) / \tau_i$. In recent experimental research, it has been shown that this equation indeed correctly reproduces the motion of a single pedestrian walking in a corridor, having the relaxation time $\tau_i = 0.54$ s [15].
- A set of repulsive forces $\sum_{j \neq i} \vec{R}_{ij}$, which makes pedestrian i avoid other pedestri-

ans j by moving away from them. In its simplest form, the term \vec{R}_{ij} is defined as a gradient of a repulsion potential, resulting in $\vec{R}_{ij} = A_i e^{-d_{ij}/B_i} \vec{d}_{ij}$, where \vec{d}_{ij} is the normalized vector pointing from j to i , and d_{ij} is the distance between the pedestrians; A_i and B_i are model parameters reflecting the strength and the range of the interaction, respectively. Nevertheless, many other specifications have been suggested (e.g. 9, 14, 15). Because it reflects how one individual reacts during interactions with other people, this component is the key element determining how the pedestrian behaves in the crowd.

- A set of repulsive forces $\sum_k \vec{W}_{ik}$, which makes pedestrian i to keep a certain distance from walls and physical obstacles k of the environment. The influence of an obstacle k is defined as a function of the distance d_{ik} to the closest point of that obstacle: $\vec{W}_{ik} = A_k e^{-d_{ik}/B_k} \vec{d}_{ik}$, where \vec{d}_{ik} is the normalized vector pointing from k to pedestrian i , A_k and B_k are model parameters.

While the very first specifications of the social force model had only qualitative connections to empirical observations, many recent studies made use of tracking algorithms to reconstruct trajectories of interacting pedestrians from video recordings taken in streets, train stations, or highly crowded areas, and to elaborate and calibrate increasingly precise specifications of the model [14–17]. Today, the most recent specifications are able to generate realistic crowd behavior, and to reproduce – at least qualitatively – every known crowd behavior, including lane formation, oscillation at bottlenecks [11], social groups' behavior [8], stop-and-go waves [18], and crowd turbulence [19].

2.2 Strength and Limitations of Physics-Based Approaches

One of the greatest advantages of force-based models is their versatility, which probably explains the large variety of existing specifications in the literature. In fact,

the social force framework is very easy to adapt by adding new parameters, changing their values, modifying the shape of the equation the forces involved, or adding new attractive or repulsive components. For example, many different specifications of the model only differ in the formulation of the equation of the main repulsive force \vec{R}_{ij} . Therefore, it is not difficult to extend the model to new kinds of interactions by adding a new term to the final equation. Thus, social interactions can be implemented by adding attraction forces among group members [8], indirect interactions with the active walker model [10], or imitation by means of a herding force in situations of panics [9]. Another important strength of the social force framework is that it benefits from all the existing tools of statistical physics, which favors its development in the literature. For example, the transformation of the individual-based model into a macroscopic description based on partial differential equations is facilitated.

Nevertheless, the force-based approach exhibits some theoretical limitations. First, although force-based models can reproduce any empirical observation, it is important to notice that this often requires a modification, an adjustment, or a recalibration of the model. In fact, force-based models have excellent *fitting* capabilities, in the sense that a model can reproduce almost any observation after adjusting the equation of motion accordingly. However, they offer relatively low *predictive* power: a model that has been previously calibrated on a given dataset often fails to quantitatively predict another set of observations. One example is the experimental specification of the model presented in Ref. [15]. This force-based model was specifically designed to reproduce individual avoidance trajectories as observed under experimental conditions (we call it dataset A). However, it failed to quantitatively reproduce the complex dynamics of lane formation observed in Ref. [3] (dataset B). Nevertheless, a recalibrated model finally allowed to reproduce correctly the dataset B, but did not work any longer for dataset A. Therefore, this particular specification was not able to reproduce the features of dataset A *and* dataset B at the same time. Likewise, the recent simulation of crowd turbulence required the use of very strong inter-individual repulsive forces that would probably not be adapted for the simulation of pedestrian movements at low density [19]. Thus, even through this specification is an extremely valuable tool for the planning of mass events where crowd turbulence often occurs, it implies using different specifications of the model depending on the expected crowd density level.

Another issue with force-based models is that quantitative agreement with empirical data often requires rather sophisticated movement equations. In particular, it seems from the past decade that crowd models have tended to become increasingly more complex in an attempt to reproduce the growing amount of new empirical observations. The specification presented in Ref. [15], for instance, is a good illustration of how sophisticated the model equations have to be to precisely reproduce individual avoidance trajectories. In fact, it is not a trivial problem to find a proper balance between attractive and repulsive effects that would correctly reproduce the speed and direction changes during an avoidance manoeuver. In Ref. [15], this was achieved at the cost of using sophisticated equations of motion,

which is also the case for many other force-based specifications. Although the high complexity of a model does not undermine its simulation capabilities, it might reduce the model's usefulness for deciphering the dynamics of the system.

2.3 *Outcome Models and Process Models*

One possible reason explaining the above limitations is that force-based models aim at describing directly the observed movements of pedestrians, rather than the *internal cognitive processes* leading to the observed movement. In other words, force-based models are excellent at reproducing observations under specific conditions, but do not capture the intrinsic cognitive mechanisms operating at the level of the individual. It is very unlikely that pedestrians would be *really* under the influence of attractive and repulsive forces. Instead, it seems more plausible that they rely on simple and unconscious rules and navigation strategies, which let them act *as if* they were subject to external forces.

This is the distinction between so-called “*outcome models*” describing directly the observed behaviour, and “*process models*” describing the cognitive processes that give rise to the observed behaviour [20, 21]. To illustrate the difference between outcome models and process models, consider the following example: Imagine the problem of modelling the movements of a baseball outfielder trying to catch a ball in the air. One can imagine two distinct modelling approaches. The first consists in measuring the expected landing point of the ball according to its current trajectory and other environmental variables, and to use an attraction force to describe the player's motion toward that point. Even through this modelling approach would require sophisticated equations and the use of many parameters, it would probably reproduce the movements of the player in a realistic manner. The second method is to elaborate a process model that relies on the so-called gaze heuristic – a simple rule-of-thumb that is used by people and animals to catch a moving target [20, 22]. The gaze heuristic consists of three steps: Fix your gaze on the ball, start running, and adjust your running speed and direction so that the angle of gaze remains constant. A simple model implementing these three rules would also reproduce the movements of the player, but it can ignore all causal variables necessary to compute the landing point of the ball, such as the velocity, angle, air resistance, or speed and direction of wind among others. Interestingly, both methods would probably predict a similar trajectory. Nevertheless, the process model generates the motion from the bottom-up, and is easier to formulate than the outcome model.

The above example can be easily put in parallel with the modelling of pedestrian movements. Existing force-based models are outcome models. Yet, a consistent framework for the development of a process model is still lacking. In the following, we describe a first attempt to elaborate such a framework based on Ref. [23], and discuss its strength and limitations.

2.4 A Process Model of Pedestrian Behaviour

The elaboration of a process model requires addressing and answering two key questions:

1. *What kind of information does the pedestrian use?*
2. *How is this information processed?*

To answer the first question, there is no doubt that a pedestrian relies on visual cues as primary source of information to decide where to walk [24, 25]. Similar vision-based approaches to describe people's movement in complex buildings have been undertaken in the past [26–29]. While interactions *among individuals* are the most important for the study of crowd dynamics, these studies only concern interactions between the individual and the physical environment. Recently, there have been several attempts to elaborate models of pedestrians' behaviour in crowds based on visual cues [30], among which is the heuristic model that we will present in the next section.

2.4.1 Formalization of Visual Cues

What would be the simplest way to describe the visual cues that a pedestrian uses to navigate in a dynamic environment? Some simplifications have to be made here, as it would be impossible to describe the entire complexity of the human visual system. Therefore, we assume that the relevant information is the distance before collision with surrounding people, objects and obstacles. Therefore, we describe the input information of a pedestrian i by a function $f(\alpha)$ describing the distance that the pedestrian can walk toward the direction α at his or her comfortable walking speed S_i^0 before a collision occurs. Because the function $f(\alpha)$ describes the visual information of the pedestrian, it is only defined for values of α in the interval $[-\phi, \phi]$ delimiting the vision range of the individual. Here, the value $\alpha = 0$ corresponds to the looking direction represented by a unit vector \vec{H}_i and the vision field of the pedestrian is ϕ degrees to the left and to the right of the direction \vec{H}_i . If no collision is found toward the direction α , then the value of $f(\alpha)$ is set to a default maximum value d_{\max} , which represents the horizon distance of the pedestrian as sketched in Fig. 1. Even though the computation of the collision distances with other people requires complex geometrical calculations, it remains a reasonable assumption as collision anticipation is a core capacity of the human brain [24, 31]. It is important to note here that this formulation requires some other simplifying assumptions, such as the fact that pedestrians have a circular body of radius r_i (although it is possible to adapt the model to elliptical body shapes as we will mention later in this article, in the 'Possible improvements' section).

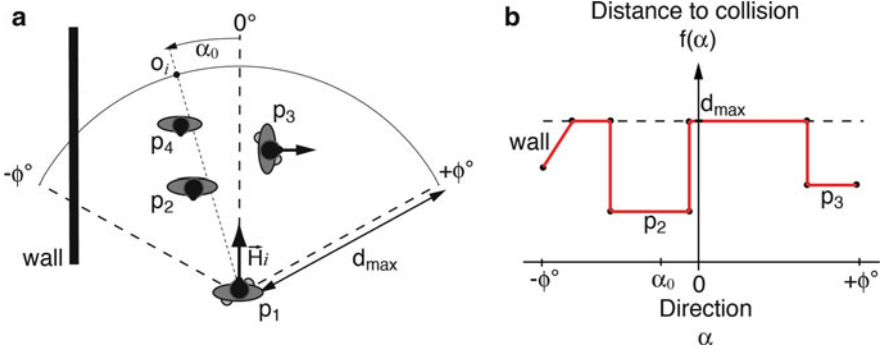


Fig. 1 (a) Illustration of a pedestrian p_1 facing three other individuals and a wall, trying to reach the destination point O_i . (b) Graphical representation of the function f reflecting the distance to collision with any obstacle when moving into different directions. The wall covers the *left-hand* side of the vision field. Pedestrian p_4 is not visible because it is hidden by p_2 . Pedestrian p_3 is moving away, so a collision would occur only if p_1 moves toward the *right-hand* side

2.4.2 Two Simple Heuristics and Body Contacts

The second question that needs to be answered concerns the processing of this visual information. Having described the surrounding visual information, we need now to define a set of rules describing how the pedestrian exploit visual cues to navigate toward a destination point O_i . For this, we assume that the pedestrian relies on two simple cognitive procedures, called heuristics [20]. The first one delineates how the pedestrian adapts their *direction of motion* according to the occupancy of the visual field, and the second describes how the pedestrian adapts their *walking speed* as a function of the available walking space.

Minimizing Detours

The first movement heuristic concerns the relative angle α_{des} of the chosen walking direction. Empirical evidence suggests that pedestrians seek an unobstructed walking direction, but dislike deviating too much from the direct path to their destination [32, 33]. A trade-off therefore has to be found between avoiding obstacles and minimizing detours from the most direct route. Accordingly, our first heuristic is defined as follows:

The chosen walking direction α_{des} is the one that minimizes walking towards the destination point.

In this way, the pedestrian chooses the unobstructed direction that deviates least from the destination point. Formally, the chosen direction $\alpha_{des}(t)$ is computed through the minimization of the distance to destination $d(\alpha)$:

$$d(\alpha) = \sqrt{d_{max}^2 + f(\alpha)^2 - 2d_{max}f(\alpha)\cos(\alpha_0 - \alpha)}.$$

Here, α_0 is the direction of the destination point.

Keeping a Safe Distance

The second heuristic determines the desired walking speed $v_{des}(t)$. Since a reaction time τ is required for the pedestrian to stop in the case of an unexpected obstacle, pedestrians should compensate for this delay by keeping a safe distance ahead [34]. Therefore, we formulate the second heuristic as follows:

The pedestrian reduces the walking speed to keep the time to collision with the nearest obstacle above τ seconds.

Formally, the desired speed is given by:

$$v_{des}(t) = \min(v_i^0, d_h/\tau),$$

where d_h is the distance between pedestrian i and the first obstacle in the desired direction α_{des} at time t .

Finally, the vector \vec{v}_{des} of the desired velocity points in direction α_{des} , and has the norm $\|\vec{v}_{des}\| = v_{des}$. The change in the actual velocity \vec{v}_i at time t under normal walking conditions is given by the acceleration equation $d\vec{v}_i/dt = (\vec{v}_{des} - \vec{v}_i)/\tau$, where $\tau = 0.5$ s as determined in previous experimental measurements [15], and the location $\vec{x}_i(t)$ of pedestrian i at time t is the first derivative of the velocity $d\vec{x}_i/dt = \vec{v}_i$. The looking direction \vec{H}_i is constantly adjusted toward the desired direction α_{des} .

Pushing Behavior

The above model has very good simulation performance at low density. For instance, it quantitatively reproduces the features of individual avoidance trajectories [23], as well as the emergence of unstable dynamics during lane formation [3]. However, simulation results at higher densities are not satisfying. The reason for this is that the *nature* of interactions involved is different. In fact, when the density is high enough, physical contacts may occur as well, causing unintentional movements that are not determined by the above heuristics. Therefore, it is necessary to distinguish between *intentional* avoidance behaviors based on strategic navigation heuristics, and *unintentional* movements resulting from pushing forces caused by body contacts. Hence, it is necessary to extend the above description by considering a physical contact force that applies *only* when people are in physical contact:

$$\vec{f}_{ij} = kg(r_i + r_j - d_{ij})\vec{n}_{ij},$$

where the sub-function $g(x)$ is zero if the pedestrians i and j do not touch each other, and otherwise equals the argument x . Here, \vec{n}_{ij} is the normalized vector pointing from pedestrian j to i , and d_{ij} is the distance between the pedestrians' centers of mass [9].

The final model allows for simulations of crowd movements at any density level, and is capable of quantitatively reproducing a large range of phenomena, such as the fundamental diagram, stop-and-go waves, some features of crowd turbulence, and evacuation times [23]. In contrast to force-based approaches, the repulsive interaction term \vec{f}_{ij} used in the cognitive model is not an analogy, but reflects the physical pressure among bodies that actually takes place in crowded environment. It is interesting to note that most existing models in the literature do not make a clear distinction between physical interactions and collision avoidance interactions, trying to describe both of them with the same tool. But these two kinds of interaction arise from fundamentally different processes: the physical pressure on the one hand, and the navigation strategy on the other hand.

2.5 Benefits and Drawbacks of the Heuristic Model

Beside the fact that the heuristic model is based on plausible hypotheses and offers a new perspective on existing literature, it is interesting to note that it actually solves a long-standing open issue about how to combine multiple simultaneous interactions [35]. For example, in a situation where an individual A is facing three other individuals B, C, and D, force-based models typically assume that A sums up the repulsive effects that B, C and D would have separately in the absence of the others. However, this approach raises several theoretical issues. First, it is not obvious that simultaneous influences are additive. One can also integrate them in different ways such as averaging over them, or combining them nonlinearly. Second, it is unclear how to determine the influential neighbors and how to weight their influence. For example, it has been suggested that only the k closest individuals should be taken into account, or only those located in a certain interaction radius R [35–37]. But the values of k and R remain unclear and seem to vary with increasing density level. Another subsequent problem is that the repulsive effect in force-based models is necessarily proportional to the number of interacting partners. Consider the example in which a person is avoiding a group of standing pedestrians. Because repulsive forces typically cumulate, the shape of the avoidance trajectory will change according to the number of people in the standing group, which often generates inconsistent simulations. In contrast, in the heuristic model, interactions cannot be reduced to the superimposition of pair interactions because individuals react to a visual pattern in an integrative way. Therefore, rather than balancing multiple repulsion effects originating from other individuals, the simulated pedestrian *detects* an efficient free way to the destination and follows it, which generates realistic behaviour from the bottom-up. Therefore,

it is not necessary to define explicit rules for combining simultaneous interactions or setting a fixed number of interacting partners in advance. These problems vanish naturally when using an integrated visual input, such as the pedestrian's visual field.

Nevertheless, the cognitive model exhibits technical limitations due to the difficulty of its implementation. In fact, the calculation of the function $f(\alpha)$ describing the visual pattern of the pedestrian is a complex algorithm that requires heavy computational power and is prone to programming errors. The program typically needs to identify the first collision point between one moving object (the focus pedestrian) and many others (the other individuals), and to repeat this step for all directions α of the vision field, for all pedestrians i , and at every time step t . Therefore, simulations of the cognitive model are systematically longer than simulations of a force-based model, and may reach unreasonable computation time for simulations of large crowds (e.g. higher than 1,000 individuals). Even through this technical limitation does not directly challenge the validity of the model, it can hinder or slow down its future development, and dissuade the use of the model in commercial software. In the next section, we will suggest the search-and-stop rule as a future improvement that is likely to reduce the needed computational power. Advances in programming techniques and particularly in ray-casting algorithms may also help in resolving this issue.

Another issue with the cognitive model is that it is more difficult to extend than force-based models. With the social force approach, modeling a new component of pedestrians' behavior, such as the side preference, the herding behavior during panics, or the movements of pedestrians in social groups, always consists of adding a new force component and calibrating this force with empirical data [8–10, 15]. This systematic methodology facilitates the development of the model. Updating the cognitive model, however, always requires some deep questioning about the cognitive processes involved in the situation being studied. For example, the cognitive model fails to correctly reproduce the situation where two pedestrians are facing each other at a narrow bottleneck, such as a door. In this situation, the visual field of each individual indicates that there is no empty space where it is possible to move, and therefore both pedestrians stop moving and wait endlessly for an opportunity to move ahead. Of course, this situation would never happen in real life because people have learnt that one has to step back and let the other one go first. But implementing this improvement in the model is more complicated, as simulated pedestrians need to identify the problem first, and solve it afterward.

2.6 Possible Improvements

As we mentioned earlier in this article, the cognitive approach described above should be considered as an initial basic framework rather than a final model. We have deliberately kept the model in its simplest form so far, to highlight the most basic heuristics needed to reproduce the fundamental features of crowd dynamics.

But this first attempt certainly requires many improvements. In this section, we describe some possible improvements that could be considered in the future.

The first modification that could be undertaken is the implementation of elliptical body shape. Although the circular body shape seems to be a reasonable simplification in the first place (as demonstrated by the accurate predictions of the model), it may be relevant to use an elliptical body shape instead in the future [38]. In fact, at high densities, elliptical bodies may reduce the collision frequency and therefore affect the density threshold at which stop-and-go waves and crowd turbulence form. The implementation of elliptical body shape would also constitute a first step for modeling movements of pedestrians' shoulders, which is known to facilitate avoidance maneuvers in crowded areas [39]. This improvement is expected to be important even at low density because it may help unblocking some face-to-face situations, such as the one described in the previous section. However, this update remains challenging, as it will require even more sophisticated algorithms for the detection of collisions.

Another important improvement would be the elaboration of a search-and-stopping rule [20, 40]. The current version of the model presumes that pedestrians select the best walking direction among all directions within their field of view (i.e. the direction that minimizes the distance to the destination point). However, it might be more realistic to assume that the pedestrian instead searches a good walking direction in his visual pattern and stops searching when a good enough solution is found, without exploring the complete vision field. This would require the implementation of a search rule (what is the starting point of the searching? What is the exploration sequence?), and a stopping rule (what is a good enough solution? When to stop searching?). Ideally, this rule would predict the kinds of eye movements that pedestrians engage in, based on theoretical principles and empirical data [41]. For example, one may assume that the individual starts searching in front of him (around $\alpha = 0$), explores the visual pattern toward the sides, and stops when a satisficing walking direction is found. In addition, biased exploration patterns toward the right-hand side could possibly reproduce the features of the side preference [15]. The search-and-stop rule could also drastically reduce the computational power, as the complete field of vision would not need to be computed in advance, and might produce approximate decisions in a way that is closer to the pedestrian's actual decision process.

Finally, it could also be interesting to include noise and fluctuations in the simulated behavior of the pedestrian. In particular, most existing modeling approaches rely on an "extrinsic" source of fluctuations, in the sense where random fluctuations of the movement are added after the deterministic behavior has been calculated. In force-based models, for instance, the equation of movement typically includes a random component that causes the pedestrian to deviate randomly from a pre-calculated position (e.g. the term $\vec{\varepsilon}(t)$ in the original equation of the social force model).

When using a heuristic-based approach, however, it becomes possible to inject an *intrinsic* source of stochasticity. In such a way, the noise is not added after the movement is computed, but directly included in the cognitive process that generates

the movement. For example, one may add random errors when the pedestrian estimates the expected collision points with other pedestrians, with less precise estimations on the sides than in the center of the visual field. The precision of the estimates in the model could even be based on data on the relative area that the visual cortex devotes to processing stimuli at a particular distance from the center of the visual field [42]. When the pedestrian makes eye movements (fixations) to particular parts of the visual field, the precision of their estimates of the location and behavior of stimuli near that part of the visual field would increase the most.

3 Conclusion

In this article, we have described and compared two modelling frameworks for simulating crowd dynamics. While an outcome model can make use of attractive and repulsive forces to describe a pedestrian's movements, a process model based on concepts of cognitive science describes the internal processes underlying the movement. We underlined the fact that different kinds of interaction, namely collision avoidance and physical interactions, should be described with different tools that account for the specific nature of each type of interaction: simple heuristics to describe the pedestrian's navigation strategy, and a repulsive force to account for body contacts in dense crowds.

When comparing the cognitive approach to the classical social force framework, it seems that each method complements the other, and has its own benefits and drawbacks. Each approach has similar performance in simulations, but the cognitive approach offers the greater potential for connecting pedestrian decision processes with individual and aggregate pedestrian behaviour. Nevertheless, we believe that outcome- and process-based models, by existing in parallel, will facilitate the development of comprehensive theories of crowd dynamics that could not arise from either approach alone.

References

1. Helbing D, Molnar P, Farkas IJ, Bolay K (2001) Self-organizing pedestrian movement. *Environment and Planning B: Planning and Design* 28:361–383.
2. Yamori K (1998) Going with the flow: Micro-macro dynamics in the macrobehavioral patterns of pedestrian crowds. *Psychological review* 105:530–557.
3. Moussaïd M et al. (2012) Traffic Instabilities in Self-Organized Pedestrian Crowds. *PLoS Comput Biol* 8:e1002442.
4. Kretz T, Grünebohm A, Kaufman M, Mazur F, Schreckenberg M (2006) Experimental study of pedestrian counterflow in a corridor. *Journal of Statistical Mechanics: Theory and Experiment* 2006:P10001–P10001.
5. Helbing D, Buzna L, Johansson A, Werner T (2005) Self-Organized Pedestrian Crowd Dynamics: Experiments, Simulations, and Design Solutions. *Transportation Science* 39:1–24.

6. Helbing D, Johansson A, Al-Abideen H (2007) The Dynamics of crowd disasters: an empirical study. *Physical Review E* 75:46109.
7. Camazine S et al. (2001) *Self-Organization in Biological Systems* (Princeton University Press).
8. Moussaïd M, Perozo N, Garnier S, Helbing D, Theraulaz G (2010) The Walking Behaviour of Pedestrian Social Groups and Its Impact on Crowd Dynamics. *PLoS ONE* 5:e10047.
9. Helbing D, Farkas I, Vicsek T (2000) Simulating dynamical features of escape panic. *Nature* 407:487–490.
10. Helbing D, Keltsch J, Molnar P (1997) Modelling the evolution of human trail systems. *Nature* 388:47–50.
11. Helbing D, Molnar P (1995) Social force model for pedestrian dynamics. *Physical Review E* 51:4282–4286.
12. Helbing D (1991) A mathematical model for the behavior of pedestrians. *Behavioral Science* 36:298–310.
13. Yu WJ, Chen R, Dong LY, Dai SQ (2005) Centrifugal force model for pedestrian dynamics. *Physical Review E* 72:26112.
14. Johansson A, Helbing D, Shukla P (2007) Specification of the social force pedestrian model by evolutionary adjustment to video tracking data. *Advances in Complex Systems* 10:271–288.
15. Moussaïd M et al. (2009) Experimental study of the behavioural mechanisms underlying self-organization in human crowds. *Proceedings of the Royal Society B: Biological Sciences* 276:2755–2762.
16. Johansson A, Helbing D, Al-Abideen HZ, Al-Bosta S (2008) From crowd dynamics to crowd safety: A video-based analysis. *Advances in Complex Systems* 11:479–527.
17. Hoogendoorn S, Daamen W (2007) in *Traffic and Granular Flow*, pp 329–340.
18. Helbing D, Johansson A, Mathiesen J, Jensen M, Hansen A (2006) Analytical Approach to Continuous and Intermittent Bottleneck Flows. *Physical Review Letters* 97:168001.
19. Yu W, Johansson A (2007) Modeling crowd turbulence by many-particle simulations. *Physical Review E* 76:46105.
20. Gigerenzer G, Todd P (1999) *Simple Heuristics That Make Us Smart* (Oxford University Press).
21. Gigerenzer G, Brighton H (2009) Homo Heuristicus: Why Biased Minds Make Better Inferences. *Topics in Cognitive Science* 1:107–143.
22. Bennis W, Pachur T (2006) Fast and frugal heuristics in sports. *Psychology of Sport and Exercise* 7:611–629.
23. Moussaïd M, Helbing D, Theraulaz G (2011) How simple rules determine pedestrian behavior and crowd disasters. *Proceedings of the National Academy of Science* 108:6884–6888.
24. Gibson J (1979) *The Ecological Approach To Visual Perception* (Houghton Mifflin).
25. Gibson JJ (1958) Visually controlled locomotion and visual orientation in animals. *British Journal of Psychology* 49:182–194.
26. Hillier B, Hanson J (1984) *The Social Logic of Space* (Cambridge University Press).
27. Garling T, Garling E (1988) Distance minimization in downtown pedestrian shopping. *Environment and Planning A* 20:547–554.
28. Penn A, Turner A (2002) in *Pedestrian and Evacuation dynamics*, eds Schreckenberg M, Sharma S (Springer), pp 99–114.
29. Turner A (2007) in *6th International Space Syntax Symposium*, eds Kubat AS, Ertekin O, Guney YI, Eyuboglu.
30. Ondřej J, Pettré J, Olivier A-H, Donikian S (2010) A synthetic-vision based steering approach for crowd simulation. *ACM Trans Graph* 29:1–9.
31. Cutting JE, Vishton PM, Braren PA (1995) How we avoid collisions with stationary and with moving obstacles. *Psychological Review* 102:627–651.
32. Batty M (1997) Predicting where we walk. *Nature* 388:19–20.
33. Turner A, Penn A (2002) Encoding natural movement as an agent-based system: an investigation into human pedestrian behaviour in the built environment. *Environment and Planning B: Planning and Design* 29:473–490.
34. Johansson A (2009) Constant-net-time headway as a key mechanism behind pedestrian flow dynamics. *Physical Review E* 80:26120.

35. Ballerini M et al. (2008) Interaction ruling animal collective behavior depends on topological rather than metric distance: Evidence from a field study. *Proceedings of the National Academy of Sciences* 105:1232.
36. Steffen B (2008) in *Conference proceedings of PED2008* (Springer, Berlin).
37. Ma J, Song W, Zhang J, Lo S, Liao G (2010) k-nearest-neighbor interaction induced self-organized pedestrian counter flow. *Physica A* 389:2101–2117.
38. Still K (2000) Crowd Dynamics.
39. Daamen W, Hoogendoorn S (2002) Controlled experiments to derive walking behaviour. *Journal of Transport and Infrastructure Research* 3:39–59.
40. Hutchinson J, Gigerenzer G (2005) Simple heuristics and rules of thumb: Where psychologists and behavioural biologists might meet. *Behavioural Processes* 69:97–124.
41. Nelson J, Cottrell G (2007) A probabilistic model of eye movements in concept formation. *Neurocomputing* 70:2256–2272.
42. Sereno MI et al. (1995) Borders of multiple visual areas in humans revealed by functional magnetic resonance imaging. *Science* 268:889–893.

The Characteristics and Needs of Pedestrians with Mobility Impairments

How to Move Around Comfortably and Safely with a Reduced Ability to Walk, See, Hear, Feel or Process

Marjolein de Jong

Abstract Mobility is one of the preconditions for being able to participate in social life: individuals perform activities because of economic, social, recreational and other personal reasons. Mobility constraints may lead to a decreased participation. Making the mobility landscape more inclusive is not an easy task at all: the whole travel chain has to be designed and organized in such a way that the specific needs of several groups are taken into account. The accessibility of an environment is not only determined by the barrier context of the person, but also by the environment and the activity undertaken. Depending on these constraints, people with reduced abilities to walk, see, hear, feel or process information can move around more or less independently.

Keywords Pedestrians • Reduced mobility • Accessibility • Mobility impairments

1 Mobility as a Precondition to Participate in Social Life

The *European Disability Strategy 2010–2020* (a Barrier-Free Europe) that was launched in November 2010 should ensure an effective implementation of the *UN Convention on the Rights of Persons with Disabilities* [31] within Europe and the individual countries. In relation to mobility, the recent *White Paper on Transport* [13], issued by the EU, stresses the importance of quality and reliability as key elements for an efficient and integrated mobility system.

Mobility is one of the preconditions for being able to participate in social life: individuals perform activities because of economic, social, recreation and other

M. de Jong (✉)

Transportation Research Institute (IMOB), Hasselt University, Hasselt, Belgium
e-mail: marjolein.dejong@uhasselt.be

personal reasons. Taking part in activities implies to be able to travel to various destinations where specific activities take place. If the travel possibilities don't allow someone to participate in social life in an adequate manner, this person will suffer from a decreased participation [34] due to "transportation poverty" [7] meaning that one has to live with disadvantages concerning his/her own out-door mobility and reduced access to relevant points in the public space.

Older persons or disabled persons have not that often been the specific focus of travel behaviour research (see e.g. [38]), but it can be expected that they will be confronted with similar constraints as other people, but of a different nature or degree [23]. The constraints older or disabled people have to deal with, influences the travel behaviour pattern of themselves and those they travel with in a fundamental way and also the decision making process related to making a trip. The following three dimensions need to be accounted for when modelling for people with mobility impairments:

- *Individual decision level*: physical problems or signs of fatigue or bad weather conditions influence the individual itself.
- *Mobility system*: physical accessibility of the public domain or travel service
- *Social network and household*: 'companions' (other disabled persons), friends, care givers and others may induce, alter or reduce mobility by forming the physical and emotional support system [28].

1.1 Dis-abilities

The World Health Organization [34] recognizes disability "as a complex interaction between features of a person's body and features of the environment and society in which he or she lives." Adopting the WHO's classification, impairment refers to "a problem in a body function or structure," whether permanent or temporary, motor, sensory, or cognitive. Most people, if not everybody, deals at least once in his life with permanent, temporary or even situational functional impairments.

Being *situational impaired* as concept has been introduced by Goldsmith [18] and is based on the concept of architectural disability. It is not exclusively a property of physically disabled people, but a property of the environment we have to move in. Lack of toilets for example (and this is even more problematic for women than for men) is one of the reasons people avoid going to unknown places. By advocating "access for everyone" instead of "access for disabled" all kind of handicap situations should be addressed, also for those without a typical impairment, but nevertheless feeling dis-abled. The way in which activities are limited by the environment or society has impact on the social participation of an individual. Persons are therefore disabled by the society they live in, not directly by their impairment, which is an argument for using the term *disabled persons*, rather than *persons with disabilities*.

So in other words: the accessibility of an environment is not only determined by the barrier context of the person, but also by the environment and the activities

undertaken. Depending on these constraints, people with reduced abilities to walk, see, hear, feel or process information can move around more or less independently. Participation in social life is an equal right for all citizens. By starting from a **design for all approach**, an inclusive built environment can be realised without stressing specific impairments too much and avoiding the creation of dis-abling situations.

1.2 Incidence of Disabilities

Mobility related impairments are very wide spread. In Europe (population of 800 million) around 15 % of the population has an impairment affecting mobility:

- 26 million (3.25 %) sensory impairments (hearing, seeing, . . .)
- 55 million (6.9 %) cognitive impairments (understanding, . . .)
- 35 million (4.4 %) dexterity impairments (arms, hands, fingers)
- 30 million (4 %) mobility impairments (moving)

If we also consider the ageing and de-greening of our society – trend we can't ignore – the group of people mobility impairments increases considerably. Prognoses for 2050 indicate that the number of 0–59 year-olds will diminish while the number of 65+ will rise by more than 50 % and the number of 80+ will even more than double. Ageing itself is not a disease, but often comes with a number of physical, psychological, social and financial changes. Approximately 50 % of the over 65 s have a disability having impact on their mobility. It is often a gradual accumulation of multiple minor impairments resulting in difficulties to maintain an active and independent lifestyle. As a result, a growing proportion of the population find themselves increasingly disabled and may acquire, regardless of age, a temporary or permanent impairment during the course of life.

2 Pedestrians Need a Safe and Secure Environment

Safety is a fundamental and essential need for the human organism and as important as the need for social interaction and sex (Fig. 1). As human beings we are always interested in maintaining our own safety and that of those around us. Still, feeling safe is only one of our fundamental needs. Often we find ourselves having to deal with conflicts of interest, and we have to trade off between the perceived benefits and risks of our actions [16].

If we talk about the needs of pedestrians with mobility impairments, safety is an important issue. Actually it is not only important for those with impairments, but for all pedestrians the perceived security and safety plays a crucial role in the decision to walk, as well as on the actually routes chosen [16]. Pedestrians are very vulnerable and the chance to survive a collision with a car depends strongly on the



Fig. 1 *Left:* Level access offering comfort to all kind of users. *Right:* lack of platform and stairs lead to ‘situational-impairments

speed of the vehicle. If the speed is around 30 km/h, there is still a chance of 80 % the pedestrian will survive meanwhile a speed of around 50 km/h reduces the chance to survive to only 20 % [35].

2.1 *Fear of Accidents*

Feelings of unsafety can be related to fear of accidents (safety-related risk perception) as well as to fear of crime, violence and strangers (security-related risk perception). A survey from Backer-Grøndahl et al. [3] on the perceived safety and security for ten different modes of transport revealed that for walking, people reported higher perceived risk for security issues than for safety issues. People appear to be more afraid of situations where they think they are likely to be exposed to threats, violence, and other unpleasant situations, than of being involved in an accident as a pedestrian. If we look at the safety-security risk profile of the ten modes of transport we find pedestrians in the cluster of public transport modes Fig. 2. This indicates that pedestrians are, like users of public transport modes, highly exposed to what is happening in the public domain. Also statistically, they run a far greater risk of being exposed to violence than bicyclists, car drivers, and motorcyclists (Fig. 3).

2.2 *Safety and Security as a form of Comfort*

Within the PROMPT project (New means to PROMote Pedestrian Traffic in cities) pedestrians on the street have been interviewed about their actual trip and the way they perceived the situation. Based on interviews in six European countries two main types of pedestrians can be distinguished [24]:

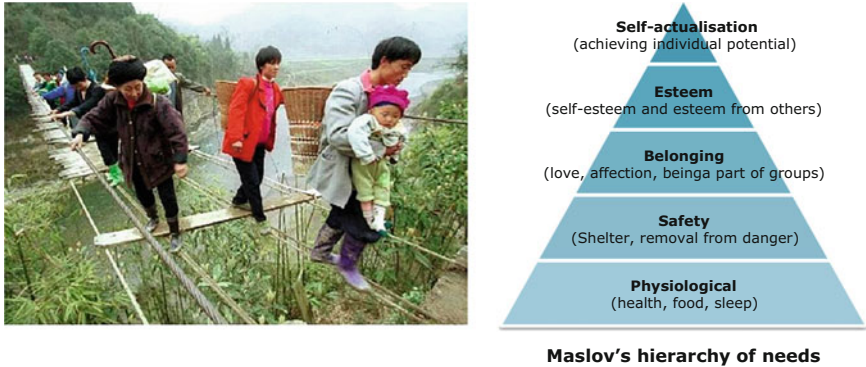


Fig. 2 If the physiological needs are not fulfilled, safety risks are being taken

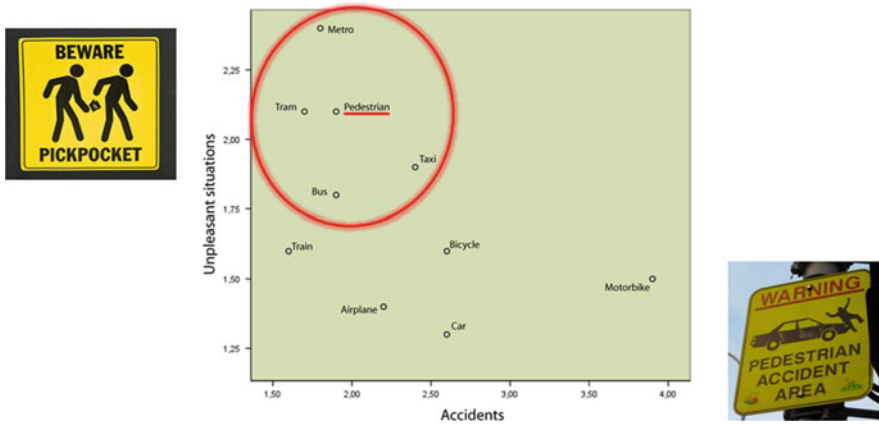


Fig. 3 ‘Risk profile’ of ten modes of transport. Respondents’ perception of worry for accidents and for being involved in an unpleasant situation (crime, violence, harassment). Mean scores from 1 to 5 (From Backer-Grøndahl et al. [2])

- Pedestrians seeking ease and social pleasure: For them presence of other people is important as well as places to sit, requirements met, weather and light conditions, surface conditions, the open/narrowness and layout of the surroundings.
- Pedestrian seeking security away from traffic: The important factors are safety, noise level, comfort, air conditions and traffic conditions.

As reason for the specific route they had chosen, the most common answers were time use (38 %) and walking distance (33 %), while as many as 15 % mentioned the surroundings. However, the most important factor to explain comfort when walking was to feel *safe* and *secure*. Walking in general and use of public transport are the two modes of transport with the highest fear of crime. In both cases physical contact with strangers is possible but there is often no quick escape. The perceived risk of

becoming a victim of crime seems to be higher after dark and in enclosed spaces [10, 30]. Women normally report more fear than men. This corresponds with research by Greene [19], who found two basic characteristics of the built environment, which play an important role in the perception of risk: the visual field (how much can I see?) and the visual control (can I be seen?). People feel the safest if they have a good overview of the space in which they are moving and if they have the feeling that they are supported by other users.

If we come back to the needs of pedestrians, creating a safe and secure environment is part of inviting people to use the space as a pedestrian. In that respect, both safety and security should be taken into consideration when looking at pedestrian behaviour and when aiming at a design for all approach.

3 Our Future Selves: Getting Older

“Our future selves” is introduced by Coleman and Pullinger [9], to emphasize the understanding of disability as inherently woven into the human lifecycle, as dynamic and environmentally related. Disability shouldn’t be understood as something that only happens to a minority of people, but as a universal human experience we are all confronted with, sooner or later. For elderly, walking is a way to maintain their mobility and overall health situation. The ability to go on foot to destinations like shops, doctors and public transport increases their level of independence. However, older people may experience mobility restrictions like moving slower than before, hearing or visual perception may deteriorate and reaction and decision time may increase [25].

It is interesting to realize that almost all pedestrians, regardless of age, try to save energy by choosing short routes. The Dutch photographer van der Burg was fascinated by the phenomenon of people choosing the shortest route, also when it just means a gain of a few seconds (Facebook page: [14, 33]) (Fig. 4).

3.1 A Safe Environment

Older people mentioned in several studies that they stay at home because they are afraid of the road traffic which is, in their view, too dangerous [4, 6, 17]. Senior citizens wish an attractive environment with low speed zones (max 30 km/h), traffic islands to cross the street in two phases and enlargement of sidewalks at crossings. These aspects are considered very important to increase – the feeling of – comfort and safety for older people. Furthermore there is the wish for continuous pavements and the avoidance of underpasses or footbridges as they have a positive impact on the life quality in road-areas [17].

Fig. 4 ‘Elephant trails’ appear when the routes are not considered to be logical. But sometimes it is just rounding a corner resulting in an almost negligible gain . . .



3.2 Possibilities to Have a Rest

Another important aspect that is coming back again and again in surveys and focus groups, is the need for enough places to rest and toilets. Senior citizens wish enough possibilities to sit down and have a rest or to use a public toilet, both making it possible to cover longer walking-distances [29]. According to elderly, there are often not enough seats offered in public space. However, places to rest are not only important for senior citizens, but make walking more convenient for all age groups [37]. When people sit on a bench they can observe the environment, look at people walking, running or strolling by, and they can establish social contacts through small-talks which may help feeling more connected to society. Offering these facilities in the direct living-area of elderly allows them to get involved in appropriate mental and/or physical activities [27].

3.3 Fear for Falling

In a random sample of elderly between 65 and 80 years old in the United States, 9 % reported a serious fear of falling. Although more women than men reported fear, for both groups the fear of falling increased with age. As a result they seldom left the building where they lived [1]. Research shows that among women between 54 and 77 years of age in the UK, 10 % were afraid of falling One third had already fallen on the street. Australian research of women between 70 and 85 shows that fear of falling was larger than fear of being robbed on the street [8]. Fear of falling has an

impact on the amount of outdoor walking elderly engage in and their activity pattern as loss of confidence and fear of falling often leads to adapting the mobility pattern to less walking and consequently a more limited activity pattern [5].

4 Visual Impairments

4.1 Incidence

For people with visual impairments, the way how the walking environment is designed has an important impact on the possibilities to move and to participate in activities. At a certain moment in life almost everybody has to deal with problems with sight: at the age of 50 around 95 % of the population has to use glasses permanently or in specific situations to be able to see good enough. Not everybody with glasses or contact lenses is visual impaired, although it may be very inconvenient to enter a station with fogged glasses and to find out which train you have to take. Problems with sight become a visual impairment if the problems can't be remediated adequately with an optimal correction with glasses or contact lenses. About 1 % of the population experiences serious visual impairments due to loss of central sight, tunnel vision, loss of visual acuity or sight with patches. A much smaller part of the population is considered blind, meaning that the visual field is less than 10° or an absence of light perception [20]. The eye diseases macular degeneration and cataract account for about half of the people getting blind at later age and are also an important reason for poor eyesight. About 82 % of all people who are visually impaired are age 50 and older which means that the amount of visual impaired persons will increase with the aging of society due to getting older in general and aging related diseases like diabetes [36]. This means that a significant group of the – aging – population has to deal with the consequences of bad eyesight having immediate consequence on travel options.

4.2 Visual Information

The travel options of bad sighted people are reduced as driving a car themselves is in most cases not possible. Therefore, the ability to walk is an essential factor for being able to move independently, not only as a pedestrian, but also as a public transport user. Thus, design of public space and public transport play a crucial role in allowing blind and visual impaired persons to participate in social life. However, when travelling we rely very much on visual information and having a good sight is almost a necessary precondition for all travel modes. As most information related to orientation and travel possibilities is collected through visual channels [26] moving around in everyday life is not easy for this group of people. Reading messages on



Fig. 5 Example of a crossing with visual and tactical guidance on different levels

the street or from paper is an important barrier for sight impaired persons and braille is in most cases not considered as an alternative; just 10 % of the blind read it and an even smaller group of the visually impaired uses this form of information [21]. Special devices for the blind like long canes or guide dogs are often not used by visual impaired, especially not by those who got the problems at higher age.

4.3 *Comfort Prevails Above Length: An Example from Leuven*

An experiment in Leuven revealed some interesting points about the impact of the quality of the route and the route choice [11, 32]. The routes chose by the test group were tracked and the participants were followed on distances and questioned afterwards about their decisions. With the choice of their route, visual impaired people rely very much on information they have gained during travel training or previous trips. An important element for route choice is to avoid unknown situations or places with little guidance. Instead of crossing an open place it is perceived safer to follow the row of houses until a known street and continue from there. Lack of visual and tactile guidance also leads to walking around an open space instead of crossing it. It is worth walking a bit more as long as you can go from point to point following routes that are perceived safe. In general, people with visual impairments are depending very much on their memory when choosing a route and gathering information during the trip. Reading signs or information displays is for most of them very difficult and therefore of no or little help during a trip. Good guidance is therefore a necessary element on a route, like the example in Fig. 5

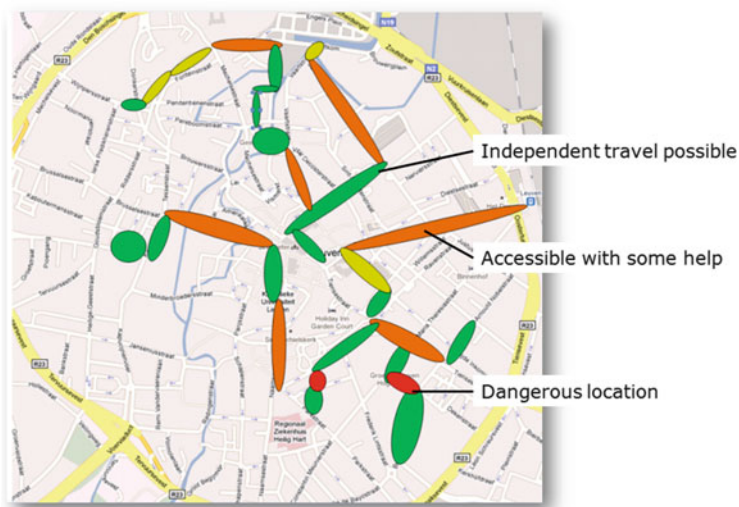


Fig. 6 Leuven: accessibility map for visual impaired based on the opinion of the test group

For Leuven we have made an accessibility map for visual impaired (Fig. 6) based on the results of the test routes and the interviews afterwards. This kind of maps could be an interesting means of help for people with visual impairments, but also could be a ‘road map’ for governments to take away the most important bottle necks.

Although the participants of our test group still have the ability to distinguish shades, colours, forms or even parts of the surrounding environment, a white stick is considered as a useful tool to show the public they don’t see very well; in general people respond on it in a positive way by clearing the route. Special facilities for blind persons like tactile lines or strong colour contrast are considered very useful, and are often used as boundary of the walking route. Bicycles, signposts, and other clutter on the walking route are considered as a problem. Although potholes and puddles often can be detected in time when using a white stick they form a problem when walking with guidance of someone or alone without a stick. Another thing most participants seem to avoid are places where traffic can be expected everywhere. The participants don’t like it when a clear pedestrian area is lacking. Cyclists are very silent and feared because they are suddenly there, often unexpected and unannounced. Especially in mixed used areas, this is considered problematic.

In general we can see that there is a strong connection between the experiences while walking (operational level), route choice (tactical level) and the decision prior to conducting a trip. Bad experiences during the trip like very narrow sidewalks, too much obstacles, a lot of potholes, difficult crossings, too much other traffic or big open spaces lead to other decisions on strategic level and even might lead to another mode of transportation if it is considered too difficult to walk independent or to look for help during the trip. For visual impaired it is of crucial importance that there are obstacle free walking routes marked with colour contrasts or tactile guidance with

a surface in good condition. As soon as one these elements is missing, it is likely that it will lead – on the shorter or longer term – to another route choice, another transport mode and eventually to the decision not to travel at all.

5 Doing It Right When No One Is Looking

5.1 Treat-as-normal Approach as the Standard

Pedestrians are very sensitive for the quality of the public space in which they have to move around. For people who experience mobility impairments, it is even more important that ‘design for all’ principles are applied for pedestrian routes and public transport. As discussed in this paper, it is often the environment itself that “dis-ables” people or makes people more aware of possible – and often slight – impairments they have. To turn it around: we are all challenged to provide public space that allows people to move around as independent as possible, no matter what kind of impairments someone has to deal with.

During the last decades a change in perception can be noted in the professional attitude towards the diversity of impairments and capacities people have and the handicap-situations associated with it. Instead of a treat-as-different approach, a treat-as-normal approach is gaining importance in Europe [15]:

- MICRO approach (treat-as-different): wheelchair accessible building, Assistive Technology, Design for Special Needs, Barrier free Design etcetera. These are categorical design principles based on the medical model. This medical model has a strong base in the European culture of welfare and social services (service-led).
- MACRO approach (treat-as-normal): Universal Design, Design for All, Inclusive Design etcetera. These concepts express the new design paradigm that anticipates on social ‘handicap-situations’. Especially in the United States this model of self-help culture is leading (grievance-led).

By taking the treat-as-normal approach as the starting point for design, more inclusive environments will be realized, also anticipating on all kind of possible smaller or larger discomforts we, as our future selves, have to deal with sooner or later.

5.2 Some Rules of Thumb

In this paper, I’ve just mentioned some of the elements that have to be taken into account when designing public spaces that are usable for all kind of users (Fig. 7). In the presentation more examples can be found and for details concerning an



Fig. 7 Pedestrians like a smooth surface: the larger tiles are preferred by strollers. The pattern also gives a guidance for the terrace: till there and not further

actual design, guidelines from the national or local government can be consulted (for example [10, 22]). However, a good design is more than summing up ‘best practices’ for different kind of impairments. The main challenge is to integrate the needs from the different impairment groups in such a way that they are more or less ‘invisible’, but yet usable for all kind of users, including our future selves (Fig. 7). As Henry Ford once said: “Quality means doing it right when no one is looking”, which is very important starting point for total quality management [12]. A good accessible design can be used by wheelchair users, elderly with a walking stick, by people with reduced sight, and also by people suffering from ‘claudation’ (in the US the severity is indicated according to the amount of blocks someone can walk without problems). There are four main groups of problems we have to deal with: mental, acoustical, visual and physical, each with their typical problems and measures. In general, each design should be assessed according to those four main groups of problems and solution-directions considering a whole family from the children till the grand parents (Fig. 8).

Although there are a lot of requirements a good design for the public space has to fulfill, there are four easy to remember basic rules:

1. Easy to recognize logical routes
2. Proper designed routes
 - (a) Width
 - (b) Surface
 - (c) Height differences






	Problem		Measures
	Mental	Uptake of information	Understandable information
	Acoustical	Hearing impairments	Visual guide-system
	Visual	Visual impairments	Tactile and acoustical guide-system
	Physical	Limited mobility	Walking routes <ul style="list-style-type: none"> • Width • Surface • Level access
	consider a family, from children till the grand parents		

Fig. 8 The main problems and associated generic measures

3. Only special facilities for people with impairments if necessary (often not needed if design is ‘smart’)
4. Count with longer waiting times and slower speeds

These basic rules can be seen as a framework for the different requirements a design has to comply with. Those four rules of thumb deal with the actual design of public spaces. Also other facilities like ticketing machines or waiting facilities have to be designed in such a way that they are usable for all, taking the different (potential) users into account. Sometimes it is not possible to make a route or area accessible for all user groups. In those cases, clear communication is very important. Users like to know what they can expect and how they can use a space. On the other hand, their opinion is also very valuable as feedback to gain new knowledge for further designs or improvements of current situations.

References

1. Arfken, C. L., H. W. Lach, et al. (1994). “The prevalence and correlates of fear of falling in elderly persons living in the community.” *American Journal of Public Health* **84**(4): 565–570.
2. Backer-Grøndahl, A., A. H. Amundsen, et al. (2007). *Trygt eller truende? Opplevelse av risiko på reisen. 913/2007* Oslo, Transportøkonomisk institutt (TØI).
3. Backer-Grøndahl, A., A. Fyhri, et al. (2009). “Accidents and unpleasant incidents: Worry in transport and prediction of travel behaviour.” *Risk Analysis* **29**: 1217–1226.
4. Bernhoft, I. M. and G. Carstensen (2008). “Preferences and behaviour of pedestrians and cyclists by age and gender.” *Transportation Research Part F* **11**(2008): 83–95.
5. Bertera, E. M. (2008). “Fear of falling and activity avoidance in a national sample of older adults in the United States.” *Health and Social Work* **33**(1).

6. Borst, H. C., H. M. E. Miedema, et al. (2008). "Relationships Between Street Characteristics and Perceived Attractiveness for Walking" *Journal of Environmental Psychology* **28**(4): 353–361.
7. Bourgeois, M. (2002). *Vervoersarmoede in Vlaanderen*. Brussel, Belgium, Koning Boudewijnsstichting
8. Bruce, D. G., A. Devine, et al. (2002). "Recreational physical activity levels in healthy older women: the importance of fear of falling. ." *Journal of the American Geriatrics Society* **50** (1): 84–89.
9. Coleman, R. and D. J. Pullinger (1993). "Designing for our future selves." *Applied Ergonomics* **24**(1): 3–4.
10. CROW (2002). *Toegankelijkheid van de openbare ruimte*. Ede, CROW.
11. de Jong, M., C. Kaufman, et al. (2010). What does walking mean for groups with special needs? - Tasks and how they are perceived. *Pedestrians' Quality Needs. Final Report of the COST project 358*. Methorst R., Monerde i Bort H., Risser R. et al. Cheltenham, Walk21: 22.
12. de Jong, M. and W. Sweers (2010). *Self Assessment Tool - Manual. Deliverable 4.2*. Mediate – Methodology for Describing the Accessibility of Transport in Europe.
13. European Commission (2011). *WHITE PAPER Roadmap to a Single European Transport Area – Towards a competitive and resource efficient transport system*.
14. Facebook page: Olifantenpaadjes (2012).
15. Froyen, H., C. Asaert, et al. (2006). *Ontwerpen voor Iedereen. Integraal en Inclusief*.
16. Fyhri, A., T. Hof, et al. (2010). The Influence of Perceived Safety and Security on Walking. *Pedestrians' Quality Needs. Final Report of the COST project 358*. Methorst R., Monerde i Bort H., Risser R. et al. Cheltenham, Walk21: 22.
17. Glasl, P., W. Rauh, et al. (1993). *Vorrang für Fußgänger*. Wien: VCÖ Verkehrsclub Österreich.
18. Goldsmith, S. (1997). *Designing for Disabled: The New Paradigm*. Oxford, Architectural Press.
19. Greene, E. (2003). *Urban safety in residential areas: spatial variables in crime and feeling of (in)security*. Paper presented at the World Bank Urban Research Symposium 2003, Washington D.C., U.S.A.
20. KMBS (2012). "Koninklijke Maatschappij voor Blinden en Slechtienden vzw." Retrieved 2012, from <http://www.kmbstvzw.be/>.
21. Kraushar, M. F., V. J. DeSantis, et al. "Enabling Blind and Visually Impaired Patients to Achieve Maximal Personal and Occupational Goals: The Importance of Nonvisual Skills." *American Journal of Ophthalmology* **149**(5): 695–696.e692.
22. Liv Øvstedal, Tone Øderud, et al. (2010). *Indicators describing the accessibility of urban public transport. Deliverable 2.2*. Mediate – Methodology for Describing the Accessibility of Transport in Europe.
23. Mercado, R., A. Páez, et al. (2010). "Transport policy and the provision of mobility options in an aging society: a case study of Ontario, Canada. ." *Journal of Transport Geography* **18**: 649–661.
24. Øvstedal, L. and E. Olaussen Ryeng (2002). Who is the most pleased pedestrian? *Walk 21*. San Sebastian, Spain.
25. PROMISING (2011). *Measures for pedestrian safety and mobility problems. Final report of Workpackage 1 of the European research project PROMISING (Promotion of Measures for Vulnerable Road Users), Deliverable D1*. National Technical University of Athens NTUA, Athens.
26. Sánchez, J. and M. Sáenz (2010). "Metro navigation for the blind." *Computers & Education* **In Press, Corrected Proof**.
27. Schlansky, A., R. Hasenstab, et al. (2006). *Gehen bewegt die Stadt: Nutzen des Fußverkehrs für die urbane Entwicklung, (Broschüre)*. Berlin: FUSS e.V. Fachverband Fußverkehr Deutschland.
28. Sharmeen, F., T. Arentze, et al. (2010). Modelling the dynamics between social networks and activity-travel behavior: Literature review and research agenda. *12th WTCR*. Lisbon.

29. SIZE (2005). "SIZE - Life quality of senior citizens in relation to mobility conditions. 5th Framework programme." from www.factum.at/size-project.
30. Stafford, J. and G. Pettersson (2004). *People's perceptions of personal security and their concerns about crime on public transport: research findings*. Department for Transport, UK.
31. UN (2012). "UN Convention on the Rights of Persons with Disabilities." Retrieved June, 2012, from <http://www.un.org/disabilities/convention/conventionfull.shtml>.
32. Van den Wyngaert, H. (2010). Toegankelijkheid visueel gehandicapten in de stad. *Traffic and Transportation sciences*. Hasselt, Hasselt University.
33. van der Burg, J.-D. and M. 't Hart (2012). *Olifantenpaadjes. Desire lines*.
34. WHO (2001). *International Classification of Functioning, Disability and Health: ICF*, World Health Organization. Geneva.
35. WHO (2004). *World report on road traffic injury prevention*. Geneva, World Health Organization.
36. WHO (2009). "Factsheet nr 282. Visual impairments and blindness." 2010, from www.who.int/mediacentre/factsheets/fs282/en/index.html.
37. Wunsch, D., G. Haindl, et al. (2007). *Gehen in der Donaustadt. Was das Gehen attraktiv macht und was es erschwert: Kommunikation mit Bürgerinnen und Bürgern in ausgewählten Gebieten des XXII. Wiener Gemeindebezirks*. Im Auftrag der MA 18 Stadtentwicklung und Stadtplanung, Wien.
38. Ziegler, F. and T. Schwanen (2011). "'I like to go out to be energised by different people': an exploratory analysis of mobility and wellbeing in later life. ." *Ageing & Society* **31**: 758–781.

Part II

Experiment and Evacuation

An Evacuation Validation Data Set for Large Passenger Ships

Edwin Richard Galea, Steven Deere, Robert Brown, and Lazaros Filippidis

Abstract An evacuation model data set collected as part of the EU FP7 project SAFEGUARD is presented. The data was collected from a RO-PAX ferry operated by ColorLine AS called SuperSpeed 1 during a semi-unannounced assembly at sea involving 1,349 passengers. The trial took place at an unspecified time however, passengers were aware that on their voyage an assembly exercise would take place. The validation data set consists of passenger; response times, starting locations, routes taken and arrival times in the assembly stations. The validation data was collected using a novel data acquisition system consisting of ship-mounted beacons, each emitting unique Infra-Red (IR) signals and data logging tags worn by each passenger. The results from blind simulations using maritimeEXODUS for this assembly exercise are presented and compared with the measured data. Three objective measures are proposed to assess the goodness of fit between the predicted model data and the measured data.

Keywords Experiment • Ship evacuation • Ship evacuation model • Validation

E.R. Galea (✉) • S. Deere • L. Filippidis

Fire Safety Engineering Group, University of Greenwich, London, UK

e-mail: e.r.galea@gre.ac.uk; s.deere@gre.ac.uk; l.filippidis@gre.ac.uk

R. Brown

Fire Safety Engineering Group, University of Greenwich, London, UK

Offshore Safety & Survival Centre, Fisheries and Marine Institute, Memorial University,
St. John's, Canada

e-mail: robert.brown@mi.mun.ca; r.c.brown@gre.ac.uk

1 Introduction

In 2002 the International Maritime Organisation (IMO) introduced guidelines for undertaking full-scale evacuation analysis of large passenger ships using ship evacuation models [1]. These guidelines, known as IMO MSC Circular 1033, were to be used to certify that the passenger ship design was appropriate for full-scale evacuation. As part of these guidelines it was identified that appropriate full-scale ship based evacuation validation data was not available to assess the suitability of ship evacuation models. As suitable validation data was not available, a series of test cases were developed which verified the capability of proposed ship evacuation software tools in undertaking simple simulations. However, these verification cases were not based on experimental data. Furthermore, successfully undertaking these verification cases does not imply that the evacuation model is validated or capable of predicting real evacuation performance. In 2007 IMO MSC Circular 1238 (MSC1238) [2], a modified set of protocols for passenger ship evacuation analysis and certification were released however, the issue of validation of passenger ship evacuation models was not addressed. The IMO Fire Protection (FP) Sub-Committee in their modification of MSC Circ. 1033 at the FP51 meeting in February 2007 [3] invited member governments to provide, “. . . further information on additional scenarios for evacuation analysis and full scale data to be used for validation and calibration purposes of the draft revised interim guideline.” The EU framework seven project SAFEGUARD aims to address this requirement by providing full-scale data for calibration and validation of ship based evacuation models.

As part of project SAFEGUARD, a series of five semi-unannounced full-scale assemblies were conducted at sea on three different types of passenger vessel. From these trials five passenger response time data sets were collected and two full-scale validation data sets. This paper will concentrate on the first Safeguard Validation Data Set (SGVDS1) which was generated from an assembly trial conducted on a large RO-PAX ferry operated by ColorLine AS called SuperSpeed 1 [4]. The vessel can carry approximately 2,000 passengers and crew and over 700 vehicles. The route taken by the vessel is from Larvik in Norway to Hirtshals in Denmark, a trip of 3 h and 45 min. Data from a sailing from Larvik to Hirtshals in early September 2009 was collected with 1,349 passengers on board. The trial consisted of the ship's Captain sounding the alarm and crew moving the passengers into the designated assembly areas. The trial took place at an unspecified time on the crossing however, passengers were aware that on their crossing an assembly exercise would take place. The data collected during the assembly trial consisted of passenger: response time data, starting locations, arrival time at the designated assembly stations and the paths taken. Some 30 digital video cameras were used to collect the response time data. The other validation data was collected using a novel data acquisition system consisting of ship-mounted beacons, each emitting unique Infra-Red (IR) signals and IR data logging tags worn by each passenger [4].

The generated ship validation data set is unique for a number of reasons. Unlike most evacuation model validation data sets, the SGVDS1 incorporates regional information relating to the starting locations of the population in addition to the actual response time distribution for the population. Most evacuation validation data sets lack these essential details allowing modellers the opportunity to tune their predictions in order to obtain the best fit to the experimental results. Furthermore, the trials were conducted on a real ship, at sea and were semi-unannounced making the results relevant, credible and realistic. In addition, as the start and end location for the population is known, it is also possible to utilise the data set to evaluate the capabilities of evacuation model route planning and wayfinding algorithms. In this paper we will present the SGVDS1, the blind results from the maritimeEXODUS modelling and an assessment of the level of agreement between model predictions and trial data.

2 The Ship Geometry

The ship contains a mixture of spaces spread over three decks (deck 7–9) including; business and traveller class seating areas (airline style seating), large retail and restaurant/cafeteria areas, bar areas, indoor and outdoor general seating areas and general circulation spaces (see Fig. 1). The cabins located on deck 9 are intended for lorry drivers only and not for regular passengers. Thus only the airline seating portion of deck 9 is available to regular passengers. Also, the hatched region shown on deck 8 represents crew only areas. A CAD DXF file is provided to define the layout of the ship within the evacuation model. The ship has four Assembly Stations (AS), three located on Deck 7 (AS A, B and C) and one located on Deck 8 (AS D). AS B and C are located on the outer decks while AS A and D are internal. AS A is located within the ship's reception/lobby area and AS D is located within the ship's self service restaurant (see Fig. 1). The outer AS B and C have two exits/entrances. Internal AS A, located in the ship's lobby area, can be accessed by three routes including stair 3 while internal AS D, located in the ship's self service restaurant can be accessed by two routes.

The vessel has four main vertical zones and four sets of primary passenger stairs. The aft most stair (stair 1) is located in the bar on deck 7 and extends up to the bar on deck 8 and is 1.0 m wide. The next stair (stair 2) is located just outside the bar on deck 7 and extends to deck 9. From deck 7 to deck 9 the stair consists of two lanes separated by a banister with landings located between deck 7 and deck 8 and deck 8 and deck 9. The width of each stair lane is 1.35 m. The next stair (stair 3) is located between the reception area and the 1st Street general seating area and also extends between decks 7 and 9. From deck 7 to deck 8 the stair consists of two lanes separated by a banister with a landing located between deck 7 and deck 8. From deck 8 to deck 9, there is only a single stair lane with a landing located between deck 8 and deck 9. As with stair 2, the width of each stair lane is 1.35 m. The final stair (stair 4) is located outside the duty free shop/buffet restaurant in the

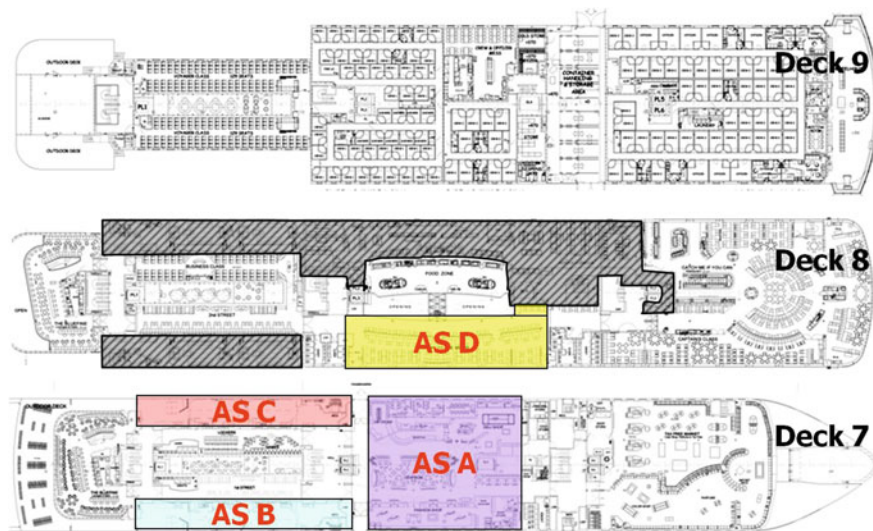


Fig. 1 Layout of Superspeed 1 showing assembly stations

forward part of the ship and extends between deck 7 and deck 8. The stair consists of two lanes separated by a banister with a landing located between deck 7 and deck 8. As with stairs 2 and 3, the width of each stair lane is 1.35 m.

3 The Initial Population Distribution

The initial distribution of the population was determined through the use of an Infra-Red (IR) tracking system. The system is based on the TagMobile system developed by the RFID Centre Ltd. The RFID Centre worked with FSEG to modify this system to make it more appropriate for use in evacuation applications [4]. The system deployed on the ColorLine vessel consists of 30 IR beacons strategically located throughout the vessel, and IR data logging tags worn by each passenger (see Fig. 2a). Each beacon generates a unique IR light field. As a tagged individual passes through the IR field, IR light sensors in the tag detect the IR light and log its ID and the time at which it was detected in the tag's internal memory. Following the test, all the tags must be retrieved in order to determine the occupant's route data. The IR beacons are strategically placed at the main locations where passengers congregate; key junctions such as the entrances to stairs, and at the entrances to each of the AS (see Fig. 2b). In this way the initial location of each tagged passenger can be determined, their route to an AS, which AS they go to and at what time they enter the AS.

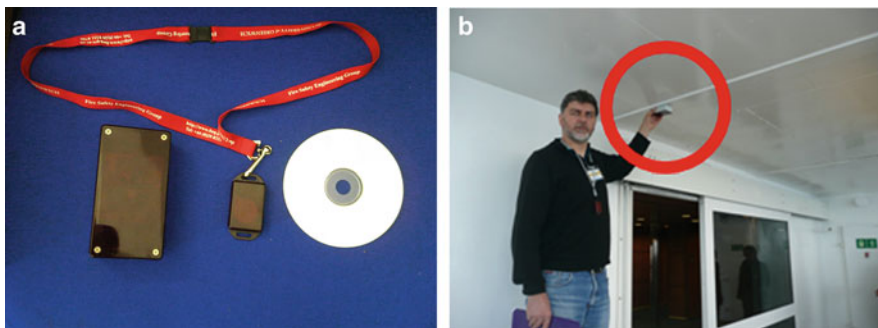


Fig. 2 IR beacon and tag (a) and installing IR beacon at the entrance to an external AS (b)

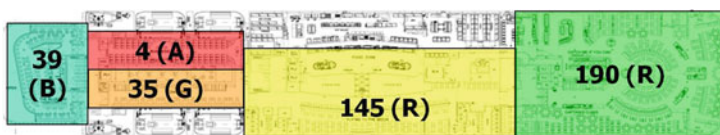


Fig. 3 Initial distribution of tagged passengers on deck 8

Using the IR tag information, the initial location of each tagged passenger was determined using data related to the first IR field that the tagged passengers passed through. Using this information the initial location of each tagged passenger can be confined to a region of space defined by the IR beacons.

The starting location of 764 tagged passengers was determined using this approach. The starting locations of 413 tagged passengers located on deck 8 are shown in Fig. 3. The initial starting location regions are defined by the coloured rectangles in Fig. 3 with the number of people initially located in the region indicated. For example, 39 tagged passengers were initially in the aft bar on deck 8, while 4 tagged passengers were located in the airline seating area on deck 8 (see Fig. 3). The lettering in Fig. 3 indicates the type of space occupied, with B standing for Bar, R standing for Restaurant, A standing for Airline seating and G standing for General seating.

4 The Trial Results

4.1 Final Locations of Tagged Passengers at the End of the Assembly Trial

Of the 1,349 passengers on board the SuperSpeed 1, 780 wore tags and so were tracked throughout the trial. In addition to identifying the starting location of the tagged passengers, the IR tracking system enabled the determination of the route

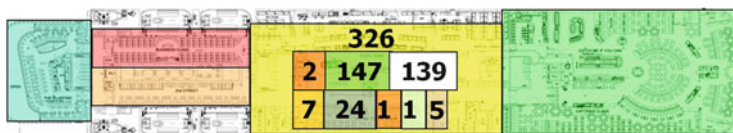


Fig. 4 Location of 326 tagged passengers on deck 8 at the end of the assembly trial

taken by each tagged passenger and which AS the passenger ended up in. Presented in Fig. 4 are the locations of the tagged passengers on completion of the assembly trial on deck 8. As deck 8 only has one AS, AS D, Fig. 4 indicates that 326 tagged passengers ended up in this AS. Furthermore, the colour coding around each number provides a breakdown of the number of tagged passengers who arrived at AS D from the various starting locations (indicated by the different colours). For example; 147 tagged passengers (green background) entered AS D from the neighbouring forward restaurant on deck 8 (also coloured green), 7 tagged passengers (orange background) from the neighbouring general seating area to the aft of AS D (also coloured orange) entered AS D while 139 tagged passengers who were already located in the AS (white background) at the sounding of the alarm remained in AS D.

4.2 Passenger Response Time Distribution

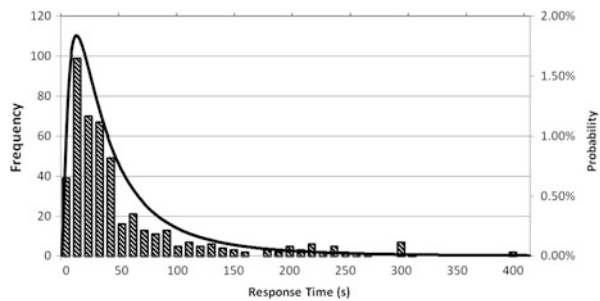
The passenger response time distribution was determined from data collected from the 30 digital video cameras located throughout the vessel [4]. Shown in Fig. 5 is a video camera used to record response phase behaviours of passengers located in the airline seating area on deck 8. In total the response times for 470 passengers was determined. The response times were determined on a regional basis and associated with the type of space that was occupied. Thus a response time distribution was determined for passengers located in the airline seating areas, bars, restaurants, shops and general seating areas (see Fig. 3). In addition, an overall response time distribution was also determined making a total of six response time distributions. Each response time data set was fitted with a log normal curve, producing for each response time distribution; the minimum and maximum observed response times, the natural log of the mean response time and the natural log of the standard deviation.

Using this information the log normal response time distribution for each region and the overall response time distribution can be constructed (see Fig. 6). For example, for the overall response time distribution, the minimum and maximum response times are 0 and 402.4 s, while the log of the mean response time is 3.578 s while the log of the standard deviation is 0.975 s.

Fig. 5 Video camera positioned to collect passenger response time data



Fig. 6 Overall log normal response time distribution for the Superspeed 1 assembly trial



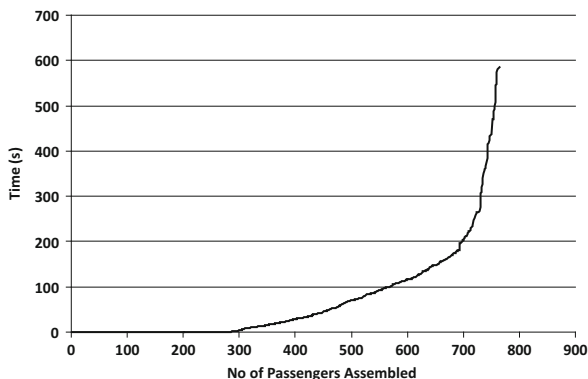
4.3 Assembly Times

The Captain officially ended the assembly exercise 10 min after its start. The IR tracking system recorded the time that each tagged passenger entered an AS providing a good indication of the overall assembly time. The IR data suggests that the last tagged passenger arrived in AS A after 585 s (9 min 45 s). In addition, the IR tracking system enables the generation of the arrival curve for each AS and hence the overall arrival curve (see Fig. 7). As such the SGVDS1 provides a means of not only determining how well an evacuation model can predict the overall assembly time, but more importantly, how well the evacuation model can predict the overall assembly process and hence the overall assembly time.

In principle this data set is ideal for validation purposes, as the starting locations and response times of each participant is known. This means that it should be possible to remove most of the uncertainty associated with input parameters associated with response time and starting location. However, there are several complications associated with the validation data set.

First, of the 1,349 passengers on board, 780 wore the IR tags and participated in the assembly trial. Of these 16 appeared in the AS after the trial ended and so are not included in the analysis, making a total of 764 tagged passengers included in the assembly exercise. The majority of the 569 passengers who did not take the tags indicated that they did not want to participate in the assembly exercise – which was not compulsory for ethical and legal reasons. A small number indicated that they

Fig. 7 Overall measured assembly curve for the Superspeed 1 trial



did not want to wear the tag. However, of the 569 passengers who did not take tags, a significant number did eventually decide to participate in the assembly exercise. This was determined by a combination of analysis of video footage, passenger post assembly survey responses and team members who were in the assembly stations collecting the IR tags from the participants. By participating in the trial, the presence of the untagged individuals in the evacuation routes will have had an impact on the overall evacuation, especially in the highly congested areas. However, their assembly times will not have been recorded in the overall assembly data.

Secondly, the exact starting location of the tagged participants was not known, but the region where they were located was known. Spatial regions were between 24 and 48 m long; thus not knowing the precise starting location of an individual may increase/decrease their arrival time by 25–50 s. Thirdly, the response time is not associated with a unique individual but to a region. Thus the precise response time of each unique individual is not known, but the response time distribution associated with a starting region is known. All of these factors must be taken into consideration when determining how well the evacuation model predicts the assembly exercise.

5 Modelling Procedure

The results presented in this paper are generated from blind simulations using the maritimeEXODUS V4.1 software [5, 6]. The bulk of the parameters used in the simulation are compliant with those specified in MSC1238 [2] with the exception of the response time distribution and the initial location of the passengers. These are determined from the trial data. For the simulations presented here, the regional response time data is used (see Sect. 4.2) and the initial starting locations of the passengers as defined in Sect. 3 are used. Furthermore, given the starting zone that an agent is assigned to, the AS that they should use is known. This information is also imposed on the simulations presented here. Thus, the validation simulations presented here do not examine the route finding or wayfinding capabilities of the

model. The agent will go to the correct AS as defined by the trial. However, the route taken by the agent to the assigned AS is not prescribed.

As already noted, of the 569 passengers that did not wear IR tags, an unknown number actually participated in the trial and so had an effect on the movement of those passengers wearing the IR tags during the assembly exercise. It is not known how many of the 569 passengers participated in the trial but we cannot ignore the fact that a large number of passengers, who were not wearing IR tags participated in the assembly exercise and so had an impact on the overall assembly exercise. In an attempt to take this into account, it is assumed that 250 of these passengers, approximately half, did actually participate in the assembly exercise. These passengers are included in the evacuation simulation as moving passengers, BUT are not included in the analysis of the AS arrival curves and the total assembly times. These 250 agents are distributed throughout the vessel according to the population distribution of the known 764 passengers. As is required by MSC1238 [2] a total of 50 repeat simulations are produced, where the starting locations of the passengers within the various starting regions are randomised and the 95th percentile case is selected to represent the prediction of the assembly process. The regulations assume that evacuation models will under-predict the likely total assembly time by 25 % and so requires that an additional 25 % is added to the predicted total assembly time.

6 Comparing Model Predictions with Trial Results

The numerical predictions for the assembly process are presented in Fig. 8 along with the experimental data. Presented are the measured and predicted arrival curves for each AS (Fig. 8a–d) and the overall arrival curve (Fig. 8e).

As can be seen from Fig. 8, the numerical simulations under-predict the Total Assembly Time (TAT) for each AS and the overall assembly process. The simulations under-predict the TAT for each AS by; 18 %, 26 %, 27 % and 26 % respectively and the overall TAT is under-predicted by 18 % (see Table 1). Thus the error in predicting the overall TAT is 18 % while the error in predicting the TAT for each assembly station varies from 18 % to 27 %. However, as can be seen from Fig. 8, the number of passengers in the tail of the distributions, producing the under-predictions in the TATs, is very small and is possibly caused by a few strugglers exhibiting behaviours not represented within evacuation models, for example stopping on the way to the AS to talk or make some observation. Furthermore as described earlier, there are several other uncertainties introduced into the experimental data which may contribute to these differences. The uncertainty in the exact starting location of the passengers can introduce an error of 25–50 s in the prediction of the assembly times. This uncertainty alone introduces a possible error of some 9 % in the overall TAT and an error of some 11 % in the prediction of the TAT for the individual AS. In addition, in analysis of the performance of the IR system, it was noted that the IR measured assembly times can lag the actual assembly times by up to 5 s. This would

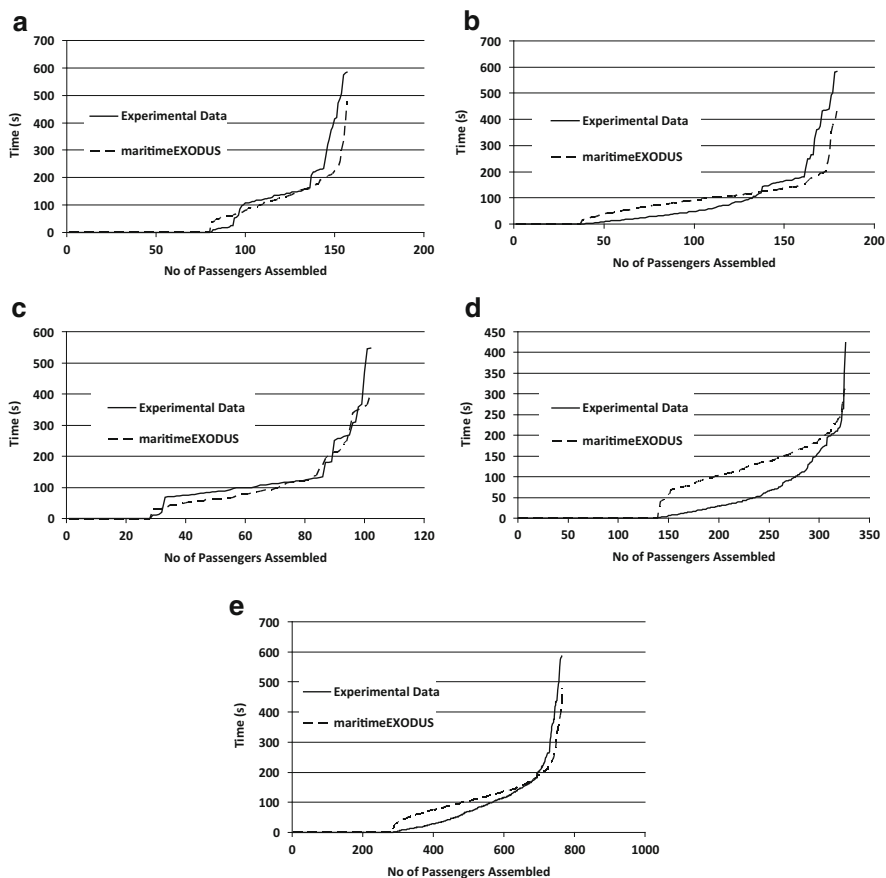


Fig. 8 Comparison of model predictions with experimental data. (a) Assembly station A. (b) Assembly station B. (c) Assembly station C. (d) Assembly station D. (e) Overall assembly

introduce a 1 % error in the estimation of the measured assembly times. Finally, the error associated with the assembly of the non-tagged passengers is difficult to estimate. While the analysis has attempted to take this into account by introducing half the untagged passengers into the simulation, it is not clear if this is sufficient as the starting location and AS used by the non-tagged passengers is not known. Taking this uncertainty into consideration, the errors in the predicted assembly times appear reasonable.

In addition, it is also noted that the numerical simulations correctly identifies that the last AS to assemble is AS A. This is an important result as MSC1238 requires that the simulations identify which vertical fire zone is the last to assemble – which is driven by the last AS to assemble – and makes use of this information to formulate additional scenarios to be investigated. It is thus desirable that the evacuation model can correctly identify which AS has the longest TAT.

Table 1 Metric values for maritimeEXODUS prediction of SGVDS1

s/n	SC					n	ERD	EPC	% diff TAT
	0.01	0.03	0.05	0.07	0.09				
Overall	0.8	0.9	0.9	1.0	1.0	480	0.3	1.1	18
AS A	0.4	0.7	0.7	0.7	0.8	77	0.4	1.4	18
AS B	0.6	0.7	0.7	0.8	0.9	142	0.4	1.2	26
AS C	0.3	0.4	0.6	0.7	0.9	74	0.2	1.1	27
AS D	0.7	0.8	0.8	0.9	0.9	187	0.6	0.7	26

Furthermore, simply predicting the time for the overall assembly within an acceptable tolerance is not sufficient to determine whether or not the simulations provide an accurate representation of the assembly process. It may be possible for a reasonable prediction of the overall assembly time to be generated while the evacuation dynamics is misrepresented by the evacuation simulation. To determine if the evacuation simulation is a good representation of the evacuation dynamics it is necessary to look at how well the predicted arrival curves match the measured arrival curves. By sight, the predicted and measured assembly curves for the overall assembly appear to be in good agreement (see Fig. 8e). With the exception for AS D (see Fig. 8d), the predicted arrival curves for each of the AS (Fig. 8a–d) also appear to be in good agreement with the measured curves. This suggests that the evacuation model is doing a reasonable job of predicting the overall assembly process. However, it is desirable to have objective measures of the level of agreement between predicted and measured performance rather than subjective assessments. This is particularly important if the validation analysis is to be used by regulatory authorities to determine the suitability of the evacuation modelling tool. Thus it is necessary to quantify the level of agreement between predicted and measured performance.

In [7] several metrics are presented which can be used to quantify the level of agreement between predicted and measured values. However, the mathematical formulations presented in [7] have a number of typographical errors [8] and are here presented correctly. Before presenting the formulation of the metrics it is necessary to introduce some terminology. The series of measured experimental data is represented by the n -dimensional vector $E = (E_1, E_2, \dots, E_n)$, where E_i represents the measured assembly time for the i th passenger. Similarly, the series of predicted model data is represented by the vector $m = (m_1, m_2, \dots, m_n)$, where m_i represents the predicted assembly time for the i th agent. The metric used to quantify the level of agreement between predicted and measured values consists of three measures. The first is the Euclidean Relative Difference (ERD) defined by Eq. 1. This is used to assess the distance between the experimental data (E_i) and the model data (m_i). This value should return a value of 0 if the two curves are identical in magnitude. The smaller the value for the ERD, the better the overall agreement. An ERD of 0.2 suggests that the average difference between the model and experimental data points, taken over all the data points is 20 %.

$$\frac{\|E - m\|}{\|E\|} = \frac{\sqrt{\sum_{i=1}^n (E_i - m_i)^2}}{\sqrt{\sum_{i=1}^n E_i^2}} \quad (1)$$

$$\frac{\langle E, m \rangle}{\|m\|^2} = \frac{\sum_{i=1}^n E_i m_i}{\sum_{i=1}^n m_i^2} \quad (2)$$

$$\frac{\langle E, m \rangle}{\|E\| \|m\|} = \frac{\sum_{i=s+1}^n \frac{(E_i - E_{i-s})(m_i - m_{i-s})}{s^2(t_i - t_{i-1})}}{\sqrt{\sum_{i=s+1}^n \frac{(E_i - E_{i-s})^2}{s^2(t_i - t_{i-1})} \sum_{i=s+1}^n \frac{(m_i - m_{i-s})^2}{s^2(t_i - t_{i-1})}}} \quad (3)$$

The second measure is the Euclidean Projection Coefficient (EPC) defined by Eq. 2. The EPC calculates a factor which when multiplied by each model data point (m_i) reduces the distance between the model (m) and experimental (E) vectors to its minimum. Thus the EPC provides a measure of the best possible level of agreement between the model (m) and experimental (E) curves. An EPC of 1.0 suggests that the difference between the model (m) and experimental (E) vectors are as small as possible. The third measure is the Secant Cosine (SC) defined by Eq. 3. Unlike the other two measures, it provides a measure of how well the shape of the model data curve matches that of the experimental data curve. It makes use of the first derivative of both curves. An SC of 1.0 suggests that the shape of the model (m) curve is identical to that of the experimental (E) curve.

The t in Eq. 3 is a measure of the spacing of the data. For the assembly data presented in Fig. 8, the spacing of the data is 1 i.e. there is a data point for each passenger/agent that enters an AS. Thus the difference in t consecutive values in Eq. 3 is 1. The s in Eq. 3 is a factor that represents the period of noise in the data, or variations in the experimental data resulting from microscopic behaviour not possible to reproduce in the model. Selecting a value of s which is greater than the period of the noise in the data provides a means to smooth out the effect of the noise. However, care must be taken in selecting the value of s . If s is too large the natural variation in the data may be lost, while if s is too small, the variation in the data created by noise may dominate the analysis. Selecting an appropriate value of s is dependent on the number of data points in the data set, given by n . Thus it is desirable to keep the ratio s/n as low as possible.

For data sets in which an experimental and model data point are available for each person, if the ERD = 0.0, then it would not be necessary to consider other measures

as the two data sets would be identical. In all other cases it is necessary to consider the three measures together in order to get a good indication of how well the two data sets match each other. As the model data curve can cross the experimental data curve one or multiple times (as shown in Fig. 8) EPC can return a value close to 1.0 while there is a difference between the two curves. Similarly, the SC can return a value of 1.0 even though the model and experimental data curves are off set by a constant value. In general, for the model and experimental curves to be considered a perfect match, it is necessary to have all three measures at their optimal values i.e. $ERD = 0.0$, $EPC = 1.0$ and $SC = 1.0$.

If the metric is applied to the data shown in Fig. 8 it produces the values presented in Table 1. First consider the data relating to the overall assembly curve. The values for the SC suggest that the shape of the overall assembly curve closely resembles that of the experimental data, even with s/n as low as 0.01. This is consistent with the conclusion drawn from a visual inspection of Fig. 8e. Note that an s/n of 0.01 represents 1 % of the data set and implies $s = 5$ for this data set. Thus for the 480 point data set, the gradients used in the evaluation of Eq. 3 are spread over five data points, which is considered reasonable. Furthermore, the ERD for the overall assembly is quite low (0.3) and the EPC is close to 1.0 suggesting that the overall predicted assembly curve is quite close to the measured curve, again consistent with a visual inspection of Fig. 8e. It is also noted that the overall TAT is within 18 % of the measured value.

Next consider the AS. Here we find that for an s/n of 0.05, the SC values for all the AS are close to 1.0 suggesting that the shapes of the predicted curves are in good agreement with the measured curves, again supporting the conclusions of the visual inspection. This s/n value, represents 5 % of the data set, is larger than that for the overall assembly curve, but is still considered to be small. For the smallest of the AS data sets (AS C), this represents an s value of 4, while for the largest of the AS data sets (AS D), this represents an s value of 9. With the exception of AS D, the ERD values are reasonably low, and the EPC values are reasonably close to 1.0 with the exception of that for AS A and D. These values suggest that, with the exception of AS D, the predicted values are reasonably close to the measured values, which again is consistent with a visual inspection of Fig. 8.

Based on this analysis, a set of acceptance criteria can be defined for SGVDS1 that takes into consideration the uncertainties in the experimental data and that the maritimeEXODUS predictions presented in Fig. 8 are arguably a reasonable match for the experimental data based on a visual inspection of the data. A general two step validation protocol is suggested based in part on the philosophy of MSC1238, which focuses on the overall assembly process.

In the first step of the validation protocol, the acceptance criteria are applied to the model predictions of the overall assembly. To be deemed to be acceptable, the model predictions must satisfy all elements of the acceptance criteria. If successful, the second step of the validation protocol is considered. In the second step, the acceptance criteria are applied to each of the four AS with a minimum of 10 passes out of a possible 12 being deemed to be acceptable. Furthermore, no more than one failure can occur in any one AS. The suggested acceptance criteria are as follows:

- (i) $ERD \leq 0.4$
- (ii) $0.6 \leq PC \leq 1.4$
- (iii) $SC \geq 0.6$ with $s/n \leq 0.05$
- (iv) Predicted TAT for the overall assembly to be within 30 % of the measured value. This criterion is only applied to step 1 of the acceptance process.

Applying the suggested validation protocol to the maritimeEXODUS data presented in Table 1, we note that in the first step the model predictions satisfy all four criteria and hence the second step of the validation protocol is considered. In the second step, AS D fails to meet criteria (i) but all other criteria are satisfied. As the model predictions have satisfied all four criteria in step 1 and 11 of the 12 criteria in step 2, the model is considered to have satisfied the acceptance criteria.

The validation protocol described above is being applied to two other ship evacuation models, EVI and ODEGO (by their developers), as part of the SAFE-GUARD project. Once this is completed the validation protocol will be finalised and acceptance criteria for SGVDS1 will be finalised. In addition, a second SAFEGUARD validation data set, SGVDS2, is being prepared based on a similar semi-unannounced assembly at sea for the cruise ship “Jewel of the Seas”. The assembly data associated with SGVDS2 was not subject to the level of uncertainties associated with SGVDS1. Thus, it is expected that while the validation protocol established for SGVDS1 will be applied to SGVDS2, the acceptance criteria associated with SGVDS2 will be more demanding than that for SGVDS1.

7 Conclusions

Data from a semi-unannounced assembly at sea for a Ro-Pax ferry has been collected consisting of passenger: response time data, starting locations, arrival time at the designated assembly stations and the paths taken by the passengers. The response time data was collected using some 30 digital video cameras while the other data was collected using a novel data acquisition system consisting of ship-mounted beacons, each emitting unique Infra-Red (IR) signals and IR data logging tags worn by each passenger. The collected data is used to define a unique validation data set for ship evacuation models. The data set is considered unique for a number of reasons, primarily because unlike most validation data sets, it contains information defining; occupant response times, starting locations, final arrival times and paths taken. Furthermore, the trials were conducted on a real ship, at sea and were semi-unannounced making the results relevant, credible and realistic.

A validation protocol and acceptance criteria have been proposed based on the collected data. The acceptance criteria are objective and are determined by a metric consisting of three measures, the Euclidean Relative Difference, Euclidean Projection Coefficient and Secant Cosine. Collectively the metric measures the magnitude of the distance between the predicted and experimental data and the similarity of the shapes of the predicted and experimental arrival time curves.

The proposed acceptance criteria take into consideration uncertainties associated with the measured data.

In a blind application of the validation protocol to the maritime EXODUS ship evacuation software, the software was found to satisfy the acceptance criteria, suggesting that it is capable of predicting the outcome of the assembly process for this vessel to a given level of accuracy. This work is being continued with the application of the validation protocol to two other evacuation tools, EVI and ODIGO. Furthermore, a second validation data set is currently being developed based on the evacuation of a large cruise ship.

It is proposed that the suggested validation protocol and the acceptance criteria could be used by IMO as part of a validation suite to determine acceptability of maritime evacuation models in a future enhancement to MSC1238. In this way we hope to improve the reliability of the assessment of ship evacuation capabilities based on computer simulation and hence safety at sea for all those who travel and work on passenger ships.

Acknowledgement Project SAFEGUARD (contract 218493) is funded under the European Union Framework 7 Transport initiative. The authors acknowledge the co-operation of their project partners. This paper was completed 100 years, almost to the day, after the sinking of the Titanic with the loss of over 1,500 lives and 100 days following the grounding of the Costa Concordia with the loss of 32 lives. We dedicate this paper to all those who have lost their lives at sea in the 100 years between these two tragic accidents and hope that this work will contribute to improving safety at sea.

References

1. IMO, "Interim Guidelines for Evacuation Analyses for New and Existing Passenger Ships", IMO MSC/Circ 1033, 6 June 2002.
2. "Guidelines for Evacuation Analysis for New and Existing Passenger Ships", IMO MSC/Circ 1238, 30 Oct 2007.
3. IMO Fire Protection Sub-Committee, 51st session, Work Package 3, FP 51/WP.3, 8 Feb 2007.
4. Galea, E.R., Brown, R.C., Filippidis, L., and Deere, S.: Collection of Evacuation Data for Large Passenger Vessels at Sea, Pedestrian and Evacuation Dynamics 2010. 5th International Conference. Proceedings. March 8–10, 2010, Springer, New York, NY, Peacock, R.D., Kuligowski, E.D., and Averill, J.D., Editor(s), 163–172, (2011).
5. Deere, S., Galea, E.R., Lawrence, P., Filippidis, L. and Gwynne, S.: The impact of the passenger response time distribution on ship evacuation performance, *International J of Maritime Eng*, Vol 148, Part A1, 35–44, (2006).
6. Galea, E.R., Deere, S., Sharp, G., Filippidis, L., Lawrence, P., and Gwynne, S.: Recommendations on the nature of the passenger response time distribution to be used in the MSC 1033 assembly time analysis based on data derived from sea trials." *International J of Maritime Eng*, Vol 149, Part A1, 15–29, (2007).
7. Peacock, R.D., Reneke, P.A., Davis, W.D., Jones, W.W.: Quantifying Fire Model Evaluation Using Functional Analysis, *Fire Safety Journal*, 22, 167–184, (1999).
8. Peacock, R.D.: Private Communication with E.R.Galea, 23 November 2011.

An Information Processing Based Model of Pre-evacuation Behavior for Agent Based Egress Simulation

Vaisagh Viswanathan and Michael Lees

Abstract During a fire evacuation, evacuees do not start evacuating immediately on hearing a fire alarm. This delay in reaction is often the cause of unnecessary deaths. However, it is hardly ever considered in computational models of egress. In this paper, an agent based computational model for pre-evacuation behavior is proposed and implemented by modeling cue perception and communication. Through experiments, the significant impact that pre-evacuation behavior modeling can have is also demonstrated.

Keywords Agent-based simulation • Evacuation • Pre-evacuation • Behavior • Model • Communication • Cue perception

1 Introduction

Ideally, when a fire starts a fire alarm goes off; all occupants hear this alarm and use the nearest safe exit to leave the building. However, this is hardly the norm. In many cases, occupants are desensitized from hearing false alarms and often do not start to evacuate until they are completely sure that it is needed. On January 19, 2000, a fire in Boland Hall in Seton Hall University killed three students because they had ignored the fire alarms assuming they were false [1]. This uncertainty about the authenticity of the first sign of danger isn't an isolated incident [9, 11, 13]. Hence, when studying the behavior of evacuees, it is necessary to study and understand their actions from the time at which the fire started right up until the point where the last person evacuated [13]. Modeling and simulation is one approach for analyzing and understanding egress behavior.

V. Viswanathan (✉) • M. Lees
School of Computer Engineering, Nanyang Technological University, Singapore
e-mail: vaisagh1@e.ntu.edu.sg; mhlees@ntu.edu.sg

Software that simulates crowd egress is necessarily very complex because crowd egress from a building is itself a very complex system with lots of interacting elements (people, fire, alarms, etc.) each of which can cause different complications in the system. One of the most popular methods for studying and modeling complex systems is through Agent Based Models (ABM). In ABM, a set of heterogeneous, intelligent entities called agents are programmed with behavior approximating humans and placed in a partially observable environment. Asynchronous interactions between agents result in macro-level dynamics which can help observers learn more about the system.

Pre-evacuation uncertainty and investigation are features of human behavior during egress that are rarely considered in models. Pre-evacuation refers to the period of time that elapses after the start of the fire alarm before the person starts evacuating. While some models [15] do have a simplified model of pre-evacuation behavior, they fail to model it in enough detail to enable their extension to more general cases. For example, a fire alarm could have different effects based on the clarity and believability of the alarm [3, 7]. This variability is hard to model in existing models of pre-evacuation behavior. Also, during an evacuation people exchange event and environment related information with other evacuees. Evacuees are unlikely to follow blindly any and all messages that they receive. There is a variability in the *trust* in messages received that can have different effects on egress. This is rarely considered in existing models.

In this paper, we present one aspect of a behavioral model for Agent Based Modeling of crowd egress which we call the IBEVAC (Information Based Evacuation) model. This behavioral model models evacuees as information processing entities. More specifically, in this paper we introduce the information-based event identification and communication system that is used in IBEVAC. The evacuees identify and process information in terms of event cues which exist throughout the environment. The importance of modeling pre-evacuation behavior and a communication system is illustrated through experimentation.

2 Related Work

A fire evacuation is a complex situation to model and simulate. One large component of this complexity is the need to understand the behavior and decision making of the people taking part in it. There are a lot of conflicting theories on how humans behave in emergencies and why they behave as they do. However, there are also certain parts of human nature that are generally accepted to be true, such as the constant search for information [6, 9, 12, 13]. This section first summarizes the existing knowledge of human behavior during egress with special emphasis on pre-evacuation behavior. Following this, some existing models of pre-evacuation behavior and communication is presented.

2.1 *Pre-evacuation Behavior*

Several studies of human behavior during emergency egress [4, 6, 10], have shown that an evacuee's first reaction after realizing that there is an unusual situation is to investigate and gather more information about the situation. Evacuation starts only once the need for evacuation is established. *Cues* are the key to understanding this transition from realization to investigation and, eventually, to evacuation. Cues are certain changes in the environment that indicate that something is wrong or different from normal [12]. They come in a variety of different forms. Fire and smoke are the typical and most unambiguous cues for an evacuation. Fire alarms and people running about are examples of more ambiguous cues. According to Proulx [10], an ambiguous cue by itself does not cause a person to initiate investigation. Rather, the cue has to persist for a period of time before investigation begins.

There have been several surveys, interviews and other studies of the factors that influence evacuation and pre-evacuation behavior. Kuligowski [5] summarized the key findings of these studies and compiled a list of factors that influence pre-evacuation behavior. She suggested that the period that we term as pre-evacuation itself consists of two phases. Phase 1 is called *perception*. This refers to the perception of some unusualness in the current situation. Kuligowski calls the next phase *interpretation*. During this phase, the person searches for more information to verify whether a fire has actually started and if it actually poses a threat that needs to be handled. Several others [6, 10, 13] have also emphasised the importance of this phase though sometimes under different names. Regardless of what it is called, this phase consists of two parts (1) defining the situation as a fire and (2) defining the risk that the situation poses.

Kuligowski categorized the factors that influence these phases into two types: occupant based factors and cue based factors. Occupant based factors are intrinsic characteristics of the evacuee like age, experience, gender, etc. One of the factors that encourage the programmatic implementation of cue based factors is the fact that the effect of a cue can be explained to be caused by the nature and characteristics of the cue rather than the specific cue. In other words, each cue can be described in terms of its ambiguity, consistency with other cues and its source and it is this description that determines the effect of the cue.

2.2 *Existing Models*

As mentioned in Sect. 1, there are very few existing models that take the pre-evacuation period into consideration. Pires [8] modeled the pre-evacuation decision making of an individual using a simple Bayesian Belief Network (BBN). França et al. [2] created a simulation model of the development of panic behavior during emergency egress. This model implemented the hysterical belief theory [14] and modeled how panic first develops and then evacuation happens. It also had a basic

communication system through which agents exchanged mood information (which is a key factor in the development of panic) by using the grid based environment as a medium for communicating messages. Despite pre-evacuation behavior being modeled in some detail, it is not possible to extend this model to replicate the heterogeneity in people's reaction to cues. ESCAPES [15] is a fairly recent model that takes into account some factors like the spread of knowledge, fear and emotion between the different evacuees. These factors are used to create a simplistic model of pre-evacuation behavior. The event identification and communication model proposed in this paper have been influenced by these models but is unique in the way that the diversity of cues and their effects can be considered.

3 The IBEVAC Model

This section gives an overview of the modular IBEVAC agent architecture. Figure 1 shows this architecture. There are many objects or actions that an agent can sense or observe in the environment. We call these *raw percepts*. According to their sources, they can be classified as *observations* from the environment and *messages* from other agents. The Information Based Perception (IBP) Module is the only gateway through which the agent receives information from the environment. This module is explained in more detail in [16]. The IBP Module passes a percept to the Knowledge Base.

The *Environment Knowledge Module* stores a representation of the layout of the environment that is formed as a result of the observations of the agent. Information regarding accessibility of links is also stored. As a detailed discussion of this module is beyond the scope of this paper, all agents are assumed to have complete knowledge of the layout. However, agents can learn about inaccessible links only through direct observation or through messages from other agents. The *Event Knowledge Module* is the focus of research in this paper. It stores the agent's beliefs about the current state of the environment. Cue perception alters these beliefs and triggers a state change in the agent which is then handled by the Planning Module. This Module is explained in more detail in Sect. 4.

The intrinsic characteristics of the agent like the agent's size, speed, mass and social role are stored in the *Agent Description Module (ADM)*. It is also responsible for determining the strategies and actions taken by the Planning Module and in determining the effects of the cues on the Event Knowledge Module (Sect. 4). The *Planning Module* stores the current state of the agent i.e. whether it is exploring, milling or escaping and creates a plan of action for the agent as a set of goals. Each goal is a location that is passed to the Navigation Module. For the purpose of this paper, three kinds of behavior are modeled: normal behavior where the goal is the center of the *home* room of the agent, for milling behavior the agent gathers with other agents at the nearest *corridor* (See Fig. 2) and during escape the agent heads towards the nearest exit.

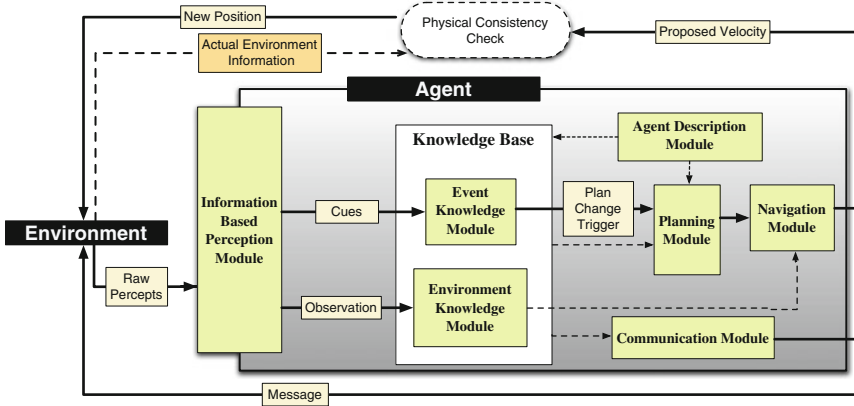


Fig. 1 An illustrated representation of the IBEVAC agent architecture

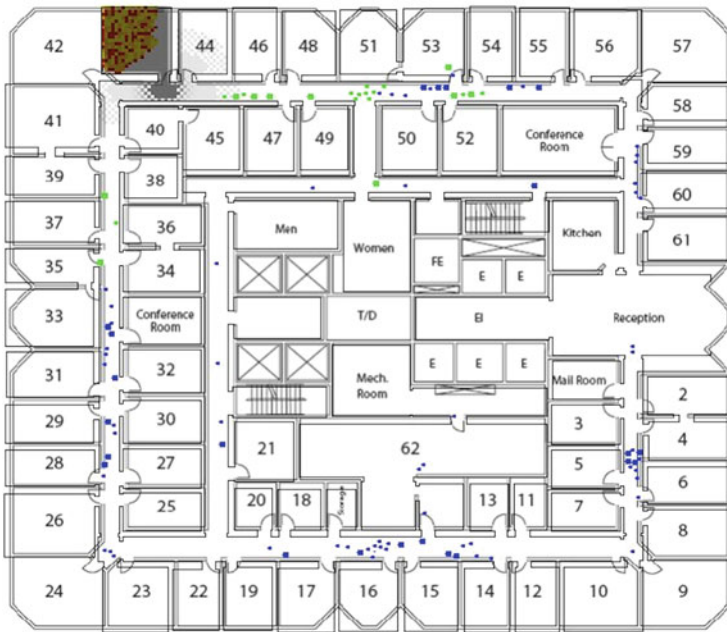


Fig. 2 First of two floors from World Trade Center, California. Fire is started in the corner room and generates smoke. Fire kills agents. Smoke depending on concentrations slow or kill agents. The longer rectangles are corridors connecting rooms and the open area on the right center is the exit

Communication between agents is facilitated by the *Communication Module*. It transmits messages to agents within a communication range. The working of this communication is explained in more detail in Sect. 4. The *Navigation Module* uses a four level navigation system. At the highest level, a logical path is determined

in terms of rooms to be crossed from the agents current location to the goal. From this logical path, spatial way points or locations are extracted by the next level. The third level determines a possible collision free path to the farthest visible spatial way point. Finally, a physics engine ensures that objects don't pass through other objects.

4 Event Identification and Pre-evacuation Behavior

It is known that the ambiguity, source and consistency of the cue [4, 12, 13] are the key factors (Sect. 2.1) in determining the effect of a cue. In the IBEVAC model, this is used in modeling all cues in the same way. Each object or event that is to be perceived as a cue implements a *Cue interface* which ensures that each cue can be explained in terms of its ambiguity, source and consistency. This is one of the key novelties of IBEVAC's approach to behavior modeling. Each cue is located at a particular location in the environment and is sensed by agents when within their perception range.

Once perceived, these cues are passed to the Event Knowledge Module. The module has a *bucket* of information corresponding to *uncertainty* and another corresponding to *fire*. When a cue is perceived, appropriate amount of information is added to the appropriate bucket(s) based on the ambiguity level. A less ambiguous cue contributes more information. For each bucket, a *threshold* is initially fixed by the ADM. When the amount of information in a bucket overflows the threshold, a trigger is sent to the Planning Module to change the agent's state and strategy.

Communication is implemented as *messages* sent from one agent to the other. Each message has a message cue and environment information. The message cue works just as other cues. Here the term ambiguity is used to refer to the trustworthiness of the source of the information. In this paper, the environment information that is passed is only about the inaccessible paths in the map. During an IBEVAC simulation, a cellular automata based fire model and a simple finite difference smoke model are executed. This creates fire and smoke cues at locations near the fire. As soon as the fire starts, fire alarm cues are placed all over the environment. Agents react to these cues and mark observable pathways that are blocked as inaccessible in their Environment Knowledge Module. All agents either escape or are killed at the end of the simulation.

5 Results

Experiments were conducted using IBEVAC to demonstrate the effect that cue perception and communication can have on egress. Both experiments were conducted on the two floor office environment shown in Fig. 2. Simulations were

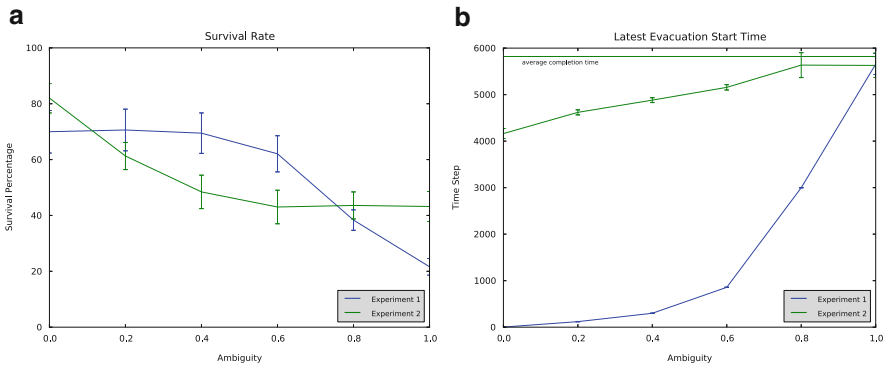


Fig. 3 Observations from 100 replications of each setting of the IBEVAC simulation. **(a)** Average survival rate. **(b)** Last agent start time

conducted with 200 agents randomly distributed all over the environment and data was collected after averaging over 100 replications of the simulation.

5.1 Experiment 1: The Effect of Fire Alarm Clarity

In this experiment, the effect that fire alarm cue clarity and ambiguity has on egress was examined. It is assumed that the fire alarm can be heard clearly at every location on the map; so cues are placed in every room. A fire alarm with a simple ringing sound is much less clear and more ambiguous than a public announcement system that explicitly states that it is not a drill and gives real time updates about the situation. To examine the effect of this difference in clarity, the experiment was repeated for different values of ambiguity (from 0.0–1.0). The blue curves in Fig. 3a show the error plot of the survival percentage and the one in Fig. 3b the average time taken for last agent to start evacuating for this experiment. As expected there is a significant drop in number of survivors as the ambiguity of the alarm increases. Also, the later an agent starts evacuating, the lesser is his chance for survival.

5.2 Experiment 2: The Importance of Communication

In this experiment, the effect of message trustworthiness (ambiguity) is modeled. The fire alarm ambiguity is kept at 1.0 to minimize its interference with the effect of message cues. Similar to Experiment 1 (Sect. 5.1) the cue ambiguity is varied from 0.0 to 1.0. The green curves in Fig. 3a, b show the results for this experiment. However, both these data are collected for agents in the lower floor only. This is because none of the agents on the higher floor start evacuating as they neither

observe the fire nor get a message from other agents about the fire. A similar trend can be observed where the survival rate decreases with increasing ambiguity. The green curve in Fig. 3b flattens out towards the end because in both these cases, the agent's trust in other agents is so less that the only reason they start evacuating is because of the smoke or fire itself. Another thing to note is that even if all agents are completely trusted (ambiguity = 0), the last agent still takes a long time to start evacuating because it takes a long time for the information to propagate to it. This can also explain why there is such a dramatic change in the effect of slight change in ambiguity of the fire alarm cue as opposed to a change in ambiguity of the message cue.

6 Conclusion and Future Work

In this paper, the IBEVAC agent architecture for agent based simulation of emergency egress was introduced. A novel cue modeling and perception system which enables the detailed modeling of pre-evacuation behavior has been described and its working demonstrated.

Only preliminary experiments and results were presented in this paper. Further experiments are being conducted in examining the effect of partial knowledge, variability in trustworthiness and other factors. An interesting extension to the cue perception system would be the implementation of a cue memory. This can be used to model agents forgetting about certain cues or being desensitized to cues due to overexposure.

Acknowledgements This research has been funded by the NTU SU Grant M58020019 and (AcRF) Tier 1 Grant RG10/10(M52020103)

References

1. Berry, D., Hanley, R.: Questions About Fire Safety After Deaths at Seton Hall (Jan 2000)
2. França, R.d.S., Marietto, M.d.G.B., Steinberger, M.B.: A Multi-Agent Model for Panic Behavior in Crowds. Fourteenth Portuguese Conference on Artificial Intelligence (Oct 2009)
3. Kobes, M., Helsloot, I., de Vries, B., Post, J.G.: Building Safety and Human Behaviour in Fire a Literature Review. *Fire Safety Journal* 45(1), 1–11 (Dec 2009)
4. Kuligowski, E.D.: Review of 28 Egress Models. In: Proceedings of Workshop on Building Occupant Movement During Fire Emergencies. pp. 68–90 (Jan 2005)
5. Kuligowski, E.D.: The Process of Human Behavior in Fire. Tech. rep., NIST (May 2009)
6. Ozel, F.: Time Pressure and Stress as a Factor During Emergency Egress. *Safety Science* 38, 95–107 (2001)
7. Paulsen, R.: Human Behavior and Fires: an Introduction. *Fire Technology* 20, 15–27 (May 1984)
8. Pires, T.T.: An Approach for Modeling Human Cognitive Behavior in Evacuation Models. *Fire Safety Journal* 40(2), 177–189 (Mar 2005)

9. Proulx, G.: Playing with Fire Understanding Human Behavior in Burning Buildings. *ASHRAE Journal* 45(7), 33–35 (Jul 2003)
10. Proulx, G.: High-Rise Office Egress the Human Factors. In: *Symposium on High-Rise Building Egress*. pp. 1–6. Institute of Research in Construction, National Research Council, Canada (May 2007)
11. Purser, D., Bensilum, M.: Quantification of Behaviour for Engineering Design Standards and Escape Time Calculations. *Safety Science* 38(2), 157–182 (Jul 2001)
12. Sime, J.D.: Affiliative Behavior During Escape to Building Exits. *Journal of environmental psychology* 3, 21–41 (1983)
13. Tong, D., Canter, D.: The Decision to Evacuate a Study of the Motivations which Contribute to Evacuation in the Event of Fire Theoretical deficiencies. *Fire Safety Journal* 9, 1–9 (1985)
14. Torres, M.R.: Every Man for Himself? Testing Multiple Conceptual Approaches of Emergency Egress on Building Evacuation During a Fire. Ph.D. thesis, University of Delaware (Apr 2010)
15. Tsai, J., Fridman, N., Bowering, E., Brown, M.: ESCAPES-Evacuation Simulation with Children, Authorities, Parents, Emotions, and Social comparison. In: *10th Int. Conf. on Autonomous Agents and Multiagent Systems* (May 2011)
16. Viswanathan, V., Lees, M.H.: Modeling and Analyzing the Human Cognitive Limits for Perception in Crowd Simulation. In: Gavrilova, M.L., Tan, K.C., Phan, C.V. (eds.) *Transactions on Computational Science*. Springer (2012)

An Innovative Evacuation System for Multiplex Cinemas

Case Study “Village Roadshow Group of Companies Athens: Greece”

Athanasios Kosmopoulos and Stavros Katsoulis

Abstract This paper addresses the organizational, training, awareness, behavioral, procedural as well as the technological issues related with an innovative evacuation system for Village Road show Company in Athens Greece. The paper depicts the requirements needed for this case study system to ensure proper and safe evacuation plan for the public in a multiplex cinema. A well designed evacuation system should produce clear optical directional signaling in order to guide the audience towards the assigned exit doors and routes in case of an emergency. Statistical data show, with respect to audience behavioral movements, that the strong majority of all audience in an emergency prefers to follow the previous entry routes rather than the indicated exit ones. In such a case serious injury probability occurs with the conflicting routing of entering and exiting audience. The system responds significantly to the aforementioned risk, ensuring the integrity, and safety of both people involved and infrastructure. It is not to be neglected an 5 % of all audiences refusing to move in an emergency process, and the proper system should motivate them towards the proper direction. The paper discusses the procedures deployed for the operation and support of the system involving the human resource factors in terms of training, monitoring and control. As critical factor emerges the need for immediate response of the system partially or totally in the multiplex as far as Decision making process is concerned. The paper analyses and answers to the plethora of emergency risks imposed in a multiplex cinema (fire, earthquake, bomb threat, hostage situation etc.) and the different related types of evacuation process should be followed respectively. It assesses and forecasts the impact of an evacuation failure both to the company continuity as well as the specific damages to be caused. The case study includes a

A. Kosmopoulos (✉)

Audit and Regulatory Compliance, SIGMANet SA, Athens, Greece

e-mail: kosmopouloa@intertech.gr

S. Katsoulis

Village Roadshow Operations SA, Athens, Greece

e-mail: Stavros_Katsoulis@village.com.gr

software simulation of different evacuation situations regarding different audience presence in the multiplex. Conclusively the paper focuses on the specific attributes an evacuation system for multiplexes should respect and ensure such as accuracy, verifiability, accountability, security and quality assurance in relation to the relevant international standards in force such as ISO.

Keywords Evacuation • Multiplex • Cinema • Optical signs • Routing • ISO

1 Introduction

In multiplex cinemas audience may encounter the need to follow emergency evacuation procedures. There is general agreement amongst social scientists, who have studied the subject that escape behavior to an exit, often attributed to panic, is accounted for primarily by a serious delay in people becoming and being made aware of a threat.¹ A central concern has been to understand the main factors that each agent in an audience decides his next behavior (movement).

These Factors are²:

- **Information gathering**
- **Destination choice**
- **Route choice**
- **Local movement**

It appears that the first and most essential factor is the one related to the Information gathering, especially prior to signal an evacuation than during it.

The literature review³ also outlined common assumptions about exit choice behavior as follows:

- People's safety cannot be guaranteed since in certain circumstances they "panic" leading to "inappropriate" escape behavior
- Individuals almost (but not) always start to move as soon as they hear an alarm
- The time taken for people to evacuate a floor is primarily dependent on the time it takes them to physically move to and through an exit
- Movement in emergencies is characterized by the aim of escaping
- People are most likely to move towards the exit they are nearest to;

¹45/1992: Human Behaviour in Fires, Department for Communities and Local Government Eland House, Bressenden Place, London (1992).

²Pedestrian Behaviour Modelling: An Application to Retail Movements using a Genetic Algorithm, KAY KITAZAWA and MICHAL BATTY, Centre for Advanced Spatial Analysis, University College London, DDSS (2004).

³Sime J D, Creed C, Randall J and Powell J A (1986a) Report to the Home Office (Stage 1): Escape behaviour in fires (Stage 1 of Project: January 1985–March 1986). BUSRU (Building Use and Safety Research Unit), School of Architecture, Portsmouth Polytechnic, (1987).

- People move independently of each other (unless in a dense crowd);
- Fire exit signs help to ensure people find a route to safety
- People are unlikely to use an obstructed or smoke filled escape route
- Most of the people present are equally capable of physically moving to an exit
- As long as an exit is not seriously obstructed, people have a tendency to move in a familiar direction, even if further away, rather than to use a conventional unfamiliar fire escape route.

This last one assumption has been widely verified in drills and evacuation exercises in Village at the Mall cinemas in Athens,⁴ where it was observed that the majority of audience when informed about the necessity of an immediate evacuation has chosen his previous entry route/door, although sufficient signaling was provided to the emergency exit doors.⁵

In our study context, we utilized simulation software as to define pedestrian behavioral attitudes, bottlenecks in addition to important infrastructure points to consider.

On the other hand an important finding is that the startup time (i.e. people's reaction to an alarm) is as (if not more) important as the time it takes physically to reach an exit. In our theatres, during drills⁴, considerable amount of time from the onset of an alarm to reaching exits was spent by people not moving at all. This led to the conclusion that important information must be communicated prior the start of every film in order to familiarize audience with all existing exit doors.

2 Establishing System Design Methodology

The first critical factor observed in the conduct of the research was the need to establish an “evacuation readiness” culture among primarily the members of the staff as well as the audience. This was achieved through “focused on the issue” training as well as with specific guidance on adopting emergency/critical response policies and procedures.

Another important factor was the ensuring that the proper and officially pre-approved exit and evacuation routes were made appropriately demonstrated for the public and the audience prior their entry into the auditoriums. This was accomplished by admitting and implementing the **ISO 23601** requirements regarding “**Safety identification – Escape and evacuation plan signs**”. Additionally to that it was predicted special illumination with Green Led Light Strips fixed on the perimeter of all the exit doors panels since the existing emergency light system

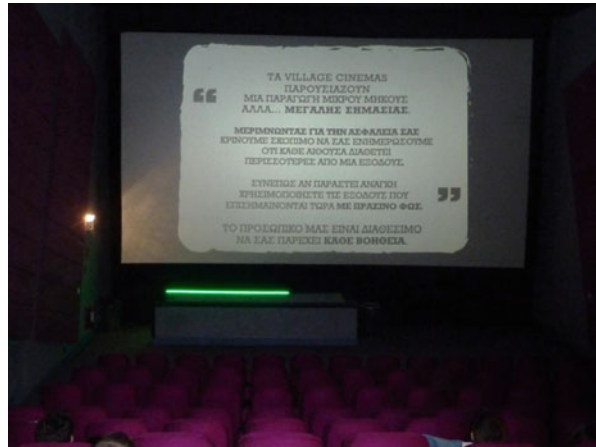
⁴Evacuation Drill, Conclusions Report ,Village at the Mall, 9.12.2011.

⁵Movement toward the Familiar, Person and Place Affiliation in a Fire Entrapment Setting, Jonathan D. Sime, Environment and Behavior, November 1985 vol. 17 no.6 697–724.

Fig. 1 Evacuation system activated at the beginning of the film



Fig. 2 Illuminating the emergency exits



was considered not sufficient in case of immediate evacuation necessity under low visibility circumstances (i.e. black out, smoke etc.) Figs. 1 and 2.

Decision-making during an emergency is different from day-to-day decision-making for three main reasons. First, there is much more at stake in emergency decisions – often the survival of the person and of the people he or she values the most is at play. Second, the amount of time available is limited to make a decision before crucial options are lost. Third, the information on which to base a decision is ambiguous, incomplete and unusual, further it is usually impossible to look for more appropriate information due to the lack of both time and means to get information.

The innovative idea in our design is to display to the audience, on an ordinary basis, the respective exit doors and routes before the projection of the film begins at each auditorium. This procedure is repeated every time a film begins in every theater. In this context a short video clip describing briefly the emergency plan is projected. During this short projection all emergency lights are activated for 10 s. In this respect each and every one of our spectators are acquainted with the existing

exit doors and in case of an emergency they would have to spend less time to identify them, especially should they find themselves in a stressful situation.⁶

On the other hand normal distribution of evacuating people is achieved with respect to the existing doors, since they are already familiar with the nearest to them exit door and there is no need to just follow the outgoing crowd.

As major handicap on the design phase was observed the fact that staff numbers fluctuate during the day. This fact led to the need to implement the system in such a way that would remain independent of the staff availability at the time of an event. This was achieved by introducing specific procedures to apply assuming the minimum staff availability.

Parallel use of the central announcement system was incorporated in order to inform the audience that an evacuation procedure should begin.

The expectation of 'panic' has been a favored argument put forward to delay warning of the public during emergencies. Such delays in informing the occupants have contributed to subsequent stressed behavior and crush of people, who had only a few seconds left to react and escape, once the situation unexpectedly got out of hand. Consequently, researchers are pleading for early warning to the public, providing occupants with as much information as possible to support them in their decision making process.⁶

Finally the system is designed to provide partial evacuation activation for one or more theaters successively or for the total multiplex immediately.

3 Determining the Final Evacuation System

The traditional way of designing an evacuation system is based on well defined procedures. To support that we developed detailed procedures that describe specific actions and patterns to follow before, during and after an emergency event.

Next were the infrastructure preparation, panel and cabling installation and technical/computerized controls of the system. Specific care was taken for the system to be activated with the minimum staff requirements. Both optical and sound provisions were included.

Based on our observations we categorized pedestrian behavior during an evacuation as follows:

- **Wait – Seek Information**

People in this category don't have a specific intention/ target to move. For example, people are waiting (seated or standing) for other person(s) to move or are just gathering information. People in this category are assumed to stay in one place for a longer time.

⁶Understanding Human Behaviour in Stressful Situations, G. Proulx, National Research Council Canada 45394, (2002).

- **Finding the way**

Even if a person has a clear purpose for evacuating the auditorium, sometimes his/her destination is still unclear. For instance, when a person starts moving, he/she may not have decided which particular door to use yet and just follows the mob. In this case, the person will look around to choose a door while moving.

- **Going straight**

When a person clearly recognizes both his/her exit destination and route, he/she is expected to move directly to the goal.⁷

The most time consuming phase is the first (wait & seek) and this is the reasoning for our decision to focus on making people familiar with the emergency plan before an actual event occurs.

Staff training is set out in a policy document and is manifested through videos shown at induction, subsequent refresher training, a guided tour of fire related facilities within the premises, and regular fire evacuation drills. The induction video provides a basic introduction to how fire/earthquake safety is managed in the company, fire prevention, what to do on discovering a fire, how to use a fire extinguisher and what to do in response to an earthquake in the multiplex. Earthquake/fire evacuation drills are normally conducted in the absence of customers. A record is kept of drills and staff who have participated. The company policy is that 75 % of staff will have taken part in drills within a 6 month period. To a greater or lesser extent, this is dependent upon the nature of the position they hold in the company as well as the training they have already received in relation to safety issues.

Prior the training we categorized staff behavior as follows⁸:

- **Ignore:** staff made no visible reaction to the alarm,
- **Wait/seek information:** staff did not take any positive evacuation action sometimes they continued to serve customers (concession), sometimes they appeared to be discussing the situation with colleagues or trying to communicate with the manager,
- **Evacuate customers:** staff's response was to initiate the evacuation of customers
- **Evacuate self:** this action represents the cases where the staff member could be seen evacuating the premises without assisting customers,
- **Left area:** in several cases, on hearing the alarm, staff members (sometimes ignoring customers in the area) left the area. The most probable reason for this action is that they were actively seeking further information or alerting, but it is recognized that they could have been evacuating themselves.

Six months after the training, staff's emergency awareness and readiness improved significantly and no "left area" cases were observed.

⁷Classification of pedestrian behavior in a shopping Mall based on LRF and camera observations, Kotaro Okamoto, Akira Utsumi, MVA2011 IARP Conference on Machine Vision Applications, June 13–15, 2011, Nara, Japan.

⁸An investigation into Staff Behavior in Unannounced Evacuations of Retail Stores - Implications for Training and Fire Safety Engineering, Dmitry SAMOCHINE, Karen BOYCE, Proceedings of the Third International Symposium on Human Behaviour in Fire", Belfast, 2004, pp. 355–366.

4 Conclusions

The most important conclusions regarding the design and application of our system are:

1. This prototype system institutes a low cost but very effective/efficient solution with regard to safe and rapid evacuation needs of an auditorium, theater as well as large multiplexes.
2. It is a first of its kind model that incorporates aviation and maritime standards, regarding emergency procedure briefings for passengers, to multiplex audiences.
3. It requires a minimum staff and personnel number for its operation.
4. It contributes to a safety awareness and emergency readiness culture both for the public and the staff.
5. Last but not least it constitutes a *res judicatum* concerning similar problems in large public areas as shopping Malls, event venues etc.

References

1. 45/1992: Human Behaviour in Fires, Department for Communities and Local Government Eland House, Bressenden Place, London (1992).
2. KAY KITAZAWA and MICHAL BATTY, Pedestrian Behaviour Modelling: An Application to Retail Movements using a Genetic Algorithm, Centre for Advanced Spatial Analysis, University College London, DDSS (2004).
3. Sime J D, Creed C, Randall J and Powell J A (1986a) Report to the Home Office (Stage 1): Escape behaviour in fires (Stage 1 of Project: January 1985-March 1986). BUSRU (Building Use and Safety Research Unit), School of Architecture, Portsmouth Polytechnic, (1987)
4. Evacuation Drill, Conclusions Report ,Village at the Mall, 9.12.2011
5. Jonathan D. Sime, Movement toward the Familiar, Person and Place Affiliation in a Fire Entrapment Setting, Environment and Behavior, November 1985 vol. 17 no.6 697–724
6. G. Proulx, Understanding Human Behaviour in Stressful Situations, National Research Council Canada 45394, (2002)
7. Kotaro Okamoto, Akira Utsumi, Classification of pedestrian behavior in a shopping Mall based on LRF and camera observations, MVA2011 IARP Conference on Machine Vision Applications, June 13–15, 2011, Nara, Japan.
8. Dmtry SAMOCHINE, Karen BOYCE, An investigation into Staff Behavior in Unannounced Evacuations of Retail Stores - Implications for Training and Fire Safety Engineering, Proceedings of the Third International Symposium on Human Behaviour in Fire”, Belfast, 2004, pp.355–366.

An Innovative Scenario for Pedestrian Data Collection: The Observation of an Admission Test at the University of Milano-Bicocca

Mizar Luca Federici, Andrea Gorrini, Lorenza Manenti,
and Giuseppe Vizzari

Abstract The investigation of crowd dynamics is a complex field of study that involves different types of knowledge and skills. Due to the difficulty in reaching an exhaustive definition of the notion of crowd, we propose to analytically investigate this phenomenon focusing on pedestrian dynamics in medium-high density situations, and, in particular, on proxemic behavior of walking groups. In this work we will present several results collected during the observation of the incoming pedestrian flows to an admission test at the University of Milano-Bicocca. In particular, we collected empirical data about: level of density and service, spatial arrangement, composition (size, gender) and walking speed of groups. The analysis of video footages of the event showed that unexpectedly a large majority of the incoming flow was composed of groups, and that group size significantly affects walking speed.

Keywords Pedestrians • Groups • Proxemics • Level of service • Walking speed

M.L. Federici (✉)

Crowdyxity s.r.l. – Crowd Dynamics and Complexity, Via Ventura 3, Milan 20134, Italy
e-mail: m.federici@crowdyxity.com

A. Gorrini

Information SOCIETY Ph.D. Program, University of Milan-Bicocca, Via Bicocca degli Arcimboldi 8, Milan 20126, Italy
e-mail: a.gorrini@campus.unimib.it

L. Manenti • G. Vizzari

CSAI – Complex Systems and Artificial Intelligence Research Center, University of Milan – Bicocca, Viale Sarca 336, Milan, Italy
e-mail: manenti@disco.unimib.it; vizzari@disco.unimib.it

1 Introduction

The investigation of crowd dynamics is a complex field of study, and it involves different types of knowledge and skills. Its scientific relevance is related to the growing need of applicative results, strictly linked with the management of large events (e.g., celebrations, concerts, sports events) and the design of public spaces (e.g., square, stadium, station). From the socio-psychological perspective the definition of crowd is still controversial, because of the lack of standard guidance for data collection. The empirical investigation of the phenomenon is indeed made difficult by ethical-practical reasons and its variability with respect to size and typology of the observed situation.

Early interest in studying crowd behavior started from the pioneering study of Gustave Le Bon [1] who defined a crowd as a potential threat to society: as members of a crowd people display an altered state of consciousness, with a consequent loss of sense of self-awareness, and an increase of irrational and violent behaviors. In complete opposition, the ESIM-Elaborated Social Identity Model [2] proposes a social-normative conception of collective behavior, arguing that social norms continue to shape behavior of people also within the crowd, by means of the spontaneous transition from an individual identity to a common social identity [3].

Starting from these contrary theoretical assumptions, the most accepted definition of crowd cites: “A crowd can be defined as a gathering of 20 people (at least), standing in close proximity at a specific location to observe a specific event, who feel united by a common social identity, and who are able to act in a socially coherent way, despite being strangers in an ambiguous or unfamiliar situation” [4, p.43].

Because of the difficulty to reach an exhaustive definition of what a crowd actually is, we propose to analytically investigate the phenomenon¹ focusing on pedestrian dynamics in medium-high density situations. In particular, we focus on: *groups*,² which are the basic elements which the crowd is composed of, and *proxemics* [5], an analytical indicator of crowd behavioral dynamics, thanks to its ability to model social relationships among people and groups in the crowd, by means of the dynamic regulation of interpersonal distances.³

Proxemic behavior reveals the psychological bonding among group members, and, in high-density situation, it represents an adaptive stress-reducing behavior

¹And hopefully contribute to the above discussion by producing scientifically sound observations and data.

²A group can be defined as two or more people who interact for a shared goal, perceiving a membership based on a shared social identity [3].

³The regulation of spatial distances (intimate, personal, social, and public distances) is influenced by age, gender, culture, and personality [6].



Fig. 1 The typical pattern of proxemic behavior of walking group: from the *left*, the Line-abreast pattern, the V-like pattern and the River-like pattern

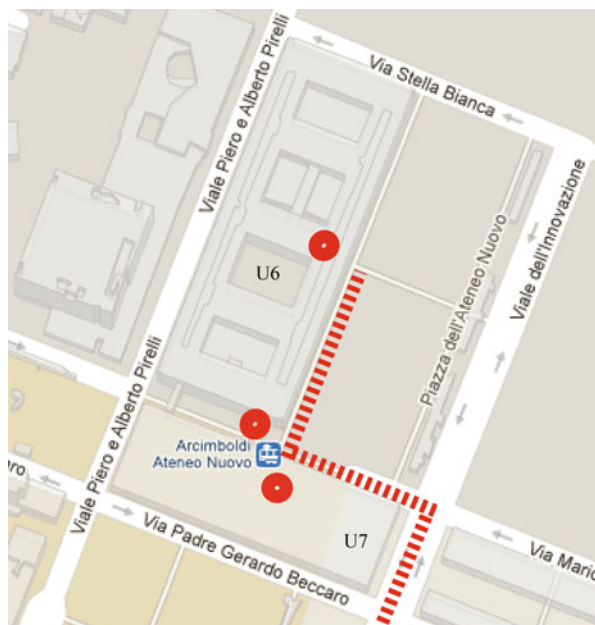
to crowding,⁴ by producing spatial boundaries that shield group members from the invasion of personal space [7]. In motion situation, group proxemic behavior generates typical patterns (see Fig. 1), which allow communication and spatial cohesion among members [8]. At low density, group members tend to walk side by side, forming a line perpendicular to the walking direction (line-abreast pattern); as the density increases, the linear walking formation turns into a V-like pattern, with the middle individual positioned slightly behind in comparison to the lateral individuals; in situation of high density, the spatial distribution of group members leads to river-like pattern, characterized by the presence (or emergence) of a leader that guides the group members to cross the space [9]. This kind of dynamic has only recently been investigated by pedestrians and crowd modelers, and also on the observation and analysis side much work is still necessary to achieve a comprehensive characterization of this kind of phenomenon.

To further investigate pedestrian dynamics in medium-high density situation, we propose to detect the behavior of walking group, focusing on the relation among: level of density and service, proxemic spatial arrangement (degree of alignment and cohesion), group size and composition (gender) and walking speed. In particular, in this work we will present several results collected during the observation of the incoming pedestrian flows to the admission test of the Faculty of Psychology at the University of Milano-Bicocca (September 1, 2011). In the context of crowd studies carried out by the CSAI research center, the survey was aimed to enhance existing knowledge and results achieved from several early observations [10, 11], and first modeling proposals [9, 12, 13].

This work is organized as follow: after a briefly description of the scenario and the methodological approach (Sect. 2), a preliminary analysis will be proposed (Sect. 3); in particular we will focus on flow composition (Sect. 3.1) and walking speed analysis (Sect. 3.2); finally, some conclusions and final remarks will be presented in order to underline future developments (Sect. 4).

⁴Psycho-physiological responses of arousal and stress, cognitive performance decrements, and aggressive response [7].

Fig. 2 The scenario: buildings U6 and U7, which were the venues of admission test; counting points for video footage (represented by *circles*); the main incoming flow from public transports (represented by *dotted line*)



2 Scenario Analysis and Methodological Approach

About 2,000 prospective students attended the last admission test to the Faculty of Psychology at the University of Milano-Bicocca.⁵ The survey was aimed at observing individual and group pedestrian behavior during the last phases of arrival and entrance processes in the U6 Building (one of the venues of the admission test – see Fig. 2). In particular, data collection was focused on level of density, group composition (size and gender), group spatial arrangement and walking speed. The incoming pedestrian flow was measured minute by minute⁶; the identification of groups in the streaming of passers-by was assessed considering verbal and non verbal communication indicators: talking, gesticulation, visual contact, body orientation and, in particular, on spatial arrangement and cohesion of group members (in reference to typical proxemic patterns). A topographical analysis of the scenario was performed to support the detecting of the level of density, the level of service and the walking speed analysis.

⁵The subscription list of the participants to the admission test was composed of 2,094 students, including 437 males (29 %), and 1,657 females (79 %), on average 19 years old; it must be noticed that not all subscribers actually participated the test.

⁶Each observer wrote down the counted number of pedestrians or groups every 60 s to prevent errors due to the counting operations.

The team was composed of two supervisors and six observers (distributed on different counting points). Each counter was equipped with: a pre-printed blank table that was necessary to note data, a counting device, a chronograph and a special pass provided by University Authorities. Preliminary surveys were performed to define the best counting points, trying not to hinder the activities of the organizers, and not to influence the behavior of observed subjects. To ensure more validity to the research, video-recording tools were employed in addition to human counters. The equipment for video footage consisted of full HD video cameras with stands. Existing legislation about privacy was also consulted to exceed some ethical issues about the video recording of the event.

3 Data Analysis

The starting point of data analysis consisted of a preliminary investigation about data collected by the counters (e.g., realization of charts and frequency of arrival tables). Then, a post process analysis of the video-recorded images was performed by two independent persons to perform a cross-checking of their conclusions and therefore to further reduce errors averaging out their results. A preliminary comparison of the results obtained by the two techniques (head-counting and video footages) showed that the video analysis, although time consuming, is a useful technique to reduce human error, ensuring more validity to the research. Even if expert counters were employed during the activities, the video footages analysis highlighted the presence of an over estimation error in determining the pedestrians flow (around 4 %) and the presence of groups (around 10 %) in the incoming flow. For this reason we decided to rely on the video footages of the event. In the following, we will introduce the results of several analyses about: pedestrians flow, level of density and service, group spatial arrangement, gender and walking speed.

3.1 Flow and Composition

The incoming pedestrian flow was composed of 1,897 persons, which reached the venues of the admission test between 7:35 a.m. and 8:40 a.m.. The 34 % of them arrived alone, while the 66 % arrived in groups: 77 % of groups were couples, 19 % triples and 4 % larger groups.

In relation with the average low-level of density observed (0.05 persons/m²), the analysis of spatial patterns of walking groups showed that:

- Ninety seven percent of couples was characterized by line-abreast pattern, 3 % by river-like pattern;
- Sixty six percent of triples was characterized by line-abreast pattern, 33 % by V-like pattern, and 1 % by river-like pattern;

- Groups with four members were usually structured into sub-units of dyads, or triads and individuals: 30 % of four-person groups was characterized by rhombus-like pattern (one person leading the group, followed by a dyad and ended by an another single person), 21 % of the groups split into two dyads, 21 % line-abreast pattern; 14 % triad followed by a single person, 7 % single individual followed by a triad, 7 % by V-like pattern.

3.2 Walking Speed Analysis

In this section an analysis of a selected portion of the incoming flow is proposed, considering people that reached Building U6 (745 persons, 39 % of the total incoming flow). We propose below a data analysis of the walking speed of single pedestrians and groups, and, in particular, we focused on: level of service (referred to a precise area of 146.4 m²), group size, group spatial arrangement and gender of individuals and group members.

According to the existing HCM Walkway Level of Service Criteria [14], the flow rate was measured as the relationship among pedestrian/minute/meter: the average flow rate (5.09 pedestrian/min/m) is associated to A-level, while several isolated time intervals were instead associated to B-level. It has to be underlined that the available space was huge in relation to the flow and, therefore, free flow situations were dominant as expected.

Since we are interested in characterizing group dynamics in medium-high density situations, we focused on the time intervals characterized by a B-level: this category is not really associated to medium density, but it is not even completely free-flow. A subset of 201 pedestrians was extracted. Since large groups were not regularly detected in these situations, we focused the analysis on singles (50 single pedestrians – 25 % of the subset), couples (50 couples – 50 %) and triples (17 triples – 25 %). A first analysis was devoted to the identification of the average walking speed for singles ($\bar{M} = 1.38$ m/s), couples ($\bar{M} = 1.30$ m/s) and triples ($\bar{M} = 1.21$ m/s). By means of an one-way analysis of variance (ANOVA, see Table 1), the difference of walking speed among singles, couples and triples was tested: the results showed that a significant size of group affects walking speed ($p < 0.05$). More in detail, the differences in walking speed between singles and couples, singles and triples, couple and triples, were investigated with a *T*-test, which confirmed a significant effect of group size ($p < 0.01$).

In conclusion, the results showed that, at a low-medium level of density, a greater size of the pedestrian groups is associated to a lower walking speed. This conclusion is in tune with previous observations [8, 15, 16].

Further ANOVA analyses were focused on spatial arrangement and gender: no significant differences in walking speed ($p > 0.05$) between line-abreast and river-like couples, and among line-abreast, V-like and river-like triples; no significant differences in walking speed ($p > 0.05$) between females and males walking alone (i), same and mix gender couples (ii), same and mixed gender triples (iii).

Table 1 ANOVA analysis of the difference of walking speed among single, couple and triple (the analysis was performed by means of *IBM SPSS Statistics v.18*)

ANOVA						
Walking_speed						
	Sum of squares	df	Mean square	F	Sig.	
Between groups	0.435	2	0.218	9.678	0.000	
Within groups	2.563	114	0.022			
Total	2.998	116				
Post hoc tests						
Multiple comparisons						
Walking speed						
LSD						
(I) N_people	(J) N_people	Mean difference (I-J)	Std. error	Sig.	95 % confidence interval	
					Lower bound	Upper bound
1	2	0.08660*	0.02999	0.005	0.0272	0.1460
	3	0.17386*	0.04210	0.000	0.0905	0.2573
2	1	-0.08660*	0.02999	0.005	-0.1460	-0.0272
	3	0.08726*	0.04210	0.040	0.0039	0.1707
3	1	-0.17386*	0.04210	0.000	-0.2573	-0.0905
	2	-0.08726*	0.04210	0.040	-0.1707	-0.0039

*The mean difference is significant at the 0.05 level

4 Discussion and Future Works

The analysis of the video footages of event showed that the incoming flow to the admission test was composed of almost two thousands of people, and that a large majority of it was composed of groups (couples, triples and groups of four members). The results can be compared to others similar observations [8, 15, 16], taking into account the different context where the observations took place. Although the admission test is individual, we detected a pervasive presence of groups: this confirms our hypothesis of dominance of groups as basic constitutive elements of crowds. The results achieved at a low-medium level of density, showed that the greater the size of the pedestrian groups, the lower their walking speed is.

Future works are aimed at collecting further empirical data about the relationship between walking speed and proxemic behaviour of walking groups in high-density situation (taking into account also age and gender differences, and larger groups). In high-density scenarios, the degree of freedom of spatial distribution of walking groups is affected by the need to avoid physical contact with other individuals or groups. Although it could be more difficult to detect groups in this kind of scenario, we will focus on queues and lane formation: when people move in opposite directions in a crowded environment, they spontaneously organize themselves into different lanes for each direction of travel [17].

Moreover, additional analyses on the process of entrance to the University buildings, will support the definition of a set of recommendations aimed at achieving a more efficient management of people who attend every year the admission test (e.g. reduction of waiting times, better organization of queues and guidance information to the attendees), with specific reference to pedestrian circulation dynamics and physical layout of the environment.

Acknowledgement This work is partially been funded by the University of Milano-Bicocca, within the project “Fondo d’Ateneo per la Ricerca – anno 2010/2011”.

References

1. Le Bon, G.: *The Crowd: A Study of the Popular Mind*. Ernest Benn, London (1895, trans. 1947)
2. Reicher, S.: The psychology of crowd dynamics. In *Blackwell handbook of social psychology: Group processes*, Wiley-Blackwell, 182–208 (2001)
3. Turner, J.: Toward a cognitive definition of the group. *Cahiers de Psychologie Cognitive/Current Psychology of Cognition*, 15–40 (1982)
4. Challenger, W., Clegg, W. C., Robinson, A. M.: *Understanding crowd behaviours: Guidance and lessons identified*. Technical Report prepared for UK Cabinet Office, Emergency Planning College, University of Leeds (2009)
5. Hall, E. T.: *The Hidden Dimension*. Doubleday, New York (1966)
6. Aiello, J. R.: Human spatial behavior. *Handbook of environmental psychology*, 1, 389–505 (1987)
7. Baum, A., Paulus, P. B.: Crowding. *Handbook of environmental psychology*, 1, 533–570 (1987)
8. Costa, M.: Interpersonal Distances in Group Walking. *Journal of Nonverbal Behavior*, 34(1), 15–26 (2010)
9. Moussaïd, M., Perozo, N., Garnier, S., Helbing, D., Theraulaz, G.: The walking behaviour of pedestrian social groups and its impact on crowd dynamics. *PLoS One*, 5(4), e10047 (2010)
10. Kachroo, P., Al-Nasur, S. J., Wadoo, S. A., Shende, A.: Pedestrian dynamics: Feedback control of crowd evacuation. Springer Verlag (2008)
11. Peacock, R. D., Kuligowski, E. D., Averill, J. D.: *Pedestrian and Evacuation Dynamics*. Springer Verlag (2011)
12. Bandini, S., Manzoni, S., Vizzari, G.: Modeling, Simulating, and Visualizing Crowd Dynamics with Computational Tools Based on Situated Cellular Agents. *Pedestrian behavior: models, data collection and applications*, pp.45. (2009)
13. Waş, J.: Crowd dynamics modeling in the light of proxemic theories. *Artificial Intelligence and Soft Computing*, 683–688 (2010)
14. Milazzo II, J. S., Roupail, N. M., Hummer, J. E., Allen, D. P.: Quality of service for interrupted-flow pedestrian facilities in Highway Capacity Manual 2000. *Transportation Research Record: Journal of the Transportation Research Board*, 1678(-1), 25–31 (1999)
15. Willis, A., Gjersoe, N., Havard, C., Kerridge, J., & Kukla, R. (2004). Human movement behaviour in urban spaces: Implications for the design and modelling of effective pedestrian environments. *Environment and Planning B Planning and Design*, 31(6), 805–828
16. Schultz, M., Schulz, C., Fricke, H.: Passenger Dynamics at Airport Terminal Environment. *Pedestrian and Evacuation 17 Dynamics 2008, Part 2*, 381–396, Springer Berlin Heidelberg (2010)
17. Schadschneider, A., Kirchner, A., Nishinari, K.: CA approach to collective phenomena in pedestrian dynamics. *Cellular Automata*, 239–248 (2002)

Trajectory Analysis of Pedestrian Crowd Movements at a Dutch Music Festival

Dorine C. Duives, Winnie Daamen, and Serge Hoogendoorn

Abstract Major pedestrian crowd movements have proven to be volatile in the past. The contribution of this paper is to assess a new recording and a new analysis technique to improve the currently limited theoretical knowledge on the movement of individual pedestrians within a crowd. Using a camera attached to a UAV, footage of pedestrian crowd movements has been recorded at the major music festival Lowlands in the Netherlands. This paper describes a detection and tracking tool, resulting in trajectory information for all pedestrians visible within the footage. Footage recorded at Lowlands is used to assess the new techniques' contribution, resulting in trajectory analyses of individual pedestrian movements in a crowd.

1 Introduction

Several pedestrian crowd events that turned into disasters occurred in the last decade. Even though pedestrian crowd events are organized frequently, not a lot is known about pedestrian crowd movements. Simulation models might be able to help predicting where, when and why a hazardous event arises. However, literature shows that pedestrian crowd modeling is a relatively young field of study in which not a lot is known. The fundamental diagrams used for calibration show a lack of conformity (e.g. Ando et al. [1]; [15]). Besides that, it is questionable whether a fundamental diagram established for single-file walking movements can be used in the simulation of congested pedestrian crowd situations. Last of all, one might wonder whether during microscopic pedestrian flow experiments

D.C. Duives (✉) • W. Daamen • S. Hoogendoorn
Department of Transport and Planning, Faculty of Civil Engineering and Geosciences,
Delft University of Technology, Delft, The Netherlands
e-mail: d.c.duives@tudelft.nl; w.daamen@tudelft.nl; s.p.hoogendoorn@tudelft.nl

pedestrians display the same behaviour as when walking in a crowd. Very limited data are available to derive theories or calibrate pedestrian crowd models. It can be concluded that a lack of data on individual movements within crowds exists.

In this paper new data gathering and analysis tools are introduced. By means of unique data of undisturbed pedestrian crowd movements recorded at a Dutch music festival using a UAV the proposed technique is assessed. Accordingly, conclusions are drawn about the opportunities of the new technique. The main research objective of this paper is to development the new airborne recording technique and an offline (semi-)automatic analysis technique capable of analyzing pedestrian crowd movements.

2 Background

The previously mentioned lack of data is partly caused by the lack of stable and long time coverage of high-density pedestrian crowd movements. Therefore equipment is needed that is able to capture these movements from a stable high vantage point, such as video. This research seeks whether a light-weight high-speed high-resolution (HDHS) camera attached to a UAV can provide the means to do so.

However, the lack of knowledge on pedestrian crowd movements is also caused by the laborious process of video image analysis needed. Many aids have been used to make the automatic tracking of pedestrians in traffic flow experiments easier, such as coloured caps and white t-shirts [5], contrasting walls and floors and predefined limited areas of movement [8, 9, 11]. Since crowd movements often take place at outdoor locations, most of the above described tricks cannot be used to improve pedestrian detection and tracking. A few software programs have been developed specifically for the analysis pedestrian movement footage recorded in outdoor environments (for instance [7, 12]). For most software programs detection and tracking becomes problematic for footage recorded using an unstable recording medium featuring dynamically changing pedestrian flows in changing light conditions from a very high vantage point (>50 m). Occlusion during high density situations further aggravates the detection and tracking difficulties.

The alternative, manual detection is a very laborious task. To improve the data processing a new software tool is needed that detects and tracks pedestrians based on very limited information per pedestrian in medium and high density situations. This research proposes a software package containing the whole footage analysis process (from initial UAV image sequences to final movement analysis). Footage recorded at one of the largest pop festivals in the Netherlands (Lowlands) is used to test the proposed chain of software programs.

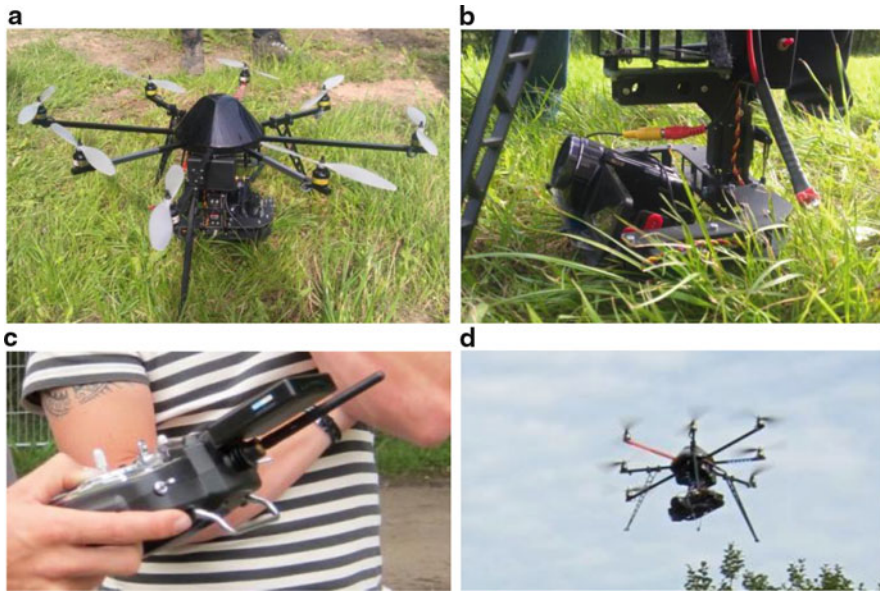


Fig. 1 Octa-copter with filming equipment (a) octa-copter, (b) camera suspension, (c) steering equipment, (d) airborne UAV

3 UAV Recording Set-up

With a new data collection method – an octa-copter (UAV) equipped with a lightweight high-speed high-definition camera with a F3.45 41.4 35 mm Leica lens (Fig. 1) – we are able to record pedestrian crowd movements in an outdoor environment without interfering with the natural movement of the pedestrian crowd. Unlike most CCTV, an air borne camera records a top-view from a height of 50 m or higher, which ensures limited occlusion of pedestrians (occlusion is predominantly visible at the rims of the recording area) and a large recording area. This is however dependent on the lens used (for a 180° lens the occlusion is more problematic but the on film captured area is larger).

The data were collected at the 20th of August 2011 at a Dutch music festival named Lowlands at Biddinghuizen. The footage consists of eight video sequences, six of which have a duration of 9 min and are shorter (5 min). Only three video sequences of 9 min featuring ‘low’, ‘medium’ and ‘high’ density crowd movement footage were finally used. The separate PNG images of the footage have a resolution of $1,080 \times 1,900$ pixels, with a image recording speed of 50i. Figure 2 displays the images recorded at Lowlands. The total area covered by the camera is 150 by 30 m and it was recorded under an angle of approximately 49°. On average 250–1,100 pedestrians are visible in every frame. In Fig. 2 the origins and destinations are indicated by the rectangular boxes. The three exits on the left lead to festival stages.

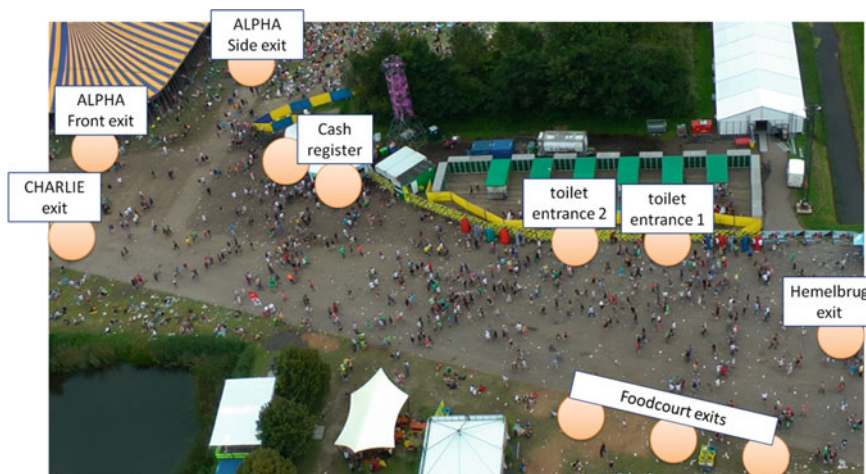


Fig. 2 Recorded terrain displaying origins and destinations, low density

The elongated exit on the right leads towards the rest of the festival terrain. The predominant pedestrian flows are left-right and right-left.

3.1 Recording Technique

Due to the method of recording using a UAV, interlacing is visible when the subject of the recording moves too fast through the image (high walking velocities) or when the recording medium is itself unstable. However, in the parts of the footage where the UAV is kept stable at one position, the influence of interlacing is limited with respect to the subject.

Because the camera is mounted to an octacopter, the raw footage is not entirely recorded from the same stable position due to wind and rotor vibrations. Both large movements and small vibrations are clearly present within the footage. Both work in six directions, being rotation around the x -, y -, and z -axis and translation in the x -, y - and z -direction. The GPS system of the octacopter was not exact enough to record these movements.

3.2 Lighting Conditions

The footage is recorded between 4:42 p.m. and 8:19 p.m. During the data collection the sun was on its way down. It is clearly visible that the spectral power of the sun decreases throughout the recordings. Due to sundown more grey influences are added into the images' colour histogram. During the data collection a slight

Fig. 3 Blown-up of footage recording showing three pedestrians (two with a *red shirt* and one with a *black shirt*)



haze was continuous present. As such, lightning shifts due to clouding are not visible within the footage.

3.3 Recorded Subject

Due to the relatively small dimensions of a singular pedestrian only limited information is available on each pedestrian. Singular pedestrians are mainly distinguishable through about the pedestrians is available. Figure 3 shows a magnification of Fig. 3. It can be seen that the outline of each pedestrian is very vague. The pedestrians can only be identified by their distinctive pixel colour and movement with respect to the image background.

The movements of the pedestrians are very diverse in both x- and y-direction. There is no standardized flow through the image.

At low densities almost no occlusion is visible. However, when people are standing almost shoulder to shoulder, the body of pedestrians in the background is almost completely obscured by other surrounding bodies. Due to the small amount of pixels available per individual at high densities, the exact number of individuals becomes impossible to determine directly from the number of occupied pixels.

4 Chain of Software Programs

Based on the footage characteristics discussed above a chain of software programs has been put together. In Fig. 4 the flowchart of the total software framework is shown.

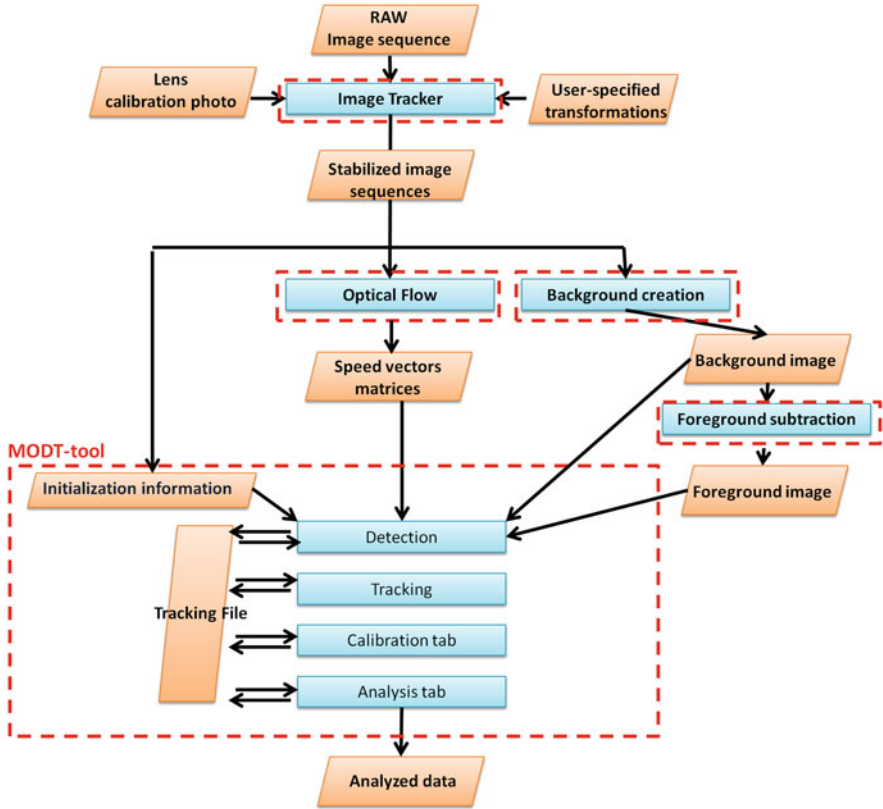


Fig. 4 Organisation diagram proposed software chain

The red striped boxes are separate software programs that need to be run to convert the RAW image sequence into analyzed data. Image Tracker and the Optical Flow method are software programs developed by a third party. The combination of VirtualDub, ImageTracker and the newly developed Moving Object Detection and Tracking-tool (MODT) has been used to analyze the footage. The latter two will be further elaborated upon below.

4.1 ImageTracker

For the stabilization of the image sequences an, at the TU Delft developed, software package is used. ImageTracker [6] corrects for lens distortion, searches for the transformation necessary to match sequential images and applies this transformation to stabilize the image with respect to a reference image. The software assumes that no interlacing is present within the image files that are read into the software

Fig. 5 Flow chart MODT

program and thus does not correct for this. Therefore the most heavily interlaced sequences have been disregarded in this paper.

4.2 *MODT-tool*

The software developed for the detection and tracking of the pedestrians consists of three parts (Fig. 5).

Firstly the pedestrians are detected in one of the images of an image sequence. After detection the pedestrians are tracked across the total image sequence. Subsequently visual data analysis is possible by means of the analysis module. For the numerical data analysis a separate script was used. The MODT-tool runs as a Windows executable, which provides the end-user with easy access to the software without the need to work directly in the command line interface/source code.

4.2.1 Detection

The detection of moving objects in a sequence is possible in two ways: either via manual detection or by means of an automated procedure that detects the majority of moving objects. The input of the manual detection consists of the stabilized image. During the manual detection the user will be asked to indicate the approximate position of pedestrians within the stabilized image.

For the computer detection also a set of foreground images (computed using background modelling (e.g. [17])) is necessary. The automated detection procedure assumes that all moving objects are pedestrians. As such it can be assumed that all foreground pixels are part of a moving object. By recording the contour of each blob of foreground pixels (Fig. 6) all moving objects are identified. To filter out the white noise, it is assumed that a blob of less than 4 pixels in width and 8 in height does not represent a pedestrian but noise. For blobs that are bigger than one pedestrian no special reservations have been made (that is, the whole group is detected as one person). The automatic detection does not adapt noise filter depending on the location within the image where a pedestrian is detected. Ultimately this also needs to be integrated to improve detection. Automatic detection of pedestrian groups with high levels of occlusion would need to be considered when further developing this software tool. The automated detection will, depending on the density, detect 90 % (less crowded circumstances) or less

Fig. 6 Registered blobs of foreground pixels



(20 %) (very crowded circumstances – 4 P/m²) pedestrians. However, using the combination of both procedures detection rates of more than 60 % minimum can be reached for high density situations.

4.2.2 Tracking

During the tracking procedure pedestrians are tracked based on their current position, the mixture of the pixel colour and the velocity vector at their current position. In the procedure the new location is first predicted by means of a Kalman Filter that implements Optical flow data [13, 14] and the pedestrian's previous positions. In the second step, their current position is found by means of a local search (within a 20×20 pixel region) that searches for the correlating pixel colour nearest to the predicted location.

The tracking method does not allow rapid changing pixel colours to be followed since this would allow the software to shift focus too easily. The software is allowed to shift the focus on the pixel colour slowly because slight variations in colour of the pedestrian focus do occur. However, occlusion generally occurs only for short periods of time (2–3 s) in the footage. By allowing the software program to loose a pedestrian and tracking its predicted location based on the last known velocity and pixel colour, the software has the possibility to recover a pedestrian's location when it reappears after the occlusion. While the pedestrian is temporarily lost, its last detected pixel colour is used to locally search for the pedestrian at the predicted location. A disadvantage of tracking based on predicted locations and set pixel colours is the risk of mismatching reappearing pedestrians. Occasionally also mismatching is introduced when two pedestrians with exact the same surface reflection pass in close vicinity of each other.

4.2.3 Computation of Visual Analysis

In order to better understand the implications of the tracked movements, also visual data analysis is necessary. In the Analysis tab several plots can be made, namely macroscopic velocity plots, individual velocity vector plots, density plots, flow characteristic scatter plots and trajectory visualizations. The macroscopic velocity plot shows the average movement direction at each location within an image. Its computation is based on the methodology used by Helbing et al. [4]. The individual velocity plot computes the current movement direction of each individual detected in an image. The trajectory visualization depicts the trajectory of specified individuals during a specified time interval. Last of all, the MODT tool can determine the local flow characteristics (walking velocity, density and flow) at any location within an image. Based on the trajectory data also individual flow characteristics can be plotted. However, these are currently written as a loose Matlab script to make adaptation easier.

5 Lowlands Test Case

We were able to deduct individual trajectories from the recordings. The recorded pedestrian movements can be translated into time series of the macroscopic flow characteristics.

5.1 Velocity

Based on the trajectory information, the pedestrian movements have been analyzed for three of the three best of the in total eight footage sequences, namely sequences 5, 7 and 8. The visible velocities in sequence 5 range between 0.3 and 1.2 m/s (see Fig. 7). This is significantly lower than was expected based on previous research [1, 10, 15, 16]. Although these studies have not been deducting during a festival. In sequences 7 and 8, where higher densities are observed, also higher walking velocities are observed in the low-density regions. Often even higher walking velocities than in the free flow conditions of sequence 5. On average, walking velocities ranging between 0.4 and 1.8 m/s are found (Figs. 8 and 9). It is hypothesized that contrary to sequence 5, the pedestrians in sequences 7 and 8 display goal-oriented behaviour.

In Table 1 Gaussian estimates of all velocity distributions are presented. The velocity distributions display the same discrepancies with respect to previous research as the graphs. The mean walking velocities of sequences 7 and 8 are both significantly higher than the mean walking velocity of sequence 5, while their standard deviations are on average equal. This can be an indication that two different behavioural profiles are visible at the Lowlands grounds.

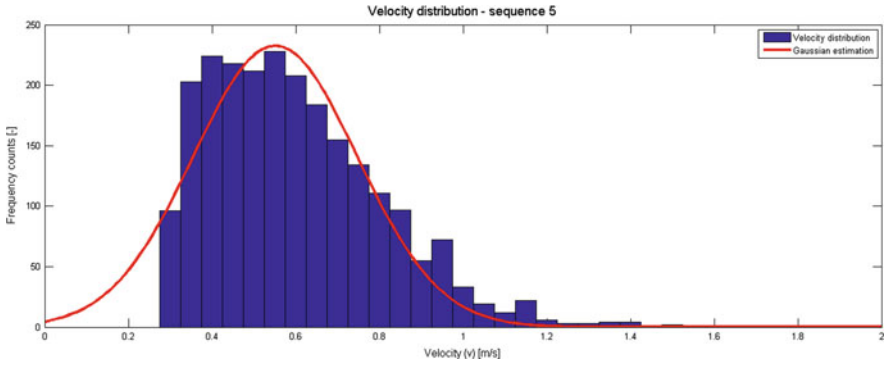


Fig. 7 Velocity frequency counts sequence 5

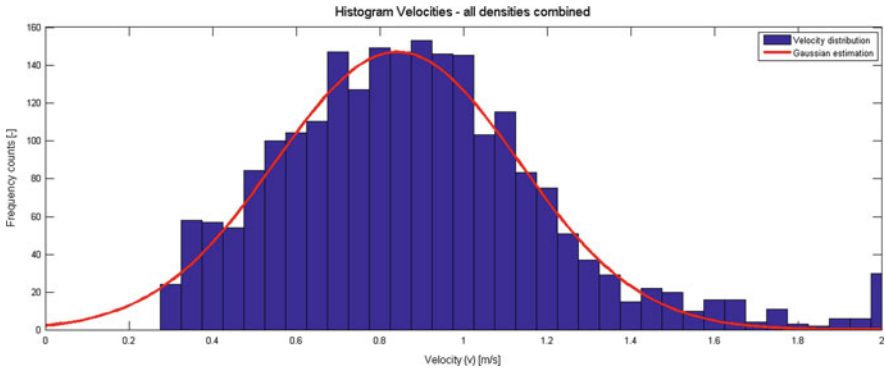


Fig. 8 Velocity frequency counts sequence 7

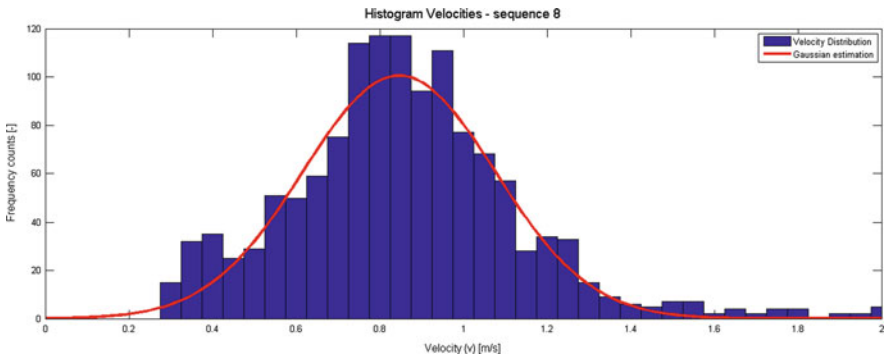


Fig. 9 Velocity frequency counts sequence 8

Table 1 Velocity distributions

	Mean (confidence interval) [m/s]	Std (confidence interval) [m/s]
Sequence 5	0.55 (0.53–0.57)	0.20 (0.17–0.22)
Sequence 7	0.84 (0.82–0.86)	0.29 (0.27–0.31)
Sequence 8	0.85 (0.83–0.87)	0.23 (0.21–0.25)

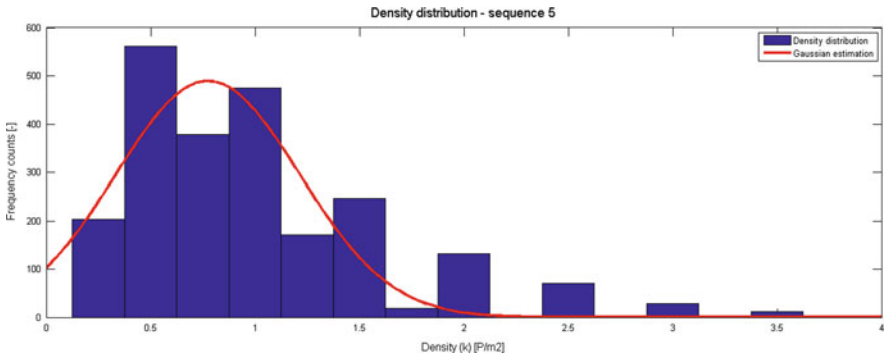


Fig. 10 Density frequency counts – sequence 5

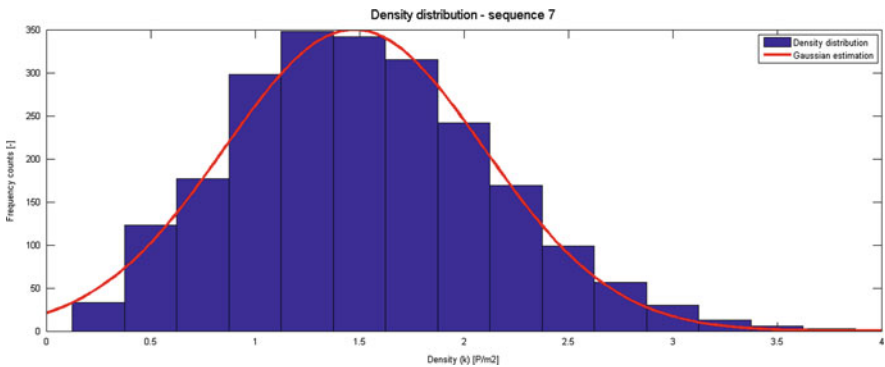


Fig. 11 Density frequency counts – sequence 7

5.2 Density

At the experiment area densities range from 0–2.5 P/m² in sequence 5 (Fig. 10) to 0.5–4 P/m² in sequences 7 and 8 (Figs. 11 and 12). In sequences 7 and 8 large high density regions are visible, while low density regions also remain present, (though smaller and fewer in number).

An estimation of the Gaussian distribution (Table 2) for each of the histograms displays the same trend as seen for the walking velocity. The mean densities of the distribution of sequences 7 and 8 are significantly higher than the mean density of sequence 5. Furthermore in sequences 7 and 8 higher standard deviations are found.

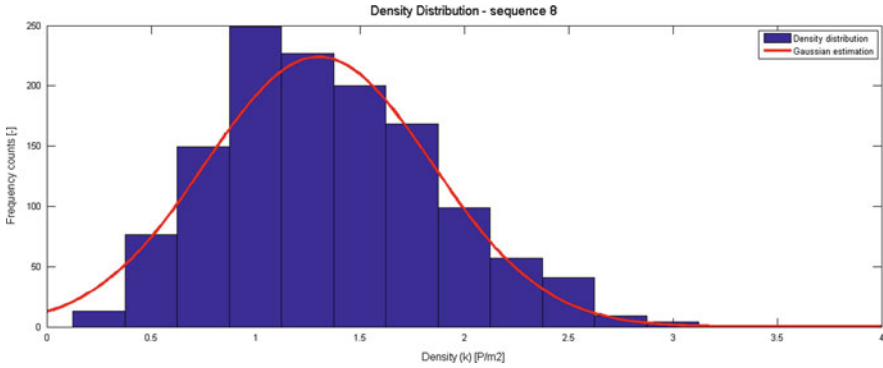


Fig. 12 Density frequency counts – sequence 8

Table 2 Gaussian estimations of density distributions

	Mean (confidence interval) [P/m ²]	Std (confidence interval) [P/m ²]
Sequence 5	0.77 (0.66–0.88)	0.44 (0.32–0.55)
Sequence 7	1.48 (1.45–1.51)	0.62 (0.59–0.65)
Sequence 8	1.30 (1.25–1.35)	0.54 (0.49–0.59)

This shows that even though the average density is higher, low densities are still encountered frequently in the recordings.

5.3 Fundamental Diagram

When looking at the density-velocity graphs of both sequence 5 and sequences 7 and 8, it becomes visible that indeed different behaviours are found within the footage. For sequence 5 it is seen that at low densities (where unconstrained movements are possible) the walking velocity is far lower than in sequences 7 and 8. For higher densities the walking velocities of pedestrians in sequences 5 and 7 are on average equal.

Parallel to the density and velocity histograms, a difference in behaviour is also visible in the fundamental diagrams. However, the site is the same and the pedestrians are similar. It is hypothesized that the difference in behaviour is rooted in the schedule of the festival. Sequence 5 was recorded while all concerts were ongoing, while sequences 7 and 8 are recorded in between concerts. The lower walking velocities might be explained by the natural tendency of people to walk slower when they have no direct goal in mind (given the fact that the footage was taken during a performance).

The velocity results, density results and the fundamental diagrams showed that the proposed technique produces usable pedestrian movement data. Therefore it can be concluded that footage recorded by UAV can be used to capture pedestrian crowd

Fig. 13 Fundamental diagram (velocity-density relation) – sequence 5

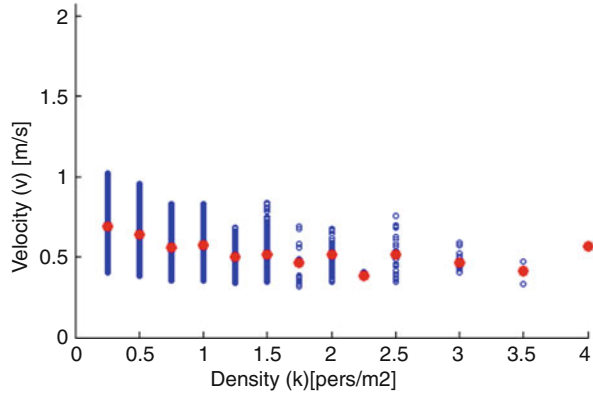
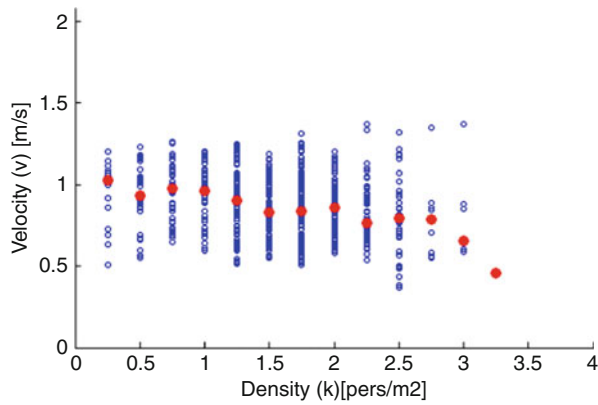


Fig. 14 Fundamental diagram (velocity-density relation) – sequence 7



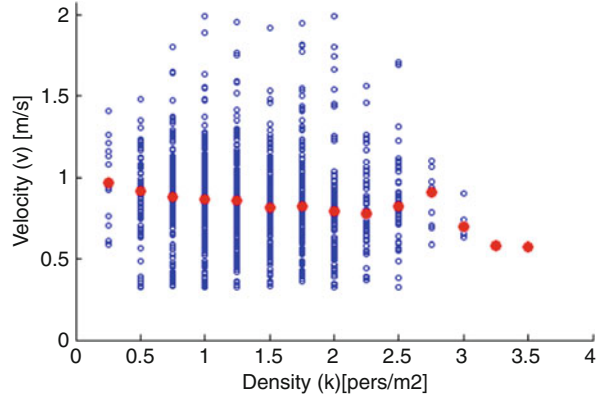
movements. It can furthermore be concluded that the proposed chain of software does allow the footage to be interpreted.

5.3.1 Uncertainties

Figures 13, 14, and 15 show that the scatter within the plots is quite large. This scatter is partly due to the natural heterogeneity in pedestrian movement, but also partly due to measurement uncertainties. This second source of noise is introduced by a combination of still present slight movements in the stabilized footage, slight misinterpretations in the tracking technique and misdetection during the tracking phase. However, because lots of pedestrians have been detected and tracked the large amount of data points allows us to draw conclusions about pedestrian high density crowd behaviour.

Due to a combination of unstable stabilized footage and several tracking errors, uncertainties are introduced in the velocity calculation. Based upon the movement estimations of stationary pedestrians the remaining uncertainty in the velocity

Fig. 15 Fundamental diagram (velocity-density relation) – sequence 8



calculation was estimated to be about 0.1 m/s. For walking movements (where the average velocity is 1.00 m/s) this uncertainty is quite high.

Furthermore during the manual detection of pedestrians in very dense crowds errors are made ($< 1 P/m^2$).

Both errors introduce a deformation of the fundamental diagrams found. The uncertainty in the density calculations is expected to be of more influence on the lower end of the density scale. While the uncertainty in the velocity calculation is randomly distributed over all points.

6 Conclusion

This research assessed a new recording and analysis tool. It is found that the UAV recording method can indeed be used to study pedestrian crowd movements. Since the method captures areas with large dimensions, this method is uniquely equipped to record pedestrian crowd motions. However, the developed software is very sensitive to scaling and rotations of the recorded footage. Therefore, it is also concluded that the UAV, because it vibrates, rotates and translates, is not the most stable equipment available to record footage. But because the UAV can reach great heights, can respond quickly to commands from the ground and has a recording installation that is easily adaptable, it is a piece of equipment that can certainly help to improve the understanding of crowd movements.

The footage recorded using the UAV equipped with a HDHS camera can currently not be stabilized entirely. Therefore, slow processes ($v < 1$ m/s) recorded from great heights (> 50 m) proof reasonably good (but not impossible) to analyze automatically with the developed chain of software programs. It can therefore be concluded that the developed chain of software programs provides a basic tool for moving object (i.e. pedestrian) analysis of footage with limited information per pedestrian, as long as the raw footage is reasonably stable.

The robustness of the UAV equipment is currently inadequate, thereby making the UAV recording technique currently less suitable for the crowd management practice. The UAV recording technique is however very easy to implement. When one has the luxury to use a generator and multiple batteries (and do not need continuous eyes in the air), the UAV recording technique is a footage recording technique to take into consideration. Besides pedestrian movements, the UAV recording method can also be used to record other moving ‘object’ phenomena where a large recording area is important.

The stability of the recordings currently influences the precision of the data analysis in a negative manner. This can be improved by means of better stabilization software. The combination of Image tracker and the MODT tool allows for a next step in pedestrian crowd research. Next to pedestrian research, the MODT tool is especially designed to track objects about which limited information (<20 pixels per object) is available, that have a distinctive colour with respect to their immediate background, have variable surface areas throughout the footage and have unrestricted motion.

References

1. Ando, K., Ota, H., Oki, T.: Forecasting the flow of people (in Japanese). *Railway Research Review*: vol. 45, nr. 48, 14–48 (1988)
2. Daamen, W., Hoogendoorn, S.P.: Capacity of Doors during Evacuation Conditions. *Procedia Engineering*. vol. 3, 53–66 (2010)
3. Duives, D. C. Analysis of Pedestrian Crowd Movements at Lowlands. MSc., Delft University of Technology. (2012)
4. Helbing, D., Johansson, A., Al Abideen, H.Z.: The dynamics of crowd disasters: an empirical study. *Physics Review Part E*: vol. 75, 046109 (2007)
5. Hoogendoorn, S. P., Daamen, W., Bovy, P.: Extracting Microscopic Pedestrian Characteristics from Video Data. *Transportation Research Board 2003 Annual Meeting*. (2003).
6. Knoppers, P., Lint, H. van, Hoogendoorn S.P.: Automatic Stabilization of Aerial Traffic Images. *Proceedings of TRB 2012*. (2012)
7. Kratz, L., Nishino K.: Anomaly detection in extremely crowded scenes using spation-temporal motion pattern models. *Computer Vision and Pattern Recognition*. 1446–1453 (2009).
8. Kretz, T., Hengst, S., Vortish P.: Pedestrian Flow at bottlenecks - validation and calibration of VISSIM’s social force model of pedestrian traffic and its empirical foundations, 3rd Int. symposium on Transport Simulation. Queensland, Australia, Monash University (2008)
9. Navin, F.P.D., Wheeler, R.J.: Pedestrian Flow Characteristics. *Traffic Engineering*. vol. **39**, 30–36 (1969)
10. Predtetschenski, W.M., Milinski, A.I.: *Personenströme in Gebäuden*. Berlin, Staatsverslag der Deutschen Demokratischen Republik. (1971)
11. Seyfried, A., Steffen, B., Klingsch, W., Boltes, M.: The fundamental diagram of pedestrian movement revisited. *Journal of Statistical Mechanics: Theory and Experiment*. vol. 10, P10002 (2005)
12. Spengler, M., Schiele, B., Toward robust multi-cue integration for visual tracking. *Machine vision and applications*. vol. 14, no. 11, 50–58 (2003)
13. Sun, D., Roth, S., Black, M.J.: Secrets of Optical Flow Estimation and Their Principles. *Computer Vision and Pattern Recognition (CVPR)*. 2432–2439 (2010)

14. Sun, D., Roth, S., Lewis, J.P., Black, M.J.: Learning Optical Flow. LNCS: vol. 5304, pp. 5383–5397 (2008)
15. Thompson, P., Marchant, E.: A computer model for the evacuation of large building population. *Fire Safety Journal*. vol. 24, 131–148 (1995)
16. Turner, F. S. P.: Preliminary planning for a new tube railway across London. *Prod. Institution of Civil Engineers*: 19–38 (1959)
17. Yin, J. H., Velastin, S.A., Davies, A.C., Image processing techniques for crowd density estimation using a reference image. *Second Asian Convergence on Computer Vision*. (1995)

An Experimental Study on the Correlation Between “Attachment to Belongings” “Pre-movement” Time

Marco D’Orazio and Gabriele Bernardini

Abstract Many studies show that people carry out activities not directly connected with the evacuation after hearing a fire alarm. In this study we analyze the behavior of two groups of students in a Faculty of Engineering, following the activation of a fire alarm. The study shows that in these types of buildings, due to the fact that students are involved in activities with electronic devices, “pre-movement times” are very high and are strongly influenced by users’ attachment to their belongings. In particular this study allows the distribution of pre-movement time and the speed of people during the evacuation to be calculated.

Keywords Evacuation • Fire safety • Pre-movement time • Movement-time • Public buildings

1 Introduction

Several studies have been conducted in the past on social and environmental factors that influence the “evacuation time” of a building during a fire [1–5]. A review of these studies was conducted recently by Kobes et al. [6].

D. Helbing [7, 8] describes such behavior in terms of attractive and repulsive social forces that lead individuals to achieve their goal (evacuation time) on the basis of interactions with other people and the environment. This can be represented as the equation of motion as shown in Eq. 1.

$$m' \cdot \frac{d\vec{v}}{dt} = \vec{F}_{obj}(t) + \vec{F}_{ij}^{rep} + \vec{F}_{iW}^{rep} + \vec{F}_{swarm} + \vec{F}_{swarm}^p + \varepsilon \quad (1)$$

M. D’Orazio (✉) • G. Bernardini
DICEA Department, Università Politecnica delle Marche, via di Brece Bianche,
Ancona 60131, ITALY
e-mail: m.dorazio@univpm.it; inmedioshostes@hotmail.com

Where:

m' = people mass;

$\frac{d\vec{v}}{dt}$ = acceleration;

$\vec{F}_{obj}(t)$ = force that pushes the individual to their aim (evacuation);

\vec{F}_{ij}^{rep} = repulsion force which expresses the fact that moving people tend to keep a certain distance from each other;

\vec{F}_{iW}^{rep} = repulsion force which expresses the fact that moving people tend to keep a certain distance from obstacles;

\vec{F}_{swarm} = alignment, cohesion and repulsion force that occur when individuals move in groups;

\vec{F}_{swarm}^p = force that reflects the fact that the “psychology” of people changes from “individual psychology” to “collective psychology” as the density of the group increases;

ε = gaussian noise related to accidental variations.

Although this formulation is generally recognized, and used for commercial and research software Lizhong et al. [9], Zheng et al. [10], Ko et al. [11], showed that before people really move there is a phase (after the time to detect the fire and alert the occupants) called “pre-movement”, where they perform actions preliminary to moving Shen [12]: they try to interpret any information received about the dangers by interacting with other individuals present too Nilsson e Frantzich [13]; they are wait for other people; they try to retrieve things to which they are attached .

Analyses carried out on people’s behavior during previous incidents Proulx [4], show that this phase delays the evacuation and that it has contributed to numerous deaths [14–16].

Purser e Bensilum [14] analyze in detail the behavior of people during this phase in a series of fires. On the basis of their analysis, these authors show how the pre-movement process can be divided into two stages: “recognition” (when people try to interpret any information received) and “response” (when people carry out activities prior to evacuation).

Since the “pre-movement time” strongly influences the overall evacuation time [1], several experiments have been conducted with the aim to quantify this value in offices [17], stores [18], hotels [19], cinema and theaters [20], schools [21–23], flats [24]. On the basis of experimental data, Purser e Bensilum [14] report the average response time for the “recognition” and “response” phases in different types of building. In particular, they show an average time ranging between 0.03 and 1.05 (decimal minutes) for the “recognition phase” and between 0.13 and 0.67 (decimal minutes) for the “response phase”. The maximum “pre-movement” time measured in experiments is 3.92 decimal minutes for a theater (from the voice announcement).

However, the data reported by Purser e Bensilum [14] show a wide dispersion, depending on the type of building and on the activities in which the people are engaged [25]. In fact, some authors agree that, although the “pre-movement time” could be exemplified as an explicit value, it is a random variable following some kind of probability distribution.

Purser e Bensilum [14] suggest a unimodal distribution characterized by a positive skewness. Normal and lognormal distributions are also given.

Finally, studies by various authors agree in highlighting how the “pre-movement” time can vary significantly depending on the type of building and the activities in which people are engaged [26]. Furthermore, the authors show that the “pre-movement” time could be significantly influenced by the phenomena of “attachment to people” (waiting to be reunited with family members and friends) and “attachment to things” [10]. Although the latter (“attachment to things”) is recognized to be a major cause of delay in people’s movement in the event of evacuation this aspect has not yet been sufficiently investigated, as indicated by Kobes et al. [6]. This is a security issue not only for elderly people or for people with disabilities but for every man or woman. Therefore it was considered necessary to further investigate this issue by conducting a simulated evacuation experiment in university classrooms. University classrooms are places where this phenomenon could be important. In fact current teaching methods make increasing use of these devices in classrooms and, therefore, the evacuation of a school building may be strongly affected by this factor. In the experiment we evaluated the influence of “attachment to things”, in particular to electronic devices (notebooks, tablets) that are now commonly used in these environments for educational activities. The results are compared with previous studies conducted by Zhang et al. [23].

2 Phases, Materials and Methods

This study is based on the analysis of the evacuation time in two classrooms in the Faculty of Engineering at the “Università Politecnica delle Marche” (Italy). Usually in these classrooms, students attend lectures, study and do exercises that require the use of electronic devices (notebooks, tablets). The experimental work was conducted in two phases. The first phase consisted in gathering information through a questionnaire, about the hypothetical behavior that students would adopt during a fire-evacuation. The questionnaire was submitted to approx. 200 students while they were engaged in lectures in classrooms or in study activities in the university library (all submitted questionnaires were collected). In the second phase we conducted an experimental evacuation of two classrooms (not simultaneously) without giving the students any prior warning. The students who participated in the experiment were enrolled on two different degree programs and were in the age range 19–24 years. At the time of the experiment, there were 42 students in classroom 155/D3 and 62 in classroom 140/5. No people with disabilities were present, so we have to expect an high motion speed. Table 1 shows the dimensions of the two classrooms used for the experiment.

Figure 1 shows the plan of the two classrooms.

In order to determine the pre-movement time and to calculate the people’s movement speed three cameras were set up for each classroom. Two cameras were

Table 1 Classroom dimensions and characteristics

Experiment	Class-room	Width [m]	Length [m]	Corridors length [m]	Width tables [m]	Distance between seats [m]	Area [m ²]	Seats [-]	Width emergency exit [m]
A	155/D3	8.95	12.65	1.20	0.55	0.60	111.6	68	1.50
B	140/4	9.45	18.40	1.20–1.90	0.55	0.60	168.8	98	1.60

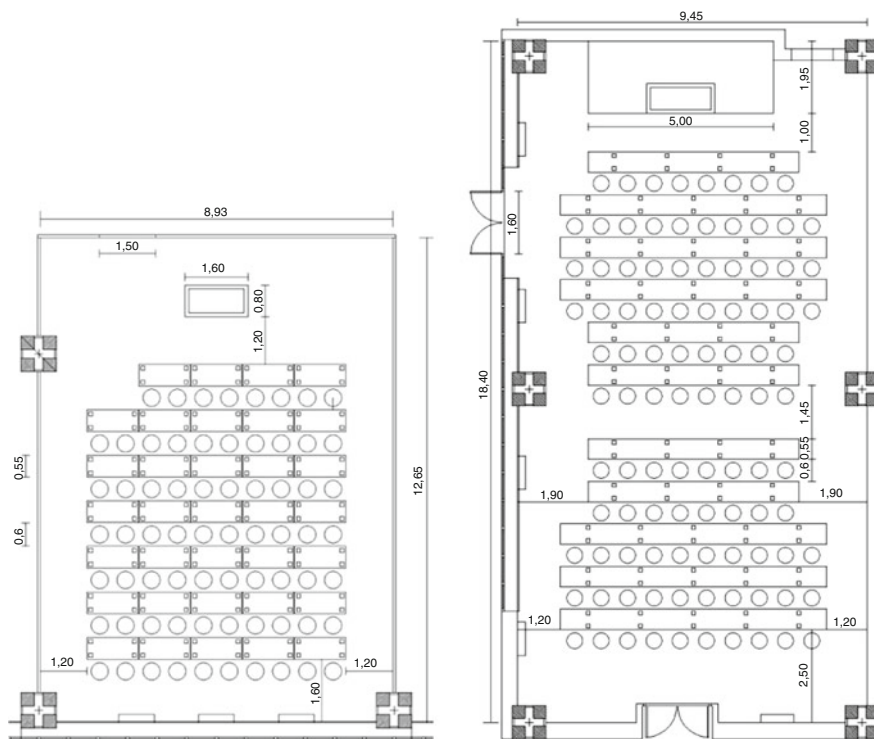


Fig. 1 Plans of classrooms 155/D3 and 140/5

Table 2 Distribution of students in the classroom

Experiment	People	Gender		Classroom
		Male	Female	
A	42	16 (38 %)	26 (62 %)	155/D3
B	62	33 (53 %)	29 (47 %)	140/4

put in each classroom in two opposite corners while the third was positioned outside the exit in order to reconstruct the time needed to evacuate the room. Table 2 summarizes information about the people present in the classrooms who participated in the experiment.

At the sound of the alarm bell, the lecturer asked the students to follow the proper evacuation procedures. They were asked to stand up and to walk out of the room.

Table 3 Students’ response to the questionnaire

Questions/room		Classroom 155 (%)	Classroom 140 (%)	Library (%)	Mean (%)	St.dev. (%)
Have you conducted in the past a fire emergency evacuation?	Yes	33	32	7	24	15
What would you do after hearing the alarm bell?	Nothing	67	68	93	76	15
	I would go immediately to the exit	10	9	29	16	11
	I collect the things that belongs to me then i go to the exit	21	35	32	29	7
	I act like other people	67	45	32	48	18
Do you wait for other people before going to exit?	I continue to study	2	11	7	7	5
	Yes	52	26	30	36	14
How much time do you spend usually in this room?	No	48	74	70	64	14
	1 or 2 h	–	–	15		
	4 h	–	–	42		
	All the day	–	–	43		

The analysis of the films and the trajectories of all the students has allowed us to observe the behavior of students and to obtain “pre-movement” and “movement” time.

3 Declared Behavior

Table 3 shows the results of the questionnaire given to students a few weeks before the experiments. The questionnaire was provided in order to collect information about the type of behavior that the students would hypothetically adopt in a similar case (fire-evacuation).

Analyzing the data collected, we noted that only 24 % of the subjects stated that they had previously been in a similar situation (real fire emergencies and/or evacuation connected to false alarms). However, there appear to be differences in the responses depending on the group considered. With regard to the behavior declared during the evacuation (question 2) the responses were more uniform. More than 90 % of the students said that they would behave like the others (sense of belonging to a group) and retrieve their things first (attachment). Only 10 % of the sample stated that they would leave the building immediately. This behavior can be explained by the response to question 6. Over 93 % of the students (in the two classrooms) use personal electronic devices and therefore in the event of a fire they

Table 4 Basic statistics for the variables “Pre-movement time”, “Movement time”, “Total Time”, “Velocity”

Data	Premovement time [s]	Movement time [s]	Total time [s]	Velocity [m/s]
Minimum	5.6	4.6	12.2	0.35
Maximum	71.4	34.2	81.5	2.17
Median	21.6	14.2	40.9	0.84
Arithmetic mean	25.9	15.5	41.4	0.92
Standard deviation	15.8	6.7	15.4	0.33
Skewness (G1)	1.0	0.8	0.4	0.98

would not leave this type of instrumentation in the classroom because of the effect that the loss of these tools, and the data stored on them, would have on their future activities.

4 Observed Behavior in a Classroom Evacuation Experiment

Subsequently, as previously mentioned, we carried out an evacuation experiment for the two classrooms. The experiment confirmed the typical behavior already described by D. Helbing [8].

Table 4 presents a summary of the data collected. The pre-movement time was significantly greater than the exit time (the time required to leave the classroom). In particular, we found a different value per person, going from a minimum of 5.6 s to a maximum of 71.4 s. This maximum value corresponds to students who, during the evacuation, returned to the room to collect their belongings. The average “pre-movement” time was 21.6 s. The movement time was between 4.6 and 34.2 s.

Figure 2 shows the distribution of the pre-movement times for the two classrooms. The distributions are similar (weibull) to those reported by Purser e Bensilum [14]. Nevertheless some differences (skewness) can be seen which are presumably due to the different sizes of the classrooms and to a “queue”, with values of over 40 s. This was caused by the fact that some students in classroom 140/5 initially moved towards the exit but then went back into the room in order to collect their personal belongings.

Figure 3 shows the results of the qualitative correlation of the values measured. It is interesting to note that the total motion time in this case appears to be more related to the “pre-movement” time than to real time motion. This highlights how the actions that people carry out before moving have a greater impact on evacuation time than the speed at which they then proceed during the evacuation.

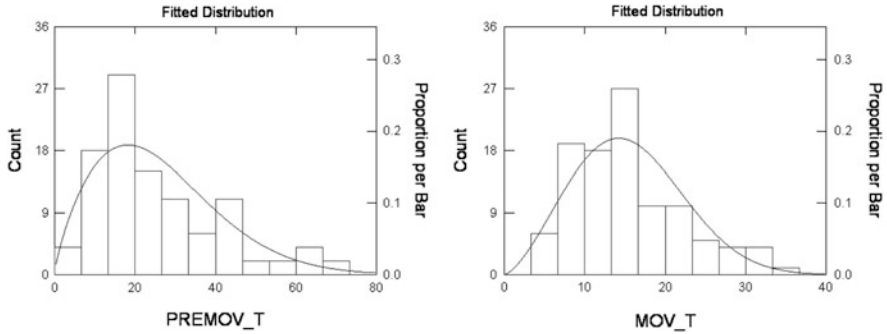


Fig. 2 Pre-movement time distribution, classrooms 140/5 and 155/D3

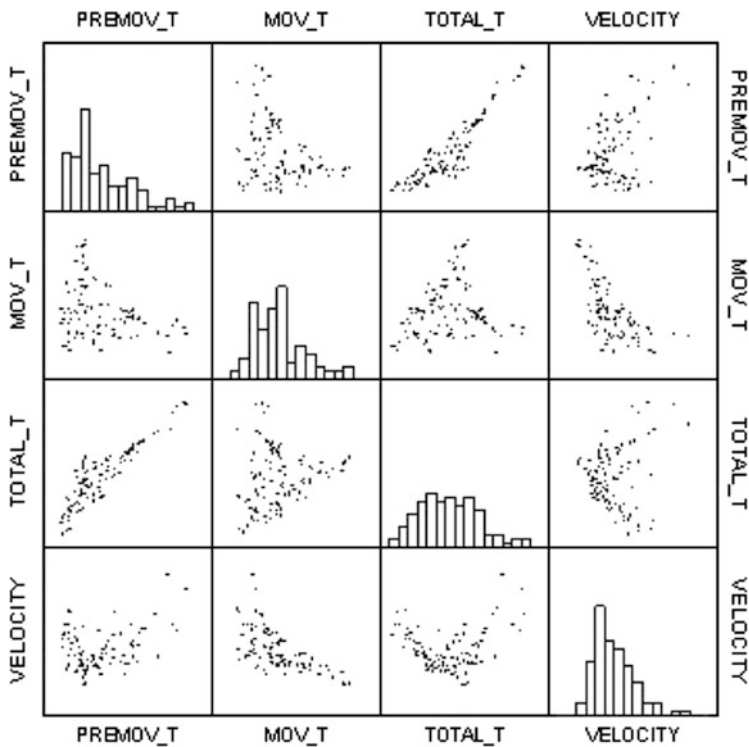
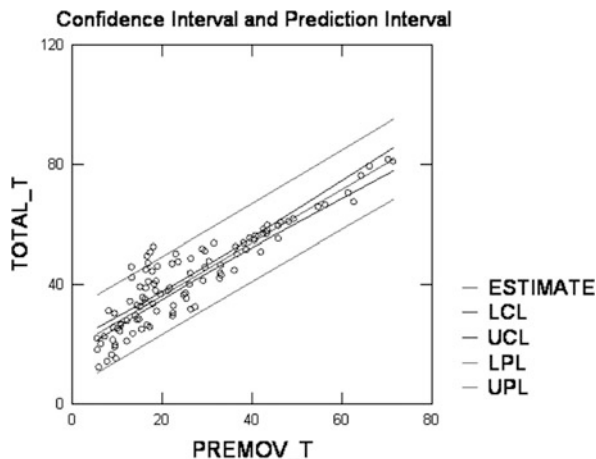


Fig. 3 Analysis of the correlation between the values measured for classrooms 140/5 and 155/D3 (premovement-time, movement-time, total evacuation time, velocity)

Figure 4 shows the results of the least squares regression for the variables “pre-movement” time and “total movement” time and the limits of the confidence intervals. It is possible to observe a high degree of correlation with a value of $R^2 = 0.82$. Greater dispersion of data is observed for low values of “pre-movement”

Fig. 4 Pre-movement times measured for classrooms 140/5 and 155/D3



and “total movement” time. This highlights, as reported below, how, after a fire alarm, some students behave as “individuals” and do not interact with the others. Moreover they do not stay in the classroom to retrieve their belongings.

Figure 5 completes the analysis of the experimental data. This figure shows the distribution of velocities detected in experiments A (classroom 140/5) and B (classroom 155/D3) divided by gender (male/female). It can be seen that the average speed recorded is about 0.95 m/s, with slight differences between males and females. This average speed value is lower than data found in literature as average speed under “normal” conditions, but it’s high if compared with average speed values reported for educational buildings (0.25–0.33 m/s) or generic public places (0.5–0.7 m/s) [27].

However it is necessary to consider that a number of factors can have an impact on the speed of movement, including the characteristics of the occupants, such as age, gender, grouping, clothing and physical ability [28]. All people involved in experimental activity were young and with good physical ability. In fact if we compare our results with Fahy R.F. [27] regarding average speed values found in experiments conducted in hotel corridors (with able-bodied participants – during daytime) we can find similar results.

5 Reasons for Pre-movement Time

In order to understand the reasons for these results we analyzed the photographs taken during the evacuation. After the fire alarm, with no distinction between the two classrooms, all of the students, first spent most of the time in activities not connected with the evacuation. In particular students (those with the shortest “pre-movement time”), hesitated by interacting with each other in order to understand what to

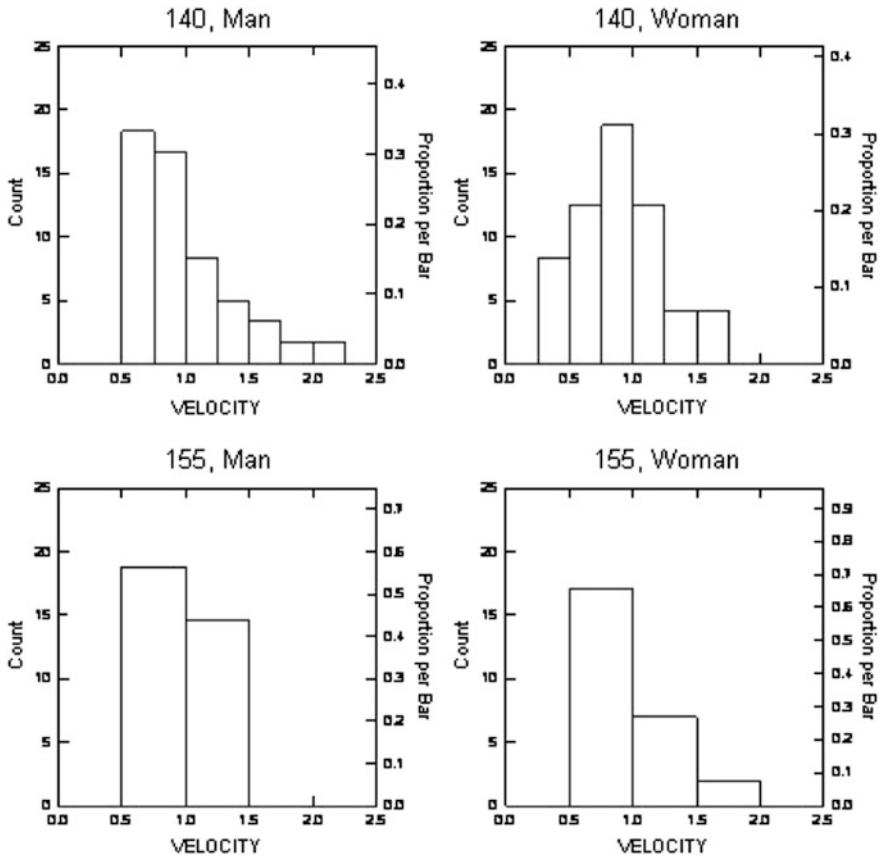


Fig. 5 Distribution of velocities detected in the two experiments, A (room 140/5) and B (classroom 155/D3) divided by gender (male/female)

do [6] as shown in Fig. 6a. In addition, many students considered it necessary to dedicate time to saving data and retrieving personal electronic devices. In particular we noticed an increased “pre-movement” time with respect to literature, caused by saving files, turning off and putting away electronic devices (notebooks, tablets).

It is interesting to notice that, while in literature the minimum “pre-movement” time observed is approximately 1 s, in our case the first student moves only after 9–11 s (depending on the experiment).

Figure 6b also shows the queue during the evacuation. It is clear that some students are still engaged in extremely slow data-rescue operations and the collection of their belongings.

It is interesting to note that students who have spent time saving data and turning off their PCs have, in fact, blocked the exit (Fig. 7a, b), thereby slowing down the movement of the other students and forcing them to leave from the opposite side of the room.



Fig. 6 Photograph from the video recording (**a**: 9 s, **b**: 49 s). It is possible to see (**a**: *left*) the presence of people who are asking each other what to do and who are interacting with their PC, (**b**: *right*) the movement of people along the evacuation route

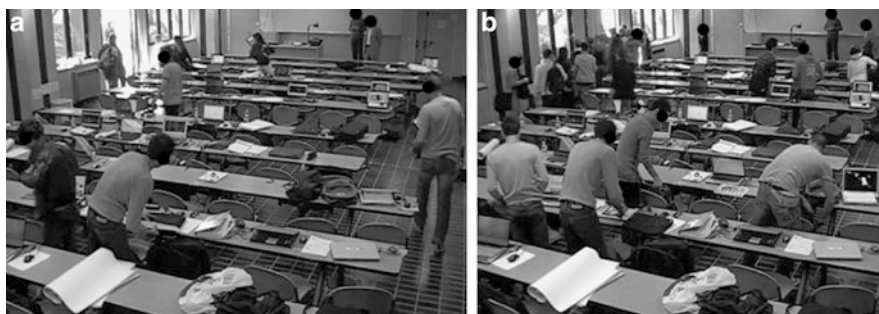


Fig. 7 Photograph from the video recording. It is possible to observe people (**a**: *left*; **b**: *right*) engaged in saving data and retrieving electronic devices

Conversely, some students seated in the most external rows near the exit, in addition to being facilitated by their location, minimized the time to recover their belongings. Moreover, these students behaved as “individual entities”, without any social interaction with the others. Similar behavior was also found for classroom 140/5.

We observe in conclusion that the attention dedicated by students to saving data and personal electronic devices was particularly high (attachment to belongings). In classroom 140/5, 57 students (of the 62 present), equivalent to 92 %, were using personal electronic devices at the time of the evacuation.

After the evacuation 20 electronic devices, 35 % of the total, were left in the classroom. Therefore 65 % of the students secured their electronic devices, after saving the data. A similar situation was found in classroom 155/D3. In this case, 40 of the 42 students present, i.e. 95 %, were using electronic devices at the time of the evacuation. Only 22 electronic devices were left in the classroom after the evacuation, therefore 45 % of the students saved their electronic devices.

6 Conclusions

The study confirmed the behavior reported in the literature characterizing the initial stages of evacuation in the event of fire. In particular, we detected, as described in literature, the existence of a “recognition phase” and a “response phase” (in which individuals perform preparatory work: turning off electrical equipment, etc.).

In particular we show how these activities, at universities, because of the introduction of teaching methods that use personal electronic devices, affect the “pre-movement” time and also represent an obstacle for the rapid evacuation of students who did not wish to proceed before saving their data and tools. Specifically, we confirm that the “pre-movement time” measured can be described by a Weibull-type distribution with a positive skewness. Results regarding average speed during evacuation differ slightly from literature data. But it is necessary to consider that all people involved in experimental activities were young and without disabilities and that in the space visibility was good during evacuation.

References

1. Canter, D., 1980. Fires and human behaviour. J. Wiley. ISBN 9780471277095.
2. Sime, J. D., 1995. Crowd psychology and engineering. *Safety Science*, 21(1):1–14. ISSN 0925-7535. doi:DOI: [10.1016/0925-7535\(96\)81011-3](https://doi.org/10.1016/0925-7535(96)81011-3).
3. Guylene and Proulx, 1993. A stress model for people facing a fire. *Journal of Environmental Psychology*, 13(2):137–147. ISSN 0272-4944. doi:[10.1016/S0272-4944\(05\)80146-X](https://doi.org/10.1016/S0272-4944(05)80146-X).
4. Proulx, G., 2002. Movement of People: The Evacuation Timing, in *SFPE Handbook of Fire Protection Engineering*. 3. National Fire Protection Association.
5. Guanquan, C. and Jinhua, S., 2006. The effect of pre-movement time and occupant density on evacuation time. *Journal of Fire Sciences*, 24(3):237–259. doi:[10.1177/0734904106058249](https://doi.org/10.1177/0734904106058249).
6. Kobes, M., Helsloot, I., de Vries, B., and Post, J. G., 2010. Building safety and human behaviour in fire: A literature review. *Fire Safety Journal*, 45(1):1–11. ISSN 0379-7112. doi:DOI: [10.1016/j.resaf.2009.08.005](https://doi.org/10.1016/j.resaf.2009.08.005).
7. D. Helbing, T. V., I Farkas, 2000. Simulating dynamical features of escape panics. *Nature*, (407):487.
8. D. Helbing, T. V., I Farkas, 2009. Social force model for pedestrian dynamics. *Phys.Rev.*, E(51):42–82. 10
9. Lizhong, Y., Weifeng, F., and Weicheng, F., 2003. Modeling occupant evacuation using cellular automata - effect of human behavior and building characteristics on evacuation. *Journal of Fire Sciences*, 21(3):227–240. doi: [10.1177/0734904103021003004](https://doi.org/10.1177/0734904103021003004).
10. Zheng, X., Zhong, T., and Liu, M., 2009. Modeling crowd evacuation of a building based on seven methodological approaches. *Building and Environment*, 44(3):437–445. ISSN 0360-1323. doi:DOI: [10.1016/j.buildenv.2008.04.002](https://doi.org/10.1016/j.buildenv.2008.04.002).
11. Ko, S., Spearpoint, M., and Teo, A., 2007. Trial evacuation of an industrial premises and evacuation model comparison. *Fire Safety Journal*, 42(2):91–105. ISSN 0379-7112. doi:DOI: [10.1016/j.resaf.2006.07.001](https://doi.org/10.1016/j.resaf.2006.07.001).
12. Shen, T.-S., 2006. Building egress analysis. *Journal of Fire Sciences*, 24(1):7–25. doi:[10.1177/0734904106052549](https://doi.org/10.1177/0734904106052549).
13. Nilsson, D. and Frantzich, H., 2010. Design of voice alarms.the benefit of mentioning fire and the use of a synthetic voice. In S.-V. B. Heidelberg, editor, *Pedestrian and evacuation dynamics 2008*. doi:[10.1007/978-3-642-04504-2_10](https://doi.org/10.1007/978-3-642-04504-2_10).

14. Purser, D. A. and Bensilum, M., 2001. Quantification of behaviour for engineering design standards and escape time calculations. *Safety Science*, 38(2):157–182. ISSN 0925-7535. doi:DOI: [10.1016/S0925-7535\(00\)00066-7](https://doi.org/10.1016/S0925-7535(00)00066-7).
15. McConnell, N., Boyce, K., Shields, J., Galea, E., Day, R., and Hulse, L., 2010. The uk 9/11 evacuation study: Analysis of survivors' recognition and response phase in wtc1. *Fire Safety Journal*, 45(1):21–34. ISSN 0379-7112. doi:DOI: [10.1016/j.firesaf.2009.09.001.11](https://doi.org/10.1016/j.firesaf.2009.09.001.11)
16. Kuligowski, E. D. and Mileti, D. S., 2009. Modeling pre-evacuation delay by occupants in world trade center towers 1 and 2 on September 11, 2001. *Fire Safety Journal*, 44(4):487–496. ISSN 0379-7112. doi:DOI: [10.1016/j.firesaf.2008.10.001](https://doi.org/10.1016/j.firesaf.2008.10.001).
17. Oven, V. and Cakici, N., 2009. Modelling the evacuation of a high-rise office building in Istanbul. *Fire Safety Journal*, 44(1):1–15. ISSN 0379-7112. doi:DOI: [10.1016/j.firesaf.2008.02.005](https://doi.org/10.1016/j.firesaf.2008.02.005).
18. Shields, T. J. and Boyce, K. E., 2000. A study of evacuation from large retail stores. *Fire Safety Journal*, 35(1):25–49. ISSN 0379-7112. doi:DOI: [10.1016/S0379-7112\(00\)00013-8](https://doi.org/10.1016/S0379-7112(00)00013-8).
19. Kobes, M., Helsloot, I., de Vries, B., and Post, J., 2010. Exit choice, (pre-) movement time and (pre-)evacuation behaviour in hotel fire evacuation - behavioural analysis and validation of the use of serious gaming in experimental research. *Procedia Engineering*, 3:37–51. ISSN 1877-7058. doi:DOI: [10.1016/j.proeng.2010.07.006](https://doi.org/10.1016/j.proeng.2010.07.006). 1st Conference on Evacuation Modeling and Management.
20. Nilsson, D. and Johansson, A., 2009. Social influence during the initial phase of a fire evacuation - analysis of evacuation experiments in a cinema theatre. *Fire Safety Journal*, 44(1):71–79. ISSN 0379-7112. doi:DOI: [10.1016/j.firesaf.2008.03.008](https://doi.org/10.1016/j.firesaf.2008.03.008).
21. Sime, J., 1988. *Safety in the built environment*. E. & F.N. Spon. ISBN 9780419144809.
22. Liu, S., Yang, L., Fang, T., and Li, J., 2009. Evacuation from a classroom considering the occupant density around exits. *Physica A: Statistical Mechanics and its Applications*, 388(9):1921–1928. ISSN 0378-4371. doi:DOI: [10.1016/j.physa.2009.01.008.12](https://doi.org/10.1016/j.physa.2009.01.008.12)
23. Zhang, J., Song, W., and Xu, X., 2008. Experiment and multi-grid modeling of evacuation from a classroom. *Physica A: Statistical Mechanics and its Applications*, 387(23):5901–5909. ISSN 0378-4371. doi:DOI: [10.1016/j.physa.2008.06.030](https://doi.org/10.1016/j.physa.2008.06.030).
24. Guylene and Proulx, 1995. Evacuation time and movement in apartment buildings. *Fire Safety Journal*, 24(3):229–246. ISSN 0379-7112. doi: [10.1016/0379-7112\(95\)00023-M](https://doi.org/10.1016/0379-7112(95)00023-M).
25. Liu, M. and Lo, S., 2011. The quantitative investigation on people's preevacuation behavior under fire. *Automation in Construction*, In Press, Corrected Proof:-. ISSN 0926-5805. doi:DOI: [10.1016/j.autcon.2010.12.004](https://doi.org/10.1016/j.autcon.2010.12.004).
26. Augustijn-Beckers, E.-W., Flacke, J., and Retsios, B., 2010. Investigating the effect of different pre-evacuation behavior and exit choice strategies using agent-based modeling. *Procedia Engineering*, 3:23–35. ISSN 1877-7058. doi:DOI: [10.1016/j.proeng.2010.07.005](https://doi.org/10.1016/j.proeng.2010.07.005). 1st Conference on Evacuation Modeling and Management.
27. Fahy R.F., P. G., 2001. Toward creating a database on delay times to start evacuation and walking speeds for use in evacuation modeling. In 2nd International Symposium on Human Behaviour in Fire, pages 175–183.
28. Kady, R. A. and Davis, J., 2009. The impact of exit route designs on evacuation time for crawling occupants. *Journal of Fire Sciences*, 27(5):481–493. doi: [10.1177/0734904109105320](https://doi.org/10.1177/0734904109105320).

Bottlenecks in Evacuation Design Considering Both Structural and Human Behavioural Aspects: An Experimental Study

Tuomo Rinne, Timo Korhonen, and Peter Grönberg

Abstract Evacuation experiments were performed in February and in March 2012 in Finland. The first set of experiments was done at Aalto University, where 83 university students were used as test persons in a setup where counter flows in corridor was examined. The second and third sets of experiments were conducted in Kuopio, where the persons attending the tests were students of Finnish emergency services college and conscripts, in total 60 persons. These later tests included a geometry related to stairs, where fatigue, fire fighters' and normal people counter flows, and fire fighters' rescue operations in stairs are examined. Trials were also performed using different door geometries. Two other scenarios were conducted in corridors, where density of smoke, different lightning conditions, and counter flows are examined on both group and individual levels. The preliminary results of the test series without throughout statistical analysis are presented in this paper.

Keywords Evacuation • Counterflow • Spiral stairs • Smoke conditions • Specific flow

1 Introduction

Usually dimensioning problems in evacuation situations relate to bottlenecks, e.g., door geometries, stairs, merging flows, counter flows, and emergency rescue personnel operations. These issues can be demonstrated through fully controlled experimental set-ups. VTT is a coordinator in a project “Evacuation and rescue operations in fire conditions” that will produce experimental data in four different

T. Rinne (✉) • T. Korhonen • P. Grönberg
VTT Technical Research Centre of Finland, P.O. Box 1000, Espoo, VTT FI-02044, Finland
e-mail: tuomo.rinne@vtt.fi; timo.korhonen@vtt.fi; peter.gronberg@vtt.fi

scenarios and geometries. The first geometry relates to stairs, where fatigue, fire fighters' and normal people counter flows, and fire fighters' rescue operations in stairs are examined. The second trial will be performed using different door geometries, where the aim is to monitor how prone people are to form a new queue near the doors when selecting a doorway, how certain geometrical arrangements increase specific flows, and what is the effect of door opening forces and angles to the specific flows. Two other scenarios are conducted in corridors, where density of smoke, different lightning conditions, route selections and counter flows are examined on both group and individual levels. The instrumentation consists of normal DV-cameras, and sensors measuring angular acceleration and door opening forces, and physical stress of the fire fighters. In addition, questionnaires will bring more detailed information to explain individual data and behavioural phenomena.

Experiments were performed in March 2012 and the persons attending the tests were students of Finnish emergency services college and conscripts, in total 60 persons. Most of the test persons were males, aged 20–30 years old. Depending on the nature of the experiment, the group size varies from 15 to 40 persons. In addition, some of the tests were conducted on an individual level. The results will be published in the final report that is freely available on internet in the end of year 2012. The preliminary results of the test series without throughout statistical analysis are presented in this paper.

2 Case A: Visibility in a Corridor

The consequences a partial or total loss of visibility has on evacuation times and walking speed has been studied in many different contexts [1–6]. This includes varying aids for exit in the form of lights and signs, the presence of smoke and possible irritants, different levels of lighting, exit route topologies etc. Looking at the previous work and results in this field, a test series was planned to study the effect of a gradual loss of visibility due to an increase of smoke in a long corridor (39 m) that was a part of the exit route (Fig. 1).

The exit route was unknown for the people attending the test. Four groups performed the evacuation test only informed, that this was an evacuation drill and they were supposed to exit the premises by following exit signs. They were told that the evacuation would take place under conditions simulating an increasing level threat and they were motivated to try to exit even if they would observe signs of risk that normally would make them hesitant. All alternative exit routes were blocked, simulating the scenario and thus only one exit could be used.

The groups consisted of 10–12 persons who performed the test as individuals i.e. one by one. The perceived visibility in the test were maintained at levels of >40, 10–12, 5–7 and <1 m by using non-irritant white smoke. Lights and exit signs were used in all but the last test (visibility <1 m) where only the exit signs were used.

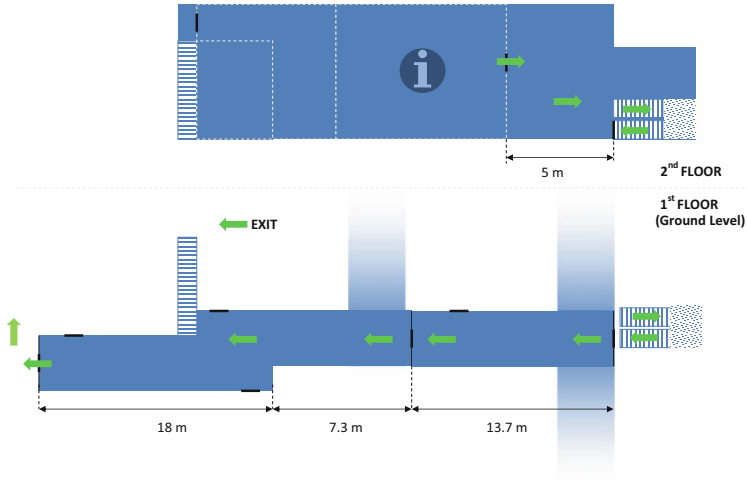


Fig. 1 The geometry used in the visibility test

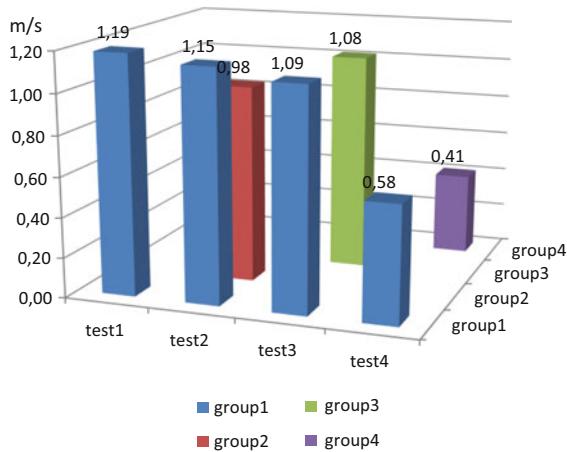


Fig. 2 Average walking speeds during test 1–4 for groups 1–4

Group 1 performed first the test with normal visibility level (only small amounts of smoke to illustrate “threat”). They then attended all the remaining test so by having prior knowledge of the exit route topology demonstrating the effect of familiarity of the building. Groups 2–4 only performed the corresponding tests 2–4 thus having no prior knowledge of the route or presentiment of the conditions they would observe during the test. Figure 2 presents the preliminary average walking speed results of the tests. The walking speed is an average over the 39 m distance on the ground level corridor (Fig. 1).

The course of the test was monitored visually, by cameras (normal and thermal imaging) and light gates. By this arrangement it will be possible to break up the different phases of the evacuation and to find explaining factors for occurring phenomena. People attending were also asked about how stressful they considered the test to be, by what means they did decisions and what aided their strategy of escape.

At the time of writing it is already possible to see that in the presence of no real danger (even though the stress factor of lack of knowledge, unfamiliarity with surroundings and decreasing visibility) and the motivation to “find the way out”

- The differences between tests with visibility of 10–12 m versus 5–7 m were not substantial as in this topology the persons could effectively see the side walls of the corridor (width 1.5–2.8 m) as a guidance for direction and the maintained average speeds of approx. 1 m/s gave them enough time to react to obstacles (corners and recesses). Never the less, the situation was considered to be more demanding and stressful.
- Loss of these means for orientation has a substantial effect on effective speed and evacuation time.
- Familiarity of the exit route yields consistency i.e. smaller deviations in the times and speeds during the evacuation.

A more thorough analysis of the phases and phenomena of the observed evacuation tests are under work at the time of writing.

3 Case B: Experiments in a Door Geometry

The evacuation situation itself affects the usage of doors, for example motivation has a clear role to subjects' behaviour [7]. In a technical point of view, the door geometry has its effective width, but also other features which contribute to the use of doors and specific flows. These include, for example, the door leaf opening angle and the torque needed to open the door leaf. Daamen and Hoogendoorn [8] have studied the effect of the door leaf. They noticed the decay observed in the flow was 20 % lower in the case where the door leaf was rotated 90° from the direction of movement compared to the case where there was no door leaf.

Gwynne et al. [9] discussed the dynamic door leaf concept. They found the door leaf to open about 50–80 % of total capacity. This was concluded to affect the people passing through the door opening. The torque related experiments have not been performed very much. One such study involved disabled people's ability to open the door with different opposed forces [10]. In all subjects through the door spend more time with higher opening force of (21 N . . . 70 N). Failures increased about 2 % . . . 5 % the higher the force was.

In our studies the door geometry related experiments are aimed at finding explanatory factors and the phenomena of the subjects' use of exit doors. In all, six experiments were conducted and one of these is represented in this paper.

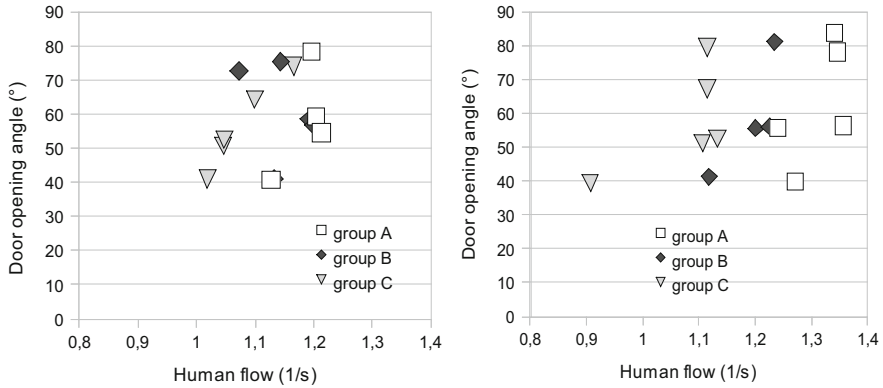


Fig. 3 Effective mean door opening angle versus human flow in scenarios, where subjects had to push (left side) and pull (right side) the door open

In the first configuration we examined the door leaf opening angle effect to specific flow (or human flow) and in the second test we studied the torque effect to the specific flow. The subjects were divided into three groups A, B, and C in DOOR6 experiment. The number of persons in groups was 17, 19, and 19, respectively. In all, 30 tests were conducted, in which 18 were door opening tests with increasing torque (first six with torque 30 Nm, the following 18 Nm, and the last 77 Nm; door opening was 90°). The rest 12 experiments were performed with different door opening angles (45° and 60°; torque 30 Nm). The door angle test data with 90° was taken from the first test series.

Each individual group (A, B, and C) walked through twice the door opening in one specific test scenario. First the group had to push the door leaf open and the second trial was conducted in opposite direction (meaning as pulling the door open). For example, the test scenario with 30 Nm torque was performed with three groups times two directions (in all six trials). The instrumentation was carried out using door leaf angular measurement, torque measurement (before tests, not during the actual tests), and digital video cameras on both sides of door.

Results of specific flows are shown in Fig. 3. As we can see, the human flow through the door opening decreases with decreasing door opening angle (in all 30 tests). Surprisingly, when subjects had to pull the door leaf the human flow values seem to be higher compared to case when pushing the door leaf. On the other hand, the data is more dispersed in the previous (“push”) case. The torque effect on the door opening angle can be seen in Fig. 4, where the results are quite natural to first expectations. The more the torque is the less the door leaf is opened during tests. This also affects the specific flows, because less free clear door width is present. (The plots below do not include the door opening trials with maximum opening angles 45° and 90°.)

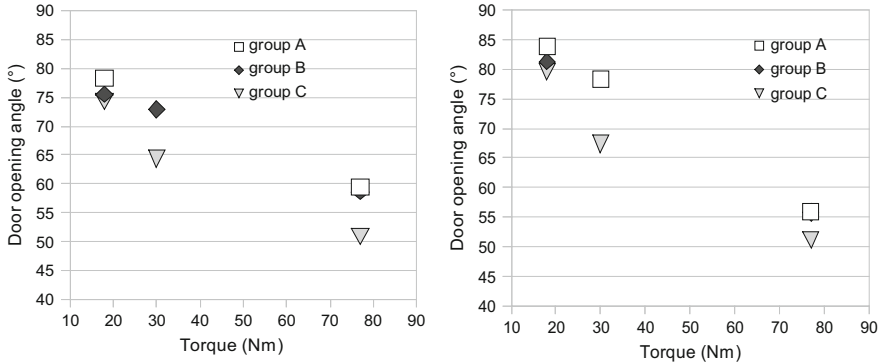


Fig. 4 Effective mean door opening angle versus torque of the door leaf in scenarios, where subjects had to push (*left side*) and pull (*right side*) the door open

4 Case C: Counterflow in a Corridor

A number of theoretical analyses have been published on pedestrian counterflow [10–13], but only a few sets of data of actual experiments are available [14, 15]. Isobe et al. [14] ran experiments with university students in a 12 m by 2 m corridor. Initially, the students were randomly located in the left and right half of the corridor. As the experiment started, the students in the right half tried to walk to the left end of the corridor and vice versa. Kretz et al. [15] ran counterflow experiments in a corridor in a different setting. While there was no space in between the groups of right walkers and left walkers in the initial setting of Isobe et al., Kretz et al. had the two groups standing 20 m apart each other. The flows measured by Kretz et al. were significantly faster than those of Isobe et al. Because both experiments were ran with university students, a likely reason for the difference is the settings of the experiments. The 20 m gap between the groups is significant, as the test persons are able to form lanes already before the two groups encounter, and thus, the encounter is much smoother.

For this reason, an experiment was planned which could test this hypothesis, i.e., the influence of the geometry and the ability of the persons to adjust their walking direction and speed to encounter the counterflow. The experiment took place in an intersection of two corridors where one part of the corridors was blocked by tables so that the test geometry formed a “L” shaped corner so that the groups going to different directions could not see each other before the counterflow situation at the corner, see Fig. 5. The experiments took place in February 2012 at the Aalto University School of Science and Technology at Espoo, Finland. A mixed-sex group of 83 undergraduate students participated in the experiments. In total, 16 trials with counterflow groups were carried out and a couple of “zero experiments” without any counterflow were also recorded in order to get the normal corridor speed of the sample population.

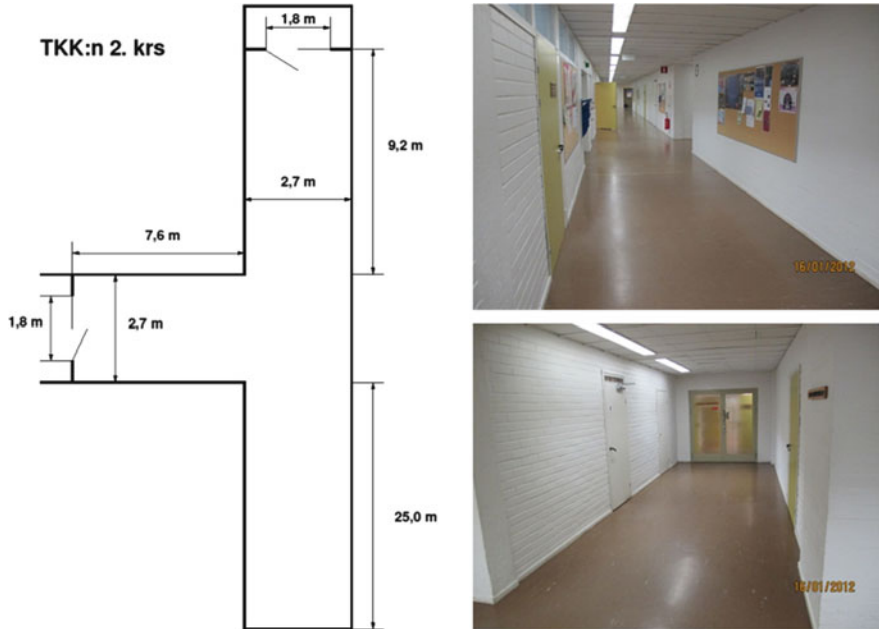


Fig. 5 The geometry used in the counterflow experiments. The *top* corridor was blocked with tables so just the horizontal and *bottom* part was used in the experiments, i.e., a “L”-shaped corridor was used. The photos on the *right hand side* are taken before the experiments showing the corridors as they are in daily use

The students were divided in the majority and minority groups. The majority group had always 35 students whereas the minority group had either four or eight students. The minority group had different objectives in different trials. They could have instructions to move as a “single person” or as a “small group”. If the order was to move as a small group then the minority persons should try to move together through the majority group, e.g., like family members. The minority students were randomly picked before there trials and for the first trials the minority group members were not used in the majority group, i.e., the minority group members waited their turn in a classroom and returned there after their trial, whereas the majority group was the same in each trials. At the midpoint of the trials, i.e., after the first 8 trials, the minority and majority group members were interchanged and the trials were duplicated in order to have more data for the statistical analysis. Due to the fact that there were only 83 students in total, some of the former minority group members were randomly picked to join the minority groups once again so that about 27 % had previous experience as a member of a minority group in the eight last trials (trials 9–16). Each trial lasted until all participants had passed the finish lines that also served as the starting lines for the opposing direction moving crowd. The trials were recorded with six digital video cameras located in the corridor.

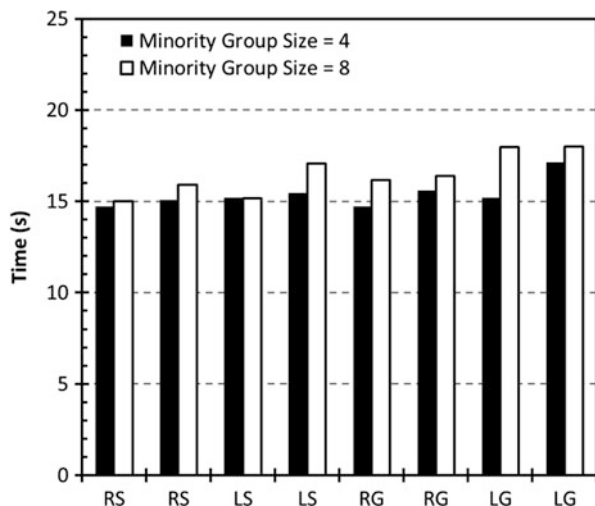


Fig. 6 The passing time of the majority group that had 35 members in each experiment. The first letter (*R*: right or *L*: left) of the horizontal axis labels refers to the turning direction of the majority group at the corner. The second letter refers to the motivation of the minority group members, *S* means as an individual and *G* as a member of a small group

From the recordings, the times from the whistle to the moment of the last person of the majority group to cross the finish line were recorded.

The first results of the performed experiments are summarized in Fig. 6, where the passing times for the majority groups are shown. The statistical analysis of the results is still going on and nothing can yet be said about the statistical significance of the findings. The passing time of the majority group for a right turn was on the average 15.5 s (st.dev. 0.7 s) for a left turn 16.4 s (st.dev. 1.3 s). The passing time of the majority group without any opposing minority group were 15.5 and 14.3 s for the trials for right and left turn, respectively, that were done before the counterflow trials in order to train the majority students. The motivation and the size of the minority group seem to have some effect on the passing times of the majority group. The passing times are longer for larger minority groups as expected and the minority group behavior might also make the passing times of the majority group slightly longer.

Acknowledgements This work has been funded and acknowledged by the Finnish Fire Protection Fund, the Ministry of the Environment, the Ministry of the Interior, Abloy Ltd., L2 Paloturvallisuus Ltd., and VTT Technical Research Centre of Finland. Karelia Air Command of the Finnish Defense Forces and the Finnish Emergency Services College are specially acknowledged for their help, person hours, and the use of the premises.

References

1. Frantzych, H., Nilsson, D., 2003. Utrymning genom tät rök: beteende och förflyttning. Department of Fire Safety Engineering, Lund University, Sweden, Report 3126.
2. Isobe, M., Helbing, D., and Nagatani, T., 2004. Experiment, theory, and simulation of the evacuation of a room without visibility. *Physical Review E* vol. 69.
3. Jeon, G.-Y., Kim, J.-Y., Hong W.-H. and Augenbroe, G., 2011. Evacuation performance of individuals in different visibility conditions. *Building and Environment* 46(2011) 1094–1103.
4. Jin T., 1978. Visibility through fire smoke. *Journal of Fire & Flammability*, Vol 9.
5. Kobes, M., Helsloot, I., de Vries, B., Post, J.G., Oberije', N., Groenewegen, K., 2010. Wayfinding during fire evacuation; an analysis of unannounced fire drills in a hotel at night. *Building and Environment*.
6. Nilsson, D., Johansson, M., Frantzych, H., 2009. Evacuation experiment in a road tunnel: A study of human behaviour and technical installations. *Fire Safety Journal* vol. 44.
7. Heliövaara, S., Kuusinen, J.-M., Rinne, T., Korhonen, T. & Ehtamo, H. 2012. Pedestrian behavior and exit selection in evacuation of a corridor – An experimental study. *Safety Science* 50, pp. 221–227.
8. Daamen. W. & Hoogendoorn. S.P. 2010. Emergency Door Capacity: Influence of Door Width, Population Composition and Stress Level. *Fire Technology*.
9. Gwynne, S. M., Kratchman, J., Kuligowski, E. D., & Milke, J. A. 2009. Questioning the Linear Relationship Between Doorway Width and Achievable Flow Rate. *Fire Safety Journal* 44 (2009) 80–87.
10. Helbing, D., Molnar, P. Social force model for pedestrian dynamics. *Physical Review E* 1995;51(5):4282–4286.
11. Schadschneider, A., Burstedde, C., Kirchner, A., Klauck, K., Zittartz, J.. Cellular automaton approach to pedestrian dynamics - Applications. In: Schreckenberg, M., Sharma, S., editors. *Pedestrian and Evacuation Dynamics*. Springer; 2001, p. 87–97.
12. Tajima, Y., Takimoto, K., Nagatani, T.. Pattern formation and jamming transition in pedestrian counter flow. *Physica A* 2002;313:709–723.
13. Blue, V.J., Adler, J.L.. Cellular automata microsimulation for modeling bidirectional pedestrian walkways. *Transportation Research Part B: Methodological* 2001;35:293–312.
14. Isobe, M., Adachi, T., Nagatani, T.. Experiment and simulation of pedestrian counter flow. *Physica A* 2004;336:638–650.
15. Kretz, T., Grünebohm, A., Kaufman, M., Mazur, F., Schreckenberg, M.. Experimental study of pedestrian counterflow in a corridor. *Journal of Statistical Mechanics: Theory and Experiment* 2006;:2527–2539. P10001.

Comparison of Evacuation Simulation Models

Aseri, BuildingExodus, FDS+Evac, and PedGo Applied to Auditorium

Burkhard Forell, Hubert Klüpfel, Volker Schneider, and Sören Schelter

Abstract In this paper we present simulation results for an auditorium. The results have been obtained by the programs Aseri, buildingExodus, FDS+Evac, and PedGo. Additionally they are compared to hand calculations based on Predtetschenski's and Milinski's model and a capacity analysis. Beside the calculation of RSET the focus of this paper is on the predicted locations of congestions.

Keywords Simulation • Evacuation • Aseri • BuildingExodus • FDS+Evac • PedGo • Predtetschenski & Milinski • GFPA • Auditorium

1 Safe Egress

The condition for safe egress can be formulated by the following equation:

$$\text{RSET} < \text{ASET} \tag{1}$$

B. Forell (✉)

Gesellschaft für Anlagen- und Reaktorsicherheit (GRS) mbH, Cologne, Germany
e-mail: burkhard@forell.de

H. Klüpfel

TraffGo HT GmbH, Duisburg, Germany
e-mail: kluepfel@traffgo.de

V. Schneider

IST GmbH, Frankfurt, Germany
e-mail: schneider@ist-gmbh.net

S. Schelter

BFT Cognos GmbH, Aachen, Germany
e-mail: soeren.schelter@freenet.de

Table 1 Summary of models used

Type	Model
Capacity analysis	GFPA-Guidelines, “moderate demand”
Dynamic flow model	Predtetschenski & Milinski, (“mid-season street dress”, “normal conditions”)
Discrete model	buildingExodus (Ver. 4.00) (standard population)
Discrete model	PedGo (Vers. 2.5) (standard population)
Continuous model	Aseri (Vers. 4.8) (“Egress”, inhomogeneous population)
Continuous model	FDS+Evac (Vers.: FDS 5.5.3, Evac 2.3.1) (standard population “adult”)

The safe egress must be completed when the conditions become unsafe as given by the available safe egress time (ASET). The required safe egress time (ASET) is the sum of the intervals for detection, alarm reaction and movement time [1].

$$RSET = \text{Detection} + \text{Alarm} + \text{Reaction} + \text{Movement} \quad (2)$$

In addition to the time criterion, the formation of severe congestion must be avoided or contained temporarily and spatially to a short time span and small area. In this paper, we compare different models for the determination of RSET and additionally focus on the different predicted locations of congestions (cf. Table 1).

2 Simulation of the Required Safe Egress Time

2.1 Models Used

The models used are shown in Table 1. These are two hand calculation methods, a simpler one called “Capacity Analysis” [1] and the more complex one of Predtetschenski und Milinski (P&M) [2] taking into account the non-linear dependence of the flow on the density (“Dynamic Flow Modell”). Additionally, four computer based simulations were used. Two of them are with discrete geometry (buildingExodus and PedGo) and two with continuous geometry (Aseri and FDS+Evac). All different models have different parameters e.g. on the population or on the flow conditions to set which are for the most part not directly comparable. Therefore all models were used with their standard conditions or default settings to achieve a high level of comparability.

3 Description of the Geometry

The auditorium for which the evacuation time is determined is $34 \times 29 \times 12$ m ($L \times W \times H$) and has 20 rows with 32 seats each. Up to 640 persons seating and 360 standing might occupy the venue. There are two stairs in the middle and two

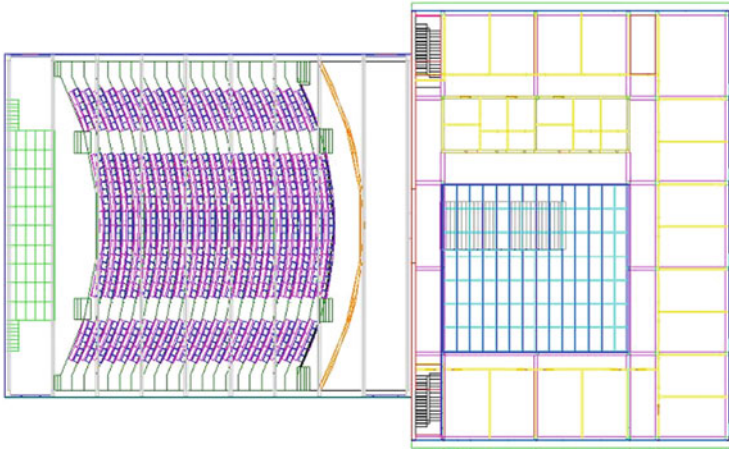


Fig. 1 Layout of the auditorium (*left*) with adjoining foyer (*right*) (Courtesy A. Weilert)

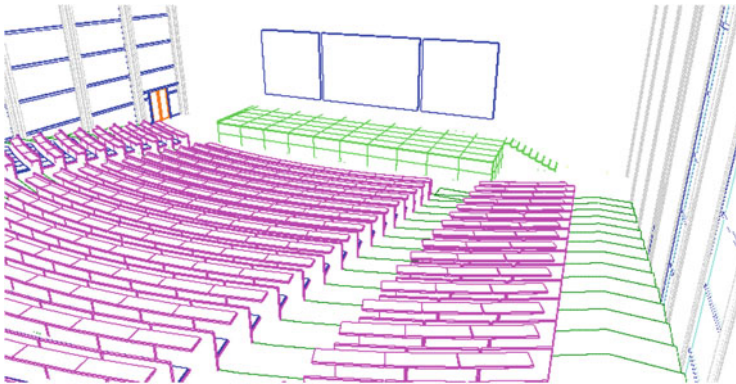


Fig. 2 Inside of the auditorium (Courtesy A. Weilert)

stairs at the side. The auditorium has two main entrance doors which lead (in case of egress) to the first floor of the adjoining foyer-building which is considered the safe area. The egress route in the foyer-building is further via one downward stair to the ground floor and outside. Additionally, two emergency exit doors are provided in the auditorium on the left and right side of the podium. The escape routes fulfill the German guidelines. The simulations with all six models were conducted for the emergency egress via escape route 1 (main entrance) and escape route 2 (emergency exits). Reaction times are not set, i.e. the evacuees are assumed to react immediately to the alarm signal. The time obtained is then the movement time.

Figure 1 shows the general layout of the building. The auditorium is shown on the left. The right part of Fig. 1 shows the main staircase in the foyer of the building in the center. The escape route is either upwards into the foyer or downwards to the emergency exits at the side (cf. Fig. 2). The everyday access to the auditorium and therefore the familiar entrance and exit to the room is route 1 (Fig. 3).

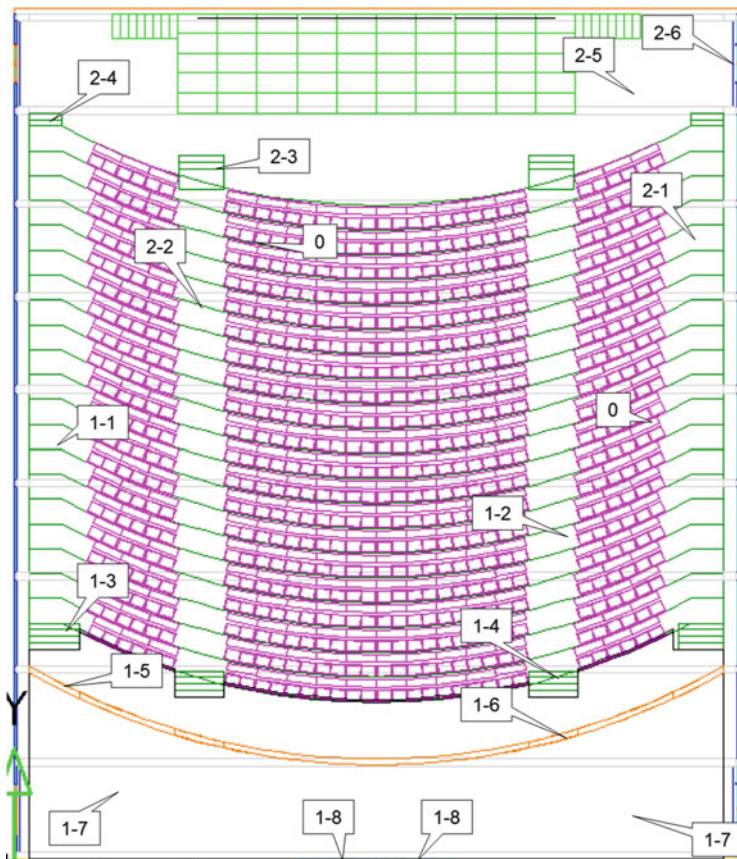


Fig. 3 Detailed view with numbering of route elements and exits

4 Flow-Based Calculations

Two different methods for flow based calculations are applied to calculate the overall movement time for the scenario described in the previous section: (1) Capacity Analysis and (2) Dynamic Flow Model. In both cases, the free widths of the escape route elements are multiplied with the specific flow to obtain the effective flow (column 6 in Table 2).

4.1 Results of the Capacity Analysis

For the Capacity Analysis the movement parameters shown in Table 2 were used which are given in the GFPA-Guidelines [1] and had been derived from [11]. For route 1, the overall evacuation time is 304 s. For route 2, the time is 298 s.

Table 2 Input parameters and results for the capacity analysis

1	2	3	4	5	6	7	8	9	10
No.	Route element	Number [-]	Effective width [m]	Specific flow [P/(m*s)]	Flow [P/s]	Total flow [P/s]	Maximum length [m]	Velocity [m/s]	Walking time [s]
0	Aisle	120	0.42	— ^a	0.63 ^a	75.60	—	—	—
1-1	Outer stairwell	2	1.20	0.8 ^b	0.96	1.92	10.0	0.6	16.7
1-2	Central stairwell	2	1.80	0.8	1.44	2.88	10.0	0.6	16.7
1-3	Stair	2	1.60	0.8	1.28	2.56	1.5	0.6	2.5
1-4	Stair	2	2.00	0.8	1.60	3.20	1.5	0.6	2.5
1-5	Through pass	2	1.40 ^c	0.9	1.26	2.52	0.3	1.0	0.25
1-6	Door	2	2.00	0.9	1.80	3.60	0.3	1.0	0.25
1-7	Floor	4	2.50	1.1	2.75	11.00	15.0	1.0	15.0
1-8	Main exits	2	2.00	0.9	1.80	3.60	0.5	1.0	0.5
1-9	Stair in foyer	2	2.40	0.8	1.92	3.84	15.0	0.6	25.0
2-1	Stair down	2	1.20	0.8	0.96	1.92	10.0	0.6	16.7
2-2	Central stair down	2	1.80	0.8	1.44	2.88	10.0	0.6	16.7
2-3	Stair	2	2.00	0.8	1.60	3.20	0.7	0.6	1.17
2-4	Stair	2	1.20	0.8	0.96	1.92	0.7	0.6	1.17
2-5	Floor to exit	4	1.20	1.1	1.32	5.28	10.0	1.0	10.0
2-6	Exit doors front	2	2.00	0.9	1.80	3.60	0.5	1.0	0.5

^aThe capacity in the rows does not depend on the width [2]. The values are for normal movement

^bStairwells are modelled as stairs (error on the safe side). No distinction is made between down and up

^cIf this area is used for exhibition, the minimal width must be ensured

For the escape route 1, the walking time of the first people to escape is the sum of the values of column 10 of Table 2 for the route elements 1-i. As of the outer stairwell (element 1-1) only about 5 m are used by the head of the group, only about 8.3 s are needed for this element instead of 16.7 s. The sum of the walking times is 26.6 s.

The alternative route via 1-4 and 1-6 for the other part of the auditorium is faster. Please note that we did not take into account the outside stair in the foyer (1-9), since the foyer is already considered to be the safe area. We did not calculate the time for leaving the building but for leaving the auditorium. The elements 1-1 and 1-2, 1-3 and 1-4, and 1-5 and 1-6 are assessed “in parallel” for the calculation of the flow time. Escape route element 1-8 is used by all 1,000 persons. Therefore, this is the bottleneck; since it has the lowest ratio of N/F (N is shown in column 3 and F in column 6 in Table 1). In summary, the flow time is therefore 1,000 Persons divided by 3.6 Persons per second, which results in 278 s. The total movement time is then the sum of the walking time and the flow time, i.e. 304 s.

For the alternative escape route (2-1 to 2-6 in Table 1) a similar calculation gives 20 s for the walking time and 278 s for the flow time, i.e. 298 s for the movement time.

4.2 *Predtetschenski's and Milinski's Flow Model*

The model is based on a group specific projection area, which is in our case 0.113 m²/person. This corresponds to person's mid-season street dress. Due to the symmetry of the auditorium, it is sufficient to focus on the escape of 500 persons via the side stairs (200 persons) and the central stairs (300 persons).

For the stairs (route element 1-1 and 1-2) the density is 8.14 persons per square meter. This value is used to determine the flow rate from the fundamental diagram in [3]. The velocity is 0.11 m/s (upstairs) and the specific flow 0.89 P/m/s. Since the specific inflow for the stairs 1-9 is 1.12 P/m/s, congestion occurs on the stairs. The inflow is determined as

$$f_{in} = \sum_{in} F_{in}^i / w_{in} \quad (3)$$

and compared to the maximum specific outflow

$$f_{out} = f_{out,max} / w_{out} \quad (4)$$

where w_{out} is the clear width of the downstream escape route element and $f_{out,max}$ is the maximum specific flow of the route element type obtained from the fundamental diagram, i.e. its capacity. If

$$f_{out} > f_{in} \quad (5)$$

Table 3 Summary of the movement times

Model	Route 1		Route 2	
	Time [s]	Congestion	Time [s]	Congestion
Capacity analysis	304	Exit doors (1-8)	298	Exit doors (2-6)
P&M	295	Stairs (1-1 & 1-2), Stairs in foyer (1-9)	318	Stairs (2-1 & 2-2)
Exodus	382	Stairs (1-1 & 1-2)	266	Stairs (2-1 & 2-2)
PedGo	348	(Stairs (1-1 & 1-2)), Exit doors (1-8) (Stairs in foyer (1-9))	276	Stairs (2-1 & 2-2) (Exit doors (2-6))
ASERI	324	Stair (1-1 & 1-2) Exit doors (1-8)	311	Stair (2-1 & 2-2) Exit doors (2-6)
FDS+Evac	373	(Stairs (1-1 & 1-2)), Exit doors (1-8)	239	Stairs (2-1 & 2-2)
Mean	338		285	

a congestion occurs and the congested flow value $f_{out,congested}$ is used for the further calculation. Since for stair 1-9 this is the case, i.e. there is congestion, the value for $f_{out,congested}$ is 0.65 P/m/s at the maximum density is applied. The 500 persons using stair 1-8 then need $500/0.65 * 2.4$ s, i.e. 318 s to pass. Adding the walking time of 39 s, and overall movement time of 347 s is obtained.

For the alternative escape route (2-1 to 2-6), an overall time of 295 s results.

5 Simulation Models

BuildingExodus was developed by the Fire Safety Engineering Group at the University of Greenwich. Model details can be found in [3]. It is a grid based model with a cell size of 0.5 m. There are various individual parameters.

PedGo is based on a square grid. The length of the square cell is 0.4 m, which allows for a maximum density of 6.25 persons per square meter. A detailed description of the model can be found on <http://www.traffgo-ht.com> where the users' manual is available for download.

ASERI is based on each agent searching for the shortest path. Details can be found in [10].

FDS+Evac is an extension of the Fire Dynamics Simulator (FDS) [6]. Additional model details are described in [7, 8].

6 Summary, Conclusion, and Outlook

The results are summarized in Table 3.

References

1. GFPA (German Fire Protection Association, vfdb): *Leitfaden Ingenieurmethoden des Brand-schutzes (Guidelines of Fire Safety Engineering)*. Technical Report TB 04/01, 2. ed. Braun-schweig/Altenberge. 2009. <http://www.vfdb.de>
2. Predtetschenski, V.M.; Milinski, A.I.: *Personenströme in Gebäuden - Berechnungsverfahren für die Projektierung*. Verlagsgesellschaft Rudolf Müller, Köln. 1971.
3. Galea, E.R. et al.: *Building Exodus 4.00, Users Guide and Technical Manual*. University of Greenwich. Greenwich. 2004.
4. PedGo Handbuch: TraffGo HT GmbH, Version 2.5. Duisburg, 2011. <http://www.traffgo-ht.com/downloads/pedestrians/downloads/documents/Handbuch.pdf>
5. Hebben, S. und Klüpfel, H.: *Eingabe- und Ergebnisdaten des Beispiels der Räumung eines Hörsaalgebäudes mit PedGo*. 2011 <http://www.traffgo.ht/slinks/vfdbJFT11>
6. Korhonen, T.; Hostikka, S.: *Fire Dynamics Simulator with Evacuation: FDS+Evac, Technical Reference and User's Guide (FDS 5.5.3, Evac 2.2.3)*, VTT Technical Research Centre of Finland, 2010.
7. Korhonen, T.; Hostikka, S.; Heliövaara, S.; Ehtamo, H.: *FDS+Evac: An Agent Based Fire Evacuation Model*. In: Klingsch, W. et al. (Hrsg.) PED2008, Tagungsband zur 4th International Conference on Pedestrian and Evacuation Dynamics, Wuppertal, Februar 2008, Springer Verlag, Berlin 2008.
8. Heliövaara, S.: *Computational Models for Human Behavior in Fire Evacuations*, Master-thesis, Department of Engineering Physics and Mathematics, Helsinki University of Technology, 2007.
9. Harding, P.J.; Gwynne S.M.V.; Amos, M.: *An early warning method for crush*. Preprint, arXiv:1008.2160v1, 2010.
10. Referenzhandbuch ASERI, Ausgabe 30. Mai 2008.
11. Proulx, G.: *Movement of People: The Evacuation Timing*. In: The SFPE Handbook of Fire Protection Engineering, Third Edition, Quincy, Massachusetts. 2002.
12. Weidmann, U.: *Transporttechnik der Fußgänger - Transporttechnische Eigenschaften des Fußgängerverkehrs (Literaturauswertung)*. Schriftenreihe des Instituts für Verkehrsplanung, Transporttechnik, Strassen- und Eisenbahnbau, ETH Zürich, Nr. 90, 2., ergänzte Auflage Zürich, März 1993.
13. ARGEBAU: Begründung und Erläuterung zur Musterverordnung über den Bau und Betrieb von Versammlungsstätten. Fachkommission Bauaufsicht, Juni 2005. <http://www.is-argebau.de>
14. DIN EN 13200: *Zuschauertribünen, Teil 1: Kriterien für die räumliche Anordnung von Zuschauerplätzen - Anforderungen*. 2004.
15. Draft ISO-WD_16738: *Evaluation of behaviour and movement of people*. 03-2007.
16. Autorenkollektiv: *Richtlinie für Mikroskopische Evakuierungsanalysen*. RIMEA, Version 2.2.1. 2009. <http://www.rimea.de>
17. Forell, B.; Klüpfel, H.; Schneider, V.; Schelter, S. (2011): *Vergleichende Anwendung verschiedener Räumungsmodelle*. Tagungsband zur 59. vfdb Jahresfachtagung 2011, 30. Mai bis 1. Juni, Berlin.

Crowd Guidance in Building Emergencies: Using Virtual Reality Experiments to Confirm Macroscopic Mathematical Modeling of Psychological Variables

Kerry L. Marsh, Christian T. Wilkie, Peter B. Luh, Zhenxiang Zhang,
Timothy Gifford, and Neal Olderman

Abstract A general challenge during a building emergency evacuation is guiding crowd to the best exits, given potential hazards and blockages due to high density use. Although computer simulation programs such as FDS+Evac allow researchers to evaluate various guidance policies under different circumstances, computational complexity limits their use during an actual emergency. A second limitation of such programs currently available is that they can only model certain psychological variables that affect evacuation. We suggest two innovations to address these difficulties. First, using macroscopic models, mathematical techniques can allow for rapid optimization of guidance that could eventually be used to provide real-time use during emergencies. Second, we conduct virtual reality experiments using human participants to provide confirmation of our models, and offer insights into

K.L. Marsh (✉)

Department of Psychology, University of Connecticut, Storrs, CT, USA

e-mail: Kerry.L.Marsh@uconn.edu

C.T. Wilkie • P.B. Luh

Department of Electrical and Computer Engineering, University of Connecticut, Storrs, CT, USA

e-mail: Christian.Wilkie@uconn.edu; Peter.Luh@uconn.edu

Z. Zhang

Advanced Interactive Technology Center (AITC), Center for Health, Intervention, and Prevention, University of Connecticut, Storrs, CT, USA

e-mail: Zhenxiang.Zhang@chip.uconn.edu

T. Gifford

Department of Psychology, University of Connecticut, Storrs, CT, USA

Advanced Interactive Technology Center (AITC), Center for Health, Intervention, and Prevention, University of Connecticut, Storrs, CT, USA

e-mail: Timothy.Gifford@uconn.edu

N. Olderman

Center for Continuing Studies, University of Connecticut, Storrs, CT, USA

e-mail: Neal.Olderman@uconn.edu

how psychological factors not yet available in FDS+Evac will affect evacuation outcomes. Results of an initial VR experiment are presented.

Keywords Building emergency egress • Evacuation stress • Virtual reality experiments • Crowd guidance • Macroscopic modeling • Mathematical optimization • Social force model

1 Introduction

Crowd evacuation behaviors including disorder and blocking have been observed in tragedies such as the 2003 Rhode Island and 2009 Bangkok nightclub fires [1, 2]. Behavioral studies of evacuees have shown that psychological stress plays an important part in the emergence of disorder and blocking [3, 4]. However, there is a gap between theories that explain the behavior of evacuees and the methods of providing effective guidance to evacuees in building emergencies. With recent advances in fire detection methods and crowd communication, there is potential to alleviate these kinds of injuries and deaths in the future. Some advanced building designs incorporate sophisticated systems that monitor a wide range of building conditions, and sense locations and possibly densities of people. Such systems could be integrated with dynamic emergency guidance systems (signs that could be made more salient or less prominent, audio/signage/text messages that could be updated dynamically given the changing circumstances) to provide better guidance during an emergency evacuation. However, the lynchpin in such an approach is that a computerized modeling, optimization and simulation system need also be in place that would allow emergency personnel to, in rapid time, run optimization and simulation that determines the best way evacuees should be guided through buildings given relevant physical and psychological factors. In sum, two critical issues for determining optimal guidance is elucidating important psychological factors that influence egress and reducing the computational challenge such that these factors can be optimized and simulated rapidly.

2 Current Model

As a starting point for our model, Helbing's social force model [5] is used as the psychological basis for understanding the motivational/arousal state that propels people to move slowly or fast during an evacuation, and leads people to reduce or increase their desired velocity when the condition has been worsened (or when that initial velocity is being impeded). However, these dynamically changing variables or parameters are modeled macroscopically in our approach to reduce computational burdens.

Second, selected factors currently known about informational, psychological and cognitive factors that affect egress are included in our model. The challenge with

using simulation programs available (e.g., FDS+Evac) to test our model is that not all of these factors are currently incorporated in the programs. In the table below, the crucial features of our model, as presented recently [6] are highlighted. In the final column of the table we suggest how these features already included in the simulations would be tested and validated using immersive virtual reality experiments. We also suggest ways in which VR could be used to extend the simulations by exploring features not yet included in FDS+Evac to account for them. One additional feature of our model not in the table is the social bond or cooperativeness factor [6, 7]. We postulate that social bonds among people (e.g., evacuating with familiar others) can reduce the impatience that can lead to competitive-appearing behavior postulated by Helbing (continued pressure on people at blockages, because of the nervousness due to failure to achieve desired speed). This is supported by substantial evidence provided by considerable accounts of evacuation that prosocial behavior during evacuations is more commonly experienced than competitive, self-interested behavior [8]. Although it is not yet clear how to incorporate this feature into FDS+Evac, there are well-established ways in psychological experiments of experimentally manipulating degree of cooperative vs. competitive behavior.

3 Using Optimization to Determine How to Guide Crowds

To address the problem of providing effective guidance to crowds, an optimization problem was formulated in our previous work [6, 7]. The underlying equations were chosen to follow a macroscopic model, where crowds are treated as a fluid [11, 12] to reduce the computational complexity for optimization. Our model improves upon existing fluid-type models by capturing psychological phenomena that previously have been examined only within computation-intensive microscopic models. In particular, one novel parameter, the desired flow rate (evacuees' feeling of urgency to move), was developed as a macroscopic counterpoint to Helbing's desired velocity [5]. This can help explain the emergence of disorder and blocking during an emergency event. It is an important factor since it can be affected by perceptions of imminent danger, or lack of information about narrowed passageways or obstacles that cannot be seen by pedestrians far from the source of the disorder or blocking. It can also be affected by introducing front-to-back communication in such situations [13] either by providing visual information to reduce impatience, or by social sources of guidance (a leader who requests people to slow down). Thus the first focus of our optimization and validation studies was on this psychological variable. The eventual goal is to use validated models and methods to solve the guidance problem in real-time, allowing effective guidance of evacuees during an actual emergency event. Although the current state of crowd guidance falls far short of such an objective, confirming our ideas to validate optimized procedures is a major step towards realizing this goal (Table 1).

Table 1 Comparison between simulation models and virtual reality procedures

Feature	FDS+Evac 2.3.1 [9]	Our model [6, 7]	Beta FDS+Evac [10]	Procedures for virtual reality experimentation
Social force	Helbing's desired velocity implemented via the so called unimpeded walking speed which remains constant except when vision is reduced by smoke	Translates Helbing's microscopic desired velocity into a macroscopic version: the desired flow rate	FDS+Evac 2.3.1 features but with unimpeded walking speed changing dynamically based on nervousness due to waiting times	<i>Basic validation:</i> Have participants experience a trajectory from a simulation and assess satisfaction with movement; also, experimentally heighten desired velocity via physical information (visible, auditory, and/or odor) or social information See <i>Basic validation</i> procedure above; also, experimentally manipulate Helbing's nervousness by reducing uncertainty via visual or auditory information or via leadership
Effects of failure to achieve desired velocity	Effects of a discrepancy between desired and actual velocity does not recursively impact desired velocity	Consistent with Helbing's nervousness parameter: failure to achieve desired velocity can dynamically increase desired velocity	FDS+Evac 2.3.1 features but with Helbing's nervousness equation dynamically determining desired velocity	Use experimental inductions of trust, source of information (expert leader versus peer versus standard audio message) along with <i>Basic validation technique</i>
"Faster is slower" effect	Implemented by incorporating Helbing's equations for forces between evacuees	Translates this blocking effect into a macroscopic feature, using a probability distribution to determine flow rate	Same as FDS+Evac 2.3.1	<i>Basic validation technique</i> , but implemented as a massive multiple player online simulation
Exit selection	Exists ranked based on disturbing conditions at the exit, familiarity, visibility, and estimated queuing time	Use models to optimize guidance based on blocking, impatience due to hazards, and trust in guidance	Same as FDS + Evac 2.3.1.	Use experimental inductions of trust, source of information (expert leader versus peer versus standard audio message) along with <i>Basic validation technique</i>

4 Using Virtual Reality in Evacuation Research

One important advance in the area of emergency egress from buildings is the use of virtual reality (VR) to examine how individuals would evacuate a building under given circumstances [14, 15]. For instance, researchers have examined the impact of different kinds of emergency signs and different features of the escape route on virtual evacuations [16, 17], and have used VR to examine the impact of social bonds on evacuation behavior [18]. One novel way to use virtual reality is introduced in this paper – namely, tightly integrating its use with the output of simulation models such as FDS+Evac, and, in our next step, integrating with optimized guidance found using our model and methods. The position outputs for every agent throughout the course of simulated evacuation can be used to model the behavior of avatars in a virtual environment. One of these agents can then be replaced by a human participant (or multiple participants, in a massive multiplayer online version) with his/her actual behavior compared to the output of the program as a means of validating the FDS+Evac output, or developing additional insights into the adequacy of the simulation or optimization. We provide a first step toward doing this in the study detailed below.

5 Methods and Results

5.1 Optimization and FDS+Evac Simulations

In this paper we analyze the effects of one key psychological factor from Helbing's model, desired speed, which is the microscopic counterpart to the macroscopic desired flow rate used in our model. To examine this factor, a virtual reality testing platform was created. This allowed us to run many trials with participants and to better recreate the psychological effects of an emergency event by making the evacuation an embodied, immersive experience. The participant experienced the evacuation from a first-person perspective and provided us continual feedback about their reactions to that evacuation. For the virtual reality environment, a university library was chosen due to the potential benefits of guidance at this location. In particular, this library is often crowded with college students who are unfamiliar with the locations of emergency exits. Although peripheral exits are usable by patrons for inter-floor movements and they lead to stairwells which then lead to emergency exits out of the library, almost no students ever use these exits and they are not familiar with them. A 3D model of one floor was constructed and used in the evacuation simulator Fire Dynamics Simulator with Evacuation (FDS+Evac) [9] to determine the evacuation routes and speeds of agents. Graphical avatars were created in VR with their routes calculated using position data imported from FDS+Evac and displayed during the experiment. The participant, one for each trial, was immersed in the virtual environment through the use of a head mounted

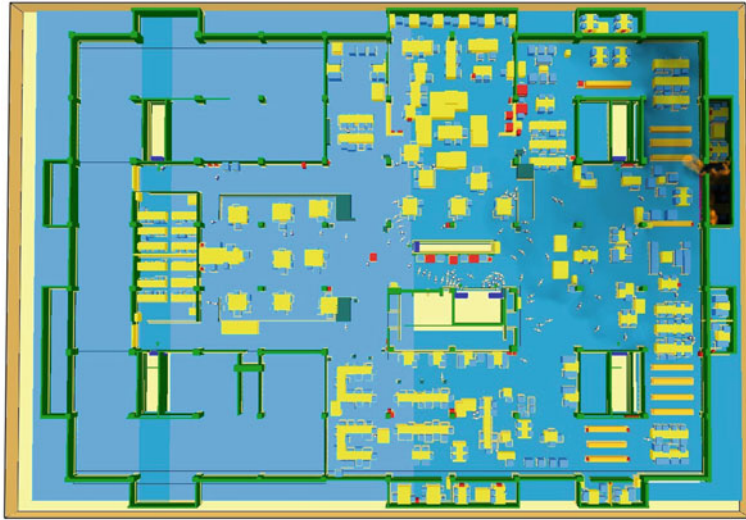
display and tracking equipment which updated the display based on the actual head movements of the participant. The camera position and orientation that generated the image being displayed to the participant was a combination of real-time tracking data and the pre-computed FDS+Evac agent position and orientation data. The participant's experience was thus as if he/she was being passively moved through the evacuation (as if he/she was walking at some computer-determined speed and direction).

5.2 Virtual Reality Experiment

Virtual reality experiments are valuable in the following aspects: (a) It provides a way to partially validate the output of FDS+Evac. For instance, we can confirm whether VR participants would want to move in the direction and speed that FDS+Evac is simulating they would do. (b) It also provides a way to develop or adjust parameters that are difficult to determine a priori in FDS+Evac. For instance, it may be difficult to determine how strong of a tendency there would be in a given situation to use the main, familiar exit, over nearby, unfamiliar exits. We can attempt different parameter settings in FDS+Evac and then confirm the adequacy of them by getting feedback from people who are immersed in first-person virtual simulations of that environment. (c) It also allows us to examine the underlying psychological mechanisms that are assumed to explain the behavior of simulated evacuees. For instance, during a virtual evacuation, joystick direction could be used to assess various psychological states such as how anxious they feel. Other states might also be assessed immediately after the evacuation, for instance, by using a questionnaire to assess how much trust an evacuee had in the guidance information provided during the evacuation.

The initial pilot experiment was designed to provide a test of whether (a) presented above was possible. One of the most basic assumptions in Helbing's social force model about psychological factors during evacuation is that perception of hazards will elicit the desire to move faster. To test whether VR experiments will provide a good platform for validating this psychological assumption, we examined the effects of hazard on desire to move rapidly. Specifically, we wanted to determine whether participants would show greater dissatisfaction with their evacuation speed when there was a mismatch between hazard conditions and evacuation speed. For a given trial, the participant was moved at a speed and direction based on what was specified by an FDS+Evac simulation. The participant was not able to control his/her movements during the virtual evacuation; instead a joystick was used to indicate whether the speed that he/she was being moved was satisfactory. Although the focus of the experiment was on the microscopic level (desired speed), the simultaneous movement of avatars around the participant during the evacuation would provide a visual flow of information that should correspond to the macroscopic flow rate.

Smokeview 5.8 - Oct 29 2010



Frame 481

Time: 22:55

*101 (XMM3)

Fig. 1 In this screenshot of an FDS+Evac simulation, a fire has broken out in a room on one end of the library that contains the writing center for the library. Smoke has begun to spread

5.2.1 Procedure

FDS+Evac Simulation

Evacuation simulations were created based on three different walking speeds in which 150 adults were evacuating a large upper floor of a university library with floor dimensions of 175×250 ft (53.34×76.2 m), where a fire was modeled to break out at one end of the floor. A screenshot of the simulation is illustrated in Fig. 1. For the medium speed condition, the unimpeded natural walking speed for adults of $U(0.95, 1.55$ m/s) [9] was used, with speeds for the 150 agents uniformly distributed across this range. In slow and fast walking speed simulations, the agents' speeds were uniformly distributed from $U(0.325, 0.925$ m/s) and $U(1.3, 3.7$ m/s), respectively. These distributions of speeds used in the slow and fast simulations were centered around unusually slow walking speeds (from about half normal walking speed to two-thirds of normal walking speed), and very fast walking speeds (from a fast-normal speed, to jogging and running speeds). The parameters in the FDS+Evac program for exit strategy were set to give these agents 100 % probability of being familiar with the two doorways of the central staircase that library patrons use almost exclusively. In addition, familiarity with peripheral exits leading to emergency exits was set to 20 % probability. The positions for agents throughout the simulations were used as the basis for determining the trajectories of all avatars used in the virtual experiment. Not all trajectories were entirely usable

in virtual reality. For instance, approximately 15 agents were typically trapped in an FDS+Evac simulation in unrealistic ways because of the geometric limitations of FDS+Evac modeling and the cluttered library. Similar numbers of valid agent trajectories produced by FDS+Evac could not be fully implemented in VR because the avatar's movements in a cluttered environment led them to have difficulties escaping (e.g., an avatar trapped in-between what is modeled as an unmovable chair and a bookcase). After eliminating the trajectories of these agents/avatars, a total of 120 FDS+Evac trajectories were used to model the movements of 120 virtual persons (avatars) evacuating the library in virtual reality. Up to 30 % of these trajectories, each with a corresponding starting position, were available as options for the VR participant's trajectory during a virtual reality trial. The actual number, however, could be considerably less in some conditions. For instance, if the participant was to see a fire, then certain options had to be eliminated. With those constraints, the participant's starting position was chosen at random from these possible starting positions for each trial in the experiment. Figure 1 is a screen shot of a simulation from FDS+Evac.

Virtual Reality Experiment

Twenty-five undergraduate students participated in this experiment for experimental credit in their introductory psychology course. They participated in the experiment alone, in a cubicle room equipped with a computer, a Polehmus motion tracker, and a head mounted display (HMD). After the experimenter fitted a head-mounted display (HMD) with head tracker attached (see Fig. 2) to the participant's head, participants were told that they would be moving through some environment during each trial of the experiment. To familiarize the participant with being in a first-person perspective virtual environment, participants first experienced an introductory scene in which they were in what appeared to be a foyer of an apartment building. In this room, a virtual person (avatar Victor) explained that the experiment would involve the participant being moved through a virtual environment. Although they would not be able to control their movement, they would use the joystick to convey how they would normally have wanted to move in this situation.

Specifically, Victor said: "In this virtual world we have created situations in which you will be moved in the virtual world along with other people at a fixed speed: What we want to know is how well we are moving you in that virtual world. Are you moving about right? Or too fast? Or too slow? To tell us how satisfied you are with the movement, you will move this joystick." The participant then explored pushing the joystick forward and back, while seeing the display on the screen changing accordingly. Victor said "The visual display on the screen will let you tell us that you wish you were being moved faster or slower. The display will show you how much you are moving the joystick" As Fig. 2 indicates, up and down arrows conveyed whether the participant wished to be moving faster or slower to a slight, moderate, or considerable degree. Keeping the joystick at the middle, neutral point, indicated comfort with the speed of movement. Joystick position



Fig. 2 Participants viewed the virtual library evacuation through a HMD with position tracker attached. When the participant moved the joystick forward, *up arrow(s)* were displayed, representing a desire to move faster; *down positions* indicated a desire to slow down. When the participant was moving at a comfortable speed, only the bar in the neutral position was lit

was recorded as a value between 1 and 7, with values below 4 indicating desire to move slower and values above 4 indicating desire to move faster. Participants gave real-time continuous feedback on their relative desired speed during each trial by moving a joystick forward or backward. The position was recorded 20–30 times a second, with less updating in conditions that required more computation (e.g., smoke conditions). Thus, joystick position was updated every 2.4 ms on average during a trial.

After the introductory scene, the participant went through a series of library evacuation trials in which participant’s speed was varied as slow, medium (natural speed), or fast as presented before. Moreover, hazard conditions were varied: no smoke or fire was visible, or only smoke was visible, or both smoke and fire were visible. When fire was visible, the sound of a crackling fire could be heard faintly. In sum, the design of the experiment was a 3 (Hazard) \times 3 (Walking speed) within-subjects design, with the dependent measure being the desired speed scores (of 1–7) assessed continuously during the trial. All participants completed one block of nine trials, and for exploratory purposes participants completed as many as nine additional trials. In the second block, trials could be taken from any of the conditions (chosen at random, but with replacement), thus few participants had complete data for all nine conditions that would allow for analysis of the second block. Therefore only the results of the first block are analyzed. The order of the nine trials was counterbalanced across participants, with the restriction that the first three conditions (presented in random order) were the natural speed conditions. As each trial opens, the participant is already in motion (along with other avatars) during an evacuation of the university library, thus avoiding the complications caused by “evacuation initiation delay.” As Fig. 3 illustrates, library details were reproduced



Fig. 3 An overhead view of the virtual floor of the library used in the experiment. The ceiling has been moved for illustration; the beams indicate whether the ceiling would normally begin

with a high degree of fidelity, including locations of all exit signs, the appearance of doors and images on the walls, and the organization of furniture (e.g., the location, size and shape of tables, movable boards, chairs (in fixed positions), lounge chairs, and bookcases) in different areas of the library. This floor is a high use, familiar floor to the student participants, and a wide range of studying activities (including centers for quantitative and writing tutoring) are conducted in areas that are differently structured. There are no traditional “stacks.” Instead, there are about a dozen low-height book cases. The open floor plan and wide range of diverse areas can make it feel confusing to a visitor. The section of the floor accessible to only library staff was not modeled in detail. Participants saw fire alarms flashing and heard fire alarm and automated evacuation messages (recorded from actual library messages) throughout the trial. In any given trial, a participant could be near or far from a number of different exits in the library. When smoke was present, it spread horizontally as well as downward as a trial progressed. Screen shots during various hazard and speed trials are illustrated in Fig. 4. Each trial ended (faded to black) when the participant was propelled by the program into a stairwell.

5.2.2 Hypotheses

It is hypothesized that greater hazard conditions would lead participants to indicate greater feelings of discomfort with their speed than less hazardous conditions. It is also hypothesized that unnaturally slow speeds would lead to less satisfaction with one’s speed than would natural speed conditions.

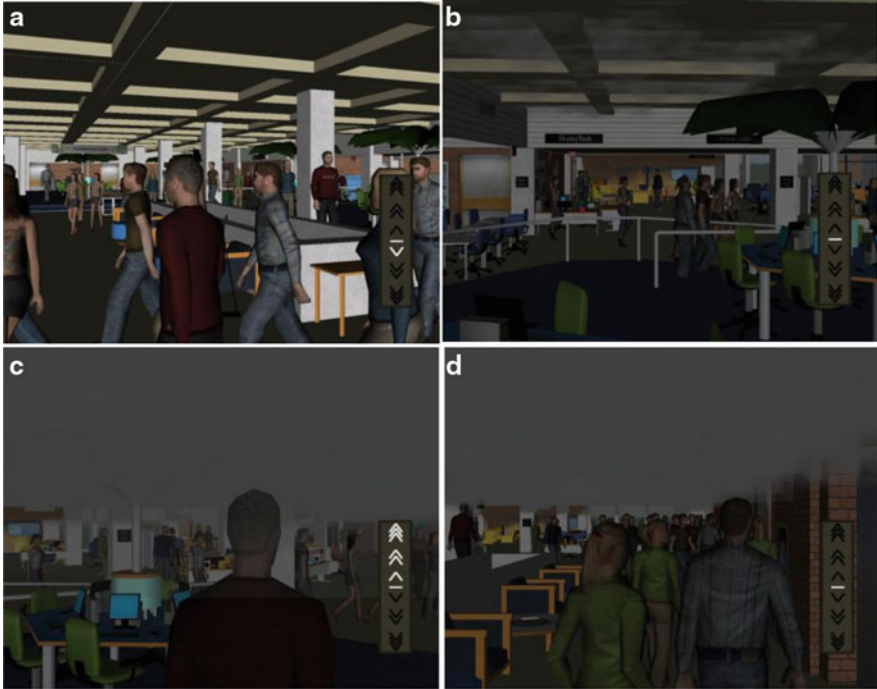


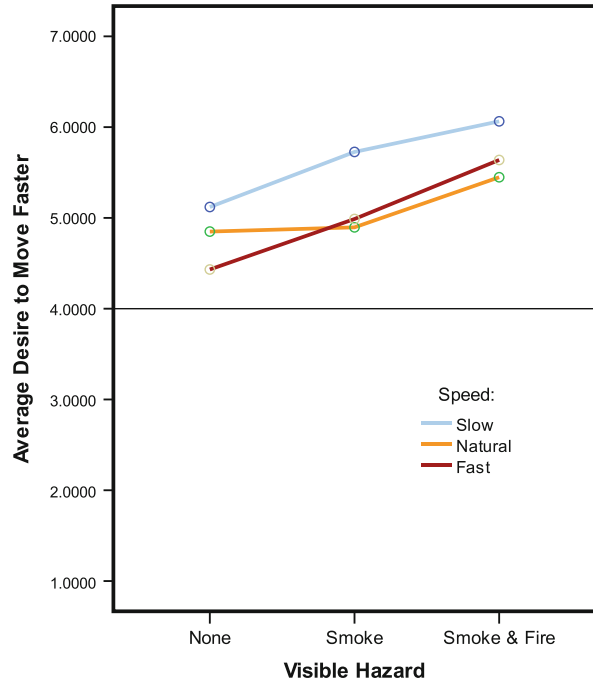
Fig. 4 Screen shots of situations (from *upper left*, clockwise) where (a) there was no visible hazard; (b) it is early in a trial, a fire was visible, but smoke was just beginning; (c) it was late in a smoke & fire trial where participant is reaching the crowded exit; and (d) smoke has progressed and participant desires to move fast

6 Results

A participant's desired speed scores throughout a given trial were used to produce a mean score for that participant, and a maximum value as well. Mean and maximum desired speed scores were analyzed in separate 3×3 within-subjects Analyses of Variance (ANOVAs). For exploratory purposes, epoch analyses were also conducted of the early, middle, and last segment of a given trial. Trials varied in length from 12 to 94 s (mean = 41.57, standard deviation = 23.05, median = 34.34). Responses in the first, middle, and last three seconds of a trial were used for these analyses.

For the maximum desired speed, there were significant main effects of both Hazard, $F(2, 48) = 31.56$, $p < .001$, and Walking Speed, $F(2, 48) = 6.53$, $p = .003$. As expected, when participants were walking through the environment slowly, they had the strongest desire to move faster, with an average value of 6.48 out of 7. When they were walking at medium and fast speed, averages for maximum desired speed approached 6 (means of 5.95 and 5.89, respectively). Moreover, hazard heightened participants' discomfort with the speed as anticipated. On average, participants'

Fig. 5 A Hazard \times Speed interaction moderated the main effects of Hazard and Speed on desired speed

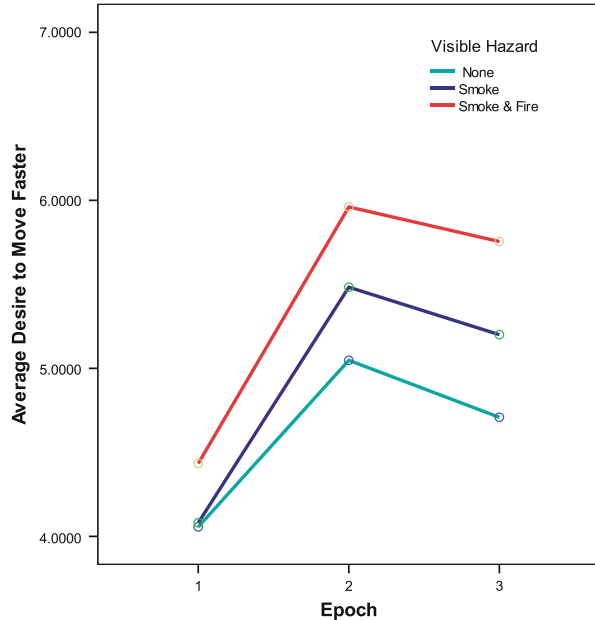


maximum score when no hazard was present was 5.57. In contrast, participants' maximum value was typically over 6 when hazards were present (means were 6.11 for smoke visible, and 6.64 for smoke and fire visible).

The ANOVA on average desired speed similarly revealed main effects of Hazard $F(2, 48) = 15.81, p < .001$, and Walking Speed, $F(2, 48) = 10.53, p < .001$ as expected. Average desired speed was lowest when evacuating with no visible hazard (mean = 4.80) relative to evacuating when smoke (mean = 5.20) or smoke and fire (mean = 5.72) were visible. When individuals were moved slowly the average desired speed was higher (mean = 5.64) than when they were moved at a natural or fast walking speed (means = 5.06 and 5.02, respectively). As Fig. 5 illustrates, there was also an unanticipated Hazard \times Walking Speed interaction that moderated these main effects, $F(2, 48) = 2.52, p = .046$. Only when no hazards were visible were fast speeds associated with the lowest levels of desired speed; with hazards present participants' desired speed showed no distinction between natural and fast speeds. Somewhat surprisingly, no means were below the midpoint – that is, even during the fast trials, participants did not indicate, on average, that the speed was uncomfortably fast.

Finally, a 3 (Epoch) \times 3 (Hazard) \times 3 (Walking Speed) within-subjects ANOVA replicated the main effects of Hazard and Walking Speed found on the other measures, each $F(2, 48) \geq 4.84$, with each $p < .013$. A main effect of Epoch, $F(2, 38) = 48.36, p < .001$, revealed, as anticipated, that participants were more

Fig. 6 Effects of Hazard by Epoch interaction on desired speed. At the beginning of trials, participants’ joystick position indicated they were comfortable with the speed (i.e., at the midpoint of 4) except when fire was visible. Effects of Hazard on desire to move faster intensified during the trial. In the last third of the trial, there was typically a decreased urgency to go faster



comfortable with the speed at the beginning of a trial (mean = 4.19) relative to the middle (mean = 5.50) and end of a trial (mean = 5.22). Interestingly, a Hazard × Epoch interaction, $F(4, 96) = 5.43, p = .001$ was unexpectedly also significant. As Fig. 6 reveals, Hazard’s impact on their desire to move faster increased as the trial progressed.

7 Discussion

Our hypotheses regarding the effects of hazard and speed were mostly supported by the results of the virtual reality experiment. Desired speed increased when hazards were visible, indicating the effectiveness of the virtual environment to induce appropriate psychological responses. Being moved at an unusually slow speed also led participants to desire to move faster, but contrary to predictions, the distinctions between natural and high speed were minimal. Participants’ responses were also responsive to the dynamic changing circumstances of the environment – as a trial progressed, desire to move faster was heightened, particularly as smoke was spreading. At the end of trials, desire to move was unexpectedly reduced, a phenomena which should be examined in further research.

7.1 Limitations of this Experiment

There are several limitations of this virtual reality experiment, some are specific to the details of this particular procedure, while others suggest broader limitations of virtual reality. One localized limitation concerns the way the joystick was used. Using a joystick to convey “this is faster than I’d like to go” or “this is slower than I’d like to go” is a rather unfamiliar use of the joystick for the participants. Despite the artificiality of this, the joystick measure was sensitive to dynamically changing aspects of the experience such as the slowdown at the exits. In subsequent experiments, participants will be able to use the joystick more actively, to deviate from the FDS+Evac plotted trajectory and directly choose a different speed or even different exit. Another limitation of the current experiment is that it may only generalize to situations of relatively high density in the library. Having over 100 people around already in motion toward exits is a different experience than evacuating with fewer avatars present. At high density phenomena such as “herding” (conforming to others’ behavior regarding choice of exits, presumably because others’ behavior is informative) are likely to be stronger, as social psychological theorizing would predict [20]. Moreover, others in motion decrease the attentional and cognitive resources available to search for and consider other exits. Having more people moving in the environment also increases occlusion of signage (such as signs directing one to unfamiliar exits). This limit on generalizability, however, is easily remedied by replicating such procedures with different numbers of avatars. It is also useful to note that even though the experience of evacuating with 120 other people on the floor in motion can feel moderately crowded, during final exams the actual number of students on the floor could be double this number, as observed by library staff.

7.2 Limitations of this Virtual Reality Paradigm

A more pervasive limitation of this method is that even though it is an immersive, first-person evacuation experience preserving a tight integration between perception and action, there still are some limitations on perception that make it more difficult to ideally examine variables such as evacuation speed. First, if the avatar’s vertical displacement (i.e., with each step they take) is fully modeled veridically, it is physically uncomfortable to a participant (nauseating) because the display seems to jitter up and down as if watching a poorly shot hand-held camera scene. Humans do not experience this when actually moving up and down with each step, because the continuous haptic information about our motion is tightly integrated with the visual flow field. Thus, it was essential to remove the jitter for participants to be comfortable moving through the environment. On the other hand, removing this seemingly artificial jitter does remove a source of information that the participant is “walking.” Because a participant has no other haptic information about how fast

they are moving (subtle changes in sound as they move, feeling of air on one's face moving fast, and the feel of the ground beneath one's feet), an unnaturally fast movement was not necessarily experienced as running. This was likely exacerbated by the fact that participants did not need to worry about running into a table or stumbling because the program was moving their body: they did not have to navigate themselves. To have a sufficiently strong manipulation of movement speed, the upper range on fast walking was set unnaturally high (i.e., a running pace). Even so, in Fast Walking Speed conditions, the average desired speeds were not below the comfort midpoint of 4. One way to overcome this limitation would be to use a 360° treadmill that participants could walk on during their evacuation, rather than using a joystick. This would not provide perfectly integrated haptic information, but would be quite close.

7.3 Conclusion

Given the promising results of the above findings, we plan to test other psychological factors. For instance, we will attempt to understand when there will be excessive urgency to move due to blocking. A slowing that can seem unreasonable when no information is available may heighten anxiety or increase “nervousness” as Helbing’s model suggests. We will examine whether providing visual information can change the psychological experience of slowing that can occur when obstacles at the front of a crowd are unseen by participants at the back of a crowd. Therefore we hypothesize that reducing uncertainty by providing visual information about the causes of the slowing, or social information about what is occurring, may lead to predictions that deviate from Helbing’s model. Participants may be able to tolerate greater discrepancy between actual and desired speed, provided information is available and the participant is not under immediate danger. We will also examine other key factors of our model including trust in social over nonsocial information, and the effects of leadership and social bonds. Optimized guidance will be incorporated and tested. We are also planning to conduct a fire drill in the same library our virtual environment is created from. This could provide an opportunity to estimate parameters that are difficult to infer without realistic data from a large group of individuals. Such data could provide the basis for setting the initial value of parameters that are otherwise challenging to determine for running a FDS+Evac simulation, in addition to tuning the parameters in our macroscopic model.

Acknowledgements This work was supported in part by the National Science Foundation under Grant CMMI-1000495. We thank library staff members Susanna Cowan, David Avery, other AITC staff members, and the University of Connecticut Fire Department for their assistance on this project.

Disclaimer: The views expressed in this paper are solely those of the authors and do not necessarily represent those of NSF.

References

1. Grosshandler, W. L., Bryner, N. P., Madrzykowski, D., Kuntz, K.: Report of the technical investigation of the Station Nightclub fire. NIST NCSTAR 2, vol. 1. (2005)
2. Mydans, S.: At least 59 die in Bangkok club fire. *New York Times* (2009)
3. Proulx, G.: A stress model for people facing a fire. *Journal of Environmental Psychology*. 13, 137–147 (1993)
4. Fahy, R. F., Proulx, G.: Human behavior in the World Trade Center evacuation. In: 5th International Symposium on Fire Safety Science, pp. 713–724. Melbourne, Australia, (1997)
5. Helbing, D., Farkas, I., Vicsek, T.: Simulating dynamical features of escape panic. *Nature*. 407, 487–490 (2000)
6. Luh, P. B., Wilkie, C. T., Chang, S. C., Marsh, K. L., Olderman, N.: Modeling and Optimization of Building Emergency Evacuation Considering Blocking Effects on Crowd Movement. *IEEE Transactions on Automation Science and Engineering*. (2012). Digital Object Identifier [10.1109/TASE.2012.2200039](https://doi.org/10.1109/TASE.2012.2200039)
7. Wang, P., Luh, P. B., Chang, S. C., Sun, J.: Modeling and optimization of crowd guidance for building emergency evacuation. In: 4th IEEE Conference on Automation Science and Engineering, pp. 328–334. Washington DC, August (2008)
8. Averill, J. D., Mileti, D. S., Peacock, R. D., Kuligowski, E.D., Groner, N., Proulx, G., Reneke, P. A., Nelson, H. E.: Federal Building and Fire Safety Investigation of the World Trade Center Disaster: Occupant Behavior, Egress, and Emergency Communications. NIST NCSTAR 1–7. National Institute of Standards and Technology. Gaithersburg, MD, 2005
9. Korhonen, T., Hostikka, S.: Fire Dynamics Simulator with Evacuation: FDS+Evac - Technical Reference and User's Guide. VTT Technical Research Centre of Finland. Espoo, Finland (2009)
10. Korhonen, T.: "Issue 1547: Variable Unimpeded Walking Speed - Nervousness Parameter." FDS-SMV Issue Tracker, <http://code.google.com/p/fds-smv/issues/detail?id=1547>
11. Chalmet, L. G., Francis, R. L., Saunders, P. B.: Network Models for Building Evacuation. *Management Science*. 28, 86–105 (1982)
12. Hamacher, H. W., Tjandra, S. A.: Mathematical Modeling of Evacuation Problems – A State of the Art. In: Schreckenberg, M., Sharma, S. D. (eds.) *Pedestrian and Evacuation Dynamics*, pp. 227–266. Springer, Berlin, (2002)
13. Challenger, R., Clegg, C. W., Robinson, M. A.: *Understanding Crowd Behaviours: Supporting Documentation*. Cabinet Office, London (2009)
14. Gamberini, L., Cottone, P., Spagnoli, A., Varotto, D., Mantonani, G.: Responding to a Fire Emergency in a Virtual Environment: Different Patterns of Action for Different Situations. *Ergonomics*. 46, 842–858 (2003)
15. Mol, A. C. A., Jorge, C. A. F., Couto, P. M.: Using a Game Engine for VR Simulations in Evacuation Planning. *IEEE Computer Graphics and Applications*, 28, 6–12 (2008)
16. Koutamanis, Alexander: Multilevel Analysis of Fire Escape Routes in a Virtual Environment. In: 6th International Conference on Computer-Aided Architectural Design Futures, pp. 331–342. National University of Singapore, Singapore (1995)
17. Tang, C., Wu, W., Lin, C.: Using virtual reality to determine how emergency signs facilitate way-finding. *Applied Ergonomics*. 40, 722–730 (2009)
18. Drury, J., Cocking, C., Reicher, S., Burton, A., Schofield, D., Hardwick, A., Graham, D., Langston P.: Cooperation versus competition in a mass emergency evacuation: A new laboratory simulation and a new theoretical model. *Behavior Research Methods*. 41, 957–970 (2009)
19. Helbing, D., Farkas, I., Molnar, P., Vicsek, T.: Simulation of Pedestrian Crowds in Normal and Evacuation Situations. In: Schreckenberg, M., Sharma, S. D. (eds.), *Pedestrian and Evacuation Dynamics*, pp. 21–58. Springer, Berlin (2002)
20. Latane, B.: The psychology of social impact. *American Psychologist*. 36, 343–356 (1981)

Development of Smoke Control System Ensuring Safe Evacuation Through Stairwell for High-Rise Building in Korea

Jung-Yup Kim, Hyun-Joon Shin, and Ji-Seok Kim

Abstract In general, the pressure differential smoke control system has been used as a smoke control system on the emergency stairs of high-rise buildings, but it can fail to achieve the purpose of pressure differential system due to high possibility of overpressure between the lobby and the accommodation or pressure drop in the lobby in case the leakage and supplementary air flow is supplied at the same time through one air supply path. In connection with improvement of this problem, we suggested device configuration and methods to conduct supply of leakage and supplementary air flow through different flow passages, thereby providing safe evacuation environment in case of a fire in high-rise buildings.

Keywords Smoke control system • High-rise building • Evacuation stairwell • Field experiment

1 Introduction

With increased advancement and integration of the cities, the demand for large-scale, high-rise and complex buildings has been on the rise, and the number of buildings vulnerable to fire has also increased (Table 1). In this connection, the need for of effective prevention measure of fire is urgently required. In particular, the importance of smoke control system is highlighted in the recognition that the smoke is the main cause to disturb evacuation and fire fighting activities and the biggest threat to human life in case of a fire (Table 2).

In the recognition that suffocation due to smoke spread is the main cause of human deaths as in the cases of fires in MGM Grand Hotel, Roosevelt Hotel and

J.-Y. Kim (✉) • H.-J. Shin • J.-S. Kim
Fire Research Center, Korea Institute of Construction Technology, Goyang, Gyeonggi-Do, South Korea
e-mail: jykim1@kict.re.kr; hjshin@kict.re.kr; gorapadk@kict.re.kr

Table 1 Status of annual high-rise building construction (Korea), Unit: number of buildings [1]

Year	2006	2007	2008	2009	2010	2011
Number of floors						
21–30 floors	428	1,235	816	689	876	669
More than 31 floors	51	115	173	80	170	134

Table 2 Design criteria for smoke control system of emergency stairs by major countries

Nation	Fire safety standards (smoke control system part)	Remarks
The U.S.	NFPA 92A IBC (1022.9, 909.20)	
Europe	EN 12101-6	
China	GB 50045 (8.3)	

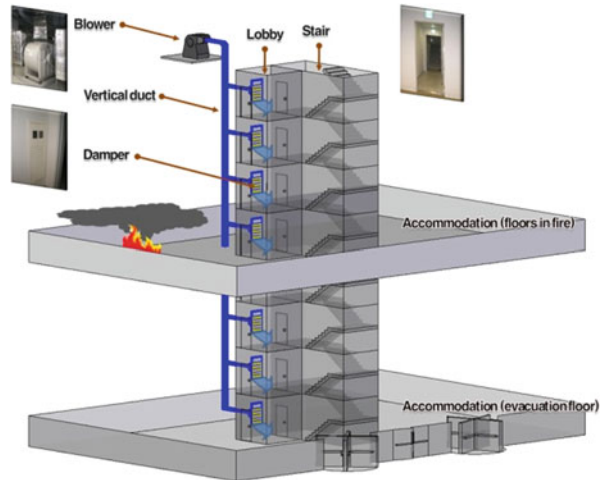
Johnson City Retirement Center, and reliable smoke control system is needed to cope with this situation, major countries have developed design technologies for smoke control systems through a variety of real-scale experiments and establishment of a theoretical foundation for smoke generation, diffusion and control applications and made continuous investments in the establishment of multiple criteria that ensure efficiency and applicability [2, 3].

In particular, they have suggested standards for smoke control on the emergency stairs as in Table 2, recognizing the importance of protecting the emergency stairs from smoke for safe evacuation in case of a fire in high-rise buildings [4–6].

In Korea, “fire safety standards of smoke control facilities in the special emergency stairs” of NFSC501A is presented as one of the fire safety standards designed to secure the smoke safety of high-rise buildings and prevent penetration of the smoke into the restricted areas. In line with this, the pressure differential smoke control system to increase the pressure inside the lobby between accommodation and staircase using smoke control blower and air supply damper shown in Fig. 1 has been used in Korea. In the pressure differential smoke control system, the differential pressure of between lobby and accommodation has to be maintained within a certain range to prevent penetration of the smoke and make it easier for evacuees to open doors, and to this end, flap dampers and differential pressure control dampers are being adopted in terms of equipment installation.

As above, the main design criteria for emergency stairway smoke control system of high-rise buildings used in major countries including Korea was established in the 1970s and 1980s, and it is reflected in fire safety standards by countries. The importance of smoke control system of emergency stairs has been highly recognized in terms of protection of the stairs from the smoke, but it is sometimes reported that the existing smoke control system of stairs don’t meet the performance requirements suggested in the international standards. That is, internationally prestigious papers and reports conclude that the smoke control system of emergency stairs which is currently applied is not effective in terms of providing evacuees with

Fig. 1 Conceptual diagram on the pressure differential smoke control system of emergency stairs



safe evacuation environment in case of a fire since it increases the force required to open doors of emergency stairs, thereby disturbing evacuees' activities to enter the stairs.

In this study, field experiments were conducted, targeting multiple high-rise buildings which are currently in operation to perform performance evaluation of the smoke control systems on the emergency stairs of high-rise buildings. In addition, the results deduced from field experiments on the performance evaluation were analyzed, and development directions of separated air supply system to perform air supply of leakage and supplementary amount through different flow passages were suggested.

2 Field Performance Evaluation on the Pressure Differential Smoke Control System

2.1 Field Experiment Methods

In this study, we evaluated operating performance of the pressure differential smoke control systems, targeting multiple high-rise buildings which are actually in operation and reviewed the results of measuring the indoor pressure in the accommodation, lobby and stairs during the operation of the smoke control systems.

Figure 2 shows air supply blower installed in each building and differential pressure control damper installed inside of the lobby is shown in Fig. 3. In Fig. 4, pressure gauge to measure the pressure formed in the interior through an operation of the smoke control system is shown in a graphic form.

Fig. 2 Air supply blower



Fig. 3 Lobby and damper



Fig. 4 Pressure sensor



2.2 Results of Field Performance Evaluation

2.2.1 The Condition that All Doors Are Closed

As shown in Fig. 5a, the indoor pressure was measured in the accommodation, lobby and stairs of the 2nd, 11th and 18th floors with all doors closed in 21-story Building A. Figure 5b, c show some results of the performance evaluation experiments. Figure 5b represents indoor pressure fluctuations in the accommodation, lobby and stairs depending on the time of measurement during the operation of the smoke control systems, and Fig. 5c the differential pressure between the accommodation and lobby.

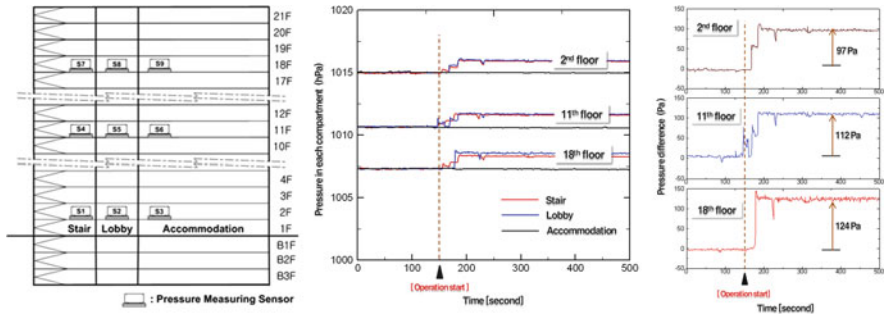


Fig. 5 Field experiment results on the condition that the door of lobby is closed

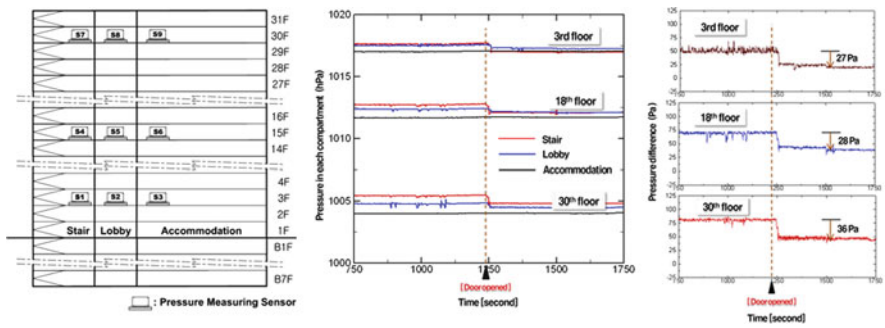


Fig. 6 Field experiment results on the condition that the door of lobby is open

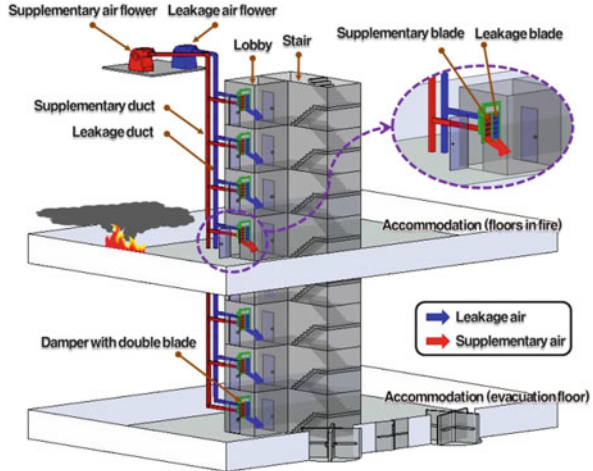
As identified in the figures, the differential pressure between the accommodation and lobby was 97 Pa on the 2nd floor after the operation of the pressured air supply system, and the differential pressure between the accommodation and lobby was recorded within the range of 112 and 124 Pa, which is much higher figure than design criteria value of 40 Pa. As above, in case high differential pressure is formed between the accommodation and lobby, it is likely that occupants have a difficulty opening the emergency exit in case of evacuation.

2.2.2 The Condition that the Door of a Lobby Is Open

As shown in Fig. 6a, the indoor pressure was measured in the accommodation, lobby and stairs of the 3rd, 15th and 30th floors with all doors open in 31-story Building B. Figure 6b, c show some results of the performance evaluation experiments.

As identified in the figures, the differential pressure between the accommodation and lobby was 48 Pa on the 3rd floor with all doors closed, but it was decreased to approximately 23 Pa with door of lobby open. In case of the 30th floor, the differential pressure was decreased from about 82 to 46 Pa. As clarified above, if the door of lobby is open in case of the current pressure differential smoke control system, the problem that the pressure of lobby on each floor drops may occur.

Fig. 7 Conceptual diagram of the pressure differential smoke control system for separation of leakage and supplementary air flow



3 Development of the Pressure Differential Smoke Control System for Separation of Leakage and Supplementary Air Flow

As identified above, the existing pressure differential smoke control systems can have the problem of the lobby pressure drop and formation of overpressure between the accommodation and lobby depending on the status of the lobby doors. With respect to this improvement, the development of the pressure differential smoke control system for separating the leakage air flow and the supplementary air flow through different flow passages are introduced in this study as follows.

3.1 Separated Air Supply-Based Design Methodology

In the pressure differential smoke control system for separation of leakage and supplementary air flow, the independent leakage air flow and the supplementary air flow is supplied to the lobby of each floor through different flow passages. That is, the leakage air flow is supplied to the lobby on each floor through the leakage air flow control blade of air supply damper, duct and blower for leakage air flow supply, and the supplementary air flow is supplied to the lobby on each floor through the supplementary air flow control blade of air supply damper, duct and blower for supplementary air flow supply as shown in Fig. 7. If this concept of separate air supply is introduced, a reasonable air supply status can be formed under the terms of opening and closing the doors of the lobby as shown in Table 3.

Table 3 Concept and effect of separate air supply

Status of the door of lobby	Status of air supply to lobby	Effect
Closed	Only leakage air flow is supplied	Maintaining the proper differential pressure Preventing overpressure between the accommodation and lobby
Open	Only supplementary air flow is supplied	Forming air critical velocity Preventing outflow of the leakage air flow into the open door

**Fig. 8** Complete view of double-blade air supply damper

3.2 Development of Double-Blade Air Supply Damper

To operate the pressure differential smoke control system for separation of leakage and supplementary air flow effectively, the air supply damper to provide and control the leakage and supplementary air flow according to the pressure formation conditions of an lobby needs to be developed as a key component. In this connection, the intelligent air supply damper of double-blade type was developed in this study. As shown in Fig. 8, the double-blade air supply damper is composed of pressure sensor, opening regulator and controller in addition to double blade for leakage and

Table 4 Operating conditions of double-blade air supply damper

Door state	Closed	Open
Status of differential pressure between the accommodation and lobby	Differential pressure (ΔP) between the accommodation and lobby is higher than ΔP_1	Differential pressure (ΔP) between the accommodation and lobby is lower than ΔP_1
Operating conditions of leakage air flow control blade	Open in case ΔP is higher than ΔP_1 PID is controlled to maintain ΔP to be ΔP_2	Closed in case ΔP is lower than ΔP_1
Operating conditions of supplementary air flow control blade	Closed in case ΔP is higher than ΔP_1	Completely open in case ΔP is lower than ΔP_1

supplementary air flow control. In double-blade air supply damper, the leakage air flow control blade is connected to the vertical air duct for the leakage air flow supply, and the supplementary air flow control blade is connected to the vertical air duct for the supplementary air flow supply. The double-blade air supply damper is controlled to perform switching operation of the blades for leakage and supplementary air flow control depending on the differential pressure (Δp) of the lobby pressure (Δp_L) and accommodation pressure (Δp_A) (Table 4).

4 Conclusion

In recent years, the importance of smoke control system has been highlighted in the recognition that the smoke is the main cause to disturb evacuation and fire fighting activities and the biggest threat to human life in case of a fire. In line with this, the pressure differential smoke control system to prevent penetration of the smoke into the emergency stairs has generally been used in Korea.

The evaluation on the operating performance of the pressure differential smoke control system was carried out, targeting multiple high-rise buildings which are currently in operation. And it was found that the purpose of the pressure differential smoke control system may not be achieved due to high possibility of overpressure between the lobby and the accommodation or pressure drop in the lobby in case the leakage and supplementary air flow is supplied at the same time through one air supply path.

In connection with improvement of this problem, we introduced the key concepts of the pressure differential smoke control system for separating the leakage air flow and supplementary air flow through different flow passages, and also suggested the operating principles and structure of the double-blade air supply damper that is a key component for providing separate air supply effectively.

Acknowledgement This study has been conducted by the relevant study to “(2012) Study of Advanced Performance-Based Fire Safety” Project, a major project of Korea Institute of Construction Technology subsidiary supported by Ministry of Knowledge Economy.

References

1. Statistics of the Ministry of Land, Transport and Mari-time Affairs in Korea. (2012)
2. Tamura, G.T. : Fire Tower Tests of Stair Pressurization Systems with Overpressure Relief, *ASHRAE Trans.*, Vol. 96. (1990)
3. Tamura, G.T. : Assessment of Stair Pressurization System for Smoke Control, *ASHRAE Trans.*, Vol. 98. (1992)
4. BS EN12101-6.: Smoke and heat control system – Part6 : Specification for pressure differential systems, British Standards Institution. (2005)
5. NFPA 92A. : Standard for Smoke-Control Systems Utilizing Barriers and Pressure Differences, National Fire Protection Association. (2006)
6. GB 50045-95.: Code for Fire Protection Design of Tall Civil Building, China Planning Publishing House. (2005)

Early-Stage Egress Simulation for Process-Driven Buildings

Gabriel Wurzer

Abstract Many complex buildings such as hospitals, airports and industrial facilities are process-driven, meaning that their design is conceived around the daily work routines of the staff, usually captured using business processes (e.g. by using flowcharts or Business Process Modeling Notation). The main idea and contribution of our approach is to leverage such a static process model in order to facilitate a dynamic egress simulation. In detail, we perform a process simulation until a specified time t is reached. As result, we get the typical location of the working staff as well as occupancy of all areas of the building, which we then feed into an agent-based egress simulation. As result, we can obtain the evacuation performance at time t under consideration of the building's process model, i.e. different usage scenarios throughout the day. This hybrid approach between process simulation and pedestrian simulation is especially suited for early stages of building design, when different spatial configurations and process variants are under consideration. In this context, the approach is just one part of many lines of architectural reasoning, covering foremost the problem of accessibility and adjacency by means of pedestrian simulation.

Keywords Process Simulation • Pedestrian Dynamics • Functional Design

G. Wurzer (✉)

Architectural Sciences, Vienna University of Technology, Vienna, Austria
e-mail: gabriel.wurzer@tuwien.ac.at

1 Introduction

The planning of process-driven buildings is occupied foremost with the production of a spatial design that facilitates the daily work routines of the building users. Especially in the early phases of the design project, architects and organization planners work in close cooperation to achieve this goal:

- **Organization planners** define the operational model of the organization, which takes the form of a hierarchy of business processes (processes and sub-processes), an organizational schema containing the responsibilities for each process (i.e. process roles), and, ultimately, a definition of staffing needs arising out of the process model.
- **Architects** define a spatial configuration that satisfies the organizational requirements, most prominently: the business processes. In this context, multiple variants of a preliminary design (also called architectural schema) are being evaluated, the key criterion being the adjacency of areas which exhibit a high degree of cooperation (as described by the process model).

In previous work [1], business process simulation (BPS) has been used to superimpose processes over the preliminary design, in order to constrain the spatial concept so that it fulfills the process model and at the same time visualize work routines of the staff. This paper extends on these concepts, by introducing a (dynamic) egress simulation that is based on the state of the aforementioned (static) process simulation at a time t . More specifically,

1. The state of the process simulation at time t gives the usage of each space.
2. An egress simulation takes this usage and computes the pedestrian flow to the nearest exits.
3. The recorded density and evacuation times can then be visualized and subsequently used to get an insight into bottlenecks occurring because of the spatial arrangement and expected occupation of the building at time t , at quite an early stage.

The inner mechanics of this hybrid simulation are detailed in Sect. 3. Apart from the actual communication between BPS and ABS, we also contribute a look at the required synchronization constructs used (see Sect. 3.3).

2 Related Work

Our approach is based on connecting a Business Process Simulation (BPS) to an Agent-Based Simulation (ABS). We are aware of many approaches following this hybrid approach (e.g. [2, 3]), but none seems to be specifically focused on the early planning of process-driven buildings, which is central to our work. What makes this context special is that it requires statements about circulation and adjacency of the preliminary design [4] on a qualitative (rather than quantitative) level. Simulation as

means for such insights, especially concerning dynamic aspects of movement and occupancy remains an area where previous work is extremely scarce; one example in this respect concerns user simulation of space utilisation [5], using the (three-dimensional) circulation network within the planned building as basis. In contrast to our work, the emphasis here is on office buildings and user behaviour (rather than planned processes), which can be used as basis for design optimization when simulating physical movement and subsequent space utilization [6, 7]. A similar approach focusing on sensitivity of a circulation network towards congestion and blockage [8] forms the basis of the evacuation simulation presented herein.

3 Inner Mechanics of the Hybrid Egress Simulation

3.1 Preparing the Process Model

Our simulation is based on Microsoft Visio, a modeling platform commonly used by organization planners for process modeling. Classically, the notation employed for this task has been based on flowcharts, in which nodes of the flow graph are annotated with additional data, either through data contained within a shape (see Fig. 1a), activity nodes with additional visual elements to hold metadata (Fig. 1b) or comments (Fig. 1c).

In our case, this metadata is important because it has to contain the physical location within the preliminary design (i.e. “where” an activity is taking place). We used unique room stamps such as “1E01” which had to be manually attributed, and later mapped to locations via a table.

It is also important to note that we employ a special style of process modeling in which each process represents one role – e.g. patient, staff, etc.; while this is not true for the common case – but almost always done in the context of planning of process-driven buildings. The reason for this lies in the communication between architects and building organization planners, which happens mostly by tracing these processes on preliminary floor-plans, one at a time.

3.2 Invoking the Simulations from the Modeling Platform

Using Visio’s scripting support, we first export the process flowcharts in a custom format (see Fig. 2a) for use in our own (external) process simulation (see Fig. 2b). In parallel to the process simulation, an agent-based simulation (ABS) which computes pedestrian flow (Fig. 2c) is also started. Process simulation and agent-based simulation (Fig. 2d) work synchronized, with messages being passed bidirectionally: Upon reaching a specified time t , the process simulation issues such a simulation request, passing all active processes (instance names, room stamp associated with currently

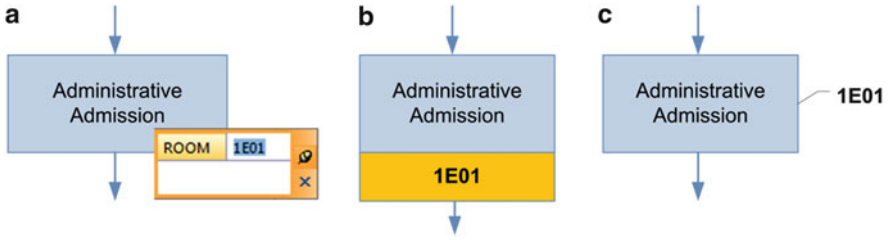


Fig. 1 Metadata for nodes within a process (a) as additional shape data, (b) attached graphical element or (c) comment

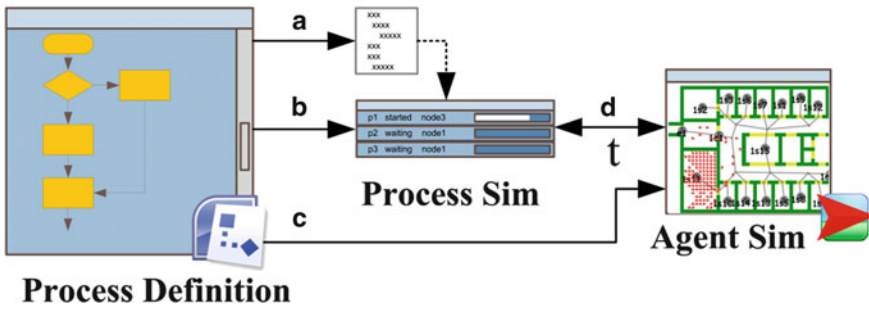


Fig. 2 Interaction between different parts of proposed approach. (a) Export of processes from Visio as input to (b) process simulation. (c) Agent simulation is opened in parallel and receives (d) simulation requests at time t from process simulation

executing nodes). The agent simulation generates an agent for each supplied process instance, and starts the egress simulation, employing whatever physical movement algorithm to move all agents to the nearest exit. In our concrete case, we use the cell-based movement model given by Blue and Adler [9]. As result of a model run, the ABS records simulated densities and the Required Safe Egress Time (RSET) for that instance t . Trivially, the outlined procedure can be repeated for a whole day, giving planners a clear picture over evacuation performance of their process-driven building at a single glance.

3.3 Communication Between Process Simulation and Agent Simulation

Our process simulation is an adaptation of a widely used business process engine [10], for the sake of showcasing our approach. The same goes for our agent simulation, which is based on the popular NetLogo ABS platform [11]. Both simulations act as servers and clients, performing bidirectional data exchange over sockets using a fixed protocol.

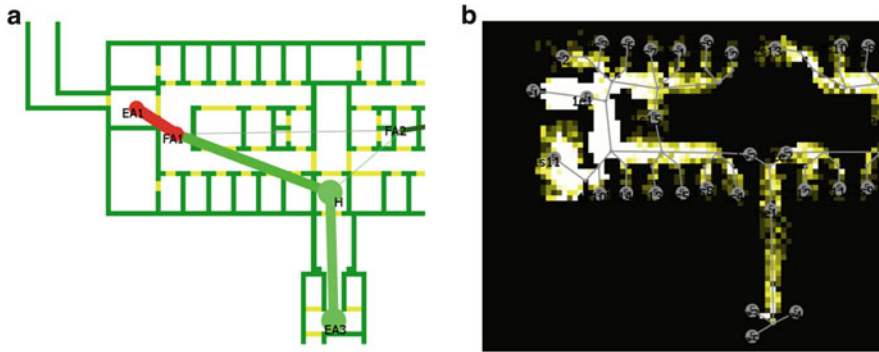


Fig. 3 Depicting results. (a) Bubble diagram with throughput (b) space utilization for a single timestep

Communication between BPS and ABS requires some synchronization construct, since these simulation types differ in their time bases (future event list versus simulation in seconds). In simplest approach, which we have undertaken, BPS and ABS both progress in seconds. For each time step, the BPS executes processes scheduled at that instance. Once time t is reached, it issues the command to begin simulating to the ABS, passing the active processes and their respective process states (including the attributed room stamp of the current node) for subsequent instantiation of agents. On the side of the ABS, the passed room stamps are used for obtaining a location for a new agent within the design, which (in our case) is composed of a cell-based floor plan and a superimposed graph-based route network that is used in conjunction with the Blue-Adler physical movement model to simulate the passage from one space to the other. The results (Densities per cell, RSET) can be communicated back, e.g. for use in a report covering the span of a day.

4 Outcome for the Design Process

As Rittel is often quoted, design is a “wicked” problem [12] that is hard to describe without reference to some solution. The presented evacuation analysis represents a step into this direction, albeit in a qualitative manner:

- The variation of the computed RSET throughout the day can be taken as overall measure of complexity/congestive tendency of the proposed design. Alternative designs can be considered when comparing two such RSET curves at equal sampling points.
- The congestive tendency within the design can be visualized by (1) assignment of all spaces to a functional area (2) counting the passages between different functional spaces and (3) visualization of these as a bubble diagram (see Fig. 3a) with weighted line and node thicknesses. Because the flow is measured for a

whole day, the variability in throughput can be furthermore color coded to depict areas of high sensitivity to congestion.

- Space utilization can be counted and visualized as well, by means of a color scale (see Fig. 3b). Furthermore, as in the previous case, areas of high variability in usage throughout the day could be highlighted, since these are probable candidates for multi-functional use. Depicting space utilization visually is very important for ensuring proper separation between private/public areas. Another possibility for further work is the explicit depiction of types of process participants (e.g. patient, staff), in order to spot possible flow crossings which are unwanted (e.g. because of hygienic or again privacy considerations).

5 Summary

We have proposed a hybrid approach linking static process simulation to dynamic egress simulation, in order to visualize bottlenecks and accessibility problems for the design process-driven buildings, based on occupancy provided by the process model. In contrast to existing egress simulations, our efforts are targeted at early stages of design and act as qualitative means rather than giving quantitative statements. The choice of process simulation and pedestrian algorithm is up to the implementers – the authors use an own process simulation linked to a Blue-Adler model.

Acknowledgements This work was supported by the “Österreichische Forschungsgemeinschaft” under the program “Internationale Kommunikation” (Project 06_12685).

References

1. Wurzer, G.: Schematic Systems -Constraining Functions Through Processes (and Vice Versa), In: *International Journal of Architectural Computing*, Vol. 08 (2010).
2. Remondino, M.: Agent Based Process Simulation and Metaphors Based Approach. In: Müller, J.-P., Seidel, M.-M. (eds.) *Proceedings of the 4th Workshop on Agent-Based Simulation*, Montpellier, France, 28–30 April 2003, Society for Computer Simulation, pp. 93–97 (2003)
3. Borshchev, A., Filippov, A.: From System Dynamics and Discrete Event to Practical Agent Based Modeling: Reasons, Techniques, Tools. In: Michael Kennedy (ed.) *Proceedings of the 22nd International Conference of the System Dynamics Society*, (2003)
4. White, E. T.: *Space Adjacency Analysis*, Architectural Media, Tucson (1986)
5. Tabak, V.: *User Simulation of Space Utilisation*, PhD. Thesis, TU Eindhoven (2008)
6. Sharma, S., Tabak, V.: Rapid Agent Based Simulation of People Flow for Design of Spaces. In: Timmermans, H.J.P., de Vries, B. (eds.) *Design & Decision Support Systems in Architecture and Urban Planning*, ISBN 978-90-6814-173-3, University of Technology Eindhoven (2008)
7. Joyce, S., Tabak, V., Sharma, S., Williams, C.: Applied Multi-Scale Design and Optimization for People Flow, In: *Proceedings of the 28th eCAADe*, pp. 633–639 (2010)

8. Wurzer, G., Ausserer, M., Hinneberg, H., Illera, C.: Sensitivity Visualization of Circulation under Congestion and Blockage, In: Proceedings of Pedestrian and Evacuation Dynamics 2010, Gaithersburg (2010)
9. Blue, V., Adler, J.: “Cellular automata model of emergent collaborative bidirectional pedestrian dynamics”, In Proceedings of Artificial Life VII, Portland (2000).
10. Rucker, B.: Building an open source Business Process Simulation tool with JBoss jBPM, Master Thesis, Stuttgart University of Applied Science (2008)
11. Wilensky, U.: Netlogo, Center for Connected Learning and Computer-Based Modeling, Northwestern University, <http://ccl.northwestern.edu/netlogo> (1999)
12. Rittel, H., Webber, M.: Dilemmas in a General Theory of Planning, In: Policy Sciences, Vol. 4, pp. 155–169 (1973)

Effect of Guidance Information and Human Relations Among Agents on Crowd Evacuation Behavior

Masaru Okaya and Tomochi Takahashi

Abstract Evacuating people during emergency situations or natural disasters is a complex task. In simulation systems, evacuees have been treated equally, or at least physical difference such as the evacuees' ages and genders are considered as parameters of simulations. We believe the content of guidance information influences their mental states, as well as helps to alleviate anxiety about their own and their family's safety, and leads to evacuation behaviors based on their situations. The effect of guidance information as it relates to family relationships among agents is simulated with our ABS evacuation simulation system. Three evacuation scenarios involving different types of disasters are simulated and the results are discussed.

Keywords Simulation • Phased evacuation • Mental state • Evacuation guidance

1 Introduction

Evacuating of people during emergency situations or natural disasters is a complex task. It is difficult to conduct physical experiments that involve many people and real environments, or to make effective plans for predictable situations based on the data of past disasters. Disaster simulation systems are employed to develop prevention plans for disasters and to test the plans. In simulation systems, evacuees are treated equally, or at least physical differences such as the evacuees' ages and genders are considered as the parameters of simulations [1].

M. Okaya (✉) • T. Takahashi

Department of Information Engineering, Meijo University, 1-501 Shiogamaguchi, Tempaku,
Nagoya 468-8502, Japan

e-mail: m0930007@ccalumni.meijo-u.ac.jp; ttaka@meijo-u.ac.jp

We know how people evacuated during disasters from reports published by those in authorities. They involve the following phenomena: people begin evacuation based on their preset circumstances; announcements from those in authority are not always clearly heard; and people communicate and share information among themselves and adjust their actions and behaviors accordingly. The phenomena present features that are addressed by crowd simulation systems.

We focus guidance information and human relations on agents involved in the disaster to control the behaviors exhibited during evacuations. The guidance information is broadcast by those in authority to achieve a more efficient evacuation process. As a result, better evacuation results in less damage caused by the disasters. An agent-based crowd evacuation simulation is proposed in this paper; the features of the systems are as follows: the guidance information is presented as a method of communication to and among agents, and their actions emerge from BDI (Belief-Desire-Intention) models. The guidance information is fed to the BDI models so that human relations factors of the agents are represented.

Background and related works are described in Sect. 2. Section 3 introduces our simulation system, which can provide guidance for agents to rely on during their evacuation. The agents behave according to their circumstances. Three scenarios of different evacuation types are shown. The simulation results are discussed in Sect. 4, and the summary is described in Sect. 5.

2 Background and Related Works

Disasters can occur anywhere and anytime, and can result in serious damage. Several disasters that caused serious damages in this decade immediately come to mind; for example, the September 11, 2001, attacks on the World Trade Center (WTC), the East Japan earthquake, along with the resulting tsunami, that occurred on March 11, 2011, and so on. Although they were different types of disasters and different types of evacuation behaviors were shown, evacuation simulation is one of the key factors necessary to decrease the damages that result from emergencies.

Bandini et al. cited three future research topics on crowd simulation: data acquisition using new technologies, such as GPS and RFID, validation techniques advancing beyond empirical studies, and the integration of psycho/sociological consideration in crowd models [6]. Pelechano presented an agent-based simulator for which both physical interactions and communication between individual agents are introduced [7]. A detailed report on occupant behavior in the World Trade Center (WTC) disaster has been published by the National Institute of Standards and Technology (NIST), and a related study has been carried out by Galea et al. [2, 4]. Survey results on evacuation behavior during the East Japan Earthquake are available as conference documents to the Japanese Government [5].

3 2001 World Trade Center

NIST organized evacuation studies of the WTC disaster through interviews and questionnaires. In the reports, the behaviors of people differed between WTC tower 1 and tower 2, and these also differed among people who had experienced the 1993 WTC bombing incident. Some occupants started to evacuate as soon as WTC1 was hit, while others performed specific activities that they wished they had performed in 1993, such as calling home and the like. The following phenomena were reported in the report.

1. Rescuers who entered a building moved in the opposite direction of occupants who were exiting the building. These movements resulted in human interactions during the evacuations. Family-minded human behaviors, such as parents searching for their children, may also have caused similar interactions during crowd evacuation.
2. Evacuation guidance information leads people to evacuate safely and efficiently. While some people begin to evacuate immediately after hearing evacuation guidance information, others may continue working if the guidance is not clearly announced. In a worst case scenario, others may not hear the guidance information.

4 2011 Great East Japan Earthquake

After the earthquake, announcements of the impending tsunami attack and requests for quick evacuations were broadcasted throughout towns by various administrative offices. In the report, people who heard the announcements are categorized into three types: (1) individuals who evacuated immediately upon hearing the announcement; (2) individuals who evacuated after first completing tasks that they had been working on, and (3) individuals who evacuated when they really felt that their life was being threatened [5].

3. Teachers guided their students to a refuge after they heard the tsunami warning along with the earthquake warning. During the evacuation, someone on the way to the refuge informed them that the refuge was not safe, so they went to the other refuge. However, they did not have enough time to make it to the second refuge.

NIST assessed the evacuation time from the WTC and analyzed the behavior of people during the evacuation using the following simulation systems: EXODUS, EXIT89, Simulex and ELVAC [2]. They reviewed the features of the egress models of simulators [1]. Although the above three points are important features of evacuation behaviors, the features have not been supported by the existing evacuation simulations.

We believe getting information guidance information to evacuees is one of the key factors that affect their evacuation behaviors. Table 1 presents the issues

Table 1 Features of models in evacuation simulations and their purposes

Model of evacuation behaviors
Traffic simulation
Travel speed model
Congestion model
Counter flow, obstacle model
Space model
Grid/network/continuous space
2D or 3D model
Actions involving individual behavior
Sensing model
Delays in evacuating
Receiving information
Action model
Selfish/altruistic actions
Information seeking task
Choosing and locating exit routes
Group behaviors
Leadership/ human relations
Sharing information
Purposes of simulations
Risk management
Preventions planning
Experience and training rescuer/rescuee

discussed in the report. The ‘-’ marked features are important in simulating following process: the contents of guidance influence evacuees’ mental states and affects their anxiety levels concerning their own and family’s safety, which in turn leads to evacuate behaviors based on their individual situations. The simulators in the reports do not have the functions of announcing evacuation guidance information to occupants, and presenting their human relationship that affect the behaviors of evacuation.

5 Simulation with Guidance Information for Evacuees and Human Relations Among Agents

5.1 Features of Our System

There are various scenes for rescue and search operations during disasters, and evacuation behavior is different for each scene. Figure 1 illustrates typical scenes that may occur when disasters strike are, for example,: (1) the disaster-prevention departments broadcast emergency announcements; (2) people exit rooms and proceed to the ground level using the stairs and elevators; (3) people evacuate to safe places; and (4) rescuers start their operations.

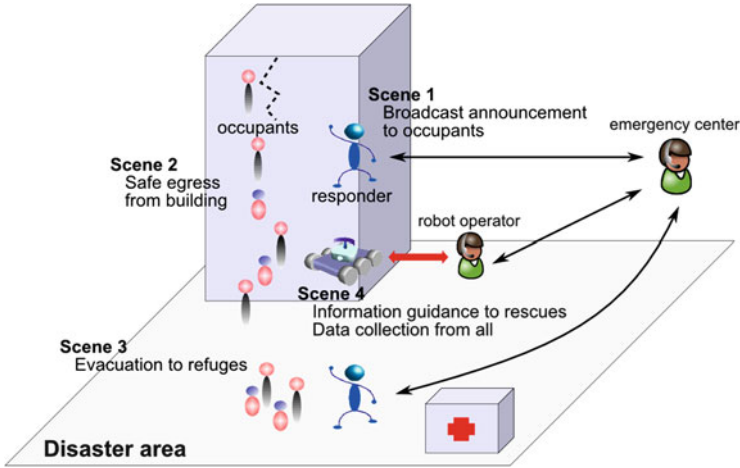


Fig. 1 Emergency scene and evacuation scenarios

We propose a crowd evacuation system for which human relations among agents and guidance announcements during emergencies are taken into consideration. Features of the system are as follows:

1. During emergencies, people behave differently than they normally would. Their behaviors are affected by mental conditions. A BDI model is employed to show how agents select their actions based on particular situations during the sense-reason-act cycle.
2. Some people engage in altruistic behavior. For example, parents may take care of their children at the risk to their own safety. They move against the major flow of other people to reach their child. The counter movement may become a blockade to others who are hurrying to refuges.
3. During disasters, there are two types of information propagations: announcements from those in authority to evacuees and communication among evacuees. They are introduced as communication among agents during simulations.

5.2 Agent-Based Simulation System

Figure 2 shows the architecture of our agent based system.

5.2.1 BDI Model Representation of an Evacuee State

During emergencies, people feel unusual events are taking place and, become anxious about their own safety and that of their family and take various actions

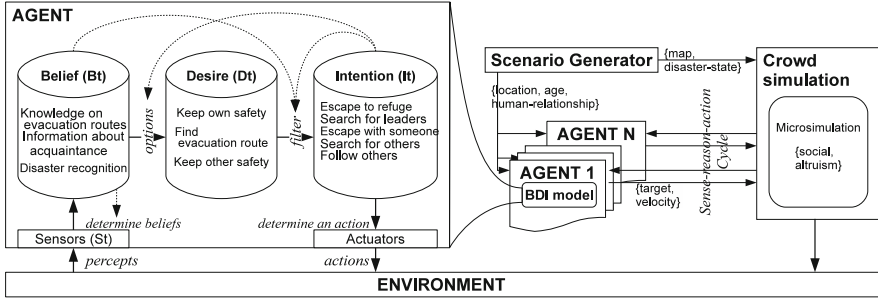


Fig. 2 System architecture of ABS evacuation system

based on information received. Some people may only trust information that is disseminated by an authority figure, while others will trust their neighbors or heed messages sent from their acquaintances. During the Great East Japan Earthquake, it is reported that approximately 30 % of people began their evacuation by taking advice from acquaintances who themselves had taken the evacuation guidance information seriously [5].

We categorize these behaviors as an awareness of danger. The degree of awareness of danger differs among different people, and these differences influence their behaviors when they start evacuating. The BDI model has been adapted to represent such behaviors.

- **Belief (B_t):** $B_t = belief(S_t, B_{t-1})$
When a person feels the shock of the earthquake or hears evacuation instructions, he/she considers his/her safety to be more important than other jobs. Some agents who do not feel they are in danger might feel differently when they hear evacuation instructions. The awareness of danger as it relates to beliefs changes according to the mindset of the agent.
- **Desire (D_t):** $D_t = option(B_t, I_{t-1})$
The changes in beliefs affect desires. Most people are in the middle of performing a job when a disaster strikes. They may have the desire to finish the task, or they may have other desires to keep themselves and others safe.
- **Intention (I_t):** $I_t = filter(B_t, D_t, I_{t-1})$
Agents filter one action from suitable actions to achieve their own desires. Agents have their own preferences depending on their personality and social norms. An agent might intend to evacuate or to save an injured person.

S_t is a set of sensor data that an agent receives at time t , and B_t , D_t and I_t represent the status of beliefs, desires and intentions, respectively. B_t consists of rules of action, knowledge, and states. The differences in agent types are implemented by using different *belief*, *option*, and *filter* functions.

5.2.2 Evacuation Guidance Information to Agents

Authorities announce information that will help make evacuations efficient and smooth, and agents try to share information. The agent hears the evacuation guidance information as sensor data. The guidance is transmitted through two methods: (1) emergency announcements from authorities and (2) communications from other agents.

The guidance consists of the targeted persons, evacuation routes, and other pertinent information. Announcements are implemented in a form of Agent Communication Language (ACL). The following example shows evacuation instructions in which a rescuer guides an occupant on the first floor to use route *R1* byway of points *A1* and point *A2*.

```
(inform
:sender Rescue-1
:receiver Anonymous
:time 20110311-100000
:content (evacuation-guidance
:target-area 1F
:move A1-A2-R1))
```

The text announced by the rescuer may not be audible to all target agents, and some agents may not hear the complete message. These situations are simulated by two parameters in the communication protocol to agents: (a) the distance up to which the message can be heard and (b) the percentage of loss in the message.

5.2.3 Crowd Simulation on Continuous 3D Space

Agents determine their intentions at every simulation step at which they receive new sensor data, and send their targets position to a crowd simulator. The crowd simulator calculates the movements of the agents in the step. The motions of the agent at one simulation step t is calculated by micro simulation using a model in that altruism force that comes from his/her own human relations and is added to a social force in Helbing's model [3, 8].

5.3 Evacuation scenarios

The following three scenarios are presented to showcase our features that traditional evacuation systems do not possess.

Scenario 1. Pairs of parent–child evacuations from campus:

Agents act according to their conduct codes or wills. Parents tend to act on their own child's behalf at the risk to their own safety. During emergencies, they

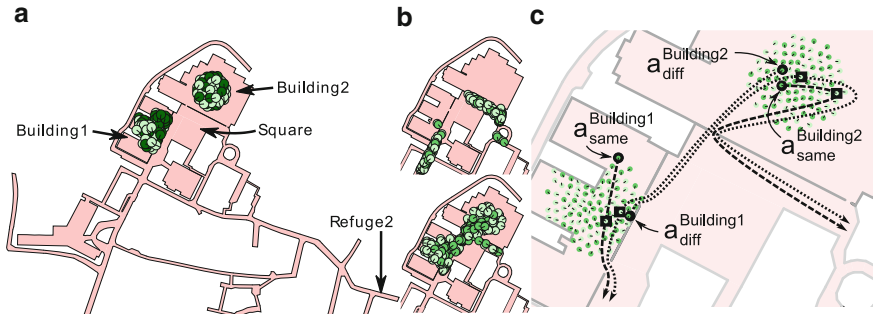


Fig. 3 Layouts of buildings and snapshots of simulations. (a) Layout. (b) Snapshots. (c) Trajectories of parent agents

evacuate together, and the parent goes to his/her child if they are separated when the disasters strike.

Scenario 2. Evacuations with guidance information provided by those in authority and communication among evacuees:

During an emergency, people go to a refuge. Authorities announce the location of refuges, along with routes that they assume safe. Some agents follow the guidance information, while others do not for various reasons.

Scenario 3. Phased evacuation from a library building:

Authorities of buildings prepare texts to be announced to the building occupants during emergencies. The texts may contain different messages based on the needs of people on different floors to ensure evacuees move quickly and efficiently.

6 Simulation Results

6.1 Scenario 1: Pairs of Parent-Child Evacuations from Campus

The scenario is evacuation from a campus (Fig. 3a). Fifty pairs of parents and children participated in an event that was held in two buildings on the campus. The features of the agents are as followings:

- Parent agents move autonomously and can look for exits when they have no knowledge of escape routes. They have one child and are anxious about their child
- Child agents have no data on escape routes and no ability to ask others for help. They can distinguish and follow their parents.

They are divided into two groups: 25 parent agents and 25 child agents are in both Building 1 and Building 2, respectively. They evacuate to a nearby refuge location during emergencies. Refuge 1 is near Building 1 and Refuge 2 is near Building 2.

The following three cases are simulated:

1. Parents and their children from all pairs are in the same building.
2. Agents are divided so that a parent and his/her child of 25 pairs are in the same building, and the other 25 pairs are in the other buildings, respectively.
3. For all parent–child pairs, parents and their children are indifferent buildings.

Parent–child pairs evacuate smoothly in case 1 (Fig. 2b up). In case 2 and 3, parents whose children are in the other building move to their child (Fig. 2b bottom). The lines in Fig. 2c show the trajectories of parent agents who evacuated last from both buildings in case 3. a_{same}^* s and a_{diff}^* are parents whose children are in the same buildings and different buildings, respectively. The trajectories of a_{diff}^* show that parents go to the other building, meet their child, and escape together, respectively. The parents' movements cause congestion in the square and in the entrances to the buildings. The congestion in case 3 is more of a problem than in case 2, and it takes more time for people to evacuate from campus.

6.2 Scenario 2: Evacuation with Guidance Information from an Authority and Communication Among Evacuees

The second scenario is modeled after a tragedy that happened at Ookawa Elementary School during the tsunami that occurred along with the East Japan Earthquake. Most of the students were engulfed by the tsunami and died, even though they had heard the tsunami warning 1 h before it struck. When the earthquake occurred, all students evacuated to the ground floor. The school was located 5 km from the sea, so they did not expect the tsunami to reach the school and did not have a specific manual for evacuation. Teachers talked and decided that they would go to Refuge 1. During their evacuation to Refuge 1, they knew that the tsunami was coming and that Refuge 1 would not be a safe place; therefore they decided to go to Refuge 2, which was located on a hill. Unfortunately, it was too late.

We tested two evacuation cases.

Case 1 Agents receive guidance information from an authority only (Fig. 4a). Some evacuees follow the guidance information from the authority, while others do not.

Case 2 Agents receive guidance information from the authority and share the information through communication. Some evacuees meet others who go to refuge 2 by following the authority's guidance information. Some of the evacuees trust what the others say and change their destination before they hear the guidance from the authority.

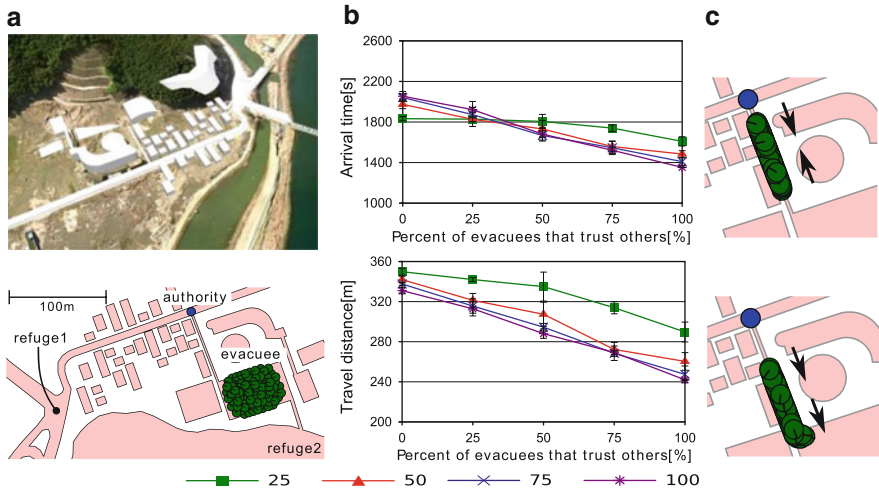


Fig. 4 Ookawa elementary school after Tsunami, results and snapshots of simulations. (a) Disaster area and initial state. (b) Simulation results. (c) Congestions

Figure 3b shows the travel distance and average arrival times of the evacuees arrive at Refuge 2. The X axis of the graph shows the percentages of evacuees who trust messages delivered by other evacuees. The messages are the guidance information received from the authority, and the marks on the lines indicate how many evacuees follow the guidance when they hear it from the authority. The followings can be assumed from the graph:

1. More evacuees trust the message of others, thus, the arrival time and travel distance become shorter. Figure 3c illustrates the flows of evacuees as it changes from a counter flow (up graph) to a direct flow (bottom graph), and the effects form congestion are lessened.
2. More evacuees follow the guidance information received from the authority; the same results as above are applied even when they share the information at the same rate among evacuees.

6.3 Scenario 3: Phased Evacuation from a Library Building

Figure 5 shows a library building at our university. The square footage of the library is about 2,000 m², and 1,400 occupants are allowed inside the building, according to the Fire Service Law. It has five stairways: two stairways run through from the fifth floor to the first floor, and four stairways run between neighbor floors. There are two exits: a front exit on the second floor and an emergency exit on the first floor.



Fig. 5 Phased evacuation from library building. (a) Floor layout. (b) Without guidance. (c) With guidance

The announcements are modeled for a phased evacuation according to the WTC emergency guidelines (p. 35 [2]) and the content differs according to the floors. Agents who are on the first and fourth floors are guided to egress through the stairway and go out through the emergency exit, while agents who are on the second, third and fifth floors are guided to egress from the front entrance. Without the announcement, all agents normally exit through the front entrance because they do not know about the emergency exit.

Three types of agents who responded differently to the same emergency announcement are cited according to the report of the Great East Japan Earthquake [6].

- Agent Type 1: (instant evacuation) People who feel anxious after experiencing accidents that have involved extreme shaking initiate their own evacuation.
- Agent Type 2: (evacuation after tasks) People who do not feel anxious after accidents and evacuate after completing their current activity. They do, however, feel anxious when they hear the guidance information announcement.
- Agent Type 3: (emergent evacuation) People who do not feel anxious and do not evacuate after completing their current activity, and after hearing the evacuation guidance information initiate evacuation when they become extremely anxious after receiving newly information from others.

We simulated three emergency cases, each with 100 people on each floor, for a total of 500 people who would be evacuating from the building. The differences among three cases are as follows:

1. In case 1, all agents are type 1 and initiate their own evacuation immediately at the starting time. In cases 2 and 3, each agent is either type 1, 2 or 3. Type 2 and 3 agents evacuate 5 min after they receive the evacuation guidance information.
2. The difference between cases 2 and 3 is with and without the loss of guidance information. The rates of information losses are set according to the report [2].

Figure 6 shows a comparison of the simulation results for cases 1, 2 and 3. In the case of evacuating without guidance information of cases 2 and 3, the number of agents who egress from the front entrance is less than 500. This is because some agents of type 2 and 3 agents did not feel they were in the danger and thus did not evacuate. In case 3, the case with guidance, the number of agents who exited

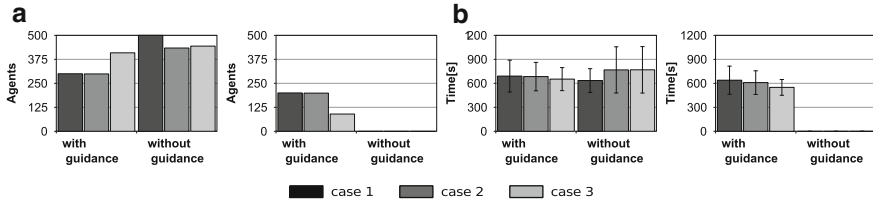


Fig. 6 Simulation results of evacuation from library. (a) Number of agent. (b) Evacuation time

from the front entrance was greater than those who exited from the emergency exit. This is because some type 3 agents, who did not hear the announcement, decided to egress based on their own BDI model. As a result, there were more people egress from the front entrance than from the emergency exit, and therefore the evacuation time was longer than the others.

7 Summary

Recently, people have been eager to assess society's safety after having experienced several disasters and the analysis of evacuation behavior has received increased attention. Agent-based simulation provides a platform for computing individual and collective behaviors in crowds.

We present two ideas; an agent behavior model presented with BDI and information propagation through communication to generate the phenomena observed in crowd evacuations. The BDI model shows how human relations among agents, the degree of trust in others' information, and the loss of text in information dissemination affect the patterns of the behaviors. The simulation results of the evacuation scenarios reveal the followings:

1. The properties of human relations and guidance information affect evacuation behaviors. The behaviors are different from those of people how much information they get from the announced guidance or from who they get the information.
2. The behaviors of some agents affect the evacuation behaviors of all agents. Some behaviors are known to cause congestion, requiring extra time to evacuate, just as in real life.

These results demonstrate that our model provides an effective simulation method of crowd behavior in emergency situations, and that test the evacuation plans and announcements of guidance information.

Acknowledgements Our platform has been developed based on RoboCup Rescue Simulation System. We greatly appreciate the contribution of the RoboCup Rescue Community. This research was supported by KAKENHI 24500186 and fund from Meijo University.

References

1. E. D. Kuligowski, R. D. Peacock: Review of Building Evacuation Models. NIST Technical Notes 1471; July 2005
2. J.D.Averill: NISTncstar 1-7: Occupant behavior, egress, and emergency communication, Sep. 2005.
3. D.Helbing, et.al: Simulating dynamical features of escape panic, NATURE,487–490, Sep. 2000.
4. Edwin R. Galea, et.al. The uk wtc9/11 evacuation study: An overview of the methodologies employed and some preliminary analysis. In Pedestrian and Evacuation Dynamics, 2008, pages 3–24. Springer, 2008.
5. the Great West Japan Earthquake Cabinet Office, Government of Japan: Prevention Disaster Conference and Tsunami. Report on evacuation behavior of people (in Japanese). <http://www.bousai.go.jp/jishin/chubou/higashinihon/7/1.pdf>, date: 9. Feb. 2012.
6. S. Bandini, S. Manzoni, G. Vizzari: Crowd Behavior Modeling: From Cellular Automata to Multi-Agent Systems, in Multi-Agent Systems, Simulation and Application (ed. A. M. Uhrmacher & D.Weyns), pp.301–32, CRC Press, 2009
7. N. Pelechano, A. Malkawi: Comparison of crowd simulation for building evacuation and an alternative approach, in Proc..The 10th International Building Performance Simulation, pp.1514–1521, 2007
8. M. Okaya, T. Takahashi: BDI Agent model Based Evacuation Simulation (Demonstration), The Autonomous Agents and MultiAgent Systems (AAMAS) 2011, P. 1297–1298, 2011, May

Empirical Fundamental Diagrams for Bidirectional Pedestrian Streams in a Corridor

J. Zhang, A. Schadschneider, and A. Seyfried

Abstract In this study, series of experiments under laboratory conditions were carried out to study uni- and bidirectional pedestrian streams in a straight corridor. The software *PeTrack* is used to extract pedestrian trajectories from video recordings automatically. From these trajectories the characteristics of bidirectional flow are analyzed using the Voronoi method. The fundamental diagram for various types of bidirectional streams agree well and no large differences are found in observed density range $\rho < 2.5 \text{ m}^{-2}$. By comparing the diagram between uni- and bidirectional stream, it is shown that the density-flow relationships agree well for the free flow state. However, the maximum specific flow in unidirectional streams is significantly larger than that in bidirectional streams.

Keywords Bidirectional flow • Voronoi method • Fundamental diagram

J. Zhang (✉)

Computer Simulation for Fire Safety and Pedestrian Traffic, Bergische Universität Wuppertal, Pauluskirchstrasse 7, Wuppertal D-42285, Germany
e-mail: jun.zhang@uni-wuppertal.de

A. Schadschneider

Institut für Theoretische Physik, Universität zu Köln, Köln D-50937, Germany
e-mail: as@thp.uni-koeln.de

A. Seyfried

Computer Simulation for Fire Safety and Pedestrian Traffic, Bergische Universität Wuppertal, Pauluskirchstrasse 7, Wuppertal D-42285, Germany

Jülich Supercomputing Centre, Forschungszentrum Jülich GmbH, Jülich D-52425, Germany
e-mail: seyfried@uni-wuppertal.de

1 Introduction

In recent years, considerable studies of uni- and bidirectional pedestrian flow in corridors have been performed. However, discrepancies exist among previous studies and currently there is no consensus on the origin of these differences. Even for the fundamental diagram, the basic relation between density, velocity and flow rate, obvious differences can be observed especially for densities $\rho > 2.0 \text{ m}^{-2}$. Moreover there is no consensus whether the fundamental diagrams of uni- and bidirectional flows are different or not. Predtechenskii and Milinksii [1] and Weidmann [2] neglected the differences in accordance with Fruin, who states that the fundamental diagrams of multi- and uni-directional flow differ only slightly [3]. In contrast, Helbing et al. [4] concluded that counterflows at bottlenecks are significantly more efficient than unidirectional flows. Besides, the flow ratio of pedestrian in opposite streams is also an important topic in bidirectional stream. Navin and Wheeler [5] found a reduction of the flow in dependence of directional imbalances. Pushkarev et al. [6] and Lam et al. [7, 8] found that bidirectional flow is not substantially different from unidirectional flow as long as the densities of the opposite streams are not too different. However, Older et al. state that different ratios of the total flow in either direction, from 80 %: 20 % to 50 %: 50 %, do not show any significant effect on the walking speed [9].

To resolve these discrepancies series of experiments under laboratory conditions were carried out to study the characteristics of uni- and bidirectional pedestrian streams in a corridor. Bidirectional streams with different kinds of lanes are observed in our experiment. In Sect. 2, the setup of the experiment is described. The main results including the pedestrian trajectories and fundamental diagrams of different kinds of flows are shown in Sect. 3. The findings are summarized in Sect. 4 which concludes the paper.

2 Experiment Setup

Up to 400 persons, mostly students participated in the experiments. Their free velocity $v_0 = 1.55 \pm 0.18 \text{ m/s}$ was obtained by measuring 42 participants' free movement. Figure 1 shows the sketch of the experiment setup and snapshots of the bidirectional flow in a straight corridor. Two groups of participants located in the waiting areas at the left and right side of the corridor entered the corridor through the entrances when a run started. The width of the entrance b_l and b_r were changed in each run to regulate the densities in the corridor. We gave the participants two types of instructions on which exit to choose in different runs. One is asking the test persons to choose the exit freely; the other is letting them choose the exit according to a number given to them in advance. The persons with odd numbers chose the left exit in the end, while the ones with even number were asked to choose the exit in the right side. With freely choosing of exits the stable separated lanes (SSL)

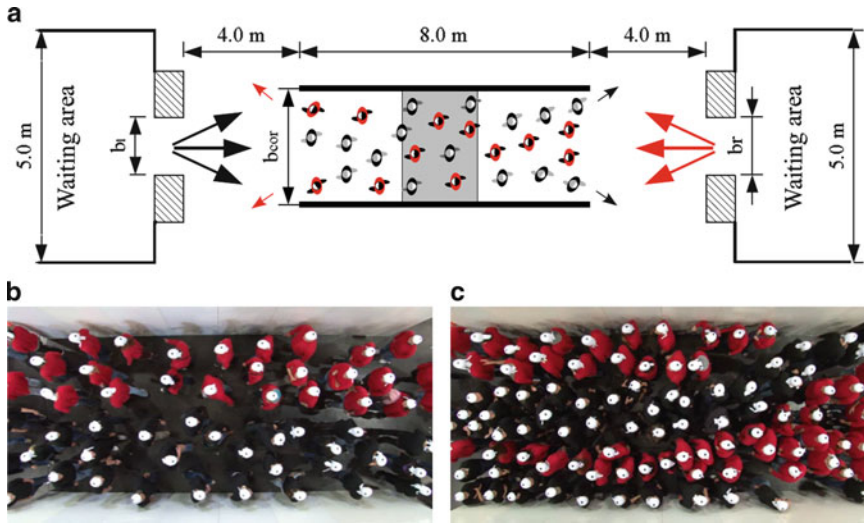


Fig. 1 Setup and snapshots of bidirectional flow experiment. (a) The *gray area* in the sketch shows the location of measurement area. Two kinds of lanes are shown in the snapshots: (b) stable separated lanes (SSL) and (c) dynamic multi lanes (DML)

are observed, whereas the dynamical multi lanes (DML) are obtained by specifying the exits in advance. Altogether 22 runs of bidirectional pedestrian streams were performed in corridors with widths of 3.0 and 3.6 m respectively.

3 Results

3.1 Extraction of Trajectories

For a precise analysis, pedestrian trajectories were automatically extracted from video recordings using the software *PeTrack* [10]. Lens distortion and perspective view are taken into account. Figure 2 shows the pedestrian paths of bidirectional flow with stable separated lanes (SSL) and dynamical multi lanes (DML) respectively. The gap between two adjacent lanes is clearer in the flow with SSL than in the flow with DML. From these trajectories, pedestrian characteristics including flow, density, velocity and individual distances at any time and position can be determined. All the analysis below is based on these trajectories.

3.2 Fundamental Diagram

In [11] and [12] the effect of different measurement methods on the fundamental diagram of pedestrian flow has been compared. Minor influences are found for the

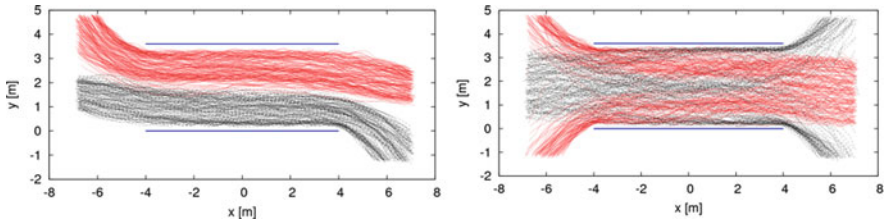


Fig. 2 Trajectories of the pedestrians in two runs of the experiments. The trajectories of *right* and *left* moving pedestrian are represented in different colors. The gap between two adjacent lanes is clearer in the flow with SSL

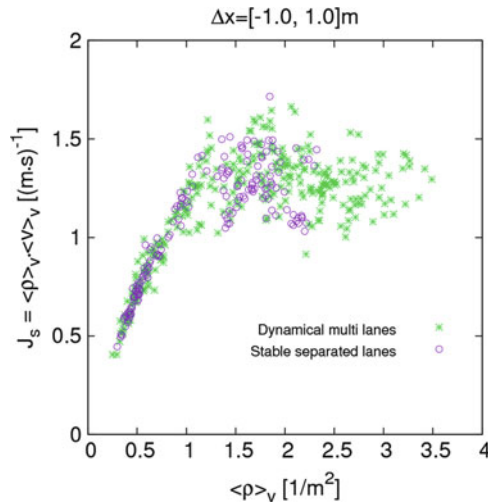
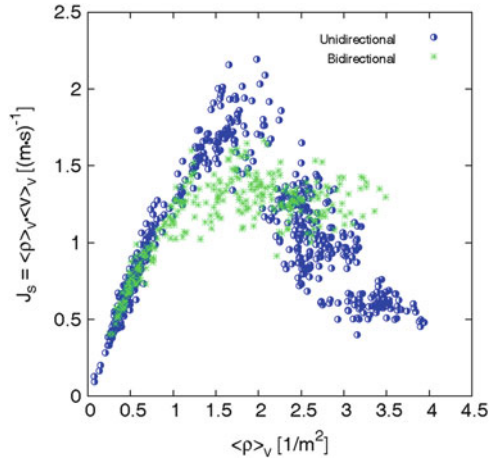


Fig. 3 Comparison of fundamental diagrams of bidirectional flow with different types of lanes. These data are for the runs in 3.6 m wide corridor

density ranges observed in the experiment but only the Voronoi method is able to resolve the fine structure of the fundamental diagram. Consequently, in this study we focus on the Voronoi method for its high spatial resolution in combination with low fluctuations.

Head-on and cross-directional conflicts commonly occur in bidirectional pedestrian flow, especially for the DML case. To investigate their influence on the flow we compare the fundamental diagram of flow with SSL and DML for $b_{cor} = 3.6$ m in Fig. 3. It can be seen that the fundamental diagrams of these two types of bidirectional flow are consistent at least for the density $\rho < 2.0 \text{ m}^{-2}$. The lower degree of ordering in the flow with DML has no effect on the fundamental diagram which agrees with the findings of Older [9]. This might be taken as an indication that head-on conflicts in multi-lanes have the same influence on the fundamental diagram as the conflicts at the borders in the flow with SSL. On the other hand, the self-organized lanes increase the order and make pedestrian movement smoother.

Fig. 4 Comparison of the fundamental diagrams between uni- and bidirectional pedestrian flow. Note that the data for unidirectional flow is obtained from the runs in 3 m wide corridor, whereas the other is for the bidirectional flow with DML in 3.6 m wide corridor



Whether the degree of ordering has an influence on the fundamental diagram at higher densities cannot be decided from our data.

According to the study in [11] and [14], the specific concept works well for both uni- and bidirectional flow at the density ranges in our experiments. Thus, we are free to choose the experiments with a larger range of density to compare their characteristics. Figure 4 shows the relationship between density and specific flow for uni- and bidirectional pedestrian flow. The data for unidirectional flow is obtained from the runs in 3 m wide corridor (for details see [11]), whereas the other is for the bidirectional flow with DML in 3.6 m wide corridor. At densities of $\rho < 1.0 \text{ m}^{-2}$, no significant difference exists. For $\rho > 1.0 \text{ m}^{-2}$, however, the specific flows for unidirectional flows are higher than that of bidirectional flows. In the bidirectional case a plateau is formed starting at a density $\rho \approx 1.0 \text{ m}^{-2}$ and the flow becomes almost independent of the density. Such plateaus are typical for systems which contain “defects” which limit the flow and have been observed e.g. on bidirectional ant trails [13] where they are a consequence of the interaction of the ants. In our experiments the defects are conflicts of persons moving in the opposite direction. These conflicts only happen between two persons but the reduction of the velocity influences those following.

4 Summary

Series of well-controlled laboratory experiments were carried out in this study. The characteristics of pedestrian streams in a straight corridor are investigated. The fundamental diagrams of bidirectional flow with different kinds of lanes are compared and no large differences are found in observed density range. It means the number and form of lanes in corridor does not have an obvious influence on the

pedestrian flow at least for $\rho < 2.5 \text{ m}^{-2}$. The self-organized lanes can help to reduce the head-on conflicts effectively and increase the ordering of the stream. However, these conflicts do not affect the fundamental diagram of bidirectional flow. The properties of uni- and directional flow show clear differences in the experiment. The maximal flow value is about $2.0 (\text{m}\cdot\text{s})^{-1}$ for unidirectional flow while $1.5 (\text{m}\cdot\text{s})^{-1}$ for bidirectional flow. For $\rho < 1.0 \text{ m}^{-2}$ the flow seems independent on the density. In addition, the jamming transition from free flow state to jammed state, which is found in many theoretical models, was not observed in our experiment covering a density range up to $\rho = 3.5 \text{ m}^{-2}$.

References

1. V. M. Predtechenskii and A. I. Milinskii, *Planning for Foot Traffic Flow in Buildings*. Amerind Publishing, New Delhi, 1978, translation of: Proekttirovanie Zhdaniis Uchetom Organizatsii Dvizeniya Lyuddskikh Potokov, Stroizdat Publishers, Moscow, 1969
2. U. Weidmann, "Transporttechnik der Fussgänger," Institut für Verkehrsplanung, Transporttechnik, Strassen und Eisenbahnbau, ETH Zürich, Tech. Rep. Schriftenreihe des IVT Nr. 90, 1993, zweite, ergänzte Auflage.
3. J. J. Fruin, *Pedestrian Planning and Design*. Elevator World, New York, 1971
4. D. Helbing, L. Buzna, A. Johansson, and T. Werner, "Self-Organized Pedestrian Crowd Dynamics: Experiments, Simulations, and Design Solutions," *Transportation Science*, vol. 39, pp. 1–24, 2005
5. F. D. Navin and R. J. Wheeler, "Pedestrian flow characteristics," *Traffic Engineering*, vol. 39, pp. 31–36, 1969
6. B. Pushkarev and J. M. Zupan, "Capacity of Walkways," *Transportation Research Record*, vol. 538, pp. 1–15, 1975
7. W. H. K. Lam, J. Y. S. Lee, and C. Y. Cheung, "A study of the bi-directional pedestrian flow characteristics at Hong Kong signalized crosswalk facilities". *Transportation*, vol. 29, pp. 169–192, 2002
8. W. H. K. Lam, J. Y. S. Lee, K. S. Chan, and P. K. Goh, "A generalised function for modeling bi-directional flow effects on indoor walkways in Hong Kong". *Transportation Research Part A: Policy and Practice*, vol. 37, pp. 789–810, 2003
9. S. Older, "Movement of Pedestrians on Footways in Shopping Streets," *Traffic Engineering and Control*, vol. 10, pp. 160–163, 1968
10. M. Boltes, A. Seyfried, B. Steffen, and A. Schadschneider, "Automatic Extraction of Pedestrian Trajectories from Video Recordings," in *Pedestrian and Evacuation Dynamics 2008*, Springer-Verlag Berlin Heidelberg, pp. 43–54, 2010
11. J. Zhang, W. Klingsch, A. Schadschneider, and A. Seyfried, "Transitions in pedestrian fundamental diagrams of straight corridors and T-junctions," *Journal of Statistical Mechanics: Theory and Experiment*, vol. P06004, 2011
12. B. Steffen and A. Seyfried. "Methods for measuring pedestrian density, flow, speed and direction with minimal scatter". *Physica A*, 389(9):1902–1910, 2010
13. A. John, A. Schadschneider, D. Chowdhury, and K. Nishinari. "Collective effects in traffic on bi-directional ant trails". *J. Theor. Biol.*, 231:279, 2004
14. J. Zhang, W. Klingsch, A. Schadschneider, and A. Seyfried, "Ordering in bidirectional pedestrian flows and its influence on the fundamental diagram". *Journal of Statistical Mechanics: Theory and Experiment*, vol. P02002, 2012

Empirical Study and Modelling of Pedestrians' Route Choice in a Complex Facility

Armel Ulrich Kemloh Wagoum, Armin Seyfried, Frank Fiedrich,
and Ralph Majer

Abstract This paper presents an empirical analysis of pedestrians' route choice in a complex facility. The study has been done within the framework of a real-time evacuation assistant. The investigated facility is part of the promenade of the ESPRIT arena in Düsseldorf, Germany. The route choice data are obtained from an automatic person counting system consisting of cameras. The collected data are presented in terms of frequencies, i.e. the number of persons passing a counting line or exit per minute in the direction "in" and "out" of a section. Using that information, the proportional usage of the different exits is calculated. Also the global route profiles of spectators for entering and leaving the arena are obtained. The results for different football games are presented and analysed in details. A modelling approach based on a quickest path algorithm is used to reproduce the exit choosing behaviour of the spectators.

Keywords Route choice • Empirical study • Modelling

A.U.K. Wagoum (✉)

Jülich Supercomputing Centre, Forschungszentrum Jülich GmbH, Jülich 52428, Germany
e-mail: u.kemloh@fz-juelich.de

A. Seyfried

Jülich Supercomputing Centre, Forschungszentrum Jülich GmbH, Jülich 52428, Germany

Computersimulation für Brandschutz und Fußgängerverkehr, Bergische Universität Wuppertal,
Pauluskirche 7, Wuppertal 42285, Germany

e-mail: a.seyfried@fz-juelich.de

F. Fiedrich

Bevölkerungsschutz, Katastrophenhilfe und Objektsicherheit, Bergische Universität Wuppertal,
Lise-Meitner-Str. 11-13, Wuppertal 42119, Germany

e-mail: fiedrich@uni-wuppertal.de

R. Majer

Vitracom AG, Erbprinzenstr. 4-12, Gebäude A, Karlsruhe 76133, Germany

e-mail: ralph.majer@vitracom.de

1 Introduction

In order to calibrate and later validate models, empirical data are needed. In the field of pedestrian dynamics (and especially for route choice), there are three main sources of data. The first source is surveys. The issue with this method is usually the size of samples obtained and their representativeness. Besides, many types of information cannot be captured by surveys and information always has to be acquired afterwards. This can be the criteria influencing the choice of a particular route asked at the end of the trip for instance. The interrogated person might not be able to give accurate responses or to remember all details. An example of a survey conducted after an unannounced evacuation of four retail stores is presented by Shields and Boyce [1]. The second source is controlled indoor/outdoor experiments. A study is presented by Heliövaara et al. [2] where the exit choosing behaviour of a group of people is analysed and used to validate a model based on a game theoretical approach. The results obtained from such experiments are not always directly applicable to real life situation, because they are controlled. It is likely that people behave differently under laboratory conditions. In addition extreme cases might not be reproduced for ethical or safety reasons. But only under well controlled laboratory conditions, some features can be analysed without endangering the crowd, for instance the emergence of critical states by high densities. Another reason speaking in favour of controlled experiments is that the study can be focussed on the influences of a particular parameter. For example the flow through exits of different widths can be studied without worrying on the influences of other external parameters like the individual motivations. Also, different configurations of scenarios are easily performed. In this context Kobes et al. [3] performed some evacuation experiments from a hotel and study the influences of smoke and exit signs. The third source is observations from real life scenarios. In comparison to experiments, there are many factors that are needed to fully understand the observations, for instance the motivation of the individual pedestrians. Independently of the source of data (surveys, experiments, observations), the information has to be extracted. For surveys participants may be asked to draw their trip on a map. For experiments and observations video surveillance are often used. Other alternatives include the tracking of digital gadgets like cell phones or GSM (Global System for Mobile Communications) log files [4] or Bluetooth devices [5, 6]. While accurate data can be obtained, the number of sample depends on the number of devices present in the investigated areas.

In this contribution we are interested in indoor empirical data. The technique used here for collecting data is an automatic person counting system based on video monitoring. There are basically two main categories of events which are held in the arena: football games and concert performances. The differences can be summarised in two points. The events feature different types of visitors. Visitors for concerts are usually first/one time visitors. The contrary can be assumed for football game visitors. The number of season tickets provides a proof to this assumption. The second point is the occupancy of the stadium. For concerts people are allowed in the field and the entrances and exits configurations are different and are subjected

to continuous changes. Although the promenade and the tribune areas are entirely covered by the cameras, we only investigate the promenade area. The motivation is that the promenade serves as distributor for the tribune and actually shows the most interesting route choice patterns. We analyse several football matches which took place between the 18th July and the 4th November 2011 in the ESPRIT arena in Düsseldorf, Germany.

This contribution is structured as follows: Sect. 2 presents the automatic person counting system. Section 3 presents the filtering process applied on the data. Detailed route choice patterns for one match are presented in Sect. 4. The summary for nine other matches are presented in Sect. 5. The work is concluded in Sect. 6.

2 Automatic Person Counting System

The counting system consists of 45 mono and 51 stereo cameras installed in the tribune and the promenade. Each camera is merely responsible for one exit, which means that at each time the information (in this case the number) about the pedestrians passing through that exit is available. Also, the passing direction for each exit is identified, making it possible to calculate the number of pedestrians inside a specific section. The position of 52 cameras in the promenade is presented in Fig. 1. They are represented with green filled circles. The cameras are all connected to a server in a local area network. The server collects and aggregates the data in real-time and makes them available through web services. The data are presented in terms of frequencies, i.e. the number of persons passing the corresponding counting line or exit per minute in the direction “in” and “out” of a section. Using that information the proportional usages of the different exits of the promenade are calculated. In order to comply with privacy regulations, no images are stored by the system. The images are directly processed by the camera itself (embedded system) and only the counting values are given out. The geographical situation of the promenade is shown in Fig. 2. The location of the parking lots and the train station are marked. This information is needed to correctly interpret the route choice patterns obtained.

The distribution of the cameras at main entrances, exits and passages leads to a logical partitioning of the promenade area in five sections (S1–S5, see Fig. 1) totalling approx. 5,200 m² with a maximal allowed capacity of approx. 10,350 persons. The gates connecting the promenade and the tribune area have a width of 2.5 m and a length of 5 m. The connections between the sections have a width of 7.4 m. The exits to the outside have a width of 2.4 m.

3 Data Filtering

A first look at the data as given by the system is presented in Fig. 3. The data are recorded in the arrival phase prior to the beginning of the event between 16:00 and 18:00. Figure 3 (left) shows the number of spectators entering the section and Fig. 3

Fig. 1 Location of the cameras (green circles) for the automatic person counting system. The most cameras are distributed in the promenade and some cover the playing field area

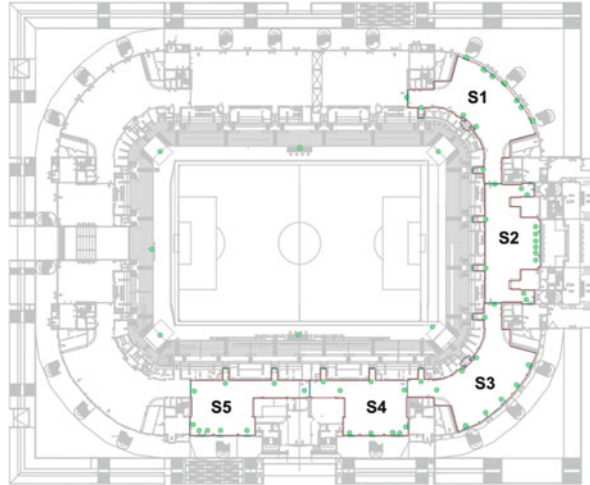
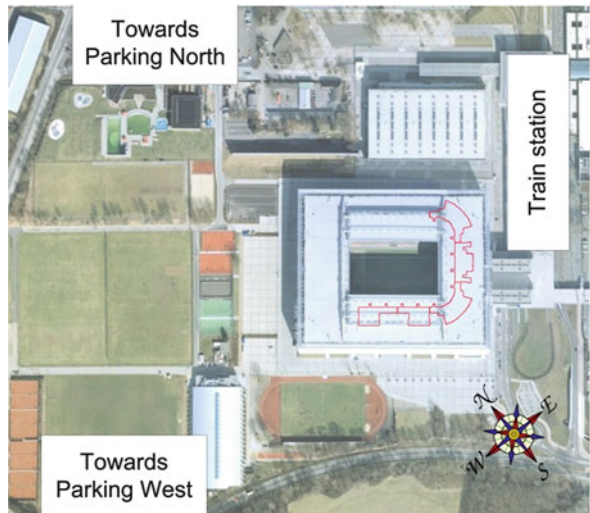


Fig. 2 Geographical location of the ESPRIT arena (Image made with Google Earth™, Feb. 2012). The investigated part of the promenade, the direction to the parking places and the train station are marked



(right) the number of spectators leaving the section for the same period of time. A naive approach to determine the occupancy of the section would be to sum up the data from each door. For this particular section the amount of pedestrians entering would be $\sim 13,664$ and the amount of pedestrian leaving would be $\sim 13,502$. But a closer look at Fig. 3 (left) reveals that ~ 907 spectators are coming from the tribune. This makes sense since many spectators first go to their seats and then come out again for buying some articles and food or going to the toilets for instance. The same applies for spectators leaving the section at the beginning, some walk out for smoking and then come in again. The resulting effects are the bidirectional flows observed at the exits.

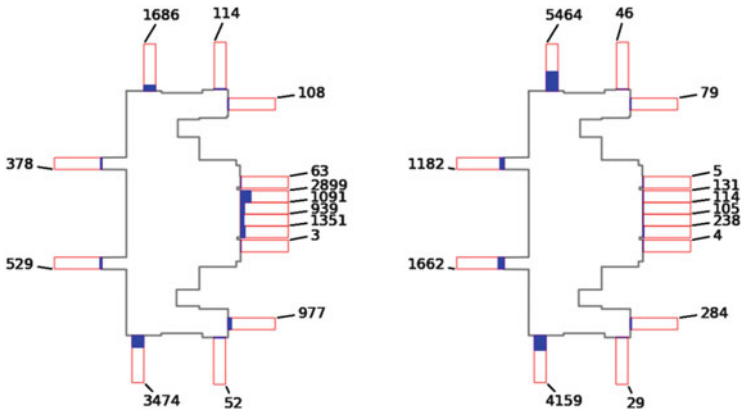


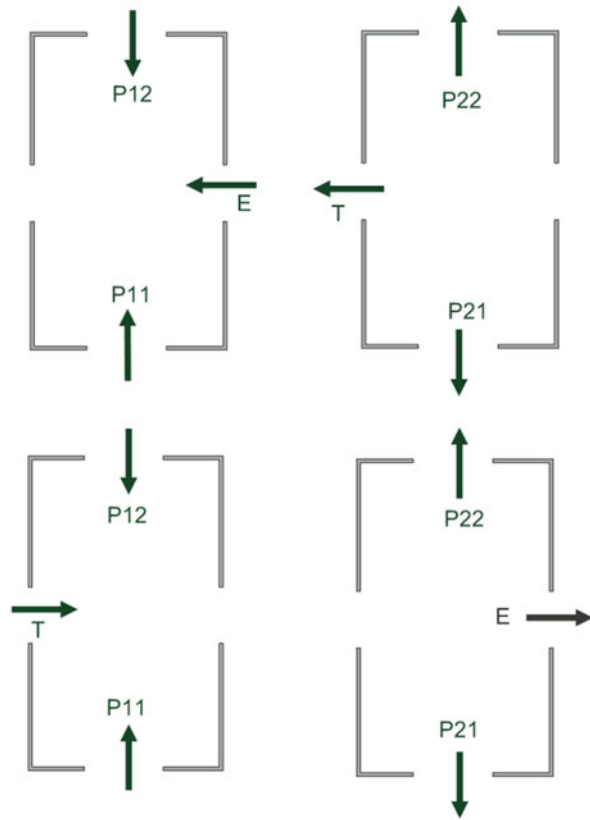
Fig. 3 Frequency data given by the counting system in the arrival phase prior to a football match for a specific section. *Left:* entering the section. *Right:* leaving the section. The bars indicate the exit location and the fill level indicates the percentage usage of the exits in relation to the total number of occupants in the section

These unwanted effects can be mitigated by applying a two stages filtering process. In a first stage the event running is divided in different phases. In a second stage the bidirectional flows observed are removed by using a simplified model of a section as presented in Fig. 4. In this model only the main flow directions are considered. The described filtering steps are required since a later comparison with a route choice model is envisaged and the model only considers a clearing scenario. In addition we are only interested in this case study in the general pedestrians' profile, which can be resumed to entering the promenade and going to the tribune at the beginning and leaving the tribune, passing through the arena towards the parking lots or the train station. Therefore it is logical to divide the event running in different phases corresponding to the different main flow directions. Following phases are considered (for matches taking places between 18:00 and 19:45):

- Phase I: entering the arena between 16:00 and 18:00
- Phase II: first Half between 18:00 and 18:45
- Phase III: half time break between 18:45 and 19:00
- Phase IV: second half between 19:00 and 19:45
- Phase V: leaving the arena between 19:45 and 20:30

The interesting sequences are the entering (Phase I) and the leaving (Phase V) of the promenade at the beginning and the end of the event. The pedestrian flow at the beginning of the event, when entering a section, is given in Fig. 4 (top left). The flow direction when leaving the section is given in Fig. 4 (top right). The sources for the occupancy of the section are the spectators coming from outside E and the spectators coming from other sections P_{12} and P_{11} . The sinks for the section are the spectators going to the tribune T and the spectators leaving to other sections P_{21} and P_{22} .

Fig. 4 Model of a section of the promenade showing the main flow directions at different phases of the events. In the arrival phase spectators enter each section as presented in the subfigure *top left*. They leave the section as presented in the subfigure *top right*. In the departure phase the flow directions are inverted. They entered the section as presented in the subfigure *bottom left* and they leave the section as given by the subfigure at the *bottom right*



The contrary applies at the end of the event and the flow directions are inverted as presented in Fig. 4 (bottom left) for entering and Fig. 4 (bottom right) for leaving the section. The sources for the occupancy of the section are T pedestrians coming from the tribune together with the P_{11} and P_{12} spectators coming from other sections. The sinks for the section are the spectators going outside E and the spectators leaving to other sections P_{21} and P_{22} .

Let's assume the following values for a section S for an observation period Δt as provided by the counting system:

- E_1 : the number of pedestrians coming from the outside and entering the section S.
- E_2 : the number of pedestrians leaving the section S and going to the outside.
- T_1 : the number of pedestrians coming from the tribune and entering the section S.
- T_2 : the number of pedestrians leaving the section S and going to the tribune.
- P_{11}, P_{12} : the number of pedestrians entering the section S and coming from other sections.
- P_{21}, P_{22} : the number of pedestrians leaving the section S and going to other sections.

The following effective values are derived for the section S during the period Δt :

- $E = E_1 - E_2$: the effective number of pedestrians coming from the outside.
- $T = T_1 - T_2$: the effective number of pedestrians entering the tribune.
- $P_{in} = P_{11} + P_{12}$: the effective number of pedestrians entering the section and coming from other sections.
- $P_{out} = P_{21} + P_{22}$: the effective number of pedestrians leaving the section and going to other sections.

At the beginning of the event valid sources for the occupancy of the section S are E and P_{in} . The redundant data given by T_1 and E_2 are automatically eliminated by the subtraction. This is straightforward since for accessing the tribune area one first has to pass through the promenade, it means that those spectators are both accounted in T_1 and T_2 n-times they crossed the section. Thus by subtracting both values from each other, they are accounted only once and the redundant data are eliminated. The same applies for spectators leaving the section for a small round outside. The sinks are T and P_{out} . These results are summarised by the flow given in the equation:

$$\begin{aligned}\Phi_{in}(\Delta t) &= E + P_{in} \\ \Phi_{out}(\Delta t) &= T + P_{out}\end{aligned}\quad (1)$$

The contrary applies at the end of the event. The valid sources are T and P_{in} and the valid sinks are P_{out} and E. The results are summarised by the equation:

$$\begin{aligned}\Phi_{in}(\Delta t) &= -T + P_{in} \\ \Phi_{out}(\Delta t) &= -E + P_{out}\end{aligned}\quad (2)$$

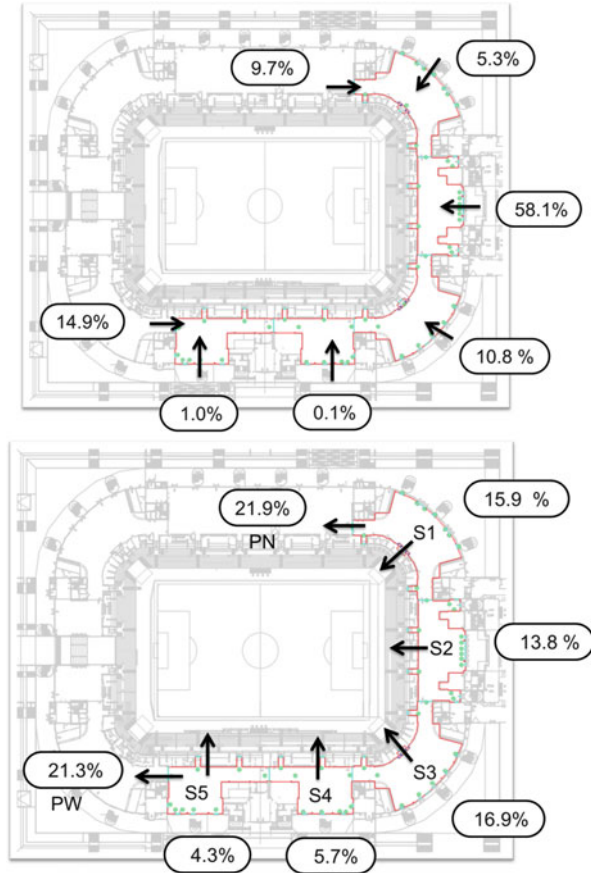
For both cases we assume the approximate occupancy given in Eq. 3. In an ideal case $\Phi_{in} = \Phi_{out}$. This is rather infeasible in this case since the estimations do not take into account the initial occupancy of the section before the observation time. This is not necessarily zero. In addition the accuracy of the counting system has to be accounted. Nevertheless valid qualitative statements can be made with the defined value of Φ .

$$\Phi(\Delta t) = \frac{(\Phi_{in}(\Delta t) + \Phi_{out}(\Delta t))}{2}\quad (3)$$

4 Analysis 1: Football Match

The profiles for entering the promenade before the beginning of the game are presented in Fig. 5 (top). Approximately 13,000 spectators have been registered by the counting system. The results are based upon the total occupancy of the promenade and do not take into consideration the different route choice options within the promenade itself. Also, we should mention here that this number is not the

Fig. 5 Pedestrians profile in the arrival phase of a football game



total number of spectators in the arena during that game, which was approximately 32,000 based on official sources. Under these considerations it can be taken from the figure that more than the half of the spectators (58 %) comes through the section S2 and distributes themselves into the other sections. They are using the train station to access the arena.

S2 is directly connected to the train station and is also the main entrance to the arena. Fifteen percent are coming from the direction parking west (PW) and 9.7 % are coming from the direction PN. The values should be considered as lowest boundaries. For instance it is unclear whether or not the 10.8 % entering through section S3 came by train, although this would be the most reasonable assumption to consider here. The distribution to the tribune areas is then straightforward and is proportional to the capacity of the corresponding areas. The tribune areas connected to section S4 and S5 have the lowest capacity and accordingly fewer spectators are going there. 43.2 % of the spectators transfer to the other parts the arena, which are not covered by the counting system.

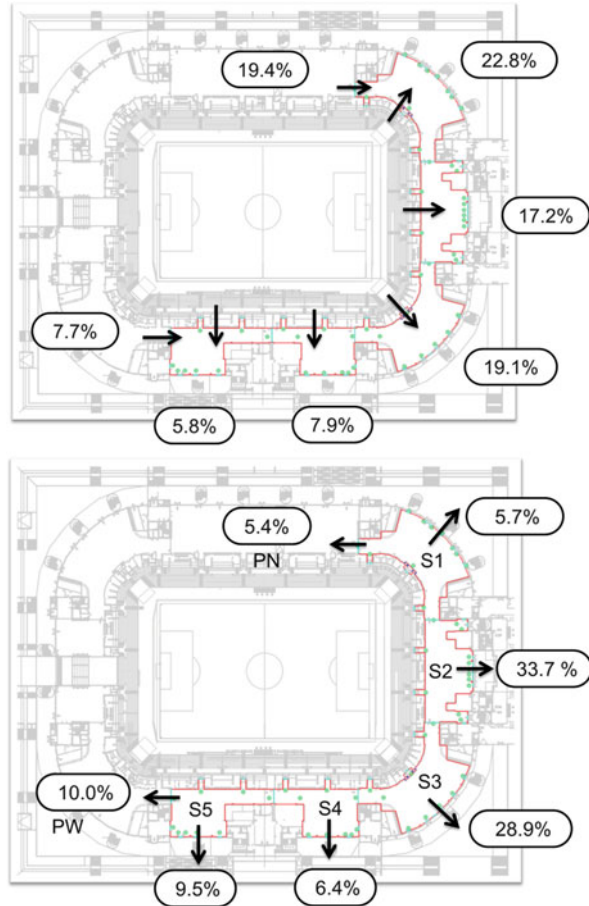
At the departure phase 11,000 spectators are recorded by the counting system. This number does not include the initial occupancy of the promenade before the end of the game since the data have been analysed in the period from 19:45 to 20:30 (see Sect. 2 about filtering the data). The profiles are presented in Fig. 5 (bottom). At the end of the event many spectators (about 33 %) still leave the promenade through the section S2 directly accessing the train station. But this is far less than the original percentage of spectators (58 %) who entered the arena through that section in the arrival phase. 9.7 % came at the beginning from the direction parking north (PN) and 5.4 % went in that direction at the end of the game. For the parking West direction the values are 15 % for coming and 10 % for going. We notice that the percentage at the end are lower than the percentage at the beginning. This is attributed to the fact that many spectators left the area through other sections. Also, the parking west (PW) is larger than the parking north (PN), this is the reason why more spectators came from and went to that direction. In addition at the end of the events, some of the exits which are normally closed during the arrival phase are opened. The highest disparity between arrival and departure phases is observed in the sections S4 and S5. 15.9 % left through that section whereas they were used by less than 1 % in the arrival phase. This is a clear indicator that spectators do not necessarily choose the same route for entering and for leaving a facility. This is also a clear indicator that the shortest path, as already assumed in many simulation tools, plays an important role. This is also the preferred route from pedestrians unless motivated by other factors as analysed by Golledge [7].

To summarise, at the end of the game there are more spectators who first go out of the promenade using the shortest path and then find their way back to the train station and the parking areas. This also implies that route choice behaviour outside the promenade has to be taken into account in simulations. From the presented data it can be inferred that the common assumption that spectators choose the same route for accessing and leaving a facility is not necessarily true. Although it is not quantifiable from our data the shortest path to leave the building plays an important role and should be accounted. This idea is supported by the fact that all sections are relatively well used for leaving the arena independent on their locations (Fig. 6).

5 Analysis 2: Football Matches

In the previous section the analysis of route choice patterns and exits choosing behaviour of spectators for a specific football game has been presented. In the following a comparison across different football games is performed. We only analysed the profiles for entering and leaving the promenade during the arrival and the departure phase. The same filtering process described in Sect. 3 is applied. A total of nine games has been recorded in the time ranging from July 2011 to November 2011. The average number of recorded spectators is 13,000 and the average number of total spectators in the arena during the games is 30,000 except for the game on the 2011-10-11 where more than 50,000 spectators were present

Fig. 6 Pedestrians profile in the departure phase of a football game



in the arena (and 15,000 were recorded by the counting system). The game on the 2011-10-11 was a national game opposing Germany and Belgium accounting for the European Cup qualifiers 2012. All other games were games from the 2nd division of the German Bundesliga involving the regional team Fortuna Düsseldorf. Recall that the data are recorded in the ESPRIT arena in Düsseldorf. Also, two games were played at 13:00, four games at 18:00, two games at 19:00 and one game at 20:15. Thus a certain distribution of the games, even though very scarce, can be assumed.

The usage of the different sections (expressed in % of the total occupancy) for entering the promenade in the arrival phase are given in Fig. 7 (top). The first noticeable pattern here is the clustering of the data independent of the events. The data all shows similar patterns. Fifty to sixty percent of the spectators always gain access to the investigated promenade area via the section connected to the train station. This number is very low (less than 5 %) for the sections S1, S4 and S5. Also,

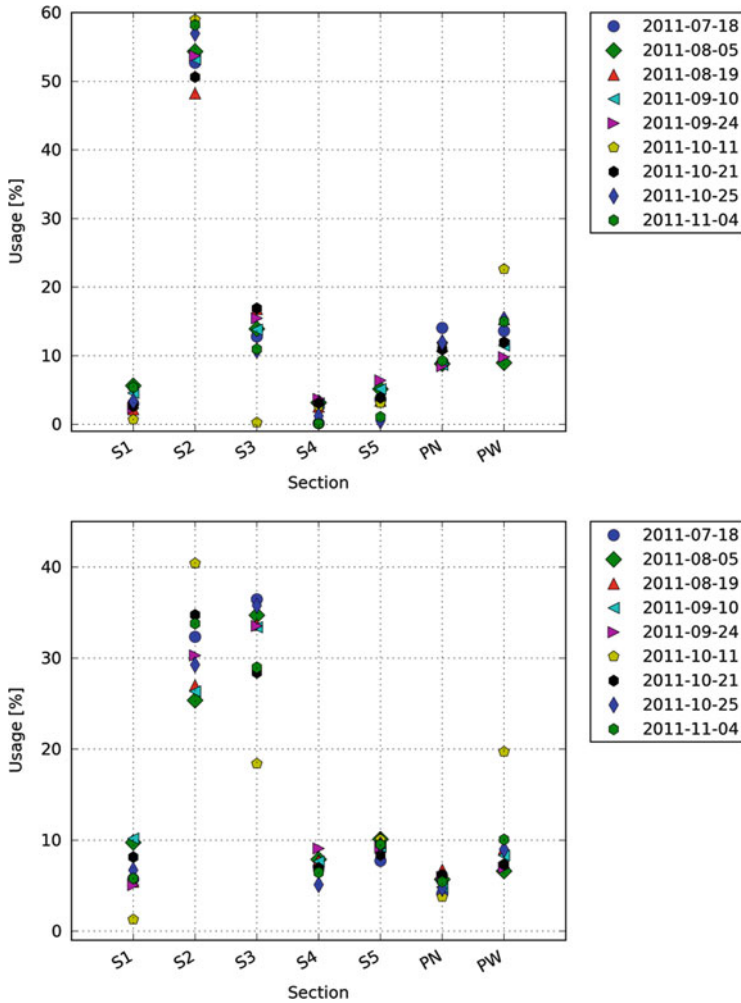


Fig. 7 Comparison of different football matches in the arrival phase (*top*) and the departure phase (*bottom*)

the number of spectators coming from the direction parking north (PN) and parking west (PW) is uniform between 10 % and 15 %. Only the national game shows some outliers. The figure infers that no pedestrian has entered the promenade through the sections S1 and S3. A closer look at the data however has shown that during the analysis period from 17:00 to 19:00, almost 3,800 pedestrians left the promenade and 3,840 came in, resulting in a ~ 0 % usage by applying the filtering process. The discrepancies can be attributed to the general audience during that national game which differs from the other events. This assumption is also supported by the fact that more spectators (than usual) came by cars from the parking west side. For all

other events the same audience can be assumed mostly made of the local supporters of Fortuna Düsseldorf and some supporters from the visiting team.

The profiles for leaving the promenade during the departure phase are given in Fig. 7 (bottom). The data shows a strong clustering of the section usage. Similar to the observations during the other phases, the outliers are also from the national game. There are more spectators going to the parking West direction, probably to their cars. By fading out the outliers we can make following general assumptions about the egress of this section of the arena during football games. The sections S2 and S3 are relatively equally used. Whereas the sections S2 is directly connected to the train station and is also the main entrance, the section S3 provides a more attractive view to the outside. Once in that section, spectators are more probable to directly go out. The other sections S1, S4 and S5 are also well used (from 5 % to 10 %) compared to the data from the arrival phase, where they were used by less than 5 %. This also expresses the trend of first going to the outside at the end of the event and from there to take new orientation steps, while having more overview. Also, we can assume that the data are not related to the period of the day, since some games were played at noon and the others in the evening.

The implications of these results for an evacuation scenario are straightforward. The audience type plays an important role and mostly their familiarity with the location. We have seen from the data that the behaviour was almost identical across the games played by the local team. We have assumed that these games were attended by the same audience as observed during local home games in the arena. The data were not collected during an actual evacuation, but the similarity between the data suggests that even in a case of a real evacuation with the same audience, the egress pattern might be similar. Also, the strategy of preferring the local shortest path to the outside in simulation tools is to some extent supported by the data. A considerable percentage of spectators left during the departure phase through sections that were not used during the arrival phase, implying that they have preferred the shortest path out and then orientated themselves towards their final destinations.

6 Modelling

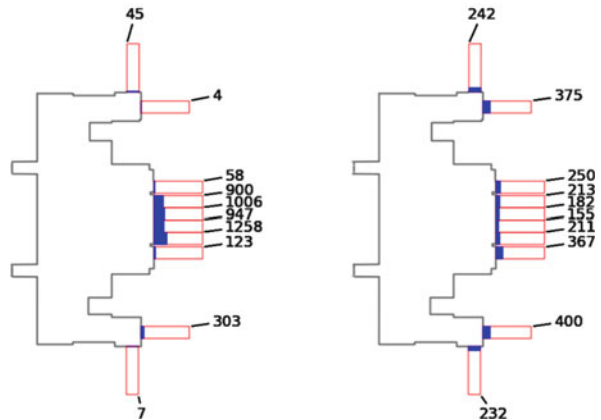
In the previous sections the pedestrians' route choice profile for entering and leaving the promenade part of the arena has been analysed for various football games and concert performances. In this section we compare the results with our route choice modelling approach. The framework used for describing pedestrian traffic is divided in a three-tier structure. One distinguishes between the strategic, the tactical and the operational level [8]. The start and the end point for each pedestrian are usually known in advance. At the strategic level pedestrians choose their self-estimated best route, among a collection of different alternatives. This can be done based on experience. Examples could be the global shortest path or the familiar path to a

given destination. Short term decisions are taken at the tactical level, avoiding jams or switching to a faster route for instance. Basic rules for motions are defined at the tactical level; these include accelerating, decelerating, and stopping. The pedestrian model at the operational level is a force based model and is described in [9] and the model at the strategic level which is a quickest path model is presented in [10]. As already mentioned in the introduction, we are only simulating an emergency clearing. This has two major impacts on the simulation. The first impact is that all pedestrians only have the same goal which is exiting from the facility. In a routine clearing, at the end of an event for instance, they may have a preferred destination, the parking lots or the train station for instance as demonstrated by the previous study. The second impact is that the pedestrians will choose the quickest path to reach the outside. The quickest path will result in a strictly unidirectional flow. The main output of profiles analysis was that the shortest path in the departure phase played an important role, even if the case of a routine clearing. Therefore we can assume that this effect will be reinforced in the case of an emergency evacuation. If the aim is to simulate a routine clearing the output from the previous section can be used as input for the route choice model with some restrictions. The study did not provide the route choice patterns inside the promenade itself, for instance how many spectators move from one section to the other. Another restriction is that the type of the event has to be taken into account.

For the initial configuration of the simulation 2,800 pedestrians are homogeneously distributed in the promenade and another 9,000 pedestrians are homogeneously distributed in the tribune. Similar to the empirical study the investigated values are E which denotes the number of using this section to reach the outside, P which is the number of pedestrians transiting through this section and T the number of pedestrians coming from the tribune. The route choice strategy applied is the quickest path and the analysis will mainly focus on the exit choosing behaviour.

If we first concentrate on the main six front exits on Fig. 8 (left), the first behaviour we notice is that not all exits are well used. The two exits on the outer part (used by 123 and 58 pedestrians) are not used. This typically occurs whenever a door is closed (not locked) and a nearby exit is open. The tendency is to walk towards the open exit as it is more inviting. The behaviour can be reversed if one spectator opens one of the exits, then other spectators will also start using it. This behaviour is not taken into account in our model and this is shown by the balanced usage of the main front exits (see Fig. 8 (right)). The second noticeable difference is the usage of the four side exits. They are used by pedestrians in our simulation following the quickest path. They lead in a shorter way to the outside than the other exits, although their position is not favourable. These discrepancies can be mitigated for instance by extending the model and adding an attractiveness parameter for all exits. Also, the network outside the building has to be considered as well.

Fig. 8 Comparison of pedestrians' profiles passing through the section S2 of the promenade at the end of the match. *Left*: observation, *right*: simulation



7 Conclusion

In this contribution an empirical study of pedestrians' route choice in an arena has been presented. The study has been done for different football games. Usually it is assumed in evacuation simulations that evacuees choose the shortest path to leave the facility. In this study, we have shown that even not in an evacuation scenario, people tend to choose the shortest path to leave the facility. These results may be an argument for the use of that strategy in evacuation software. It has also been found that the same type of spectators, regular supporters of a local team for instance, has the same route choice pattern. The results were the same across different football games played at different times in the day. After evaluating the shortest path strategy as suitable for an evacuation scenario, a simulation has been performed and with some restrictions compared with data from the empirical study. The exit choosing behaviour has shown some discrepancies where some exits giving the impression of being closed were not well used by spectators, whereas they were used in the simulation. By extending the pedestrian model to recognize attractive exits this gap can be closed. Finally it is necessary to also consider the network outside the facility for a more accurate route choice.

Acknowledgments The researches performed in this contribution have been done within the program "Research for Civil Security" in the field "Protecting and Saving Human Life" funded by the German Government, Federal Ministry of Education and Research (BMBF). The project has been supported under the grant no. 13N9952.

References

1. T.J. Shields, K.E. Boyce, "A study of evacuation from large retail stores," *Fire Safety Journal*, vol. 35, Issue 1, July 2000, pp 25–49
2. S. Heliövaara, J.-M. Kuusinen, T. Rinne, T. Korhonen, H. Ehtamo, "Pedestrian behavior and exit selection in evacuation of a corridor – An experimental study," *Safety Science*, vol. 50, Issue 2, Feb. 2012, pp 221–227
3. M. Kobes, I. Helsloot, B. de Vries, J. Post, "Exit choice, (pre-)movement time and (pre-)evacuation behaviour in hotel fire evacuation – Behavioural analysis and validation of the use of serious gaming in experimental research," *Procedia Engineering*, vol. 3, 2010, pp 37-51
4. F. Giannotti and D. Pedreschi, Eds., *Mobility, Data Mining and Privacy – Geographic Knowledge Discovery*. Springer, 2008.
5. S. Leitinger, S. Gröchenig, S. Pavelka, and M. Wimmer, Erfassung von Personenströmen mit der Bluetooth-Tracking-Technologie. In: *Angewandte Geoinformatik 2010*, 15th ed. New York: Addison Wesley Longman Inc., 2010.
6. T. Liebig and A. U. Kemloh Wagoum, "Modelling microscopic pedestrian mobility using bluetooth," in 4th International Conference on Agents and Artificial Intelligence, 2012.
7. R. Golledge, "Path selection and route preference in human navigation: A progress report," in *Spatial Information Theory A Theoretical Basis for GIS*, ser. LNCS, A. Frank and W. Kuhn, Eds. Springer Berlin / Heidelberg, 1995, vol. 988, pp.207–222
8. S. P. Hoogendoorn, P. Bovy, and W. Daamen, "Microscopic Pedestrian Wayfinding and Dynamics Modelling," in *Pedestrian and Evacuation Dynamics*, M. Schreckenberg and S. Sharma, Eds., 2002, pp. 123–155.
9. M. Chraïbi, U. Kemloh, A. Seyfried, and A. Schadschneider, "Force-based models of pedestrian dynamics," *Networks and Heterogeneous Media*, vol. 6, no. 3, pp. 425–442, 2011.
10. A. U. Kemloh Wagoum, A. Seyfried, and S. Holl, "Modelling dynamic route choice of pedestrians to assess the criticality of building evacuation," *Advances in Complex Systems*, vol. 15, no. 3, 2012.

Evacuation Analyses for Venues

Systematic Approach and Comparison to Evacuation Trials

Sven Hebben, Patrick Gessler, and Hubert Klüpfel

Abstract This paper illustrates a systematic approach for evacuation simulations and the comparison of the results to real world data for calibration and validation. An evacuation exercise in a venue of the trade fair Graz is presented. The results show that the reaction time of the evacuees is decisive for the overall evacuation duration. Additionally an evacuation analysis of the situation is presented. The simulation parameters were adapted to represent the circumstances of the exercise. The results of the exercise and the simulation are comparable.

Keywords Evacuation exercise • Evacuation analysis • Evacuation simulation • PedGo

1 Introduction

Evacuation Analyses are often used in Fire Safety Sciences to assess building layouts and venue locations. One area of application is the optimization of person flows. Another one is to assess deviations from prescriptive guidelines, e.g. concerning the dimensions of escape routes. For certain types of buildings, prescriptive guidelines are not applicable. This might be the case for architecturally demanding buildings, for sports stadiums, etc. In that context, problems of comparing different procedures or definitions of acceptance criteria might arise [1]. The reason is that prescriptive guidelines for buildings in Germany and Austria do not provide any criteria concerning evacuation simulations, evacuation durations or maximum densities for escape routes.

S. Hebben (✉) • P. Gessler • H. Klüpfel
TraffGo HT GmbH, Bismarckstr. 142, Duisburg 47057, Germany
e-mail: hebben@traffgo-ht.com

In Germany two projects develop a framework to standardize the procedures of evacuation analyses. One is the RiMEA project (Guideline for Microscopic Evacuation Analyses) [2], which defines the required aspects to be considered while preparing and analyzing a building. The second one is chapter “[An Innovative Evacuation System for Multiplex Cinemas](#)” of the vfdb Guideline for fire safety engineering (in German) [3]. The guideline specifies some basic parameters for the input of evacuation calculations.

In the following an evacuation exercise of a venue is described and its results are compared to an evacuation analysis. The evaluation of the simulation results is carried out according to the specifications given in the described guidelines.

2 The Trade Fair Graz Evacuation Trial

The exercise was planned and conducted in August 2011 by the fire brigade of Graz. It took place at the Trade Fair Graz in Styria/Austria on the upper floor of exhibition hall A. This exercise was embedded into an entertainment event, consisting of several talks and a comedy show [4].

2.1 Scenario Description

The rectangular room (room A) of the show was about 34 m wide and 67 m long. Emergency exits were located on all sides of the room. The emergency exit on the west side, which was also the main entrance, led into the west foyer. The exits on the north and south side led into staircases. The exits of the east side led into a neighboring room (room B). From there two staircases and a freight elevator were available. All staircases led directly outwards in the level of the ground floor. The floor plan of the building and the schematic escape routes are illustrated in the following Fig. 1.

The persons in room A were seated in 28 seating rows in front of a raised stage. The overall capacity of the seats was 1,232 persons. The event was not fully booked, about 1,100 persons were present. One thousand and twenty of them were registered by the event stewards. There were also several wheelchair users in the audience. These had to be evacuated separately. For the evacuation of the wheelchair users, the freight elevator near to emergency exit 2 in room B was available.

The mock-up scenario was a bomb threat with a following explosion in the west foyer. To create a realistic situation, pyrotechnics, smoke generators, and sound effects were used. The smoke generators and loud speakers were arranged in front of the doors of the west foyer (Fig. 2). Prior to the event, the audience was informed about the evacuation exercise, but they were unaware about its beginning.

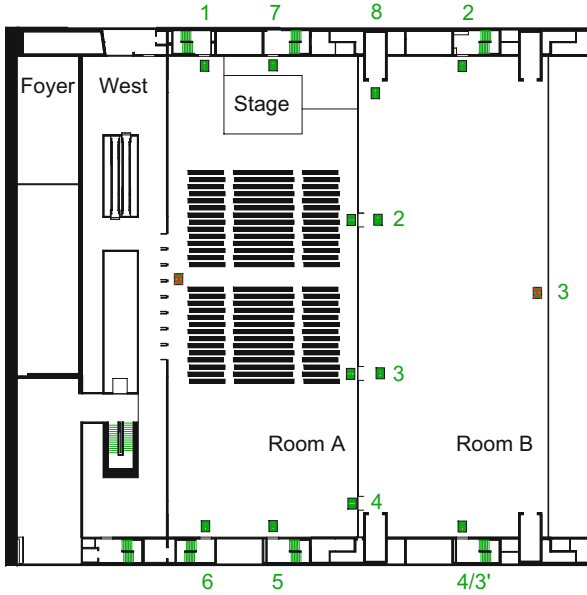


Fig. 1 Floor plan and illustration of escape routes



Fig. 2 Installation of smoke generators and speakers in the west foyer (left); ignition of smoke powder (right) (Photos by courtesy of fire brigade of Graz [5])

Since the event was not fully booked, the screenshot of the video recordings show, that most of the persons were seated in front of the stage. Some of the rear seating rows and the rows at the east side remained almost empty (Fig. 3).

Fig. 3 Screenshot of the video, showing the seated participants (room A) (Videos by courtesy of fire brigade of Graz [6])



To record the exercise, stationary as well as mobile cameras were used. The stationary cameras were mostly focused on the emergency exits. Another stationary camera was located below the ceiling to get a long shot of all persons in the hall. The mobile camera recorded the escape from the view of a wheelchair user. Additionally, several observers were positioned at the emergency exits, to document the egress flows during the exercise.

2.2 Evacuation

The emergency situation was mimicked by a bomb threat. Additionally, a piece of luggage was positioned in the west foyer. The crisis management group took measures for an evacuation. In consequence of the threat, the emergency exits to the west foyer were closed. Furthermore, emergency exit 3 was considered to be not accessible, so the persons had to be rerouted to exit 4. Event stewards were positioned inside room A in front of the remaining accessible emergency exits and in the corridors between the seating rows, to assist the evacuation.

After the simulated explosion of the bomb in the west foyer the crisis management group decided to evacuate the venue. The show stopped a few seconds after the ignition. The presenter informed the audience that something happened, which could be the result of a bomb threat. Afterwards the chief of the in-house fire safety team entered the stage and urged the persons to leave the building. The announcement took about 30 s. While the persons were informed about the incident and listened to the evacuation message, the lights were slowly turned on. The persons were instructed to leave the building immediately and to use the emergency exits on the north, east and south. Wheelchair users were instructed to use the emergency exit on the east side.

Directly after the end of the evacuation announcement, all persons stood up within about 10 s and moved towards the emergency exits. The persons mainly moved away from the smoke, which was pouring into the room from the west foyer. It was noticeable, that congestions occurred at emergency exit 2. Due to its

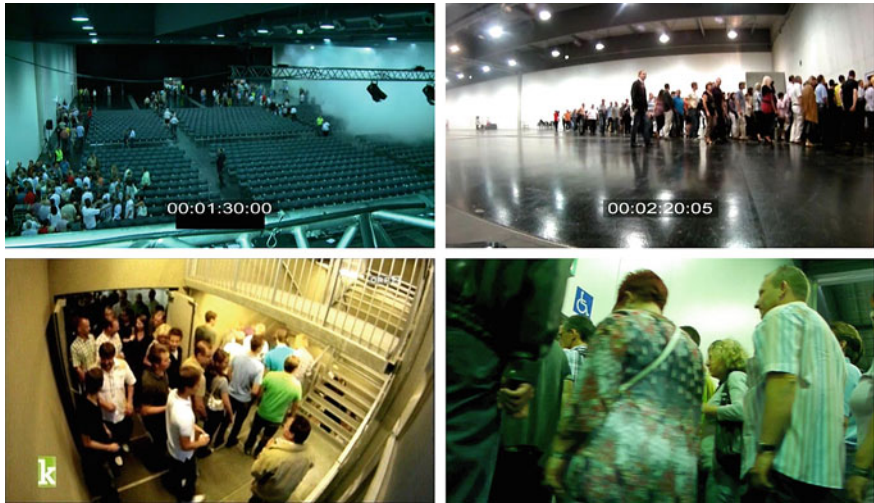


Fig. 4 Room A after 1:30 min (*top left*) [6]; Queue at staircase 2 in room B (*top right*) [6]; Landing area of a staircase (*bottom left*) [7]; View of a wheelchair user during the evacuation (*bottom right*) [6]

Table 1 Evacuation durations derived from the video recordings

Emergency exit	1 (A)	2 (A)	3 (A)	4 (A)	5 (A)	6 (A)	2 (B)	4 (B)
Time/min:s	~1:57	~2:08	~2:06	~2:07	~2:15	~2:06	~4:40	~3:40
Persons	~130	~260	~180	~100	~150	~200	~260	~280

attractiveness, emergency exit 2 was the nearest and therefore most frequently used. After having noticed, that only few persons were waiting at the neighboring exit 3, the stewards advised some persons to use exit 3. Furthermore it became obvious, that as a result of its isolated position, emergency exit 4 was rarely used. After passing through exits 2, 3 and 4, the persons waited at the entries to the staircases in room B, forming a queue. Since the widths of the stair cases were smaller than those of the exit doors, the person flow decreased (Fig. 4).

The assignment of persons to the exits and the evacuation times taken from the video recordings are illustrated in Table 1. The times are taken, when the last persons passed the exits.

Although all evacuation durations of room A are in the same range, the utilization of the exits was very uneven. Especially at the end of the evacuation, exit 4 was idle and only used sporadically by a few persons.

In the course of the evacuation, wheelchair users received a preferred treatment. Using exit 2, the stewards kept their path free in order to let them pass unhampered. Having reached room B, they were advised to move to the freight elevator, through which they were transferred to the first floor. In summary, the evacuation was calm without any major problems.

Table 2 Parameters of the simulated population

	Min	Max	Mean	Stddev	Distr.	Entity
VMax	2	5	3	1	Normal	c/s
Sway	1	3	2	1	Normal	–
Reaction	26	36	31	2	Normal	s
Dawdle	0	20	10	5	Normal	%
Inertia	1	5	3	2	Normal	–
Clustering	None					–

3 Evacuation Simulation

3.1 Evacuation Model

The model used to perform the evacuation analyses was PedGo. PedGo is a multi agent model, which is based on a cellular automaton [8]. The agents are represented individually and their characteristics are defined by individual parameters like walking speed, reaction duration, dawdling, swaying, inertia, and group behaviour. The geometry of the buildings, is imported through CAD drawings, which are projected onto a cellular grid with a cell size of 0.4×0.4 m.

3.2 Scenarios

The scenario simulated in the analysis is equivalent to the exercise. The exits to the western foyer are blocked. Only the exits to the north, south and east are accessible.

3.3 Input Parameters

The parameters chosen for the analysis are adapted to the scenario of the evacuation exercise illustrated in the previous chapter. These are e.g.: Information about the persons (number, initial location, demographics, specification of reaction durations) and the description of the route choice.

One thousand and twenty five persons are simulated. The initial locations of the persons are approximated to the seating of the venue. The exit assignment of the agents is assumed corresponding to the notes of the event stewards. The parameters of the population are adapted to the exercise and are illustrated in the following Table 2.

To consider the wheelchair users, a slower walking speed and an increased place requirement is assigned to five of the 1,025 agents.

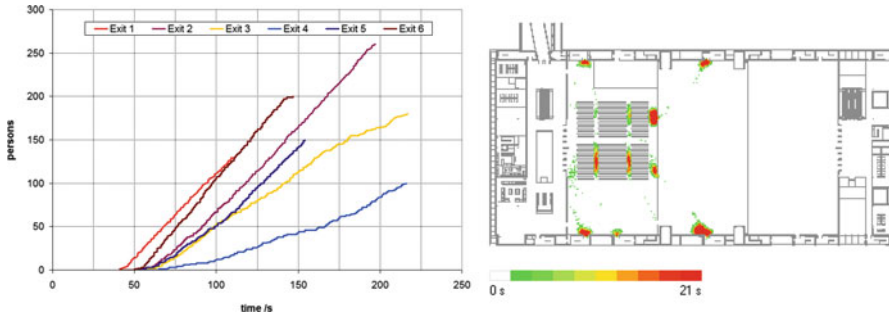


Fig. 5 Evacuation curves of each exit for the significant run (*left*), density plot of the significant run (*right*)

Table 3 Evacuation durations from the significant simulation run

Emergency exit	1 (A)	2 (A)	3 (A)	4 (A)	5 (A)	6 (A)	2 (B)	4 (B)
Time/min:s	1:50	2:20	1:57	2:15	2:33	2:26	3:16	3:36
Persons	130	260	180	100	150	200	260	280

The reaction duration is chosen according to the findings of the exercise (26–36 s). According to the RiMEA and vfdb guidelines, the reaction duration would be significantly longer (0.5–2.5 min).

3.4 Results

The following results show the evaluation of the significant run (95 %-quantile) taken from 100 stochastic simulation runs. According to RiMEA at least 10 stochastic simulation runs have to be performed.

The results of the simulation show, that the evacuation durations of the exits are in the same range. Exit 2 in room B forms an exception (Fig. 5). Compared to the results of the evacuation exercise, the simulation results are significantly shorter (Table 3). Apparently, there was a delay in the staircase at exit 2 in the exercise. The reason could be, that some persons reported to have difficulties due to their footwear on the steel grating of the stairs.

The density plot illustrates identified congestions according to the specifications given in RiMEA. The areas marked red represent areas for which densities of more than 4 p/m² persist for a period longer than 10 % of the evacuation duration. Significant congestions occur especially in the corridors between the seats and at emergency exit 2 in room A. In room B significant congestion is identified at the entries to the staircases. There is only minor congestion noticeable at emergency exit 2 in room B. As mentioned, the situation at emergency exit 2 in room B is the only place, which significantly deviates from the exercise.

4 Conclusion

The exercise shows, that the presence of event stewards can have a significant influence on the evacuation. Furthermore it is remarkable, that the persons of the evacuation exercise had a very narrow range of reaction durations. A possible reason for this, could be the fact that this was an announced evacuation trial. The view from a wheelchair user shows, that persons can have difficulties to orientate. Therefore organizational measures have to be taken for the evacuation of mobility impaired persons.

The results of the evacuation exercise and the simulation are comparable. A significant difference at emergency exit 2 in room B occurred. This is due to a delay during the exercise. To achieve the results of the exercise, the simulation parameters had to be adapted.

Acknowledgements We would like to thank the fire brigade of Graz, especially Alfred Pözl and Stefan Schnepf, for the invitation to follow the exercise and the supply of comprehensive material, such as video footage and scripts.

References

1. Hebben, Sven: Leitfaden für die Erstellung von Evakuierungsgutachten auf der Grundlage von Personenstromsimulationen und deren Bewertung durch die Genehmigungsbehörde, Diploma thesis, University Duisburg-Essen, 2008.
2. RiMEA-Project, Guideline for Microscopic evacuation analyses, version 2.2.1, 08.06.2009, www.rimea.de.
3. Vfdb (German Fire Protection Association): Guideline for fire safety engineering, Technical Report, second edition, 05/2009, www.vfdb.de.
4. Feuerwehr Graz: Script "Praxistag der Grazer Feuerwehren 2011", 19.07.2011
5. Feuerwehr Graz: Photo documentation about the evacuation exercise at the trade fair Graz, www.flickr.com/photos/feuerwehrgraz/sets/72157627443188057/.
6. Feuerwehr Graz: Video footage of the Evacuation Exercise at the Trade Fair Graz, Courtesy of Fire Brigade Graz.
7. ORF 2: Konkret: Das Servicemagazin, TV documentary, 01.09.2011.
8. PedGo Users Manual, Version 2.5.0, TraffGo HT GmbH, 2008, www.traffgo-ht.com.
9. Gessler, Patrick: Entfluchtungsanalyse von TV Studioproduktionen mit Zuschauern beim Westdeutschen Rundfunk Köln, Bachelor Thesis, Cologne University of Applied Sciences, 2010.

Influence of Spreading Hazardous Material in Macroscopic Evacuation Dynamics: A Proof of Concept

Simone Göttlich, Sebastian Kühn, Jan Peter Ohst, and Stefan Ruzika

Abstract In this article, an evacuation model describing the egress in case of danger is considered. The underlying evacuation model is based on continuous network flows, while the spread of some gaseous hazardous material relies on an advection–diffusion equation. A proof of concept shows differences to the usually used macroscopic evacuation models.

Keywords Evacuation • Dynamic network flows • Optimization

1 Introduction

Evacuation modeling is an important way to describe an evacuation process in order to estimate the total evacuation time and optimize evacuation strategies (see [1, 2]). The approaches to evacuation modeling divide into microscopic and macroscopic approaches. Whereas microscopic models consider each evacuee individually, macroscopic approaches model evacuees as part of a homogeneous group. Using optimization techniques as a basis to design macroscopic models allows for finding optimal evacuation plans concerning the minimal possible evacuation time or fastest evacuation routes. Therefore such models also allow for the computation of lower bounds on the true evacuation time [1].

Partial differential equations (pde) are widely used in the analysis of pedestrian movements on 1d- or 2d corridors (e.g. [3]) and also evacuation aspects can be

S. Göttlich (✉)

School of Business Informatics and Mathematics, University of Mannheim, Mannheim D-68131, Germany

e-mail: goettlich@uni-mannheim.de

S. Kühn • J.P. Ohst • S. Ruzika

Department of Mathematics, University of Kaiserslautern, Kaiserslautern D-67663, Germany

e-mail: skuehn@mathematik.uni-kl.de; ohst@mathematik.uni-kl.de;

ruzika@mathematik.uni-kl.de

found therein. The mapping of the pdes on networks can be done, if the coupling conditions at vertices ensure the conservation of mass. For example, this is done in traffic flow [4, 5] or supply chain modeling [6].

In this work, we are interested how the propagation of some hazardous material (e.g. a gas cloud) influences the evacuation process. This means, the evacuation model under consideration is combined with an equation for the hazardous material in an innovative way.

The remainder of this article is organized as follows. In Sect. 2, we state the macroscopic continuous evacuation model used for the proof of concept following in Sect. 3.

2 Continuous Evacuation Model

For an evacuation model we use the continuous network model proposed in [7], which is restated here for better referencing.

2.1 Network Definition

For a time horizon T let $\mathcal{G} = (V, A)$ be a directed graph with node set V and arc set A . The node set is assumed to subsume a source $s \in V$ and a sink $d \in V$. For a node $i \in V$, $\delta^-(i)$ and $\delta^+(i)$ is the set of all arcs starting and ending at i , respectively. An arc $e \in A$ is associated with an interval $[a_e, b_e]$ of length L_e . The constant times needed to traverse an arc e are called travel times τ_e and correspondingly the travel velocities are $v_e = L_e/\tau_e$. Arc capacities are denoted by piecewise constant functions $\mu_e(t, x)$ and storage capacities at nodes by time-dependent functions $M_i(t)$.

For the case study we extend this definition to multiple sinks by defining a set of sinks $D \subset V$.

To model the evacuation process we use a macroscopic model composed of ordinary and partial differential equations. Those describe the dynamics of the density of evacuees ρ_e on the arcs $e \in A$ of the network and the queues q_i in the vertices $i \in V$

$$\min / \max \Phi(\rho, q) \quad (1a)$$

$$\text{s.t. } \partial_t \rho_e(t, x) + \partial_x f_e(\rho_e(t, x)) = 0 \forall e \in A, x \in [a_e, b_e], t \geq 0 \quad (1b)$$

$$\text{where } f_e(\rho_e(t, x)) = v_e \rho_e(t, x)$$

$$\partial_t q_i(t) = \sum_{e \in \delta^-(i)} f_e(\rho_e(t, b_e)) - \sum_{e \in \delta^+(i)} f_e(\rho_e(t, a_e)) \forall i \in V, t \geq 0 \quad (1c)$$

$$q_i(0) = q_{i,0} \quad \forall i \in V \tag{1d}$$

$$\rho_e(0, x) = \rho(x)_{e,0} \tag{1e}$$

$$0 \leq q_i(t) \leq M_i(t) \quad \forall i \in V, t \geq 0 \tag{1f}$$

$$0 \leq f_e(\rho_e(t, x)) \leq \mu_e(t, x) \quad \forall e \in A, x \in [a_e, b_e], t \geq 0. \tag{1g}$$

The choice of the objective function (1a), which may depend on the density of evacuees ρ_e and the load of the queues q_i , is discussed below. The transport of the evacuees along the arcs and conservation of mass is ensured by the advection equation (1b). In contrast to the usual traffic flow models [4] or [8] a linear dependence of the flux f_e on the density ρ_e is assumed, which is a first order approximation yielding lower bounds. Furthermore we showed [7] that the linear structure enables the use of fast solution methods. The ordinary differential rate equation (1c) determines the load of the queue q_i in node i by measuring the total incoming $\sum_{e \in \delta^-(i)} f_e$ and outgoing flux $\sum_{e \in \delta^+(i)} f_e$ into this node. The distribution of the flux is subject of optimization to determine the best routing of evacuees through the network. Equations 1d and 1e define the initial conditions to the differential equations, where we assume the streets to be empty, i.e. $\rho(x)_{e,0} = 0$ for all arcs e , and $q_{i,0}$ represents the number of residents in vertex i to be evacuated. Capacity constraints (1f) and (1g) bound the queues and flow from above.

Remark 1 The problem (1) is inspired by the evacuation model motivated in [1]. Due to its linear nature, it is the simplest approach to model an evacuation process. This means, either the evacuees move forward towards their safety destination as long as capacity constraints permit escape or, if the capacity is reached, the evacuees have to stay in nodes. Therefore, congestions on arcs are avoided. However, a more sophisticated model should allow for bottleneck situations on arcs, cf. traffic flow models [4, 8].

In evacuation modeling the task is to lead a given number of evacuees to safety. In order to find a lower bound on the evacuation time we use the following, so-called *quickest flow objective function*

$$\min \Phi(\rho, q) = \sup \left\{ t \in [0, \infty) \mid f_e(\rho_e(t, b_e)) \neq 0 \text{ for some } e \in \delta^-(d) \right\}. \tag{2}$$

To ensure that all evacuees are indeed sent through the network an additional condition is introduced

$$\int_0^T \sum_{e \in \delta^-(d)} f_e(\rho_e(t, b_e)) dt = q_{s,0}. \tag{3}$$

Thus we find the minimal evacuation time by setting $q_{i,0} = 0$ for all $i \in V \setminus \{s\}$ and $q_{s,0} > 0$ and solve the *quickest flow problem*

$$\min (2) \tag{4a}$$

$$\text{s.t. (1b) – (1g) and (3).} \tag{4b}$$

We like to compare the fastest possible evacuation time found by solving problem (4) to a safest possible evacuation plan. Therefore we compute the propagation of some hazardous material (e.g. a gas cloud from a chemical blow out) by an advection–diffusion equation and use the mapping presented in [7] to map the concentration as costs onto the network. The resulting optimization problem is shown in the subsequent section.

2.2 Evacuation Influenced by Hazardous Material

The evacuation model presented until now relies on a general graph. However for any application the vertices are specified by coordinates in $\Omega \subset \mathbb{R}^2$. So we assume that the concentration of the hazardous material ω obeys the following linear advection–diffusion equation in the domain Ω

$$\partial_t \omega - \kappa \Delta \omega + d \cdot \nabla \omega = 0 \text{ in } \mathbb{R}^+ \times \Omega \tag{5}$$

with diffusion constant $\kappa > 0$ and wind vector field $d = (d_1, d_2) \in \mathbb{R}^2$. As we consider a deflagration, we do not have a time dependent source term but only impose initial conditions for the concentration of 100 (life-threatening value) in the area of the source Ω_0 and 0 elsewhere. As boundary conditions we use Dirichlet conditions with $\omega = 0$.

We include the concentration level of the hazardous material ω as an additional parameter in the evacuation model (1) by introducing time-dependent concentration parameters $c_e(t)$ and $c_i(t)$ defined on arcs e and vertices i , respectively, and a new objective function Φ .

Therefore, we map the concentration value ω to the corresponding positions in the network, e.g. $\omega|_e$ means that the values of ω are restricted to the arc e and fix a certain point in time t . The value of the hazardous material on an arc e at time t is normalized yielding the inner integral of equation (6). To include the possible change of the level of the hazardous material in the time the evacuees traverse an arc, we also regard all times within the interval $[t, t + \tau_e]$ yielding

$$c_e(t) = \int_t^{t+\tau_e} \int_{a_e}^{b_e} \frac{\omega|_e}{L_e} dx d\hat{t}. \tag{6}$$

For a vertex $i \in V$ the concentration parameter at time t represents the exposure of evacuees to the hazardous material when waiting in the vertex for one time step. Thus, we get

$$c_i(t) = \int_t^{t+1} \omega \Big|_i d \hat{t}. \tag{7}$$

An appropriate possibility for including the costs in the evacuation model is to minimize the level of concentration to which the evacuees are exposed. This can be done with the definition of new cost-dependent objective function $\Phi(\rho, q, c)$, yielding the minimization of the accumulated hazard to which the evacuees are exposed

$$\Phi(\rho, q, c) = \int_0^T \left(\sum_{e \in A} c_e(t) f_e(\rho_e(t, a_e)) + \sum_{i \in V} c_i(t) \partial_t q_i(t) \right) dt. \tag{8}$$

This objective function is useful when the hazard is harmful if the accumulated level exceeds a critical level (e.g. low levels of radiation). It can be used to extend the evacuation model (1) by solving the optimization problem

$$\min (8) \tag{9a}$$

$$\text{s.t. (1b) – (1f)}. \tag{9b}$$

Generally, this type of optimization problem can be solved using adjoint-based methods due to the continuous nature of the problem. In case of a linear objectives and constraints or only ‘mild’ nonlinearities, it is possible to reformulate the original problem into a mixed-integer program or a dynamic network flow problem.

3 Proof of Concept

Finally, we present a numerical example for the evacuation models (4) and (9). Therefore we first calculate the transport of the hazardous material by solving (5) using a Crank-Nicolson method. Then we compute the mapping onto the network according to (6) and (7). The optimal evacuation plan is the computed by solving the optimization problems (4) and (9) using an appropriate discretization as a dynamic network flow problem.

The network under consideration is shown in Fig. 1 with the source of the hazard located in the upper left corner. The vertex in the upper right corner marked by a green + is the safe destination. The evacuees are initially located in the vertex in the lower left marked by an red X ($y_{s,0} = 24$). The direction of the arcs is indicated by the arc head and either right or up.

Fig. 1 Network of the example. The *red X* shows the initial location of the evacuees whereas the *green +* marks the safe destination

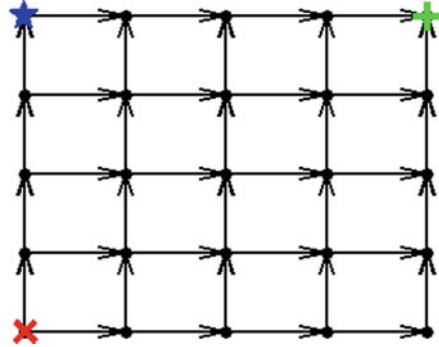
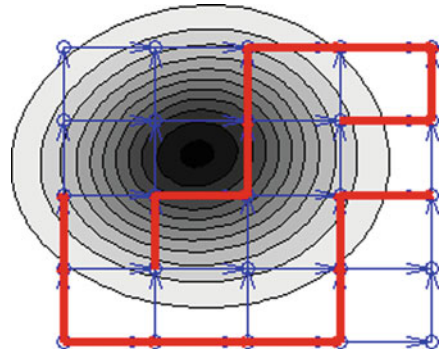


Fig. 2 Quickest flow solution at time step 8. The maximal value of the hazard is 22.42



As this is just a proof of concept the capacities as well as the velocities are chosen to be 1 for all arcs. This can later be easily adapted to a non-academic case study by taking the average velocities on different types of streets, the number of lanes and the assumed distance between cars into account to calculate these parameters.

For the hazardous material we assume it to be blown southeast crossing the network in the diagonal. The initial area Ω_0 of the cloud is located in the northwest of the network and centered at the blue star in Fig. 1.

Solving the *quickest flow problem* (4) is independent of the direction and strength of the wind and yields the fastest evacuation time. A snapshot of the solution is shown in Fig. 2 and shows the drawback of the solution as the evacuation routes are covered by the hazard.

Computing the optimal evacuation plan according to the minimization of the accumulated sum objective (9) yields highly different results (see Fig. 3), as this objective seeks for solutions avoiding the hazardous material. So, as long as the hazard is in the upper left part of the graph the evacuation routes first head right and then up. As time approaches and the hazard reaches the lower right part of the graph, the evacuation routes change and now first head up and then right. This way the evacuation strategy is adapted to the dynamics of the hazard in order to ensure an evacuation as safe as possible.

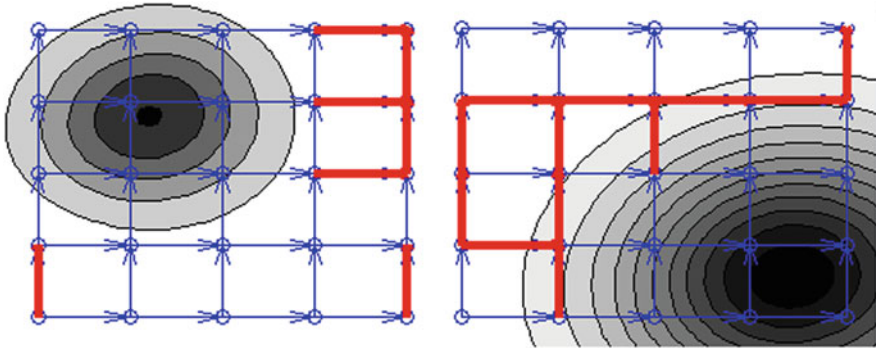


Fig. 3 Solution for accumulated sum objective. Time steps 7 (left) and 16 (right). Maximal value of the hazard is 25.36 (left) and 11.68 (right)

Table 1 Comparison of evacuation times and accumulated sum of hazard for different objective functions (2) and (8)

Problem	Accumulated concentration [a.u.]	Evacuation time [a.u.]
Quickest flow	1,670	19
Safest flow	370	25

In this network the evacuation time of both solutions presented differs only slightly whereas the difference considering the accumulated concentration is large (see Table 1). This shows the enormous advantage of the accumulated sum objective over the quickest flow objective when the safety of the evacuees is first priority.

Acknowledgements S. Ruzika is partially supported by BMBF, Project REPKA, FKZ 13N9961 (TU KL). S. Kühn and J.P. Ohst are supported by Stiftung Rheinland-Pfalz für Innovation, Project EvaC, FKZ 989.

References

1. H. W. Hamacher and S. A. Tjandra, “Mathematical modelling of evacuation problems - a state of the art,” in *Pedestrian and Evacuation Dynamics*, M. Schreckenberger and S. D. Sharma, Eds., Berlin, Springer, 2002, pp. 227–266.
2. A. Schadschneider, W. Klingsch, H. Klüpfel, T. Kretz, C. Rogsch and A. Seyfried, “Evacuation dynamics: Empirical results, modeling and applications,” in *Encyclopedia of Complexity and System Science*, B. Meyers, Ed., New York, Springer, 2009, pp. 3142–3176.
3. D. Helbing, “A mathematical model for the behavior of pedestrians,” *Behavioral Science*, vol. 36, pp. 298–310, 1991.
4. G. M. Coclite, M. Garavello and B. Piccoli, “Traffic flow on a road network,” *SIAM Journal on Mathematical Analysis*, no. 36, pp. 1862–1886, 2005.
5. M. Herty and A. Klar, “Modeling, simulation, and optimization of traffic flow networks,” *SIAM Journal on Scientific Computing*, vol. 25, pp. 1066–1087, 2003.

6. S. Göttlich, M. Herty and A. Klar, "Network models for supply chains," *Communications in Mathematical Sciences*, vol. 3, pp. 545–559, 2005.
7. S. Göttlich, S. Kühn, J. P. Ohst, S. Ruzika and M. Thiemann, "Evacuation dynamics influenced by spreading hazardous material," *Networks and Heterogeneous Media*, vol. 6, no. 3, p. 443, September 2011.
8. H. Holden and N. H. Risebro, "A mathematical model of traffic flow on a network of unidirectional roads," *SIAM Journal on Mathematical Analysis*, vol. 26, pp. 999–1017, 1995.

Evacuation Exercises in a TV Studio

Comparison to Simulation Results

Patrick Gessler and Sven Hebben

Abstract This paper presents results on two evacuation exercises in a TV studio. The results are compared to evacuation simulations. The parameters for the simulation were adapted to represent the population and behaviour characteristics observed in the exercise. The times and other results are comparable.

Keywords Evacuation exercise • Evacuation analysis • Evacuation simulation • PedGo

1 Introduction

The two exercises were performed in a German TV studio [1]. The width of the studio was 50 m, the length 30 m. Therefore, the total area was 1,500 m². In the studio each show had its own backdrop and a grandstand for 450 persons. The grandstand was opposite to the stage. The tribune consisted of three blocks, which were approximately equal in size. In total, there were four flights of stairs available.

In the evacuation exercise, three emergency exits were accessible. These were marked as exit 1, 2, and 3 in the studio (cf. Fig. 1).

In exercise 1 (during the recording of the show “Die große ARD Weltreise”), two emergency exits were located on the lower level and one emergency exit at the top of the podium (top floor). In exercise 2 (during the recording of the childrens’ show “Frag’ doch mal die Maus”) there was one emergency exit located on the lower level and two emergency exits at the upper side of the grandstand on the top floor. The two exercises were carried out differently. The details are described in the next section.

P. Gessler (✉) • S. Hebben
TraffGo HT GmbH, Bismarckstr. 142, Duisburg 47057, Germany
e-mail: gessler@traffgo-ht.com

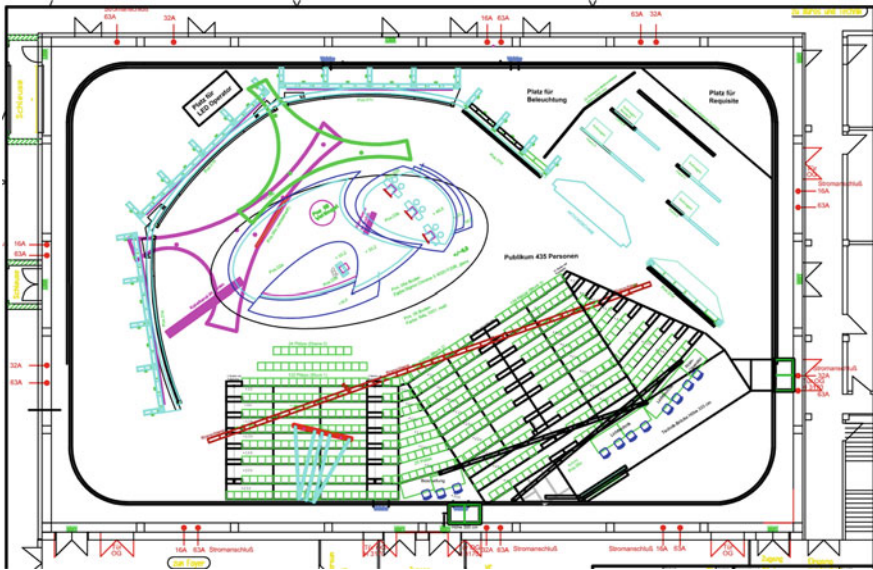


Fig. 1 Floorplan of the studio for the first exercise

2 Exercises

2.1 Description of Exercise 1

Before the beginning of the program the audience was informed that an evacuation exercise will take place after recording the show. At the end of the show the audience was requested to wait and not to leave their seats, while the cameras were placed to record the following exercise. When the preparations were completed, the persons were asked to leave the studio immediately. All persons had to choose their way out of the studio by themselves, no details about the emergency routes were given. Figure 2 illustrates the mainly chosen routes of the persons depending on the location of their seating on the grandstand. The flow of the persons inside the studio and at the emergency exits was recorded, so that an analysis of the exercise and a comparison to the evacuation simulation could be performed.

2.2 Description of Exercise 2

In the second exercise the audience was not informed about an evacuation exercise taking place after the recording of the show. When the recordings of the show were finished, the persons were asked to remain seated while the cameras were

Fig. 2 Route decision by seating (Photos by courtesy of WDR)



put back into record position. When the preparations were completed, the audience was informed about the evacuation exercise and urged to leave the studio through all emergency exits immediately. With the alarm sign (“Ladies and Gentlemen, please leave the studio now!”) which was also the beginning of the exercise, the audience was informed the first time, so that it was an unannounced exercise. The setup of the recording of the exercise has been carried out in the same manner as described in exercise 1.

2.3 Situation

In both cases the audience was already sitting in the studio for several hours and watching the recording of the TV show. Both shows were entertainment shows. The show “Die große ARD Weltreise” (exercise 1) is a game and quiz show, where celebrities have to answer difficult, but interesting questions about countries all over the world.

The show “Frag doch mal die Maus” (exercise 2) is an entertainment quiz show for children. In the program children’s issues are addressed to celebrities and are clearly explained by experiments.

2.4 Population Characteristics

The audience was selected by a casting agency to cover all age and person groups. Each exercise had a total of 450 persons on the considered tribune.

In Table 1 the age distribution for both shows is illustrated.

Table 1 Population parameters in the exercise

Category	Total	Total
Minimum age	7 years	7 years
Maximum age	84 years	84 years
Average age	46 years	38.7 years
Standard deviation	15 years	20 years
Men/Women	46 %/54 %	47 %/53 %
Disabled persons	5 persons	4 persons

2.5 Results

Exercise 1 The audience was guided only through the exits in the lower level to enter the studio, the upper exit was only known in theory (the audience was given a safety advise before the show started, but they could not walk through it except in the case of emergency). The total evacuation time for exercise 1 was 2:40 min. In this trial essentially the emergency exits in the lower floor were used by the audience (for 2:10 and 2:40 min). The exit at the top of the grandstand was only rarely used (the emergency exit was only used for 1:15 min by the persons).

Exercise 2 Right after the beginning of the second exercise, the evacuation exercise was cancelled, because most of the persons thought, that this would be a final joke of the show. The problem was, that the main character of the show, a large orange mouse, was still to see in the scenery in front of the grandstand. It was also a seen problem, that the evacuation order was given by the so called “warm-upper”, who had to entertain the audience in breaks of the recording. These circumstances led to the situation that especially the children did not follow the evacuation order. Instead of evacuating, they rushed to the front to take pictures and to get autographs. Therefore no evacuation times were measured for the emergency exits.

3 Simulation

The evacuation simulation was performed by the use of PedGo [2]. The floor plan of the studio with the installations of the show has been projected onto the grid of the discrete model. Due to the short reaction time of the audience in exercise 1, the reaction time was set as 0–10 s. The remaining parameters were set as default, because the characteristics of the age distribution diagram was similar to the default one given by the specifications of RiMEA [3].

3.1 Comparison of Simulation and Empirical Results

The results are compared in Table 2.

The comparison of the results show, that the evacuation time of the exercise is in the same range of the results of the simulation.

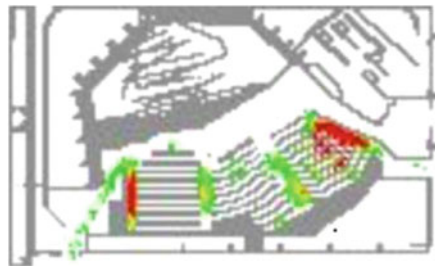
Table 2 Comparison of simulation and empirical results

	Simulation	Evacuation exercise
Minimum time	02:37	–
Maximum time	03:36	–
Average time	03:01	02:40
Significant time	03:17	–

Fig. 3 Crowding at the exits
(Photos by courtesy of WDR)



Fig. 4 Illustration of the congestion of the simulation of exercise 1



As a problem of every tribune the stairs were the bottleneck. In the following illustration of the exercise it is obvious, that the outer stairs were jammed by persons leaving the studio. Although the persons could use free stairs in the middle of the tribune, they lined up to the outer stairs. One reason could be clustering, when persons know or are related to each other (Fig. 3).

From the density plot, shown in Fig. 4, can be seen, that these areas are marked in red, to illustrate significant congestions according to the definition given in RiMEA.

4 Conclusion

Seen from the second exercise, one of the most important facts of a successful evacuation exercise, and maybe also in a real evacuation, is, that the situation has to be announced in a serious way. It is necessary, that the audience is able to notice the evacuation announcement in a clear and also serious way. It might be a problem, if an precautionary evacuation is planned in a venue in a jolly moment of a show. Persons may not notice a dangerous situation (e.g. a bomb threat). Measures have to be taken for such situations to reach the persons, so that they will follow the evacuation order.

If an evacuation is conducted, no celebrities, performers or players shall be present on the stage or be seen by the audience. It could happen, that some of the persons try to take pictures or get autographs, instead of evacuating. Persons in the illustrated exercises also tried to find their friends and relatives before they left the studio. Thus some persons crossed the main evacuation flow or hampered it by standing in the way of others.

It had a major influence on the choice of the evacuation route, on which way each person entered the studio. Persons rather used the exit they have already taken for entry than using a nearer emergency exit. The reason is, that nearer exits were not noticed by the persons.

References

1. Gessler, Patrick: Entfluchtungsanalyse von TV-Studioproduktionen mit Zuschauern beim Westdeutschen Rundfunk Köln, Bachelor Thesis, Cologne University of Applied Sciences, 2010.
2. PedGo Users Manual, Version 2.5.0, TraffGo HT GmbH, 2008, www.traffgo-ht.com.
3. RiMEA-Project, Guideline for Microscopic evacuation analyses, version 2.2.1, 08.06.2009, www.rimea.de.
4. Vfdb (German Fire Protection Association): Guideline for fire safety engineering, Technical Report, second edition, 05/2009, www.vfdb.de.

Experimental Study and Modelling of Pedestrian Space Occupation and Motion Pattern in a Real World Environment

F. Zanlungo, Y. Chigodo, T. Ikeda, and T. Kanda

Abstract In this work we tackle the statistical study and modelling of the usage of space by pedestrians in a real world environment. A large amount of pedestrian trajectories is collected in a corridor used just as a transition place, and the density and velocity distributions are analysed as functions of the distance from the walls. The empirical data are fitted to a model assuming the density and velocity to be determined through a Boltzmann factor by a comfort function depending on the distance from the walls and assuming a maximum on the left side of the corridor (Japanese traffic convention). The empirical data are then compared to numerical simulations using pure collision avoidance models, to better analyse the influence of the environment on the pedestrian distribution and to investigate how to introduce in collision avoiding the bias that makes people walk preferentially on a given side of a corridor.

Keywords Pedestrian social norms • Macroscopic and microscopic behaviour simulation • Real world data collection

F. Zanlungo (✉) • T. Ikeda • T. Kanda

Intelligent Robotics and Communication Laboratories, Department of Communication Robots, ATR 2-2-2 Hikaridai, Seika-cho, Soraku-gun, Kyoto 619-0288, Japan

e-mail: zanlungo@atr.jp

Y. Chigodo

Intelligent Robotics and Communication Laboratories, Department of Communication Robots, ATR 2-2-2 Hikaridai, Seika-cho, Soraku-gun, Kyoto 619-0288, Japan

Department of Multimedia Engineering, Graduate School of Information Science and Technology, Osaka University, Osaka 565-0871, Japan

1 Introduction

There is still a gap in pedestrian studies between analyses based on controlled experiments [1] and real world data collection [2]. The former are performed in very simple environments, data are recorded with high precision and usually allow for an effective modelling of the results and comparison with simulations. Nevertheless these experiments may deviate strongly from real world behaviour, both for the artificial nature of the environments in which they are performed, and for the unnatural behaviour that subjects may exhibit. On the opposite real world data collection presents lower data quality, and real world environments are usually too complex to allow mathematical analysis and modelling, making a generalisation of the obtained information very difficult.

This work is an attempt to create a bridge between these two approaches, analysing pedestrian behaviour in a real world environment which is simple enough to be described with a mathematical model. We study the density and velocity patterns of pedestrians in corridors used only as transition places, checking that these quantities depend only on the distance from the walls. In Japan, where data were collected, people walk on the left side of corridors [2], and our analysis, that divides them according to their walking direction, confirms this tendency. We found that the pedestrian density in each flow goes to zero close to the walls, and assumes a maximum in a point closer to the left wall than to the right one. The pedestrian velocity does not change more than 10% from the minimum value, assumed close to the walls, to the maximum, located on the right of the density maximum.

We model the data assuming that the pedestrian density distribution is given by a Boltzmann factor, whose “Hamiltonian” is a (dis)comfort function, assuming a minimum value where pedestrians can walk more easily. We also model the velocity distribution as a Gaussian centred around a preferred value that depends on the distance from the walls.

Pure collision avoiding behaviour leads to emergent self-organisation [1], and it has been proposed that a bias in the perceived position of other pedestrians may be a way to account for the (culture dependent) tendency to walk on a given side of a corridor [3]. We use computer simulations to understand to which extent the observed position and velocity distributions may be obtained using a pure collision avoiding model.

2 Environment

The purpose of this work is to study the behaviour of pedestrians in a real world environment with a simple geometry. Ideally, we would like to study a uniform corridor used just as a transition place, and since such an environment is expected to be invariant along the direction of the corridor, we want to study the density and velocity dependence on the only distance from the walls. We expect two flows to be present, i.e. identifying the x axis of the Cartesian system with the direction of the

corridor, one flow will be given by pedestrians with a positive x component velocity, $v^x > 0$, the other by pedestrians with $v^x < 0$.

As an approximation to this ideal environment we studied an underground area in Umeda (Osaka) where some corridors connect a shopping area with a railway station. These corridors are quite uniform, without any shop, and used almost only by people transiting between the station and the shopping area, and thus their structure is quite similar to the ideal one. The pedestrian positions were recorded in two working day afternoons using 2D laser range finders, a technology that allows for tracking with an error of order 60 mm [4]. The tracked trajectories were smoothed in a time window $\delta t = 200$ ms, and the velocity obtained from the smoothed trajectories as $\mathbf{v}_i(t) = (\mathbf{x}_i(t + 2\delta t) - \mathbf{x}_i(t))/(2\delta t)$.

3 Observables

We divide the environment in 2D cells of size $\Delta = 0.25$ m and area $A = \Delta^2$, and record in each cell and for each time step the number of pedestrians detected and their velocity. Assuming the observation to be performed on a time span Δt , the number of time instants at which data are recorded is given by $T = \Delta t/\delta t$. Let us assume N_k pedestrian positions to be recorded on cell k , and $\{\mathbf{v}_i\}$ with $1 \leq i \leq N_k$ to be set of their velocities. Based on these microscopic observables, it is straightforward to define the macroscopic density ρ on k as

$$\rho_k = N_k / (TA) \tag{1}$$

The macroscopic vectorial velocity and speed are

$$\mathbf{V}_k = \frac{\sum_{i=1}^{N_k} \mathbf{v}_i}{N_k} \quad \mathcal{V}_k = \frac{\sum_{i=1}^{N_k} |\mathbf{v}_i|}{N_k} \tag{2}$$

In principle $\mathcal{V}_k \neq |\mathbf{V}_k|$. After fixing the orientation of our Cartesian system, we divide the pedestrian velocities in two sets,

$$P^+ = \{\mathbf{v}_i | v_i^x > 0\} \quad P^- = \{\mathbf{v}_i | v_i^x < 0\}$$

respectively with cardinalities N_k^+ and N_k^- , and define

$$\rho_k^+ = N_k^+ / (TA) \quad \rho_k^- = N_k^- / (TA) \tag{3}$$

$$\mathbf{V}_k^+ = \frac{\sum_{i=1}^{N_k^+} \mathbf{v}_i}{N_k^+} \quad \mathbf{V}_k^- = \frac{\sum_{i=1}^{N_k^-} \mathbf{v}_i}{N_k^-} \tag{4}$$

$$\mathcal{V}_k^+ = \frac{\sum_{i=1}^{N_k^+} |\mathbf{v}_i|}{N_k^+} \quad \mathcal{V}_k^- = \frac{\sum_{i=1}^{N_k^-} |\mathbf{v}_i|}{N_k^-} \tag{5}$$

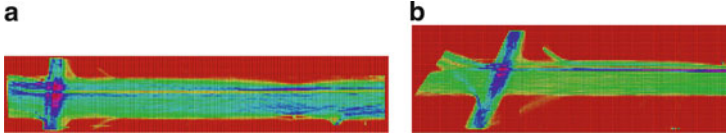


Fig. 1 ρ_k for pedestrians with $|\mathbf{v}| > 500$ mm/s in $E1$ (a) and $E2$ (b). Red corresponds to $\rho = 0$, yellow to low ρ , violet to high ρ . $E1$ measures 60×12 m, $E2$ 52×17 m

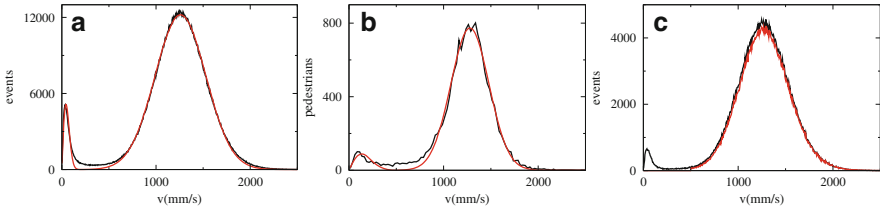


Fig. 2 (a) Velocity distribution (black) in $E1$ compared to the best-fit to a model assuming the sum of a Gaussian plus a Rayleigh distribution (red). (b) Average velocity distribution (black) in $E1$ compared to the best-fit to the same model as in (a). (c) Black line, velocity distribution in $E1a$ before filtering as in Eq. (6). Red line, after filtering

3.1 Data Filtering

We recorded data in two different corridors connecting the shopping area to the station (environments $E1$ and $E2$, Fig. 1). Both recording campaigns lasted around 6 h ($\approx 10^5$ time recordings). In $E1$ we tracked 17,188 pedestrians ($\approx 1.8 \cdot 10^6$ recordings) while in $E2$ we tracked 11,124 pedestrians ($\approx 1.1 \cdot 10^6$ events). Figure 2a shows the $v = |\mathbf{v}|$ distribution (as total number of events in a 5 mm/s histogram) in $E1$. The empirical distribution can be described as the sum of a Gaussian distribution (pedestrians walking along the corridor) plus a Rayleigh distribution (standing pedestrians assuming white Normal noise in their x, y position recordings). We find, by best-fit, for the Gaussian velocity distribution $\sigma_G = 270$ mm/s and $\mu = 1,260$ mm/s in $E1$, $\sigma_G = 260$ mm/s and $\mu = 1,250$ mm/s in $E2$. For the Rayleigh distributions, we have $\sigma_R = 44$ mm/s in $E1$, $\sigma_R = 28$ mm/s in $E2$. Assuming also the Gaussian distribution of moving pedestrian velocities to be affected by noise with intensity $\approx \sigma_R$, we expect the estimation of σ_G not to be strongly affected by noise. Let us assume $\sigma_R/\sigma_G \approx 1/5$, and the observed velocity distribution to be given by the sum of two stochastic Gaussian processes, the actual velocity distribution plus the random noise. It follows for the “true” value $\sigma_T = (\sigma_G^2 - \sigma_R^2)^{\frac{1}{2}} \approx 49/50\sigma_G$.

Figure 2b shows the empirical and best fitted distribution for average pedestrian velocities (i.e. the average value of v for each pedestrian over the tracked trajectory). We obtain $\sigma_G = 200$ mm/s, $\mu = 1,280$ mm/s for both $E1$ and $E2$. Both environments present a larger corridor crossed by a smaller one on the left (Fig. 1). On the right we observe areas in which the flow of pedestrians gets narrower, due to

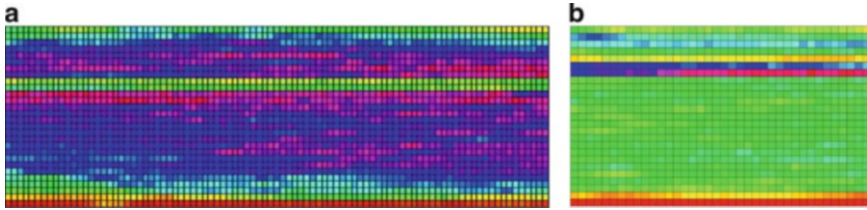


Fig. 3 ρ_k in the “ideal corridors” *E1a* (a, 22×7 m) and *E2a* (b, 10×6 m)

the presence of columns. In the central portion, the pedestrian density is almost invariant along the x axis, i.e. the environment corresponds to our definition of ideal corridor. We consider in our analysis only these portions (shown in Fig. 3 and denoted as *E1a* and *E2a*). By doing this we remove the portions in which the members of our staff, responsible for the largest part of the resting pedestrians peaks, were present. To further remove from our analysis standing pedestrians or pedestrians not behaving as commuters along the corridor, we filter our data keeping only velocities that satisfy

$$|v^x|/|v^y| > 3 \qquad |v| > 500 \text{ mm/s} \qquad (6)$$

(from now on, the observables in Eqs. (1–5) will be computed only for pedestrians satisfying Eq. (6)). Our corridors can be considered close to be ideal only if the amount of data removed by filtering (6) is negligible. Figure 2c shows the velocity distributions of pedestrians in *E1a*, before and after filtering; 8,497 pedestrians are tracked in *E1a*, corresponding to $\approx 6 \cdot 10^5$ events ($\approx 5.5 \cdot 10^5$ after filtering) while 4,586 pedestrians are tracked in *E1b* ($\approx 1.5 \cdot 10^5$, $\approx 1.35 \cdot 10^5$ after filtering). We also clipped the areas corresponding to the small corridors on the left of Fig. 1, and, after a proper rotation of the axes, filtered the data using Eq. (6) (environments *E1b* and *E2b*). These environments are far from being ideal corridors (in *E1b* $1.0 \cdot 10^5$ events over $2.3 \cdot 10^5$ remain after filtering, 12,452 pedestrians; $1.5 \cdot 10^5$ events over $2.5 \cdot 10^5$, 8,751 pedestrians in *E2b*). Even if the amount of filtered data is large, since the density of pedestrians is low and inter pedestrians interactions are scarce, we assume the behaviour of filtered pedestrians to be close to the ideal one. *E1b* measures 12×4 m and *E2b* 17×4 m.

4 Empirical Data

We integrate filtered data on the x direction to obtain 1D observables depending only on the distance from one of the walls, y . We notice the presence of an area, whose size is around 500 mm, in which ρ is much lower (see also Fig. 3), corresponding to the location of tactile paving for the visually impaired, omnipresent in Japan. Since walking on these areas is uncomfortable, their presence causes a fluctuation

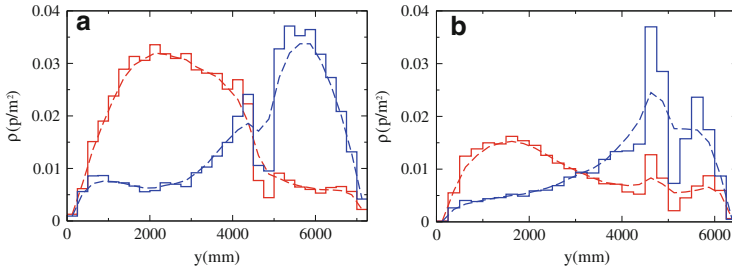


Fig. 4 Comparison between the original data (*continuous histogram*) and their smoothed versions (*dashed line*) for $\rho^+(y)$ (*blue*) and $\rho^-(y)$ (*red*). **(a)** *E1a*; **(b)** *E2a*. The axes are chosen in such a way that the Japanese traffic condition corresponds to have the P^- flow on the left

in the density patterns. To simplify our analysis we will consider data smoothed with a filter of length higher than 500 mm, which removes almost completely their effect. Figure 4 shows a comparison between the ρ^\pm distributions in *E1a* and *E2a* and their smoothed versions. The empirical data show clearly the presence of two distinct flows, since ρ^- presents a single peak located on the left, while ρ^+ presents a single peak located on the right. Density drops to zero close to the walls, and decreases quickly far from the maximum, until reaching an almost constant value. The \mathcal{V}^\pm and V_x^\pm distributions (not shown) are convex functions assuming a maximum in the centre of the corridor and minima close to the walls, with differences between the maximum and the minima around 10 %. The maximum is close to the centre of the corridor, i.e. on the right of the ρ maximum, suggesting a tendency to overcome on the right.

The analysed environments do not show enough variation in time to justify a time dependent analysis, and thus we will just perform a time-integrated analysis in order to use the maximum amount of data available. The stability in time of the observed patterns suggests that they represent some sort of equilibrium state that does not change significantly during the day and it is stable to the small density fluctuations observed in the environment.

5 Model

The empirical data present in every environment the separation between the two flows, together with a clear dependence of the density and velocity patterns on the distance from the walls. The observed environments do not present a wide variation nor in width (7.25 m in *E1a*, 6.5 m in *E2a*, 4 m in *E1b* and *E2b*), average density (0.033 ped/m² in *E1a*, ≈ 0.02 elsewhere) or relative density between the flows (≈ 1 everywhere), nevertheless the similar shape and stability suggest some “universality” in the empirical distributions. We are going to develop a model to describe these distributions, a model that is intrinsically empirical, since it is not derived by first principles about the pedestrian behaviour, but only as a function

that tries to describe the observed distributions. Nevertheless, since these patterns arise from the behaviour of individual pedestrians, in describing the (macroscopic) empirical distributions, we will try to create a connection with the individual behaviour. We will assume that the pedestrian feels more or less (un)comfortable according to the position and velocity he has (this comfort depending also on the expectation of finding pedestrians walking in the opposite direction), and that this (dis)comfort can be expressed through an ‘‘Hamiltonian’’ function. The term Hamiltonian is used here because we make the hypothesis that, as in statistical mechanics, the microscopic behaviour and macroscopic observables are connected through a Boltzmann factor, i.e. the probability of observing pedestrians with given velocity and position is determined by a negative exponential of the Hamiltonian.

5.1 Density Model

Denoting with $0 < y < L$ the distance of the pedestrian from one of the walls, we introduce an energy (or a (dis)comfort) function

$$U(y) = \frac{a}{y} + \frac{a}{L - y} + \left(\frac{\delta}{bL}\right)^2 \quad \delta = \begin{cases} y - cL & \text{if } |y - cL| < dL \\ dL & \text{if } |y - cL| \geq dL \end{cases} \quad (7)$$

$U(y)$ assumes a minimum (maximum comfort) in cL , while it increases (in a bounded way) with the distance from cL and diverges on the walls. Assuming that the probability distribution of pedestrians is given by a Boltzmann factor

$$p(y) \propto e^{-U(y)} \quad (8)$$

we expect results in good agreement with the ρ distribution in our data, since Eqs.(7–8) describe a function that behaves as a Gaussian close to its maximum, drops to zero on the walls and reaches a constant value far enough from the walls and the maximum. Parameter c accounts for the maximum position, a regulates the distance to walls, b the width of the flow, while d is introduced to explain the finite probability of walking on the ‘‘wrong’’ side of the corridor.

Using environment and flow specific parameters, the best fits of Eqs.(7–8) describe very well the empirical data (Fig. 5). To check the universality of the proposed law, it is more interesting to see to which extent the same parameters can describe all environments and ρ^\pm distributions (overall eight density distributions). To avoid an over-fitting problem, we fixed $a = 300$ mm (which is very close to the value we found when we fitted the model to single curves, and is easily understandable as a tendency to maintain a distance from walls of the order of the human body size), and found the best fitted parameters to be $b = 0.40$, $c = 0.28$, $d = 1.1$. The best fit curves are shown in Fig. 6. Even if there is clearly a difference between the description of the larger ($E1a$ and $E2a$) and smaller ($E1b$ and $E2b$) environments, the model appears to be quite general.

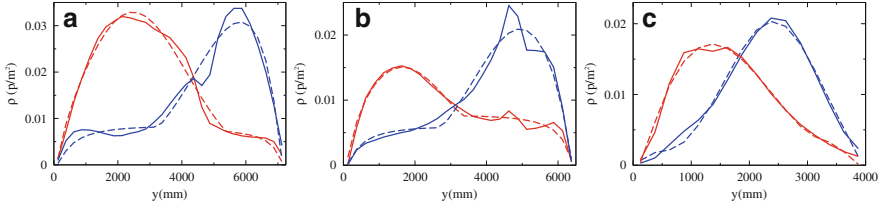


Fig. 5 Best fit of ρ^\pm in: (a) *E1a*; (b) *E2a*; (c) *E1b*

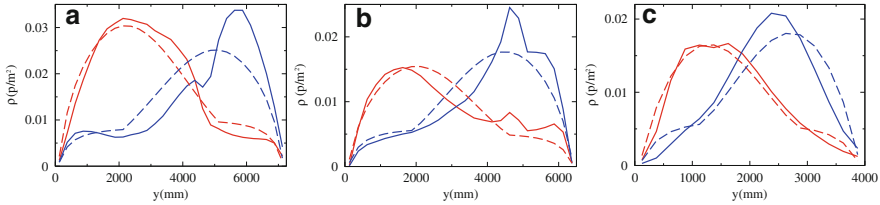


Fig. 6 Comparison between the ρ^\pm distributions and the best fits of Eq. (8) using $a = 300$ mm, $b = 0.40$, $c = 0.28$, $d = 1.1$. (a) *E1a*; (b) *E2a*; (c) *E1b*

5.2 Velocity Model

To generalise our (dis)comfort function to the velocity space, we must obtain velocity distributions as those shown in Fig. 2 for different points of the corridor (i.e., values of y). The original discretisation using $\Delta = 250$ mm was too refined to have a significant statistics, so we divide each corridor in 5 lanes of width $L/5$ and obtain the velocity distribution for each lane (we use 5 lanes on the basis of the information obtained in the previous section, since the maximum of the density for each flow should be located in the centre of the second lane from left if $c \approx 0.3$). As reported in literature [2] and in Fig. 2, the pedestrian velocity can be described with good approximation by a Gaussian function. According to this, we may extend the “Hamiltonian” for our pedestrian system introducing a quadratic term in the velocity, which takes in account the fact that our pedestrians have a preferred velocity directed along the corridor. We can assume the maximum of the Gaussian as given by a parameter v_0 depending on y , and extend Eq. (7) as

$$H(y, \mathbf{v}) = U(y) + T(y, \mathbf{v}) \quad T(y, \mathbf{v}) = \frac{(v^x - v_0(y))^2}{2\sigma_x^2} + \frac{(v^y)^2}{2\sigma_y^2} \quad (9)$$

v_0 is the pedestrians’ preferred velocity, directed along the corridor (the macroscopic velocity distribution in y will be given by the negative exponential of T , as for Eq. (8)). In Eq. (9) we have considered the possibility that the spread in velocity along and orthogonal to the corridor may be different. We calibrate Gaussian distributions to each v^x and v^y distribution in all lanes to obtain the v_0 , σ_x and

Table 1 Parameters calibrated using a best fit method. v_0 and σ in mm/s

<i>E1a</i>							<i>E2a</i>						
	v_0^+	σ_x^+	σ_y^+	v_0^-	σ_x^-	σ_y^-		v_0^+	σ_x^+	σ_y^+	v_0^-	σ_x^-	σ_y^-
1	1,233	275	171	1,237	255	156	1	1,172	252	160	1,264	250	157
2	1,259	255	186	1,267	252	158	2	1,229	257	177	1,275	254	164
3	1,283	265	171	1,288	250	160	3	1,271	254	174	1,262	250	174
4	1,264	259	159	1,291	263	167	4	1,250	249	164	1,266	225	170
5	1,226	259	158	1,218	280	163	5	1,218	238	163	1,245	274	155
<i>E1b</i>							<i>E2b</i>						
	v_0^+	σ_x^+	σ_y^+	v_0^-	σ_x^-	σ_y^-		v_0^+	σ_x^+	σ_y^+	v_0^-	σ_x^-	σ_y^-
1	1,201	350	223	1,212	313	170	1	1,203	313	207	1,228	269	197
2	1,262	314	224	1,267	299	194	2	1,253	272	229	1,265	255	211
3	1,301	286	181	1,277	283	182	3	1,260	260	215	1,264	265	208
4	1,281	280	183	1,243	308	204	4	1,260	256	208	1,267	263	223
5	1,217	286	202	1,206	318	226	5	1,239	266	207	1,202	290	223

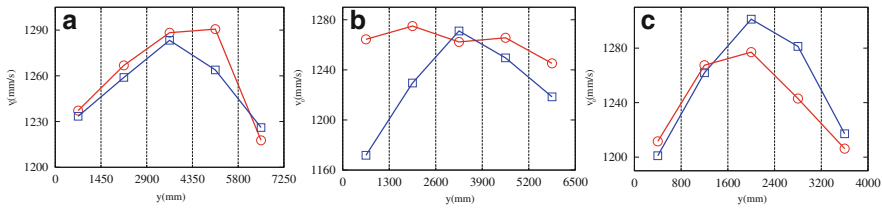


Fig. 7 $v_0(y)$ for P^+ (blue) and P^- (red). (a) *E1a*; (b) *E2a*; (c) *E1b*

σ_y parameters of Eq. (9), whose values are shown in Table 1 and Fig. 7. With the exception of P^- in *E2a*, all data show a tendency to have maximum velocity on the right of the ρ maximum cL . We notice that $\sigma_x > \sigma_y$, due to the fact that while σ_y includes only deviations from the preferred velocity (since for all pedestrians $v_0^y = 0$) σ_x includes also individual variation in v_0^x , which can be estimated to have a standard deviation around 200 mm/s (Fig. 2b). Assuming the individual variation to be ≈ 150 mm/s as for v_0^y , the overall deviation for v_0^x should be ≈ 250 mm/s (in agreement with the data).

6 Simulations

Microscopic collision avoiding behaviour is known to give rise to pedestrian organisation in lanes [1, 3]. Even if a realistic collision avoiding behaviour could hardly generate an organised pattern in the small environments and at the low densities observed in this work, these environments are part of a pedestrian area that may be large enough to generate such patterns even at low densities. In this section we use numerical simulations to investigate this possibility.

6.1 Collision Avoiding Models

In simulations we use a corridor with periodic boundary conditions and study the equilibrium distributions as density and velocity patterns that appear to be stable on the time scale relevant for pedestrian studies (10^3 – 10^4 s). In our paper [5] we investigated the extension and calibration of the Social Force Model (SFM) to describe low pedestrian densities, and verified that the Elliptical specifications using relative velocities [6] are those that better describe low densities, provided that a large enough parameter τ is used. In the original work this parameter was presented as the time length of a stride (≈ 0.5 s) but our calibration suggested a value close to 2 s to describe low densities. We hypothesised that τ actually represents the average time to the next collision, and proposed a new specification, called Collision Prediction, that explicitly computes such time (more precisely, the time to the maximum approach between pedestrians). This specification outperformed the Elliptical specifications at low density, and does not need tuning τ to be used at different densities. In this section we use the Elliptical Specification 2 (ES) and Collision Prediction (CP) models as described in [5]. We introduced a modification to CP as a maximum and minimum value for the time to the next collision (t_i in [5]), i.e. $\Delta t \leq t_i \leq t_{max}$, where Δt is the integration time of the method (0.2 s in this paper), while t_{max} is a new parameter. The introduction of these constraints is not relevant to the current work, but it is useful to extend CP to higher densities and to more realistic simulations. Since in CP the force of the pedestrian is modulated by the term v_i/t_i , i.e. it is strong enough to stop in t_i , $t_i \geq \Delta t$ is an obvious request for numerical stability (it disappears in the continuous limit). The t_{max} constraint is useful to describe pedestrians walking in the same direction at similar speeds and it is important to describe, for example, the fundamental diagram using our method.

The interaction with the walls is realised in ES through a velocity independent repulsion force (as in the original Circular Specification of the SFM, [6]), while in CP the collision time to the walls is explicitly computed in the same way as it is for pedestrians (in both methods the values of the parameters for the interaction with walls are possibly different from the pedestrian interaction ones). Furthermore we introduce in both methods a maximum distance of interaction, r_I , to reduce possible interaction effects between pedestrians in different lanes, which seem unrealistic and could represent a difficulty in obtaining the empirical distributions. We notice that in the CP specification this limit can be introduced in an elegant way as acting on the predicted distance at the time of collision, i.e. it is realised as a “cognitive process” more than a limit in perception.

6.2 Cultural Bias

Being symmetrical, the models in [5] cannot describe the cultural bias that leads Japanese people to walk on the left side of the corridor. By simplifying the model

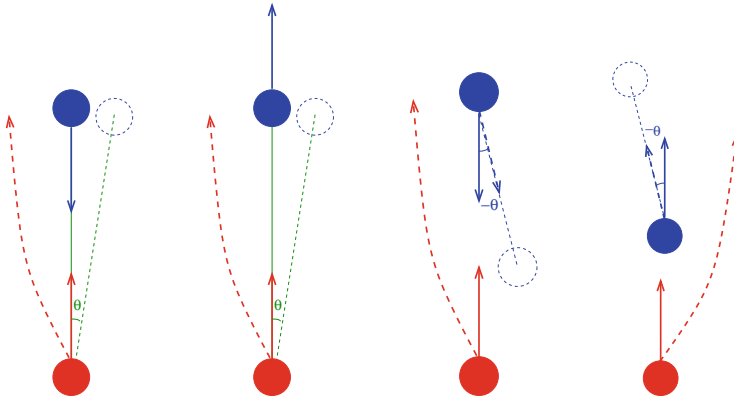


Fig. 8 Tilting the perceived position with respect to the real one leads to a bias towards left in both avoiding and overcoming, while tilting the perceived velocity leads to avoiding on the left while overcoming on the right

proposed in [3], we can introduce such a bias tilting the perceived relative position of other pedestrians. While this bias could describe well the observed lane formation, we don't expect it to describe the observed velocity distribution, since, as shown in Fig. 8, it leads not only to avoiding on the left, but also to overcome on the left. We thus propose also a different mechanism, based on rotating not the relative position but the other pedestrian's velocity, which should lead to avoiding on the left while overcoming on the right, see Fig. 8. This rotation corresponds to the expectation that the "opponent" applies the same cultural bias avoiding on the left or moving to the left if walking slower. We refer to the position tilt bias as TP, while to the velocity one as TV, and notice that the left-side bias of Japanese walkers is obtained by rotating position of a clockwise angle θ_t in TP, while it is obtained using a counter clockwise angle, $-\theta_t$, in TV. For overcoming to work properly in TV as used in this paper the pedestrian on the front should interact weakly ($\lambda \approx 1$, [6]), while a possible improvement in TV could be to multiply the tilt perceived by pedestrian i by $(\mathbf{d}_{ji} \cdot \mathbf{v}_i) / (|\mathbf{d}_{ji}| |\mathbf{v}_i|)$ to obtain a more realistic behaviour in any setting.

6.3 Noise

We calibrated models in [5] assuming them to be deterministic, i.e. virtual pedestrians always behave in the same way given the same stimulus. Obviously this is not true for real pedestrians, who have limited precision perception capabilities and arbitrary response. A good deterministic pedestrian model should provide the average behaviour, while the complex mechanism that leads to the richness of human response can be (statistically) approximated adding the right amount of noise to the model output. To estimate the amount of noise necessary to reproduce

the variety of human behaviour, we first ran simulations using the parameter values of [5], assuming the preferred velocity distribution to be centred in 1.28 m/s with deviation 0.2 m/s (see Fig. 2b). The resulting standard deviations in velocity distributions were $\sigma_x \approx 0.2$ and $\sigma_y \approx 0.03$, much lower than the observed ones (Table 1). To obtain values similar to the empirical ones, we added in all simulations to both components of the models' velocity output a Gaussian white noise with standard deviation 0.12 m/s.

6.4 Calibration

Our calibration process consists in simulating environments $E1a$, $E2a$ and $E1b$ at the observed densities and to find the parameters that better describe the observed distributions (we omit $E2b$ due to its similarity with $E1b$). In calibration we allow the collision avoiding parameters to assume stronger values than in [5], since in that paper we didn't use noise, and freely calibrate the wall interaction parameters and other parameters not calibrated in the previous work. For simulations, we use three different binary conditions, resulting in eight possible settings: the model condition (ES or CP), the bias condition (TP or TV) and the interaction with wall condition (W0, no interaction with walls, and W1). We introduce this latter condition to differentiate between the distribution given just by collision avoiding between pedestrians and the effect of walls which is to some extent "environmental". To calibrate parameters we use a genetic algorithm, with 30 generations and 30 genomes. Each genome (possible solution) is tested on all 3 environments 100 times. Each repetition lasts 5,000 s, and the "equilibrium distribution" is defined as the average density distribution in the last 2,500 s, averaged over all repetitions. All repetitions use the same number of pedestrians, chosen in such a way that the overall density (sum of the two directions) in each environment is always equal to the experimental average density in each environment. Nevertheless, the number of pedestrians in each direction is chosen in a probabilistic way, such that the average density over repetitions in each direction approaches the observed one, but the number of pedestrian for each direction present at any given time may be different (which is a more realistic setting that using always a balanced distribution). We run the GA 8 times for each condition, and for each best solution (i.e. the best solution for each condition over the 8 runs) we perform a test on 1,000 repetitions to obtain better statistical significance. This test is performed also using repetitions of length 10,000 s, to check the stability of the simulated distribution. The fitness function was defined as follows. Let $\rho_i^\pm(j\Delta)^s$ be the simulated density distribution in environment i (1 stands for $E1a$, 2 for $E2a$ and 3 for $E1b$) and $\rho_i^\pm(j\Delta)^e$ the experimental one, $\langle \rho_i^\pm \rangle$ the average density and L_i the width of the three environments; the fitness, a mean square distance weighted in such a way that all environments, regardless of size and density, contribute the same, is

Table 2 \mathcal{F} and θ_t for different methods and conditions after calibration (average and standard deviation are over different GA repetitions)

ES	TV W0	TV W1	TP W0	TP W1
Average \mathcal{F}	0.4562 ± 0.0008	0.2305 ± 0.006	0.4654 ± 0.005	0.2495 ± 0.007
Best \mathcal{F}	0.4546	0.2210	0.4572	0.2377
Average θ_t	-0.290 ± 0.016	-0.281 ± 0.022	0.139 ± 0.030	0.112 ± 0.047
CP	TV W0	TV W1	TP W0	TP W1
Average \mathcal{F}	0.4251 ± 0.002	0.2304 ± 0.021	0.4428 ± 0.011	0.2630 ± 0.020
Best \mathcal{F}	0.4218	0.2073	0.4278	0.2335
Average θ_t	-0.221 ± 0.099	-0.137 ± 0.106	0.038 ± 0.022	0.042 ± 0.030

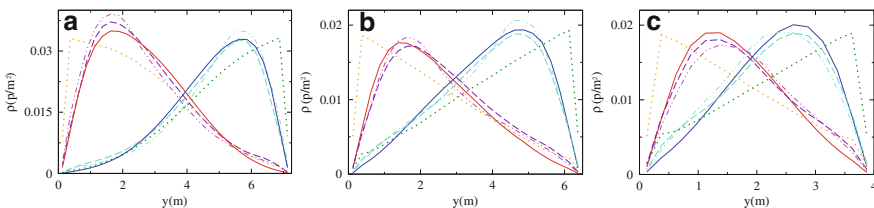


Fig. 9 Comparison between the simulated distributions using different methods and conditions. *Continuous*: CP, TV, W1. *Dotted*: CP, TV, W0. *Dashed*: CP, TP, W1. *Dash-dotted*: ES, TV, W1. **(a)** E1a; **(b)** E2a; **(c)** E1b

$$\mathcal{F} = \sqrt{\left(\sum_{i=1,3;k=\pm} \left(\sum_j \left(\frac{\rho_i^k(j\Delta)^s - \rho_i^k(j\Delta)^e}{\langle \rho_i^k \rangle} \right)^2 \right) / \frac{L_i}{\Delta} \right) / 6} \quad (10)$$

This fitness function, taking in account only the density distributions, was used also to calibrate the model (8), for which we obtained as a best solution 0.248. Once the parameters that best fit the density distribution are found, the velocity distribution generated by these parameters is tested.

6.5 Results

Table 2 shows the values of \mathcal{F} and θ_t under different conditions, while Figs. 9 and 10 compare some of the best solutions between themselves and with observed and theoretical curves. Solutions resulted to be very stable under the increase of simulation time from 5,000 to 10,000s, i.e. they describe an “equilibrium distribution” at the time scales of interest. Table 2 shows that under condition W1 the simulations achieve a quantitative performance similar to that of the theoretical model, even outperforming it under the TV condition. From a qualitative point of view, the simulated distributions have problems in describing both large spreads

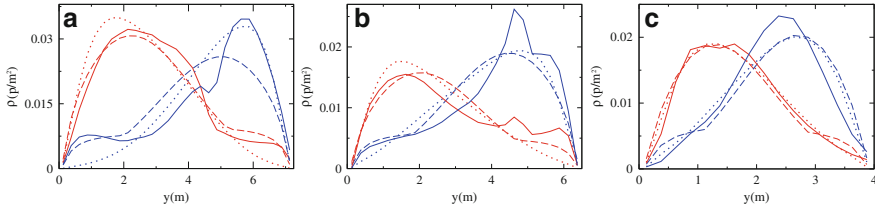


Fig. 10 Comparison between the empirical distributions (*continuous*), the simulated ones (*dotted*) and the theoretical ones (*dashed*). For simulated densities, we show the overall best simulation (CP,TV,W1). (a) $E1a$; (b) $E2a$; (c) $E1b$. P^+ in blue, P^- in red

around peaks and relatively high density corresponding to the location of the other flow's peak. The difference between W0 and W1 (Table 2 and Fig. 10) conditions shows the importance of the interaction with walls in obtaining a distribution with a significant spread around a peak at a significant distance from the wall. This means that this pattern can be obtained only by introducing some kind of environmental effect, since only collision avoiding leads, at these low densities, to the formation of lanes very close to the walls. There is also a weaker but clear tendency of TV to outperform TP, which is once again (Fig. 10) given by a better ability of describing the position and spread of the peak. This effect is probably due to the tendency of faster pedestrians to walk closer to the middle of the corridor in TV.

Both in ES and CP the best solutions had low values of r_I , probably to reduce the interaction between the two lanes. While in ES r_I represents a limit for the pedestrians' perception, and thus it cannot be set to values smaller than a few meters (we used 4 m as a limit in our calibrations), in CP it can be set to values close to the size of the human body (or of their social space) to discriminate between behaviours leading to actual collisions or just approaching behaviours that cannot cause collisions [7]. The other parameters did not seem to be relevant for the problem under study.

6.6 Velocity

The velocity distributions for best solutions under all conditions present values of σ_x between 0.25 and 0.3 m/s and of σ_y between 0.15 and 0.23 m/s, in good agreement with the values in Table 1. Figure 11 shows the average value of v^x in different "lanes" (defined as and compared to the results of Fig. 7) in P^- under W1. In $E1b$ there is almost no qualitative difference between the TV and TP conditions, while there is a clear difference between CP and ES, since the latter describes a flat distribution over the corridor. Our hypothesis is that at this low density overcoming occurs very seldom and the mechanism described in Fig. 8 does not produce macroscopic effects, while the difference between CP and ES is due to the fact that the former uses a velocity dependent interaction with the walls, and

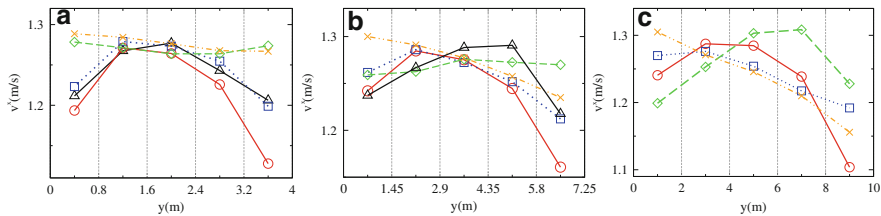


Fig. 11 Average values of v^x for P^- under W1, compared to the results of Fig. 7 (black, triangles). Red, circles and continuous: CP, TV. Blue, squares and dotted: CP, TP. Green, diamonds and dashed: ES, TV. Orange, crosses and dot-dashed: ES, TP. (a) E1a; (b) E2a; (c) E3 (virtual environment, no experimental data)

thus the quickest pedestrians have a tendency to stay farther from the walls. In E1a, due to the higher density ($\langle \rho \rangle \approx 0.021$ in E1b, $\langle \rho \rangle \approx 0.033$ in E1a) and larger size (i.e. more overcoming and less influence from walls) the difference between TV and TP is more clear. To further test this hypothesis we simulate also virtual environment E3 ($\langle \rho \rangle \approx 0.09$, $L = 10$) in which the macroscopic effect of the different bias conditions is evident. We expect the differences between the experimental data and the TV condition to be solved with the proposed enhancement $\theta'_i = \theta_i (\mathbf{d}_{ji} \cdot \mathbf{v}_i) / (|\mathbf{d}_{ji}| |\mathbf{v}_i|)$.

7 Discussion and Conclusions

Simulations based on collision avoiding reproduce quite well the observed density distributions, even if the “environmental” role played by interaction with walls is important in the attainment of such a task. Also the tendency of faster pedestrians to walk in the middle of the corridor can be obtained using a proper velocity dependent interaction with the walls. The values of the bias θ_i was much higher than the one reported in [3]. This could be due to the fact that they observed an artificial environment in which such a bias is not necessary, and also could be related to the fact that this bias is particularly strong in Japanese culture. Nevertheless such a strong value could be unrealistic, suggesting that the observed patterns cannot be obtained by using pure collision avoiding. We leave for future work the comparison between the microscopic behaviour of real and simulated pedestrians to clarify this point.

If pedestrians have, as we suggested, a tendency to overcome on the right, this can be simulated by using TV, while TP could lead to unrealistic behaviours, in particular at high densities where overcoming happens more often.

Based on these results, we believe that a pure collision avoiding behaviour using the TV bias (with values of θ_i lower than those reported in this paper) could describe properly the behaviour of pedestrians in (relatively) high density corridors, while at low density their distribution is given by a non emergent behaviour that can be

expressed using Eq. (7). The fact that a strong bias leads to distributions similar to those described by Eq. (8) suggests according to us that the pedestrians use at low density a behaviour similar to the one that they “have learnt” at higher ones (see also Figs. 7 and 11, walking with high velocity on the right is probably necessary only at high densities, but pedestrians have this tendency also at low ones). To clarify these points we want to collect data at different densities and compare microscopic and macroscopic behaviours to better understand the consistency of the θ_i values. We expect the microscopic bias values to be compatible with the observed macroscopic patterns only at densities considerably higher than those observed in this work.

The model (8) may be used as a boundary condition for the simulation of more complex environments, assuming for example that if pedestrians are entering the environment from some kind of corridor, the given distribution can be considered as the spatial distribution of entering pedestrians, supposing no further knowledge is available. From a microscopic point of view, this function could be seen as “the external potential” acting on the pedestrian (influence of the environment) and thus the force perceived by the pedestrians from the environment could be modelled as the negative gradient of U .

We also plan to observe the effect of group behaviour on simulations.

Acknowledgements This work was supported by JST, CREST.

References

1. T. Kretz, A. Grünebohm, M. Kaufman, F. Mazur, and M. Schreckenberg, *Experimental study of pedestrian counterflow in a corridor*, Jour. Stat. Mech. Theory and Experiment P10001 (2006).
2. D. Helbing, I. J. Farkás, P. Molnár, and T. Vicsek (2002) *Simulation of pedestrian crowds in normal and evacuation situations*, pg. 21–58 in *Pedestrian and Evacuation Dynamics* (2002).
3. M. Moussaïd, D. Helbing, S. Garnier, A. Johansson, M. Combe and G. Theraulaz, *Experimental study of the behavioural mechanisms underlying self-organization in human crowds*, Proc. Roy. Soc. B: Biological Sciences, **276**, 1668, 2755–2762 (2009)
4. D.F. Glas, T. Miyashita, H. Ishiguro, N. Hagita, *Laser-Based Tracking of Human Position and Orientation Using Parametric Shape Modeling*, Advanced Robotics, **23** (4), 405–428 (2009)
5. F. Zanlungo, T. Ikeda and T. Kanda, *Social Force Model with explicit collision prediction*, Europhysics Letters, **93**, 68005 (2011).
6. D. Helbing, A. Johansson (2010) *Pedestrian, Crowd and Evacuation Dynamics*. Encyclopedia of Complexity and Systems Science 16, 6476–6495.
7. F. Zanlungo, *Microscopic dynamics of artificial life systems*, Ph.D Thesis in Physics, University of Bologna, 2007

Experimental Study of the Following Dynamics of Pedestrians

C. Appert-Rolland, A. Jelic, P. Degond, J. Fehrenbach, J. Hua, A. Cretual, R. Kulpa, A. Marin, A.-H. Olivier, S. Lemercier, and J. Pettre

Abstract We report some experimental study of the behavior of pedestrians when they follow each other. In the frame of the PEDIGREE project, trajectories of pedestrians walking along a one-dimensional path were tracked through a high-precision motion capture. Data analysis allowed to obtain the fundamental diagram at different scales. Two unexpected transitions in the way pedestrians follow each other have been evidenced. The interest of the experiment is to capture at the same time microscopic and macroscopic characteristics of the flow. Indeed, macroscopic structures such as stop-and-go waves can also be studied from the data. Eventually,

C. Appert-Rolland (✉) • A. Jelic

Laboratory of Theoretical Physics UMR 8627, CNRS, Bâtiment 210, ORSAY Cedex F-91405, France

Laboratory of Theoretical Physics, University Paris-Sud, Bâtiment 210, ORSAY Cedex F-91405, France

e-mail: Cecile.Appert-Rolland@th.u-psud.fr

P. Degond • J. Fehrenbach

Institut de Mathématiques de Toulouse, Université de Toulouse; UPS, INSA, UT1, UTM, Toulouse F-31062, France

Institut de Mathématiques de Toulouse UMR 5219, CNRS, Toulouse F-31062, France

J. Hua

Institut de Mathématiques de Toulouse, Université de Toulouse; UPS, INSA, UT1, UTM, Toulouse F-31062, France

Institut de Mathématiques de Toulouse UMR 5219, CNRS, Toulouse F-31062, France

Laboratory Jean Kuntzmann, Université de Grenoble, CNRS, BP 53, 38041 Grenoble Cedex, France

A. Cretual • R. Kulpa • A. Marin

M2S – MimeTIC – University Rennes 2, Rennes, France

A.-H. Olivier • S. Lemercier • J. Pettre

INRIA Rennes – Bretagne Atlantique, Campus de Beaulieu, Rennes F-35042, France

a data-based following model has been proposed. Its calibration/validation can be performed both at the microscopic or macroscopic level. It is possible to extend the model to quasi-one-dimensional flows for the modeling of pedestrian flows in corridors.

Keywords Pedestrian traffic • Following behavior • Microscopic model • Fundamental diagram • Modeling

1 Introduction

There has been a growing interest for pedestrian modeling in the past decades, raised by various motivations ranging from the production of virtual crowds for graphics animation to the design of buildings optimizing both evacuation times in case of emergency evacuation, and comfort and efficiency of the flow in the case of normal use. The understanding of the pedestrian dynamics involves different scales – individuals or crowds. There is a need to understand how pedestrians interact, and how self-organized structures emerge from individual interactions [1, 2].

Several families of models have been proposed to describe the interactions between pedestrians [3–6]. Compared to road traffic, one difficulty comes from the two-dimensional nature of the flow. Pedestrians can adapt both their velocity amplitude and direction to navigate around [7]. Though there is still a need for experimental evidence, some models use a decoupling between amplitude and direction adaptation [6, 8].

It is possible to realize this decoupling experimentally by considering some special configurations. In this paper, we focus on experimental one-dimensional pedestrian flows, where the only adjustable variable for the pedestrians is the speed amplitude. The use of periodic boundary conditions allows to avoid boundary effects. Previous experiments of this kind were already performed on an oval trajectory [9, 10] and partial reconstruction of the trajectories was obtained from video tracking.

Here we present new experiments that were realized along two circular paths. The full trajectories were obtained from a high precision motion capture system, as explained in Sect. 2. The data analysis (Sect. 3) gave in particular several informations about the fundamental diagram [11], stepping behavior [12], and the structure of stop and go waves. It allowed to point out some transitions in the way pedestrians follow each other [11] for various density ranges. In Sect. 4, we describe how, based on the data analysis, some following model has been proposed [13, 14], and calibrated against the data both at the microscopic [15] and macroscopic scale.

Fig. 1 The experiment room. Two cylindrical walls limit the walking area, surrounded by infra red cameras



Fig. 2 Each pedestrian is equipped with four markers: two on the right shoulder, one on the right, and one on top of head



2 The Experiment

The aim of the experiment was to observe pedestrians when they follow each other, in order to extract the dynamical characteristics of their following behavior. Several realizations of the experiment were performed, with different global densities.

To do so, pedestrians were asked to walk in a natural way along a one-dimensional circular path, without passing each other. They were not allowed to speak with one another. Two circular paths of radii 2.4 and 4.1 m were used. Actually, pedestrians were asked to walk along two cylindrical walls, shown in Fig. 1 (inside for the outer wall and outside for the inner wall). Varying the path length and the number of pedestrians (from 8 up to 28) allowed us to vary the global density from 0.31 to 1.86 ped/m. Experiments durations were typically 1 min (and possibly more for higher densities).

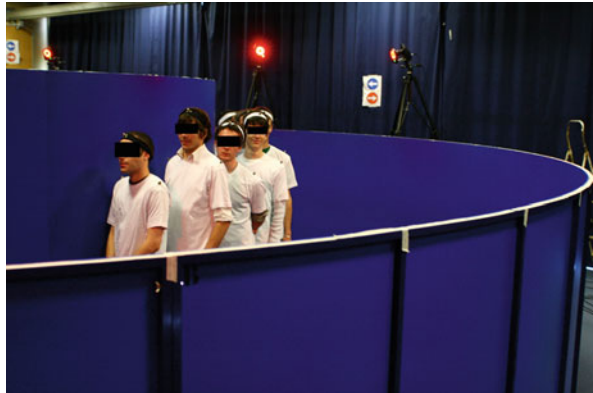
Several replicas (up to 8) were realized for the same set of parameters, if possible with different sets of participants. Before the start of the experiment, pedestrians were placed either at equal distances around the circle, or packed all together (Figs. 4 and 5). The memory of the initial condition was lost after a short transient.

The pedestrians – all volunteers – were equipped with four markers (Fig. 2). The three-dimensional motion of each marker was tracked by 12 infra-red cameras (Fig. 3) which are part of a VICON MX-40 motion capture system (see Fig. 1 for a global picture of the installation). The reconstruction software VICON IQ allows to

Fig. 3 One of the 12 infra-red cameras of the VICON system that allow to track the markers throughout the experiment



Fig. 4 Packed initial condition for the experiment along the inner circular path



convert the raw data into explicit three-dimensional coordinates for each marker, at a frequency of 120 frames/s. A second reconstruction stage had to be performed, to identify markers properly and extract the mean position of each pedestrian [16]. Except for the study of the stepping behavior, steps were filtered out.

In the experiment, some markers may be occluded for some time window, due to the presence of walls and of other pedestrians. In our analysis, we have been careful in taking into account the possible impact of the missing markers, in order to keep only reliable results.

3 Data Analysis

3.1 *Fundamental Diagrams*

The fundamental diagram is usually the first characteristics measured in any setting. It is often used as a basis for modeling, as it exhibits transition from free flow to jamming. It is often used to compare various experiments, though it was shown that it depends quite significantly on the precise geometry of the set-up [17, 18].

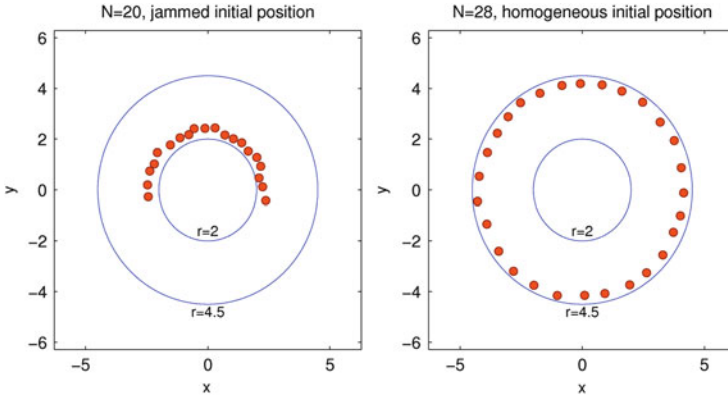


Fig. 5 Top view reconstructed through MATLAB post-treatment. Each *red circle* indicates the central position of a pedestrian. Two types of initial conditions are shown. (*left*) Packed initial condition along the inner circular path. (*right*) Homogeneous initial condition along the outer circular path

This is why we have compared our experiments only with previous one-dimensional ones [9].

As we have the full trajectories of the pedestrians, we could define densities and average velocities at different scales. In Fig. 6, we plot three types of fundamental diagrams. First, global values are obtained by an average over the whole system and the whole duration of the experiment (densities may slightly vary among realizations with the same number of pedestrians, as the experimentally measured averaged path radius was used to obtain the global density). The velocity dispersion is higher at low densities, as pedestrians are less constrained and can walk at their desired velocity – which varies from one individual to the next one.

Then we plot also local measurements, obtained by following exactly the same procedure as in [9]. We find the same tendency to reduce the velocity dispersion at higher densities. Due to the spontaneous formation of spatial inhomogeneities, the local densities could cover a larger range than the global ones. The comparison with Seyfried’s data gives a good agreement, though the velocity in our data is always slightly above. Global and local fundamental diagrams are quite similar for densities less than 1.2 ped/m. For higher densities, inhomogeneities are present due to the appearance of stop-and-go waves, and the way averages are performed starts to have an influence.

Eventually, as we have the whole trajectories of all pedestrians, we defined also some instantaneous individual density for each pedestrian, as the inverse of the distance with its leader. In [11], we have carefully discussed the data, and in particular we have excluded less reliable data due to marker occlusions. As a result, we have kept instantaneous data for densities up to 3.1 ped/m. We have not found any significant difference for the data obtained on the two circular paths.

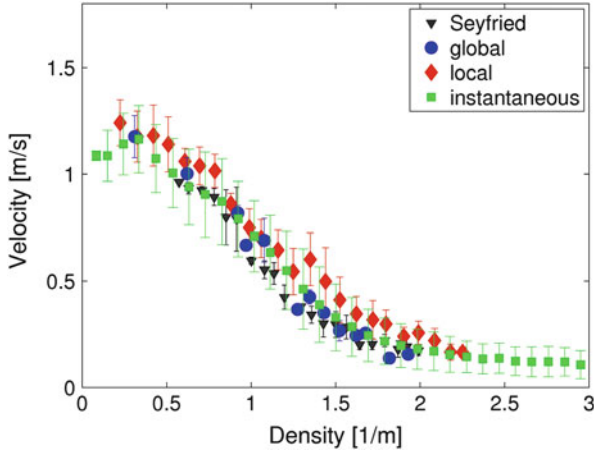


Fig. 6 Fundamental diagrams. A binning procedure was applied to the data in order to make the comparison between different measurements more easy. Bars give the standard deviation. *Blue circles, red diamonds and green squares* refer respectively to global, local and instantaneous averages. *Black triangles* indicate Seyfried et al. data [9, 19] for comparison (From [11])

3.2 Transitions in the Following Behavior

It had been noticed in [9] by Seyfried et al. that the velocity of individuals was depending linearly of the spatial headway. As our experiments are covering a larger range of densities, we found [11] that actually the velocity-headway relation was linear by parts, separated by sharp transitions. These transitions occur respectively for headways around 1.1 and 3 m and separate three regimes:

- Free flow regime: for a spatial headway larger than 3 m, pedestrians walk with their preferred velocity;
- Weakly constrained regime: for a spatial headway between 1.1 and 3 m, the velocity depends only weakly on the spatial headway.
- Strongly constrained regime: for a spatial headway less than 1.1 m, the velocity depends strongly on the spatial headway.

In each phase, the velocity-spatial headway relation is linear, but the slope differs from one phase to the other.

In the figure presented in [11], however, it was not possible to distinguish which data were obtained on the inner and outer circle, and one could have suspected that the change of curvature could be responsible for these transitions. Here we show that this is not the case. Actually, as one can see in Fig. 7, the transitions are seen on the outer circle, as the densities on the inner circle do not extend towards low enough values. On the outer circle, there are data on both sides of the transitions. Besides, the agreement is very good with independent data obtained by Seyfried et al., with a transition that seems to occur at the same place (around a headway

Fig. 7 Velocity as a function of the spatial headway. *Red circles* (respectively *yellow triangles* and *green diamonds*) were obtained along the inner (resp. outer) circular path. A binning on the velocity was used for both circular paths (*circles* and *diamonds*), but for the outer circle a binning on the headway was also used (*triangles*) so as to make the second transition, around 3 m, visible

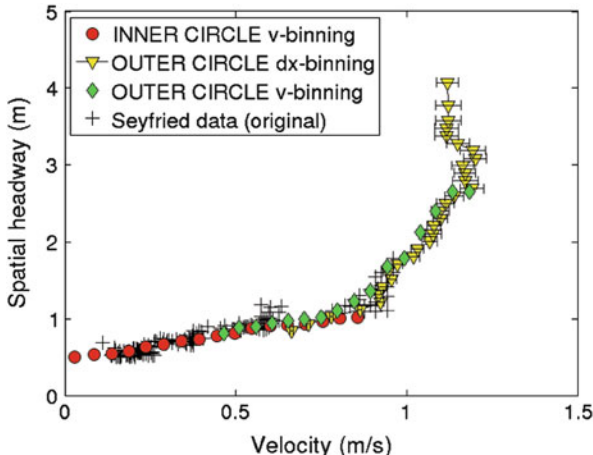
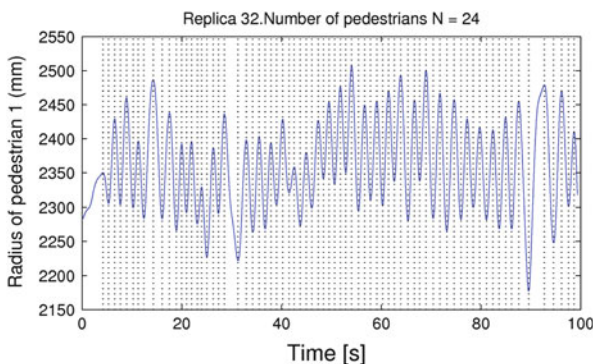


Fig. 8 Oscillations of the radial coordinate due to the steps, for one given pedestrian

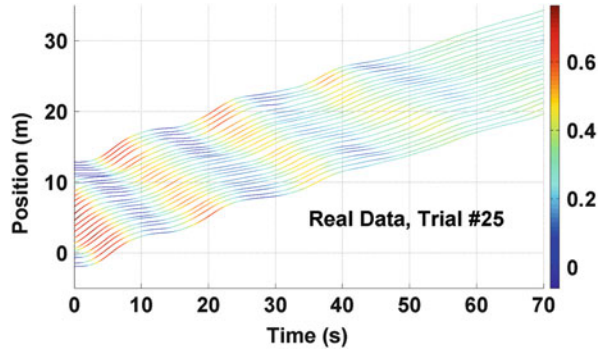


of 1.1 m). Of course it would be interesting to confirm that it also occurs in other set-ups under other experimental conditions.

3.3 Stepping Behavior

If data are not filtered, the oscillations due to the stepping behavior are clearly visible, especially on the radial coordinate (see Fig. 8 for an example). Some laws can be found that relate the step length and amplitude to the velocity of the pedestrian. We find that pedestrians mostly keep their pace, while modifying very strongly the step length [12]. This seems to indicate that the range of paces that are comfortable is not so large, and pedestrians are reluctant to modify it.

Fig. 9 Spatio-temporal plot representing the individual trajectories of all pedestrians, for an experiment realized with a global density 1.59 ped/m (From [13])



3.4 Stop-and-Go Waves

Stop and go waves can be clearly seen in spatio-temporal plots, as seen in Fig. 9. A systematic study of their properties will be published later. However, we see already in the figure that a criterium based on the velocity of the pedestrians allows to extract quite efficiently the compressed domain inside the wave. We can extract not only the propagation velocity of the waves, but also the damping of the signal inside the wave, the width of the wave, the characteristics of the pedestrians inside the wave, etc

4 A Data-Based Following Model

As road traffic is essentially one-dimensional, some car-following models have been proposed to describe how drivers react to the behavior of their predecessor. This kind of approach seemed relevant for our experiment, though it was not clear a priori which form of the following model would be most relevant in the case of pedestrians.

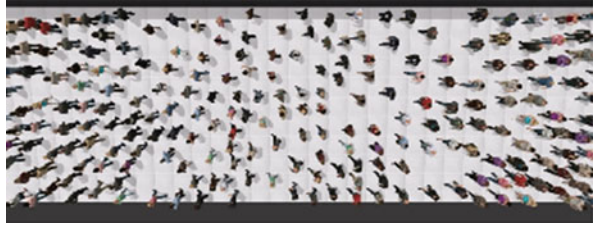
Inspired by the model proposed in [20], we tried to measure systematically in our data the correlation between various terms, e.g. the acceleration, velocity, velocity divided by the spatial headway, etc. We chose to relate the terms that had the highest correlation coefficient, over the largest range of densities – and especially in the range where stop-and-go waves are produced.

As a result, we have proposed as a ped-following model:

$$a(t) = C \frac{\Delta v(t + \tau)}{[\Delta x(t)]^\gamma} \quad (1)$$

We found that an important feature to include was the time delay inside the velocity difference term. Indeed, it seems that pedestrians need a longer time to

Fig. 10 Snapshot of the multi-lane model for a pedestrian flow inside a corridor (From [13])



evaluate a velocity difference than a distance – a finding that indeed meets common sense.

A first evaluation of the coefficients, performed over the whole range of density values, yields for the parameters of the model $\tau = 0.658 \pm 0.45$ s, $\gamma = 0.5$, $C = 0.809 \pm 0.355 m^{1/2} s^{-1}$.

More refined estimates will be yield in [15]. A perspective would be to use the knowledge of the transitions found in Sect. 3.2 to take different sets of parameters for the various regimes.

It is possible to compare models and experiments either at the microscopic level, or at a macroscopic level, based on the characteristics of stop and go waves [13].

4.1 *Extension to a Bi-dimensional Corridor Flow*

The following model defined above can be directly applied only for one-dimensional flows. For a pedestrian flow in a corridor, in order to capture the possible structuration of the flow in the transverse direction, a multi-lane model has been defined [13]. The ped-following model of Eq. 1 has been complemented by some lane changing rules, and pedestrians may step aside when they meet an obstacle.

Some simulations of the model (see supplementary material in [13] and Fig. 10) show that this simple model allows recovering important properties:

- Spatial inhomogeneities of the flow are naturally recovered
- Stop-and-go-waves emerge spontaneously.

5 Discussion and Conclusion

We have presented some experiments exploring the following behavior of pedestrians in lines. Data analysis has revealed some unexpected transitions occurring for spatial headways around 1.1 and 3 m. This finding could open new perspectives in terms of modeling.

Based on the data, a following model has been proposed to account for the following behavior of pedestrians. One advantage of our setting is that the

comparison of the model and data can be performed both at the microscopic and macroscopic level. However, we have found that the calibration done at the microscopic and macroscopic levels [13] give somewhat different parameter values. It would of course be more satisfying to have a single calibration for all scales. This may be obtained by incorporating the finding of [11] that there are actually some switches between several following behaviors. Indeed, a more detailed observation of the microscopic calibration results as in [15] seems to confirm also that different parameters for the following behavior should be used below a certain density threshold. We plan to explore this modeling direction in the future.

Having one-dimensional experimental data allows to test the following behavior of bi-dimensional models [21]. On the other hand, there is still a need to evaluate how much of the following behavior found here is retained in more general situations. One would expect to have some similar following behavior in narrow corridors [22], or in larger corridors when opposite flows organize themselves spontaneously into one-directional lanes [23, 24]. It is encouraging that a quasi one-dimensional simulation based on our following model seems to give quite realistic features [13]. Further investigations of the following behaviors to two-dimensional spaces would however be needed.

The data obtained from this experiment will be made available for the scientific community on a web platform in a near future.

Acknowledgement This work has been supported by the French' Agence Nationale pour la Recherche (ANR)' in the frame of the contract PEDIGREE (contract number ANR-08-SYSC-015-01). The project involves four research teams in Rennes (INRIA), Toulouse (IMT, CRCA), and Orsay (LPT). Experiments were organized and realized by the PEDIGREE partnership [25] at University Rennes 1, with the help of the laboratory M2S from Rennes 2.

A.J. acknowledges support from the RTRA Triangle de la physique (Project 2011-033T).

References

1. A. Schadschneider. Modelling of transport and traffic problems. In H. Umeo, S. Morishita, K. Nishinari, T. Komatsuzaki, and S. Bandini, editors, *Cellular automata, Proceedings. Book Series: Lecture Notes in Computer Science*, volume 5191, pages 22–31, 2008.
2. D. Helbing. Traffic and related self-driven many-particle systems. *Reviews of Modern Physics*, 73:1067–1141, 2001.
3. D. Helbing and P. Molnár. Social force model for pedestrian dynamics. *Phys. Rev. E*, 51:4282–4286, 1995.
4. C. Burstedde, K. Klauck, A. Schadschneider, and J. Zittartz. Simulation of pedestrian dynamics using a 2-dimensional cellular automaton. *Physica A*, 295:507–525, 2001.
5. J. Pettré, J. Ondřej, A.-H. Olivier, A. Cretual, and S. Donikian. Experiment-based modeling, simulation and validation of interactions between virtual walkers. In *SCA '09: Proceedings of the 2009 ACM SIGGRAPH/Eurographics Symposium on Computer Animation*, pages 189–198. The Eurographics Association, 2009.
6. J. Ondřej, J. Pettré, A.-H. Olivier, and S. Donikian. A synthetic-vision based steering approach for crowd simulation. *ACM Trans. Graphics*, 29(123), 2010.

7. S. Paris, J. Pettré, and S. Donikian. Pedestrian reactive navigation for crowd simulation: a predictive approach. *Computer Graphics Forum - Eurographics*, 26(3):665–674, 2007.
8. M. Moussaïd, D. Helbing, and G. Theraulaz. How simple rules determine pedestrian behavior and crowd disasters. *Proc. Nat. Acad. Sci U.S.A.*, 108:6884–6888, 2011.
9. A. Seyfried, B. Steffen, W. Klingsch, and M. Boltes. The fundamental diagram of pedestrian movement revisited. *J. Stat. Mech.*, page P10002, 2005.
10. U. Chattaraj, A. Seyfried, and P. Chakroborty. Comparison of pedestrian fundamental diagram across cultures. *Advances in Complex Systems*, 12:393–405, 2009.
11. A. Jelić, C. Appert-Rolland, S. Lemerrier, and J. Pettré. Properties of pedestrians walking in line – fundamental diagrams. *Phys. Rev. E*, 85:036111, 2012.
12. A. Jelić et al. Properties of pedestrians walking in line – stepping behavior. *preprint*, 2012.
13. S. Lemerrier, A. Jelic, R. Kulpa, J. Hua, J. Fehrenbach, P. Degond, C. Appert-Rolland, S. Donikian, and J. Pettré. Realistic following behaviors for crowd simulation. *To appear in Comput. Graphics Forum-Eurographics*, 2012.
14. S. Lemerrier, A. Jelic, J. Hua, J. Fehrenbach, P. Degond, C. Appert-Rolland, S. Donikian, and J. Pettré. Un modèle de suivi réaliste pour la simulation de foules. *Revue Électronique Francophone d'Informatique Graphique*, 5:67–76, 2011.
15. J. Hua, J. Fehrenbach, S. Lemerrier, A. Jelic, C. Appert-Rolland, S. Donikian, J. Pettré, and P. Degond. Identification of a model of pedestrian following behavior. *preprint*, 2012.
16. S. Lemerrier, M. Moreau, M. Moussaïd, G. Theraulaz, S. Donikian, and J. Pettré. Reconstructing motion capture data for human crowd study. *Lecture Notes in Computer Science*, 7060:365–376, 2011.
17. J. Zhang, W. Klingsch, A. Schadschneider, and A. Seyfried. Transitions in pedestrian fundamental diagrams of straight corridors and t-junctions. *J. Stat. Mech.*, page P06004, 2011.
18. W. Daamen and S.P. Hoogendoorn. Experimental research of pedestrian walking behavior. *Transportation Research Record*, 1828:20–30, 2003.
19. A. Seyfried, B. Steffen, W. Klingsch, T. Lippert, and M. Boltes. Steps toward the fundamental diagram - empirical results and modelling. In N. Waldau, P. Gattermann, H. Knoflacher, and M. Schreckenberg, editors, *Pedestrian and Evacuation Dynamics 2005*. Berlin, Springer, 2007.
20. A. Aw, A. Klar, T. Materne, and M. Rascle. Derivation of continuum traffic flow models from microscopic Follow-the-Leader models. *SIAM Journal on Applied Mathematics*, 63:259–278, 2002.
21. A. Seyfried, B. Steffen, and T. Lippert. Basics of modelling the pedestrian flow. *Physica A*, 368:232–238, 2006.
22. M. Chraïbi, A. Seyfried, and A. Schadschneider. Generalized centrifugal-force model for pedestrian dynamics. *Phys. Rev. E*, 82:046111, 2010.
23. M. Moussaïd, E. Guillot, M. Moreau, J. Fehrenbach, O. Chabiron, S. Lemerrier, J. Pettré, C. Appert-Rolland, P. Degond, and G. Theraulaz. Traffic instabilities in self-organized pedestrian crowds. *PLoS Computational Biology*, 8:1002442, 2012.
24. J. Zhang, W. Klingsch, A. Schadschneider, and A. Seyfried. Ordering in bidirectional pedestrian flows and its influence on the fundamental diagram. *J. Stat. Mech.*, page P02002, 2012.
25. More information can be found at <http://www.pedigree-project.info>.

FDS+Evac Model Validation for Seated Row Arrangements: Aircraft and Cinema Theatre

K. Naveesh Reddy, A.K. Babbar, and Timo Korhonen

Abstract Fire Dynamics Simulator (FDS) is open source computational fluid dynamics software for modeling practical fire problems. FDS includes a capability for the simulation of human egress process with and without the effects of fire, under the name of FDS+Evac. The human movement algorithm of FDS+Evac has been validated with experimental evacuation data and other evacuation models. But it is not yet validated on how to model evacuation process for seated row arrangements like aircraft, auditorium etc. Here an attempt has been made to model evacuation of humans in seated row arrangements with the help of two known experimental data, i.e., evacuation studies of a blended wing body aircraft (BWB) and a cinema theatre. The fire drill evacuation tests were modeled using FDS+Evac and validated with the experimental data and other human egress models. An appropriate set of FDS+Evac input parameters that seem to be well suited for the BWB case is presented in this paper. For the cinema theatre case the default parameter sets of FDS+Evac were seem to be appropriate.

Keywords Fire dynamics simulator • Evacuation • Seated row • Blended wing body aircraft • Cinema theatre

K.N. Reddy (✉) • A.K. Babbar
Engineering Services Division, PM Dimensions Pvt. Ltd., Gandhinagar 382009, India
e-mail: naveesh.reddy@pmdimensions.com; vikrambabbar12@gmail.com

T. Korhonen
VTT Technical Research Centre of Finland, P.O. Box 1000, Espoo, VTT FI-02044, Finland
e-mail: timo.korhonen@vtt.fi

1 Introduction

Fire Dynamics Simulator (FDS, version-5.5.3) (<http://fire.nist.gov/fds>) is open source computational fluid dynamics software for modeling practical fire problems [1]. It is developed by the National Institute of Standards and Technology (NIST), USA (<http://www.nist.gov/>) in cooperation with the Fire and Evacuation Safety Team at VTT Technical Research Centre of Finland (<http://www.vtt.fi/>). FDS includes a capability for the simulation of human egress process with and without the effects of fire, under the name of FDS+Evac (<http://www.vtt.fi/proj/fdsevac/>) [2]. FDS is currently the most widely used fire simulation software in the world, and FDS+Evac has also found a wide user base within the evacuation safety engineers. FDS can be used in a wide range of different operation systems and computational infrastructures, ranging from simple laptop computers to high-performance clusters and super-computers.

The human movement algorithm of FDS+Evac model [3] has been validated with experimental evacuation data and other evacuation models. But it is not yet validated on how to model the evacuation process for seated row arrangements like aircraft, auditorium etc. It is important to know whether FDS+Evac is capable of modeling aircraft, auditorium and stadium evacuation etc. If yes, what are the parameters in FDS+Evac which control the human egress process and what should be there values. Recently, authors have performed validation studies for Blended Wing Body Aircraft [4] with the help of published experimental data.

In this paper, the fire drill evacuation for aircraft and cinema theatre are modeled using FDS+Evac and validated with the help of known experimental data. Appropriate sets of FDS+Evac input parameters that seem to be well suited for the seated row arrangement in the aircraft and the cinema cases are presented in this paper.

2 FDS+Evac

The starting point of the pedestrian movement in FDS+Evac is the method of Helbing et al. This method introduces so-called “social force”, which is used to keep reasonable distances between pedestrians and pedestrians, between pedestrians and walls. The original model of Helbing et al. [5–8] uses one circle to represent the elliptical cross sectional shape of the human body, but FDS+Evac uses a more realistic representation with three circles, where one large circle describes the torso and the two smaller ones the shoulders, along the lines given in the paper by Langston et al. [9]. The movement of the agents is found by solving a coupled differential equation system consisting of equation of motions for the translational and rotational degrees of freedom of each agent. FDS+Evac can be classified to be a continuous time and space type egress model. Because FDS+Evac models the human movement using a two-dimensional geometry that represents the humans about their shoulder level, or at the torso level, the seated row arrangements might

not be modeled well, e.g., the seat cushions and backs cannot be modeled separately. The humans can have up to 0.58 m shoulder widths by default in FDS+Evac and the agents representing the evacuating humans are not turning their body angle to fit the narrow space at the seated rows. Thus, seated rows should be modeled at least about 0.7 m wide aisles. The agents in FDS+Evac also consider the obstacles in the two-dimensional geometries are like walls, i.e., full height from floor to ceiling. This might not be a too good approximation for the airplane nor cinema theatre aisles, where the seat backs are not reaching the shoulder level. So the effective width of the aisles might be a little bit wider in these geometries than in normal buildings.

3 Blended Wing Body Aircraft

A Blended Wing Body (BWB) aircraft (<http://www.twitt.org/bldwing.htm>) is the most promising future aircraft to transport passengers and cargo in a large volume. It is also very economical in operation, because of its efficient design with high lift to drag capability. It consumes 20 % less fuel than compare to conventional aircraft. A blended wing body aircraft model, configuration FW1-1-1, shown in Fig. 1 is a single-deck aircraft which can accommodate as much as 1,020 passengers, with 25 cabin crews and 20 floor level Type-A exits for evacuation. The exits present on the right hand side of the aircraft from front to rear are denoted as R1–R10 and on the left hand side as L1–L10 respectively.

Considering full-scale evacuation trails of BWB involving 1,000 people is expensive, so Galea et al. [10] decided to undertake full scale trails using a portion of BWB cabin as shown in yellow box of the Fig. 1. A total of 375 passengers evacuated with access to exits L6–L10 on the rear side of the aircraft. Some 88 participants were seated in the mockup and 146 participants were brought into the mock-up section via two cross aisles feeding the mock-up section. The airEXODUS model was validated with the help of the above experiments.

3.1 FDS+Evac Model Predictions for BWB Evacuation

The fire drill evacuation test of BWB was modeled using FDS+Evac. The test case considered was a standard aviation evacuation certification where half of the usable exits are blocked and a standard opening time of 11.1 s for Type-A exits is used. Total 10 out of 20 exits were made available on the left side (L1–L10) of the aircraft for evacuation. Since the BWB cabin layout information with internal dimensions, aisles width, seat dimensions etc. are not available in the paper by Galea et al. [10], these dimensions were estimated as well as could drawn from the figures of that paper. The BWB internal cabin layout of 70×34 m with a grid size of 0.25×0.25 m is generated as shown in the Fig. 1 by only using the available information of the aircraft model. All passengers in this test are considered as adults only since no information is given on the proportion of male and female passengers present.

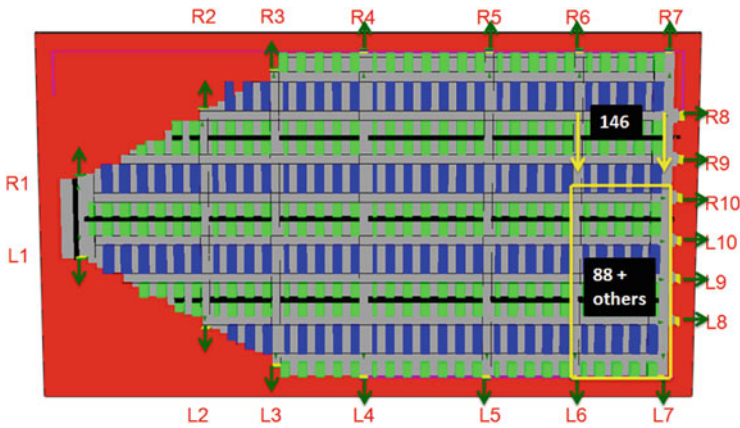


Fig. 1 Cabin layout for Blended Wing Body aircraft showing exits (green arrows) and evacuation experiment portion (yellow box)

Table 1 BWB evacuation time for different cabin layout geometries calculated by FDS+Evac model

FDS+Evac Test case	Evacuation time (s)	Remarks (door width = 1.0 m)		
		Space in front of doors	Vertical aisles width	Horizontal aisles width
BWB	123.9	1.0 m	1.0 m	1.0 m
BWBTC1	118.75	L8–L10 is 1.25 m	1.0 m	1.0 m
BWBTC2	120.65	L8–L10 is 1.50 m	1.0 m	1.0 m
BWBTC3	118.15	L4–L7 is 1.25 m, L8–L10 is 1.5 m	1.0 m	1.0 m
BWBTC4	115.45	1.5 m	1.0 m	1.0 m
BWBTC5	105.75	L4–L7 is 1.25 m, L8–L10 is 1.5 m	1.25 m	1.0 m
BWBTC6	100.5	1.5 m	1.5 m	1.0 m
BWBTC7	102.7	1.5 m	1.5 m	Two aisles as 1.25 m only
BWBTC8	101.0	1.5 m	1.5 m	Two aisles as 1.50 m only
BWBTC9	101.55	1.5 m	1.5 m	1.25 m
BWBTC10	100.25	1.5 m	1.5 m	1.5 m

Initially, the BWB layout considered in this work has the space in front of doors as 1.0 m, vertical aisles width as 1.0 m and horizontal aisles width as 1.0 m. A total of 11 BWB test cases (BWB, BWBTC1 to BWBTC10) are considered by varying the above dimensions from 1.0 to 1.25, and 1.5 m and evacuation time is calculated for all the cases. It was noticed that the variation of horizontal aisles width did not effected the evacuation time much as shown in Table 1. The final layout accepted is BWBTC6, i.e., space in front of doors as 1.5 m, vertical aisles width as 1.5 m and horizontal aisles width as 1.0 m.

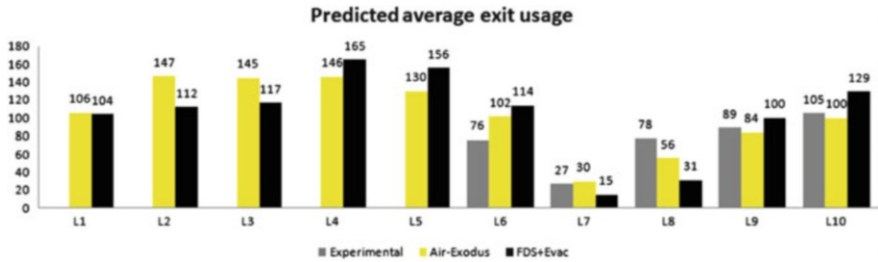


Fig. 2 Predicted average exit usage of 1,046 passengers in BWB using FDS+Evac for BWBTC6

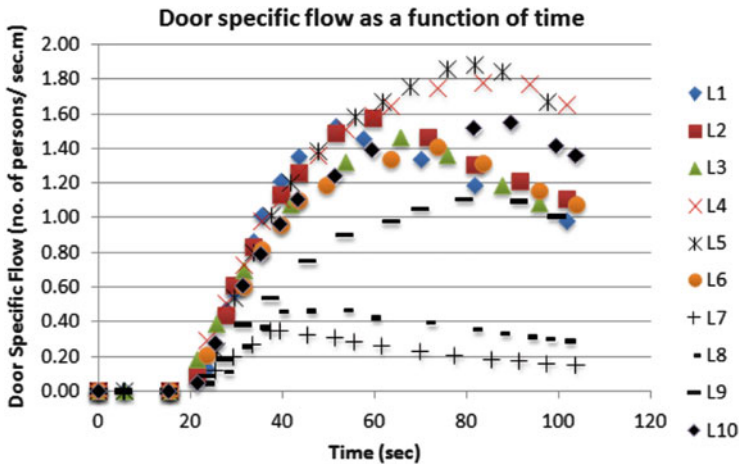


Fig. 3 Door specific flow as a function of time for BWBTC6 using FDS+Evac

FDS+Evac is a stochastic model and will get different results every time the model runs, hence the model calculations are repeated for 10 times and the average values are taken. The total evacuation time of 1,046 passengers in BWB (BWBTC6) is varying from 96.6 to 103.5 s with an average of 100.5 s. The predicted average exit usage of complete BWB model carrying 1,046 passengers using FDS+Evac is compared with airEXODUS model and it shows similar trends in exit usages as shown in Fig. 2.

Figure 3 shows the number of humans evacuating through different doors per unit time per unit width of door as a function of time. The door specific flow for exit L7, L8 and L9 are low when compare to other exits. The results for a single run are shown in this figure.

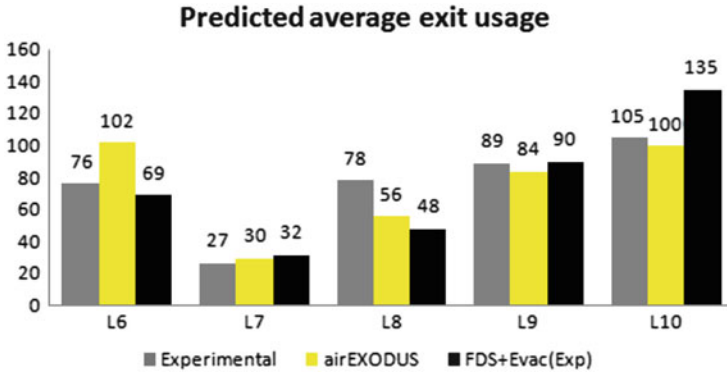


Fig. 4 Predicted average exit usage of 376 passengers as per experiment in BWB using FDS+Evac for BWBTC6

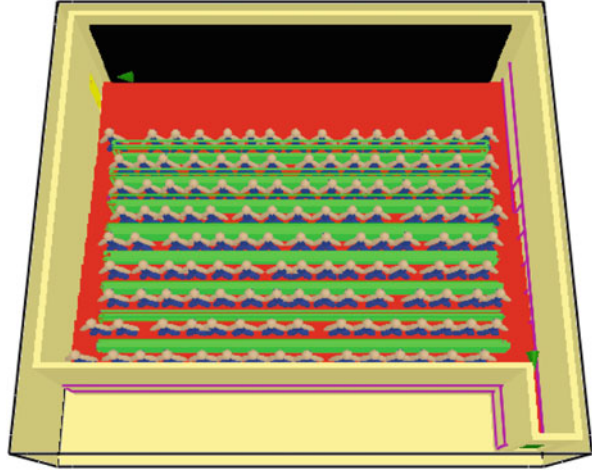
3.2 FDS+Evac Model Predictions as per Experiment for BWB Evacuation

BWTC6 layout is now modeled as per the experiment conducted by Galea et al. [10] and FDS+Evac model predictions are compared to the experiment and airEXODUS model. The trends of predicted average exit usage of 376 passengers look similar as shown in Fig. 4. The average exit usage of passengers when compared to the experimental data is more for the exit-L10 in FDS+Evac and for exit-L6 in airEXODUS model. Since the passengers are moving from the right wing to left wing they choose the nearest exit which is the exit L10. It was noticed that the passengers are unable to see above the seats in the present version of FDS (FDS-5.5.3), whereas in the forthcoming version of the model [11] this is possible due to the fact that the obstacles for visibility and movement could be independent of each other. The exit-L7, which is present at the corner, is the least used by the passengers and both models predicted nicely.

4 Cinema Theatre

The cinema theatre consists of 135 participants with two exits one at the front side and one at the back side. It consists of nine rows with fifteen seats each. The space for human movement is present on the each side of the seat rows as steps from front to back. A total of 18 evacuation experiments using various types of alarms were conducted in a cinema theatre to investigate the social influence during emergency evacuation. The purpose of these experiments was to test how different alarms effect the pre-movement time. The different alarms tested by Nilsson and Johansson [12] were alarm bell and pre-recorded human voice. Similarly two out of 18 experiments with known pre-movement times were validated using STEPS and

Fig. 5 Layout of cinema theatre showing humans and exits (*green arrows*)



SIMULEX models [13]. The two experimental cases (Case-A and Case-B) with recorded pre movement times [13] were considered in this paper for the purpose of validation studies.

4.1 FDS+Evac Model Predictions for Cinema Theatre

The layout information of the cinema theatre is known. It is 11.5×10 m with two 0.8 m wide exits and 1.0 m free space for human movement on either side of the seat rows. The space in between the seat rows is 0.5 m and the dimensions of the seats are also known. The cinema theatre model with a grid size of 0.1×0.1 m is developed from the above known information using FDS+Evac as shown in Fig. 5. In total of 135 participants are considered in this test out of which 53 % are males and remaining 47 % are females.

The default experimental pre movement times are used as the inputs to the FDS+Evac model (as per experiment) for case-A and case-B. The different values have been set for the social force term i.e. L_NON_SP parameter. The model calculations are repeated for seven times and the average values are taken. The average values of evacuation time and the number of humans present in rows 2–9 at the times 40, 50 and 60 s after activation of alarm is shown in Table 2. The number of persons evacuated as a function of time for different L_NON_SP parameters for cinema theatre (case-A) is shown in Fig. 6. The results for a single run are shown in this figure.

We have noticed that the FDS+Evac model is able to predict the total evacuation time nicely along with other models when the default FDS+Evac human movement parameters are used. The FDS+Evac model prediction on number of humans present in rows 2–9 at the times 40, 50 and 60 s after activation of alarm are close to experimental data as shown in Figs. 7 and 8 respectively.

Table 2 Average number for persons in rows 2–9 as a function of time, total evacuation time for case-A and case-B using FDS+Evac

Type	Average no. of persons in rows 2–9 as a function of time (sec)			Total evacuation time (sec)	Remarks (Tau = 0.8–1.2)
	40	50	60		
Case-A					
Experimental	70	42	27		
FDS+Evac	65	46	28	131.6	L_NON_SP = 0.3
	61	39	21	122.9	L_NON_SP = 0.4
	55	34	15	109.8	L_NON_SP = 0.5
Case-B					
Experimental	74	45	25		
FDS+Evac	70	48	32	138.8	L_NON_SP = 0.3
	67	44	27	125.9	L_NON_SP = 0.4
	61	35	18	114.8	L_NON_SP = 0.5

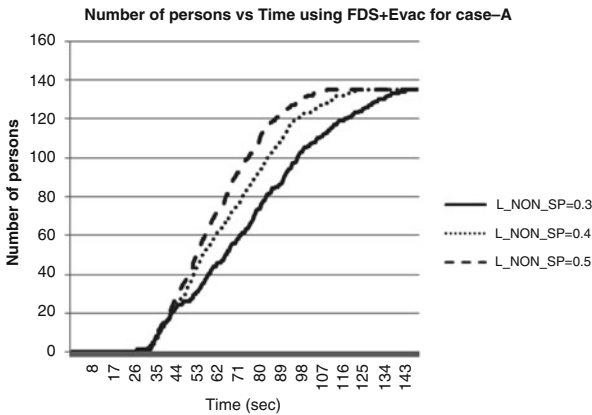


Fig. 6 Number of persons evacuating with time in a cinema theatre (case-A) using FDS+Evac

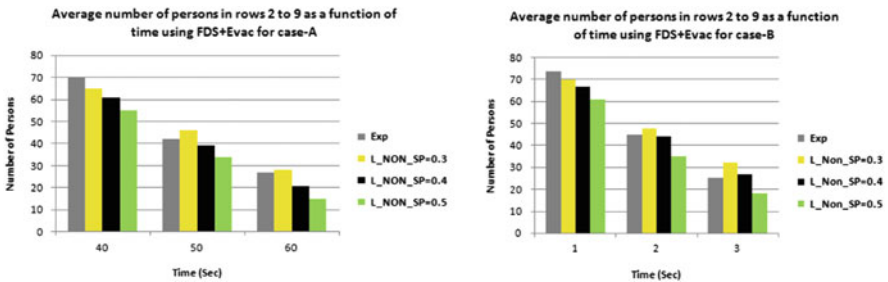


Fig. 7 Average number of persons in rows 2–9 as a function of time for case-A and case-B for different evacuation parameters using FDS+Evac

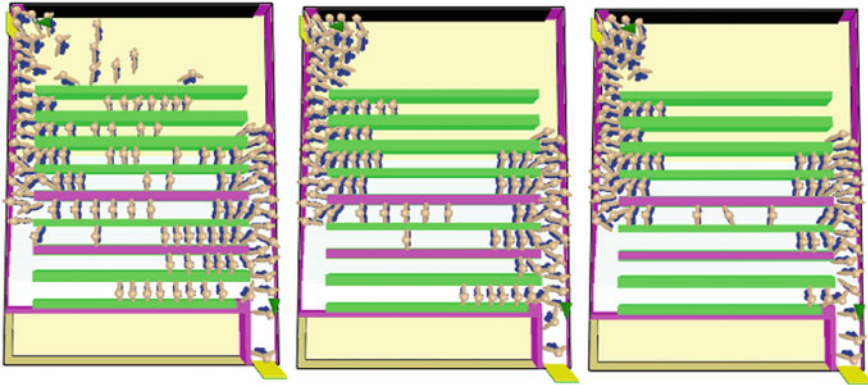


Fig. 8 Number of persons in rows 2–9 at 40, 50 and 60 s for case-A using FDS+Evac (for $L_NON_SP = 0.3$)

5 Discussions

The motive force, agent-agent, agent-wall interaction terms which controls the human egress process in FDS+Evac are given as PERS name list in FDS input file. The PERS name list parameters are shown in Table 3 can be used to model the similar kind of seated row arrangement of evacuation process in aircrafts and cinema theatre. The term L_NON_SP controls the social force in front and behind the passenger. $L_NON_SP = 0.5$ mean that the passengers feel more push from the other agents at their back than with $L_NON_SP = 0.3$ and the egress is faster. The term TAU is relaxation time parameter controls the strength of the motive force, lower the value of TAU higher the motive force of the passengers to evacuate. It was noticed that the average motive force ($TAU = 0.5$) of humans in aircraft evacuation is very much higher than compare to other emergency evacuation process ($TAU = 1.0$, FDS default value). The detection (DET) time was 5–15 s uniform distribution and same for the reaction (PRE) time. These are situation dependent parameters, not really FDS+Evac motion related parameters.

For cinema theatre case, the experimental pre movement time (as PRE_MEAN and $PRE_EVAC_DIST = 0$) for each participant is given as input in &EVAC line of the FDS input file. So this pre movement time in &EVAC line will overwrite the pre movement time, whatever may be the value, given in &PERS line and hence produce a realistic simulation similar to the experiment. The default FDS+Evac human movement parameters $L_NON_SP = 0.3$ and $TAU = 1.0$ ($TAU_LOW = 0.8$ and $TAU_HIGH = 1.2$) are able to produce close results when compared to experimental data and other egress model as shown in Fig. 9. The person name list parameters of FDS+Evac for cinema theatre evacuation given in Table 3 can be used to model similar kind of human egress process.

Table 3 PERS name list parameters in FDS+Evac for aircraft evacuation

PERS name list parameters in FDS+Evac	Aircraft	Cinema theatre
L_NON_SP	0.5	0.3
TAU_LOW	0.4	0.8
TAU_HIGH	0.6	1.2
PRE_LOW	5.0	22.5
PRE_HIGH	15.0	46.5
PRE_MEAN	N.A.	32.03
PRE_PARA	N.A.	4.19
DET_LOW	5.0	0.0
DET_HIGH	15.0	0.0

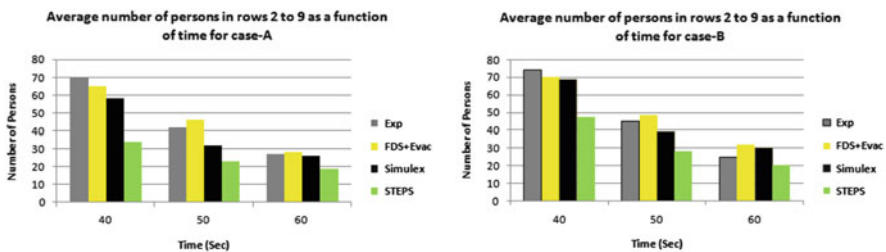


Fig. 9 Comparison of number of persons in rows 2–9 as a function of time using FDS+Evac (for L_NON_SP = 0.3) for case-A and case-B with experimental data and other egress models

6 Conclusions

The FDS+Evac model is validated for seated row arrangements by considering two experimental evacuation cases. FDS+Evac is able to predict well for both the cases. Though much information on the pre-movement times was not provided in the case of aircraft, it was noticed that the motive force for human evacuation in aircraft is faster when compared to the cinema theatre. The FDS+Evac parameters, which takes care of input like human speeds, pre-evacuation times and social influence forces etc. for the aircraft and the cinema theatre cases are presented in this paper. The default human movement parameters worked well for the cinema theatre cases whereas for the aircraft case parameter sets that produce faster and more eager egress should be used.

Acknowledgement The corresponding author thanks management of PM Dimensions and VTT for their support and encouragement to work in this area. The corresponding author would also like to thank Mr. Dinesh Nath, Ph.D., Indian Institute of Technology (IIT) Kanpur for his kind help and encouragement.

References

1. McGrattan, K., Klein, B., Hostikka, S., Floyd, J.: Fire Dynamics Simulator (Version 5) User's Guide. NIST Special Publication 1019-5, National Institute of Standards and Technology, Gaithersburg, Maryland (2008)
2. Korhonen, T., Hostikka, S.: Fire Dynamics Simulator with Evacuation: FDS+Evac - Technical Reference and User's Guide. VTT Working Papers 119, VTT Technical Research Centre of Finland (2009)
3. Korhonen, T., Hostikka, S., Paloposki, T., Rinne, T., Matikainen, K., Heliövaara, S.: Development and Validation of FDS+Evac for evacuation simulations. VTT Research Notes 2421, VTT Technical Research Centre of Finland (2008)
4. Reddy, Naveesh, K., Babbar, A.K., Korhonen, T.: FDS+Evac model validation for seated row arrangements: Blended wing body aircraft experimental evacuation. National Evacuation Conference 2012, New Orleans (2012)
5. Helbing, D., and Molnár, P.: Social Force Model for Pedestrian Dynamics. *Physical Review E*, Vol. 51, pp. 4282–4286 (1995)
6. Helbing, D., Farkas, I., and Vicsek, T.: Simulating Dynamical Features of Escape Panic. *Nature*, Vol. 407, pp. 487–490 (2000)
7. Helbing, D., Farkas, I., Molnár, P., and Vicsek, T.: Simulating of Pedestrian Crowds in Normal and Evacuation Situations. *Pedestrian and Evacuation Dynamics*, Springer, pp. 21–58 (2002)
8. Werner, T., Helbing, D.: The Social Force Pedestrian Model applied to Real Life Scenarios. *Pedestrian and Evacuation Dynamics – Proceedings of the Second International Conference*, University of Greenwich, London, pp. 17–26 (2003)
9. Langston, P.A., Masling, R., Asmar, B.N.: Crowd Dynamics Discrete Element Multi-Circle Model. *Safety Science*, Vol. 44, pp. 395–417 (2006)
10. Galea, E.R., Filippidis, L., Wang, Z., Lawrence, P.J., Ewer, J.: Evacuation analysis of 1000+ seat Blended Wing Body aircraft configurations: Computer Simulations and Full-Scale Evacuation Experiment. *Pedestrian and Evacuation Dynamics*, Springer, pp. 151–161 (2010)
11. Korhonen, T.: FDS+Evac Evacuation model: Recent developments. *Proceedings of the Fire and Evacuation Modeling Technical Conference 2011*, Baltimore, Maryland (2011)
12. Nilsson, D., Johansson, A.: Social influence during the initial phase of a fire evacuation - Analysis of evacuation experiments in a cinema theatre. *Fire Safety Journal* 44, pp. 71–79 (2009)
13. Frantzich, H., Nilsson, D., Eriksson, O.: Evaluation and validation of evacuation programs. Report 3143, Lund: Dept of Fire Safety Eng. and Systems Safety, Lund University (2008)

Fundamental Diagram of Stairs: Critical Review and Topographical Measurements

Sebastian Burghardt, Armin Seyfried, and Wolfram Klingsch

Abstract In this contribution an overview about the fundamental diagram for stairs is given. First we discuss discrepancies of fundamental diagrams of well-known planning handbooks for pedestrian facilities and evacuation routes like Predtechenskii and Milinskii (Planning for foot traffic flow in buildings. Amerind Publishing, New Delhi, 1978. Translation of: Proektirovanie Zhdanii s Uchetom Organizatsii Dvizheniya Lyuddskikh Potokov, Stroiizdat Publishers, Moscow, 1969), Nelson HE, Mowrer FW (Emergency movement. In: PJ DiNenno (ed) SFPE handbook of fire protection engineering, 3rd edn., Chap 14. National Fire Protection Association, Quincy, pp 367–380, 2002), Fruin Fruin (Pedestrian planning and design. Elevator World, New York, 1971), and Weidmann (Transporttechnik der Fussgänger. Institut für Verkehrsplanung, Transporttechnik, Strassen- und Eisenbahnbau, ETH Zürich, Tech. Rep. Schriftenreihe des IVT Nr. 90, 1993, zweite, ergänzte Auflage). To proof the correspondence to real measurements, we present published measurements available in literature.

S. Burghardt (✉)

Computer Simulation for Fire Safety and Pedestrian Traffic, Bergische Universitaet Wuppertal, Pauluskirchstr. 11, 42285 Wuppertal, Germany
e-mail: s.burghardt@uni-wuppertal.de

A. Seyfried

Computer Simulation for Fire Safety and Pedestrian Traffic, Bergische Universitaet Wuppertal, Pauluskirchstr. 11, 42285 Wuppertal, Germany

Juelich Supercomputing Centre, Forschungszentrum Juelich GmbH, 52425 Juelich, Germany
e-mail: seyfried@uni-wuppertal.de

W. Klingsch

Fire Safety Science, Bergische Universitaet Wuppertal, Pauluskirchstr. 11, 42285 Wuppertal, Germany
e-mail: klingsch@uni-wuppertal.de

In the second part we derive a fundamental diagram for stairs downwards based on precise trajectories. To check whether our experiments performed under laboratory conditions are comparable with characteristics of motion of every day situations, we present a comparison with a field study carried out at the same staircase. Furthermore the contribution shows a method to gain topographical information of density, velocity, and specific flow structures to get a microscopic insight into pedestrian dynamics on stairs. This information could be used to identify effective bottlenecks.

Keywords Pedestrian dynamics • Fundamental diagram • Topographical measurements

1 Introduction

One consequence of urbanization is the growing complexity of buildings (high-rise buildings, shopping centres, pedestrian areas). Today, tall skyscrapers and deep underground railway stations are common buildings in large cities, therefore stairs have to be considered as part of the egress routes.

The fundamental diagram is the basic relation to characterize transport properties of traffic systems. For stairs there is no consensus which are the most important factors influencing this relation. Some handbooks distinguish between up- and downwards motion [1, 3, 4] others focus on the slope of stair [2]. Of course, the flow density relation for different geometries is important, but the availability of microscopic analysis also offers the opportunity to take a deeper look at influences of measurement method and selected measurement area. Thus further analysis like spatial and temporal development of the basic quantities velocity, density and flow should be considered. Up to now, these influences are not scrutinized and the fundamental diagram for stairs, even the shape of the function, has not been completely understood.

One can assume, that stairs have lower flow values compared with horizontal routes, because often congestion appears in front of a stair. This is not analyzed in detail. It's not clear if the slightly decreased maximum flow on a stair is the most influencing factor or maybe the transition from horizontal way to stair. However, this delay must be considered in evacuation planning.

This paper begins with a discussion of discrepancies of fundamental diagrams published in well-known planning handbooks. In the second part of Sect. 2 we are facing the question, if these specifications are supported by experimental data. The setup of our experiments will be briefly described in Sect. 3. Macroscopic and microscopic analysis of experiments performed is presented in Sects. 4 and 5. Main results of this contribution are in Sect. 6.

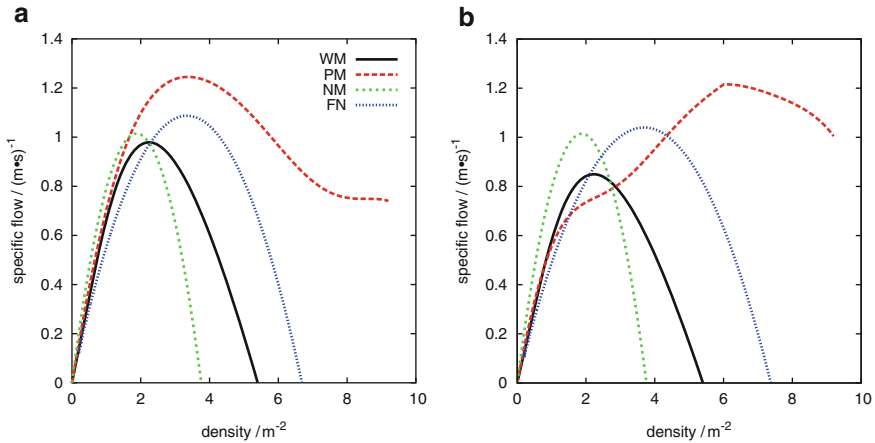


Fig. 1 Comparison of fundamental diagrams published in planning handbooks. (a) Downwards. (b) Upwards

2 Review of the Literature

2.1 Planning Handbooks

In four well-known planning handbooks for pedestrian facilities and evacuation routes like Predtechenskii and Milinskii (PM), Nelson and Mowrer (NM), Fruin (FN), and Weidmann (WM) different fundamental diagrams for stairs are presented. WM, PM, and FN distinguish between up- and downwards motion and do not consider the angle of stairs, NM focus on different angles and not on direction. In this comparison a stair of 32.47° for NM and an area of horizontal projection $f = 0.1 \text{ m}^2$ for PM is chosen.

Figure 1a shows the different specifications for the fundamental diagram downwards published in the handbooks. Up to 1.5 persons per square meter the functions are close to each other. Maximum specific flow ranges from 0.98 to 1.25 (m · s)⁻¹. NM/WM measured maximum specific flow at a density around 2 m⁻² whereas PM/FN see maximum specific flow at higher densities of 3.4 m⁻². At this density, the peak of the functions NM/WM is exceeded and the specific flow decreases. Maximum possible density ranges from 3.8 to 9.2 m⁻². In contrast to the other authors, PM do not assume a maximum density where the flow stops.

For upwards motion (see Fig. 1b) the uncertainty about maximum specific flow becomes larger and ranges from 0.85 to 1.22 (m · s)⁻¹. Compared with downwards motion, NM/WM measured maximum specific flow at the same density of about 2 m⁻² whereas PM/FN state values of 6.1 and 3.7 m⁻². The range of maximum density is equal to the movement downstairs. Basic quantities for both directions are

Table 1 Overview of basic parameters for stairs given in handbooks. Direction of movement is marked with subscript u for upstairs and d for downstairs

Handbook	$v_{0,hor}$ in $\frac{m}{s}$	ρ_{max} in m^{-2}	$\rho(J_{s,max})$ in m^{-2}	$J_{s,max}$ in $(m \cdot s)^{-1}$
PM	0.63_u	9.2_u	6.1_u	1.22_u
	0.70_d	9.2_d	3.4_d	1.25_d
WM	0.61_u	5.4_u	2.2_u	0.85_u
	0.69_d	5.4_d	2.2_d	0.98_d
NM	0.8_u	3.8_u	1.9_u	1.01_u
	0.8_d	3.8_d	1.9_d	1.01_d
FN	0.55_u	7.4_u	3.7_u	1.04_u
	0.63_d	6.7_d	3.4_d	1.09_d

summarized in Table 1. The discussion of published fundamental diagrams leads to three basic questions:

1. Are the presented maximum specific flow values realistic?
2. At which density appears maximum specific flow?
3. At which density does the flow break down?

The handbooks PM, WM and FN are common planning handbooks for pedestrian traffic. The chapter *Emergency Movement* of NM is part of the SFPE [5].

2.2 Experimental Data

In the previous chapter specifications for the fundamental diagram of stairs are discussed. All authors (except FN) do not present measurement points on which their given functions are derived. To evaluate whether these specifications are supported by data from experiments or field studies, we collect data available in the literature. In these contributions [6–20], information about the fundamental diagram for stairs are published, but we only refer to those presenting measurement points (see Fig. 2). Some authors describe the fundamental diagram as density dependence of velocity, therefore we used the flow equation to calculate specific flow; $J_s = v_{hor} \cdot \rho$ respectively. The horizontal component of velocity is used in all cases because it is independent of the slope of stair.

Beside focussing on transport properties of stairs, some work has been spent to optimize vertical evacuation strategies in large buildings. Safety aspects are taken into account and the combining of stairs with elevators are discussed. These topics are not considered in this contribution but should be mentioned. Therefore we refer to [21–26].

For downwards motion all measurement points show good accordance for low densities. Up to approx. $1.2 m^{-2}$ a linear increase of the specific flow is observable with slightly differences of the incline. The incline represents the free velocity $v_{0,down}$ and ranges from 0.6 to 0.85 m/s. Most measurement points present a fundamental diagram up to a maximum density of $3.5 m^{-2}$ with maximum specific

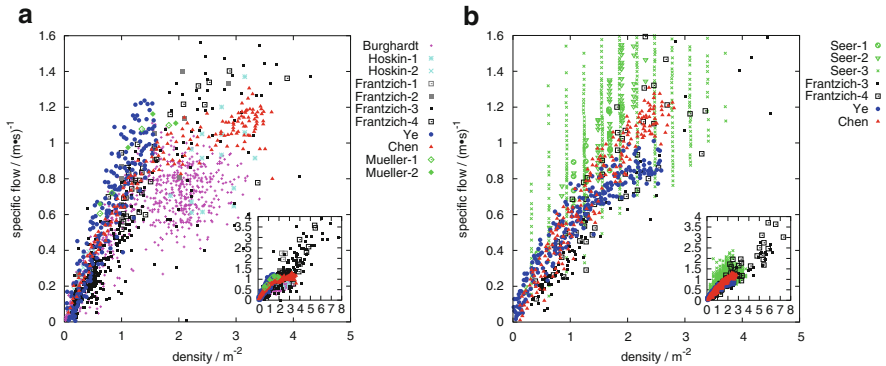


Fig. 2 Measurements of the fundamental diagram for stairs. The included small diagrams show the entire range of all measurement points. **(a)** Downwards. **(b)** Upwards

Table 2 Ranges of basic quantities obtained from experimental data

Quantity	Downwards	Upwards
v_0 in $\frac{m}{s}$	[0.6:0.9]	≈ 0.6
$J_{s,max}$ in $(m \cdot s)^{-1}$	[1.1:1.4]	[1.0:1.3]
$\rho(J_{s,max})$ in m^{-2}	[1.0:3.2]	[2.4:2.5]
ρ_{max} in m^{-2}	[1.7:3.5]	[2.6:2.8]

flow values of $1.2 (m \cdot s)^{-1}$. In two publications of Frantzich [8, 9] for $\rho > 2 m^{-2}$, maximum specific flow values are measured three times larger than results of other authors [6, 7, 12, 15, 20], also for maximum density a factor of 2 can be observed. Frantzich [9] states in his publication, that measured velocities higher than 1.5 m/s are probably errors. Over the large range of measurement points there is not an explicit decrease of flow due to overcrowding observable.

Regarding the measurement points for upwards motion it is obvious, that Seer et al. [17] used a different measurement method than the other authors [7, 9, 20]. There are only measurement points presented for a fixed grid with large fluctuations. Chen, Ye and Frantzich show a similar development of the fundamental diagram with slightly differences of the according specific flow values up to a density of approximately $2.7 m^{-2}$. A linear increase of specific flow is also observable for low densities (leaving the measurement points of Seer unconsidered due to large fluctuations). Free velocity $v_{0,up}$ measured is about 0.6 m/s. Maximum densities of $2.8 m^{-2}$ are measured and a decrease of flow due to overcrowding is not apparent.

The comparison of experimental data allows us to define ranges for the basic quantities (see Table 2 and Table 3).

Maximum specific flow values presented by the specifications of the handbooks are realistic and proven by experimental measurements. The density range where maximum specific flow appears is much larger for downwards- than for upwards motion. Densities higher than $3.5 m^{-2}$ are not observed and a decrease of flow due to overcrowding is not visible. For downwards motion it seems, that for densities higher than $1.8 m^{-2}$ the specific flow fades into a plateau.

Table 3 Information about measurements presented in Fig. 2

Author	Year	Experiment type	Direction/slope	Additional information	Flow equation used?
Burghardt [6]	2010	Field study	↘ / 32.7°	Footballstadium	No
Hoskin-1 [12]	2004	Field study	↘ / -	Incline not stated	Yes
Hoskin-2	2004	Field study	↘ / -	Incline not stated	Yes
Frantzych-1 [8]	1994	Exp./students	↘ / 32°		No
Frantzych-2	1994	Exp./students	↘ / 26°	Theatre	No
Frantzych-3 [9]	1996	Exp./students	↗↘ / 45°	Slope speed assumed	Yes
Frantzych-4	1996	Exp./students	↗↘ / 32°	$v > 1.5 \frac{\text{m}}{\text{s}}$ prob. error	Yes
Ye [20]	2008	Field study	↘ / 26.6° ↗ / 25.1°	Metro station Shanghai	No
Chen [7]	2010	Field study	↘ / 24.4° ↗ / 25.8°	Metro station Shanghai	No
Mueller-1 [15]	2010	Exp./students	↘ / 33°	Stands stadium	No
Mueller-2	2010	Exp./students	↘ / 27°	Stands stadium	No
Seer-1 [17]	2010	Exp./students	↗ / -	Subway station	No
Seer-2	2010	Exp./students	↗ / -	Subway station	No
Seer-3	2010	Field study	↗ / -	Stadium	No

3 Experiment Setup

In 2009, field studies after two football matches and experiments under laboratory conditions have been performed in the ESPRIT arena Düsseldorf. The geometry of the staircases used is exactly the same, thus a direct comparison of data is possible.

The experiments under laboratory conditions have been performed within the HERMES project [27]. In May 2009 about 350 subjects, mostly composed of students, took part. For further information we refer to [28].

Figure 3 shows the sketch of the experiment and a snapshot of the tracking tool PeTrack [29]. The staircase is roofed over, sheltered from the wind and has good lighting conditions. At the inner surface the handrail reduces the effective width w of the stair by 7 cm while at the outer face the handrail is set on top of the stair-rail and does not reduce the width of stair.

Overall seven runs (S1 to S7) have been performed (see Table 4). To guarantee some initial conditions, we used a holding area to ensure a fixed initial density. Pedestrian density on the stair was regulated by the width of the entrance b , i.e. the incoming flow, which was changed from 0.8 to 2.4 m. After passing the entrance, the participants had to walk along a 2.5 m long podium. This distance allows that the participants are able to choose their desired velocity and spread over the whole width. The geometry of the stair is characterized by the tread = 0.28 m and riser = 0.18 m which results in a slope of 32.7°.

The external staircase includes two different kinds of transitions: the transition from/to horizontal way to/from stair (numbered as 1–4) and the turning. Transition 1

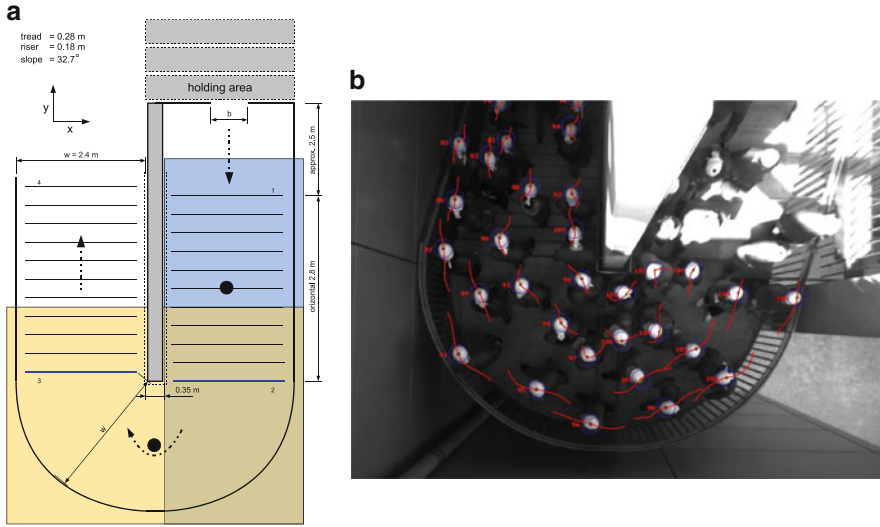


Fig. 3 (a) Shows a sketch of the experiment. The field of view of each camera is marked: camera 1 = blue, camera 2 = yellow and the overlapping area is visualized as green. (b) Tracked pedestrians of camera 2 using software PeTrack

Table 4 Parameters for the experiment stair downwards

Run	Width of entrance	N	Note
S1	b = 2.4 m	300	–
S2	b = 1.4 m	200	–
S3	b = 1.2 m	200	–
S4	b = 1.0 m	200	–
S5	b = 0.9 m	100	–
S6	b = 0.75 m	100	–
S7	b = 0.8 m	100	Free velocity

and 4 cannot be analyzed with the microscopic measurement method (see Sect. 5.1) due to insufficient trajectory data around the transitions in both y-directions. Thus, in our experiment, we can only analyze the transitions 2 and 3 (marked as blue lines) in combination with the turning.

The experiments were recorded by two cameras (16 frames per second) mounted at a fixture above the stair. To cover the complete region, one camera was positioned over the first part of the stair and the second over the landing (see the circles in Fig. 3a). The field of view of each camera is marked as colored areas. Pedestrian trajectories with high precision were extracted automatically from video recordings. All trajectories were corrected manually to ensure accurate raw data and combined automatically. Using these trajectories, pedestrian characteristics like flow, density and horizontal velocity are determined.

4 Macroscopic Measurements

4.1 Measurement Method

During the video recordings by holding a ruler in 1.8 m height (measured perpendicular to the surface) over the third step from the top and horizontal in 2 m downstairs in 1.8 m height a point was marked. Both markers combined with the effective width of the stair describe a horizontal measurement area of 4.88 m². By using a computer program two measurement lines through the markers and parallel to the edge of tread were applied. To calculate the density, entrance t_{in} and exit times t_{out} of all persons are used. The criterion for time recording was the congruence of shoulder axis with the measurement lines. With help of a computer program, density and flow were calculated by these times. For each person entering the measurement area a counter was incremented by 1 and for each person passing the exit line the counter was decremented by 1. The actual number of persons N divided by the measurement area A gives the classical density ($\rho = \frac{N}{A}$). Using this method it is possible to define a value for density for each frame of the video.

Flow J was calculated by the average of $\Delta t_i = t_{i+1} - t_i$ where t_i is the frame when a person crosses the measurement line. Timegaps were added over 125 frames (≈ 5 s) plus the following timegap of the next person:

$$J = \frac{1}{\overline{\Delta t_i}} \quad \text{with} \quad \overline{\Delta t_i} = \frac{1}{N} \sum_{i=0}^N \Delta t_i. \quad (1)$$

This method allows to observe the whole video without losing information. One negative consequence are large timegaps at the beginning and the end of the clearing period out of steady state. Combining specific flow J_s with mean density $\bar{\rho}$ for the time interval Δt gives the fundamental diagram $J_s(\bar{\rho})$ (see Fig. 4a).

It was only detected the time when one person enters and leaves, not a personal entrance and exit time. Hence, a direct calculation of individual velocity is not possible, only the mean value by using the formula $\bar{v} = \frac{J}{\rho b}$ where b is the width of the stair.

4.2 Comparison of the Fundamental Diagram obtained from Field Study and Experiment

Figure 4a shows a comparison of fundamental diagram derived from field study and experiment under laboratory conditions. The measurement points show good accordance over the whole range of density, with a trend to higher specific flow values for the experiments. During the experiments a maximum specific flow of

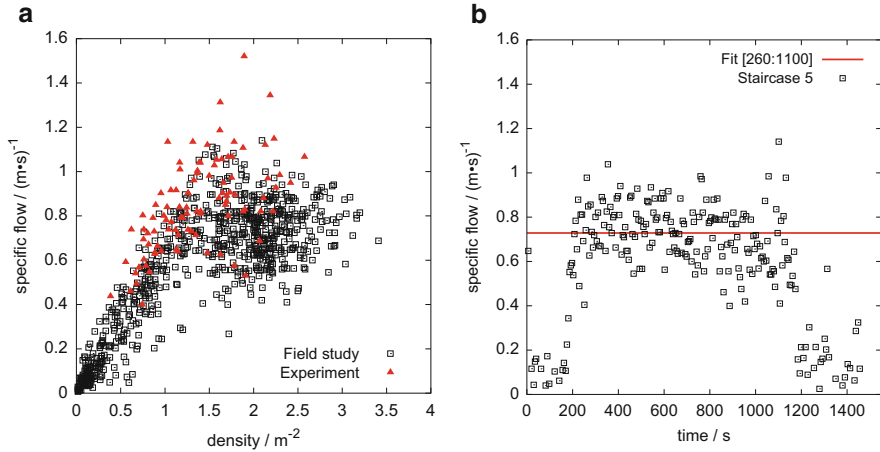


Fig. 4 (a) Fundamental diagram of stairs downwards obtained from field study and experiment using macroscopic measurement method. (b) Time development of specific flow measured at staircase 5 within field study. Over 14 min a mean specific flow of $\bar{J}_s = 0.73 \text{ (m} \cdot \text{s)}^{-1}$ is observable

about $1.1 \text{ (m} \cdot \text{s)}^{-1}$ (single value $1.52 \text{ (m} \cdot \text{s)}^{-1}$ at 1.9 m^{-2}) is measured over the density range from 1 to 2 m^{-2} . Maximum density measured is 2.6 m^{-2} . In the field study, a higher maximum density of 3.4 m^{-2} is observed. The maximum specific flow amounts $1.1 \text{ (m} \cdot \text{s)}^{-1}$, leaving one outlier unconsidered, and appears at a density of 1.5 m^{-2} . Within the observed density range, a decrease of flow due to overcrowding is not found. For densities higher than 2 m^{-2} the mean specific flow fades into a plateau.

The time development of the specific flow at staircase 5 within the field study is shown in Fig. 4b. Three phases can be observed: increase of flow at the end of the football match, a steady state from second 260 to 1,100 followed by a decrease of flow. Over 14 min, during steady state, a mean specific flow of $\bar{J}_s = 0.73 \text{ (m} \cdot \text{s)}^{-1}$ is measured. Due to normal emptying of the stadium, the visitors tend to walk relaxed without any special mood to leave the arena as fast as possible.

5 Microscopic Analysis

5.1 Measurement Method

Different measurement methods could be used to calculate the basic quantities. By using trajectories with high precision for detailed analysis, the influence of different measurement methods on the results could be studied.

In [30] it is shown, that different measurement methods can lead to differences in the fundamental diagram. Zhang et al. [31] analyzed four methods and compared them with each other. It is found, that only the range of fluctuation is affected, not the shape of the resulting fundamental diagram. The Voronoi method is able to produce a good resolution in time and space in combination with reduced fluctuations. For further information about the Voronoi method we refer to [32, 33].

The extracted trajectories from video recordings provide the exact position of pedestrians for every time step Δt as a three dimensional vector $\mathbf{x}_i = (x, y, z)$. For the complete run the set of trajectories can be written as:

$$\{\mathbf{x}_i(t_0), \mathbf{x}_i(t_0 + \Delta t), \mathbf{x}_i(t_0 + 2\Delta t), \dots, \mathbf{x}_i(t_0 + m\Delta t)\} \quad (2)$$

where m is the number of frames the person i is tracked and $\Delta t = 1 \text{ frame} = \frac{1}{16} \text{ s}$.

Using the notation of Eq. 2 the velocity \mathbf{v}_i for every frame is defined as:

$$\mathbf{v}_i(t_j) = \frac{\mathbf{x}_i(t_j + \Delta t) - \mathbf{x}_i(t_j)}{\Delta t}. \quad (3)$$

In this paper we use a horizontal projection on the floor of vector \mathbf{x}_i , thus the z-coordinate, which describes the height of the trajectory point, is disregarded. Using Eq. 3 may lead to large fluctuations due to head swaying, therefor we calculate a mean value of the instantaneous velocity $\mathbf{v}_i(t_j)$ by use of the displacement of pedestrian i in a small time interval $\Delta t' = 0.625 \text{ s}$ (corresponding to ten frames) around t_j :

$$\overline{v}_i(t_j) = \frac{\sum_{k=t_j - \frac{\Delta t'}{2}}^{t_j + \frac{\Delta t'}{2}} |\mathbf{v}_i(t_k)|}{\Delta t'}. \quad (4)$$

The idea of the Voronoi diagram is to allocate every point, in our case the position of every pedestrian, the area closer to this point than to any other one. Thus for every Voronoi cell the area A_i can be obtained and the density as well as velocity distribution $\rho_{x,y}$ and $v_{x,y}$ can be determined. Definitions of quantities are taken from [31, 32]:

$$\rho_{x,y} = \frac{1}{A_i} \quad \text{and} \quad v_{x,y} = \overline{v}_i(t_j) \quad \text{if} \quad (x, y) \in A_i \quad (5)$$

where $\overline{v}_i(t_j)$ is the instantaneous velocity for each person (see Eq. 4).

The Voronoi mean density $\overline{\rho}_v$ for the measurement area is defined as:

$$\overline{\rho}_v = \frac{\iint \rho_{x,y} dx dy}{\Delta y \cdot \Delta x}. \quad (6)$$

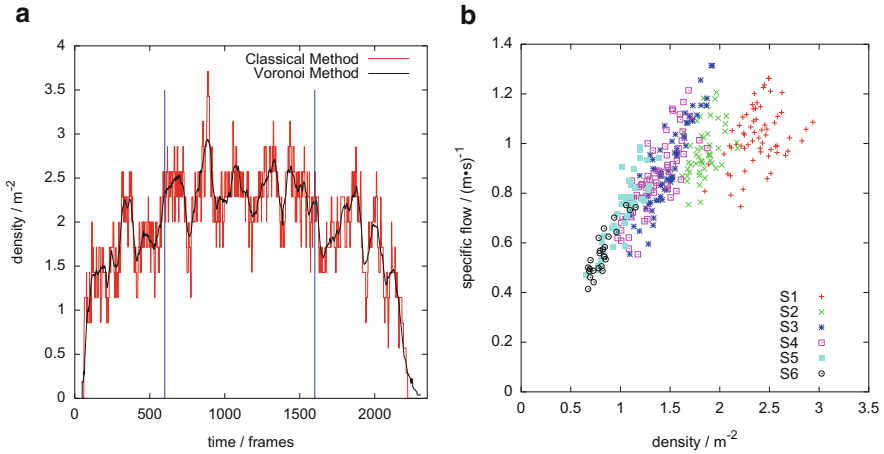


Fig. 5 (a) Time series of density and (b) fundamental diagram for stairs downwards. The flow equation is used to calculate specific flow: $J_s = v_{hor} \cdot \rho$

Δy is the length and Δx the width of the measurement area. Similarly, the Voronoi mean velocity $\overline{v_v}$ is defined as:

$$\overline{v_v} = \frac{\iint v_{x,y} \, dx dy}{\Delta y \cdot \Delta x}. \tag{7}$$

5.2 Fundamental Diagram

We already introduced the applied Voronoi method in Sect. 5.1. The fundamental diagram is determined during steady state. By analyzing time series of density the range of steady state, beginning and end are marked with vertical blue lines (see Fig. 5a), was selected manually. To decrease the number of data points and represent results more clearly, we use 1 point per second.

In our experiments we are able to analyze the fundamental diagram in a density range from 0.6 to 2.9 m^{-2} . Up to 1.5 m^{-2} a linear increase of specific flow is observable which leads to a free velocity of about 0.6 m/s. Maximum specific flow is measured of about 1.2 $(\text{m}\cdot\text{s})^{-1}$ at densities of about 1.9 and 2.5 m^{-2} . A decrease of flow due to overcrowding is not found in our experiments, but for densities higher than 2 m^{-2} the specific flow fades into a plateau.

The video recordings of the controlled experiments have been analyzed with the presented macroscopic and microscopic method. Even though the macroscopic method is more simple and needs less preparation work, the measured basic

Table 5 Comparison of basic quantities obtained from controlled experiments measured with macroscopic and microscopic method. Some outliers are unconsidered

Quantity	Macroscopic method	Microscopic method
ρ_{max} in m^{-2}	2.6	2.9
$\rho(J_{s,max})$ in m^{-2}	1.9	1.9
$J_{s,max}$ in $(m \cdot s)^{-1}$	1.1	1.2

quantities (see Table 5) only differ slightly from the microscopic analyzed ones. Thus, for a first overview, the macroscopic method gives adequate results.

5.3 Profile Analysis

In contrast to standard measurements, the Voronoi method offers the ability to measure areas smaller than pedestrians. For the experiments under laboratory conditions, we divided the complete geometry in 10 cm squares (see Fig. 6). Density and velocity are calculated frame-wise for every square. The profiles Fig. 6a–c present time average values over steady state in the density. Cells near the boundary area, especially at the turning, may be defective, because the cells are cut by walls.

In Fig. 6 topographical information for the basic quantities are provided. These include the profiles of density, horizontal velocity and specific flow. Already a first glance shows that these profiles are inhomogeneous and change significantly with the load. In S1 the maximal density reaches $3 m^{-2}$, while in S3 and S6 the highest values are 2.2 and $1.2 m^{-2}$ respectively.

The first column shows the change of the density profiles. In S1 the load is highest and maximum densities are apparent at the center of the first stair and the inner side of the bend. For lower loads and lower densities the region of highest density observable in the run moves to the second stair. In the turning, five areas are visible: red, yellow, green, light blue and dark blue. The region of low densities (dark blue area) increases for decreasing loads (S1 to S6). Column two shows the corresponding velocity profiles. These profiles show nearly the inverse behavior of the density profiles.

Specific flow profile is calculated by the product of the corresponding density and velocity cells. Here the location of highest values is not so sensible on the load than the density or velocity. Highest flow values are located at the bend. Only for low load the highest flow appears at the inner side of the bend while for higher load the region is in the center of the bend. For S1, related with the highest load, the specific flow reduces and shows a strong change at the transition from the stair to landing and from landing to stair ($y = 0.17$ m and $y = 0.44$ m). The topographical variation of the specific flow does not violate the continuity equation but indicates an effective bottleneck of the facility. We checked that the mean value over the width of facility agrees at different locations.

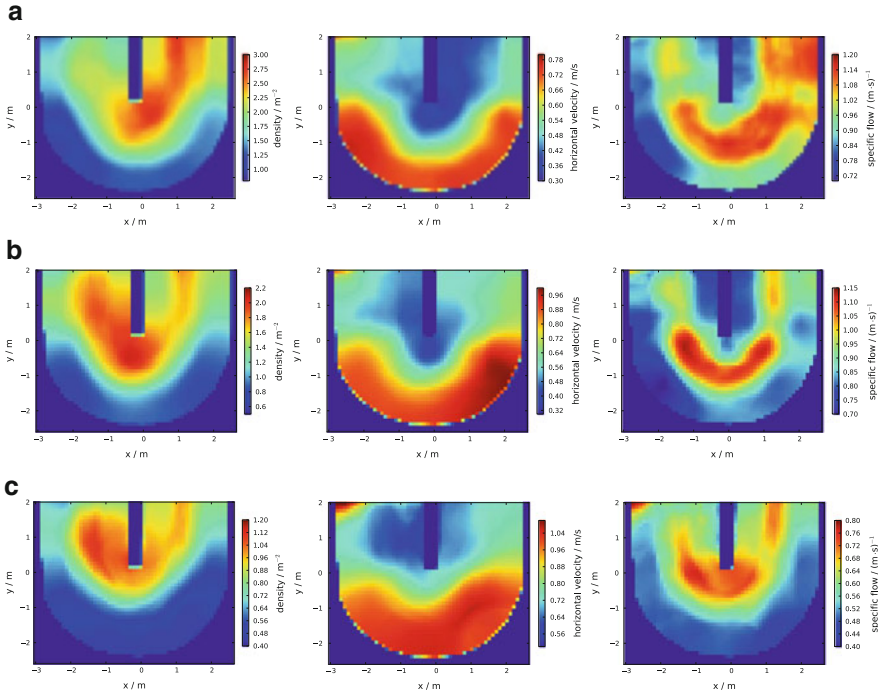


Fig. 6 Topographical analysis of run S1, S3 and S6 during steady state with $\Delta x = \Delta y = 10\text{ cm}$. For each experiment run the range of scale changes to emphasize differences in the profiles. Transition 2 and 3 are located at $y = 0.17\text{ m}$ and $y = 0.44\text{ m}$. **(a)** S1. **(b)** S3. **(c)** S6

6 Conclusion and Outlook

This contribution summarizes the actual knowledge about the fundamental diagram for stairs. An overview is given by the four stated planning handbooks, but basic quantities differ significantly (see Table 1). Maximum specific flow values up to $1.25\text{ (m} \cdot \text{s)}^{-1}$ for downwards- and $1.22\text{ (m} \cdot \text{s)}^{-1}$ for upwards motion are presented and confirmed by experimental data. PM present a fundamental diagram up to 9.2 m^{-2} , but experimental data only show maximum values up to 3.5 m^{-2} . Frantzych measured densities up to 8 m^{-2} but states, that the corresponding velocities $> 1.5\text{ m/s}$ are probably measuring errors. Regarding the functions of WM/NM, a decrease of flow at $\approx 3\text{ m}^{-2}$ due to overcrowding should be observable, but whether the experimental data base nor our experiments confirm this. For downwards motion, it seems that for densities higher than 2 m^{-2} the specific flow fades into a plateau.

Mueller and Frantzych analyzed the influence of different slopes of stairs. Comparing the measurement points shows, that changes of the slope of about 10° only have a minor effect on the fundamental diagram. Regarding the direction of movement, Ye found that the direction has an influence on the maximum specific

flow. Contrary Chen's measurement points don't support the reduced maximal flow for upwards motion.

By performing experiments under laboratory conditions as well as field studies at the same staircase, a direct comparison of data is possible. In the field study, densities up to 3.4 m^{-2} and in the experiments up to 2.9 m^{-2} are measured. The corresponding flow values at a certain density are slightly higher in experiments. Up to now, an accurate automatic tracking of persons is not feasible without prepared hats, thus characteristics of motion during field study cannot be analyzed by use of extracted trajectories.

Overall, field studies don't offer the opportunity for analysis on a microscopic scale, but to gain an overview about the basic quantities, they are helpful. The used macroscopic method gives adequate results and can be proposed for future work.

The analysis of the characteristic of the profiles leads to following questions and conclusions. It is in question whether the limiting factor for the flow of stair is given by the stair itself or by the bend of the landing. That is indicated by the reduction of the specific flow at the transition from stair to landing and from landing to stair. Moreover the significant inhomogeneities of the profiles suggest that the location of the measurement area on a stair could influence the resulting relations. Critical spots under congested conditions can be expected in front of the turning at the landing. Thus it should be analyzed if for safety issues and capacity increase, stairs without bends are preferable.

Acknowledgements This work has been performed within the program *Research for Civil Security* in the field *Protecting and Saving Human Life* funded by the German Government, Federal Ministry of Education and Research (BMBF).

References

1. V. M. Predtechenskii and A. I. Milinskii, *Planning for Foot Traffic Flow in Buildings*. Amerind Publishing, New Dehli, 1978, translation of: Proekttirovanie Zhdanii s Uchetom Organizatsii Dvizheniya Lyuddskikh Potokov, Stroizdat Publishers, Moscow, 1969.
2. H. E. Nelson and F. W. Mowrer, "Emergency Movement," in *SFPE Handbook of Fire Protection Engineering*, 3rd ed., P. J. DiNenno, Ed. Quincy MA: National Fire Protection Association, 2002, ch. 14, pp. 367–380.
3. J. J. Fruin, *Pedestrian Planning and Design*. Elevator World, New York, 1971.
4. U. Weidmann, "Transporttechnik der Fussgänger," Institut für Verkehrsplanung, Transporttechnik, Strassen- und Eisenbahnbau, ETH Zürich, Tech. Rep. Schriftenreihe des IVT Nr. 90, 1993, zweite, ergänzte Auflage.
5. P. J. DiNenno, *SFPE Handbook of Fire Protection Engineering*, 3rd ed. Quincy MA: National Fire Protection Association, 2002.
6. S. Burghardt, A. Seyfried, and W. Klingsch, "Improving Egress Design through Measurement and Correct Interpretation of the Fundamental Diagram for Stairs," in *Developments in Road Transportation*, M. Panda and U. Chattaraj, Eds., Proceedings of the International Conference on Developments in Road Transportation, October 8–12, 2010, NIT Rourkela, Odisha, India. Macmillian Publishes India Ltd, 2010, pp. 181–187.

7. X. Chen, J. Ye, and N. Jian, "Relationships and characteristics of pedestrian traffic flow in confined passageways," *Transportation Research Record: Journal of the Transportation Research Board*, vol. 2198, pp. 32–40, 2010, doi: 10.3141/2198-05.
8. H. Frantzych, "A model for performance-based design of escape routes," Department of Fire Safety Engineering, Lund Institute of Technology, Tech. Rep. 1011, 1994.
9. Frantzych, H., "Study of movement on stairs during evacuation using video analysing techniques," Department of Fire Safety Engineering, Lund Institute of Technology, Tech. Rep., 1996.
10. E. Graat, C. Midden, and P. Bockholts, "Complex evacuation; effects of motivation level and slope of stairs on emergency egress time in sports stadium," *Safety Science*, vol. 31, pp. 127–141, 1999.
11. B. D. Hankin and R. A. Wright, "Passenger Flow in Subways," *Operational Research Quarterly*, vol. 9, pp. 81–88, 1958.
12. K. Hoskin, "Fire Protection and Evacuation Procedures of Stadia Venues in New Zealand," Masterthesis, University of Canterbury, Department of Civil Engineering, University of Canterbury, Private Bag 4800, Christchurch, New Zealand, apr 2004.
13. T. Kretz, A. Grünebohm, A. Kessel, H. Klüpfel, T. Meyer-König, and M. Schreckenberger, "Upstairs walking speed distributions on a long stairway," *Safety Science*, vol. 46, no. 1, pp. 72–78, jan 2008.
14. W. H. K. Lam and C.-y. Cheung, "Pedestrian Speed/Flow Relationships for Walking Facilities in Hong Kong," *Journal of Transportation Engineering*, vol. 126, pp. 343–349, 2000.
15. M. Müller, "Fundamentaldiagramme von Personenströmen auf Tribünenstiegen – Vergleich unterschiedlicher Steigungen am Beispiel der ESPRIT arena; Fundamental diagram of stairs in grandstands – Comparison of different slopes using the ESPRIT arena as example," Bachelor Thesis, Bergische Universität Wuppertal, 2010.
16. I. Sadatoshi and K. Koichiro, Eds., *Observation of the Crowd Flow in a Building*, March 1937.
17. D. B. N. Seer, S. Bauer and M. Ray, "Estimating Pedestrian Movement Characteristics for Crowd Control at Public Transport Facilities," in *11th International IEEE Conference on Intelligent Transport Systems*, oct 2008.
18. Y. Tanaboriboon, S. S. Hwa, and C. H. Chor, "Pedestrian Characteristics Study in Singapore," *Journal of Transportation Engineering*, vol. 112, pp. 229–235, 1986.
19. J. A. Templer, *The Staircase: Studies of Hazards, Falls, and Safer Design*, M. I. of Technology, Ed. The MIT Press, 1992.
20. J. Ye, X. Chen, C. Yang, and J. Wu, "Walking behavior and pedestrian flow characteristics for different types of walking facilities," *Transportation Research Record: Journal of the Transportation Research Board*, vol. 2048, pp. 43–51, 2008, doi: 10.3141/2048-06.
21. J. Pauls, "Are functional handrails within our grasp?" *Building Standards*, vol. 60, pp. 6–12, 1991.
22. J. Pauls, A. J. Gatfield, and E. Juillet, "Elevator use for egress: the human-factors problems and prospects," *Elevator World*, pp. 63–75, 1992, paper for Symposium on Elevators and Fire to be held February 19–20, 1991, in Baltimore, Maryland.
23. J. Pauls, "Vertical Evacuation in Large Buildings: Missed opportunities for research," *Disaster Management*, vol. 6, no. 3, pp. 128–132, 1994.
24. Pauls, J., "Have We Learned the Evacuation Lessons? A Commentary," *Fire Engineering*, vol. 155, no. 10, pp. 113–122, oct 2002.
25. J. Pauls, "Photographic representation of visual fields just before missteps and falls involving stairs," in *Contemporary Ergonomics 2005*, P. D. Bust and P. T. Mc Cabe, Eds. Taylor and Francis Books, 2005, pp. 419–423, international Symposium on Slips, Trips and Falls, held as part of the Ergonomics Society 2005 Annual Conference, Hatfield, UK.
26. Pauls, J., "Elevators and Stairs for Evacuation: Comparisons and Combinations," *Elevator World*, vol. LIII, no. 1, pp. 69–74, jan 2005, proceedings of Workshop on Use of Elevators in Fires and Other Emergencies, American Society of Mechanical Engineers, 2004.
27. "Hermes – investigation of an evacuation assistant for use in emergencies during large-scale public events," <http://www.fz-juelich.de/jsc/hermes>, March 2011.

28. S. Holl and A. Seyfried, "Hermes – an Evacuation Assistant for Mass Events," *inSiDe*, vol. 7, no. 1, pp. 60–61, 2009. [Online]. Available: http://inside.hlrs.de/pdfs/inSiDE_spring2009.pdf
29. M. Boltes, A. Seyfried, B. Steffen, and A. Schadschneider, "Automatic Extraction of Pedestrian Trajectories from Video Recordings," in *Pedestrian and Evacuation Dynamics 2008*, W. W. F. Klingsch, C. Rogsch, A. Schadschneider, and M. Schreckenberg, Eds. Springer-Verlag Berlin Heidelberg, 2010, pp. 43–54.
30. A. Seyfried and A. Schadschneider, "Empirical Results for Pedestrian Dynamics at Bottlenecks," in *PPAM 2009, Part II*, R. Wyrzykowski, J. Dongarra, K. Karczewski, and J. Wasniewski, Eds. Springer-Verlag Berlin Heidelberg, 2010, pp. 575–584.
31. J. Zhang, W. Klingsch, A. Schadschneider, and A. Seyfried, "Transitions in pedestrian fundamental diagrams of straight corridors and T-junctions," *Journal of Statistical Mechanics: Theory and Experiment*, 2011, arXiv:1102.4766. [Online]. Available: <http://arxiv.org/abs/1102.4766>
32. B. Steffen and A. Seyfried, "Methods for measuring pedestrian density, flow, speed and direction with minimal scatter," *Physica A*, vol. 389, no. 9, pp. 1902–1910, may 2010.
33. G. M. Voronoi, "Nouvelles applications des paramètres continus à la théorie des formes quadratiques," *Journal für die reine und angewandte Mathematik*, vol. 133, pp. 198–287, 1908.

Hermes: An Evacuation Assistant for Large Arenas

Stefan Holl, Andreas Schadschneider, and Armin Seyfried

Abstract As part of the German Government's high-tech strategy, the Federal Ministry of Education and Research (BMBF) has launched a programme on "Research for Civil Security". The field of "Protecting and Saving Human Life" in this programme includes funding for the Hermes Project. The project with a three year duration was completed in December 2011. The aim of the collaborative project was to improve safety for people in large multifunctional buildings and also at big events by exploring the effectiveness of an evacuation assistant. In this project, we realized a real-time simulation for the reliable prediction of evacuation process.

Keywords Hermes • Pedestrian dynamics • Evacuation assistant • Automated person counting • Real-time simulation • Communication module

1 Introduction

The trend towards large multifunctional buildings as well as the dimensions of public events makes new demands on the quality of security concepts. In case of emergency, all the attendees must be able to evacuate the danger area rapidly. Although this is generally ensured by the application of building regulations, it can result in a dangerous crush and long queues in case of overcrowding or if some of the emergency exits are blocked. In recent years we have seen an increasing number

S. Holl (✉) • A. Seyfried

Jülich Supercomputing Centre, Forschungszentrum Jülich GmbH, Jülich 52425, Germany
e-mail: st.holl@fz-juelich.de; a.seyfried@fz-juelich.de

A. Schadschneider

Institute for Theoretical Physics, Universität zu Köln, Köln 50937, Germany
e-mail: as@thp.uni-koeln.de

of crowd disasters with many injured persons, e. g. Love Parade 2010 in Duisburg (Germany).

In order to prevent such critical situations optimal crowd management needs accurate and up-to-date information about the current state in the arena. In the three-year research project Hermes – funded by the German Federal Ministry of Education and Research (BMBF) – we have developed an evacuation assistant. In the project a total of 13 partners have worked together. In addition to the research institutions and business enterprises the end users (police, fire fighters and security guards) were involved in the exploration of the evacuation assistant:

1. Forschungszentrum Jülich GmbH
2. University of Wuppertal
3. University of Bonn
4. Cologne University
5. Imtech Deutschland GmbH & Co. KG
6. Multifunktionsarena Immobiliengesellschaft mbH & Co. KG (ESPRIT Arena)
7. PTV Planung Transport Verkehr AG
8. TraffGO HT GmbH
9. Vitracom AG
10. Düsseldorf Fire Brigade
11. Düsseldorf Police Headquarters
12. North Rhine-Westphalia State Office for Central Police Services
13. Special Security Service SSSD GmbH

The aim of the assistant was to incorporate the current state of the building, but also the number and distribution of persons present in the simulation. So for the first time it became possible to obtain real-time simulation results based on the actual risk situation.

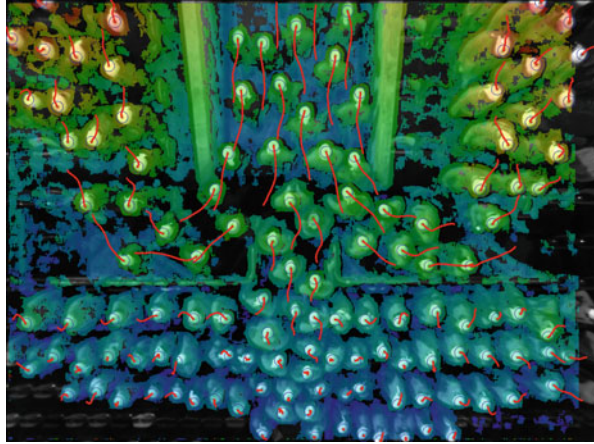
The ESPRIT Arena in Düsseldorf (Germany) provided a venue for implementing the evacuation assistant. The example of this multifunctional area with a capacity of more than 60,000 spectators showed how crowds of people at big events can be guided so that optimal use can be made of the emergency exits. The aim of the Hermes Project is to produce a real-time simulation for a reliable forecast of the evacuation behavior. The task forces will receive important information, but the decision on the optimal strategy will be taken in each case by the forces themselves.

2 Functions of the Evacuation Assistant

The project Hermes consists of several components:

- Safety and security management system
- Video-based person counting
- Real-time simulation core
- Communication module

Fig. 1 Schematic diagram of the evacuation assistant



The safety and security management system provides information about the condition of the building. So we know if escape routes are smoky or whether parts of the building were closed e. g. because of a bomb threat. The video-based person counting provides reliable data on the number of people who are currently in the parts of the building. Data privacy is taken very seriously here: we do not store video images, but only the count data will be passed. Based on these data, the system operator can now define a scenario that will be calculated from the simulation tools.

3 Modeling and Validation

In our project Hermes, three different models are combined to obtain reliable predictions from the simulations and achieve an optimal performance. One approach relies on a macroscopic model allowing a routing recommendation [1]. Additionally we use two microscopic models (floor field cellular automaton model [2] and the generalized centrifugal force model [3]) which provide rather detailed predictions about the development of an evacuation. To increase the reliability of the forecast large-scale experiments have been performed in the laboratory and the arena itself. These data are complemented by field studies.

The position vs. time curves (trajectories) of each individual was recorded in these experiments with stereo cameras (Fig. 1). With the method developed at the Research Center Juelich [4, 5], it was possible to analyze these trajectories automatically and to use for calibration and validation of simulation models (Fig. 2).

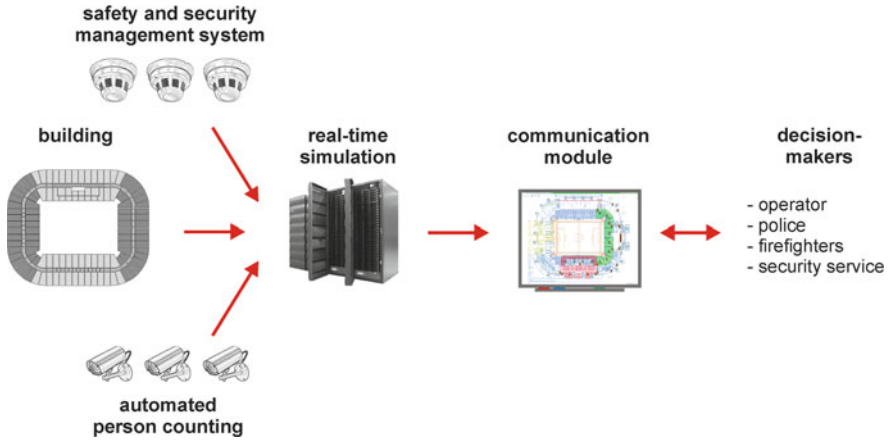


Fig. 2 Laboratory experiments, extraction of the trajectories, calibration of simulation models

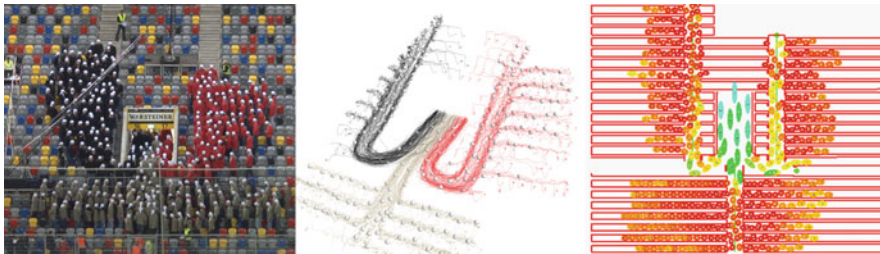


Fig. 3 Graphical interface of the communication module (Source: PTV AG)

4 Visualization of Results

Essential for the practicality of the evacuation assistant is the treatment of the resulting data. The front end of the system is therefore a communication module. The type of visualization has been jointly developed and tested with the end users (Fig. 3). With a traffic light system (red, yellow, green) it can be determined on a first glance whether the allowable number of occupants is exceeded in some areas of the building. Based on the micro-simulation it is shown, where critical traffic jams will arise during the next 15 min. Due to these results the responsible team leaders have the opportunity to deploy their employees so that pedestrian traffic can be directed optimally.

In 2011, the evacuation assistant was successfully tested during several concerts and football games.

References

1. A. Schomborg, K. Nöckel and A. Seyfried. Evacuation Assistance for a Sports Arena Using a Macroscopic Network Model. In: R. Peacock, E. Kuligowski and J. Averill (ed.), *Pedestrian and Evacuation Dynamics 2010*, Springer, p. 389–398 (2011)
2. C. Burstedde, K. Klauck, A. Schadschneider, and J. Zittartz. Simulation of pedestrian dynamics using a two-dimensional cellular automaton. *Physica A*, 295:507525, 2001.
3. M. Chraibi, A. Seyfried, and A. Schadschneider. Generalized centrifugal force model for pedestrian dynamics. *Physical Review E*, 82:046111, 2010.
4. M. Boltes, A. Seyfried, A.; B. Steffen, A. Schadschneider. Using Stereo Recordings to Extract Pedestrian Trajectories Automatically in Space. In: *Pedestrian and Evacuation Dynamics*, ed./ R.D. Peacock, E.D. Kuligowski, J.D. Averill, Springer, 2011. - 978-1-4419-9725-8. -. S. 751–754
5. M. Boltes, A. Seyfried, B. Steffen, B.; A. Schadschneider. Automatic Extraction of Pedestrian Trajectories from Video Recordings. In: *Pedestrian and Evacuation Dynamics 2008*,/ed.: W.W.F. Klingsch, C. Rogsch, A. Schadschneider, M. Schreckenberg, Berlin/Heidelberg, Springer, 2010. - 978-3-642-04503-5. - S. 43–54

Influence of Emissions on Pedestrian Evacuation

Hermann Mayer, Dirk Hartmann, Wolfram Klein, and Oliver Zechlin

Abstract Emissions like fire, smoke, noxious gases etc. have a crucial impact on the evacuation of large buildings in case of an emergency. Given static egress plans, the predefined escape route might be blocked by any of these emissions. Since the exact location of an emission is not known during planning stage, it is not possible to include this phenomenon into static egress plans. However, if the building is equipped with an adequate selection of detectors and sensors, egress plans can be dynamically adapted during an emergency. Optimal escape routes are calculated by a pedestrian simulation. The results of the simulation will be communicated to the occupants (by means of dynamic signage, hand-held devices, voice evacuation).

Keywords Pedestrian simulation • Fire simulation • Egress models • NIST FDS

1 Introduction

We have developed a pedestrian simulation, which is capable of integrating an emission model that influences the movement of pedestrians. Two alternatives, online and offline coupling have been implemented. Offline coupling can be employed to integrate data generated by accurate, but time-consuming methods like NIST FDS (Fire Dynamics Simulator developed by the National Institute of Standards and Technology). The distribution of substances is calculated by a separate tool and afterwards the results are prepared to synchronize them with the

H. Mayer (✉) • D. Hartmann • W. Klein
Siemens AG, CT T DE TC3, Otto-Hahn-Ring 6, München 80200, Germany
e-mail: hermann-georg.mayer@siemens.com; dirk.hartmann@siemens.com;
wolfram.klein@siemens.com

O. Zechlin
Siemens AG, IC BT FSS IIA, Gubelstrasse 22, Zug 6300, Switzerland
e-mail: oliver.zechlin@siemens.com

downstream pedestrian simulation. In contrast for online coupling, the emission is not pre-calculated by a standalone model, but directly integrated into the main loop of the pedestrian simulation. Therefore, an immediate interaction between occupants and the effects of a certain emission is feasible. In addition, the applied algorithms are optimized for performance while still providing acceptable accuracy. This feature is essential for online simulation planning as demanded by fire alarm systems: both fire spread and pedestrian motion can be simulated faster than real-time. In case of a fire, the simulation calculates situational, individual egress routes for each occupant (or each group of occupants). By employing calculation methods, which are faster than real-time, the updated egress route can be communicated to the occupants immediately.

2 Materials and Methods

In this chapter we describe two possibilities of integrating a fire dynamics model into a pedestrian simulation. The first option, offline coupling will be shown using the example of NIST FDS. However, the proposed method can be easily generalized in order to include the results of every smoke simulator, which is based on the finite volume method. The second possibility, online coupling, employs a simplified but fast method to calculate the spatial distribution of smoke. Later, in the conclusion, both methods are compared to each other and the advantages of both are summarized.

2.1 Pedestrian Simulation

Pedestrian simulation is supposed to be a key element in the management of the cities of the future. Therefore, we have found various factors to motivate an investment into the research on pedestrian simulation:

- Dangerous situations (for example during an evacuation) can be simulated and results can be integrated into the design of new buildings (e.g. layout of exit doors).
- If integrated into a facility management system, pedestrian simulation can assist in online routing of occupants (e.g. switch dynamic exit signs).
- Each year people die at mass events, in critical infrastructures and in emergency situations when crowds get out of control. Pedestrian simulation can assist first responders in the emulation and identification of critical situations.
- Knowing the behavior of crowds can reduce costs: for example, massive police deployment is necessary to maintain control even at routine events: 370 police officers and 150 private security guards survey a “regular” soccer game. Knowing critical spots can help to deploy resources more efficiently.
- Simulation capabilities are not yet used for efficient logistical planning and staff allocation.

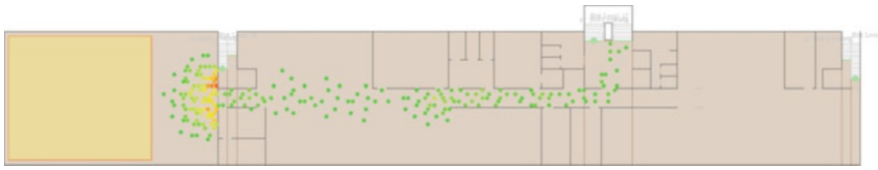


Fig. 1 Evacuation Simulation: the leftmost room is evacuated through a narrow door. By means of microscopic simulation, the positions of individual pedestrians are calculated. In contrast to macroscopic simulation, the shape of the congestion can be derived from the results, and therefore, employed for planning reasons (e.g. to find a safe location to place objects like tables or poster stands). This result does not depend upon the reproducibility of the position of an individual person

Based on these prerequisites, we have developed a pedestrian simulator, which is integrated into an intuitive user interface. A first version of the pedestrian simulator without coupling to a fire simulation has already been published, for example in [1] and [2]. The simulator has been developed within the last 3 years by the research and development department of Siemens AG. The software comprises the actual simulation kernel, a graphical user interface, a tool for statistical evaluation and a 3D visualization. Scenarios for a simulation can be extracted from architectural drawings or data bases and augmented by the user with relevant data description (e.g. locations of sources and destinations of occupants). In addition, it is possible to couple the simulation with third party tools (like data export to Microsoft Excel). The tool has already been assessed by experts in the field (e.g. [3]) and various new action items have been defined in order to extend the functionality of the simulator.

The simulator implements a discrete, microscopic model for the movement of pedestrians. In comparison to continuous simulation, a discrete model is much faster and does not suffer from instability factors like oscillations. In addition, it is easier to include interactions of the pedestrian with dynamic events like fire spread, since calculations can be restricted to discrete events in time. While macroscopic pedestrian simulation is predominantly focused on producing statistical data (like flows and densities), microscopic simulation can help to identify the behavior of single pedestrians. However the behavior of an individual can never be anticipated, but the interaction of many individuals can be emulated by microscopic simulation. The following example (cf. Fig. 1) clarifies the description above:

The implementation of the pedestrian simulation is based on a cellular automaton, which operates on a hexagonal grid. The pedestrians are passive elements (in contrast to agents), which are moved from cell to cell after an equidistant, discrete amount of time. The movement of pedestrians is influenced by a social force model, where pedestrians are attracted by a destination and repelled by obstacles and by each other.

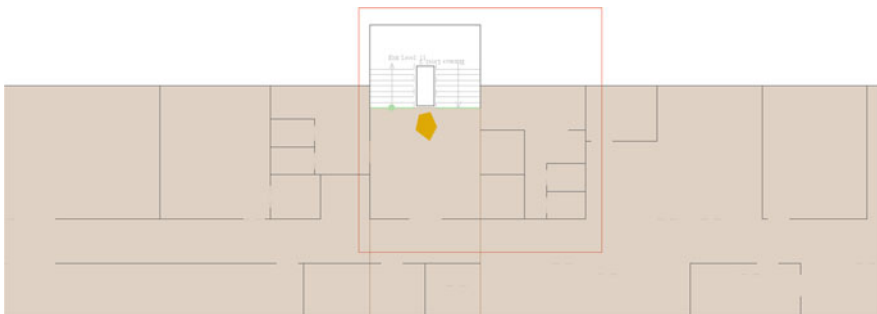
2.2 *Offline Coupling: NIST FDS*

For the accurate offline simulation, fire and egress computations are performed separately and sequentially. First, the propagation of a fire is simulated by a

dedicated fire model (we have integrated NIST FDS, which is based on computational fluid/gas dynamics: CFD). The CFD method requires the environment to be subdivided into a grid of finite volumes. In case of FDS, the simulation environment is subdivided into rectangular cuboids. The selection of a resolution for the subdivision predominantly influences both accuracy of the calculation and computation time (cf. [4]). Pertinent literature suggests an edge length of about 0.1 m for each direction of the cuboids (e.g. [5]). In addition, this resolution provides a sound representation of oblique walls (see below). However, resolution recommendations differ depending on the field of application. For instance, large-scale tunnel simulation is performed at a resolution of 0.25–0.5 m [6]. In contrast, a realistic sooth output in the vicinity of the plume of a fuel fire requires a resolution of down to 0.05 m [7, 8]. To our knowledge the version of FDS we have employed does not support monolithic multi-scale grid approaches. However it is possible to use different conjoined grids, each with a dedicated resolution (cf. [4]). Due to the nonconformity of our simulation environment this approach cannot be exploited. Therefore, the whole simulation environment has to be subdivided using a sufficient resolution to represent even delicate features in the environment regardless of their contribution to the current smoke distribution (because the influence of an element cannot be assessed a priori). Afterwards, the result of the fire simulation is fed into a model for pedestrian simulation. The temporal distribution of the fire is modeled by potential fields, repelling pedestrians.

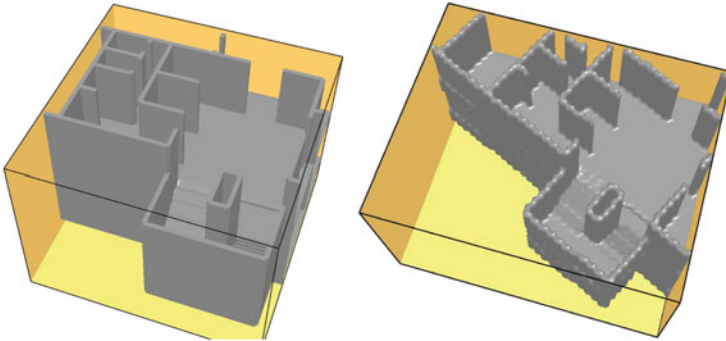
The following steps are necessary to integrate NIST FDS into the Siemens pedestrian simulator:

1. A section of the simulation environment is defined, which is cut out for the fire simulation. Usually this section should be delimited by walls and well-defined boundary conditions (like open doors) in order to yield realistic results. However, in general the horizontal projection of the section is an arbitrarily rotated rectangle. In a context menu of the rectangle, the height of the section can be defined (a multiple of building floors).



2. The section selected for fire simulation is clipped from the scenario and converted to the NIST FDS input file format. The fire source (orange) is converted to a NIST

FDS burner, which is placed on the floor of the corresponding level. Afterwards, the NIST FDS tool is started on the converted scenario. The right picture below shows issues, which might occur if the boundaries of the simulation area are not aligned with the major axes. In this case the walls suffer from discretization artifacts, unexpected holes in the topology might occur and the boundaries of the fire simulation are not well-defined. Therefore, at least the dominant walls should be aligned with the major axes of the NIST FDS input file.



3. After the NIST FDS simulation has finished, the produced results can be loaded into the pedestrian simulator and are referenced to the underlying scenario. Each smoke cell of the NIST simulation is mapped to a hexagonal cell of the pedestrian simulator (nearest neighbor). In order to map the three-dimensional NIST grid to the two-dimensional simulation environment, the user can select in which tier of the room smoke afflicts the occupants. Another value controls the density of smoke that is considered harmful or obstructing sight. In this case, smoke cells are inserted into the simulation environment (orange cells). In the picture below, three occupants are deflected by the smoke.



2.3 Online Coupling: Fast Marching Method

However, since the distribution of the fire is computed separately, a direct interaction between the pedestrians and the fire can hardly be modeled. Therefore, we also provide online coupling of fire and egress simulation, i.e. after each time step of the fire simulation, the pedestrian simulation is updated and vice versa. Due to the computational complexity of models based on CDF, those approaches cannot be performed in real-time, which however is a strict requirement for incorporating the simulation into a fire alarm system. Real-time simulation is a must for time critical applications like voice evacuation and dynamic egress routes: an optimal egress plan is calculated by a simulation and communicated to the occupants online. Otherwise, the high accuracy of a fire model based on computational fluid dynamics is not necessarily required for the controller of such a fire alarm system. A more important prerequisite is a smooth integration of the fire model into the existing simulation environment. Therefore, and since we have chosen a cellular automaton for the movements of pedestrians, our approach for integrating a fire simulation is also based on that grid model. The area of interest is discretized into hexagon cells, where each cell can be occupied by only one person. The size of a hexagon cell is based on literature on pedestrian dynamics (e.g. [9]). Given this discretization, the pedestrian model can be influenced by the fire model in each time step and vice versa. For example, if additional cells are afflicted by the distribution of smoke or fire, those cells will be marked as obstacles for the next step in pedestrian simulation. This might contingently result in a recalculation of the best egress path for some pedestrians.

An efficient method to couple a continuous model with a discretized simulation environment is constituted by the so-called Eikonal equation:

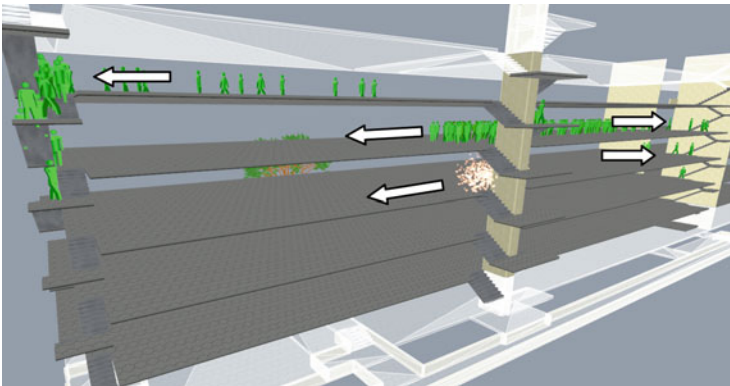
$$F(x, y) \left| \nabla T(x, y) \right| = 1.$$

The Eikonal equation is used to calculate the arrival time of waves, which are propagated by a certain speed. The speed of wave propagation is not limited to a constant value, but can take any function depending on the position in the simulation area. Our implementation establishes a dependency of the wave propagation on material parameters, or on external parameters like wind speed or elevation profiles – or whatever might influence the distribution of a fire. Apart from those advantages, it is also possible to couple a simulation with more than one Eikonal equation, for example if different models for the propagation of fire and smoke are required. Furthermore, obstacles can be included into the simulation environment by simply setting the speed of wave propagation to zero inside these areas. Although the simulation based on an Eikonal equation is a continuous method, the numerical solution of the equation is subject to a certain discretization on a computer. However, a fine discretization can be chosen, since effective methods are provided to solve the Eikonal equation. For example in [10] the so-called Fast Marching Method is proposed, an algorithm that solves the Eikonal equation in

$O(n \log(n))$ steps, where n is the number of points in the discretization. Given these features, the distribution of fire and smoke (and other harmful substances) can be coupled to a real-time pedestrian simulation. In addition, those simulation models provide a high accuracy, since relevant information can already be pre-calculated in detail during the initial phase of the simulation, which can be performed offline (non real-time).

3 Examples

We have used our software to simulate the evacuation of occupants from a multi-storey building, where a fire breaks out in the staircase. The goal of the simulation is finding an optimum egress route for each of the occupants (i.e. the simulation calculates the optimum egress route for each individual person). The optimum egress route might differ from person to person, since the occupants are located in different parts of the building with different accessibility to the exits. This kind of simulation could be directly linked to an intelligent fire alarming system, which advises each individual occupant how to exit the building in case of an emergency. Possible channels of notification are, for example, sending a short message on the mobile, displaying the exit route on the individual desktop, or using voice evacuation and dynamic lighting. The most important feature of such a system is its reactivity towards dynamic events in real-time. In this case, the simulation can always update the optimum egress route, based on the state of the environment (e.g. a fire blocking the staircase). Therefore, regarding this example, the fire alarming system has to be connected to a variety of sensors, like occupancy detection (e.g. cameras, sensitive floor plates) or fire/smoke detection. Again, all these actions require a calculation of the simulation results in real-time, which was reached by the proposed online coupling method.



4 Conclusion

In the chapters above, we have proposed methodologies for an offline and online coupling of egress simulation and fire simulation (or more general: simulation of the spatial spread of emissions). While the first approach incorporates a third-party CFD-tool (computational fluid dynamics), we have also developed a novel method, which is capable of online fire simulation. This allows for the performance of the simulation in real-time, which is an indispensable prerequisite for the inclusion of egress simulation into fire alarm systems. In addition, the exchange of relevant parameters between egress simulation and fire simulation is possible after each time step, which leads to more realistic results compared to offline calculation of fire/smoke fields. The methodology is based on the Eikonal equation, which allows for the integration of parameters like flammability of different materials, direction and speed of laminar airflows and the inclusion of different elevation profiles for outdoor applications. The employed Eikonal equation can be solved effectively by approved algorithms. In addition, those simulation models provide a high accuracy, which is sufficient for application in online evacuation. However, the high accuracy of fine-gridded CFD based models like NIST FDS cannot be reached this way, i.e. the offline mode is still the favorable option for detailed planning purposes. We expect for the future, that computers with higher performance allow for a merging of online and offline approaches, or that it is even possible to run accurate CFD models in real-time for large environments (whole building).

References

1. Köster, G., Hartmann, D., Klein, W.: Microscopic pedestrian simulations: From passenger exchange times to regional evacuation. In: International Conference on Operations Research - "Mastering Complexity", pp. 571–576. Conference Proceedings, Munich (2010)
2. Davidich, M., Köster, G.: Towards Automatic and Robust Adjustment of Human Behavioral Parameters in a Pedestrian Stream Model to Measured Data, In: Safety Science Vol. 50, Iss. 5, pp. 1253–1260, Elsevier Ltd., Amsterdam (2012)
3. Kneidl A., Borrmann, A.: How Do Pedestrians find their Way - Results of an experimental study with students compared to simulation results. In: Emergency Evacuation of people from Buildings, W. Jaskółowski and P. Kepka eds., pp. 163–172, Warsaw (2011)
4. McGrattan, K., McDermott, R., Hostikka, S., Floyd, J.: Fire Dynamics Simulator Version 5 Users Guide. National Institute of Standards and Technology, Gaithersburg (2010)
5. Hadjisophocleous, G.V., McCartney, C.J.: Guidelines for the Use of CFD Simulations for Fire and Smoke Modeling. In: ASHRAE Transactions Vol. 111, No. 2, pp. 583–594. American Society of Heating, Refrigerating and Air-Conditioning Engineers, Atlanta (2005)
6. Mawhinney, J.R., Trelles, J.: Performance Testing of Fire Protection Systems in Tunnels: Integrating Test Data with CFD Simulations. In: Fourth International Symposium on Tunnel Safety and Security, pp. 297–309. Conference proceedings, Frankfurt am Main (2010)
7. Floyd, J., Siamak, R., Mealy, C., Gottuk, D.: Modeling of and Requirements for Parallel Beamed, Flat Ceiling Corridors and Beamed, Sloped Ceilings. In: Smoke Detector Spacing Requirements Complex Beamed and Sloped Ceilings – Volume 2. The Fire Protection Research Foundation, Baltimore (2008)

8. Ma, T.G., Quintiere, J.G.: Numerical simulation of axi-symmetric fire plumes: accuracy and limitations. In: *Fire Safety Journal* Vol. 38, Iss. 5, pp. 467–492. Elsevier Ltd., Amsterdam (2003)
9. Weidmann, U.: *Transporttechnik der Fussgänger*. In: *Schriftenreihe des Instituts für Verkehrsplanung*. ETH, Zürich (1993)
10. Sethian, J.A.: *Level Set Methods and Fast Marching Methods: Evolving Interfaces in Computational Geometry, Fluid Mechanics, Computer Vision, and Materials Science*. Cambridge Monograph on Applied and Computational Mathematics. Cambridge University Press (1999)

Large-Scale Multi-modal Evacuation Analysis with an Application to Hamburg

Dirk Durst, Gregor Lämmel, and Hubert Klüpfel

Abstract Evacuation is one possible option when facing natural or man-made risks. The evacuation of a building block, part of a city, or even a whole city or region is a far-reaching measure. It is usually the last measure and only taken when a social catastrophe is impending. The Free and Hanseatic City of Hamburg was hit by flooding in 1961. The homes of 50,000 people were destroyed and a total of 315 persons died. The situation today is not comparable to the situation in the early 1960s. Back then, many buildings were still barracks and built or repaired just after World War II. First and foremost, an elaborated early warning system was established. Nevertheless, evacuation might still be necessary when dikes are damaged. These few considerations show the complex context, in which decisions about evacuations are made. In order to reduce the complexity for the decision makers, simulations for the prediction of evacuation times and potential congestion or delays are one option. They can provide objective criteria and make the consequences of certain alternatives more intuitive by visualizing them based on well-known representations of the city like street maps. We present an example for Hamburg Wilhelmsburg, i.e. the simulation of multi-modal regional evacuation, in this contribution.

Keywords Evacuation • Civil protection • Simulation

D. Durst (✉)

Federal Office of Civil Protection and Disaster Assistance, German Joint Information and Situation Centre (GMLZ), Provinzialstraße 93, Bonn 53127, Germany
e-mail: dirk.durst@bbk.bund.de

G. Lämmel

TraffGo HT GmbH, Bismarckstraße 142a, Duisburg 47057, Germany
e-mail: kluepfel@traffgo.ht

H. Klüpfel

Technische Universität Berlin, Verkehrssystemplanung, Salzufer 17, Berlin 10123, Germany
e-mail: laemmel@tu-berlin.de

1 Introduction

In this paper we will present results on a multiagent evacuation simulation, combined with different “paper and pencil” calculations. The result is the overall evacuation time in case of multi-modal transport, i.e. the *Required Safe Egress Time* (RSET). This is later compared to the *Available Safe Evacuation Time* (ASET). This ASET is an external parameter provided by the civil protection authorities and obtained from hazard calculations and risk analyses.

Four different modes of transport are taken into account for the RSET calculation: walking, busses, railway, and cars. In detail: walking to shelters, walking to bus and train stations, bus shuttle and local trains, and finally motorized individual transport by car. The major result is a range of the overall evacuation time for Hamburg-Wilhelmsburg, a district of the Free and Hanseatic City of Hamburg with approx. 50,000 inhabitants. The time obtained by the simulation and calculations is in the order of 3–4 h. This fits in the overall time-frame of 9 h for the ASET, which was adopted by the civil protection authorities in Hamburg. ASET consists of three parts: 3 h for preparation and warning, 4 h for evacuation, and 2 h as buffer, as shown in Fig. 5. ASET must be larger than the RSET, which is in our case determined by the simulations and calculations. The ASET is limited first of all by the external risk. In our case, the external risk is flooding. To be more specific: we assumed a leakage of one of the dams. Hydrological and hydrodynamic simulations are routinely performed by the civil protection authorities in Hamburg.

2 Problem Definition and Deferral

The planning of civil protection measures is in most cases based on experience from previous events. The Tsunami in Indonesia, hurricanes in the southern United States, the earthquake in Haiti, and the Tsunami in Japan are recent examples, where the evacuation of cities or regions was necessary. At this point, the distinction between natural hazard and social catastrophe is important.

A natural hazard evolves from a “natural” event like an earthquake, a tsunami, hurricane, strong wind, flooding etc. The catastrophe is always a social phenomenon in the sense that the human settlements that are affected by the natural events are social constructs. Furthermore, the consequences are only catastrophic, if the preparation for or the reaction to the event fails and people are injured or killed. The connection between natural phenomena, hazards, events, and vulnerability is shown in Fig. 2.

The exposure to threats and the coping capacities determine the environmental, social, and economic risk. The situation in Hamburg Wilhelmsburg has changed drastically since 1962. As can be seen from Fig. 1, in 1962 the buildings were mainly barracks. Taking into account the risk reduction by vulnerability reduction as illustrated in Fig. 2 it is obvious that the risk is by far lower today for Hamburg Wilhelmsburg than it was back in 1962. There are two main strategies to reduce vulnerability: (1) increase preparedness and (2) enhance the intervention system.



Fig. 1 The flooding in Wilhelmsburg in 1962 (Photo: G. Pietsch)

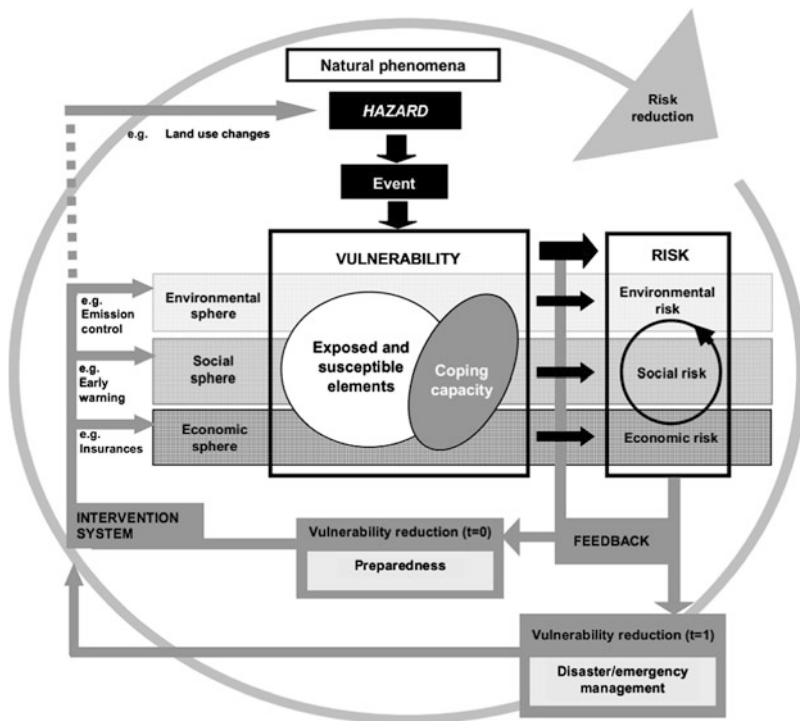


Fig. 2 The BBC framework [1]

3 The Threat: Flooding

Wilhelmsburg is an “island” surrounded by the river Elbe in Hamburg (cf. Fig. 3). Therefore, the area potentially affected by flooding can be left via bridges only.

Fig. 3 The “island”
Wilhelmsburg



Table 1 Possible decisions and consequences

	No evacuation	Evacuation, assumptions correct, time estimate correct	Evacuation, assumptions wrong, time estimate wrong
Event happens	Responsibility for damages	Right decision	Responsibility; Worst case: more persons are injured than in case of no action
Event does not happen	Right decision?	Responsibility for production losses etc.	Responsibility for production losses etc.

The possible decisions that can be taken for the evacuation are shown in Table 1. Depending on the realization of the event (there is a flooding or not), the outcome differs. There are two “worst” cases: (1) no decision and the occurrence of the threat, and (2) the decision is made too late and persons are affected by the threat while still evacuating.

Of course, the prognosis about the development of the threat, i.e. the dynamics of the flooding is a key ingredient for the decision making process.

The simulation model takes into account the weather conditions and allows investigating scenarios such as, e.g., a damaged dyke. A screenshot can be seen in Fig. 4. The planning is based on a “dry evacuation”. The evacuees must have left the endangered area before the water level rises.

The rationale behind that planning paradigm is to avoid the “worst case” shown in Table 1: persons are endangered while still evacuating.

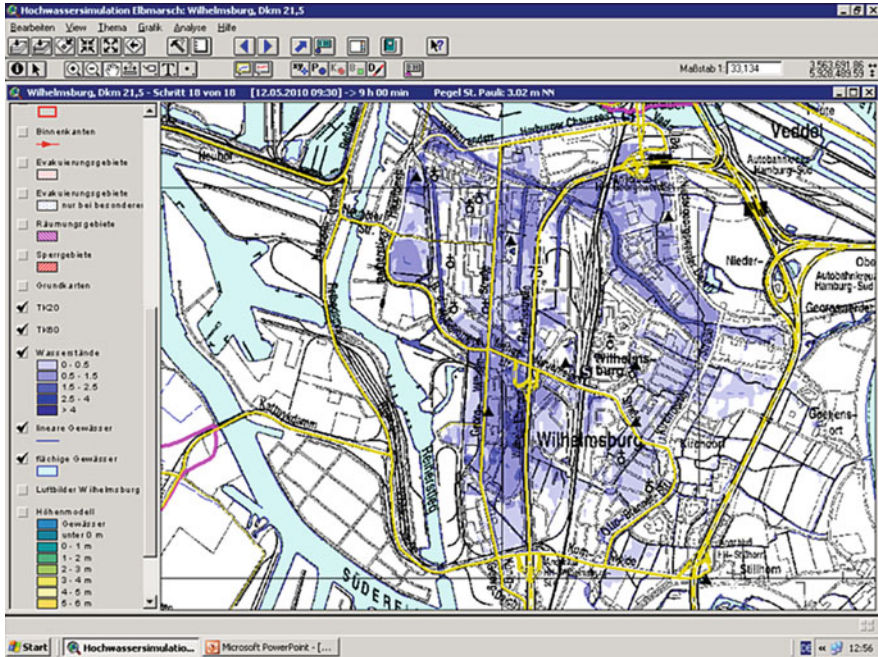


Fig. 4 Flooding simulation

4 Evacuation Phases and Overall Evacuation Time

When assessing evacuation processes, many different phases of information gathering, decision making, communication, and feedback collection have to be taken into account. These phases to some extent can overlap. In general, the overall time can be divided into the following parts:

$$t_{\text{evac}} = t_{\text{detect}} + t_{\text{decide}} + t_{\text{alarm}} + t_{\text{prepare}} + t_{\text{move}} \quad (1)$$

4.1 Pre-movement Time

One major uncertainty is the individual preparation time. It might be influenced by the warning mechanisms and messages. We know that cultural influences and awareness of possible nature disasters, has influence on people behaviour. So inhabitants on the Florida Keys will be better in preparation for leaving their homes than for example inhabitants of a city without the permanent risk to be concerned by a natural disaster. An example of a cultural influence is a case study, of the Indonesian city of Padang. Up to 50 % of the population stated they would stay in

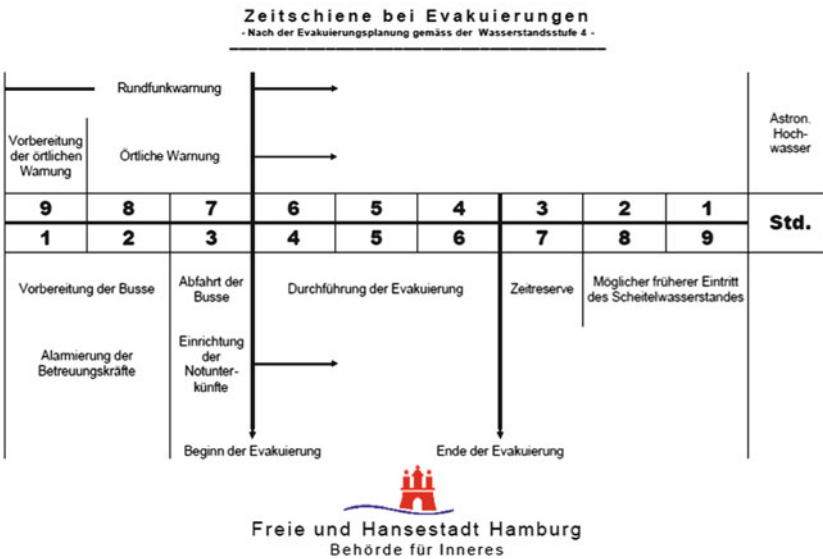


Fig. 5 Time frame for the evacuation

case of a Tsunami warning [7]. This could be explained by the fear of looting. In the Free and Hanseatic City of Hamburg, the inhabitants are more sensitive to possible natural disasters because of a variety of flooding took place during the flooding period between September and March. Inhabitants are addressed by different media, in different languages and informed how to behave in the case of flooding.

The pre-movement or preparation time is a major influence on the overall evacuation time in Eq. 1 and therefore the RSET. It can be influenced by the information of the population, especially by the warning mechanisms (see the next section). Additionally, the coping capacity will also influence the preparation time. Be a person that has a place to go and strong social bonds will be more willing to leave her home than someone who will have to his evacuated to a public place of refuge [5].

4.2 Warning Mechanism

There is a plethora of warning mechanisms planned for this scenario, ranging from radio messages and SMS to canon-shots, sirens, individual phone calls, etc [3].

4.3 Places of Refuge

Safe places are within the evacuation area as well as outside. In Hamburg-Wilhelmsburg, places of refuge are either higher floors of private buildings or public buildings prepared as evacuation shelters. The places of such shelters are shown in the warning brochure distributed to all inhabitants [4]. Further places of refuge which are situated outside the evacuation require transportation. Several modes of transport are employed: motorized individual means of transport, bus shuttle, and local trains.

5 Simulation Model and Results

Totally 50,601 evacuees were considered. 35,041 of them were planned to be evacuated by approximately 17,000 cars (agents). 4,250 could find refuge in buildings used as shelter. The rest, 11,310 evacuees had to be transported by busses and trains. Therefore, we used a “paper and pencil” calculation. For more detailed information see also [2]. In the simulation, 17,000 agents were distributed in the area of the Elbe Island (Fig. 3). The simulations are based on MATSim [6]. The street network was imported from Open Street Map.

MATSim was used as it was offered for downloading in August 2010. The simulation was part of a comprehensive assessment taking into account public transport (by local trains and busses), traffic to shelters on foot, and motorized individual traffic on the one hand. On the other hand, capacities of shelters and infrastructure, first responders, and information dissemination were taken into account. The traffic simulation module was used to determine the overall evacuation time for motorized individual traffic. Since the movement to shelters and the transportation by public transport (local trains and busses) is independent thereof, the maximum of the time for the different evacuation modes can be regarded as the overall evacuation time. In the scenario analyzed an advance warning of 3 h was assumed. This time is also used for the preparation of the emergency and rescue service. For motorized individual traffic the overall evacuation time is < 90 min. However, transportation by public transport takes about 4 h, which uses up the ASET given by the local authorities. In order to improve the situations and increase of the available transport infrastructure (i.e. number of busses/trains), a more effective use of the existing transport infrastructure is needed. This would mean to increase the number of persons per bus or train. It has to be noted that the number of persons per bus was less than 20 % than under normal conditions, based on an evacuation exercise performed in Cologne. This is due to the extensive amount of luggage carried by the evacuees. The results presented here are embedded into a larger context, which is the GRIPS research project. See Bakilah et al. (in these proceedings).

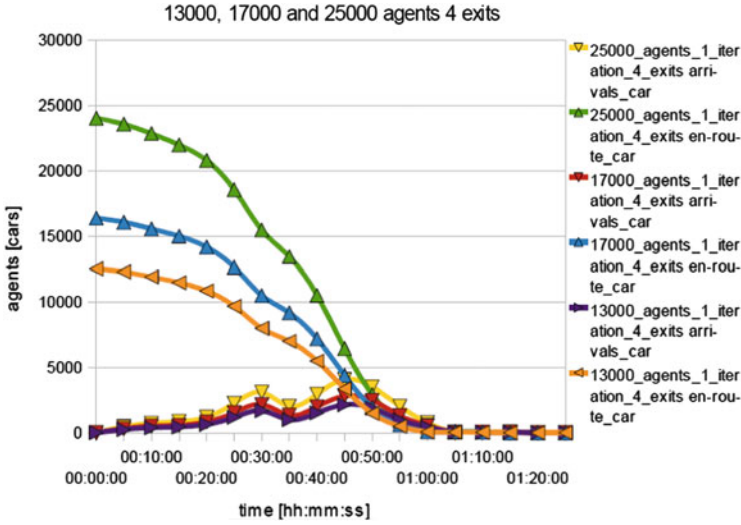


Fig. 6 Simulation with 13,000, 17,000 and 25,000 agents

6 Interpretation of Results

The results themselves do not contain information about which strategy is the best to prepare for a flooding, to increase the coping capacity, or decrease vulnerability (Fig. 6). These strategies have to be developed by the persons responsible for disaster preparedness, i.e. by the civil protection authorities.

This is only part of the solution. Preparedness and coping capacity are based on the individual preparation and resources. As can be seen from Fig. 5, the time frame determined by the simulation is sufficient. RSET was estimated to be less than 4 h. The plan for ASET shows an available time of 3 h plus 1 h buffer. Therefore, the condition $RSET < ASET$ holds and safe evacuation is possible. We emphasize the fact that the assumptions for determining RSET were all taken to err on the safe side. Most of all, the total number of evacuees was to be 50,601, i.e. the total population number.

7 Summary, Conclusion, and Outlook

In this paper we have presented simulation results for the evacuation of Hamburg Wilhelmsburg. The scenario was the flooding after dyke damage. The simulation results were obtained by the Multi-Agent Transport Simulation MATSim. The overall result is: **ASET < RSET. Therefore, the current evacuation plan is sufficient.**

There are a few questions that should be researched in further works. Is the result of the exercise done in Cologne valuable that only 20 % of the space in busses and trains could be used for the evacuees, because of the bulky luggage they carried with them? What about persons with special needs, elder and disabled persons, and children and so on? Are the specific plans correct and practicable?

These results will be transferred to other cities in Germany within the research project GRIPS, Gis-based Risk assessments, information, and Planning System.

References

1. Birkmann, J. (2006): Measuring vulnerability to promote disaster-resilient societies: Conceptual frameworks and definitions, In: *Measuring Vulnerability to Natural Hazards – Towards Disaster Resilient Societies*, edited by: Birkmann, J., New York, UNU, 9–54, 2006.
2. Durst, D. (2010): Thesis: Large-scale Multi-Modal Evacuation Analysis with an Application to Free and Hanseatic of Hamburg, Hamburger Fern-Hochschule (HFH), URL: <http://www.traffgoht.com/downloads/research/studies/Durst2010.pdf>
3. Freie und Hansestadt Hamburg, Behörde für Inneres und Sport (2010): Sturmflutbroschüre, URL: <http://www.hamburg.de/contentblob/569738/data/sturmflutbroschuere.pdf>
4. Freie und Hansestadt Hamburg, Behörde für Inneres und Sport (2010): Sturmflutmerkblatt Wilhelmsburg, URL: <http://www.hamburg.de/contentblob/562890/data/-sturmflutmerkblatt-wilhelmsburg-2008.pdf>
5. Lämmel, G., Nagel, K. (2008): Working paper: Multi agent based large-scale evacuation simulation, TU Berlin <http://preview.tinyurl.com/d7snfsk>
6. Nagel, K. et. al. (2010): MATSim - Multi-Agent Transport Simulation Toolkit, TU Berlin und ETH Zürich, URL: <http://www.MATSim.org/> [accessed: 03.03.2010]
7. Taubenböck, H. et al. (2009) Final report Last Mile – Numerical Last-Mile Tsunami Early Warning and Evacuation Information, ISSN 1619-7399, Geotechnologien Science Report, Helmholtz-Zentrum, Potsdam

Measuring Individual's Egress Preference in Wayfinding Through Virtual Navigation Experiments

Jan Dijkstra, Qunli Chen, Bauke de Vries, and Joran Jessurun

Abstract There is an underestimation of the influence of architectural information on individual's navigation in the built environment. In the presented studies, an experiment was conducted where participants were asked to choose their preferred egress in a list of specially designed isolated virtual convex rooms with only visual architectural cues provided. With data collected from the experiment, variable levels influencing individual's decision making on the egress were analyzed. The findings indicate that individuals tend to choose brighter and wider egress, especially brighter and wider corridors in wayfinding.

Keywords Egress preference • Wayfinding • Virtual navigation

1 Introduction

Finding one's way to a certain destination is one of the most compulsive behaviors in our daily life. This has been extensively studied in the last 50 years. Originally raised by Lynch [1], the term "wayfinding" is defined by Golledge [2] as "the process of determining and following a path or route between an origin and destination." Arthur and Passini [3] suggest that different types of information can be used in wayfinding tasks, namely the verbal (information obtained from the reception, staff members, etc.), the graphic (map of the environment, signage showing the location or pointing to certain location, etc.), the architectural (e.g. doors, corridors, texture, elevators) [4, 5], and the spatial (spatial relationship of objects in the environment) [6, 7]. The significance of these types of information on wayfinding processes has been investigated. In most studies, however, the function of the architectural

J. Dijkstra (✉) • Q. Chen • B. de Vries • J. Jessurun
Design Systems Group, Eindhoven University of Technology, Eindhoven, The Netherlands
e-mail: j.dijkstra@tue.nl; q.chen@tue.nl; b.d.vries@tue.nl; a.j.jessurun@tue.nl

information was underestimated compared to other types of information – it was often treated as limiting the architectural space.

In reality, human feelings about the color of an object are influenced by different factors, such as the physical condition of the object, the color contrast between the object and its background, our mental state at that moment, etc. Moreover, different colors have a different psychological effect for different people. In this study, a greyscale model is applied to describe this psychological effect. Therefore, egress choices are only influenced by grey contrast between egresses, and between the egress and its background.

In this paper, a study will be presented where subjects' egress choices are collected given different settings of selected egresses (door or corridor) in a list of architectural spaces. In this context architectural spaces are independent spaces with only visual architectural information provided. The main objective of this study is to research the utility effect of variables that would influence individual's egress choices in architectural spaces. The *utility effect* is defined as the contribution of part-worth values of variable levels. Moreover, it is assumed that a preference function can be deduced to predict the probability of an individual to choose the left egress of the egresses pair (left, right) in architectural spaces.

This paper focuses on the individual's egress choosing behavior in the built office environment. Note that “*egress*” mentioned in this paper is specified as a linkage between rooms, or a linkage between a room and a space, rather than the linkage between a built environment and the world outside of this built environment.

This paper gives in Sect. 2 a brief description about architectural cues in wayfinding. Section 3 provides the experimental design, and Sect. 4 presents the results of the experiment. A discussion about the conclusions and future directions will conclude this paper.

2 Architectural Cues in Wayfinding

In built environments are different kinds of designed cues. When people interact with the environment, they perceive information and acquire knowledge from surrounding spaces. Therefore, these cues are important for individual's perception of the built environment. Based on investigation on various visual cues that would be acquired from surrounding spaces in the context of wayfinding, Rapoport [8] summaries these visual cues into three categories with clearer framework, namely Non-fixed cues, Semi-fixed cues, and Fixed-cues. Non-fixed cues are defined as pieces of information that can be perceived from dynamic objects (e.g. interaction between humans). Located in the built environment, Semi-fixed cues are some special objects that can be reconstructed with ease. Objects like maps, signs, and different decorations are semi-fixed cues. These cues will provide information on egress direction in the built environment. The last cue category, the Fixed-cues, also offer information on egress direction in the built environment. However these cues are part of the built environment and thus they are difficult to be reconstructed.

A Fixed cue is also called architectural cue, and according to Passini's argument on wayfinding strategies [7], it can be divided into the categories global architectural cue and local architectural cue.

Global architectural cues can be perceived from building forms, and these cues provide information on the spatial relationships between different parts of the built environment. Four types of sources in the built environment can provide global architectural information: the circulation system, the exterior form of the building, the visible structural frameworks, and the atrium. An individual will have certain familiarity of the built environment when he perceives the global architectural cues. Based on his familiarity of the entire environment, he could split the wayfinding task into sequential parts. In other words, the individual could plan his wayfinding when he perceived global architectural cue of the built environment.

Local architectural cues however, are perceived from the abstract three-dimensional geometric features of the local architectural elements (e.g. stairs, entrances, corridors, etc.) in the built environment. Sun [9] summaries four sources where local architectural cues can be obtained in a built environment: the characteristics of the architectural element in the circulation system, the feature of distance from the architectural elements to the individual, the feature of the scale of the architectural element, and the feature of the angular position of the architectural elements in the individual's view.

3 Design of Experiment

In this section, we start with the discussion of the approach. Then, we will discuss the left egress probability and the data collection effort.

3.1 Approach

The study focuses on the individual's egress choosing behavior in the built office environment. After a study on the egress types in the office environment, two common used egresses are selected for the experimental design: *door* and *corridor*. In addition, three different sizes are designated for each assigned egress referred to as narrow (80 cm by 200 cm), normal (150 cm by 200 cm), and large (194 cm by 246 cm).

Four characteristics are identified for these two egress types, which could influence visitor's choice on the egresses, resulting in four variables for designing the rooms in the experiment: the distance from the egress to the entrance point (D), the width of the egress (W), the grey level of the egress (G), and the angle between the view direction and the egress in the view (A). Table 1 shows these attributes and their corresponding levels of the egresses in the designed rooms. In our experiment, the grey level of an egress was computationally defined, ranging

Table 1 Variable attributes and attribute levels of the egresses in the experiment

	Grey level	Angle (degree)	Distance (m)	Width (cm)
Door	25,50,75	10,20,30	7,15,25	80,150,194
Corridor	25,50,75	10,20,30	7,15,25	120,190,280

**Fig. 1** Three types of rooms in the experiment: door and corridor, two doors, and two corridors

from 0 to 100, indicating the brightness of the grey of the egress. The change of room illumination in the virtual built environment would affect the grey level of the egresses. The higher the grey level of an egress, the brighter of the egress's grey will be.

The type of room is another related variable, which is also taken into account in the experimental design phase. In the experiment, each designed room consists of two egresses. As a result, there are three types of room layouts: a room with two corridors, a room with two doors, and a room with a door and a corridor. This result is shown in Fig. 1.

The designed rooms are of three different sizes, namely small (4 m by 6 m), medium (9 m by 12 m), and large (15 m by 20 m). Each designed room contains two egresses: one on the left, and one on the right. The orientations of the egresses in these rooms vary systematically. Furthermore, the aspect ratio of the screen is preset such that the application (the experiment is VR application based) could be run on any computer with the same aspect ratio. Based on the variable attribute levels of the egresses and types of the rooms, fractional factorial design is employed to determine the number of convex rooms that is required for the experiment. We found a minimal number of 81 rooms should be designed: each room in the experiment was a unique combination of the variable attributes of the egresses and the room types. These 81 convex isolated spaces with different sizes were rendered by Vizard, a versatile reality development interface.

The sequential order of the rooms presented in the experiment is randomly generated for each subject once they start the experiment. In this experiment, as long as one subject chooses an egress in the current room and within a certain distance to the chosen egress, the next room would be generated and linked to the chosen egress automatically according to the generated sequential order of the rooms for this subject. In other words, each subject has to make 81 decisions on the egress

pairs in total and subject’s egress choice in the current room has no consequence on the room linked to the chosen egress.

3.2 Egress Preference

Within the discrete choice framework, the subject’s decision can be described as a choice between two options: choose the left egress or not choose the left egress (choose the right egress). In this paper, we look at the utility of choosing the left egress, the left egress probability (p^{left}) and then estimate the parameters of the variables included in the utility of choosing the left egress (v^{left}). Equation 1 shows the left egress utility:

$$v^{left} = \beta_0 + \sum_{i=1}^4 \beta_i c_i + \sum_{j=1}^2 \beta_j s_j \tag{1}$$

where:

β_0 is the parameter for the intercept,

β_i is the parameter for the variable c_i ,

c_i indicates the variable of the egress preference (Width, Distance, Angle, Grey level),

β_j is the parameter for the variable s_j ,

s_j indicates the individual’s characteristics (Age and Gender).

Equation 2 shows the probability of choosing the left egress, Eq. 3 shows the probability of not choosing the left egress, and Eq. 4 shows the binary logit model for estimating the parameters.

$$p^{left} = \frac{\exp\left(\beta_0 + \sum_{i=1}^4 \beta_i c_i + \sum_{j=1}^2 \beta_j s_j\right)}{\exp\left(\beta_0 + \sum_{i=1}^4 \beta_i c_i + \sum_{j=1}^2 \beta_j s_j\right) + 1} \tag{2}$$

$$p^{null} = \frac{1}{\exp\left(\beta_0 + \sum_{i=1}^4 \beta_i c_i + \sum_{j=1}^2 \beta_j s_j\right) + 1} \tag{3}$$

$$\ln\left(\frac{p^{left}}{p^{null}}\right) = \beta_0 + \sum_{i=1}^4 \beta_i c_i + \sum_{j=1}^2 \beta_j s_j \tag{4}$$

In this paper, we are interested in the utility effect of the variable levels, namely the levels as indicated as attribute levels for the variable attributes *width*, *distance*, *angle* and *grey level* in the previous mentioned Table 1 for the variables *door* and *corridor*. That means, we are interested in the part-worth values of the attribute levels, Using binary logistic regression and the use of dummy coding for the respective levels of the variable attributes we can estimate their utility effect. This will be performed for male and female group in different types of room. The next section describes the collection of the necessary data.

3.3 Data Collection

This experiment was conducted in Jiangyin in China by 102 participants. These participants are the subjects in this experiment. Most of them were working in the same office building, and their ages ranged from 13 to 54 years ($Mean = 31$). With 60 males and 42 females, all these subjects had normal or corrected-to-normal (with glasses) vision.

In this experiment, subjects were asked to sit 30 cm in front the monitor screen, and then run the VR application. The English interpretation of the task information presented on the monitor screen in the experiment was as follows:

In this experiment, we assume that you are heading for an interview in a new building. There are a set of rooms in this experiment. Each room is an experiment on its own with no relationship to previous rooms. As long as you enter a room you will see two possible egresses (linkage between rooms, or linkage between a room and a space). You need to choose an egress that will most likely lead you to the interview room. At the end of the experiment, you will see a message 'Congratulations, this is the end'. You are in a hurry; therefore you cannot spend too much time in each room and must make your decision intuitively. You can use the mouse or arrow keys to navigate in the rooms.

In the experiment, each room had a unique entrance, which was fixed at the middle of an empty wall. The middle line of the entrance in the current room was linked to the middle line of the egress chosen in previous room. As a result, each time a participant stepped into a new room, the start position of this subject was the midpoint of the entrance in the new room. From this position, both egresses in the new room would fall into the view angle range of this subject. Thus, subjects could quickly make a decision on the egresses, rather than spending additional time to figure out the locations of the egresses in the new room. Furthermore, subjects could not turn back and change their choice.

The subjects were aware that they would go through a total number of 81 rooms and in each of these rooms they would choose an egress based on the visual architectural cues perceived in the current room. Furthermore, they were clear that in each room they should choose an egress that holds the highest probability to bring them to the destination according to their feelings based on the perceived information. Before the experiment, subjects were instructed on how to navigate in the virtual environment using the mouse or arrow keys prior to their participation in

the experiment. However, a number of subjects could not get used to the navigation in the application due to their lack of experience of navigating in a 3D virtual environment. As a consequence, they were asked to sit in front of the monitor screen, and make the decision on the egresses in each room, while the navigation through the virtual environment was operated by the author.

Apart from the issues mentioned above, some other small factors, such as the various subjects' eye heights when they were sitting in front of the monitor, and the time each subject took to get used to the virtual environment, can influence their choice made in each room. These effects were reduced by adjusting seat height and assigning more time on navigation in a similar virtual environment before the experiment for each subject.

4 Analysis of the Experiment

In this section, we will report the utility effect of the variable attributes (the distance from the egress to the entrance point, the width of the egress, the grey value of the egress, and the angle between the view direction and the egress in the view) for male and female group in different type of the room by using binary logistic regression in SPSS.

Table 2 shows the estimation results of the respective attribute levels for the variable attributes for male and female and the different room types (corridor-corridor, door-corridor, and door-door). It is striking that almost all cases, the grey level is significant at 0.05 level ($\alpha \leq 0.5$). Further, it is striking that all attribute levels for the variable attribute Angle have no significance.

Figure 2 shows the utility effect of the variable *Distance* for male and female in different types of the room. In these figures the utility effect of 25 m is set as the reference base. It shows that, in a corridor-corridor room, the utility effect of Distance (relative to 25 m) for female is larger than for male. The utility effect of 15 m is much larger than the utility effect of 7 m for both genders. This indicates that, in a corridor-corridor room, the medium distance to the egress is more preferred over the short and large distance to the egress, regardless of the gender. In the case of the utility effect of the variable attribute *Distance* (relative to 25 m) in a door-corridor room, given different gender, the utility effect of 15 m is higher than the utility effect of 7 m for male. However, the utility effect of 15 m is lower than the utility effect of 7 m for female. In other words, in a door-corridor room, males tend to choose the egress with medium distance to the entrance, while females would like to choose the egress with the short distance to the entrance. By comparing the total utility effect (utility effect including male and female) of *Distance* (relative to 25 m), the total utility effect of 15 m (0.087) is higher than the utility effect of 7 m (0.058). In a door-door room, the utility effect of the variable *Distance* (relative to 25 m) shows that males will tend to choose the door with the long distance to the entrance in the office environment. By contrast, females will choose the door with

Table 2 Estimation results of the variable attributes and their attribute levels of the egresses in the experiment

	Corridor-corridor		Door-corridor		Door-door	
	Female		Male		Female	
	β	Sig.	β	Sig.	β	Sig.
Distance						
7 m	-.001	.992	.058	.701	.002	.988
15 m	.155	.209	.323	.031*	.134	.280
Grey level						
25	-.048	.703	-1.075	.000*	-.250	.044*
50	-.229	.062	-.810	.000*	-.288	.020*
Angle						
10°	-.150	.219	.040	.791	-.174	.158
20°	-.104	.409	.268	.072	-.078	.531
Width						
80 cm					-.467	.007*
150 cm					-.213	.499
194 cm					-.461	.226
120 cm	-.599	.000*	-.379	.013*	-.118	.590
190 cm	-.088	.476	-.014	.928	-.093	.008*

*Significance at 0.05 level

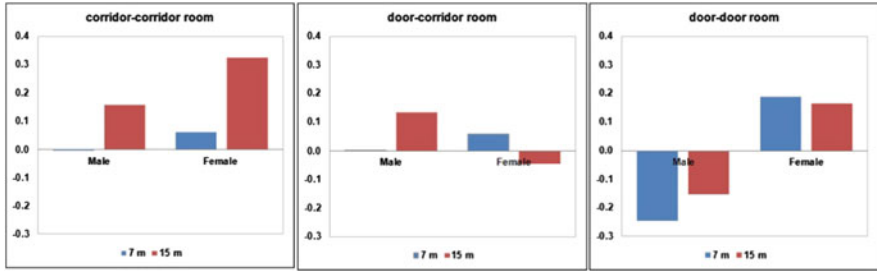


Fig. 2 The utility effect of the variable *Distance* for male and female group with the reference base of '25 m' for the corridor-corridor, door-corridor and door-door room respectively

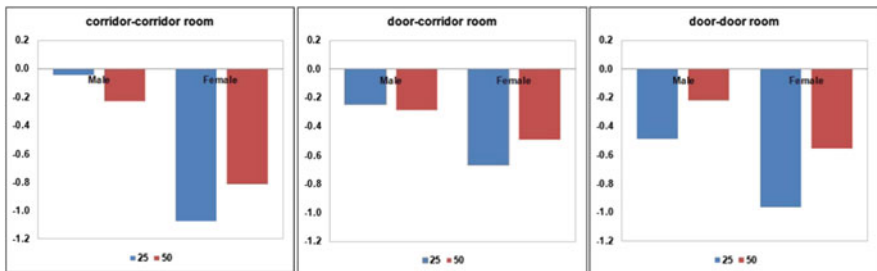


Fig. 3 The utility effect of the variable *Grey level* for male and female group with the level reference base '75' for the corridor-corridor, door-corridor and door-door room respectively

the short or medium distance to the entrance. Moreover, the total utility effect of 15 m (0.013) is higher than the total utility effect of 7 m (-.059).

The utility effect of the variable attribute *Grey level* in different room types with gender difference are presented in Fig. 3. In this figure we can find that the total utility effect is higher for the brighter egress (Grey level = 50). In other words, the bright egress is preferred by most of the subjects. In addition, the total utility effect of Grey level increases as we raise the grey value of the egress. Further, it is remarkable that this effect is stronger for the door-door type of room.

Next, we will look at the utility effect of the variable attribute *Angle* for male and female in different types of room. Figure 4 shows the utility effect of Angle (relative to 30°) in different types of room for different gender groups. It is striking that for the room types corridor-corridor and corridor-door the female group has the highest utility effect. Her utility effect is exactly opposite for the door-door room type. This indicates that, when the egress types in current room are different, females will tend to choose the egress with narrow angle, and males prefer the egress with broad angle.

This figure also shows the utility effects for different angle levels in a door-door room for both genders. The utility effect of 10° and 20° for males are higher than zero, the utility effect of 10° and 20° in a door-door room for females are lower than zero.

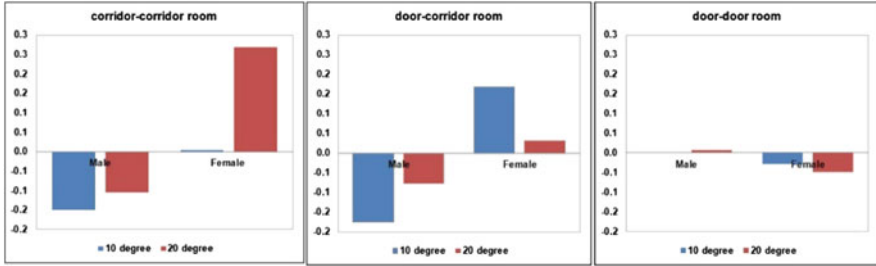


Fig. 4 The utility effect of the variable *Angle* for male and female group with the reference base '30 degree' for the rooms corridor-corridor, door-corridor and door-door respectively

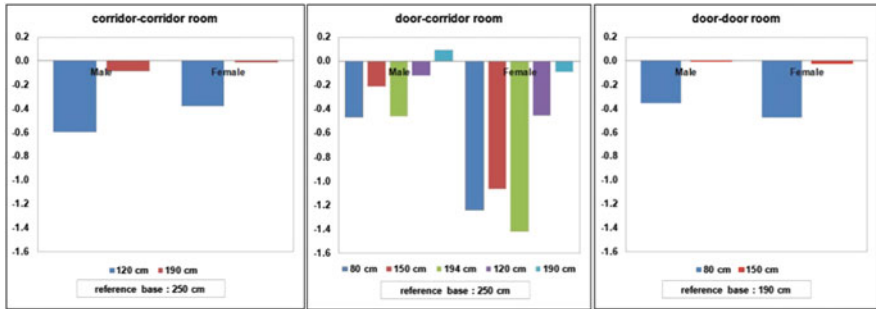


Fig. 5 The utility effect of the variable *Width* for male and female group for the room types corridor-corridor, door-corridor and door-door respectively

The last variable that we will analyze is the variable attribute *Width* of the egresses. In our experiment, each egress type has three levels of width. As a consequence, in a door-corridor room, there are six levels of width. For all presented plots in Fig. 5 on the utility effect of the attribute *Width*, the possible largest width in the room is applied as the reference base. In the corridor-corridor room type, 250 cm has the highest utility effect for both genders. Besides, the narrowest corridor level (120 cm) holds the lowest utility effect for both genders. It is clear that subjects have a favor of wider corridor. For the corridor-room type, 80, 150 and 194 cm are the three width levels for door, and 120, 190 and 250 cm are the three width levels for corridor. It is obvious that female's tendency to choose door is less the male's, given the fact that the utility effect of 80, 150 and 194 cm (relative to 250 cm) for female are lower than for men. In the case of a door-door room type, the utility effect of 80 cm has large negative values for both gender, compared with the utility effect of 150 cm and the utility effect of 190 cm (the reference base). Moreover, the utility effect difference between 150 cm and the reference base 190 cm is relatively small for both genders. In general, the narrow width door is the last choice for most of the subjects.

5 Discussion

Our primary motivation for this study was to find out how individuals would make their choices in a built environment with only visual architectural cues provided when they visited the space for the first time. As a consequence, in our experiment, our subjects' decisions on the egresses were purely based on the visual architectural cues they perceived of the built environment.

In the result session, figures are plotted of the utility effect of the attributes (the distance from the egress to the entrance point, the width of the egress, the grey value of the egress, and the angle between the view direction and the egress in the view) for male and female group in different type of the room. From these figures, we find that gender difference and type of the room have significant influence on the utility effect of the attributes. The average utility effect of the attributes reveal that the average utility effects of the medium Distance (15 m), the brighter Grey (75), and wider Width (250 cm for the corridor, and 190 cm for the door) have the highest values in all types of rooms. In other words, majority have a preference on wider egresses, medium distance to the egresses, and brighter egresses. Additionally, doors are less preferred over corridors.

In recent years, Sun [9] researched the influence of the attributes that effect human choice on the architectural cues in the underground space, and concluded that distance from the egress to the observation point had a higher weight than the width of the egresses on influencing individual's choice in a exit-exit room, and egress width would have higher significance than the distance from the egress to the observation point in a corridor-corridor room. Furthermore, egress with larger width and shorter distance to the observation point was in favor of more subjects. We had some expectations based on Sun's findings before our experiment: egresses with shorter distance to the entrance, and egresses with larger width would be preferred by the majority. Furthermore, we expected that most of the subjects would choose the relatively brighter egresses, regardless of their gender.

In contradiction to our expectation, the average utility effect of short distance (7 m) is lower than the average utility effect of medium distance (15 m) in all types of rooms based on the data from our experiment. This could due to the different virtual environmental settings between our experiment and Sun's experiment. In our experiment, our subjects navigated in a virtual office environment, where the room sizes would be much smaller than the room sizes in the underground space. Although the physical performance of the subjects in both experiment were of little difference, the attribute Distance (D) was of different utility effect.

Our analysis also reveals subjects' preference on the wider egresses, which consistent with our expectation. However, when there are a door and a corridor in current room, the subjects, especially females, tend to choose the corridor other than the door, even though the door is wider than the corridor. One explanation could reside in the individual's uncertainty of the egress behind. When the individuals are not sure whether the destination is behind the egress, they would prefer to choose

the corridors: at least certain information of the next room can be perceived when they stand before the corridors.

Analysis of the attribute grey value of the egress (G) shows that brighter egress is preferred by a large number of the subjects. One possible explanation is that when we assign different grey value to the egresses, these egresses would have different meanings: darker egress is likely linked to insignificant destination in the environment and brighter egress might relate to a frequently used destination.

Compared with previous researches in wayfinding, gender difference in our research is not related to spatial ability: our subjects made a decision on the egresses in each room, however their decisions could not be used for configuration of their position in the virtual environment due to the isolation of each room in the experiment. Gender difference in our research reflects the individual's preference on the egresses given various combination of different attributes. Our analysis shows dark egresses and narrow egresses have significant negative utility effect on female's decision making.

6 Conclusion

Unlike past researches, our study focuses on the influence of visual architectural cues in the built environment on wayfinding. From the analysis one can conclude that visual architectural information has a significant utility effect on individuals' behaviors. Given diverse wayfinding tasks in the built environment, attributes forming architectural information are of different utility effect on individual's choice making. In general, wider and brighter egresses, especially wider and brighter corridors, are in favor of most people. If the wayfinding goal is to find certain destination in the built environment, medium distance to the egress has the highest average utility effect; in contrast, egresses with short distance to the observing point are preferred when the wayfinding goal is to get out of the built environment in a short time, especially in evacuation. Furthermore, gender difference has certain indispensable effect on individual's decision making.

In our further research, a preference function with the width of the egress, the distance from the egress to the entrance point, the angle between the view direction and the egress in the view, the grey value of the egress and the gender of an individual as input will be deduced to predict this individual's choice of egress given different types of rooms in a built environment with only visual architectural cues provided. The simple egress types in isolated convex rooms in our experiment did not represent the real world built environment. It is unclear whether room types in reality will yield different outcomes. However, our deduced preference function will provide basic indications for architects on what kind of egresses will attract more individual's attention during their wayfinding process in the reality.

References

1. Lynch K.: *The Image of the city*. London: Harvard University Press (1960)
2. Golledge R.G.: *Human Wayfinding and Cognitive Maps*, in *Wayfinding behavior: Cognitive Mapping and other Spatial Processes* R.G. Golledge, Editor. The Johns Hopkins University Press. 5-45 (1999).
3. Arthur P. and Passini R.: *1-2-3 Evaluation and Design Guide to Wayfinding*. Ottawa (1990)
4. Passini R.: *Wayfinding Design: Logic, Application and some Thoughts on Universality*. *Design Studies*. **17**(3): 319-331 (1996)
5. Dogu U. and Erkip F.: *Spatial Factors Affecting Wayfinding and Orientation*. *environment and behavior*. **32**(6): 731-755 (2000)
6. Arthur P. and Passini R.: *Wayfinding: people, signs, and architecture*: McGraw-Hill Companies (1992).
7. Passini R.: *Wayfinding in architecture*. *Environmental Design*. Vol. 4: John Wiley & Sons Inc. (1984)
8. Rapoport A.: *The meaning of the Built Environment - a Nonverbal communication approach*. London: Sage (1982)
9. Sun C.: *Architectural cue model in evacuation simulation for underground space design.* Thesis, Eindhoven: Technische Universiteit Eindhoven (2009)

Modelling Evacuation Using Escalators: A London Underground Dataset

Michael J. Kinsey, Edwin R. Galea, and Peter J. Lawrence

Abstract This paper presents a brief analysis of an escalator human factors dataset collected in a London Underground (subway) station in England. The data analysis highlights and quantifies a variety of escalator human factors. Using the buildingEX-ODUS evacuation software, a series of evacuation scenarios of a hypothetical underground station are then presented. The simulation results demonstrate that escalator strategies and associated human factors can have a considerably influence upon an evacuation compared to using stairs alone.

Keywords Escalator • Evacuation • Modeling • Pedestrian • Human factors • Underground • Subway • Transit station

1 Introduction

The development and expansion of underground (subway) stations, often located deep underground, has been possible with the introduction of escalators capable of efficiently transporting large volumes of people [1]. As a result, underground stations are reliant upon escalators for circulation and in many cases emergency evacuation. Despite this, few studies have attempted to quantify human factors associated with escalator usage (microscopic analysis), the majority of past studies focusing on establishing capacity (macroscopic analysis) rather than usage behaviours [2–4].

As such, it is uncertain how human factors associated with escalator usage impact escalator performance in both circulation and evacuation situations. It is also uncertain whether human factors associated with escalator usage has a cultural

M.J. Kinsey (✉) • E.R. Galea • P.J. Lawrence
Fire Safety Engineering Group, University of Greenwich, Greenwich, UK
e-mail: m.j.kinsey@gre.ac.uk; e.r.galea@gre.ac.uk; p.j.lawrence@gre.ac.uk

component. To address these issues, escalator human factors data within three underground station environments in Spain (Barcelona) [5], China (Shanghai) [6] and England (London) have been collected. In each location the same methodology for data collection and analysis was used. This paper presents an overview of the analysis for the London dataset. This data has been implemented within the buildingEXODUS escalator model [7]. In addition, a series of evacuation scenarios has then been simulated using the buildingEXODUS evacuation software [7]. These explore the influence of the escalator human factors and operational strategies upon an evacuation.

2 Data Collection

The data was collected in the Paddington Underground station in London, England. The station links the underground rail network to the mainline national rail services and also forms part of the Heathrow airport express/connect coach service. In addition, it links four underground tube lines (Bakerloo, Circle, District, and Hammersmith & City). As such many commuters and international travellers pass through the station every day. The footage of two adjacent escalators and an adjacent stair was collected over a period of 2 days. The escalators were moving in opposite directions. Each escalator had a vertical drop of 3.65 m with a horizontal length of 8.78 m and horizontal speed of 0.5 m/s. The adjacent three lane stair (separated by two hand rails) comprised of two flights connected via a single landing (see Fig. 1). The escalators/stair linked the ticket hall level of the underground station to the adjoining mainline railway station platform level.

Data was collected via video footage in approximate 20 min segments during the morning rush-hour, afternoon non-rush hour and evening rush-hour for 2 days ($2 \times 3 \times 20 = 120$ min of footage).

3 Data Analysis

The following section presents a brief overview of the data analysis. In total, 11,019 pedestrians were recorded: 6,123 on the escalators and 4,896 on the stair. More males (59.3 % (3,629)) than females (40.7 % (2,494)) were observed using each escalator.

3.1 Escalator/Stair Usage

Combining the data from the three measurement periods, the majority of pedestrians travelling in the up direction elected to use the escalator (67.0 %) compared the adjacent stair ($\chi^2 = 620.0$, $p < 0.05$). However, in the down direction the majority

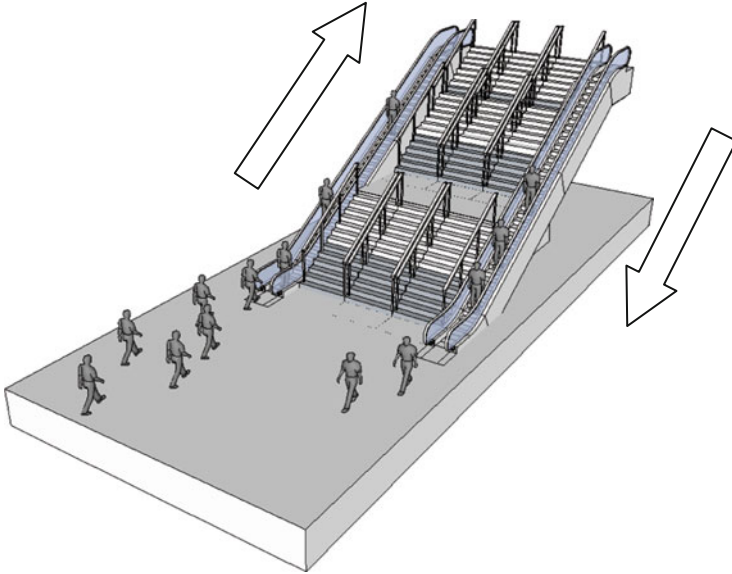


Fig. 1 Escalator/stair configuration (not to scale)

of pedestrians elected to use the adjacent stair (55.3 %) ($\chi^2 = 63.0$, $p < 0.05$). Considering each period separately, in the morning, the overall trend of the escalator being more preferential in the up direction (75.3 %) ($\chi^2 = 539.1$, $p < 0.05$) and stair in down direction (64.0 %) ($\chi^2 = 63.0$, $p < 0.05$) was also observed. However, during both the afternoon and evening periods, the escalator was the most preferred device irrespective of direction (afternoon (65.9 %): $\chi^2 = 105.2$, $p < 0.05$, evening (53.7 %): $\chi^2 = 4.6$, $p < 0.05$). Overall, the results highlight that the escalator was the most used device in all time periods for both directions with the exception of the morning down direction.

3.2 Walker/Rider Usage

Of the 6,123 escalator users recorded, the majority rode the escalator (74.9 %) with the remaining electing to walk. Significantly more males (29.2 %) elected to walk compared to females (19.3 %) ($\chi^2 = 77.0$, $p < 0.05$). There was a significant difference between the number of walker/riders in each period ($\chi^2 = 1.8$, $p < 0.05$). Regardless of direction, in the evening periods there were significantly more walkers (21.0 %) than in the afternoon periods (15.6 %) ($\chi^2 = 16.3$, $p < 0.05$). In the morning periods there were significantly more walkers (33.5 %) than in the afternoon ($\chi^2 = 147.9$, $p < 0.05$) and evening periods ($\chi^2 = 91.404$, $p < 0.05$).

Overall there were approximately the same proportion of walkers for both the up (25.2 %) and down (25.1 %) directions ($\chi^2 = 0.03$, $p > 0.05$). Considering time period, this trend continued for the morning periods where a similar proportion of walkers for both the up (34.5 %) and down escalator (32 %) ($\chi^2 = 1.8$, $p > 0.05$) was observed. Similarly for the afternoon periods there was a comparable proportion of walkers for both the up (15.3 %) and down escalator (15.9 %) ($\chi^2 = 0.09$, $p > 0.05$). However, during the evening significantly more walkers were observed on the down escalator (23.6 %) than on the up escalator (19.1 %) ($\chi^2 = 5.8$, $p < 0.05$).

The results show that time period influences the proportion of walkers/riders. Pedestrians during the rush-hour periods appear more motivated (reflected in the higher proportion of walkers) than during the non-rush hour periods. The combination of time period and direction of travel only appeared to influence the proportion of walkers/riders in the evening. Here significantly more walkers were recorded in the down direction.

3.3 Side Usage

Analysis of the side usage data identified that there was a common side preference for riders to typically use the right side (88.4 %) and walkers to use the left side (78.2 %) of each escalator ($\chi^2 = 5,853.6$, $p < 0.05$). This trend was more strong for the up direction ($\chi^2 = 4284.5$, $p < 0.05$) (91.6 % riders right/82.9 % walkers left) than in the down direction ($\chi^2 = 1699.9$, $p < 0.05$) (83.7 % riders, right/71.4 % walkers left). This suggests that those on the up escalator conformed more to the common side preference behaviour than those on the down escalator. This may be due to more pedestrians typically simultaneously using the escalator in the up direction. In turn this may have prompted more pedestrians to conform to either riding on the right side or walking on the left side through not wanting to inconvenience other escalator users.

3.4 Walker Speeds

In total 810 escalator walker speeds were recorded. The walker speeds were calculated using the horizontal distance travelled and represent the relative speed that pedestrians walked in relation to the escalator (i.e. do not include the escalator speed). A large majority of walkers were male (70.7 % (572)). More walkers were observed in the morning (54.3 % (441)) and evening (32.2 % (261)) than in the afternoon (13.4 % (108)). Overall average walker speeds were faster in the down direction (0.82 m/s) than in the up direction (0.70 m/s) ($p < 0.05$). On average males walked 13.33 % (0.1 m/s) faster than females ($p < 0.05$). There was no significant difference between walker speeds between each period ($p > 0.05$). The

results suggest that gender and direction of travel influence escalator walker speeds; however, time period does not.

3.5 *Flow-Rates*

The maximum escalator flow-rate was 75 ped/min in the up direction during the morning rush-hour period. During this period pedestrians moving in the up direction were funnelled into using the escalator due to the adjacent stairs being crowded with pedestrians moving down in the opposite direction. As such, pedestrians moving in the up direction had little choice to use the adjacent stair. During this peak-flow rate period there were a high proportion of riders (68 %) with approximate even usage of both the left and right side of the escalator: each side was fully utilised. A slightly higher proportion of males (62.8 %) were also recorded during this period. The majority of pedestrians (60.7 %) carried items of luggage during this period. However, most were small items (i.e. only a rucksack (26.0 %) or only a handbag (20.8 %)). As such it is expected that this did not contribute to decreasing the flow-rate.

4 Evacuation Simulations

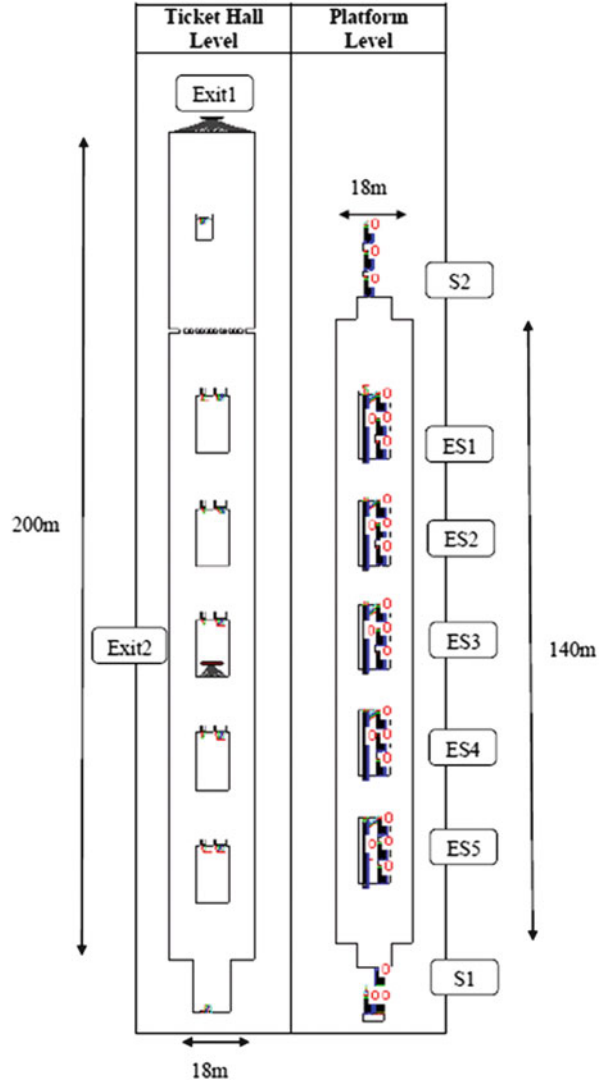
A series of evacuation scenarios have been performed using the building EXODUS evacuation software [7]. This software includes an escalator and associated agent model which have been described in other publications [6–8]. A description of the geometry, escalator attributes, population and scenarios are presented followed by the simulation results.

4.1 *Geometry*

The building used for the simulations was a hypothetical underground station (see Fig. 2).

The geometry consisted of two levels. The lower level contained a double-sided platform below ground connected via five escalators, each with adjacent stairs, to a ticket hall level above. The ticket hall level is where the exits of the station are located. In addition, an emergency stair was positioned at either end of the platform. The platform was 18 m wide and approximately 140 m long. Each escalator/stair enclosure linking the platform to the ticket level was approximately 7.5 m in width and 15 m in length. The total area of the platform was 2,407.5 m². Each escalator had a width of 1.0 m, height of 6.29 m and horizontal length of 15.5 m with a horizontal speed of 0.5 m/s. Each stair had a width of 2.3 m, height of 6.29 m and

Fig. 2 Hypothetical underground station geometry (ES escalator/stair, S stair)



horizontal length of 13.62 m; consisting of three flights of stairs connected via two landings.

The geometry had two exits (Exit 1 and Exit 2) both located on the ticket hall level (see Fig. 2). Exit 1 was 18 m in width and Exit 2 was 7 m in width, both representing an open plan exit without doors. The maximum travel distance to Exit 1 and 2 was 67.3 m and 68.3 m respectively from the platform level.

4.2 Population

Within each scenario agents were modelled as non-connected individuals and were not constrained by groups. The demographics of the agent were assigned according to the default population within buildingEXODUS, representing a broad cross-section of attributes and capabilities [7]. The default stair walker speeds used in buildingEXODUS [7] were derived from those collected by Fruin [9]. The escalator walker speeds used in the scenarios were derived from the London Underground dataset (see above).

The NFPA 130 Standard for Fixed Guideway Transit and Passenger Rail Systems 2010 [10] includes recommendations for maximum occupancy levels within train stations. It states that the maximum agent load for a train station shall be based on trains simultaneously arriving at each platform within a station plus the simultaneous arrival of individuals entering the station for each train during peak times. The 1996 Rolling Stock 7 car design (currently used on the Jubilee line in the London Underground) spans a length of approximately 124 m which is similar to the platform length in the hypothetical geometry. Such trains allow a maximum train capacity of 964 passengers (234 sitting, 730 standing) [11].

In addition to representing occupants simultaneously arriving on trains at each platform, those occupants that would already be waiting on each platform was also represented. The platform waiting occupancy has been proposed to be 50 % of the maximum train capacity. In the given geometry this equates to $2 \times 482 = 964$ agents (for two trains on either side of the platform). This waiting occupancy frequency is considered to be the upper limit of the maximum platform occupancy. All occupants initially on the platform level were assumed to be located on the platform itself and no representation of occupants disembarking trains is represented. Combined with the maximum capacity for a train on each platform gives a total platform level occupancy of 2,892 agents. The total occupancy on the platform is considered maximal and meant that on average the platform effectively had approximately 1.2 ped/m^2 which corresponds to Fruin's level of service E described as "Standing in physical contact with others is unavoidable" [9].

Within all scenarios, approximately an even number of agents initially on the platform level elect to use each of the five escalators/stairs to traverse to the ticket hall above as part of their egress. The initial agent starting locations on the platform were specified such that these frequencies for device usage were achieved with agents using their nearest escalator/stair. This was to ensure that any single escalator/stair was not disproportionately oversubscribed (so extending the evacuation). Though uneven escalator/stair loading would decrease the efficiency of an evacuation, the focus of this investigation is how escalator strategies and human factors influence an evacuation. Approximately 10 % (388) of all platform agents were assumed to use the emergency stairs at either end of the platform. This represents the decreased usage (compared to the main escalators/stairs) due to the expected lack of familiarity with stairs due to not being used during normal circulation situations.

The ticket hall level above was assumed to be initially occupied by the same number of waiting agents on a single platform (964). This was intended to represent both entering and exiting agents to the station. The frequency of agents initially on the ticket level were assigned to use each exit according to the proportion of the aggregated width each exit provided; with 28.0 % (270) assigned to Exit 1 and 72.0 % (694) assigned to Exit 2. As with the escalator/stair assignment on the platform level, this was to minimise the influence of uneven usage of exits and the potential decrease in evacuation efficiency caused. Combining the total platform and ticket level occupancy, the entire occupancy of the station was 3,856 agents.

Passenger response times for underground station environments are not well documented and so response times were specified using the Chinese Design Code for Subway stations [12]. This specifies an average evacuation response time of 60 s for people in a transit station. Such specifications have been typically used to assess upper limit design requirements. With this in mind, agents within the modelled scenarios were randomly uniformly assigned a response time range between 0 and 120 s (0–2 min) with an average of 60 s.

4.3 Scenarios

A series of 12 evacuation scenarios were performed exploring the influence of different escalator strategies and escalator human factors upon the evacuation (see Table 1). The scenarios investigated are:

- Scenario 1: Only the stairs were used with the escalators not being used.
- Scenario 2: The stairs and escalators could be used however, the escalators were static: agents could walk up the escalators if they chose to. No data was collected with regards to static escalator walker speeds in each of the studies. As such agents assessed whether to use a static escalator based on their stair walker speed. If agents elected to use the static escalator they would use their stair walker speed to traverse the escalator.
- Scenarios 3–8: Explored the impact of different human factors upon an evacuation. This included analysing the influence of the number of escalator/stair users, number of walkers/riders, ride side usage, and different congestion threshold values [7].
- Scenarios 9–11: Focused on the influence of escalators/stairs being unavailable.
- Scenario 12: Employed the escalator human factors data collected from the London Underground presented in Sect. 3. The proportion of escalator/stair users, walkers/riders and side usage values were derived from the up morning rush-hour data [8]. This was considered appropriate considering potential increased levels of motivation during such periods.

Each scenario was run a total of five times and the average results are presented in Table 2.

Table 1 Evacuation scenarios with attribute values for the escalator model

Scenario	Escalator motion (moving/static)	Escalator/stair (% of agents)		Walker/rider (% of agents)		Rider side usage (% of agents)		Congestion threshold (CT) (ped/m ²)
		Escalator	Stair	Walker	Rider	Left	Right	
1	-	0	100	-	-	-	-	-
2	Static	-	-	-	-	-	-	0
3	Moving	50	50	0	100	-	100	-
4	Moving	-	-	100	0	-	-	0
5	Moving	-	-	0	100	50	50	0
6	Moving	-	-	0	100	0	100	0
7	Moving	50	50	100	0	0	0	1
8	Moving	50	50	100	0	0	0	2
9	Moving	-	-	100	0	-	-	0
10	Moving	-	-	100	0	-	-	0
11	Moving	-	-	100	0	-	-	0
12	Moving	75.3	24.7	34.5	65.5	5.4	94.6	1

Table 2 Average TET, PET, CWT, platform clearance time, Door 1 and 2 exit times for each scenario (average of five simulations)

Scenario	Avg TET (s)	Avg PET (s)	Avg CWT (s)	Platform clearance time (s)	Overall: % time saved compared		Platform: % time saved compared	
					to stairs only	to stair+static escalator	to stairs only	to stair+static escalator
1	429	199	67.6	337	-	-21.6	-	-23.4
2	353	170	40.5	273	17.8	-	19.0	-
3	380	174	42.7	307	11.5	-7.7	8.8	-12.6
4	325	163	36.3	246	24.3	8.0	27.0	10.0
5	339	170	36.6	268	21.1	4.0	20.4	1.7
6	361	175	40.9	291	15.8	-2.4	13.5	-6.8
7	321	160	32.6	247	25.1	9.0	26.7	9.6
8	315	159	31.5	229	26.7	10.8	31.9	15.9
9	367	173	46.2	270	14.4	-4.1	19.9	1.1
10	421	183	56.9	327	1.9	-19.3	2.9	-19.9
11	564	230	95.7	468	-31.4	-59.8	-39.0	-71.6
12	336	167	35.1	254	21.6	4.7	24.5	6.9

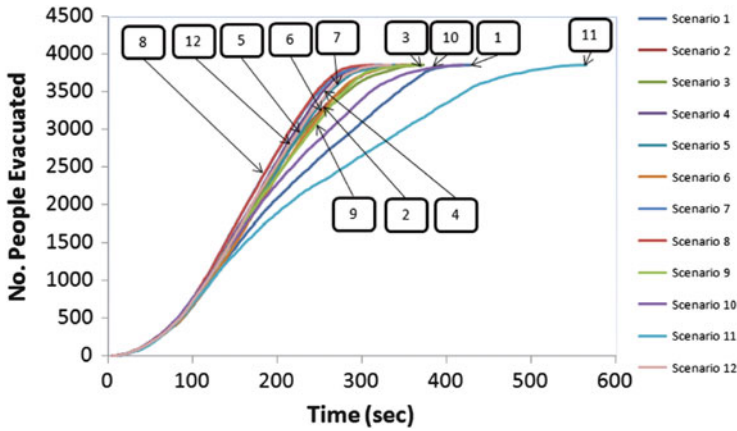


Fig. 3 Evacuation curves for each scenario

4.4 Results

A summary of results for each scenario is presented in Table 2 with evacuation curves shown in Fig. 3. Scenario 1 represents a situation akin to potential practice in an actual evacuation whereby the escalators are not used and people are required to use only the stairs. This scenario produced the second longest Total Evacuation Time (TET) of 429 s with the platform taking 337 s to clear. On average agents spent just over 1 min waiting in congestion with the average Cumulative Wait Time (CWT) being 67.6 s. Another common practice during an evacuation is to turn the escalators off, but allow agents to walk on the devices. If it is assumed that agents elect to use a device based on the shortest time system (Scenario 2), the TET reduces to 353 s, a decrease of 17.8 % (76 s). In addition, the platform clearance time also reduced to 273 s, a decrease of 19.0 % (64 s). On average approximately a quarter of agents (26.1 %) who made an escalator/stair choice, used an escalator. This reflects the influence of the increased width of the stairs compared to the static escalator.

In Scenario 3 the escalators were active, agents were evenly assigned to use both the escalators/stairs and all escalator users rode on the right side. During this scenario a small increase (7.7 % (27 s)) in TET to 380 s was observed compared to the static escalator case (Scenario 2). If it is now assumed that agents elect to use a device based on the shortest time system with all escalator users walking (Scenario 4), the TET reduces even further to 325 s. This represents a decrease of 24.3 % (104 s) compared to the stair only scenario and was one of the fastest scenarios. Similarly the platform clearance time also decreased by 27.0 % (91 s) to 246 s compared to the stair only scenario. A reduction in average CWT by almost a half (46.3 % (31.3 s)) to 36.3 s was also recorded compared to the stair only scenario. On average a higher proportion of agents elected to use the escalator (59.5 %) compared to the stairs (40.5 %). An increased overall average flow-rate

of agents onto the escalators (87.7 ped/min) was observed compared to Scenario 3 (68.3 ped/min) where agents were only allowed to board the right side and ride the escalator.

In Scenario 5 all escalator users were assumed to ride with an even number adopting each side. In this scenario an average decrease in TET of 10.8 % (41 s) and 12.7 % (39 s) in platform clearance time can be seen compared to when escalator users all rode on the right side (Scenario 3). Compared to when all escalator users walked (Scenario 4), only a slight increase in TET (5.2 % (17 s)) and platform clearance time (9.2 % (23 s)) was recorded.

Scenario 6 is identical to Scenario 3 where all escalator users rode on the right side, except that agents selected to use a device according to which one they expect they could traverse in the shortest time (i.e. the shortest time system [7]) instead of evenly being assigned. A slight decrease in TET by 4.7 % (18 s) was observed compared to Scenario 3 with a similar reduction (5.1 % (16 s)) in platform clearance times. Approximately an even number of agents used each escalator/stair with the average PET/CWT being similar in both scenarios.

Scenario 7 extended Scenario 4 by using the hybrid device selection system [7]. In this scenario a Congestion Threshold (CT) value of 1 ped/m² was set with even usage of each escalator/stair imposed before the CT was reached. The scenario produced one of the shortest TETs (321 s) and platform clearance times (247 s). It was comparable to Scenario 4 where all agents used the shortest time system when choosing to use an escalator/stair. In Scenario 4 approximately an even number of agents used each escalator/stair. As such assigning an even proportion of agents to use each device before a given level of congestion was reached in Scenario 7 had little effect. A similar phenomenon occurred in Scenario 8 where the altered CT of 2 ped/m² had little influence upon the overall evacuation compared to Scenario 4.

The concept of reducing escalator/stair availability is introduced in Scenario 9. In this scenario ES1 was unavailable with agents who would have used ES1 evenly using the remaining escalators/stairs. In addition, the shortest time system was used with all escalator users walking. Both the TET and platform clearance times were marginally longer by 12.9 % (42 s) and 9.8 % (24 s) respectively compared to when all escalators/stairs were available (Scenario 4). Scenario 10 extends the escalator/stair unavailability concept to two escalator/stairs (ES1 and ES5) being unavailable at either end of the platform. Here an average TET of 421 s and platform clearance time of 327 s was recorded which is similar to the time taken to evacuate the station in the stair only scenario (Scenario 1). Despite this, the evacuation rate was notably higher than the stair only case for a large proportion of the TET: between approximately 42.8 % (180 s)–87.9 % (370 s) of the TET (see Table 2). This was due to the added vertical throughput afforded by the available escalators and escalator users all walking. The TET from Scenario 10 increased by 29.6 % (96 s) compared to Scenario 4 where all escalators/stairs were available. The final scenario involving escalator/stair unavailability was Scenario 11 where 3 escalators/stairs were unavailable. This scenario produced the longest TET of all scenarios at 564 s, representing a 73.6 % (239 s) increase compared to Scenario 4 where all escalator/stairs were available. In all scenarios involving escalators/stairs

being unavailable approximately an even number of agents used each device. The escalator/stair availability results suggest that there may not be a linear increase in time with linear decrease of escalators/stairs availability. This demonstrates that escalator human factors impact the extent to which platform clearance times are increased when escalators/stairs are unavailable.

The final scenario incorporated the data presented in Sect. 3 into the escalator model in buildingEXODUS [7]. Overall average results (see Table 2) and evacuation curves (see Fig. 3) were similar to that of Scenario 5 where all agents rode on both sides of the escalators. This reflects the similar influence of having separate walker/rider lanes compared to all agents riding using both sides. Since only 5.4 % of riders in the data were observed to use the walker lane, in the model this meant that few agents that were riders would have blocked walkers from walking up the walker lane (i.e. this further contributed to the similarities with Scenario 5). In addition, since the levels of congestion increased quickly at the base of each escalator/stair, the influence of the CT being set to 1 ped/m² was reduced. Thus, most agents selected a device using the shortest time system in both Scenario 5 and Scenario 11.

In all scenarios agents initially on the ticket hall level were among the first to evacuate the station so varying escalator strategies or associated human factors had little influence on those agents. Consequently the evacuation curves for all scenarios (see Fig. 3) are similar for the first 964 agents in each scenario (i.e. the total ticket hall population). The remaining agents evacuated from the platform level below so were influenced by the different escalator strategies and escalator agent behaviour. As such the evacuation curves begin to differ after approximately the ticket hall agents evacuated.

5 Conclusion

This paper has presented a brief overview of the analysis of an escalator human factors dataset collected in a London Underground station. The analysis showed the escalators to be the most used devices compared to the adjacent stairs with most escalator users electing to ride rather than walk. Escalator users were observed to strongly adopt a common side preference whereby riders used the right side and walkers use the left side. Escalator users typically walked faster in the down direction and males walked faster than females. When peak flow-rates were observed, approximately an even number of escalator users occupied both the right and left sides with a higher proportion of walkers typically carrying small items e.g. handbags, rucksacks etc. Some human factors were shown to be influenced by direction of travel and time period.

Results from a series of evacuation simulation scenarios were presented, based on the buildingEXODUS escalator model which explored the influence of escalator strategies and human factors upon evacuation efficiency. The evacuation analysis demonstrated that even the provision of static escalators can have a considerable

influence upon an evacuation compared to using stairs alone. Furthermore, the provision of a moving escalator has been shown to decrease overall evacuation times by up to approximately 25 % compared to using stairs alone and around 10 % compared to using static escalators. Results have shown that little decrease in TET was observed when all escalator users walked compared to if they all rode. This is an important observation and suggests that there is little added benefit if the population walk up the moving escalator – as this reduces tread utilisation. Thus, urging escalator users to ride on both sides of an escalator, rather than walking up the moving escalator, has the advantage of reducing the likelihood of users tripping on the escalator without significantly increasing the TET.

Scenarios where escalators/stairs were rendered unavailable had a considerable impact upon the evacuation, as expected. In those scenarios, increases in TET of up to 60 % and platform clearance times of up to 72 % compared to stairs alone were recorded. Such findings highlight the severity caused by the unavailability of escalators/stairs (e.g. due to fire/smoke, code stipulations, etc.), and the need to consider additional provision of vertical egress capacity.

Further investigation is required to assess the extent to which the results are generally applicable. In addition, the human factors escalator data collected from Shanghai, Barcelona and London is being examined to estimate the possible impact of culture on human behaviour associated with the use of escalators.

Acknowledgements Michael Kinsey gratefully acknowledges the support of the Fire Safety Engineering Group of the University of Greenwich and the Engineering and Physical Science Research Council (EPSRC) for providing him with a bursary under their Ph.D. bursary scheme. The authors gratefully acknowledge the support of Kingfell, London Underground Limited and British National Rail in providing access to the facilities for the collection of the escalator data.

References

1. Strakosch, G., Caporale, R.S.: *The Vertical Transportation Handbook*, The Third Edition, John Wiley & Sons Inc (2010)
2. Al-Sharif, L.: *Escalator Handling Capacity: Standards Versus Practice*, Elevator World (1996)
3. Cheung, C., Lam, W.: Pedestrian Route Choices Between Escalator and Stairway in MTR Stations, *Journal of Transportation Engineering*, Vol. 124, No. 3, pp227–285 (1998)
4. Davis, P., Dutta, G.: *Estimation of Capacity of Escalators in London Underground*, No 2002-11-01, IIMA Working Papers from Indian Institute of Management Ahmedabad, Research and Publication Department (2002)
5. Kinsey, M.J., Galea, E.R., Lawrence, P.J., Blackshields, D., Hulse, L., Day, R. and Sharp, G.: *Modelling Pedestrian Escalator Behaviour, Pedestrian and Evacuation Dynamics (PED) Conference*, pp689–695 (2008)
6. Kinsey, M.J., Galea, E.R., Lawrence, P.J.: *Extended Model of Pedestrian Escalator Behaviour Based on Data Collected within a Chinese Underground Station*, *Proceedings of the Human Behaviour in Fire Conference*, pp173–182 (2009)
7. Galea, E.R., Lawrence, P.J., Gwynne, S., Filippidis, L., Blackshields, D., Cooney, D.: *BuildingEXODUS V5.0 User Guide and Technical Manual*, Fire Safety Engineering Group, University of Greenwich (2011)

8. Kinsey, M.J.: Vertical Transport Evacuation Modelling', PhD Thesis, University of Greenwich (2011)
9. Fruin, J.J.: Pedestrian Planning and Design, Metropolitan Association of Urban Designers and Environmental Planners (1971)
10. NFPA – National Fire Protection Association: NFPA 130: Standard for Fixed Guideway Transit and Passenger Rail Systems, Technical Report (2010)
11. Transport for London (TfL): '1996 Rolling Stock', <http://www.tfl.gov.uk/corporate/modesoftransport/londonunderground/rollingstock/1630.aspx> (2010)
12. Planning Press of China: Code for Design of Subway. GB 50157-2003 (2003)

Observations from Student Exercises to Collect Human Behavior and Movement Data

Majed Almejmaj and Brian J. Meacham

Abstract Experiments and field observations have been the main source for data used to develop empirical models and inputs for evacuation computer software. Although researchers have been highlighting the need to gather additional data from various building and occupancy types, across a broader spectrum of occupant demographics, data remain scarce. There have been some attempts to develop a general framework for data collection especially during fire drills. However, specifics about the architectural settings and conditions under which data are collected are often not addressed.

As a means to help students learn more about the importance of various human and building factors on occupant use of egress systems, and to help generate additional data for analysis and use in evacuation modeling, students in the Worcester Polytechnic Institute course, *FPE 580M, People and Fires*, were asked to undertake an experiment-based project related to human behavior, pedestrian movement and identify a human behavior or movement attribute by observing people in public spaces under normal conditions. This study discusses the suggested experimental setups given to students, some of the student project findings, some of the challenges faced during data collection and analysis, and suggestions for others embarking on similar exercises in the future.

Keywords Data collection • Human behavior • Experimental setup • Movement speed • Exit choice

M. Almejmaj (✉) • B.J. Meacham
Department of Fire Protection Engineering, Worcester Polytechnic Institute, 100 Institute Road,
Worcester, MA 01609, USA
e-mail: mejmaj@wpi.edu; bmeacham@wpi.edu

1 Introduction

Much of the data on human behavior and movement used in fire engineering and evacuation analysis have been collected through drills and interviews/surveys following actual incidents. These data are used to help construct correlations and equations for evacuation analysis, and are also used as input in various computational models. However, several challenges exist [1]. Data are scarce because it is technically and ethically challenging, as well as costly, to collect. In addition, the settings in which the currently available data have been collected are not always detailed and are often misused [2]. Also, although guidance exists of setting up data collection for evacuation exercises [3], such guidance is not always followed to a degree necessary.

To introduce fire protection engineering students to the challenges of collecting data on human behavior and movement, as well as to add to the data that are available to model developers and engineers, students in the Worcester Polytechnic Institute (WPI) graduate fire protection engineering course, FPE 580M, *People and Fires*, were assigned a small project to collect data by observing the movement of people in public spaces, analyze the data, and develop a report detailing their findings. To guide the projects a set of target 'experimental scenarios' was defined. To obtain diversity in the data, students were given the freedom to choose the location and occupancy type. This resulted in seventeen projects covering various university buildings, five on rail terminals, two on airports, two on churches and two studied on sporting arenas. Outcomes yielded some insights for further observational studies.

2 Suggested Scenarios

Scenario 1 was outlined with the objective of having students observe human behavior and movement speed along a straight corridor. Requirements were that the corridor have minimum dimensions of 1.5×7.6 m (5×25 ft.) and be such that occupants are moving across the entire corridor distance of the corridor towards a door. A target was to collect data on individuals and groups, noting demographics. Cameras and markers would be located as needed to assess speed and flow in the corridor and through a door, if readily achievable.

Scenario 2 was outlined with the objective of having students observe human behavior and movement speed through a 90° turn in a corridor. Requirements were that the corridor should have a minimum of 1.5 m (5 ft.) in width and 4.5 m (15 ft.) straight travel distance before and after the turn. A target was to collect data on individuals and groups, noting demographics. Cameras and markers would be located as needed to assess speed and flow around the corner.

Scenario 3 was outlined with the objective of having students observe a group of occupants leaving an assembly-type space of any size with any number of

occupants. The aim of this scenario is to observe human behavior and movement of large numbers of people through limited size openings, with occupants starting evacuation from a normal state such as sitting in a lecture seat or work space and continuing through an exit access doorway. Cameras and markers would be located as needed to assess start of exit, speed, flow and density, and time to leave the room.

Scenario 4 was outlined with the objective of having students observe human behavior and movement speed up or down a stairway of at least 1.2 m (44 in.) in width. The aim of this scenario is to observe human behavior and movement of individuals and small groups as they move up and down stairs as well as entry/exit from the stair. Cameras and markers would be located as needed to assess speed and flow up or down the stairs and as they enter/exit the stairwell.

3 Scenarios Covered by the Students

Since students were given the freedom to choose the scenario for their projects, this resulted in a range of focus areas, configurations and data. Though none of the student groups chose scenario 2, the collected data addressed different types of building spaces, such as university classrooms, auditoriums and transportation terminals, covering scenarios involving movement speed, crowd behavior and exit selection. Results from selected projects are discussed in the following sections. While the outcomes of these projects do not necessarily constitute complete or repeatable data sets, some insights were developed, which may help inform future experimental plans and data collection exercises.

3.1 Scenario 1: Occupant Movement Speed through Corridors

There are numerous elements affecting occupant movement speed [4, 5]. One of these elements is counter flow especially when emergency responders use the same exit stairwell as the occupants [6]. In an evacuation drill of a six-story building, emergency responders counter flow reduced occupant speed from 0.83 to 0.73 m/s (2.72 to 2.4 ft./s) [7].

One of the groups that chose to address Scenario 1 collected data in corridors from at a church sanctuary, with a particular focus on occupants' walking speeds and the effects of counter flow. The setup and results of the data sets are discussed in the following section.

Occupant movement speeds were observed between classrooms and a sanctuary at a local church. The corridor is 19.5 m (64 ft.) long and has a clear width of 1.83 m (6 ft.) with four classrooms and the large sanctuary connected to the corridor. Figure 1 illustrates the location of the two cameras used to record the observations at both ends of the corridor as well as the directions of occupant flow.

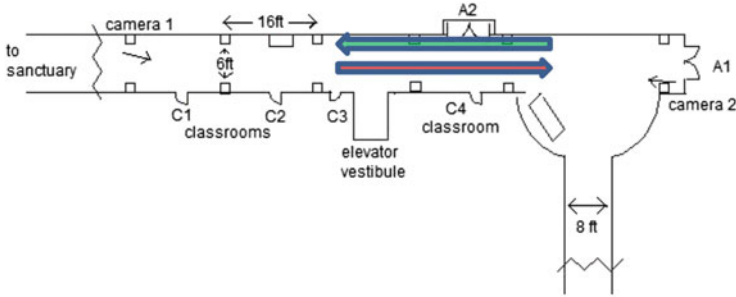


Fig. 1 Group 1 corridor layout, location of cameras and travel path

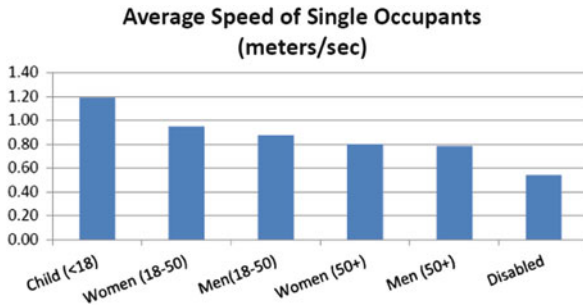


Fig. 2 Group 1 average speed of single occupants

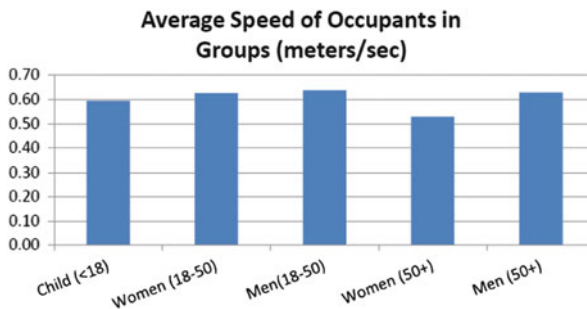


Fig. 3 Group 1 average speed of occupants in groups

The population distribution of the 158 occupants composed of 32 children (age < 18), 32 males (age 50+), 22 males (ages 18–50), 38 females (age 50+), 29 females (ages 18–50) and four disabled occupants with a cane or walker. The travel speeds of the occupants was determined by measuring the time it takes an occupant traveling individually or with a group between two columns spaced 16 ft apart. The observed average speeds can be seen in Figs. 2 and 3.

Table 1 Group 1-different age groups average speed

Demographic	Group 1 church study	Lord et al. 2005
	Average speed of occupants m/s (ft/s)	Average speed of occupants m/s (ft./s)
Child (<18)	0.63 (2.07)	0.88 (2.89)
Women (18–50)	0.70 (2.3)	1.12 (3.67) ^a
Men(18–50)	0.75 (2.46)	1.12 (3.67) ^a
Women (50+)	0.66 (2.17)	0.86 (2.82) ^a
Men (50+)	0.54 (1.77)	0.86 (2.82) ^a

^aProvided only as ‘adults’ and not identified by gender

It was concluded from the observed data that the average speeds of occupants traveling in groups was relatively close since that each group contained more than one category of occupants. Also, groups moving with children tend to have the slowest travel speed. However, the observed data for individual occupants’ speed differs significantly the published results by Lord et al. [8] for different age groups covering apartment buildings, retail stores, shopping malls, and transportation terminals. This is illustrated in Table 1.

Due to the limited availability of data for such occupancy (church), the results from Group 1 were compared to results of different occupancies found in the literature. Group 1 identified adults between the ages of 18 and 50 as one group which seems to be a valid assumption since that the average speed of adults between 18–29 and 30–50 in the Lord et al. [8] study were similar. It can be seen that the average walking speeds from Group 1 study are significantly lower which can be attributed to the counter flow of occupants trying to access different parts of the building after a sermon. The occupancy type might also be contributing factor to the differences in walking speeds which would raise a concern regarding the applicability of applying data across different occupancies. Additional research efforts are needed to determine the effects of the occupancy type on walking speeds.

3.2 Scenario 3: Exit Selection from Assembly Space

Occupants’ ability to select an exit during an emergency is greatly affected by their familiarity with the space [9]. Occupants will choose to evacuate a space through a familiar route when in a stressful situation such as a fire emergency [10]. People exhibit this behavior because using a familiar route is easier than the process of finding another route and involves less effort [11]. There are various factors that affect occupants’ decision to redirect to another exit such as length of the queue, severity of smoke and distance to exit [12].

One of the groups that chose to address Scenario 3 collected data from an auditorium at WPI, with a particular focus on occupants’ exit choice. The setup and results of the data sets are discussed in the following section. Students observed

Fig. 4 Group 2 auditorium layout and camera location

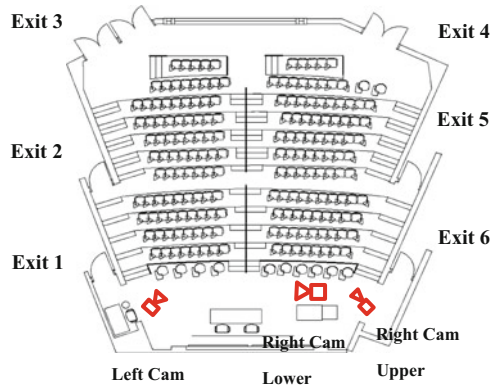


Table 2 Group 2 auditorium exit selection

Selected exit	Number of people
Exit 1	13
Exit 2	8
Exit 3	20
Exit 4	11
Exit 5	0
Exit 6	0
Total	52

exit choice at an auditorium at the end of class session to determine occupants’ exit choice. The auditorium serves as a classroom lecture hall as well as a movie theater during the weekend. It is also considered as one of the largest lecture halls on the WPI campus with a capacity of 193 students. There are three stair aisles extending from the lower level of the auditorium to the upper level. Two of those aisles are located at both sides while the third aisle is located in the middle of the auditorium. Three cameras were located at the lower level of the auditorium to collect data from the right half of the lecture (left Cam), the top side of the lecture hall (Right Cam Upper) and exit 1 (Right Cam Lower). The layout of the auditorium can be seen in Fig. 4.

In order to simplify data analysis, each exit was assigned a number as illustrated in Fig. 4.

Exits 1, 2, 5 and 6 have a width of 105.4 cm. (41.5 in.) while exits 3 (two double leaf doors) and 4 (double leaf door) have a width of 360.7 cm. (142 in.) and 180.3 cm. (71 in.) respectively. The videos were analyzed to determine the exact number of occupants using each exit. The results are shown in Table 2.

The results illustrate that 38.5 % of the occupants chose to leave the auditorium through exit 3. Also, the majority of the occupants exited through exits one, two and three which are located on the western side of the auditorium. This is due to occupants’ previous knowledge of these exits and where they lead. In addition, none of the occupants used exits five and six, though they lead to the outside of

the building. This is attributed to the fact that students cannot use these doors to enter the auditorium.

3.3 Scenario 4: Movement on Stairs

Stairs are used to evacuate occupants as well as by emergency responders to access upper floors during emergency conditions especially in high-rise buildings [13]. As firefighters try to access a building using the stairs while occupants are evacuating, counter flow becomes an issue where the flow of descending occupants is restricted by the ascending emergency responders [6].

While most of the data available for people movement over stairs and published in the SFPE Handbook dates back to the 1970s and 1980s [4], many researchers argue that such data is not applicable nowadays due to changes in demography [5]. This is also applicable to escalators where there is limited data available on how people behave around escalators though it is widely used in underground train stations. Escalators are usually turned off or blocked during emergency to prevent occupants from accessing them as stairs; However, survivors of the World Trade Center reported using the escalators while they were moving or as stationary stairs (shutdown) while evacuating the buildings on 9/11 [14]. This would indicate the probability of using escalators during evacuation especially for underground train stations.

Two groups of students observed occupants' movement and behavior at an on-campus building at WPI to broaden the amount of data available for occupants' speed while descending and ascending stairs using one camera located at the top of the stairs.

Both experiments covered the longest section of the stairs which is 161.3 cm (63.5 in.) wide and consists of 17 steps with 17.8 cm (7 in.) riser and 30.5 cm (12 in.) tread depth.

The student recorded the time it takes a single occupant to descend or ascend the entire length of the stair section, which is 5.5 m (18 ft) to calculate the travel speed. The average walking speeds for both groups are listed in Table 3 along with published values in the SFPE Handbook.

The average stairs ascending speed reported by both groups are relatively close to the values in the SFPE Handbook. When comparing the average stairs descending speed, the SFPE Handbook states that it is the same as that for ascending the stairs [5]. However, the values reported by both groups contradict that statement. Group 3's descending speed was 20 % higher than that of the SFPE Handbook and group 4's reported speed was 12 % higher. The reported range for group 3 is much higher than that of group 4 and the SFPE Handbook. This is due to the large number of people included in the experiment (1,726 individuals) compared to the range of group 4 (469 individuals).

Both groups reported behaviors that affected occupants speed while traversing the stairs. Group 3 indicated that texting decreased travel speed up or down the

Table 3 Group 3 and 4 average walking speeds on stairs comparison

Walking speeds on stairs			
Source	Mean m/s (ft./s)	Standard deviation m/s (ft./s)	Range m/s (ft./s)
Group 3 experimental data – up stairs	0.68 (2.23)	0.19 (0.62)	0.22–1.88 (0.72–6.17)
Group 4 experimental data – up stairs	0.63 (2.07)	0.19 (0.62)	0.36–1.83 (1.18–6.0)
SPFE HB – up stairs [5]	0.70 (2.30)	0.24 (0.79)	0.55–0.82 (1.8–2.70)
Group 3-experimental data – down stairs	0.85 (2.79)	0.19 (0.62)	0.20–1.71 (0.66–5.61)
Group 4-experimental data – down stairs	0.79 (2.59)	0.24 (0.79)	0.24–1.83 (0.79–6.0)
SPFE HB–down stairs [5]	0.7 (2.30)	0.26 (0.85)	0.45–1.10 (1.48–3.61)

stairs to 0.51 m/s (1.67 ft./s). Group 4 also reported that texting students stopped right before the stairs or in the middle which caused other students to maneuver around them.

4 Potential Areas for Data Usage

Researchers have been calling on the life safety community to increase their efforts in collecting much needed data on human movement and behavior [1]. Though there have been great advances in bridging this data gap, certain aspects of human behavior and movement were falling behind. This can be attributed to the ethical challenges and cost associated with collecting such data [2]. In addition, a substantial amount of data collected in the past has not been published [1].

Specifying certain scenario setups for data gathering would provide the research community with the opportunity to compare data from different occupancy and cultures. It will also provide much needed data for egress models verification and validation and egress analysis model inputs for RSET results for PBD. Such data can also be used to develop empirical correlations [2] that can be implemented in various computer models.

These results are a first step in collecting data from mainly university and transient terminal settings to create a database for occupants' walking speed and various evacuation behaviors. Additional results will be published in more detail once the analysis is complete and after refining the scenarios based on feedback from the research community. Such database would coincide with previous suggestions made by Fahy and Proulx [15].

References

1. *Available Data and input into Models*. Fahy, Rita F. s.l. : National Research Council, 2002. National Research Council Workshop to Identify Innovative Research Needs to Foster Improved Fire Safety in the United States, Session on Human Behavior.
2. Gwynne, S. M. V. *Conventions in the Collection and Use of Human Performance Data*. s.l. : NIST GRC 10-928, 2010.
3. Proulx, Guylène. *Methodology for Evacuation Drill Studies*. Ottawa, Ontario : National Research Council Canada, 1996.
4. Gwynne, Steven M. V. and Rosenbaum, Eric R. Employing the Hydraulic Model in Assessing Emergency Movement. [book auth.] Society of Fire Protection Engineers. *The SFPE Handbook of Fire Protection Engineering*. Bethesda, MD : National Fire Protection Association, 2008, pp. 3-373 to 3-396.
5. Proulx, Guylène. Evacuation Time. [book auth.] Society of Fire Protection Engineers. *The SFPE Handbook of Fire Protection Engineering*. Bethesda, MD : National Fire Protection Association, 2008, pp. 3-355 to 3-370.
6. Tubbs, Jeffrey S. and Meacham, Brian J. *Egress Design Solutions*. Hoboken, NJ : John Wiley and Sons, 2007.
7. *Stairwell Evacuation from Buildings: What We Know We Don't Know*. Averill, Jason D., Peacock, Richard D. and Kuligowski, Erica D. Wuppertal, Germany : Springer-Verlag Berlin Heidelberg, 2008. Pedestrian and Evacuation Dynamics. pp. 55-66.
8. *Uncertainty in Egress Models and Data: Investigation of Dominant Parameters and Extent of Their Impact on Predicted Outcomes-Initial Findings*. Lord, James, et al. Luxembourg : Society of Fire Protection Engineers, 2004. The 5th International Conference on Performance-Based Codes and Fire Safety Design Methods. pp. 342-353.
9. *Movement Towards the Familiar: Person and Place Affiliation in a Fire Entrapment Setting*. Sime, Jonathan D. 1985, *Environment and Behavior*, pp. 697-724.
10. *Human Response During Fire Situations: A Role for Social Engineering*. Keating, J. P. Los Angeles : American Institute of Architects, 1985. Research and Design 85: Architectural Applications of Design and Technology Research. pp. 285-288.
11. Passini, Romedi. *Wayfinding in Architecture*. New York : Van Nostrand Reinhold Company Inc., 1984.
12. *Daptive Decision-Making in Response to Crowd Formation in building Exodus*. Gwynne, S., et al. 1998-99, *Journal of Applied Fire Science*, pp. 301-325.
13. *Selecting Appropriate Evacuation Strategies for Super Tall Buildings: Current Challenges and Needs*. Tubbs, Jeffrey. Cambridge, UK : Interscience Communications Limited, 2009. 4th International Symposium on Human Behaviour in Fire. pp. 41-50.
14. *Extended Model of Pedestrian Escalator Behaviour Based on Data Collected Within a Chinese Underground Station*. Kinsey, Michael J., Galea, Edwin R. and Lawrence, Peter J. Cambridge, UK : Interscience Communications Limited, 2009. 4th International Symposium on Human Behaviour in Fire. pp. 173-182.
15. *Towards Creating a Database on Delay Times to Start Evacuation and Walking Speeds for use in Evacuation Modeling*. Proulx, G. and Fahy, R. F. Boston, MA : s.n., 2001. 2nd International Symposium on Human Behaviour in Fire. pp. 175-183.

On Measuring Pedestrian Density and Flow Fields in Dense as well as Sparse Crowds

Matthias Plaue, Günter Bärwolff, and Hartmut Schwandt

Abstract In the framework of macroscopic human crowd models, pedestrian dynamics are described via local density and flow fields. In theory at least, these density and flow fields are often required to have a certain degree of regularity such as being smooth. In this paper, we describe a new method for the calculation of spatio-temporally smooth, locally defined density and flow fields from pedestrian trajectories. This method is based on kernel density estimation with variable bandwidth and—for a large range of scale—yields spatially averaged values close to the density or flow defined in the standard way.

In order to evaluate our approach and compare with other techniques such as the fixed-bandwidth estimator or the Voronoi estimator, we use a data set of intersecting pedestrian flows extracted from a human crowd experiment that we conducted at Technische Universität Berlin.

Finally, we argue that the proposed model may be interpreted as to not only describe the transport of pedestrian mass via particle flow but also as the result of variations in the pedestrians' personal space in crowded situations. We suggest that this approach may be useful for the description and/or visualization of clogging phenomena, or crowd disasters which may be thought of as events where a sudden compression of personal space occurs.

Keywords Pedestrian density and flow measurement • Kernel density estimation • Human crowd experiments • Intersecting pedestrian flows

M. Plaue (✉) • G. Bärwolff • H. Schwandt
Institut für Mathematik, Technische Universität Berlin, Straße des 17. Juni 136, 10623 Berlin,
Germany
e-mail: plaue@math.tu-berlin.de; baerwolf@math.tu-berlin.de; schwandt@math.tu-berlin.de
<http://www.math.tu-berlin.de/projekte/smdp>

1 Introduction

The study of pedestrian dynamics has important applications in crowd management such as devising strategies for the evacuation of buildings or public places. In order to evaluate the predictive power of mathematical models designed to emulate human crowd behavior, it is a common procedure to compare numerical simulations based on these models with empirical data. These empirical data are usually extracted from video recordings of either naturally occurring human crowds [7] or pedestrian flows that have been produced by controlled experiments [2, 3, 23]. In general, the latter are devised to demonstrate crowd behavior in special situations such as evacuation or passing through a bottleneck. In our work, we put a particular emphasis on analyzing intersecting pedestrian flows, and in Sect. 2 we describe experiments that were conducted with this purpose.

Furthermore, different modeling approaches demand the extraction of different types of data: For example, the social force model [6] and the cellular automaton model [1] aim at predicting pedestrian trajectories, whereas continuum methods [8] adopted from fluid mechanics describe the dynamics via a density and flow field associated with the crowd. The computation of the density on a large range of spatial scale from a crowd consisting of only a few pedestrians is a challenging task because of the low number of samples. In this context, we propose a variable-width kernel density estimation described in Sect. 3 and apply this algorithm to our experimental data (Sect. 4).

We conclude with a short summary and an overview of remaining problems in Sect. 5.

2 Experiments

In the experiment which we use here to illustrate our method, two pedestrian flows (group *A*, 142 subjects, and group *B*, 83 subjects) intersected at an angle of 90° for 1 min in a region of about 25 m^2 , reaching a peak density of about five pedestrians per square meter. The scene was recorded from a gallery at a height of about 6 m with five networked and temporally synchronized JVC VN-V25U surveillance video cameras. Here, we analyze the data provided by the three central cameras which covered the area where the actual intersecting of the pedestrian flows took place, see Fig. 1. A similar experiment with this purpose has been conducted in [4]. However, we process data from multiple cameras, and therefore, a larger field of view covering a larger portion of the observation area than one camera view could be captured. Also, in our experiments, the pedestrians did not move along specified, confined corridors.

The cameras were calibrated by applying a pinhole model to the world and image coordinates of about 30 reference points in the scene. After camera calibration, the spatio-temporal positions of the pedestrians were extracted by photogrammetric

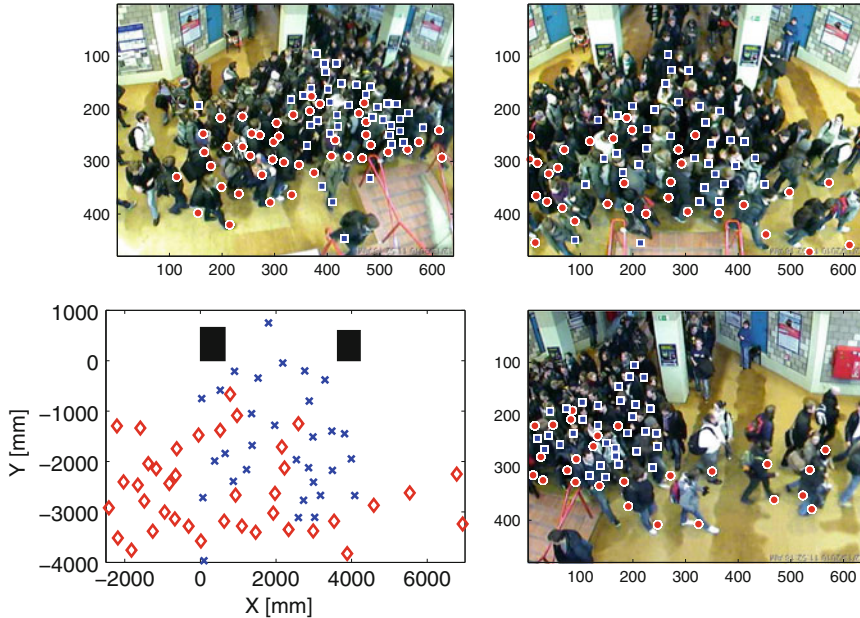


Fig. 1 Intersecting pedestrian flows. *Red diamonds*: group A, *blue crosses*: group B

means—a particular challenge was presented by the fact that due to constructional limitations the scene could not be captured from a bird’s eye view. For more details, we refer to [14, 15]. First, for each frame, the heads of the pedestrians were marked manually, aided by the Lucas–Kanade tracking algorithm [11, 18]. Then, for each pedestrian the floor position was marked in (at least) one frame in order to compute the height of the respective pedestrian via the homography determined from camera calibration. This information is sufficient to calculate the pedestrians’ world coordinates above ground for each frame. Smooth trajectories were then obtained via approximation with cubic B-splines. Finally, the trajectories extracted from different cameras were merged by combinatorial assignment with the Kuhn–Munkres algorithm, also known as the Hungarian method [9, 13].

The experimental data, i.e., videos and extracted trajectories, can be downloaded at <http://www.math.tu-berlin.de/projekte/smdpc/>.

3 Density and Flow Estimation

Empirical data of human crowd behaviors are usually represented by the trajectories of the pedestrians. Probably the most basic way to compute a density from such trajectories would be to divide the number of pedestrians in a given region by the area of that region, at a given point in time. However, this “standard” density

estimator yields data with large scatter—let alone a smooth density function defined at every point. Very similar problems occur when estimating the flow by counting pedestrians that pass through a given cross section.

At least two approaches for computing the density have been suggested in the literature as alternatives:

1. In [7], a local density field is computed via the sum of Gaussians with a fixed standard deviation (typically 0.7 m) centered at each pedestrian. Formally, this approach may be recognized as a kernel density estimation with fixed bandwidth, which is a basic tool in statistical data analysis (see [19], for example). This method results in a smooth density field defined at every point. Of course, the kernel estimator yields the same result as the standard density when spatially averaged across large regions. However, for isolated pedestrian groups of “mesoscopic” size one typically observes values that are significantly lower than the standard density since a large portion of the “pedestrian mass” is located outside of the respective region.
2. The authors of [20] propose two similar estimators, both of which are based on the Voronoi diagram defined by each pedestrian’s position as a Voronoi site. The Voronoi method has been successfully applied to study pedestrian flows through observational areas that feature a constrained geometry, such as corridors or the vicinity of bottlenecks, see also [23]. The main idea in this approach is to account for the personal space occupied by each pedestrian, and this personal space is represented by the area of the corresponding Voronoi cell. The values for the Voronoi density are very close to standard densities, but with significantly less scatter. However, the Voronoi estimator does not yield a smooth local density function defined at every point. Also, for sparse and unconstrained crowds, a significant number of Voronoi cells may be quite large (in fact, may even have infinite area) resulting in densities that are lower than expected. However, a more recent suggestion is to mitigate this problem by introducing a fixed limit to the size of the cells [10]. In this paper, we only consider the original definition for the Voronoi density that is denoted in [20] as “ D_V ”.

In this work, we propose yet another method, based on kernel estimation with a variable bandwidth defined by Eq. (3) below. This method is conceptually a blend of the Voronoi estimator (accounting for personal space) and the fixed-bandwidth kernel estimator (yielding smooth density fields).

3.1 Standard and Voronoi Density

At a given point in time t , suppose we observe a (large) number N of pedestrians labeled by some suitable index set J such that $|J| = N$. The positions of these pedestrians are denoted by $x_j(t) \in \mathbb{R}^2$, $j \in J$. We may then define a local density distribution

$$\rho(t, \mathbf{x}) = \sum_{i \in I} k_i(t, \mathbf{x}) = \sum_{i \in I} \delta(\mathbf{x} - \mathbf{x}_i(t)) \tag{1}$$

where δ denotes the Dirac delta function. The index set $I \subset J$ labels the pedestrians of interest—for example, the whole crowd, in which case $I = J$, or a group of pedestrians with a common destination. For this density field—which is obviously not smooth but highly singular—the spatial average across some region $\Omega \subset \mathbb{R}^2$ is simply given by the number of pedestrians contained in Ω divided by the area of Ω :

$$\langle \rho(t, \cdot) \rangle_{\Omega} = \frac{1}{|\Omega|} \int_{\Omega} \rho(t, \mathbf{y}) \, d^2 \mathbf{y} = \frac{1}{|\Omega|} \sum_{i \in I} \int_{\Omega} \delta(\mathbf{y} - \mathbf{x}_i(t)) \, d^2 \mathbf{y} = \frac{|I_{\Omega}(t)|}{|\Omega|}$$

with $I_{\Omega}(t) := \{j \in I | \mathbf{x}_j(t) \in \Omega\}$. We will refer to this way of computing the density as the standard density.

The Voronoi method also defines a local density field which—like the standard density, or the kernel density defined in the next subsection—may be written in the form $\rho(t, \mathbf{x}) = \sum_{i \in I} k_i(t, \mathbf{x})$. In this case, we have

$$k_i(t, \mathbf{x}) = \begin{cases} \frac{1}{|V_i(t)|} & \text{if } \mathbf{x} \in V_i(t), \\ 0 & \text{if } \mathbf{x} \notin V_i(t), \end{cases}$$

where $V_i(t)$ is the Voronoi cell the seed of which is given by $\mathbf{x}_i(t)$. Obviously, this local density field is, in general, not continuous. Also note that without the introduction of some upper bound to the size of the cells, the local Voronoi density is not properly normalized, i.e., $\int_{\mathbb{R}^2} \rho(t, \mathbf{y}) \, d^2 \mathbf{y} \neq |I|$.

3.2 Kernel Density and Flow Estimators

In order to obtain a smooth density field instead of the distribution given by Eq. (1), one way is to replace the Dirac distribution by suitable nascent Dirac functions. One may understand this technique as a smoothing procedure that replaces the singular Dirac peaks by peaks of finite height and non-zero width. The main difficulty is given by the problem to choose appropriate widths for the new peaks. To this end, consider a kernel pedestrian density estimator with isotropic kernel function:

$$\rho(t, \mathbf{x}) = \sum_{i \in I} k_i(t, \mathbf{x}) = \sum_{i \in I} \frac{1}{(\lambda d_i(t))^2} \cdot K\left(\frac{\mathbf{x} - \mathbf{x}_i(t)}{\lambda d_i(t)}\right).$$

The dimensionless number $\lambda > 0$ is a global smoothing parameter. In the following, we will always assume $\lambda = 1$, and that the kernel is given by a Gaussian function:

$$K(\mathbf{y}) = \frac{1}{2\pi} \exp\left(-\frac{\|\mathbf{y}\|^2}{2}\right).$$

Probably the most natural formula for computing a corresponding flow field would be given by:

$$\mathbf{j}_m(t, \mathbf{x}) = \sum_{i \in I} k_i(t, \mathbf{x}) \cdot \frac{d\mathbf{x}_i(t)}{dt}. \quad (2)$$

However, the continuity equation is generally not satisfied with \mathbf{j}_m as the only flow component. Instead, we have

$$\frac{\partial \rho(t, \mathbf{x})}{\partial t} + \operatorname{div}(\mathbf{j}_m(t, \mathbf{x}) + \mathbf{j}_c(t, \mathbf{x})) = 0$$

with an additional, irrotational flow

$$\mathbf{j}_c(t, \mathbf{x}) = \sum_{i \in I} k_i(t, \mathbf{x}) \cdot \frac{d \ln(d_i(t))}{dt} \cdot (\mathbf{x} - \mathbf{x}_i(t)).$$

Note that \mathbf{j}_c vanishes if, for each label $i \in I$, the corresponding bandwidth $d_i(t)$ is fixed, i.e., it does not depend on the point in time t . Thus, if we wish to enforce a law of “pedestrian mass conservation”, a sensible choice for the total flow is given by $\mathbf{j} = \mathbf{j}_m + \mathbf{j}_c$. Furthermore, Eq. (2) also applies to the limiting case $d_i \rightarrow 0$, i.e., the standard density, to provide a standard flow. The spatial average of the standard flow with respect to some region Ω is simply given by the sum of the pedestrians’ individual velocities divided by the area of that region:

$$\frac{1}{|\Omega|} \sum_{i \in I} \int_{\Omega} \delta(\mathbf{y} - \mathbf{x}_i) d^2 y \cdot \frac{d\mathbf{x}_i(t)}{dt} = \frac{1}{|\Omega|} \sum_{i \in I_{\Omega}(t)} \frac{d\mathbf{x}_i(t)}{dt}.$$

As for the choice of bandwidth, one may assume it to be fixed—for example, $d_i(t) \equiv 0.7 \text{ m}$ [7]. More generally, the numbers $d_i(t)$ can be computed from the current positions of the pedestrians in a suitable way—a formal analogue of this procedure in statistical data analysis is known as a sample smoothing estimator [21]. For the nearest-neighbor kernel estimator we previously proposed in [14], we have:

$$d_i(t) = \min_{j \in I, j \neq i} (\|\mathbf{x}_i(t) - \mathbf{x}_j(t)\|).$$

Note, however, that in general, the functions $t \mapsto d_i(t)$ defined in this way are not differentiable, yielding a density field that is not smooth with respect to the time variable t . Therefore, for some fixed additional parameter $p \in \mathbb{R}$, $p > 1$, we propose the following functions instead (cf. [15]):

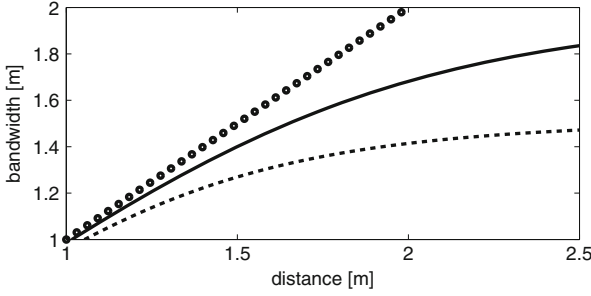


Fig. 2 The bandwidth, defined by Eq. (3), assigned to a particular pedestrian A as a function of the distance to another individual pedestrian B . *Dotted line*: with no other pedestrian present. *Solid line (dashed line)*: with one other pedestrian C (three other pedestrians C , D and E) located at a constant distance of 2 m to A

$$d_i^{(p)}(t) = \left(\sum_{j \in J, j \neq i} (\|\mathbf{x}_i(t) - \mathbf{x}_j(t)\|)^{-p} \right)^{-\frac{1}{p}}. \quad (3)$$

The bandwidths thus defined are smooth functions and at the same time generalize the nearest-neighbor kernel as its limiting case of $p \rightarrow \infty$. In the following, when we speak of variable bandwidth, we will always assume that Eq. (3) applies, with $p = 4$. Figure 2 shows a toy-model calculation for a single pedestrian: The bandwidth decreases with the number of pedestrians located in the near vicinity, and their respective distance. We interpret this behavior as the compression of personal space in crowded situations, see Sect. 4.

3.3 Modeling Obstacles

In order to model obstacles, we propose the following additional procedure to be implemented when computing smooth density and flow fields via kernel estimation. Note, however, that we choose not to use this method for the computations presented here since the computational overhead is barely justified for the few obstacles present in the area where we conducted our experiments. Nevertheless, for more constrained geometries—such as a corridor, for example—we expect this method to be of some value. First, define the characteristic function of the experimental area:

$$\chi(\mathbf{x}) = \begin{cases} 0 & \text{if } \mathbf{x} \text{ is inside an obstacle,} \\ 1 & \text{if } \mathbf{x} \text{ is not inside an obstacle.} \end{cases}$$

Then, define a smoothed characteristic function by convolution with a suitable mollifier:

$$\chi_\epsilon(\mathbf{x}) := (\chi * \psi_\epsilon)(\mathbf{x}) = \int_{\mathbb{R}^2} \chi(\mathbf{x}) \cdot \psi_\epsilon(\mathbf{y} - \mathbf{x}) \, d^2y.$$

For example,

$$\psi_\epsilon(\mathbf{x}) = \begin{cases} \frac{1}{\epsilon^2} \exp\left(-\frac{\epsilon^2}{\epsilon^2 - \|\mathbf{x}\|^2}\right) & \text{if } \|\mathbf{x}\| < \epsilon, \\ 0 & \text{if } \|\mathbf{x}\| \geq \epsilon. \end{cases}$$

For each fixed time t and pedestrian $i \in I$, compute (by any method of choice) the function $k_i(t, \mathbf{x})$ associated with this pedestrian's position, and correct this function so that it vanishes inside of obstacles:

$$k_i^{(\text{corr})}(t, \mathbf{x}) = \frac{k_i(t, \mathbf{x}) \cdot \chi_\epsilon(\mathbf{x})}{\int_{\mathbb{R}^2} k_i(t, \mathbf{y}) \cdot \chi_\epsilon(\mathbf{y}) \, d^2y}.$$

Calculate the density ρ and the flow component \mathbf{j}_m with these corrected kernel functions. In order to compute the corresponding value for \mathbf{j}_c , numerically solve the Poisson equation

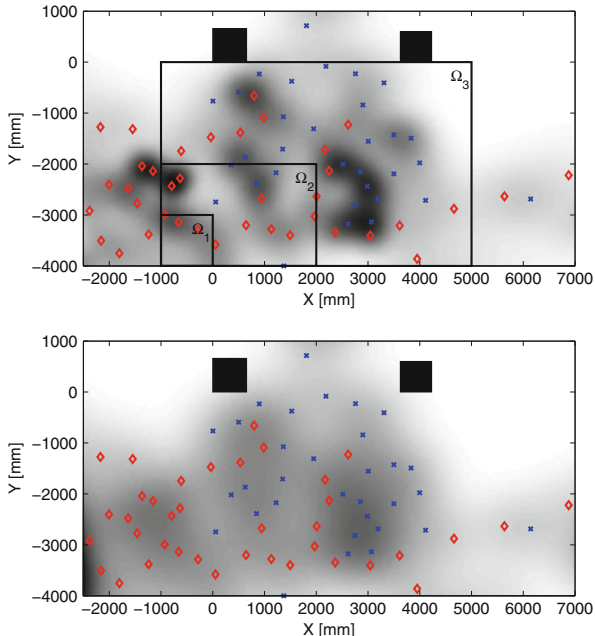
$$\Delta u = \frac{\partial \rho}{\partial t} + \text{div}(\mathbf{j}_m),$$

and define $\mathbf{j}_c = -\text{grad}(u)$. In order to solve this equation, one may use, for example, finite-differencing [16, pp. 1024–1030], and choose a constant Dirichlet boundary condition far away from the observation area to enforce uniqueness.

4 Results and Discussion

Figure 3 illustrates how the variable-bandwidth estimator distributes pedestrian mass to favor densely crowded regions. Probably any sensible macroscopic crowd model provides a mechanism that prevents pedestrian mass to be distributed to regions of already high density since pedestrians generally avoid crowded areas. On the other hand, as opposed to this repulsive short-range action, it is often assumed that there is also an attractive long-range action (similar to the effect of chemotaxis, cf. [17]). Our method of computing densities is in fact consistent with this assumption: Consider two single pedestrians approaching one another. At long distances, they will not regard each other as obstacles since their personal space is still large, and their mass is distributed over a large region. At shorter distances, however, they will avoid entering the personal space of each other since this would lead to a very large local density.

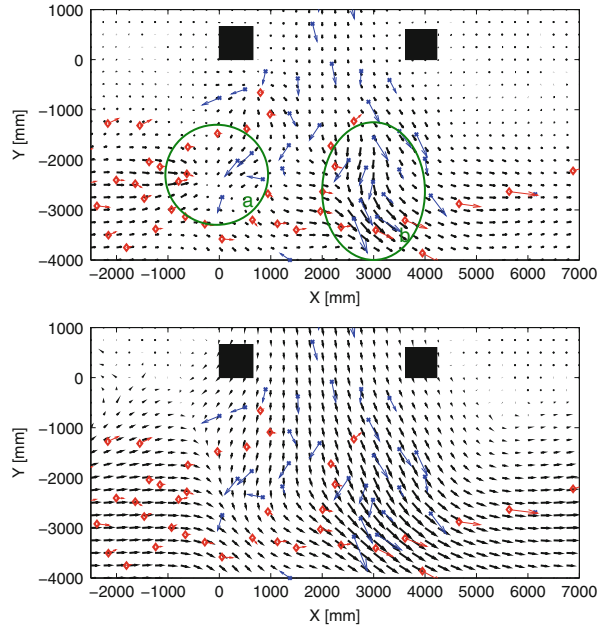
Fig. 3 Pedestrian density field at a fixed point in time. *Top*: variable-bandwidth estimator, *bottom*: fixed-bandwidth estimator ($d_i = 0.7$ m). Max. value: 7.1 m^{-2} . *Red diamonds*: group A, *blue crosses*: group B



Also, this tendency to highlight pedestrian clusters may prove to be advantageous for (visually) identifying (social) groups in naturally occurring human crowds, the study of which is also an important task; see, for example, [12].

As for the flow computed via the variable-bandwidth method, the additional component \mathbf{j}_c arises from the shrinking or expanding of the Gaussians due to the change in distance between pedestrians. In other words, \mathbf{j}_c describes the transport of mass via compression of the pedestrians’ personal space in crowded situations. On the other hand, one might be tempted to think of \mathbf{j}_m as the “actual” transport of pedestrian mass due to the displacement of pedestrians. However, one has to be careful with this interpretation since the length scale determined by Eq. (3) is to be understood as a free path and not an approximation of the physical size of the pedestrian. Nevertheless, in the context of crowd disasters, we suggest that this distinction between the flow components may be an appropriate way to identify panic situations: Even if regions with large density ρ or flow \mathbf{j} exist, this does not necessarily indicate a (potentially) dangerous situation—imagine, for example, an elevator full of people or a large marathon event, respectively. However, it has been noted that panic situations can be characterized by a number of typical features, a comprehensive list of which is given in [5]. These features include physical interactions between people, clogging and incoordinated movement—all of which are indicated by large changes in density due to the compression of personal space (Fig. 4). In Fig. 3, a comparison of the fixed-bandwidth and variable-bandwidth flow is given by example. The fixed-bandwidth flow appears as a simple superposition of the pedestrian flows A and B. Both computation methods yield a free flow of

Fig. 4 Pedestrian flow field at a fixed point in time. *Top*: variable-bandwidth estimator, *bottom*: fixed-bandwidth estimator ($d_i = 0.7$ m). *Blue and red arrows* indicate the velocities of individual pedestrians



pedestrian mass exiting the observation area in the region marked (b). In contrast to this, in region (a), the variable-bandwidth estimator shows a sink of pedestrian mass which is due to the compression of personal space when one lane of the bifurcating flow *B* meets the dominant flow *A* almost head on.

Figure 5 shows the functions $\text{div } \mathbf{j}$ and $\text{div } \mathbf{j}_c$ spatially averaged across a microscopic region, plotted against time. We see that temporal changes in density are more pronounced with the variable-bandwidth method. It can also be noted that the temporal changes of personal space indicated by $\text{div } \mathbf{j}_c$ have a larger amplitude when the two pedestrian flows actually meet. However, we acknowledge that this observation is not fully conclusive since the large scatter might also be caused by random measurement errors.

4.1 Comparison with Other Methods

In the following, we would like to compare the different methods mentioned in this work as to their ability to represent the mean density and flow on different spatial scales. To this end, the spatially averaged density and flow is plotted versus the time in Fig. 6, computed via different methods in three regions of different size. One may characterize these regions as microscopic, mesoscopic and macroscopic—although we do not wish to claim that this terminology should generally be applied to regions of the respective size.

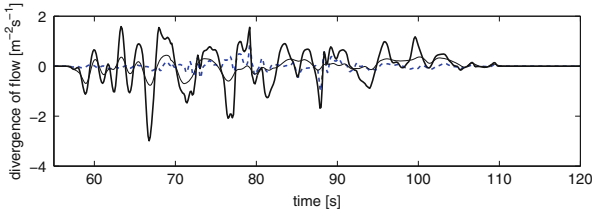


Fig. 5 Divergence of the flow vs. time, spatially averaged across the microscopic region Ω_1 marked in Fig. 3, $|\Omega_1| = 1 \text{ m}^2$. *Thin black line*: fixed-bandwidth estimator, *thick black line*: variable-bandwidth estimator, *dashed blue line*: divergence of the flow component j_c

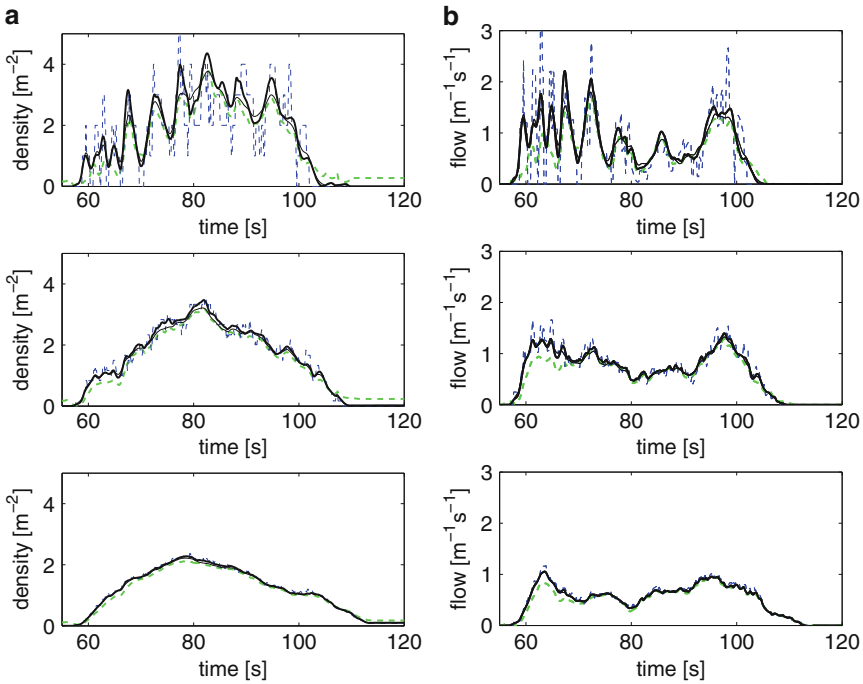


Fig. 6 Spatial average across the rectangular regions marked in Fig. 3. From top to bottom: region with area $|\Omega_1| = 1 \text{ m}^2$, $|\Omega_2| = 6 \text{ m}^2$ and $|\Omega_3| = 24 \text{ m}^2$. *Thin black line*: fixed-bandwidth estimator, *thick black line*: variable-bandwidth estimator, *thin dashed blue line*: standard density/flow, *thick dashed green line*: Voronoi density/flow. (a) Density vs. time. (b) Flow of pedestrian group A in x -direction vs. time

For the computations, we assumed that the pedestrians stop and cease to move once they exit the area covered by the cameras. This was to avoid outliers in the flow measurement because of incomplete trajectories—cf. the first issue noted in the concluding section of this work. Also, this workaround assures a fairer comparison with the Voronoi method that we implemented in its unmodified form that was

originally proposed in [20] and which was not designed for sparse, unconstrained crowds.

Naturally, the methods yield very similar values for the macroscopic region. However, for microscopic regions a significant difference can be noted: the standard density shows large scatter while all three alternative methods appear as smoothed versions of this standard density. Therefore, these methods may be used to reliably compute the density and flow for sparse or dense crowds, and work well on any scale.

While there is not much difference in the total values of the density, the temporal variation, and therefore the divergence of the flow, may show vast differences between fixed and variable bandwidth method as illustrated by Fig. 5.

5 Conclusion

In this paper, we have demonstrated that kernel estimation methods provide an attractive alternative to the standard or the Voronoi method of measuring densities or flows. Also, these kernel methods naturally yield smooth density and flow fields. We argue that estimating such fields from experimental data is helpful in evaluating macroscopic crowd models which yield precisely this type of data. Also, we have shown that even kernel methods with variable bandwidth may be designed in such a way that the resulting density and flow field satisfy the continuum equation.

Moreover, the kernel estimator with variable-bandwidth proposed by us may provide a useful model for changes in personal space, which is also a key idea when formulating the approach based on Voronoi diagrams. These changes in personal space reflect in the dynamic density and flow fields and may be used to effectively visualize effects such as clogging or counter flows.

However, there are some practical and theoretical issues that particularly concern the variable-bandwidth kernel method:

1. In human crowd experiments, trajectories are often incomplete as pedestrians leave the area observed by the cameras. This circumstance usually results in the computation of temporally discontinuous densities and very large flows because of the sudden change in density when pedestrians leave the observation area and “vanish”. Although this problem may potentially present itself with any computation method, the variable-bandwidth kernel method is particularly susceptible to it.
2. It would be preferable to obtain the parameter values λ and p in a data driven, automatic manner—for example, by techniques already known from statistical data analysis. We suggest that one approach to obtain the parameter λ , at least, might be given in [22]. On the other hand, analogies relating probability and pedestrian densities only extend to a certain degree and one might think that these parameter values should be fixed as they are inherent to any crowd configuration.

3. We have to acknowledge that the variable-bandwidth estimator lacks robustness against errors in the measurement of the pedestrians' trajectories. For example, if the spatio-temporal positions of two different pedestrians were to (almost) coincide due to a measurement error, very large, factually incorrect density values may occur. If no reliable data is available, a workaround would be given by enforcing a lower limit on the bandwidth.
4. In some circumstances, the variable-bandwidth estimator yields large local density values ($> 10 \text{ m}^{-2}$) that—in principle—cannot be predicted by macroscopic models which usually have a restricted range of density values. However, this might only reflect the fact that macroscopic models are designed to describe crowds at large scales.
5. As already noted earlier, the divergence of the flow depends significantly on the type of kernel used for computation, at least when averaged across microscopic regions (see Fig. 5). It also largely depends on the chosen parameters, and the relationship of such graphs to discrete analogues based on the standard density remains unclear.

We conclude by noting that the measuring techniques presented here may be understood as particular smoothing procedures based on the standard definition of a particle density, which do not seem to add any particularly relevant information to the data. In fact, if one is solely interested in the spatial average across macroscopic regions of dense crowds, probably any technique would suffice. However, even an artificial increase in spatio-temporal resolution may prove to be insightful when visualizing data based on sparse pedestrian flows and/or microscopic regions of a crowd, resolving fine-structure that would otherwise remain unseen (cf. [23]).

Acknowledgements We would like to thank all university staff and students who helped with conducting the experiments, and we especially thank C. Neumann for carrying out the data analysis and implementing the density/flow estimation algorithm based on Voronoi diagrams.

The authors gratefully acknowledge the support of Deutsche Forschungsgemeinschaft (German Research Foundation) for the project SCHW548/5-1 + BA1189/4-1. The numerical calculations were made with the computing software MATLAB by MathWorks.

Finally, we would like to thank the organizers of the 6th International Conference on Pedestrian and Evacuation Dynamics 2012, ETH Zurich, Switzerland.

References

1. Burstedde, C., Klauck, K., Schadschneider, A., Zittartz, J.: Simulation of pedestrian dynamics using a two-dimensional cellular automaton. *Physica A* 295, 507–525 (2001)
2. Daamen, W., Hoogendoorn, S.P.: Experimental research on pedestrian walking behavior. In: Transportation Research Board annual meeting. pp. 1–16 (2003)
3. Galea, E.R., Filippidis, L., Wang, Z., Lawrence, P.J., Ewer, J.: Evacuation analysis of 1000+ seat blended wing body aircraft configurations: Computer simulations and full-scale evacuation experiment. In: *Pedestrian and Evacuation Dynamics 2010*. pp. 149–151 (2011)
4. Guo, R.Y., Wong, S., Huang, H.J., Zhang, P., Lam, W.: A microscopic pedestrian-simulation model and its application to intersecting flows. *Physica A* 389, 515–526 (2010)

5. Helbing, D., Farkas, I.J., Molnár, P., Vicsek, T.: Simulation of pedestrian crowds in normal and evacuation situations. In: Proc. PED 2001. pp. 21–58 (2002)
6. Helbing, D., Molnár, P.: Social force model for pedestrian dynamics. *Phys. Rev. E* 51(5), 4282–4286 (1995)
7. Helbing, D., Johansson, A., Al-Abideen, H.Z.: Dynamics of crowd disasters: An empirical study. *Phys. Rev. E* 75, 046109 (2007)
8. Hughes, R.L.: A continuum theory for the flow of pedestrians. *Transportation Research Part B* 36, 507–535 (2002)
9. Kuhn, H.W.: The Hungarian method for the assignment problem. *Naval Research Logistic Quarterly* 2, 83–97 (1955)
10. Liddle, J., Seyfried, A., Steffen, B., Klingsch, W., Rupperecht, T., Winkens, A., Boltes, M.: Microscopic insights into pedestrian motion through a bottleneck, resolving spatial and temporal variations (2011), arXiv:1003.5465v1 [physics.soc-ph]
11. Lucas, B.D., Kanade, T.: An iterative image registration technique with an application to stereo vision. In: Proc. of Imaging Understanding Workshop (1981)
12. Moussaïd, M., Perozo, N., Garnier, S., Helbing, D., Theraulaz, G.: The walking behaviour of pedestrian social groups and its impact on crowd dynamics. *PLoS ONE* 5(4), e10047 (2010)
13. Munkres, J.: Algorithms for the assignment and transportation problems. *Journal of the Society for Industrial and Applied Mathematics* 5(1), 32–38 (1957)
14. Plaue, M., Chen, M.J., Bärwolff, G., Schwandt, H.: Trajectory extraction and density analysis of intersecting pedestrian flows from video recordings. In: ISPRS Conf. on Photogrammetric Image Analysis 2011. *Lecture Notes in Computer Science*, vol. 6952, pp. 285–296. Springer (2011)
15. Plaue, M., Chen, M.J., Bärwolff, G., Schwandt, H.: Multi-view extraction of dynamic pedestrian density fields. *Photogrammetrie, Fernerkundung, Geoinformation* (2012), accepted
16. Press, W.H., Teukolsky, S.A., Vetterling, W., Flannery, B.P.: *Numerical recipes: The art of scientific computing*. Cambridge University Press, 3rd edn. (2007)
17. Schadschneider, A., Kirchner, A., Nishinari, K.: CA approach to collective phenomena in pedestrian dynamics. In: Proc. ACRI 2002. *LNCS*, vol. 2493, pp. 239–248 (2002)
18. Shi, J., Tomasi, C.: Good features to track. In: Proc. of the IEEE Comp. Soc. Conf. on Computer Vision and Pattern Recognition. pp. 593–600 (1994)
19. Silverman, B.W.: *Density Estimation for Statistics and Data Analysis*. Chapman and Hall (1986)
20. Steffen, B., Seyfried, A.: Methods for measuring pedestrian density, flow, speed and direction with minimal scatter. *Physica A* 389, 1902–1910 (2010)
21. Terrell, G.R., Scott, D.W.: Variable kernel density estimation. *Ann. Statist.* 20(3), 1236–1265 (1992)
22. Wu, T.J., Chen, C.F., Chen, H.Y.: A variable bandwidth selector in multivariate kernel density estimation. *Statistics Probability Lett.* 77(4), 462–467 (2007)
23. Zhang, J., Klingsch, W., Schadschneider, A., Seyfried, A.: Transitions in pedestrian fundamental diagrams of straight corridors and T-junctions. *J. Stat. Mech.* p. P06004 (2011)

On the Simulation for Rail Tunnel Evacuation with Cross-Passageways

S.B. Liu, S.M. Lo, and J. Ma

Abstract To study the evacuation from rail tunnels is vital for saving human lives when trains are forced to stop inside the tunnel due to fire or other incidents. Although NFPA 130 standard has given limited suggestions on the design of means of egress in rail tunnels, very rare other references can be found about the tunnel evacuation so far. In this paper, an agent based continuous crowd simulation model was developed to study the evacuation from rail tunnel with cross-passageways. This study has focused on the influence of the walkway width and cross-passageway spacing on the egress time and queuing patterns during the evacuation. In our simulation, it was found that if the width of walkway was added by every 100 mm, the egress time would decrease accordingly, but with different sensitivity at different width. The continuous model was proved to be eligible for identifying the continuously change of the dimensions of egress element. The study also revealed that the distance between cross-passageways was highly relevant to the optimized evacuation route choice strategy and certainly was an important parameter for egress time.

Keywords Agent-based model • Cross-passageway • Evacuation • Rail tunnel

S.B. Liu • S.M. Lo (✉)

Department of Civil and Architectural Engineering, City University of Hong Kong, Kowloon Tong, Hong Kong

e-mail: boliu9@student.cityu.edu.hk; bcsmli@cityu.edu.hk

J. Ma

Department of Civil and Architectural Engineering, City University of Hong Kong, Kowloon Tong, Hong Kong

School of transportation and Logistics, Southwest Jiaotong University, Chengdu 610031, China
e-mail: majian@mail.ustc.edu.cn

1 Introduction

It has been reported in the book “The handbook of tunnel fire safety” [1] that hundreds of serious tunnel fires had caused the loss of tens of thousands of lives during the past few decades. It indicated that tunnels, with their particular geometry nature, have added new dimensions to the already complex process of egress from fire or other emergencies.

Accompanying with the boom of fire safety research started from the last century, studying the behavior of evacuees in tunnel fires has also attracted researchers’ interests. Real tunnel fire incidents surveys [2] as well as tunnel evacuation experiments in laboratory scale [3] and full scale [4] have been conducted to study the human or facility factors during tunnel evacuations. Some standards or engineering references such as the NFPA(National Fire Protection Association) 130 standard [5] and the SFPE(Society of Fire Protection Engineers) hand book [6] also have provided much knowledge on tunnel design for the purpose of evacuation and fire protection. Computer simulation software such as Building Exodus [7], STEPS [8] etc. have also been used to study the evacuation from tunnels. However, detailed studies on this topic, especially on the sensitivity analysis of different dimensions of tunnel egress route elements, are still vital important because of the special nature of the tunnel geometries, e.g. different walkway widths or different spacing between cross-passageways etc. Many pedestrian flow or evacuation simulation models developed so far, including the discrete models and continuous models [9] may be usable for investigating this problem. But the discrete models usually discretize the floor plan into uniform rectangular grids which may be difficult to distinguish the difference when changes of the dimension are less than the grid size, such as 100 mm’s change of the width of a walkway. On the contrary, the continuous models treat the space continuously and thus are able to handle any minor changes of the dimension [10].

In this paper, a continuous agent based pedestrian simulation model will be used to investigate the tunnel egress problem. The research has focused on identifying the egress time and the pattern of the pedestrian flow under different tunnel egress element dimensions. Means of egress in rail tunnels, including the walkway alongside the track and the cross-passageway which leads to “safety points” such as another twin-tunnel or an open space have been considered in this research. Different walkway width and spacing between two cross-passageways have been examined by simulating different tunnel evacuation scenarios.

2 The Simulation Model

The architecture of the model has been shown in Fig. 1. Human behaviors in crowd movement can typically be distinguished at three levels: the strategic level, the tactical level and the operational level [11]. Here, the strategic and tactical

Fig. 1 Architecture of the simulation model in overview

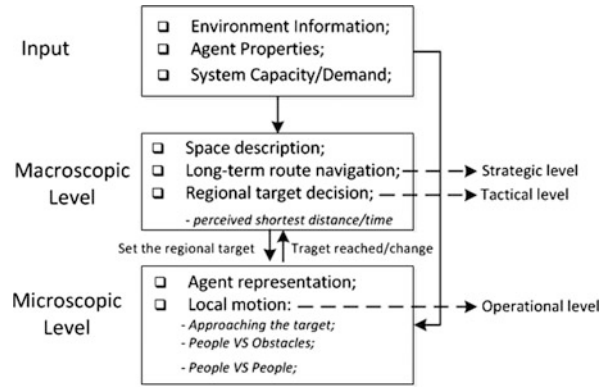
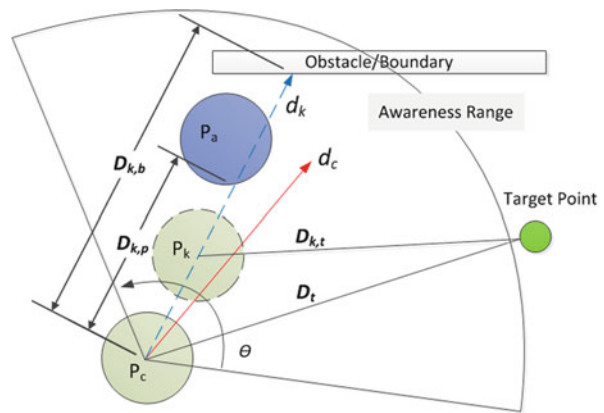


Fig. 2 Representation of the agent and the variables defined for direction d_k



level of behaviors can be implemented on a macroscopic level. First, the floor plan will be divided into separate zones with connections serving as portals to adjacent zones. Then the agent could navigate its route through different zones by a list of connections. On the operational level, an agent is represented as a circle (Radius = 20 cm) with movement direction, awareness angle and awareness distance (Fig. 2). The awareness angel θ is discretized into sub-angles every $\Delta\theta$. Then if the current moving direction is θ_c , the possible moving direction k may be denoted as $d_k = \theta_c \pm \Delta\theta$. We assume that if d_k has been selected, the agent would move one step towards this direction based on its moving speed and the time gait size. And if the regional target has been reached, the agent will be transferred from the current zone to the next zone and recalculate the new target point. The probability of choosing direction d_k is defined by the following factors:

1. The efficient of approaching the target point: this factor is measured as the relative value of D_t and $D_{k,t}$; where, D_t means the distance from the current position P_c to the target point; $D_{k,t}$ means the distance from the future position P_k to the target point;

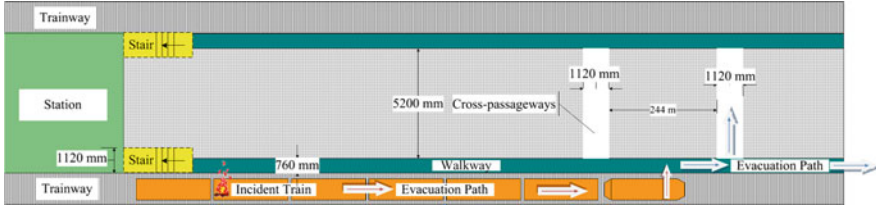


Fig. 3 Schematic illustration of the tunnel evacuation scenario setup: W denotes the width of evacuation walkway, S represents the interval of cross-passageway (CP), and C is the width of the cross-passageway

2. $D_{k,b}$: the distance from the nearest obstacles or the geometry boundaries;
3. $D_{k,p}$: the distance from the nearest agent on the direction d_k ;

In the next two sections, the model will be used to study the evacuation time and crowd flow pattern under different dimensions of tunnel egress elements.

3 The Tunnel Evacuation Scenarios

A schematic illustration of evacuation scenario from tunnel is showed in Fig. 3. According to the NFPA 130, the walkway width W shall be not less than 610 mm, and the cross-passageways shall not be farther than 244 m apart and shall not be further than 244 m from the station or tunnel portal. Cross-passageways shall be a minimum of 1,120 mm in clear width and 2,100 mm in height [5].

Since the cross-passageways are regarded as the emergency exit, the passenger is considered safe if he walk through the cross passage and reach the twin tunnel. Detailed information of the train in the simulation is shown in Table 1.

Our study has focused on the influence of the different walkway width W and cross-passageways spacing S on the evacuation results. Two scenarios, scenario A and B, each with 11 cases, have been setup to study the influences of W and S , correspondingly. The cross-passageway width C in both scenarios is set to be 1,620 mm. The dimensions of the two key egress elements in Case A1–A11 and Case B1–B11 have been shown in Tables 2 and 3.

4 Simulation Results and Discussions

To keep the consistency of simulations for different cases, the optimized route selection strategies are used in all of these cases in our simulations.

Table 1 Train car details

Train Dimension	3 × 25 m per car (8 cars, 211 m in length)
Train exit doors	1,500 mm width (five exit per car on each side)
Intercar gangway	1,600 mm width
Train capacity	2,500 people (about 63 passengers every car in average)

Table 2 Dimensions of cross-passageway spacing and walkway width set for Case A

Case	A1	A2	A3	A4	A5	A6	A7	A8	A9	A10	A11
<i>S</i> (m)	211	211	211	211	211	211	211	211	211	211	211
<i>W</i> (mm)	610	710	810	910	1,010	1,110	1,210	1,310	1,410	1,510	1,610

Table 3 Dimensions of cross-passageway spacing and walkway width set for Case B

Case	B1	B2	B3	B4	B5	B6	B7	B8	B9	B10	B11
<i>S</i> (m)	244	294	269	244	211	194	169	144	120	90	60
<i>W</i> (mm)	610	810	810	810	810	810	810	810	810	810	810
Number of CP used	2	2	2	2	2	2	3	3	3	3	5

CP cross-passageway, *S* cross-passageways spacing, *W* walkway width

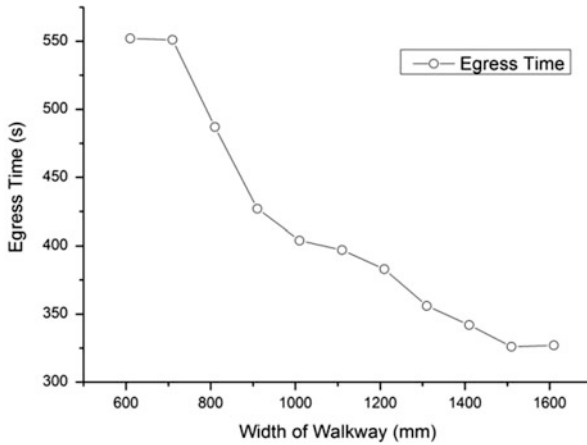


Fig. 4 Egress times as a function of walkway width in simulations of Case A1–A11

4.1 Influence of Different Walkway Width (Study of Scenario A)

Simulation scenario A (case A1–A11, see Table 2) is designed to study the influence of different walkway width. First, the egress times for the 11 cases are recorded (See Fig. 4). It is clear that a wider walkway would lead to a shorter egress time, and larger flux (see Fig. 5), but the sensitivity of the 100 mm’s change varies at different walkway width. It can be seen that the egress time is more sensitive to this change when *W* = 710–1,010 mm. This is probably due to the relative width of the walkway and the cross-passageway.

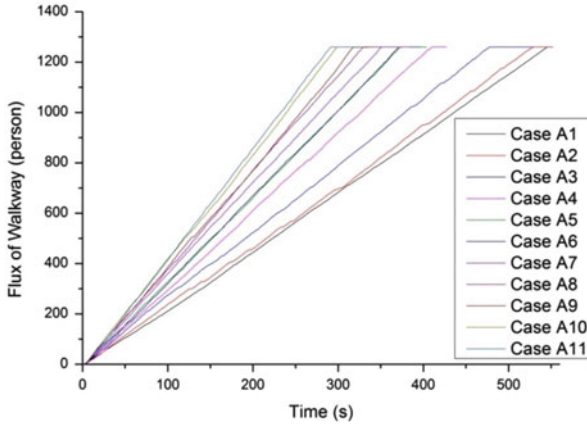


Fig. 5 Pedestrian flux on the walkway

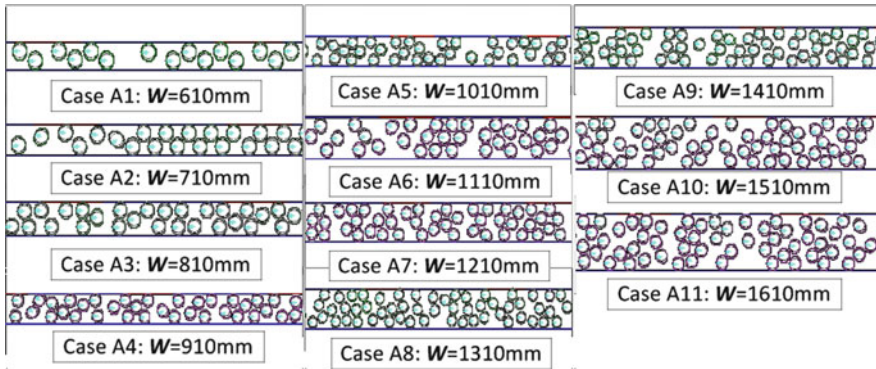


Fig. 6 Queuing patterns in walkways with different dimensions

Besides, we can see from Figs. 4 and 5 that, every 100 mm’s change has resulted in a different egress time and walkway flux. For example, walkways with width of 810 and 910 mm perform very different in our simulation, because different dimensions of walkways have led to different queuing patterns during the evacuation. As what is shown in Fig. 6 (Case A1)–(Case A11), when $W = (n \times 400 + 10)$ mm ($n = 2, 3, 4$) Fig. 6 (Case A3, A7, A11), people may walk side by side and regular parallel queue will show up since the radius of the agent in our model is 200 mm, otherwise, the queue will be shown in an irregular staggered pattern.

4.2 Influence of Different Cross-Passageway Spacing (Study on Scenario B)

The distance between every two cross-passageways is another sensitive parameter for the tunnel evacuation. It is recommended in the NFPA 130 standard that

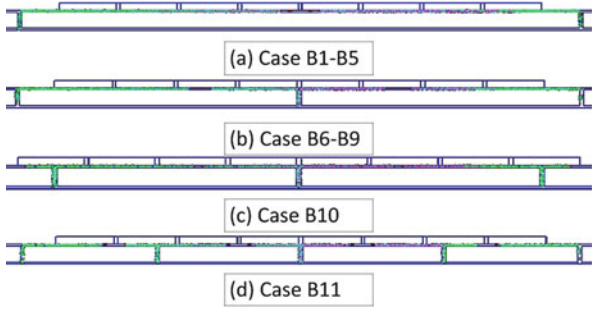


Fig. 7 Number of cross-passageway used and the optimized route selection strategy for case B1–B11

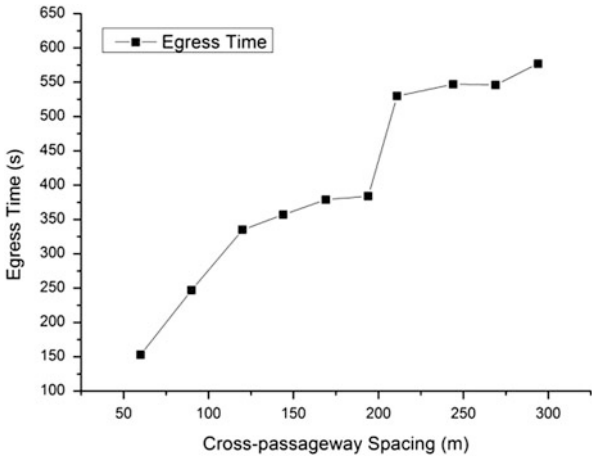


Fig. 8 Egress times as a function of the different value of cross-passageway spacing S in simulation of Case B2–B11

the maximum spacing between two cross-passageways is 244 m, but without mentioning any time based criteria. Here, scenario B (simulation case B1–B11, see Table 3) is designed to give an elementary discussion on the evacuation under various cross-passageway spacing.

It is assumed all the evacuees know the environment well and can take the optimized evacuation strategy. As shown in Fig. 7, the number of cross-passageways used and the evacuation route selection strategies in Fig. 7a–d are corresponding with the situations in Case B1–B5, Case B6–B9, Case B10, and Case B11, respectively. Besides, the egress time for each case are recorded (see Fig. 8). There is no doubt that the nearer the value S is, the easier the evacuation becomes, since a smaller S will lead to either shorter travel distance or more available emergency exits. However, the distance which is equal to the length of a train (Case B5) may serve as a critical value for deciding the maximum spacing between every

two cross-passageways. Because if the $S >$ length of a train, there will become at most two cross-passageways for use under our assumptions. And the further the two cross-passageways apart to each other, the longer the egress distance will be.

5 Conclusions

By referring to the literature on the tunnel evacuation study and the requirements stated in NFPA 130 standard, this paper studied the tunnel evacuation problem by means of simulation. The study has focused on the influence of the width of walkways and the cross-passageway spacing. An agent based continuous pedestrian flow simulation model has been developed to simulate a serial of different tunnel egress scenarios.

Two scenarios, namely scenario A and B have been simulated. In scenario A, walkways with different width which range from 610 to 1,610 mm have led to different egress times and queuing patterns. It has been found that the increase of walkway width will reduce the egress time but with a more sensitive effect between 710 and 1,010 mm. Continuous models have been approved to be more flexible on dealing with the change of egress element dimension by 100 mm. In scenario B, different cross-passageway spacing has resulted in different travel distances and the number of cross-passageways available for evacuation. And it is recommended that the distance which is equal to the length of a train be a critical value for the cross-passageway spacing evaluating.

Acknowledgement The work described in this paper was fully supported by a grant from the Research Grant Council, Government of the Hong Kong Administrative Region, China: No. CityU119011.

References

1. Carvel, R. and G. Marlair, A history of fire incidents in tunnels, in *The handbook of tunnel fire safety*, Alan Beard and R. Carvel, Editors. 2005, Thomas Telford: Heron Quay, London. p. 3–37.
2. Shields, J., Human Behavior in Tunnel fires, in *The handbook of tunnel fire safety*, Alan Beard and R. Carvel, Editors. 2005, Thomas Telford: Heron Quay, London. p. 323–341.
3. Oswald, M., H. Kirchberger, and C. Lebeda, Evacuation of a High Floor Metro Train in a Tunnel Situation: Experimental Findings, in *Pedestrian and Evacuation Dynamics 2008*. 2008. p. 67–81.
4. Oswald, M., et al., Full-Scale Evacuation Experiments in a smoke filled Rail Carriage - a detailed study of passenger behaviour under reduced visibility, in *Pedestrian and Evacuation Dynamics 2005*. 2007. p. 41–55.
5. NFPA, NFPA 130-Standard For Fixed Guideway Transit and Passenger Rail Systems 2010 Edition, in Chapter 6 Trainways. 2009: Batterymarch Park, Quincy, MA.

6. Bryan, J.L., Behavioral Response to Fire and Smoke, in SFPE Handbook of Fire Protection Engineering, P.J. DiNenno and W.D. Walton, Editors. 2002, National Fire Protection Association: Quincy, Massachusetts. p. 315.
7. Hao, S.Q., et al., Tunnel Fire Staff Evacuation Channel Distance Design based on EXODUS. 2009 International Conference on Networking and Digital Society, Vol 1, Proceedings. 2009. 269–272.
8. Zhang, N., et al., Research on the Disaster Prevention and Rescue and the Numerical Simulation of Safety Evacuation in the Super-Long Railway Tunnel. International Symposium on Emergency Management 2009, ed. J. Huang and L. She. 2009. 569–574.
9. Erica D. Kuligowski and R.D. Peacock, A Review of Building Evacuation Models, in National Institute of Standards and Technology Technical Note 1471. 2005, National Institute of Standards and Technology.
10. Schadschneider, A., et al., Evacuation Dynamics: Empirical Results, Modeling and Applications, in Encyclopedia of Complexity and System Science. 2009, Springer: Berlin Heidelberg New York.
11. Hoogendoorn, S.P. and P.H.L. Bovy, Pedestrian route-choice and activity scheduling theory and models. *Transp. Res., Part B: Methodologies*, 2004. 38(169).

Pedestrian-Vehicles Interaction During Evacuation: Agent-Based Hybrid Evacuation Modelling of Southeast Asian Cities

Manuela Di Mauro, Michael Lees, Kusnowidjaja Megawati,
and Zhenhua Huang

Abstract Southeast Asian cities such as Jakarta (Indonesia) present traffic patterns that differ importantly from ‘Western’ cities. This includes the typology of vehicles, lane utilization and distinctions between pedestrian and vehicular routes. Such differences are maintained, and sometimes accentuated, during a sudden evacuation, such as the one that might occur as consequence of a (actual or perceived) tsunami hazard. Most of the commonly used traffic models are not designed for reproducing these patterns, assuming that the vehicles would follow queuing patterns or lane divisions, and allowing a limited interaction between pedestrians and vehicles. In reality, during a non-staged sudden evacuation, the portion of the road occupied by pedestrians can vary significantly, seemingly depending on the ratio between pedestrians and vehicles. This paper presents the results of a study aiming to develop a hybrid evacuation model able to target these issues. In particular, the model aims to describe the vehicular traffic consistently with the local traffic patterns, and represent a strong interrelationship between vehicular and pedestrian traffic, under the constraint of modelling a large number of evacuees. Results from preliminary applications are presented and compared with existing models.

Keywords Mass evacuation • Mixed models • Vehicle-pedestrians interaction

M. Di Mauro (✉) • K. Megawati • Z. Huang
Earth Observatory of Singapore, Nanyang Technological University, Singapore, Singapore

Civil and Environmental Engineering, Nanyang Technological University, Singapore, Singapore
e-mail: manuela@ntu.edu.sg; kusno@ntu.edu.sg; zh Huang@ntu.edu.sg

M. Lees
Computer Engineering, Nanyang Technological University, Singapore, Singapore
e-mail: mhlees@ntu.edu.sg

1 Introduction

Most of the commonly used models for traffic (both macro and micro scale) are designed for specific orderly traffic, assuming that the vehicles follow queuing patterns or lane divisions. These features are not applicable to many cities in Southeast Asia, which also present a very specific traffic composition, including a high rate of motorbikes and smaller vehicles (for example, see [1]).

Another important feature of the traffic in Southeast Asian cities concerns the interaction between pedestrian and vehicles. In modelling mass evacuation, vehicles and pedestrians are usually modelled separately: allowing for some transversal interactions, to simulate pedestrian crossing the roads; and/or longitudinal interactions, by introducing some degree of reduction in the road capacity when pedestrian temporarily hop off and on the footpath (e.g. [2, 3]). Such models assume that pedestrians will mainly remain within the delimited footpath during an evacuation. However, in many cities, particularly in Southeast Asia, pedestrian and vehicular traffic flows are not rigidly separated, even in normal (non-emergency) situations, see for example [4]. In many cases, urban roads do not have footpaths, and both vehicles and pedestrians tend to occupy any possible free space in the roads. This coupling of pedestrian and traffic dynamics can greatly impact any large scale evacuation in such cities, especially in the case of a non-staged evacuation following, for example, a short-term warning. To model this form of evacuation it is therefore necessary to capture the impact that traffic has on pedestrians and vice versa.

This paper presents the preliminary results of a study aiming to produce a novel model that is able to simulate the interaction between vehicles and pedestrians, and in general capturing the specific conditions of the traffic in many Southeast Asian cities.

2 Description of the Model

The main objective of the model is to be able to capture and analyze the following aspects of the evacuation:

- Evacuation times and critical points on the road network;
- Benefits/consequences of application of emergency management measures;
- Sensitivity of the results to different evacuees behaviours.

Further than being consistent with the local traffic conditions and representing the interaction between pedestrian and vehicles, the model must be able to handle a large number of vehicles and pedestrians. In fact, the population density of Southeast Asian cities is larger than the average world density [5], while a degree of urbanization around and over 30 % (except only Cambodia) confirms that this high density mainly occurs in the cities [6]. Major cities like Jakarta, Manila,

and Bangkok have a population over ten million people, while ‘minor’ cities such as Hanoi, Bandung and Medan gravitate well over two millions [7]. Hence, the principle requirements for such model are:

- To be able to handle a large (over 10,000) number of evacuees.
- To represent the vehicular traffic consistently with local traffic patterns;
- To model a strong(er) interaction between pedestrian and vehicular traffic;

This section describes the technical features of the novel model that was developed as part of this study, aiming to fulfil these requirements.

2.1 Traffic Algorithms

Traffic can be modelled using different techniques that loosely fall in the classification of macro, meso and micro models. Macromodels employ averaged traffic parameters and their governing equations are usually based on extensive traffic measurements, both characteristics leading to a potentially limited uncertainty in the calculated (averaged) traffic patterns. They can also handle a large number of vehicles. On the other hand, they usually cannot satisfactory model heavy traffic conditions, as their equations usually do not converge when the road is close to its full capacity [8]. Also, these models do not allow modelers to follow the trajectories of specific vehicles [9] and cannot represent individual route choices or other behaviours.

Micromodels are able to represent individual behaviours such as route choices and overtaking, to assign and track individual trajectories. However, the representation of the individual behaviours might lead to oversensitivity of some parameters; and the uncertainty in each single assigned behaviour might resolve in a non-linear growth of the uncertainty in the results. They also require greater computational resources to model the same volume of traffic, when compared to macromodels.

The desired outcomes from the model presented in this paper are consistent with the choice of a macro-scale model. However, the instability of the macroscale equations at high density conditions and the desired ability of the model to explore different behaviours of the evacuees favour the preference for a micro approach.

To incorporate the advantages of both modelling approaches, we chose to develop a mesoscale model. In the resulting model, the vehicles and pedestrian are modelled as individual entities (agents). The model in this sense is ‘agent-based’, because the entities are modelled individually, they occupy a physical space in the model domain and they can assume individual behaviours.

The traffic at the road junctions (nodes), including the ‘start’ and ‘end’ points, is modelled with a micro-scale approach, by assigning a maximum capacity to the junction (traffic volume per unit of time) according to which each vehicle (or pedestrian) can or cannot enter the junction. Empirical fundamental diagrams for the intersections are used to model the relationships between the capacity and actual inflow, which determine the effective inflow and waiting time at the intersections.

For the vehicles, these are inferred from local Highway Capacity Manuals. For pedestrians, the nodes are treated as bottlenecks, and their capacity is determined according to [10]. If the vehicle (pedestrian) cannot enter the junction, it will be forced to wait on the upstream road, contributing to the current capacity of that road.

Each road also has a maximum capacity that is calculated from local Highway Capacity Manuals. According to the continuity equation, the flow of vehicles (or pedestrians) exiting a node will equal the flow entering the downstream node. If the maximum capacity is reached, the agent is forced to wait at the node, contributing to the capacity of the node itself.

The model therefore allows the spillback of vehicles (or pedestrians) from a node to the upstream road (if it cannot enter the node), and from a downstream road to the node (if it cannot enter the downstream road). In a macromodel, to ensure the continuity equation is respected, the spillbacks are managed by performing iterations at each time step, this allows the full traffic ‘spillback’ to be resolved in one time step. This is necessary to satisfy the continuity equation. In reality, the spillback does not occur instantaneously and the nodes have a certain storage capacity (e.g. [11, 9]). Therefore, we can assume that, if the timestep is small enough, the spillback occurs within one time step, meaning that the effect of the spillback is felt by the network in the subsequent timestep. This assumption holds if two conditions are respected: (1) the spillback volume in the timestep has to be lower than the maximum traffic volume per timestep (that is the maximum capacity of the road or the node) and (2) the nodes have to be allowed a storage capacity equal to the maximum traffic volume per timestep. If these conditions cannot be respected, the time step should be reduced or an error will occur. These conditions, however, are not applicable at the source nodes (where the vehicles\pedestrians start) and the arrival nodes, as these nodes are assumed to be able to store a larger number of vehicles. The arrival nodes thus maintain a limited capacity, which regulates the entrance rate to the node. The agents are modelled following a macro-modelling approach to represent their movements along each road. All the vehicles in the road link are assumed to have the same average speed, calculated using locally sourced empirical fundamental diagrams to represent the flows at the road links. At each time step, the vehicles move along the road links with a speed that is function of the actual flow (assumed constant during the time step) and the maximum capacity of the road. Similarly, the pedestrians move with the same average speed, calculated using Weidmann’s diagram for pedestrian in the links [12].

2.2 *Hybrid Model*

The main challenge for the implementation of the model is to represent the interaction between pedestrian and vehicular traffic. Footages of evacuation recorded in Cebu, Philippines (from the post-earthquake tsunami false alarm occurred the 6th February 2012) and in Padang, Indonesia (from the post-earthquake tsunami

false alarm of 30th September 2009) were examined. Although the duration and quality of these footages are too limited to extract formal measurements, it can be observed that the portion of the road occupied by pedestrians seems to depend on the ratio between pedestrians and vehicles. One piece of footage shows the pedestrian traffic engaging the entire road breadth, forcing the vehicles to proceed alongside the pedestrians, (apparently) assuming the same average speed.

To represent this interaction, the capacities of roads for both vehicles and pedestrian are modelled as variable. These variable capacities are calculated at each time step as functions of the total number of agents (pedestrians and vehicles) and the ratio pedestrian\vehicles. Three stages of traffic are modelled:

- *Vehicle-dominated*, when vehicles predominate and occupy the whole road (if they need to), and the pedestrian walk at the side, one following the other;
- *Balanced*, when vehicles and pedestrian traffic balance each others, and the pedestrians are left 1 m each side of the road;
- *Pedestrian-dominated*, when the pedestrians' volume is such that the vehicles are forced to proceed the same average speed as the pedestrians.

The transitions between each stage are regulated by thresholds that are functions of the ratio between the traffic volumes of vehicles and pedestrians (Eq. 1).

$$\begin{aligned}
 V_p/V_v \leq T_1 & \rightarrow w_p = 0.6 \text{ [m]}; & w_v = w_r - 0.8 \text{ [m]} \\
 T_1 < V_p/V_v \leq T_2 & \rightarrow w_p = 2 \text{ [m]}; & w_v = w_r - 2.4 \text{ [m]} \\
 V_p/V_v > T_2 & \rightarrow w_p = w_r - 1.6 \text{ [m]}; & w_v = 1.6 \text{ [m]}
 \end{aligned} \tag{1}$$

where:

$$\begin{aligned}
 V_p &= \text{volume of pedestrian traffic [m}^2/\text{s]} & V_v &= \text{volume of vehicular traffic [m}^2/\text{s]} \\
 w_p &= \text{road width engaged by pedestrians [m]} & T_1, T_2 &= \text{thresholds} \\
 w_v &= \text{road width engaged by vehicles [m]} & w_r &= \text{total width of the road [m]}
 \end{aligned}$$

It is assumed that the minimum distance between a vehicle and a pedestrian is 0.2 m. This distance does not apply when the traffic is pedestrian-dominated. This representation is based on qualitatively assumptions, and it needs to be improved and validated with empirical data. In absence of such data, the implemented model can however be used to provide an initial assessment of the impact that these assumptions have to the overall evacuation times, and to appraise the sensitivity to the thresholds.

2.3 Modelling Platform

The algorithms described in Sects. 2.1 and 2.2 were implemented using the java-based modelling platform MASON [13]. The platform allows defining a spatial domain for the model and implementing classes of agents.

Table 1 Parameters used in the model

Parameter description	Value and/or source
Road capacity – vehicles	Function of road type and width, [15]
Intersection capacity – vehicles	Function of intersection type and width, [15]
Road capacity – pedestrians	Function of road width, [15]
Intersection capacity – pedestrians	Function of intersection width, [10]
Vehicle's size (cars and motorbikes)	[4]
Person's size	[16]
Free flow speed – vehicles	[15]
Free flow speed – pedestrians	[12]
Time step	60 s

3 Application

The first pilot site for this model is the city of Padang, Indonesia, which was chosen for several reasons. First, the city is expected to be affected by an earthquake and subsequent tsunami in the next decades. Although evacuation studies have been carried on in the past, our consultations with local emergency planners showed the need for more detailed analysis and assistance in translating them into actual evacuation plans. Secondly, the city is often affected by earthquakes, recent ones triggering mass evacuations. The last event occurred on the 11th April 2012. These events showed the typical traffic characteristics observed for Southeast Asian cities described above (see, for example, [14]). This application was carried on thanks to the collaboration with the local emergency planners and NGOs.

Preliminary tests were carried out to assess the sensitivity of the results to the variation of the parameters regulating the interaction pedestrian-vehicles. In order to test the model, some simple base scenarios were developed, in which either pedestrian or vehicles evacuate. In all these scenarios, the agents are required to follow the same 6.5 Km path. The parameters used in this model are shown in Table 1.

The results of these base scenarios are showed in Table 2.

These results are consistent with the expected evacuation times given the model's parameters and the network characteristics. The standard deviation provides information on the traffic conditions: the higher the standard deviation, the higher the variation of the arrival times among the agents, which means that the first agents departing can almost travel at their free-flow speed (accounting for the delays at the intersections and the limited ingress rate of the arrival node). These results are used as basis for comparison with scenarios in which both vehicles and pedestrians engage the road network. Three combinations of pedestrian-vehicles composition are implemented, aiming to test different ratios between pedestrian and vehicles (Table 3). Variations of the thresholds T_1 and T_2 were also studied. T_1 is varied between 0.2 and 0.7; T_2 is varied between 1.2 and 3.

Figure 1 shows the results of the sensitivity analysis. It can be noted that the variation in T_1 does not produce important differences in the results. This is because the

Table 2 Base scenarios, either pedestrian or vehicles in the network

No.	No. pedestrians	No. vehicles	Max evacuation time (h)	Min evacuation time (h)	Avg evacuation time (h)	St Dev %
20	0	6,000	4.05	0.28	2.16	50.6
21	20,000	0	1.97	0.98	1.47	19.7
34	0	500	0.58	0.38	0.42	21.4
35	10,000	0	1.47	0.98	1.22	12.0
67	0	1,000	0.90	0.28	0.58	31.2
68	20,000	0	1.97	0.98	1.47	19.7

Table 3 Assumed traffic distributions

Distribution name	No. pedestrians	No. vehicles
TD1	10,000	6,000
TD2	20,000	1,000
TD3	20,000	500

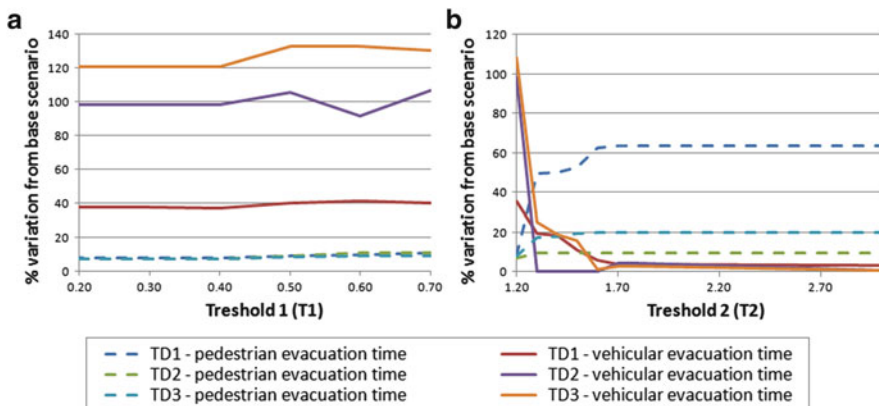


Fig. 1 Results of scenarios implementing different traffic distributions (*TD1*, *TD2* and *TD3*), varying the threshold *T1* (a) and *T2* (b), as % variation of average evacuation time

minimum space allowed to the pedestrian is capped to allow at least one pedestrian to move along the road. Also, the width of the roads is limited, that varying between 5 and 10 m. Therefore the vehicles can only gain an increase in available road width from 2.6 to 4 m and from 7.6 to 9 m, which does not result in an important increase in the capacity. Similarly, the pedestrians ‘lose’ a portion of the road width that does not significantly influence the overall capacity, and thus the average evacuation time remains similar. The results shows that the most important parameter is the actual proportion between vehicles and pedestrians, with the vehicular traffic increasing the average evacuation time from about 40 % to about 120 %, corresponding to a decrease in the ratio vehicles/ pedestrian from 60 % to 2.5 %.

On the other hand, the results show a higher sensitivity to threshold *T2*. This threshold in fact causes the vehicles to move at the same speed as the pedestrians,

if the space occupied by the pedestrians is such to “trap” the vehicles, and therefore has an important effect to the overall traffic. This also has an impact on the average evacuation time for the pedestrians, as the capacity of the road is reduced by the presence of the vehicles. These results are qualitatively consistent with the reality. The value of threshold T2 was shown to be important to the final results, therefore attention should be paid in choosing this threshold, possibly based on observed data. However, there are currently no available measurements taken during a real evacuations, and the retrieved footages are not sufficiently long or do not have a sufficient quality to allow a better estimation of this threshold.

4 Conclusions

The implemented model was shown to perform well in modelling either vehicular or pedestrian evacuation, using traffic parameters consistent with the traffic in Southeast Asian cities. The model is capable of representing the important interaction between pedestrian and vehicles. The results are consistent with what would be expected, as the average evacuation time increases with the increase of the overall traffic, and that the vehicular traffic is the one suffering the higher increase in evacuation time, being the vehicular traffic more sensitive to the road capacity than the pedestrian traffic. The higher is the ratio between pedestrians and vehicles, the higher the level of congestion of the vehicular traffic. However, this implementation of hybrid evacuation is based on qualitative assessments, and should require an extensive validation against observed data. The next step of this study includes the implementation of the full evacuation for the city of Padang (Indonesia), the comparison with previous models for the city (which, however, only include pedestrians, such as [17]) models, and the research on possible validation cases for the hybrid model.

References

1. Hoang, T.L., et al., *Simulating Motorbike dominated Traffic*, in *12th World Conference on Transport Research 2010 Lisbon, Portugal*.
2. Meschini, L. and G. Gentile. *Simulating car-pedestrian interactions during mass events with DTA models: the case of Vancouver Winter Olympic Games*. in *90th annual meeting of the Transportation Research Board*. 2011. Washington D.C.
3. Wu, H. and W. Wu. *Microscopic Dynamic Simulation Model for Pedestrian-Vehicle Mixed Traffic*. in *IEEE International Conference on E-Health Networking, Digital Ecosystems and Technologies*. 2010.
4. Chandra, S. and U. Kumar, *Effect of lane width on capacity under mixed traffic conditions in India*. *Journal of Transportation Engineering-Asce*, 2003. **129**(2): p. 155–160.
5. The World Bank, *World Development Indicators*, 2011.
6. Asian Development Bank, *Key Indicators for Asia and the Pacific 2009*, 2009: Mandaluyong City, Philippines.

7. Brinkhoff, T. *The Principal Agglomerations of the World*. 2012; Available from: www.citypopulation.de.
8. Helbing, D. and M. Treiber, *Numerical simulation of macroscopic traffic equations*. Computing in Science & Engineering, 1999. **1**(5): p. 89–99.
9. Kerner, B.S., *Introduction to modern traffic flow theory and control* 2009, Berlin Heidelberg: Springer-Verlag.
10. Hoogendoorn, S.P. and W. Daamen, *Pedestrian behavior at bottlenecks*. Transportation Science, 2005. **39**(2): p. 147–159.
11. Gordon, R.L., *Technique for control of traffic at critical intersections*. Transportation Science, 1969. **3**(4): p. 279–288.
12. Weidmann, U., *Transporttechnik der Fussgänger*, in *Schriftenreihe des IVT* 1993, ETH: Zurich
13. Luke, S., et al., *MASON: A multiagent simulation environment*. Simulation-Transactions of the Society for Modeling and Simulation International, 2005. **81**(7): p. 517–527.
14. Andriani, D.C. *Gempa Susulan Memaksa Warga Padang Mengungsi*. 2012 [Accessed 17 April 2012]; Available from: <http://www.zamrudtv.com/sumbar-4510-gempa-susulan-memaksa-warga-padang-mengungsi.html>.
15. Departemen Pekerjaan Umum, *Manual Kapasitas Jalan Indonesia (Indonesian Highway Capacity Manual)*, 1997, Direktorat Jenderal Bina Marga, Indonesia.
16. Korhonen, T., et al., *FDS+Evac: An Agent Based Fire Evacuation Model*. Pedestrian and Evacuation Dynamics 2008, 2010: p. 109–120.
17. Lammel, G., et al., *Emergency Preparedness in the Case of a Tsunami-Evacuation Analysis and Traffic Optimization for the Indonesian City of Padang*. Pedestrian and Evacuation Dynamics 2008, 2010: p. 171–182.

PedGo Guardian: Evacuation Decision Support System for Events

H. Klüpfel and T. Meyer-König

Abstract Modern societies are characterized by urbanization. Large scale entertainment and mass gatherings are ubiquitous. Venues accommodating large numbers of persons and large and complex multi-functional arenas are part of most large cities. The guidance of pedestrian flows in such buildings is a challenge. Within the Hermes research project, funded by the German Federal Ministry of Education and Research within the Security Research Program, an “evacuation assistant” for the quick and safe evacuation of stadiums was developed as a prototype. The aim was to be provide guidance for visitors and safety and security forces more quickly and more safely than currently possible. The PedGo Guardian is an implementation of such a system (evacuation assistant) based on the Hermes results. It is designed to use information about the current situation to predict the future positions of the occupants. It involves feeding in data about the availability of rescue routes, fire protection systems, and the distribution of people as determined using an arbitrary detection system. This allows for flexible reactions to the actual situation for which usually no special emergency plans exist.

1 Design of Evacuation Systems

In Germany, the dimensions of escape routes are specified in building design codes. The regulations concerning the width and length of escape routes are laid down in the “Versammlungsstättenverordnung” (resp. SBauVO, part 1, for the state of North-Rhine-Westphalia). The title of this guidelines could be translated “Regulation for Venues”. It applies to large stadiums, convention centers, concert halls, etc. For a non-roofed sports stadium, an escape route and emergency exit width of 1.20 m

H. Klüpfel (✉) • T. Meyer-König
TraffGo HT GmbH, Bismarckstraße 142a, Duisburg 47057, Germany
e-mail: kluepfel@traffgo.ht

per 600 persons is required. The minimum is 1.20 m, increasing in steps of 0.60 m for every additional 300 persons. For roofed sports stadiums the requirements are different. A width of 1.20 m is required for the first 200 persons and an additional 0.60 m for every 100 additional persons. In addition to the requirements concerning the width of escape route elements, the maximum distance to a safe area must not exceed 35 m. For high roofed rooms, the length is increased up to 60 m depending on the height of the ceiling.

The “safe area” might, for example, be a fire protected staircase. When deviating from those specifications, fire safety engineering methods are used to assure an equivalent level of safety [19]. For sports stadiums, especially the second aspect regarding the maximum walking distance to a safe area sometimes collides with architectural objectives. Fire safety engineering methods can be used to justify a relief from that requirement. To that end, calculations or simulations have to be performed, to assess the escape routes and their use by the visitors in case of an emergency. The required safe egress times (RSET) obtained from those evacuation simulations are compared to the available safe egress times (ASET). These are usually determined on the basis of an assessment of the hazards originating from fire and smoke. To do this, the ventilation and smoke extraction is either calculated or simulated by Zone models or CFD. As soon as smoke or combustion products like toxic or irritant gases are potentially inhaled by the evacuees, the conditions for safe evacuation no longer exist. As soon as this is the case, the ASET ends. One requirement for the acceptance of the design is then:

$$ASET > RSET \quad (1)$$

In (1), no safety factor is used, since the available time is called “safe”, therefore, it is assumed to contain a safety factor or margin. Additionally, the formation of queues or congestion during the evacuation process has to be assessed. The criterion in (1) is accompanied by criteria for the maximum size and density of congestion, and for the maximum pressure, respectively force, experienced by the evacuees,

$$f(t_{\text{congestion}}, A_{\text{congestion}}, p_{\text{congestion}}, \dots) < f(t_{\text{congestion}}, A_{\text{congestion}}, p_{\text{tenable}}, \dots) \quad (2)$$

The function f is some strictly and monotonically increasing function, i.e. for increasing t , A , or p the value of f also increases. Both conditions (1) and (2) have to be met for approval of the design.

The general design process for pedestrian traffic shown in Fig. 3, also applies to route elements of an evacuation system. As mentioned above, the design criteria according to the prescriptive codes are the length and width of escape route elements. Therefore, prescriptive codes are static approaches not taking into account the crowd dynamics aspects of an emergency evacuation. This can be taken into account by evacuation simulations as often used in day to day fire engineering work.

However, although simulations significantly improve the analysis method, they still only analyse the evacuation with static input data. The users of such software tools take well defined initial data and analyze it with the simulation, thereby trying

to identify the worst case scenarios in order to provide a reliable safety level with their results. All possible scenarios which can occur in the day to day operation of e.g. a large stadium cannot be covered by such a method.

An evacuation assistant like the PedGo Guardian is designed to tackle this problem. The input it constantly uses reflects the real and actual situation. Thus it supervises reality and delivers results, which helps operators of the stadium, e.g. the crowd management.

Based on the forecast of the simulation, the security staff can prepare for events to come and can test different strategies to handle potentially hazardous or very uncomfortable situations. In order to assess the different strategies and their consequences, a level of hazard concept based on the level of service and the crowd density and movement characteristics is used.

2 Level of Service

The service standards for an evacuation differ from the level of service used for pedestrian walkways, which is based on the notion of comfort [3]. The following table shows the level of service for waiting areas which allows higher densities than for walking areas. It also shows a simple, traffic light like, classification in red, yellow, and green.

3 Layout of the Stadium

The example of application and test scenario is the ESPRIT Arena in Düsseldorf, Germany. It is a multi-functional arena, where sports (e.g. football) and cultural events (rock concerts, etc.) take place.

The general arrangement of the stadium is shown in Fig. 1. A lounge area is integrated in the western grandstand. Most persons access the stadium via the tram station located in the south next to the stadium (see Fig. 1, the station is denoted “U” for underground).

4 Components of the Real-Time Evacuation Guidance System

As shown in Fig. 2, the Guardian uses two kinds of input data. The basic geometry of the building is static. It consists of walls, stairs and doors which form rooms which form the stadium. The danger management system delivers data about the status of doors and rooms. E.g. if smoke is detected in a room, it is assumed, that

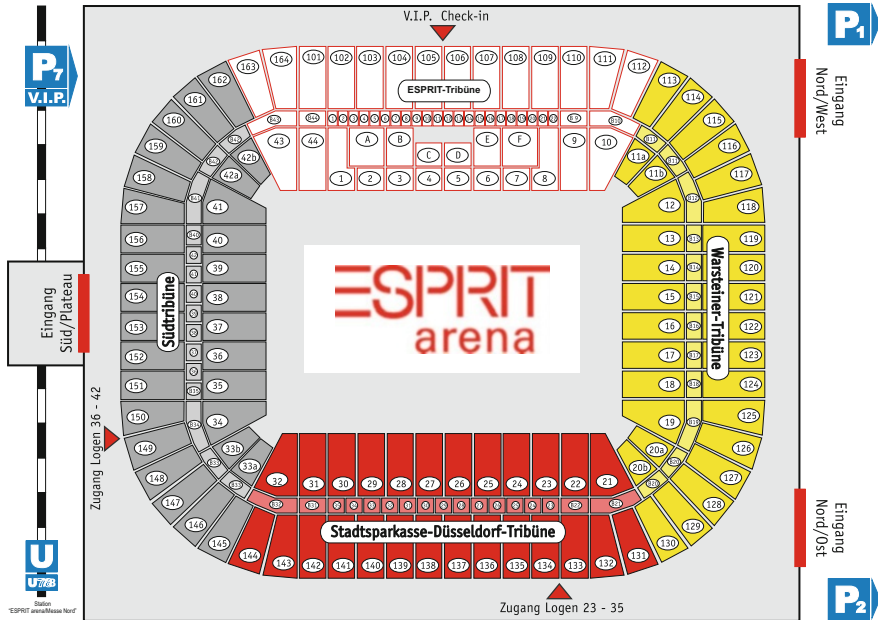


Fig. 1 Layout of the ESPRIT arena (Courtesy: espritArena Verwaltungs GmbH)

this room will not be entered. Thus the doors leading into the room are blocked. Thus, the geometry and resulting the route choice is adapted to the real situation.

For distributing the population, the guardian connects to a person counting system. This could be a manual fed database, but automatic (and expensive) systems are available as well. Within HERMES, the German company Vitracom implemented their detection system. It consists of specially developed cameras detecting and counting in and outflow of persons. The information from video cameras is used to extract person flows and determine the occupancy of the rooms in the stadium. Those values are stored in a database for further analysis and at the same time fed into the evacuation simulation. Therefore, the simulation can at any time be triggered based on the actual occupancy of the stadium.

Another detection method successfully used by the Guardian was the detection system of the British company Crowd Vision. In contrary to Vitracoms method, the Crowd Vision Software uses conventional CCTV video feeds and counts the detected persons. The combination of the PedGo Guardian and Crowdvisions detection method was demonstrated during the British *Instinct* event, held in London in 2009.

Since the costs of automatic detections systems is a factor, only half of the lower ranks and the adjacent promenade could be supervised by the detection system. This resulted in a maximum of approximately 10,000 persons.

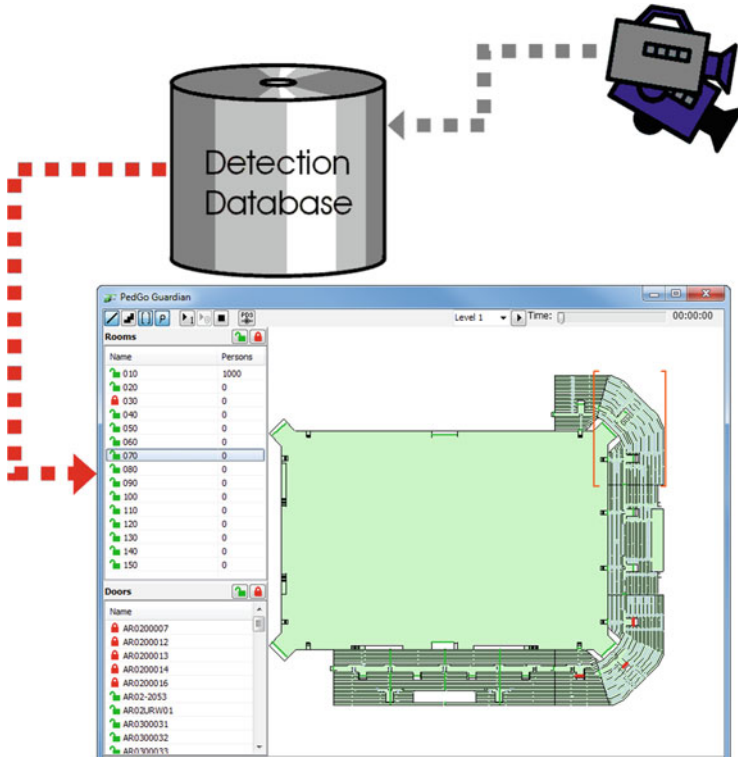


Fig. 2 Software architecture of PedGo Guardian

The architecture is not only used in the PedGo Guardian implementation of the evacuation assistant, but a general result of the Hermes research project. Further details about Hermes can be found in another publication in these proceedings by Holl [18]. Of course, the data obtained from the CCTV can also be used to calibrate other models like macroscopic flow models. This was actually done within Hermes [18].

5 Integration in the Design and Operation Process

The role of the operator is central for the successful use of the PedGo Guardian. The operator processes the information from the security staff, the police, and the fire brigade. Based on that information and the information fed in by the building management system (the smoke detectors and other detectors and actors), the operator initiates a simulation showing the overall evacuation time and the formation of congestion. All that is based on the current situation, i.e., the actual

Table 1 The level of service concept for waiting areas [3]. The levels A and B are fine (*green*), levels C and D require attention (*yellow*), and levels E and F intervention (*red*). The densities are given in square feet per person, square meter per person and person per square meter

Fruin LoS		ft/m	0.3048
Waiting Area	sq ft / P	sqm/P	P/sqm
A	13	1.2	0.83
B	10	0.93	1.1
C	7	0.65	1.5
D	3	0.28	3.6
E	2.5	0.23	4.4
F	2	0.19	5.3

number of persons in each room and the availability of escape route elements. Due to its high speed (10,000 persons in $100 \times$ real time), the simulation can be finished within seconds for the scenario under consideration. The Guardian can also be run continuously. That is: the initial population distribution and the state of the escape route elements (e.g., closed doors) is updated every fixed time interval (e.g., 10 s) and a simulation is performed for that situation. The result is then compared to some threshold value for the *ASET*. If this is exceeded, intervention or prevention measures are required. The same applies for the identification of significant congestion during the simulation evacuation process.

Within Hermes there was an additional component based on a network flow algorithm. This component provided by PTV and based on their software Visum can calculate an optimal rerouting of the evacuees and show bypasses for areas not accessible due to smoke, fire, or other incidents [18].

For the sake of instructing and supporting the security forces, i.e. the stewards, security service, police, and fire brigade, the areas observed can be categorized in the guardian based on the levels A to F shown in Table 1. These six levels of comfort are grouped into three broader categories. “Green”, “yellow”, and “red” are the levels used in the safety context. The “green” areas do not require any special attention or intervention, the “yellow” areas do require attention and preventive measures, i.e. the re-directing of persons that wish to access those areas. This might prevent further congestion. Finally, the “red” areas require intervention, i.e. the active mitigation of dangerous congestion by directing persons out of this area.

For a summary of crowd management techniques and the distinction between crowd management and crowd control, please refer to the contribution of Klüpfel (in these proceedings) (Fig. 3) [19].

5.1 Evacuation Simulation

Evacuation simulation is a core part of the PedGo Guardian. Microscopic simulations predict the motion of more than 500,000 persons, taking into account individual properties. The information of the detection system about the position of all persons in the arena is processed by the simulation kernel. Similar to a weather

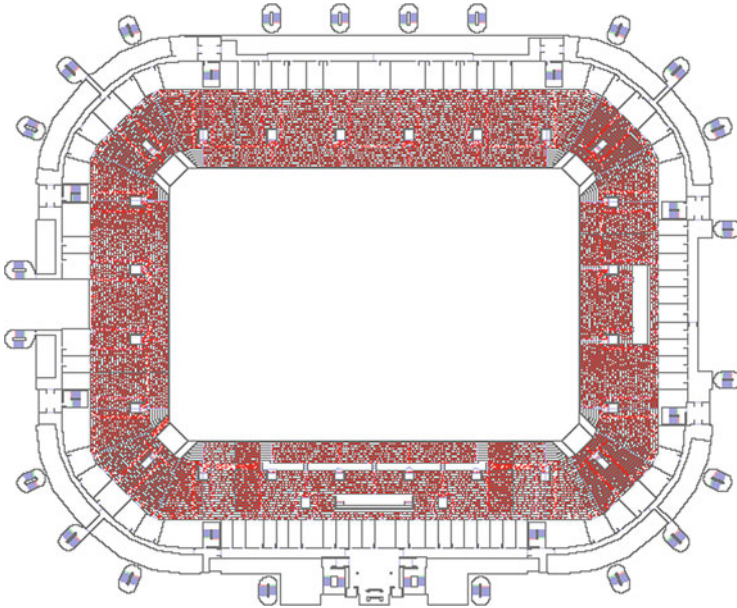


Fig. 3 Floor plan of the ESPRIT Arena used in the simulation with PedGo. *Red dots* show the initial locations of the (non-moving) spectators

forecast, the kernel then computes a prognosis for the situation 15 min in the future. An example for the initial situation for a football match with all persons placed initially on the stands is shown in Fig. 3.

The red dots indicate persons sitting on their seats. The cumulative local density is one major criterion for identifying congestion. In Fig. 4 the areas where this cumulative local density exceeds 3.5 persons per square meter for more than 10 % of the overall egress time is marked red.

5.2 Classification of Risk

The evacuation assistant will be used by the staff in the command and control center (called “skybox” in the arena) to assess the situation and plan the operation of the security staff and forces. As shown in Table 1, the six levels of comfort are grouped into three categories (green, yellow, and red).

This categorization is also present in Table 2. The density criterion is only one for assessing critical situations. Equations (1) and (2) contain further criteria. As stated above, overall evacuation time, waiting times and identification of significant congestion are some of those criteria. Significant congestion can be determined by the density and the temporal or spatial extent of the congestion. Concerning spatial

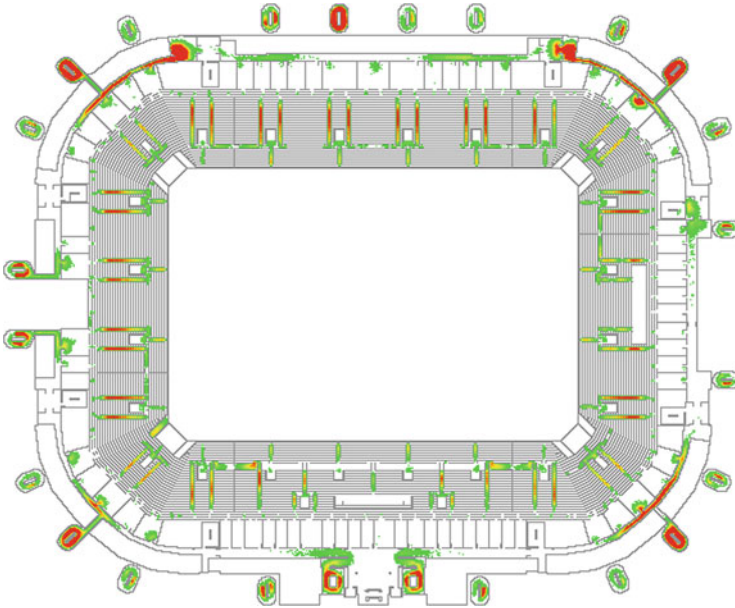


Fig. 4 Simulation result: The 0.1 T cumulative density exceeding 3.5 P/m^2 for $t_{\text{evacuation}}$ (i.e. significant congestion [4, 14]) is shown in red

Table 2 Risk classification for sports events [12]

Class	Risk	Threat	Intervention	Action
5	Severe	Cancel	Secured	Stop Access
4	High	Maximum	Controlled by authorities	Comprehensive Control
3	Raised	Raised	Restrictive	Pat down
2	Watch	Medium	Protective	Restricted Access
1	Low	Minimum	Routine	No Action

extent, a dense congestion reaching back 10 m might be considered too severe. The reason is that in that case, the persons pushing from behind might exert a pressure leading to severe asphyxia.

6 Summary, Conclusion, and Outlook

In this paper, we have presented an evacuation assistant called PedGo Guardian, which is based on the results of the Hermes research project [20]. Based on real-time observation data and a connection to the building management system, evacuation processes can be simulated.

A traffic-light scheme of green/yellow/red is used to categorize densities and risks relevant for crowd management. This scheme might be implemented in a future version of the PedGo Guardian. It would then assist the security personnel to focus their attention. As long as a situation is “green”, no specific attention is necessary. Yellow requires special attention and preparation for crowd management measures and other interventions. Finally, red situations are not acceptable and require specific and immediate action like crowd control. Of course, the challenge is the definition of the demarcation criteria between the different regimes and the calibration of the intervention and action catalogue. Such criteria can be found in Tables 1 and 2.

The, the role of the operator of the system, i.e. the evacuation assistant, is central to its success and usefulness. The operator must be able to integrate the different sources of information and to communicate the results to the stewards, security service, police, and fire brigade.

References

1. S. Buchmüller and U. Weidmann: Parameters of pedestrians, pedestrian facilities, and walking facilities. IVT, Technical report 132, ETH Zurich, 2007.
2. W. Daamen, S. Hoogendoorn, and P.H.L. Bovy: First-order Pedestrian Traffic Flow Theory. In: Transportation Research Board Annual Meeting 2005, Washington DC: National Academy Press, 2005.
3. J.J. Fruin: Pedestrian Planning and Design. New York: Metropolitan Association of Urban Designers and Environmental Planners, 1971.
4. International Maritime Organization (IMO), Guidelines for Evacuation Analyses for New and Existing Passenger Ships, MSC.1/Circ.1238, November 2007.
5. A. Johansson; D. Helbing; H.Z. Al-Abideen; and S. Al-Bosta: From Crowd Dynamics to Crowd Safety: a Video-based analysis. *Advances in Complex Systems (ACS)*, Volume 11, Issue 4, p.497–527, 2010.
6. W. Klingsch, C. Demirel, and G. Adam: Gebäudetechnischer Brandschutz für die Multifunktionsarena Düsseldorf. In: *Bauphysik 27* (2005), Heft 1, Ernst & Sohn, Berlin.
7. H. Klüpfel: A Cellular Automaton Model for Crowd Movement and Egress Simulation, Dissertation, Universität Duisburg, 2003.
8. H. Klüpfel: Models for Crowd Movement and Egress Simulation. In: S. Hoogendoorn et. al.: *Traffic and Granular Flow 2003*. Springer, Berlin, 2004.
9. G. Lämmel, H. Klüpfel, and K. Nagel: Risk minimizing evacuation strategies under uncertainty. 5th International Conference on Pedestrian and Evacuation Dynamics, Washington, DC, Mar 8–10, 2010.
10. PedGo Users Manual, TraffGo HT GmbH, 2007/2010. Available for download at: www.traffgo-ht.com/de/pedestrians/downloads.
11. W.M. Predtetschenski and A.I. Milinski (1971): *Pedestrian Flow in Buildings*. Müller, Köln-Braunsfeld, 1971.
12. L.B. Perkins: *Athlete and Athletic Facility Security*. Presentation available for download at: www.ManagingCrowds.com, 2003.
13. D. Purser and M. Bensilium: Quantification of Behaviour for Engineering Design Standards and Escape Time Calculations, *Safety Science* 38(2), 158–182, 2001.
14. RiMEA-Projekt: Richtlinie für Mikroskopische Entfluchtungsanalysen, www.rimea.de
15. A. Schadschneider, W. Klingsch, H. Klüpfel, T. Kretz, C. Rogsch, and A. Seyfried. Evacuation dynamics: Empirical results, modeling and applications. In: *Encyclopedia of Complexity and System Science*. Springer, Berlin and Heidelberg, 2009.

16. Vfdb-Leitfaden, Ingenieurmethoden des vorbeugenden Brandschutzes“. D. Hasser (Hrsg.), Altenberge, 2009.
17. U. Weidmann, Transporttechnik der Fußgänger, Transporttechnische Eigenschaften des Fußgängerverkehrs, Literaturlauswertung, Schriftenreihe des IVT 90, ETH Zürich, Jan. 1992.
18. Stefan Holl: *Hermes – an evacuation assistant for large arenas*. (in these proceedings)
19. Hubert Klüpfel: Special requirements for crowd management at large events. (in these proceedings)
20. Klüpfel, H and Seyfried, A and Holl, S and Boltes, M and Chraibi, M and Kemloh, U and Portz, A and Liddle, J and Rupprecht, T and Winkens, A and others. HERMES – Evacuation Assistant for Arenas, Future Security, 2010.

RiMEA: A Way to Define a Standard for Evacuation Calculations

Christian Rogsch, Hubert Klüpfel, Rainer Könnecke, and Andreas Winkens

Abstract Since many years the RiMEA-Richtlinie (**R**ichtlinie für **M**ikroskopische **E**vakuirungs **A**nalysen – Guideline for Microscopic Evacuation Analyses; RiMEA-Guideline) is a guideline for German-speaking authorities to check evacuation analyses of complex buildings. Based on the RiMEA-Guideline expert reports are written to ensure that the fundamental questions of an evacuation analysis are answered. Since April 2012, a German DIN Specification (like a pre-Standard) for evacuation calculations (DIN Spec 91284:2012-04) is available. This DIN Specification is based on the RiMEA-Guideline and was developed together with the RiMEA society (RiMEA e. V.). The paper will show how this DIN Specification (DIN Spec 91284:2012-04) was developed and what kind of requirements have to be fulfilled to transform the RiMEA-Guideline to this German DIN Specification. Additionally we will show what are the differences between this DIN Specification and the RiMEA-Guideline. Furthermore paper gives an overview about the actual RiMEA-Guideline and shows a short comparison between the RiMEA-Guideline

C. Rogsch (✉)

RiMEA e.V., Executive Committee, Grabenstr. 133, D-47057 Duisburg, Germany
e-mail: christian@rogsch.de; email@rimea.de

H. Klüpfel

RiMEA e.V., Executive Committee, Grabenstr. 133, D-47057 Duisburg, Germany

TraffGo HT GmbH, Duisburg, Germany

e-mail: kluepfel@traffgo.ht; email@rimea.de

R. Könnecke

RiMEA e.V., Executive Committee, Grabenstr. 133, D-47057 Duisburg, Germany

IST GmbH, Hamburg, Germany

e-mail: r.koennecke@ist-net.de; email@rimea.de

A. Winkens

RiMEA e.V., Executive Committee, Grabenstr. 133, D-47057 Duisburg, Germany

BPK Brandschutz Planung Klingsch GmbH, Frankfurt, Germany

e-mail: a.winkens@bpk-mail.de; email@rimea.de

U. Weidmann et al. (eds.), *Pedestrian and Evacuation Dynamics 2012*,

DOI 10.1007/978-3-319-02447-9_38,

© Springer International Publishing Switzerland 2014

and the IMO-Guideline MSC.1/Circ.1238 (Guidelines for Evacuation Analyses for New and Existing Passenger Ships). At the end we will give an overview about test cases, which are implemented in the RiMEA-Guideline.

Keywords RiMEA • Evacuation • Standardization • Test scenarios

1 What Is RiMEA e. V.?

RiMEA e. V. (e. V. means registered society in Germany) is a German-speaking society which has different aims in the field of pedestrian and evacuation dynamics, in general these aims are

- To host and to proceed further development of the RiMEA-Guideline,
- To support (young) scientists in the field of pedestrian and evacuation dynamics and also fire safety,
- To support collaboration of science and industry,
- To host scientific meetings and/or conferences, and
- To develop new ways in the field of evacuation analyses.

RiMEA e. V. was founded on November, 10th, 2010 in Munich, Germany. It actually consists of 29 members which are from different German-speaking countries.

The RiMEA-Guideline [5] was originally initiated by six people (Tim Meyer-König and Michael Schreckenber from Germany, Peter Gattermann and Nathalie Waldau from Austria, and Christian Morage and Martin Schwendimann from Switzerland) in 2004. These six people developed the first version of the RiMEA-Guideline and were responsible for further developments in the first years of this guideline. Later on the interest of other German-speaking people on this guideline grows thus it was more difficult to handle comments or wishes in a way which is acceptable for all persons. The idea to found RiMEA e. V. was especially to ensure that the RiMEA-Guideline will be further developed and that the process of this development is open to everyone. With founding of RiMEA e. V. this development process has now a new structure and authorities or companies have now a contact organization for questions and/or other inquiries.

2 The RiMEA-Guideline

The RiMEA-Guideline (in German: RiMEA-Richtlinie, Richtlinie für Mikroskopische Evakuierungs Analysen – Guideline for Microscopic Evacuation Analyses; RiMEA-Guideline) is a guideline for German-speaking authorities to check evacuation analyses of complex buildings. Based on the RiMEA-Guideline expert reports are written to ensure that the fundamental questions of an evacuation analysis are answered.

The guideline itself will be changed or further developed during at least annual meetings of the members of the RiMEA Society. Before each meeting so called

“contribution rounds” (in German: Beitragsrunde) are performed where all people (not only members of the society) are allowed to post changes or comments for further development via email. At the meeting itself all contributions are discussed and if accepted by the members, the RiMEA-Guideline will be changed based on the accepted contribution. The guideline can be downloaded by everyone via Internet (www.rimea.de).

2.1 Structure of the RiMEA-Guideline

The actual RiMEA-Guideline version number is 2.2.1 and it was published on June, 8th, 2009. The RiMEA-Guideline consists of eight topics and seven appendices, which will be introduced in the following.

2.1.1 Preface (German: Allgemeines)

The Preface gives a short definition about simulation based evacuation analyses.

2.1.2 Objectives (German: Ziele)

Objectives of the described methods of the RiMEA-Guideline are

- To evaluate evacuation times in the context of a selected building,
- To confirm that existing evacuation routes, which differ from the building regulations, are sufficient for evacuation of people out of the building,
- To show that evacuation routes are flexible enough if parts of the evacuation routes are not accessible,
- To identify areas where congestions are possible in a case of evacuation.

The main objective of the RiMEA-Guideline is to define a minimum standard of an evacuation analysis, based on

- Input parameters,
- Model usage and development,
- Simulation,
- Analysis of the results, and
- Documentation of the analysis.

With usage of the RiMEA-Guideline it should be possible to evaluate escape routes as part of a building.

2.1.3 Scope (German: Anwendungsbereich)

The RiMEA-Guideline is actually focused on the German building regulations for places of assembly, the so called Musterversammlungsstättenverordnung [1], this means the RiMEA-Guideline is mainly focused on

- Assembly places with assembly rooms, which have a total capacity of more than 200 persons,
- Assembly places (open-air) with a capacity of more than 1,000 persons,
- Sport stadiums with a capacity of more than 5,000 persons, and
- Buildings for special usage (in German: Gebäude besonderer Art und Nutzung (Sonderbauten))

But in general, the RiMEA-Guideline could be used for all kind of buildings.

2.1.4 Definitions (German: Begriffe)

The fourth section of the RiMEA-guideline is about definitions of keywords which are used in the guideline. In total, actually 17 keywords are defined.

2.1.5 Characteristics of Simulation Models (German: Eigenschaften der Simulationsmodelle)

The RiMEA-Guideline shows in this section different input parameters which can be used for an evacuation analysis. These parameters are

- Age distribution of a standard population,
- Response times,
- Free walking velocity (horizontal movement),
- Free walking velocity (stair movement), and
- Initial density for different kind of buildings.

Also simplified assumptions, which can be used for an evacuation analysis, are presented (like pedestrians will move only on escape routes, defined groups of people use the same escape route).

2.1.6 Evacuation Analysis (German: Entfluchtungsanalyse)

The section about evacuation analysis defines steps which should be used to perform a comprehensible evacuation analysis, in general these steps are

- Description of influencing parameters and boundary conditions, like geometry, population, safe areas, or organizational issues,
- Investigated scenarios, like usage of the building e.g. different kind of events (party or museum, for example),
- Significant total evacuation time (based on statistical issues), and
- Identification of congestions.

The statements about investigated scenarios and significant evacuation times are discussed in more details in the RiMEA-Guideline. This is necessary because

different views of the results and input parameters must be done, thus it is important not to forget any of the detailed steps because the evacuation analysis must be comprehensible, at least for the local building authorities.

2.1.7 Corrective Methods (German: Korrekturmaßnahmen)

Corrective Methods are used if results of an evacuation analysis are not compatible to the protection objectives of the building regulations, e. g. evacuation times are too long if the building differs from the building regulations compared with a building, which is conform to the building regulations. As corrective methods

- Changes in the building,
- Plant-engineering changes, or
- Organizational changes

are possible to get the investigated building conform to the building regulations.

2.1.8 Documentation (German: Dokumentation)

In the documentation section different points are listed which have to be defined or explained based on statements of the local building authorities. These points are

- Assumptions, which are used, and why are these assumptions used (especially when they differ from values (like free walking velocity) which are described in the guideline),
- Variables used in the model description,
- Influence of parameters on movement,
- Kind of update scheme used in the software-tool,
- Input of stairs, doors, or other building specific parts and their influence on pedestrian movement,
- A user's guide of the software,
- Software version, which was used for the analysis, and
- Details of the analysis, like calculation, total evacuation time, and congestions.

2.1.9 Appendices (German: Anhänge)

The RiMEA-Guideline has seven appendices, three of seven will be presented in more detail, the other appendices are

- Bibliography,
- RiMEA-Members,
- RiMEA-Initiators, and
- RiMEA-Contributions.

In the following, the three other appendices will be presented in more detail.

Structure and Minimum Content of an Evacuation Survey Report (German: Gliederung und Mindestinhalt eines Evakuierungsgutachtens)

- In this part of the appendix an examples is given for a structure of an evacuation survey report to ensure that this kind of paper contains at least a minimum of information about the analysis:
 - Title page,
 - Motivation and problem,
 - Description of the building,
 - Description of the software-tool used,
 - Description of evacuation scenarios,
 - Results and specifics,
 - Interpretation of results, and
 - Summary and conclusion.

Interim Guideline for Validation and Verification of Software-Tools (German: Vorläufige Anleitung zur Validierung/Verifizierung von Simulationsprogrammen)

In this part of the appendix different test scenarios for software-tools are provided. These scenarios are used to show that a software-tool is able to reproduce at least the simplest requirements for an evacuation analysis, in total 14 test cases are available:

- Test case 1: Keep velocity in a floor
 - Create a 2 m wide and 40 m long floor. Place one pedestrian at the beginning of the floor and let him walk through the floor. The time to reach the end of the floor should be as expected based on the free walking velocity.
- Test case 2: Keep velocity upstairs
 - Create a 2 m wide and 10 m long stair (10 m of sloped distance) and place at the beginning one pedestrian to walk upstairs. Results should be the same as in test case 1, only with different values based on the upstairs walking velocity.
- Test case 3: Keep velocity downstairs
 - Like test case 2, only downstairs.
- Test case 4: Specific flow through an opening
 - Based on a periodic boundary system with a width of 4 m the specific flow should be measured based on different densities inside the system. The results should be as shown in Fig. 1. Actually this test case in discussion.

Fig. 1 Specific flow (y-axis) and density (x-axis) based on [6]

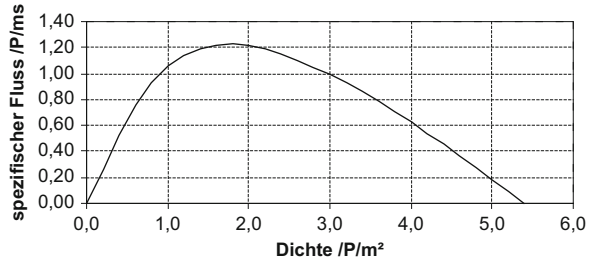
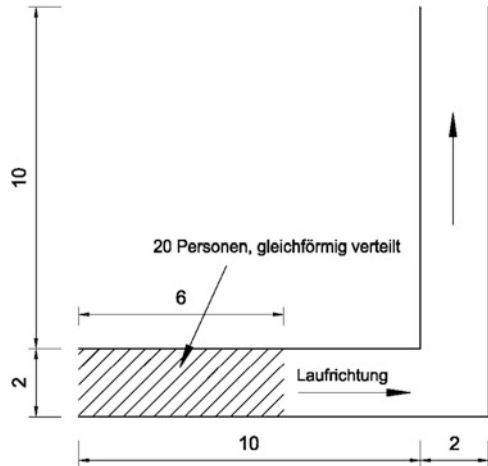


Fig. 2 Twenty pedestrians should be placed in the crosshatched area and walk around the corner without crossing walls and corner. All measures are in m [5]



- Test case 5: Response time
 - Ten pedestrians should be placed with uniform distribution of their response time (10–100 s) in a 8–5 m room with a 1 m wide exit. Verify, that every 10 s a pedestrian starts to move.
- Test case 6: Moving around a corner
 - Twenty pedestrians should move around a corner without “crossing” walls and the corner. See Fig. 2.
- Test case 7: Assignment of demographic parameter
 - Based on a given distribution of free walking velocity, 50 pedestrians should be initiated with this distribution. Verify, that the distribution is correct as expected.
- Test case 8: Parameter study
 - To show the influence of different parameters, create the building as shown in Fig. 3 (Erdgeschoss = ground floor, 1. und 2. Stock = first and second level). Place four pedestrians in every room. Make one simulation run with fixed

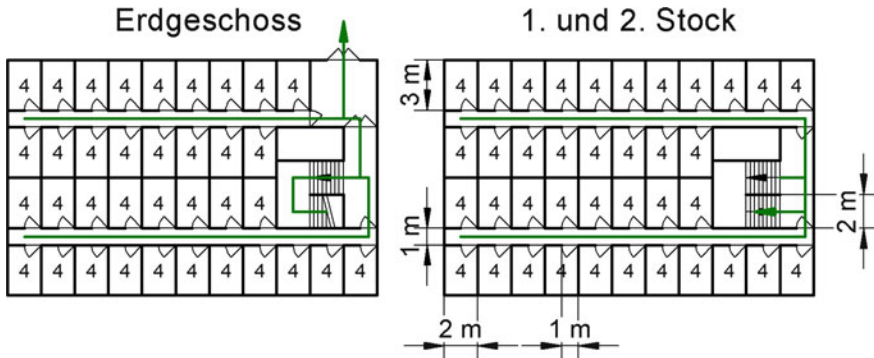


Fig. 3 Building for test case 8. The 2nd level has no stairs upstairs, thus it is different from the 1st level. Four pedestrians should be placed in every room [5]

parameters (e. g. free walking speed for all pedestrians 1 m/s) and one with variation (e. g. 0.75–1.25 m/s). Write the results down in a report and show graphs. These results should be placed on the RiMEA website (www.rimea.de).

- Test case 9: Evacuation of a large room
 - One thousand pedestrians should be placed in the crosshatched area without response time. Run one simulation with all open doors, and one simulation with door 1 and 2 closed (Tür 1 and Tür 2). In the second case (two doors closed), the evacuation time should be ca. a factor of 2 larger as in case 1 (all doors open). See Fig. 4.
- Test case 10: Assignment of evacuation routes
 - Based on Fig. 5, in total 23 pedestrians should be placed in the building. Pedestrians in room 1, 2, 3, 4, 7, 8, 9, and 10 should use the main exit (“Hauptausgang”), pedestrians in room 5, 6, 11, and 12 should use the secondary exit (“sekundärer Ausgang”). This is the expected result. If the result is different, it should be explained why pedestrians choose another exit.
- Test case 11: Choosing an evacuation route
 - A room (see Fig. 6) has two exits (“Ausgang 1” and “Ausgang 2”). Pedestrians should be placed in the crosshatched area without response time. As expected result most of the pedestrians should use “Ausgang 1” and a congestion should appear in front of this exit. Only a few pedestrians should use “Ausgang 2” as an alternative.
- Test case 12: Effects based on bottlenecks
 - Place 150 pedestrians in the crosshatched area (see Fig. 7) without response time. Show, if at the exit (“Ausgang”) a congestion appears or not. This is just to show what kind of results the model calculates, because it is not clear what really happens (a congestion or no congestion) at the exit.

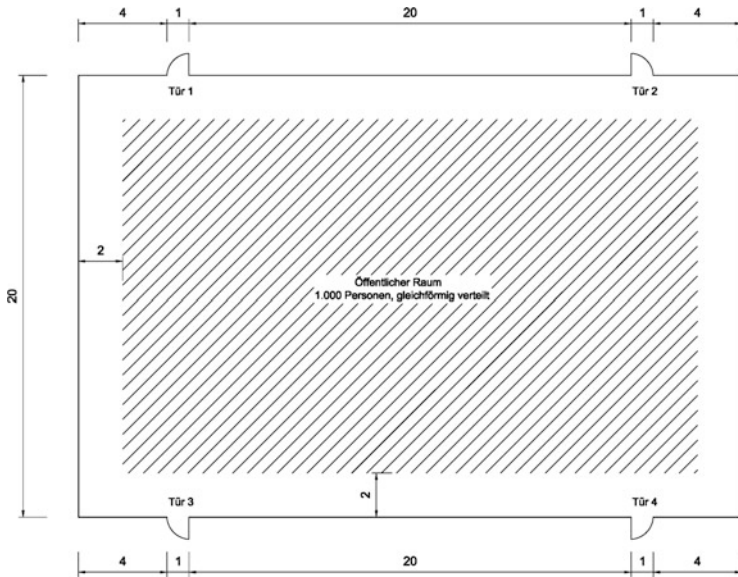


Fig. 4 Evacuation of a large room (test case 8). Measurements are in m [5]

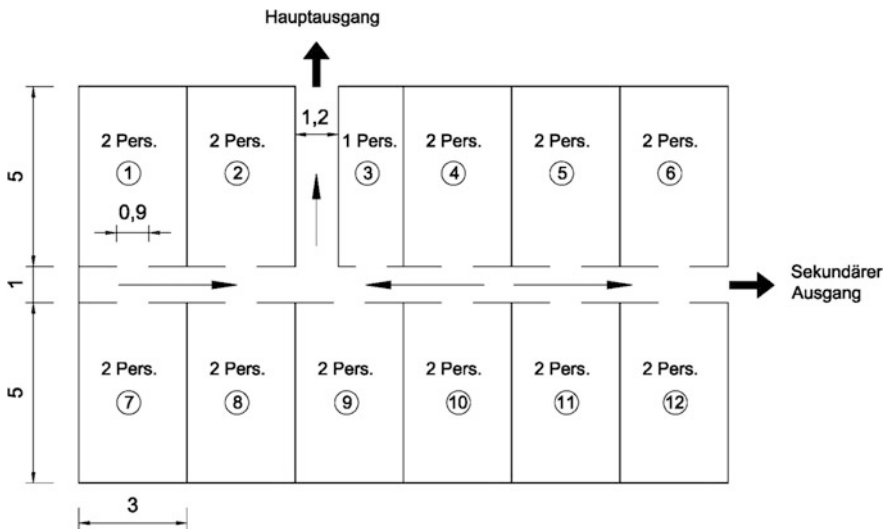


Fig. 5 Room scenario for test case 10. Measurements are in m [5]

- Test case 13: Congestion in front of stairs
 - As shown in Fig. 8, a room with floor and stair (upstairs) should be created. One hundred and fifty pedestrians should be placed in the crosshatched area without response time and walk through the floor upstairs. First a congestion

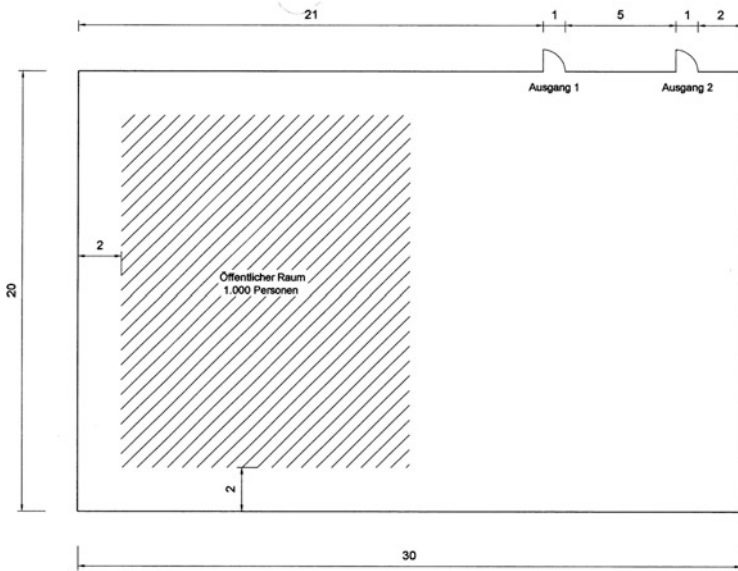


Fig. 6 Floor plan for test case 11. Measurements are in m [5]

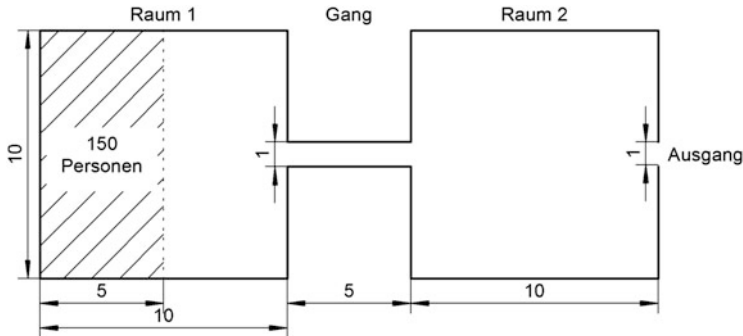


Fig. 7 Scenario for test case 12. Measurements are in m [5]

at the floor should appear, later on a congestion should appear at the beginning of the stairs, because the flow upstairs is smaller as the flow through the floor.

- Test case 14: Route choice
 - At one corner the exit has to be placed, at the next corner the user has to place some pedestrians (see Fig. 9). The shortest way between pedestrians and exit has to be the way using an lower level with two stairs (one from start level to lower level and one from lower level to exit level, which is equal to start level). The longer way has to be in the same level. It should be documented which way to the exit pedestrians prefer. If it is possible to “configure” which way pedestrians use, this should be also documented.

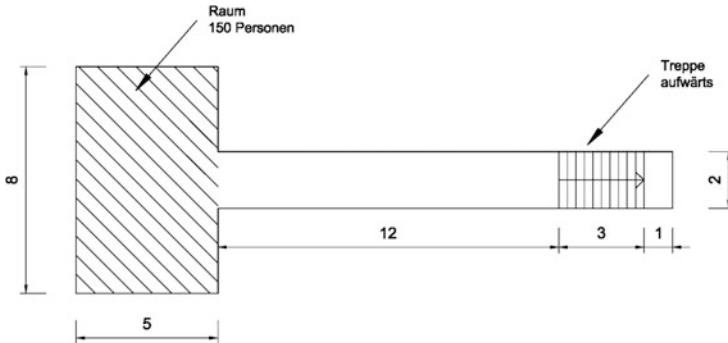


Fig. 8 Floor plan for test case 13. Measurements are in m [5]

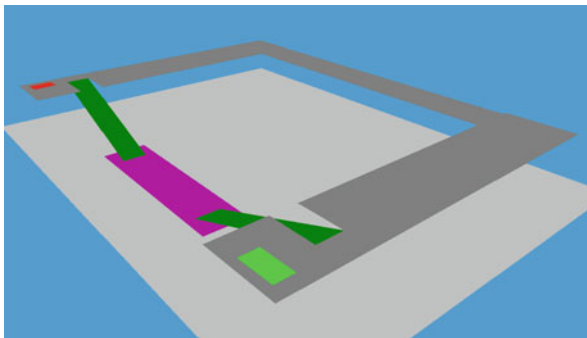


Fig. 9 Floor plan for test case 14. Pedestrian should start at the green area and walk to the red area [5]

Distribution of Individual Response Times (German: Verteilung der individuellen Reaktionsdauern)

Based on the work of Purser [4] some response times are presented in the appendix of the RiMEA-Guideline. This should help the user to choose a “correct” response time as an input parameter for an evacuation simulation.

3 Comparison with IMO MSC.1/Circ. 1238

The RiMEA-Guideline and the IMO MSC.1/Circ.1238 Guideline [3] are similar. Both guidelines define a structure of an evacuation analysis and they provide some information about input data, like response times or free walking velocities. Also both guidelines provide simple test scenarios to test evacuation software tools, some of them are identically. A difference of the two guidelines is that the IMO-Guideline presents a sample analysis of a ship with multiple decks and different

initial densities. Also the IMO-Guideline has fixed response times for day and night cases, the IMO-Guideline also presents four scenarios which should be considered for an evacuation analysis. Contrary to that, the RiMEA-Guideline does not present some “fixed” scenarios like the IMO-Guideline.

In general, both guidelines are “in the same range”, the IMO-Guideline has its focus on the evacuation of ships, the RiMEA-Guideline is more focused on buildings in general. However, the first version of the RiMEA-Guideline was based on the IMO MSC/Circ.1033 Guideline [2], but based on several years of development it has now its own structure and input parameters which are different from the IMO-Guideline MSC.1/Circ.1238, which supersedes the MSC/Circ.1033 Guideline.

4 Development of DIN Spec 91284:2012-04

Based on the RiMEA-Guideline a German DIN Specification (DIN Spec 91284:2012-04) was developed. This was based on a project called “Infranorm”, which was sponsored by the German Government. A DIN Spec can be compared to a pre-standard, but the creation process is a little bit different compared to a German Standard, the so called “DIN Norm”. Like a DIN Norm, the announcement is official, thus everybody who is interested is able to participate. Contrary to a DIN Norm, a DIN Spec is like a manual, where a process is described, but it has no “hard coded numbers”, which means that the reader have to choose the values he or she needs for e. g. an evacuation calculation by himself. A short example should help to understand the difference. In a DIN Norm it is possible to write “. . . if pedestrians walk, they should have a free walking velocity of 1.34m/s . . .”, in a DIN Spec you only write “. . . if pedestrians walk, they should have a free walking velocity, which is chosen by the user . . .”, so in a DIN Norm you can write some numbers precisely, in a DIN Spec you do not write any numbers. Also the publishing process of a DIN Norm is different compared to a DIN Spec. If a DIN Norm is published, first a draft is published (so called “yellow-print” (“Gelbdruck” in German)) thus the public is able to sent comments or caveats to the committee. Contrary to that, if a DIN Spec is published, no draft is necessary. If the committee decides, that the DIN Spec is OK, it will be published without any possibility to send comments or caveats. In case of DIN Spec 91284:2012-04 a draft was presented to the members of RiMEA e. V. thus they can send comments about this draft. All comments were checked and implemented in the draft. After that, the draft was published as the final specification.

Because this difficult process of draft, comments and caveats are not necessary, a DIN Spec can be created and published very quick, in case of DIN Spec 91284:2012-04 the writing process itself had a duration of round about half a year. After 3 years there will be a check, if the DIN Spec is still necessary and if “yes”, it will be checked if the content is still OK or if there are some updates or changes necessary.

5 Future of the RiMEA-Guideline

With founding of RiMEA e. V. the RiMEA-Guideline has the chance to be a well-accepted guideline for evacuation analysis in the German-speaking area, because with this new society which is open to everyone it is possible to include remarks and comments from all interested groups, like the process of creating a German or International Standard (“DIN-Norm” or “ISO Standard”). The development of DIN Spec 91284:2012-04 was the first process, which was developed together with RiMEA e.V.

Acknowledgements The authors thank all members of RiMEA e. V. for their willingness to contribute and to develop the RiMEA-Guideline in the future. Also the authors thank the original initiators of the RiMEA-Guideline, without their encouragement this guideline would not have been possible.

References

1. Argebau (2005), Musterverordnung über den Bau und Betrieb von Versammlungsstätten (Muster-Versammlungsstättenverordnung – MVStättV), Fassung Juni 2005), available online www.is-argebau.de
2. IMO (2002), Interim Guidelines For Evacuation Analyses For New And Existing Passenger Ships, International Maritime Organization, MSC/Circ.1033, 6 June 2002
3. IMO (2007), Guidelines For Evacuation Analyses For New And Existing Passenger Ships, International Maritime Organization, MSC.1/Circ.1238, 30 October 2007
4. Purser, D. (2003), Behaviour and Travel Interactions in Emergency Situations and Data Needs for Engineering Design, Proceedings of the 2nd International Conference on Pedestrian and Evacuation Dynamics 2003, Greenwich, U.K., S. 355 – 369
5. RiMEA (2009), Richtlinie für Mikroskopische Entfluchtungsanalysen, Version: 2.2.1, 2009, June, 8th, available online www.rimea.de
6. Weidmann U (1992)., Transporttechnik der Fußgänger, Schriftenreihe des Institut für Verkehrsplanung, Transporttechnik, Strassen- und Eisenbahnbau Nr. 90, S.35–46, Zürich, Januar 1992.

Simulation Model of Evacuation Behavior Following a Large-Scale Earthquake that Takes into Account Various Attributes of Residents and Transient Occupants

Toshihiro Osaragi, Takayuki Morisawa, and Takuya Oki

Abstract Understanding human behavior, such as waiting, returning home, and evacuation, after a great earthquake is very critical in establishing detailed disaster prevention planning. In the present paper, we construct a simulation model to describe how human behavior varies as a function of physical damage, such as the spread of urban fires and street blockage due to collapsed buildings. The proposed model is applied to a densely built-up area of Tokyo using a database of the spatiotemporal distribution of railroad passengers, automobile users, and pedestrians. Using the model, we attempt to demonstrate some new findings that can be applied to disaster prevention planning by examining evacuation plans and various settings in earthquake simulations.

Keywords Evacuation • Earthquake • Spatiotemporal distribution • Transient occupants

1 Introduction

1.1 Background and Objectives of Research

In recent years, people's daily lives are becoming busier due to rapid urbanization and the growth of rapid transit networks. Therefore, it is difficult to predict the effects of a large-scale earthquake on the population. The authors have investigated methods of estimating the spatiotemporal distributions of people inside/outside

T. Osaragi (✉) • T. Morisawa • T. Oki
Department of Mechanical and Environmental Informatics, Graduate School of Information Science and Engineering, Tokyo Institute of Technology, Tokyo, Japan
e-mail: osaragi@os.mei.titech.ac.jp; morisawa@os.mei.titech.ac.jp; oki@os.mei.titech.ac.jp

buildings and the people in transit with the aim of constructing the necessary database for analyzing disaster prevention plans [1–4].

In this paper, we consider not only the spatiotemporal distribution of occupants inside buildings, but also of transient occupants, (i.e., people who are walking or otherwise in the process of using transportation in the city) in order to construct a simulation model for evacuation efforts following a large-scale earthquake. The model takes into consideration the behavioral characteristics of a variety of people, some of whom are constantly moving and some of which remain in a single location within the city. We have attempt to account for the influence both people whose movement paths stay within the city and those returning home (e.g., from offices/schools) on the number and spatial distribution of stranded people. This influence has not been addressed in previous studies.

1.2 Comparison with Previous Studies

Early spatial models representing urban spaces were raster data models [5, 6], but those models were replaced with block models to clarify aspects of different actual urban areas. More recently, it has become more common to employ spatial models using detailed digital maps. Attempts have also been made to build models based on multi-agent simulations (MAS), in which stranded people, fires, and other factors are treated as agents. The range of applications for MAS, which originated in the life sciences, has expanded with the advance of computer technology, and MAS has come into wide use in the field of evacuation behavior simulations in recent years. Highly versatile procedures have been proposed, including analyses of simulations of evacuation activities that model activities for the rescue of people requiring aid during seismic fires [7] and models based on commercially available digital maps [8]. Many proposals have also been made for evacuation activities following tsunamis [9–11].

However, the source data for previous research, namely, spatial distributions of populations, have been static data obtained from the population census or other similar sources that do not account for human behavior characteristics, which change dynamically with time and location. Also, depending on the time and place, one can expect the coexistence and intermingling of stranded people and those attempting to return home. No studies have simultaneously discussed evacuation activities and return home travel. Therefore, in this report, the authors have combined a model for estimating the spatiotemporal distributions of occupants remaining in the city and transient occupants [1–4] with a model describing the intention to return home and the associated return activities [12], and incorporated this into a new model describing evacuation behavior.

There are many studies presenting models for describing property damage. Models relating to the urban spread of fire and the collapse of buildings, include the 2001 Tokyo Fire Dept. model [13], and the model for building collapse by Murao and Yamazaki [14]. The present report uses these models in an attempt to provide

a micro-simulation analysis on a unit building basis, taking into consideration the attributes of buildings.

The simulation model proposed here can be summarized as follows: (1) blockage of streets by collapsed buildings is modeled; (2) the progress of fire is predicted using an urban fire spread model; (3) the spatiotemporal distribution of train passengers, automobile users, and pedestrians is incorporated; (4) the movement of people returning home who enter or exit the region under analysis are modeled; and (5) stranded people are categorized using a detailed profile based on their, for example, the purpose of their movements.

2 Analytical Data

2.1 People and Regions Under Analysis

The region employed in this analysis was the Setagaya Ward of Tokyo (Fig. 1). Setagaya has areas that are densely crowded with wooden structures, and thus are very vulnerable to housing collapse and urban conflagration in the event of an earthquake. In addition, many workers and students live in Setagaya and commute within the Tokyo region (i.e., they would be counted as transient occupants). The subjects under analysis included all individuals residing and traveling within the ward during a disaster, not only those who live in Setagaya. This population also includes people re-entering Setagaya from outside the ward at various times after a disaster (people returning home).

Data from a Person-trip Survey (PT data) conducted in 1998 were employed to compile the daily trip destinations for Setagaya residents. It was found that approximately 96 % of the trips remain within metropolitan Tokyo and these return travel activities took place across the whole of the Tokyo region.

2.2 Spatiotemporal Distribution of Occupants

Location data for occupants remaining in the city (occupants of any facility, including residences) were represented by building locations or intersections. Specifically, the location of each occupant of Setagaya was determined by selecting the building probabilistically, using the floor area of each building, the purpose of travel PT data, and the building type noted in the digital maps. For residents outside Setagaya, locations were determined by selecting positions at random from among intersections in area units (small zones) used in the PT data.

Location data for the railway passengers [2], automobile users [3], and pedestrians [12, 15] were predicted by employing the results of previous research together with the detailed data available on individual attributes.

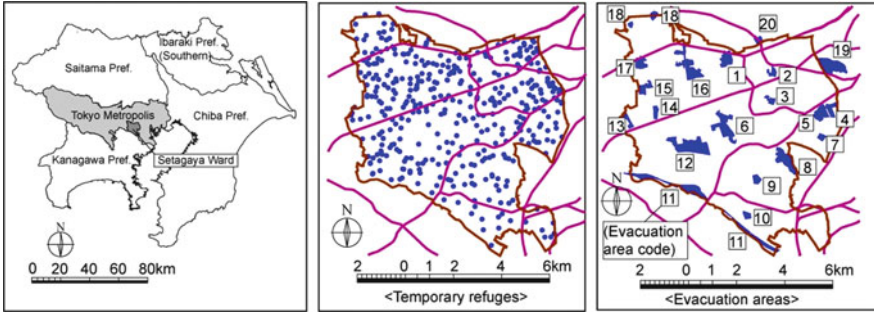


Fig. 1 Study area

2.3 Spatial Model Used in Simulation

The street network was extracted from the digital map to use as the spatial model. People were assumed to be walking on the sidewalks, and so sidewalk widths were extracted from the traffic census data (2005). In order to prevent confusion during evacuation and encourage orderly evacuation behavior, the Tokyo Regional Disaster Prevention Plan [16] is based on a two-stage evacuation, which calls for people initially to gather in temporary refuges and then to move from there to (official, wide and safe) evacuation areas. The study area consisting of 392 temporary refuges (Fig. 1, center panel) and 20 evacuation areas (Fig. 1, right-hand panel) connected with a street network was created in order to examine the effectiveness of this evacuation scheme.

3 Modeling Property Damage

3.1 Building Collapse Model and Street Blockage Model

In building collapse models, the probability of collapse can be estimated for each building unit based on its year of erection or its construction type (wood, reinforced concrete, steel frame construction, or light steel frame construction) (Fig. 2, left-hand panel) [14]. According to the damage forecast for Tokyo Metropolis [17], a North Tokyo Bay Earthquake (7.3M) would cause shaking of a weak 6 on the Japanese seismic scale in Setagaya. Using an empirical equation [18] relating seismic intensity to seismic velocity, a velocity of $PGV = 60.0$ (cm/s) was assumed. We used data on building heights and street widths to make a forecast of street blockage caused by building collapse (Fig. 3).

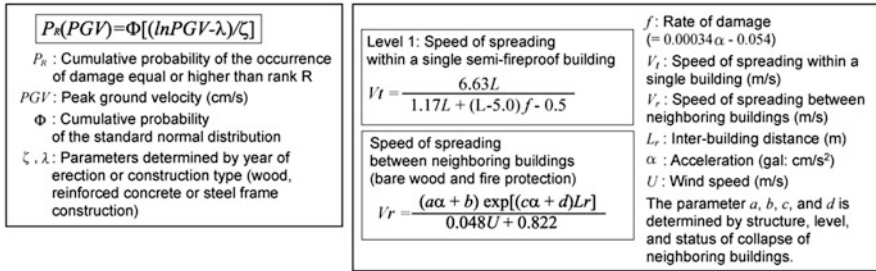


Fig. 2 Building collapse model and fire spread speed model

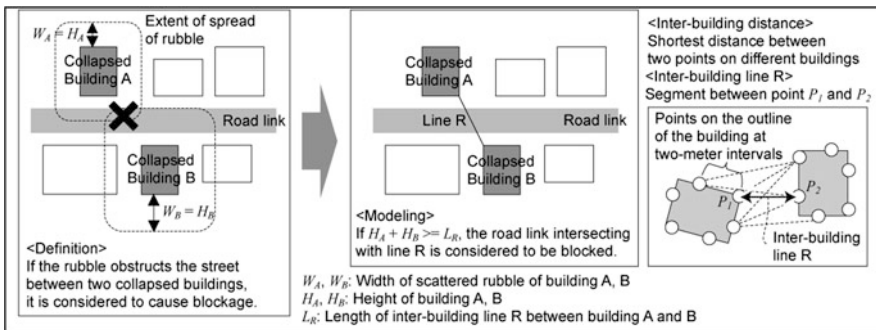


Fig. 3 Street blockage model

3.2 Fire Outbreak Model and Urban Fire Spread Model

In this study, we considered a fixed number of 58 fires breaking out in Setagaya, on the basis of the numbers of fires predicted for the area (18:00 o'clock) in the damage estimate for Tokyo Metropolis [17]. The specific locations of fire outbreak can be broken down by building use, season, daytime vs. nighttime occurrence, and typical acceleration (gal: cm/s²); we used the building-type-based outbreak rates of the Tokyo Fire Dept. [13] to estimate these locations.

The fire spread speed model of the Tokyo Fire Dept. [13] was employed; this model can account for different modes of fire spread and different structural building types. “Spreading speed” has two categories, speed of spreading within a single building and speed of spreading between neighboring buildings (Fig. 2, right-hand panel), the latter of which depends on the distance between the two buildings.

3.3 Basic Analysis Using the Property Damage Model

After the above preparations, we carried out 10 Monte Carlo simulations using the models of building collapse and street blockage (each a different combination of building collapse and street blockage). The fractions of blockage in relation to

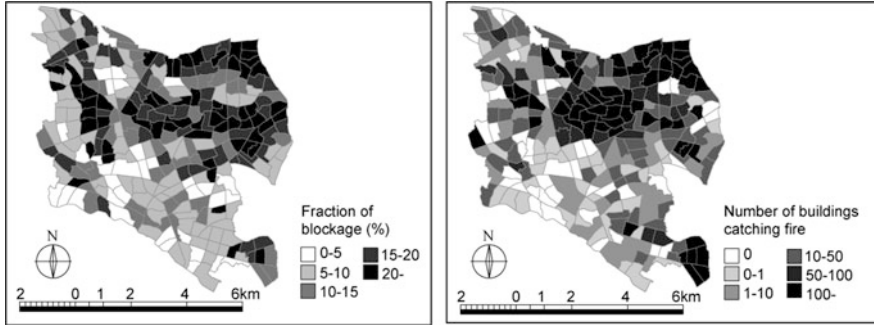


Fig. 4 Fraction of blockage and the number of buildings catching fire

the total number of streets were calculated (mean numbers of streets by units of neighborhood and block) and are shown in Fig. 4 (left-hand panel). As shown, areas with many narrow streets suffered a relatively high rate of street blockage.

Next, we carried out Monte Carlo simulations using the fire outbreak model and the urban fire spread model, taking as given building collapse and assuming the conditions: winter, nighttime, and a 6 m/s north wind. The parameter of maximum acceleration in the fire spread speed model (Fig. 2, right-hand panel) was assumed to be 500 gal, which is based on an empirical formula [18] relating seismic intensity and maximum acceleration. The number of buildings catching fire within 48 h after the earthquake (mean numbers by units of neighborhood and block) were determined and are shown in Fig. 4 (right-hand panel). As shown, the number of buildings was higher in areas in which buildings of wood construction were dense.

4 Modeling Human Behavior

The typical series of human behaviors when an earthquake strikes were categorized and modeled. Figure 5 shows an example of the behavior modeled for occupants at home, from the perspective of initial reactions, searching for routes, methods of evacuation (direct evacuation versus two-stage evacuation), walking in a crowd (walking speed), and activities while waiting. Specifically, the model incorporated the following: (1) a time is set for the start of evacuation after the earthquake; (2) in the case of a two-stage evacuation, the stranded people move to temporary refuges; (3) a time is set for beginning movement of stranded people from the temporary refuges to evacuation areas; (4) evacuation is complete when the stranded people have arrived at an evacuation area; and (5) the stranded people proceed directly to the evacuation area when a two-stage evacuation is not followed. Figures 6 and 7 show the details of how the walking speed is set, how routes are sought, and the time to begin activities, respectively.

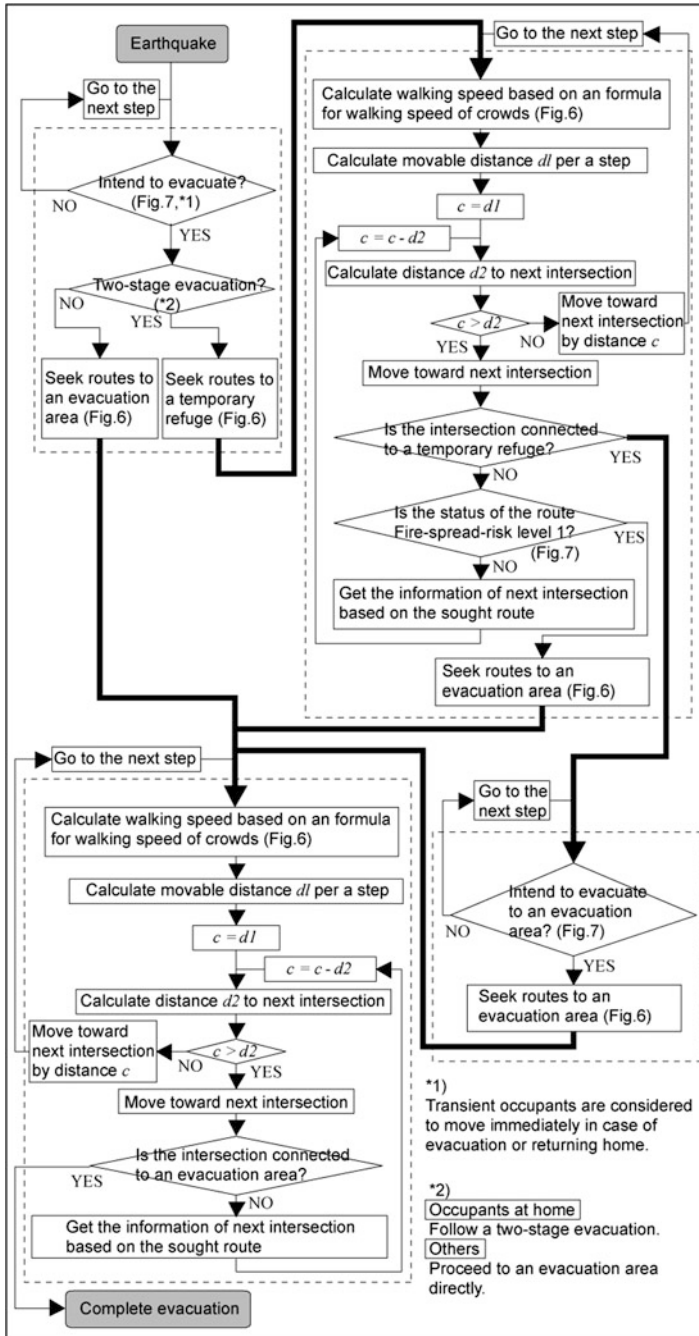


Fig. 5 Human behavior model for occupants at home

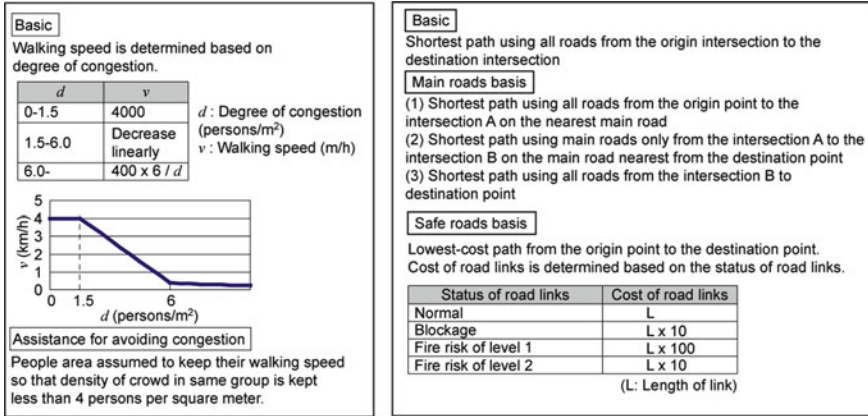


Fig. 6 Walking speed and route search

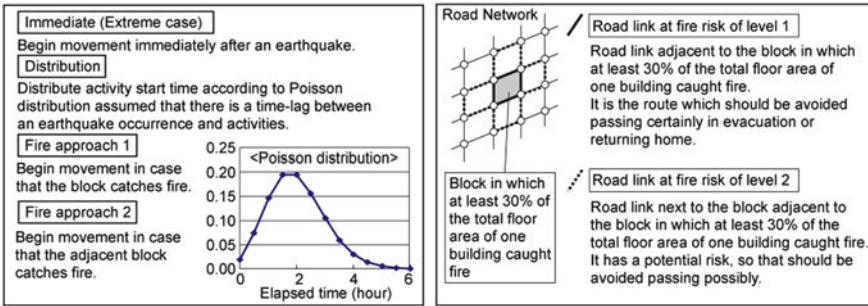


Fig. 7 Definition of activity start time and risk based on fire-spreading risk

The activities of transient occupants (railway passengers, automobile users, and pedestrians) are modeled as follows: (1) they decide whether to attempt to return home (the outcome is determined by the model of intention to return home) [12]; (2) if they decide not to return home, they are treated as occupants at home at the time of the earthquake; (3) if they decide to attempt to return home, they do so using the main streets. The routes from their location at the time of earthquake back to their homes are determined (Fig. 6, right-hand panel); (4) if they encounter fire on their way home, they take refuge in an evacuation area; (5) if they complete their journey home, subsequently, they act in the same way as the occupants already at home at the time of the earthquake.

Occupants in facilities other than their own residences are modeled as follows: (1) they decide whether to return home; (2) if they decide not to return home, they wait in the current facility until the time to begin evacuation, and after that, they act in the same way as occupants at home; and (3) if they decide to return home, they subsequently act in the same way as the transient occupants.

Table 1 Definition of risk assessment indices

Risk	Method for calculating risk
Risk1	The number of road links blocked by collapsed buildings, which stranded people passed through
Risk2	The number of road links at fire risk of level 1, which stranded people passed through
Risk3	The number of road links at fire risk of level 2, which stranded people passed through

Table 2 Conditions for simulation (Basic pattern in this paper)

Direct evacuation	First evacuation start time	At once, [Distribution] + [Fire approach 1], Fire approach 2
	Search routes using safe roads?	[Yes], No
Two-stage evacuation	First evacuation start time	[Distribution] + [Fire approach 1], Fire approach 2
	Avoid congestion?	[Yes], No
	Search routes using safe roads?	[Yes], No
	Second evacuation start time (after the occurrence of an event)	0 min, 15 min, 30 min, [Fire approach 1], Fire approach 2

5 Execution of the Simulation Model

5.1 Performance Indicators and Settings

The danger imposed by road links was defined (Fig. 7, right-hand panel) in order to make an assessment of the effect of urban fire spreading on safety during evacuations. It was assumed, as an approximation, that once at least 30 % of the total floor area of one building in a certain block had caught fire, the radiated heat would endanger adjacent routes. However, streets that border large open areas (at least 10,000 m²), such as parks or vacant lots, were considered to be safe. Next, risk assessment indices were set (Table 1) in order to quantify risks during evacuation. From the standpoint of safety, it is desirable if the above risk of evacuations should be reduced.

Evacuation methods, walking speed, path search methods, and activity start times could each be varied in the simulation model constructed. To prioritize examining the influence of transient occupants and persons returning home, however, the data were analyzed under the conditions given below in Table 2.

5.2 Preliminary Analysis of Return Home Travel

We determined fluctuations (over time) in the number of persons returning home passing through Setagaya, for different combinations of starting points and arrival points, to learn about return home travel (Fig. 8). These fluctuations depended

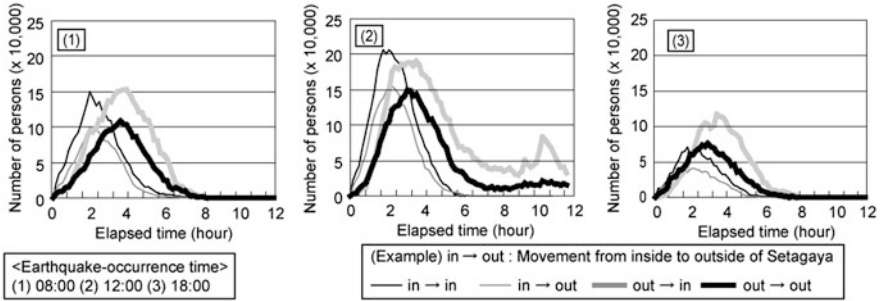


Fig. 8 Fluctuations in the number of persons returning home passing through Setagaya ward

heavily on the timing of the disaster and on the combination of starting point and destination. We also found an unexpectedly large number of stranded people would be returning to homes in Setagaya from outside the ward, even several hours after the occurrence of the disaster.

5.3 Observations on Characteristics of the Simulation Model

In order to examine the importance of accounting for the presence of transient occupants and persons returning home, we analyzed the variations in people input into the simulation for three specific cases: (1) the population consisting only of occupants remaining in the area, (2) that population plus transient occupants, and (3) that population plus transient occupants and persons returning home. Figure 9 shows the increases in stranded people in comparison to the first population. This figure indicates that, in case (2), the time-based changes in transient occupants strongly affect the number of stranded people, specifically, including them increases the number of stranded people, and in case (3), the number of stranded people is greatly increased by the inclusion of persons returning home in the daytime, when there would be many persons returning home. Examining the results by age group, there is an increase in child stranded people (5–12 years) in the morning and evening, but the elderly population (65 or more years) showed little variation. In contrast, the reader can see that stranded people in the 13-to-64-year age group grew by about 20 % during the 08:00-to-17:00 time frame. More specifically, the presence of transient occupants and persons returning home, which has previously been unaccounted for, may cause an approximately 20 % increase in the number of stranded people estimated for the peak hours period. This is an amount that cannot be ignored.

Next, we consider the number of stranded people in evacuation areas. Figure 10 indicates the evacuation areas with high rates of increase in cases (2) and (3). There appeared a large influx of railway passengers at the evacuation areas around

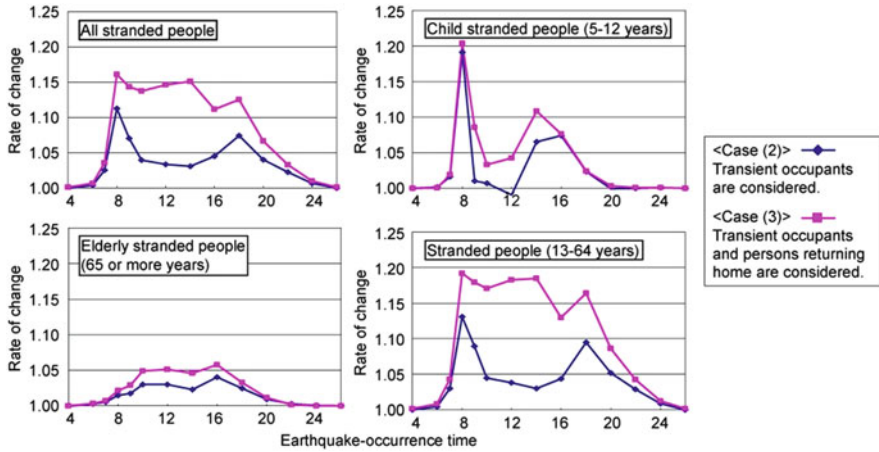


Fig. 9 Increase in stranded people by considering transient occupants and persons returning home (attribute-based)

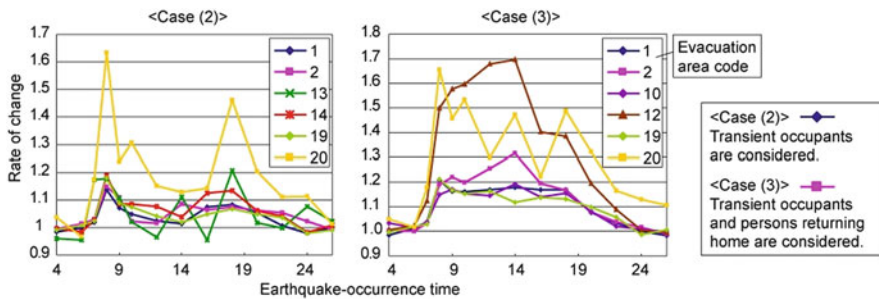


Fig. 10 Increase in stranded people by considering transient occupants and persons returning home (in evacuation area)

locations with high densities of railway lines. Previous investigations regarding the numbers and locations of evacuation areas have usually been based on the numbers of local residents, but in an urban area with a highly developed transportation network, it seems essential for the planning of evacuation areas to account for the presence of transient populations on railways and other traffic arteries, especially during the morning and evening rush hours.

We analyzed the effects of incorporating property damage into the simulation model to address the closure of streets due to urban fires and building collapse. Most previous simple simulations of evacuation activities did not incorporate property damage or the timing of evacuations in order to keep the models from becoming too large and complicated. In actuality, however, because the timing and routes of evacuations would vary with the extent of property damage, there is a large element of chance in the safety and efficiency of any evacuation. Therefore, the composition ratios of the stranded people was compared (Fig. 11) in terms of each sub-group of

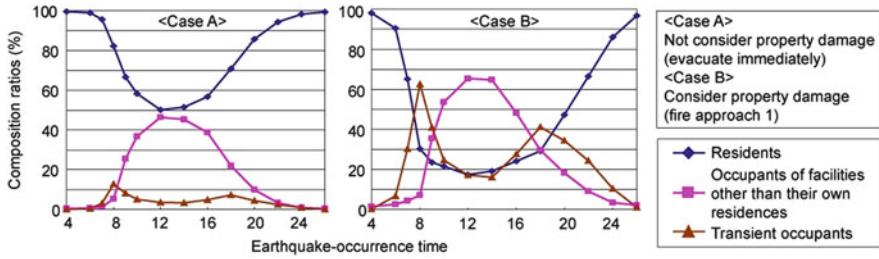


Fig. 11 Effect by considering property damage

stranded people (residents, occupants of facilities other than their own residences, and transient occupants) between the case when everyone in some area is evacuated without taking into consideration property damage and the case when the time for beginning evacuation was decided after considering the property damage situation. We can see that there is a greater fraction of non-resident stranded people, especially during the day, if planners take property damage into account.

5.4 Risk Assessment in Travel to Evacuation Areas

The simulation was executed, accounting for all occupants (whether in buildings, transient, or on their way home), and the risks during evacuation to open areas were evaluated. The cases of two-stage evacuation and direct evacuation were compared (Fig. 12). Residents at home make up a majority of the stranded people at night, and so in this case, the risk is greatly reduced by organizing a two-stage evacuation. During the day, however, many of the stranded people, specifically occupants who are not home residents, would not comply with a two-stage evacuation; therefore, ordering a two-stage evacuation would have relatively little effect on risk. That is to say, planners must anticipate that during the daytime, a sizeable fraction of the occupants are occupants of facilities other than their own homes and that these transient occupants will not know where the temporary refuges are and will head directly to evacuation areas. Walking time to refuges can be longer in a two-stage evacuation, depending on how stranded people are directed, in order to avoid congestion. However, because there are many individuals who would not evacuate to an evacuation area and whose routes would terminate at temporary refuges near their homes, if we evaluate walking time averaged over all stranded people, travel time would be about the same in the two-stage case as in the direct evacuation case.

The numbers of stranded people moving to evacuation areas in a two-stage evacuation were compiled in terms of stranded people’s attributes. Figure 13 shows the results for different situations at the time of a disaster. In the early morning, many transient occupants would go to an evacuation area (6, 11, 12). During the day, many stranded people would go to an evacuation area from their business

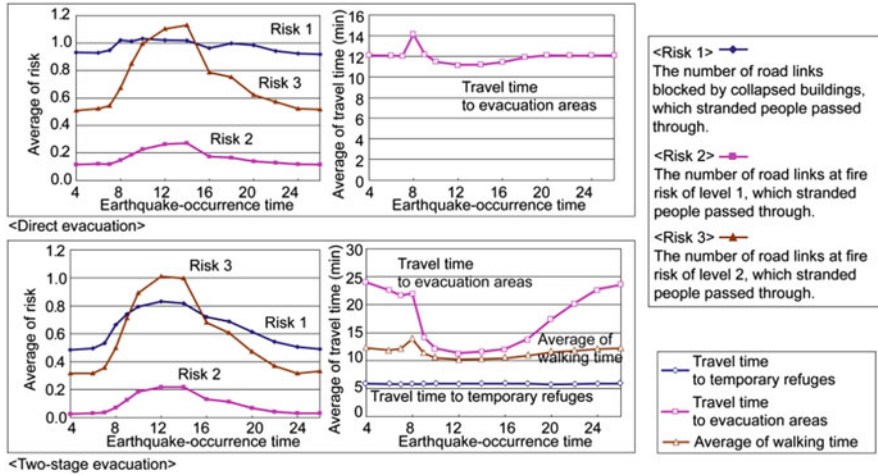


Fig. 12 Comparison between direct evacuation and two-stage evacuation

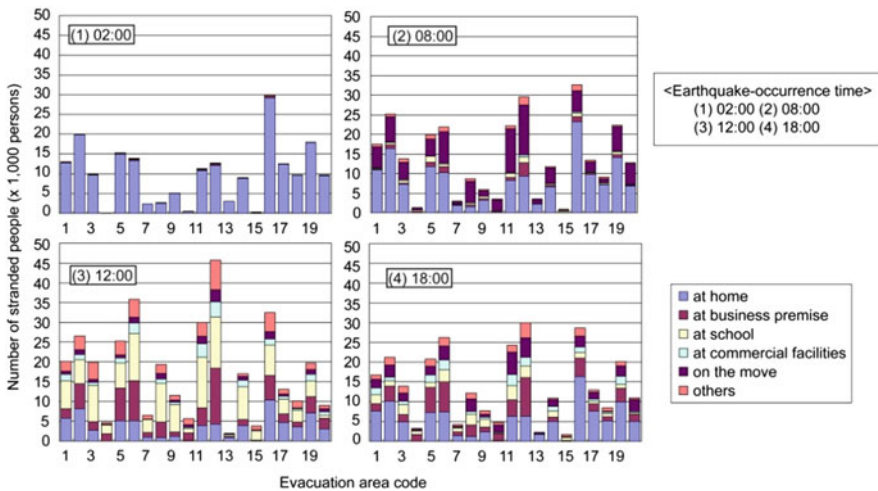


Fig. 13 Number of stranded people in evacuation areas in terms of situation of persons

premises (5, 6, 12). Many would also go there from commercial facilities (6, 11, 12). Figure 14 shows the results in terms of age group. The reader can see that not only the number of stranded people, but also the stranded people’s profile varies greatly with the timing of a disaster. Comparing the cases of a disaster occurring at 2:00 AM and one occurring at noon (Fig. 15), nearly all the evacuation areas show increased numbers of stranded people in the latter case. The evacuation areas in locations surrounded by multiple railways and serving large regions tended to show particularly high differences between night and day.

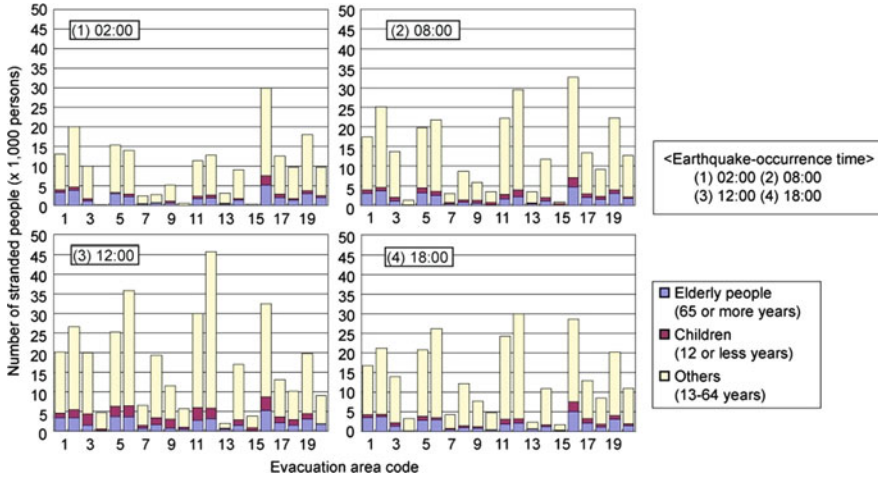


Fig. 14 Number of stranded people in evacuation areas in terms of age group

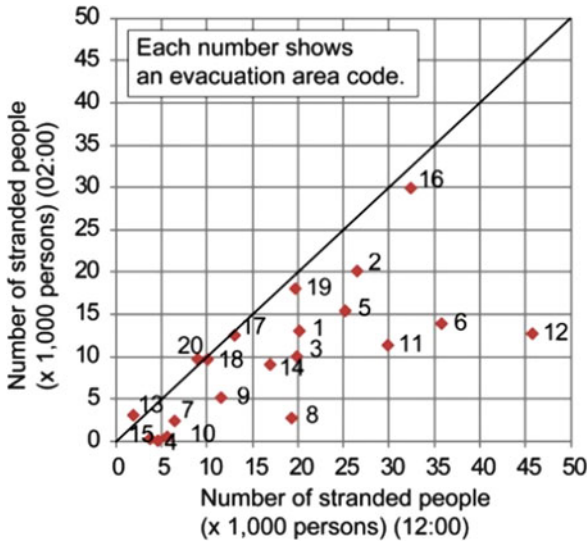


Fig. 15 Difference of the number of stranded people in evacuation areas by earthquake-occurrence time

All of the above results were due to the inflow into evacuation areas of transient occupants and persons returning home, who were not incorporated into previous evacuation simulations. A disaster mitigation planning must account for the fact that the numbers and types of stranded people will vary with the location of the evacuation area and the timing of the disaster.

6 Conclusion

A simulation model was constructed to describe human actions (waiting, returning home, and evacuating) after a devastating earthquake, taking into account property damage. A numerical simulation of people's reactions after a disastrous earthquake in Setagaya Ward of Tokyo was employed to verify the importance of accounting for the presence of transient occupants and that of persons returning home, and the importance of combining such a model with one describing property damage. Our analysis has revealed that the presence of transient occupants and persons returning home, who have not formerly been included in disaster prevention planning, may add about 20 % to the numbers of stranded people during morning and evening peak periods, a quantity that cannot be ignored. Two-stage evacuations were also evaluated from the viewpoint of risks during evacuation to open areas. This indicated large variations in the numbers and attribute profiles of stranded people, depending on the location of evacuation area and the timing of the disaster.

Acknowledgements This research was part of an effort supported by a Grant-in-Aid (21310105) from the Ministry of Education, Culture, Sports, Science and Technology Health and Labor Sciences Research Grant, Scientific Research (B).

References

1. Osaragi, T., Hoshino, T.: Predicting Spatiotemporal Distribution of Transient Occupants in Urban Areas. In: J. Gensel et al. (eds.) 2012, Part 6. Lecture Notes in Geoinformation and Cartography, Bridging the Geographic Information Sciences, pp. 307–325. Springer, Heidelberg (2012)
2. Osaragi, T.: Estimating Spatio-temporal Distribution of Railroad Users and Its Application to Disaster Prevention Planning. In: M. Sester et al. (eds.) 2009, Lecture Notes in Geoinformation and Cartography, Advances in GIScience, pp. 233–250. Springer, Heidelberg (2009)
3. Osaragi, T., Shimada, R.: Spatio-temporal Distribution of Automobile Users for Disaster Prevention Planning (in Japanese). *Journal of Architectural Planning and Engineering*. 641, 1561–1568 (2009)
4. Osaragi, T., Shimada, R.: Spatio-temporal Distribution of Population on Weekdays and Holidays for Estimating Human Damages from Devastating Earthquake (in Japanese). *Journal of Architectural Planning and Engineering*. 635, 145–152 (2009)
5. Okada, K., Yoshida, K., Kashihara, S., Tsuji, M.: Presumption of Human Injury in Case of Earthquake's Fire and Consideration on Its Countermeasure: Part 1 Structure of Computer Simulation Model and Its Assumptions (in Japanese). *Journal of Architecture, Planning and Environmental Engineering*. 275, 141–148 (1979)
6. Aoki, Y., Osaragi, T., Hashimoto, K.: A Simulation Model of Evacuation Behavior in the Fire-spread Urban Area Following Earthquake: Effects of Hearsay Information Process and Geographical Urban Image (in Japanese). *Journal of Architecture, Planning and Environmental Engineering*. 440, 111–118 (1992)
7. Ueda, R., Seo, K., Motoki, K.: A Simulation of Rescue Activity for Weak People in Disaster during Post-earthquake Fire Focusing on Local Disaster Mitigation: A Case Study at a Densely-populated Wooden District in Asagaya and Koenji, Sugunami, Tokyo (in Japanese). *Journal of Architectural Planning and Engineering*. 622, 137–144 (2007)

8. Muraki, Y., Kanoh, H.: The Effectiveness of Communication on Wide Area Simulation of Disaster Evacuation Using Multiagent Model (in Japanese). IPSJ SIG Technical Report. 130, 69–72 (2004)
9. Fujioka, M., Ishibashi, K., Kaji, H., Tsukagoshi, I.: Multi Agent Simulation Model for Evaluating Evacuation Management System against Tsunami Disaster (in Japanese). Journal of Architectural Planning and Engineering. 562, 231–236 (2002)
10. Suzuki, T., Imamura, F.: Simulation Model of the Evacuation from a Tsunami in Consideration of the Resident Consciousness and Behavior (in Japanese). Journal of Japan Society for Natural Disaster Science. 23–4, 521–538 (2005)
11. Ohata, D., Takai, N., Kagami, H.: Spatial Evaluation of Tsunami Refuge Facilities in the Central Kushiro City: Simulation of Evacuation Behavior from Tsunami Utilizing Multi Agent System Part 2 (in Japanese). Journal of Architectural Planning and Engineering. 612, 87–91 (2007)
12. Osaragi, T.: Modeling a Spatiotemporal Distribution of Stranded People Returning Home on Foot in the Aftermath of a Large-scale Earthquake. Nat Hazards, DOI [10.1007/s11069-012-0175-8](https://doi.org/10.1007/s11069-012-0175-8) (2012)
13. Tokyo Fire Dept.: The Development and Practical Use Policy of Assessment Technique of Disaster Prevention for Earthquake Fires (in Japanese), Tokyo Metropolis (2001)
14. Murao, O., Yamazaki, F.: Development of Fragility Curves for Buildings Based on Damage Survey Data of a Local Government after the 1995 Hyogoken-nanbu Earthquake (in Japanese). Journal of Architectural Structure and Construction. 527, 189–196 (2000)
15. Nishimura, K., Osaragi, T.: Spatio-temporal Distribution of Railroad Users in the Vicinity of Terminal Station (in Japanese). Proceedings of Geographical Information Systems Association. 18, 5–8 (2009)
16. Tokyo Regional Disaster Prevention Plan: Tokyo Regional Disaster Prevention Plan: Earthquake Disaster (in Japanese), Tokyo Metropolis (2003)
17. Tokyo Regional Disaster Prevention Plan: Summary on the Damage Assessment of Earthquake Directly under Tokyo (Interim report) (in Japanese), Tokyo Metropolis (2006)
18. Midorikawa, S., Fujimoto, K., Muramatsu, I.: Correlation of New J.M.A. Instrumental Seismic Intensity with Former J.M.A. Seismic Intensity and Ground Motion Parameters (in Japanese). Journal of Social Safety Science. 1, 51–56 (1999)

Simulation of City Evacuation Coupled to Flood Dynamics

A.S. Mordvintsev, V.V. Krzhizhanovskaya, M.H. Lees, and P.M.A. Slood

Abstract Crowd modeling is one of the key components of risk analysis and evacuation planning in emergency situations. This paper presents a simulation environment for experimenting with different city evacuation scenarios. The simulation couples a flood model with a crowd escape model. The developed agent-based crowd model mimics the behavior of pedestrians escaping from dangerous regions towards safe areas. The system is evaluated through a series of experiments, modeling the flooding of an area in St. Petersburg, Russia.

Keywords Crowd dynamics • Evacuation • Urban flood • Agent based simulation • Decision support

A.S. Mordvintsev (✉)
National Research University ITMO, St. Petersburg, Russia
e-mail: A.S.Mordvintsev@gmail.com

V.V. Krzhizhanovskaya
National Research University ITMO, St. Petersburg, Russia

University of Amsterdam, Amsterdam, Netherlands
e-mail: V.Krzhizhanovskaya@uva.nl

M.H. Lees
Nanyang Technological University, Singapore, Singapore
e-mail: mhlees@ntu.edu.sg

P.M.A. Slood
National Research University ITMO, St. Petersburg, Russia

University of Amsterdam, Amsterdam, Netherlands
Nanyang Technological University, Singapore, Singapore
e-mail: P.M.A.Slood@uva.nl

1 Introduction

Global warming and rising sea levels have seen an increase in the severity and frequency of urban floods worldwide. Governments are now struggling to understand and provision for possible future emergencies that may involve mass evacuation of large cities. This problem is especially true for countries with cities that lie close to sea level, and those cities with large surrounding water mass. St. Petersburg, Russia is one such city. With a large sprawling river system and a central island surrounded by water, the city has historically experienced a number of major floods, many of which have had significant impact [1]. In order to better prepare for such floods it is possible to use simulation as a means of understanding how different flooding scenarios might impact the city and how the flow of water might be controlled to mitigate the overall impact [2–8].

In some cases, particularly with increasing severity of flooding, there is real risk of fatalities in the city population. Understanding how best to evacuate or manage the people of the city should help reduce the likelihood and level of danger in such scenarios. Again, simulation can be used to help analyze these questions. In this context crowd modeling is one of the key components of risk analysis and evacuation planning for emergency situations. However, to fully analyze and prepare the correct evacuation measures it is essential to understand the interacting dynamics of the flood and the human populations. In particular we want to be able to understand for a variety of possible flood scenarios, what the best strategy is for ensuring the safety of the population, and how to adapt the environment in order to increase the survivability of the city populous.

There are several well-known methods to assess the impact of the flood to the urban areas. Some of them consider the economical effects of flooding [9], while others focus on estimation of the number of fatalities [10–12]. Some of these use empirical models which try to predict the number of casualties by some heuristic rules. For example [11] uses numerical flood simulation to estimate the flood characteristics (depth, flow speed and so on) in the modeled area. They apply an empirical formula to estimate the fraction of fatalities (mortality function) for each spatial location. Given the initial population distribution this can provide a useful estimate of the number of loss of life events.

Some authors use agent-based modeling (ABM) to employ more details of population behavior into the simulation. For example [10] uses ABM to model the cycle of daytime routines being interrupted by a flood. The authors consider the case of vehicle evacuation over a road network. The Life Safety Model [12] is another agent-based model of flood evacuation; it uses a sophisticated set of rules to predict loss-of-life events depending of agent's health condition and actual location (building, vehicle, pedestrian).

In this paper we present an egress model which is coupled to the output of a flood simulation. This coupling of models provides a simulation environment with which different city evacuation scenarios can be evaluated. The main difference of this paper to the previous work is the strong orientation towards pedestrian

crowd dynamics. Our model tries to reproduce the effects of junctions and different pedestrian path planning strategies. The simulation couples a flood model with a crowd escape model for a scenario of flooding of a region in St. Petersburg, Russia.

The model consists of two main parts: a hydrodynamic flooding model and a crowd escape model. We use a Flood Simulator [9] adapted by the UrbanFlood project [2] from a DRFSM code developed by HR Wallingford for simulation of floodwater propagation. It receives water flow rates discharged into floodplain areas from breached or overtopped flood defenses and then spreads the water over the floodplain according to the city topography. The primary outputs of the Flood Simulator are water levels and flow velocities in the area of the city. These outputs form the inputs to an agent-based model of egress that mimics the behavior of pedestrians heading from dangerous regions towards safe areas. More explicitly, it uses the output of the flood simulation to trigger the evacuation process, to compute available evacuation paths and to identify those agents trapped in, or killed by, the flood.

The remainder of this paper is organized as follows: in Sect. 2 we give an overview of our modeling approach; Sect. 3 describes the details of flood model interoperation; Sect. 4 explains the crowd behavior model, including the path planning and collision avoidance algorithms; in Sect. 5 we show simulation results for several evacuation scenarios and model parameters; Sect. 6 concludes the paper.

2 Modeling Approach

The novelty of our work is that we essentially couple two simulations: water spreading on the lands due to overtopped defenses or breached dams, and an agent-based simulation of pedestrians trying to avoid the flood and to reach the safe areas. This section briefly describes both of those models and outlines the execution flow of the combined simulation environment.

The basic outline of the simulation execution is shown in Fig. 1. The first stage is to run a flood simulation, which generates output containing details of the flood dynamics in the city. This data is used to instantiate the environment of the agent-based crowd model.

Every agent in the crowd model is characterized by the following set of attributes:

- Spatial position in continuous 2D space
- Behavior state, one of: *idle*, *running*, *safe*, *drowned*
- Desired speed.

Other agent parameters are given in Table 1.

Initially all agents are considered to be in the *idle* state. Currently we use a uniform initial distribution of agents in empty areas of the modeled region.

The crowd model proceeds in a time-stepped fashion and takes the following actions at each time step of the simulation:

Fig. 1 Outline of flood/evacuation simulation

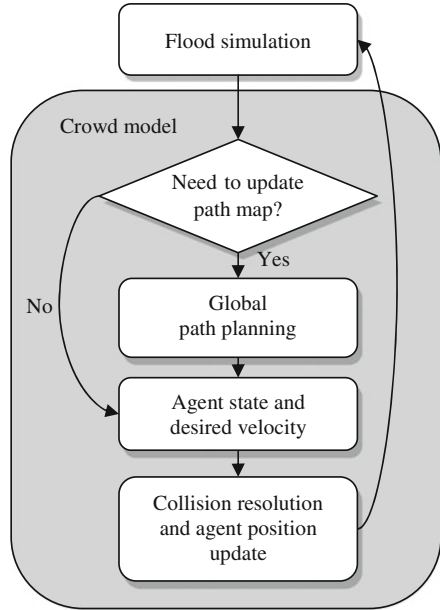


Table 1 Default model parameters

Model parameter	Value
Number of simulated agents	10,000
Grid size (height map, path map, obstacle map)	782 × 531
Grid step	9.42 m
Agent preferred velocity (mean, std)	4.0, 0.2 km/h
Agent maximum velocity	8.0 km/h
Probability of a <i>running</i> agent to alert the neighbors within a second	0.02
Agent alert neighborhood radius	36 m
Crowd simulation time step	0.5 s
Radius of a circle approximating agent body size	0.5 m
Path map update interval	30 s of model time

- Flood simulation.** Our model treats the flow simulator as an external component, which provides information about the flood at each time step. Currently the Flood Simulator described in [9] is used, but in principle it is possible to couple the agent-based simulation with any code for flood simulation. The output of the Flood Simulator is converted into a raster flood map, which is a binary image, marking grid sites that are considered to be flooded. Time steps of the flood simulation output may be much longer, than the steps of agent-based crowd model, so we adopt a simple method of interpolation between subsequent generated flood maps. More details about the flood model and associated interpolation are given in Sect. 3.

- **Global path planning.** Next, a global path map to the safety zones is updated. We use a potential function path planning approach [13]. For this we compute a potential function on an obstacle map, combining static obstacles with non-traversable flooded areas. For performance reasons this calculation is performed only in a subset of the iterations. Currently we specify a fixed predefined model time interval to define the frequency of this calculation. We cache the results of each execution of this step for use in subsequent runs of the model (with the same flood and path planning parameters). The use of global path planning rests on the assumption that all agents know the entire city map and the current flood situation. Such an ideal scenario is in principle possible, but would require some technology capable of providing complete real-time information transfer between the agents. A more detailed description of our path planning algorithm and its variants can be found in Sect. 4.1.
- **Agent state and desired velocity update.** Following behaviours are executed:
 - (a) *Idle* agents are stationary. If an agent senses the approaching water, its state is changed to *running*. We sample the state of the flood at the agent's current position at a time shifted 5 min into the future. This way we emulate prediction capabilities of an agent. If an agent observes another agent in the *running state* then the observing agent transits to a *running* state too with some predefined probability.
 - (b) *Running* agents are heading towards the Safe Heavens. The potential-based navigation model causes agents to simply try to follow the negative gradient of the potential function, computed at the path planning stage.
 - (c) Agents that manage to reach the Safe Heavens change their state to *safe*. Agents that happen to be in flooded areas are assumed *drowned*. Agents in either of these states will be removed from the simulation.

The output of this stage is a desired velocity vector for each agent. For *running* agents this vector points in a direction suggested by the path planning approach and has a magnitude equals to agent's desired speed.
- **Collision resolution and agent position update.** We use the RVO2 library [14] to implement agent-agent and agent-obstacle collision avoidance logic. The library uses the vector obstacle map to compute agent velocity vectors avoiding collisions. The details of scene data preparation and RVO operation are given in the Sect. 4.2. We then use the computed velocities to obtain new positions of agents for the next iteration of the simulation.

3 Flood Simulation

The flood simulation model receives water flow rates discharged into floodplain areas from breached or overtopped flood defenses and then spreads the water over the floodplain according to the city topography. We use a Rapid Flood-Spreading model, described in [9] for floodwater propagation. The model inputs are:

- Raster height map of modeled area,
- Positions and rates of floodwater discharges.

The simulation splits the modeled region into so called *impact zones* (IZ); aggregations of a number of adjacent height map cells. The model iteratively updates the state of the impact zones. Periodically the model stores the amount of discharged water, water level and flux for each IZ affected by spreading flood into a database table. We convert the model data so as to form an output raster map of water levels on grid cells. Any other source of data which could be converted to this form can be used by the simulation. Each grid cell is classified as traversable or not traversable, depending on its flood condition. Currently we simply consider raster map cells with water level greater than zero as flooded and not traversable.

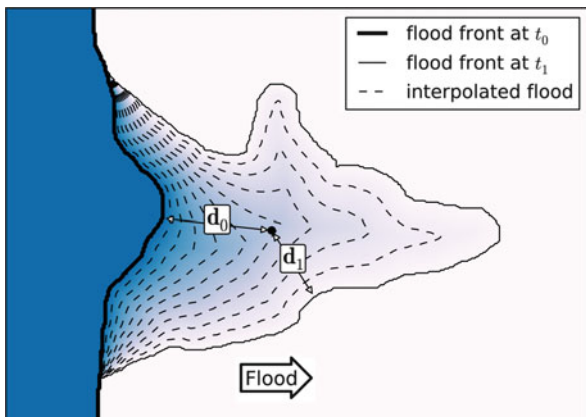
As previously stated, the agent-based pedestrian crowd and flood models (in general) may work on significantly different time-scales. A typical reasonable time step for an agent-based simulation of pedestrian behavior would be in the order of seconds (or sub-seconds). Large-scale flood models on the other hand will usually adopt a time-step on the order of minutes or even tens of minutes. Moreover, in some cases one might want to use historical flooding data, or data acquired from real world (life) observations, so low temporal resolution might be an inherited property of the data used. For these reasons it is desirable to have a method capable of interpolating between coarse flooding time steps. We use the following strategy to do this. Consider two consecutive flooding time steps at t_0 and t_1 . Proceed through following steps to interpolate between them:

- Build raster traversability maps for each of them: $f_0(x,y)$ and $f_1(x,y)$, where $f_i(x,y) = 1$, if raster grid cell is not traversable (flooded) and 0 otherwise. We make an assumption that $\forall x, y f_0 \leq f_1$ i.e. flooded areas don't become traversable again during the simulation. We need to interpolate smoothly between binary functions f_0 and f_1 for values of $t \in [t_0, t_1]$.
- Build two *distance transforms*: $d_0(x,y)$ of function $1 - f_0(x,y)$ and $d_1(x,y)$ of function $f_1(x,y)$. Distance transform computes the distance to nearest zero pixel for each pixel of the input image in terms of given distance function (we use Euclidian norm). We use an OpenCV [19] implementation of an algorithm described in [15] for the construction of the distance transform.
- Compute a *morph coefficient* $w = d_0/d_0 + d_1$ for each pixel in the transition zone, where $f_0 \neq f_1$. Then the interpolated traversability function:

$$f_t(x, y) = \begin{cases} f_0, & |f_0 = f_1 \\ 1, & |f_0 \neq f_1, w \leq w_t \\ 0, & |f_0 \neq f_1, w > w_t \end{cases}$$

where $w_t = (t - t_0)/(t_1 - t_0)$ is a *morphing* threshold for a particular time value (Fig. 2).

Fig. 2 Flood map
spatio-temporal interpolation



4 City Evacuation Model

Our agent-based crowd model mimics the behavior of pedestrians heading from dangerous regions towards the predefined safe areas. Inputs of the model are:

- City topography data, including raster height map (also used for flood modeling), and a vector obstacle map, which contains locations of buildings, fences and other obstacles. Some buildings or map areas are marked as Safe Havens.
- Demographics data, including population distribution of people across the modeled area, the distribution of walking speeds and other agent characteristics.
- Results of hydrodynamic modeling of the flood in the form of a traversability mask for a current time step, as described in Sect. 3.

We use the raster height map as a topography model of the region. This is the same height map that is used by the flood simulation. We classify all grid cells as either obstacles or empty spaces. In a used height map all elevations higher than 3 m belong to buildings, this produces a reasonable obstacle map. For regions with more complex obstacles (high fences and low buildings) a more sophisticated strategy is necessary with tracking steep elevation gradients.

Pedestrian behavior models often separate the logic of agent behavior into several layers [17, 18], where each subsequent layer controls the underlying layer and receives feedback from it. The decisions made by each layer depend of the agent state (memory) and perception. In our model we split the agent motion model into path planning and collision avoidance. Every time step, the path-planning subsystem computes a *desired velocity vector* for each agent. Currently in our model this vector is guaranteed to lead *running* agents to the Safe Havens. This is a simplified approach that can be replaced by a suboptimal path planning with intermediate destinations. The magnitude of the *desired velocity vector* is equal to the agent's preferred speed. For agents in other states their desired velocity is assumed to be zero. Desired velocity vectors are passed to the collision avoidance subsystem,

which assigns agents new, real velocities based on their desired velocities and current velocities of their neighbor agents. In the following subsections we describe approaches to control the agent's behavior on both layers used in the model.

4.1 Path Planning

We use the Artificial Potential Fields (APF) method for the agents' path-planning. This is a well-known path-planning tool [13], here the basic idea is to define a potential function φ over the modeled space in a way that following the negative gradient of φ leads agents to the destination, while avoiding collisions with static obstacles. There are many methods for constructing such functions discussed in the robotics literature [20]. Many of those papers discuss simple yet efficient techniques like using a superposition of attractive APFs of one or more targets and repulsive APFs from obstacles.

The advantages of such techniques are computational efficiency, implementation simplicity and the ability to produce smooth and safe paths. One of the major drawbacks is the sensitivity to unwanted local minima of the used potential functions. There are some suggested strategies for addressing this issue that try to detect when the agent is stuck in spurious minimum and modify the APF in an attempt to eliminate it (e.g. by varying obstacle repulsive fields or avoiding previously visited locations).

Another way to avoid the local-minima problem is to explicitly construct an APF with minima in destination points only. Several approaches for the construction of such functions (sometimes called *navigation functions* [21]) are commonly used, methods based on *eikonal* [23] or *Laplace* [22] equations are particularly popular. Examples of different navigation functions are shown in Fig. 3.

In our work, the Eikonal equation is used. We solve a partial differential equation that governs the behavior of a potential function φ in spatial domain D :

$$\nabla\varphi(x) = c(x), \quad c(x) > 0, \quad x \in D \setminus T \quad (1)$$

$$\varphi(x) = 0, \quad x \in \partial T,$$

where T denotes target regions and $c(x)$ is a positive cost function. The cost function is equal to infinity in obstacle regions. In traversable space regions $c(x)$ equals to unit cost (in time or fuel) of passing through a particular point. It is possible to modify an agents' path-planning strategy by varying this cost function. For example, Fig. 3a shows an example of heading to a destination while avoiding moving too close to obstacle boundaries. Figure 3b shows an alternative strategy, where the agent tries to move along the obstacle boundaries. This is achieved by setting the cost function near obstacles to higher or lower value than in the open space.

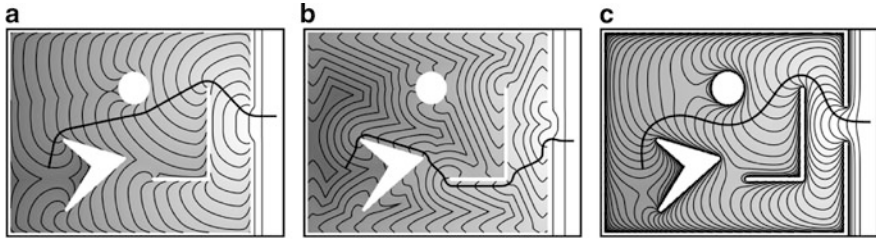


Fig. 3 Potential functions contour lines for: (a) eikonal equation with wall avoidance, (b) eikonal equation with wall following, (c) Laplace equation

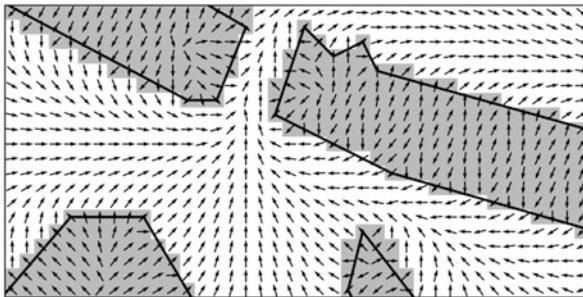


Fig. 4 Part of obstacle map (buildings are shown in grey) with vectorized obstacles and navigation map directions

It can be shown [21], that for any point in D following the direction of $-\nabla\varphi$ will lead to a given destination region by a minimal cost path. Absence of unwanted local minima is guaranteed by explicitly setting $\nabla\varphi \neq 0$ for all traversable space points.

We use a numerical solver based on a modified Dijkstra algorithm to solve Eq. 1 on a two-dimensional Cartesian grid. Intuitively it can be described as a model of shock-wave propagation. The algorithm starts from target sites and adds nodes to a visited set one-by-one. Every time step, it takes a node with the smallest estimated wave front arrival time and re-calculates arrival time for the unvisited neighbors. More details can be found in [23]. While being reasonably efficient, this algorithm suffers from poor scalability due to its sequential nature. Parallel methods of solving Eq. 1 are preferable; some methods can even be adapted for GPU computing [24].

Figure 4 shows a close-up picture of an obstacle map. Black arrows indicate the direction of the steepest decrease of the potential function. Grey cells indicate grid sites marked as obstacles. It can be seen on the figure that the navigation function is defined even for obstacle cells. This is done because we approximate raster obstacle contours with simplified polygons used by the collision avoidance model. Some cells, marked as obstacles may fall of this approximation. We use the Douglas–Peucker algorithm [16], which guaranties that the resulting polygonal approximation lies within a certain given threshold from the initial contour. Very low thresholds generate contours that follow the raster defects of the obstacle map.

To avoid this we use a higher threshold value (one pixel in this example), which gives a more realistic contours but causes some boundary obstacle pixels to fall off the polygonal obstacle boundary approximation. If an agent gets to such point it still needs a defined navigation direction to continue its motion. However our path planning algorithm stops on raster obstacle boundaries and does not provide any meaningful direction inside them. To avoid confusion we provide some reasonable moving direction for grid sites marked as obstacles. To do this, we run two path planning passes: one for empty spaces with destinations in the Safe Heavens and the other one for obstacles with destination in empty spaces. The combined navigation map is shown in Fig. 4.

4.2 Collision Avoidance

We use the collision method implemented in the Optimal Reciprocal Collision Avoidance (ORCA) method [14] for local collision avoidance between agents. The implementation uses RVO2 library. The library analyses each agent's neighborhood and for each neighboring agent or obstacle the library computes a subset of allowed velocities, which avoid collision with this particular agent or obstacle in a given time interval. If the intersection of these subsets is non-empty, the library uses 2D convex linear programming to find allowed velocity vector closest to the agent's preferred velocity. Otherwise it tries to find a velocity that minimizes the overlap of the agents. In this case the new agent's velocity doesn't depend on its preferred velocity and it "goes with the flow". In our simulations interpenetrations between agents were reasonably small even in crowded conditions.

The standard RVO2 library uses polygonal representations for static obstacles. We use the vectorization procedure described earlier. Note that we vectorize static obstacles only. Avoiding flooded regions is achieved by path planning only, not using collision avoidance.

5 Results

In this section we describe the results of extensive runs of our model with varying sets of parameters. An example of simulation results is shown in Fig. 5. At the beginning of the simulation all agents are IDLE and evenly distributed in the streets. Then some agents start evacuating as the alert zone (shown in grey) spreads from the left part of the scene.

Agents move towards the safe zones and alert other agents of their way. This process spawns an avalanche of evacuating agents. Our default simulation settings are based on trying to provide reasonable values for all parameters. Table 1 gives a list of used model parameters:

Fig. 5 Two time steps of the evacuation simulation. Evacuation is triggered as a reaction to the flooding of Vasilievsky Island in St. Petersburg. *Dark regions* show the flooded zones. *Gray zones* are “alert zones” where agents see the flood and start evacuating. *Orange points* are the running agents. *Grey points* are agents unaware of the approaching flood

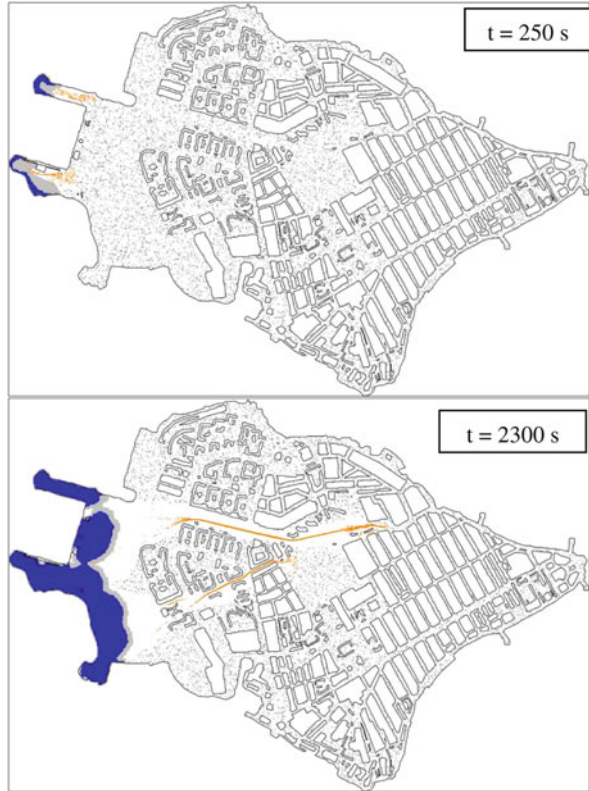
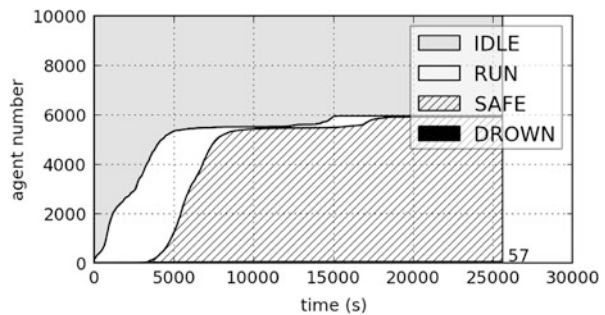


Fig. 6 Agents’ states evolution in time for default model parameters

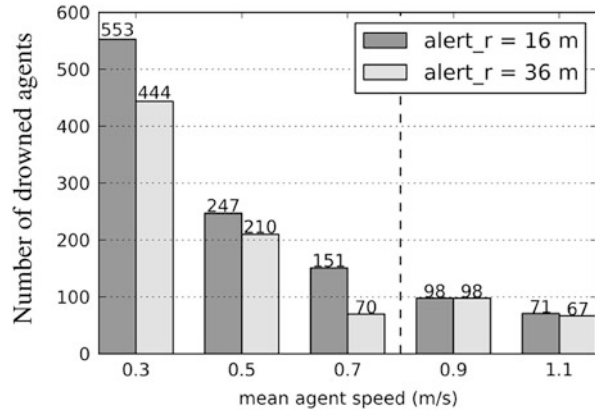


Our default settings allowed almost all agents to escape the flood. The evolution of agents’ states over time is shown in Fig. 6.

The number of casualties equals 57 for this simulation. Interestingly, most of these casualties are the result of agents being cut off from the evacuation routes due to the rapid flood spreading.

To study the influence of simulation parameters on the simulation results, we conducted a series of model runs with varying mean agent desired velocities and

Fig. 7 Number of drowned agents for different agent parameters



alert radices. Resulting numbers of casualties for different simulation parameters are shown in Fig. 7.

As expected the number of drowned agents decreases as mean velocity increases. It can be observed that for small agent velocities (or a rapidly approaching flood) the ability of agents to spread information about the flood can play an important role in decreasing the number of casualties. For example, for a mean velocity equal to 0.7 m/s, increasing the alert radius leads to more than a twofold decrease in casualties.

The agent alerting capability is far less important when the velocity of agents is sufficient to avoid the approaching flood water, even without preliminary notification. These cases are shown to the right of the dashed line in Fig. 7.

The current distance-based alerting approach is quite sensitive to the initial distribution of agents. The experiments were conducted by initializing agents using a uniform distribution in empty areas of the modeled region. Results may become very different for different agent density (this currently depends on the number of agents) or distribution structure (e.g., sparse set of dense clusters).

5.1 Junction Effects

Our simulation region has enough room to provide uncongested flow of agents evacuating from the flooded areas to the safe zones. In order to test the behavior of our model in crowded scenarios we reduced the grid step parameter of the simulation from 9.5 to 2.0 m, leading to a more than 22 times region area decrease. This led to a rapid spread of the flood alert, since the agent alert radius was not modified. As Fig. 8 shows, all the agents quickly run towards the exits, causing congestion in narrow passages.

Road junctions limit the rate of agents leaving the modeled area. The line separating the IDLE and RUNNING zones is much steeper than the RUN-SAFE

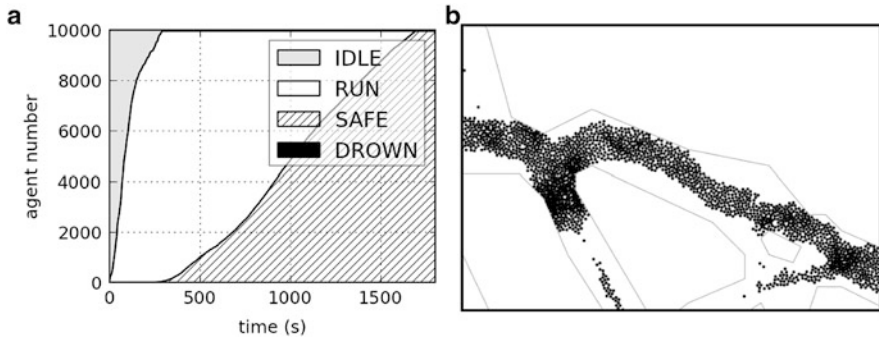


Fig. 8 (a) Agents' states evolution for a crowded scenario. (b) Crowd flow junction

line in Fig. 8a. Compare this to Fig. 6, where the number of evacuated agents almost follows the number of alerted agents up to the delay introduced by agents traveling time.

Figure 8b shows an example of a close up of such road junction. While the RVO collision avoidance model behaves reasonably well in low and medium crowd density conditions, it allows some agent interpenetration at high density condition. Such zones of crowd “thickening” might be the signs of dangerous regions, where high pressure levels may cause injuries. However, the geometrical nature of the RVO model does not consider such agent properties as mass, force, friction, etc. Therefore it does not provide a quantitative way to measure the level of pressure inside a crowd.

5.2 Performance

Our system handles scenarios containing up to 10,000 evacuating agents at 77 computational time steps per second. With a time step of 0.5 s, we simulate evacuation 38 times faster than real time. We run path map update procedures every 30 s of model time. Calculations of the path map took about 22 % of the execution time. Note that we cache computed path maps, so subsequent runs of our model with the same environment and path planning parameters ran about 20 % faster. The remaining execution time is dominated by sensing (querying agent neighbors) and avoiding collisions. Performance was measured on an Intel Core i7 2.93GHz quad-core CPU.

6 Conclusion and Future Plans

In this paper we have presented a model of city-scale evacuation which is coupled to a rapid flood dynamics model. Through experimentation we have shown that the proposed model is capable of producing visually adequate simulations of

crowd evacuation. Beyond this, our experiments offer a number of interesting insights which we plan to investigate in the future. Below we summarize these key observations.

While an increase in agent velocities allows more agents to escape the flood, there is still a residual number of casualties (Fig. 7). Some of these may be avoided by improving the agent path planning strategy, both in the model and reality. For example, avoiding zones that are expected to be flooded soon, via some form of forecast, might be one way to improve the survival rate. Another important source of casualties is groups of agents trapped in isolated areas due to initial rapid spreading of the flood. These observations emphasize the importance of careful evacuation path planning, especially when considering the possible scenarios of flood development. One important factor that was shown to influence the results of evacuation is the ability of agents to sense the approaching flood. Related to this observation, we found the ability of agents to spread the flood alert further around the island can improve survival in some cases. The importance of this ability decreases to being almost insignificant in cases where agents are able to run fast enough to escape the approaching flood, hence reducing the need for prior alert.

In future we plan to make a few important extensions to our model, such as individual randomized graph based path planning, more sophisticated information transfer between agents, incorporation of social relations and walking-in-water models. One final, and most important, open question is the model validation. We plan to investigate the possibility of conducting an experiment by reproducing some historical events (e.g. [1]).

Acknowledgement This work is supported by the *Leading Scientist Program* of the Russian Federation, contracts 11.G34.31.0019 and 13.G25.31.0029; by the EU FP7 project *UrbanFlood*, grant N 248767; and by the *BiGGrid* project BG-020-10 # 2010/01550/NCF with financial support from the Netherlands Organisation for Scientific Research NWO.

References

1. K.S. Pomeranets. Three centuries of floods in Petersburg (in Russian: Три века петербургских наводнений). St. Petersburg: Iskusstvo-SPB, 2005.
2. V.V. Krzhizhanovskaya et al. *Flood early warning system: design, implementation and computational modules*. Procedia Computer Science, V. 4, pp. 106–115, 2011. <http://dx.doi.org/10.1016/j.procs.2011.04.012>
3. A.L. Pyayt et al. *Artificial Intelligence and Finite Element Modelling for Monitoring Flood Defence Structures*. Proc. 2011 IEEE Workshop on Environmental, Energy, and Structural Monitoring Systems. Milan, Italy, September 2011, pp. 1–7 <http://dx.doi.org/10.1109/EESMS.2011.6067047>
4. B. Pengel, G.S. Shirshov, V.V. Krzhizhanovskaya, N.B. Melnikova, A.R. Koelewijn, A.L. Pyayt, I.I. Mokhov. *Flood Early Warning System: Sensors and Internet*. IAHS Red Book series, 2012 (in print)
5. N.B. Melnikova, G.S. Shirshov, V.V. Krzhizhanovskaya. *Virtual Dike: multiscale simulation of dike stability*. Procedia Computer Science, V. 4, pp. 791–800, 2011. <http://dx.doi.org/10.1016/j.procs.2011.04.084>

6. N.B. Melnikova et al. *Virtual Dike and Flood Simulator: Parallel distributed computing for flood early warning systems*. Proc. Int'l Conference on Parallel Computational Technologies (PAVT-2011). Publ. Centre of the South Ural State University, Chelyabinsk, pp. 365–373. <http://goo.gl/MPLfk>
7. A.L. Pyayt et al. *Machine Learning Methods for Environmental Monitoring and Flood Protection*. World Academy of Science, Engineering and Technology, Issue 78, pp. 118–124, June 2011. <http://www.waset.org/journals/waset/v78/v78-23.pdf>
8. B. Gouldby et al. *Multiscale modelling in real-time flood forecasting systems: From sand grain to dike failure and inundation*. Procedia Computer Science, V. 1, p. 809. <http://dx.doi.org/10.1016/j.procs.2010.04.087>
9. B. Gouldby et al. A methodology for regional-scale flood risk assessment. Proceedings of the Institution of Civil Engineers, 2008.
10. Dawson R.J., Peppe R. & Wang M.A. Agent-based model for risk-based flood incident management. Nat Hazards 2011, 59, 167–189.
11. M. Di Mauro, K.M. de Bruijn. Application and validation of mortality functions to assess the consequences of flooding to people. Journal of Flood Risk Management. Volume 5, Issue 2, pages 92–110, June 2012.
12. M. Di Mauro and D. Lumbroso. Hydrodynamic and loss of life modelling for the 1953 Canvey Island flood, in the proceedings of the International Conference on FloodRisk, 30 September to 2 October 2008, Oxford, UK
13. Khatib, O. Real-time obstacle avoidance for manipulators and mobile robots. Proceedings. 1985 IEEE International Conference on Robotics and Automation, 1985.
14. Jur van den Berg, Stephen J. Guy, Ming C. Lin, and Dinesh Manocha, “Reciprocal n-body collision avoidance,” in Cédric Pradalier, Roland Siegwart, and Gerhard Hirzinger (eds.), Robotics Research: The 14th International Symposium ISRR, Springer Tracts in Advanced Robotics, vol. 70, Springer-Verlag, Berlin, Germany, May 7, 2011, pp. 3–19.
15. P. Felzenszwalb, D. Huttenlocher. Distance Transforms of Sampled Functions. Computing and Information Science Technical Reports, Cornell University, 2004.
16. D. Douglas, T. Peucker. Algorithms for the reduction of the number of points required to represent a digitized line or its caricature. Cartographica: The International Journal for Geographic Information and Geovisualization, V. 10, N 2. (1 October 1973), pp. 112–122.
17. C. Reynolds. Steering Behaviors for Autonomous Characters. 1999.
18. Suiping Zhou, Dan Chen, Wentong Cai, Linbo Luo, Malcolm Yoke-Hean Low, Feng Tian, Victor Su-Han Tay, Darren Wee Sze Ong, Benjamin D. Hamilton: Crowd modeling and simulation technologies. ACM Trans. Model. Comput. Simul. 20(4): 20 (2010).
19. G. Bradski. The OpenCV Library. Dr. Dobb's Journal of Software Tools, 2000.
20. C.W. Warren. Global path planning using artificial potential fields. IEEE International Conference on Robotics and Automation, 1989.
21. S. LaValle. Planning Algorithms (First ed.), Cambridge University Press, 2006.
22. C. I. Connolly, J. B. Burns, R. Weiss. Path Planning Using Laplace's Equation. In Proceedings of the IEEE International Conference on Robotics and Automation, 1990.
23. L. C. Polymenakos, D. P. Bertsekas, J. N. Tsitsiklis. Implementation of efficient algorithms for globally optimal trajectories. IEEE Transactions on Automatic Control In Automatic Control, Vol. 43, No. 2., pp. 278–283, 1998.
24. Won-ki Jeong, Ross, T. Whitaker. A fast eikonal equation solver for parallel systems. In SIAM conference on Computational Science and Engineering, 2007.

Large Scale Outdoor Events

Specific Requirements Concerning Evacuation Analysis

Hubert Klüpfel and Sven Hebben

Abstract In this paper, the evacuation of a large scale outdoor event is described. The assessment is based on determining the required safe egress time by evacuation simulation. This paper argues that the method used is applicable to the evacuation simulation of outdoor events in general. The major acceptance criteria for the evacuation safety are: (1) the comparison of the available safe egress time ASET and the required safe egress time RSET and (2) the identification of congestion.

Keywords Large scale outdoor events • Safety • Evacuation simulation • Required safe egress time • Available safe egress time • Identification of congestion

1 Introduction

The evacuation simulation of large scale outdoor events has specific requirements. These can be divided into three areas:

- Method
- Interpretation of simulation results
- Assessment

The simulation is usually performed to determine the required safe egress time. This is part of the assessment of the event safety (safety concept). One acceptance criterion for the assessment of the evacuation safety is given in (1).

$$RSET = t_{\text{detect}} + t_{\text{alarm}} + t_{\text{react}} + t_{\text{movement}} < ASET \quad (1)$$

H. Klüpfel (✉) • S. Hebben
TraffGo HT GmbH, Duisburg, Germany
e-mail: kluepfel@traffgo.de

The required safe egress time must be smaller than the available safe egress time. This is not the only criterion, though. Another one is the identification of congestion. The waiting time in congestion during evacuation processes might lead to frustration and stress. This might provoke pushing and crowd surges. The pressures build up by the crowd can then reach dangerous values. Therefore, the size and duration of congestion must not exceed certain threshold values. A rule of thumb for the duration of congestion is 1 min. For the size of congestion, 10 m in length can be considered a maximum in front of exit doors, stairs, or barriers. The rationale behind that value is the force a crowd that size might exert a force that make breathing difficult in front.

2 Large Scale Events

There are usually more restrictive requirements for the safety of large scale outdoor events than for “normal” events. As a rule of thumb, we use a number of 5,000 visitors as a demarcation. This is applicable for the situation in Germany, the general statement is nevertheless most probably true in other contexts, too. The safety measures can be characterized by two general principles:

- Contain the spread of fire and smoke for a certain time
- Extinction of fire or threat in a restricted area without causing disproportional damage

The second principle will then require evacuation if the health or safety of the audience is affected by an incident. The German Council of Fire Brigades (AGBF) has issued a checklist for safety concepts for large scale events consisting of nine chapters:

1. Introduction
2. Crisis Management
3. Procedure when safety relevant issues arise
4. *Evacuation*
5. Large number of injured persons
6. Concept for security staff
7. Concept for medical first responders
8. Concept for fire safety watch keeping
9. Appendices
 - (a) Check lists
 - (b) Fire Safety Regulation according to DIN 14096 (optional)
 - (c) Fire Safety Plans according to DIN 14095 (optional)
 - (d) Escape Plans according to DIN 4844 (optional)

Part 4 is concerned with evacuation which underlines the fact that the evacuation analysis is only valid as part of a more comprehensive safety concept. We will describe an event on the next section, where such an evacuation analysis has been performed as part of a safety concept.



Fig. 1 General plan of the festival [2]

Table 1 Total number of persons

Lower Reichsstraße	2,887	Visitors
	86	Staff
Sum:	2,973	
Central Reichsstraße	2,356	Visitors
	62	Staff
Sum:	2,418	
Upper Reichsstraße	3,266	Visitors
	58	Staff
Sum:	3,324	
Central court	129	Families
	15	Staff
Sum:	144	
Total Sum:	8,859	

3 Example of Application

The example of application described here is the “Reichsstraßenfest” in Donauwörth, Bavaria, Germany. The general plan is shown in Fig. 1. The Reichsstraßenfest is a street festival. It mainly takes place between the main church and the market place. The total number of persons taken into account in the evacuation simulation is 8,859. The assumptions concerning the distribution of persons can be seen from Table 1. Assuming a maximum average density of two persons per sqm, the area occupied by the audience would be about 17,700 square meters. The area available is larger.

The audience is divided into three groups in the simulation: visitors, staff, and families. The demographic parameters for visitors and staff are equal (see Table 2).

Table 2 Demographic parameters

PedGo demographics	log file			Version	2.4.3.1
	Min	max	mean		
Group 0:					
Families					
VMax:	2	4	2	1	Normal
Sway:	1	5	3	2	Normal
Reaction:	60	180	120	25	Normal
Dawdle:	0	30	15	5	Normal
Inertia:	1	5	3	2	Normal
Clustering:	None				
Group 1: Staff					
VMax:	2	5	3	1	Normal

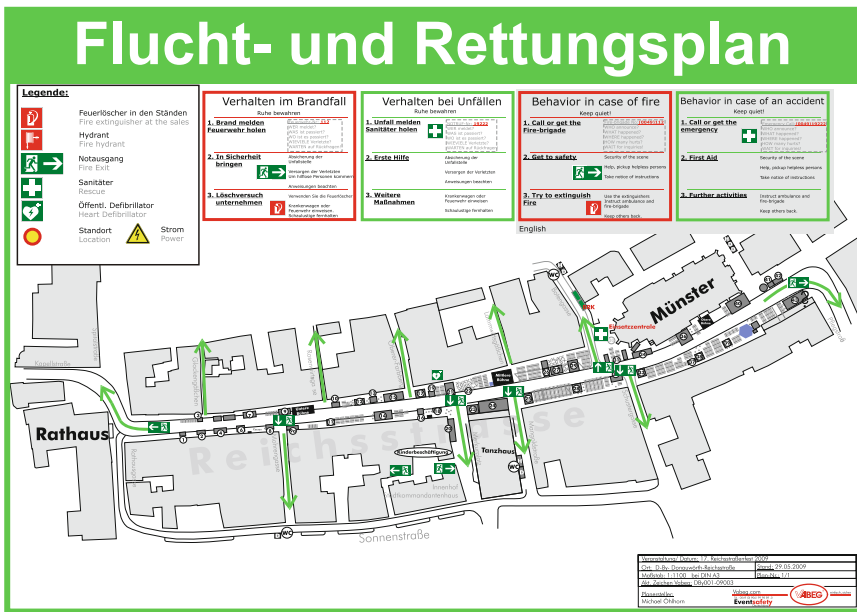


Fig. 2 Escape route plan [2]

The escape routes and the directions for the movement of the persons from their initial location are shown in Fig. 2. The route choice in the simulation is based on the escape route plan, i.e. the assumption is that all evacuees are following the assigned routes. This can of course be disputed. What is shown here is a reference case. Based on that reference case, further cases can be developed by varying the assumptions concerning route choice, reaction time, demographic parameters, etc.

The original CAD plan is pruned to make it suitable for import in the simulation program PedGo (Fig. 4). The demographic parameters are summarized in Table 2.



Fig. 3 Situation in the main street during day (*left*) and at night (*right*) [2]

The escape route plan in the previous figure is the basis for the route choice in the simulation. The case simulated is the day case (see Fig. 3, left). Further cases have not yet been investigated but can easily be implemented based on the reference case.

4 Simulation Input

The simulation is based on the general plan as shown in Fig. 1. This plan is pruned (Fig. 2), imported in the simulation and transformed into the geometric, cell-based model. The population is added in the simulation program (i.e., PedGo Editor) directly (Fig. 4).

The demographic parameters (“reaction time”, etc.) are normally distributed (Table 2). The cell size is 0.4 m, therefore, v_{\max} is 0.8–2.0 m/s [3, 4].

5 Simulation Results

The simulation results are summarized in Table 3. Figure 5 shows the evacuation curve, Fig. 6 screenshots for 2, 4, 6, and 8 min. Dark areas are those where the density exceeds 3.5 persons per square meter for more than 10 % of the overall time, in our case 57 s [4]. The density is measured locally. For each cell of size 0.4×0.4 m the eight cell neighborhood (i.e. an area of nine cells in total) is used to calculate the density.



Fig. 4 Plan for import into the simulation program

Table 3 Simulation results

	/s	/(min:s)	seed
Mean	568	09:28	4711
stddev	14	00:14	--
95% <	591	09:51	4809
Min	524	08:44	4750
Max	605	10:05	4716

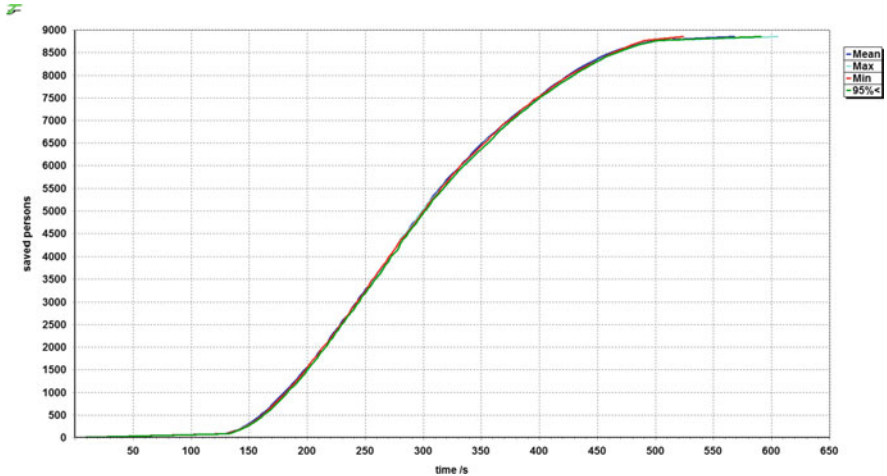


Fig. 5 Evacuation curve (persons saved vs. time/s)

The overall movement time is about 10 min. Please note that short reaction time (1–3 min, see Table 2) was assumed. Furthermore, the exits are 2.5 times as wide as required by the regulations. In order to obtain the overall evacuation time, the times for detection and alarm have to be added. We should a simple scenario providing a

Fig. 6 Situation after 2, 4, 6, and 8 min



reference case. Based on that reference case, further scenarios can be developed and investigated. Those will provide more insights in what could happen, what the consequences of different reaction time distributions or route choice decisions would be and how sensitive the results are with respect to those parameters.

The evacuation curve shown in Fig. 5 illustrates several facts. The egress starts slowly after about 60 s (1 min minimum for the reaction time).

After about 150 s (2.5 min) the curve becomes steeper. The last person starts evacuation after 3 min. This is not directly visible due to the scale of the y-axis. Then the evacuation is rather smooth and the rate of persons evacuating is roughly 8,000 persons/400 s, i.e. 20 per second or 1,200 per minute. After 10 min, the whole area is completely evacuated.

6 Summary, Conclusion, and Outlook

In this paper the results for the evacuation simulation of a large scale event have been presented. The simulation result, e.g. the overall time, can be used to determine the required safe egress time *RSET* via (1). The detection and alarm phase are not covered by the simulation, though. Those two components have to be derived separately. The *RSET* can then be compared to the available safe egress time *ASET*. For outdoor events, the risk of fire is not as high as rooms. The danger of visitors being exposed to smoke and combustion products like irritant and toxic gases is less severe than for venues inside buildings. Therefore, the available safe egress time is usually larger. This is also reflected in the regulations, which allow for Germany thrice as many persons (with respect to the width of the escape routes) outdoors than indoors. There is also no requirement concerning the maximum length of the escape route for outdoor events. Indoors, the maximum walking distance to a safe area (e.g. a fire protected staircase) is restricted by law and regulations. The simulation result for the movement time of 10 min (including an individual reaction time of 1–3 min) is therefore very fast.

References

1. Arbeitsgemeinschaft der Leiter der Berufsfeuerwehren in der Bundesrepublik Deutschland (AGBF): *Sicherheitskonzepte für Versammlungsstätten*, 28.03.2008. (PDF available for download at http://www.agbf.de/f08_loveparade-i01.htm)
2. Vabeg Eventsafety GmbH: *Referenzprojekt "Reichsstraßenfest Donauwörth"* (www.vabeg.de, accessed April 23th, 2012)
3. TraffGo HT GmbH: *PedGo Handbuch*. www.traffgo.ht/slinks/handbuch
4. RiMEA – Richtlinie für Mikroskopische Enfluchtungsanalysen. Version 2.2.1, 8. Juni 2009. www.rimea.de
5. Erlass des Innenministers NRW vom 11.08.2010, Az. 71/38.05.01. (<http://www.im.nrw.de/sch/819.htm>, in German, accessed April 30th, 2012).
6. dokument/MMA15-7.pdf
7. Gattermann, P. et al.: *Handbuch für die Sicherheit von Großveranstaltungen*. Österreichisches Institut für Schul- und Sportstättenbau (ÖISS), Wien, 2005.
8. Widmer, P. et al.: *Handbuch Sicherheit bei Veranstaltungen*. Schweizerische Stiftung für Risikoberatung, Zürich, 2005. (PDF)

The Study on the Effects of the Counter-Flow on the Evacuation of People from Tall Buildings

Piotr Tofilo, Marcin Cisek, and Krzysztof Lacki

Abstract The counterflow condition on the escape stairs is a situation that may occur during the evacuation from buildings when the downward flow of evacuating occupants passes the upward flow of firefighters heading to the fire floor. The aim of this work is to study the effects of counterflow in connection with the requirements of fire regulations. The second aim is to provide data for numerical modeling and calculations. A series of experiments was conducted on a staircase with and without a simultaneous counter flow of ascending firemen. The experimental results are compared to simulations performed with current popular evacuation packages: Building EXODUS, Pathfinder, STEPS.

Keywords Modeling • Experiments • Egress • Counter-flow

1 Introduction

Condition of counter-flow does not always take place because in majority of lower buildings evacuation starts and ends before fire brigade arrives on the scene. In case of taller buildings the conflict between the two movements is more likely to happen due to certain factors: the firefighting and evacuation strategy adopted for the building, the use and purpose of the building, the number of staircases and sizing of the stair, fire warning systems available, the quality of management and staff training, the availability of firefighters lifts and the distance to the fire station.

The evacuation strategy in taller buildings is usually either simultaneous or phased. In case of simultaneous evacuation the counterflow condition is more likely in case of long pre-movement times that are usually the result of inadequate warning

P. Tofilo (✉) • M. Cisek • K. Lacki
The Main School of Fire Service, Warsaw, Poland
e-mail: piotr.tofilo@sgsp.edu.pl; m.cisek@sgsp.edu.pl

systems or poor training. In this case the movements are more likely to coincide. An important issue here is the sizing of the stairs and the philosophy here varies slightly from country to country. For example in UK the sizing of the stairs for simultaneous evacuation is directly related to the whole number of occupants in the building which implies that the total number of people must have enough standing space within the staircase. In most countries however stairs are sized to the highest floor population based on assumption that floors are well compartmented and only the fire floor must be evacuated immediately while other floors will have more time. This concept is quite close to the phased evacuation which allows narrower stairs, however phased evacuation is usually gradual and controlled by warning system, internal communication, well trained staff and the fire control centre. In case of phased evacuation, due to a delayed evacuation of some floors, the likelihood and the impact of counterflow increases.

In British regulations this is acknowledged by a requirement for checking whether the effect of fire fighters on phased evacuation is possible. This should be taken into account while deciding for the number of staircases in the building assuming that one may be discounted due to fire brigade activities. In most of new buildings it is not necessary because there are usually fire fighter lifts provided, however some older buildings still do not meet the required standard of lift protection and cannot be safely used by fire fighters. In practice the most likely occasions where counterflow is expected are tall offices, hotels and the buildings that are not tall enough to have firefighting lifts while having significant population. The problem of counterflow can be even bigger in cases where disabled people are evacuated.

The aim of this work is to study the effects of counterflow in connection with the requirements of regulations and most common evacuation strategies. The second aim is to provide data for numerical modeling and calculations. To achieve these goals a series of experiments was conducted.

2 Experiments

2.1 Main Assumptions and Initial Conditions

The building selected for an experiment was a 10 storey office. Experiments were conducted outside of office hours in one of the two staircases. The general view of the building, the staircase and its dimensions are presented on pictures below (Figs. 1 and 2).

2.2 Experiment Description

In the experiment 78 people were involved – 73 as evacuees and 5 as firefighter. They were the students from Main School of Fire Service in Warsaw but with exception



Fig. 1 Building and the staircase

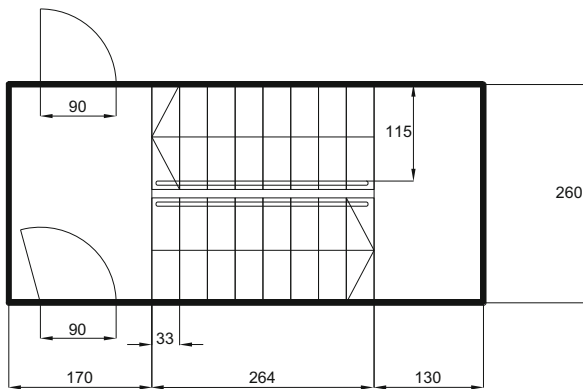


Fig. 2 Staircase dimensions

of firefighters they were not trained and this experiment was the first evacuation training for most of them. Firefighters were fully equipped with typical equipment used during office, hotel or apartment building fire. They were also wearing but not using breathing apparatuses. Next figure shows the firefighters with their equipment. In the experiment one of the firefighters was also carrying movie camera. The firefighters were moving in a row close the wall on their right side. They were asked to not to hurry but also not to stop. Before the main part of experiment the time required for firefighters to ascend to every floor was measured (without the opposing flow). In every run of experiment that firefighters were taking part, they were registering the time required to pass by the evacuees and the segment of

Table 1 Plan of experiments

Run no.	Initial floor density [p/m^2]	Firefighters
1.	4	No
2.	4	Yes
3.	3	No
4.	3	Yes
5.	2	No
6.	2	Yes
7.	1	No
8.	1	Yes

**Fig. 3** Fire fighting team

the staircase on which they did it. In the experiment the firefighters went upstairs five times – once without any evacuees and four times with people evacuating downstairs.

During the experiment eight runs with evacuees were carried out. The variables were the floor density and the counter movement of climbing firefighters. Table 1 shows the variables for every run of experiment.

In every run the same number of students was involved but to simulate different floor densities, they were placed on different segment of the stair case. The lower floor density was applied the more levels of the staircase were occupied. Table 3 shows the people placement on every segment of the staircase before start of every run. The start of every run was signaled by loud whistle audible for all people on the stair case. The evacuees were asked to move calmly and not to run downstairs. They were also asked to move all at once at the start of every run to keep the floor density from the beginning of the run to the moment when they meet firefighters (Fig. 3, Tables 2 and 3).

2.3 Data Collection

For data collection full measuring installation was prepared. It was composed of two IR directional sensors (one for every exit door) connected with the counting

Table 2 Initial conditions

	Length	Width	Area	Target density/students per segment			
				4	3	2	1
Landing A	1.7	2.6	4.42	18	14	9	5
Fly 1	2.7	1.15	3.105	13	10	7	4
Landing B	1.3	2.6	3.38	14	11	7	4
Fly 2	2.7	1.15	3.105	13	10	7	4

Table 3 Schedule of the distributions of occupants in the stairwell

	Numbers of students in segments			
	Exp 1 & 2	Exp 3 & 4	Exp 5 & 6	Exp 7 & 8
6 floor				
5 floor				5
				4
				4
				4
4 floor				5
				4
				4
				4
3 floor			4	4
			9	5
			7	4
		4	7	4
		10	7	4
2 floor	15	14	9	5
	13	10	7	4
	14	11	7	4
	13	10	7	4
1 floor	18	14	9	5
Ground				
Sum	73	73	73	73

unit to the computer with software. presents picture of the installation. The sensors were mounted on the top of both door openings and they were giving impulse to the counting unit any time when the person was passing the door in the outside direction. The sensors were calibrated to measure anybody who is at least 140 cm tall and they should recognize every people even in high floor density. The calculating unit was set up to give information to the computer about number of evacuated people in 1 s time steps. Additionally video cameras were used. One was placed on first floor which was the best place to observe the influence of firefighters movement on the evacuation process. The second video camera was used by one of the firefighters to record the fireman’s perspective during the counter flow movement (Figs. 4 and 5).

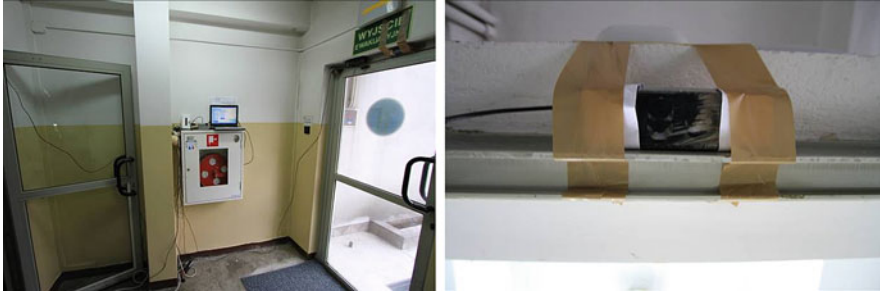


Fig. 4 Data logging system and the sensor attached at the top of the door opening



Fig. 5 Experiment in progress

3 Experimental Results

The following figures present collected data and calculated results (Table 4).

4 Numerical Simulations

4.1 Assumptions

The authors, after carrying out experiments, performed a simulation of the problem using computer software. The following software programs were available for the simulation: STEPS, building EXODUS, Pathfinder and EVAC.

After performing the initial tests and after discussion with a designer of the EVAC software, it was decided not to use this software program for further simulations. The foresaid was due to lack of possibility to reconstruct the experiment.

Table 4 Results

	Exp 1	Exp 2	Exp 3	Exp 4	Exp 5	Exp 6	Exp 7	Exp 8	Firemen free ascent
Time of clash	-	2.38	-	4.27	-	3.48	-	3.38	Floor Last fireman
End of counterflow	-	40.84	-	48.11	-	53.33	-	49.4	0
First person out of staircase	3	4	6	5	4	8	8	9	1 7.06
Last person out of staircase	45	58	61	77	61	67	76	84	2 15.86
Beginning of counterflow (segment)	-	2	-	2	-	2	-	2	3 26.69
End of counterflow (segment)	-	9	-	11	-	12	-	14	4 37.51
									5 50.36

In case of building Exodus software and its newest version 5.0, which has a new model of stairs included, the authors were forced to use the previous method of stairs modelling. The reason for the above was the new version didn't have an option to locate people on the stair flies.

The remaining settings of the entry data consisted in general reconstruction of all elements of the experiments including:

- Characteristics of evacuees;
- Characteristics of fire fighters;
- Instant time of commencing the movement by all individuals;
- A geometry of the building;
- Initial position of people in the staircase.

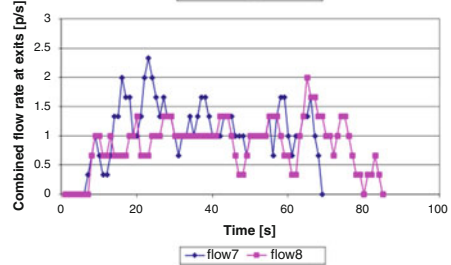
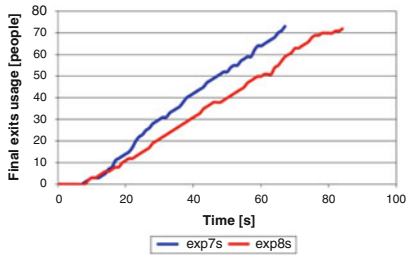
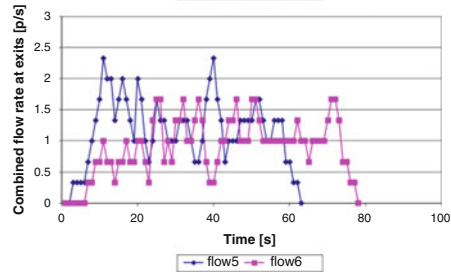
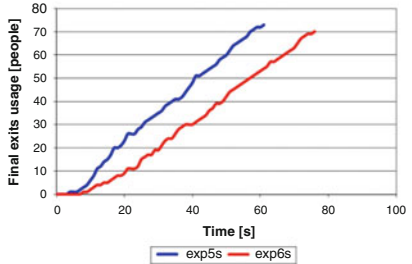
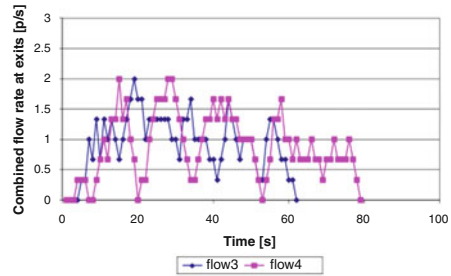
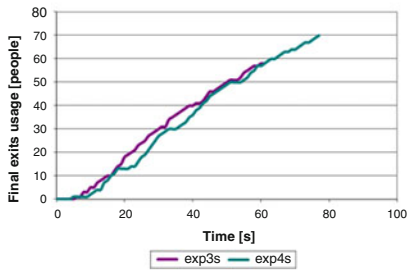
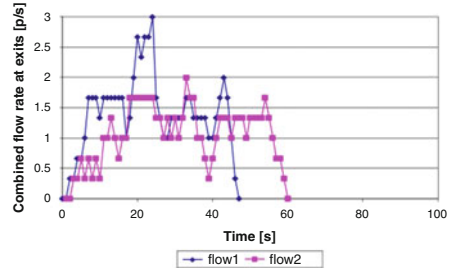
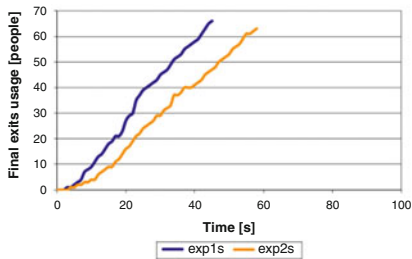
With regards to the actual experiment, the below has not been not reconstructed during the simulation:

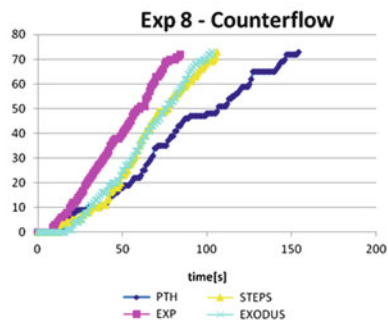
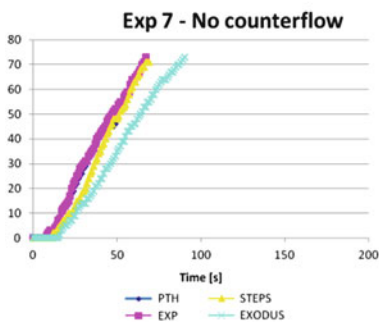
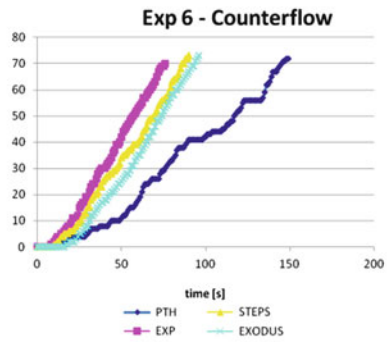
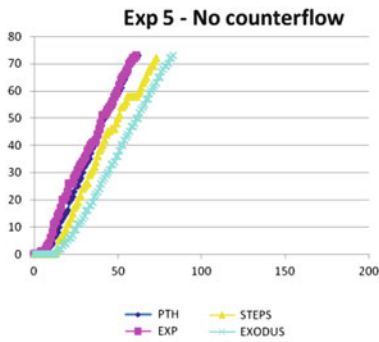
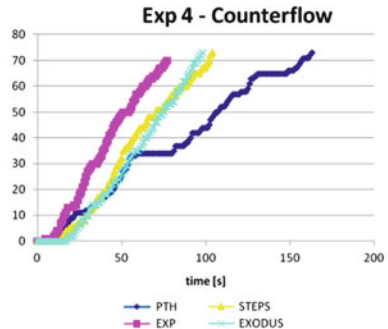
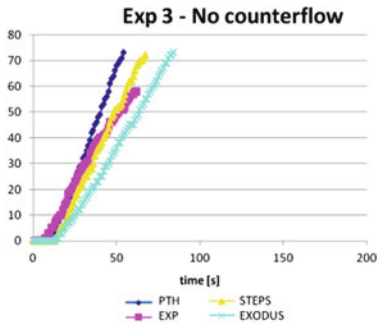
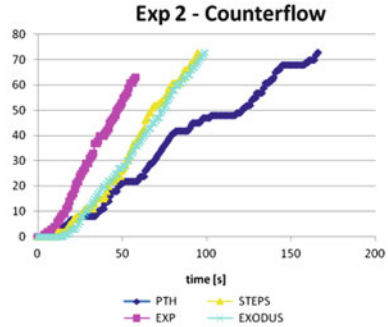
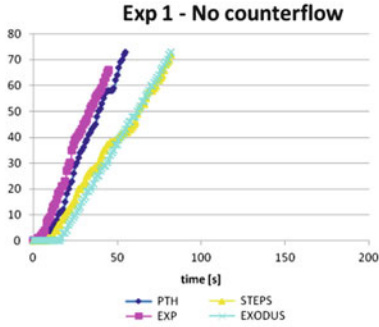
- Fire fighters' movement in a line;
- Fire fighters' movement by the wall when going up the stairs – it refers to STEPS and building EXODUS software
- Progressing tiredness of people participating in the experiment (during the actual experiment the signs of boredom and weariness were noticed among participants of the study).

The simulations were performed according to the best knowledge of the authors, and the software settings, which can affect the final results of the evacuation time, were aimed at most accurate reconstruction of the experiment. However, some social and individuals behaviours were impossible to reconstruct. The same issue concerned the equipment carried by the fire fighters and its impact on their movement – remodelling it in the simulation was not possible.

4.2 Results

The following curves represent results of simulations versus the experimental data.





4.3 Comments to the Results

Based on the conducted simulations and after compilation of the experiment results, the following was observed:

- The results of the experiments without the fire fighters (the experiments no. 1, 3, 5, 7) may be recognized as convergent; in this case it should be emphasized that in most cases the longest evacuation times were recorded in the simulation performed by the building EXODUS software.
- The Pathfinder software recorded the shortest evacuation times in the experiments no. 1, 3, 5, 7 when compared to the other software programs.
- The results of the experiments with the fire fighters (the experiments no. 2, 4, 6, 8) can be split into three groups in all cases. The shortest evacuation time results from the experiment. The results of the simulations performed by STEPS and building EXODUS software are higher up to around 30 %. The Pathfinder results are higher up to around 100 %.
- Applying different methods of modelling explains differences in the results among these software programs.
- In the experiments no. 1, 2, 3 and 4, during the actual study the evacuees were moving considerably faster than the evacuees during the real evacuations and trainings. It resulted directly from social behaviours and some sort of euphoria felt by some participants.
- In case of experiments with the fire fighters, the graphs provided by the Pathfinder software were showing flattening effect that resulted from congestion occurring when the fire fighters were passing by the evacuees.
- Differences between the results coming from STEPS and building EXODUS (apart from experiments 3 and 7) stand at around 10 %.
- In majority of cases (apart from the experiment no. 3) the shortest evacuation time was measured during the actual study.

5 Conclusions

Compilation of all the results and their qualitative and quantitative comparison allows the following general conclusions to be made:

The employed software programs managed the staircase counter-flow problem in various ways. Some of the available software programs couldn't handle this issue at all.

It depends on the applied method of people and space modelling. The incorrect modelling may happen particularly in case of software programs that don't use fine mesh of connected nodes or programs in which the dimensions of the human body cannot be changed. In such cases the results are significantly different from the data of the actual experiment. Given the foregoing, using a software program for modelling this sort of problem should be confirmed by earlier validation.

When comparing the results of the actual experiment and the computer simulation, the simulation results are placed on the conservative side – the evacuation time is longer.

5.1 Further Studies

In order to better understand the staircase counter-flow problem, the further study is required which would take into account the following variables:

- The width of the staircases. It is true that the staircase of the width 1.2 m, which was used in the study, is the most frequently used in many countries; however, the popular width is also 1.5 m up to 2.4 m.
- A number of people going up the stairs. In some cases a number of people going up against the current may be higher. The number of 5 fire fighters used in the study is based on the fire fighting standards.
- More diversified population of evacuees that takes into account different age of people and their ability to move.

5.2 Counter Flow in the Context of Fire Regulations

Applying the computer software, which is validated against the staircase counter-flow problem, is essential for analysis of the evacuation time in the following instances:

- Fire fighting intervention during evacuation in tall buildings where it is not possible to use elevators during existing hazardous conditions.
- Evacuation of people out of stadiums, sport and event buildings, during which the emergency services must proceed towards the source of hazard.
- Evacuation of shopping malls, during which some people return to find their family that occupy the higher levels of the building (e.g. to fetch children which were left in a play room).

The above phenomena are occurring in reality and their accurate reconstruction is necessary for correct computing of the evacuation time.

6 Summary

The actual experiment aimed at estimating what is the influence of people going up the stairs on the time required to evacuate people out of the building. In some cases, when fire brigades arrive at premises where the fire has been detected still during the evacuation process, or other cases mentioned in this article, it could happen that some people would be using the stairs to move in the direction opposite to

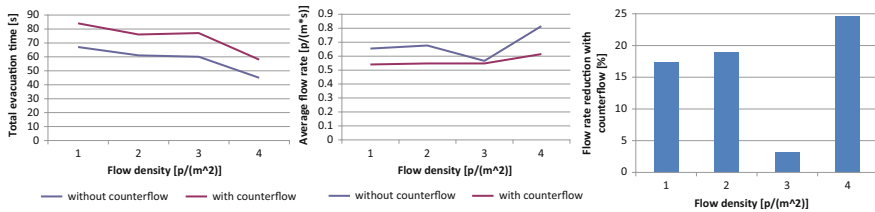


Fig. 6 Differences in occupant flow for cases with and without the counter-flow as derived from the experimental data

the evacuation flow. Based on the conducted measurements, the authors estimated a difference in the evacuation time at the level up to 25 % between the evacuation with counter-flow issue and without it.

A simple recommendation can be proposed that in evacuation calculations, for stair movement, when counter-flow is probable, it is recommended to assume the flow (or available stair width) in one stair to 75 % of its nominal rate. This recommendation is subject to many limitations as discussed, but with current data it is seen as an appropriate measure to account for a counter-flow condition during evacuation.

Further research is required for other sizes of staircases. Improvements in data collection technique are necessary to obtain more precise data.

Additionally the performed experiments and simulations were an engineering attempt to examine dispersion in results of the computer simulations and the actual study for non-standard and difficult problem when modelling the evacuation. The final conclusions from the analysis of the graphs depend on which computer software has been employed. Among available software programs designed for evacuation simulation, there are software programs that are not able to cope with this issue at all and there are programs that generate results very close to the data coming out of the experiments.

For better understanding of the counter-flow influence on the time needed to evacuate people out of the building, it is necessary to conduct further study on variables that may also affect the evacuation, such as a change of the staircase width or a change in the number of people moving in the direction opposite to the evacuation flow. Implementation of these results in the evacuation simulation software is important due to considerable impact of the counter-flow issue on the evacuation time, which currently is very often omitted when analysing the evacuations out of the buildings (Fig. 6).

Reference

1. E.R.Galea, S.Gwynne, P.J.Lawrence, L.Filippidis and D Blackshields, buildingEXODUS V5.0 User Guide and Technical Manual, Fire Safety Engineering Group, University of Greenwich, UK, 2011.

Study of Human Behavior Before Evacuation

Tao Chen, Lili Pan, and Guoquan Zhang

Abstract Computer simulation is the main method to study evacuation during fire or other disasters. In the evacuation simulation, one of the most important initial parameters is the occupant characteristics, such as the age, gender, education, distribution, accompanied status and pre-movement time. In practice, these parameters are based on assumption and experience. However, due to lack of evacuation and pedestrian data, validation or calibration of evacuation models is still a challenging problem which has not got a good solution. We conducted six unannounced evacuation drills in a lecture hall, and three drills of which are used to discuss the human behavior before evacuation, especially for the pre-movement time. Also, questionnaire survey is conducted to make a qualitative analysis of evacuation behavior. Analyzed and compared with data from three evacuation drills, it comes to results as follows. Firstly, people in different groups respond differently, which results in some difference of pre-movement time. Secondly, according to data from the video information, bimodal distribution of pre-movement time is gotten. Thirdly, analysis by gender identity, pre-movement time of women is shorter than that of men, which could be one of the reasons of bimodal distribution of pre-movement.

Keywords Evacuation drill • Human behavior • Pre-movement times • Bimodal distribution

T. Chen (✉) • L. Pan
Institute of Public Safety Research/Department of Engineering Physics, Tsinghua University,
Beijing 100084, China
e-mail: Chentao.a@tsinghua.edu.cn

G. Zhang
IKEA China, Beijing 100102, China

1 Introduction

Safety evacuation is the key solution to ensure the safety of people in an emergency situation. Since 1970s, evacuations in fire emergency have attracted more and more considerable attentions. With the accumulation of fire cases investigations, the abroad conduction of evacuation experiments and surveys, the evacuation behavioral features of occupants and some important parameters of the movement have been abstracted. Computer simulation is the main method to study evacuation during fire or other disasters. Some evacuation models are being built and improved as the computer and modeling technologies develop [1–5].

In the evacuation simulation, one of the most important initial parameters is the occupant characteristics, such as the age, gender, education, distribution, accompanied status and pre-movement time. In practice, these parameters are mainly based on assumption and experience. It is necessary and significant for researchers in different countries to conduct evacuation drills and questionnaire surveys to obtain results and study different behaviors due to their own culture and building construction regulation. Shields conducted four unannounced evacuations of four Marks and Spencer stores between June 1995 and January 1997 [6]. The information of human behavior is collected by CCTV cameras and questionnaires, which provide input for the SIMULEX simulations [7]. Proulx [8, 9], Purser [10], Gwynne [11] et al. have also done some important research and gotten useful information for understanding occupants' behaviors in emergency.

In China, the work of evacuation and pedestrian data collection and study from experiments and real events is less than the European and American countries. Evacuation behavior during evacuation has strong dependence on human characteristics, such as physical feature, cultural backgrounds, habits and emergency training. Obviously, there are must be some differences between Chinese and foreigner for evacuation behavior. Using foreign data to study evacuation of Chinese crowd will inevitably greatly reduce the accuracy and credibility of computer simulation of evacuation. So, it is necessary to conduct research work on data collection and analysis of evacuation behavior in China. Observation of passengers in metros [12, 13], questionnaire surveys of survivors in fires [14], students [15] and residents [16] as well as some announced drills [17–19] have been conducted. But unannounced evacuation drills as well as investigation of actual cases are still rare in China up to now. Due to lack of evacuation and pedestrian data, validation or calibration of evacuation models is still a challenging problem which has not got a good solution.

In this manuscript, data collection and analysis of evacuation behavior is carried out by means of questionnaire survey and evacuation drill. We focus on human behavior before evacuation through questionnaire survey and video information, and pre-movement time is discussed in-depth.

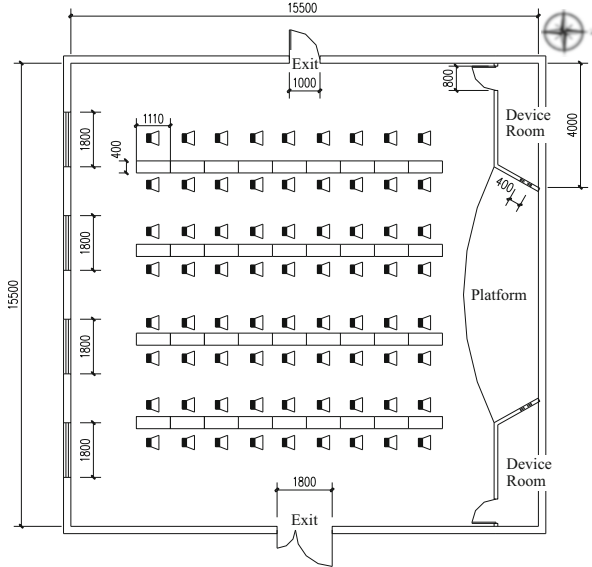


Fig. 1 Layout of the meeting-room for evacuation drills

2 Evacuation Drills

2.1 Drill Place Description

The evacuation drill place is a multifunctional lecture hall, which is in the fifth floor of a hotel in Tianjin. The plan of the room is shown in Fig. 1. The lecture hall area is about 240 m². There are 120 sets of removable wooden tables and chairs in the hall. There is a device room in the northwest corner, which can control the projector, sound and lighting in the hall. The lecture hall has two entrances, one on the east side, 1.8 m wide, and another on the west side, 1 m wide. Both entrances were set significantly evacuation signs, and the east side entrance is the day-to-day commonly used entrances and exits, while the west entrance is mainly used by staff.

2.2 Experimental Materials

During the evacuation drill, smoke cakes were used to simulate smoke during fire, and wireless cameras were used to record human behavior during drill. The smoke cakes are safe, non-toxic, non-gunpowder explosion sources, which can produce harmless smoke rapidly. The smoke cake technical parameters are shown in Table 1.

Table 1 The technical parameters of smoke cake used during drill

Parameter type	Value
Radius	40 mm
Length	88.5 mm
Delay time	0.6–1 s
Affect scope	≥50 m ²
Weight	150 g
Smoke duration time	15–20 s
Normal action rate	≥96 %
Working temperature	−30 °C–45 °C
Diffusion time	60 s

Fig. 2 Wireless camera used for the evacuation drills



Table 2 The technical parameters of wireless camera

Parameter type	Value
Image sensor	1/3 in. CMOS
Effective pixels	PAL: 682 × 582
Delay time	0.6–1 s
visual range	62°
Transmitting frequency	ISM2400-2,438 MHZ
Transmitting power	10 mw
Battery capacity	500 mAh
Receiving frequency	2,414 MHZ 2,432 MHZ 2,450 MHZ 2,468 MHZ

We conduct six times of unannounced drills in the same lecture. In the first drill, two handset HD cameras were used to record the drill process. Unfortunately, Someone participated in the drill found the camera soon, and many people refuse to evacuate. Therefore, several wireless cameras of 300 line level resolution were used in the next five drills, shown in Fig. 2. Built-in rechargeable lithium batteries, the wireless camera can continuous work up to 2 h, whose barrier-free work range is up to 100 m. The technical parameters of wireless camera are shown in Table 2.

Table 3 Detailed description of the six unannounced evacuation drills

No.	Number of attendees	Detailed description
1	78	Recorded by handset HD camera, which found by the attendee, evacuation not finished
2	40	One man attendee tried put out fires with fire extinguisher, which influenced the drill. Several staff got into the hall to direct evacuation
3	57	Fire extinguisher was hidden; two staff help to keep order, evacuation finished
4	56	Someone tried to find out fire, many people stayed around the entrance and looked around, evacuation finished
5	96	The same situation as drill 4, many people stayed around the entrance, evacuation finished
6	51	The same situation as drill 4

2.3 *Experimental Organization*

From March 2nd to June 1st, we conducted six unannounced evacuation drills in the lecture hall where the fire fighting lecture was held. The drill was held during the rest time between two lectures. After every drill, we did questionnaire surveys to obtain some human physical characteristics, such as age, gender, education. The accumulative total of attendee was 378 for the six drills, and 374 effective questionnaires were received.

The first drill was recorded by handset HD camera, and the other five drills were recorded by the wireless cameras. All the evacuation drills were unannounced. When the attendees began to have a rest after a lecture, we released the smoke in the device room of the northwest corner, and some noise was produced by the audio equipment to simulate the fire noise. So, during the drill, all the people in the lecture hall would see the ‘fire’ smoke and hear the sound of ‘fire’, but they wouldn’t directly face the fire. It seems that all the attendees didn’t find the wireless camera during drills. So, the five drills were unannounced for a certainty. The detailed description is list in Table 3.

The six evacuation drills have two characteristics:

1. All the drills were unannounced. Unannounced here means that the attendees had no prior knowledge of the evacuations and were not informed by voice communication systems during the evacuations.
2. These drills were comparable. The drill place, drill plan and the questionnaire after drill were all same. And the attendees for each drill had almost uniform distribution of physical characteristic.

Table 4 The age distribution of the attendees

Age range	18–25	26–35	36–45	>45	Total
Number	73	110	93	98	374
Percentage	19.5 %	29.4 %	24.9 %	26.2 %	

Table 5 The education state of the attendees

Education degree	Junior high school	Technical secondary school or high school	Collage or undergraduate	Bachelor or above	Total
Number	44	118	175	37	374
Percentage	11.8 %	31.6 %	46.8 %	9.9 %	

3 Data Analysis

3.1 Questionnaires Analysis

From questionnaires surveys, some physical characteristics were gotten. Among the 374 attendees who filled out the questionnaire, there were 298 men (about 79.7 %) and 76 women (about 20.3 %). The age distribution of these attendees is shown in Table 4, and the education state is shown in Table 5.

From the analysis of questionnaire surveys, it seems that these evacuation drills have certain representing significance.

3.2 Video Analysis

The key to guarantee the human safety in building is that the Required Safe Egress Time (RSET) must be smaller than the Available Safe Egress Time (ASET, viz. the time period from fire breaking out to endangering human safety). The universal criterion of safe evacuation time-line is shown in Fig. 3.

The RSET means the time period from the moment of fire breaking out to the moment that all the people reach the safe area. The RSET includes the detecting and alarm time t_{alarm} , the pre-movement time t_{pre} and the movement time t_{move} , expressed as (1).

$$RSET = t_{alarm} + t_{pre} + t_{move} \quad (1)$$

Because of the visual range restriction of wireless camera, we couldn't get the whole human behavior before evacuation. But the captured video successfully recorded the move time for attendee from beginning evacuates till he reach the entrance. For all the people in the lecture hall would see the 'fire' smoke and hear

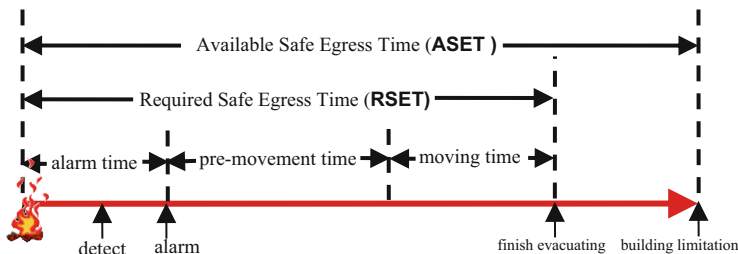


Fig. 3 Universal criterion of safe evacuation time-line

the sound of ‘fire’, fire alarm time was ignored in this paper. So the pre-movement can be gotten as (2).

$$t_{pre} = RSET - t_{move} \tag{2}$$

where $RSET$ is the time period from “fire” occur to attendee reach the entrance, and t_{move} is the time period for attendee from beginning evacuates till he reach the entrance.

Because there are some problems in the previous three evacuation drills, here we mainly analyze the pre-movement of the latter three evacuation drills. The pre-movement time distribution of the latter three evacuation drills are shown in Figs. 4, 5 and 6. Obviously, it can be gotten from these results, the pre-movement time for these drills present a bimodal distribution characteristic, which is different from the traditional normal distribution or logarithmic normal distribution. Although the drills were comparable for the same personnel, there are still large differences for the pre-movement time.

3.3 Comparative Analysis

Statistics from the questionnaire surveys and literature material [20], women tend to evacuate earlier than men. So, we comparative analyze the difference of pre-movement between man and women. Also, the videos of latter three evacuation drills were used to study. The results are shown in Figs. 7, 8 and 9. The figures show that the pre-movement time of woman is obviously shorter than that of man, which is one of the reasons for bimodal distribution.

In order to see clearly, the relations of pre-movement time and gender are list in Table 6. A total of 203 people took part in the latter three drills, with 160 men and 43 women. Accounted for 53 %, 43 women began evacuating in the first phase, and only 28 % of the total men began evacuating in the first phase.

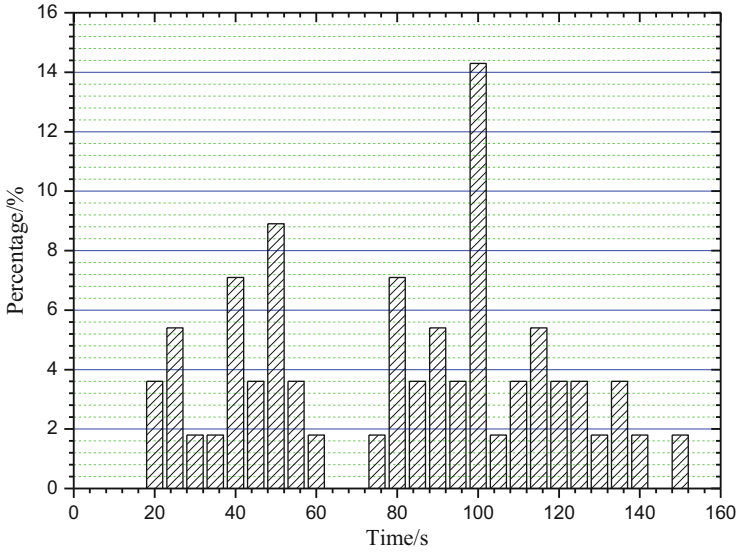


Fig. 4 The pre-movement time distribution of drill 4

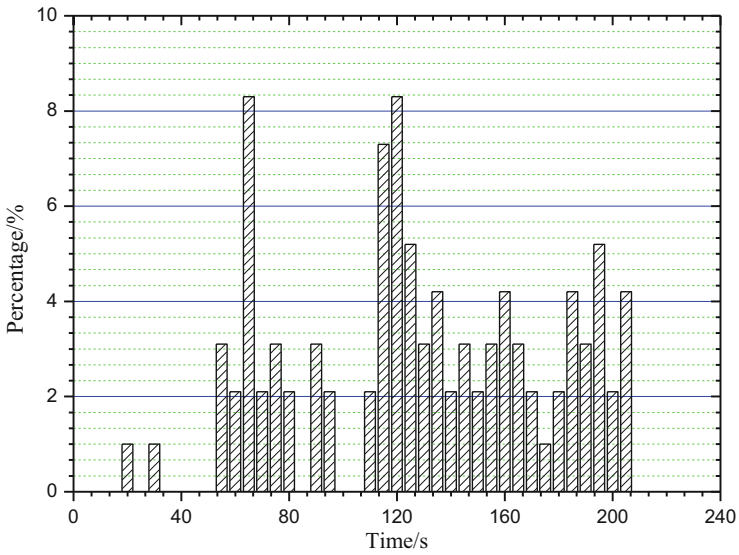


Fig. 5 The pre-movement time distribution of drill 5

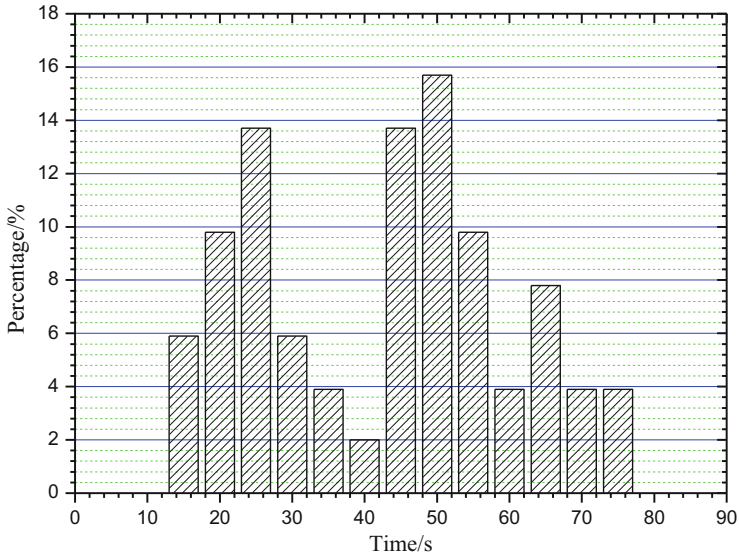


Fig. 6 The pre-movement time distribution of drill 6

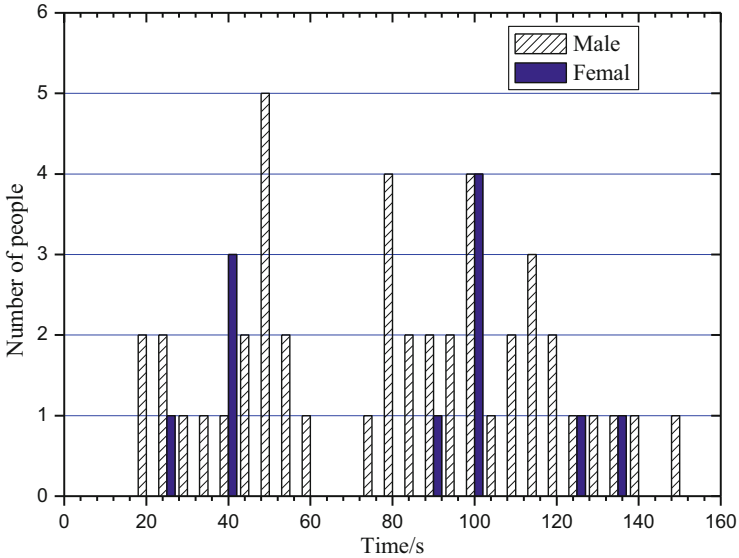


Fig. 7 The comparison of pre-movement time for men and women in drill 4

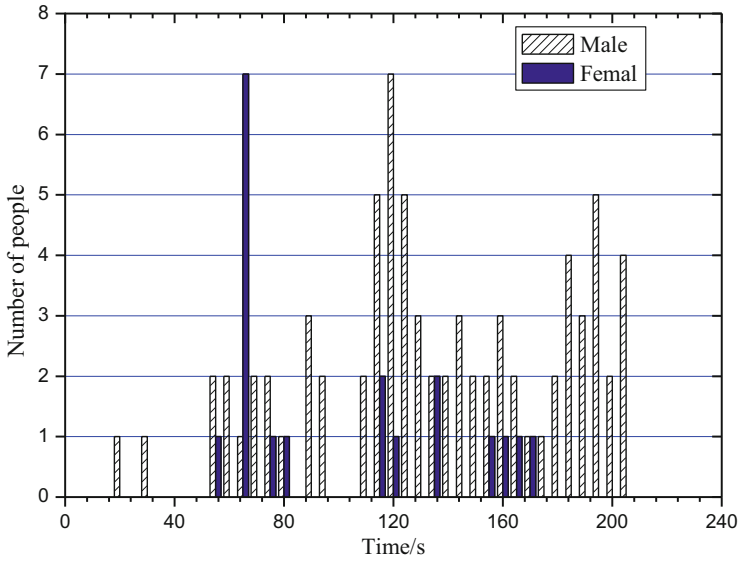


Fig. 8 The comparison of pre-movement time for men and women in drill 5

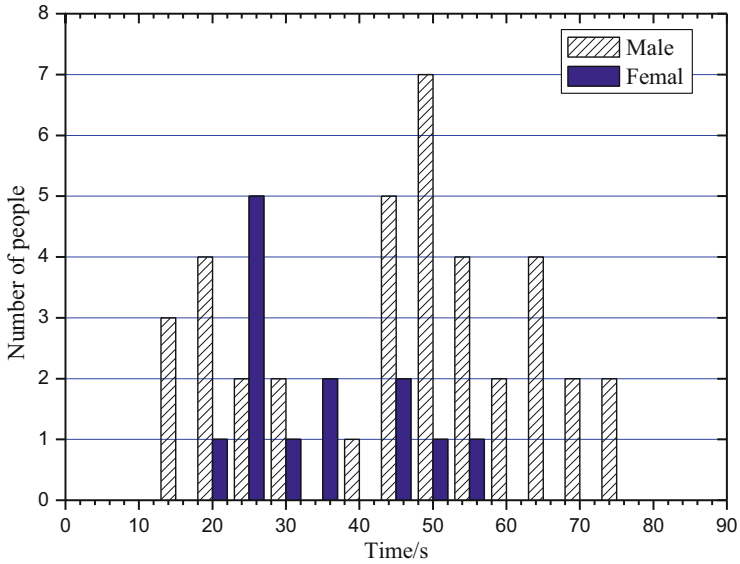


Fig. 9 The comparison of pre-movement time for men and women in drill 6

Table 6 The relations of pre-movement time and gender

No.	First normal distribution		Second normal distribution	
	Men	Women	Men	Women
4	17(38 %)	4(36 %)	28(62 %)	7(64 %)
5	17(22 %)	10(53 %)	60(78 %)	9(47 %)
6	11(29 %)	9(69 %)	27(71 %)	4(31 %)
Total	45(28 %)	23(53 %)	115(72 %)	20(47 %)

4 Conclusion

Computer simulation is the main method to study evacuation during fire of other disasters. In the evacuation simulation, one of the most important initial parameters is the occupant characteristics, such as the age, gender, education, distribution, accompanied status and pre-movement time. So, it is necessary to conduct research work on data collection and analysis of evacuation behavior, especially for the pre-movement time. Data collection and analysis of evacuation behavior is carried out by means of questionnaire survey and evacuation drill. We focus on human behavior before evacuation through questionnaire survey and video information, and pre-movement time is discussed in-depth.

We conducted six unannounced evacuation drills in the lecture hall where the fire fighting lecture was held. The accumulative total of attendee was 378 for the six drills, and 374 effective questionnaires were received. After the analysis of questionnaires survey and video analysis, we got some interesting results about pre-movement time.

Firstly, from the study of unannounced evacuation drills, we got pre-movement time distribution for each drill. For all their differences, it shows the same bimodal distribution, which is different from the traditional normal distribution and log-normal distribution. This finding will helpful for computer simulation of evacuation, especially for those who simulate whole process of evacuation.

Secondly, from the questionnaires analysis and video comparative analysis, the results were obvious that the pre-movement time of women is shorter than that of men. It is due to the characteristic of the gender that women are more sensitive to fire.

Because of space and time cause, the pre-movement time of real fire cases didn't discuss in this paper, which will be described and used to compare in later work.

Acknowledgements The authors appreciate the project 70973062 supported by NSFC and the National Basic Research Program of China 2012CB719705 support by MOST.

References

1. John L Bryan. Human Behavior in Fire: The Development and Maturity of a Scholarly Study Area. *Fire and Materials*, 1999, 23: 249–253
2. S. Gwynne, E. R. Galea, M. Owen, P. J. Lawrence and L. Filippidis. A Review of the Methodologies Used in Evacuation Modelling. *Fire and Materials*, 1999, 23: 383–388
3. J. D. Sime. An occupant response shelter escape time (ORSET) model. *Safety Science*, 2001, 38:109–125
4. Hubert Klüpfel, *Models for Crowd Movement and Egress Simulation*, 2003
5. Gabriel Santos, Benigno E. Aguirre, *A Critical Review of Emergency Evacuation Simulation Models*, 2005
6. T.J.Shields, K.E.Boyce, A study of evacuation from large retail stores,*Fire Safety Journal* 35 (2000) 25–49.
7. B. Ashe and T. J. Shields, Analysis and modelling of the unannounced evacuation of a large retail store, *Fire & Materials* 23 (1999) 333–336.
8. G. Proulx, Evacuation Time and Movement in Apartment Buildings, *Fire Safety Journal* 24 (1995) 229–246.
9. G. Proulx, Occupant Response During a Residential Highrise Fire, *Fire and Materials* 23 (1999) 317–323.
10. D.A. Pursler, M. Bensilum, Quantification of behavior for engineering design standards and escape time calculations, *Safety Science* 38 (2001) 157–182.
11. S. Gwynne, E.R. Galea, J. Parke, and J. Hickson, The Collection and Analysis of Pre-evacuation Times Derived from Evacuation Trials and Their Application to Evacuation Modelling, *Fire Technology* 39 (2003)173–195.
12. J.R. Tian, Study on human behavior in metro fire and risk analysis, master's thesis (In Chinese) 2006.4, Guangzhou University.
13. X.M. Li, T. Chen, S.F. Shen and L.L. Pan, Experiment Study on pedestrian flow on stairwells, *ISSST* 2008, 546.
14. S.P. Zhang, Y.Z. Zhang, Z.M. Lu and L. Yang, Research of human behavior reaction in the building fires, *Fire Science and Technology (In Chinese)* 24 (2005) 563–566.
15. W.D. Yan, B.Z. Chen, and M.H. Zhong, Research on time model of personnel evacuation in building fires, *Journal of Safety Science & Technology (In Chinese)* 2 (2006) 20–23.
16. X.L. Zhang, S.X. Lu, J.H. Wang et al, Study the evacuation time of occupant pre-movement in resident building, *Fire Safety Science (In Chinese)* 17 (2008) 40–43.
17. P.H. Zhang, B.Z. Chen, and L.Z. Liu, Study on the behavior of population dispersion during the fire of a big public building, *China Safety Science Journal (In Chinese)* 11 (2001) 22–26.
18. X.M. Li, T. Chen, L.L. Pan et al. Lattice gas simulation and experiment study of evacuation dynamics, *Physica A* 387 (2008) 5457–5465.
19. X.D. Cheng, H.P. Zhang et al, Study of announced evacuation drill from a retail store, *Building & Environment* 44 (2009) 864–870.
20. J.L. Bryan, Behavioral response of fire and smoke, *SFPE Handbook of Fire Protection Engineering*, 2nd edition, Society of Fire Protection Engineers, 1995

Tracking People in Crowded Scenes

Maik Boltes and Armin Seyfried

Abstract For the collection of trajectory data of pedestrian movement in crowds we are developing software for the automatic extraction of accurate trajectories out of video recordings. In this paper a newly introduced method for a markerless detection is presented. This method identifies people by comparing the shape of the top part of their body with the perspective depth field of overhead stereo recordings. Features to match are pyramidal stacks of ellipses, which approximate isolines of the same distance to the camera.

Keywords Field study • Crowd • People detection • Stereo imaging

1 Introduction

For the proper understanding and modelling of pedestrian dynamics, reliable empirical data is necessary. Collecting the trajectories of every person with a high temporal and spatial resolution allows a detailed analysis of movement and the calibration and verification of microscopic models in space and time [3, 4].

In recent years we have performed an extensive series of well-defined experiments with up to 350 people to study the movement of pedestrians in different situations [5, 6]. These laboratory experiments give us the opportunity to analyse the influence of single parameters under controlled conditions.

For the analysis of these experiments we have developed software to automatically extract trajectories from video recordings of marked people on plane ground [7] and uneven terrain [8].

M. Boltes (✉) • A. Seyfried
Jülich Supercomputing Centre, Forschungszentrum Jülich GmbH, 52425 Jülich, Germany
e-mail: m.boltes@fz-juelich.de; a.seyfried@fz-juelich.de

Despite the above mentioned advantages the experiments under laboratory conditions have also drawbacks. The number of experiments is limited due to the costs of the test persons and for building the artificial environments. Thus, the variance of the studied parameter is limited. Studying some influences of group structures (e.g. football fan or visitor of a classical concert, sober or drunken persons) can only be accomplished by field studies.

Therefore we present a new approach to detect pedestrians without markers also in crowded scenes to facilitate field studies and the easier realization of moderated experiments in real environments, where we use independent gatherings which happen anyway (e.g. works meetings). Thus, we can increase the amount of trajectory data with less time and effort.

The newly introduced method based on the analysis of the depth field of stereo recordings taken from overhead of the pedestrians. The overhead recordings perpendicular to the floor allow a view without occlusion for a range of body heights, so that a microscopic detection and tracking without estimation of the persons' route can be performed.

1.1 Related Work

There has already been done a lot of work in the field of pedestrian detection. Most of the approaches are for monocular cameras and slanted views like from surveillance cameras, and densities which result only in temporary or partly occlusion. These methods are not as robust as techniques using stereo cameras. Publications like [9–11] all report a false detection rate of more than 10 %. Typically the decrease of the false detection rate induces the increase of false positive detections. One of the best results for these scenarios can be found in [12].

Existing techniques for trajectory extraction for stereo cameras, such as [13, 14], depend on accurate segmentation of foreground objects. For dense crowds, where we especially are interested in, these methods would not be applicable or would only detect groups of people. Other techniques use motion patterns of human beings [15, 16] like periodic leg movement or additionally take skin colour [17] into account or use a face detector [18], which is only applicable from side view because of visibility. The side view is also needed by [19], because they assign a region to one person, if the region has the same distance to the camera.

For our studies we want to know the detailed position of every person at any time also in crowded scenes, so that the video recordings have to be done overhead to avoid occlusions. Thus, often no extremity or skin is visible. This perpendicular view also disengages us from a decelerating plan-view statistic like in [20]. Algorithms using motion like [21] cannot be adopted, because in dense situations stagnant flow often occurs. In [22] a method for people tracking in dense situations with multiple cameras is suggested. The combined data from several views is used to calculate the height and thus the position of peoples' head. A robust detection and tracking algorithm also for crowded scenes is described in

[23]. The detection process based on a clustering procedure using bio-metrically inspired constraints. In [24] the detection is done by searching for clusters inside the point cloud of a depth map, which are arranged in a sphere that is proportional in size to human heads. For people walking close together van Oosterhout et al. obtain a precision of 0.97 taking tracking into account, which is nearly as high as our precision (see Sect. 3).

2 Detection and Tracking

The goal of the extraction process are trajectories as exact as possible from every person at any time in particular in crowded scenes.

Before extracting metric information the video has to be calibrated. For the correction of the lens distortion a model of a pinhole camera with distortion is adopted (considering radial and tangential distortion up to fourth order).

For the description of the detection process and in the results we use two experiments performed in the project Hermes [6]: movement around a corner and a merging flow through a T-junction. Details of the artificial setup and the analysis results of the T-junction experiment can be found in [26].

Both experiments have been recorded with two synchronized stereo cameras of type Bumblebee XB3 (manufactured by Point Grey) with the viewing direction perpendicular to the floor. The overlapping field of view of the stereo system is 64° at the average head distance of about 6 m from the cameras. Thus all pedestrians with the discovered height range can be seen without occlusion at any time. Stereo recordings are needed to get spatial trajectories for experiments e.g. at stairs but also for experiments on plane ground to take the perspective distortion into account.

2.1 Detection

The detection method directly uses the perspective depth field, and does not use laborious plan-view statistics to speed up and simplify the extraction step. The identification of the people is done only using the shape of the top part of their body especially the head and shoulders.

Depth Field The depth field h contains the distance of every pixel to the camera and is inversely proportional to the disparity map, $d \propto 1/h$ which describes the pixel offset of both camera views of the stereo camera for every pixel.

Figure 1 shows on the right an overlay of the disparity map on the left picture. The disparity map is restricted to the distance of the upper body part colour coded from red to blue according to the distance of 570–735 cm to the camera.

Background subtraction To identify people only by their shape, before a background subtraction has to be performed to reduce the number of false positive

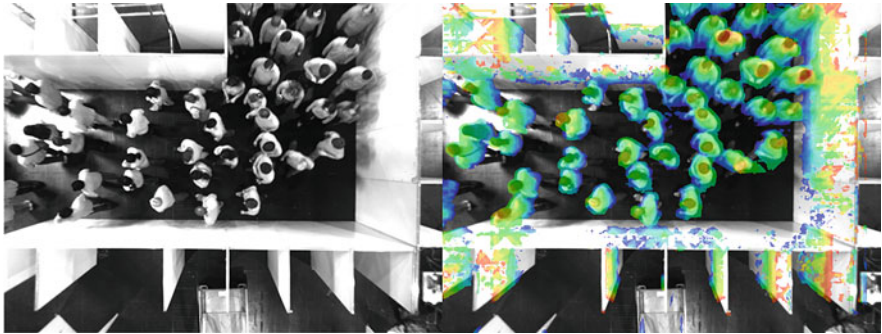


Fig. 1 *Left*: Rectified image of one image from a stereo camera of a corner experiment. *Right*: Colour coded disparity map restricted to the distance of the upper body part (570–735 cm)

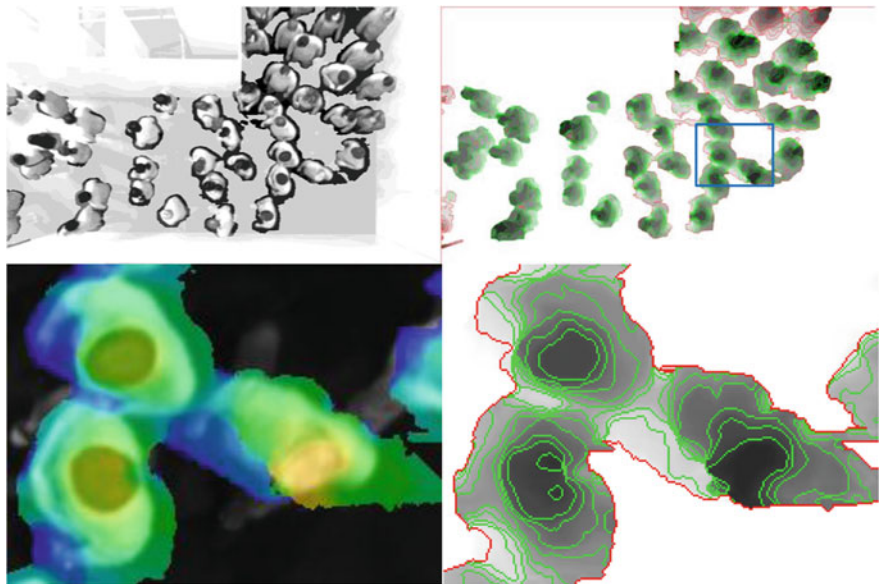


Fig. 2 *Top Left*: Background greyed out. *Right*: Isolines of the same distance to the camera at intervals of 5 cm (coloured according to the orientation) drawn on the grey scaled perspective depth field. *Bottom*: Zoomed view of the *top right* blue labeled region from the disparity map and the isolines

detections. Pixels are part of the background and thus are ignored in the detection process, if the distance to the perspective depth field of the background is smaller than a threshold value without generating a rectified depth field. The chosen distance threshold is 40 cm and cannot be increased for robustness, since people near walls would be eliminated due to the omitted plan-view statistic. This effect can already be seen in the left of Fig. 2 at the walls forming a corner, where the greyed out part is indicating the background.

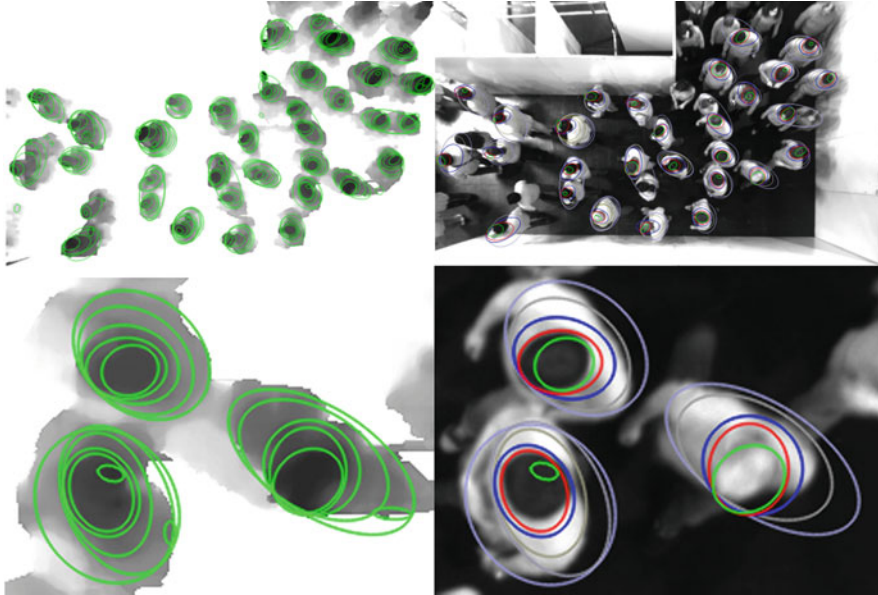


Fig. 3 *Left: Ellipses approximating the isolines of Fig. 2. Right: Pyramidal stacked ellipses identifying pedestrians. Green ellipses correspond to the isoline nearest to the camera, following by red and blue. Bottom: Zoomed view corresponding to Fig. 2*

Small regions of missing values inside the perspective depth field of the background are interpolated linearly within the row. Small regions inside the segmented foreground are added to the background to erase noise and regions that cannot be occupied by a person.

Directed Isolines To extract features identifying pedestrians inside the depth field, directed isolines of the same distance to the camera are used. The step size of the iso-value scanning the depth field is 5 cm. Beforehand the depth field is adapted by replacing values covered by the background mask with the furthest value which belongs to the foreground.

In Fig. 2 red isolines surround regions further away. They can be ignored. Green isolines encircle regions which are nearer to the camera. To improve the visibility of the isolines the colour coding of the disparity map is replaced by a grey scale one.

Approximating Ellipses The remaining isolines enclosing a minimum and maximum of pixels and with a small ratio between the length of the isoline and the enclosed area (to eliminate isolines with big dents) are approximated by ellipses as seen in Fig. 3. The ellipses allow an easier access to values characterising the global shape.

Small ellipses with a large eccentricity are discarded. Large ellipses can have a bigger eccentricity to enclose multiple people also visible in Fig. 3. The values used for the selection of isolines and ellipses have been chosen heuristically considering the number of pixel covered by one person.

Ellipses Pyramids By scanning the depth field downwards in steps of 5 cm a pyramid of ellipses (Pyramidal Ellipses Stack) for every person is build up.

Thus for every new depth level an ellipse is assigned to that pyramid, whose centre is located inside the new ellipse. If no PES fits, the new ellipse starts a new pyramid. For multiple ellipses on the same level covering the identical pyramid that one is chosen, whose centre is the closest to the pyramid centre. New ellipses can cover multiple PES, if the pyramids have already a substantial number of ellipses from previous depth levels. Otherwise the small pyramids are rejected or, if there are only small ones, the pyramid with the closest centre is chosen.

Finally we neglect PES with a

- Small (≤ 4) number of ellipses,
- Large (semi-major axis ≥ 40 cm) second ellipse (corresponding to the head),
- Small (semi-major axis ≤ 14 cm) third ellipse (to reject e.g. lifted arms),
- Small (area ≤ 500 cm²) last ellipse (corresponding to the body).

We prefer a strict deletion to avoid false detections since for tracking it is not necessary to detect a person every frame. The values again are chosen heuristically taking peoples' shape into account.

At the end the centre of the second ellipse of every PES represents a pedestrian and thus is tracked (red ellipse on the right of Fig. 3). The first ellipse is not chosen, because the location varies too much, especially due to the fact that the heads are detected at different depth the first time.

The resulting pyramids are shown on the right of Fig. 3. The ellipses are coloured according to their level in the pyramid. The topmost ellipse has a green, the second a red and the third a blue colour. The latter ellipses can cover more than one person.

2.2 Tracking

For tracking of detected pedestrians the robust pyramidal iterative Lucas Kanade feature tracker [25] is used to join the same detected pedestrian in successive frames or bypass over frames where a specific pedestrian could not be located.

After analysing the complete video recording trajectories are rejected, which do not cross the given test area, or have only few frames where the supposed pedestrian is identified. The left of Fig. 4 shows the tracked people and their path during the last second. The right shows trajectories of 162 pedestrians attending a corner experiment.

3 Results

All resulting trajectories for the pictured experiment around a corner can be seen in Fig. 4. The strict deletion leads to four missing persons (2.4 %) and no false detections. The complete number of passing people is 166. Less restrictive

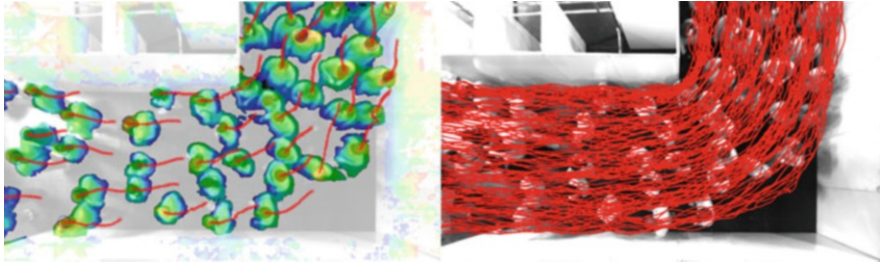


Fig. 4 *Left:* Tracked people and their identified position in the last second shown by 16 small red circles. *Right:* Red trajectories of 162 pedestrians attending this experiment

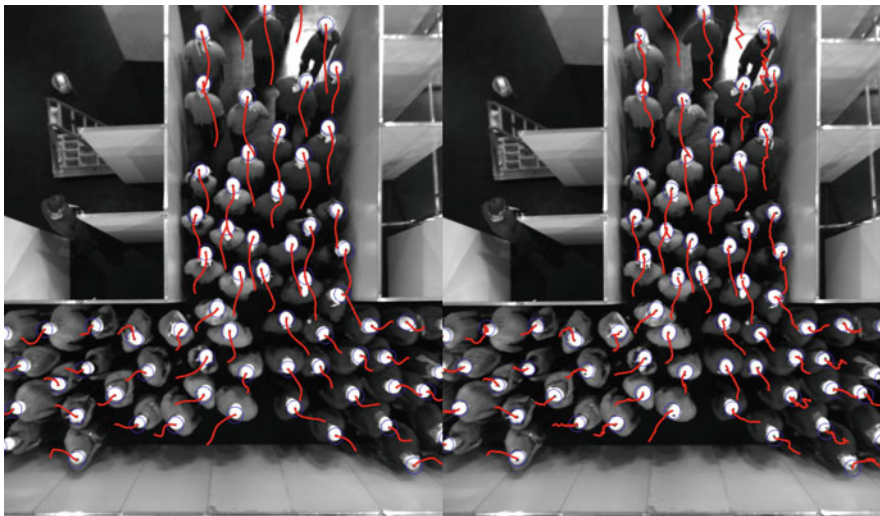


Fig. 5 *Left:* Tracked people by markers and their smooth path during the last second. *Right:* Tracked people without markers and their more unsettled path during the last second

regulation may detect the lost people, but may produce false detections, which are more difficult to discover inside a crowded scene within a subsequent manual revision.

Figure 4 also shows that the trajectories are unsettled, but the smoothness of the trajectories is important for the analysis, e.g. for the microscopic velocity calculation. To estimate the smoothness we consult a T-junction experiment with markers and extract the trajectories by using and also without using the markers. The right of Fig. 5 shows the tracked people and their unsettled path during the last second in comparison to the left picture showing the path of the people detected by markers. To quantify the smoothness the average microscopic acceleration can be used.

Table 1 Comparative results of the detection methods

Method	Detected	False positive	False negative	Avg. acc. [m/s ²]
Corner				
Markerless	162	0	4	3.6 ± 4.8
T-junction				
Markerless	300	0	3	6.5 ± 6.8
With markers	304	1	0	1.2 ± 0.7
Combination	303	0	0	1.2 ± 0.7

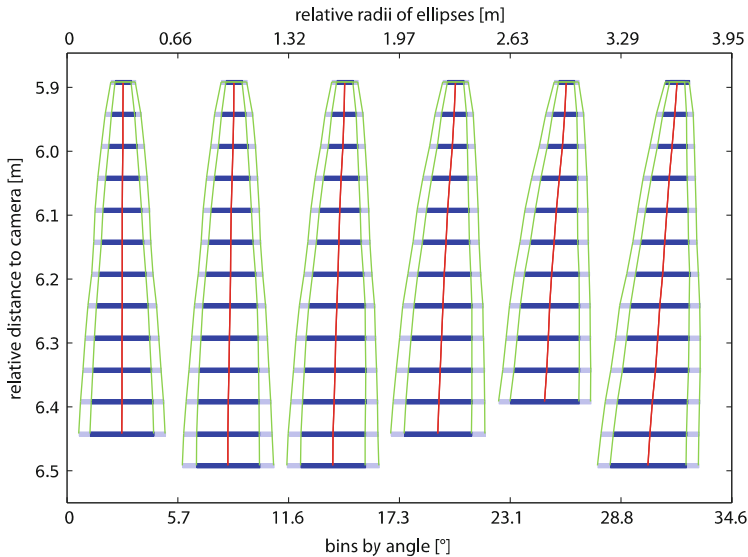


Fig. 6 Side view of mean pyramids binning by the angle to the optical axis of the camera. The *blue ellipses* are surrounded by *green lines* at the major and minor radius. The *red pyramid axis* connects the centre of the ellipses stack

Quantitative results of the detection with and without markers are shown in Table 1. The one misleading match of the detection using markers traces back to an area similar to the easy structured marker. The strict heuristic of the markerless detection deletes some correct trajectories.

Besides this, the markerless detection can improve the robustness of the marker based detection, as detected markers not lying on an elevation describing a persons' head can be rejected. The combination of both methods has no false detection.

To illustrate the shape of the PES, Fig. 6 shows six bins of all PES detected during an experiment according to their angle to the optical axis from side view. The lowest ellipses are neglected, if they cover more than one person. All PES have been adjusted to one camera distance before a mean pyramid for each bin was calculated. The red lines concatenate the centre of the blue ellipses of successive height level and depict the pyramid axes. The green lines surround the ellipses stack at the major

and minor radius. One can see that the red centre line of the mean pyramids is tilted according to the angle, but less than one would expect from the perspective view, because the based isolines of the latter ellipses have to cover the higher ones due to the not performed plan view statistic. The radii increase slightly for larger angle. The size of the radii can be read from the top diagram axis.

Acknowledgements This study was performed within the project funded by the project Hermes funded by the Federal Ministry of Education and Research (BMBF) Program on “Research for Civil Security – Protecting and Saving Human Life”.

References

1. Klingsch, W. W. F., Rogsch, C., Schadschneider, A. and Schreckenberg, M. (Eds.), *Pedestrian and Evacuation Dynamics 2008*, Springer Berlin Heidelberg (2010)
2. Peacock, R. D., Kuligowski, E. D. and Averill, J. D. (Eds.), *Pedestrian and Evacuation Dynamics 2010*, Springer Berlin Heidelberg (2011)
3. Steffen, B., Seyfried, A. and Boltes, M.: Reliability issues in the microscopic modeling of pedestrian movement. In: *Mathematical results in Quantum Physics*, Pavel Exner, H. K. (Ed.), pp. 254–259 (2011)
4. Chraïbi, M., Seyfried, A. and Schadschneider, A.: Generalized centrifugal force model for pedestrian dynamics. In: *Physical Review E*, vol. 82, pp. 046111 (2010)
5. Seyfried, A., Boltes, M., Kähler, J., Klingsch, W., Portz, A., Rupprecht, T., Schadschneider, A., Steffen, B. and Winkens, A.: Enhanced empirical data for the fundamental diagram and the flow through bottlenecks. In: [1], pp. 145–156 (2010)
6. Holl, S. and Seyfried, A.: Hermes - an Evacuation Assistant for Mass Events. In: *inSiDe*, vol. 7, pp. 60–61 (2009)
7. Boltes, M., Seyfried, A., Steffen, B. and Schadschneider, A.: Automatic Extraction of Pedestrian Trajectories from Video Recordings. In: [1], pp. 43–54 (2010)
8. Boltes, M., Seyfried, A., Steffen, B. and Schadschneider, A.: Using Stereo Recordings to Extract Pedestrian Trajectories Automatically in Space. In: [2], pp. 751–754 (2011)
9. Leibe, B., Seemann, E. and Schiele, B.: Pedestrian detection in crowded scenes. *Computer Vision and Pattern Recognition 2005*, pp. 878–885 (2005)
10. Saadat, S., Teknomo, K. and Fernandez, P.: Automation of Tracking Trajectories in a Crowded Situation. In: *Fire Technology*, pp. 1–18. Springer Netherlands (2010)
11. Johansson, A., Helbing, D., Al-Abideen, H. Z. and Al-Bosta, S.: From Crowd Dynamics to Crowd Safety: A Video-Based Analysis. In: *Advances in Complex Systems*, vol. 11 (2008)
12. Schwartz, W. R., Kembhavi, A., Harwood, D. and Davis, L. S.: Human detection using partial least squares analysis. In: *IEEE International Conference on Computer Vision 2009*, pp. 24–31 (2009)
13. Rittscher, J., Tu, P. and Krahnstoever, N.: Simultaneous estimation of segmentation and shape. In: *IEEE Computer Society Conference on Computer Vision and Pattern Recognition*, Vol. 2, Schmid, C., Soatto, S. and Tomasi, C. (Eds.), pp. 486–493. IEEE Computer Society (2005)
14. Hu, W., Zhou, X., Tan, T., Lou, J. and Maybank, S.: Principal axis-based correspondence between multiple cameras for people tracking. In: *IEEE Transactions on Pattern Analysis and Machine Intelligence*, vol. 28, pp. 663–671. IEEE Computer Society (2006)
15. Cutler, R. and Davis, L.: Robust real-time periodic motion detection, analysis, and applications. In: *IEEE Transactions on Pattern Analysis and Machine Intelligence*, vol. 22, pp. 781–796. IEEE Computer Society (2000)

16. Pai, C., Tyan, H., Liang, Y., Liao, H. and Chen, S.: Pedestrian detection and tracking at crossroads. In: *Pattern Recognition*, vol. 37, pp. 1025–1034. Pergamon Elsevier Science Ltd (2004)
17. Darrell, T., Gordon, G., Harville, M. and Woodfill, J.: Integrated person tracking using stereo, color, and pattern detection. In: *International Journal of Computer Vision*, vol. 37, pp. 175–185. Kluwer Academic Publ (2000)
18. Muñoz-Salinas, R., Aguirre, E. and Garca-Silvente, M.: People detection and tracking using stereo vision and color. In: *Image Vision Computing*, vol. 25, pp. 995–1007. Butterworth-Heinemann (2007)
19. Hou, Y.-L. and Pang, G. K. H.: Multi-cue-Based Crowd Segmentation. In: *Stereo Vision. International Conference on Computer Analysis of Images and Patterns*, Real, P., Daz-Pernil, D., Molina-Abril, H., Berciano, A. and Kropatsch, W. G. (Eds.), vol. 6854, pp. 93–101. Springer (2011)
20. Harville, M.: Stereo person tracking with adaptive plan-view templates of height and occupancy statistics. In: *Image and Vision Computing*, vol. 22, pp. 127–142 (2004)
21. García-Martín, A., Hauptmann, A. and Martínez, J. M.: People Detection Based on Appearance and Motion Models. In: *8th IEEE International Conference on Advanced Video and Signal-Based Surveillance 2011* (2011)
22. Eshel, R. and Moses, Y.: Homography based multiple camera detection and tracking of people in a dense crowd. In: *IEEE Computer Society Conference on Computer Vision and Pattern Recognition*, pp. 1–8. IEEE Computer Society (2008)
23. Kelly, P., O'Connor, N. E. and Smeaton, A. F.: Robust pedestrian detection and tracking in crowded scenes. In: *Image and Vision Computing*, vol. 27, pp. 1445–1458. Elsevier Science BV (2009)
24. Van Oosterhout, T., Bakkes, S. and Kröse, B.: Head Detection in Stereo Data for People Counting and Segmentation. In: *International Conference on Computer Vision Theory and Applications*, pp. 620–625 (2011)
25. Bouguet, J.-Y.: Pyramidal Implementation of the Lucas Kanade Feature Tracker. In: *OpenCV Documents*. Intel Corporation, Microprocessor Research Labs (1999)
26. Boltes, M., Zhang, J., Seyfried, A. and Steffen, B.: T-junction: Experiments, trajectory collection, and analysis. In: *IEEE International Conference on Computer Vision Workshop on Modeling, Simulation and Visual Analysis of Large Crowds*, pp. 158–165 (2011)

Validation and Calibration of the EXIT89 Evacuation Model for Road Tunnel Evacuation Applications

Enrico Ronchi, Rita Fahy, Pasquale Colonna, and Nicola Berloco

Abstract The validation of an evacuation model is generally performed through testing its predictive capabilities within a set of standard environments (e.g. buildings) or standard layouts. Unfortunately, non-expert users could consider model results as reliable in unique environments as well, such as road tunnels, and extend their use to applications where no ad hoc validation tests have been performed. This paper focuses on the applicability of the EXIT89 model for road tunnel evacuations. The predictive capabilities of EXIT89 are tested by comparing the model results with a tunnel evacuation experiment. A case study has been then analysed, namely the Condò tunnel in Lecce (Italy). The evacuation times produced by the model are also compared with the results produced by the capacity method described in the Society of Fire Protection Engineering Handbook. Conclusions focus on model strengths and limitations in the reproduction of human behaviour aspects related to road tunnel evacuations.

Keywords Egress model validation • Tunnel evacuation • Road tunnel safety • EXIT89 • Human behaviour in fire • SFPE capacity method

1 Introduction

The definition of validation in the context of simulation models is a controversial point in the scientific community [16]. The validity of a tool generally refers to the correctness of the results produced. But, how to define if these results are correct?

E. Ronchi (✉) • P. Colonna • N. Berloco
Polytechnic University of Bari, Via Orabona 4, 70100 Bari, Italy
e-mail: Enrico.Ronchi@brand.lth.se

R. Fahy
National Fire Protection Association, Quincy, MA, USA

The first step should be the definition of the system in which the tool is going to be employed as well as the basic hypothesis/assumption – often defined in engineering terms as boundary conditions – on which the model is based. Validation may not necessarily be a simple procedure for testing scientific theory or certifying the correspondence between the model and reality, i.e. the current understanding of a problem. Rather, validation, in a more general sense, can mean that a simulation model is suitable for its intended use. A simulation model should therefore meet specified performance requirements [7]. The process of egress model validation should be addressed taking into account several aspects, such as (1) the purpose of the model, (2) the performance criteria and (3) the specific context(s) of use of the model. Validation may either be a part of the model building process [11] or validation tests are required after the model has been created. The key objectives are (1) to define if the model is acceptable for its intended use, i.e., if the model is able to reproduce reality well enough for its intended purpose [5] and (2) to check if the modelling assumptions are accurate enough to represent reality, i.e., how much confidence to be placed in its representation of the real system [2]. In order to provide an example of these issues, this paper is focused on the application of a model that has been originally created and validated for high-rise buildings – the EXIT89 evacuation model [3] – to a different context of use, i.e., road tunnel evacuation scenarios. EXIT89 is a network-based model able to simulate the evacuation of large populations through complex infrastructures. The model permits the simulation of different aspects related to human performance under fire conditions, such as travel paths, delay times, merging flows, counter-flows, etc. Travel speeds are considered within the model as a function of the changing crowdedness of spaces during the evacuation [3, 4, 8]. Walking speeds are then calculated in accordance with people density as well as occupant characteristics, using the equations provided by Predtechenskii and Milinskii [12]. Road tunnels are environments where the crucial factors during an evacuation scenario could then be related to the occupants' behaviour during the pre-evacuation phase more than on the people movement itself [13, 14, 15]. Thus, there is a need of testing the predictive capabilities of models where speeds are based on other factors (i.e. people density) for the specific case of road tunnel evacuation scenarios. The example provided has been made in order to show that a safety analyst should always evaluate the ability of a model to reproduce reality as well as check its usability in its specific context of use. Empirical data and measures are then necessary to perform these two analyses. A data-set relating to a tunnel evacuation experiment performed by the Department of Fire Safety Engineering and Systems Safety at Lund University [10] has been used to validate the results produced by EXIT89. This validation exercise is focused on the validation and calibration of this model for the specific use of EXIT89 in road tunnel environments. In a second stage, the predictive capabilities of EXIT89 were used to study another road tunnel, namely the Condò tunnel in Lecce (Italy). This case study is focused on investigating different agent speeds by following the guidelines provided in the Italian legislation framework [1]. EXIT89 results are then also compared with the results produced by the capacity method provided in the Society of Fire Protection Engineering Handbook [6, 9].

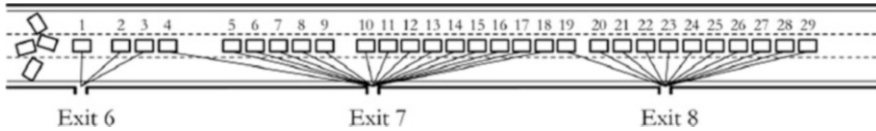


Fig. 1 Schematic representation of Network A, based on experimental observations [10]

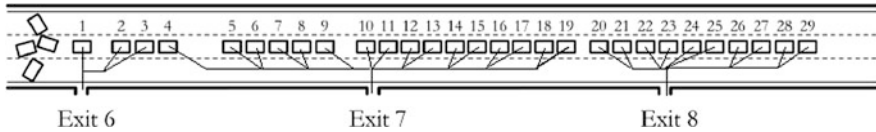


Fig. 2 Schematic representation of Network B

2 Validation Test: The Göta Tunnel

A validation test was conducted by comparing the results produced by EXIT89 and an evacuation experiment in a twin bore road tunnel. This experiment was performed by the Department of Fire Safety Engineering and Systems Safety at Lund University in 2006 [10] in the Göta tunnel in Göteborg. The length of the tunnel is approximately 1.6 Km with 15 emergency exits. The experiment consisted of the evacuation of 29 car drivers involved in a simulated crash inside the tunnel. Participants were partially informed during the experiments i.e. they were only told they were taking part in a study about driving behaviour, thus permitting the analysis of participants' behaviours in case of an unannounced evacuation. Further information about the tunnel layout, experimental procedures, participant demographics, etc. can be found in the paper by Nilsson et al. [10].

The evacuation experiment has been simulated using EXIT89. Different scenarios have been simulated. Two different networks were employed:

- Network A: The network is simulated through straight arcs connecting the nodes of the cars to the emergency exits. In this case, the simulated path represents people walking straight towards the emergency exit. The emergency exit picked by each occupant is selected in line with the experimental paths recorded (see Fig. 1).
- Network B: The network consists of nodes linking the doors of the cars to an intermediate set of nodes along the virtual corridor (e.g. a sidewalk) between the cars and the emergency exits (see Fig. 2).

These two networks were used in order to try to approximate as much as possible the paths observed during the evacuation experiment (Network A) and check the effect of different people densities in nodes (Network B).

Two different types of node dimensions were employed, that represent two possible threshold values for the areas of a node. The first node size employed was 8 m² that represents the area effectively available. The second area is 1 m² that represents an artificial reduced area chosen in order to check the effect of

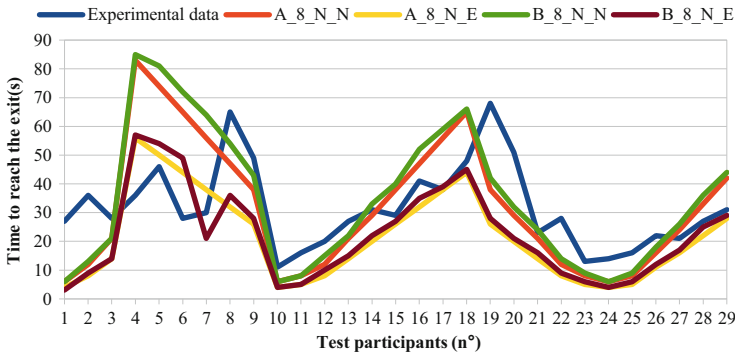


Fig. 3 Comparison between results produced employing Network A and B (area of nodes = 8) and experimental data when the speed factor function is not enabled

the dimensions of the nodes on the results produced by EXIT89. The delay time observed during the evacuation experiment was assigned to each occupant in order to simulate the evacuation process.

EXIT89 also embeds a speed factor function S_f . S_f is a coefficient that can be assigned as an input in EXIT89 and multiplied by the agent speed (calculated by the model), it returns a modified value of speed. It may be employed to modify the speed of the agents in relation to pre-defined conditions (e.g. people with disabilities, individual characteristics of the agents, etc.). In this case, this function has been used to try to match the speeds recorded during the experimental observations. In addition, EXIT89 simulates different types of conditions that are reflected in agent speeds, namely normal conditions and emergency conditions (i.e. the walking speeds employed are higher in this case).

A total of 12 scenarios have been studied varying the combination of the above described variables (i.e. type of network, area of the nodes, speed factor, speed conditions). A four place naming convention is used for these scenarios. The first place indicates the assumed type of network (either A or B). The second place shows the area of the nodes (either 8 or 1). The third place indicates if the speed factor has been employed (either Y = Yes or N = No). The final place shows the speed conditions employed (either N = normal conditions or E = Emergency conditions). For instance, scenario [A_8_Y_N] represents a scenario where Network A has been employed, the area of the nodes is 8, and the speed factor has been employed and normal speed conditions have been simulated.

In order to provide a direct comparison between the results produced by the model and the experiments, delay times are removed from the comparison, i.e. the time to reach the exit is the benchmark value. The time to reach the exit is defined here as the time from which the occupants open the door until they reach an emergency exit. This is obtained by removing the delay times from the evacuation times produced.

Figures 3 and 4 show that the results produced by EXIT89 are in some cases different than the experimental results. This is mainly due to the different walking speeds produced by the model with default. For this reason, the speed factor function

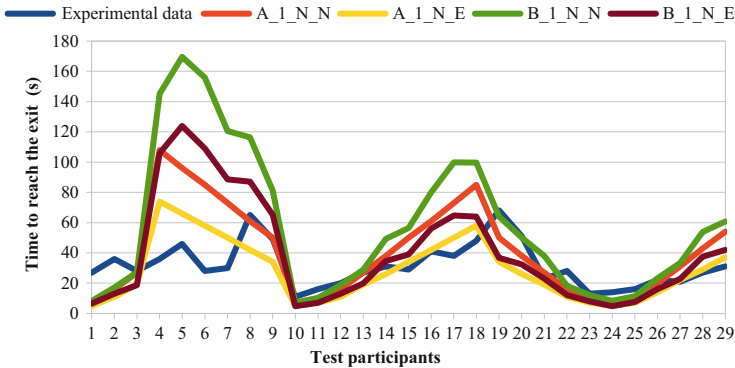


Fig. 4 Comparison between results produced employing Network A and B (area of nodes = 1) and experimental data when the speed factor function is not enabled

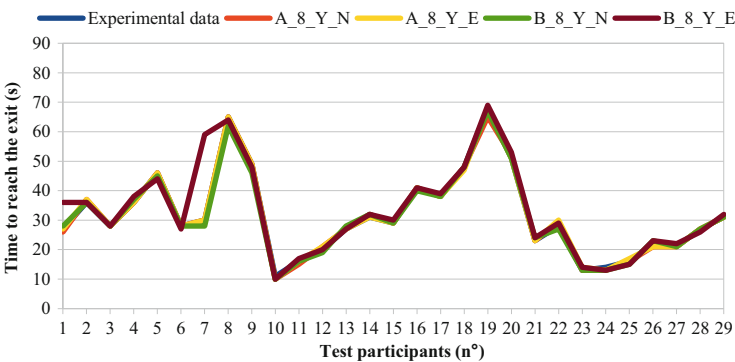


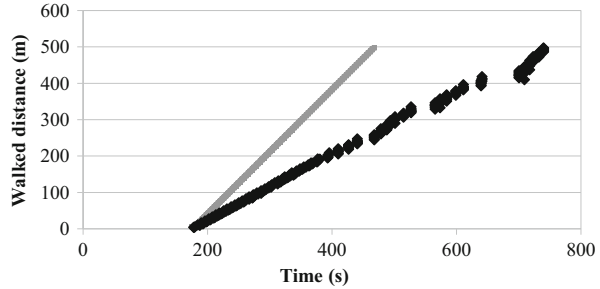
Fig. 5 Comparison between results produced employing Network A and B (area of nodes = 8) and experimental data in the case the speed factor function is enabled to match the recorded experimental speeds

has been enabled in order to give evidence of the better correspondence between the model and the experimental data-set when the walking speeds are comparable (see Fig. 5). Results are in fact reasonably similar for all the occupants. Few differences occur for Network B where more than one occupant may be in one node, thus causing some further delay in the time produced.

3 Case Study: The Condò Tunnel

The predictive capabilities of EXIT89 have been used to analyse a case study, namely the Condò tunnel in Lecce (Italy). This tunnel has been selected since it is part of a crucial network of the city of Lecce (i.e., it belongs to the city ring road and to the National Company of Road Networks in Italy). In addition, a crash involving

Fig. 6 Comparison between the results produced employing walking speed S1 using the capacity method described by Gwynne and Rosenbaum [6] (grey line) and EXIT89 (black dots)



several vehicles recently occurred (2011) calling the attention of the public opinion to its safety conditions. In this example, the tunnel has been the object of one of the analyses defined in the ANAS technical guidance [1, 15] about the safety design of road tunnels. In fact, Italian fire safety codes permit the use of evacuation models to perform this type of analysis. At the same time, the study of the evacuation process was also tested using the capacity method described in the SFPE Handbook by Gwynne and Rosenbaum [6]. This method has been already used and tested against evacuation models by the authors of the paper to reproduce road tunnel evacuations [14].

The Condò tunnel is a two-bore road tunnel with an emergency link between the two bores. The length of the bores is approximately 1 Km. The emergency link is located approximately in the middle of the tunnel.

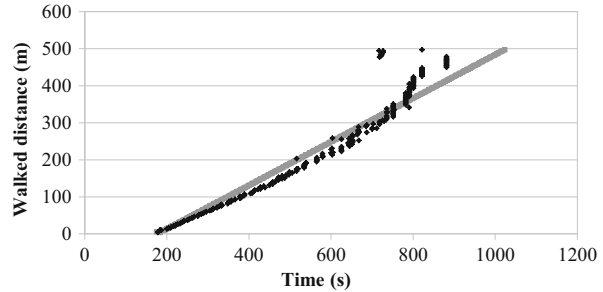
A hypothetical emergency scenario has been considered. A set of assumptions has been taken into account:

- There is a crash occurring near the tunnel link and the emergency exit linking to this tunnel is not available.
- A queue of cars is placed behind the crash. A high occupant load has been considered (5 people/cars) distributed in two rows of parallel cars. This produces a total of 900 people inside the tunnel. These assumptions have been employed to consider an extremely severe emergency situation.
- Different types of occupant speeds have been simulated in accordance with ANAS Guidelines. S1 is the speed automatically generated by the model according to the equations provided by Predtetschenski and Milinskii [12], then a speed factor is used to produce a more conservative speed, namely $S2 = 0.5$ m/s.

The capacity method has been also employed, using the same assumptions (if possible), i.e. two different walking speeds were adopted. The evacuation times produced with the two methods have been summarised in Figs. 6 and 7.

Results produced by EXIT89 are more conservative than the SFPE capacity method when speed factors are not employed (S1 walking speed) and the model is simulating the speed of the agents in accordance with the algorithm embedded in the model by default. The use of speed factors substantially reduce the difference

Fig. 7 Comparison between the results produced employing walking speed S2 using the capacity method described by Gwynne and Rosenbaum [6] (*grey line*) and EXIT89 (*black dots*)



in terms of time needed by the agent to walk down the tunnel (see Fig. 7). This is because the speed of the agents is here adjusted to fit with the desired walking speeds.

4 Discussion and Conclusion

This paper presents an example of model validation for a unique environment, i.e. road tunnels. The validation test shows how the EXIT89 model needs to be accurately calibrated in order to provide reliable results. In this context, the use of speed factors is recommended to simulate the desired walking speeds. Evidence of the methods to perform the validation and calibration of a model has been provided. The process included (1) comparison with experimental data and (2) cross comparison with another evacuation model, namely the capacity method by Gwynne and Rosenbaum [6]. The paper showed the need of performing accurate validation tests before employing a model beyond its validation evidence. The use of appropriate modelling assumptions and validation tests would permit use of the predictive capabilities of evacuation models with more confidence and increase the reliability of the results produced.

Acknowledgment The authors wish to thank Daniel Nilsson for providing the data-set of the experiments in the Göta tunnel and for his valuable help in its interpretation. The authors also thank the National Administration of Roads and Highways (ANAS) in Bari for providing technical support on the study of the Condò tunnel here under consideration.

References

1. ANAS [National administration of roads and highways]: Guidelines for the road tunnel safety design, II Edition, Direzione Centrale Progettazione (2009)
2. Curry, G.L., Deuermeyer, B.L., Feldman, R.M.: Discrete Simulation, Holden-Day, Inc., pp. 297 (1989)

3. Fahy, R.F.: Enhancement of EXIT89 and analysis of World Trade Center data, NIST-GCR-95-684, Fire Analysis and Research Division (1996)
4. Fahy, R. F.: Update on the Features and Demonstrated Predictive Capability of EXIT89. Engineered Fire Protection Design. Applying Fire Science to Fire Protection Problems, International Conference. Proceedings. Co-organized by: Society of Fire Protection Engineers (SFPE) and National Institute of Standards and Technology (NIST). June 11–15, 2001, San Francisco, CA, pp. 303–314 (2001)
5. Giere R.N.: Understanding Scientific Reasoning. Harcourt Brace Jovanovich College Publishers, New York, 322 pp (1991)
6. Gwynne S.M.V., Rosenbaum, E.: Employing the Hydraulic Model in Assessing Emergency Movement. In the SFPE Handbook of Fire Protection Engineering, 4th Edition. National Fire Protection Association, Quincy, MA, pp. 3-396–3-373 (2008)
7. International Maritime Organization: Guidelines for Evacuation Analyses for New and Existing Passenger Ships, MSC/Circ.1238, International Maritime Organization, London, UK (2007)
8. ISO/TC 92/SC 4 N622: Fire Safety Engineering – Example on verification and validation of a calculation method – Part 4: Egress model (2011)
9. Jin T.: Visibility and Human Behavior in Fire Smoke. In the SFPE Handbook of Fire Protection Engineering (fourth edition). National Fire Protection Association, Quincy MA, USA (2008)
10. Nilsson D., Johansson, M., Frantzich, H.: Evacuation experiments in a road tunnel: A study of Human Behaviour and technical installations, Fire Safety Journal 44, pp. 458–468 (2009)
11. Overton, S.: A strategy of model construction. In: C. Hall and J. Day (Editors), Ecosystem Modeling in Theory and Practice: An Introduction with Histories. John Wiley & Sons, New York. Reprinted 1990, University Press of Colorado, pp. 49–73 (1977)
12. Predtetschenski, W.M., Milinskii, A.L.: Planning for foot traffic flow in buildings, Amerind Publishing, New Dehli (1978)
13. Purser, D.A.: Application of human behaviour and toxic hazard analysis to the validation of CFD modelling for the Mont Blanc Tunnel fire incident. In Proceedings of the Advanced Research Workshop on Fire Protection and Life Safety in Buildings and Transportation Systems 2009, Santander, Spain, pp 23–57 (2009)
14. Ronchi, E., Colonna, P., Capote, J., Alvear, D., Berloco, N., Cuesta, A.: The evaluation of different evacuation models for assessing road tunnel safety analysis. Tunnelling and Underground Space Technology. DOI: 10.1016/j.tust.2012.02.008 (2012a)
15. Ronchi, E., Colonna, P., Berloco, N. Reviewing Italian Fire Safety Codes for the analysis of road tunnel evacuations: Advantages and limitations of using evacuation models. Safety Science DOI: 10.1016/j.ssci.2012.03.015 (2012b)
16. Rykiel, E.J.: Testing ecological models: the meaning of validation, Ecological modelling Vol. 90 No. 3 pp. 229–244 (1996).

Waiting Zones for Real Life Scenarios: A Case Study Using a German Railway Station as an Example

Maria Davidich, Florian Wilhelm Geiss, Hermann Mayer,
Alexander Pfaffinger, and Christian Royer

Abstract Simulations of pedestrian dynamics aim to reproduce and predict the natural behaviour of pedestrians in different situations. In most models it is assumed that pedestrians constantly walk towards their destinations. Here we investigate the legitimacy of this assumption using data, collected during a field experiment and obtained from analysis of video recordings, at a major German railway station. Our observations suggest that a substantial proportion of people stand at certain locations for some time. In order to reproduce the observed behaviour adequately, we enhance an existing cellular automata framework with a new element to model standing persons, the so called waiting zones. Through simulations, we demonstrate how standing persons influence the overall dynamics. We also analyse how the developed model can be used for analysis of critical situations.

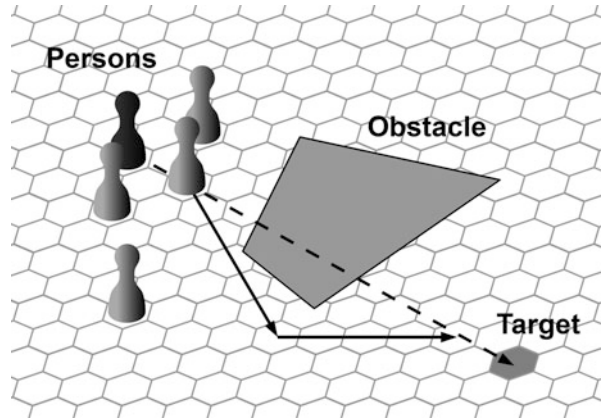
Keywords Pedestrian simulation • Cellular automata • Waiting zone

1 Introduction

The model of pedestrian stream aims to reflect the real behavior of pedestrians. The developed models cover a large number of aspects of pedestrian behavior, such as bottlenecks, forming of lanes, deceleration with increasing density and many others [1–3]. Surprisingly in most models it is assumed that pedestrians constantly move towards their destinations. However, our observations at a railway station show that a significant part of pedestrians stands and does not walk all the time, while waiting for other people, a train or for some other reason.

M. Davidich (✉) • F.W. Geiss • H. Mayer • A. Pfaffinger • C. Royer
Siemens AG, CT PRO, Virtual Design, Otto-Hahn-Ring, 6, 81739 Munich, Germany
e-mail: maria.davidich@siemens.com

Fig. 1 Schematic sketch of a cellular automaton simulating microscopic pedestrian dynamics



In this article we present our analysis of pedestrian motions at a major German railway station, which includes a field experiment and the analysis of video recordings. We propose a model that uses waiting zones and show with simulations how standing pedestrians influence the overall dynamics.

This article is organized as follows. In the first section we introduce a cellular automaton model and its improved version with the waiting zone model. Then we present the results from analysis of pedestrian motions at the railway station followed by examples of modeling a train station using waiting zones. In the conclusion part the impact of the waiting zone element is discussed.

2 Model

We choose a microscopic cellular automaton model with hexagonal grid (c.f. Fig. 1) according to [4, 5], for its high performance even for large scenarios and its reliability to model pedestrian dynamics [6–8].

In model [4, 5] each cell has a certain state: cells can be empty or occupied by a pedestrian or an obstacle. Positions of pedestrians are updated according to a set of rules, which are described in the following. The model uses a potential-based approach, in which pedestrians are treated as electrons, i.e. they are attracted by positive charges – the targets, and repelled by other negatively charged particles – obstacles and other pedestrians. The forces between pedestrians, targets and obstacles are represented by scalar functions: the potentials. Every pedestrian moves at each time step towards the cell where the potential is smallest and the cell is not already occupied. The details of the model are described in [4, 5, 8]. Apart from that, each pedestrian has his/her assigned free-flow velocity with which he or she moves in the absence of other persons. This velocity is adjusted during the simulation,

e.g. pedestrians slow down with increasing crowd density. The model is calibrated in accordance with measured values [9–11].

Here, we improve our simulation by including waiting areas into our model. The waiting area model allows simulating pedestrians, not only walking towards a target, but also the ones that keep standing.

A waiting zone is modelled as a polygonal area, and can be considered as an intermediate target for pedestrian motion. As soon as a pedestrian arrives at his/her prescribed waiting zone, some arbitrary location within this area is chosen as a next destination. The pedestrian walks to this location and stands there for a determined period of time. After this time, the pedestrian walks to the final target, for example, towards a train.

3 Observations

We validated the proposed model on a real life scenario. As an example scenario we take a large German railway station with complex infrastructure and typical topology.

The data sources, on which our investigations are based on, were threefold. We used video recordings of several cameras in various parts of the railway station, conducted a 2½ day field experiment and the Deutsche Bahn (DB) provided information on the arrival and departure rate at this station.

On the video recordings several tracks and a part of the station's main hall were visible. We analyzed several video recordings with a runtime of at least 1.5 min and about 400 recognized pedestrians on each recording. The video provided information on the density and velocities distribution as well as the relation between density and velocity. In [10] the results are presented in detail.

A two and a half day field experiment at this station served the data on pedestrian arrival and departure rates and the time span pedestrian need to walk from one point to the other. Furthermore we investigated the essential behavior patterns at this station: The mainly observed behavior is that pedestrians enter the railway station and go straight to some track and that arriving pedestrians go directly to one of the exists. We also observed that a significant part of pedestrian were standing. We examined where they tend to stay and found out that a great part of pedestrians stands waiting for a train, waiting for arriving persons or crowd near kiosks or shops. Typical waiting areas are in front of tracks, kiosks, ticket machines which are often awkward locations in the sense that by standing in these areas passing pedestrians are blocked and therefore slow down the pedestrian flow. By high densities of pedestrians the waiting pedestrians influence the overall dynamics by building bottlenecks themselves. Our observations showed that the interference of standing persons with crowd motions cannot be disregarded in realistic simulations.

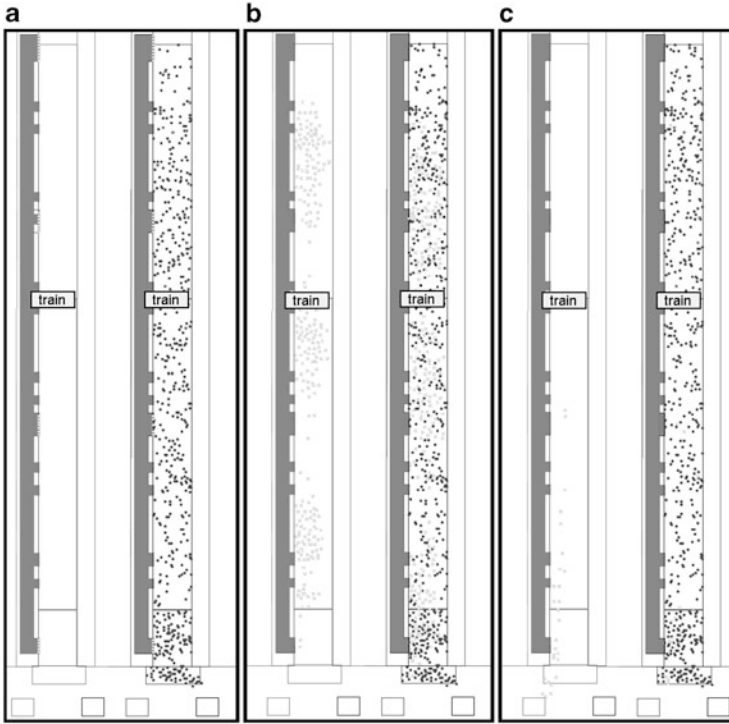


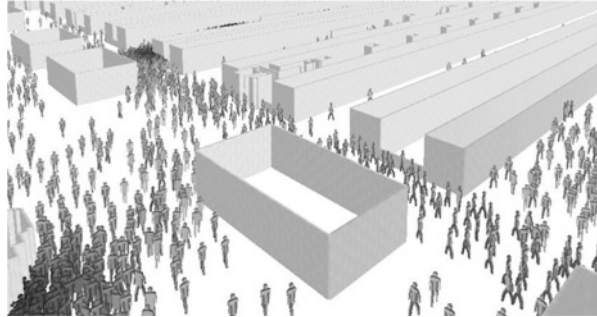
Fig. 2 A comparison of simulations with waiting persons to a simulation without waiting pedestrians. On each figure, two scenarios are show, on the *left* a scenario without waiting persons and on the *right* a scenario with 450 waiting pedestrians. The initial situation is shown in (a), (b) and (c), illustrates the simulation results 50 s and 200 after train arrival respectively. Waiting pedestrians are represented by *dark grey dots* and the arriving one by *light grey dots*. (a) 0 s. (b) 50 s. (c) 200 s

4 Results

We test the waiting zone model on a realistic scenario with high pedestrian densities. The tested scenario represents the worst imaginable situation on a Friday evening, for example, during a mass event: A crowded ICE train arrives at a track, where passengers are waiting for this train, but also for another train arriving on a neighboring track. Using the observation data the following scenario has been worked out: A crowded train arrives with 400 passengers, where 485 persons are waiting for this train, but also for another train arriving on a neighboring track (Fig. 2). We compare this scenario to a scenario in which no pedestrians are waiting at the track. The number of travelers, their velocity distribution and deceleration with increasing density, the source-target distributions, and the number of waiting passengers is in accordance to empirical observations.

Our simulations predict that the waiting persons increase the walking time, necessary to leave the track, up to 18 %, compared to the situation with no waiting

Fig. 3 An example of 3D simulation of the railway station. Pedestrian accumulate near the entrance (left bottom) and in front of tracks (top left)



persons. In particular, the time required for 95 % of the arriving persons to leave the track takes 349 s, in average, but without waiting persons only 297 s in average. This is due to the fact that the average velocity of arriving pedestrians decreases if persons block their way and the paths deviate from the ones without waiting pedestrians.

The results of the simulation reproduce the observations and give evidence to the importance of considering waiting persons in scenarios with high density.

The described scenario is illustrated in Fig. 2, whereas 450 persons are standing at the track and 300 persons arrive by train. The influence of waiting pedestrians on the time span, arriving pedestrians need to leave the track, is shown in (Fig. 2).

As a second step we run several scenarios for the entire railway station. The input parameters were based on collected data (field experiments, video data and information from DB) with different numbers of arriving and waiting persons, which correspond to different weekdays. Our simulations suggest that critical situations are more likely to appear if pedestrians accumulated in front of tracks or next to different “attracting locations”, such as kiosks, ticket machines, etc., which are placed next to the entrance of a track (Fig. 3). (For security reasons we cannot demonstrate the results in detail). Simulation of the entire railway station reveal the possible bottlenecks and “weak” places of topology, where eventually pedestrian jams tend to appear due to an awkward placement of points of interest such as kiosks, coffee shops, bistros, etc.

Finally, different operation scenarios in case of high density waiting zones have been tested. For example, what will happen if a platform is crowded with waiting persons and a crowded train arrives? When will it lead to a large pedestrian jam and in which case is it better to change the track number of a coming train? The waiting zone model allows playing through a number of virtual scenarios and support the decision making process.

5 Conclusions

During our experiments we found that waiting is an essential aspect in predicting behavior of pedestrians – just like walking and running. Since research in the field of pedestrian dynamics is predominantly focused on emergency evacuation (which

of course does not include waiting), only little data is available on that specific topic [9, 12–19].

However, during a large-scale research project we had a chance to get real-life data on pedestrian motions at the railway station. The data was evaluated and revealed the importance of including waiting pedestrians in the models of crowd dynamics. Therefore, using the framework of a cellular automata model [4, 5], we developed a new simulation element – the waiting zone.

We performed tests of the element itself and simulated several real-life scenarios using waiting zones. In particular, we studied the impact of waiting pedestrians on overall crowd dynamics and observed that strongly crowded platforms may extend the time that arriving pedestrians need to leave the platform by up to 18 %. Furthermore, we demonstrated that awkwardly located kiosks or ticket machines next to highly frequented areas may cause accumulations and critical situations.

Finally, we have shown how the model can be used as a decision supporting tool for design of public transport stations and time tables as well as to predict scenarios where the overall situation may become dangerous due to waiting persons in awkward locations. Particularly, we have shown for critical infrastructures such as railway stations, that waiting zones play a significant role and cannot be omitted in a realistic reproduction of critical scenarios.

Acknowledgments This work is supported by Ministry for Education and Science (BMBF), SinoVE Project.

References

1. Helbing, D., Molnár, P., Farkas, I.J., Bolay, K.: Self-organizing pedestrian movement. *Environment and Planning B: Planning and Design* 28, pp. 361–383 (2001)
2. Helbing, D., Johansson, A., Al-Abideen, H.: The Dynamics of crowd disasters: an empirical study. *Physical Review E* 75, 046109 (2007)
3. Hoogendoorn S., Daamen, W.: Self-Organization in Pedestrian Flow. *Traffic and Granular Flow* 3(4), 373–382 (2005)
4. Köster, G., Hartmann, D. and Klein, W.: Microscopic pedestrian simulations: From passenger exchange times to regional evacuation. *Proceedings of the International Conference of Operations Research* (2010)
5. Klein W., Koester G. and Meister A.: *Towards the Calibration of Pedestrian Stream Models*, Lecture Notes in Computer Science: PPAM 2009. Springer Verlag, 2010.
6. Nagel K. and Schreckenberg M.: A Cellular Automaton Model for Free-way traffic. *J. Phys. I France*, 2, 2221–22229 (1992)
7. Burstedde C., Klauck K., Schadschneider A and Tittartz J.; Simulation of Pedestrian Dynamics Using a 2-dimensional Cellular Automaton. *Physica A*, 295 (4), 507–525 (2001)
8. Kinkeldey C.: *Fussgängersimulation auf der Basis zellularer Automaten: Studienarbeit im Fach Bauinformatik* (2003)
9. Kneidl A., Bormann A: How Do Pedestrians find their Way - Results of an experimental study with students compared to simulation results. In: *Emergency Evacuation of People from Buildings Proceedings* (2011)

10. Davidich, M.I., Köster, G.: “Verification of Pedestrian Stream Models Based on Video Analysis”, talk at 6th International Conference on Pedestrian and Evacuation Dynamics, Zurich, Switzerland, 2012. Peer-reviewed paper accepted in conference proceedings (2012)
11. M. Davidich, G. Köster: Towards Automatic and Robust Adjustment of Human Behavioral Parameters in a Pedestrian Stream Model to Measured Data, *Safety Science* 50, pp. 1253–1260 (2012)
12. Schadschneider A., Klingsch W., Kluepfel H, Kretz T, Rogsch C. and Seyfried A: Evacuation Dynamics: Empirical results, Modeling and Applications. *Encyclopedia of Complexity and System Science*, Robert A. Meyers (Ed.), Springer, 2009, ISBN 978-0-387-75888-6, Vol. 3 pp. 3142 (2009)
13. Hamacher H.W. and Tjandra S.A.: *Mathematical Modelling of Evacuation Problem: A State of the Art*. Springer Verlag (2002)
14. Proulx, G.: Occupant Response During a Residential High-Rise Fire, *Fire and Materials*, **23**, 317–323 (1999)
15. Fruin, J. J.: *Pedestrian Planning and Design*. (Revised Edition), Elevator World, Inc., Mobile, AL (1987)
16. *Handbook of Fire Protection Engineering* (Second ed., pp. 3-263–3-285). Society of Fire Protection Engineers, Bethesda, MD (1995)
17. Nelson, H. E. and Mowrer, F. W.: Emergency Movement. In: P.J.Denno & W. D. Walton (Eds.), *The SFPE Handbook of Fire Protection Engineering* (Third ed., pp. 3-367–3-380). Society of Fire Protection Engineers, Bethesda, MD (2002)
18. Proulx, G.: Movement of People: The Evacuation Timing. In: P.J.DiNenno & W. D. Walton (Eds.), *The SFPE Handbook of Fire Protection Engineering* (Third ed., pp. 3-341–3-366). Society of Fire Protection Engineers, Bethesda, MD (2002)
19. Kuligowski, E. D. and Peacock, R. D., Review of Building Evacuation Models, Technical Note 1471, Natl. Inst. Stand. Technol., Gaithersburg, MD (2005)

Part III
Simulation and Modeling

A Data-Driven Model of Pedestrian Following and Emergent Crowd Behavior

Kevin Rio and William H. Warren

Abstract Pedestrian following is a common behavior, and may provide a key link between individual locomotion and crowd dynamics. Here, we present a model for following that is motivated by cognitive science and grounded in empirical data. In Experiment 1, we collected data from leader-follower pairs, and showed that a simple speed-matching model is sufficient to account for behavior. In Experiment 2, we manipulated the visual information of a virtual leader, and found that followers respond primarily to changes in visual angle.

Finally, in Experiment 3, we use the speed-matching model to simulate speed coordination in small crowds of four pedestrians. The model performs as well in these small crowds as it did in the leader-follower pairs. This cognitively-inspired, empirically-grounded model can serve as a component in a larger model of crowd dynamics.

Keywords Cognitive science • Data • Dynamics • Experiment • Following

1 Introduction

Crowds are complex systems, made up of individual pedestrians who interact with one another and their environment to exhibit emergent collective behavior [1]. One of the most successful methods for studying crowd behavior is simulation with individual-based models of locomotion [2], such as the social force model [3, 4]. By specifying the local behavior of pedestrians, and the interactions between them, large-scale patterns emerge at the level of the crowd, such as lane formation [3, 5], jamming [6], stop-and-go waves [3, 7], and turbulence [8].

K. Rio (✉) • W.H. Warren
Department of Cognitive, Linguistic, and Psychological Sciences, Brown University,
Providence, RI, USA
e-mail: kevin_rio@brown.edu

Existing crowd models stand to benefit from two underutilized sources of information. First, they should take into account findings from cognitive science, which yields results about the human capabilities for perception, action, and cognition that can be used to inspire new models [9, 10], and generate constraints which limit the space of possible models. Second, models should be tested with experimental and observational data. This has been recognized since the earliest work on crowd locomotion [12], but despite recent efforts [13–17], such empirical validation remains uncommon.

To address these concerns, we have adopted a modeling program motivated by cognitive science and grounded in experimental data. We utilize the behavioral dynamics framework [18], which integrates an information-based approach to perception [19] with a dynamical systems approach to action [20, 21]. A full understanding of behavior in this framework consists in specifying how information about the environment is picked up by the agent and used to control action (a *control law*), and a low-dimensional description of the global behavior that arises as a result (a *behavioral strategy*). We use experimental data on human locomotion to test hypotheses about these processes, and to generate models of pedestrian behavior [22, 23].

This paper applies our approach to the case of pedestrian following. Following is a common behavior, and may provide a key link between individual locomotion and crowd dynamics [24]. Successful followers must control their speed to stay behind the leader, and control their heading to stay on course with the leader. Here we focus on speed control. Our goal is to model the behavioral strategy and visual control law governing following in dyads, and then use this model to simulate the emergent behavior of small crowds.

In Experiment 1, we test candidate behavioral strategies against data collected from leader-follower pairs. In Experiment 2, we test candidate sources of visual information against data collected from pedestrians following a leader in virtual reality. In Experiment 3, we extend the model to simulate speed coordination in small crowds.

2 Experiment 1: Behavioral Dynamics of Following

2.1 Background

The goal of Experiment 1 was to determine the behavioral strategies used to control pedestrian following. There are a number of candidate strategies, many of which have been studied in the context of car following [25].

Distance One strategy is for the follower to maintain a preferred distance from the leader. The follower’s acceleration \ddot{x}_f at each time step is given by:

$$\ddot{x}_f = c \cdot [\Delta x - \Delta x_0] \quad (1)$$

where Δx is the current distance between the leader and follower, Δx_0 is the preferred distance, and c is a free parameter. Δx_0 might be chosen in various ways. It could be a constant, such as the initial distance between leader and follower, or it could vary with velocity [26, 27]. In the latter case, the preferred distance is equal to:

$$\ddot{x}_f = c \cdot [\Delta x - \alpha - \beta \dot{x}_f] \quad (2)$$

where \dot{x}_f is the follower's speed and α , β , and c are free parameters.

Speed Another strategy is for the follower to match the speed of the leader. Follower acceleration is given by:

$$\ddot{x}_f = c \cdot [\dot{x}_l - \dot{x}_f] \quad (3)$$

where \dot{x}_l is the leader's speed and c is a free parameter. An equivalent expression can be written in terms of the relative speed $\Delta \dot{x}$, which is the difference in speed between the leader and follower:

$$\ddot{x}_f = c \cdot [\Delta \dot{x}] \quad (4)$$

One advantage of this strategy is that it does not require a preferred value for distance, like the previous model does. This is an advantage both for the follower (who does not need to store a fixed distance in memory) and for the model (which does not require an additional parameter).

Ratio The GHR model [28] is “perhaps the most well-known model” of car-following [25]. We use a simplified version, which incorporates a ratio of speed and distance, where follower acceleration is given by:

$$\ddot{x}_f(t) = c \cdot \dot{x}_f^M \cdot \frac{\Delta \dot{x}}{\Delta x^L} \quad (5)$$

and c , M , and L are free parameters.

Linear A linear combination of the speed and distance models was proposed in the context of car-following [29]. Again we use a simplified version, which we call the linear model, where follower acceleration is given by:

$$\ddot{x}_f(t) = c_1 [\Delta \dot{x}] + c_2 [\Delta x - \alpha - \beta \dot{x}_f] \quad (6)$$

where c_1 , c_2 , α , and β are free parameters.

Thus there are several hypotheses for the behavioral strategy used to control speed during following. The follower could (1) maintain a particular distance, (2) match the speed of the leader, or (3) combine speed and distance information. Experiment 1 was designed to test these strategies against empirical data collected from real leader-follower pairs.

2.2 Methods

Participants 10 students (4 male, 6 female), participated in Experiment 1.

Apparatus Experiment 1 was conducted in the Virtual Environment Navigation Laboratory (VENLab) at Brown University. Participants walked in a 12×12 m area, and wore bicycle helmets to which tracking units were affixed. Head position and orientation were recorded at a sampling rate of 60 Hz by a hybrid inertial-ultrasonic tracking system.

Procedure A confederate acted as the ‘leader,’ and the participant as the ‘follower.’ The initial separation was 1 or 3 m. When each trial began, the leader began walking at a comfortable speed in a straight line. After 2, 3, or 5 steps, the leader would speed up, slow down, or remain at the same speed for 3 steps. Finally, the leader would return to his comfortable speed.

Design Experiment 1 had a 2 (initial separation) $\times 3$ (speed up, slow down, or constant speed) $\times 3$ (number of steps) factorial design, with 3 trials per condition, for a total of 54 trials per participant. All variables were within-subject, and trials were presented in a random order.

Data Analysis The time-series of leader and follower head position were filtered, using a forward and backward 4th-order low-pass Butterworth filter with a cutoff frequency of 0.6 Hz, to reduce the effects of side-to-side gait oscillations. The filtered position data were differentiated, to produce time-series of leader and follower speed and acceleration.

2.3 Results and Discussion

For each trial, five models were used to simulate follower acceleration in response to the human leader. Root-mean-squared error (RMSE) was used as a measure of goodness of fit for each model and was used to calculate best fit parameters. Pearson’s r was used as a second measure of goodness of fit. An optimization algorithm (BFGS Quasi-Newton method [30]) was used to find the set of parameter values that minimized mean RMSE for each model.

Figure 1 shows a plot of the acceleration predicted by each of the five models for a single trial, generated using the best fit parameters.

Table 1 lists mean RMSE and r values for each model.

A one-way ANOVA showed significant differences in RMSE between the models, $F(4,45) = 365.03$, $p < .001$. Post hoc tests using the Bonferroni correction revealed significant differences between all pairwise combinations of models, $p < .01$, except between the speed ($M = 0.26$, $SD = 0.033$) and linear ($M = 0.25$, $SD = 0.029$) models, which were not significantly different, $p > .05$.

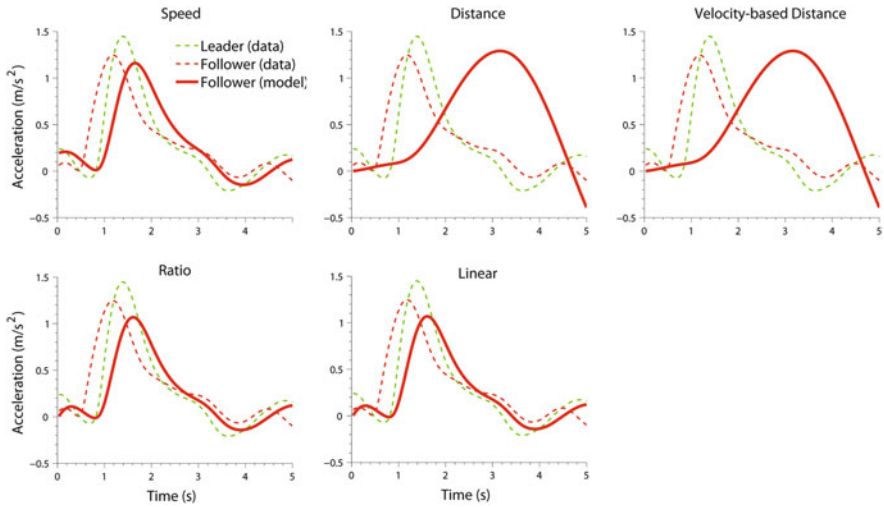


Fig. 1 Time-series of acceleration for a single trial

Table 1 Number of parameters, mean RMSE, and mean r values for five models

Model	# Parameters	Mean RMSE	Mean r
Speed	1	0.26	0.84
Distance	1	0.74	-0.05
Velocity-based distance	2	0.43	0.25
Ratio	3	0.32	0.20
Linear	4	0.25	0.85

These results indicate that the speed model performs as well as the more complicated linear model, and significantly better than the distance, velocity-based distance, and ratio models. A model based on speed provides a better fit to the data than a model based on distance, and adding distance information in the ratio and linear models does not improve performance. Taken together, the results of Experiment 1 support the hypothesis that pedestrian followers rely on a simple strategy of matching the leader’s speed.

Several factors constrained followers’ behavior in Experiment 1, which could limit the generalizability of our model. First, trials were fairly short, lasting only about 8 s. It is possible that followers adopt a different behavioral strategy when following for longer durations. Second, followers started fairly close to the leader; at longer initial separations, distance information may play a role in addition to or instead of speed information. Despite these constraints, our model is useful because it performs well in the situation that is most relevant to everyday locomotion, following behind a nearby leader, and is robust to changes in initial separation.

3 Experiment 2: Visual Information for Following

3.1 Background

The behavioral strategies described in Experiment 1 are defined in terms of real-world variables, like speed and distance. But observers do not have direct access to these real-world variables; instead, they must rely on information in the optic array. The goal of Experiment 2 was to determine which source(s) of information followers use to control behavior. There are a number of candidate sources; following previous work [31–34], we focus on two of these sources: binocular disparity and visual angle.

Visual Angle The visual angle of the leader has been used to model car-following [35]. The leader's visual angle, α , is a function of the distance between leader and follower, Δx , and the leader's diameter, d . Assuming the leader's height is constant, visual angle depends only on the distance between leader and follower, so maintaining a constant distance behind the leader (a behavioral strategy) is consistent with keeping the leader at a constant visual angle. The change in visual angle, $\dot{\alpha}$, is a function of the relative speed (and distance) between the leader and follower, so a constant relative speed can be achieved by nulling changes in the leader's visual angle.

Binocular Disparity These strategies can also be implemented using binocular disparity. Binocular disparity refers to the difference in retinal images that result from the eyes' horizontal separation; it is a function of an object's distance from an observer. Followers can maintain a constant distance by keeping the relative disparity between the leader and the background constant, and maintain a constant relative speed by nulling changes in disparity.

When the leader speeds up relative to the follower, its binocular disparity increases and its visual angle decreases. Typically, these variables are coupled, but in virtual reality, they can be dissociated [35]. Disparity and visual angle can be manipulated independently by expanding or shrinking the leader as it moves relative to the follower. If followers rely on only one variable, they should speed up when it specifies an increase in leader speed (or vice versa), but not be affected by changes in the other. Conversely, if they rely on both variables, behavior will be sensitive to changes in either one.

Thus there are several hypotheses for the optical information that could be used to control real-world variables like relative speed. The follower could (1) use visual angle, (2) use binocular disparity, or (3) use some combination of the two. Experiment 2 was designed to test these hypotheses against experimental data collected from real pedestrians following a virtual leader.

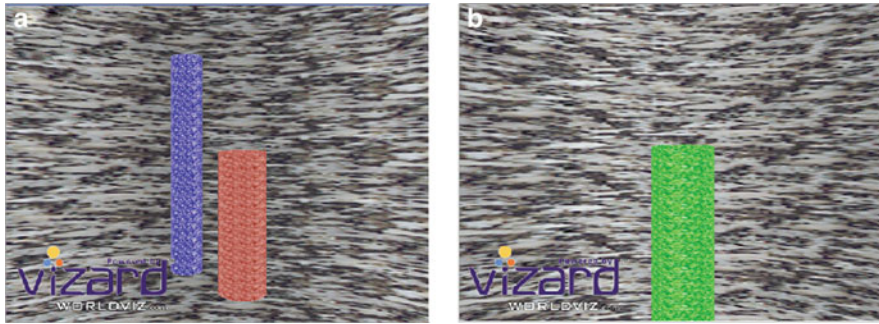


Fig. 2 First-person view of the virtual display used in Experiment 2. **(a)** The blue ‘home’ pole; participants walk into it and face the red ‘target’ pole. **(b)** The ‘target’ pole during following; the pole turns green and begins moving after a button press by the participant

3.2 Methods

Participants 12 students (6 male, 6 female), participated in Experiment 2.

Apparatus Experiment 2 was conducted in the VENLab. Participants walked in a 12×12 m area while viewing a virtual environment through a head-mounted display (HMD), which provided stereoscopic viewing with a 68° horizontal \times 53° vertical field of view with a resolution of $1,280 \times 1,240$ pixels. Displays were generated at a frame rate of 60 fps using the Vizard software package. Head position and orientation were tracked as in Experiment 1, and used to update the display with a latency of approximately 50 ms (three frames).

Displays The virtual environment was sparse, consisting of a vertical cylindrical surface (radius 20 m) mapped with a grayscale granite texture and no ground plane. A blue home pole (radius 0.2 m, height 3.0 m) with a granite texture appeared at the center of the environment, and a green/red target pole (radius 0.3 m, height 1.7 m) appeared 1 m away. Figure 2 shows a first-person view of the virtual environment.

Procedure Before each trial, participants stood at the home pole and faced the target pole. To begin a trial, participants pushed a handheld button, which caused the target pole to turn green. After 1 s, the target pole began moving through the environment horizontally in depth. For the first 0.5 s of the trial, the pole’s velocity increased linearly from 0 to 0.8 m/s. Its speed then remained constant for a variable amount of time ($M = 2.5$ s, $SD = 1$ s) until a “manipulation” lasting 3 s changed the visual angle and/or the binocular disparity of the target pole. Participants were instructed to follow the pole; no further instructions were given regarding speed or distance.

Binocular disparity was manipulated by having the pole speed up (to 1.2 m/s) or slow down (to 0.4 m/s), or by having it remain the same speed. Visual angle was manipulated by having the pole expand or shrink such that its visual angle

Table 2 List of conditions for Experiment 2

		Visual angle-specified speed (m/s)		
		0.4	0.8	1.2
Disparity-specified speed (m/s)	0.4	Speed up	Disparity manipulation	Conflict
	0.8	Visual angle manipulation	Constant speed	Visual angle manipulation
	1.2	Conflict	Disparity manipulation	Slow down

was consistent with a pole of the original dimensions (radius 0.6 m, height 1.6 m) moving at 0.4, 0.8, or 1.2 m/s. There were three possible manipulations for each cue, which were fully crossed, for a total of nine manipulations. These conditions are shown in Table 2.

Design Experiment 2 had a 3 (disparity) \times 3 (visual angle) factorial design, with 8 trials per condition, for a total of 72 trials per participant. All variables were within-subject, and trials were presented in a random order.

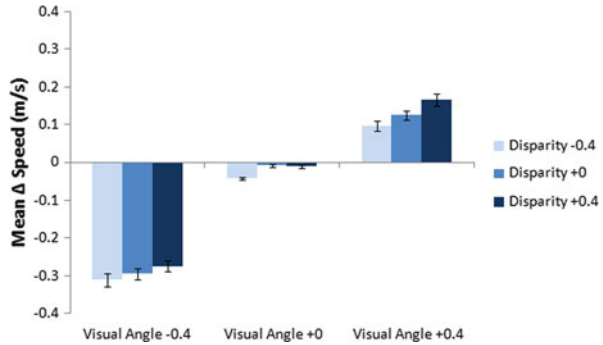
Data Analysis Data was filtered and differentiated as in Experiment 1. For each trial, the mean change in the follower's speed (Δ Speed, or Δ S) during the visual manipulation was computed by subtracting the participant's mean speed in the 2 s interval from 1 s after the onset of the visual manipulation until its offset from their mean speed in the 2 s interval prior to the manipulation. A positive value specifies that the participant sped up during the manipulation. The mean of these Δ S values, averaged across participants, was used as a measure of behavioral response to each manipulation.

3.3 Results and Discussion

The mean Δ Speed values are shown in Fig. 3. In the visual angle manipulation, participants speed up (Δ S = 0.13 m/s) relative to baseline (Δ S = -0.01 m/s) when visual angle-specified speed increases, and slow down (Δ S = -0.29 m/s) when visual angle-specified speed decreases. This is not the case for the binocular disparity manipulations, however. There is no significant difference in speed when disparity-specified speed increases (Δ S = -0.04 m/s) or decreases (Δ S = -0.09 m/s) relative to baseline.

This same pattern of results is observed, regardless of whether a single cue was manipulated, both cues were congruent, or the cues were in conflict. When visual angle decreases, for example, mean changes in speed do not differ when disparity increases (Δ S = 0.10 m/s), remains constant (Δ S = 0.12 m/s), or decreases (Δ S = 0.17 m/s). A two-way ANOVA showed a significant main effect of

Fig. 3 Mean Δ Speed values for the nine visual manipulation conditions, across trials and participants. Positive values represent an increase in walking speed as a result of the manipulation; negative values represent a decrease. Error bars represent standard error of the mean



visual angle, $F(2,81) = 99.55, p < .001$, no main effect of disparity, $F(2,81) = 1.14, p > .05$, and no interaction, $F(4,81) = .12, p > .05$.

These results suggest that visual angle is the primary source of optical information used to regulate human following. The follower’s speed changed significantly only when visual angle was manipulated. Changes in disparity did not result in changes in speed. Even in the conflict condition, the behavioral response was always in the same direction as visual angle, and it was the same magnitude as when disparity was congruent or unchanged. This indicates that these two cues are not combined.

It is important to note that only a limited range of values were tested. We examined visual angle and disparity manipulations which corresponded to speed changes of +0.4 m/s and lasted 3 s. This created a rather large conflict between the two sources of information, such that the visual system may have ‘vetoed’ [37] the weaker disparity information rather than integrating it with visual angle. However, the tested values are realistic for the case of pedestrian following, so the results indicate that following is primarily controlled by changes in visual angle.

4 Experiment 3: Following in Small Crowds

4.1 Background

So far, we have provided evidence that pedestrian followers match leader speed (Experiment 1) by nulling changes in visual angle (Experiment 2). In Experiment 3, our goal is to use this model to predict the acceleration of pedestrians in small crowds. Specifically, we ask whether pedestrians follow neighbors in a crowd as they do in dyads.

Small crowds represent a vital link between studies of individual locomotion and larger crowds of hundreds or thousands of pedestrians, and have been the subject of observational [38] and experimental [16, 39–41] investigations. Studying small

crowds permits experimental control, which can be difficult in large crowds (see [40]), and allows for a richer set of interactions between pedestrians than studies of individuals or dyads.

We collected data from small crowds of four pedestrians walking toward a common goal. In a preliminary analysis [42], we found evidence for collective behavior, such as the adoption of a common speed and the appearance of a preferred density. Here, we extend this analysis by applying the speed-matching model derived from Experiments 1 and 2.

4.2 *Methods*

Participants 20 students (8 male, 12 female) participated in Experiment 3.

Apparatus Experiment 3 used the same apparatus as Experiment 1.

Procedure An overhead view of the experimental geometry is shown in Fig. 4. Before each trial, participants were assigned to individual starting positions, at the corners of a square, with lengths of 0.5, 1.0, 1.5, or 2.5 m on a side. This resulted in four initial densities. Participants were instructed to walk toward one of three goal posts (radius 0.15 m, height 2, 2 m apart).

To begin each trial, an experimenter verbally instructed the participants to begin walking forward (“Start!”). When the last participant traveled 1 m from the starting positions, an experimenter verbally instructed the participants toward one of the three goals (e.g. “Three!”). Participants walked toward the goal and touched it with their hand. An experimenter signaled that the trial was over (“Stop!”), and starting positions were assigned for the next trial.

Design Experiment 3 had a 4 (density) \times 3 (goal position) factorial design, with 8 trials per condition, for a total of 96 trials per group (480 total). All variables were within-group, and trials were presented in a random order.

Data Analysis Data was filtered and differentiated as in Experiment 1.

4.3 *Results and Discussion*

The present analysis focuses on the goal 2 condition, in which the goal was located directly ahead of the starting positions. Thus, the primary mode of coordination between participants was in speed, rather than heading. Participants can be divided into six pairs, which represent front-back, side-side, and diagonal couplings. Correlations between the time-series of speed for all six pairs are high ($M = 0.77$, $SD = 0.23$), providing evidence for coordination.

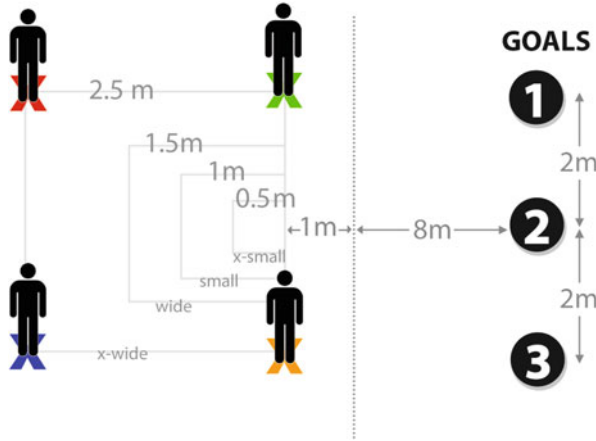


Fig. 4 Overhead view of Experiment 3 geometry (not to scale)

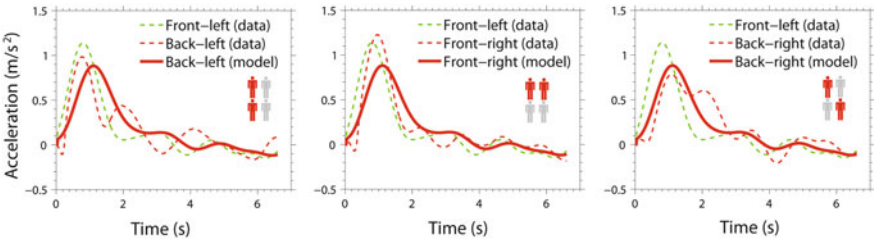


Fig. 5 Time-series of acceleration (data and model predictions) for a single trial

The speed-matching model derived from Experiments 1 and 2 was used to predict the acceleration of one participant as a function of another’s speed. Front-back and diagonal couplings are assumed to be unidirectional, so the participant in front always served as the ‘leader’ in the model. Side-side couplings are bidirectional, so two simulations were performed and then averaged, with each participant serving as ‘leader’ and ‘follower,’ respectively. The speed-matching model performs as well on the front-back pairs (RMSE = 0.19 m/s², $r = 0.78$) as on the following data from Experiment 1 (RMSE = 0.26 m/s², $r = 0.84$) using fixed parameters. This shows that our model generalizes to speed coordination in small crowds. Figure 5 shows a plot of observed and predicted follower acceleration for 3 pairs of pedestrians.

Some caution is warranted in interpreting these findings. First, Experiment 3 included an acceleration at the beginning, rather than a speed change in the middle of the trial, as in Experiment 1. This may have reduced variability in speed, leading to improved model performance. Second, the common Go signal may have produced spurious correlations. Despite these limitations, the model presented here represents an important first step in linking individual locomotion with coordinated locomotion in small crowds.

5 Conclusion

Empirical validation is necessary for the development of realistic models of human crowds. Here, we have presented a data-driven model of speed control in pedestrian following, derived from experimental results on the behavioral strategy (Experiment 1) and visual information (Experiment 2) in leader-follower pairs. We then showed that this model generalizes to more complex scenarios involving small crowds (Experiment 3) with fixed parameters. Pedestrians appear to follow neighbors in crowds just as they do in dyads.

This model exemplifies our bottom-up approach to understanding crowd dynamics as an emergent phenomenon. By deriving empirical models of local pedestrian interactions, we seek to account for crowd behavior while producing realistic individual trajectories. The speed-matching component generates a form of spatiotemporal coordination that many models [2] have taken to be a primary behavior, along with attraction and repulsion. Our group has developed similar data-driven components for steering and obstacle avoidance based on human experiments [22, 23]. Taken together, they are building toward a model of crowd dynamics in which each individual component has been derived from data, rather than postulated ad hoc [43].

References

1. Goldstone, R.L., Gureckis, T.M.: Collective Behavior. *Top. Cogn. Sci.* 1(3), 412–438 (2009)
2. Reynolds, C.W.: Flocks, Herds, and Schools: A Distributed Behavioral Model. *Comp. Graph.* 21(4), 25–34 (1987)
3. Helbing, D., Molnár, P.: Social Force Model for Pedestrian Dynamics. *Phys. Rev. E.* 51(5), 4282–4286 (1995)
4. Helbing, D., Farkas, I., Vicsek, T.: Simulating Dynamical Features of Escape Panic. *Nature* 407(6803), 487–490 (2000)
5. Piccoli, B., Tosin, A.: Pedestrian Flows in Bounded Domains with Obstacles. *Continuum Mech. Therm.* 21(2), 85–107 (2009)
6. Muramatsu, M., Irie, T., Nagatani, T.: Jamming Transition in Pedestrian Counter Flow. *Physica A*, 267(3–4), 487–498 (1999)
7. Portz, A., Seyfried, A.: Modeling Stop-and-Go Waves in Pedestrian Dynamics. In: Wryzkowski, R., Dongarra, J., Karczewski, K., Wasniewski, J. (eds.) LNCS, vol. 6068, pp. 561–568. Springer, Heidelberg (2010)
8. Yu, W., Johansson, A.: Modeling Crowd Turbulence by Many-Particle Simulations. *Phys. Rev. E* 76(4), 046105 (2007)
9. Ondřej, J., Pettré, J., Olivier, A.-H., Donikian, S.: A Synthetic-Vision Based Steering Approach for Crowd Simulation. *ACM T. Graphic.* 29(4), 123 (2010)
10. Moussaïd, M., Helbing, D., Theraulaz, G.: How Simple Rules Determine Pedestrian Behavior and Crowd Disasters. *Proc. Natl. Acad. Sci. USA* 108(17), 6884–6888 (2011)
11. Lakoba, T.I., Kaup, D.J., Finkelstein, N.M.: Modifications of the Helbing-Molnár-Farkas-Vicsek Social Force Model for Pedestrian Evolution. *Simulation* 81(5), 339–352 (2005)
12. Henderson, L.F.: The Statistics of Crowd Fluids. *Nature* 229, 381–383 (1971)

13. Kretz, T., Grünebohm, A., Schreckenberg, M.: Experimental Study of Pedestrian Flow through a Bottleneck. *J. Stat. Mech.* P10014 (2006)
14. Moussaïd, M., Helbing, D., Garnier, S., Johansson, A., Combe, M., Theraulaz, G.: Experimental Study of the Behavioral Mechanisms Underlying Self-Organization in Human Crowds. *P. Roy. Soc. B.* 276(1688), 2755–2762 (2009)
15. Robin, T., Antonini, G., Bierlaire, M., Cruz, J.: Specification, Estimation, and Validation of a Pedestrian Walking Behavior Model. *Transport. Res. B.* 43(1), 36–56 (2009)
16. Moussaïd, M., Perozo, N., Garnier, S., Helbing, D., Theraulaz, G.: The Walking Behaviour of Pedestrian Social Groups and Its Impact on Crowd Dynamics. *PLoS One* 5(4), e10047 (2010)
17. Schadschneider, A., Seyfried, A.: Empirical Results for Pedestrian Dynamics and Their Implications for Modeling. *Netw. Heterog. Media* 6(3), 545–560 (2011)
18. Warren, W.H.: The Dynamics of Perception and Action. *Psychol. Rev.* 113(2), 358–389 (2006)
19. Gibson, J.J.: *The Ecological Approach to Visual Perception*. Psychology Press, New York (1979)
20. Kugler, P., Turvey, M.: *Information, Natural Law, and the Self-Assembly of Rhythmic Movement: Resources for Ecological Psychology*. Erlbaum, Hillsdale (1987)
21. Kelso, S.: *Dynamic Patterns: The Self-Organization of Brain and Behavior (Complex Adaptive Systems)*. The MIT Press, Cambridge (1995)
22. Fajen, B.R., Warren, W.H.: Behavioral Dynamics of Steering, Obstacle Avoidance, and Route Selection. *J. Exp. Psychol. Human* 29(2), 343–362 (2003)
23. Fajen, B.R., Warren, W.H.: Behavioral Dynamics of Intercepting a Moving Target. *Exp. Brain Res.* 180(2), 303–319 (2007)
24. Li, T.-Y., Jeng, Y.-J., Chang, S.-I.: Simulating Virtual Human Crowds with a Leader-Follower Model. In: *Proceedings of the Fourteenth Conference on Computer Animation*, pp. 93–102 (2001)
25. Brackstone, M., McDonald, M.: Car-Following: A Historical Review. *Transport. Res. F.* 2(4), 181–196 (1999)
26. Pipes, L.A.: An Operational Analysis of Traffic Dynamics. *J. Appl. Phys.* 24(3), 274 (1953)
27. Herman, R., Montroll, E.W., Potts, R.B., Rothery, R.W.: Traffic Dynamics: Analysis of Stability in Car-Following. *Oper. Res.* 7(1), 86–106 (1959)
28. Gazis, D.C., Herman, R., Rothery, R.W.: Nonlinear Follow-The-Leader Models of Traffic Flow. *Oper. Res.* 9(4), 545–567 (1961)
29. Helly, W.: Simulation of Bottlenecks in Single Lane Traffic Flow. In: *Proceedings of the Symposium on Theory of Traffic Flow*, pp. 207–238. Elsevier, New York (1959)
30. Fletcher, R.: *Practical Methods of Optimization*. Wiley, Hoboken (2000)
31. Regan, D., Beverley, K.I.: Binocular and Monocular Stimuli for Motion in Depth: Changing-Disparity and Changing-Size Feed the Same Motion in Depth Stage. *Vision Res.* 19, 1331–1342 (1979)
32. Heuer, H.: Estimates of Time-to-Contact Based on Changing Size and Changing Target Vergence. *Perception* 22(5), 549–563 (1993)
33. Gray, R., Regan, D.: Accuracy of Estimating Time To Collision Using Binocular and Monocular Information. *Vision Res.* 38, 499–512 (1997)
34. Rushton, S.K., Wann, J.P.: Weighted Combination of Size and Disparity: A Computational Model for Timing a Ball Catch. *Nat. Neurosci.* 2(2), 186–190 (1999)
35. Anderson, G.J., Sauer, C.W.: Optical Information for Car Following: The Driving by Visual Angle (DVA) Model. *Hum. Factors* 49(5), 878–896.
36. Tarr, M.J., Warren, W.H.: Virtual Reality in Behavioral Neuroscience and Beyond. *Nat. Neurosci.* 5, 1089–1092 (2002)
37. Bühlhoff, H.H., Mallot, H.A.: Integration of Depth Modules: Stereo and Shading. *J. Opt. Soc. Am. A* 5(10), 1749–1758 (1988)
38. Costa, M.: Interpersonal Distances in Group Walking. *J. Nonverbal Behav.* 34(1), 15–26 (2010)
39. Dyer, J.R.G., Johansson, A., Helbing, D., Couzin, I.D., Krause, J.: Leadership, Consensus Decision Making and Collective Behaviour in Humans. *Phil. Trans. R. Soc. B.* 364(1518), 781–789 (2009)

40. Dyer, J.R.G., Ioannou, C.C., Morrell, L.J., Croft, D.P., Couzin, I.D., Waters, D.A., Krause, J.: Consensus Decision Making in Human Crowds. *Anim. Behav.* 75(2), 461–470 (2008)
41. Faria, J.J., Dyer, J.R.G., Tosh, C.R., Krause, J.: Leadership and Social Information Use in Human Crowds. *Anim. Behav.* 79(4), 895–901 (2010)
42. Bonneaud, S., Rio, K., Chevaillier, P., Warren, W.H.: Accounting for Patterns of Collective Behavior in Crowd Locomotor Dynamics for Realistic Simulations. In: Pan, Z., Cheok, A.D., Müller, W., Chang, M., Zhang, M. (eds.) *Transactions on Edutainment VIII, LNCS*, vol. 7145, pp. 1–12. Springer, Heidelberg (2012)
43. Bonneaud, S., Warren, W.H.: A Behavioral Dynamics Approach to Modeling Realistic Pedestrian Behavior. In: Weidmann, U., Kirsch, U., Puffe, E., Weidmann, M. (eds.) *Pedestrian and Evacuation Dynamics*. Springer, Heidelberg (2012)

A Macroscopic Model for Bidirectional Pedestrian Flow

Cécile Appert-Rolland, Pierre Degond, and Sébastien Motsch

Abstract We present a macroscopic model for pedestrian dynamics in a corridor (or in any quasi one-dimensional system). The model is inspired from the Aw-Rascle model of car traffic but here, a two-directional flow is considered: in each point, two densities are defined, for left and right going pedestrians. The challenge is to bound the density even under congestion. This is enforced by a pressure term, modeling the interactions between pedestrians, that diverges when the density approaches the maximal density. The intensity of the divergence is controlled by a small parameter epsilon. In the limit where epsilon tends to zero, the system exhibits coexisting congested and uncongested phases separated by sharp interfaces.

The lateral extension of the corridor can be taken into account through a multi-lane model, with appropriate lane changes. A characteristic of two-way models is that they can lose their hyperbolicity in some cases. Actually, this could be the counterpart of phenomena observed in real crowds, namely the instability of homogeneous flows towards lane-formation, or even crowd turbulence as observed at very high crowd densities.

C. Appert-Rolland (✉)

Laboratory of Theoretical Physics UMR 8627, CNRS, Bâtiment 210, F-91405 Orsay Cedex, France

Laboratory of Theoretical Physics, University Paris-Sud, Bâtiment 210, F-91405 Orsay Cedex, France

e-mail: Cecile.Appert-Rolland@th.u-psud.fr

P. Degond

Institut de Mathématiques de Toulouse, Université de Toulouse; UPS, INSA, UT1, UTM, F-31062 Toulouse, France

Institut de Mathématiques de Toulouse UMR 5219, CNRS, F-31062 Toulouse, France

e-mail: pierre.degond@math.univ-toulouse.fr

S. Motsch

Department of Mathematics, University of Maryland, College Park, MD 20742-4015, USA

e-mail: smotsch@cscamm.umd.edu

Keywords Pedestrian traffic • Two-way traffic • Multi-lane traffic • Macroscopic model • Aw-Rascle model • Congestion constraint

1 Introduction

Pedestrian modelling has known a growing interest in the past decades. Several levels of description can be considered. Agent-based models consider each individual pedestrian. In this paper, we shall rather consider macroscopic models, hence consider large scales at which individuals are not visible anymore, and crowds can be described as a continuous fluid. More precisely, an average density and velocity of pedestrians is defined in each point, and its time evolution is given by a set of partial differential equations, completed by phenomenological closure relations.

Actually such approaches have been proposed to describe road vehicular traffic since the 50s [20], and many variants have been proposed so far. There are several new features to include in order to extend these approaches to pedestrian traffic. In particular, while road traffic is uni-dimensional, pedestrians are in general walking in a bi-dimensional space. Besides, pedestrians sharing the same walking space may have different goals, and as a consequence may walk in different directions. Hence different types of pedestrians will have to be considered in the model. A consequence of these features is that a special care must be given to the implementation of the congestion constraint: in order to be realistic, a macroscopic crowd model must enforce an upper bound for the density.

Different models have already been proposed, that consider one or the other of the above features. A first approach has been proposed in [16]. Some models have been derived from gas-kinetics models [1, 14], from optimal control theory and differential games [17–19], or inspired by the analogy with road traffic [4, 8, 9]. Though some models consider discrete time [24, 25], we shall stick in this paper to a continuous time description.

In this paper, we shall propose a two-way one-dimensional model, that can be extended to multi-lanes in order to describe a bi-directional pedestrian flow in a long corridor. Our focus will be on the handling of congestions. While pedestrian counter-flows have already been considered in [27], multi-lane traffic in [26], and the treatment of congestions in [21, 22], we would like now to include all these features in a single model. Besides, our method to implement the congestion constraint should allow for parameter fitting to data. It is inspired by earlier work for vehicular traffic [5, 6, 11], following a procedure initiated in [7]. This paper is an abridged version of a more technical paper [2], to which the reader can refer to get more details on the model, and the full derivation of its properties.

2 Two-Way One-Lane Traffic Model

In this section, we introduce a one-dimensional model, for bidirectional pedestrian flow. This means that we consider two populations of pedestrians, going in opposite directions, each described by a density and a velocity field. This model can be seen as a generalisation of the one-way Aw-Rascle model [3] which was proposed in the frame of vehicular traffic. This is why we shall refer below to our model as the 2 W-AR model.

More precisely, we shall indicate with an index + the quantities referring to the right-going pedestrians and – for the left-going ones. Let ρ_{\pm} be the density of pedestrians, u_{\pm} their velocity, w_{\pm} their desired velocity and p an auxiliary function that we shall call the pressure and which shall be defined later. Then the 2 W-AR model for 2-way traffic is written:

$$\partial_t \rho_+ + \partial_x (\rho_+ u_+) = 0, \tag{1}$$

$$\partial_t \rho_- + \partial_x (\rho_- u_-) = 0, \tag{2}$$

$$\partial_t (\rho_+ w_+) + \partial_x (\rho_+ w_+ u_+) = 0, \tag{3}$$

$$\partial_t (\rho_- w_-) + \partial_x (\rho_- w_- u_-) = 0, \tag{4}$$

$$w_+ = u_+ + p(\rho_+, \rho_-), \tag{5}$$

$$w_- = -u_- + p(\rho_-, \rho_+). \tag{6}$$

The first two equations (Eqs. 1 and 2) can be recognized as conservation laws for each population of pedestrians.

It can be shown from these equations that the w_{\pm} variables verify

$$\partial_t w_+ + u_+ \partial_x w_+ = 0,$$

$$\partial_t w_- + u_- \partial_x w_- = 0.$$

i.e. w_+ is transported with the flow of + pedestrians, and the same holds for w_- . This justifies the interpretation of these variables as the desired velocities of the pedestrians, as it is a quantity that indeed pedestrians carry along with them (at least as long as they do not go through a shock).

Then the pressure in Eqs. 5 and 6 appears as a velocity offset between the desired and the actual velocities of the pedestrians of a given type. It will have to be prescribed later. It is through the pressure terms that the two flows of pedestrians are coupled.

We took here the convention that the desired velocities w_{\pm} and the velocity offsets $p(\rho_{\pm}, \rho_{\mp})$ are magnitudes, and as such, are positive quantities. The actual velocities u_{\pm} are signed quantities: $u_+ > 0$ ($u_- < 0$) when right-going (left-going) pedestrians are going to the right (to the left).

It is instructive to rewrite the equations of the model under another form, namely

$$\begin{aligned}\partial_t (\rho_+ u_+) + \partial_x (\rho_+ u_+ u_+) &= -\rho_+ \left(\frac{d}{dt} \right)_+ [p(\rho_+, \rho_-)], \\ \partial_t (\rho_- u_-) + \partial_x (\rho_- u_- u_-) &= \rho_- \left(\frac{d}{dt} \right)_- [p(\rho_-, \rho_+)],\end{aligned}$$

where the material derivatives $(d/dt)_\pm = \partial_t + u_\pm \partial_x$ depend on what type of particles is concerned. These equations mean that pedestrians react to the *Lagrangian* derivative of the pressure. It was already shown for vehicular traffic that reacting to local gradients was leading to various deficiencies in second order models [10] and that this problem could be solved by using rather material derivatives [3].

In [2], we have shown that the 2 W-AR model is not always hyperbolic. Non-hyperbolicity may occur at the onset of congestion. This is not completely surprising, as this is quite common in systems involving two counter-propagating flows. In the context of pedestrians, this instability could actually describe the crowd turbulence that was shown to occur in extreme density conditions [15].

3 Introduction of the Congestion Constraint in the 2 W-AR Model

3.1 Congestion Model with Smooth Transitions

As mentioned before, the form for the pressure term has to be prescribed independently to close the model equations (Eqs. 1, 2, 3, 4, 5 and 6). In principle, this form should be obtained from experiments such as those described in [23] and obtained in the frame of the PEDIGREE project [28].

Here we propose a form that allows to illustrate how an adequate pressure can implement the congestion constraint:

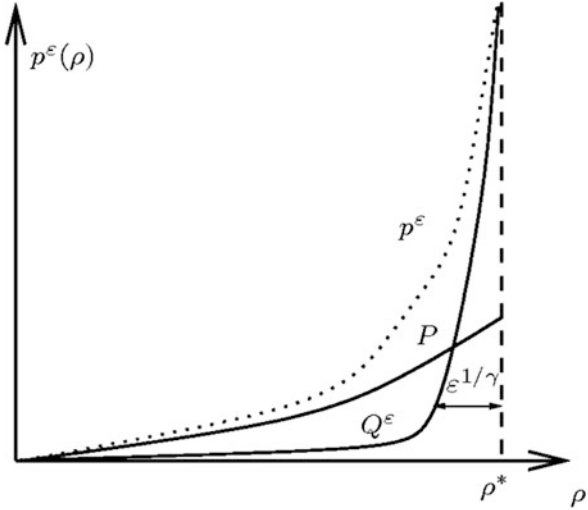
$$p(\rho_+, \rho_-) = p^\varepsilon(\rho_+, \rho_-) = P(\rho) + Q^\varepsilon(\rho_+, \rho_-), \quad \text{with } \rho = \rho_+ + \rho_- \quad (7)$$

$$P(\rho) = M\rho^m, \quad m \geq 1, \quad (8)$$

$$Q^\varepsilon(\rho_+, \rho_-) = \frac{\varepsilon}{q(\rho_+) \left(\frac{1}{\rho} - \frac{1}{\rho^*} \right)^\gamma}, \quad \gamma > 1. \quad (9)$$

The choice for this form was justified as follows. $P(\rho)$ is the background pressure of the pedestrians in the absence of congestion (and is taken in the form of an isentropic gas dynamics equation of state). In uncongested regime, we expect that the velocity offsets of the right and left going pedestrians are the same. Thus, the uncongested flow pressure P given by Eq. 8 is a function of ρ only. Q^ε is

Fig. 1 Schematic representation of $Q\varepsilon$, P , and $p^\varepsilon = P + Q\varepsilon$, as a function of ρ



a correction which turns on when the density is close to congestion (i.e. $\varepsilon \ll 1$ is a small quantity), and modifies the background pressure to have it match the congestion condition $p(\rho) \rightarrow \infty$ as $\rho \rightarrow \rho^*$ (Fig. 1).

Indeed, as long as $\rho - \rho_*$ is not too small, the denominator in Eq. 9 is finite and $Q\varepsilon(\rho)$ is of order ε . Thus the pressure p is dominated by the P term. However, a crossover occurs when congestion is approached, and the diverging term $Q\varepsilon(\rho)$ takes over.

The prefactor $q(\rho_+)$ takes into account the fact that the velocity offset for the majority particle is smaller than that of the minority particle. In other words, the flow of the majority category of pedestrians should be less impeded than that of the minority one. Therefore, we prescribe q to be an increasing function of ρ_+ .

Physically relevant expressions of $q(\rho_\pm)$ can be obtained from real experiments. A possible extension would be to have different functions $q_+(\rho_+)$ and $q_-(\rho_-)$. This could model the fact that for example, a crowd heading towards a train platform could be more pushy than the one going in the opposite direction.

With the choice Eqs. 7, 8 and 9 of the pressure, we anticipate that the constraint

$$\rho = \rho_+ + \rho_- \leq \rho^*$$

will be satisfied everywhere in space and time, though this still has to be checked.

3.2 Congestion Model with Abrupt Transitions

While for a finite ε , the transition to congestion is smooth, this is not the case in the limit $\varepsilon \rightarrow 0$ considered here.

In this limit, as long as the flow is uncongested, it is unperturbed and the flow is compressible. It is only when the density hits ρ_* that the congestion suddenly turns on, and that the flow becomes incompressible. It must be specified by a specific relation how the left and right going pedestrians share the available space in the congested state – and this sharing relation depends upon the choice of the function q .

4 Two-Way One-Lane Model with Constant Desired Velocity

In this section, we considered a simpler version of the model, called 2 W-CAR model, for which all the pedestrians have the same desired velocity

$$w_+ = w_- = V, \tag{10}$$

and thus

$$u_+ = V - p(\rho_+, \rho_-), \quad u_- = -V + p(\rho_-, \rho_+). \tag{11}$$

The 2 W-CAR model is written:

$$\partial_t \rho_+ + \partial_x (\rho_+ (V - p(\rho_+, \rho_-))) = 0, \tag{12}$$

$$\partial_t \rho_- - \partial_x (\rho_- (V - p(\rho_-, \rho_+))) = 0. \tag{13}$$

These are two first-order models coupled by a velocity offset which depends on the two densities.

Now that the desired velocity is a fixed value and not a continuum, it is possible to interpret this model in terms of moving (densities g_{\pm}) and steady (densities s_{\pm}) particles. Note that even when they are stopped, pedestrians still keep their desired velocity oriented either toward the left or right direction, and thus densities of steady pedestrians must indicate to which population they refer. We have

$$\rho_{\pm} = g_{\pm} + s_{\pm} \quad \text{and} \quad \rho_{\pm} u_{\pm} = \pm V g_{\pm}.$$

and we can show that

$$\frac{s_+}{\rho_+} = \frac{p(\rho_+, \rho_-)}{V}, \quad \frac{s_-}{\rho_-} = \frac{p(\rho_-, \rho_+)}{V}.$$

Therefore, the offset velocities $p(\rho_+, \rho_-)$ and $p(\rho_-, \rho_+)$ scaled by the particle velocity V represent the proportions of the steady particles s_+ / ρ_+ and s_- / ρ_- respectively.

If we derive the equations for the steady and moving densities directly from the 2 W-AR model, we find that the transitions from the steady to moving states or

vice-versa depend on the derivatives of the concentrations of moving pedestrians. In reality, moving pedestrians are not impeded by other pedestrians moving in the same direction. Thus the model could here be modified so that the pressure rather depends on the density of obstacles constituted by the sum of the densities for the steady and the oppositely going pedestrians. Again, this modification could be performed only in the case of the 2 W-CAR model, and not for the 2 W-AR model, for which only pedestrians moving faster than a given pedestrian would not impede its motion.

Also for the 2 W-CAR model, the congestion constraint can be implemented, in a similar way as in Sect. 3. Again, a smooth or an abrupt constraint can be implemented.

5 A Two-Way Multi-Lane Model of Pedestrians

In order to allow for a spatial structuration of the flow in the direction transverse to the corridor axis, one may define a multi-lane model, for which the dynamics on each lane is defined by the above 2 W-AR model. The model must be completed with lane-changing rules, for which a choice has been given in [2]. The way the congestion constraint must be extended to account for these lane changes is also described.

6 Conclusion

In this paper, following [2], we have presented a macroscopic model for quasi-one-dimensional two-way pedestrian traffic. Our main focus was on the treatment of the congestion constraint, according to which the pedestrian density must be bound even in congested states. We provide a methodology to handle this congestion, by the introduction of a pressure term which reduces the pedestrian velocities when the density reaches this maximal density. This pressure term could be thought of as representing the contacts between pedestrians that prevent the density to exceed a limit density.

This pressure term may act progressively as the density increases, or occur on an arbitrarily small range of densities. Then the model may exhibit abrupt transitions from uncongested compressible regions and congested incompressible ones.

Besides, we have found that the two-way models proposed here may lose their hyperbolicity in certain conditions and that this may be linked to the generation of large scale structures in crowd flows. It was shown by numerical simulations in [2] that adding diffusion could help to stabilize the small scale structures and favor the development of large scale structures which may be related to observations.

Here the model is defined first on one single lane, and then extended to a corridor like geometry through a multi-lane structure involving lane changes. It would be interested to extend it to two-dimensional flows.

Implementing numerically the congestion constraint is not an easy task, and special methods have to be designed, as for example in [12, 13] for the case of Euler system of gas dynamics.

Future work should provide mathematically rigorous proofs that the upper-bound for the density is indeed respected in all regimes. It would also be useful to obtain approximate equations for the interfaces between congested and uncongested regions. Eventually, a derivation of the macroscopic model from a microscopic model is in preparation.

References

1. S. Al-nasur & P. Kachroo: A Microscopic-to-Macroscopic Crowd Dynamic model. Proceedings of the IEEE ITSC 2006, 2006 IEEE Intelligent Transportation Systems Conference Toronto, Canada, September 17–20 (2006).
2. C. Appert-Rolland, P. Degond, and S. Motsch: Two-way multi-lane traffic model for pedestrians in corridors. *Networks and Heterogeneous Media* **6** (2011) 351–381.
3. A. Aw, M. Rascle: Resurrection of second order models of traffic flow. *SIAM J. Appl. Math.*, **60** (2000), 916–938.
4. N. Bellomo, C. Dogbe: On the modelling crowd dynamics: from scaling to second order hyperbolic macroscopic models. *Math. Models Methods Appl. Sci.*, **18** (2008), 1317–1345.
5. F. Berthelin, P. Degond, M. Delitala, M. Rascle: A model for the formation and evolution of traffic jams. *Arch. Rat. Mech. Anal.*, **187** (2008), 185–220.
6. F. Berthelin, P. Degond, V. Le Blanc, S. Moutari, J. Royer, M. Rascle: A Traffic-Flow Model with Constraints for the Modeling of Traffic Jams. *Math. Models Methods Appl. Sci.*, **18**, **Suppl.** (2008), 1269–1298.
7. F. Bouchut, Y. Brenier, J. Cortes, J. F. Ripoll: A hierarchy of models for two-phase flows. *J. Nonlinear Sci.*, **10** (2000), 639–660.
8. C. Chalons: Numerical approximation of a macroscopic model of pedestrian flows. *SIAM J. Sci. Comput.*, **29** (2007), 539–555.
9. R. M. Colombo, M. D. Rosini: Pedestrian flows and nonclassical shocks. *Math. Methods Appl. Sci.*, **28** (2005), 1553–1567.
10. C. Daganzo: Requiem for second order fluid approximations of traffic flow. *Transp. Res. B*, **29** (1995), 277–286.
11. P. Degond, M. Delitala: Modelling and simulation of vehicular traffic jam formation. *Kinet. Relat. Models*, **1** (2008), 279–293.
12. P. Degond, J. Hua, L. Navoret: Numerical simulations of the Euler system with congestion constraint. *J. of Computational Physics*, **230** (2011), 8057–8088.
13. P. Degond, M. Tang: All speed scheme for the low Mach number limit of the Isentropic Euler equations. *Commun. Comput. Phys.*, **10** (2011), 1–31.
14. D. Helbing: A fluid dynamic model for the movement of pedestrians. *Complex Systems*, **6** (1992), 391–415.
15. D. Helbing, A. Johansson, and H.Z. Al-Abideen: The dynamics of crowd disasters: An empirical study. *Phys. Rev. E* **75**, 046109 (2007).
16. L. F. Henderson: On the fluid mechanics of human crowd motion. *Transportation Research*, **8** (1974), 509–515.
17. S. Hoogendoorn, P. H. L. Bovy: Simulation of pedestrian flows by optimal control and differential games. *Optimal Control Appl. Methods*, **24** (2003), 153–172.
18. R. L. Hughes: A continuum theory for the flow of pedestrians. *Transportation Research B*, **36** (2002), 507–535.

19. R. L. Hughes: The flow of human crowds. *Ann. Rev. Fluid Mech.*, **35** (2003), 169–182.
20. M. J. Lighthill, J. B. Whitham: On kinematic waves. I: flow movement in long rivers. II: A theory of traffic flow on long crowded roads. *Proc. Roy. Soc.*, **A229** (1955), 281–345.
21. B. Maury, A. Roudneff-Chupin, F. Santambrogio: A macroscopic crowd motion model of gradient flow type. *Math. Models Methods Appl. Sci.*, **20** (2010), 1787–1821.
22. B. Maury, J. Venel: A mathematical framework for a crowd motion model. *C. R. Acad. Sci. Paris, Ser. I*, **346** (2008), 1245–1250.
23. M. Moussaïd, E. Guilloit, M. Moreau, J. Fehrenbach, O. Chabiron, S. Lemerrier, J. Pettré, C. Appert-Rolland, P. Degond, and G. Theraulaz: Traffic Instabilities in Self-organized Pedestrian Crowds. *PLoS Computational Biology*, **8** (2012) 1002442.
24. B. Piccoli, A. Tosin: Pedestrian flows in bounded domains with obstacles. *Contin. Mech. Thermodyn.*, **21** (2009), 85–107.
25. B. Piccoli, A. Tosin: Time-evolving measures and macroscopic modeling of pedestrian flow. *Arch. Ration. Mech. Anal.*, **199** (2010), 707–738.
26. V. Shvetsov, D. Helbing: Macroscopic dynamics of multi-lane traffic. *Phys. Rev. E* **59** (1999), 6328–6339.
27. W. G. Weng, S. F. Shena, H. Y. Yuana, W. C. Fana: A behavior-based model for pedestrian counter flow. *Physica A* **375** (2007), 668–678.
28. More information can be found at <http://www.pedigree-project.info>.

A Macroscopic Multiple Species Pedestrian Flow Model Based on Heuristics Implemented with Finite Volumes

Frank Huth, Günter Bärwolff, and Hartmut Schwandt

Abstract We present a macroscopic model for pedestrian movement and its implementation. The focus is on the simulation of multiple interacting pedestrian streams. The number of different species is potentially unrestricted. Tunability is provided by parameters common to all pedestrian species as well as species-specific parameters.

The primary goal of our model is the description of pedestrian motion in non-panic circumstances but we expect that an extension to panic scenarios is feasible.

The implementation uses a finite volume method in order to enforce mass conservation, and method-specific optimizations model certain aspects of pedestrian behavior. Furthermore, we apply a set of heuristics to obtain a particularly simple model.

The intent to simulate human crowds in realistic environments implies the need to manage arbitrary domain and cell shapes. Development flexibility suggests to use open source code. These requirements, and its code maturity, made OpenFOAM® our choice to base the implementation on.

Keywords Macroscopic pedestrian model • Human crowd simulation • Intersecting pedestrian flows

F. Huth (✉) • G. Bärwolff • H. Schwandt
Institut für Mathematik, Technische Universität Berlin, Sekr. MA 6-4, Straße des 17. Juni 136,
10623 Berlin, Germany
e-mail: huth@math.tu-berlin.de; baerwolf@math.tu-berlin.de; schwandt@math.tu-berlin.de;
<http://www.math.tu-berlin.de>

1 Introduction

The need to simulate pedestrian streams arises from the planning and safe operation of complex infrastructures dedicated to pedestrian use, which is a complex task. See, for example, [1] for more details.

Two major approaches to pedestrian traffic simulation can be identified: microscopic models (which represent the pedestrians as individual agents) and macroscopic models (which describe the pedestrian crowd via continuous density and flow fields). Both methodologies have their advantages and disadvantages in specific situations and should be considered complementary. For a view on the limitations of the latter approach, which we also apply here, and details on the following discussion, see [1]. We argue that the following assumptions are instrumental in formulating our model.

Assumption 1. *Pedestrian movement is determined by a field that affects their walking direction and speed. Every considered aspect (like the planned path to a target, obstacles like walls or other pedestrians, and so on) has an effect on the environment of the pedestrians generating an interaction field of distant forces. The data described by this field can be represented by partial differential equations (PDEs).*

Assumption 2. *The information base that is processed by individual pedestrians to make decisions is not purely factual but a perception or even a (re-)constructed image (based on the experiences of these individuals) of reality. Speed and walking direction are the product of heuristic decision making of individual pedestrians to avoid collisions.*

Finally, we remark on the following:

Remark 1. We argue that there is a particular finite spatial resolution that can be applied to simulations sensibly, and therefore a certain minimal spatial volume. We remark on the following concerning the existence of such a representative elementary volume (REV): At points where the density of a particular species is very low, an REV cannot exist since the volume of the REV would tend to be very large, potentially infinite. This is the point when a macroscopic model produces unreliable or even useless results. On the other hand, if densities are very low, interactions between pedestrians are rare and, consequently, the predefined path to a target will probably be followed by the pedestrians in a very predictable way.

2 Setting Up the Model

In order to achieve the goal of applying our model to real-life settings, we define the following primary requirements:

- Robustness,
- Simplicity (as far as possible),

- Stand-alone usability, and integrability with other models or software,
- Flexibility to
 - Provide for adaptability during the research process,
 - Be able to serve as a module in the framework of the MATSim project (see <http://www.matsim.org/>),
 - Be able to couple with a microscopic model,
- Heuristics to describe important features.

It has to be noted that much vital information to finish the model is (yet) missing.

Recent research on pedestrian dynamics has recognized that it is beneficial to base models on well-founded heuristics (see, for example, [2–5]).

Assumption 3. *The heuristics that apply in pedestrian traffic should be sufficiently simple in order to be accessible by the majority of pedestrians. If several simple strategies are considered, the one that proves most effective is likely to be preferred since pedestrians are supposed to seek efficiency, too.*

2.1 The Transport Equation

Perceiving pedestrian flows as a transport problem, we start with the governing equation that describes the mass flow:

$$\frac{\partial \rho_i}{\partial \vartheta} + \nabla \cdot (\rho_i v_i) = 0. \quad (1)$$

In this document, ϑ denotes the time, and $i \in \{1, \dots, n\}$ where n is the number of pedestrian “types” or “species” distinguished by certain properties. The desired velocity would be a frequent example of such a property. Furthermore, ρ_i is the current density and v_i the current velocity of a species in a given computational domain.

Since pedestrian dynamics cannot be entirely described as a physical phenomenon, the parts of the equation can do well with some discussion.

2.2 Measuring Pedestrian Density

In physics, mass density ρ has units $[\rho] = \frac{\text{mass}}{\text{volume}}$. However, this does not seem to be the best fit for the problem considered here. The definition $[\rho] = \frac{\text{mass}}{\text{area}}$ used, for example, in [3] similarly includes “mass” which the authors need to model inertial effects, which are not included in our model.

Concerning pedestrian inertial mass, we require the following:

Assumption 4. *Due to the smoothness of the controlling fields (see Assumption 1) we assume that it is not necessary to describe mass (inducing inertial behavior in the model). This way we assume that the pedestrians may follow (adapt speed and heading) to the controlling fields without significant lag by means of internal impetus, decision and physical strength.*

Therefore, one natural way to measure the pedestrian density in this setting is to use $[\rho] = \frac{\text{pedestrians}}{\text{area}}$, which implicitly relies on a certain amount of homogeneity of the pedestrian crowd in the considered sample. An even smarter approach is presented in [6] by defining the area that a specific pedestrian occupies. This area depends on, e.g., whether the pedestrian is a child, an adolescent or an adult, which cloths the pedestrian wears (summer or winter cloths), how much luggage the pedestrian carries and so on. This yields an appropriate dimensionless measure $[\rho] = \frac{\text{pedestrians'neededarea}}{\text{availablearea}}$. Since the area occupied by a pedestrian is not always readily available for input, we choose the former definition of density as pedestrians per area.

In our model we use normalized densities: $\rho_i, \rho \in [0, 1]$ with $\rho = \sum_{i=1}^n \rho_i$. A value of $\rho = 1$ would for instance mean $5.4 \frac{\text{pedestrians}}{\text{area}}$ according to [7] and up to $10 \frac{\text{pedestrians}}{\text{area}}$ according to other sources (see, e.g., [8] for a discussion).

2.3 Transport Velocity

The primary goal is to find a sensible functional relationship $v_i = v_i(\rho_1, \dots, \rho_n)$ that yields a nonlinear system for realistic cases.

In the literature, one frequently discriminates between a planned (e.g., “external” in [2] or “tactical” in [8]) and an instantaneous (e.g., “intelligent” in [2] or “operational” in [8]) velocity. In our opinion, this differentiation makes sense in the context of categorizing the cause of an action taken by a pedestrian.

Our approach is slightly more pragmatic and accounts for three different types of decisions. Pedestrians:

1. Choose a direction they wish to go,
2. Choose a speed for walking in the chosen direction based on local conditions,
3. Alter speed and walking direction in order to locally avoid densely populated areas (prefer the direction of $-\nabla\rho$).

Therefore, we decompose the velocity as follows:

$$v_i = a_i V d_i^i - b_i W d^1, \quad (2)$$

where:

$V \in [0, 1]$ is a normalized speed determined by a fundamental diagram (see below).

d_i^i is a unit vector field pointing into the direction of the desired heading.

d^1 is a directional vector field for local correction (not necessarily of unit length, see below). Since it depends on the total density ρ , it is common to all pedestrian species.

a_i and b_i are constants: a_i stands for the absolute value of the wished velocity, b_i is a measure for avoiding regions of high density.

$W = 1 - V$ reflects the operational shift from wanting to reach the desired target to reacting to local encounters with other pedestrians at high densities.

Summarizing this the term $a_i V d_i^i$ stands for the gradient driven part of the velocity and $b_i W d^1$ describes the influence of high density regions on the velocity of pedestrians.

A model for two pedestrian species with just the $a_i V d_i^i$ term present has been investigated in [9] with a focus on discussing the mathematical foundation. This investigation highlights some shortcomings of the model with respect to the simulation of real-world scenarios. The authors suggest to introduce (cross) diffusion terms in order to solve these problems. Since the meaning of these terms in the context of real-life applications seems to be obscure, here we prefer to introduce the $b_i W d^1$ term.

2.3.1 Desired Heading

The term d_i^i describes the pedestrian’s choice of a walking direction, and is based on spatial information from the vicinity and the global environment of the pedestrian:

$$\Delta \phi_j^{(i)}(\vartheta) = r_j^{(i)}(\vartheta), \tag{3}$$

$$\phi_i(\vartheta) = \sum_j \phi_j^{(i)}(\vartheta), \tag{4}$$

$$d_i^i(\vartheta) = \begin{cases} \frac{\nabla \phi_i(\vartheta)}{|\nabla \phi_i(\vartheta)|} & \text{if } |\nabla \phi_i(\vartheta)| \neq 0, \\ \text{random unit vector} & \text{if } |\nabla \phi_i(\vartheta)| = 0. \end{cases}$$

With the formula (4) we add the different potentials coming from global influences like the shape of the considered domain or local influences like the local density.

The subscripted character j of $\phi_j^{(i)}(\vartheta)$ denotes the influence type (for example global, local etc.), and the superscripted character i denotes the considered species.

Therefore, according to Assumption 1, d_i^i is based on source and boundary terms of j (partially) solved Poisson equations for each pedestrian species i (reflecting j different influencing factors). The $\alpha_j^{(i)}$ are constant weights, and the $f_j^{(i)}(\vartheta)$ are source terms derived from spatially distributed information—for example, the

density $\rho_k(\vartheta)$ of some pedestrian species. This kind of flow, the direction of which is derived from a potential, has been investigated in [10].

The parameters in the above equations have to be chosen very specifically, and finding appropriate settings is one of the open tasks for the application of this model.

In the following we specify the right hand side of the Eq. (3).

Global Potential Field

This field includes the following data:

- The geometry of the computational domain, e.g., as introduced in [11], by requiring appropriate boundary conditions.
- Congestion detection by introducing a source term into (3):

$$\tilde{f}_j^{(i)}(\vartheta, x) = \begin{cases} \rho(\vartheta, x) & \text{if } \rho(\vartheta, x) \geq \tau, \\ 0 & \text{else,} \end{cases}$$

$$f_j^{(i)}(\vartheta, x) = \tilde{f}_j^{(i)}(\vartheta, x) - \int_{\Omega} \tilde{f}_j^{(i)}(\vartheta, x) \, dx / |\Omega|.$$

Here, $\alpha_j^{(i)} \leq 0$ is for “normal”, and $\alpha_j^{(i)} > 0$ is for “rubberneck” behavior. The number $\tau = \rho_{congestion}$ is a threshold determining when jam perception occurs. For $\tau = 0.5$ this means, e.g., $2.7 \frac{\text{pedestrians}}{m^2}$ (see [7, p. 62]).

With the weighting parameters $\alpha_j^{(i)}$ and the density fluctuations $f_j^{(i)}(\vartheta, x)$ the right hand side of (3) is defined as

$$r_j^{(i)}(\vartheta) = \alpha_j^{(i)} f_j^{(i)}(\vartheta).$$

Data propagated this way is carried around corners, therefore it might be unrealistic in that respect. As a solution to this problem we suggest splitting the computational domain into convex sub-domains.

Local Effect Field

The only effect currently implemented is an attraction and/or repulsion between the individual pedestrian species. This effect is implemented through source terms in Eq. (3):

$$r_j^{(i)}(\vartheta) = \sum_{k=1}^n \varpi_k^{(i)} \rho_k(\vartheta, x)$$

where $\varpi_k^{(i)}$ is the inter-pedestrian attraction for different species. A setting of

$$\alpha_{j,k}^{(i)} \begin{cases} > 0 & \text{if } i = k, \\ = 0 & \text{if } i \neq k \end{cases}$$

seems to produce qualitatively sensible results. This setting generates an intra-species attraction generating dynamic clustering and lane formation, and leads to the clustering of some of the pedestrians moving in the same direction. A setting of

$$\alpha_{j,k}^{(i)} \begin{cases} > 0 & \text{if pedestrian } i \text{ and pedestrian } k \text{ share their target(s),} \\ = 0 & \text{else} \end{cases}$$

adds even more realism to the simulation (see [12]).

The boundary conditions for the potential equation (3) in the case of the local potentials are of Dirichlet type with a value of zero.

In order to keep the effects local, we have implemented a small number of Jacobi smoother steps to just “dent” the initial values ($\equiv 0$ in this case) of the iteration. Since the Jacobi iteration propagates data at a rate of one cell per iteration, an estimate of the locality of the data is provided. This implies that the cell sizes should be sufficiently similar to avoid local differences in the range of the propagated data.

The tuning of the iteration count is clearly a question of the pedestrians’ behavior to be modeled in conjunction with the spatial resolution.

Another alternative were to introduce source terms which are designed such that the result of the smoothing steps are the result of a complete solution of (3). This approach would be more expensive and—given the other open modeling problems and inaccuracies—most probably overkill.

Furthermore, scale plays a vital role when it comes to the question which aspects to model and how (as has been seen in [1]). A large scale (with spatially large cells) is very likely to cancel structures that emerge at the local level that are modeled in this section. This means that the effects of such structures should rather be modeled by an appropriate fundamental diagram (see [12]).

2.3.2 Introducing the Gradient Term

There are a number of possible approaches to introduce a gradient term. Notable are the following two:

$$d^1(\vartheta, x) = \begin{cases} \frac{\nabla\rho(\vartheta, x)}{|\nabla\rho(\vartheta, x)|} & \text{if } |\nabla\rho(\vartheta, x)| > 0, \\ 0 & \text{if } |\nabla\rho(\vartheta, x)| = 0, \end{cases} \tag{5}$$

$$d^1(\vartheta, x) = \begin{cases} \frac{\nabla\rho(\vartheta, x)}{|\nabla\rho(\vartheta, x)|} & \text{if } |\nabla\rho(\vartheta, x)| > 1, \\ \nabla\rho(\vartheta, x) & \text{else.} \end{cases} \quad (6)$$

Concerning (5) it has to be noted that $d^1(\vartheta, x)$ is not necessarily continuous with respect to x at points where $|\nabla\rho(\vartheta, x)| = 0$ holds. Another problem obviously present with this term is that it may show large scatter where the density is high. This can lead to the violation of the condition $\rho_i, \rho \in [0, 1]$ because of numerical overshooting. Another risk is the numerical oscillation of the solution (which might be interpreted as remaining erratic pedestrian activity at high densities in certain situations).

This term might be viewed as carrying some random disturbances as discussed in [13, 14], which produces less effective motion (stronger clogging tendency due to the “freezing by heating effect” discussed there). The measurement of the mobility there did not show an increase of flux with more “thermal” motion at all. This is due to the inhibition of lane formation because the effect of lane formation yields an enhancement of flux. The observed “freezing by heating effect” has been considered for modeling panic situations, where it might well make sense. However, such scenarios are beyond the scope of this paper.

The gradient term defined by (6) is more likely to be the rule applied by pedestrians under normal conditions, because it is more efficient than the term given by Eq. (5) (see Assumption 3).

Another argument in favor for (6) is given by the fact that the key idea of the macroscopic approach is to average the behavior of several pedestrians and thus smoothing out random disturbances caused by single pedestrians at sufficiently large scales.

2.3.3 Walking Speed and Fundamental Diagram

A uni-directional flux can be defined by $J = \rho_i V(\rho_1, \dots, \rho_n) d_i$. For the case of $J = \rho V(\rho) d$ the three quantities are related by a fundamental diagram. Fundamental diagrams have been determined by a number of authors, with a relatively wide range of different results that cannot be used to deduce a general law. According to [8], the values found in the literature for the maximum pedestrian density, where movement is possible at all, vary from 3.8 to 10/m². Another controversially discussed issue is how V depends on whether movement is uni-directional or multi-directional.

For more details, see [1] and [12].

Despite the issues described above, we have evaluated the impact of different fundamental diagrams on quantitative and qualitative properties of the solutions. The differences are large enough to indicate the need for a better approximation in this respect. The fundamental diagrams that we have tested are:

$$V(\rho) = 1 - \rho, \quad (7)$$

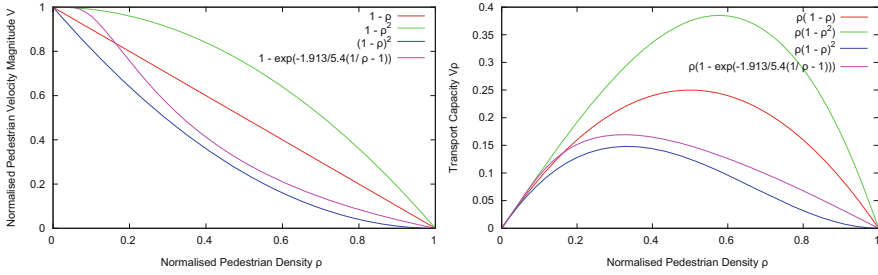


Fig. 1 *Left*: V-profiles of (7)–(10) in comparison; *right*: transport capacities for the given V-profiles

$$V(\rho) = (1 - \rho)^2, \tag{8}$$

$$V(\rho) = 1 - \rho^2, \tag{9}$$

$$V(\rho) = 1 - \exp(-1.913/5.4(1/\rho - 1)), \tag{10}$$

see also Fig. 1. Note that, compared to [7, p. 65], Eq. (10) employs the normalization conditions $V \in [0, 1]$ and $\rho \in [0, 1]$.

2.4 Some Aspects of Setting Boundary Conditions

Boundary conditions usually include the entry/exit points of the simulation domain. Since doorways have a great impact on the capacity of the spatial configuration, special care has to be taken when setting them.

Due to the fact that data at the boundaries cannot be derived from the model itself to a larger extend, assumptions on the configuration beyond the boundary have to be made. We distinguish the following types of boundary segments:

$$\Gamma_w := \{ \Gamma_k \mid \Gamma_k \text{ is a wall} \},$$

$$\Gamma_{i,i} := \{ \Gamma_k \mid \Gamma_k \text{ is an entry for } \rho_i \},$$

$$\Gamma_{o,i} := \{ \Gamma_k \mid \Gamma_k \text{ is an exit for } \rho_i \},$$

$$\Gamma_f := \{ \Gamma_k \mid \Gamma_k \text{ confines the domain with walls sufficiently far away} \}$$

or Γ_f is a boundary of far field type.

Here we discuss some aspects of selecting sensible boundary conditions. Several settings are available, and when a choice qualifies as “sensible” depends on the aspect that is intended to be modeled.

In the following, we assume that ν is the outward-pointing normal at Γ_k , which is part of the boundary:

$\Gamma_k \in \Gamma_w$. One obvious aspect is that pedestrians do not move through walls—which means that the flux through a wall is zero. As can be seen from the the flux part of Eq. (1), the condition of $v \cdot v_i = 0$ and/or $\rho_i = 0$ is sufficient to ensure this behavior. Equation (2) implies the following possible choices:

- Setting $V = 0$ and $W = 0$ will surely inhibit any flux at the wall. This is a good choice if we do not only suspect that pedestrians do not move through walls, but also that they are not located so close to the wall that they can be considered as moving “into” the wall.
- Setting $d_i^1 = 0$ has the same effect as $V = 0$, implying $v \cdot d_i^1 = 0$, which would leave the walking-into-the-wall scenario a possibility.
- If $b_i \neq 0$, one way to control the gradient term appropriately is for instance to set $v \cdot \nabla \rho = 0$ due to Eq. (6).

$\Gamma_k \in \Gamma_{i,i}$. One certain restriction is that an influx $V\rho_i$ beyond the critical value is not applicable. Setting $v \cdot d_i^1 = -1$ would be a natural choice.

- Setting $(V\rho_i)(\vartheta, x)$ to a certain constant and $Wd^1 = 0$ can be used to account for an experimentally measured flux through an entrance.
- The conditions $\rho|_{\Gamma_k} = \sum_j \rho_j|_{\Gamma_k}$ and $W|_{\Gamma_k} = 1 - V(\rho|_{\Gamma_k})$ would imply that the rules of the inner domain are extended beyond the boundary, and backflux is permitted through the entrance.

$\Gamma_k \in \Gamma_{o,i}$. Setting $v \cdot d_i^1 = 1$ is a natural choice. Beyond that, we have to make assumptions on what is happening beyond the boundary. Some examples:

Unimpeded flux of pedestrians beyond the exit. In case that $V|_{\Gamma_k} = V(\rho|_{\Gamma_k})$, setting $\rho|_{\Gamma_k} = \sum_{\{j| \Gamma_k \notin \Gamma_{o,j}\}} \rho_j|_{\Gamma_k}$ would inhibit the influence of the densities of the exiting species’ at (and beyond) the boundary.

Near Γ_k , the situation is the same as inside Ω . This can be achieved by setting $v \cdot \nabla \rho = 0$ and applying $V|_{\Gamma_k} = V(\rho|_{\Gamma_k})$ again. This implies that congestions at such exits would not resolve.

These are only a few examples of boundary conditions which we give here as motivation.

2.5 Assembly of the Full Model

In the following we describe the full set of equations that constitute our model. Let Ω be an open domain with $\bigcup_{1 \leq k \leq m} \Gamma_k$ its sufficiently smooth boundary (segments) for $m \in \mathbb{N}$. Further necessary conditions like, e.g., $\Gamma_k \cap \Gamma_l; \quad k \neq l \in \{1, \dots, m\}$ have a measure of zero, are expected to be satisfied. Additionally, let $\vartheta \geq 0$ denote the time variable.

Now, by assuming $\vartheta > 0$ and inserting (2), (10), (4), (3) into (1), we get:

$$\begin{aligned} \frac{\partial \rho_i}{\partial \vartheta} + \nabla \cdot (\rho_i (a_i V d_i^i - b_i W d^1)) &= 0, \\ \rho &= \sum_i \rho_i, \\ a_i &= \text{const}, \\ V(\rho) &= 1 - \exp(-1.913/5.4(1/\rho - 1)), \\ b_i &= \text{const}, \\ W &= 1 - V, \\ d^1 &= \begin{cases} \frac{\nabla \rho(\vartheta, x)}{|\nabla \rho(\vartheta, x)|} & \text{if } |\nabla \rho(\vartheta, x)| > 1, \\ \nabla \rho(\vartheta, x) & \text{else,} \end{cases} \\ d_i^i &= \begin{cases} \frac{\nabla \phi_i(\vartheta)}{|\nabla \phi_i(\vartheta)|} & \text{if } |\nabla \phi_i(\vartheta)| \neq 0, \\ \text{random unit vector} & \text{if } |\nabla \phi_i(\vartheta)| = 0, \end{cases} \\ \phi_i(\vartheta) &= \sum_j \phi_j^{(i)}(\vartheta), \\ \tilde{\Delta} \phi_j^{(i)}(\vartheta) &= \alpha_j^{(i)} f_j^{(i)}(\vartheta), \end{aligned}$$

with the domains $D(\rho) = D(\rho_i) = D(V) = D(d_i^i) = D(W) = D(\phi_i) = D(d^1) = \Omega$.

Now we consider the case of two kinds of potentials. The subscript 1 denotes the global and the subscript 2 denotes the local potentials.

$$\begin{aligned} \tilde{\Delta} \phi_1^{(i)} &= \Delta \phi_1^{(i)} = \begin{cases} \alpha_1^{(i)} \rho & \text{if } \rho \geq \tau = \rho_{\text{congestion}}, \\ 0 & \text{else,} \end{cases} \\ \alpha_1^{(i)}, \rho_{\text{congestion}} &= \text{const}, \\ \tilde{\Delta} \phi_2^{(i)} &= \hat{\Delta} \phi_2^{(i)} = \sum_o \varpi_o^{(i)} \rho_o, \\ \varpi_o^{(i)} &= \begin{cases} \text{const} > 0 & \text{for inter - pedestrian species attraction,} \\ \text{const} < 0 & \text{for inter - pedestrian species repulsion,} \end{cases} \\ \hat{\Delta} &:= \text{Laplacian smoothed by a few Jacobi steps.} \end{aligned}$$

For $\vartheta = 0$, we require $\rho_i = \rho_i^{(0)}$ on Ω for all i . For this example we assume $\rho_i^{(0)} = 0$ by default.

Concerning the boundary conditions, a vast variety of sensible choices are available, depending on assumptions at a specific boundary segment Γ_k (see Sect. 2.4). In the following, we give an example setting for a simulation that can be initiated with data obtained from a real-world experiment.

The boundary conditions $\text{BC}(\varphi, \Gamma_k)$ applied for a variable φ at Γ_k are:

$$\text{BC}(\rho_i, \Gamma_k) \text{ is } \begin{cases} \rho_i = \rho_i(\vartheta, x, y) & \text{if } \Gamma_k \in \Gamma_{i,i}, \\ \rho_i = 0 & \text{if } \Gamma_k \in (\Gamma_w \cup \Gamma_f), \\ \nu \cdot \nabla \rho_i = 0 & \text{if } \Gamma_k \in \Gamma_{o,i}. \end{cases}$$

$$\text{BC}(\phi_1^{(i)}, \Gamma_k) \text{ is } \begin{cases} \phi_1^{(i)} = \text{const} > 0 & \text{if } \Gamma_k \in (\Gamma_w \cup \Gamma_{i,i}), \\ \phi_1^{(i)} = \text{const} < 0 & \text{if } \Gamma_k \in \Gamma_{o,i}, \\ \nu \cdot \nabla \phi_1^{(i)} & \text{if } \Gamma_k \in \Gamma_f. \end{cases}$$

$$\text{BC}(\phi_2^{(i)}, \Gamma_k) \text{ is } \phi_1^{(i)} = 0 \text{ if } \Gamma_k \in (\Gamma_{i,i} \cup \Gamma_{o,i} \cup \Gamma_f \cup \Gamma_w).$$

$$\text{BC}(d_i^i, \Gamma_k) \text{ is } \begin{cases} d_i^i = 0 & \text{if } \Gamma_k \in (\Gamma_w \cup \Gamma_f), \\ \nu \cdot d_i^i = -1 & \text{if } \Gamma_k \in \Gamma_{i,i}, \\ \nu \cdot d_i^i = 1 & \text{if } \Gamma_k \in \Gamma_{o,i}. \end{cases}$$

$\text{BC}(\rho, \Gamma_k)_i$ has specific boundary conditions for different pedestrian species i (see Sect. 2.4 for a discussion).

$$\text{Therefore, we set } \text{BC}(\rho, \Gamma_k)_i \text{ to } \begin{cases} \rho = \sum_j \rho_j & \text{if } \Gamma_k \in \Gamma_{i,i}, \\ \rho = \sum_{j \neq i} \rho_j & \text{if } \Gamma_k \in \Gamma_{o,i}, \\ \nu \cdot \nabla \rho = 0 & \text{if } \Gamma_k \in (\Gamma_w \cup \Gamma_f). \end{cases}$$

$$\text{BC}(V, \Gamma_k) \text{ is } \begin{cases} V = 1 - \exp(-1.913/5.4(1/\rho - 1)) & \text{if } \Gamma_k \in \Gamma_{i,i}, \\ V = 1 & \text{if } \Gamma_k \in \Gamma_{o,i}, \\ V = 0 & \text{if } \Gamma_k \in (\Gamma_w \cup \Gamma_f). \end{cases}$$

$$\text{BC}(W, \Gamma_k) \text{ is } \begin{cases} W = 1 - V & \text{if } \Gamma_k \in (\Gamma_{i,i} \cup \Gamma_{o,i}), \\ W = 0 & \text{if } \Gamma_k \in (\Gamma_w \cup \Gamma_f). \end{cases}$$

$$\text{BC}(d^1, \Gamma_k) \text{ is } \nu \cdot \nabla d^1 = 0 \text{ if } \Gamma_k \in (\Gamma_{i,i} \cup \Gamma_{o,i} \cup \Gamma_f \cup \Gamma_w).$$

3 Implementation

We used a finite volume method to implement our model. This approach has been chosen in order to produce excellent, realistic results based on a sound mathematical foundation. The most important advantages of finite volume methods in this respect are mass conservation and the flexibility in flux modeling that cannot be matched, for instance, by a finite element method.

The model used in [2] presumably yields better preservation of the flux direction, but the following benefits of the OpenFOAM[®] library and tools outweigh this advantage:

- Finite volume method toolbox,
- Code maturity,
- Primarily a C++ library for field operations, therefore conceptually open (most features are related to physics, especially transport phenomena),
- Open source, thus fully accessible,
- Many preprocessing, solving and post-processing utilities are already implemented,
- Many code examples can be extended/adapted to serve specific tasks,
- Extremely powerful and flexible considering code complexity,
- Capable of handling convex cells with arbitrarily shaped polygons as faces.

4 Example Simulations

4.1 Academic Example $\Omega = (-1, 1)^2$

In the following examples we consider two pedestrian groups (the superscripts run from 1 to 2) and global and local potentials (the subscripts run also from 1 to 2).

4.1.1 180° Encounter

Figure 2 shows the results of a simulation with the parameter setting:

$$\begin{aligned}
 a_i &= b_i = 1, \\
 \rho_i(\vartheta = 0) &= 0.3, \\
 \Phi_1|_{\Gamma \setminus \Gamma_{\text{out}}} &= 100, \\
 \Phi_1|_{\Gamma_{\text{out}}} &= -100, \\
 \varpi_1^{(1)} &= 1,000, \\
 \varpi_2^{(1)} &= 0, \\
 \rho_i|_{\Gamma_{\text{in}}} &= 0.19, \\
 \alpha_1^{(1)} &= \alpha_1^{(2)} = -500.
 \end{aligned}$$

Formation of dynamically reconfiguring lanes can be observed.

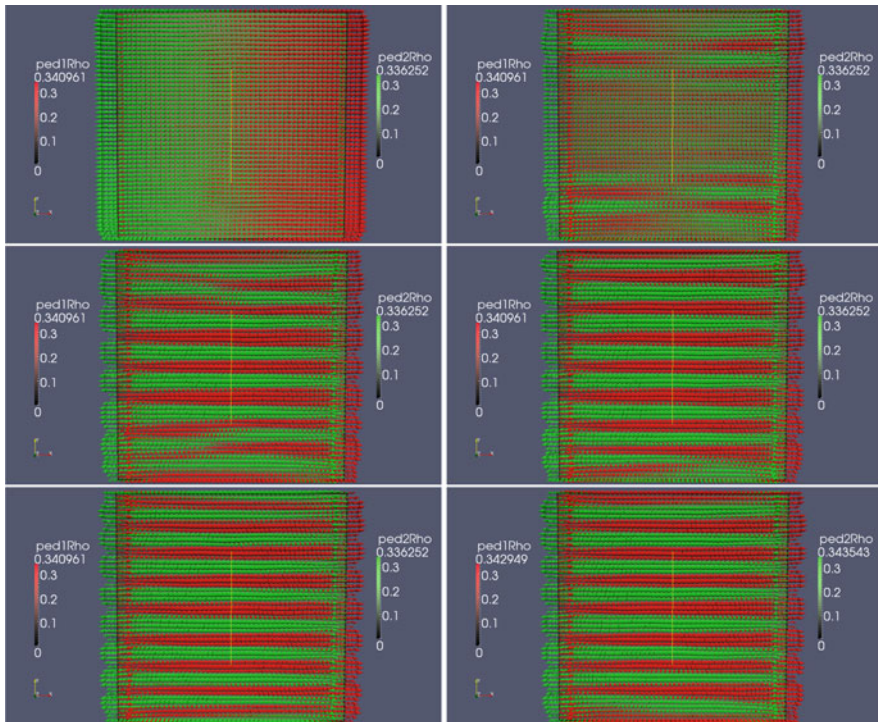


Fig. 2 Time steps 1, 20, 40, 60, 80 and 100 of the simulation of a 180° encounter. Shown are densities and flux. The length of the *arrows* indicate flux strength, *color* indicates species displayed

4.1.2 90° Encounter

Figure 3 shows the results of a simulation with the parameter setting:

$$\begin{aligned}
 a_i &= b_i = 1, \\
 \rho_i(\vartheta = 0) &= 0, \\
 \Phi_1|_{\Gamma \setminus \Gamma_{\text{out}}} &= 100, \\
 \Phi_1|_{\Gamma_{\text{out}}} &= -100, \\
 \varpi_1^{(1)} &= 10,000, \\
 \varpi_2^{(1)} &= 0, \\
 \rho_i|_{\Gamma_{\text{in}}} &= 0.125, \\
 \alpha_1^{(1)} = \alpha_1^{(2)} &= -1,000.
 \end{aligned}$$

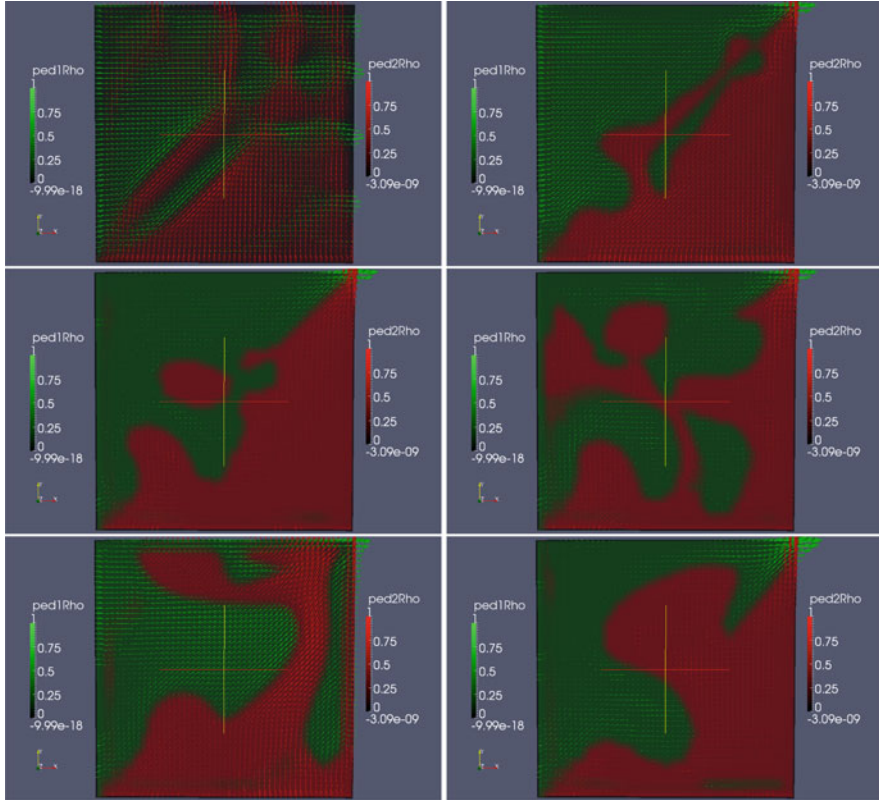


Fig. 3 Time steps 5, 10, 20, 40, 60 and 80 of the simulation of a 90° encounter of two (*red* and *green*) species. Shown are densities and flux. The length of the *arrows* indicate flux strength, *color* indicates species displayed

Formation of dynamically reconfiguring clusters can be observed. See Fig. 4 for the fluxes at the boundaries.

5 Conclusion

For appropriate parameter settings, the medium-scale simulations presented here are able to reproduce the commonly expected qualitative phenomena like lane formation, clustering of pedestrians and congestion. The simulations have been run with up to four interacting pedestrian species.

Due to how the model is constructed, it describes the dynamics of the total density and the density assigned to individual pedestrian species, while maintaining

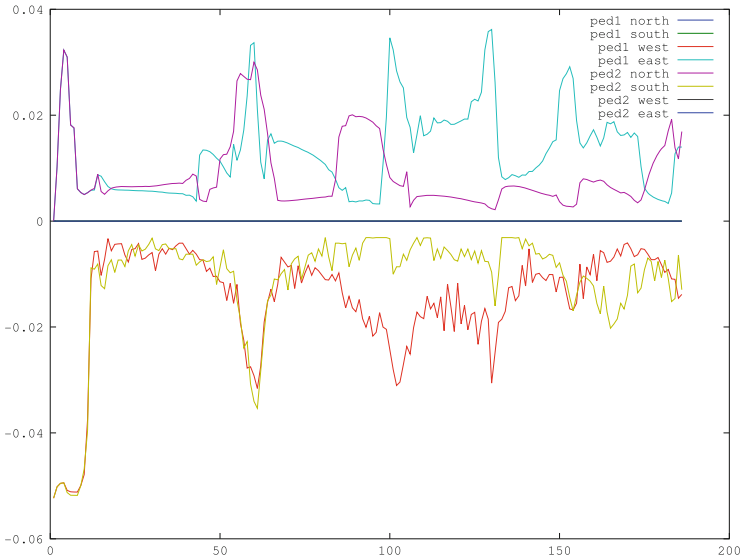


Fig. 4 Boundary fluxes of the 90° simulation

the assumed maximum and minimum density limits for appropriate parameter settings.

These results have been achieved by a fairly simple set of rules. A quantitative comparison with real-life data is still work in progress.

Acknowledgements The authors gratefully acknowledge the support of Deutsche Forschungsgemeinschaft (German Research Foundation) for the project SCHW548/5-1 + BA1189/4-1.

An invaluable contribution to this research has been committed by the open source software community. Notably, we used OpenFOAM[®] by the OpenFOAM Team at Silicon Graphics International Corp. for the simulations and ParaView, supported by Kitware and several collaborators, octave and gnuplot for the processing and visualization of the results.

Finally, we would like to thank the organizers of the 6th International Conference on Pedestrian and Evacuation Dynamics 2012, ETH Zurich, Switzerland.

References

1. Huth, F., Bärwolff, G., Schwandt, H.: Some fundamental considerations for the application of macroscopic models in the field of pedestrian crowd simulation. Preprint ID 2012/16 at http://www.math.tu-berlin.de/menue/forschung/veroeffentlichungen/preprints_2012 (2012)
2. Cristiani, E., Piccoli, B., Tosin, A.: Modeling self-organization in pedestrians and animal groups from macroscopic and microscopic viewpoints. In Bellomo, N., Naldi, G., Pareschi, L., Toscani, G., eds.: *Mathematical Modeling of Collective Behavior in Socio-Economic and Life Sciences. Modeling and Simulation in Science, Engineering and Technology*. Birkhäuser Boston (2010) 337–364

3. Moussaïd, M., Helbing, D., Theraulaz, G.: How simple rules determine pedestrian behavior and crowd disasters. *PNAS* **108** (2011) 6884–6888
4. Bierlaire, M., Antonini, G., Weber, M.: Behavioral dynamics for pedestrians. In Axhausen, K.W., ed.: *Moving Through Nets: The Physical and Social Dimensions of Travel*. Elsevier (2003) 81–106
5. Gigerenzer, G.: Why heuristics work. *Perspectives on Psychological Science* **3** (2008) 20–29
6. Predtechenskii, V.M., Milinskii, A.I.: *Planning for Foot Traffic Flow in Buildings*. Amerind Publishing, New Delhi (1978) translation of *Proekktirovanie Zhdanii s. Uchetom Organizatsii Dvizheniya Lyudskikh Potokov* (Moscow: Stroizdat, 1969).
7. Weidmann, U.: *Transporttechnik der Fußgänger – transporttechnische Eigenschaften des Fußgängerverkehrs (Literaturstudie)*. Schriftenreihe der IVT **90** (1993) in German.
8. Schadschneider, A., Klingsch, W., Kluepfel, H., Kretz, T., Rogsch, C., Seyfried, A.: Evacuation dynamics: Empirical results, modeling and applications. *Encyclopedia of Complexity and Systems Science* (2009) 3142–3176
9. Berres, S., Ruiz-Baier, R., Schwandt, H., Tory, E.M.: An adaptive finite-volume method for a model of two-phase pedestrian flow. *Networks and Heterogeneous Media (NHM)* **6** (2011)
10. Hughes, R.L.: A continuum theory for the flow of pedestrians. *Transportation Research Part B* **36** (2002) 507–535
11. Piccoli, B., Tosin, A.: Pedestrian flows in bounded domains with obstacles. *Continuum Mechanics and Thermodynamics* **21** (2009) 85–107
12. Huth, F., Bärwolff, G., Schwandt, H.: Fundamental diagrams and multiple pedestrian streams. Preprint ID 2012/17 at http://www.math.tu-berlin.de/menue/forschung/veroeffentlichungen/preprints_2012/ (2012)
13. Helbing, D., Farkas, I.J., Vicsek, T.: Freezing by heating in a driven mesoscopic system. *Phys. Rev. Lett.* **84** (2000) 1240–1243
14. Radzihovsky, L., Clark, N.A.: Comment on “Freezing by heating in a driven mesoscopic system”. *Phys. Rev. Lett.* **90** (2003) 189603

Quantitative Validation of the Generalized Centrifugal Force Model

Mohcine Chraibi, Armin Seyfried, and Andreas Schadschneider

Abstract Mathematical models for pedestrian dynamics contribute increasingly to the process of understanding the dynamics of crowds, which has a positive impact in designing building and enhancing their level of safety. In order to improve their validity and maximize the significance of their predictions, several experiments were conducted and evaluated. The results of these experiments give authentic insights into the dynamics of pedestrians and serve as a benchmark for the models. Therefore, the quantitative validation of mathematical models is an important step in their development and eases their application in real-world scenarios. In this article we briefly introduce the generalized centrifugal force model (GCFM). Computer simulations with the GCFM are compared with different empirical data obtained in controlled experiments. In order to test the quality of the model, several scenarios are simulated without changing the parameters of the underlying model.

1 Introduction

Each time a crowd gathers to attend an event, e.g. of sportive, musical or religious nature, there are some security concerns. This was dramatically showcased in 2010 when 21 people died while trying to attend the 2010 love parade in Duisburg Germany. Several projects [1] were realized with the aim to develop new strategies

M. Chraibi (✉) • A. Seyfried

Jülich Supercomputing Centre, Forschungszentrum Jülich, 52425 Jülich, Germany

Computer Simulation for Fire Safety and Pedestrian Traffic, Bergische Universität Wuppertal, Pauluskirchstraße 11, D-42285 Wuppertal, Germany

e-mail: m.chraibi@fz-juelich.de; a.seyfried@fz-juelich.de

A. Schadschneider

Institute for Theoretical Physics, Universität zu Köln, D-50937 Köln, Germany

e-mail: as@thp.uni-koeln.de

and tools that supply security people with deeper insights into the dynamical changing state of a crowd, hence, they are able to better predict a possible overcrowded situation and precociously react on probable danger.

One of the most serious difficulties in mathematical modelling of pedestrian dynamics is the complexity and richness of the human walking behaviour. To predict and study the behaviour of a crowd, several models were developed. This allows an extensive examination of the dynamics under different conditions and in complex buildings.

In pedestrian dynamics many collective phenomena were observed, e.g. lane formations in bi-directional flow, oscillations at bottlenecks, clogging at exits. To explain those phenomena and others several models, based on physical hypotheses were formulated. See [2] for a brief overview of the most established models. From a qualitatively point of view, most of the models show a good capability of explaining and reproducing those phenomena. As the crucial part of any reasonable scientific approach is validation and verification of the hypothesis and/or models several experiments under controlled laboratory conditions were prepared and realized. Therefore, a detailed quantitative evaluation of the mathematical models was possible.

There are various reasons for this issue. First, that state of the art of camera techniques is not mature enough to extract trajectories automatically with high precision from videos, e.g. security recordings in railway-stations. Second, and this is maybe the most important reason, is to reduce the complexity of the studied system. For example well prepared experimental environments in basic geometries are useful to study the dynamics of pedestrians and to extract valuable knowledge that can be generalized to more complex geometries. Despite the fact that the experimental data basis is relatively narrow, there are important discrepancies in the extracted data and any comparison between experiments should take this fact into account. The reason of this state is difficult to determine, since some experiments are poorly documented. However, it was indicated in [3] that cultural factors lead to differences in the characteristics that emerge from the empirical data. The discrepancies of reported empirical data can also be explained by human properties related to the attendees of the experiments, e.g. age, motivation, homogeneity of the group. Other factors are more technical and are directly related to the realisation of the experiments, extraction of the data and their measurement.

In this sense several experiments have been performed [4, 6–10] to investigate specific issue like flow in bottlenecks, the fundamental diagram in narrow and wide corridors in comparison to T-junctions. In this work some of those experimental data will serve as a validation basis of simulation results.

2 Generalized Centrifugal Force Model

Force-based models are microscopic models, which predict the movement of pedestrian by a set of non-linear differential equations. The general definition of such models leans on the second Newtonian law

$$m_i \ddot{\vec{R}}_i = \vec{F}_i = \vec{F}_i^{\text{drv}} + \sum_{j \in \mathcal{N}_i} \vec{F}_{ij}^{\text{rep}} + \sum_{w \in \mathcal{W}_i} \vec{F}_{iw}^{\text{rep}}, \quad (1)$$

with m_i the mass of pedestrian i and \vec{R}_i the vector of its coordinates in space.

Given a small time constant Δt the update rule reads

$$\begin{pmatrix} \vec{R}_i(t + \Delta t) \\ \vec{v}_i(t + \Delta t) \end{pmatrix} = \int_t^{t+\Delta t} \begin{pmatrix} \vec{v}_i(t) \\ \vec{F}_i(t)/m_i \end{pmatrix} dt + \begin{pmatrix} \vec{R}_i(t) \\ \vec{v}_i(t) \end{pmatrix} \quad (2)$$

and is repeated step-wise as necessary.

Since the force-based models iteratively compute the state of the system step-wise, they are able to describe the constantly changing state of a crowd. The question that should be asked is whether a *in silico* description of the dynamics of a system corresponds to reality. In order to address this issue it should be noticed that force-based models and in general microscopic models are of an explorative nature. That means they show how complex phenomena converge from simple rules [11–14]. For security relevant issues, the application area of a model should go beyond this explorative level.

In this work the GCFM will be investigated quantitatively by comparing its results with empirical data. Hereby, different basic geometrical scenarios are simulated. For the sake of completeness, the next section introduces GCFM.

2.1 The Repulsive Forces Between Two Pedestrians

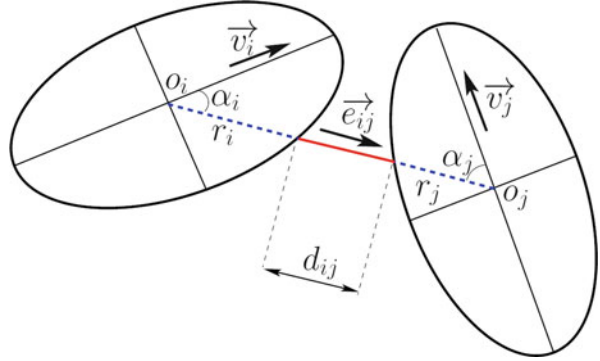
The GCFM [14] is a force-based model that describes the movement of pedestrian by means of superposing small-range forces. Space requirement of pedestrians including their body is defined asymmetrically by an ellipse with two velocity-dependent axes a and b . The first semi-axis models the dynamical space requirement in the direction of motion, which increases with increasing velocity. In the GCFM a is defined by a linear relation of the velocity.

$$a = a_{\min} + \tau_a v_i. \quad (3)$$

The second axis, describes the space requirement of pedestrians in the direction of shoulder. It results from the shoulder length plus an extra amount giving the swaying [4] of pedestrians while moving. The definition of b reads

$$b = b_{\max} - (b_{\max} - b_{\min}) \frac{v_i}{\|\vec{v}_i^0\|}. \quad (4)$$

Fig. 1 The direction of the repulsive force between pedestrians i and j



b_{\min} represents the shoulder length and $b_{\max} > b_{\min}$ is a constant to consider the lateral swaying. $\|\vec{v}_i^0\|$ is the desired velocity of i .

Given two pedestrians at position \vec{R}_i resp. \vec{R}_j , the unit direction vector between i and j is defined as

$$\vec{R}_{ij} = \vec{R}_j - \vec{R}_i, \vec{e}_{ij} = \frac{\vec{R}_{ij}}{\|\vec{R}_{ij}\|}, \quad (5)$$

The repulsive force reads

$$\vec{F}_{ij}^{\text{rep}} = -m_i k_{ij} \frac{\left(\eta \|\vec{v}_i^0\| + v_{ij}\right)^2}{d_{ij}} \vec{e}_{ij}, \quad (6)$$

with the relative velocity

$$v_{ij} = \Theta \left(\left((\vec{v}_i - \vec{v}_j) \cdot \vec{e}_{ij} \right) \cdot (\vec{v}_i - \vec{v}_j) \cdot \vec{e}_{ij} \right), \quad (7)$$

and the effective distance between i and j

$$d_{ij} = \|\vec{R}_{ij}\| - r_i(v_i) - r_j(v_j). \quad (8)$$

r_i is the polar radius of pedestrian i (Fig. 1).

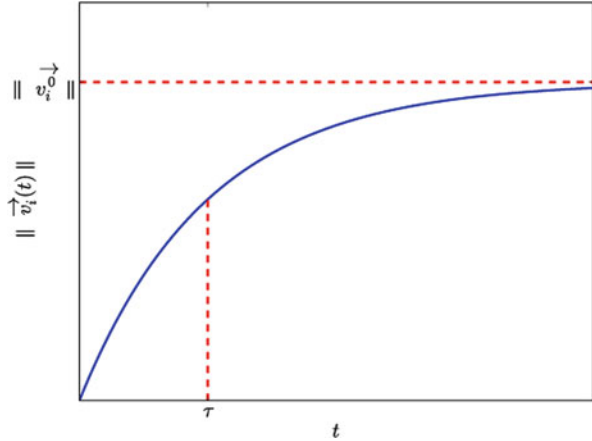
The term

$$k_{ij} = \Theta \left(\vec{v}_i \cdot \vec{e}_{ij} \right) \cdot \left(\vec{v}_i \cdot \vec{e}_{ij} \right) / \|\vec{v}_i\| \quad (9)$$

reduces the action field of the force to 180° in the direction of motion.

The special definition in Eq. 8 with the Heaviside function $\Theta()$ ensures that pedestrian i is less influenced by slower pedestrian than by faster ones.

Fig. 2 Exponential behaviour of the free acceleration



The strength of the force can be adjusted by means of the free parameter η .

The repulsive forces between pedestrians and walls are defined similarly. For further details we refer to [14].

2.2 The Driving Force Towards an Exit

Assuming an exponential nature of pedestrian’s free acceleration [15] the driving force of pedestrian i towards a predefined direction \vec{e}_i^0 is given by

$$\vec{F}_i^{\text{drv}} = m_i \frac{\vec{e}_i^0 \cdot \|\vec{v}_i^0\| - \|\vec{v}_i\|}{\tau}, \tag{10}$$

with a time constant τ . In Fig. 2 the evolution of the free acceleration defined by Eq. 10 is depicted.

This mathematical expression of the driving force is systematically used in all known force-based models and describes well the free movement of pedestrians. The desired direction \vec{e}_i^0 is defined differently depending on the simulated scenario.

3 The Measurement Method

In this work we consider the $\rho - v$ – form of the Fundamental Diagram (FD). Given the trajectory of pedestrian i the velocity v_i reads

$$v_i(t) = \frac{x_i(t + \Delta t) - x_i(t - \Delta t)}{2\Delta t}, \tag{11}$$

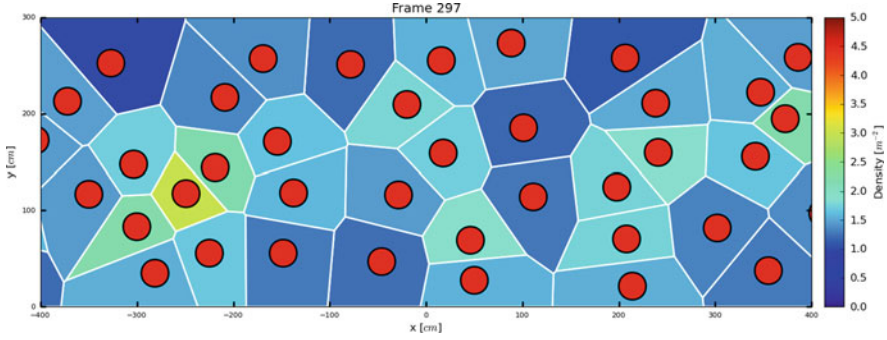


Fig. 3 Voronoi-diagrams for a set of point in the space

with $\Delta t = 10$ s. In order to measure the density, we make use of the Voronoi method. In [17] it was shown this method reduces the fluctuations of the density in a given measurement area. Following, a brief definition of the Voronoi method is given.

For a set of points $(x_i, y_i), i = 1, \dots, n$, one can define a partition of the space, giving cells A_i . Each cell A_i represents the set of points closest to (x_i, y_i) than to all other points $(x_j, y_j), j \neq i$. See Fig. 3.

The density distribution is defined for all pedestrians as

$$p_i(\vec{x}) = \begin{cases} \frac{1}{|A_i|} & : \vec{x} \in A_i \\ 0 & : \text{otherwise.} \end{cases} \tag{12}$$

Integrating the overall density distribution

$$p(\vec{x}) = \sum_{i=1}^n p_i(\vec{x}), \tag{13}$$

over a given measurement area A yields

$$\rho = \frac{\int_A p(\vec{x}) d\vec{x}}{|A|}. \tag{14}$$

The flow through a measurement line during a measurement time of Δt is given by

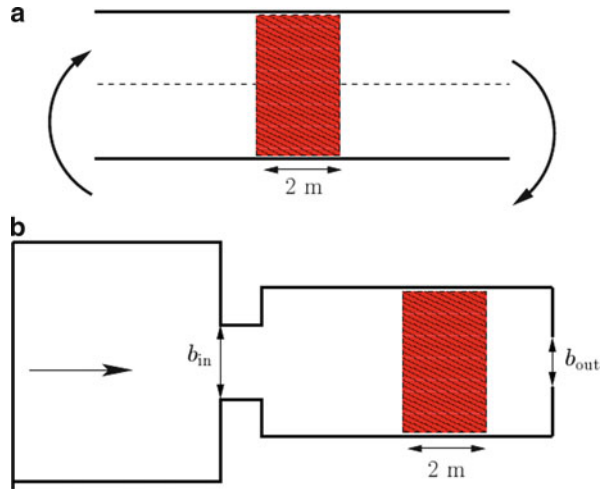
$$J = \frac{N_{\Delta t} - 1}{\Delta t}, \tag{15}$$

where $N_{\Delta t}$ is the number of pedestrian that passed the line in the time period Δt .

Table 1 Parameter set for the simulations of the different scenarios

Parameter	Eq.	Value
η	6	0.2
a_{\min}	3	0.18 m
τ_a	3	0.43 s
b_{\min}	4	0.20 m
b_{\max}	4	0.25 m
τ	10	0.5 s

Fig. 4 Different geometrical scenarios (a) Corridor. (b) Bottleneck



4 Validation and Numerical Results

Simulations in different geometrical scenarios are performed with one set of parameter (Table 1).

The desired speeds of pedestrians are Gaussian distributed with $\mu = 1.34$ m/s and standard deviation $\sigma = 0.26$ m/s. For simplicity, the mass m_i is set to unity.

In Fig. 4. A schematic description of the simulated scenarios is given.

4.1 Single-File Movement

To simulate single-file movement pedestrians are distributed in a corridor along the dashed line (Fig. 4). Since the direction of the forces have no components in the axis perpendicular to the movement direction, the pedestrians perform a one-dimensional movement. In order, to guarantee a steady state we consider closed boundary conditions. Figure 5 shows the result of the simulation in comparison with experimental data.

Fig. 5 FD for one-single movement in comparison with experimental data [18]. Length of the corridor is 25 m

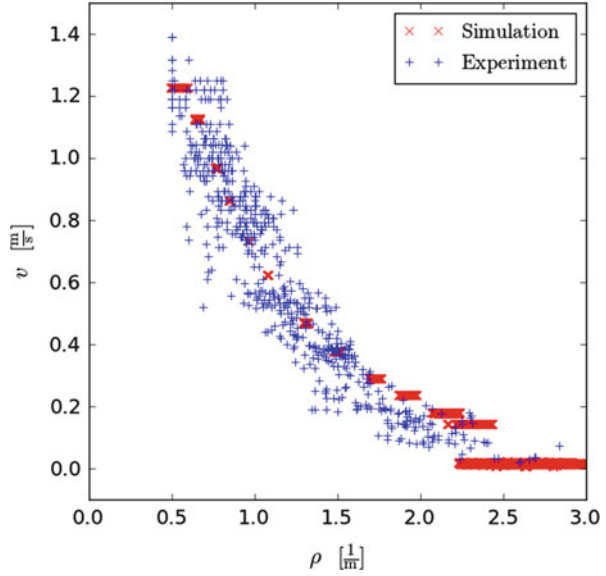
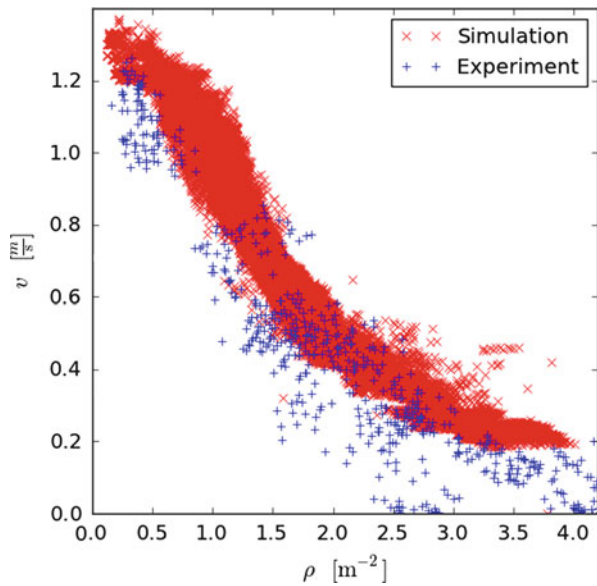


Fig. 6 FD in a 1.8 m wide corridor with closed boundary conditions in comparison with experimental data from the HERMES-project [1, 19]

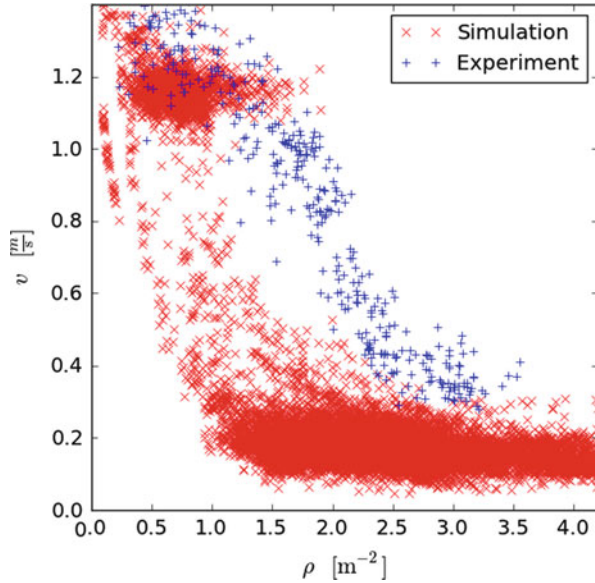


4.2 FD in Wide Corridors Closed Boundary Conditions

In the second step we consider the same corridor with a width of 1.80 m. Initially pedestrians are randomly distributed in the corridor. After 300 s we measure the density in an area of $2 \times 1.80 \text{ m}^2$ situated in the middle of the corridor.

The results of the simulations are presented in Fig. 6.

Fig. 7 FD in a 1.8 m wide corridor with open boundary conditions in comparison with experimental data from the HERMES-project [1, 19]



4.3 FD in Wide Corridors: Open Boundary Conditions

As in Sect. 4.2 we study the movement of pedestrians in wide corridors, but this time with open boundary conditions. In order to produce a wide spectrum of densities it is necessary to trigger the input- and the output flow to the corridor. For this concern we simulate a bottleneck-like geometry with a $1.8 \times 12 \text{ m}^2$ corridor. Similarly to the simulation in Sect. 4.2 the measurement area is situated in the middle of the corridor and is 2 m long and 1.8 m wide. The results of the simulation in comparison with experimental data are shown in Fig. 7.

5 Discussion

In this paper we performed several simulations with the GCFM with the purpose to quantitatively validate its results. The goal of this validation process is to verify whether or not the model is able to describe with one set of parameter the dynamics emerging from different geometrical scenarios.

The first scenario is single-file movement. Here pedestrians move in a narrow 25 m long corridor without overtaking. Considering closed boundary conditions, after 300 s of simulation the system settles on a steady-state. The FD is measured with the Voronoi method, which minimizes scattering in density measurements. The results show good agreement to experimental data. Having a parameter set with which the single-file movement is reproduced; we make the second step

towards wide corridors. The difference of this scenario to the first one is that lateral movement is now observed in the system. Here again the simulated FD show good agreement with the experimental data.

The third step of the validation is considering the same geometrical corridor as in the previous scenario but with open boundary conditions. Here care should be taken then a steady-state system is no longer possible, which may lead to results majorly influenced by initial conditions. Furthermore, it is not obvious to reproduce a wide spectrum of densities by incrementing the number of simulated pedestrians. In order to deal with these issues, especially the second, we considered the same set-up of experiment as performed in HERMES [1]. That is to simulate a bottleneck-like geometry with a 12 m long corridor. The density can be triggered by changing the input and output rate to and from the corridor. The simulation results show relatively good agreement with experimental data. However the FD reacts abruptly on geometrical changes, which increases the discrepancy to the experimental data.

This result is important and makes clear that pedestrian's reaction and their perception of geometrical changes in their neighborhood influences their movement. This component of the human behavior is not yet builds in the GCFM which explains the discrepancy of the FD in corridors with open boundary conditions with experimental data.

Acknowledgement This work is within the framework of two projects. The authors are grateful to the Deutsche Forschungsgemeinschaft (DFG) for funding the project under Grant-No. SE 1789/1-1 as well as the Federal Ministry of Education and Research (BMBF) for funding the project under Grant-No. 13 N9952 and 13 N9960.

References

1. Holl, S., Seyfried, A.: Hermes - an evacuation assistant for mass events. inSiDe, 7(1), 60–61 (2009)
2. Schadschneider, A., Chowdhury, D., Nishinari, K.: Stochastic Transport in Complex Systems. From Molecules to Vehicles. Elsevier Science Publishing Co Inc. (2010)
3. Chattaraj, U., Seyfried, A. and Chakroborty, P. Comparison of pedestrian fundamental diagram across cultures, *Advances in Complex Systems*(3), 393–405, 2009
4. S. P. Hoogendoorn and W. Daamen. Pedestrian behavior at bottlenecks. *Transport. Sci.*, 39(2):147–159, 2005.
5. J. Liddle, A. Seyfried, W. Klingsch, T. Rupprecht, A. Schaschneider, and A. Winkens. An experimental study of pedestrian congestions: Influence of bottleneck width and length. *ArXiv e-prints*, 2009, 0911.4350. Conference proceedings for Traffic and Granular Flow 2009.
6. X. Liu, W. Song, and J. Zhang. Extraction and quantitative analysis of microscopic evacuation characteristics based on digital image processing. *Physica A*, 388(13):2717–2726, 2009.
7. M. Moussaid, D. Helbing, S. Garnier, A. Johansson, M. Combe, and G. Theraulaz. Experimental study of the behavioural mechanisms underlying selforganization in human crowds. *Proc. R. Soc. B.*, 276(1668):2755–2762, 2009.
8. A. Seyfried, M. Boltes, J. Kähler, W. Klingsch, A. Portz, T. Rupprecht, A. Schadschneider, B. Steffen, and A. Winkens. Enhanced empirical data for the fundamental diagram and the flow through bottlenecks. In W. W. F. Klingsch, C. Rogsch, A. Scha schneider, and

- M. Schreckenberg, editors, *Pedestrian and Evacuation Dynamics 2008*, pages 145–156, Berlin Heidelberg, 2010. Springer.
9. J. Zhang, W. Klingsch, A. Schadschneider, and A. Seyfried. Transitions in pedestrian fundamental diagrams of straight corridors and t-junctions. *J. Stat. Mech.*, 2011.
 10. A. Kirchner, K. Nishinari, and A. Schadschneider. Friction effects and clogging in a cellular automaton model for pedestrian dynamics. *Phys. Rev. E*, 67:056122, 2003.
 11. W. J. Yu, L. Chen, R. Dong, and S. Dai. Centrifugal force model for pedestrian dynamics. *Phys. Rev. E*, 72(2):026112, 2005.
 12. D. R. Parisi, M. Gilman, and H. Moldovan. A modification of the social force model can reproduce experimental data of pedestrian flows in normal conditions. *Physica A*, 388(17):3600–3608, 2009.
 13. M. Moussaïd, D. Helbing, and G. Theraulaz. How simple rules determine pedestrian behavior and crowd disasters. *P. Natl. Acad. Sci. USA.*, 108(17):6884–6888, 2011, 1105.2152.
 14. D. Helbing and P. Molnar. Social force model for pedestrian dynamics. *Phys. Rev. E*, 51:4282–4286, 1995.
 15. M. Chraïbi, A. Seyfried, and A. Schadschneider. The generalized centrifugal force model for pedestrian dynamics. *Phys. Rev. E*, 82:046111, 2010.
 16. J. J. Fruin. *Pedestrian Planning and Design*. Elevator World, New York, 1971.
 17. L. A. Pipes. An operational analysis of traffic dynamics. *J. Appl. Phys.*, 24(3):274–281, Mar 1953.
 18. B. Steffen and A. Seyfried. Methods for measuring pedestrian density, flow, speed and direction with minimal scatter. *Physica A*, 389(9):1902–1910, 2010. flow, speed and direction with minimal scatter.
 19. A. Seyfried, M. Boltes, J. Kaehler, W. Klingsch, A. Portz, T. Rupperecht, A. Schadschneider, B. Steffen, and A. Winkens. Enhanced empirical data for the fundamental diagram and the flow through bottlenecks. In W. W. F. Klingsch, C. Rogsch, A. Schadschneider, and M. Schreckenberg, editors, *Pedestrian and Evacuation Dynamics 2008*, pages 145–156, Berlin Heidelberg, 2010. Springer.
 20. A. Schadschneider. I'm a football fan . . . get me out of here. *Physics World*, 21, 2010.

An Econometric-based Model of Pedestrian Walking Behavior Implicitly Considering Strategic or Tactical Decisions

Daisuke Fukuda, Toru Seo, Kaoru Yamada, Hideki Yaginuma,
and Nobuhiro Matsuyama

Abstract We propose an econometric-based model for the behavior of pedestrian walking that implicitly considers strategic or tactical decisions. In real situations, it is only possible to observe pedestrian trajectories and final choices of destination (e.g., the ticket gate they have actually chosen) and the targeted destination en route is latent and unobservable. To reflect this, a model of dynamic latent plans was extensively used by assuming destination choice as a decision at the planning level and walking at the action level. The latent plans (destinations) of pedestrians may dynamically change subject to the environment, leading to a dynamical and structural change in their action choices (walking trajectories).

Keywords Pedestrian walking behavior • Discrete choice model • Plan–action model • Pedestrian tracking • Particle filter

1 Introduction

Analyzing pedestrian behavior is important for the better design of facilities and evacuation planning. As a specific example, congestion in the Tokyo metropolitan railway system is rapidly rising. Not only is congestion annoying but it also has severe social costs such as delayed trains, increased transfer time and safety risks.

D. Fukuda (✉) • T. Seo • K. Yamada

Transport Studies Unit, Tokyo Institute of Technology, Tokyo, Japan

e-mail: fukuda@plan.cv.titech.ac.jp; t.seo@plan.cv.titech.ac.jp; yamada.k@plan.cv.titech.ac.jp

H. Yaginuma

Highway Planning Inc., Tokyo, Japan

e-mail: yaginuma@doro.co.jp

N. Matsuyama

Merrill Lynch Japan Securities, Tokyo, Japan

Congestion can be thought of as a social issue, and reduction measures are widely required. One solution to such pedestrian congestion is the expansion of railway infrastructure (e.g., expansion of pedestrian walkways and installation of extra entrance gates). However, owing to a lack of analysis methods, it is difficult to analyze beforehand the effectiveness of planned measures. Therefore, there is an obvious need to describe pedestrian behavior.

Previous traditional approaches of modeling pedestrian behavior can be classified into two types: (1) cell-based spatial representation (e.g., a cellular automata model); and (2) continuous spatial representation (e.g., a social force model). As a third type, econometric-based pedestrian behavior analysis using a discrete choice model (e.g., [1,2]) has recently attracted attention. This approach is attractive because various factors of walking behavior can be easily incorporated into utility functions and the calibration of model parameters based on econometric theory is rigorous.

Existing econometric pedestrian models, however, only consider walking behavior at the operational level and do not deal with any choice decision at the strategic level (e.g., destination) or tactical level (e.g., route). It is usually assumed that strategic and tactical decisions are made exogenously. In various real situations, however, pedestrians intermittently make a decision to change their destinations or routes. For example, video observation at train stations shows that pedestrians passing through a ticket gate tend to change their target gate en route when the station plaza and the area neighboring the gate are crowded.

Another issue relating to the use of econometric pedestrian modeling is that, in calibration, it is costly to collect pedestrian trajectories, which are usually manually tracked from video sequences. To some extent, automation in data collection of pedestrian trajectories is expected.

In this study, we propose an econometric behavior model of pedestrian walking that implicitly considers strategic or tactical decisions. In real situations, it is only possible to observe pedestrian trajectories and the final choice of destination (e.g., the ticket gate they actually choose) and the targeted destination en route is latent and unobservable. To reflect this, a model of dynamic latent plans [3] is extensively used by assuming the destination choice as a decision at the planning level and walking at the action level. The latent plans (destinations) of pedestrians may dynamically change subject to the environment, leading to dynamical and structural changes in action choices (walking trajectories).

The proposed model is validated with video sequences of pedestrian behavior recorded around a ticket gate at a crowded rail station in Tokyo. For efficient data collection, a generalized state-space modeling approach (particle filter method, see [4]) is applied to automatically track walking behaviors from video sequences. The parameter calibration result indicates that the proposed model fits the real data much better than the simple model of walking behavior. Finally, a pedestrian simulator is implemented and tested to evaluate pedestrian movements at a larger and more crowded station.

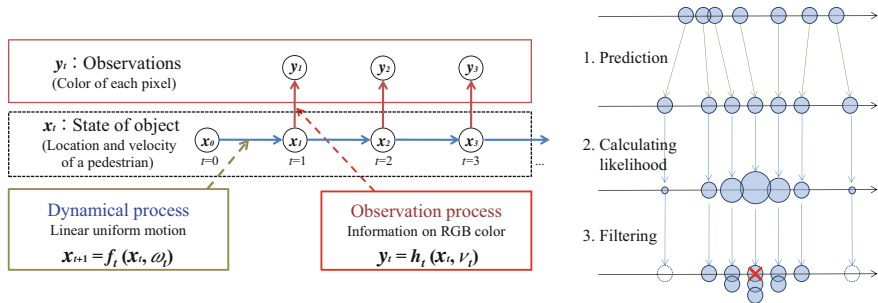


Fig. 1 Process of state-space modeling for pedestrian tracking (left) and particle filter (right)

2 Semi-Automated Data Collection of Pedestrian Trajectories

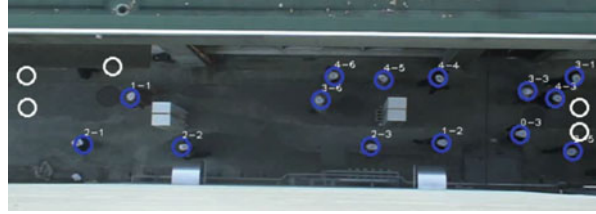
2.1 Outline

We discuss to what extent it would be possible to automate the data collection in pedestrian detection and tracking. To estimate the parameters for our pedestrian behavior model that will be outlined later, we require the trajectory data of each pedestrian. A useful approach to obtain such data is to use dynamic picture images with background subtraction. However, manually tracking pedestrian coordinates is time-consuming work because of the need to extract coordinate data for each person and for each frame of video images. Expanding the versatility of our modeling framework, automation (or semi-automation) of the tracking phase is an important step in our study.

Therefore, we implement an image-processing program that is able to automate pedestrian tracking using a particle filter, which is called condensation in the field of image processing [4]. A particle filter is a form of generalized state-space modeling, the purpose of which is to estimate the state of objects through continuous observations. In our case, the location of a pedestrian corresponds to the state, and RGB brightness data represent the observation (Fig. 1).

A detailed procedure was presented by Yaginuma et al. [5], and the four steps to the algorithm are summarized as follows.

- Step 0 Generate sample particles (i.e., ensembles) according to the initial distribution.
- Step 1 Use the system model to relocate these particles as prediction samples in the next time step.
- Step 2 Weight each prediction sample according to the observation model.
- Step 3 Resample particles considering the weight of each sample.

Fig. 2 Tracked pedestrians

2.2 Tracking Results

We validate the tracking program using a pedestrian experiment video (see Fig. 2). The dynamic picture image has an interval length of 50 s and contains 90 pedestrian trajectories. The detection rate is calculated as 99.8 %. The average difference (error) between the position coordinates obtained by the above-mentioned procedure and the true coordinates is 2.48 pixels, and the standard deviation is calculated as 1.35 pixels, corresponding to 5.46 and 2.97 cm in real space, respectively. These results imply that the proposed algorithm is helpful in pedestrian tracking with a certain level of accuracy. In particular, we compare two methods: the standard background subtraction method and the newly proposed particle filter method.

Although the proposed method would have sufficiently high accuracy to be practically applicable, we find that, to apply the image-processing program, video images should satisfy two requirements: (i) the point of view (angle) needs to be directly above the pedestrian; and (ii) the pedestrian in the video should not be covered by another pedestrian or obstacles. In a real situation such as a station yard or building, however, it would be difficult to obtain videos that satisfy these requirements. Hence, we need to improve our algorithm so that it can be applied to more general videos.

3 Pedestrian Behavior Model

3.1 Concept of a “Plan–Action” Decision Structure

The plan–action model is a recently developed behavioral model (see Choudhury et al. [3] for details). It is a particular formulation of discrete choice models that have been widely used in the analysis of travel behavior.

In the plan–action model, an individual’s behavior is composed of two-step choices: a (latent) plan choice and an (observable) action choice. The plan represents an individual’s specific objective, purpose or goal. Considering the environmental conditions, the subject implicitly chooses one plan. On the other hand, the action is an observable behavior intended to achieve or approach the plan. Therefore,

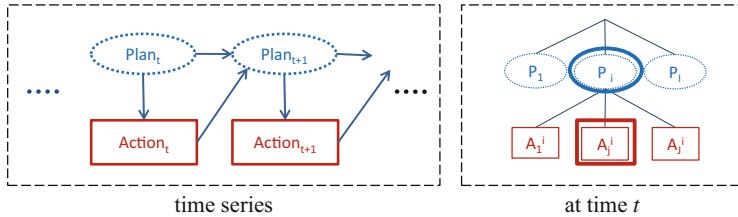


Fig. 3 Concept of the plan–action model

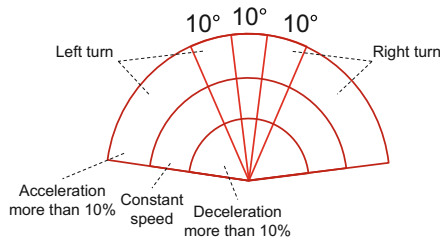


Fig. 4 Pedestrians' action choice set

analysts only know the action result, and cannot know which plan is actually chosen. However, it is estimable which plan is likely to explain the current action (Fig. 3).

3.2 Pedestrian Behavior Model Based on Random Utility

In our study, the plan choice is assumed to be a pedestrian’s destination choice, and the action choice is regarded as a pedestrian’s movement (route) to approach their chosen destination.

The plan model takes the form of a multinomial logit model (MNL; see [6]) that can consider various factors such as the distance to the target destination, declination between the current movement and the destination, and congestion level near the destination. The action behavior, on the other hand, can be taken as walking behavior. We apply a pedestrian behavior model by extensively applying the work of Antonini et al. [1], which is also based on a discrete choice model. The behavior model hypothesizes that pedestrians choose their direction and speed at the next instant from the choice set shown in Fig. 4. All pedestrians choose their movement for each period of 0.5 s. In our study, we also apply the MNL to action choice behavior.

The choice probabilities of the plan and action are formulated as

$$P_{plan}(i) = \frac{\exp(V_{plan}(i))}{\sum_{i=1}^5 \exp(V_{plan}(i))}, \tag{1}$$

$$P_{action}(j|i) = \frac{\exp(V_{action}(j|i))}{\sum_{j=1}^{15} \exp(V_{action}(j|i))}, \quad (2)$$

where i is the plan alternative, j is the action alternative, V_{plan} is the utility for the plan and V_{action} is the utility for action. In our case study, we assume five latent plans and 15 actions (Fig. 4).

Since the plan choice result is not observable, we consider the joint probability of action j of pedestrian n at time t for any possible plan as

$$P_n(j_t) = \sum_{i_t=1}^5 P_{action}(j_t|i_t) P_{plan}(i_t). \quad (3)$$

In parameter estimation for utilities, the corresponding log-likelihood for all samples is defined as

$$L = \sum_{n=1}^N \sum_{t=1}^{T_n} \ln \sum_{i_t=1}^5 P_{action}(j_t|i_t) P_{plan}(i_t) \quad (4)$$

By maximizing the log-likelihood, it is possible to estimate parameters in utility functions for both plan and action.

4 Model Calibration

4.1 Data Collection

Data collection was carried out at the Tama-Plaza station in the Tokyo Metropolitan Area, where there are many commuters. This station has a terrace over its ticket gates, and it is thus easy to observe pedestrian movements and interactions near the ticket gates. We took several video images around the ticket gates (Fig. 5).

4.2 Model Specification

The utility functions are specified as

$$V_{plan}(i) = \beta_{gap} dist_i \Delta angle_i + \beta_{congestion} congestion_i + I_{out} \beta_{oneway}, \quad (5)$$

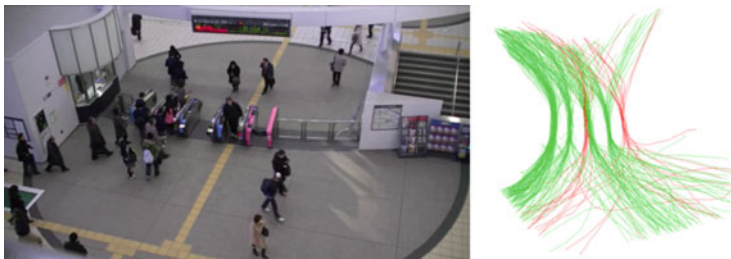


Fig. 5 View of the Tama-Plaza station (left) and examples of pedestrian trajectories (right)

Table 1 Estimation summary

		Type	Name	Value	Std. err.	t-test	p-value
		Plan	β_{gap}	-0.352	0.317	-1.117	0.264
		Plan	$\beta_{congestion}$	-2.799	2.376	-1.178	0.239
		Plan	β_{oneway}	17.952	16.235	1.106	0.269
		Action	β_{dist}	-0.087	0.015	-5.658	0.000
		Action	$\beta_{angle, little}$	-0.627	0.053	-11.85	0.000
		Action	$\beta_{angle, large}$	-2.086	0.112	-18.58	0.000
Number of parameters	11	Action	β_{acc}	-68.258	3.317	-20.58	0.000
Number of samples	1740	Action	β_{dec}	-23.339	1.919	-12.19	0.000
Initial log-likelihood	-4537.4	Action	β_{wall}	10.417	0.899	11.58	0.000
Final log-likelihood	-3386.4	Action	$\beta_{collider}$	6.141	2.876	2.135	0.033
ρ^2	0.254	Action	β_{leader}	0.617	0.745	0.828	0.408

$$\begin{aligned}
 V_{action}(j|i) = & \beta_{dist}dist_j + I_{angle, little}\beta_{angle, little} + I_{angle, large}\beta_{angle, large} \\
 & + I_{acc}\beta_{acc}\left(\frac{v}{v_{max}}\right)^{2.42} + I_{dec}\beta_{dec}\left(\frac{v}{v_{max}}\right)^{2.42} \\
 & + \beta_{wall}walldist_j + \beta_{collider}colliderdist_j + \beta_{leader}leaderdist_j,
 \end{aligned}
 \tag{6}$$

where β values are unknown parameters, $dist_i$ is the distance to the gate, $\Delta angle_i$ is the angle difference, $congestion_i$ is the level of crowding, I_{**} are the dummy variables for each particular situation, $walldist_j$ is the distance to the wall (obstacles), $colliderdist_j$ is the distance to the collider, and $leaderdist_j$ is the distance to the leader. All parameters are of reasonable sign and value (Table 1).

5 Simulating Pedestrian Behavior

5.1 Medium-Scale Simulation

To check our model’s reproducibility, we develop a pedestrian simulator that represents our data collection site (around the ticket gate at the Tama-Plaza station).

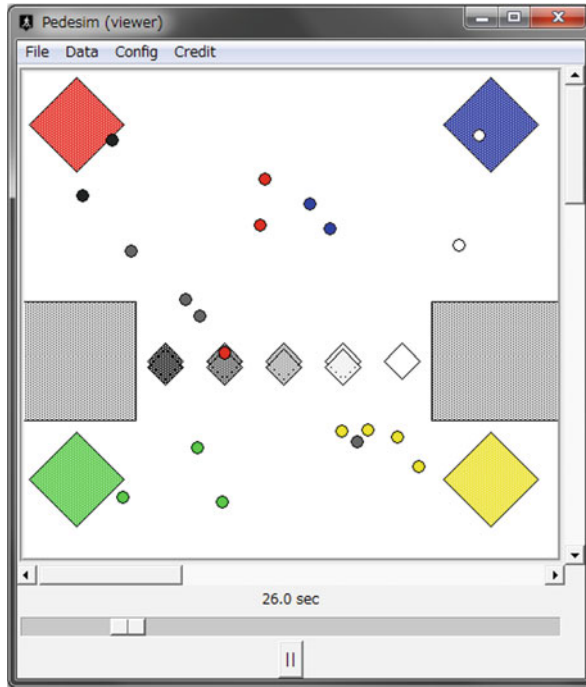


Fig. 6 The simulator

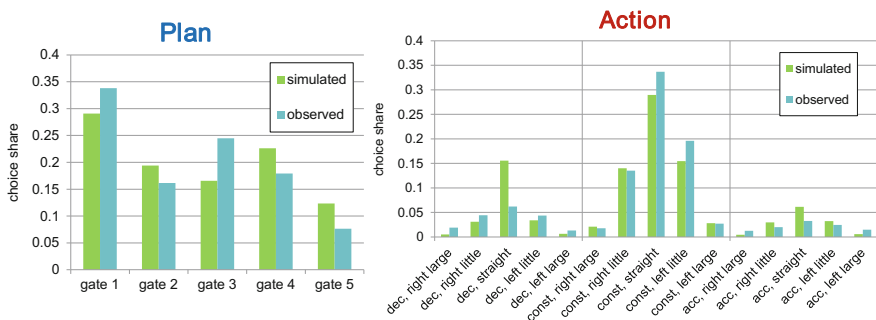


Fig. 7 Reproducibility check for the plan and action

Figure 6 is a snapshot of the simulator. The two gray squares denote walls, the diamonds are destinations such as ticket gates and entrances, and small circles represent pedestrians.

Figure 7 shows the predictive accuracy of the proposed model. The tendency of choice share seems to be roughly the same between simulation and observation. In particular, the most frequently used ticket gate is simulated as gate #1 as in the real world.

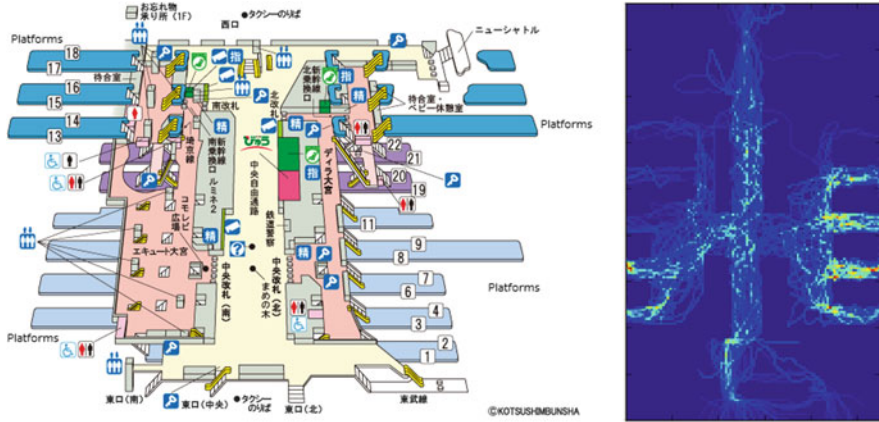


Fig. 8 Plan of Oomiya station (Source <http://www.jreast.co.jp/estation/stations/350.html> left) and simulation results of the pedestrian distribution (right)

5.2 Large-Scale Simulation

We further test our model and simulator for a large-scale station (Oomiya station). Oomiya station is one of the largest stations in Japan. There are 12 platforms and 320,000 users per day.

Figure 8 shows the plan of Oomiya station and the results obtained with the simulator. The simulation results show the pedestrian distribution during the entire simulation period. It is seen that the most congested areas are the stairs leading to the platforms.

6 Conclusions

We proposed an econometric-based model for the walking behavior of pedestrians that implicitly considers strategic or tactical decisions. A model of dynamic latent plans was extensively applied to model pedestrian behavior at rail stations by assuming the destination choice as a decision at the planning level and walking at the action level.

References

1. Antonini, G., Bierlaire, M., Weber, M.: Discrete choice models of pedestrian walking behavior. *Transportation Research Part B: Methodological*. 40 [8], 667–687 (2006)
2. Robin, T., Antonini, G., Bierlaire, M., Cruz, J.: Specification, estimation and validation of a pedestrian walking behavior model. *Transportation Research Part B: Methodological*. 43 [1], 36–56 (2009)

3. Choudhury, C., Ben-Akiva, M., Abou-Zeid, M.: Dynamic latent plan models. *Journal of Choice Modelling*. 3 [2], 50–70 (2010)
4. Isard, M., Blake, A.: Condensation–conditional density propagation for visual tracking. *International Journal of Computer Vision*. 29 [1], 5–28 (1998)
5. Yaginuma, H., Fukuda, D., Yamada, K., Matsuyama, N.: Automated pedestrian data collection for the estimation of discrete-choice-based pedestrian behavior model. *Journal of Japan Society of Civil Engineers, Ser. D3*. 67 [5], I_787–I_800 (2011)
6. Ben-Akiva, M., Lerman, S.: *Discrete Choice Analysis: Theory and Applications to Travel Demand*. MIT Press, Cambridge (1985)

An Empirically-Grounded Emergent Approach to Modeling Pedestrian Behavior

Stephane Bonneaud and William H. Warren

Abstract Realistic models of locomotion, accounting for both individual pedestrian behavior and crowd dynamics, are crucial for crowd simulation. Most existing pedestrian models have been based on ad-hoc rules of interaction and parameters, or on theoretical frameworks like physics-inspired approaches that are not cognitively grounded. Based on the cognitively-plausible behavioral dynamics approach, we argue here for a bottom-up approach, in which the local control laws for locomotor behavior are derived experimentally and the global crowd behavior is emergent. The behavioral dynamics approach describes human behavior in terms of stable, yet flexible behavioral patterns. It enabled us to build an empirically-grounded model of human locomotion that accounts for elementary locomotor behaviors. Based on our existing components, we then elaborate the model with two new components for wall avoidance and speed control for collision avoidance. We show how the model behaves with many stationary obstacles and interacting agents, and how it can be used in agent-based simulations. Five scenarios show how complex individual behavioral patterns and crowd dynamics patterns can emerge from the combination of our simple behavioral strategies. We argue that our model is parsimonious and simple, yet accounts realistically for individual locomotor behaviors while yielding plausible crowd dynamics, like lane formation. Our model and the behavioral dynamics approach thus provide a relevant framework for crowd simulation.

Keywords Empirically-grounded model • Pedestrian behavior • Behavioral dynamics • Individual based model

S. Bonneaud (✉) • W.H. Warren

Virtual Environment and Navigation Laboratory, Department of Cognitive, Linguistic, and Psychological Sciences, Brown University, Providence, RI, USA
e-mail: stephane_bonneaud@brown.edu

1 Introduction

Crowd simulation would greatly benefit from models accounting reliably for both individual pedestrian behavior and crowd dynamics. The ability to accurately reproduce human locomotor dynamics and paths of travel, as well as self-organized patterns of crowd dynamics is necessary for urban planning, disaster management, or any research and application requiring artificial pedestrians to mimic human behavior [26]. As has recently been emphasized [18, 22, 26], realistic crowd simulation calls for stronger theoretical and empirical grounding in principles inspired by cognitive science research. Yet, as of today, building a realistic model, demonstrating that a model is realistic, or quantifying the extent to which it is realistic, are unsolved problems. When modeling crowd dynamics, one may measure and try to reproduce global crowd parameters, and yet the resulting individual trajectories can be highly unrealistic. We argue for a converse bottom-up approach, in which the local control laws for locomotor behavior are derived experimentally and the global crowd behavior is emergent, and also evaluated empirically. Such a generative model will not only produce accurate trajectories at the individual level, but is also likely to yield realistic collective behavior.

Thus, our focus here is on modeling human locomotor behavior, and investigating the properties of crowd behavior that emerges from local interactions. The first challenge to modeling locomotion is understanding the dynamics of an individual interacting with its environment to move toward goals and avoid obstacles. Hence, the modeling needs to be grounded in observations of human locomotion and based on theoretical principles governing human perception and action [27]. The second challenge is understanding what makes a model realistic, when it is impossible to validate its predictions in all possible crowd scenarios of locomotion. Hence, the model not only needs to behave realistically in particular scenarios, but it needs to capture the general behavioral dynamics of human locomotion [28]. Arguably, a prominent feature of human locomotion is our capacity to effortlessly locomote in highly unpredictable environments with stable, yet flexible behavioral patterns. In consequence, we believe that the theoretical framework of the model has to describe human behavior in broader terms than those of locomotion only, and should provide cognitively plausible conceptual tools for modeling stable, yet flexible behavior.

Most existing pedestrian models have been based on ad-hoc rules of interaction and parameters [18, 24], or on theoretical frameworks like physics-inspired approaches that are not cognitively grounded [13]. Recently, articles introducing approaches inspired by cognitive science and psychology have led the way to more plausible simulations [21, 23]. Moussaïd et al. [21] advocate in particular for a synthetic modeling of the pedestrian perception system providing information to cognitively inspired heuristics controlling the movement. Their Gibsonian description of the agent's perception system [11], which others [23] have also advocated, explicitly base visual control on the information provided by the optic flow [29]. Ondrej et al. [23] went further in linking their model to the theory and data by arguing for a dynamical approach to modeling locomotion and by using behavioral

strategies found in the cognitive science literature, namely the constant bearing strategy for avoiding obstacles [5, 28] and the tau-dot strategy for decelerating to avoid collisions [19, 30]. In doing so, these models have been able to simulate a rich range of behavioral patterns, from the individual level of the pedestrian to patterns of collective behavior in crowds. Yet, while providing more plausible models, these approaches haven't shown why and to what extent they produce realistic patterns of crowd dynamics based on empirical observations. Furthermore, their assumptions are not always consistent with human data, e.g. the path of least energy hypothesis [21] may not fully account for preferred human trajectories [9], and the use of the constant bearing strategy [23] rather than a heading error strategy [7] to steer toward a stationary goal leads to unrealistic spiral trajectories.

By experimentally deriving the local control laws for locomotor behavior, we built a model that generates reliable individual trajectories in the general locomotor scenarios of moving towards a goal, while avoiding stationary and moving obstacles. The model is motivated by the cognitively-plausible behavioral dynamics approach [27], which synthesizes the ecological approach to perception [12] and the dynamical approach to action [15, 17]. The behavioral dynamics approach aims to provide a theoretical framework that accounts for the stable and flexible nature of human behavior. Applied to locomotion, it translates into a parsimonious model accounting for general human locomotor dynamics [7, 8, 28]. In this presentation, we first briefly describe the behavioral dynamics approach. Then, we describe our locomotion model and the control laws for four elementary locomotor behaviors. Finally, we show how the model can be used in agent-based simulations of crowd scenarios, including *many* stationary obstacles and *many* interacting agents. We discuss the performances of our model in terms of behavioral patterns in the context of computer simulation and animation.

2 A Behavioral Dynamics Approach to Locomotion

The behavioral dynamics approach [27] is an ecological, emergent, and distributed approach to behavior. Based on the ecological approach to perception and action [12], the individual is seen as coupled to its environment through information and control variables, such that action is governed by behavioral strategies or control laws. The locomotor trajectory is not prescribed by an internal planning process, but emerges from the interactions of the individual agent with its environment. The temporal evolution of behavior is thus not determined by either the agent or the environment alone, but control is distributed across both, through the conjunction of the agent-environment state, given the task constraints and the effective control laws. As such, control lies in the agent-environment system [12] and is distributed and self-organized.

The coupling between the agent and the environment is both mechanical, through forces exerted by the agent, and informational, through information fields in the environment that specify the state of affairs to the agent. From that coupling emerges

a pattern of behavior, with a dynamics characterized by stable states, bifurcations, hysteresis, attractors and repellers. As such, the approach characterizes the agent-environment interaction as a dynamical system, and the unfolding behavior as a trajectory in the state space of the system. It is this emergent behavior that is called the behavioral dynamics [27].

Locomotor behavior is thus treated as a particular case of agent-environment coupling. Understanding locomotion dynamics in this framework means explicating (1) the visual information used by the agent and (2) the control laws that use this information to modulate the agent's action so as to reach a goal while avoiding obstacles. To derive and test hypotheses about the informational variables and control laws, we depend on controlled experiments with human participants in real and virtual worlds [7, 8]. The results yield control laws of locomotion, which can then be implemented in model simulations of human behavior.

3 A Pedestrian Model

3.1 Empirically-Grounded Components

Both the theory and the empirical observations enabled us to describe a parsimonious model using behavioral rules under different environmental conditions that humans use when locomoting in an environment. We propose to decompose locomotion into a set of elementary behaviors that can be modeled individually. As a first approximation, these include (a) steering to a stationary goal, (b) avoiding a stationary obstacle, (c) intercepting a moving target, and (d) avoiding a moving obstacle. Subsequently, we hypothesize components for (e) wall following and (f) speed control. Our strategy [7] is to model each elementary behavior as a nonlinear dynamical system and then attempt to predict human behavior in more complex environments by linearly combining these components. We determined the behavioral variables as the heading (ϕ) or direction of travel of the agent (with respect to an allocentric reference axis), and the current turning rate ($\dot{\phi}$), assuming for the moment a constant speed of travel v .

The general idea of the model is to consider the directions of goals and obstacles as attractors and repellers, respectively, for the agent's heading. The simplest description of steering toward a stationary goal is for the agent to align its heading ϕ with the direction of the goal ψ_g , that is to bring the target-heading angle to zero ($\phi - \psi_g = 0$) as it moves forward, which defines an attractor in state space at $[\phi, \dot{\phi}] = [\psi_g, 0]$. The law controlling the angular acceleration of the agent's heading is then:

$$\ddot{\phi} = -b\dot{\phi} - k_g(\phi - \psi_g)(e^{-c_1 d_g} + c_2) \quad (1)$$

First, the equation is a second order dynamical system with a damping term $-b\dot{\phi}$, because a first-order system generates a turning rate that is unrealistic and unconstrained. Second, the backbone of the behavioral strategy is found in the term $k_g(\phi - \psi_g)$ which serves to null the heading error. Finally, a distance term $(e^{-c_1 d_g} + c_2)$ exponentially decreases the goal's attraction with distance d_g ; the (positive) c_2 constant keeps it greater than zero, making the goal always attractive whatever the distance.

Conversely, for a stationary obstacle that lies in a bearing direction (ψ_o) at a distance d_o , the simplest description of obstacle avoidance is to magnify the obstacle-heading angle $(\phi - \psi_o > 0)$, which defines a repeller at $[\phi, \dot{\phi}] = [\psi_o, 0]$. The dynamics of angular acceleration induced by the obstacle is given by:

$$\ddot{\phi}_o = k_o(\phi - \psi_o)(e^{-c_3|\phi - \psi_o|})(e^{-c_4 d_o}) \quad (2)$$

where $k_o(\phi - \psi_o)(e^{-c_3|\phi - \psi_o|})$ is the underlying law, specifying an exponential decay of the repulsion as the agent turns away from the obstacle and the obstacle-heading angle increases, so the agent bypasses the obstacle rather than spinning around. $(e^{-c_4 d_o})$ is the distance term. If the agent encounters an obstacle en route to a goal, these two components are superposed, such that the agent turns away from the obstacle locally while simultaneously attempting to null the heading error with the goal. The agent's path thus emerges from the evolving competition between attractors and repellers as it moves through the environment.

Steering toward a moving goal turns out to yield a different solution from the stationary case. Rather than turning toward the target, pedestrians try to keep the target in a constant bearing direction [3, 5, 20, 27] as it moves forward. Sailors have long used this strategy: if another ship remains at a constant compass bearing, one is on a collision course. The law controlling the agent's heading is thus to null change in the bearing direction of the moving target (ψ_m) :

$$\ddot{\phi} = -b\dot{\phi} + k_m\dot{\psi}_m(d_m + c_1) \quad (3)$$

$(d_m + c_1)$ is a simple linear distance term, which compensates for the decrease in angular velocity with target distance; c_1 prevents the target's influence from dropping to zero as distance decreases.

Conversely, for a moving obstacle, the agent follows the inverse strategy by avoiding a constant bearing with the obstacle.

$$\ddot{\phi}_{mo} = k_{mo}(-\dot{\psi}_{mo})(e^{-c_5|\dot{\psi}_{mo}|})(e^{-c_6 d_{mo}}) \quad (4)$$

The term $k_{mo}(-\dot{\psi}_{mo})(e^{-c_5|\dot{\psi}_{mo}|})$ constitutes the core of the strategy, which serves to repel the agent's heading from the collision point, again with an exponential decay in repulsion as the agent turns away. The distance term $(e^{-c_6 d_{mo}})$ exponentially reduces the repulsion with distance from the target. In addition, we implemented

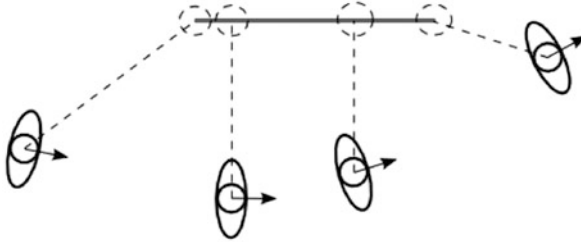


Fig. 1 An individual considers a barrier as a punctual obstacle which position depends on its relative position to the barrier. The figure shows different points on the barrier with which the individual is interacting depending on its own position

this component so the repulsion would drop to zero as the agent passed the obstacle, when the obstacle-bearing angle was greater than $\pi/2$: $\left(1 - \frac{\text{sgn}(|\phi - \psi_{mo}| - \frac{\pi}{2}) + 1}{2}\right)$.

3.2 Wall Avoidance

We have considered several models to account for how humans interact with walls, e.g. walls are treated as a set of point-obstacles whose repulsion is a weighted distribution along the barrier length [10], or as a solid obstacle with a repulsion term based on the barrier's visual angle [14]. Our model accounts for obstacle avoidance in general terms, and we propose to have agent interact with walls using an analogous control law. As shown in Fig. 1, we make the assumption that an individual interacts with a “virtual” point-obstacle, that corresponds to the wall's closest point. This point is treated as a repeller for the agent's heading following the stationary obstacle component described previously. A similar approach was used in other models, including Helbing's original model [13]. We are in the process of testing it against human data.

3.3 Tau-Dot Based Speed Control

Lee [19] showed that the visual system might control behavior based on the temporal proximity of objects, rather than their distance per se. He showed that the time-to-collision with an object is specified by its relative rate of optical expansion, the optical variable “tau”, under certain conditions. Further, the rate of change in this variable, “tau-dot”, can be used to prevent collision by decelerating to hold tau-dot constant at a value of -0.5 [19]. As shown in [16, 30], the tau-dot strategy seems to be used by humans to control deceleration during braking, even when spatial information is available (but see [6] for a related strategy).

We propose here to use a strategy equivalent to the tau-dot strategy to provide agents with a speed control and collision avoidance component. For purpose of simulation, we compute the equivalent value of deceleration from physical variables [30] (Appendix A12), rather than using the tau-dot variable itself as input. This differs in its formulation and implementation from [23] a compact model with an exponential function of tau-dot. Let's consider an agent walking with an object in its field of view. The general idea is for the agent to adopt a preferred speed v when there is no risk of imminent collision, and to decelerate to avoid collision based on \dot{z} when the object is in its path. We therefore express the dynamics on \dot{v} as follows:

$$\dot{v} = s_g (v_{pref} - v) - s_o \frac{v^2}{2z} e^{(-c_s|\phi-\psi|)} \quad (5)$$

With z the distance to the perceived object, v the agent's velocity, ϕ the agent's heading, and ψ the bearing angle with the perceived object. s_g , s_o , and c_s are constants.

The first term, $s_g(v_{pref} - v)$, describes an attractor for the agent's speed in state space at $[v, \dot{v}] = [v_{pref}, 0]$. The second term computes the required deceleration $s_o \frac{v^2}{2z}$. The term $e^{(-c_s|\phi-\psi|)}$ exponentially increases as the obstacle-heading angle ($\phi - \psi$) goes to zero. Its formulation comes from our moving obstacle component, making the agent slow down only if the risk of collision is located in front of it.

4 Simulations

Fajen and Warren [7,8] and Warren and Fajen [28] extensively review and detail how the model accounts for observations of human behavior. Therefore, we propose to show how adding our wall avoidance and tau-dot-like components produce credible simulations of pedestrian locomotion. And, we study five complex scenarios of crowd behavior. Three scenarios focus on interactions between pedestrians walking in corridors. The last two focus on a pedestrian finding its way on a crowded plaza with (1) N stationary obstacles, and then (2) M agents walking in various directions.

4.1 Elementary Scenarios of Interaction

(Scenario S1) *Travel in a corridor*

This scenario sets an agent at one end of a corridor with its goal outside of the corridor at the opposite end. The corridor is made up of six short walls, making up a winding corridor structure. The agent is initially located at the entrance of the corridor, and its goal is positioned so that the agent, following the walls of the corridor, in some places has to walk away from the goal's position. Figure 2a shows the resulting spatial trajectory of the agent, which is centered in the first segment of

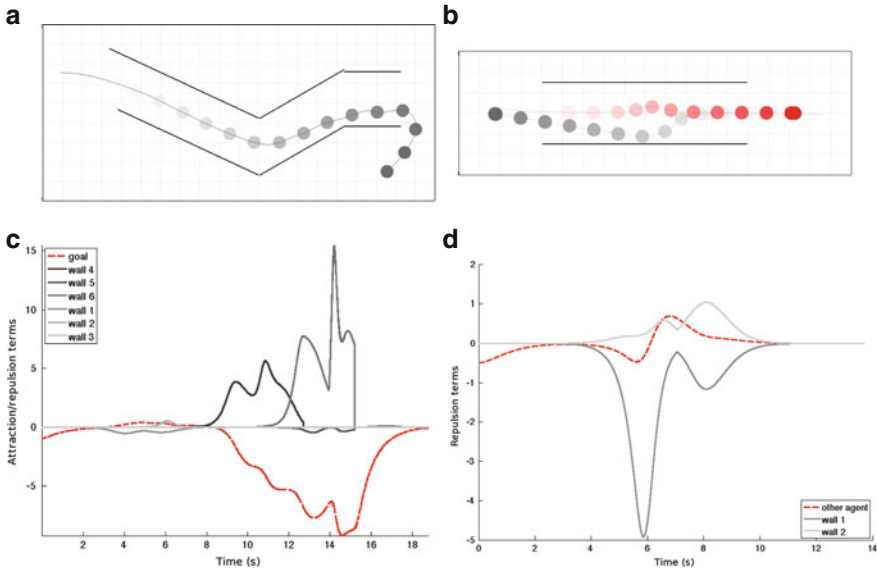


Fig. 2 Scenarios S1 (*left*) and S2 (*right*). **(a)** and **(b)** Agent spatial trajectories for S1 and S2: agent locations are visualized with colored disks, which value is function of time: most recent locations have the highest color value. **(c)** and **(d)** Time series of the model’s components (attraction and repulsion terms) for S1 and S2. On the *left*, temporal evolution of wall repulsion (*grey plots*) and goal attraction (*red plot*). On the *right*, temporal evolution of the wall repulsion (*grey plots*) and other agent repulsion (*red plot*)

the corridor and then follows one wall until it reaches the corridor’s end and turns towards its goal. Figure 2c represents the temporal evolution of wall repulsion and goal attraction: the time series of the repulsion components for each of the six walls are in grayscale, and that for the attraction of the goal is in red. Walls 4 and 5, which are located between the agent and the goal, provide the dominant repulsion components.

(Scenario S2) Two pedestrians walking towards each other in a corridor

Two agents are set at each end of a linear corridor (3 m wide and 10 m long) with their respective goals at the opposite end. The agents’ initial positions are centered in the corridor, but noise is introduced to slightly randomize their initial locations and initial headings. Figure 2b shows sample spatial trajectories. We can see that the agents avoid each other while also remaining within the corridor’s walls. Figure 2d takes the perspective of the “red” agent in Fig. 2b, and shows the time series of each of its obstacle avoidance components. We can see how its repulsion from the other agent evolves in time, and how its behavior is influenced. As the “red” agent tries to avoid the other agent, the repulsion of the walls increases.

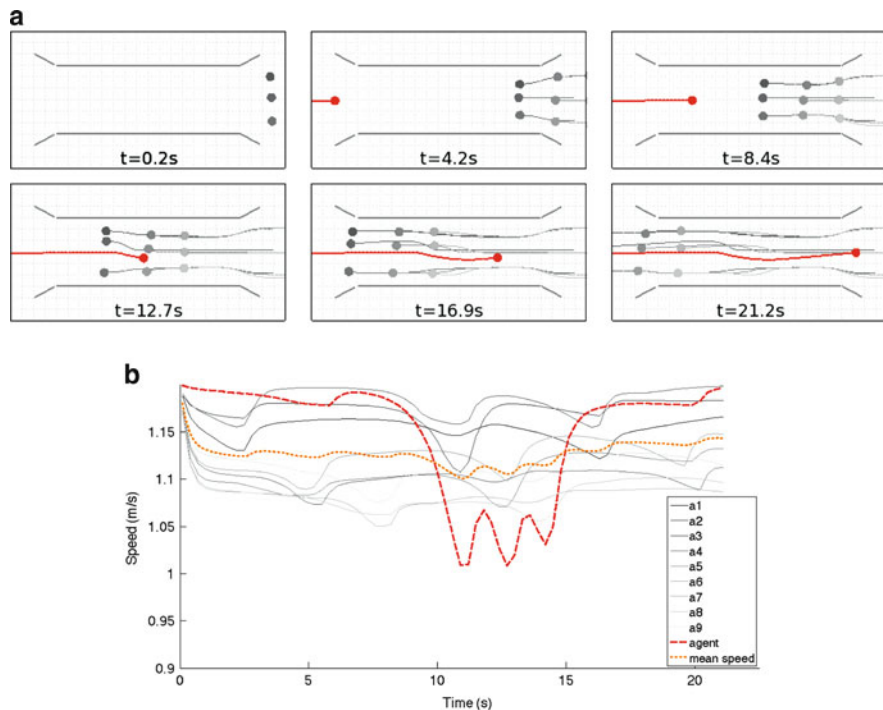


Fig. 3 Scenario S3. (a) Snapshots of different simulation time steps showing the spatial trajectories and positions of the different agents. (b) Speed time series, for the agents in the group in grey, and the “red” agent in red; the orange plot is the mean speed of all agents

4.2 Complex Scenarios of Interaction

(Scenario S3) One pedestrian passing through a crowd in a corridor

This scenario is comparable to scenario 2 except that a group of nine agents is at one end of the corridor. Figure 3a shows the evolution in time of the simulation. Results show how the agent on the left finds its way through the middle of the group, and how the others avoid it while remaining within the corridor. Figure 3b shows the speeds of each agents. The red plot shows the time series of the speed of the “red” agent in the top figures, and the orange plot is the time series of the mean speed of all agents. In this figure, gray level codes the position of agents in the group, with the darkest grays indicating the front row. At the beginning of the trial, all agents slow down very slightly when entering the corridor. The front row keeps a nearly constant speed, whereas the second and third rows slow down more to avoid the front row. As the front row moves ahead, the second row slowly increases its speed, followed by the third row. As the group meets the “red” agent coming from the opposite direction, the front row slows down and moves aside – particularly a2,

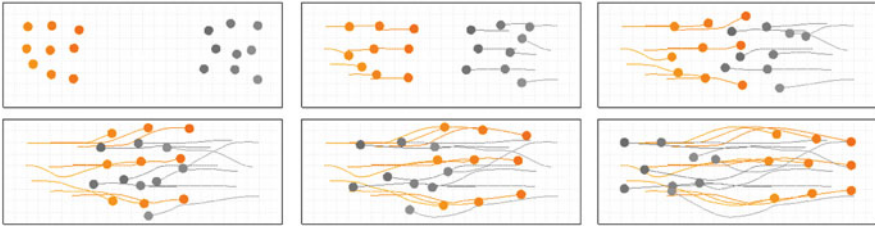


Fig. 4 Scenario S4. Snapshots of different simulation time steps showing the spatial trajectories and positions of the agents

avoiding a head-on collision – followed by the second and third rows as they avoid agents who have moved in front of them.

(Scenario S4) *Two crowds passing through in opposite directions*

The scenario puts two groups of nine agents each walking towards each other. Their positions and headings are initialized with a slight noise to generate more irregular group configurations. Figure 4 shows the evolution in time of the agents' spatial trajectories. Note that agents naturally form lanes.

(Scenario S5) *N stationary obstacles*

In this scenario, 30 stationary obstacles are randomly distributed in between the initial position of the agent and its goal. Figure 5a shows how the agent finds its way through the obstacles.

(Scenario S6) *M moving obstacles*

Finally, the last scenario shows how an agent finds its way in an hall where many other agents are walking. Four flows of agents are used as shown in Fig. 5b. Each flow is set on one of the side of the hall and generates agents that have to cross the hall to a goal on the other side. The figure shows how agents steer through the crowd toward their respective goals without collisions.

5 Discussion

We argue that our model is parsimonious, with few parameters. Each component is based on empirical data and built in the coherent theoretical framework of behavioral dynamics. Components have fixed parameters, and generalize to new scenarios. Only the parameter of the distance term c_6 of the moving obstacle component has been slightly modified to account for the dynamics of small groups, and we are currently investigating this collective behavior [1, 2, 25]. Both the theoretical approach and the components therefore provide a fruitful ground for finding realistic description of human behavior in complex scenarios of locomotion. We show that our model produces plausible individual trajectories in various

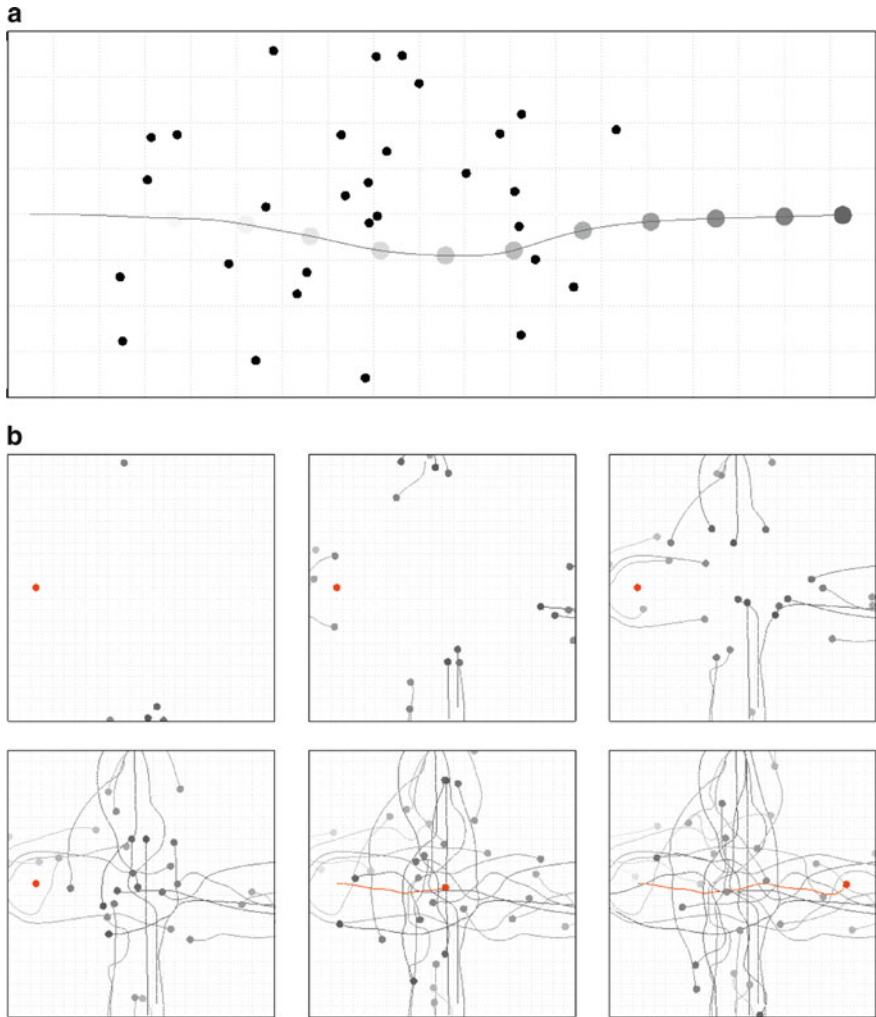


Fig. 5 Scenarios S5 (*top*) and S6 (*bottom*). (a) Agent spatial trajectories (low color value corresponds to older timesteps) with black disks corresponding to stationary obstacles. (b) Snapshots of different time steps showing agent spatial trajectories and positions

scenarios from wall avoidance to crowd dynamics. The different scenarios show that agents follow walls without collision (S1), even when avoiding oncoming agents (S2). Individual agents exhibit smooth trajectories around obstacles with plausible paths to their goals (S5), even in highly dynamic environments (S6). Scaling up to groups of agents, the model still produces plausible trajectories. Groups smoothly split to avoid oncoming agents (S3), or intermingle without collisions, self-organizing into lanes (S4).

Yet, further studies of human behavior are required. The wall avoidance component is not based on observations of human behavior. And it is unknown how humans interact with walls in different situations: walls may be alternatively wide obstacles to walk around or long barriers to follow. The tau-dot-like strategy is based on human experiments, but our component is not fully linked to data, and the ratio of deceleration to turning still has to be adjusted to recent observations [4]. While humans avoid collisions by both decelerating and changing their heading, how they combine these two strategies is currently being modeled. The behavioral dynamics approach explains how locomotion emerges from the interactions of the agent with its environment, and, in this case, that the combination of speed and heading control is an online process from which emerges the locomotor path. And as the agent turns to avoid a collision, it might have to slow down less, or as it slows down, it might have to turn less. The model, by combining simple strategies, yields complex agent behavioral patterns. Yet, complex human behavioral patterns are still not described and quantified sufficiently to know if we fully account for them.

Arguing for the realism of a locomotion model for crowd simulation is still an unsolved problem. Our four elementary components account for individual locomotor paths in various scenarios. As such, these elementary components provide a platform for the design of new components. For obstacle avoidance for instance, our component has been built using observations of individuals interacting with poles, i.e. obstacles that can be assimilated to punctate objects. With more complex objects, e.g. a long table, it is likely that the stationary obstacle components have to be revised. This may have a cognitive reality, and if humans have simple behavioral strategies to locomote, they probably use them from within highly adaptive behaviors. Last, we show that our model scales up smoothly to scenarios of crowd dynamics and reproduces in particular lane formation patterns. Yet, crowd dynamics in general requires further empirical study, e.g. we don't know how to fully characterize lane formation. Further experimental investigation of patterns of crowd dynamics is necessary, which we have started doing with small groups of pedestrians [1, 2, 25].

6 Conclusion

One of the main issues in crowd simulation is the lack of human data to constrain and validate pedestrian models. We described here a locomotion model grounded in observations of human behavior, that generates the same spatial trajectories as humans in four elementary tasks. We then elaborated our model with two new components to account for wall avoidance and speed control for collision avoidance. These two components were not built directly from observations of human walking as were the four others. For the wall avoidance component, we assumed our elementary stationary obstacle component to be a general formulation for avoiding the closest point on the obstacle. For the speed control component, we used a tau-dot-like strategy based on human data for the control of braking [30]. We then

formulated these components within the behavioral dynamics framework, inspired by our previous model [28].

Finally, we showed how our model generates plausible trajectories and crowd patterns. Our two new components for wall avoidance and speed control for collision avoidance produce realistic results and scale up smoothly with several agents avoiding each other while remaining inside a corridor. Scenarios of crowd dynamics show that our model scales up when many agents are simulated. Smooth spatial trajectories of groups of agents intermingling without collisions show realistic patterns like lane formation. Yet, further observations and characterization of patterns of crowd dynamics are required. However, we believe that building an empirical model of individual locomotor behavior and using it, bottom-up, to account for emergent crowd behavior is a promising path to a realistic model of crowd dynamics. In this effort, a scientific theoretical framework accounting for the dynamics of human perception and action [27] offers a coherent modeling framework. By deriving the components from empirical data, we can maintain the parsimony of the model while accounting for human behavior.

References

1. Bonneaud, S., Rio, K., Chevaillier, P., Warren, W.: Accounting for patterns of collective behavior in crowd locomotor dynamics for realistic simulations. In: Z. Pan, A. Cheok, W. Muller, M. Chang, M.E. Zhang (eds.) *Transactions on Edutainment VII, LNCS*, vol. 7145, pp. 1–12. Springer, Heidelberg (2011)
2. Bonneaud, S., Warren, W.H., Chevaillier, P.: Multi-agent modeling of the collective behavior of groups of pedestrians. 2012 (in preparation)
3. Chardenon, A., Montagne, G., J Buekers, M., Laurent, M.: The visual control of ball interception during human locomotion. *Neuroscience Letters* **334**(1), 13–16 (2002)
4. Cohen, J.A., Bruggeman, H., Harrison, H., Warren, W.H.: Behavioral dynamics of moving obstacle avoidance. 2012 (in preparation)
5. Cutting, J.E., Vishton, P.M., Braren, P.A.: How we avoid collisions with stationary and moving obstacles. *Psychological Review* **102**, 627–651 (1995)
6. Fajen, B.: Calibration, information, and control strategies for braking to avoid a collision. *Journal of Experimental Psychology: Human Perception and Performance* **31**(3), 480–501 (2005)
7. Fajen, B.R., Warren, W.H.: Behavioral dynamics of steering, obstacle avoidance, and route selection. *Journal of Experimental Psychology: Human Perception and Performance* **29**, 343–362 (2003)
8. Fajen, B.R., Warren, W.H.: Behavioral dynamics of intercepting a moving target. *Experimental Brain Research* **180**, 303–319 (2007)
9. Fajen, B.R., Warren, W.H.: Route selection in complex scenes emerges from the dynamics of steering and obstacle avoidance. Poster at the VSS 2010 conference, Naples, Florida (2010)
10. G erin-Lajoie, M., Warren, W.H.: The circumvention of barriers: Extending the steering dynamics model. *Journal of Vision* **8**(6), 1158a (2008)
11. Gibson, J.: Visually controlled locomotion and visual orientation in animals. *Ecological Psychology* **10**, 161–176 (1998). (Reprinted from *British J. of Psychology*, 49, 182–194, 1958)
12. Gibson, J.J.: *The ecological approach to visual perception*. Lawrence Erlbaum (1986)
13. Helbing, D., Moln r, P.: Social force model for pedestrian dynamics. *Physical Review E* **51**, 4282–4286 (1995)

14. Huang, W.H., Fajen, B.R., Fink, J.R., Warren, W.H.: Visual navigation and obstacle avoidance using a steering potential function. *Robotics and Autonomous Systems* **54**, 288–299 (2006)
15. Kelso, J.A.S.: Dynamic patterns: the self-organization of brain and behavior, chap. Intentional dynamics, pp. 137–158. MIT Press (1995)
16. Kim, N.G., Turvey, M., Carello, C.: Optical information about the severity of upcoming contacts. *Journal of Experimental Psychology: Human Perception and Performance* **19**(1), 179–193 (1993)
17. Kugler, P., Turvey, M.: Information, natural law, and the self-assembly of rhythmic movements. Hillsdale, NJ: Lawrence Erlbaum Associates (1987)
18. Lakoba, T.I., Kaup, D.J., Finkelstein, N.M.: Modifications of the helbing-molnár-farkas-vicsek social force model for pedestrian evolution. *Simulation* **81**, 339–352 (2005)
19. Lee, D.N.: A theory of visual control of braking based on information about time-to-collision. *Perception* **5**, 437–459 (1976)
20. Lenoir, M., Musch, E., Janssens, M., Thiery, E., Uyttenhove, J.: Intercepting Moving Objects During Self-Motion. *Journal of Motor Behavior* **31**(1), 55–67 (1999)
21. Moussaid, M., Helbing, D., Theraulaz, G.: How simple rules determine pedestrian behavior and crowd disasters. *Proceedings of the National Academy of Sciences of the United States of America* **108**(17), 6884–6888 (2011)
22. Moussaid, M., Perozo, N., Garnier, S., Helbing, D., Theraulaz, G.: The walking behaviour of pedestrian social groups and its impact on crowd dynamics. *PLoS ONE* **5**(4), e10,047 (2010). DOI 10.1371/journal.pone.0010047
23. Ondrej, J., Pette, J., Olivier, A.H., Donikian, S.: A synthetic-vision based steering approach for crowd simulation. *ACM Transaction on Graphics* **4:123** (2010)
24. Reynolds, C.W.: Flocks, herds, and schools: A distributed behavioral model. In: *Proceedings of the SIGGRAPH conference* (1987)
25. Rio, K., Warren, W.H.: A data-driven model of pedestrian following and emergent crowd behavior. In: U. Weidmann, U. Kirsch, E. Puffe, M.e. Weidmann (eds.) *Pedestrian and Evacuation Dynamics*. Springer, Heidelberg (2012)
26. Thalmann, D., Musse, S.R.: *Crowd simulation*. Springer (2007)
27. Warren, W.: The dynamics of perception and action. *Psychological review* **113**, 358–389 (2006)
28. Warren, W., Fajen, B.: Behavioral dynamics of visually guided locomotion. In: A. Fuchs, V. Jirsa (eds.) *Coordination: Neural, Behavioral and Social Dynamics, Understanding Complex Systems*, vol. 17, pp. 45–75. Springer Berlin / Heidelberg (2008)
29. Warren, W.H., Kay, B.A., Zosh, W.D., Duchon, A.P., Sahuc, S.: Optic flow is used to control human walking. *Nature Neuroscience* **4**, 213–216 (2001)
30. Yilmaz, E.H., Warren, W.H.: Visual control of braking: a test of the $\dot{\tau}$ hypothesis. *Journal of Experimental Psychology: Human Perception and Performance* **21**, 996–1014 (1995)

Calibrating a General Pedestrian Stream Simulation Model According to a Specific Real Life Scenario of a German Railway Station

M. Davidich and G. Köster

Abstract Pedestrian stream simulations are used to mitigate risks for people in buildings and at public events. They allow gaining virtual experience for situations where it is impossible to gather real experience. At some point even short term predictions may become possible. However, simulations remain useless if the simulation tool does not reliably reproduce the true phenomena. Hence, one of the biggest challenges in the applied research field of crowd motion is the validation of the proposed models. Up to now very little data from real-life scenarios has been available and calibration attempts have mostly relied on literature values or, at best, laboratory measurements. Instead, we propose to extract key data from live video records as a part of a methodological approach that makes possible to calibrate a simulation tool against video data. We re-enact a real-life scenario observed at a major German railway station with a benchmark simulator and compare the results to the video observations to give a proof of concept for our approach.

Keywords Pedestrian simulation • Cellular automata • Real-life scenario • Validation

1 Introduction

Pedestrian stream simulations have become an integral part of planning public buildings and large events [1–7, 10]. They are seen as means to mitigate risk for life and limb of people visiting buildings or attending public mass events. Their

M. Davidich (✉)

Siemens AG, CT PRO, Virtual Design, Otto-Hahn-Ring, 6, 81739 Munich, Germany
e-mail: maria.davidich@siemens.com

G. Köster

University of Applied Sciences, Lothstr. 64, 80335 Munich, Germany

strength lies in the number of scenarios that their user can virtually enact to gather insight, in cases when it would be uneconomical, unethical or simply impossible to gain real experience.

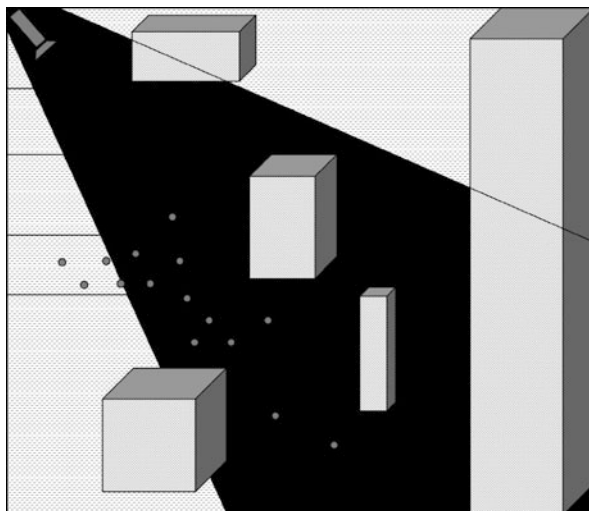
Another, yet largely unachieved goal is to produce short time predictions from real-time simulations. A time frame of only 3 min may be sufficient to act in many cases, e.g. when a station manager is faced with the decision, whether to allow a full train into an already full station. In real-time simulations of pedestrian behaviour live data is collected and a simulator is calibrated against the actual scenario. Geometry, occupation and even fundamental diagrams are used as input to enable predictions on the evolution of the scenario. But how do we know whether the prediction is trustworthy? When we re-enact a real-life scenario in a computer simulation, we expect that at least the important characteristics of the scenario are reproduced. Unfortunately most calibration attempts are still based on literature data or laboratory experiments that remain to some extent artificial and deal with isolated phenomena. Extracting data from the real-life observations is necessary to gather evidence that a complete scenario with its more varied aspects will be also reliably reproduced [8, 13–18].

In this paper we present a holistic approach to solving this problem: We gather video data through video cameras (in our example installed at a German railway station) and then combine data collection, data analysis and calibration of simulation against data from live scenario to ensure high quality predictions of pedestrian flows. In particular, we look at the free-flow velocities of pedestrians and the fundamental diagram and discuss their deviation from the classic literature values on density-flow relationships compiled in [19]. The proposed methodology is then applied to one of our sample videos. We then re-enact the scenario in a benchmark simulator and compare the evolution of the density of the simulation experiment to the performed measurements in several observation areas.

2 Gathering Data for the Scenario: A German Railway Station

We used partly automated video tracking to estimate pedestrian paths, walking speeds, schedules of appearance and disappearance of pedestrians. The examined area includes several platforms and a part of the station's main hall (Fig. 1). All data is anonymous: A single person has the size of a few pixels. We analyzed two video recordings, each of it is about 1.5 min long with about 400 paths on each video. Some trajectory parts are obscured by obstacles or far off. The obscured and distorted trajectories were excluded from the analysis. Detailed analysis of the velocity distribution and deceleration of pedestrians with increasing density was restricted to fully visible and undistorted parts. A schematic view of the experiment is shown in Fig. 1.

Fig. 1 Schematic representation of a video measurement: The *black area* corresponds to the examined area, the position of a camera is schematically shown at the *left corner*. The platforms are represented with *lines* and are on the *left part* of the scenario. The *grey parallelepipeds* correspond to the obstacles. The *grey points* are the schematic representation of pedestrian positions



3 The Benchmark Simulation Tool

As a benchmark simulation we use a simulation based on cellular automation. We choose the cellular automation approach for its simplicity and speed, especially for large scenarios with thousands of persons and difficult topology. The detailed description of our simulation can be found in [20, 21]. Here, we describe the main ideas of the model.

The whole simulation area is covered with cells. Each cell has two states: it is either empty or occupied. It can be occupied by a person, an obstacle or a source or a target. The source denotes a place from where pedestrians enter a scenario, and a target denotes pedestrian destinations. The cells have a hexagonal shape that allows pedestrians to move in six different directions. The cell size is 53 cm, which corresponds to the average shoulder width of European males.

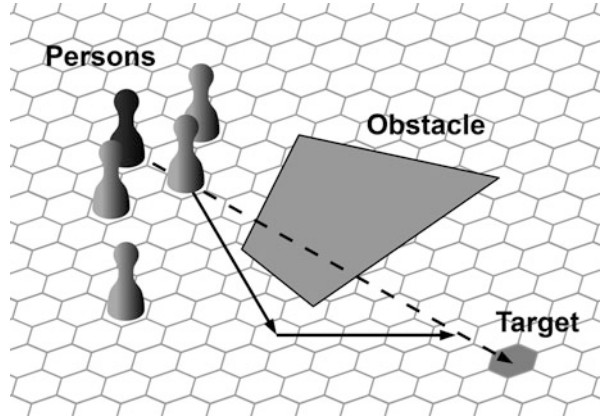
To each pedestrian a combination of potentials is applied (Fig. 2):

- A target potential, i.e. a person tries to achieve its destination/target.
- Repulsive forces of obstacles.
- Repulsive forces of other pedestrians.

These potentials are added to receive a resulting potential for each cell at each time step. Each virtual pedestrian tries to get to his or her destination and moves in accordance with a sequential update scheme, which makes collisions impossible. The speed of motion depends on the individual pedestrian speed, i.e. the speed when the path in the direction of movement is free. If there are other people present in the direction of movement, pedestrians have to decelerate.

A lot of attention was paid to the calibration of the model. A detailed description can be found in [21].

Fig. 2 Pedestrians move on a grid with hexagonal cells towards a target. Persons, targets and obstacles occupy cells. Positions are updated sequentially in each simulation step, so that collision is impossible



4 Realistic Calibration According to Video Data

In order to adjust a simulation to a certain real life scenario, as a first step, a set of relevant parameters should be selected, that capture the most vital phenomena.

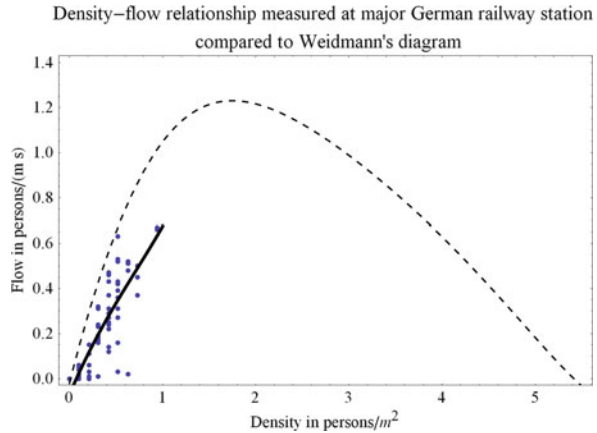
4.1 Free-Flow Velocity

It is often assumed that the distribution of pedestrian free-velocities has a Gaussian form, and that the average velocity is 1.34 m/s with a standard deviation of 0.26 m/s. The extracted data from the video footage of the railway station scenarios also suggests a normal distribution of the velocities. However, the measured velocities deviate from the standard 1.34 m/s value. The pedestrians at the railway station tend to walk slower, with an average velocity of 1.04 m/s and a standard deviation of 0.51 m/s. All results are shown for video recordings which were taken in the late afternoon at around 5.30 p.m. on a working weekday.

4.2 Flow-Density Dependence

Pedestrians tend to decelerate as density increases. When no additional information is available, it is often assumed that pedestrians decelerate in accordance with the Weidmann's fundamental diagram [19]. However, recent investigations show that deceleration can vary and depends on many factors such as, for example, nationality [22]. Information on how pedestrians decelerate is necessary to reproduce a scenario in a simulation. It is crucial especially for critical scenarios in which high densities and inability of pedestrians to move may lead to a disaster.

Fig. 3 Measured density-flow relationship at the German railway station compared to Weidmann's diagram (*dashed line*). *Dots* are the measured values of flow for a certain density. The maximum difference in flow between Weidmann's data (already given in a smooth form) and the measured data is 0.4 persons/ms. Densities above 1 person/m² did not occur. The *solid line* is a smooth approximation of the measured data



Our measurements taken at the station show that pedestrians decelerate differently than one would expect based on Weidmann's diagram. Again, the analyzed video recordings were taken during a working day at around 5.30 p.m. The results are shown in Fig. 3: The pedestrians decelerate stronger than in Weidmann's fundamental diagram. The algorithm used to calibrate our simulation model against measured flow-density diagrams is described in detail in [21].

4.3 Schedule of Pedestrians Entering and Leaving of the Scenario

The schedule of pedestrians entering and leaving is usually individual for every specific scenario. It is necessary to insert virtual pedestrians into the simulation so that it fits the scenario and to adequately remove them from the simulation.

Apart from the parameters mentioned above and the schedule of pedestrian entering and leaving of the scenario, statistical information on the distribution of trajectories and information on topology must be included into the calibration:

5 Comparison of Measured Data to Simulation Results

Once the steps described in the calibration section are completed, a comparative simulation can be started. In our case we conducted the statistical analysis described above and constructed a fundamental diagram that fits the measured data. The scenario we re-enact was recorded during the rush hour in the afternoon. A train arrives on a platform (on the left side of Fig. 4), passengers exit the train and move to different destinations to the subway entrances, food stalls, elevators and other

Fig. 4 Snapshot of a simulated scenario. *Circles* correspond to pedestrians. *Lines* represent contours of obstacles and source and target location. The *rectangle* covered by a *grid* shows the area of observation

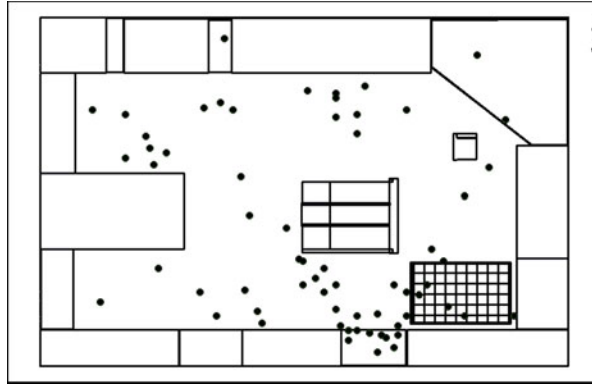
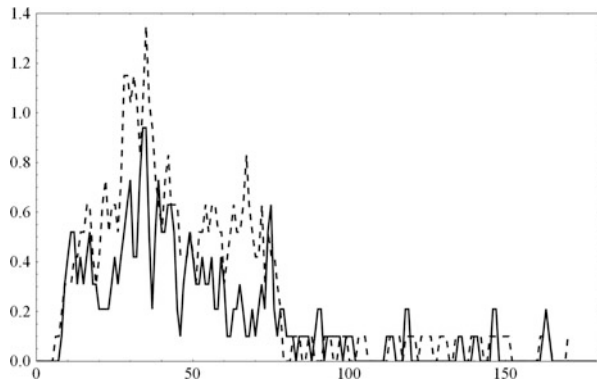


Fig. 5 Comparison of measured densities from video footage (*solid line*) simulated densities (*dashed lines*) when pedestrians are inserted into the scenario with the source/target distribution, free-flow velocities and the density-flow relationship measured at the start of the scenario. 180 s (3 min) are simulated



platforms. Clearly, the density is low at first. When the bulk of the crowd appears, a higher pedestrian density is measured for 3 min; afterwards no more passengers come from the platform. The density goes down again.

Figure 5 shows a comparison of simulated to measured densities in a time span of 3 min. Solid lines correspond to the video footage, dashed lines to the simulation. The peak density occurs in the proper area of observation, at the correct time, for the correct duration and in the correct order of magnitude, but is some-what higher than in reality. This can be partially explained by the influence of random choices in the simulation regarding velocities of the virtual pedestrians and their destinations: Only the distributions of the input and measurement parameters coincide. We also suspect that the real pedestrians coordinate their movements better than the virtual pedestrians. The virtual pedestrians are quite ‘short sighted’ and take steps to avoid collision only when they actually ‘feel’ the potential of other pedestrians. Real pedestrians are more likely to plan ahead. This is a typical disadvantage of high speed pedestrian stream simulators that need to restrict influences to the near field, so-called greedy algorithms, to keep computation times low.

The question is whether this systematic overestimation is acceptable. If we are interested in a warning system for potentially dangerous densities, than a slight overestimation can be tolerated, whereas underestimations would be unacceptable.

6 Discussion and Next Steps

In this paper, we analyzed video data gathered from the complex real-life scenario at the major German railway station and calibrated a benchmark simulation tool according to the measured data. The density evolution of the simulated data well matches the measured data in the area of observation. In that sense, the paper constitutes a proof of concept. Short term predictions of crowd densities are therefore possible, within a certain range of applications, if one carefully adjusts the input parameters to the measured parameters.

References

1. Proulx, G.: Occupant Response During a Residential High-Rise Fire, *Fire and Materials*, 23, 317–323 (1999)
2. Fruin, J. J.: *Pedestrian Planning and Design*. (Revised Edition), Elevator World, Inc., Mobile, AL (1987)
3. Pauls, J.: Movement of People. In: P.J.DiNenno, C. L. Beyler, R. L. P. Custer, W. D. Walton, J. M. Watts, D. Drysdale, and J. R. Hall (Eds.), *The SFP*
4. *Handbook of Fire Protection Engineering* (Second ed., pp. 3-263–3-285). Society of Fire Protection Engineers, Bethesda, MD (1995)
5. Nelson, H. E. and Mowrer, F. W.: Emergency Movement. In: P.J.Denno & W. D. Walton (Eds.), *The SFPE Handbook of Fire Protection Engineering* (Third ed., pp. 3-367–3-380). Society of Fire Protection Engineers, Bethesda, MD (2002)
6. Proulx, G.: Movement of People: The Evacuation Timing. In: P.J.DiNenno & W. D. Walton (Eds.), *The SFPE Handbook of Fire Protection Engineering* (Third ed., pp. 3-341–3-366). Society of Fire Protection Engineers, Bethesda, MD (2002)
7. Kuligowski, E. D. and Peacock, R. D., Review of Building Evacuation Models, Technical Note 1471, Natl. Inst. Stand. Technol., Gaithersburg, MD (2005)
8. Rogsch C. Vergleichende Untersuchungen zur dynamischen Simulationen von Personströmen, Diplomarbeit an der Bergischen Universität Wuppertal (2005).
9. Nagel K. and Schreckenberg M.: A Cellular Automaton Model for Free-way traffic. *J. Phys. I France*, 2, 2221–22229 (1992)
10. Hamacher H.W. and Tjandra S.A.: *Mathematical Modelling of Evacuation Problem: A State of the Art*. Springer Verlag (2002)
11. Burstedde C., Klauck K., Schadschneider A and Tittartz J.; Simulation of Pedestrian Dynamics Using a 2-dimensional Cellular Automaton. *Physica A*, 295 (4), 507–525 (2001)
12. John A., Schadschneider A., Chowdhury D., Nishinari K.: Characteristics of Ant-inspired Traffic Flow: Applying the social insect metaphor to traffic models. *Swarm Intelligence*, 2, 25–41 (2008)
13. A. Schadschneider, A. Seyfried: Empirical Results for Pedestrian Dynamics and their Implications for Cellular Automata Models, A. Schadschneider and A. Seyfried. In:

- H. Timmermans (ed.), *Pedestrian Behavior: Data Collection and Applications*, pp. 27–43, Emerald Group Publishing Limited, 2009.
14. Kretz T., Wölki M, Schreckenberg M, Characterizing correlations of flow oscillations at bottlenecks. *Journal of Statistical Mechanics: Theory and Experiment*, P02005, 2006.
 15. Johansson, A., Helbing, D., Al-Abideen, H. Z., and Al-Bosta, S. From crowd dynamics to crowd safety: A video-based analysis, *Advances in Complex Systems* 11 (4), 497–527, 2008.
 16. Johansson A., Helbing D., Shukla P.K.: Specification of the Social Force Pedestrian Model by Evolutionary Adjustment to Video Tracking Data. *Advances in Complex Systems. Advances in Complex Systems*, 10(4), 271–288 (2007).
 17. Hoogendoorn, SP, & Daamen, W (2004). Design assessment of Lisbon transfer stations using microscopic pedestrian simulation. In Allen, J, CA Brebbia, RJ Hill, G Sciutto & S Sone (Eds.), *Computers in railways IX (Congress Proceedings of CompRail 2004)*, Dresden, Germany, May 2004 (pp. 135–147). Southampton: WIT Press.
 18. Schadschneider A., Klingsch W., Kluepfel H, Kretz T, Rogsch C. and Seyfried A: Evacuation Dynamics: Empirical results, Modeling and Applications. *Encyclopedia of Complexity and System Science*, Robert A. Meyers (Ed.), Springer, 2009, ISBN 978-0-387-75888-6, Vol. 3 pp. 3142 (2009)
 19. Weidmann U. *Transporttechnik für Fussgänger*. Schriftenreihe des IVT, 90, 1992.
 20. Klein W., Koester G. and Meister A.: *Towards the Calibration of Pedestrian Stream Models*, *Lecture Notes in Computer Science: PPAM 2009*. Springer Verlag, 2010.
 21. Davidich M, Köster G, *Towards Automatic and Robust Adjustment of Human Behavioral Parameters in a Pedestrian Stream Model to Measured Data*, *Safety Science* 50 (2012), pp. 1253–1260.
 22. Chattaraj U, Seyfried A, Chakroborty P.: *Comparison of Pedestrian Fundamental Diagram Across Cultures*. *Advances in Complex Systems*, 12(3), pp. 393–405, 2009

Cognition-oriented Simulation of Pedestrian Dynamics

Perceptually Driven Social Force Model

Wassim Abu Abed and Volker Berkhahn

Abstract In this paper the basic preliminary form of a cognitive egocentric dynamic mathematical representation of the proximate surrounding space as perceived by humans is introduced. In this context the social force model as an example of a CAE tool is reconsidered on three different level of modelling reality: the physical level, cognitive quasi-physical level and the cognitive level. Bridging the gap between the flexibility of human representations and the precision and clarity of physical or computerised representations is a major advantage of this approach.

Keywords Cognition • Spatial perception modelling • Fuzzy sets • Social force model • Pedestrian dynamics

1 Introduction

For the simulation of pedestrian dynamics a wide variety of simulation models exists representing these dynamics analogous to physical systems. Despite the fact that most of the models currently in use reproduce many of the available empirical observations of pedestrian dynamics relatively good, the physical origin and nature of the observation strategies and the modelling approaches are responsible for an inevitably incomplete and insufficient representation of the observed system. A major reason is that the complicated behaviour of human beings cannot be realistically reproduced by just applying a physical scheme of stimulus and reaction. Significant research is still needed for a realistic simulation of pedestrian behaviour that is not rigidly coupled to the stimuli of the outside world, but rather a result of the internal cognitive processes. The reproduction of the missing flexibility

W.A. Abed (✉) • V. Berkhahn

Institute of Computer Science in Civil Engineering, Leibniz Universität Hannover, Hannover, Germany

e-mail: abuabed@bauinf.uni-hannover.de; berkhahn@bauinf.uni-hannover.de

of the human cognition and the resulting behaviour is an important development for compensating the limited analogy between pedestrian dynamics and physical processes in the mathematical models so far in use.

In this paper an egocentric dynamic mathematical representation of the proximate surrounding space as perceived by humans is presented. Motivated by the fact that human cognitive activities are approximate rather than precise in nature, the representation is based on the theory of fuzzy sets. This pedestrian-centred dynamic representation of the surrounding is then integrated in a modified version of the well-known social force model to result in a perceptually driven motion model of pedestrians.

2 Modelling the Spatial Human Perception

Spatial perception is one of the key cognitive activities of human beings. Sight and hearing are the primary senses responsible for the spatial perception of the surroundings. External stimuli usually find their way to the spatial cognitive system of a human being through this mental, physiological capability. Hence, spatial perception is an important foundation of the behaviour of pedestrians and has the primary function in facilitating interactions between the individual and its environment. The spatial representation of the environment, so far in use in the current physically inspired simulation models of pedestrian dynamics, takes a bird's-eye view of the surroundings. The exact positions, size and motion is represented in a precise Euclidean geometry. This representation satisfies the purpose of describing a motion model, but it does not help to facilitate the modelling of a perceptually guided interaction between individuals and their environment. A spatial representation from a human standpoint or perspective is needed. Each individual pedestrian interprets the spatial information he perceives in terms of his own subjective frame of reference. In contrast to the precise representation used in motion models, the desired spatial perceptual representation should take into account the subjective interpretation of the surroundings and the associated state of mind or feeling emphasising internal processes not resulting directly from the stimulus input. In the following a basic mathematical formulation for such a spatial representation is introduced.

2.1 Basic Mathematical Formulation

Hypothesis Suppose $\overline{PS} \subset R^2$ is the subset of the two-dimensional Euclidean space that represents the portion of space that is confined by a geometric engineering representation of the proximate surrounding of a human being. Since the cognitive process of the spatial localisation and orientation begins with recognising

and identifying, i.e. perceiving, the different objects comprising the proximate surrounding, let $o_i(t) \subset \overline{PS}$ be the n perceived objects with $i = 1, \dots, n$, and let the set

$$PS(t) := \{o_i(t) \subset \overline{PS} \mid i = 1, \dots, n\} \tag{1}$$

be the set of the perceived dynamic proximate surrounding. Note that the set $PS(t)$ depends on time t , since a set $o_i(t)$ can change over time, if it represents a moving object, such as another moving human being or a moving vehicle. The position of the reference human being who is perceiving her proximate surrounding is defined as the set

$$P_{ego}(t) \subset \overline{PS}. \tag{2}$$

Note that this set is also dependent on time, since the reference human being usually changes its position over time. A cognitive egocentric subjective dynamic mathematical representation of the proximate surrounding space as perceived by humans is then given by the set

$$SPeAr(t) := \left\{ \vec{d}_{ego,i} \in \tilde{V} \mid \vec{d}_{ego,i} := T(P_{ego}, o_i) : \{P_{ego}\} \times PS \rightarrow \tilde{V} \right\}. \tag{3}$$

$\vec{d}_{ego,i}$, with $i = 1, \dots, n$, are the natural egocentric vector coordinates and \tilde{V} is the set of fuzzy vectors. For more information on fuzzy sets and vectors see [1].

Basic Representation A preliminary basic representation of $\vec{d}_{ego,i}$ in the one-dimensional case is given in the following for demonstration purposes. Nonetheless, it is still a hypothetical representative example of how $\vec{d}_{ego,i}$ would look like in the context of this theoretical description.

In the scenario considered in Fig. 1 the position of the reference human being is given as the set $P_{ego}(t) = [\vec{x}_{min,ego}(t), \vec{x}_{max,ego}(t)]$. The positions of the perceived objects, a moving human $o_1(t)$ and an exit o_2 , are given in the form of the interval $o_i(t) = [\vec{x}_{min,i}(t), \vec{x}_{max,i}(t)]$. The natural egocentric vector coordinates

$$SPeAr(t) := \left\{ \vec{d}_{ego,1}, \vec{d}_{ego,2} \right\} \tag{4}$$

are given as $\vec{d}_{ego,i} := \left\{ (\vec{\delta}, \mu_{\vec{d}}(\vec{\delta})) \mid \vec{\delta} \in V, \mu_{\vec{d}}(\vec{\delta}) \in [0, 1] \right\}$, where $\mu_{\vec{d}}(\vec{\delta})$ represents the degree of attention and is given as an upper semi-continuous function over the interval $[\vec{d}_{min,i}, \vec{d}_{max,i}]$ with $\vec{d}_{min,i} :=$

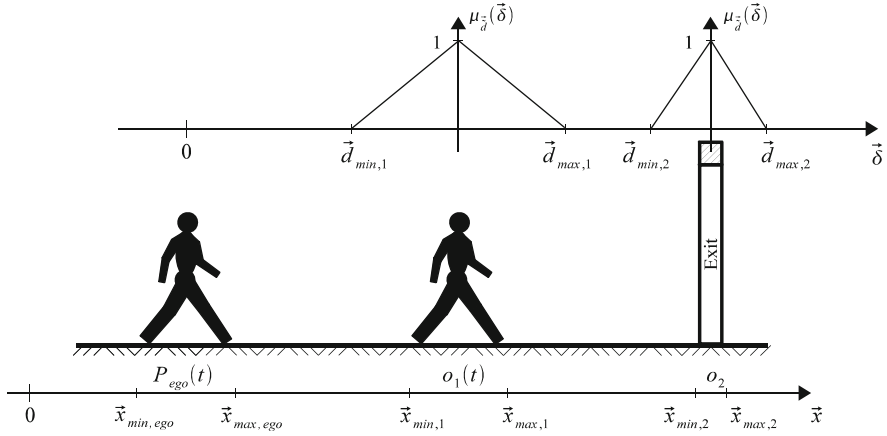


Fig. 1 Egocentric dynamic representation of the proximate space

$$\vec{x}_{\min,i} - \vec{x}_{\max,ego}, \vec{d}_{\max,i} := \vec{x}_{\max,i} - \vec{x}_{\min,ego} \text{ and } \mu_{\vec{d}}(\vec{m}_i) = 1 \text{ with } \vec{m}_i := \frac{1}{2}(\vec{d}_{\max,i} - \vec{d}_{\min,i}) + \vec{d}_{\min,i}, \text{ see Fig. 1.}$$

3 Perceptually Driven Social Force Model

The following description of the Social Force Model (abbreviated as SFM) is based on the original formulation given in [2] and [3]. Nonetheless, this description is reflecting the authors’ own interpretation that accentuates the cognitive psychological notion of the SFM. In this description the process of a pedestrian’s motion and interaction with the proximate surrounding occurs on three different levels of reality: the *physical level*, the *cognitive quasi-physical level* and the *cognitive level*, see Fig. 2. Different processes usually take place on each of these levels. Apart from the actual physical motion on the physical level a cognitive perceptual judgement process is taking place on the cognitive level. Accordingly, two different systems are separately considered. The first one is comprised of the pedestrian as a physical moving object in a physical set represented by the built-up environment and other pedestrians and objects. This system obviously resides on the physical level of reality where the actual physical motion and interaction are governed by the classical law of Physics. The other system is the human as a cognitive being that subjectively perceives and interprets its physical surrounding. These two main systems interact and communicate via a cognitive quasi-physical interface. The processes occurring on this intermediate level can be understood as those leading to the actual activation of specific body muscles after receiving the order from the cognitive system to use energy and induce a specific physical acceleration force.

Fig. 2 Physical, cognitive quasi-physical and cognitive modelling

Reality		Modelling	
Physical Level		Precise Euclidean Representation	Social Force Model
Cognitive Quasi-physical Level			Cognitive Quasi-physical Models of "Social Forces"
Cognitive Level	Decision-making	Egocentric Representation	Cognitive Perceptual Judgement Model
	Perception		

The SFM in its original basic form consists of a motion model and several cognitive quasi-physical models of “social forces”. The SFM accounts only for the processes on the physical and cognitive quasi-physical levels of reality. In accordance with this perceptually driven approach to the SFM a perceptually based decision-making model is accounting for the processes on the cognitive level. This model is based on the egocentric dynamic representation introduced in Sect. 2. The different models and quantities on all three levels are discussed in the following sections. In this account of the SFM only the functional dependencies are discussed. For the different exact formulas of the SFM in its original form see the literature [2–5].

3.1 Physical Motion Modelling

The social force model in its original basic form is a simplified model of pedestrian motion that incorporates the idea of social influences. Humans are regarded as physical objects that move according to equations of motion due to the own accelerating force. Hence, in analogy to Newton’s laws of motion the following basic equation describes the “actual physical motion” of a pedestrian α .

$$\frac{d\vec{r}_\alpha}{dt} := \vec{v}_\alpha \left(t, \frac{d\vec{v}_\alpha}{dt}, v_\alpha^{\max} \right) \tag{5}$$

In Eq. 5 \vec{r}_α is the actual physical position of a pedestrian α , $\vec{v}_\alpha(t)$ is her actual physical velocity and v_α^{\max} is the maximal physical speed “physiologically” acceptable by a pedestrian α . The temporal change $\frac{d\vec{v}_\alpha}{dt}$ of the actual physical velocity is dependent on cognitive quasi-physical quantities and hence it will be defined in the next section.

3.2 Cognitive Quasi-Physical Processes Modelling

$$\frac{d\vec{v}_\alpha}{dt} := \vec{F}_\alpha(t) + \vec{\varepsilon}_\alpha(t) \tag{6}$$

In Eq. 6 \vec{F}_α is a cognitive quasi-physical quantity interpreted as an accelerating “social” force and $\vec{\varepsilon}_\alpha$ is a pseudo-behavioural fluctuation term. The “social” force \vec{F}_α is defined as the functional

$$\vec{F}_\alpha(t) := f\left(\vec{F}_\alpha^0, \vec{F}_\alpha^{res}\right). \tag{7}$$

\vec{F}_α^0 is a cognitive quasi-physical quantity that dominates during “free motion”, i.e. when the way to a destination is completely free of any motion restraining factors, such as other pedestrians or physical objects, that may deflects the course of motion. It motivates a pedestrian α to spend her energy and move towards a specific destination. \vec{F}_α^{res} is a cognitive quasi-physical quantity accounting for the effects of a restrained motion. It motivates a pedestrian α to change her desired course of action \vec{F}_α^0 when her motion is retrained by other pedestrians or objects.

\vec{F}_α^0 is interpreted in the SFM as the main acceleration force towards a destination and is given as a function of a specific cognitive quasi-physical desired velocity \vec{v}_α^0 and the actual physical velocity \vec{v}_α , see Eq. 8.

$$\vec{F}_\alpha^0(t) := f\left(\vec{v}_\alpha^0, \vec{v}_\alpha\right) \tag{8}$$

The desired velocity can be a function $\vec{v}_\alpha^0 := f\left(\vec{d}_\alpha^0\right)$ of the cognitive quasi-physical distance vector \vec{d}_α^0 to the destination. In the original basic form of the SFM \vec{F}_α^0 is given as

$$\vec{F}_\alpha^0 := \frac{\hat{v}_\alpha^0 \cdot \vec{e}_\alpha^0 - \vec{v}_\alpha}{\tau_\alpha} \tag{9}$$

In Eq. 9 \vec{e}_α^0 is the specific cognitive quasi-physical desired direction, \widehat{v}_α^0 is the cognitive quasi-physical desired speed and τ_α is the physiologically acceptable relaxation time needed to adapt the actual physical velocity \vec{v}_α to the cognitive quasi-physical desired one \vec{v}_α^0 in case the motion was not restrained.

\vec{F}_α^{res} is interpreted in the original basic form of the SFM as a modifying acceleration force that sums up all motion restraining effects of objects β which could be either repulsive or attractive. It is given for a pedestrian α as a function of the cognitive quasi-physical distance vectors $\vec{d}_{\alpha\beta}$ to the restraining objects β and the cognitive quasi-physical velocities $\vec{v}_{\alpha\beta}$ of the restraining objects β relative to the pedestrian α , see Eq. 10.

$$\vec{F}_\alpha^{res}(t) := \sum_{\beta=1}^n f\left(\vec{d}_{\alpha\beta}, \vec{v}_{\alpha\beta}\right) \quad (10)$$

The restraining object β can be any physical object or other pedestrian in the surrounding space. The object β could be either static or dynamic in this formulation, since only the relative distance and velocity are considered. Different definitions of this function can be found in [2–5] that take into account the interaction strength and the interaction range with the restraining object. Furthermore, finding new definitions of this function is still the subject matter of many research works that fall under the so-called modifications of the SFM, see [2–5].

3.3 Cognitive Perceptual Judgement Process Modelling

The cognitive quasi-physical quantities presented in the previous section are the final result of the interaction with the physical, physiological and cognitive psychological constraints. They are mostly the result of a cognitive perceptual judgement process that is ultimately based on a subjective egocentric dynamic representation of reality. Therefore, they are not necessarily equal to the actual physical quantities they correspond to, as it is the case in the original basic form of the SFM. In this perceptually driven approach the different cognitive quasi-physical quantities are either in a functional dependency on other cognitive quasi-physical quantities or they have corresponding cognitive quantities on the cognitive level.

The cognitive quasi-physical quantities $\vec{d}_\alpha^0 := PJ\left(\vec{d}_\alpha^0\right)$, $\vec{d}_{\alpha\beta} := PJ\left(\vec{d}_{\alpha\beta}\right)$ and $\vec{v}_{\alpha\beta} := PJ\left(\vec{v}_{\alpha\beta}\right)$ are derived from their respective cognitive ones via a perceptual judgement function PJ .

The corresponding cognitive quantities \vec{d}_{α}^0 , $\vec{d}_{\alpha\beta}$ and $\vec{v}_{\alpha\beta}$ are based on the subjective egocentric dynamic representation introduced in Sect. 2. Hence, they are two-dimensional fuzzy vectors. Moreover, the cognitive quantity $\vec{v}_{\alpha\beta}$ representing the cognitive velocity of a moving object β relative to a pedestrian α is given as a functional of the cognitive relative distance vector to β at time t and the respective one at time $t - dt$, see Eq. 11.

$$\vec{v}_{\alpha\beta}(t) := \tilde{f}\left(\vec{d}_{\alpha\beta}(t - dt), \vec{d}_{\alpha\beta}(t)\right) \tag{11}$$

The perceptual judgment function that maps a cognitive quantity \vec{x} to the respective cognitive quasi-physical quantity $\vec{\hat{x}}$ can be given as the following composite function:

$$PJ(\vec{x}) := g(f(a)). \tag{12}$$

To simplify matters suppose that \vec{x} is a one-dimensional fuzzy vector, the functions f and g can be given as in Eqs. 13 and 14, respectively.

$$f(a) := \left[\vec{x}\right]^a = \left[\vec{x}_{\min}^a, \vec{x}_{\max}^a\right] = \left\{ \vec{\xi} \in V \mid \mu_{\vec{x}}(\vec{\xi}) \geq a \right\} \tag{13}$$

$$g\left(\left[\vec{x}\right]^a\right) := \begin{cases} \vec{x}_{\min}^a & \text{if } Rand([0, 1]) < 0.5 \\ \vec{x}_{\max}^a & \text{otherwise} \end{cases} \tag{14}$$

$a \in [0,1]$ is a value that stands here for attention. \vec{x}_{\min}^a and \vec{x}_{\max}^a are the vectors with the minimum and maximum norm, respectively, in the interval $\left[\vec{x}\right]^a$. $Rand([0,1])$ is a uniform random number generator over the interval $[0,1]$.

4 Validation

A preliminary validation test of a single file movement, compare to [6], showed an improvement of the behaviour of the SFM as given in [5], if the SFM was based on the presented egocentric representation, see Fig. 3. The following values of the parameters of the SFM [5] were used: $\tau = 0.5$, $A_{\alpha} = 5.0$, $B_{\alpha} = 0.4$ and $\lambda = 0.0$.

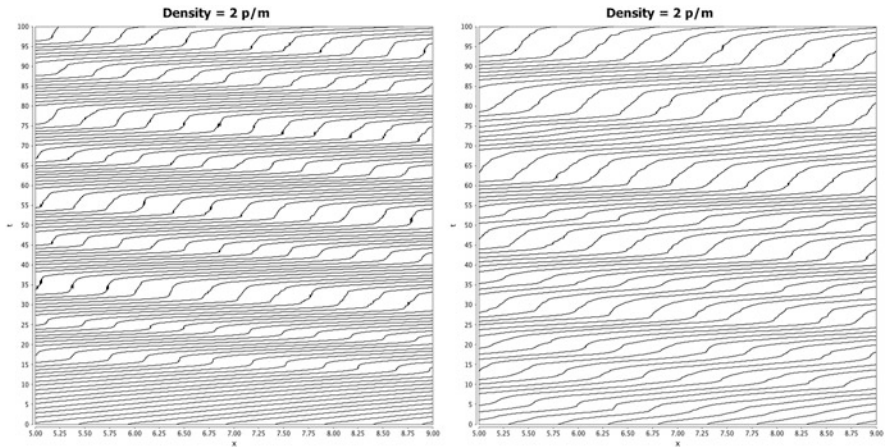


Fig. 3 Single file movement [6]: *left* SFM as in [5], *right* perceptually driven SFM

5 Conclusion and Future Work

The basic mathematical formulation of the egocentric spatial representation, so far introduced in this paper, can be regarded as a pure theoretical fuzzy geometric representation. Therefore, conducting perceptual experimentation investigating the spatial human perception from a cognitive psychological point of view are indispensable for refining and developing this basic formulation towards a fully cognitively based subjective egocentric dynamic representation.

References

1. Dubois, D., Prade, H. (eds.): Fundamentals of Fuzzy Sets. The Handbooks of Fuzzy Sets Series. Kluwer Academic Publishers (2000)
2. Helbing, D., Molnár, P.: Social Force Model for Pedestrian Dynamics. *Physical Review E* 51, 5, 4282–4286 (1995)
3. Helbing, D., Johansson, A.: Pedestrian, Crowd and Evacuation Dynamics. In: Robert, A.M. (ed.) *Encyclopedia of Complexity and Systems Science*. pp.6476-6495. SpringerScience + Buisness Media, LLC (2009)
4. Helbing, D., Farkas, I., Vicsek, T.: Simulating Dynamical Features of Escape Panic. *Nature* 407, 487–490 (2000)
5. Johansson, A., Helbing, D., Schukla, P.K.: Specification of the Social Force Pedestrian Model by Evolutionary Adjustment to Video Tracking Data. *Advances in Complex Systems* 10, 271–288 (2007)
6. Portz, A., Seyfried, A.: Modeling Stop-and-Go Waves in Pedestrian Dynamics. In: Wyrzykowski, R. et al. (eds.) *PPAM 2009, Part II, LNCS 6068*. pp.561–568. Springer-Verlag Berlin Heidelberg (2010)

Comparison of Different Calibration Techniques on Simulated Data

Christian Rudloff, Thomas Matyus, and Stefan Seer

Abstract Pedestrian simulation models are used in a multitude of ways. While model development for Social Force models is quite advanced little is known about how to calibrate a Social Force model such that the parameters are reproducing real life data in many situations. This paper tests different calibration methodologies that were previously used in the calibration of Social Force models to give an indication of the usability of such techniques. This is done on simulated data to guarantee the comparability of the different methodologies. The result will give practitioners a guideline in choosing how to use real live data in the calibration process.

Keywords Pedestrian simulation models • Model calibration • Social force model

1 Introduction

Pedestrian simulation models are used in a multitude of ways, ranging from the design of transport infrastructure [1], planning and optimization of operations [2], crowd analysis at large events [3] to evacuation of buildings [4], ships [5] and even cities [6]. Many different modeling techniques which include crowd behavior on various levels of detail are used to deal with these complex and rather different problems. While in some situations, like for large scale evacuation problems, it is often enough to use fast macroscopic models that just give hold of minimal evacuation times, for planning, operations and crowd control it is often necessary to know the position of every pedestrian separately. Thus, less coarse mesoscopic or

C. Rudloff (✉) • T. Matyus • S. Seer
Austrian Institute of Technology, Dynamic Transportation Systems, Giefinggasse 2,
A-1210 Vienna, Austria
e-mail: christian.rudloff@ait.ac.at

even microscopic methods, such as Cellular Automata [7], choice models [8] or Social Force models [9, 10] are applied to answer the relevant questions.

The Social Force model and its variants have proved to be very useful to give a rich simulation model that answers many questions successfully (see e.g. [11, 12, 2]). As a consequence it has developed into one of the main approaches for modeling and simulating pedestrian movement on a microscopic level. The model is defined by describing the acceleration of an individual pedestrian based on the sum of different attraction and repulsive forces: while an attraction force accelerates pedestrians towards their desired direction and speed, repulsion forces allow evasion from other pedestrians and boundaries.

Many papers (e.g. [9, 10, 13]) discuss model developments and calibration based on pedestrian movement observations. For that purpose real world data or data collected in experiments can provide individual trajectories which are then used to find the model parameters. In particular, when calibrating pedestrian simulation models, one has the problem that trajectories collected with automated tracking methods as well as manually annotation are noisy due to inaccuracies of both methodologies. Additionally, most data collection methods deliver trajectories based on the head of pedestrians. As a result, the trajectories include body sway caused by the side movement of the pedestrian's head during each step (see e.g. [14]). This introduces significant uncertainties as the positions and velocities of the surrounding pedestrians are used to model the acceleration of a pedestrian.

For the calibration process different methodologies are described in the literature: in [15] a maximum likelihood approach is applied for estimating the model parameters directly on the accelerations extracted from the trajectory data. However, this might lead to error-in-variables problems, possibly resulting in a bias towards zero in the parameters (see e.g. [13]) and in general suffers from the problem that errors in the data are increased by differencing them twice. Furthermore, parameter values in the calibration can be estimated based on a similarity measure between real and simulated data. By formulating this similarity measure in an objective function, for instance the mean Euclidean distance between real and simulated trajectories, one can apply optimization techniques such as genetic algorithms [16] or Nelder-Mead algorithms [13].

While most papers show that the calibrated models reproduce self organizing behavior, like lane formation, and perform well on scenarios similar to the estimation data, it is not really known how transferable the models are. In addition, most papers do not give much information about the quality and sensitivity of the parameters or the dependence of the parameter values on each other (Some first steps were taken in [17, 13]). Furthermore, it is not known what influence the choice of a specific calibration technique has on the quality of the calibrated model parameters as usually only a single calibration method is used (with the exception of [13] where three methodologies are compared). Adding to this is the fact that the velocity and acceleration are calculated by differencing the noisy position data leading to increased errors for those variables.

To give researchers a guideline when calibrating pedestrian simulation models, this paper tests several calibration techniques. Therefore, a calibration dataset was

created which originates from simulations instead of observation allowing full control over the real parameters that were estimated with the different methodologies. For more realistic data random errors and a body sway like movement were added to the trajectories.

The organization of the remainder of the paper is as follows: in Sect. 2 the model and the calibration techniques and the metrics for the comparison of results and original data are described in detail. Section 3 describes the data creation process. In Sect. 4 the results of the experiments are presented. The final section gives conclusions to the presented work as well as an outlook to open problems and future work.

2 Experimental Setup for Model Calibration

Instead of using trajectories from empirical observations, our data set for model calibration is based on simulations with the Social Force model. This allows us to create data sets where the original model parameters are known. Furthermore, different types of error characteristics, which are also included in empirical data, can be added to the trajectories for our investigations. We define different calibration techniques which were performed using a variation of optimization criteria to compare the fit of original and simulated trajectories.

2.1 Description of the Social Force model

The Social Force model, first introduced in [9] and variants of it are one of the most widespread model types in continuous, operational models for microscopic simulation of pedestrians. Assuming that a pedestrian α walking with a current velocity $\vec{v}_\alpha(t)$ wants to move in a desired direction \vec{e}_α with a desired speed v_α^0 , the Social Force model gives the acceleration $\vec{f}_\alpha(t)$ of that pedestrian α dependent on other pedestrians β and surrounding walls i as

$$\vec{f}_\alpha(t) = \frac{1}{\tau_\alpha} \left(v_\alpha^0 \vec{e}_\alpha - \vec{v}_\alpha \right) + \sum_{\beta \neq \alpha} \vec{f}_{\alpha\beta}(t) + \sum_i \vec{f}_{\alpha i}(t), \tag{1}$$

where $\vec{f}_{\alpha\beta}(t)$ is the repulsive force away from other pedestrians, $\vec{f}_{\alpha i}(t)$ the repulsion away from walls and τ_α the relaxation parameter governing the time it takes the pedestrian to accelerate from the current velocity to the desired velocity. The original formulation in [9] models the repulsive force dependent on the distance of pedestrian α from obstacles β and i . Later variants like [13] or [10] changed this formulation and added dependencies on the velocities of the pedestrians into the formulas. Due to the smaller number of relevant parameters and the popularity of

the formulation in applications, we chose to use the formulation from [10] for this study. In this formulation the repulsive forces are given as

$$\vec{f}_{\alpha\beta}(t) = w(\varphi_{\alpha\beta}(t)) \vec{g}(d_{\alpha\beta}(t)). \quad (2)$$

In the elliptic force from [10] the interaction force depends on the distance $\vec{d}_{\alpha\beta}$ of the pedestrians and their velocities $\vec{v}_{\alpha}(t)$ and $\vec{v}_{\beta}(t)$ and is given as

$$\vec{g}(d_{\alpha\beta}) = A e^{-b_{\alpha\beta}/B} \frac{\|\vec{d}_{\alpha\beta}\| + \|\vec{d}_v\|}{2b_{\alpha\beta}} \frac{1}{2} \left(\frac{\vec{d}_{\alpha\beta}}{\|\vec{d}_{\alpha\beta}\|} + \frac{\vec{d}_v}{\|\vec{d}_v\|} \right) \quad (3)$$

where A and B are parameters, $\vec{d}_v = \vec{d}_{\alpha\beta} - (\vec{v}_{\beta} - \vec{v}_{\alpha}) \Delta t$ and

$$2b_{\alpha\beta} = \sqrt{\left(\|\vec{d}_{\alpha\beta}\| + \|\vec{d}_v\|\right)^2 - \left((\vec{v}_{\beta} - \vec{v}_{\alpha}) \Delta t\right)^2}. \quad (4)$$

Furthermore, the difference between the strength of the force ahead or behind a pedestrian, also referred to as an anisotropic characteristic, is determined by

$$w(\varphi_{\alpha\beta}(t)) = \left(\lambda_{\alpha\beta} + (1 - \lambda_{\alpha\beta}) \frac{1 + \cos(\varphi_{\alpha\beta})}{2} \right) \quad (5)$$

which is dependent on the angle between the distance vector between pedestrians α and β . the strength of the force behind grows with $0 \leq \lambda_{\alpha\beta} \leq 1$ and is equal to the acceleration ahead for $\lambda_{\alpha\beta} = 1$. For the repulsion form walls the same formulation with $\vec{v}_i = 0$ is applied.

2.2 Data Creation Process

In order to have full control over the real model parameters our calibration data set was created using simulations instead of observations. Therefore, a relatively simple scenario including a corridor of 2 m width with bidirectional flows was chosen. In this scenario tactical behavior, such as route choice, which is not represented by the Social Force model, can be neglected. Overall 50 pedestrians were simulated, 25 in each direction. The two groups were placed 10 m apart into regular 4×7 grids. A position and goal in opposite grids were assigned randomly to each pedestrian out of the 28 grid squares (see Fig. 1).



Fig. 1 A 2 m wide corridor with 50 pedestrians was used as a scenario for data creation. Here a simple visualization of the simulation with pedestrians in *red* and walls in *grey*

All pedestrians were assigned desired velocities from a normal distribution (mean 1.3 m/s, variance 0.2). To get the five calibration scenarios the starting positions and goals as well as the velocities were assigned randomly to the 50 pedestrians five times.

The elliptical model as described above from [10] was chosen for both repulsion from walls and pedestrians to create our calibration data set. As the methodology does not rely on parameters found in real pedestrian behavior the parameter values were chosen using hints from literature and visual testing of the simulation. The parameters for the repulsive force between pedestrians were set to be $\tau_\alpha = 0.54$, $A = 1.7$, $B = 0.7$ and $\lambda_{\alpha\beta} = 0.4$. For walls two parameters are changed to $A = 5.5$, $B = 0.5$.

Typically, collecting trajectory data from videos introduces errors due to inaccuracies in manual annotation or of the automated tracking. To create more realistic data, different error characteristics were added to the simulated trajectories: the first error type added was a random, normally distributed error. Here, two different data sets were created, one with variance 0.05 and one with an unusually large variance 0.2.

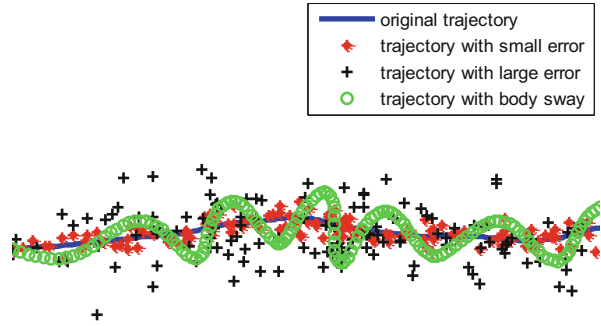
The second type of error added to the data was a “body sway” type error. Body sway can be seen in pedestrian trajectories extracted by annotating the head of pedestrians in videos, as the head sways from one side to the other during a normal walking motion. Looking at several data sets e.g. [14] it can be seen that the body sway is larger the slower the pedestrians walk. To create a similar swaying motion in the simulated data, a sine curve

$$S(t, v_\alpha, r_\alpha) = \frac{0.1}{(v_\alpha + 0.1)} \cdot \sin\left((t + r_\alpha) \cdot \frac{\pi}{0.6}\right) \tag{6}$$

is added to the data to the trajectory at time t in direction perpendicular to the current velocity. The step length of each pedestrian is set to 0.6 s and a random whole number r_α is added to t to have an offset to the body sways for different pedestrian.

Overall, we obtained four different data sets including the original and erroneous trajectories. A comparison of the resulting trajectories can be seen in Fig. 2.

Fig. 2 Comparison of different trajectories: in *blue* the original simulated trajectory, in *red* the one with a normal error with variance 0.05, in *black* one with variance 0.2 and in *green* a trajectory with added body sway



2.3 Calibration Methodologies and Metrics

For our tests the model parameters A and B in Eq. 3 governing the strength and the interaction distance of the repulsive force between pedestrians were calibrated. The remaining parameters including those in the repulsive force for walls were left at their original values as used in the data set creation process. In this work, we compare three different calibration techniques: the base method is a Maximum Likelihood Estimation (MLE) of the parameters directly derived from the calculated accelerations at each point in time. Furthermore, we applied two methodologies which fit the simulated to the original trajectories. First, all pedestrians were simulated at the same time, second, in each simulation run only one pedestrian was simulated and all remaining pedestrians were kept on their original trajectories. In all cases the desired velocities of pedestrians were calculated as the 90 % quantile of the velocities in their original trajectories.

In literature (e.g. [17, 13]) it was shown that for most realistic data sets the distance measures tested show strong interdependencies for several parameters. In particular, the parameters A and B often show large regions with similar fits on the chosen objective function. Hence, different optimization criteria were compared that match the original and the simulated trajectories within the calibration process. In particular, these were the mean Euclidian distance between the trajectories, the maximal distance between the trajectories and the differences in arrival times of the pedestrians within a meter away from the goal.

Two different MATLAB optimization algorithms were used for parameter estimation: the first function applied was `fminsearch`, which uses a Nelder-Mead optimization algorithm [18]. Here, the starting parameters for the optimization were also varied ranging from (a) the parameter values originally used to create the calibration dataset, (b) random start values. The second method was a genetic algorithm (GA) using the function `ga`, starting with a random population of 40.

3 Experimental Results

The calibration process was started for different combinations of the above described calibration techniques. The first thing that can be noticed was that there are large differences in the calibration processes in terms of computational speed. In general the Nelder-Mead algorithm finds results in a much shorter time than genetic algorithms. However, as can be seen later, in particular for the data with added errors, the Nelder-Mead algorithm is prone to finding local minima in the objective function.

The second observation was that using simulation of single pedestrians was, not surprisingly also clearly slower than the variant of simulating all pedestrians at once as 50 simulation processes have to be run successively in each calibration step. As a result not all possible combinations were run. Furthermore, due to the results from the sensitivity analysis other combinations were skipped.

3.1 *Parameter Sensitivity*

Before the actual model calibrations, we performed a sensitivity analysis on the model parameters. Thus, the different objective functions were calculated for the simulation while changing the parameter values for A and B in the range of -50% to $+50\%$ from the original values. The tests were run for all four data sets, the original data, the data with added normally distributed errors and the data set with added body sway. With respect to computational performance, all pedestrians were simulated at once.

Examining the sensitivity of single parameters one can see from Figs. 3 and 4 that both parameters are sensitive to even small changes for both mean and maximal distance between real and simulated trajectories. This behavior could be observed for all performed distance measures. Furthermore, the gradient for the maximal distance is much steeper than in the other distance measures. This single parameter sensitivity analysis already shows that for erroneous data the optimal parameter values derived from the estimation are significantly deviating from the real values. In particular one has to be very careful when a large random error has to be expected.

Next, the sensitivities of parameter pairs $[A,B]$ on the different objective functions were tested. In Fig. 5 one can see the sensitivity graphs for the four data sets applying the mean Euclidian distance between real and simulated trajectories as the objective function. The results from all objective functions indicate valleys of parameter pairs which deliver very similar values close to the optimal value. In particular, for the erroneous data local minima can be found in those valleys, which make optimization using the Nelder-Mead algorithm difficult.

The existence of such a valley is not clear as there is no easy explanation why the models deliver similar results for changing parameter values. In [19]

Fig. 3 Sensitivity of the parameters A and B to changes with respect to the **mean Euclidian distance** between input and simulated data for the tree erroneous data sets

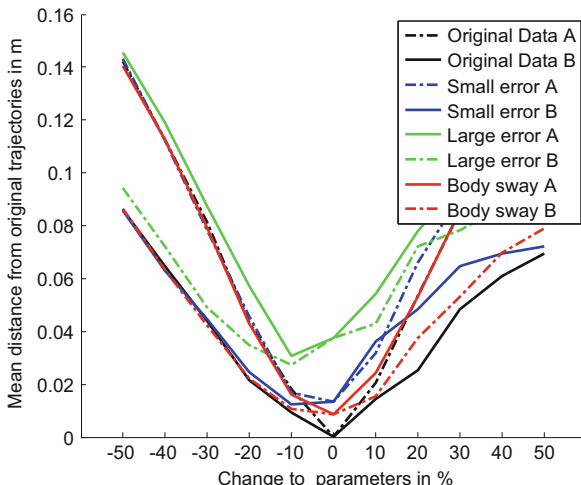
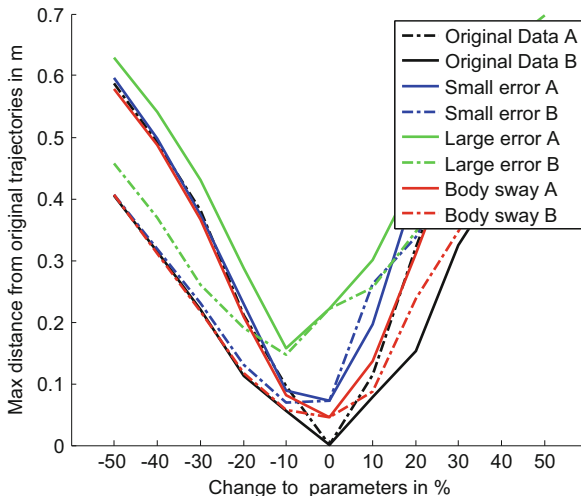


Fig. 4 Sensitivity of the parameters A and B to changes with respect to the **maximal Euclidian distance** between input and simulated data for the tree erroneous data sets



it is conjectured that there is a certain headway when people decide to evade oncoming pedestrians. This is justified as for different parameter pairs $[A,B]$ the graphs for the force dependent on the distance between pedestrians intersect in a single spot (see [19]). For further research, it is necessary to find a functional form and corresponding explanation for the valley in order to obtain an additional objective function whose fits vary more strongly along the function. In a first step a nonparametric curve was fit into the valley. This should offer a chance to find a uniquely defined parameter setting by comparing fitness functions on that curve.

The results of the sensitivity analysis also reveal that for the erroneous data the global minima is not necessarily at the original parameter values. While the data

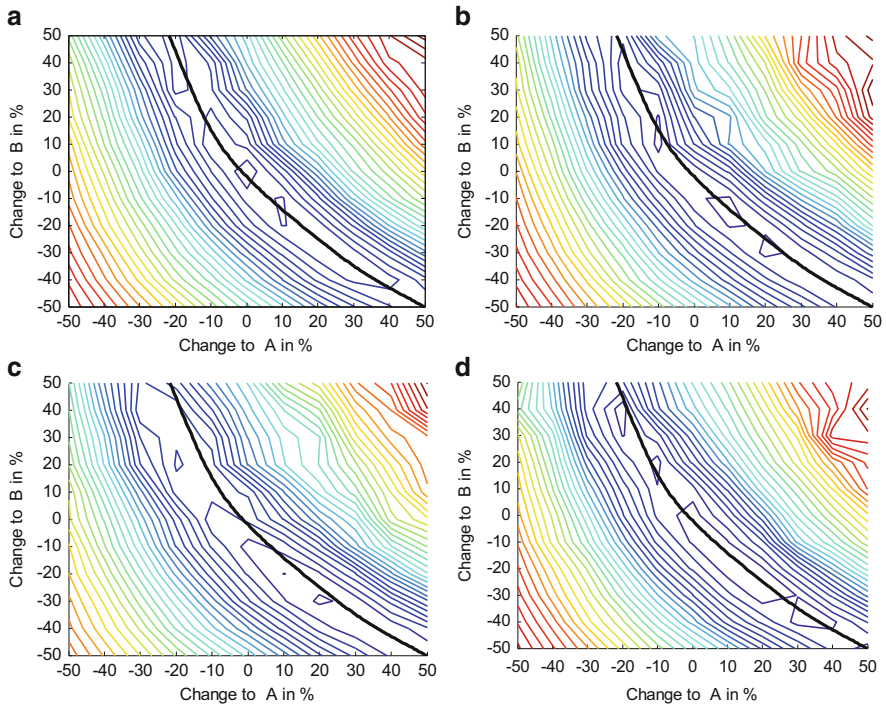


Fig. 5 Sensitivity of the parameters for the mean of the distance between real and simulated trajectories for (a) original data, (b) data with small error, (c) data with large error and (d) data with body sway. The Black line gives a non-parametric fit of the valley for the original data

with a small error has the global minimum close to those parameters for the other data sets this is not always the case. Especially the data including the large error has the minimum relatively far away from the original values.

For the maximum Euclidian distance as well as the velocity the results of the sensitivity analysis are worse. In particular, for large random errors these functions become much more unreliable, but also for an added body sway the whole valley moves away from the one that that can be observed for the original data. In Fig. 5 this is illustrated for the mean distance between original and simulated velocity calculated from the trajectories. These objective functions will therefore not be useful for calibration of pedestrian simulation models in most cases (Fig. 6).

Objective functions that are relatively independent of the added errors can also be found. For example, the time difference to reach the goal in the real and simulated data does only depend on that error in a very limited way. However, the small differences in simulation caused by staying in the valley are even less pronounced here, which makes calibration relatively difficult. Furthermore the valley proves to follow the same graph as for the other objective functions. This poses identifiability questions on the parameters A and B. However, it can be seen in Fig. 7 that

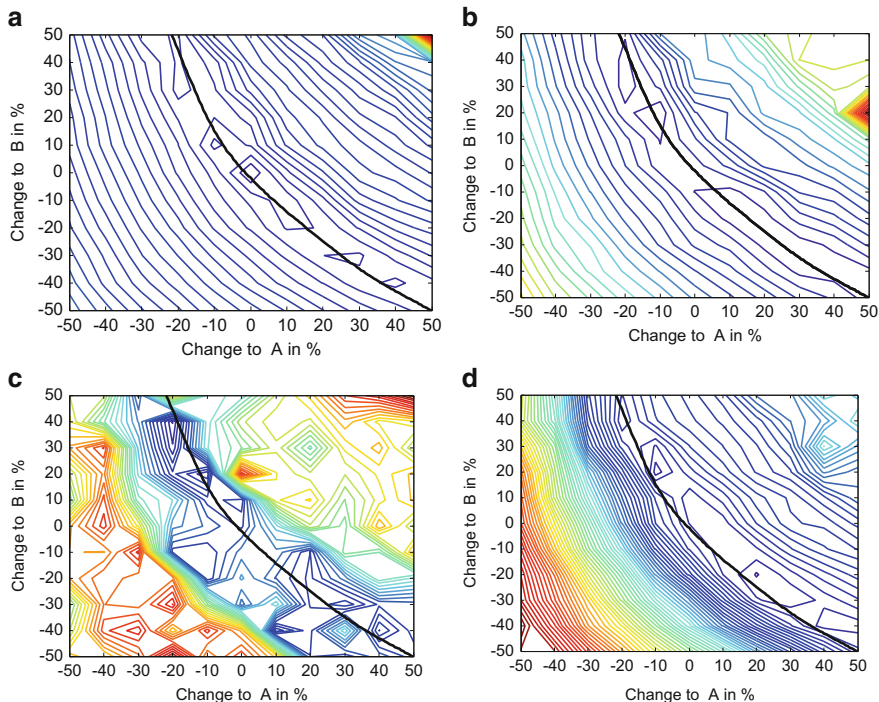


Fig. 6 Sensitivity of the parameters for the mean of the distance between real and simulated velocities for (a) original data, (b) data with small error, (c) data with large error and (d) data with body sway. The black line marks again the valley of the mean distance plot

combining this time difference with a mean distance produces a correctly position global minimum and has steep sides of the valley, but due to the flat valley, identifiably is not guaranteed with this combination, either.

3.2 Calibration Results

After the sensitivity analysis was run, the different calibration methodologies were applied. The calibration results in Table 1 show that MLE can only be feasible if very small errors can be guaranteed in the input data. Even with a small error in the trajectories, the parameter values become very large compared to the original values. This might be the case as the random error makes the measured accelerations quite large. For the body sway the parameters are not quite as conclusive. While the mean values of the parameters look relatively feasible, the standard deviations are high. Here, the parameter values were close to zero for some of the sets, while for the others, the parameters were relatively close to the valley in the fitness function.

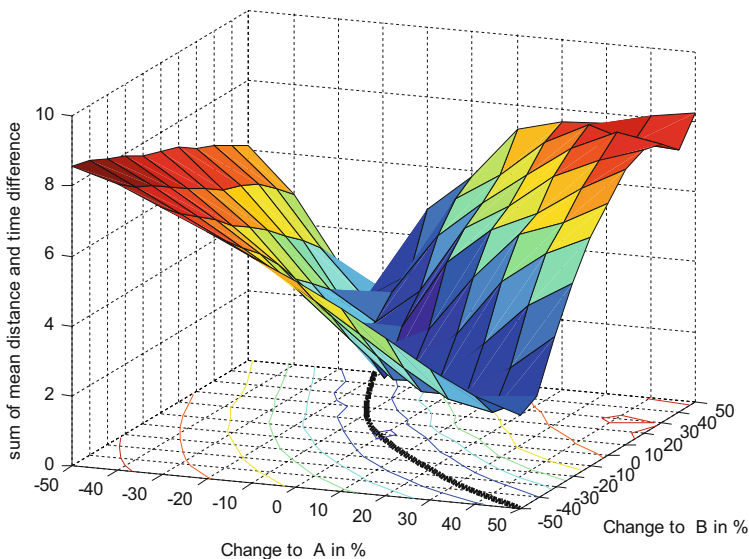


Fig. 7 Sensitivity of the sum of mean and time differences for the comparison of input and simulated data for the data set with added body sway

Table 1 Mean values and standard deviation of the estimated parameters using a MLE on the four trajectory data sets

	$\mu(\hat{A}), \text{std}(\hat{A})$	$\mu(\hat{B}), \text{std}(\hat{B})$
Original set	1.70, 0.00	0.69, 0.00
Small error	14.02, 23.28	1.16, 0.49
Large error	31.13, 1.42	7.12, 0.19
Body sway	1.62, 1.93	0.38, 0.35

Overall, the use of MLE cannot be recommended as a small random error as well as a body sway have to be expected in real data sets. In such situations, the parameters are not even close to the valley region in the fitness function, thus it is not expected that the parameters can produce valid simulation results.

For the calibration of the parameters using the simulation of a single pedestrian at a time it has to be noted that due to the large number of simulation runs in each step, (one for each pedestrian) the calibration time in our case is almost 50 times the time it takes using a simulation of all pedestrians at once. Hence, it is not feasible to combine this method with a genetic algorithm. In order to see if there is a noticeable difference in the results between these two techniques, we performed two tests using the mean Euclidean distance: first with starting values at the original values and second setting the starting value for both parameters to 3. The results in Table 2 show that the Nelder-Mead algorithm is strongly dependent on starting values. Using the real parameters as starting values both algorithms perform in a comparable way. However, when the starting values differ from the real parameter values, while both

Table 2 Mean values and standard deviation of the estimated parameters using a Nelder-Mead algorithm with different starting values on the four trajectory data sets

	All at once, real values				One at a time, real value			
	$\mu(\widehat{A}), \text{std}(\widehat{A})$	$\mu(\widehat{B}), \text{std}(\widehat{B})$	$\mu(f(\widehat{A}, \widehat{B}))$		$\mu(\widehat{A}), \text{std}(\widehat{A})$	$\mu(\widehat{B}), \text{std}(\widehat{B})$	$\mu(f(\widehat{A}, \widehat{B}))$	
Original set	1.69, 0.02	0.70, 0.00	0		1.67, 0.02	0.69, 0.01	0.004	
Small error	1.70, 0.04	0.69, 0.02	0.004		1.70, 0.02	0.69, 0.01	0.003	
Large error	1.71, 0.07	0.70, 0.02	0.006		1.74, 0.03	0.71, 0.01	0.005	
Body sway	1.73, 0.04	0.70, 0.01	0.005		1.74, 0.03	0.69, 0.01	0.004	
	All at once, starting at 3				One at a time, starting at 3			
	$\mu(\widehat{A}), \text{std}(\widehat{A})$	$\mu(\widehat{B}), \text{std}(\widehat{B})$	$\mu(f(\widehat{A}, \widehat{B}))$		$\mu(\widehat{A}), \text{std}(\widehat{A})$	$\mu(\widehat{B}), \text{std}(\widehat{B})$	$\mu(f(\widehat{A}, \widehat{B}))$	
Original set	3.47, 0.54	0.48, 0.05	0.010		12.41, 14.13	0.24, 0.10	0.084	
Small error	3.19, 3.79	0.67, 0.24	0.012		15.00, 22.51	0.25, 0.07	0.085	
Large error	4.11, 3.12	0.52, 0.24	0.032					
Body sway	5.872, 0.93	0.94, 1.17	0.046					

Table 3 Calibrated parameter values using a GA and a 2-step process where the GA results were used as starting values in a Nelder- Mead algorithm

	$\mu(\hat{A}), \text{std}(\hat{A})$	$\mu(\hat{B}), \text{std}(\hat{B})$	$\mu(f(\hat{A}, \hat{B}))$
Original set, mean Euclidean position error	1.41, 0.86	1.19, 1.01	0.011
Original set, mean Euclidean position error, 2-step process	1.71, 0.73	0.73, 0.18	0.005
Original set, time error	1.15, 0.42	0.96, 0.29	0.006
Set with small error, mean Euclidean position error	1.19, 0.86	1.39, 1.00	0.015
Set with large error, mean Euclidean position error	1.07, 0.59	1.45, 1.31	0.012
Set with body sway, mean Euclidean position error	1.17, 0.67	1.03, 0.41	0.011

versions return local minima, the ones for the individual simulation are much further away from the real values and have worse fits with respect to the mean Euclidean distance from the original trajectories. Hence, for further studies only the all at once variant was applied.

The next question to answer is if using a different objective function, like the mean Euclidean distance between original and simulated velocities or times, offers a better base for the Nelder- Mead algorithm to find the global optimum. However, starting with 3 as starting value for both A and B again, for none of the data sets did the algorithm manage to avoid the local minima in the neighborhood of the starting value.

The GA does not suffer from a starting value problem as it incorporates random changes to the parameter values. However, due to the random search the estimated parameters vary to a much larger extent if the search space cannot be restricted at all. Due to the random search method applied here, the simulation again has to be run a large multiple of times it needs to be run using a continuous optimization algorithm. Hence, not all cases were calibrated here.

To show that GA works better the Nelder-Mead algorithm for this optimization, two examples are given in Table 3. Even though there is still a large standard deviation in the parameters, the parameter values are much closer to the real values than by using the Nelder-Mead Algorithm. On the other hand, the values are not showing a vast improvement in the mean Euclidean distance fit compared to the original data. However, as can be seen in Table 3 for different objective functions the GA results can serve as good starting values for a continuous optimization algorithm as one can expect to be closer to the actual minimum. In that case, parameter values and their standard deviation as well as the fit are better compared to a random starting value for the Nelder Mead algorithm.

In accordance to the valleys in the fitness function, it can be seen from our results that a larger strength parameter results in a smaller interaction distance. This could be a sign for an identification problem for both parameters leading to a region of similar values for the objective function (see also [2]).

4 Conclusions and Outlook

In this paper we tested several calibration algorithms for a continuous operational pedestrian simulation model on simulated data. In particular, calibration procedures applied in literature were tested for their suitability for the calibration of pedestrian simulation models. Simulated data was used in the calibration process to have control over the real parameters of the simulation.

The first noticeable result is that as soon as errors are contained in the input data, MLE is not giving reliable parameter values and should be avoided in the calibration of pedestrian simulation models.

Furthermore, it can be seen that despite the effort to find a suitable fitness function none was found that does not have a large valley where the fitness is very similar for the parameter pairs within the valley.

With respect to calibration procedures, it was found that it does not pay to simulate all pedestrians separately during the calibration process. While reasonable results can be expected with respect to the mean distance fit, the parameters tend to be far away from the real values, which might be a problem when a different fitness function is applied.

It is possible to avoid this time intensive procedure by just simulating all pedestrians at once. Using this methodology it can be seen that the continuous Nelder-Mead optimization algorithm is prone to getting stuck in local minima within the valley of the fitness function and hence should be used with caution, in particular when there is no good prior knowledge of the real parameter values. Random search algorithms like GA are more suitable to find values when that knowledge is not available. They can also be used to find reasonable starting values for a subsequent continuous optimization and even work relatively well on erroneous data. However, it can be seen that it is of high importance to find good ways of avoiding or smoothing random errors and to correct body sway in the data as these errors hinder correct calibration.

In conclusion, the combination of a genetic algorithm followed by a numeric optimization step seems to be most promising. In our tests the mean Euclidean distance actually performed best and showed least dependence on errors in the data. However, a test with more simulated scenarios and with different densities is needed to verify the identifiability of the parameters.

In future work it will be vital to find objective functions that showing more variation of fitness values in the valleys of the fitness functions used at this point. Only then can reliable parameter values be found and the quality of simulation models and parameter sets is compared in more detail. However it is not clear at this

point if SFM and their parameters are independent of the density of the scenario. This will be tested in future work as well. Also, next to fitness functions that allow the comparison of SFM it will be important to find functions that can be used on a multitude of data and in many situations. Only then will it be possible to test for the best model for a certain task. Furthermore the transferability of models to different scenarios, crowd densities, speed levels, etc. needs more testing to come to a truly complete picture of which model is the best for the task at hand, which will in turn be an invaluable information for practitioners that rely on the quality and accuracy of their simulation tools for their work.

References

1. Seer, S., Bauer, D., Bröndle, N.: Design of Decision Rules for Crowd Controlling using Macroscopic Pedestrian Flow Simulation. Proceedings of the PED2008 conference. , Wuppertal, Germany (2008).
2. Rudloff, C., Bauer, D., Matyus, T., Seer, S.: Mind the gap: Boarding and Alighting Processes using the Social Force. In: IEEE (hrsg.) Proceedings of the 14th IEEE ITSC. IEEE Intelligent Transportation Systems, 402 (2011).
3. Helbing, D., Johansson, A., Al-Abideen, H.: Dynamics of crowd disasters: An empirical study. *Phys. Rev. E*. 75, (2007).
4. Zheng, X., Zhong, T., Liu, M.: Modeling crowd evacuation of a building based on seven methodological approaches. *Building and Environment*. 44, 437–445 (2009).
5. Klüpfel, H., Meyer-König, T., Wahle, J., Schreckenberg, M.: Microscopic Simulation of Evacuation Processes on Passenger Ships. In: Bandini, S. und Worsch, T. (hrsg.) *Theory and Practical Issues on Cellular Automata*. Springer, Berlin (2000).
6. Lämmel, G., Grether, D., Nagel, K.: The representation and implementation of time-dependent inundation in large-scale microscopic evacuation simulations. *Transportation Research Part C: Emerging Technologies*. 18, 84–98 (2010).
7. Schadschneider, A.: Cellular Automaton Approach to Pedestrian Dynamics - Theory. In: Schreckenberg, M. und Sharma, S. (hrsg.) *Pedestrian Evacuation Dynamics*. S. 75–86. Springer (2002).
8. Antonini, G., Bierlaire, M., Weber, M.: Discrete choice models of pedestrian walking behavior. *Transportation Research Part B: Methodological*. 40, 667–687 (2006).
9. Helbing, D., Molnar, P.: Social Force Model for Pedestrian Dynamics. *Physical Review E*. 51, 4282–4286 (1995).
10. D Helbing, Johansson, A: Pedestrian, Crowd and Evacuation Dynamics. *Encyclopedia of Complexity and Systems Science* 16.
11. Helbing, D., Molnar, P., Schweitzer, F.: Computer Simulations of Pedestrian Dynamics and Trail Formation. *Evolution of Natural Structures*. S. 229–234. Sonderforschungsbereich 230,, Stuttgart (1994).
12. Mehran, R., Oyama, A., Shah, M.: Abnormal Crowd Behavior Detection using Social Force Model. *Proc. IEEE Intl. Conference on Computer Vision and Pattern Recognition (CVPR2009)* (2009).
13. Rudloff, C., Matyus, T., Seer, S., Bauer, D.: Can Walking Behavior Be Predicted? *Transportation Research Record: Journal of the Transportation Research Board*. 2264, 101–109 (2011).
14. Steffen, B., Seyfried, A.: Methods for measuring pedestrian density, flow, speed and direction with minimal scatter. *Physica A: Statistical Mechanics and its Applications*. 389, 1902–1910 (2010).

15. Hoogendoorn, S., Daamen, W.: Microscopic Parameter Identification of Pedestrian Models and Implications for Pedestrian Flow Modeling. *Transportation Research Record*. 1982, 57–64 (2006).
16. Johansson, A., Helbing, D., Shukla, P.: Specification of the Social Force Pedestrian Model by Evolutionary Adjustment to Video Tracking Data. *Advances in Complex Systems*. 10, 271–288 (2007).
17. Steiner, A., Philipp, M., Schmid, A.: Parameter Estimation for a Pedestrian Simulation Model. *Gehalten auf der 7 th Swiss Transport Research Conference , Monte Veria (2007)*.
18. Nelder, J., Mead, R.: A Simplex Method for Function Minimization. *The Computer Journal*. 7, 308–313 (1965).
19. Johansson, A.: *Data-Driven Modeling of Pedestrian Crowds*, (2009).

Evacuation Agent Simulation in an Underground Shopping Street Adding a Floor Field Approach and Its Three Dimensional Expression

Yoshiyuki Kobayashi, Toshiyuki Kaneda, Masaki Tamada, Taichi Shimura,
and Keisuke Hata

Abstract This paper reports a trial of evacuation simulation for examining space design and evacuation strategy in an underground shopping street in downtown Nagoya in the case of electric lighting blackout. We evaluated the evacuation performance of the models of two different space based on the actual measurement survey of there through simulation using a floor field approach, which has both high operability and can be expected to save calculation volume, and to compare two results. Moreover, we employ 3D space expression intelligible for many stakeholders through each process of the simulations.

Keywords Pedestrian dynamics • Evacuation • ASPF • Underground shopping street • Floor field • 3D

1 Research Background and Objectives

In Japan, underground shopping areas are a familiar feature of large cities, and the public commonly accepts them as spaces used in the course of shopping, commuting and school-commuting. In terms of their actual construction, underground shopping areas are subject to a set of building regulations and restrictions that ensures their space design offers adequate ventilation and lighting, and that evacuation measures can cope with such disasters as fires and earthquakes.

Y. Kobayashi (✉) • T. Kaneda
Nagoya Institute of Technology, Gokiso, Showa, Nagoya, Japan
e-mail: sakurako1988@gmail.com; kaneda@nitech.ac.jp

M. Tamada • T. Shimura • K. Hata
Kozo Keikaku Engineering Co. Ltd, Nakano, Nakano, Tokyo, Japan
e-mail: tamada@kke.co.jp; taichi-shimura@kke.co.jp; keisuke-hata@kke.co.jp

This research focuses on power failures in underground shopping areas by employing a virtual underground shopping area, and examines the space design and evacuation measures; it also clarifies by conducting pedestrian simulation show the structure of underground space affects people's behavior under evacuation conditions. Moreover, a visual representation of 3D space allows experimental evacuation simulation models to be developed to explore and assess the direction of improvements.

2 An Underground Space Model for Evacuation Simulations

Prior to the research, underground space modeling was carried out by taking Unimall, one of Nagoya Station's underground shopping areas, as an example.

Figure 1 shows the Nagoya underground shopping areas and the location of Unimall.

The Unimall shopping area conforms to the Building Standards Law, and in the Enforcement Ordinance of Building Standards Law, the following excerpt stipulates some of the provisions applied to our space modeling: (1) Each construction in an underground shopping area must have a width of 2 m or more which is adjacent to an underground passage; (2) The width of an underground passage shall be 5 m or more; the height from floor to ceiling shall be 3 m or more; the passage shall have no stairs, and no slope ways with a slope exceeding 1:8; and (3) Stairs shall be installed so that the walking distance from any section of a construction that is adjacent to a passage shall be 30 m or less.

With the enforcement of the Comprehensive Decentralization Law in 2000, space design and evacuation measures for underground shopping areas has been left to the discretion of urban local governments, and in 2004 Nagoya City established the Nagoya City Underground Shopping Area Basic Policy, and since then has been giving guidance concerning underground shopping areas. The policy as applied to our space modeling is as follows: (1) The width of a public underground passage shall be 6 m or more; (2) The effective width of stairs leading to the ground shall be 1.5 m or more; and (3) Information boards and maps that are easy-to-understand and suitable for use in the case of evacuation shall be installed.

In addition, pedestrians in underground spaces tend to lose their sense of direction and need appropriate guidance; Nagoya City established the "Nagoya City Underground Space Sign Installation Guidelines" to ensure uniformity and continuity of signs in underground passages.

A representative of Unimall was interviewed, and it was confirmed that the following disaster prevention measures in the current underground shopping street are in place, and Unimall is equipped with the following facilities.

1. Emergency exit: A staircase leading to a ground level exit is installed within 30 m of any store.

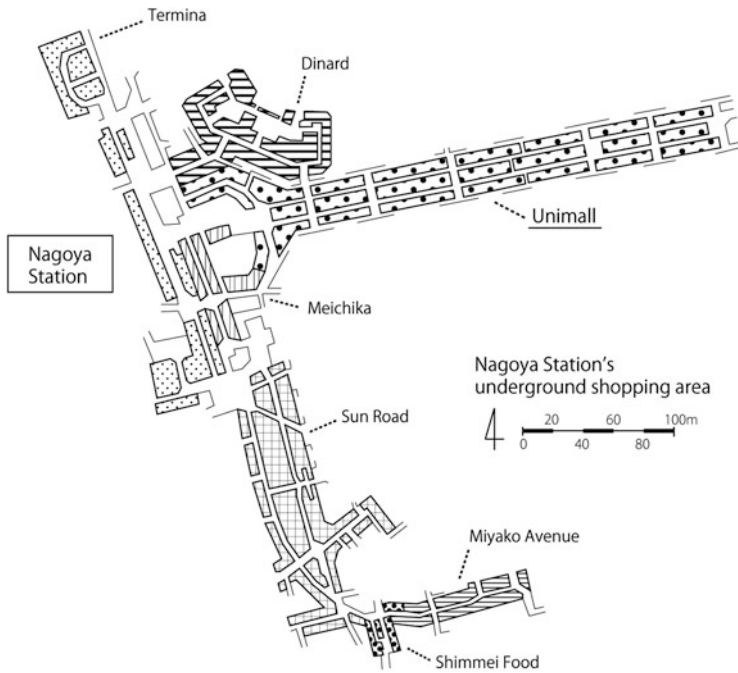


Fig. 1 Nagoya Station’s underground shopping area and the location of Unimall

2. Emergency lighting: In the event of a power failure, emergency lighting will replace the regular fluorescent lighting; emergency lights positioned about every 10 m will work for approximately 10 h, and provide sufficiently bright light to ensure safe evacuation. In addition, these facilities are powered by an independent generator, and the interviewee confirmed that in the event of an emergency, the possibility of a generator failure was very low.
3. Emergency exit signs: The signs are suspended from the ceiling and are in the form of a direction post indicating an exit. Each sign points the way towards the closest exit, which is indicated by an arrow, but no information concerning the distance is given; the signs are positioned in such a way that at least one sign is visible from any location in Unimall. Signs are also installed on passage floors.
4. Smoke hanging barrier: A smoke hanging barrier is a partition that creates a smoke compartment as stipulated by the Building Standards Law. They are covered by or made of noncombustible materials, and by hanging down from the ceiling for 50 cm or more are designed to effectively prevent the flow of smoke; in Unimall, their size ensures they will in no way hinder visibility in the case of an evacuation.
5. Smoke-extraction equipment: Unimall staff claimed that the smoke-extraction equipment ensured there was a very small possibility of Unimall being filled

with smoke. However, as the current facilities are constructed with the same ducts serving as both an air intake and a smoke outlet; there is an undeniable possibility of a reversal of smoke-extraction.

6. Installation of sprinklers and fire extinguishers: They are installed in conformity with the Building Standards Law.
7. Indoor broadcasting: In the event of a disaster such as an earthquake or fire, to ensure human safety and keep panic to the minimum, a Disaster Prevention Center will broadcast throughout Unimall.
8. Safety drills: An emergency drill and a fire drill are held twice a year. A fire is first reported to the Disaster Prevention Center, and if possible, staff members using the installed fire extinguishers fight the early stages of the fire. Unimall has organized its own fire-fighting team to rapidly provide a first line of response and to help with the evacuation of pedestrians. It should be noted that in front of the Nagoya Station, many underground shopping areas are found, but it seems that no comprehensive drill for the entire area is conducted.

In the research case example, two locations with the largest difference in space structure were selected, and these two locations are described as two space models in 3.3.

3 Pilot Development of an Evacuation Simulation Model by Adding Floor Field

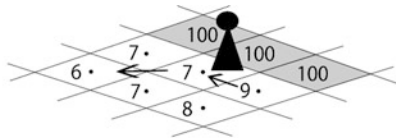
3.1 Floor Field Approach

This research aims to simulate the natural behavior of a normal crowd, and conducts evacuation simulations using a floor field approach [1, 2], which has both high operability and can be expected to save calculation volume.

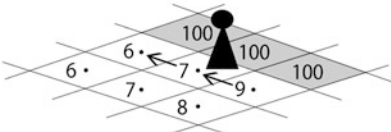
In this approach, a potential value is provided for a floor cell and agents move toward a lower potential value. Figure 2 shows an explanatory example of the potential values applied in this research. A characteristic of this approach is that from among the eight cells in the neighborhood (Moore neighborhood) of a floor cell positioned for each step, each agent updates their direction to the lowest potential value, and if there are several lowest value cells, the agent does not update its direction and continues in the same direction.

3.2 Algorithm of the Agent Model

In this research, ASPF (Agent Simulation of Pedestrian Flows) –pedestrians local behavior rules – are applied to each agent. Figure 3 shows an algorithm for an



I : Case that the agent changes its direction



II : Case that the agent continues in the same direction

I : If there is a lowest potential value cell in Moore neighborhood, the agent updates its direction to the cell.

II : If there are several lowest potential value cells in Moore neighborhood, the agent dose not update its direction and continues in the same direction.

Fig. 2 Explanatory example of the floor field potential values

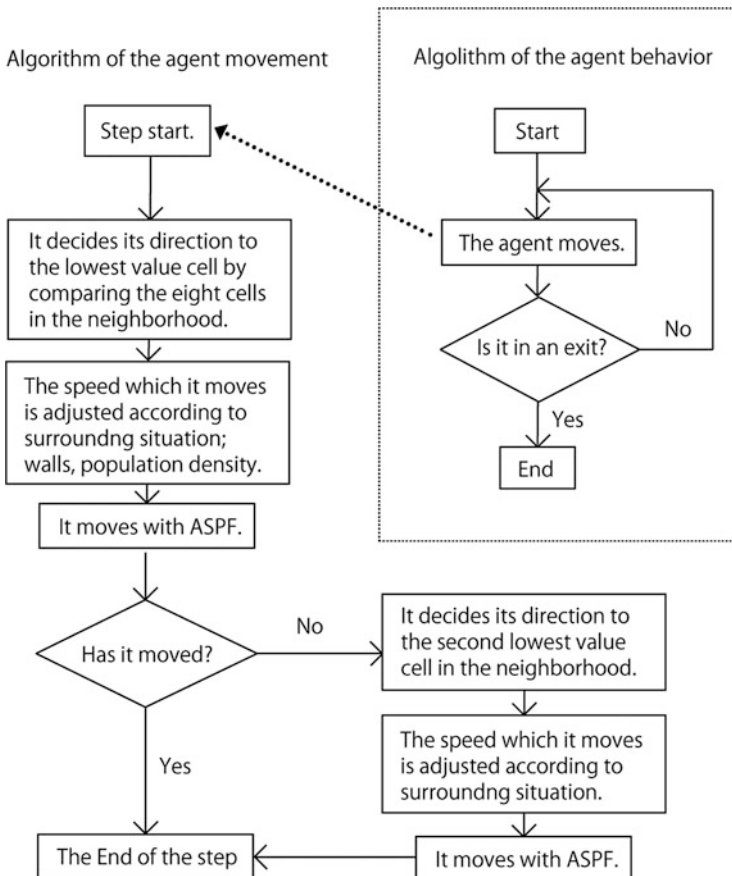


Fig. 3 Algorithm of the evacuation agent

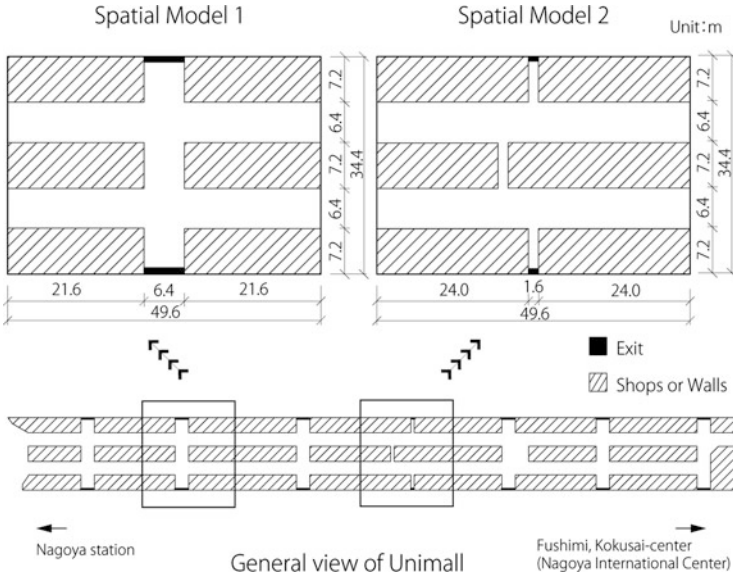


Fig. 4 Spatial models for the simulation

agent from the start to completion of the evacuation. There are 22 rules governing each agent’s behavior in relation to other agents, and 14 rules stipulating an agent’s response to walls, giving a total of 36 rules [3, 4]. From the start of evacuation, the agent decides their direction according to the above-mentioned floor field approach, and moves by following the ASPF rules; they repeat these steps until they reach an exit.

3.3 Simulation Results and Analysis

Figure 4 shows the two types of spatial models used in the research. The map model was created assuming 0.4×0.4 m per cell and consists of east–west 124 cells (49.6 m) and north–south 86 cells (34.4 m). To analyze how underground space structure affects evacuation behavior, 100 pedestrians were placed in each model, and both models used the same pedestrian start positions in the simulation of evacuation behavior. Using artisoc3.0 [5], 10 simulations were conducted for each model, and the number of steps taken for completing evacuation was measured. Figure 5 shows the comparison of the results, and indicates that Spatial Model 2 required not only more steps to complete evacuation, but also there was a greater variation among the simulations, compared to Spatial Model 1.

With regard to the large difference in the average number of steps taken to complete evacuation, it can be considered that when comparing the two models,

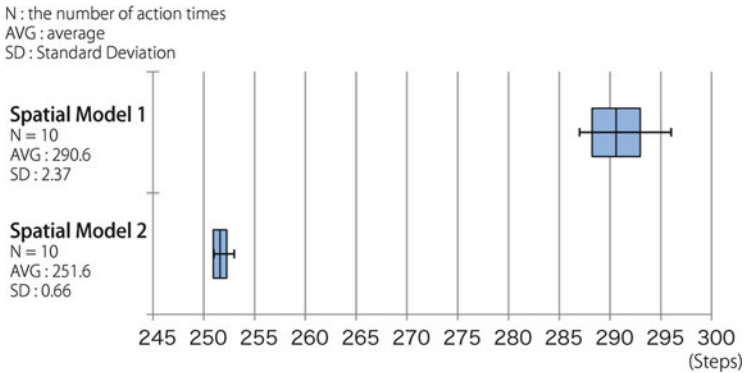


Fig. 5 Simulation result

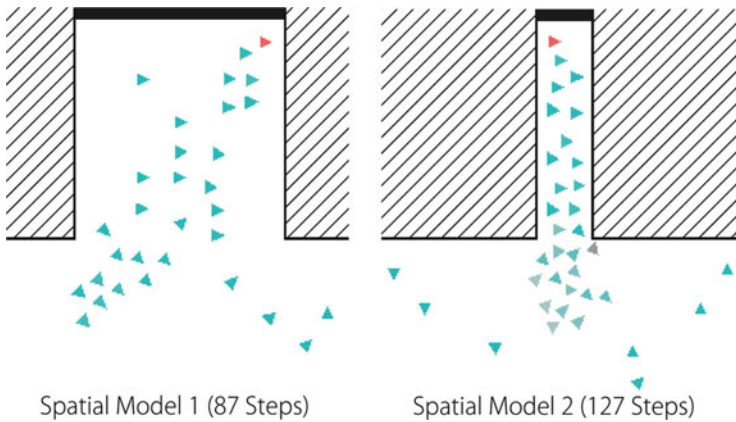


Fig. 6 Situations of the surroundings of each exit

the clear difference in the widths of exits and passages leading to the exits was directly connected to the results, which clearly demonstrated the effect of different widths when pedestrians converge. The great variation in the numbers of steps taken in Spatial Model 2 can be explained by the tendency to create local high density status, commonly known as bottlenecks; this phenomenon is different every time according to the position and timing of agents, as shown in Fig. 6.

4 Experiment of 3D Visualization of the Model

Google SketchUp Pro was used to create a three-dimensional spatial model, which was output in a 3ds file, and loaded using artisoc3.0. Figure 7 shows SketchUp images used to create the model.



Fig. 7 SketchUp image used to create the model



Fig. 8 Example of the pilot model

Figure 8 shows an example of the pilot model. The model successfully expresses such features as glass, signs, and furniture. The following areas all need to be improved: at present an agent maintains a rigid posture and appears to slide along the ground rather than walk naturally; clearer differentiation of light and dark areas; and better use of camera angles in depicting action. In addition, the file size tends to be larger (2,092 KB; 106 KB before 3D), and the model is also affected by computer processing capacity; using a MacBookAir (CPU: 1.7 GHz Intel Core i5, memory: 4 GB), it took an average of 31.7 s up to completion.

5 Conclusion

An evacuation simulation pilot model for an underground shopping street was made by introducing floor field potential, and the evacuation performance in two spatial models was confirmed. Through the simulation, it was found that the difference in exit widths caused the difference in time taken to complete evacuation, and blocking and stationary phenomena were also observed. In addition, three-dimensional visualization for this model was achieved.

References

1. C. Burstedde, et al.: "Simulation of Pedestrian Dynamics Using a Two dimensional cellular automaton", *Physica A*, pp.507–525, 2001
2. T. Wakiyama: "Searching Evacuation Strategies for High-Rise Office Buildings", in T. Kaneda et al. (eds), "Introduction to Pedestrian Agent Simulation by using Artisoc", pp.173–184, Kozo-Keikaku Engineering Inc., 2010 (in Japanese)
3. T. Kaneda: "Developing a Pedestrian Agent Model for Analyzing an Overpass accident", *Pedestrian and Evacuation Dynamics*, pp.273–284,2005
4. Y. He, et al.: "Adding Higher Intelligent Functions to Pedestrian Agent Model", *Pedestrian and Evacuation Dynamics*, pp.529–535, 2008
5. S. Yamakage: "Modeling and Expanding Artificial Societies", Hayama Publishers, 2009

Frozen Shuffle Update in Simple Geometries: A First Step to Simulate Pedestrians

J. Cividini, C. Appert-Rolland, and H.J. Hilhorst

Abstract We introduce a new type of update for cellular automata representing pedestrian traffic on a lattice. We investigate this update analytically and by Monte-Carlo simulations on a simple model. We are able to predict the fundamental diagram, and phase diagrams in several geometries.

Keywords Pedestrian traffic • Exclusion process • Shuffle update

As part of the effort to model pedestrian motion, the past years have seen the development of cellular automata based models, among which the so-called ‘floor field’ model [1, 2]. These models represent pedestrians as particles that jump from site to site on a discrete lattice, with an exclusion principle that forbids two pedestrians to simultaneously occupy the same site. In general, the pedestrians’ positions are subject to a parallel update procedure, i.e., the particles attempt to jump at the same instants of time. Although this type of update ensures a quite regular motion under free flow conditions, it creates conflicts when two or more pedestrians try to move at the same time to the same target site. Introducing an arbitrary numerical decision procedure to resolve these conflicts can be considered as a drawback and alternative update procedures have been looked for. In Ref. [3], for example, large pedestrian simulations are performed by means of a random shuffle update. In this sequential update scheme an updating order for the pedestrians is drawn at random at the beginning of each time step.

The random shuffle update was first proposed and studied in [4, 5]. It was applied there to the Totally Asymmetric Simple Exclusion Process (TASEP), which can

J. Cividini (✉) • C. Appert-Rolland • H.J. Hilhorst
Laboratory of Theoretical Physics Batiment 210, University Paris-Sud, CNRS, F-91405 Orsay
Cedex, France
e-mail: Julien.Cividini@th.u-psud.fr; Cecile.Appert-Rolland@th.u-psud.fr;
Henk.Hilhorst@th.u-psud.fr

be seen as a basic model for pedestrian traffic. A TASEP (for Totally Asymmetric Simple Exclusion Process) is a cellular automaton in which particles move on a lattice by jumping from one box to the next one, always in the same direction, say from the left to the right. This is an exclusion process, so there can be only 0 or 1 particle on each site. The TASEP does not have to be totally deterministic, the movements of the pedestrians can occur at some probability different from one, for instance. Still, in this paper, we shall only consider the case where all attempted jumps are performed if they are possible.

We decided to introduce a new type of update scheme, which seems to have interesting properties: the period of update for each pedestrian is exactly 1, it is possible to give a physical interpretation of the update – at least in the FF phase and conflicts are avoided.

It is called ‘frozen shuffle’ update, and it consists in updating the particles in a randomly chosen order, which does not change at each timestep but is fixed once for all. This order is implemented by giving each particle a “phase” τ between 0 and 1. This avoids priority issues between pedestrians: the first pedestrian to move will simply jump on its target before the other one. This update also lowers the statistical fluctuations, since all the pedestrians have barely the same velocity when they are not constrained. The dynamics is then deterministic once the order has been chosen, since the particles jump with probability 1 when they can. Besides, in the free flow phase, there exists a direct mapping between the discrete TASEP with frozen shuffle update and a model of moving rods in continuous space and time. Indeed, a particle moving at timestep t with a phase τ can be seen as a particle moving at continuous time $t + \tau$. We investigate this model analytically, and by Monte-Carlo simulation, for different boundary conditions and geometries.

1 Periodic Boundary Conditions

First, we study the TASEP with frozen shuffle update on the one-dimensional ring [8], the simplest non-trivial geometry. Our goal is to plot the fundamental diagram, i.e. the mean particle current j as a function of the density ρ of the system. The stochastic part of the model lies on the fact that one value of the density corresponds to several updating orders of the particles. As a preliminary, we see that a pair of two neighbour particles will move as a block if the first one has the smaller phase, whereas the two particles will need a hole between them to move with velocity 1 if they are ordered the other way, as seen in Fig. 1. A sequence of an arbitrary number of adjacent particles with well-ordered phases will then move as a whole, and will never be split anymore. These stable blocks of adjacent particles will be called platoons.

For the whole system, we see that there are two cases depending on the density:

- If $\rho < 1/2$, all the configurations will end up in a free flow state, a state in which all the particles can move at each timestep.

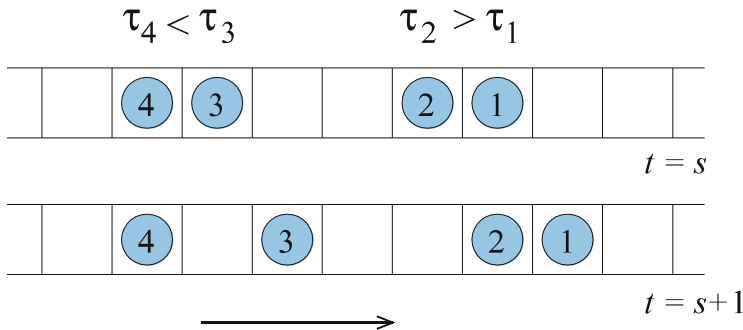


Fig. 1 Two configurations for pairs of particles. Particles 1 and 2 can move together because their phases are well ordered whereas 3 and 4 will spontaneously be separated by a hole [8]

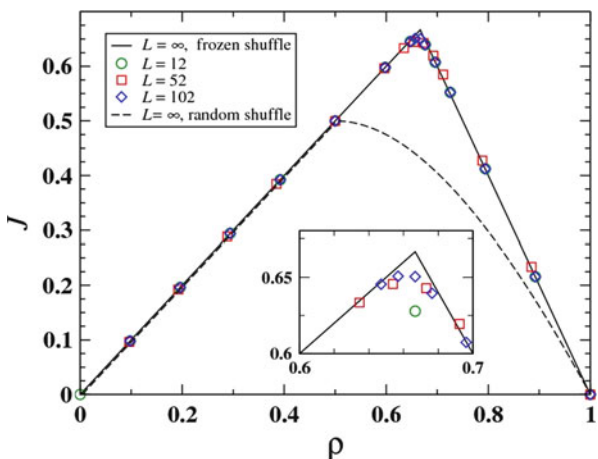


Fig. 2 Current as a function of the density in periodic boundary conditions for different system sizes. The *black lines* are the results of the theory and the *circles, squares and diamonds* are numerical data. The transition takes place for a density of $2/3$ for an infinite system. The curve becomes smooth for a finite system (From [8])

- If $\rho > 1/2$, there are configurations in which there is at most one hole between two consecutive platoons, these configurations will be called jammed.

We notice that there are more and more jammed configurations as ρ goes to 1. In the case of an infinite system, as the spatial average realizes effectively an average over the disorder, we find a phase transition separating the free flow phase and the jammed phase. A simple combinatorics argument shows that the average platoon length is 2, so that an intuitive value for the critical density would be $2/3$. We also were able to analytically predict finite-size corrections near the transition point [8]. We then carried out simulations and plotted the fundamental diagram. The results are shown in Fig. 2 with good agreement.

2 Open Boundary Conditions

Secondly, we use open boundary conditions [10] for the TASEP lane and we fix the entrance and exit probabilities, ρ and j being functions of these rates. Since we now have to create particles, we must now insert them into the already-existing particles update chain.

We use the aforementioned equivalence of the model with a continuous model of pedestrians evolving in a continuous space-time to prescribe how particles are injected in the system. In particular, it does not only determine the timestep at which a new particle enters the system, but also the phase this particle will be given.

The entrance algorithm satisfies two important properties. Firstly, the particles entering the system do not create a jam unless an exterior perturbation blocks them. In our case, they all move with velocity 1 if there is no jam at the exit. Secondly, the probability that a particle enters at a given time is constant, provided the entrance site is free. This allows us to define an entrance rate α , the probability a particle enters the system at a given timestep where the entrance site is empty. However, note that a particle may also be injected if the first site is not empty at the beginning of the timestep. The exit rate β is defined as usual: the probability that a particle occupying the exit site goes out of the system at the next timestep.

Again we expect to see a phase transition between a jammed state, in which an infinite queue of particles propagates upstream, and a free flow. The jamming transition occurs when the entering current becomes greater than the maximum current the exit can sustain. After some computation, one obtains the simple condition $\alpha = \beta$ for the transition line. We have considered only the deterministic version of the model for which pedestrians move with probability 1 when it is possible. The usual maximal-current phase is therefore reduced to a point. An unusual property of our update is that the current in the jammed phase depends not only on the exit rate, but also on the entrance rate as the latter has an effect on the average platoon length, therefore on the mean current.

Again, we were able to predict the finite-size rounding for $\rho(\alpha)$ near the critical point. We could also compute the density profile using a domain-wall approach [6, 7], which gives us the correlation length and some scaling law near the transition.

The results of the simulations are shown in Figs. 3 and 4. The agreement is very good for $\rho(\alpha)$, but some yet unexplained weak discrepancies between simulations and theory remain when it comes to the density profile.

3 Intersection

Finally, we consider a set of two open TASEP lanes sharing one site we shall refer to as the crossing. We can then vary the entrance and exit probabilities for each lane, and this should give us four possible states for the system, either lane being free or jammed. We shall refer to these regimes with the obvious abbreviations FF,

Fig. 3 Density as a function of the entrance rate for open boundary conditions, for $\beta = 0.4$. The *solid lines* represent the theory and the *dots* are the results of simulations. See [9]

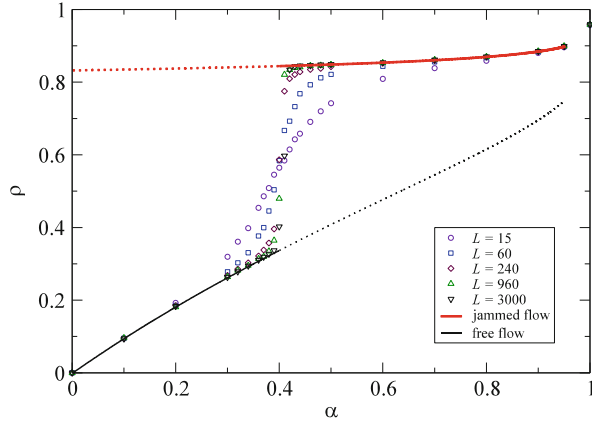
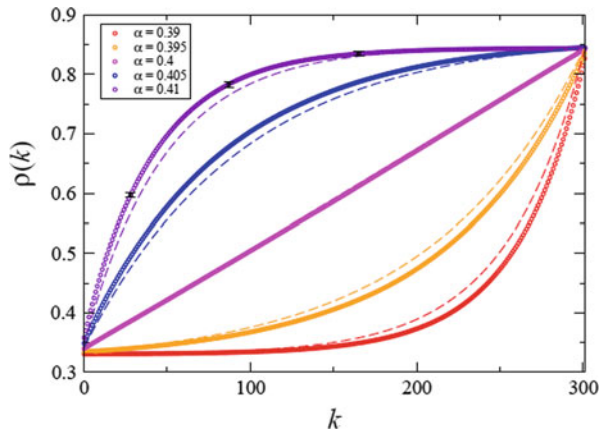


Fig. 4 Density profile in the lane across the transition for $\beta = 0.4$. k denotes the boxes of the lane. The *circles* are simulation results and the *dotted lines* are obtained using a domain wall approach (From [9])



FJ, JF and JJ. The simplest case is when the system is symmetrical between the two lanes: each lane has simply an effective exit rate of $\beta/2$. But we also studied an asymmetric system with exit probabilities set to one (in order to have only the jams created by the crossing and not by exit conditions). Eventually we vary each parameter independently.

In this geometry, the system shows an interesting property we called the pairing mechanism, explained in Fig. 5. This mechanism ensures that two incoming platoons will combine as they step in the crossing and go out at the same time. In simpler words, we have found a simple picture of the stationary JJ state, so that we can easily compute interesting properties of the system, the mean crossing occupation for example. It also gives us the outgoing current. We could obtain the current in the FJ/JF phase by similar means, and the method for the FF phase is the same as the one-dimensional case. As a summary, we computed the current (and the density) in all phases, so this gives us the analytical phase diagram as shown in Fig. 6, which agrees with numerics.

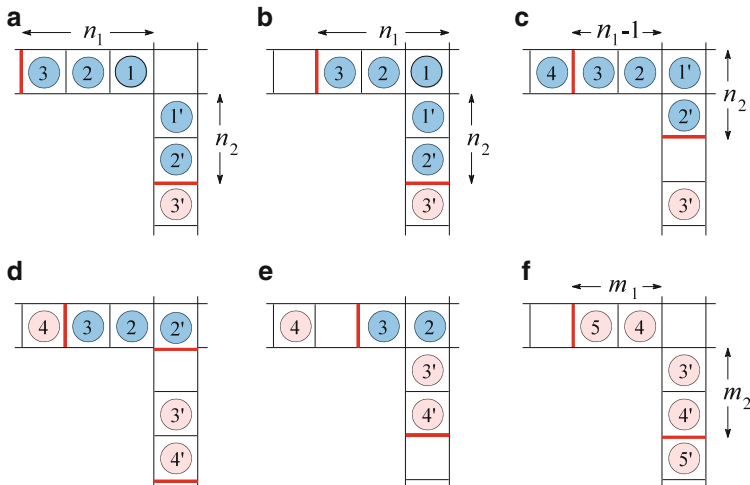


Fig. 5 Pairing effect in the crossing. The particles are represented by circles and the borders between platoons are emphasised as thick red lines. Suppose that we have two platoons P and P' waiting at the crossing (a), and that the phase of 1 is smaller than the phase of 1'. 1 will hop forward, so that all the platoon P will follow it (b). Since 1 moves before 1' and 2, the crossing will be free when either 1' or 2 tries to jump, here 1' is faster than 2 (c). This will happen until all the particles in one of the platoons go out (d). Now remember that there is necessarily a hole between the end of a platoon having jumped at the previous timestep (2') and the beginning of the next one (3'). This ensures that the platoon P will go through the crossing before the new one (e). Eventually, the system will start again the process with two new platoons (f) [10]

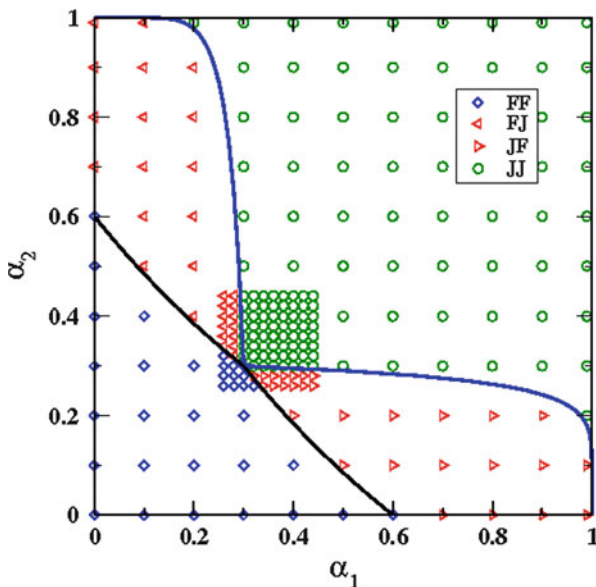


Fig. 6 Phase diagram of the crossing for $\beta = 0.6$. The lines are the theoretical boundaries and the diamonds, triangles and circles are the numerics [10]

4 Conclusion

To conclude, we have introduced in this paper a new update scheme for the TASEP, namely the frozen shuffle update, which should be appropriate, in particular, for the modeling of pedestrians. We were able to fully determine the fundamental diagram on a ring, and all the macroscopic properties of the systems with open boundary conditions. A mapping with a continuous model of hard rods exists [8], which is exact for free flow configurations, and may be useful for the interpretation of the results in terms of pedestrian motion.

In further work, we plan to take into account the width of the corridors through multilane models, and to enlarge the crossing to a bigger square. Our aim would be to understand how macroscopic structures can spontaneously emerge in such systems, and how they are modified for various modifications of the dynamical rules. Another question would be the behavior of the system with one more stochastic component, i.e. if we allowed the particles to jump with probability $p < 1$.

References

1. C. Burstedde, K. Klauck, A. Schadschneider, and J. Zittartz. Simulation of pedestrian dynamics using a 2-dimensional cellular automaton. *Physica A*, 295:507–525, 2001.
2. A. Schadschneider. Cellular automaton approach to pedestrian dynamics - theory. In M. Schreckenberg and S.D. Sharma (Eds.), editors, *Pedestrian and Evacuation Dynamics*, pages 75–85. Springer, 2002.
3. H. Klupfel. The simulation of crowds at very large events. In A. Schadschneider, T. Poschel, R. Kuhne, M. Schreckenberg, and D.E. Wolf, editors, *Traffic and Granular Flow'05*, pages 341–346, 2007.
4. M. Wolki, A. Schadschneider, and M. Schreckenberg. Asymmetric exclusion processes with shuffled dynamics. *J. Phys. A-Math. Gen.*, 39:33–44, 2006.
5. D.A. Smith and R.E. Wilson. Dynamical pair approximation for cellular automata with shuffle update. *J. Phys. A: Math. Theor.*, 40(11):2651–2664, 2007.
6. A.B. Kolomeisky, G.M. Schütz, E.B. Kolomeisky, and J.P. Straley. Phase diagram of one dimensional driven lattice gases with open boundaries. *J. Phys. A: Math. Gen.*, 31:6911, 1998.
7. C. Pigorsch and G.M. Schütz. Shocks in the asymmetric simple exclusion process in a discrete-time update. *J. Phys. A: Math. Gen.*, 33:7919–7933, 2000.
8. C. Appert-Rolland, J. Cividini and H. Hilhorst. Frozen shuffle update for an asymmetric exclusion process on a ring. *J. Stat. Mech.*, P07009, 2011.
9. C. Appert-Rolland, J. Cividini and H. Hilhorst. Frozen shuffle update for deterministic totally asymmetric simple exclusion process with open boundaries. *J. Stat. Mech.*, P10013, 2011.
10. C. Appert-Rolland, J. Cividini and H. Hilhorst. Intersection of two TASEP traffic lanes with frozen shuffle update. *J. Stat. Mech.*, P10014, 2011.

Fundamental Diagram as a Model Input: Direct Movement Equation of Pedestrian Dynamics

E. Kirik, A. Malyshev, and E. Popel

Abstract Inspiring by advantages of continuous and discrete approaches to model pedestrian dynamics a new discrete-continuous model SIGMA.DC. was developed. This model is of individual type; people (particles) move in a continuous space - in this sense model is continuous, but number of directions where particles may move is a model parameter (limited and predetermined by a user) - in this sense model is discrete. To find current velocity vector we do not describe forces that act on people. To have a value of velocity we use a fundamental diagram data; and probability approach is used to find a direction. Description of the model and some simulation results are presented.

1 Introduction

In the paper a new type of pedestrian movement model is presented.¹ Idea of the model is motivated by the following points. Nowadays computer simulations based on mathematical models are used to reproduce different phenomena. Usually real-life phenomena are continuous. At the same time computer calculations are discrete by nature; and discrete models are more convenient for computer simulation and save computational time.

The last one encouraged developing of discrete approach to model pedestrian dynamics. Discrete models are discrete by space and time. Such models operate

¹A model is of individual type when trajectories of each person are simulated.

E. Kirik (✉) • A. Malyshev
Institute of Computational Modelling SB RAS, Krasnoyarsk, Russia
e-mail: kirik@icm.krasn.ru

E. Popel
Siberian Federal University, Krasnoyarsk, Russia

with spaces sampled into cells of some size (often $40\text{cm} \times 40\text{cm}$ in size [11]), which are either empty or occupied by the only person (exclusive principle). Usually each particle can move to one of its four (the von Neumann neighborhood) or eight (Moore neighborhood) adjacent cells or stay in the present cell at each discrete time step $t \rightarrow t + 1$; i.e., $v_{\max} = 1[\text{step}]$. There are models that allow $v_{\max} > 1[\text{step}]$. Discrete models describe people dynamics (including interaction with environment) in a rule-based way. Stochasticity of the people movement is captured by calculating probabilities to move in each direction. It gives models relative mathematical simplicity, and it is the pros, and the cons are problems concerning adjusting real object sizes to discrete model space. Sometimes in a focus of engineering investigation is, for example, a changing of a door size on 5–15 cm. Discrete models can not pick up such point. But such point is very significant for the main application of pedestrian evacuation models that are fire safety problems.

Continuous models imply that people move in a continuous space. Generally there are no restrictions on directions and steps lengths except nearest people and obstacles. From practical applications continuity of a space is the pros; and cons of traditional continuous approach are problems with movement equation. In Newtonian mechanics to define trajectory of an object (person) one need to know current position and velocity vector (or its time derivative that is acceleration). Acceleration vector is given usually by forces that act on object (the second Newton's law) $m\vec{a} = \vec{F}$. There are already examples of force-based models of pedestrian dynamics such as social- [2] and generalized centrifugal- [1] force models. The main goal in such models is to describe forces \vec{F} and solve system of N differential equations in a correct way (N – number of people). One necessary (but not sufficient) condition is agreement of simulated velocity-density dependence with the empirical data (fundamental diagram - FD).

An idea of the discrete-continuous approach proposed is to omit solution of the differential equations system and to “extract” velocity scalar for each person from empirical data in accordance with local (simulated) densities. We use analytical expressions of velocity versus density by Kholshevnikov and Samoshin [3, 4]. The next step direction is proposed to be stochastic with probabilities distribution calculated. Set of possible directions is predetermined. Procedure of calculating probabilities to move to each of the directions is adopted from previously presented stochastic cellular automata floor field model [7] and gives the highest probability to direction that has most preferable conditions for movement considering other particles and obstacles and strategy of the people movement (the shortest path and/or the shortest time). Directed movement is given by using the static floor field that shows a distance from each point of the space to the nearest exit. So person at each time step is allowed to move in a continuous space - in this sense model is continuous, but number of directions where particles may move is limited and predetermined by a user - in this sense model is discrete. Such approach seems to be fruitful and useful from both mathematical statement and practical applications.

The article is organized as follows. In the next section, statement of the problem is presented. It is followed by the decision section (movement equation, choosing direction, velocity formula are presented), simulation section and conclusion.

2 Statement of the Problem

Modeling space $\Omega \in R^2$ and infrastructure (obstacles) are known.² People may move to (and thought) a free space only. To orient in the space particles use the static floor field S [11]. Let the nearest exit is assumed as a target point of each pedestrian.

Shape of each particle is disk with diameter d_i , initial positions of particles are given by coordinates of the center of the disks $\vec{x}_i(0) = (x_i^1(0), x_i^2(0))$, $i = \overline{1, N}$, N – number of particles (it is supposed that these are coordinates of mass centre projection). Each particle is assigned with the free movement velocity³ v_i^0 , square of projection, mobility group.

Each time step t each particle i may move in one of predetermined directions $\vec{e}_i(t) \in \{\vec{e}^\alpha(t), \alpha = \overline{1, q}\}$, q – number of directions, model parameter (for example, a set of directions uniformly distributed around the circle will be considered here $\{\vec{e}^\alpha(t), \alpha = \overline{1, q}\} = \{(\cos \frac{2\pi}{q}\alpha, \sin \frac{2\pi}{q}\alpha), \alpha = \overline{1, q}\}$).

The goal is to model individual people movement to the target point taking into account interaction with environment.

3 Decision

There is a preliminary step that includes calculation of static floor field S . This field stores the information on the shortest distance to the nearest exit; i.e., field S increases radially from the exit and it is zero in the exit(s) line(s). It does not change with time and is independent of the presence of the particles. The unit of this distance is meters, [m]. Here we omit procedure of calculating static field S .

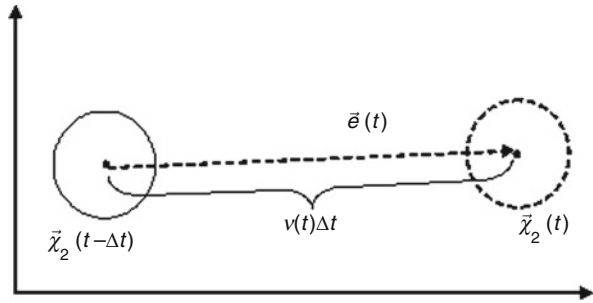
3.1 Movement Equation

In this approach a person movement equation is derived from a finite-difference expression $v(t)\vec{e}(t) \approx \frac{\vec{x}(t) - \vec{x}(t - \Delta t)}{\Delta t}$ that is given by a velocity definition.

²There is unified coordinate system, and all data are given in this system.

³We assume that free movement velocity is random normal distributed value with some mathematical expectation and dispersion [3, 4].

Fig. 1 Movement scheme



This expression allows to present new position of the particle as a function of a previous position and local particle’s velocity. Thus for each time t coordinates of each particle i are given by the following formula:

$$\vec{x}_i(t) = \vec{x}_i(t - \Delta t) + v_i(t) \vec{e}_i(t) \Delta t, \quad i = \overline{1, N}, \tag{1}$$

where $\vec{x}_i(t - \Delta t)$ – coordinates in previous time moment; $v_i(t)$, [m/s] – the particle velocity; Δt , [s] – length of time step (fixed), Fig. 1.

Unknown values in Eq. 1 for each time step for each particle are velocity $v_i(t)$ and direction $\vec{e}_i(t)$. As it was said above we omit to describe forces that act on person, solve differential equations and get velocity vector $\vec{v}_i(t)$. We propose to “extract” velocity from experimental data (fundamental diagram). In this case in contrast with force-based models we have an opportunity to divide task of finding velocity vector to two parts. At first a direction is determined; then, a velocity, according to local density in the direction chosen.

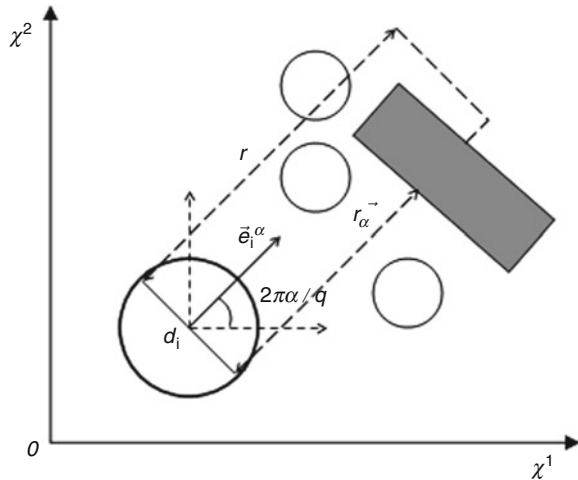
In conditions considered it’s supposed that while moving people have maximal velocity (free movement velocity), and each person maintain velocity in accordance with local density. Particles that cross target line leave the modeling space.

3.2 Direction

In this discrete-continuous model we took inspiration from our previously presented stochastic CA FF model [7]. Stochasticity of the model is realized by calculating for each person each time step probabilities to move in each direction (among all allowed) and choosing direction according to probability distribution obtained.

Probabilities in the model are not static and vary dynamically and issued from the following facts. Pedestrians keep themselves at a certain distance from other people and obstacles. The tighter the crowd and the more in a hurry a pedestrian, the smaller this distance. During movement, people follow at least two strategies: the shortest path and the shortest time.

Fig. 2 Scheme of visibility area of particle in the direction $\rightarrow e_i^\alpha(t)$



Thus personal probabilities to move in each direction each time step have three contributions: (a) the main driven force (given by destination point), (b) interaction with other pedestrians, (c) interaction with an infrastructure (non movable obstacles). The highest probability⁴ is given to direction that has most preferable conditions for movement considering other particles and obstacles and strategy of the people movement (the shortest path and/or the shortest time).

The following procedure is applied to each particle to calculate transition probabilities for the particle to move in each of predetermined directions from current position and then to choose a required direction.

Let particle i has current coordinate $\vec{x}_i(t - \Delta t)$. The probability of movement from this position to direction $\vec{e}^\alpha(t) = (\cos \frac{2\pi}{q}\alpha, \sin \frac{2\pi}{q}\alpha)$, $\alpha = \overline{1, q}$ during next time step is the following:

$$p_\alpha^i(t) = \frac{\widehat{p}_\alpha^i(t)}{Norm} = \frac{\exp\left(-k_W^i \left(1 - \frac{r_\alpha^*}{r}\right) 1(\Delta S_\alpha)\right) \exp\left(-k_P^i F(r_\alpha^*)\right) \exp\left(k_S^i \Delta S_\alpha\right)}{Norm} W\left(r_\alpha^* - \frac{d_i}{2}\right), \tag{2}$$

where $Norm = \sum_{\alpha=1}^q \widehat{p}_\alpha^i(t)$.

Visibility radius r ($r \geq \max\left\{\frac{d_i}{2}\right\}$), [m], is model parameter representing the maximum distance at which people and obstacles influence on the probability in the given direction. If it is necessary visibility radius r is reduced to a value r_α^* (Fig. 2)

⁴Mainly with value 0, 8–0, 9.

People density $F(r_\alpha^*) \in [0,1]$ is estimated in the visibility area, see bellow.

Function $1(\cdot)$ is Heaviside unit step function.

Model parameter $k_S^i > 0$ is field S -sensitive parameter. Model parameter $k_W^i > k_S^i$ is wall-sensitive parameter. Model parameter $k_p^i > 0$ is density-sensitive parameter. Information on parameters presented bellow.

$\Delta S_\alpha = S(t - \Delta t) - S_\alpha$, where $S(t - \Delta t)$ – static floor field in the coordinate $\vec{x}_i(t - \Delta t)$, S_α – static floor field in the coordinate $\vec{x} = \vec{x}_i(t - \Delta t) + 0, 1 \vec{e}_i^\alpha(t)$. With ΔS_α moving to the target point is controlled.

Function $W\left(r_\alpha^* - \frac{d_i}{2}\right) = \begin{cases} 1, & r_\alpha^* - \frac{d_i}{2} > w \\ 0, & r_\alpha^* - \frac{d_i}{2} \leq w \end{cases}$ controls approaching to obstacles,⁵ model parameter $0 \leq w \leq 0, 1, [m]$, – coefficient of inadherence to obstacles.

If $Norm = 0$ than particle does not leave present position.⁶

If $Norm \neq 0$ than required direction $\vec{e}_i(t)$ is considered as discrete random value with distribution that is given by transition probabilities obtained. Exact direction $\vec{e}_i(t) = \vec{e}_i^{\hat{\alpha}}(t) = \left(\cos \frac{2\pi}{q} \hat{\alpha}, \sin \frac{2\pi}{q} \hat{\alpha}\right)$ is determined in accordance with standard procedure for discrete random values.

3.3 Velocity

Person’s velocity is density dependant. We assume that only conditions in front of the person influence on velocity.⁷ Thus only density $F\left(r_\alpha^*\right)$ in direction chosen $\vec{e}_i(t) = \vec{e}_i^{\hat{\alpha}}(t)$ is required. According [3, 4] current velocity of the particle is

$$v_i(t) = v_i^{\hat{\alpha}}(t) = \begin{cases} v_i^0 \left(1 - a_l \ln \frac{F\left(r_\alpha^*\right)}{F^0}\right), & F\left(r_\alpha^*\right) > F^0; \\ v_i^0, & F\left(r_\alpha^*\right) \leq F^0, \end{cases} \tag{3}$$

where F^0 – limit people density until which free people movement is possible (density does not influence on speed of people movement); a_l – factor of people adaptation to current density while moving on l -th kind way ($a_1 = 0, 295$ is for horizontal way; $a_2 = 0, 4$, for down stairs; $a_3 = 0, 305$, for up stairs).

⁵Note function $W(\cdot)$ “works” with nonmovable obstacles only.

⁶Actually this situation is impossible. Only function $W(\cdot)$ may give (mathematical) zero to probability. If $Norm = 0$ then particle is surrounded by obstacles from all directions.

⁷It is motivated by a front line effect in a dense people mass when front line people move with free movement velocity while middle part is waiting a free space available to make a first step. As a result it leads to a diffusion of the flow. Otherwise simulation will be slower then real process.

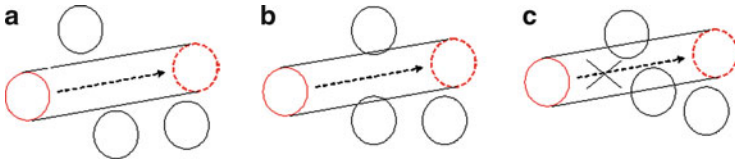


Fig. 3 Possible situations. *Dashed circle* is a desired new position (in time t) of considering particle. Positions of other particles are for previous time moment $t - \Delta t$

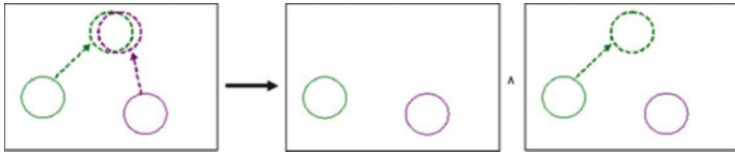


Fig. 4 Conflict situation. *Dashed circles* are desired new positions (in time t). Resolution of the conflict is leaving both particles in their places or move one of them to a new position

3.4 Collisions

Direction $\vec{e}_i(t)$ and velocity $v_i(t)$ obtained substituted in Eq. 1. If particle moves from position $\vec{x}_i(t - \Delta t)$ to a new position $\vec{x}_i(t) = \vec{x}_i(t - \Delta t) + \vec{e}_i(t)v_i(t)\Delta t$ without collisions (intersections) with other particles new coordinate for the particle is fixed. Allowed situations (when we consider that there is no collision) are presented in Fig. 3. Otherwise when situation in Fig. 3 takes place reduced step is allowed only or movement is denied at all. Note (!) that positions of other particles are taken in to account for time $t - \Delta t$.⁸

When new positions of all particles are calculated then corrections of possible collisions are applied.⁹ It takes place if there are particles l, m intended to one position: $|\vec{x}_l(t) - \vec{x}_m(t)| \leq \frac{d_l}{2} + \frac{d_m}{2} - \Delta d$, Fig. 4. In this case conflict resolution procedure is applied. Movement of all the involved particles is denied with probability μ ; i.e., pedestrians stay at their current positions with probability μ . One of candidates moves to the desired cell with probability $1 - \mu$. A person allowed to move is chosen randomly.

3.5 Discussion

In this subsection model parameters and local density estimation are presented.

⁸Parallel update scheme is used here.

⁹Only here we operate with coordinates obtained during current time step.

3.5.1 Model Parameters

There are non-dimensional model parameters: k_S^i, k_W^i, k_P^i .

Parameter $k_S^i > 0$ is field S -sensitive parameter which can be interpreted as knowledge of the shortest way to the exit or a wish to move to the exit. The equality $k_S^i = 0$ means that the pedestrian ignore the information from field S and move randomly. The higher k_S^i , the better directed the movement. For wide range of evacuation tasks that intend directed movement $k_S^i = 40$ is normal.

Parameter $k_W^i \geq 0$ is wall-sensitive parameter which determines the effect of walls and obstacles. We assume that people avoid obstacles only moving towards the destination point. When people make detours (in this case $\Delta S_\alpha^i < 0$) approaching the obstacles is not excluded.

Parameter $k_P^i > 0$ is the density-sensitive parameter which determines the effect of the people density. The higher parameter k_P^i , the more pronounced the shortest time strategy¹⁰ for the person.

Note that probabilities are density adaptive; the low people density lowers the effect of density-sensitive term, and the probability of the shortest path strategy increases automatically. But this automatic property is not enough. Ideally a time-spatial adaptation for model parameters is required. There are time-spatial conditions when it is necessary to force a reduced values to k_P^i and k_W^i .

All parameters may be assigned individually or unified for all involved particles.

3.5.2 Density Estimate

Local density is estimated for each particle in each direction each time step. So it is the most time consuming procedure over all simulation. We examined some methods. Recall that in the model density is estimated in the visibility area for each direction, Fig. 2. Coordinates of all involved particles are considered for time $t - \Delta t$.

Analytical estimate supposes to calculate total square S_2 of other particles that intersect the visibility area with square $S_1 = d_i \cdot r_\alpha^*$. There were developed an algorithm to identify positions of each disc intersecting visibility area and the geometric formulas to calculate the intersection area. Density is $F(r_\alpha^*) = S_2/S_1, [m^2/m^2]$.

Grid method supposes dividing visibility area to G_1 small cells. Density is $F(r_\alpha^*) = G_2/G_1, [m^2/m^2]$, G_2 - number of cells intersecting with some disc.

Monte Carlo method gives density estimate as a relation $F(r_\alpha^*) = M_2/M_1, [m^2/m^2]$, where M_1 - number of randomly placed points in the visibility area, M_2 - number of points intersecting with some disc.

Rozenblat-Parsen's nonparametric kernel estimate [8] gives a weighted estimate of the density. From movement conditions situations in Fig. 5 are different. In the

¹⁰For more detailed information on model parameters see in [5, 7].

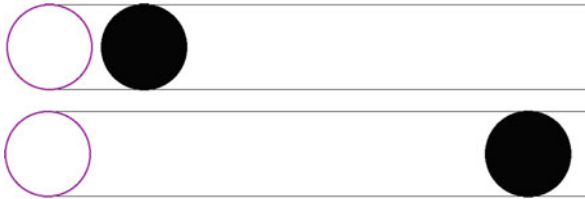


Fig. 5 Examples of possible density conditions in visibility area

Table 1 Execution time for each method in equal conditions with accuracy at least 99 %

Method	Analytical	Monte Carlo	Rosenblatt-Parzen	Grid
Time of 1,000 calculations, in seconds	0,119	0,119	1,250	1,263

first case motion in this direction is impossible; in the second, possible. Analytical, grid, and Monte-Carlo methods give the same density in both situations.

To distinguish both cases numerically is available by using weighted density estimate. Two steps are required. According to Monte Carlo method M_2 points with coordinates $(\bar{x}_j^1, \bar{x}_j^2)$, $j = \overline{1, M_2}$, are determined. Then each of these points is provided with certain “weight” that depends on a distance between a point and center $\vec{x}_i(t - \Delta t)$ of the considering person. So weighted density estimate is $F(r_\alpha^*) = \frac{1}{C^1 C^2 M_1} \sum_{j=1}^{M_2} \Phi\left(\frac{x_i^1(t - \Delta t) - \bar{x}_j^1}{C^1}\right) \Phi\left(\frac{x_i^2(t - \Delta t) - \bar{x}_j^2}{C^2}\right)$, where $C^1 =$

$$d_i \sqrt{5}, C^2 = r_\alpha^* \sqrt{5}, \Phi(z) = \begin{cases} 0,335 - 0,067z^2, & z^2 \leq 5; \\ 0, & z^2 > 5. \end{cases}$$

Among these methods the most accurate and the fastest is analytical. But it is sensitive to the shape of geometrical forms. Analytical method was used to check other methods. Numerical methods (Monte Carlo and grid) operate at about the same rate. But to achieve 99 % accuracy Monte-Carlo method needs $M_1 = 5000$ points; grid method, 100,000 cells, see Table 1

4 Simulation

There were investigated movement in straight corridor $b = 2$ m in width for periodic and open boundary conditions for the same set of initial densities, parameters $k_s^i = 40, k_w^i = 0, k_p^i = 5,^{11} q = 16$ uniformly distributed over the circle, $r = 5$ m.

¹¹Model parameters were chosen to simulate directed movement only with the shortest path strategy due to shape of the geometry

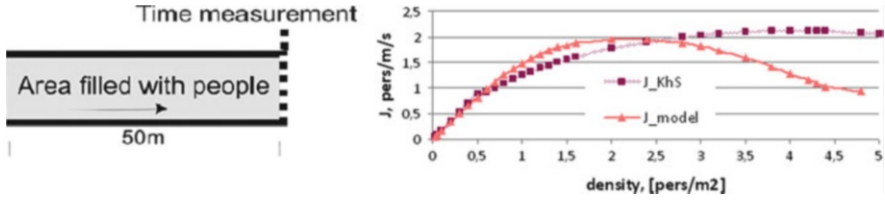


Fig. 6 Case study geometry for periodic boundary conditions (left); fundamental diagram: J_{model} is for model presented; J_{KhS} is given by product of velocity Eq. 3 and density (right)

4.1 Periodic Boundary Conditions

Case study is presented in Fig. 6. There was a control line and we measured time T that $\hat{N} = 1000$ people needs to pass this line.¹² To model periodic boundary conditions there was maintained a permanent number of people during all experiment.

Velocities $v_i^0, i = \overline{1, N}$ were normal distributed random values with $E v^0 = 1,75$ [m/s], and $\sigma(v^0) = 0,083$ [m/s], diameter of particles was $d = 0,4$ [m].

A model specific flow is $J_s = \hat{N}/T/b$, [pers/s/m]. Model fundamental diagram is in Fig. 6 (right). It is compared with fundamental diagram $J_s = v\rho$ by Kholshchikov and Samoshin [3, 4], where velocity is given by Eq. 3, $\rho = N/\max n$, $\max n$ is maximal number of particles with $d = 0,4$ that are possible to place in the corridor.

There is a perfect coincidence of the model flow with real data for low densities. For middle densities model is faster then experimental data. It seems to be a computational impact of the density estimation. Model gives lower density and consequently has faster velocity. For high densities model is considerably slower than a real flow. It seems to be an impact of the model as it is.

4.1.1 Open Boundary Conditions

Case study is presented in Fig. 7. Under open boundary conditions model flow was investigated in two corridors 50 and 100 m show diffusion of the flow.

Velocities $v_i^0, i = \overline{1, N}$ were given as a normal distributed random values with $E v^0 = 1,3$ [m/s], and $\sigma(v^0) = 0,06$ [m/s], diameter of particles was $d = 0,4$ [m].

T_{tot}^{50} and T_{tot}^{100} are average total evacuation times (in seconds) for both corridors.¹³ To compare data there were used $\tilde{T}^{50} = T_{tot}^{50}, \tilde{T}^{100} = T_{tot}^{100} - 30$.¹⁴ Corresponding

¹²One hundred simulations for each density were made, and average time is considered.

¹³Here we use average value over 100 simulations for each density and corridor.

¹⁴Thirty second is minimal time to reach control line in corridor 100 m in length.

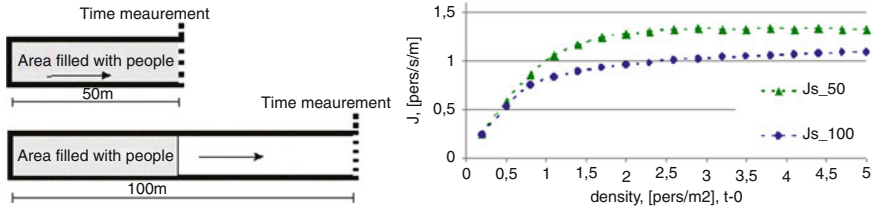


Fig. 7 Case study geometry for periodic open conditions (*left*); specific flows: J_s ₅₀ is for 50 m corridor; J_s ₁₀₀, for 100 m corridor (*right*)

specific flows are $J_s^{50} = N/\tilde{T}^{50}/2$, $J_s^{100} = N/\tilde{T}^{100}/2$, [pers/s/m] (see Fig. 7, right).

Each curve has two typical phases; it goes up until some initial density and then J_s^{50} is stable, J_s^{100} goes up very slowly. Such behavior is expected and says that capacity is reached for 50 m corridor, and in other case due to longer distance capacity may be “update” for higher densities.

Perfect coincidence of flows for low densities shows that corresponding initial density maintains during all experiment. It means that density (till 0, 5 [pers/m]) is comfortable and persons do not use an opportunity (in 100 m corridor) to decrease local density. Critical value 0, 5 [pers/m] matched with empirical data in [3, 4].

Divergence of the curves means that in 100 m corridor an opportunity to decrease density is used and flow diffusion realized.

5 Conclusion

Model SIGMA.DC allows to simulate people movement in arbitrary geometry. Free movement velocity, square of projection, mobility group, age of each person may be assigned individually.

A new approach to describe movement equation is presented. In contrast to force-based models, in model obtained velocity-density dependence is used in pure way. Instead of (3) one can use FD that is more appropriate to a task. Directions’ probabilities distribution imitates forces that act on person each time step.

Of course model is “computationally heavier” in comparing with discrete variant but this is a price for flexibility and applicability. Comparing with force-based models this model is faster considerably: $\Delta t = 0,25$ s in this model versus $\Delta t = 0,01$ s in force-based models [1, 2].

Dynamical properties of the model are good. Comparing with other fundamental diagrams [11] one can say that the model flow in periodic boundary conditions generally (quantitatively and qualitatively) coincides with an existing conception on the velocity-density dependence of people flow.

Experiments on open boundary conditions showed expected and qualitatively the same behavior that model should reproduce, and RIMEA collection presents [10].

Model parameters allow to model people movement from arbitrary to strongly directed. Time-spatial adaptation for model parameters is required. We continue to develop and investigate SIGMA.DC discrete-continuous stochastic floor field people movement model.

Acknowledgments This work is supported by the Integration project of SB RAS 2012–2014, contract 49.

References

1. Chraïbi, M., Seyfried, A., Schadschneider, A. (2010) Generalized centrifugal-force model for pedestrian dynamics // *Physical Review E*, 82, 046111.
2. Helbing, D., Farkas, I., Vicsek, T. (2000) Simulating dynamical features of escape panic // *Nature* 407, 487–490.
3. Kholoshevnikov, V.V., Samoshin, D.A. (2009) Evacuation and human behavior in fire, Moscow, Academy of State Fire Service, EMERCOM of Russia, 212 p. (Rus.)
4. Kholoshevnikov, V.V. (2011) Forecast of human behaviour during fire evacuation // In the book “Emergency evacuation of people from buildings” (EMEVAC’2011 Proceedings), Warsaw: Belstudio, 139–153.
5. Kirik, E., Yurgel’yan, T., Krouglov D. (2010) On Influencing of a Space Geometry on Dynamics of Some CA Pedestrian Movement Model // *Lecture Notes in Computer Science*, V. 6350, Cellular Automata, 474–479.
6. Kirik, E., T. Yurgel’yan, A. Malyshev (2011). On discrete-continuous stochastic floor field pedestrian dynamics model SIGMA.DC // In the book “Emergency evacuation of people from buildings” (EMEVAC’2011 Proceedings), Warsaw: Belstudio, 155–161.
7. Kirik, E., Yurgel’yan, T., Krouglov, D. (2011) On realizing the shortest time strategy in a CA FF pedestrian dynamics model // *Cybernetics and Systems*, vol.42:01, 1–15.
8. Parzen, E. (1962) On estimation of probability Density Function // *Ann.Math. Stat.*, Vol.33, 1065–1076.
9. Predtechenskii, V.M., Milinskii, A.I. (1978) Planing for foot traffic flow in buildings. American Publishing, New Dehli. Translation of: Proektirovanie Zhdanii s Uchetom organizatsii Dvizheniya Lyudskikh potokov, Stroiiizdat Publisher, Moscow, 1969.
10. Rogsch, C. Vergleichende Untersuchungen zur dynamischen Simulation von Personenströmen, Diploma thesis of the University of Wuppertal and the Research Center Julich, 2005.
11. Schadschneider, A., Klingsch, W., Kluepfel, H., Kretz, T., Rogsch, C., Seyfried, A. (2009) Evacuation Dynamics: Empirical Results, Modeling and Applications. *Encyclopedia of Complexity and System Science*. Springer.

Improving Flexibility of Agent's Path Selection in Cellular Pedestrian Flow Model

Juha-Matti Kuusinen and Sergey Kitov

Abstract Motivated by the results of an exit selection experiment, this paper presents an agent-based cellular automaton with a new path selection approach. In our model, an agent first selects a target cell within a look-ahead distance by avoiding conflict with other agents and minimizing the distance to destination. Then, the agent moves to the neighbor cell which minimizes the distance to the selected target and the repulsion induced by other agents. Simulation of the experiment with our new model gives more realistic results than with a simple model taking account of only local information. Furthermore, our model successfully simulates self-organized phenomena such as lane formation.

Keywords Cellular automata • Agent-based modeling • Path selection

1 Introduction

A popular approach for modeling pedestrian dynamics combines a cellular automaton and agent-based modeling [1–5]. In most of these models, an agent selects its next movement based on a static field which stores the distance to destination for each cell, and a dynamic field which defines the interaction between the agents. A common approach is to base movement selections on comparisons of the field values on those cells that are available as the agent's next position. This makes the agents move along the gradient of the static field, i.e. along the shortest path to the destination. Such movement decisions are optimal with respect to time to destination when the shortest path does not contain any obstacles. In reality, however, the shortest path may be blocked, e.g., by other pedestrians, and thus, another direction

J.-M. Kuusinen (✉) • S. Kitov
KONE Elevators Ltd., Keilasatama 3, Espoo, Finland
e-mail: juha-matti.kuusinen@kone.com; sergey.kitov@kone.com

in which the static field is locally increased might be selected. Such behavior cannot be reproduced with models that take into account only local information. The reason is that information about alternative paths is simply unavailable to the agents. Hence, they act as if alternative paths do not exist.

Recently, an experimental study on pedestrian exit selection in the evacuation of a corridor was conducted [6]. Motivated by the findings in this study, we suggest a new path selection model to reproduce the pedestrian exit selection behavior observed in the experiment. In our model, an agent observes the cells within a predefined look-ahead distance in nine directions and selects a target cell that minimizes the distance to destination and has the least conflict with other agents. A similar approach for direction selection was used in [7] on the top of the successful social force model [8]. Contrary to the common approach, our model is based on asynchronous updating. The agent that moves next is defined according to a priority queue containing the agents' individual updating times in an ascending order.

To account for speed variations due to crowding, we calibrate our model based on Fruin's speed-density diagram [9]. This calibration is required since our movement model is fairly simple and does not adjust speeds with respect to crowding as such. By simulating the exit selection experiment, we compare our model to a simple model that takes into account only local information. We show also that our approach is able to reproduce self-organized effects encountered experimentally in real crowds, namely, lane formation and oscillations at bottlenecks [10].

2 Model Description

2.1 Agent Updating and Movement Model

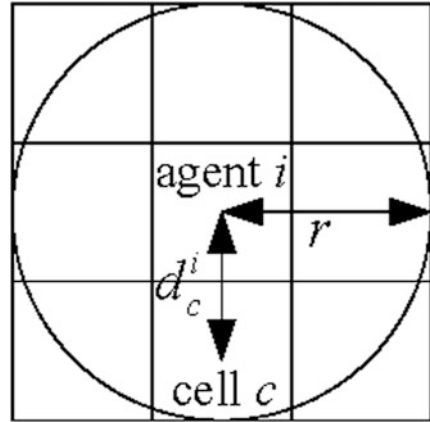
In our model, an agent can occupy only one cell at a time, and one cell can be occupied by no more than one agent. In this study, the dimensions of a cell are 40×40 cm. Movement from the current cell can be made to one of the eight neighbor cells. Diagonal moves are $\sqrt{2}$ times longer than non-diagonal moves. This corresponds to "variant 2" metric in [11].

The k th movement time of agent i is t_k^i , and the next agent that moves is the agent with the lowest movement time. After the move is made, the individual movement time of the agent i is increased by the ratio of the moved distance d_k^i to the agent's speed v_k^i ,

$$t_{k+1}^i = \begin{cases} t_k^i + \frac{d_k^i}{v_k^i}, & d_k^i > 0 \\ t_k^i + \frac{1}{v_{free}^i}, & d_k^i = 0 \end{cases}, \quad (1)$$

where v_{free}^i is the free flow speed of agent i measured in cells per second. The moved distance and speed are determined before the move is made. The speed depends on

Fig. 1 Emission of repulsion of agent i to cell c



the proximity of other agents as described below. The moved distance equals 1 for a horizontal or vertical move, $\sqrt{2}$ for a diagonal move, and 0 if the agent stays in its current cell.

With this asynchronous updating, speeds can be selected from a continuous range. The computational cost for maintaining a priority queue of the movement times has a logarithmic dependency on the number of agents. Hence, it is not computationally heavy even with a lot of agents.

Movement is determined by two fields: a static distance to destination field D which is computed before simulation, and a dynamic repulsion field R . The repulsion emitted by agent i to cell c within radius r is

$$e_c^i = r - d_c^i, \tag{2}$$

where $d_c^i \leq r$ is the distance between agent's i current position and cell c . The radius r describes the minimum comfortable distance between two agents which typically varies, e.g., between different cultures. Figure 1 illustrates the emission of repulsion of an agent.

Let C^i denote the set of cells containing the current cell of agent i and those neighbor cells that are available for movement. The value of the dynamic repulsion field affecting agent i in the adjacent cell $c' \in C^i$ is the sum of all repulsions emitted by agents other than i to cell c'

$$R_{c'}^i = \sum_{j \neq i} e_{c'}^j. \tag{3}$$

The moving speed of agent i , v^i , is determined as

$$v^i = v_{free}^i \times f(R_c^i), \tag{4}$$

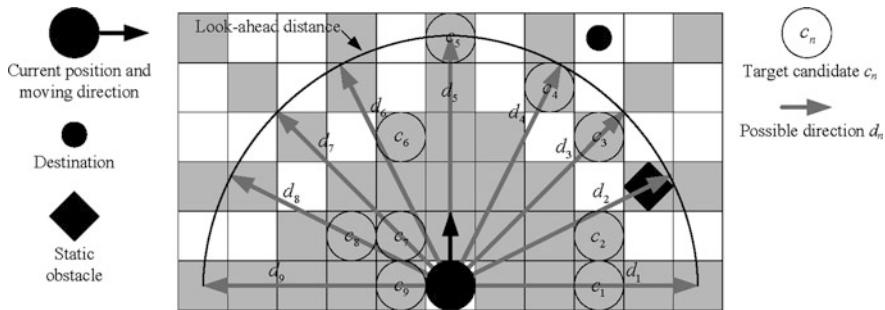


Fig. 2 Target selection

where $c \in C^i$ is the cell that agent i has selected to move to as described below, and the speed coefficient function $f(\cdot)$ is chosen in this study so that the model reproduces Fruin’s speed-density diagram [9]. This kind of calibration is needed because the movement model does not account for speed variations due to crowding as such. We describe next a simple path selection approach based only on the local information, and our improved approach.

2.2 Path Selection

In the simple approach, agent i selects the next cell c to move to as

$$c = \arg \min_{c' \in C^i} (D_{c'} + R_{c'}^i), \tag{5}$$

where $D_{c'}$ is the distance to destination from cell c' , and $R_{c'}^i$ is the value of the dynamic repulsion field affecting agent i in cell c' .

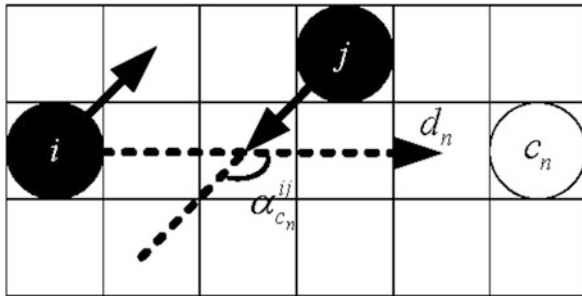
In our improved path selection approach, agent i first selects a target cell c_t from cells within a look-ahead distance in nine directions that do not deviate more than 90° with respect to the agent’s current moving direction (see Fig. 2). Then, the next cell to move to is selected as

$$c = \arg \min_{c' \in C^i} (d_{c_t}^{c'} + R_{c'}^i), \tag{6}$$

where $d_{c_t}^{c'}$ is the distance from neighbor cell c' to the target c_t .

Target Selection A target candidate $c_n, n = 1, 2, \dots, 9$, of a possible movement direction is the cell that has the shortest distance to destination in that direction, does not contain a static obstacle, and is not beyond a static obstacle or the look-ahead

Fig. 3 Conflict computation



distance. Amongst all nine target candidates, the candidate with the biggest score is selected as the final target c_t .

The score of target candidate c_n for agent i is defined as

$$S_{c_n}^i = D^i - D_{c_n} - k_{conflict}^i \times V_{conflict,c_n}^i, \tag{7}$$

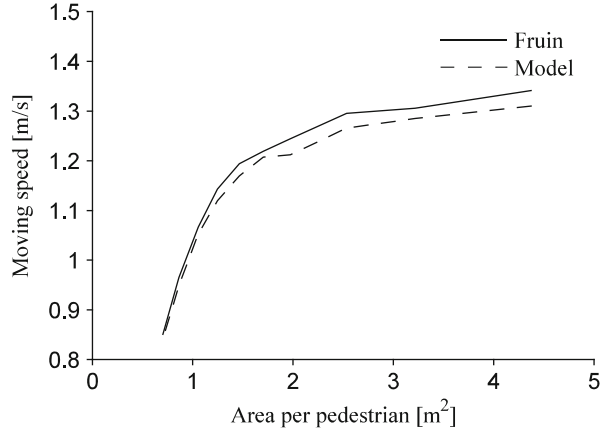
where $k_{conflict}^i$ is a weight parameter describing the tolerance of agent i to conflicting flow, and D^i and D_{c_n} are the distance to destination from the current position of agent i and target candidate c_n , respectively. Note that the closer the target candidate is to the destination, the greater the score of the candidate. Furthermore, the difference between the two distances to the destination does not depend on the agent's current position on the grid.

The value of conflict $V_{conflict,c_n}^i$ estimates the conflict of agent i with other agents on the way to target candidate c_n as

$$V_{conflict,c_n}^i = \sum_{j \in \Omega^i, j \neq i} \frac{(1 - \cos(\alpha_{c_n}^{ij}))}{2}, \tag{8}$$

where $\alpha_{c_n}^{ij}$ is the angle between the direction from the current location of agent i towards the target candidate c_n and the direction of agent j that is inside the rectangle of agent i , Ω^i , where conflicts may occur. The expression inside the sum equals its maximal value 1 when the direction of agent j is opposite to the direction from agent i to target candidate, and its minimal value 0 when the two directions are the same. The size of the rectangle depends on the distance to the target candidate such that the length of the shorter edge of the rectangle is 0.5 times the distance to the target candidate. If there is no target candidate with a positive score, the agent does not move but changes its direction with a predefined probability. A similar approach for avoiding conflicts was presented in [7] but a cone was used instead of a rectangle. The rectangular shape was selected in this study for simplicity. Figure 3 illustrates the conflict computation for two agents.

Fig. 4 Simulated and measured speed-density diagrams



3 Model Calibration and Validation

3.1 Speed-Density Diagram

The effect of increased traffic intensity on pedestrian walking speed has been studied by Fruin [9]. To fit our simulated speed-density diagram to that of Fruin's, we adjusted the free walking speed and selected a suitable form for the speed coefficient function shown in Eq. 4. In our simulations, speed-density dependency was determined by measuring average travel time in a straight corridor with different incoming flow rates. A good fit to Fruin's experimental results was obtained with the following function

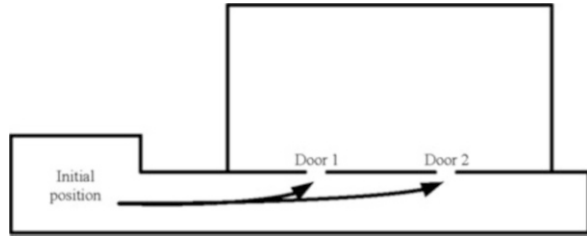
$$f(R_c^i) = \sqrt{\frac{m}{m + R_c^i}}, \quad (9)$$

where the constant m was selected during calibration. The fit is shown in Fig. 4.

3.2 Self-Organized Effects

Any simulation model should reproduce the self-organized phenomena occurring in real pedestrian crowds. Lane formation is a self-organized effect observed especially in multi-directional flows where pedestrians moving in opposite directions tend to form lines. Oscillation at bottlenecks means that in narrow passageways such as doorways, the changes in the passing direction are oscillatory [10]. Our model reproduced both of these effects.

Fig. 5 Geometry of the experiment



4 Simulation of Experiment

4.1 Description of Experiment

Our new path selection approach is motivated by an experimental study on pedestrian exit selection in the evacuation of a corridor [6]. The experiment was conducted on two different days at Aalto University School of Science and Technology in Espoo, Finland. In total, 48 and 54 students took part in the first and second experiment, respectively.

The geometry of the experiment and the initial position of the participants before each trial are shown in Fig. 5. In each, the participants were instructed to evacuate the corridor by moving to the classroom. Every trial and evacuation started from a blow to a whistle.

In the experiments, the queue clearance time for a door was defined as the time from the whistle to the moment when the last participant who used that door entered the classroom. These clearance times for all trials are reported in [6]. The numerical values for the number of participants using each door in each trial could also be obtained [12].

4.2 Simulation Results

The experiment was simulated with the simple model and our improved model of Sect. 2.2. The experimental results of the four trials in normal conditions as well as the simulated results are shown in Table 1. The values are averages computed from the trials. In total, 4 simulations with 48 and 54 agents were run with both models.

The results obtained with the improved model are much closer to the results obtained in the experiment. The reason is that with the simple model, the agents formed a crowd in front of Door 1 and only those agents that were pushed to Door 2 went through it.

Table 1 Observed and simulated results of pedestrian exit selection experiment

Source	Number of agents		Clearance time		Clearance time Door 2
	Agents Door 1	Agents Door 2	Door 1	Door 2	
Improved model	48	26.75	21.25	36.8	38.8
	54	31	23	42.7	40.6
Simple model	48	46	2	52.9	31.3
	54	51	3	57.5	33.2
Observed	48	26.5	21.5	28.68	29.97
	54	27.5	26.5	31.3	33.38

5 Conclusions

This work presents an approach for flexible pedestrian path selection in a cellular pedestrian flow model. In addition to local information about other agents and environment, movement decisions are based on traffic information and distance to destination field values further away. The simulation results show that our model is able to reproduce pedestrian exit selection behavior observed in a real experiment. A simple model based on only local information gives unrealistic results in such simulations. Furthermore, our model simulates self-organization phenomena realistically.

In our model, conflicts in a possible moving direction are considered inside a rectangular area. Other shapes and sizes should be studied in the future. Also our repulsion model for agent interactions and speed adjustment is a subject of improvement.

References

1. Gibbs, P.G., Marksjös, B.: A micro-simulation model for pedestrian flows. *Mathematics and Computers in Simulation* 27, 95–105 (1985)
2. Muramatsu, M., Irie, T., Nagatani T.: Jamming transition in pedestrian counter flow. *Physica A* 267, 487–498 (1999)
3. Klüpfel, H., Meyer-König, T., Wahle, J., Schreckenberg, M.: Microscopic Simulation of Evacuation Processes on Passenger Ships. In: Bandini, S., Worsch, T. (eds.) *ACRI 2000*. Springer, London (2000)
4. Burstedde, C., Klauck, K., Schadschneider, A., Zittartz, J.: Simulation of pedestrian dynamics using a two-dimensional cellular automaton. *Physica A* 295, 507–525 (2001)
5. Was, J., Gudowski, G., Matuszyk, P.J.: Social Distances Model of Pedestrian Dynamics. In: Yacoubi, E., Chopard, B., Bandini, S. (eds.) *ACRI 2006*. Springer, Heidelberg (2006)
6. Heliövaara, S., Kuusinen, J.-M., Rinne, T., Korhonen, T., Ehtamo, H.: Pedestrian behavior and exit selection in evacuation of a corridor – an experimental study. *Safety Science* 50, 221–227 (2012)
7. Heliövaara, S., Korhonen, T.: Counterflow Model for FDS + Evac Simulations. In: Peacock, R.D., Kuligowski, E.D., Averill, J.D. (eds.) *Pedestrian and Evacuation Dynamics*. Springer, New York (2010)

8. Helbing, D., Farkas, I., Vicsek, T.: Simulating Dynamical Features of Escape Panic. *Nature* 407, 487–490 (2000)
9. Fruin, J.J.: Pedestrian planning and design. Elevator World Inc., Alabama (1987)
10. Helbing, D., Farkas, I.J., Molnár, P., Vicsek, T.: Simulation of Pedestrian Crowds in Normal and Evacuation Situations. In: Schreckenberg, M., Sharma, S.D. (eds.) *Pedestrian and Evacuation Dynamics*. Springer, Berlin (2001)
11. Kretz, T., Bönisch, C., Vortisch, P.: Comparison of Various Methods for the Calculation of the Distance Potential Field. In: Klingsch, W.W.F., Rogsch, C., Schadsschneider, A., Schreckenberg, M. (eds.) *Pedestrian and Evacuation Dynamics*. Springer, Berlin (2008)
12. Korhonen, T.: Personal communication (2012)

Including Route Choice Models into Pedestrian Movement Simulation Models

D. Bauer and J. Gantner

Abstract Route choice models in most pedestrian movement simulation models (PMSMs) currently use shortest path algorithms for representing wayfinding of the modeled pedestrians. This is in contrast to commonly used traffic models as well as to empirical evidence hinting at various strategies that people use in real life. Moreover, the impact of guiding systems is not represented in the models. This paper reports on some experiments providing empirical evidence on strategies used for wayfinding. Furthermore a model incorporating these strategies as well as routing concepts commonly used in traffic modeling is proposed and demonstrated in a case study.

Keywords Wayfinding • Assignment • Route choice

1 Introduction

Nowadays pedestrian movement simulation models (PMSMs) are increasingly used for infrastructure planning and evaluation in particular for large hubs of mass public transport but also for recreation or cultural sites. The main purpose of these applications is to detect bottlenecks in the infrastructure reducing either the capacity of the infrastructure or at least the level of service.

Consequently the main output of such tools typically are maps (or rather the underlying quantitative data) providing the spatial dependence of pedestrian density or delays in regions of the infrastructure. Therefore the main task of the PMSMs in this context is to predict the location of pedestrians on their way through the infrastructure.

D. Bauer (✉) • J. Gantner

Department Mobility, Austrian Institute of Technology, Giefingg. 2, A-1210 Vienna, Austria
e-mail: Dietmar.Bauer@ait.ac.at

To achieve this goal recently much effort has been directed towards calibrating the operational level of the models [1–3]. Much less attention has been directed towards the tactical level and in particular in the representation of wayfinding. Here the predominant assumption is still that pedestrians use shortest path criteria for their route choice. This is in contrast to common usage in the related area of traffic modeling as well as to well established empirical facts.

While shortest path navigation might be appropriate for commuters with a profound knowledge of the infrastructure, the same definitely does not hold for persons unfamiliar with the infrastructure. Their wayfinding is supported by guiding systems which currently are not represented in PMSMs. First attempts in this direction are presented in [4].

Even for commuters familiar with the infrastructure it is questionable, if shortest path seeking is a good representation of the route choice. One of the most well known early investigations into route choice for pedestrians is constituted by [5]. The main finding here was that there are a number of strategies to be found in route choice including

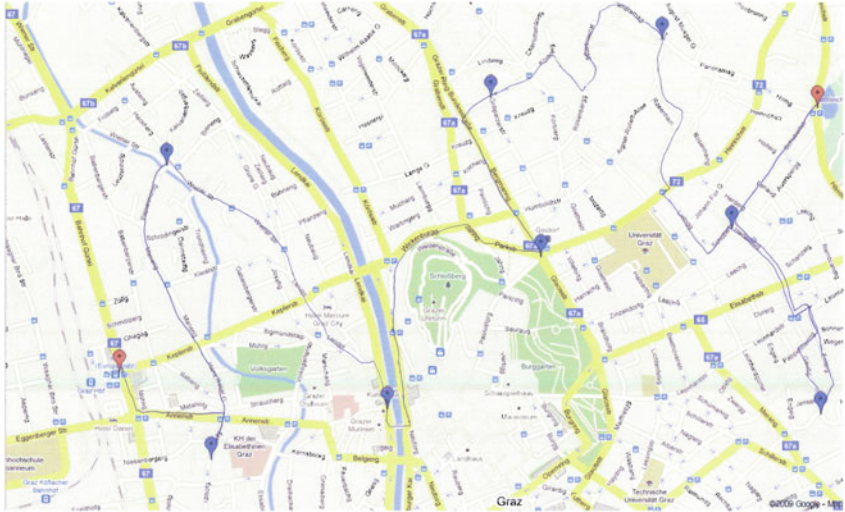
- Shortest distance
- Least time
- Fewest turns
- Stay on main roads as much as possible
- Longest leg first
- Shortest leg first

In the related area of traffic modeling much effort is devoted to the concept of route assignment which consists of route choice for individuals in a setting where individual decisions influence each other via congestion effects (see e.g. [6] for a textbook overview). In this area currently stochastic route choice models are commonly used representing differences in route choice attributed to the inability of individuals to correctly assess trip lengths and durations as well as individual differences in preferences.

For PMSMs predominantly shortest path assumptions are used. While route assignment methods based on trip duration minimization could be used and have been proposed (e.g. [7, 8]) also for pedestrian traffic it is questionable whether pedestrian route choice follows the same rules as route choice in an urban context.

Therefore this paper reports on the findings from two experiments aiming at gaining some insights into the mechanisms used for wayfinding. The discussion of the results leads to the proposition of a model for route choice incorporating the findings. This model is demonstrated using a small test case.

The paper is organized as follow: In the next section the wayfinding experiments are described. Section 3 collects the corresponding results. Section 4 proposes the new wayfinding model and Sect. 5 provides details demonstrating the application of the model. The paper concludes with a discussion on future research.



Instructions:
 Starting at the left red marker, draw a route on the map going past all 8 blue markers, ending at the right red marker.
 You may use all available roads on the map for your route.
 Please write your number on the sheet.

Fig. 1 Map of Graz with instructions for the first exercise. The *blue line* shows the answer of one of the participants (labeled number 9)

2 Wayfinding Experiments

In order to gain insights into strategies used for wayfinding two experiments have been performed with 25 persons in December 2009 during a workshop on calibration of PMSMs in Vienna. All participants are researchers in the area of pedestrian modeling.

The two tasks to be executed by the participants consisted in route choice in two different settings. The first exercise asked the participants to draw a line connecting the origin with a destination in a Google maps view of the city of Graz (no participant was familiar with the city, whose name was furthermore not indicated on the map) including eight via-points along the way. The via-points have been manually chosen in order to cover the whole map. The map (cf. Fig. 1) shows different categories of roads. Main roads are drawn in yellow, minor roads in white. The participants have been asked to mark their chosen route. The only information provided was the sentence written on the map. In particular no information on the mode used to connect the points has been given.

As a result from the first exercise a total of 25 paths drawn on the map are available. Three participants did not successfully connect all via-points. Their results needed to be eliminated leaving 22 maps. The paths were digitized and map matched using a Teletlas map. Consequently for each drawn path as a result a sequence of Teletlas link IDs is available. From this information it is possible to provide quantitative indicators of the chosen routes such as route lengths, number of

Fig. 2 Symbols on the floor for the second exercise



turns and ratio of length on main roads. For each subpath connecting two adjacent via-points it was recorded whether the first leg was the longest. Finally a quantity termed ‘retrace ratio’ has been computed indicating the percentage of path length used at least twice. As no information on travel time has been supplied, shortest time could not be calculated. Also no information on other users has been provided and hence no congestion effects are included.

The second task asked the participants to connect via-points by walking over them. To this end on the floor 11 symbols have been distributed (see Fig. 2). Each participant was given a sheet of paper showing five of these symbols. The subjects were asked to find a path connecting all of the symbols and it was pointed out, that this need not be in the sequence indicated on the sheet.

The second exercise was video taped using a camera mounted on the ceiling. Each participant wore a colored hat allowing the automatic extraction of the movement trajectory. The camera view has been calibrated using a standard 3D-calibration algorithm (for a description of the particular algorithm used see e.g. [9]). Consequently also in this case quantitative information is available sufficient to extract indicators characterizing the routes. Again route length and the number of turns has been calculated for each individual.

3 Results from Experiments

The characteristics of the various indicators for the sample of 22 maps are given in Table 1.

Already from this table it follows that no subject in the experiment follows the “longest leg first” strategy as the maximum number of subpaths where this occurs equals 5 out of 9 possible subpaths. Also the retrace ratio is small, less than 10 % in all cases with a median of only 1.2 %. Therefore in the following these two indicators are neglected.

In order to identify patterns of path finding an unsupervised k-mean clustering is performed on the indicators length, main road ratio and turns. All indicators are

Table 1 Sample characteristics of the indicators

Indicator	Length (m)	Main road ratio (%)	Turns (#)	Retrace ratio (%)	Subpaths with longest leg first (#)
Min	9,949	13.2	34	0.0	1.0
Max	13,141	49.5	57	9.9	5.0
Mean	11,100	35.1	44	2.7	2.9
Median	10,964	34.4	43	1.2	2.5
Std	875	8.1	5	3.2	1.2

Table 2 Intervals of indicators in the five clusters. Numbers are percentages i.e. normalized indicators

Cluster	Length	Ratio of main roads	Turns	Members
1	0.0–24.9	42.7–82.8	0.0–30.4	5
2	5.7–31.0	0.0–50.1	43.5–69.6	4
3	30.1–46.8	54.1–78.3	30.4–60.9	8
4	53.7–71.7	84.6–100.0	21.7–43.5	3
5	96.4–100.0	45.0–77.5	71.9–100.0	2

normalized such that the minimal indicator equals 0 % and the maximal 100 % to account for differences in location, scale and spread.

K-means clustering has been performed repeatedly using different number of clusters. Five clusters have been found to be appropriate based on the usual scree-plots. The characteristics of the clusters can be seen in Table 2 and can be given the following interpretation:

- Cluster 1 and 2 contain the individuals that minimize path length. Individuals in Cluster 1 show the smallest number of turns and a relatively high ratio on main roads, while Cluster 2 accepts more turns and avoids main roads using direct routes.
- Cluster 3 shows medium path lengths, number of turns as Cluster 2 and ratio of main roads as Cluster 1. Thus the interpretation of the behavior in this cluster is somewhat unclear.
- Cluster 4 prefers to stay on the main roads and accepts longer path lengths to achieve this goal.
- Cluster 5 contains only two individuals and is characterized by excessive path lengths and a large number of turns. It is concluded that these individuals did not use any optimality criterion.

With respect to Cluster 3 one possible hypothesis was that these persons wanted to minimize trip length but did not succeed because of the complexity of the task. There are two possible causes of longer trip lengths: The ordering of the via-points or the length of the path between the via-points. The ordering of the via-points did not show any differences between Cluster 1, 2 and 3. With regard to the length of the subpaths a new indicator has been calculated, the mean of the ratio between the lengths of the subpaths connecting two via-points divided by the shortest possible

distance. Using a two sided two sample (with equal variances) *t*-test for comparing this indicator between individuals in Cluster 1 and 2 and individuals in Cluster 3 resulted in a marginally significant *p*-value of 0.0450. This is remarkable given the small sample size and thus the small power of the test. Thus it is concluded that individuals in Cluster 3 did not reach minimum path length because of their inability to find the shortest path between two via-points in a complicated network.

This hypothesis has been further investigated with the help of the second experiment. In this setting the task of linking two adjacent via-points is trivial as there is no street network to be respected and hence any two via-points can be connected using a straight line. For each individual the corresponding path from the second experiment has been investigated. As an indicator of finding the shortest path, the ratio between the shortest possible route for the chosen sequence of symbols and the actual trip length has been calculated. A two sided two sample *t*-test of differences in mean ratio for Cluster 1 and 2 on the one hand and Cluster 3 on the other hand resulted in a *p*-value of 0.14. Hence no significant differences can be found in this simple setting. This supports the hypothesis that individuals in Cluster 3 also wanted to minimize path length, but failed to do so in the complex scenario while they succeeded in the simpler setting.

Summing up the findings from the experiments we find three groups of navigation strategies:

- Minimizing trip length by high usage of main roads and simultaneously minimizing turns,
- Minimizing trip length by using the most direct path irrespective of usage of main roads or minimizing turns,
- Staying on main roads and accepting longer paths

The two first mentioned strategies can be modeled uniformly by using a utility function consisting of the components route length, ratio of main roads and number of turns. The first strategy puts much emphasis on the number of turns as well as the trip length, while the second strategy only considers trip length. The third strategy is different in the sense that it searches for the point on main roads with smallest distance to the destination and connects the origin and this point by the shortest possible path on the major road network. This route cannot be found by using minimization strategy as maximizing the main road ratio will lead to routes of excessive lengths adding segments on main roads in order to increase the share of main roads in terms of the total distance. Therefore this constitutes a second strategy falling out of the random utility model framework.

Additionally a number of individuals appear to be trying to choose the most direct route but do not succeed in complicated settings. This calls for probabilistic approaches, where the routes are selected from a number of different routes based on subjective assessment of utility modeled using a random utility framework.

Logit models incorporating route communality factors or nested logit models to account for correlations between similar routes sharing parts of the routes have been used to this end in the traffic modeling literature (see [6] for a comprehensive discussion).

The small sample size does not allow drawing any quantitative conclusions on the relative frequencies of usage of these strategies.

4 Modeling Wayfinding

The results provided above suggest a hierarchical model for route choice consisting of an upper level selecting one of the identified strategies and a lower level where the selected strategy is applied.

The **upper level** is modeled using a discrete probability model assigning individuals randomly according to given frequencies to the various strategies discussed above. Additionally routing strategies for special needs must be included. This relates to persons not familiar with the infrastructure (which hence cannot be assumed to optimize any criterion relying on full knowledge of the infrastructure) as well as to persons with mobility impairments that are restricted in their choices (such as wheelchair users). Such special routing needs to be taken care of independently of the approach suggested below [4] provides more details on routing for these special groups of pedestrians.

The main difficulty for modeling the upper level lies in determining the frequencies of the various wayfinding strategies empirically. The results of the last section do not provide much information in this respect. Larger samples in real world applications are needed. Moreover, the frequencies are likely to be application and even temporally dependent.

Two possible strategies for obtaining data on these frequencies are a disaggregate approach classifying single pedestrians depending on their wayfinding strategy and observing the relative frequencies of the strategies and second the inference based on the observed route choice behavior and the corresponding link flows. Both approaches have been followed in the general traffic modeling community with the second approach being used predominantly.

The **lower level** for the first two strategies (compromise between trip length and number of turns or ratio of main roads respectively; additionally trip duration plays a role in route choice and hence is included below) is modeled using a nested-logit model. Hereby a hierarchical graph is used for representing the walkable space¹: The whole walkable region is partitioned into sections representing rooms or pathways or floors of a building. Each section in itself is partitioned into regions. Each region constitutes a link in the graph, while the nodes are given by the borders of the regions connecting two or more regions. Major nodes connect two or more sections while minor nodes connect regions inside a section. The graph thus contains major and minor nodes (seen as intermediate goals). A route is consequently represented as a sequence of nodes containing a subsequence of

¹This structure has been jointly developed with Thomas Matyus and Kardi Teknomo, which is gratefully acknowledged.

major nodes. In this setting the nesting structure relates to pairs of major nodes, which can be connected using different subroutes inside the corresponding section. The selection of a particular of these subroutes given that the pair of major nodes appears in the route hence constitutes the lower level in the nesting structure.

For the first strategy of maximizing a random utility the coefficients for the four influence factors trip length, trip duration, number of turns and ratio of main roads can be mixed according to some probability density function, e.g. a log-normal, in order to account for interpersonal differences. A simpler, different approach taken here consists of segmenting the population into a finite number of homogenous segments with one vector of coefficients in the utility function specific to each segment.

In addition to the coefficients in the random utility function, the model contains one other parameter as usual in nested logit models, the nesting factor determining the correlation of alternatives inside a nest.

As discussed above, within the nested logit model specification the routes must be described using a graph in order to obtain link flows which can be converted into link speeds resulting in expected link travel times. The graph needs to allow the representation of route alternatives and contain sufficient information in order to allow the conversion of flow numbers into travel times. Thus the graph needs to partition the walkable space into regions building the links of the graph, the nodes representing the borders between two adjacent regions. In the following the process of producing the graph representing the walkable space is discussed.

4.1 Graph Creation

The model for the lower level requires an underlying graph representing the walkable space and indicating “main roads”. Contrary to road networks, pedestrian infrastructures do not possess clearly defined roads and hence a decomposition of the walkable space into distinct regions needs to be performed in the modeling process [8] discusses some of the pitfalls involved in this partitioning of the walkable space.

In addition to the partitioning also characteristics of the regions must be provided which are used for the assessment of routes. These may include inter alia the length, the area covered by the regions or the capacity of throughput through the region. The length is used in the approximation of walking length, the area in the assessment of the density inside the region involved in the usage of fundamental diagrams for converting lengths into expected travel times. Alternatively, as will be done below, volume delay functions can be used in order to convert link flows into link travel times while respecting capacity constraints.

For our routing models also a classification in main roads and others and a definition of the term “turn” must be provided. In the following a number of different algorithms for defining the routing graph including the additional characteristics are described. Hereby it must be stated that each of the approaches below has

advantages and disadvantages as well as significant potential for improvement. The discussion is to be seen as a first approach rather than as finished research. The choice between the algorithms is therefore currently only guided by subjective judgment. More research in this area is needed.

4.1.1 Grid Based Approach

One approach to obtain a routing graph automatically is the superimposition of a grid of cells over the space where the walkable space is given by the cells not fully occupied by obstacles such as walls. Additionally not connected parts of a cell (e.g. separated by obstacles) must be split into two separate regions.

The definition of the area covered by each cell is straightforward. The capacity of the cells typically would be related to the smallest width in walking direction. For bidirectional or omni-directional movement the concept of volume delay function might not be appropriate as the capacity might differ depending on the walking direction.

The definition of the length of the cell depends on the definition of the neighborhood. These issues are well known from cellular automata models or queuing network models. Again omnidirectional movement might cause troubles.

The grid size is the major determinant for the properties of the resulting graph. Using a small grid size most of the regions will be identical to grid cells and hence reduce some of the difficulties in defining cell width and length. At the same time the definition of turns becomes more complicated. Also the number of possible routes grows rapidly.

For large grid size on the other hand defining turns is easier, the number of distinct routes becomes smaller. On the other hand for models involving travel time the homogeneity of the regions is less plausible. And finally more regions will not coincide with square cells due to the occurrence of obstacles covering parts of the squares and hence demand more complicated definitions of cell width, length and throughput capacity.

4.1.2 Using the Sight Graph

A different automatic method of partitioning the walkable space delineated using polygons is provided by triangularization usual in methods for calculating the visibility graph, see e.g. some of the method discussed in [10].

The purpose of these methods is to provide for an infrastructure represented by a polygon where obstacles inside the infrastructure are also represented by polygons for each corner a polygon (given as the union of triangles) such that the polygon covers all points seen from the corner. Intersecting all the triangles one obtains a partitioning of the space into distinct regions given as polygons.

Depending on the geometry of the infrastructure the resulting regions can become very complex. The definition of the area covered by the region is

again straightforward. The shape of the region might, however, render the use of fundamental diagrams for the calculation of travel speeds useless. The same applies for the application of volume delay functions and the definition of throughput capacities.

Nevertheless this partitioning may provide a useful automatic first step on which subsequently manual joining of so obtained regions can be performed potentially leading to a useful graph.

4.1.3 Manual Definition

In many cases knowledge of the usage of the infrastructure will lead to a definition of a partitioning of the walkable space that fits well with the routing models. The decomposition of the whole walkable space into sections is one such aspect. Splitting the walkable space at bottlenecks such as doors or stairs, elevators and the like moreover leads to a natural definition of throughput capacities based on the most restrictive element determining the level of congestion.

Between such bottleneck elements the walkable space can often be split in order to distinguish different routes. Also the merging of several routes for different origins and destinations needs to be taken into account as space will be utilized in omnidirectional movement in some cases.

No guidelines can be provided in this respect at this point in time and more research is needed in order to automate this process. The next section provides an example in this respect.

5 Model Demonstration

In this section the model proposed above is applied to the subway station “Stadion” of the Viennese subway network (for a map see Fig. 3) serving the main soccer stadium. The station is equipped with a special access control system developed in the run up to the UEFA Euro 2008[©] soccer championship. The control system has been described e.g. in [11].

For the spectators of a soccer game or other events in the stadium the walking path from the stadium into the subway is indicated using orange arrows in Fig. 3: the spectators arrive at the station from the lower right corner. They enter the station via one of nine so called meanders.² These are steel constructions limiting flow to one walking lane.

²In fact 15 meanders exist as shown on the map, but only nine are opened currently. This number has been specified based on the capacity of the subway system of roughly 400 persons per minute as compared to the capacity of the meanders of roughly 50 persons per minute. See [11] for details.

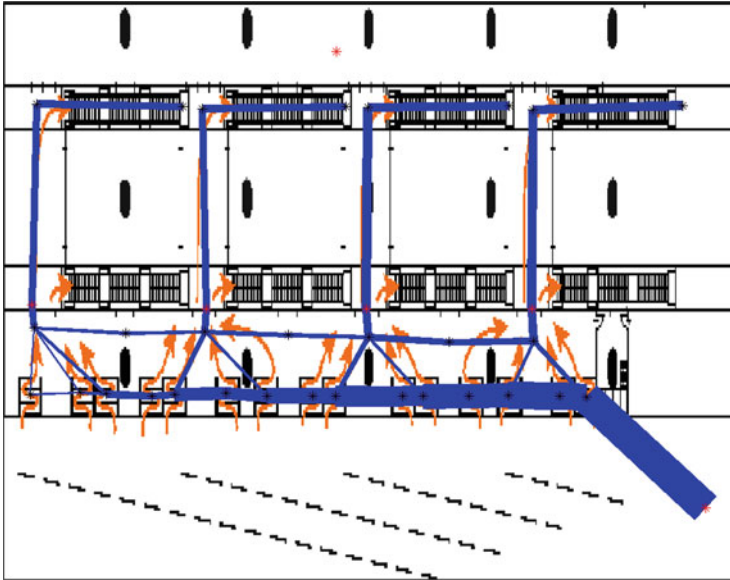


Fig. 3 One example of the link flows according to stochastic user equilibrium at the Viennese U2-station “Stadion”. Major nodes shown as *red stars*, minor nodes as *black stars*. Links are *blue lines*, the width is proportional to the link flow

Once the spectators pass the meanders they use one of four portals equipped with sliding doors to enter the station building. The portals act as crowd controllers as the sliding doors can be set to restrict access to 0, 1, 2 or 3 walking lanes. Inside the building they walk up a flight of stairs to reach the platform where the inbound trains leave.

The walkable space in this case is partitioned according to the main alternative routes linking the arrival at the station to the meanders, the meanders with the portals and the portals with the platforms. Route choice in this setting pertains to the choice of the meander and subsequently the portal. Route lengths are measured between arriving at the station and reaching the platform as the trains can be entered along the whole platform.

The graph in this case has been derived manually. The major nodes are constituted by the starting point, the meanders, the portals and the platform. The minor nodes are introduced mainly in order to account for possible overlaps between different routes. Thus e.g. the area in front of the portals will be used coming from different meanders. One node in front of each of the portals is hence necessary in order to account for joint usage of this region.

The length of the regions has been extracted as the metric distance between the nodes. This is somewhat inaccurate as it neglects the structure of the meanders. However, as each path contains the passage through exactly one meander, for the utility optimization this is irrelevant.

The capacity of the regions is calibrated to match the hourly throughput of the various bottleneck elements. These numbers are based on the fact that the transport for the spectators in reality takes approximately 1 h. The rates of the various bottlenecks (meanders, portals, stairs) have been measured empirically, see [11].

For the determination of the link travel times the walking time per meter is calculated using a conical volume delay function [12]. It is currently unclear, whether this volume delay function is the optimal choice. The link walking time then amounts to the time per meter times the length of the link. Additionally time for waiting in queue is taken into account. Hereby the links are considered acting as queues where persons arrive and are discharged. The arrival rate is determined by the link flows and the discharge rate is determined by the capacity of the links. This is appropriate for links having bottlenecks at their exit points such as the meanders, the portals and the stairs.

Turns are defined where in a loose sense significant changes of direction are expected. This occurs at the entering of the meanders, the entering of the portals, the entering of the stairs.

Finally a major route has been defined as the shortest path route of entering the rightmost open meander and following through the rightmost portal. This corresponds to the signage on the site.

Note that this situation is relatively simple as mostly one directional movement is expected. The only exception here is the area between the meanders and the portals where bidirectional traffic is possible but not likely. The regions have been defined in order to reflect the most relevant congestion effects occurring at the bottlenecks designed to limit passenger inflow.

The last element of the specification of the model requires the definition of segments of the population with homogenous utility function composed of the length of the route, the travel time, the number of turns and the ratio of main roads. Here two segments are considered: One segment that tries to minimize travel times and a second one that wants to stay on the main road as much as possible. This is equivalent in this setting to choosing the shortest path.

The stochastics in the estimation of the trip duration leads to a dispersion of the spectators onto the various routes (i.e. portals) rather than choosing only the route with the shortest trip duration. A static stochastic user equilibrium is calculated using the method of successive averages [6] in order to impose congestion effects as well as subjectivity in the utilities.

This choice of two groups of spectators is taken based on observations at the games of the European soccer championship. In all six games it was noticeable that after the bulk of spectators had already been transported away beginning from the leftmost portal the queues in front of the portals dissolved. At this time while the three other portals were already idle and walking time would have been significantly lower a large group of spectators still insisted on waiting in front of the rightmost portal. This crowd behavior, which has been observed at each single event, is not compatible with trip duration minimization but matches with the strategy to stay on the main road as well as on the shortest path in this situation. Thus this phenomenon can be explained by using a segmentation of the population into part of the group

Table 3 Percentages corresponding to stochastic user equilibrium and different choices of parameters

Percents	Portal 1	Portal 2	Portal 3	Portal 4
True	27.8	26.2	22.8	23.3
40 % shortest path, $\beta = 0.03$	40.0	25.8	19.6	14.5
5 % shortest path, $\beta = 0.03$	26.6	26.6	24.7	22.1
0 % shortest path, $\beta = 0.03$	26.5	26.6	24.8	22.1
5 % shortest path, $\beta = 0.001$	26.9	27.0	22.9	23.2
5 % shortest path, $\beta = 0.02$	26.6	26.6	24.4	22.3
5 % shortest path, $\beta = 1$	26.8	26.6	25.8	20.9

that tries to minimize walking (and waiting) time and another part who minimizes walking length (or staying on main roads) irrespective of the trip duration.

Table 3 shows the distribution of 20,000 persons onto the four major routes using different choices for two main parameters, the variance of the stochastic utility (encoded in the coefficient β for trip duration in the random utility) and the relative frequency of persons always using the shortest path. The first row of the table provides the average distribution in three games during the Euro 2008[©] soccer championship, where data has been obtained. This average serves as a benchmark.

Larger values of β here correspond to a larger systematic part of the random utility and hence to smaller variance of the random error. It can be clearly seen that for small variance of the error term the leftmost route is infrequently chosen while for large variance persons are distributed more evenly.

If the relative frequency of the persons always using the shortest route is small the distribution across all four major routes is more even, for large share of such persons the rightmost route is heavily preferred as expected. Travel times there are larger than for the other routes and hence no one minimizing travel time uses this route in this case.

Using the parameters of the model it would be possible to exactly match the relative frequencies measured. Also different volume delay functions could be used. More data is needed in order to obtain useful parameter estimates.

6 Conclusion

In this paper a model for pedestrian route choice is presented and related to empirical evidence. The main model uses a hierarchical structure where in the upper level one of several navigation strategies is chosen and in the lower level a nested-logit model is used for route choice. The logit model is based on a network graph representation of the infrastructure distinguishing between major and minor nodes as well as main “roads”. As such the model uses assignment concepts from traffic modeling in order to represent congestion effects in the distribution of persons onto the various routes.

The model as proposed in this paper uses stochastic user equilibrium concepts. Clearly such concepts only apply to stationary conditions and are not appropriate for route choice in situations where transportation demand varies largely over time. In such situations dynamic user equilibrium concepts need to be considered.

The model contains a number of parameters to be calibrated using real world information. Currently there is a lack of large scale real world data that is informative enough in order to be used to this end. Such data sets could be obtained using a mixture of different sensors: Bluetooth scanners can be used to track devices (and hence anonymously the people carrying them) on their way through the infrastructure. It is known that using this technology roughly 10 % of the persons can be tracked while this percentage varies vastly over time. Thus additionally people counting sensors must be used to obtain the number of persons at selected cross sections. Whether such a procedure is able to provide representative data on route choice is a matter for future research as the self selection involved in accessible Bluetooth devices might introduce a bias.

Alternatively experiments in virtual environments that can be changed at will may be conducted [13] presented such an environment using a head mounted display. The research project IMITATE in Austria aims to develop a similar environment based on a CAVE environment in Graz. These environments provide optimal conditions for large scale experiments on route choice behavior including the influence of guiding systems, navigation devices as well as other pedestrians.

Acknowledgments The authors thank Irmgard Zeiler, Christian Rudloff, Stefan Seer and Markus Ray for support in the data collection and analysis. Part of this work has been financed by the Austrian BMVIT in the program initiative “ways2go” in the project “IMITATE” which is gratefully acknowledged.

References

1. A. Johansson, D. Helbing, and P. Shukla, “Specification of the Social Force Pedestrian Model by Evolutionary Adjustment to Video Tracking Data,” *Advances in Complex Systems*, vol. 10, pp. 271–288, 2007.
2. M. Chraïbi, A. Seyfried, A. Schadschneider, and W. Mackens, “Quantitative Verification of a Force-based Model for Pedestrian Dynamics,” in *Traffic and Granular Flow (TGF)*, 2009.
3. C. Rudloff, T. Matyus, S. Seer, and D. Bauer, “Can walking behaviour be predicted? An analysis of the calibration and fit of pedestrian models,” in *Proceedings of the 90th Annual Meeting of the Transportation Research Board.*, 2011.
4. H. Schrom-Feiertag and T. Matyus, “Simulation of Handicapped People Finding their Way Through Transport Infrastructures,” to appear in *Proceedings of the PED2012 Conference*, 2012.
5. R. G. Golledge, “Defining the criteria used in path selection,” in *Transportation*, no. 278, Elsevier, 1995, pp. 151–169.
6. E. Cascetta, “Transportation Systems Analysis. Models and Applications,” *Springer*, 2nd ed., 2009.
7. F. Gräßle and T. Kretz, “An Example of Complex Pedestrian Route Choice,” in *Proceedings of the PED2010 Conference*, 2010.

8. V. Zachariadis, J. Amos, and B. Kohn, "Simulating Pedestrian Route Choice Behaviour under Transient Traffic Conditions," in *Pedestrian Behavior Models Data Collection Application*, H. J. P. Timmermans, Ed. Emerald Group Publishing Limited, 2009, p. 420.
9. D. Bauer, "Comparing pedestrian movement simulation models for a crossing area based on real world data," in Proceedings of the PED2010 Conference, 2010, pp. 547–556.
10. D. T. Lee and F. P. Preparata, "Computational Geometry - A Survey," *IEEE Transactions on Computers*, vol. c, no. 12, pp. 1072–1101, 1984.
11. S. Seer, D. Bauer, N. Brändle, and M. Ray, "Estimating Pedestrian Movement Characteristics for Crowd Control at Public Transport Facilities," in Proceedings of the ITSC2008, 2008, pp. 742–747.
12. H. Spiess, "Conical Volume-Delay Functions," *Transportation Science* May 1990 vol. 24 no. 2 153–158
13. A. Perez Arias, U. D. Hanebeck, P. Ehrhardt, S. Hengst, T. Kretz, and P. Vortisch, "Extended Range Telepresence for Evacuation Training in Pedestrian Simulations," in *Proceedings of the PED2010 Conference*, 2010.

Integrating Lateral Swaying of Pedestrians into Simulations

Barbara Krausz and Christian Bauckhage

Abstract Traditionally, pedestrian simulations are a standard tool in public space design, crowd management, and evacuation management. In particular, when minimizing evacuation times or identifying hazardous locations, it is of vital importance that simulations are as accurate and realistic as possible. Although today's pedestrian simulation models give satisfying results in many cases, they are not realistic in highly crowded scenes. In this paper, we describe a characteristic motion pattern that is commonly observed in areas of high pedestrian density and that has not been taken into account in state-of-the-art pedestrian models. Hence, we extend an existing pedestrian model by integrating this characteristic motion pattern and show that our proposed model gives more realistic trajectories.

Keywords Pedestrian simulation • Lateral oscillation • Trajectory • Generalized centrifugal force model • Social force model

1 Introduction

Simulations of pedestrian streams play an important role when optimizing evacuation routes or identifying hazardous locations in a building or event location in order to prevent accidents. Considering future research directions that integrate real-time information into simulations in order to foresee hazardous situations, prevent accidents, and recommend evacuation strategies in real-time, accurate pedestrian models are even more important.

In order to improve and validate models of pedestrian behavior, insights into human motion characteristics are needed. In particular, the dynamics in locations of

B. Krausz (✉) • C. Bauckhage
Fraunhofer IAIS, 53754 Sankt Augustin, Germany
e-mail: barbara.krausz@iais.fraunhofer.de; christian.bauckhage@iais.fraunhofer.de

high pedestrian density are of great interest. A very characteristic human motion pattern is lateral swaying. From common observations, it is known that people do not move along a straight line, but instead tend to swing laterally. In [1], we have shown that the relationship between the velocity and the amplitude of lateral swaying is even a linear relationship. Recently, this characteristic motion pattern has been exploited in order to detect congested areas by analyzing short-term motions from video surveillance cameras [2, 3].

However, a comparison of simulated trajectories and real trajectories reveals that lateral swaying has not been adequately taken into account in state-of-the-art pedestrian models. In this work, we extend the generalized centrifugal force model [4, 5] by superimposing an oscillation force that mimics lateral swaying of pedestrians. In addition to introducing the oscillation force, we also adapt the ellipse modeling space requirements of pedestrians to a reasonable size.

2 Related Work

Despite of many modifications of the social force model presented by Helbing and Molnár [6] and Helbing et al. [7] that have been proposed over the years [5, 8, 9], the model still cannot reproduce realistic motion behavior in areas of high pedestrian densities. Overlapping of pedestrians can hardly be avoided making a higher repulsive force between pedestrians necessary. As a consequence, oscillations occur when high repulsive forces push pedestrians back and forth. In their *centrifugal force model*, Yu et al. [9] take the relative velocity of people into account and introduce a collision detection technique in order to avoid overlappings. However, by introducing a collision detection procedure, the centrifugal force model as proposed in [9] increases the complexity of the model and counteracts the idea of a force-based system. Thus, Chraïbi et al. [4] and Chraïbi and Seyfried [5] propose the *generalized centrifugal force model* (GCFM) in which they replace the collision detection technique in favor of an improved formulation of repulsive forces.

3 The Generalized Centrifugal Force Model

In the following, we briefly describe the *generalized centrifugal force model* and use the notation of Chraïbi and Seyfried [5].

Given pedestrian i with coordinates \vec{R}_i and mass m_i , the movement of i is described as the superposition of a driving force and repulsive forces:

$$m_i \ddot{\vec{R}}_i = \vec{F}_i^{drv} + \sum_{j \in \mathcal{N}_i} \vec{F}_{ij}^{rep} + \sum_{w \in \mathcal{W}_i} \vec{F}_{iw}^{rep}. \quad (1)$$

The driving force models motion into the direction of the pedestrian's intended destination as well as his desired speed v_i^0 . Formally, the driving force of pedestrian i is given as

$$\vec{F}_i^{drv} = m_i \frac{\vec{v}_i^0 - \vec{v}_i}{\tau} \quad (2)$$

where \vec{v}_i denotes i 's current velocity and τ is a relaxation time.

Repulsive forces induced by nearby pedestrians as well as obstacles model the avoidance of collisions. In [5], the repulsive force between pedestrians i and j is given as

$$\vec{F}_{ij}^{rep} = -m_i k_{ij} \frac{(\eta_{ped} \|\vec{v}_i^0\| + v_{ij})^2}{dist_{ij}} \vec{e}_{ij}. \quad (3)$$

With \vec{R}_{ij} being the vector pointing from pedestrian i to pedestrian j , \vec{e}_{ij} is the normalized connecting vector:

$$\vec{R}_{ij} = \vec{R}_j - \vec{R}_i, \quad \vec{e}_{ij} = \frac{\vec{R}_{ij}}{\|\vec{R}_{ij}\|} \quad (4)$$

In order to model the field of perception, the coefficient k_{ij} in Eq. 3 is at its maximum when pedestrian j is in the motion direction of pedestrian i , whereas it is zero when pedestrian j is out of sight, i.e. when the angle between \vec{v}_i and pedestrian j is greater or equal to 90° :

$$k_{ij} = \begin{cases} (\vec{v}_i \cdot \vec{e}_{ij}) / \|\vec{v}_i\|, & \text{if } \vec{v}_i \cdot \vec{e}_{ij} > 0 \wedge \|\vec{v}_i\| \neq 0 \\ 0, & \text{otherwise.} \end{cases} \quad (5)$$

In addition to the field of perception, the relative velocity between pedestrians is also taken into account. If pedestrians in front of pedestrian i are walking fast, i is not affected by them:

$$v_{ij} = \begin{cases} (\vec{v}_i - \vec{v}_j) \cdot \vec{e}_{ij}, & \text{if } (\vec{v}_i - \vec{v}_j) \cdot \vec{e}_{ij} > 0 \\ 0, & \text{otherwise.} \end{cases} \quad (6)$$

However, if v_{ij} is small, the repulsive force decreases leading to overlappings. Chraïbi and Seyfried take the intended speed $\|\vec{v}_i^0\|$ into account, since pedestrians with a high desired speed require higher repulsive forces in order to prevent collisions. They introduce a parameter η_{ped} to control the influence of the desired

speed. In their experiments, they find a value of $\eta_{ped} = 0.3$ in order to minimize both overlappings and oscillations.

Next, $dist_{ij}$ in Eq. 3 denotes the distance between pedestrians i and j which are modeled as ellipses. $dist_{ij}$ is the distance of the ellipses along the vector \vec{R}_{ij} connecting the ellipse centers.

Pedestrian i is modeled as an ellipse centered on \vec{R}_i with semi-axis a_i being the semi-axis in the movement direction \vec{v}_i and b_i the semi-axis orthogonal to a_i . a_i includes physical body extensions of pedestrian i as well as space requirements in movement direction which depends on the current speed:

$$a_i = a_{min} + \tau_a \|\vec{v}_i\| \quad (7)$$

where a_{min} and τ_a are two parameters to be set.

With b_i , Chraibi and Seyfried model space requirements into lateral direction due to lateral swaying. From observations of trajectories, they model b_i as:

$$b_i = b_{max} - (b_{max} - b_{min}) \frac{\|\vec{v}_i\|}{\|\vec{v}_i^0\|} \quad (8)$$

where b_{max} is the maximum amplitude of lateral swaying which decreases to a minimum of b_{min} .

Similar to the repulsive force between pedestrians, the repulsive force exerted by the wall w is given in [5] as:

$$\vec{F}_{iw}^{rep} = -m_i k_{iw} \frac{(\eta_{wall} \|\vec{v}_i^0\| + \|\vec{v}_i^n\|)^2}{dist_{iw}} \vec{e}_{iw} \quad (9)$$

where \vec{v}_i^n is the normal component of i 's velocity vector to the wall and η_{wall} is a parameter controlling the influence of the intended speed on the repulsive force similar to η_{ped} in Eq. 3. $dist_{iw}$ is the distance between the nearest point on wall w and the nearest point on the ellipse of pedestrian i . \vec{e}_{iw} and k_{iw} are defined analogously to Eqs. 4 and 5.

4 Integration of Characteristic Human Motion Patterns

In contrast to the original social force model, the generalized centrifugal force model shows good results even in areas of high pedestrian density. However, a comparison of simulated trajectories and real trajectories reveals that lateral swaying has not been adequately taken into account. In the generalized centrifugal force model, pedestrians are modeled as ellipses which include space requirements into lateral

direction due to lateral swaying, but pedestrians do not actually perform lateral oscillations. Instead, they are walking along a straight line.

Since the observation of lateral swaying is a fundamental characteristic of human gait and crucial for the detection of congested areas, see [3], we introduce an *oscillation force*. Thus, the movement of a pedestrian i with mass m_i and position \vec{R}_i is modeled as the superposition of a driving force, repulsive forces as well as the oscillation force:

$$m_i \ddot{\vec{R}}_i = \vec{F}_i^{drv} + \vec{F}_i^{osc} + \sum_{j \in \mathcal{N}_i} \vec{F}_{ij}^{rep} + \sum_{w \in \mathcal{W}_i} \vec{F}_{iw}^{rep}. \quad (10)$$

where \vec{F}_i^{drv} , \vec{F}_{ij}^{rep} and \vec{F}_{iw}^{rep} are defined as described above and \vec{F}_i^{osc} is defined as:

$$\vec{F}_i^{osc} = -m_i (2\pi f(\vec{v}_i))^2 s(\vec{v}_i) \sin(2\pi f(\vec{v}_i)t + \phi_0) \vec{n}_i. \quad (11)$$

Here, \vec{n}_i is the unit vector normal to the moving direction \vec{v}_i and ϕ_0 is the phase of oscillation. $f(\vec{v}_i)$ and $s(\vec{v}_i)$ are the frequency and amplitude of lateral swaying where we use the findings from [1]. In this work, we analyzed real trajectories obtained from video recordings of a large scale experiment conducted under laboratory conditions. Based on the trajectories, we found a linear relationship between the velocity and the amplitude of lateral swaying as well as between the velocity and the frequency:

$$f(\vec{v}_i) = 0.44 \|\vec{v}_i\| + 0.35 \quad (12)$$

and

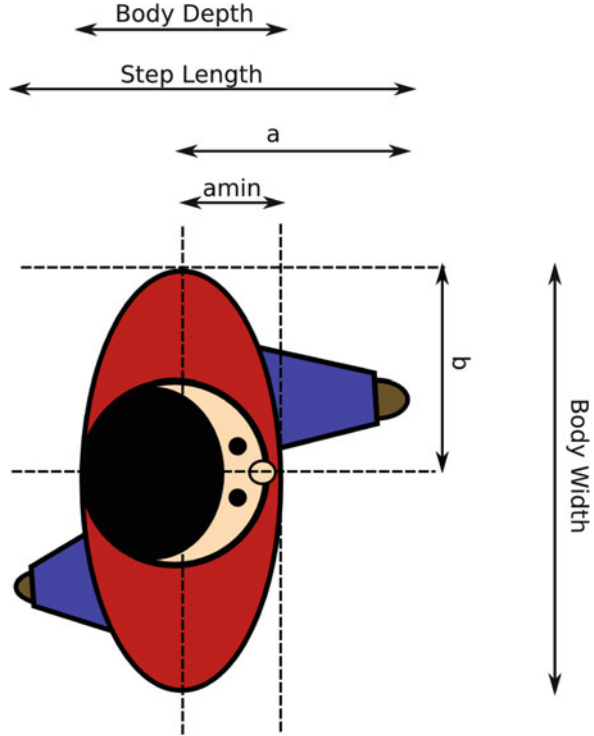
$$s(\vec{v}_i) = -0.14 \|\vec{v}_i\| + 0.21. \quad (13)$$

In addition to the introduction of an oscillation force, we adapt the ellipse modeling space requirements of pedestrians. Similar to Chraïbi and Seyfried, we model pedestrian i as an ellipse with semi-axes a_i and b_i (Fig. 1) and take empirical studies of human body dimensions into account. Weidmann [10] reports a mean value of 0.23 m for the body depth with the 97.5% at 0.27 m. Next, according to Weidmann, the step length can be computed as:

$$l(\vec{v}_i) = 0.235 + 0.302 \cdot \|\vec{v}_i\|. \quad (14)$$

First, we note that the first term in this equation is almost equal to the body depth of 0.23 m given above. The second term in Eq. 14 models space requirements of a pedestrian for taking a step. Having in mind that a_i denotes the length of the semi-axis and thus is half of the step length, we set it as follows:

Fig. 1 A pedestrian is modeled as an ellipse with semi-axis a_i being the semi-axis into the motion direction and b_i the orthogonal semi-axis. Note that b_i is half of the body width and a_i is half of the step length



$$a_i(\vec{v}_i) = 0.5 \cdot l(\vec{v}_i) = a_{min} + a_\tau \cdot \|\vec{v}_i\| \tag{15}$$

with $a_{min} \in \mathcal{N}(0.5 \cdot 0.23, 0.01) = \mathcal{N}(0.115, 0.01)$ modeling half of the body depth and $a_\tau \in \mathcal{N}(0.5 \cdot 0.302, 0.001) = \mathcal{N}(0.151, 0.001)$ modeling space requirements for taking a step.

The second semi-axis b_i is set to $b_i \in \mathcal{N}(0.5 \cdot 0.46, 0.01) = \mathcal{N}(0.23, 0.01)$, since Weidmann gives a value of 0.46 m for the body width with the 97.5 % at 0.5 m. Note that in contrast to the generalized centrifugal force model, we do not take lateral space requirements into consideration here, since they are already modeled by the oscillation force given in Eq. 11.

5 Experiments

In order to evaluate the effectiveness of our model quantitatively, we simulate pedestrian movements and test if the fundamental diagram is well reproduced. Secondly, we employ trajectories obtained from an experiment of the Hermes project [11], use their initial positions and simulate pedestrian movements.

Table 1 Parameter values used in the experiments

Parameter	Description	Value
r_c	Cutoff radius	2
v_i^0	Desired speed	$\mathcal{N}(1.34, 0.26)$
m_i	Mass	1
τ	Relaxation time	$\mathcal{N}(0.5, 0.001)$
η_{ped}	Controls influence of intended speed on repulsive force	0.3
η_{wall}	Controls influence of intended speed on repulsive force	0.2
δt	Step size for solving differential equation system	0.001
GCFM [5]		
a_{min}	Minimum length of semi-axis	$\mathcal{N}(0.2, 0.01)$
τ_a	Factor for computing length of semi-axis	$\mathcal{N}(0.53, 0.001)$
b_{max}	Maximum length of semi-axis	$\mathcal{N}(0.25, 0.001)$
b_{min}	Minimum length of semi-axis	$\mathcal{N}(0.2, 0.001)$
Modified GCFM (Sect. 4)		
a_{min}	Minimum length of semi-axis	$\mathcal{N}(0.115, 0.01)$
a_τ	Factor for computing length of semi-axis	$\mathcal{N}(0.151, 0.001)$
b_i	Length of semi-axis	$\mathcal{N}(0.23, 0.01)$

A comparison of real trajectories to the simulated trajectories reveals that our model simulates realistic trajectories. In our experiments, we use the parameters shown in Table 1.

For verification of the model proposed in Sect. 4 and to examine the influence of the two modifications (oscillation force and adaptation of ellipse), we simulate pedestrian trajectories in a corridor (26×1 m) and measure the fundamental diagram in a measurement area (2×1 m) located in the middle of the corridor.

In Fig. 2, we depict resulting fundamental diagrams in comparison to experimental data [8]. Figure 2a shows the fundamental diagram for the original GCFM. In Fig. 2b, we superimposed the oscillation force (Eq. 11), whereas in Fig. 2c, we adapt the size of the ellipses of pedestrians. Figure 2d shows the final model as proposed in Sect. 4 with oscillation force and adapted ellipse size.

When superimposing the oscillation force, the speed decreases, since pedestrians require more space for lateral oscillation. In the second case, when we just decrease the size of the pedestrians to a reasonable size, the speed increases due to less space requirements. Finally, when incorporating both modifications, the fundamental diagram fits well to experimental data.

Next, we compare simulated trajectories with real trajectories obtained from the Hermes dataset. For that purpose, we consider 30 s of a video which corresponds to the time of highest pedestrian density. We use the initial positions and velocities of 62 pedestrians and simulate their trajectories using the original GCFM as well as the modified GCFM with oscillation force and adapted ellipse size. Figure 3 shows real trajectories (green) and simulated trajectories (red).

Here, it becomes obvious that using the original GCFM, pedestrians do not perform lateral swaying. However, when using the proposed modified version of the

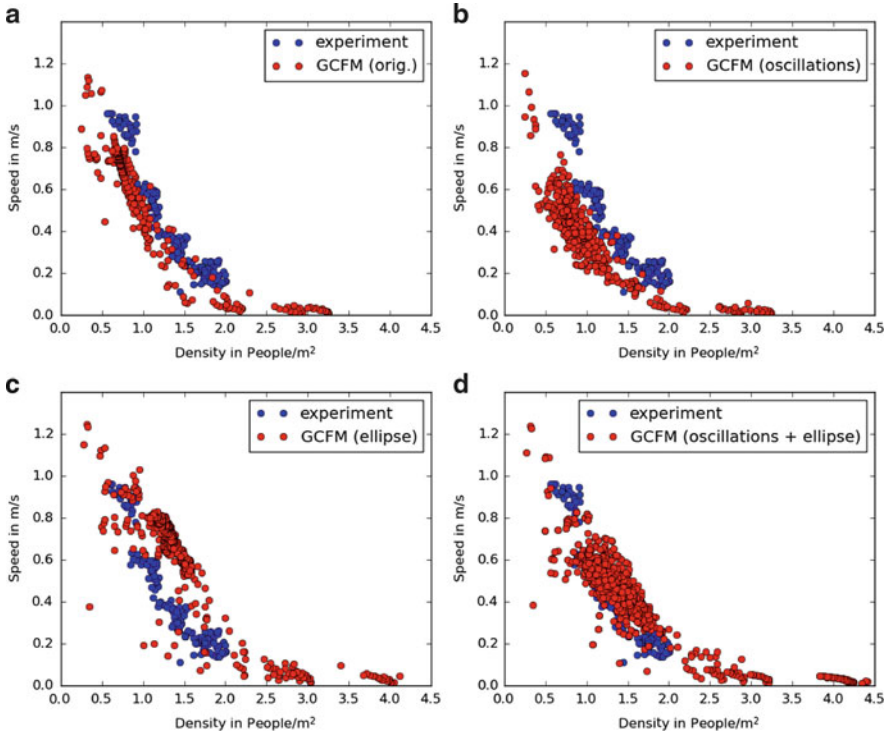


Fig. 2 Fundamental diagrams for comparing our proposed model and the original GCFM with regard to experimental data [8]. Pedestrian trajectories are simulated in a corridor (26×1 m) using the (a) original GCFM, (b) superimposing the oscillation force, (c) adapting the ellipse sizes of pedestrians, and (d) using both modifications

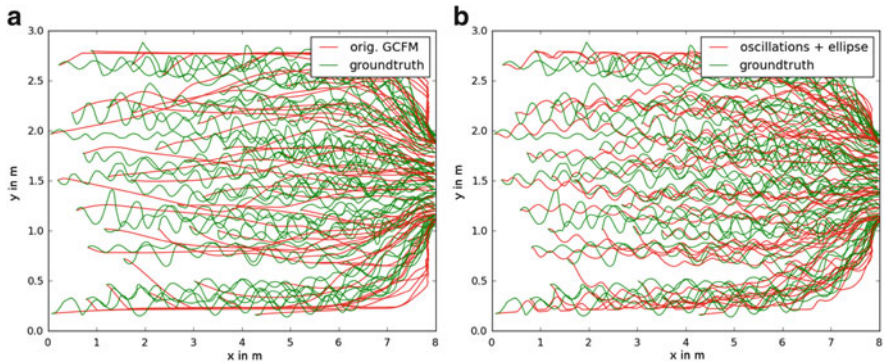


Fig. 3 Comparison of simulated trajectories to ground truth trajectories obtained from the Hermes dataset. In green, we depict the ground truth trajectories of 62 pedestrians. For simulating their trajectories, we take their initial positions and velocities and simulate their movements using the (a) original generalized centrifugal force model [5] and (b) our proposed model where we superimpose an oscillation force for including lateral oscillations and adapt the ellipse of pedestrians modeling space requirements. Note that we set the phase of lateral oscillation to 0

Table 2 Results of comparing real trajectories with simulated trajectories using the original GCFM and our modified version with oscillation force and adapted ellipse sizes. We compute mean, standard deviation and maximum of the Hausdorff distance as well as differences in trajectory lengths

		Orig. GCFM	Mod. GCFM
Hausdorff Length	Mean	0.29	0.26
	Standard deviation	0.12	0.1
	Maximum	0.73	0.64
	Mean	120	87
	Standard deviation	99	61.7
	Maximum	311	233

GCFM, lateral oscillations can be observed. Note that there are differences between real trajectories and simulated trajectories using the modified GCFM, since we do not know the phase of lateral oscillation. Instead, we assume that the phase ϕ_0 in Eq. 11 is zero.

In order to compare simulated trajectories and real trajectories, we consider the differences in trajectory lengths as well as the Hausdorff distance. Table 2 shows mean, standard deviation and maximum of the Hausdorff distance as well as mean, standard deviation and maximum value of the differences in trajectory lengths. Obviously, the modified GCFM outperforms the original GCFM.

References

1. Krausz, B., Baukchage, C.: Analyzing pedestrian behavior in crowds for automatic detection of congestions. In: ICCV Workshop on Modeling, Simulation and Visual Analysis of Large Crowds. (2011)
2. Krausz, B., Baukchage, C.: Automatic detection of dangerous motion behavior in human crowds. In: AVSS. (2011)
3. Krausz, B., Baukchage, C.: Loveparade 2010: Automatic video analysis of a crowd disaster. CVIU **116**(3) (2011) 307 – 319
4. Chraïbi, M., Seyfried, A., Schadschneider, A., Mackens, W.: Quantitative description of pedestrian dynamics with a force-based model. In: Int. Conf. on Web Intelligence and Intelligent Agent Technologies. (2009)
5. Chraïbi, M., Seyfried, A.: Generalized centrifugal-force model for pedestrian dynamics. Phys. Rev. E **82**(4) (2010) 046111
6. Helbing, D., Molnár, P.: Social force model for pedestrian dynamics. Physical Review E **51**(5) (1995) 4282–4286
7. Helbing, D., Farkas, I., Vicsek, T.: Simulating dynamical features of escape panic. Nature **407**(6803) (2000) 487–490
8. Seyfried, A., Steffen, B., Lippert, T.: The fundamental diagram of pedestrian movement revisited. Journal of Statistical Mechanics **P10002** 339–352
9. Yu, W.J., Chen, R., Dong, L.Y., Dai, S.Q.: Centrifugal force model for pedestrian dynamics. Physical Review E **72**(2) (2005) 026112
10. Weidmann, U.: Transporttechnik der Fußgänger. Schriftenreihe des IVT 90, ETH Zürich (1992)
11. Hermes: BMBF Research Programme. <http://www2.fz-juelich.de/jsc/appliedmath/ped/projects/hermes> last visited January 12, 2012.

Integration of a Multi-modal Simulation Module into a Framework for Large-Scale Transport Systems Simulation

Christoph Dobler and Gregor Lämmel

Abstract In recent years, the interest in multi-modal simulation models has increased significantly. In such models, various transport modes are simulated simultaneously, including the interactions between agents using different modes. Typical fields of application are, for example, studies on evacuations, car sharing and public transport.

Commonly used models today focus either on macroscopic simulation of large-scale scenarios with hundreds of thousands or even several million entities or microscopic simulation of small scale scenarios based on complex models for the underlying physics. While the first class only deals with vehicular traffic, the second one usually also deals with pedestrians and cyclists.

Obviously, there is a gap between these two areas that has to be closed by a multi-modal simulation. This paper presents the combination of both simulation approaches integrated a single simulation framework. Its capabilities are demonstrated on a real world large-scale scenario which includes also microscopic elements.

Keywords Force-based 2D pedestrian simulation • Large-scale transport systems simulation • Multi-modal simulation

C. Dobler (✉)

Swiss Federal Institute of Technology Zurich, Institute for Transport Planning and Systems,
Wolfgang-Pauli-Strasse 15, 8093 Zurich, Switzerland
e-mail: dobler@ivt.baug.ethz.ch

G. Lämmel

Technical University Berlin, Transport Systems Planning and Transport Telematics, Sekr. SG12,
Salzufer 17-19, 10587 Berlin, Germany
e-mail: laemmel@vsp.tu-berlin.de

1 Multi-modal Simulation

1.1 *State of the Art*

In recent years, the interest in multi-modal simulation models has increased significantly. In such models, various transport modes are simulated simultaneously, including the interactions between agents using different modes. Typical fields of application are, for example, studies on evacuations, car sharing and public transport.

Today, there are two major types of agent-based transport simulations. On one hand, models for large-scale scenarios with hundreds of thousands or even several million entities have been developed. To keep their computational effort acceptable, they are based on simplified physical representations of traffic flows as they are known from the field of dynamic traffic assignment. On the other hand, there are models with a high level of detail and a microscopic modeling of the underlying physics for small scenarios with some hundred or a few thousand agents. While the first class only deals with vehicular traffic, the second one usually also deals with pedestrians and cyclists.

Obviously, there is a gap between these two areas that has to be closed by a multi-modal simulation. Unfortunately, a model for large-scale scenarios does not provide the necessary physical accuracy which is required for a detailed pedestrian and cyclist simulation and a detailed microscopic model cannot handle several million entities. Therefore, a new approach is required which combines the best of both worlds.

One of very few approach to couple traffic-flow models with different levels of detail is presented by Sewall et al. [17]. They use a hybrid model of both continuum and agent-based methods for traffic simulations. In regions of interest, the simulation uses an agent-based approach, in the remaining parts a faster continuum model. However, in contrast to the approach presented in this paper, their model is designed only for vehicular traffic.

1.2 *Modeling Approach*

This paper presents a modeling approach that closes the gap described above by implementing a flexible multi-modal simulation that is able to handle scenarios where the level of detail varies. The implementation of this framework is done in three steps.

First, a simulation framework for vehicular traffic is extended to a simple multi-modal simulation framework with a constant level of detail. Instead of estimating travel times for non-vehicular trips, routes are created based on a multi-modal network and assigned to travelers. This extension is based on a queue model which is computationally efficient but also limited in its ability to model microscopic interactions.

Therefore, in a second step, a force-based 2D simulation module for non-vehicular trips is integrated into the framework. The agents' high-level planning (i.e. route and destination choice) is performed on a graph representing the transport system while the low level behavior (i.e. physical interaction between the participants) is simulated with a force-based model. In this force-based model, simulation entities are emitting repelling (other agents and obstacles) and attracting forces (goal locations). The force based model itself is based on existing and well established approaches.

To allow modeling different levels of detail, the simulation module has to be able to simulate different regions of the scenario with different simulation modules. An example would be a person that walks along an empty road, which can be simulated using the queue based multi-modal simulation module from step one. However, when entering a more crowded area, the person starts to interact with other people. The queue model has difficulties to deal with those situations appropriately. This is in particular true for situations with crossing pedestrian streams. To account for those interactions, people in that area can be simulated using the force-based 2D simulation module. Therefore, the possibility to dynamically switch between those two modules will be added to the simulation framework in a third step.

1.3 Application

Today, the field of application for large-scale agent-based traffic flow micro-simulations is wide spread. On one hand, such simulations create information like traffic flows and average travel times that are used traditionally in the field of transport planning and traffic management. On the other hand, those simulations produce also additional information that can be used for many interdisciplinary tasks. Due to the agent-based approach, each person in a scenario is represented as single entity. Therefore, the movement of each single person can be tracked, which is e.g. an essential requirement for evacuation scenarios and simulations.

Other fields of application for large-scale multi-modal simulations are e.g. studies that are interested in the usage of e-bikes or ride-sharing. For both of them, it is essential that also non-vehicular modes are simulated in detail.

1.4 Requirements

The proposed multi-modal simulation has to fulfill several additional requirements that result from the combination of the two different modeling approaches. Clearly, interactions between both approaches have to be included in the combined model. If, for example, pedestrians are waiting at a crosswalk, drivers have to stop and let them pass. However, this behavior is not necessary in the vehicular-only model and therefore has to be added in the multi-modal model.

Another issue is the travel time calculation for modes which are simulated using the simple model as well as the detailed 2D force-based approach. To create consistent routing results, travel times have to be estimated on a global level using information from both models.

Some further requirements result from the necessary input data which differs for the two combined models. On one hand, a vehicular model for example does not use person specific data like age or gender. A pedestrian model, on the other hand, needs this data because a person's walking speed depends on them. Another example is data representing a road network. Vehicular models typically ignore steepness information. However, a link's steepness clearly influences the speed of people using non-motorized modes. As a result, it has to be ensured that data used from either one or both models is available in the entire multi-modal simulation framework.

2 MATSim

2.1 Framework

MATSim is a framework for iterative, agent-based transport systems micro-simulations. It is currently being developed by teams at ETH Zurich and TU Berlin as well as senozon AG, a spin-off company founded by former members of both institutes. Balmer [1] gives a detailed description of the framework, its capabilities and its structure. Because of its agent-based approach, every person in the system is modeled as an individual agent in the simulated scenario. Each agent has personalized parameters such as age, sex, available transport modes and scheduled activities. MATSim's application to a large-scale Switzerland scenario (over six million agents simulated on a high resolution network with one million links) is presented by Meister et al. [11].

Figure 1 shows the structure of a typical, iterative MATSim simulation run. After creation of initial demand, plans of the agents are modified and optimized in an iterative process until a relaxed system state (typically a user equilibrium) is found. The results can be analyzed later. The loop shown in the figure contains *execution (simulation)*, *scoring* and *replanning* elements. Within the simulation module, agents' plans are executed. Afterward, the scoring module uses a utility function to calculate the executed plans' quality. Charypar et al. [2] describe the basic utility function for MATSim. Based on scoring module results, the replanning module creates new plans by varying start times and durations of activities, as well as routes and modes used to travel from one activity to another.

Simulation of traffic behavior is also part of the iterative loop. The simulation module's task is to execute agents' plans within the simulated scenario. The so-called *QSim* is a deterministic, Java based implementation of a queue model using a time step based approach with a 1-s step size. Within each time step, the state of the queues is considered.

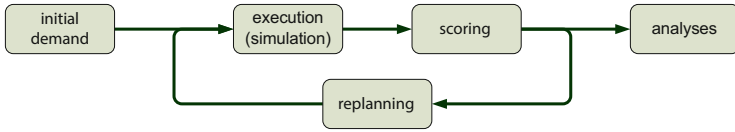


Fig. 1 Structure of the iterative MATSim loop

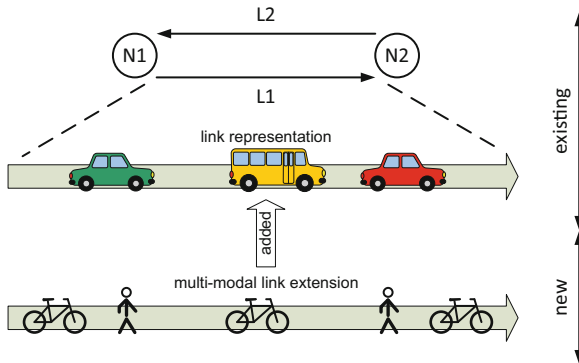


Fig. 2 Multi-modal link extension

By default, only car traffic is simulated physically. The travel times for other modes like walk, bike or public transport are estimated based on crow fly—or direct—distance. Support for public transport has been added recently [16].

2.2 Multi-modal Extension

In a first step, a multi-modal simulation framework with a constant level of detail is developed and integrated into the MATSim framework. Figure 2 shows the basic concept of the implementation. A multi-modal extension is added to each link object in the mobility simulation. While traffic flow dynamics are simulated by MATSim’s mobility simulation using a queue model, they are not taken into account in the multi-modal extension. Having a look at typical pedestrian and cyclist traffic flows shows that congestion is very rare compared to vehicular traffic and therefore justifies the application of this simplistic approach in large parts of a scenario. For regions with higher traffic flows, this simple model is replaced with a 2D force-based model, which provides a very high level of detail, including consideration of traffic flows, at the cost of additional computational effort. Besides more computational power, the 2D force-based model requires also additional information about a road’s geometry.

So far, the switch between those two approaches is performed semi-automatically. For each link, the multi-modal simulation type has to be specified (simple vs.

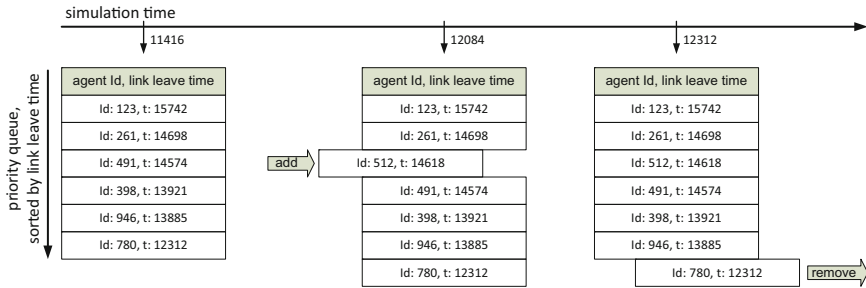


Fig. 3 Link representation in the simple model. At time 12084, agent 512 enters the link and is—based on its calculated link leave time 14618—inserted into the queue. At time 12312, agent 780 has reached its leave time and therefore is removed from the queue

detailed). Transport modes in agents’ plans are not affected by this—i.e. there is e.g. only one kind of *walk* mode. A link’s multi-modal extension then selects the corresponding model to simulate an agent traveling along that link. As part of future work, the specification of a link’s simulation model will be fully automatized. To do so, the simulation has to monitor the traffic flows on multi-modal links. If a critical level, where congestion is expected, is exceeded on a link, traffic flows on that link have to be simulated using the 2D force-based approach. When the flows drop back below the critical level, the simulation module can be switched back to the simple approach.

In the simple model, agents traveling on a link are stored in a priority queue which orders the agents based on their scheduled link leave time (see Fig. 3). This time is calculated when an agent enters a link based on parameters like the agent’s age and gender as well as the links steepness. In each time step it is checked, whether the queue contains agents who have reached their link leave time and therefore have to be moved to their route’s next link. An agent’s position on a link is not determined by the model. However, under the assumption that agents move with constant speed, their position can be interpolated. On one hand, this approach is computationally very efficient because computation effort is only created when an agent enters or leaves a link but not when the agent is traveling along a link. On the other hand, agents can travel with different speeds and therefore overtake each other.

2.3 Force-Based 2D Simulation

This sections gives a brief overview of the force based agent movement model. For a detailed discussion see [10]. We distinguish between two stages in the movement model. The first stage deals with the low level movement of the agents, meaning collision avoidance, velocity adaptation and so on. The second stage deals with the more high level movement of the agents, meaning moving along a given route.

Both stages are modeled based on additive attracting and repelling forces, which are “pushing” the agents through the environment. The general force model is defined according to Newton’s law ($F = m \cdot a$).

$$m_i \cdot \mathbf{a}_i(t) = \frac{m}{\tau} (\mathbf{v}_i^0(t) - \mathbf{v}_i(t)) + \sum_{j \neq i} \mathbf{f}_{i,j}(t), \tag{1}$$

with \mathbf{v}_i^0 is the desired velocity vector for agent i at time t . The term $\mathbf{v}_i(t)$ denotes the agent’s actual velocity at time t . The time constant τ describes the time that is needed to adjust the actual velocity to the desired velocity. The second term of the equation builds the sum over all influential entities j in the environment (i.e. other agents, walls, and obstacles). Each of those entities emit a repelling (or attracting) force to agent i .

Many different force models have been discussed in recent years (see, e.g. [12] for an overview), most of them are build on the so called social force model introduced by Helbing et al. [8]. The basic social force model implicitly reproduces collision avoiding behavior as it can be observed in real-world situations. It has been shown that the model works particularly well in high density conditions, such as one can observe in evacuation situations [7]. In this work we adapted an extension to the social force model where collisions are explicitly avoided by predicting potential collision points [20].

In the model each agent i computes for each other agent j in the environment the angle $\theta_{i,j}$ between $\mathbf{d}_{i,j}$ and $\mathbf{v}_{i,j}$. Where $\mathbf{d}_{i,j}$ denotes the vector pointing from agent i ’s position to agent j ’s position and $\mathbf{v}_{i,j}$ denotes the relative velocity between both agents. If $|\theta_{i,j}| > \pi/4$ then the time $t_{i,j} = \infty$. Otherwise $t_{i,j}$ reflects the time of closest approach which is the time when the distance of both agents is minimal by assuming that neither agent i nor agent j changes her velocity or direction of movement. The agent than takes the minimum of these times $t_i = \min_j(t_{i,j})$. Afterwards the agent computes the configuration of the environment for t_i by again assuming that none of the pedestrians changes her velocity or direction of movement. Let $\mathbf{d}'_{i,j}(t_i)$ denote the predicted vector pointing form agent i to agent j at time t_i . The agent j ’s influence on agent i (second term in Eq. 1) is

$$\mathbf{f}_{i,j}(t) = A_{env} \frac{v_i(t)}{t_i} e^{-d_{i,j}(t)/B_{env}} \frac{\mathbf{d}'_{i,j}(t_i)}{d'_{i,j}(t_i)}. \tag{2}$$

The constants A_{env} and B_{env} are free parameters in the model. Equation 2 is not only applicable for other agents in the environment but also for any none moving object like walls or obstacles. The collision avoiding model describes how the environment influences the agents’ movement. However, in order to move through the environment along a given route a “driving force”, like the velocity adaption term in Eq. 1, is needed.

In the current setup every agents start at a link in the navigation graph. A simple approach would be to let \mathbf{v}_i^0 point towards the to-node of the start link at the

beginning. As soon as the node is reached \mathbf{v}_i^0 points to the to-node of the next link and so on until the agent reaches her destination. However, in [6] it has been shown that such an approach leads to an unrealistic behavior in situations when agents are moving next to each other. The reason is that those agents are pulled together at close range to a node and after the node is passed their trajectories diverge again. The authors proposed a force system that follows the route in the navigation graph. The basic idea is that each agent keeps a shadow tag on the navigation graph, which moves along the graph as the agents move forward. Furthermore, the agents are connected by a virtual rubber strap to their corresponding shadow tag. The agents are driven by a driving force that works parallel to the link which has the shadow tag on it. The virtual rubber strap pulls the agents towards the shadow tag if they diverge to far from the link. This leads to the following force:

$$\frac{m_i}{\tau} (\mathbf{v}_i^0(t) - \mathbf{v}_i(t)) + A_{path} e^{d_i^p(t)/B_{path}} \mathbf{d}_i^p(t), \quad (3)$$

where $d_i^p(t)$ is the agent i 's distance to the current link, and $\mathbf{d}_i^p(t)$ is the perpendicular unit vector pointing from the agent to the current link.

Sticking all together the agents' acceleration at time t is given by:

$$\mathbf{a}_i(t) = \frac{1}{\tau} (\mathbf{v}_i^0(t) - \mathbf{v}_i(t)) + \frac{1}{m_i} \left(A_{path} e^{d_i^p(t)/B_{path}} \mathbf{d}_i^p(t) \sum_{j \neq i} A_{env} \frac{v_j(t)}{t_j} e^{-d_{i,j}(t)/B_{env}} \frac{\mathbf{d}'_{i,j}(t_j)}{d'_{i,j}(t_j)} \right) \quad (4)$$

This leads to a model with four free parameters (A_{env} , B_{env} , A_{path} , and B_{path}).

In the rubber strap analogy discussed above the agent would switch to the next link as soon as the shadow tag moves over the node. This means, at the end of each link is virtual perpendicular finish line and as soon as the agent crosses that finish line, the shadow tag is assigned to the next link. However, as it is pointed out in [5], this approach results in an artifact if the angle between two consecutive links is smaller than $\pi/2$. In those cases the agents will move toward the inner curve of the path, which is not plausible. The proposed solution that is implemented here is that the finish line is not perpendicular to the link but it corresponds to the bisector of the angle between both links.

The model for the agent movement defined in Eq. 4 defines the agents' acceleration in a continuous time model. However, in order to integrate the model into a computer simulation the time has to be discretized. This means an agent's velocity will only be updated at discrete time steps. There are different ways how to update velocities at discrete time steps. A common used way is the Euler-Cromer method (see, e.g. [3]), which ends up in the following equations:

$$\mathbf{v}_i(t+h) = \mathbf{v}_i(t) + h\mathbf{a}_i(t) \quad (5)$$

$$\mathbf{r}_i(t+h) = \mathbf{r}_i(t) + h\mathbf{v}_i(t+h) \quad (6)$$

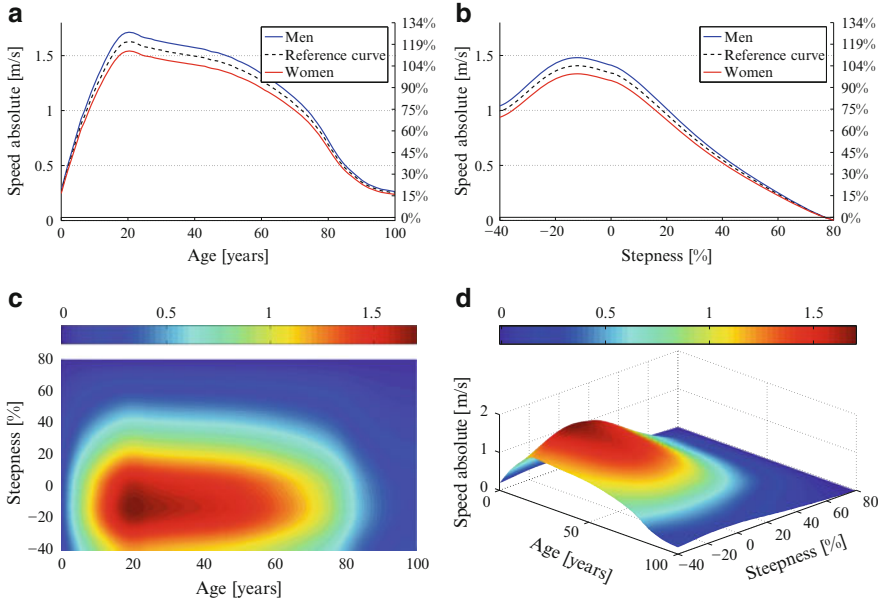


Fig. 4 Speed of pedestrians. (a) Age dependent speed. (b) Steepness dependent speed. (c) Age and steepness dependent speed. (d) Age and steepness dependent speed (3d)

Where $\mathbf{r}_i(t)$ is the agent i 's position at time t and h is the time step size.

2.4 Multi-modal Travel Times

Travel time calculation for motorized modes is already implemented in MATSim. Therefore, this section focusses on travel time calculation for non-motorized modes.

Walk travel time calculation is based on results of a comprehensive literature review presented by Weidmann [19]. Starting point is a normally distributed reference speed of 1.34 m/s with a standard deviation of 0.26 m/s, which leads to an individual reference speed for each person. References [4] and [18] report comparable but not as detailed data. If a trip's purpose is known, a person's reference value can be adjusted (commuting 1.49 m/s, shopping 1.16 m/s, leisure 1.10 m/s) [4]. Using the reference speed and respecting a person's age and gender, a personalized speed is calculated (see Fig. 4a). Finally, to calculate the person's travel time on a specific link, the influence of the link's steepness on the person's speed is taken into account (see Fig. 4b). The combination of person specific attributes and link steepness is shown in Fig. 4c, d. As a result, a person's speed on plain terrain is calculated as:

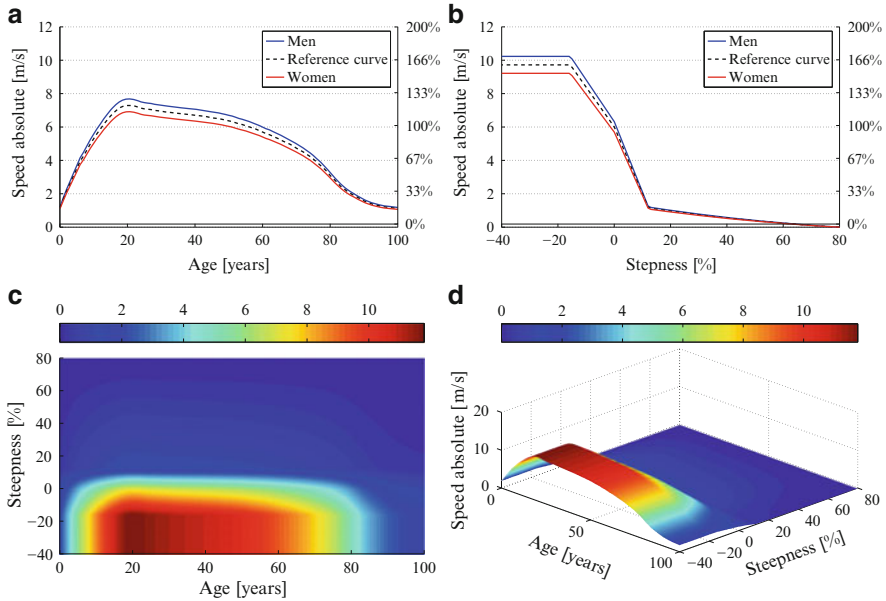


Fig. 5 Speed of cyclists. (a) Age dependent speed. (b) Steepness dependent speed. (c) Age and steepness dependent speed. (d) Age and steepness dependent speed (3d)

$$person\ scale\ factor = statistical\ spreading\ factor \cdot gender\ factor \cdot age\ factor \quad (7)$$

$$v_{person,walk} = v_{reference,walk} \cdot person\ scale\ factor \quad (8)$$

A link’s steepness is incorporated as:

$$v_{person\ walks\ on\ link} = v_{person,walk} \cdot steepness\ factor \quad (9)$$

The speed of cyclists is determined using results from [13]. Starting point is again an individual person speed based on a normal distributed ($\mathcal{N}(6.01, 1.17^2)$) reference speed. Again, a person’s speed is calculated by accounting for age and gender (see Fig. 5a).

When calculating the steepness factor, it is distinguished whether a link goes uphill or downhill. When going uphill, the person’s speed is reduced by a factor which is calculated based on the grade and a reference factor of 0.4002 m/s which is scaled by the same factor as the person’s reference speed. I.e. the speed drop of slow people is lower than the drop of fast people. When the bike speed drops below the walk speed, which happens at a grade of approximately 12 %, it is assumed that the person’s switches to walking (see Eq. 11). For downhill links a reference factor of 0.2379 m/s is used. Additionally it is assumed, that cyclists limit their speed to 35 km/h (9.7222 m/s; see Eq. 12).

$$v_{person,bike} = v_{reference,bike} \cdot person\ scale\ factor \tag{10}$$

$$v_{person,uphill} = \max \begin{cases} v_{person,bike,flat} - 0.4002 \cdot |grade| \cdot person\ scale\ factor \\ v_{person,walk,uphill} \end{cases} \tag{11}$$

$$v_{person,downhill} = \min \begin{cases} v_{person,bike,flat} + 0.2379 \cdot |grade| \cdot person\ scale\ factor \\ 9.7222 \end{cases} \tag{12}$$

Another parameter that affects the speed of pedestrians and cyclists is the crowdedness of the link where they are physically present. Data to take this effect into account is again presented by Weidmann [19]. However, to calculate the crowdedness of a link, its geometry has to be taken into account. One method of doing this is discussed in [9]. In the following we give a short description of this method. We assume that the geometry of a link is represented by a simple polygon. Important parameters of the polygon are:

- Link area A
- Link minimum width w

While the area of a polygon is straightforward to calculate, there is no obvious approach to calculate the minimum width of the link. One way is first to calculate the median, which can be derived from the medial axis of a polygon (see, e.g. [15] for a “medial axis” algorithm), and afterwards calculating the minimum border to border distance orthogonal to the median. Having this parameters we can calculate the storage capacity and flow capacity of the link. The storage capacity for pedestrians usually is given in persons per area. In Weidmann’s work a pedestrian flow comes to a stand still at a density of $\rho^{max} = 5.4 / m^2$. This means, the storage capacity of a link is $A * \rho^{max}$. The minimum width of the link defines the bottleneck and so the part with the smallest flow capacity of the link. This leads to the following definition of the flow capacity:

$$q = w * 1.33 \frac{1}{m * s} \tag{13}$$

This means, a bottleneck with a width of 1 m has a flow capacity of 1.33/s, which reflects a generally accepted value (see, e.g., [14]).

3 Scenario

The capabilities of the introduced multi-modal simulation framework are demonstrated on the model of a shopping center which is located near the main station in the city of Zurich (see Fig. 6) and can be reached either by walking, cycling, public transport (SBB) or car. People walking or using public transport have to cross a

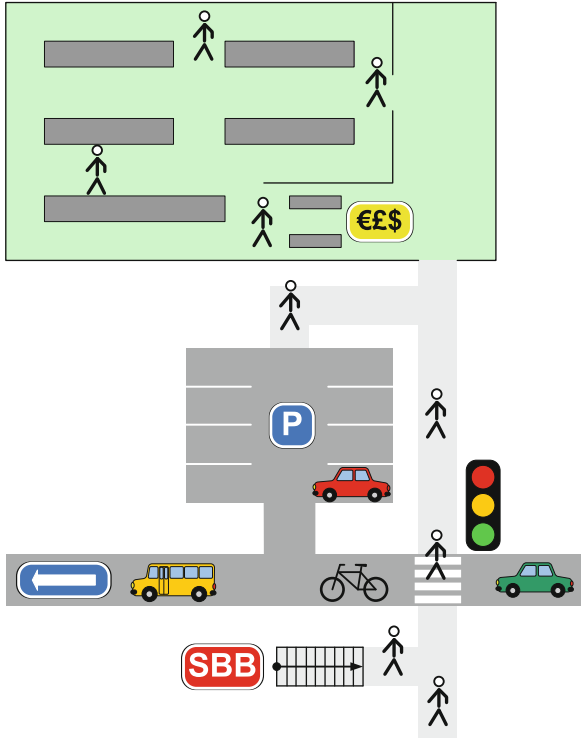


Fig. 6 Shopping center

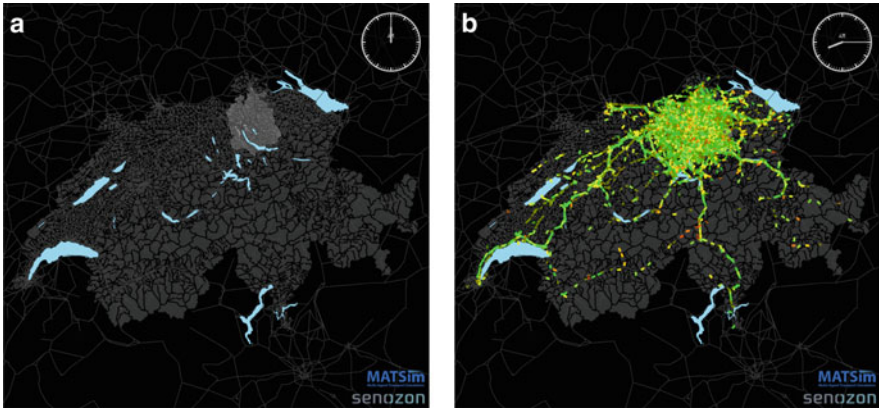


Fig. 7 Switzerland. (a) Switzerland without traffic flows. (b) Switzerland with traffic flows at 08:15 a.m.

road at a signalized crosswalk. The shopping center is embedded into a scenario of the Canton Zurich which contains 450,000 agents—a 25 % sample of the entire population—that are simulated on a planning network with 24,000 nodes and 60,000 links. Figure 7a shows a map of Switzerland containing the road network and the

Fig. 8 Canton Zurich with traffic flows at 08:15 a.m.



Fig. 9 City of Zurich with traffic flows at 08:15 a.m.



study area (colored light grey). The population consists of all people, that touch the study area during one of their activities or trips. Therefore—as shown in Fig. 7b—not only the canton’s residents but also people who cross the canton, are included. Figures 8 and 9 give a more detailed look of the study area. Vehicles are drawn as rectangulars, pedestrians and cyclists as arrows. Pedestrians simulated using the force-based approach are represented by circles. The color of a vehicle/person represents its velocity relative to its maximum allowed speed (red: min, green: max). Finally, the full capability of the multi-modal simulation becomes visible when having a look at the shopping center (see Figs. 10 and 11). Marker A shows the traffic lights at the intersection. A pedestrian (B) crosses the street while a vehicle (C) has to wait until its light signal becomes green. Marker D points to an agent which has just parked its car and is now walking to the shopping center. A vehicle leaving its parking lot is shown by marker E. Two agents inside the shopping center are shown by marker F. One walking along the floor (walking at normal speed, therefore colored green), another one picking up an article from a shelf (stopped, therefore colored red). The switch between the simulation modes is performed when agents reach the points marked with G (for walking agents) respectively when they leave/enter their car on the shopping center’s parking area.

Fig. 10 Shopping center with traffic flows at 08:15 a.m.

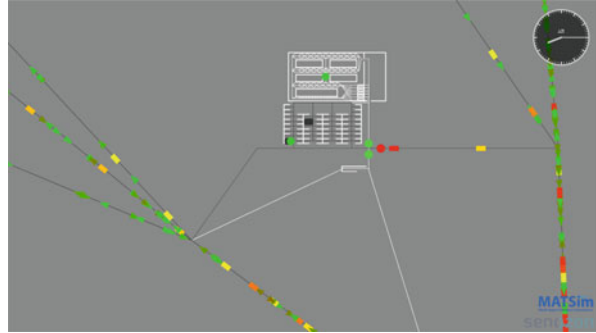
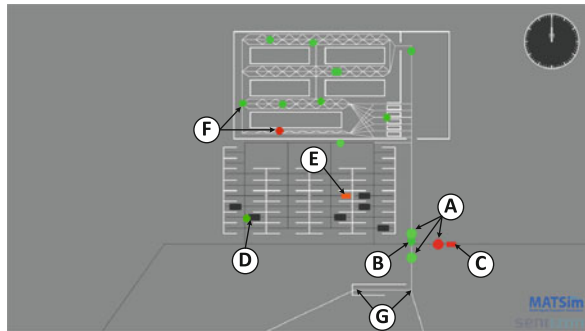


Fig. 11 Shopping center with traffic flows at 12:00 p.m.



4 Conclusions

We explained why there is a growing interest in microscopic large-scale multi-modal simulations. Existing models are limited by available computation power and therefore are either large-scaled or microscopic. Since the required level of detail varies in large scenarios, we propose an approach where the level of detail is also flexible. This allows combining a framework for large-scale simulation with a microscopic force-based 2D simulation.

Depending on an agent's position and its transport mode, it is simulated either with a faster or more details simulation approach. However, so far interactions between agents simulated with different approaches are not included in the framework. As a result, agents walking from their parking lot to the shopping center do not force cars to slow down. Therefore, the next step of development will be adding the capability to take such interaction into account to the framework.

So far, the user has to statically define the level of detail for each part of the scenario. This process will be automatized in a two step approach. First, the possibility to dynamically switch a region's level of detail during the simulated time period will be added. As a result, the shopping center from this paper's scenario could be simulated using the force-based approach only during opening hours. In a second step, the simulation will take control over the dynamic level of detail

adaption using real time data like crowdedness. As a result, the simulation will switch a link's simulation mode to the force-based model when it is too crowded and vice versa.

Acknowledgements This project was funded in part by the German Ministry for Education and Research (BMBF) under grant 13N11382 ("GRIPS") and by the German Research Foundation (DFG) under grants Na 682/5-1.

Moreover, we would like to thank Professor Kay W. Axhausen and Professor Kai Nagel, as well as our colleagues at the institutes, who supported our work on this paper. Finally, we want to thank Marcel Rieser (senozon AG), who adapted their visualization tool *via*, which allowed us visualizing pedestrian traffic flows.

References

1. Balmer, M.: Travel Demand Modeling for Multi-Agent Traffic Simulations: Algorithms and Systems. Ph.D. thesis, ETH Zurich, Zurich (May 2007)
2. Charypar, D., Nagel, K.: Generating complete all-day activity plans with genetic algorithms. *Transportation* 32(4), 369–397 (2005)
3. Cheney, W., Kincaid, D.R.: *Numerical Mathematics and Computing*. Brooks/Cole, 7. edn. (2012)
4. Forschungsgesellschaft für Straßen- und Verkehrswesen: *Handbuch für die Bemessung von Strassenverkehrsanlagen*: HBS. Forschungsgesellschaft für Straßen- und Verkehrswesen, Cologne (2009)
5. Gloor, C.D.: *Distributed Intelligence in Real World Mobility Simulations*. Ph.D. thesis, ETH Zurich, Zurich (2005)
6. Gloor, C.D., Mauron, L., Nagel, K.: A pedestrian simulation for hiking in the alps. In: STRC (ed.) 3rd Swiss Transport Research Conference. Ascona (March 2003)
7. Helbing, D., Farkas, I., Vicsek, T.: Simulating dynamical features of escape panic. *Nature* 407, 487–490 (2000)
8. Helbing, D., Molnár, P.: Social force model for pedestrian dynamics. *Physical Review E* 51(5), 4282–4286 (1995)
9. Lämmel, G.: *Escaping the Tsunami: Evacuation Strategies for Large Urban Areas. Concepts and Implementation of a Multi-Agent Based Approach*. Ph.D. thesis, Technical University Berlin, Berlin (2011)
10. Lämmel, G., Plaue, M.: Getting out of the way: collision avoiding pedestrian models compared to the real world. In: *Pedestrian and Evacuation Dynamics 2012*. Springer (2012)
11. Meister, K., Balmer, M., Ciari, F., Horni, A., Rieser, M., Waraich, R.A., Axhausen, K.W.: Large-scale agent-based travel demand optimization applied to Switzerland, including mode choice. In: WCTRS (ed.) 12th World Conference on Transportation Research. World Conference on Transport Research Society (WCTRS), Lisbon (July 2010)
12. Oleson, R., Kaup, D.J., Clark, T.L., Malone, L.C., Boloni, L.: Social potential models for traffic and transportation. In: Bazzan, A.L.C., Klügl, F. (eds.) *Multi-Agent Systems for Traffic and Transportation Engineering*, chap. VII, pp. 155–175. Information Science Reference, Hershey (2009)
13. Parkin, J., Rotheram, J.: Design speeds and acceleration characteristics of bicycle traffic for use in planning, design and appraisal. *Transport Policy* 17(5), 335–341 (2010)
14. Predtechenskii, V.M., Milinskii, R.A.I.: *Planning for Foot Traffic in Buildings*. Amerind, New Dehli (1978)

15. Preparata, F.P.: The medial axis of a simple polygon. In: Gruska, J. (ed.) *Mathematical Foundations of Computer Science 1977*, Lecture Notes in Computer Science, vol. 53, pp. 443–450. Springer, Berlin (1977)
16. Rieser, M.: *Adding Transit to an Agent-Based Transportation Simulation*. Ph.D. thesis, Technical University Berlin, Berlin (2010)
17. Sewall, J., Wilkie, D., Lin, M.C.: Interactive hybrid simulation of large-scale traffic. *ACM Transaction on Graphics (Proceedings of SIGGRAPH Asia)* 30(6) (December 2011)
18. Transportation Research Board: *Highway Capacity Manual*. Transportation Research Board, Washington, D.C. (December 2010)
19. Weidmann, U.: *Transporttechnik der Fussgänger - Transporttechnische Eigenschaften des Fussgängerverkehrs, Literaturoberwertung*. Schriftenreihe 90, IVT, ETH Zurich, Zurich (1992)
20. Zanlungo, F., Ikeda, T., Kanda, T.: Social force model with explicit collision prediction. *EPL (Europhysics Letters)* 93(6) (2011)

Merging Processes of Pedestrian Queues

Daniel Weber, Florian Knorr, and Michael Schreckenberg

Abstract We consider the merging of two pedestrian queues in a simple cellular automaton model. The scenario is restricted to the case of a minimal merging area (2 cells), which corresponds to the intersection of two small corridors in reality. We derive exact results for the flow and present numerical results.

1 Introduction

Cellular automata based models have become valuable tools for the analysis and simulation of pedestrian motion [1, 4].

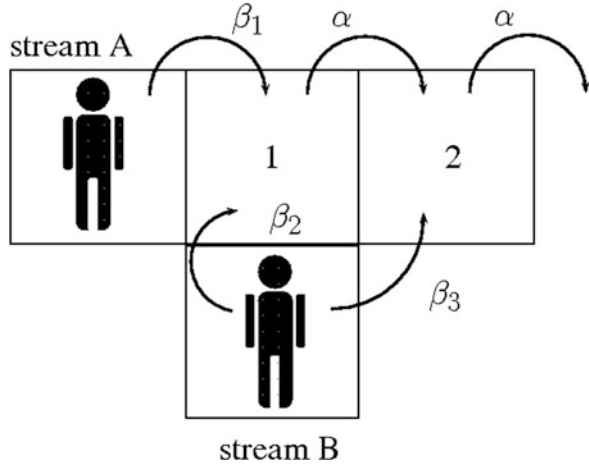
In these models both space and time are discrete: Space is divided in cells which are either empty or occupied by exactly one pedestrian. Based on the model's rules each pedestrian chooses a target cell from the set of neighboring cells. Finally, all pedestrians simultaneously move to the target cell if it is empty.

This approach allows simulating and tracking the motion of every single pedestrian. However, conflicts may occur when two pedestrian try to move to the same target cell. Motion may also dependent on cell geometry and the definition of the neighboring cells. In the case of quadratic cells there are two possible definitions for neighboring cells: In the von Neumann neighborhood all cells that share a common bond with a given cell are regarded as this cell's neighbors. The Moore neighborhood counts all cells as neighbors that share a common vertex with a given cell.

The differences resulting from neighborhood definition [3] and conflicts become especially obvious when two particle or pedestrian streams are combined. Merging processes, in general, are a crucial aspect in the modeling of various transport

D. Weber (✉) • F. Knorr • M. Schreckenberg
Physik von Transport und Verkehr, Universität Duisburg-Essen, D-47057 Duisburg, Germany
e-mail: weber@ptt.uni-due.de; knorr@ptt.uni-due.de; schreckenberg@ptt.uni-due.de

Fig. 1 Two pedestrian streams A and B move to the merging area that consists of two cells labeled 1 and 2, respectively. Particles from stream A, moving horizontally, leave the merging area via cells 1 and 2. Particles from stream B can either choose cells 1 and 2 as well to leave the merging area or skip cell 1 and go directly to cell 2. If $\beta_2 \neq 0 \neq \beta_3$, the setup corresponds to a Moore neighborhood and to a von Neumann neighborhood otherwise



phenomena. Therefore, we will use the terms pedestrian and particle synonymously for the rest of this paper.

To assess the influence of conflicts and selected neighborhood both numerically and analytically we study the merging of two separate pedestrian queues from two narrow corridors into a single-lane stream. While this setup may appear quite artificial, similar situations are encountered in the evacuation through a narrow exit or the evacuation of the tiers in a stadium. One can also think of this setup as two queues waiting for a server to become free or a T-shaped intersection in vehicular urban traffic.

The outflow from the merging area is the most important factor describing the dynamics of the merging process. Via a two-cluster approximation we obtain an estimate of the actual outflow. We compare this estimate to the results from computer simulations.

2 Problem Statement

In analogy to CA models particles move on a lattice with hard core exclusion and a parallel update scheme. The width of each lane is assumed to be one cell and particles have a maximum velocity of one cell per time step. For the sake of simplicity and similar to [5] we neglect any long range interaction, e.g., repulsion from walls, and focus on the merging area.

Figure 1 illustrates the setup for our analysis. Pedestrians from stream A (moving horizontally) enter the merging area at cell 1 with probability β_1 . Pedestrians from stream B can enter the merging area via cells 1 or 2. Within the merging area, particles move to the right with probability α . All particles leave the system through cell 2.

As each cell of the merging area can either be empty or occupied. Let τ_i ($i \in \{1,2\}$) denote the state of the i th cell and set $\tau_i = 0$ (1) if it is empty

(occupied). There are four possible configurations of the merging area that have to be considered. $P_t(\tau_i, \tau_j)$ is the probability to find the cells (1,2) in state τ_i and τ_j at time t . They obey the normalization condition $\sum_{x,y=0}^1 P_t(x,y) = 1$.

To solve conflicts we use an additional friction parameter $\mu \in [0,1]$, which was introduced in [2]. If a conflict occurs none of the two particles moves with probability μ . Otherwise, one of the two particles is randomly but with equal probability selected and allowed to move. By varying the friction parameter the merging process of pedestrians from different streams can be varied from “cooperative” to “competitive”.

The time evolution of probabilities $P_t(\tau_1, \tau_2)$ is then given by

$$\begin{pmatrix} P_{t+1}(0,0) \\ P_{t+1}(0,1) \\ P_{t+1}(1,0) \\ P_{t+1}(1,1) \end{pmatrix} = \begin{pmatrix} p_{11} & p_{12} & 0 & 0 \\ p_{21} & p_{22} & p_{23} & 0 \\ p_{31} & p_{32} & p_{33} & p_{34} \\ p_{41} & p_{42} & p_{43} & p_{44} \end{pmatrix} \begin{pmatrix} P_t(0,0) \\ P_t(0,1) \\ P_t(1,0) \\ P_t(1,1) \end{pmatrix}, \quad (1)$$

where

$$p_{11} = [(1 - \beta_1)(1 - \beta_2 - \beta_3) + \mu\beta_1\beta_2]$$

$$p_{12} = \alpha [(1 - \beta_1)(1 - \beta_2) + \mu\beta_1\beta_2]$$

$$p_{21} = (1 - \beta_1)\beta_3$$

$$p_{22} = (1 - \alpha) [(1 - \beta_1)(1 - \beta_2) + \mu\beta_1\beta_2]$$

$$p_{23} = \left[\alpha(1 - \beta_3) + \frac{1}{2}(1 - \mu)\alpha\beta_3 \right]$$

$$p_{31} = \beta_1(1 - \beta_2 - \beta_3) + \beta_2(1 - \beta_1) + (1 - \mu)\beta_1\beta_2$$

$$p_{32} = \alpha [\beta_1(1 - \beta_2) + \beta_2(1 - \beta_1) + (1 - \mu)\beta_1\beta_2]$$

$$p_{33} = [(1 - \alpha)(1 - \beta_3) + \mu\alpha\beta_3]$$

$$p_{34} = \alpha$$

$$p_{41} = \beta_1\beta_3$$

$$p_{42} = (1 - \alpha) [\beta_1(1 - \beta_2) + \beta_2(1 - \beta_1) + (1 - \mu)\beta_1\beta_2]$$

$$p_{43} = \left[(1 - \alpha)\beta_3 + \frac{1}{2}(1 - \mu)\alpha\beta_3 \right]$$

$$p_{44} = 1 - \alpha$$

In the case of parallel dynamics as it is considered here the matrix elements p_{ij} actually are transition probabilities such that the entries in each column must sum up to 1. In the steady state limit, where $P_{t+1}(\tau_i, \tau_j) = P_t(\tau_i, \tau_j) \equiv P(\tau_i, \tau_j)$, these equations can be solved analytically. As we are interested in the outflow of the merging area, we have to determine the occupation probability $p_{occ}(t)$ of cell 2 which is given by $p_{occ}(t) = P_t(0,1) + P_t(1,1)$. The average outflow $\langle J_{out} \rangle$ is then given by $\langle J_{out} \rangle = \alpha p_{occ}$.

Additionally, by solving the linear system one can also determine the inflow from stream A $\langle J_{in,A} \rangle$ and stream B $\langle J_{in,B} \rangle$, respectively:

$$\langle J_{in,A} \rangle = (P(0,0) + P(0,1)) \left[\beta_1(1 - \beta_2) + \frac{1}{2} \beta_1 \beta_2 (1 - \mu) \right] \quad (2)$$

$$\begin{aligned} \langle J_{in,B} \rangle = & (P(0,0) + P(0,1)) \left[\beta_2(1 - \beta_1) + \frac{1}{2} \beta_1 \beta_2 (1 - \mu) \right] \\ & + P(1,0) \left[(1 - \alpha) \beta_3 + \frac{1}{2} \alpha \beta_3 (1 - \mu) \right] + P(0,0) \beta_3 \end{aligned} \quad (3)$$

This enables us to determine the contribution of each stream to the total outflow $\langle J_{out} \rangle$.

3 Numerical Results

Figure 2 shows the outflow from the intersection as a function of β_1 (i.e., the inflow from stream A) and μ (i.e., the probability with which none of the particles moves in case of a conflict), where $\beta_2 = \beta_3 = 1/2$ and $\alpha = 1$. It is no surprise that the maximal outflow is obtained for $\mu = 0$ and $\beta_1 = 1$. In this case, there is always one particle allowed to move, if a conflict occurs, and the inflow from stream A is maximal.

The maximum value is also easy to understand: due to $\alpha = 1$, a particle will always move to an empty cell ahead. Hence, when cell 2 is occupied a particle will leave the system and when it is empty another particle will move to this position. (Remember that for $\beta_1 = 1$, there is always a particle to fill the gap.)

In Fig. 3 the influence of the friction parameter and of mutually blocking streams becomes obvious. It depicts the outflow as function of the inflow probabilities β_1, β_2 and β_3 , where we assumed $\beta_2 = 1 - \beta_3$, $\mu = 1/2$ and $\alpha = 1$. The outflow reaches its maximum value for $\beta_1 = 1$ and $\beta_2 = 0$ or 1. This corresponds to the situation where particles enter the intersection only via cell 1 or 2 (i.e., no conflicts occur.) The minimum outflow results from situations where the number of conflicts is maximal. This is the case when the inflow from streams A and B becomes maximal (i.e., $\beta_1 = 1$ and $\beta_2 = 0$ or 1).

Fig. 2 Dependence of the outflow from β_1 and μ , where $\beta_2 = \beta_3 = 1/2$

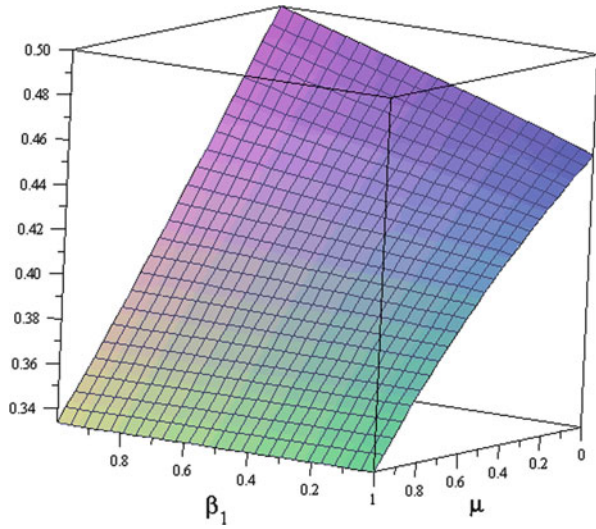
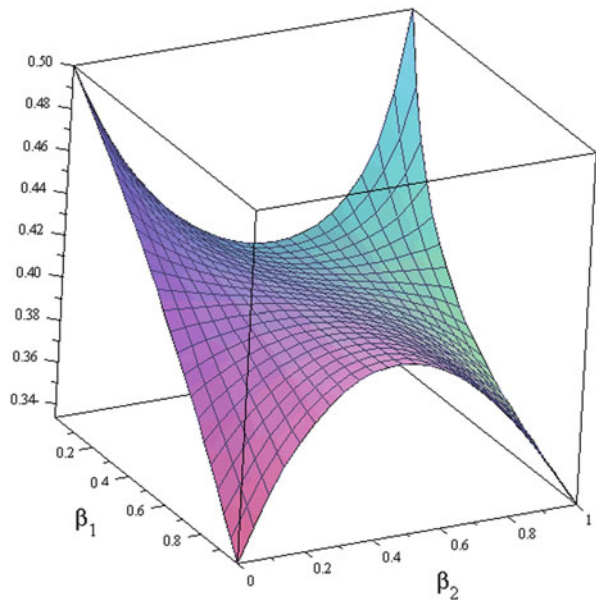


Fig. 3 Outflow $\langle J_{out} \rangle$, as a function of the inflow probabilities $\beta_1, \beta_2, \beta_3$, where $\beta_2 = 1 - \beta_3$



4 Conclusion

We have presented an analytic solution for the steady state for merging process in a simple pedestrian-CA scenario. Thereby, the influence of the CA-parameters can directly be assessed. Especially the influence of the so called friction parameter is of interest as it determines how conflicts (i.e., pedestrians trying to move to the same

target cell) are treated. The treatment of conflicts, in turn, governs the outflow of the intersection and thereby the speed of a possible evacuation. In a next step these outflow rates can be compared to empirical data.

Acknowledgement Our work has been conducted within the SPIDER-project, which is part of the nationwide security research program funded by the German Federal Ministry of Education and Research (BMBF) (FKZ 13 N10236).

References

1. Burstedde, C., Klauck, K., Schadschneider, A., & Zittartz, J. (2001). Simulation of pedestrian dynamics using a two-dimensional cellular automaton. *Physica A: Statistical Mechanics and its Applications*, 295, pp. 507–525.
2. Kirchner, A., Nishinari, K., & Schadschneider, A. (2003). Friction effects and clogging in a cellular automaton model for pedestrian dynamics. *Phys. Rev. E*, 67, p. 056122.
3. Kretz, T., & Schreckenberg, M. (2007). Moore and more and symmetry. In N. Waldau, P. Gattermann, H. Knoflacher, & M. Schreckenberg (Eds.), *Pedestrian and Evacuation Dynamics 2005* (pp. 297–308). Berlin, Heidelberg.
4. Kretz, T., & Schreckenberg, M. (2006). The F.A.S.T.-Model. In S. El Yacoubi, B. Chopard, & S. Bandini (Eds.), *Cellular Automata (Lecture Notes in Computer Science, Vol. 4173)* (pp. 712–715). Berlin, Heidelberg.
5. Yanigasawa, D., & Nishinari, K. (2007). Mean-field theory for pedestrian outflow through an exit. *Phys. Rev. E*, 76, p. 061117.

Methodology for Pedestrian Analysis in Public Spaces Based on Probabilistic Approach

Ignacio Martínez and Ana Olmeda

Abstract In the field of pedestrian simulation, there is a lack of detail in terms of the random movements of pedestrians within a public space. This is due to the use of models based on deterministic approaches, like O/D-based fixed percentage of routes which, in most cases, hardly reproduce those random patterns. The presented methodology tries to cover the need of representing the complexity of movements of such spaces, without forgetting the efficiency and effectiveness of the implementation in the model of such large amount of information. This paper describes an intuitive and innovative idea that substantially improves the modeling of random pedestrian patterns, the validation of the results and the analysis of commercial areas and future scenarios.

Keywords Passengers • Commuters • Station design • Pedestrian 2D simulation • Modeling pedestrian behavior • Random pedestrian pattern simulation

1 Introduction

Usually, during the functional design or evaluation of a public space, it is essential to have a tool that guarantees the suitable operation of the designed spaces. Modern railway stations, for instance, are increasingly becoming sophisticated spaces that combine the commercial plurality of a shopping center with the complex boarding processes of an airport.

In this kind of spaces -airports, stations, intermodal transportation hubs etc.- people find a high variety of random waypoints or intermediate activities in their journey (such as restaurants, shops, baths, cash dispensers, stands or screens, among

I. Martínez (✉) • A. Olmeda
INECO, Madrid, Spain
e-mail: ignacio.martinez@ineco.es; ana.olmeda@ineco.es

others). Those waypoints usually reach the hundred, or even more. In such cases, the number of possible routes for pedestrians along their journey towards their final destination grows exponentially. This leads to a huge combination of feasible pathways.

Modeling pedestrian methodologies are usually based on a O/D matrix with fixed percentage routes allocating people in them, so as to move around the modeled space, through one or several intermediate activities before reaching their final destination. Those conventional and simple methods are, therefore, no longer enough to represent the complexity of such spaces. They are just unable to reproduce the complexity of real-time decisions in pedestrians.

Therefore, it is important to develop and implement a comprehensive and robust methodology, able to reproduce and assess those complex pedestrian movements inside this type of spaces. Besides this and for it to be practical, the methodology has to be simple enough so it will not to be too cumbersome or calculation-intensive for a common PC.

Being said this, it is necessary to leave behind conventional deterministic solutions based on explicit approaches to the real situation – assume known routes before the simulation-, and to find a “real-modeltime” dynamic method, simple and precise enough to become a practical tool in the decision-making process.

On the basis of these principles, it has been developed a methodology which reproduces the behavior of people in public spaces. From a deep knowledge of current situation, people behavior has been analyzed and processed in each case, effectively identifying behavior-patterns that are used as the basis for validation of these pedestrian models, and for the design of future scenarios as well. This method has already been successfully applied in the two major railway stations in Madrid, Chamartín and Atocha Stations.

2 Data Acquisition

The key component of this methodology involves important field surveys campaign: O/D matrix, counts and commuter tracking, used to identify all the steps/waypoints of users inside these venues. Those surveys have achieved more than 5,000 commuters tracking in Chamartín Station and more than 11,000 tracking to commuters in Atocha Station. Those tracking imply following people from the moment they enter the studied space to the moment they left it, covering all operating hours and intermediate stops/waypoints. Final reports were expanded to the total daily demand so every user in the station had a register record with exhaustive information data about their waypoint “chain”. The tracking included all the necessary information to precisely characterize and segment every user, which is an important reason to use them over other automated processes (Wi-Fi, RFID or Bluetooth based).

Passenger daily demand of Chamartín Station in 2010 was over 39,000 people, and Atocha Station exceeded 215,000 boarding passengers a day. Having in mind those figures, it is clear that a specific methodology is required in order to effectively

solve the problem of analyzing their behavior, and its subsequent application in a pedestrian model.

As stated before, since the basic premise of this methodology is to precisely reproduce the behavior of people in public spaces, avoiding conventional solutions such as the ones based on O/D-based fixed percentages of routes, field surveys campaign represents the key step on which the later pedestrian modeling relies.

The adjustment of the simulation model requires a precise knowledge of the entering and outgoing movements of pedestrians in the different entrances/exits in the model, as well as their location and evolution over time. This data acquisition provides a complete parameterization of the pedestrian flows carried out in the studied public space, and it will be the starting point for the development and calibration of the model.

2.1 Field Surveys Tasks

This preliminary field surveys campaign consists of two sequential activities:

Counts of users entering and leaving the analyzed public space. Count stage allows quantifying the number of users in the public space, as well as being the reference for the expansion of subsequent data from the tracking campaign along the analyzed period.

Count points are located so that pedestrian flows can be recorded for every relevant entrance/exit of the public space. In case the architecture of the public space is complex enough, or if it is a multiple level venue, further observation points inside the public space are advisable to determine internal transit flows, apart from the physical activity waypoints which are analyzed in the next topic, in order to complement in/out movements for every different area/stage.

According to the needs of the study, it is interesting – if not essential- to consider full day surveys so counts and subsequent tracking provide useful information about the different patterns of behavior occurring in peak and off-peak hours.

Visual tracking to a representative sample of the users inside the public space.

The second stage consists on visual tracking to a sample of users within the space, in order to check the use of the existing services and the activities carried out in them. Those visual tracking require following people from the moment they enter the studied space to the moment they leave, and they include all the necessary information to precisely characterize every user such as:

- Time the user enter the scenario.
- No. of entrance.
- Movement 1.
- Time the user is arriving movement No. 1.
- Time the user is leaving movement No. 1.
- Movement “i”.
- Time the user is arriving movement No. “i”.

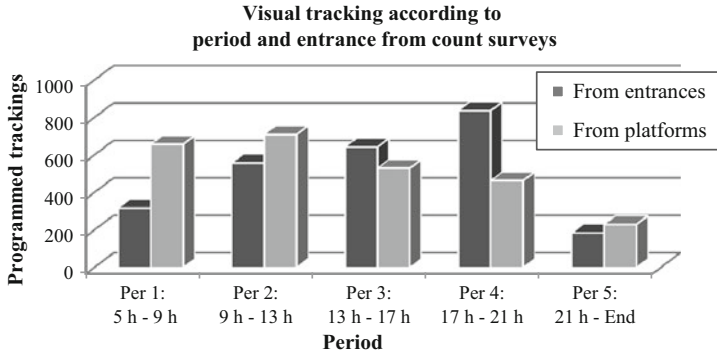


Fig. 1 Example of visual tracking with its specific control ratio in Chamartín Station-Madrid

- Time the user is leaving movement No. “i”.
- Final destination.
- Time the user reaches the final destination.
- No. of exit.
- Age range.
- Sex of the user.

In case the analyzed scenario is a specific public space such as train stations, airports, intermodal transportation hubs, stadiums etc., particular information will be required, among others:

- Train/bus/aircraft schedule.
- Track number/bus parking bay/boarding gate/stadium gate etc.
- Luggage (shoulder bag, bag, small suitcase, large suitcase etc.)
- Type of user (boarding travelers, passing users, transit users etc.)

Results from this stage will allow deep insight knowledge of entry/exit flows and their evolution over time and through the station, the time they spent in each place and its link to the activities carried out during their visits to the physical waypoints that are monitored.

People subject to observation are chosen under a random selection from the entrances with a distribution according to data from the first stage. This control ratio is based on the hourly period and locations of entrance to the space from the counts campaign.

Size of visual tracking campaign is programmed so that the sample is representative enough to be expanded according to the figures obtained from count surveys. For a 39,000 passenger/day station – for instance – more than 5,000 visual commuters tracking are required for an adequate knowledge of pedestrian behavior (Fig. 1).

Visual tracking should include all kind of waypoints, not only the visit to the different activities inside the public space (shops, bathrooms, check-in, information

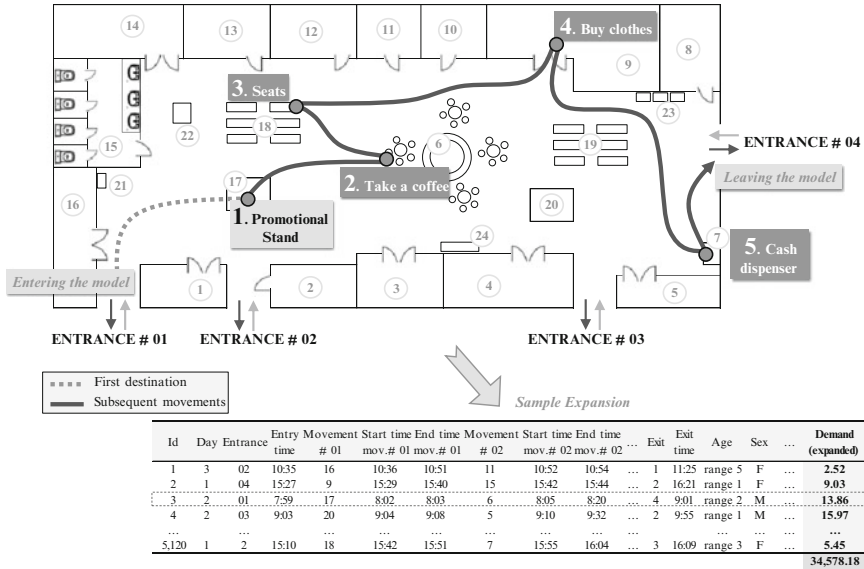


Fig. 2 Example of a navigation route and subsequent expanded data

bureau, etc.) but also activities such as “going out to smoke”, “strolling around the lobby”, “waiting for a traveler”, “looking at the information screen” and every kind of activities carried out within the studied space.

As the final step in this phase, final reports are expanded to the total demand so every user in the public space has a register with exhaustive information data about their waypoint “chain” (Fig. 2).

3 Modeling Pedestrian Behavior

3.1 Solution Approach

Since all the previous information is usually related to very large databases, a next level of data abstraction is needed for its use in the pedestrian behavior model.

This methodology aims to bring together a balanced solution between complexity (accuracy) and efficiency on the basis of a statistical analysis of the raw data surveyed. These statistical methods are to reflect – through probabilistic analysis – user decisions in their navigation among waypoints. So then, the proposed approach to develop the behavioral model is to abstract those pedestrian patterns in “next-step” probability tables. Those tables should be created for each waypoint type and pedestrian segmentation in order to have an adequate level of accuracy.

Navigation Routes Within the Model Using raw data from the tracking database, the probabilistic analysis is divided according to the following criteria:

- **First movement statistics.** A set of probabilistic tables are estimated separately considering the first movement of pedestrians immediately after they enter the public space. Therefore, for every entrance, tables reflect the probability of users heading directly towards their destination (according to the O/D matrix) or going to the first waypoint in their waypoint “chain”.
- **Statistics of navigation between waypoints.** For every internal waypoint inside the public space, probabilistic tables for next movement are obtained. Those tables statistically reflect the probability of visiting every particular waypoint type, once the user has visited a specific previous one. It is convenient to segment this analysis into navigation tables for different “groups” of users. For example, when analyzing a transportation hub, it is essential to establish different navigation tables for boarding and alighting travelers, as their behavior within these kinds of premises use to be significantly different from one case to another. Further classifications may be interesting in order to facilitate the fine-tuning of the model according to particular needs of each one, such as segregated probabilistic tables for high-speed travelers and commuters in train stations, different age ranges in a mall or for different hourly periods, for instance. The essential data for this segmentation is obtained from the visual tracking, as every register contains all the information which makes it possible to filter by required needs. This is one of the reasons why an automated tracking system has not been used as an alternative to the visual following.

The more segmented tables the modeler obtains, the more accurate the simulation model will be, but usually one or two divisions will be enough to obtain a precise simulation without it becoming too costly (Table 1).

Average Time Spent in Waypoints Activities Another important factor determining the proper functioning of the simulation model is the time that users stay in every visited waypoint in their navigation “chain”.

Not only the duration of the activities in waypoints will establish the occupancy of the public space in every specific moment, -and therefore will be related to evaluation parameters such as level of service, density etc.-, but it will be an important parameter when developing and calibrating the model.

The average time spent in every waypoint is easily obtained from the visual tracking database, adjusting it with the weight coefficient of users visiting it (expanded demand), in order to eliminate the non-significant extremes in the duration range. In order to achieve this, every register in the tracking database should include start-time and end-time for its user’s activity in every waypoint (despite it corresponding to a first or an intermediate movement in their navigation “chain”), the basic equation for obtaining the average length of stay in each waypoints is:

$$\text{Average time spent in waypoint}_i = \frac{\sum_{n=j}^{n=k} T_n \times W_n}{\sum_{n=j}^{n=k} W_n} \quad (1)$$

Table 1 Example of probabilistic tables for a group of users in an hypothetical space

		First movement					
		To destination	1 <i>(Books)</i>	2 <i>(Restaurant)</i>	3 <i>(Shoes)</i>	... <i>(Tickets)</i>	Σ
Entrance	#01	35 %		11 %	24 %	... 0 %	100 %
	#02	17 %	0 %		12 %	... 1 %	100 %
	#03	23 %	5 %	0 %		... 22 %	100 %
	#04	18 %	0 %	0 %	10 %	... 4 %	100 %
From way- point	To subsequent waypoint						
	1 <i>(Books)</i>	20 %		15 %	2 %	... 3 %	100 %
	2 <i>(Restaurant)</i>	13 %	2 %		0 %	... 9 %	100 %
	3 <i>(Shoes)</i>	1 %	10 %	23 %		... 7 %	100 %
	4 <i>(Cinema)</i>	65 %	0 %	35 %	0 %	... 0 %	100 %
	... 23 <i>(Tickets)</i>	... 100 %	... 0 %	... 0 %	... 0 % 100 %

where T_n and W_n are respectively the duration of the stay of every user “n”, and the weight of the users (expanded demand) in every register, according to the field survey campaign.

In case the simulation runs over a timeline wide enough to influence in the behavior-patterns, it may be convenient to refine the average length for every particular period, instead of using the average time corresponding to the whole timeline. This may be especially significant when modeling peak and off-peak periods in the same running. As in the treatment of navigation tables, the decision of filtering and segmenting the average length of stay according to every hourly period is up to the modeler.

Integration of the Probabilistic Behavior into the Model Modern pedestrian simulation software has considerably evolved in the past few years, developing technologies that automate and ease the model-building process. The combination between the use of one of these advanced software and the treatment of the behavior-patterns as statistic tables, results in a routing methodology that allows redirecting people inside the public space through their probabilistic routes without knowing them in advance (Fig. 3).

As a result, entities enter the model through their designated access points, according to the O/D matrix from the field surveys. After entering, the behavior model determines the next step dividing between heading directly their destination, to prevent “non-wandering” pedestrian to enter the iterative process, or selecting the next waypoint amongst the range of possibilities available. This range of possibilities is different for every entrance (and every sub-filter of entity groups the statistic tables are filtered for) (Fig. 4).

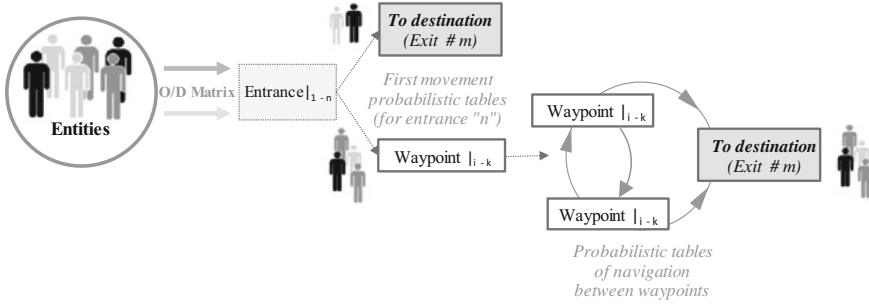


Fig. 3 Redirecting methodology of entities by probabilistic patterns

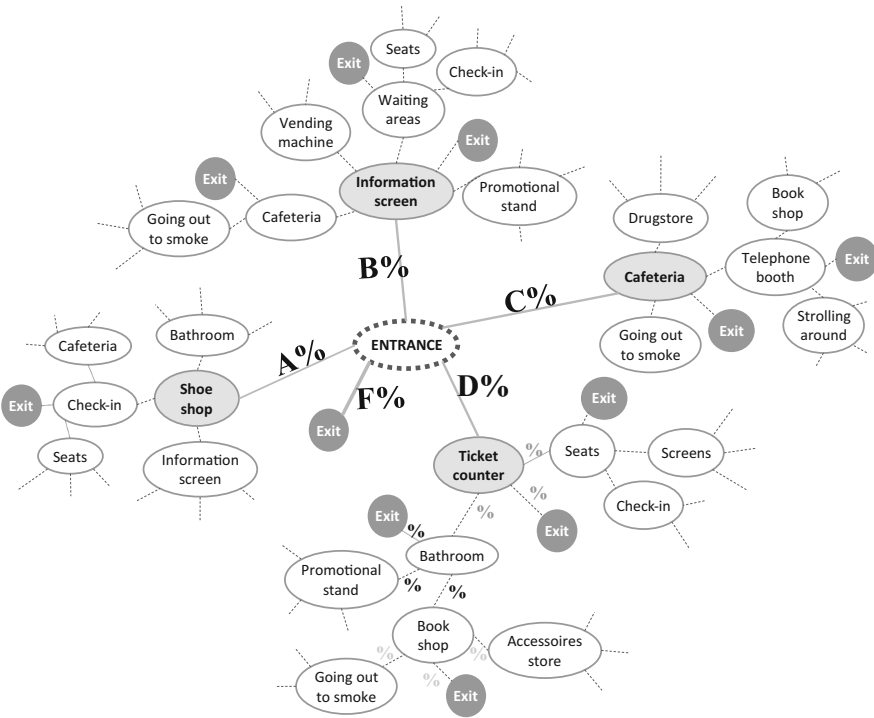


Fig. 4 Dynamic and probabilistic tree of route choice according to the previous waypoint

After this stage, once entities reach a particular waypoint, they are routed through subsequent waypoints according to navigation tables, taking into account that every waypoint is related to the others by specific probabilities. Those probabilities are also different from the ones affecting the first movement of the chain.

This way, complex and random routing is simulated inside the model as the simulation develops without needing to include all the explicit routes which is

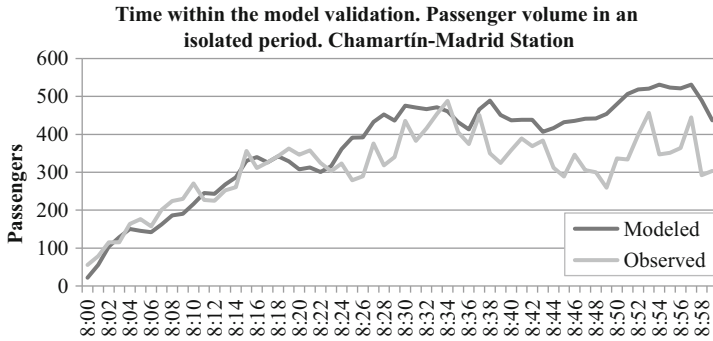


Fig. 5 Validation of user time within the model in Chamartín Station (Madrid) (Source: [31])

both inaccurate -for there are a big percentage of pedestrian not surveyed- and cumbersome.

3.2 Calibration and Validation

Before using the developed pedestrian model it is crucial to calibrate and validate it. These two tasks are use for verification purposes, to establish that its parameters are such that the simulation model comes as close as possible to reproducing the observed patterns.

Regarding transportation models, calibration and validation are usually very different processes, but in this particular case both activities go hand in hand, as many of the data to build the model has been directly obtained from surveys in an exact way. An example of this is entrance distribution in the public space, for which calibration makes no sense as far as output and input data are unfailingly the same.

These tasks try to make sure the pedestrian model is suitable for the subsequent decision-making process, checking whether it can represent a known state of the public space with sufficient accuracy.

Since the present methodology focuses on the number of “visits” amongst different waypoints and the duration that users remain in them, one of the most useful ways to test the validation of the model is to cross-check user volume within the public space in every moment along the simulation period.

In order to obtain a reliable validation, several processes are used as a complementary cross-checking mechanism to test the effectiveness of the model.

The validation of the time users stay within the public space is made on the basis of a synthetic simulation ran over an isolated hour. It is thus intended to analyze it without introducing “noise” from the users of adjacent periods. It is important to check not only the precision of the time spent within the model, but also the accuracy of fluctuations throughout the timeline (Fig. 5).

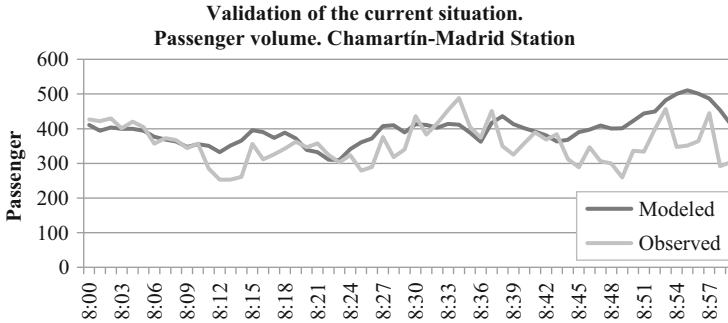


Fig. 6 Validation of passenger volume in Chamartín Station (Madrid) (Source: INECO 2010)

In a complementary manner, the real simulation with warm-up period, establishes the validation of passenger volumes within the public space which, together with the accuracy of fluctuations, ensures that the model is a sufficiently good representation of reality (Fig. 6).

Additionally, it is also desirable to conduct further calibration techniques in order to test the model from a statistic point of view, as for example through the GEH¹ Statistic.

4 Future Scenario Creation

Pedestrian simulation models built by this probabilistic routing methodology have the advantage of being relatively easy to implement – apart from the complexity of the survey field-, but being highly applicable in the decision-making process or evaluation of projected spaces.

Under these circumstances, this methodology provides a powerful tool when evaluating, for instance, scenarios with future architectonic modifications, enlargements, or changes in commercial uses compared to the current situation. In these cases, modeling pedestrian methodologies so far used, lack the necessary resources to foresee pedestrian random/commercial behaviors in these planned spaces.

This developed methodology focuses on forecasting pedestrian behavior patterns. Since the visual tracking campaign provides precise information about connections between waypoints; it is easy to group them according to their different commercial uses, in order to obtain valuable information regarding the patterns governing pedestrian behavior.

¹GEH Statistic is a formula that gets its name from Geoffrey E. Havers, used to contrast two sets of transportation volumes.

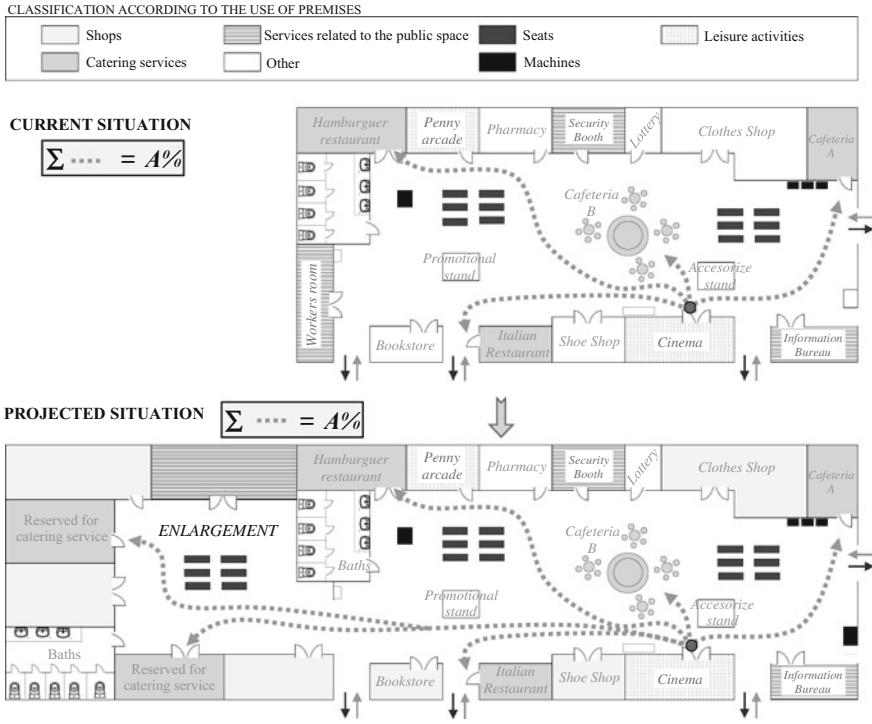


Fig. 7 Future scenario creation in a hypothetical space

Though the detailed trade premises are unknown for the future assessed venue, it is possible to evaluate the projected situation under the hypothesis of the global commercial uses in a reliable way, as they are deeply known in the current situation and global pedestrian behavior is usually maintained over the time in short terms situations.

For example in a big shopping center the percentage of people going to dinner after a night at movies is known. In a future enlargement of the mall, -no matter the new distribution of commercial uses or the number of new restaurants-, it is not likely that those physical changes in the mall affect to users behavior, and it is expected that the percentage of people visiting catering service keeps invariable (Fig. 7).

5 Conclusions

As a whole, the development of this specific methodology allowed to solve the problem of the analysis of important data in the tracking campaign database from the field survey and its direct application in the development, calibration and

validation of a pedestrian model reflecting their random behavior, a key element in the decision-making process.

The probabilistic behavior pattern methodology, based on deep knowledge of the current situation, helps to greatly enhance the realism and reliability of a pedestrian simulation model, reproducing the complexity of real-time routing for pedestrians inside a public space. Apart from this and after taking into consideration the large quantity of data from the tracking campaign used to characterize user behavior patterns, an indirect benefit that results from this methodology is the simplification in the database treatment. This also allows an agile implementation in the pedestrian simulation model, ensuring data modification once the model is built.

Finally, since the navigation between waypoints obtained from the visual tracking campaign, another important benefit of this approach is that it is highly modular, allowing it to apply known surveyed patterns over projected designs through the characterization of the different global commercial uses.

References

1. Fruin, John J., Ph.D (1987). *Pedestrian. Planning and design*. Elevator World, Inc.
2. Fruin, John J., Ph.D (1970). *Designing for Pedestrians: A Level of Service Concept*. American Society of Mechanical Engineers, American Society of Mechanical Engineers. Standing Committee on Transportation
3. Drew, Donald R. (1968). *Traffic flow theory and control*. McGraw Hill Book Company
4. Hill, Michael R. (1984). *Walking, crossing streets, and choosing pedestrian routes: a survey of recent insights from the social/behavioral sciences*. University of Nebraska
5. Cohen, J. (1988). *Statistical power analysis for the behavioral sciences*. 2nd ed. Lawrence Erlbaum Associates.
6. Zacharias J., Bernhardt T., Montigny L. (2005). *Computer-simulated pedestrian behaviour in shopping environment*. Journal of urban planning and development. ASCE
7. Uhlig K.R. (1979). *Pedestrian areas: from malls to complete networks*. Architectural Book Publishing Co.
8. Timmermans H.J.P. (2009). *Pedestrian behaviour: Models, data collection and applications*. Emerald Group Publishing.
9. Emmerich, H., Nestler, B., Schreckenberg, M. (2003). *Interface and Transport Dynamics: Computational Modelling*. Springer. Series: Lecture Notes in Computational Science and Engineering, Vol. 32
10. Hoogendoorn. S.P and Bovy, P.H.L (2004). *Pedestrian route choice and activity scheduling theory and models*. Transp. Res., Part B.
11. Schadschneider, A., Klüpfel, H., Kretz, T., Rogsch, C. and Seyfried, A. (2009). *Fundamentals of Pedestrian and Evacuation Dynamics*. Bazzan and Klugl (Eds), A.Multi-Agent Systems for Traffic and Transportation Engineering
12. Liddle, J., Seyfried, A., Klingsch, W., Rupperecht, T., Schadschneider, A. and Winkens, A. (2009). *An Experimental Study of Pedestrian Congestions: Influence of Bottleneck Width and Length*. Conference proceedings for Traffic and Granular Flow 2009
13. Zacharias, J (2001). *Path choice and visual stimuli: signs of human activity and architecture*. J. Environmental Psychology
14. Steffen, B., Seyfried, A. (2009). *Methods for measuring pedestrian density, flow, speed and direction with minimal scatter*. Physica A: Statistical Mechanics and its Applications, 2010, Vol. 389

15. Schadschneider A. and Seyfried, A. (2011). *Empirical results for pedestrian dynamics and their implications for modeling*. Networks and Heterogeneous Media, Vol. 6, Pages : 545 - 560
16. Thompson PA, Marchant EW (1993). *Modelling techniques for evacuation*. Smith RA, Dickie JF (eds) Engineering for crowd safety. Elsevier, Amsterdam, pp 259–269
17. Transportation Research Board (1985) Highway Capacity Manual, Special Report 209. Transportation Research Board, Washington DC
18. Garbrecht, D. (1973). *Describing pedestrian and car trips by transition matrices*. Traffic Q 27:89–109
19. Older SJ (1968). *Movement of pedestrians on footways in shopping streets*. Traffic Eng Control 10:160–163
20. Helbing, D. (1992). *A mathematical model for attitude formation by pair interactions*. Behav Sci 37:190–214
21. Radjai F, Roux S (2002). *Turbulentlike fluctuations in quasistatic flow of granular media*. Phys Rev Lett 89:064302
22. Le Bon G (2002). *The Crowd*. Dover, New York (1st edn: 1895)
23. Tubbs J, Meacham B (2007). *Egress design solutions: A guide to evacuation and crowd management planning*. Wiley, New York
24. Smith R.A, Dickie J.F. (1993). *Engineering for crowd safety*. Elsevier, Amsterdam
25. Waldau N, Gattermann P, Knoflacher H (2006). *Pedestrian and evacuation dynamics 2005*. Springer, Berlin
26. Helbing D, Buzna L, Johansson A, Werner T (2005). *Self-organized pedestrian crowd dynamics: Experiments, simulations, and design solutions*. Transp Sci 39(1):1–24
27. Baeck T (1996). *Evolutionary algorithms in theory and practice*. Oxford University Press, New York
28. Johansson A, Helbing D (2007). *Pedestrian flow optimization with a genetic algorithm based on Boolean grids*. In: Waldau N, Gattermann P, Knoflacher H, Schreckenberg M. Pedestrian and evacuation dynamics 2005. Springer, Berlin, pp 267 - 272
29. Canter D (ed) (1990). *Fires and human behaviour*. Fulton. London
30. Helbing D., Johansson A. *Pedestrian, Crowd and Evacuation Dynamics*. ETH Zurich. Institute for Advanced Study, Collegium Budapest, Hungary
31. INECO (2010). Construction design for the extension of the Chamartin complex in Madrid. Spain

Methods for Modeling and Simulation of Multi-destination Pedestrian Crowds

Günter Bärwolff, Minjie Chen, Frank Huth, Gregor Lämmel, Kai Nagel, Matthias Plaue, and Hartmut Schwandt

Abstract In this paper we present an overview of the four parts of a research project concerning pedestrian flow modeling. In retrospect, rapid growth in the volume of public transport in the last 20 years has urged efficient planning and optimal construction of public facilities. At the same time, the modeling of transport and pedestrian behaviors has become an important research topic as well. In the study of pedestrian behaviors, whereas evacuation scenarios (in which pedestrians all target a definite destination) and multi-agent systems (in which pedestrians are treated as heterogeneous individuals) have attracted much attention as two specific problems, comparatively little attention has been paid to pedestrian crowd behaviors in situations of multiple destinations. The objective of the present study is to investigate pedestrian behaviors in such a context. Our primary focus is the modeling of intersecting pedestrian streams. To address the problem from a practical perspective, we applied simple but realistic geometric configurations in our study, which could be independently extended, if necessary.

Keywords Microscopic • Macroscopic and hybrid models • Pedestrian density and flow measurement • Kernel density estimation • Human crowd experiments • Intersecting pedestrian flows • MATSim extension

G. Bärwolff (✉) • M. Chen • F. Huth • M. Plaue • H. Schwandt
Technische Universität Berlin, Institut für Mathematik, Straße des 17. Juni 136, 10623 Berlin, Germany
e-mail: baerwolf@math.tu-berlin.de; minjie.chen@math.tu-berlin.de; huth@math.tu-berlin.de; plaue@math.tu-berlin.de; schwandt@math.tu-berlin.de

G. Lämmel • K. Nagel
Technische Universität Berlin, Institut für Land- und Seeverkehr, Verkehrssystemplanung und Verkehrstelematik, Sekr. SG 12, Salzufer 17–19, 10587 Berlin, Germany
e-mail: laemmel@vsp.tu-berlin.de; nagel@vsp.tu-berlin.de
Project home page: <http://www.math.tu-berlin.de/projekte/smdpc>

1 Simulation Models

In the last years, several methodical approaches have been investigated for the modeling and the simulation of traffic problems. In the present context, we develop both microscopic approaches in which the pedestrian is considered as an individual in interaction with others, and macroscopic models in which the pedestrian behavior is analyzed in terms of more global properties of a continuous stream.

1.1 *Microscopic Models*

In our project two microscopic models are developed. The first one is a grid-based approach relating to traditional cellular automaton (CA) models. The second is a combination of force-based and graph-based approaches.

1.1.1 **Grid-Based Approach**

The common grid-based approaches of the simulation of pedestrian dynamics assume and request that at any position represented by a grid cell there can be either exactly one pedestrian or none present. This implies that the grid cell associated with the aforesaid geometric position can be in a state of being empty (unoccupied) or occupied by a simulation participant (i.e. pedestrian). For this reason, the state change of the grid cell (i.e. position) is employed to describe the system dynamics of the simulation in the traditional CA model and its various extensions (see [1–7] and the references therein). The typical size of the grid cell was defined to be $0.4 \cdot 0.4$ m [1]. An important issue in these models is the update strategy. A proper update strategy is essential in the case of a high density of pedestrians in which multiple pedestrians simulated to enter into a same grid position can often be observed. In a straightforward manner, [2] introduced a (pseudo-) parallel update and the random sequential update for the simulation participants. The random sequential method involved further static and dynamic floor field information induced by the environment and pedestrians [1, 3, 7].

Our approach goes in a different direction. Our previous work [8] proposed a new solution for the step calculation in the general case of velocity larger than one grid cell size in one dimension per simulation cycle. (We therefore are of the opinion that is more suitable to categorize our approach as a graph-based method rather than a CA extension, since unlike in the case of step length 1, the immediate state dynamics, at least in the theoretical sense of cellular automata, become an issue of secondary significance. We are more concerned with the position evolution of the pedestrians in the simulation.) This method disassembles a step of $(\Delta x, \Delta y)$ (with Δx and Δy denoting integers of a suitable magnitude) into a series of substeps which can be one grid cell in either direction or in both (i.e. a diagonal step). See Fig. 1.

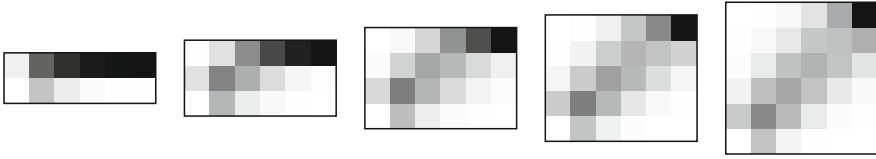


Fig. 1 Visual explanation of substeps with $\Delta x = 5$, $\Delta y = 2, \dots, 6$. The frequency of cell position's occurrence in the substep choices is displayed in a *gray scale*. The start position $(0, 0)$ and the end position $(\Delta x, \Delta y)$ are by definition in *white* and *black* respectively

In this way, small deviations on route within a local step would become possible and strictly speaking, unavoidable. But these local deviations are all under the restriction that the mathematical expectation of the substep choices should be exactly equal to the position transition in geometric sense. This in addition enables the representation of heterogeneous pedestrians.

In addition, we introduce a balancing mechanism in the simulation cycle to decide the execution sequence of the simulation participants. This improvement, along with the substep calculation, results in an enormous reduction of possible “dead-lock”s among the participants which should be addressed in the design of the simulation.

Another issue not to neglect is that, to our knowledge, the fixed grid cell size in the geometric setting poses a serious conceptual limit: the simulation participants (i.e. pedestrians) are all associated with a fixed spacial size, defined by the size of the grid cell in the model. Consequently, the pedestrians in the simulation have a fixed exclusive personal space, which is unfortunately not affirmed by empirical observations.

In our model this exclusive personal space is given additional attention. Naturally, we can reasonably assume the lower limit of this exclusive personal space to be the physical size of a typical real pedestrian (e.g. $0.3 \cdot 0.3$ m) and the upper limit to be three times three of this base size (which implies that a real pedestrian enjoys an exclusive personal space of $0.9 \cdot 0.9$ m in the leisure state). Common sense and empirical observations confirm this. We can modify the personal space thus by defining some of the grid cells in the $3 \cdot 3$ -Moore-neighborhood as unaccessible, we call this “deactivation” (abbr.: \bar{d}). A grid cell definitely not to be deactivated is “activated” (abbr.: \bar{a}). Any state between these two will be written as \bar{s} and is associated with a probability number p for its deactivation.

In the context of multi-destination pedestrian dynamics then, a pedestrian tends to “deactivate” certain positions in his or her moving direction for those pedestrians with a different destination and in a similar way, this pedestrian “deactivate”s some of the positions for the “follower”s in behind, see Fig. 2. p is defined as a linear function of the ratio of the temporary velocity to the upper limits in velocity. We list two simulation experiments in Figs. 3 and 4. For a better visual effect, we will re-compile the results into video animation and publish them on our project home page.

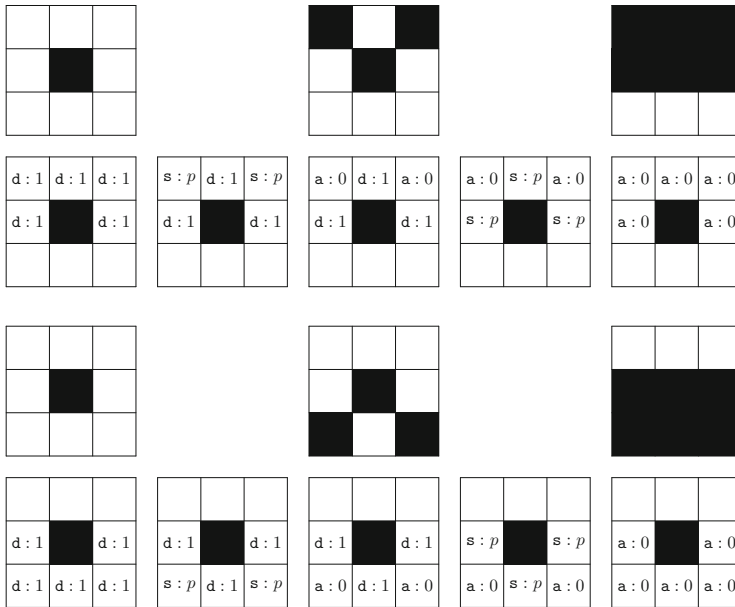


Fig. 2 Deactivation and activation of grid cells in the 3-3-Moore-neighborhood. The first two rows refer to the case for pedestrians with a different destination. The next two rows refer to the case for pedestrians with the same destination but as “followers”. The current pedestrian is assumed to be moving in the positive y -direction

1.1.2 Force-Based Approach

Force-based models employ discretized differential equations [9, 10] (“molecular dynamics (MD)”) to compute the persons’ movement. A well-known model using the MD analogy is the social force model introduced by Helbing and Molnár [11]. In the social force model, each virtual person (agent) has a desired velocity towards a desired destination. While the simulation is running, agents try to adapt their velocity to the desired ones. However, a full adaption is usually not possible since the agents have to avoid other agents and obstacles. This interaction is modeled by repelling social forces emitted by obstacles and agents. These social forces depend only on the distances and not on actual velocities. An illustration of the social force model is given in Fig. 5a. There are four agents in the scene depicted as circles i , j , k , and l . The figure demonstrates the force calculation from agent i ’s perspective. The agent has a desired velocity \mathbf{v}_i^0 . The other agents are emitting repelling forces denoted by $f_{i,j}$, $f_{i,k}$, and $f_{i,l}$ respectively. The resulting force f_i is basically a linear combination of repelling forces and the desired velocity \mathbf{v}_i^0 . (Details are given in [12].) It is shown that even agent i desires to move from left to right, the resulting force f_i exhibits a direction pointing to the left.

As has been shown that the model works particularly well in high density conditions, an example to name would be the evacuation scenarios in [12]. However,

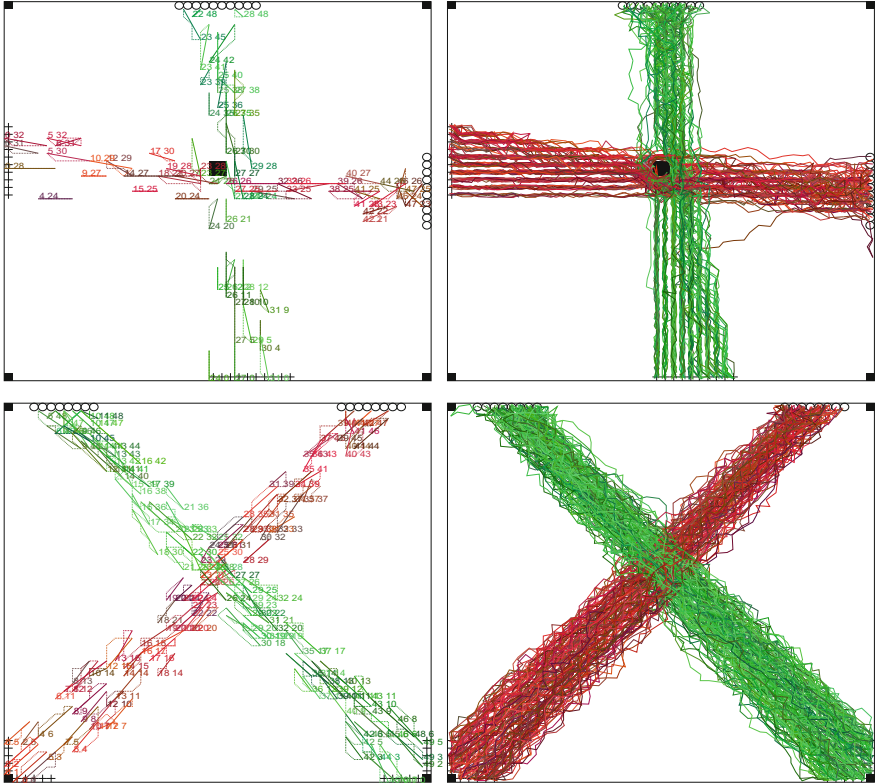


Fig. 3 The perpendicular intersection of two pedestrian groups

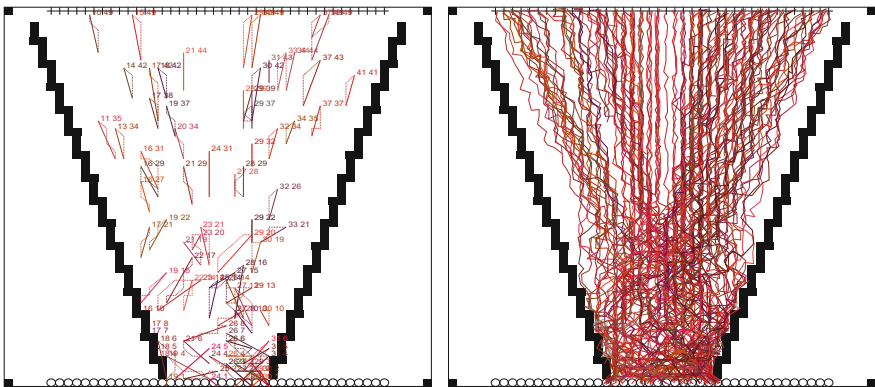


Fig. 4 A single group of pedestrians walking through a bottle-neck

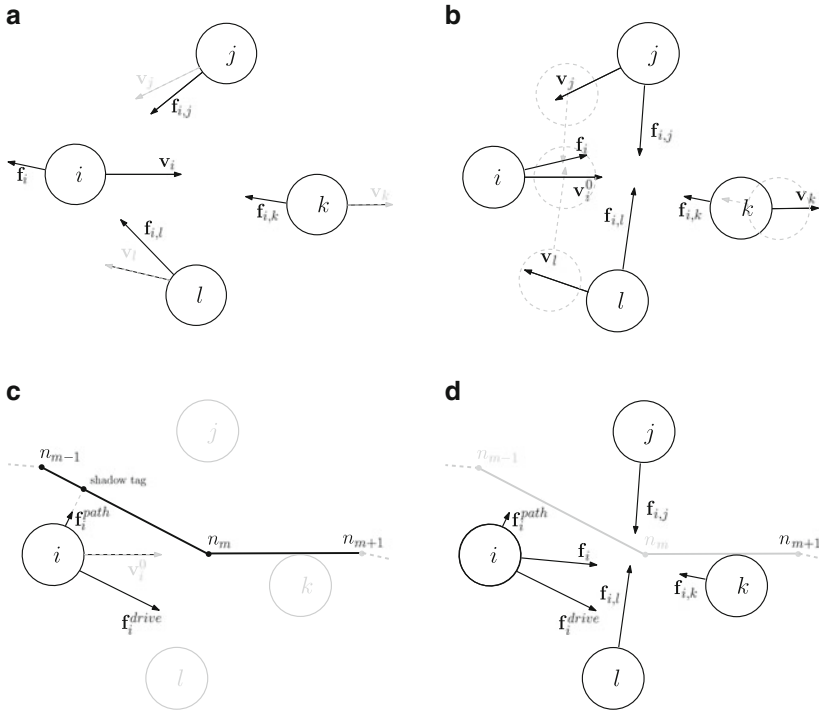


Fig. 5 Force-based models. (a) Social force model [12]. (b) Collision predicting force model [13]. (c) “Rubber strap” model for desired velocity calculation, proposed by Gloor et al. [14]. (d) Combination of Zanlungo et al. [13] and Gloor et al. [14]

when dealing with pedestrian streams which possibly cross each other, it seems necessary to consider the velocities of the moving objects.

Another model that takes velocities into consideration in order to avoid collisions has been proposed by Zanlungo et al. [13]. The basic idea of the model is to calculate potential collision points by projecting the actual scene into future under the assumption of constant movement for all agents. The repelling forces are then calculated based on this projection instead of the current situation. The basic principle of this model is depicted in Fig. 5b. The projected situation is indicated by dashed circles. The actual time to which the scene is projected depends on the individual times of closed approaches between agent i and agents j , k , and l . This approach leads, compared to the social force model, to a resulting force f_i that points in a complete different direction. In the example shown in Fig. 5b, agent i is no longer pushed to the left, but instead the agent finds a way more or less in the direction of the desired velocity v_i^0 by avoiding collisions at the same time.

Another issue which seems to puzzle the force-based models is the determination of the desired velocity vector. This is apparent, when it comes to complex way finding. Obviously it is possible to perform this on a graph. The actual route for

an agent is then described by a list of links or nodes. A straightforward solution to combine this with a force-based model would be to let the desired velocity \mathbf{v}^0 point at the beginning towards the first node of the route and incrementally switch to the next node as soon as a node has passed. However, in [14] it is shown that such an approach leads to unrealistic behaviors when agents are moving next to each other. The reason is that those agents are pulled together when they approach a node and after the node is passed their trajectories diverge again. The authors propose a force system that follows the route in the navigation graph. The basic idea is that each agent keeps a shadow tag on the navigation graph, which moves along the graph as the agents move forward. The agents are connected by a virtual “rubber strap” to their corresponding shadow tag. They will be directed by a driving force that is parallel to the link where the shadow tag is present. The “rubber strap” pulls the agents towards the shadow tag when the distance to the link becomes too large. An illustration of this approach is given in Fig. 5c.

In this project we propose a combination of the collision-avoiding model introduced by Zanlungo et al. [13] and the “rubber strap” model [14]. Implementation details and first simulation results are discussed in [15].

1.2 *Macroscopic Models*

The macroscopic approach is based on a set of pedestrian-specific coupled partial differential equations. These equations are not derived from the Euler or Navier-Stokes equations in fluid and gas dynamics. The specific situation of multi-destination pedestrian crowds as crossing streams requires the development of appropriately adapted methods. This has been targeted by means of simple heuristics.

Typical applications of these approaches include real-world scenarios like airports, shopping malls, buildings of middle to large size etc., where the participants (i.e. the pedestrians) do not exhibit an overall unanimity and may have different and multiple destinations.

Beyond the modeling techniques of the above-mentioned problems, a particular purpose of our work will be the development, implementation and test of appropriate computer-based simulation models. The assessment of the reliability of these models by a comparison with real data obtained from experiments of intersecting pedestrian groups is currently in progress.

1.2.1 **Model Equations**

Starting from the mass balance for species mixture for every species, the continuity equations

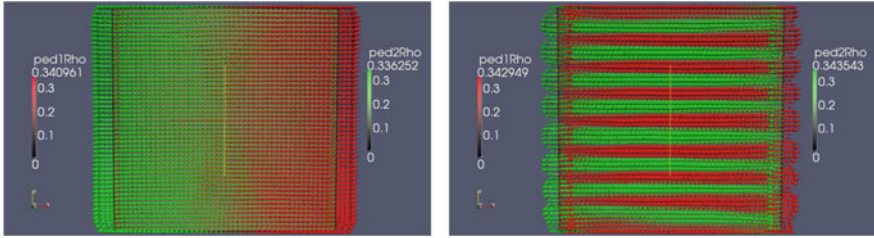


Fig. 6 Simulation of two pedestrian groups which walk in opposite directions

$$\frac{\partial \rho_i}{\partial t} + \nabla \cdot (\rho_i v_i) = 0 \quad (1)$$

will be considered. For the velocities of pedestrian group i , the following formulation

$$v_i = a_i V d_i^1 - b_i (1 - V) d^1 \quad (2)$$

is applied. A detailed discussion of the model is carried out in [16]. Here we will explain the essentials briefly. $V = V(\rho)$ stands for the velocity magnitude from a suitable velocity-density diagram where $\rho = \sum \rho_i$ is the sum of the species densities. To incorporate non-local effects on the pedestrian dynamics, we map the non-attracting spots like walls, obstacles and jams to potentials by solving a set of potential equations. These potentials are used to define the vector fields d_i^1 and d^1 which de-accelerate or accelerate the pedestrian movement. Also in (2), a_i , b_i are constants configured from the resulted numerical tests in comparison with the data acquired from experiments.

1.2.2 Some Aspects for Setting Boundary Conditions

Boundary conditions usually comprise the entries and exits of a certain region to be simulated. The fact that pedestrians are “sensitive” in their decision-making concerning spacing configurations should draw our attention. With consideration of the fact that information applied on boundaries, to a large extent, cannot be derived from the model, certain assumptions must be made. An example would be that on the boundary representing a wall, it is obvious that pedestrians are not allowed to move through it. This means that the flux through the corresponding wall is zero. In the flux part of (1), the condition of either $v \cdot v_i = 0$ or $\rho_i = 0$, as well as both simultaneously, is sufficient to guarantee this behavior (Fig. 6).

An elaborate discussion of modeling in combination with different boundary constellations is detailed in [16].

2 Experiments and Real World Data Generation

The evaluation of simulation models requires reliable and clearly defined empirical data. These empirical data may be obtained from either naturally occurring human crowds [17] or pedestrian flows that have been produced under controlled, experimental conditions [18–20]. In general, such experiments are designed to demonstrate crowd behavior in special situations such as evacuation or passing through a bottleneck or corridor.

In our case, for the access of reliable empirical data of intersecting pedestrian flows of multiple destinations, we conducted in 2010 human crowd experiments at Technische Universität Berlin.

The spatio-temporal positions of the pedestrians were obtained via photogrammetric means from video data recorded with multiple temporally synchronized network surveillance video cameras. Tracking of the pedestrians was facilitated with the Lucas–Kanade algorithm. Smooth trajectories were then obtained via approximation with cubic B-splines, and the combinatorial assignment of trajectories obtained from different camera perspectives was supported by the Kuhn–Munkres algorithm. Finally, we computed dynamic local density and flow fields via a novel method based on variable-bandwidth nearest-neighbor kernel density estimation.

In the following, we will quickly summarize the experimental setup and the methodology for the computation of trajectories and density/flow fields from the recorded video data. For more details, we refer to [21–23].

2.1 Experimental Setup

During the Lange Nacht der Wissenschaften 2010 (Long Night of the Sciences) four volunteer groups of event visitors were instructed to move from opposite sides of an observation area located in the entrance hall of the Department of Mathematics of Technische Universität Berlin, to create various scenarios: two groups and four groups intersecting from perpendicular directions, two groups meeting head-on, and two groups meeting head-on from an angle of approximately 180° .

In a follow-up experiment later that year, under similar conditions, two pedestrian groups (a group composed of 142 subjects and another with 83 subjects) intersected at an angle of roughly 90° for 1 min in a region of about 25 m^2 , reaching a peak density of about five pedestrians per square meter. In our studies, we use this experiment as the main test case. The scene was recorded from a gallery at a height of about 6 m with five networked and temporally synchronized JVC VN-V25U surveillance video cameras. We analyzed the data provided by the three central cameras which covered the area where the two pedestrian groups meet, see Fig. 7. A particular challenge concerning the photogrammetric analysis was manifested by

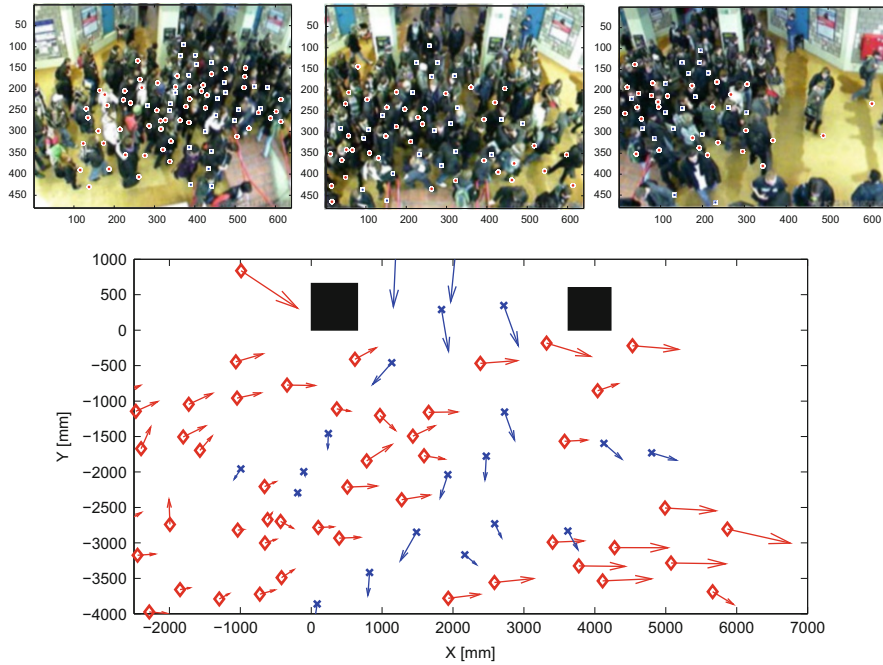


Fig. 7 Video snapshots of intersecting pedestrian groups and the retrieved positions and local velocities of the subjects. The figures (snapshots) in the first row are measured in pixel elements delivered by hardware, whereas in the overall computed result (second row) length is measured in physical unit. The conversion is not linear, for details consult the references mentioned in the text

the fact that due to constructional limitations of the building the scene could not be captured from a bird's eye view.

2.2 *Extraction of Trajectories*

After measurement of the world and image coordinates of about 30 reference points in the scene, the cameras were calibrated under the assumption of a pinhole model. Then, for each video frame, the heads of the pedestrians were marked manually, aided by the Lucas–Kanade tracking algorithm [24,25]. In the next step, we marked the floor position of each pedestrian in (at least) one frame in order to compute the height of the respective pedestrian via the homography determined from camera calibration. Given this information, the world coordinates of the pedestrians' floor positions can be computed for each frame. These spatio-temporal positions were then approximated with cubic B-splines in order to obtain smooth trajectories. Finally, the trajectories extracted from different camera perspectives were brought together by combinatorial assignment with the Kuhn–Munkres algorithm [26,27].

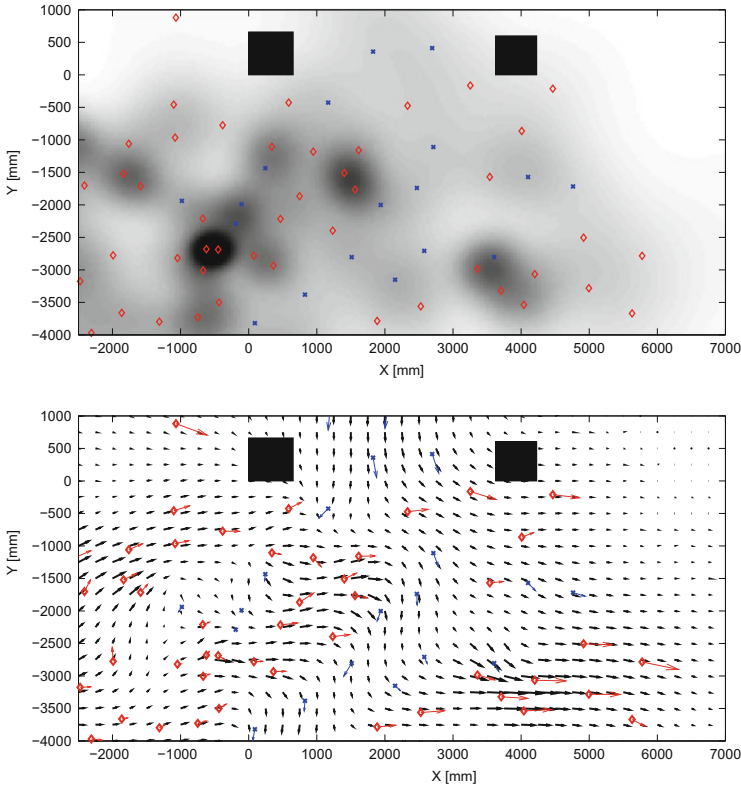


Fig. 8 Pedestrian density and flow fields at a fixed point in time. The *blue* and *red* arrows indicate the velocities of individual pedestrians

2.3 Local Density and Flow Fields

We are of the opinion that dynamic local density and flow fields as a representation of pedestrian dynamics are particularly suited for the calibration and validation of a variety of models: macroscopic simulations already produce density and flow fields, and data obtained from experiments or microscopic simulations may be converted into such fields.

In order to compute density and flow fields from pedestrian trajectories, we propose a new method based on a particular variable-bandwidth kernel estimator. Other feasible techniques include the Voronoi method [28] or kernel estimators with fixed bandwidth [17]. The bandwidth is defined in such a way that it decreases with the number of pedestrians located in the close vicinity and their respective distance. Therefore, this method supports a description of the limited range of pedestrians in particularly crowded situations. For details of the algorithm we refer to [21]. In Fig. 8, the density and flow fields are shown for the situation illustrated in Fig. 7.

Table 1 Incompatible model features of macroscopic models and MATSim and adaptation approaches

MATSim	Macroscopic model	Adaptation approach
Geometry data consists of obstacles; paths are followed on graphs of intended routes	Need for a meshed bounded area with flux-conditions at the boundaries; intended walking directions should be provided for every point in the computational domain	Cutting part of the plane used in MATSim of a subproblem, provide it with (inner and outer) boundaries and mesh it; generate a field of intended directions in the domain
Traceable agents moving on planes according to certain rules	Densities of pedestrian species are subject to transport equations modeling the “interaction” of pedestrians perceived as unstructured “matter”	Providing an interface to convert moving agents into densities and/or fluxes of “matter”, which can be considered consisting of groups of agents that are equivalent in the context, at the inflow boundaries; “re-assemble” the agents at the outflow boundaries of the macroscopic model based on thresholds and FIFO lists

3 Hybrid Ansätze

Merging the advantages of the respective microscopic and macroscopic models is a long-term objective of the present project. One possibility consists in the exploitation of the potentials generated in the macroscopic modeling to qualify the decision-making of the agents in the microscopic model not to be oversimplified. In this field, first results have been obtained and an implementation of such a model modification is feasible.

On the other hand, it is possible to employ the velocity and density fields as results of the macroscopic mathematical model in a straightforward manner to reconstruct paths of members of a pedestrian group. But unfortunately, in general, compatibility among agent-based models—as we have seen them integrated in our MATSim modeling—and macroscopic models cannot be guaranteed. The integration of macroscopic models into the framework MATSim has thus been our concern in the current project.

The techniques to adapt the data to provide the information flux between the models have been listed in Table 1. The macroscopic model applied has also been shown as an integrated module of MATSim, the implementation of which has been carried out in the OpenFOAM framework by providing a simulation utility that has to be run in a so-called case directory holding the necessary initial and

control information of the setting which is to be simulated. Thus the interaction of MATSim with the macroscopic model solver is in a master-slave-state. MATSim, as the master, generates the case directory structure, calls the simulator and re-extracts and converts the data from the slave, that is, the macroscopic model, in a form needed for further computation.

Acknowledgements The authors gratefully acknowledge the support of Deutsche Forschungsgemeinschaft (German Research Foundation) for the project SCHW548/5-1+BA1189/4-1 and project Na 682/5-1.

In addition, we would also like to thank the organizers of the Sixth International Conference on Pedestrian and Evacuation Dynamics 2012, ETH Zurich, Switzerland.

References

1. Burstedde, C., Klauck, K., Schadschneider, A., Zittartz, J.: Simulation of pedestrian dynamics using a two-dimensional cellular automaton. *Physica A* **295** (2001) 507–525
2. Keßel, A., Klüpfel, H., Wahle, J., Schreckenberg, M. [29] 193–200
3. Schadschneider, A. [29] 75–85
4. Kirchner, A., Nishinari, K., Schadschneider, A.: Friction effects and clogging in a cellular automaton model for pedestrian dynamics. *Physical Review E* **67**(5) (2003) 056122
5. Klüpfel, H.L.: A cellular automaton model for crowd movement and egress simulation. PhD thesis, Universität Duisburg-Essen (2003)
6. Kirchner, A., Klüpfel, H., Nishinari, K., Schadschneider, A., Schreckenberg, M.: Discretization effects and the influence of walking speed in cellular automata models for pedestrians dynamics. *Journal of Statistical Mechanics: Theory and Experiment* **2004**(10) (2004) P10011
7. Nishinari, K., Kirchner, A., Namazi, A., Schadschneider, A.: Extended floor field CA model for evacuation dynamics. *IEICE Trans. Inf. & Syst.* **E87-D**(3) (2004) 726–732
8. Chen, M.J., Bärwolff, G., Schwandt, H.: A study of step calculations in traffic cellular automaton models. In: 13th International IEEE Conference on Intelligent Transportation Systems. (2010) 747–752 An electronic version can be retrieved at: <http://page.math.tu-berlin.de/~chenmin/pub/cbs100709.pdf> (accessed February 24, 2014).
9. Helbing, D., Farkas, I.J., P.Molnár, Vicsek, T. [29] 21–58
10. Helbing, D., Buzna, L., Johansson, A., Werner, T.: Self-organized pedestrian crowd dynamics: Experiments, simulations and design solutions. *Transportation Science* **39** (February 2005) 1–24
11. Helbing, D., Molnár, P.: Social force model for pedestrian dynamics. *Phys. Rev. E* **51** (May 1995) 4282–4286
12. Helbing, D., Farkas, I., Vicsek, T.: Simulating dynamical features of escape panic. *Nature* **407** (2000) 487–490
13. Zanlungo, F., Ikeda, T., Kanda, T.: Social force model with explicit collision prediction. *EPL (Europhysics Letters)* **93** (2011) 68005
14. Gloor, C., Mauron, L., Nagel, K.: A pedestrian simulation for hiking in the alps. In: Proceedings of the Swiss Transport Conference (STRC). (2003)
15. Lämmel, G., Plaue, M.: Getting out of the way: Collision avoiding pedestrian models compared to the real world. (2012) to appear in the same volume.
16. Huth, F., Bärwolff, G., Schwandt, H.: A macroscopic multiple species pedestrian flow model. (2012) to appear in the same volume.
17. Helbing, D., Johansson, A., Al-Abideen, H.Z.: Dynamics of crowd disasters: An empirical study. *Physical Review E* **75** (2007) 046109

18. Daamen, W., Hoogendoorn, S.P.: Experimental research on pedestrian walking behavior. In: Transportation Research Board annual meeting. (2003) 1–16
19. Galea, E.R., Filippidis, L., Wang, Z., Lawrence, P.J., Ewer, J.: Evacuation analysis of 1000+ seat blended wing body aircraft configurations: Computer simulations and full-scale evacuation experiment. In: Proc. PED2010. (2011)
20. Zhang, J., Klingsch, W., Schadschneider, A., Seyfried, A.: Transitions in pedestrian fundamental diagrams of straight corridors and T-junctions. *J. Stat. Mech.* (2011) P06004
21. Plaue, M., Bärwolff, G., Schwandt, H.: On measuring pedestrian density and flow fields in dense as well as sparse crowds. (2012) to appear in the same volume.
22. Plaue, M., Chen, M., Bärwolff, G., Schwandt, H.: Multi-view extraction of dynamic pedestrian density fields. preprint (2012)
23. Plaue, M., Chen, M., Bärwolff, G., Schwandt, H.: Trajectory extraction and density analysis of intersecting pedestrian flows from video recordings. In: Proc. PIA11. Volume 6952 of LNCS. (2011) 285–296
24. Lucas, B.D., Kanade, T.: An iterative image registration technique with an application to stereo vision. In: Proc. of Imaging Understanding Workshop. (1981)
25. Shi, J., Tomasi, C.: Good features to track. In: Proc. of the IEEE Comp. Soc. Conf. on Computer Vision and Pattern Recognition. (1994) 593–600
26. Kuhn, H.W.: The Hungarian method for the assignment problem. *Naval Research Logistic Quarterly* **2** (1955) 83–97
27. Munkres, J.: Algorithms for the assignment and transportation problems. *Journal of the Society for Industrial and Applied Mathematics* **5**(1) (1957) 32–38
28. Steffen, B., Seyfried, A.: Methods for measuring pedestrian density, flow, speed and direction with minimal scatter. *Physica A* **389**(9) (2010) 1902–1910
29. Schreckenberg, M., Sharma, S.D., eds.: *Pedestrian and Evacuation Dynamics*. Springer-Verlag Berlin Heidelberg (2002)

Modeling Pedestrian Route Choice During Large Public Gatherings

Lei Feng and Elise Miller-Hooks

Abstract This paper describes network optimization-based modeling and solution frameworks for assessing pedestrian response to the physical layout of a venue's ingress and egress routes during large public gatherings. These approaches support the movement of both individuals and groups. They exploit concepts of utility maximization and recognize that the utility of a route depends on both fixed route characteristics, such as length or grade, and characteristics that depend on the choices made by others who simultaneously seek passage along the same routes. Results of numerical experiments are provided to demonstrate the effectiveness of the proposed methodologies and investigate the impact of groups on flow efficiency.

1 Introduction

Large gatherings of people arise for a variety of purposes and may be held in a myriad of venues, including for example, complex buildings, transportation stations, sports stadiums, commercial malls, and other type of facilities. In such gatherings, crowds are directed through passageways within the facilities. The physical layout of these passageways provides a set of route options from which pedestrians can choose for ingress or egress. The speed with which a pedestrian will move through the passageway depends on its physical capacity, the person's physical well-being, and the number of other pedestrians utilizing it at the same time. The time for ingress or egress to or from the event depends on the series of choices the pedestrian makes in navigating the physical layout and competition with other pedestrians for passageway capacities. A pedestrian's preference for an alternative route depends on the route's utility and its utility depends both on its attributes and the pedestrian's

L. Feng • E. Miller-Hooks (✉)
Department of Civil and Environmental Engineering, University of Maryland, College Park,
MD 20742, USA
e-mail: elisemh@umd.edu

sensitivity to each such attribute type. Moreover, some attributes, like travel speed, are affected by the choices made by competing system users. The selection of a route is assumed to be rational, meaning that the pedestrian will choose the route with the maximum utility based on his/her preference function. The overall problem of estimating which routes all pedestrians will take is known as a traffic assignment problem, and is referred to as a pedestrian assignment problem in this context.

The concept of route choice in vehicular traffic flow is well developed. Pedestrians, however, have more degrees of freedom in movement and often choose to travel in groups. Such groups arise in vehicular traffic scenarios, but these groups are typically housed within a single vehicle. For example, a family will travel within the same car or larger groups will travel in a bus. These groups, thus, will never be faced with the possibility of being split apart. Others who seek to access the venue together but in different vehicles will often need to be willing to meet at the destination. In the context of pedestrian movement, however, groups must make a concerted effort to move together and not be split apart. For example, parents will not wish to be separated from their children. Thus, while each person within the family is an individual (i.e. a unit of flow) and is free to make his or her own decisions in response to directives from crowd managers or the physical layout, any effective crowd management plan must facilitate the movement of all members of the family as a group. That is, the group must be permitted to stay together and accommodations must be made to support this group movement. In this work, a distinction is made between two broadly categorized group types: separable and clustered [1]. The former can be, for example, a group of friends/colleagues who have a predilection for staying together, but each person within the group is free to make his or her own decision in response to the physical environment. It is likely but not guaranteed that individuals in this group type will travel together. The latter describes groups that will not be separated, such as parent and child. Such group decisions and movements are crucial to developing realistic models of pedestrian movement [2, 3].

This paper describes a network optimization-based modeling and solution framework for estimating pedestrian flows within a network representation of a physical environment. Movements by individuals and groups must be captured in the flows produced by this method. That is, the framework involves the modeling and solution of a pedestrian assignment problem.

Assignment problems for vehicular traffic have received enormous attention in the literature. The majority of traffic assignment models seek user equilibrium (UE) solutions, where no traveler can select an alternative path with higher utility by unilaterally switching routes [4]. Deterministic user equilibrium (DUE) and stochastic user equilibrium (SUE) models are two common UE approaches. DUE assumes that travelers have perfect information on the performance of all alternative routes when choosing a route. SUE, on the other hand, presumes that each user makes his/her selection of a route based on perceived features of the alternatives. It is generally accepted that SUE approaches provide more realistic predictions of traveler route choice behavior [5]. Both modeling approaches assume that travelers are homogenous in terms of their preference functions. And both assign travelers to

paths probabilistically, with higher likelihood of choosing a path with higher utility. That is, the frequency of path use can be set by the probability of its selection. An alternative approach might be to employ a Nash equilibrium based methodology. Both pure- and mixed-strategy Nash equilibriums have been considered in the context of vehicular traffic assignment [6, 7]. In [6, 7], players have their own preference functions. Formulations seeking such equilibriums involve concepts of non-cooperative games. In these prior works, group behavior is not considered and, therefore, the developed models and algorithms for traffic assignment cannot be applied directly in the movement of pedestrians where group behavior must be considered. One reason for this is that the marginal impact of the decision of one flow unit in pedestrian assignment where group behavior is modeled must account for the impact of group size.

Several works in the context of vehicular traffic take the heterogeneity of users into consideration. For example, the assignment problem for multiclass user traffic networks is considered in [8, 9]. In this multiclass user equilibrium problem, each class of travelers (e.g. trucks, buses, passenger cars) has an individual preference function and each class makes decisions based on path utilities derived from this function. Travelers are assigned to paths probabilistically, as in DUE and SUE methods, again with higher likelihood of choosing a route with higher utility. Users in the same class will have the same probability of selecting route alternatives. Thus, the multiclass user equilibrium assignment method does not guarantee that members in the same class will make the same decisions.

While there is a significant body of work existing in the vehicular traffic assignment area, these works cannot be directly extended for use in modeling clustering (or group) behavior as is required for many pedestrian traffic assignment contexts. On the contrary, within the literature on pedestrian modeling, numerous works consider group behavior. The majority use simulation and often involve a leader and set of followers (e.g. [3]). In an alternative network flow-based approach, Hamacher et al. [2] incorporate group movements in solving a dynamic quickest cluster flow problem. However, travel times are not flow-dependent and thus competition among travelers for limited capacity is not considered.

In this paper, the effects of separable and clustered group movements on flow distributions through the physical layout are studied. Two methodologies are proposed to model these effects: an SUE pedestrian assignment approach to model separable groups and an n-player non-cooperative game seeking a pure-strategy Nash equilibrium to model clustered groups. In terms of separable groups, all group members are assumed to have identical (homogenous) preference functions, but as mentioned previously, they behave independently. In terms of clustered groups, all members of the same group make the same route decision. Note that the SUE pedestrian assignment problem used to model separable groups can be reformulated as a game in which a mixed-strategy Nash equilibrium is sought [10]. In this game, each player represents a single pedestrian. The solution produces the probability that each player chooses each strategy (i.e. route), producing the fraction of total flow distributed over the network. Numerical experiments were conducted to demonstrate the impact of pedestrian route choice under both separable

and clustered group situations on movement efficiency within the venue's physical layout. Before proceeding to descriptions of these two modeling approaches, general introduction to utility maximization concepts in the context of route choice is provided.

2 Utility Maximization in Route Choice

Route choice, sometimes referred to as wayfinding, involves choosing an option from a finite set of alternative routes for given origin–destination (O-D) pairs. The concept of route choice in vehicular traffic is well developed [11]. Utility maximization-based discrete choice models are widely used to model route decisions by drivers. The basic assumption underlying this model is that a traveler's preference for each alternative route can be described by a utility (or disutility) that is a function of the attributes of the alternative routes and sensitivity parameters of the traveler to these attributes [4]. The traveler is assumed to choose the route with maximum utility (or minimum disutility).

In the context of pedestrians, a number of works consider pedestrian route choice behavior [12–16]. A couple of these works employ utility maximization-based choice models [14–16]. Pedestrians are very sensitive to route characteristics that are related to physical effort, such as walking distance, walking time and the exertion involved in climbing stairs or ramps. As discussed in [17, 18], walking distance and time are the most important route attributes in pedestrian route choice. Furthermore, in discrete choice models, the independence of irrelevant alternatives property is assumed to hold. The concept of path size factor proposed in [19] is adopted herein to deal with overlap in alternative routes due to the sharing of arcs. In the next section, two types of utility functions that incorporate these elements (group size, travel distance, travel time and overlap) are proposed for separable and clustered groups. The pedestrian route choice problems involving separable and clustered groups are formulated as an SUE assignment problem and n-player non-cooperative game seeking a pure-strategy Nash equilibrium, respectively. Solution methodologies for obtaining flows for each problem class are also provided.

3 Two Proposed Approaches to Determining Pedestrian Routes

In this section, mathematical formulations of the SUE assignment for separable groups and pure-strategy Nash equilibrium assignment for clustered groups are provided. A logit-based Method of Successive Averages (MSA) and Best Response Dynamics-based Tabu Search heuristics are proposed for solutions to SUE assignment and pure-strategy Nash equilibrium assignment, respectively.

3.1 Mathematical Modeling Schemes for Pedestrian Route Choice

3.1.1 Variable Definitions

The physical layout is represented by a network $G = (N, A)$, where N is a set of nodes representing locations at which decisions can be taken, and A is a set of directed arcs connecting the nodes. The arcs represent passageways along which movement is possible. Let $O, D \in N$ be the set of origins and destinations, respectively. Each arc $a \in A$ has an associated length l_a , capacity c_a , and a nonnegative travel time $t_a(x_a, c_a)$, which is a continuously differentiable and strictly increasing function of arc flow x_a and capacity c_a . The BPR-based form [20] is adopted:

$$t_a(x_a, c_a) = t_a^0 \cdot \left[1 + k_a \left(\frac{x_a}{c_a} \right)^2 \right] \quad \forall a \in A, \tag{1}$$

where k_a is a coefficient that scales the rate at which congestion increases with time, and t_a^0 denotes free-flow travel time. For free-flow speed v_a , t_a^0 can be calculated as in Eq. 2.

$$t_a^0 = l_a / v_a \quad \forall a \in A. \tag{2}$$

For specific O-D pair $w \in W$, where W is the set of O-D pairs, there is a set of groups of pedestrians $G_w (g = 1, \dots, |G_w|)$ and set of routes connecting O-D pair w , $R_w (r = 1, \dots, |R_w|)$. Let S_w^g denote the size of group $g \in G_w$ between pair w .

Further, let f_w^r, T_w^r and L_w^r denote the flow, travel time and distance on route $r \in R_w$ for pair w , respectively. According to the route-arc incidence relationships, route travel time and distance on route r connecting pair w can be written as in Eqs. 3 and 4, respectively.

$$L_w^r = \sum_{a \in A} l_a \cdot \delta_w^{r,a} \quad \forall r \in R_w, w \in W \tag{3}$$

$$T_w^r (f_w^r) = \sum_{a \in A} t_a(x_a) \cdot \delta_w^{r,a} \quad \forall r \in R_w, w \in W, \tag{4}$$

where $\delta_w^{r,a}$ equals 1 if route r passes through arc a , and 0 otherwise.

3.1.2 SUE Assignment Formulation

An SUE-based assignment formulation in which separable groups can be modeled is given in program (P1). The skeleton of the formulation is from [21]. This formulation is expanded to address group movements. Thus, group assignment and group flow conservation are added as in (P1).

$$(P1) \quad \min_{\mathbf{x}} \quad Z_1(\mathbf{x}) = \sum_{a \in A} \int_0^{x_a} u_a(\omega) d\omega + \frac{1}{\theta} \sum_{w \in W} \sum_{r \in R_w} f_w^r \cdot \ln f_w^r \quad (5)$$

$$s.t. \quad \sum_{r \in R_w} f_w^{g,r} = S_w^g \quad \forall g \in G_w, w \in W \quad (6)$$

$$x_a^g = \sum_{r \in R_w} f_w^{g,r} \delta_w^{r,a} \quad \forall a \in A, g \in G_w, w \in W \quad (7)$$

$$x_a = \sum_{w \in W} \sum_{g \in G_w} x_a^g \quad \forall a \in A \quad (8)$$

$$f_w^{g,r} \geq 0 \quad \forall g \in G_w, r \in R_w, w \in W, \quad (9)$$

where $u_a(\cdot)$ is the disutility on arc a , $f_w^{g,r}$ is the flow of group g on route r between O-D pair w , and x_a^g is the flow of group g on arc a . Objective function Eq. 5 seeks to minimize the perceived disutility subject to flow conservation constraints Eqs. 6, 7 and 8. Constraints Eq. 9 restrict path flows to be non-negative. Note that the objective function does not have any intuitive economic or behavioral interpretation. It is only a mathematical structure that is used to solve the SUE problem.

Due to its closed form, a logit-based route choice model has been widely employed in computing SUE flows. In a logit-based route choice model, flows along the routes are proportionally assigned to routes according to their corresponding utility. The perceived disutility of route r to each individual in group g between O-D pair w is given in Eq. 10,

$$U_w^{g,r} = -\theta^g \cdot u_w^{g,r} + \varepsilon_w^{g,r} \quad \forall g \in G_w, r \in R_{od}, w \in W, \quad (10)$$

where $u_w^{g,r}$ denotes the measured disutility of route r to each individual in group g between O-D pair w , θ^g is positive scaling parameter indicating disutility perception variations between perceived disutility and real disutility (a higher θ^g means a smaller variation), and $\varepsilon_w^{g,r}$ is a random term presenting the perception errors which are assumed to be independent Gumbel distributed with mean zero.

At SUE equilibrium, the probability of group g choosing route r between pair w can be calculated as in Eq. 11:

$$p_w^{g,r} = \frac{\exp(-\theta^g \cdot u_w^{g,r})}{\sum_{k \in R_w} \exp(-\theta^g \cdot u_w^{g,k})} \quad \forall g \in G_w, r \in R_w, w \in W. \quad (11)$$

From conservation of flow constraints Eq. 6, flow associated with group g and assigned to route r between O-D pair w , $f_w^{g,r}$, can be deduced through Eq. 12.

$$f_w^{g,r} = S_w^g \cdot p_w^{g,r} \quad \forall g \in G_w, r \in R_w, w \in W. \quad (12)$$

Arc flows can be deduced from route flows through Eqs. 7 and 8.

From Sect. 2, the measured disutility, $u_w^{g,r}$, is further expressed as in Eq. 13.

$$u_w^{g,r} = \alpha^g L_r + \beta^g T_r + \gamma^g \ln(PS_r) \quad \forall g \in G_w, r \in R_w, w \in W, \quad (13)$$

where $\alpha^g, \beta^g, \gamma^g$ are parameters of walking distance, walking time and path size factor of group g , respectively, and represents the preference (sensitivity) of group g to these attributes. PS_r is the path size factor of route r proposed by [19],

$$PS_r = \sum_{a \in r} \frac{l_a}{L_r} \frac{1}{N_a}, \quad (14)$$

where a is index of an element arc of the route, and N_a is the number of alternative routes that pass through arc a .

Substituting Eqs. 3 and 4 into Eq. 13, $\forall g \in G_w, r \in R_w, w \in W$, leads to Eq. 15:

$$\begin{aligned} u_w^{g,r} &= \sum_{a \in A} [\alpha^g l_a + \beta^g t_a(x_a)] \cdot \delta_w^{r,a} + \gamma^g \ln(PS_r) \\ &= \sum_{a \in A} u_a^g(x_a) \cdot \delta_w^{r,a} + \gamma^g \ln(PS_r), \end{aligned} \quad (15)$$

where $u_a^g(x_a)$ denotes the disutility of group g on arc a , which is a function of arc flow, x_a . Then the arc disutility $u_a(x_a)$ in Eq. 5 can be expressed by:

$$u_a(x_a) = \sum_{w \in W} \sum_{g \in G_w} u_a^g(x_a^g) \quad \forall a \in A. \quad (16)$$

3.1.3 Pure-Strategy Nash Equilibrium Assignment

For clustered groups, the disutility of each route r connecting O-D pair w to group g can be expressed as in Eq. 17.

$$v_w^{g,r}(S_w^g, f_w^r) = S_w^g \cdot [\lambda^g L_w^r + \chi^g T_w^r(f_w^r)] \quad \forall g \in G_w, r \in R_w, w \in W, \quad (17)$$

where $v_w^{g,r}(\cdot)$ represents the disutility of route r for group g with O-D pair w . It is a function of group size, S_w^g , route distance, L_w^r , and walking time, T_w^r . λ^g and χ^g are parameters indicating group g 's sensitivity to walking distance and time, respectively.

Let lower-level decision variable $\xi_w^{g,r}$ equal 1 if group g chooses route r for O-D pair w , and 0 otherwise. Flow along route r for O-D pair w , f_w^r , is the sum of the sizes of groups that choose the route:

$$f_w^r = \sum_{g \in G_w} S_w^g \cdot \xi_w^{g,r} \quad \forall r \in R_w, w \in W. \quad (18)$$

From Eqs. 3 and 4, for each $g \in G_w, r \in R_w, w \in W$, Eq. 17 can be rewritten as Eq. 19.

$$\begin{aligned}
 v_w^{g,r}(S_w^g, f_w^r) &= S_w^g \cdot \left[\lambda^g \sum_{a \in A} l_a \delta_w^{r,a} + \chi^g \sum_{a \in A} t_a(x_a) \cdot \delta_w^{r,a} \right] \\
 &= \sum_{a \in A} S_w^g \cdot \left[\lambda^g l_a + \chi^g t_a(x_a) \right] \cdot \delta_w^{r,a} \\
 &= \sum_{a \in r} v_w^{g,a}(x_a) \cdot \delta_w^{r,a},
 \end{aligned} \tag{19}$$

where $v_w^{g,a}(x_a)$ measures the disutility incurred by group g using arc a .

The assignment of clustered groups to routes can be formulated as in program (P2). Program (P2) seeks (objective Eq. 20) the set of path flows over all O-D pairs with the minimum total disutility (weighted by group size). Derived from Eqs. 8 and 18, constraints Eq. 21 relate arc flows to path flows, thus, ensuring flow conservation. Constraints Eq. 22 force each group to choose one route. Binary restrictions are guaranteed through constraints Eq. 23.

$$(P2) \quad \min \sum_{w \in W} \sum_{r \in R_w} \sum_{g \in G_w} \sum_{a \in A} S_w^g \cdot \left[\alpha_g l_a + \beta_g t_a(x_a) \right] \cdot \delta_w^{r,a} \tag{20}$$

$$s.t. \quad x_a = \sum_{w \in W} \sum_{r \in R_w} \sum_{g \in G_w} S_w^g \cdot \xi_w^{g,r} \cdot \delta_w^{r,a} \quad \forall a \in A \tag{21}$$

$$\sum_{r \in R_w} \xi_w^{g,r} = 1 \quad \forall g \in G_w, w \in W \tag{22}$$

$$\xi_w^{g,r} = 0 \text{ or } 1 \quad \forall g \in G_w, r \in R_w, w \in W \tag{23}$$

Program (P2) can be viewed as an n-player, pure-strategy, non-cooperative game, where each group is a player, and the possible routes between each O-D pair form the strategy space. According to references [6, 7], there exists at least one pure-strategy Nash equilibrium for the game. Thus, the optimal solution to (P2) is a pure-strategy Nash equilibrium attaining the smallest total disutility, proof of which is provided in [22]. Note that there might be several pure-strategy Nash equilibria for the game. Problem (P2) seeks the one with the smallest total disutility. The formulation and solution methodology described in this subsection were introduced by the authors in [22].

3.2 Solution Schemes to Determine Chosen Routes

The solutions to programs (P1) and (P2) both begin with the generation of an efficient route set [4] for each O-D pair. It is presumed, as in [11], that when faced

with a route decision, a traveler selects his/her route from a limited choice set. Since complete enumeration of all possible routes is impractical and given that most people do not consider all alternatives in making their decisions, only the efficient route set is considered.

3.2.1 Efficient Route Set Definition

Based on [4], an efficient route is defined as a route passing only through efficient arcs, and an efficient arc is defined as follows. For each arc a connecting i to j , if $r(i) < r(j)$, for $r(k)$ the shortest distance from the origin to node k , and $s(i) > s(j)$, for $s(k)$ the shortest distance from k to the destination, then arc a is efficient ($eff(i, j) = 1$); otherwise, it is inefficient ($eff(i, j) = 0$). The efficient routes, R_w , between each O-D pair w are obtained with a depth-first-search (DFS) on the network of efficient arcs (i.e. the subgraph $G' = (N, A')$, where A' is the set of efficient arcs). Routes with cycles are not generated, because by definition any efficient arc transports travelers to locations that are further from the origin and closer to the destination.

3.2.2 Solution Approach for Program (P1)

The Method of Successive Averages (MSA) [4] has been successfully used in solving various stochastic user equilibrium problems. In this paper, a solution scheme that combines the MSA with group movements is proposed for solving the SUE assignment. The main procedure of MSA is given below.

Step 0: Initialization. For each $g \in G_w, w \in W$, use Eqs. 11 and 12 to perform a logit assignment based on the initial disutility, $u_a^g 0, \forall a \in A$. The result of this assignment is a set of route flows $f_w^{g,r} [0], \forall r \in R_w$. Generate initial arc flows $x_a^{[1]}, \forall a \in A$, through Eqs. 7 and 8 and set iteration count $n = 1$.

Step 1: Update. According to current arc flows $x_a^{[n]}, \forall a \in A$, update the arc disutility, $u_a^g [n](x_a^{[n]}), \forall a \in A, g \in G_w, w \in W$.

Step 2: Find direction. For each $g \in G_w, w \in W$, perform a logit assignment based on current disutility $u_a^g [n](x_a^{[n]}), \forall a \in A$, and find auxiliary arc flow $d_a^{[n]}, \forall a \in A$.

Step 3: Move. Compute new arc flow as $x_a^{[n+1]} = x_a^{[n]} + (1/n)(d_a^{[n]} - x_a^{[n]}), \forall a \in A$.

Step 4: Convergence check. Compute $gap^{[n]} = \sum_{a \in A} |d_a^{[n]} - x_a^{[n]}| / \sum_{a \in A} x_a^{[n]}$. If

$gap^{[n]} \leq \kappa$, stop; otherwise, $n = n + 1, \kappa = 0.001$, and go to step 1.

3.2.3 Solution Approach for Program (P2)

To solve program (P2), an adaptation given in [22] of the Best Response Dynamics-based Tabu Search procedure proposed in [23] for obtaining a pure strategy Nash equilibrium in normal form games in the context combinatorial auctions, is employed. Each group explores its potential route set. The group chooses the route that minimizes total disutility (i.e. the best choice route considering similar choices made by other groups. Details of important procedural steps can be found in [22].

4 Illustrative Example

4.1 Experimental Design

The efficiencies and differences between flows generated by modeling and solution methodologies designed for separable and clustered group behaviors are investigated on an illustrative example network representation of a facility layout.

The network consists of 14 nodes, 22 arcs and 4 O-D pairs as portrayed in Fig. 1. The capacity of each arc is indicated in the network. With the exception of arcs 4, 12 and 14, all arcs are assumed to have a length of 100 m. Arcs 4, 12 and 14 are 200 m in length. The free-flow speed is set be 1.42 m/s [24] and coefficient $k_a = 0.008$ for travel time calculations.

To explore the effects of separable and clustered groups on flow distributions over the network, four grouping scenarios listed in Table 1 are considered. Scenario 1 is an extreme case of scenario 2, where all pedestrians belong to the same group. Scenario 3 can be viewed as an extreme case of scenario 4, where each group consists of only one individual.

Table 2 gives the demand information for each O-D pair. For scenarios 2 and 4, it is assumed that for each O-D pair there are 20 groups each with group size randomly chosen on the interval [1, 40]. The preference parameters for each group in scenario 2 were generated incrementally, while λ^g in scenarios 3 and 4 is randomly generated between 0 and 1 and $\chi^g = 1 - \lambda^g$. Scenarios 1 and 3 have the same total demand (indicated in the O-D column in Table 2). In scenario 1, $\alpha^g = 0.053$, $\beta^g = 0.535$, $\gamma^g = 3.475$, and $\theta^g = 1.050$, computed from the average values of similar parameters in scenario 2.

Logit-based SUE assignment is employed for obtaining solutions under scenarios 1 and 2, while the Best Response Dynamics-Based Tabu Search procedure is used to address the n-player non-cooperative games of scenarios 3 and 4. Results are discussed in the next section.

Fig. 1 Network configuration

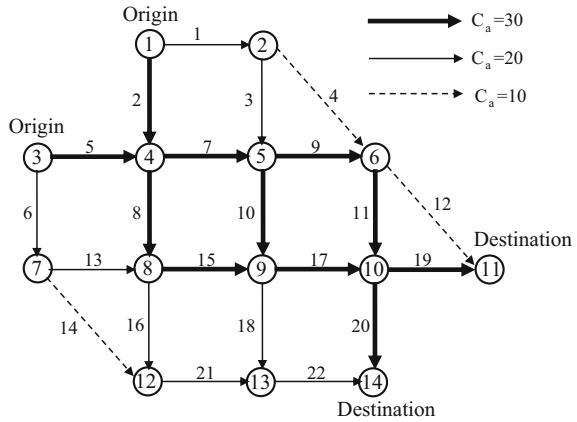


Table 1 Experiment scenarios

Separable groups	Scenario 1	All pedestrians are treated as members of one single large group and all individuals have the same preference parameters
	Scenario 2	All pedestrian can be divided into a finite number of groups composed of one or more individuals; preferences between groups are heterogeneous, but homogeneous within each group
Clustered groups	Scenario 3	Each pedestrian is viewed as a group and each has his/her own preference function
	Scenario 4	All pedestrian can be divided into a finite number of groups composed of one or more individuals; preferences between groups are heterogeneous, but homogeneous within each group; individuals within a group will stay together

4.1.1 Results and Analysis

Table 3 gives the efficient routes for each O-D pair.

Table 4 shows the arc flows by scenario. Similar arc flow results for separable single- (scenario 1) and separable variable-size groups (scenario 2). This is because scenario 1 relies on parameters taken from the average of parameter values assigned in scenario 2 – each pedestrian in scenario 1 will have identical parameter values. Note that the total travel time under the latter scenario Eq. 2 is slightly lower than that under the former scenario Eq. 1. This is because pedestrians in scenario 1 assign the same utility to every path. Thus, the lowest utility paths will be highly sought after and, therefore, highly congested. The greater variability in parameter settings of scenario 2 cause the pedestrians to disperse over a larger number of routes,

Table 2 Demand for each O-D pair

O-D	Scenario 2							Scenario 4								
	g	S_g	α^E	β^E	γ^E	θ^E	λ^E	χ^E	g	S_g	α^E	β^E	γ^E	θ^E	λ^E	χ^E
1-11 (400)	1	20	0.005	0.05	3.00	0.01	0.5	0.5	1	7	0.005	0.05	3.00	0.01	0.4	0.6
	2	23	0.010	0.10	3.05	0.02	0.7	0.3	2	27	0.010	0.10	3.05	0.02	0.3	0.7
	3	29	0.015	0.15	3.10	0.03	0.3	0.7	3	16	0.015	0.15	3.10	0.03	0.6	0.4
	4	23	0.020	0.20	3.15	0.04	0.2	0.8	4	19	0.020	0.20	3.15	0.04	0.6	0.4
	5	19	0.025	0.25	3.20	0.05	0.4	0.6	5	22	0.025	0.25	3.20	0.05	0.3	0.7
	6	25	0.030	0.30	3.25	0.06	0.6	0.4	6	27	0.030	0.30	3.25	0.06	0.1	0.9
	7	21	0.035	0.35	3.30	0.07	0.5	0.5	7	28	0.035	0.35	3.30	0.07	0.6	0.4
	8	40	0.040	0.40	3.35	0.08	0.4	0.6	8	30	0.040	0.40	3.35	0.08	0.1	0.9
	9	15	0.045	0.45	3.40	0.09	0.7	0.3	9	21	0.045	0.45	3.40	0.09	0.7	0.3
	10	1	0.050	0.50	3.45	0.10	0.7	0.3	10	16	0.050	0.50	3.45	0.10	0.2	0.8
	11	14	0.055	0.55	3.50	0.11	0.3	0.7	11	16	0.055	0.55	3.50	0.11	0.8	0.2
	12	30	0.060	0.60	3.55	0.12	0.3	0.7	12	1	0.060	0.60	3.55	0.12	0.1	0.9
	13	12	0.065	0.65	3.60	0.13	0.6	0.4	13	14	0.065	0.65	3.60	0.13	0.5	0.5
	14	30	0.070	0.70	3.65	0.14	0.7	0.3	14	18	0.070	0.70	3.65	0.14	0.3	0.7
	15	4	0.075	0.75	3.70	0.15	0.5	0.5	15	10	0.075	0.75	3.70	0.15	0.4	0.6
	16	18	0.080	0.80	3.75	0.16	0.8	0.2	16	11	0.080	0.80	3.75	0.16	0.2	0.8
	17	22	0.085	0.85	3.80	0.17	0.2	0.8	17	18	0.085	0.85	3.80	0.17	0.8	0.2
	18	14	0.090	0.90	3.85	0.18	0.6	0.4	18	1	0.090	0.90	3.85	0.18	0.2	0.8
	19	24	0.095	0.95	3.90	0.19	0.2	0.8	19	18	0.095	0.95	3.90	0.19	0.1	0.9
	20	16	0.100	1.00	3.95	0.20	0.3	0.7	20	30	0.100	1.00	3.95	0.20	0.5	0.5
3-11 (350)	1	18	0.005	0.05	3.00	0.01	0.8	0.2	1	10	0.005	0.05	3.00	0.01	0.2	0.8
	2	29	0.010	0.10	3.05	0.02	0.8	0.2	2	13	0.010	0.10	3.05	0.02	0.7	0.3
	3	29	0.015	0.15	3.10	0.03	0.8	0.2	3	16	0.015	0.15	3.10	0.03	0.1	0.9

4	15	0.020	0.20	3.15	0.04	0.2	0.8	4	13	0.020	0.20	3.15	0.04	0.7	0.3
5	27	0.025	0.25	3.20	0.05	0.4	0.6	5	19	0.025	0.25	3.20	0.05	0.8	0.2
6	20	0.030	0.30	3.25	0.06	0.4	0.6	6	18	0.030	0.30	3.25	0.06	0.5	0.5
7	17	0.035	0.35	3.30	0.07	0.3	0.7	7	29	0.035	0.35	3.30	0.07	0.5	0.5
8	20	0.040	0.40	3.35	0.08	0.1	0.9	8	24	0.040	0.40	3.35	0.08	0.0	1.0
9	19	0.045	0.45	3.40	0.09	0.6	0.4	9	28	0.045	0.45	3.40	0.09	0.4	0.6
10	6	0.050	0.50	3.45	0.10	0.2	0.8	10	6	0.050	0.50	3.45	0.10	0.3	0.7
11	19	0.055	0.55	3.50	0.11	0.6	0.4	11	12	0.055	0.55	3.50	0.11	0.7	0.3
12	27	0.060	0.60	3.55	0.12	0.5	0.5	12	17	0.060	0.60	3.55	0.12	0.4	0.6
13	8	0.065	0.65	3.60	0.13	0.2	0.8	13	15	0.065	0.65	3.60	0.13	0.8	0.2
14	1	0.070	0.70	3.65	0.14	0.3	0.7	14	9	0.070	0.70	3.65	0.14	0.3	0.7
15	20	0.075	0.75	3.70	0.15	0.6	0.4	15	20	0.075	0.75	3.70	0.15	0.8	0.2
16	22	0.080	0.80	3.75	0.16	0.2	0.8	16	28	0.080	0.80	3.75	0.16	0.3	0.7
17	21	0.085	0.85	3.80	0.17	0.8	0.2	17	8	0.085	0.85	3.80	0.17	0.8	0.2
18	7	0.090	0.90	3.85	0.18	0.2	0.8	18	1	0.090	0.90	3.85	0.18	0.7	0.3
19	23	0.095	0.95	3.90	0.19	0.3	0.7	19	8	0.095	0.95	3.90	0.19	0.3	0.7
20	2	0.100	1.00	3.95	0.20	0.1	0.9	20	6	0.100	1.00	3.95	0.20	0.2	0.8

Table 3 Efficient routes set for each O-D pair

O-D	Index	Route	O-D	Index	Route
1-11	1	1 → 2 → 5 → 6 → 10 → 11	1-14	1	1 → 2 → 5 → 6 → 10 → 14
	2	1 → 2 → 5 → 6 → 11		2	1 → 2 → 5 → 9 → 10 → 14
	3	1 → 2 → 5 → 9 → 10 → 11		3	1 → 2 → 5 → 9 → 13 → 14
	4	1 → 2 → 6 → 10 → 11		4	1 → 2 → 6 → 10 → 14
	5	1 → 2 → 6 → 11		5	1 → 4 → 5 → 6 → 10 → 14
	6	1 → 4 → 5 → 6 → 10 → 11		6	1 → 4 → 5 → 9 → 10 → 14
	7	1 → 4 → 5 → 6 → 11		7	1 → 4 → 5 → 9 → 13 → 14
	8	1 → 4 → 5 → 9 → 10 → 11		8	1 → 4 → 8 → 9 → 10 → 14
	9	1 → 4 → 8 → 9 → 10 → 11		9	1 → 4 → 8 → 9 → 13 → 14
3-11	1	3 → 4 → 5 → 6 → 10 → 11		10	1 → 4 → 8 → 12 → 13 → 14
	2	3 → 4 → 5 → 6 → 11	1	3 → 4 → 5 → 6 → 10 → 14	
	3	3 → 4 → 5 → 9 → 10 → 11	2	3 → 4 → 5 → 9 → 10 → 14	
	4	3 → 4 → 8 → 9 → 10 → 11	3	3 → 4 → 5 → 9 → 13 → 14	
	5	3 → 7 → 8 → 9 → 10 → 11	4	3 → 4 → 8 → 9 → 10 → 14	
		5	3 → 4 → 8 → 9 → 13 → 14		
		6	3 → 4 → 8 → 12 → 13 → 14		
		7	3 → 7 → 8 → 9 → 10 → 14		
		8	3 → 7 → 8 → 9 → 13 → 14		
		9	3 → 7 → 8 → 12 → 13 → 14		
		10	3 → 7 → 12 → 13 → 14		

reducing total travel time. A greater difference between arc flows exists between single-pedestrian groups (scenario 3) and clustered variable-size groups (scenario 4). The total travel time under scenario 3 is much lower than that under scenario 4. The reason is that individuals in scenario 3 have greater flexibility compared with those in scenario 4.

Figure 2a-d shows the distribution of flows by group over route alternatives between each O-D pair for the scenario involving separable variable-size groups (scenario 2). Consider for example Fig. 2d. Ten efficient routes exist for O-D pair 3-14. Of individuals in group 20, approximately 70 % chose Route 10, while only 10 % of group 1 chose a common route. For group 1, chosen routes are evenly distributed over all efficient options. This differs from group 20 in which the majority of individuals chose the same route and other routes are chosen by very few individuals. This can be attributed to differences in group preference function parameters, i.e. individual sensitivity to route attributes. Group 1's parameters are all very small. Thus, route choice is almost random, since individuals are not very sensitive to route attributes. Parameter settings for group 20 are more significant, which is also reflected in the route decisions. Also contributing to these differences in route choice between groups 1 and 20 is that the value of θ for group 1, indicating the level of discrepancy between actual and perceived utility, is smaller than for group 20. The smaller the value of θ , the larger the difference between perceived and measured disutilities. Similar patterns in flow distribution over routes can be observed for other O-D pairs.

Table 4 Arc flows for scenarios

	Scenario 1			Scenario 2			Scenario 3			Scenario 4					
	Arc	x_a	t_a	Arc	x_a	t_a	Arc	x_a	t_a	Arc	x_a	t_a			
1	342	12	165	1	341	12	165	1	340	12	164	1	357	12	187
2	408	13	192	2	409	13	191	2	410	13	197	2	393	13	179
3	217	14	81	3	217	14	81	3	219	14	84	3	243	14	84
4	124	15	381	4	124	15	380	4	121	15	387	4	114	15	348
5	378	16	148	5	378	16	148	5	369	16	154	5	387	16	152
6	272	17	502	6	272	17	501	6	281	17	498	6	263	17	494
7	449	18	134	7	449	18	134	7	435	18	132	7	459	18	120
8	337	19	585	8	337	19	585	8	344	19	586	8	321	19	563
9	411	20	287	9	411	20	287	9	411	20	280	9	436	20	294
10	255	21	228	10	255	21	229	10	243	21	238	10	266	21	236
11	370	22	363	11	370	22	363	11	368	22	370	11	363	22	356
$\sum_{a \in A} x_a \cdot t_a$	1,268,507			1,268,050			1,271,253			1,275,991					

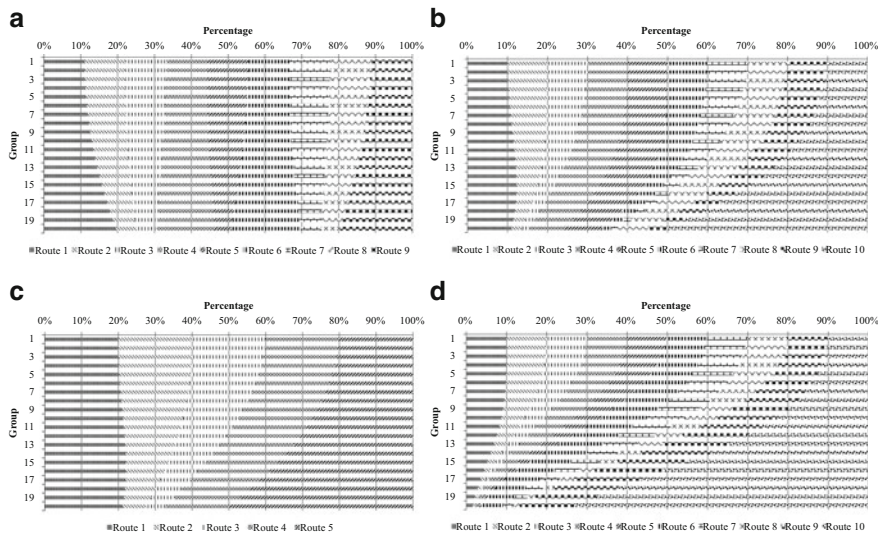


Fig. 2 Distribution of groups over routes by O-D pair for scenario 2. (a) OD 1–11. (b) OD 1–14. (c) OD 3–11. (d) OD 3–14

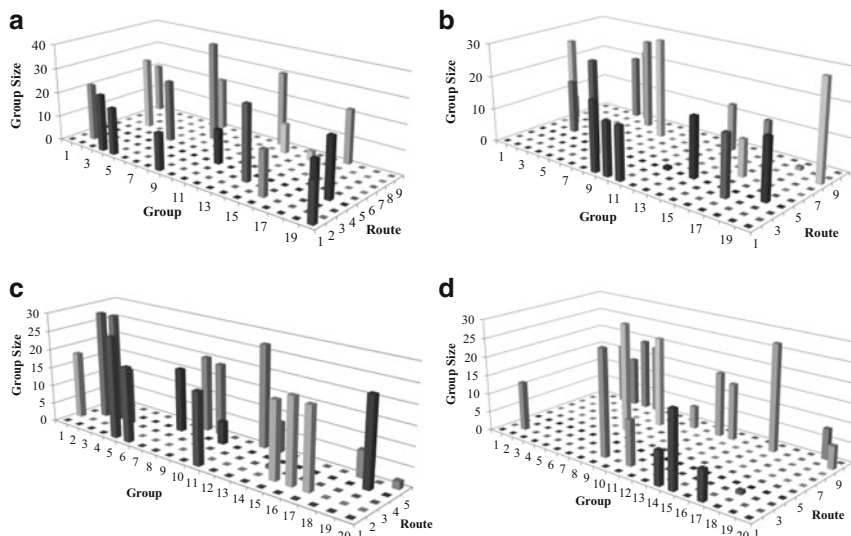


Fig. 3 Distribution of groups over routes by O-D pair for scenario 4. (a) OD 1–11. (b) OD 1–14. (c) OD 3–11. (d) OD 3–14

The distribution of flows for clustered variable-size groups (scenario 4) is depicted in Fig. 3. Although the same group size is used in scenario 4 as in scenario 2, each group in Fig. 3 selects only one route and there is no group that can decrease its total incurred disutility by unilaterally switching routes.

5 Conclusions and Future Work

In this paper, pedestrian route choice is modeled using a traffic assignment type of framework. Methods for estimating the distribution of groups and individuals over “efficient” routes for two types of groups, separable and clustered, are proposed. These methods employ formulations using logit-based SUE assignment and a pure-strategy Nash equilibrium game for separable and clustered groups, respectively. Solution methodologies for solving problems so formulated involves an MSA with groups procedure (for solution to the SUE assignment of separable groups) and a meta-heuristic scheme based on best response dynamic and tabu search (to find the pure-strategy Nash equilibrium of the game formulated for clustered groups). The conceptual framework, and specific models and corresponding solution schemes were tested on an illustrative example. The results from the experiments show the effectiveness and efficiency of the proposed approaches.

There are a number of directions in which the proposed models and solution approaches might be extended. For example, in this paper, the parameters are assumed to be homogeneous within a group. In reality, however, the parameters associated with each group might follow a distribution over individuals. This heterogeneity within each group can be further explored with the proposed models and solution schemes. Furthermore, in this paper, pedestrians make decisions based on route-based performance and once a route is selected, it is assumed that each pedestrian will follow the route in its entirety. The developed model and solution methodology might be extended to address a dynamic pedestrian assignment problem, where physical changes in the network and user goals affect the optimality and choice of routes.

References

1. Aveni, A.F.: The not-so-lonely crowd: Friendship groups in collective behavior. *Sociometry*, 96–99 (1977)
2. Hamacher, H., Leiner, K., Ruzika, S.: Quickest cluster flow problems. In: Peacock, R.D., Kuligowski, E.D., Averill, J.D. (eds.) *Pedestrian and Evacuation Dynamics*, NIST, Gaithersburg, MD, USA 2011, pp. 327–336. Springer (2011)
3. Qiu, F., Hu, X.: Modeling group structures in pedestrian crowd simulation. *Simul Model Pract Th* 18(2), 190–205 (2010)
4. Sheffi, Y.: *Urban transportation networks: Equilibrium analysis with mathematical programming methods*. Prentice Hall (1985)
5. Chen, M., Alfa, A.S.: A network design algorithm using a stochastic incremental traffic assignment approach. *Transport Sci* 25(3), 215–224 (1991)
6. Rosenthal, R.W.: A class of games possessing pure-strategy Nash equilibria. *International Journal of Game Theory* 2(1), 65–67 (1973)
7. Rosenthal, R.W.: The network equilibrium problem in integers. *Networks* 3(1), 53–59 (1973)
8. Nagurney, A.: A multiclass, multicriteria traffic network equilibrium model. *Math Comput Model* 32(3–4), 393–411 (2000)

9. Huang, H.J., Li, Z.C.: A multiclass, multicriteria logit-based traffic equilibrium assignment model under ATIS. *Eur J Oper Res* 176(3), 1464–1477 (2007)
10. Devarajan, S.: A note of network equilibrium and noncooperative games. *Transport Res B-Meth* 15(6), 421–426 (1981)
11. Bovy, P.H.L., Stern, E.: *Route choice: wayfinding in transport networks*. Kluwer Academic Publishers Dordrecht (1990)
12. Al-Gadhi, S.A.H.: A Review study of crowd behavior and movement. *Journal of King Saud University* 8(1), 77–108 (1996)
13. Løvås, G.G.: Models of wayfinding in emergency evacuations. *Eur J Oper Res* 105(3), 371–389 (1998)
14. Bierlaire, M., Robin, T.: Pedestrians choices. In: Timmermans, H. (ed.) *Pedestrian Behavior: Models, Data Collection and Applications*. pp. 1–26. Emerald Group Publishing Limited (2009)
15. Hoogendoorn, S., Bovy, P.H.L.: Pedestrian route-choice and activity scheduling theory and models. *Transport Res B-Meth* 38(2), 169–190 (2004)
16. Antonini, G., Bierlaire, M., Weber, M.: Discrete choice models of pedestrian walking behavior. *Transport Res B-Meth* 40(8), 667–687 (2006)
17. Seneviratne, P., Morrall, J.: Analysis of factors affecting the choice of route of pedestrians. *Transport Plan Techn* 10(2), 147–159 (1985)
18. Daamen, W., Bovy, P.H.L., Hoogendoorn, S.P., Van de Reijt, A.: Passenger route choice concerning level changes in railway stations. In: *Transportation Research Board Annual Meeting, Washington DC 2005*, pp. 1–18. National Academy Press (2005)
19. Ben-Akiva, M., Bierlaire, M.: Discrete choice methods and their applications to short term travel decisions. *Handbook of transportation science* 23, 5–35 (1999)
20. Branston, D.: Link capacity functions: A review. *Transportation Research* 10(4), 223–236 (1976)
21. Fisk, C.: Some developments in equilibrium traffic assignment. *Transport Res B-Meth* 14(3), 243–255 (1980)
22. Feng, L., Miller Hooks, E.: A Mathematical Modeling Approach to Managing Crowd Movements in Large Public Gatherings. In Review (2012)
23. Sureka, A., Wurman, P.R.: Using tabu best-response search to find pure strategy Nash equilibria in normal form games. In: *Proceedings of the Fourth International Joint Conference on Autonomous Agents and Multiagent Systems, The Netherlands 2005*, pp. 1023–1029. ACM (2005)
24. Thalmann, D., Musse, S.R.: *Crowd Simulation*. Springer-Verlag New York, Inc Secaucus, NJ (2007)

Pedestrian Group Behavior in a Cellular Automaton

Michael Seitz, Gerta Köster, and Alexander Pfaffinger

Abstract The study of crowd movement is very important for planning mass events and evacuations. Although many potentially critical incidents are hardly predictable, others like clogging, can be anticipated. Studies have shown that pedestrians in social groups frequently contribute the biggest part to crowds, and that these groups have a significant impact on crowd movement. Furthermore social cooperative behaviour does not stop in emergency situations, but continues or even gets stronger. We employ a cellular automaton with attractive and repulsive potentials for the simulation of individual pedestrians. Then we explain how to integrate a concise model for social groups suitable for the basic modelling techniques. Further aspects of group behavior are discussed, namely large groups and the behavior after a group separation, and we propose a model for these. These investigations lead us to the conclusion that there is a growing need of agent based modelling when facing advanced aspects of pedestrian crowd behavior.

M. Seitz (✉)

University of Applied Sciences, Lothstraße 64, 80335 Munich, Germany

Ludwig-Maximilians-Universität, Geschwister-Scholl-Platz 1, 80539 Munich, Germany

e-mail: m.seitz@hm.edu

G. Köster

University of Applied Sciences, Lothstraße 64, 80335 Munich, Germany

e-mail: gerta.koester@hm.edu

A. Pfaffinger

Siemens AG Corporate Technology, 81739 Munich, Germany

e-mail: alexander.pfaffinger@siemens.com

1 Introduction

One of the most important shortcomings in many crowd simulation tools is the lack of a model for social groups. Especially at mass events one can expect the predominance of social groups over individuals [1]. The concept of mass panic suggested the absence of cooperative social behavior in emergency situations, which is regarded as a myth by now [2]. On the contrary, social bonds dominate the behavior in emergency situations and might even hinder fast evacuation [3]. But social cooperative behavior goes further than predefined groups like families. Even strangers form social groups when faced with emergency situations [4]. However, most of the currently successful simulation models that are able to capture important characteristics of crowd movement, like density-flow relations or the formation of lanes, rely on models from physics, such as Newtonian mechanics, electrodynamics or fluid dynamics. We argue that the modelling of individual pedestrians in the form of e.g. particles is not sufficient to capture crowd movement. In the course of our model development we found that there is a need for agent-based modelling or, at least as in our case, agent-type mechanisms to supplement the physically inspired model.

2 Simulation of Individual Pedestrians with a Cellular Automaton

There are many pedestrian simulation models. Among them the social force model [5] is probably best known. It relies on physical effects, modeled through differential equations. We employ a cellular automaton for the simulation [6, 7].

In any computer simulation, time and space has to be discretized at some point. The cellular automaton divides a plane in cells, like hexagons, as in our case. Each cell is either free or occupied by a person or an obstacle of some kind. An occupied cell can not be entered. In any time step a person can move one cell forward or stay at the current cell, but cannot move more than one cell. Thus a fast person is often allowed to move when a slow person must remain at the current cell.

In this model there are two ways to influence the movement. The first is the orientation or direction of movement. This is done by attractive and repulsive potentials. The target has an attractive potential. We use the fast-marching algorithm, which calculates the travel time of a wave to the target instead of the direct Euclidean distance to determine the potential [8]. Thus pedestrians are not trapped by obstacles. Repulsive forces are placed around obstacles and other pedestrians. The second way to influence the movement is to manipulate the velocity. For further modelling details please refer to previous works, such as [9].

3 Basic Coherence of Small Social Groups

The most important observable effect of a social group is its spacial coherence. Therefore modeling groups in a pedestrian simulation has to reproduce this behavior. Singh et al. [10] model formations of social groups with attractor points, which can be given up for a short time in order to navigate around obstacles. They also use a member of the group, the so called leader, as orientation point. In our model we try to model groups more flexibly. Moussaïd et al. [11] introduce groups for social force models. The main idea is that pedestrians in a social group want to communicate with each other and thus walk abreast. When modeling this they use the center of mass of the group. We use this idea as a part for our group model [12] in the cellular automaton.

At first we also introduce a leader who carries an attractive potential, which only affects persons of the same group. The greater the distance to the leader, the greater the attraction becomes. The term leader does not mean that this person has greater knowledge of the environment or social status. In contrast to other models, the leader is not a fixed member of the group but the one closest to the target. This also implies that the leader can and does change in an ongoing simulation. Thus the other members of the group, the followers, are attracted by the leader.

$$P_l(\delta_l) = \delta_l^4 \cdot \alpha$$

is the attractive potential to the leader with δ_l as distance to the leader. The resulting direction of movement is a compromise between all influences affecting a person that. It points in the direction of steepest decent of the sum of the different potentials. Therefore α also depends on the calibration of the other potentials. In our case we choose $\alpha = 0.003$, which is rather weak in the near field, but still has a recognizable effect. Moreover the effect becomes strong with growing distance. The leader direction is not influenced by any group potential.

Secondly the velocity of the members must be adjusted in order to maintain the group coherence. We calculate the difference δ of the target potential between the center of mass and each member of the group. Members of the group ahead of the center are decelerated and members behind are accelerated. Acceleration and deceleration both increase with greater distance to the center. If a person reaches a maximum velocity it is not accelerated any more.

$$v_{adjusted} = v_{free} \cdot f(\delta_c)$$

Where $v_{adjusted}$ is the speed with which the pedestrian moves at after the consideration of his or her group. The desired speed is denoted by v_{free} scaled by a factor $f(\delta_c)$ that depends on the distance δ_c to the centroid:

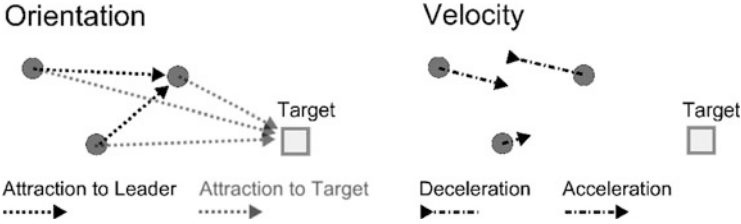


Fig. 1 Illustration of the two influences contributing to the group coherence. Each person of the group is depicted as a circle. The person closest to the target is the leader. Repulsive forces around obstacles and other persons are neglected for simplicity in the illustration. The lower person might also be decelerated depending on the calibration of the model, thus the small arrow indicates that there is only slight acceleration



Fig. 2 Simulation experiment with single pedestrians (*circles*), groups of 2 (*filled circles*), 3 (*triangles*) and 4 (*squares*) walking from *left to right* encountering a *bottleneck* in the *middle* of the path. Different shades of *gray* account for different groups or individuals. Overlapping of symbols is due to oversized depiction of pedestrians for better presentation. Groups stay together and tend to walk next to each other in a formation that facilitates communication

$$f(\delta) = \begin{cases} \beta_1 & \text{if } \delta_c > 8 \\ \beta_2 & \text{if } 8 > \delta_c \geq 1 \\ \beta_3 & \text{if } 1 > \delta_c \geq 0 \\ \beta_4 & \text{if } 0 > \delta_c \geq -1 \\ \beta_5 & \text{if } -1 > \delta_c \end{cases}$$

We obtained good results according to a classroom egress experiment [12] with the following choices: $\beta_1 = 0$, $\beta_2 = \frac{8}{17+\delta}$, $\beta_3 = \frac{1}{1+\delta}$, $\beta_4 = \frac{4}{3}$, $\beta_5 = \frac{5}{3}$.

The function $f(\delta_c)$ embodies two ideas. Firstly members walking ahead slow down and members falling behind slightly speed up to reach the group. Secondly we found that the effect of pedestrians walking abreast can be reproduced by strengthening this adjustment in the range of $-1 < \delta_c < 1$. Figure 1 illustrates both orientation and velocity of the group behavior. In Fig. 2 shows a simulation experiment with small groups of size 2–4 and individual pedestrians encountering a bottleneck.

4 A Model for Larger Groups

At mass events groups of bigger sizes are to be expected. A common assumption, yet without strong empirical evidence, is that large groups separate into smaller subgroups of size 2–4 [10, 14]. We additionally assume that large groups stay together as a whole in a less strict formation. No communication between members of two different subgroups is assumed. Otherwise we use the same mechanism we used for small groups but with weaker influence on the movement. This additional adjustment only affects group leaders. Here we use

$$f(\delta_c) = \begin{cases} \gamma_1 & \text{if } \delta_c \geq 0 \\ \gamma_2 & \text{else} \end{cases}$$

with $\gamma_1 = \frac{8}{8+\delta}$ and $\gamma_2 = 1$ as the speed adjustment function. The attractive potential to the leader of the most advanced group is the same as for small groups. The model for the subgroups stays identical to the one for small groups. Simulation runs imply a strong impact on crowd movement (see Fig. 3). The flow becomes less homogeneous. The pedestrians seem to drag each other along and clogging occurs [14].

5 Agent Aspects for Emergent Situations

The described model yields good results if there are no obstacles in the way. Groups tend to walk abreast and can neglect the group formation when navigating around other pedestrians. But when groups are separated by an obstacle they sometimes get stuck. This is because the attraction to the leader is on the line of sight. If the leader is on one side of the obstacle and a follower on the other side, the follower tries to approach the leader directly through the obstacle. Since this is not possible the follower stands still and the leader waits on the other side.

The simplest way to cope with this situation is to release followers from the group if they can not see the leader anymore, that is, the line of sight between them is intersected with an obstacle. Since this violates our objective of permanent group coherence it is not satisfactory. Another way is to let followers track back to the position where they saw the leader last [13]. If they see the leader from this point they can rejoin the group. About ten times less separations occur in an example scenario with this mechanism.

Some issues remain. Despite the improvement, there are still separations. One can argue that in reality there might also be separations of social groups. But if that is the case we would like to control them. So far we have no empirical evidence, besides our personal experience, that pedestrians deal with separations by tracking back, nor do we know how often permanent separations take place. Most likely this also strongly depends on the scenario and the kind of social

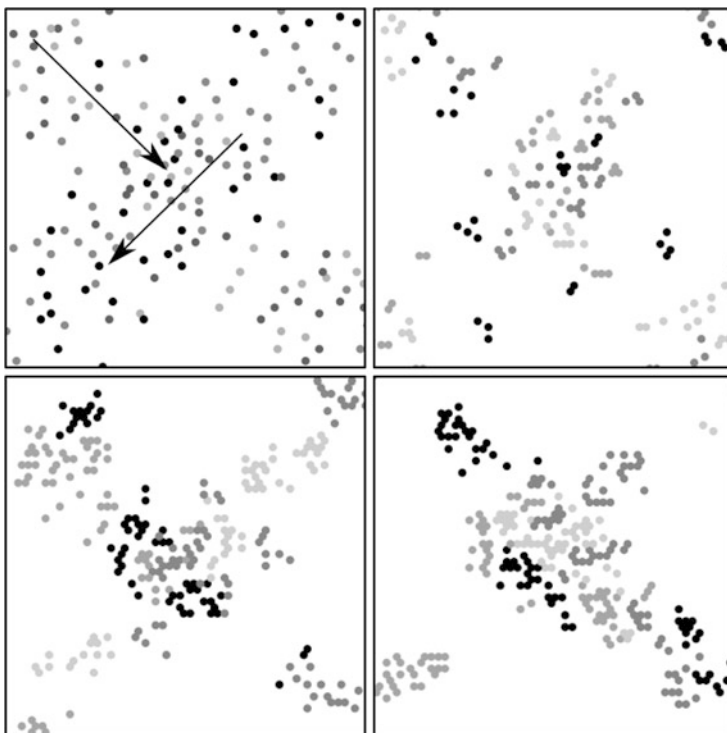


Fig. 3 Comparison of a crossing of two pedestrian streams in the simulation with different group sizes. Pedestrians walk from *top left to bottom right* and *top right to bottom left* respectively. The *two upper Figures* show streams without groups (*left*) and streams with small groups of two to four members (*right*). On the bottom only groups of 14 (*left*) and groups of 24 (*right*) are present

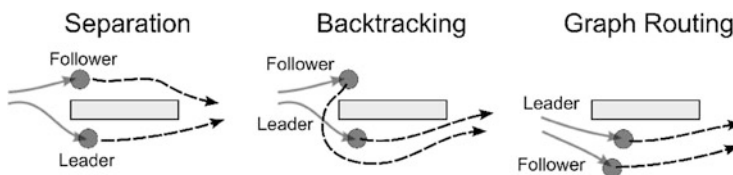


Fig. 4 The illustration shows possible ways how to treat groups with two members after a separation. The lower person is the leader of the group. The *rectangular block* is an obstacle, for instance a wall. Separation: As soon as the members are separated by an obstacle, the group influences are ignored, but are restored after the obstacle. Backtracking: The follower walks back to the position where he saw the leader last and tries to rejoin the group from this point. Graph routing: Members of a group always choose the same path in the first place, separations can be prevented completely

groups in it. With backtracking we introduce agent based modeling aspects into the simulation, which are expensive in terms of computation performance and might not be necessary. Figure 4 shows a comparison of the three approaches.

6 Conclusion

We discussed mechanisms that can be divided in two categories of decision making. The first approach combines different influences, e.g. target attraction, repulsion from other pedestrians, attraction to the leader and chooses the best compromise, most likely by adding up the potentials. This works as long as the situation is somewhat smooth. But there are situations where there is no reasonable compromise and one or more influences have to be neglected completely, as it is the case when a group member has been lost. Then the pedestrian has to decide whether to continue walking towards the target or try to find the group. We implemented this binary decision by introducing agent-type mechanisms into the model. We conclude that the ability to make decisions that cannot be expressed through a physically inspired superposition of forces is necessary when it comes to more complex social pedestrian behaviour. On the other hand we successfully used the paradigm of potentials for the coherence of large groups and even formations in small groups.

References

1. Aveni, A.F.: The Not-So-Lonely Crowd: Friendship Groups in Collective Behavior. *Sociometry* 40(1), 96–99 (1977)
2. Cocking, C., Drury, J., Reicher, S.: The psychology of crowd behaviour in emergency evacuations: Results from two interview studies and implications for the Fire and Rescue Services. *The Irish Journal of Psychology*, 30(1–2), 59–73 (2009)
3. Mawson, A.R.: Understanding Mass Panic and Other Collective Responses to Threat and Disaster. *Psychiatry* 68(2), 95–113 (2005)
4. Drury, J., Cocking, C., Reicher, S.: Everyone for themselves? A comparative study of crowd solidarity among emergency survivors. *British Journal of Social Psychology* 48, 487–506 (2009)
5. Helbing, D., Farkas, I., Vicsek, T.: Simulating Dynamical Features of Escape Panic. *Nature* 407 (6803), 487–490 (2000)
6. Burstedde, C., Klauck, K., Schadschneider, A., Zittartz, J.: Simulation of Pedestrian Dynamics Using a Two-Dimensional Cellular Automaton. *Physica A* 295, 507–525 (2001)
7. Klüpfel, H.: A Cellular Automaton Model for Crowd Movement and Egress Simulation. Doctoral Thesis, Universität Duisburg-Essen (2003)
8. Hartmann, D.: Adaptive Pedestrian Dynamics Based on Geodesics. *New Journal of Physics* 12 (4), 1367–2630 (2010)
9. Köster, G., Hartmann, D., Klein, W.: Microscopic Pedestrian Simulations: From Passenger Exchange Times to Regional Evacuation. Hu, B., Morasch, K., Pickl, S., Siegle, M. (eds) *Operations Research Proceedings 2010: Selected Papers of the Annual International Conference of the German Operations Research Society*, pp. 571–576. Springer, Berlin, Heidelberg (2011)
10. Singh, H., Arter, R., Dodd, L., Langston, P., Lester, E., Drury, J.: Modelling Subgroup Behaviour in Crowd Dynamics DEM Simulation. *Applied Mathematical Modelling* 33, 4408–4423 (2009)
11. Moussaid, M., Perozo, N., Garnier, S., Helbing, D., Theraulaz, G.: The Walking Behaviour of Pedestrian Social Groups and Its Impact on Crowd Dynamics. *PLoS ONE* 5(4) (2010)
12. Köster, G., Seitz, M., Treml, F., Hartmann, D., Klein, W.: On modeling the influence of group formations in a crowd. *Journal of Contemporary Social Science* 6(3), 397–414 (2011)

13. Seitz, M., Köster, G., Hartmann, D.: On Modeling the Separation and Reunion of Social Groups, in Proceedings of the International Conference on Emergency Evacuation of People from Buildings, Warsaw, Poland, 31. March - 1. April 2011.
14. Reuter, V., Bergner, B., Köster, G., Seitz, M., Treml, F., Hartmann, D.: On modeling groups in crowds: empirical evidence and simulation results including large groups, PED 2012.

Modeling Time Duration of Planned and Unplanned Store Visits in a Multi-Agent Simulation of Pedestrian Activity in City Centers

Jan Dijkstra, Harry Timmermans, Joran Jessurun, and Bauke de Vries

Abstract Micro-scale agent-based modeling can be used for the simulation of pedestrian movement for low and high density scenarios and for the effect of changes in an environment. Such models can also be used for pedestrian dynamics in city centers to show the design effects in the shopping environment. The main contribution of this paper is to introduce the implication of time duration of a visit to a store within a simulation framework for pedestrian movement simulation. The paper reports findings of time spent in a store.

Keywords Pedestrian activity • Pedestrian behavior • Multi-agent simulation

1 Introduction

Agent-based modeling is a computational methodology that allows us to create, analyze, and experiment with artificial worlds populated by agents. A specific research area is micro-scale agent-based modeling that can be used for the simulation of pedestrian movement for low and high density scenarios and for the effect of changes in the environment. Such models can also be used for pedestrian dynamics in city centers to show the design effects in the shopping environment. In this context [1] describe their multi-agent simulation prototype of customers' shopping behavior in a mall. Therefore, a multi-agent model to simulate pedestrian dynamic destination, route and scheduling behavior is under development, where

J. Dijkstra (✉) • J. Jessurun • B. de Vries

Design Systems Group, Eindhoven University of Technology, Eindhoven, The Netherlands
e-mail: j.dijkstra@tue.nl; a.j.jessurun@tue.nl; b.d.vries@tue.nl

H. Timmermans

Urban Planning Group, Eindhoven University of Technology, Eindhoven, The Netherlands
e-mail: h.j.p.timmermans@tue.nl

the simulation of movement patterns is embedded in a more comprehensive model of activity travel behavior.

Representation is a main issue in simulating pedestrian dynamics. One can distinguish the representation of the pedestrian environment and the representation of pedestrians. In the domain of a city center, representation of a pedestrian environment includes the geometry of the shopping environment such as stores and streets, the network as a cellular grid, and pedestrian objects. Pedestrian representation includes socioeconomic characteristics, speed, goals, familiarity with the environment, and activity agenda. It is assumed that pedestrians perceive their environment and that they are supposed to carry out a set of activities. For completing an activity, pedestrians spend time in stores. As a consequence, time duration influences their movement behavior over the network.

Although a 3D presentation of pedestrians and the pedestrian environment for the simulation of pedestrian movement is the ultimate goal, it is nevertheless meaningful to test the underlying principles in an appropriate 2D representation of pedestrians and their environment. NetLogo can be used as a simulation toolkit because it is a suitable simulation framework that supports modeling, simulation and experimentation. It also offers skeletons of agents and their environment, and interoperability (e.g. GIS). We will use shape-file information of the environment and network structure for visualizing the 2D environment and NetLogo for the actual simulation.

The main subject of this paper is to introduce the implication of time duration of a visit to a store within a simulation framework for pedestrian movement simulation. This framework involves an agent-based model that provides an activity agenda for pedestrian agents that guides their shopping behavior in terms of destination and time spent in shopping areas. In order to implement the activity agenda, pedestrian agents need to successively visit a set of stores and move over the network. It is assumed that pedestrian agents' behavior is driven by a series of decision heuristics. Agents need to decide which stores to choose, in what order and which route to take, subject to time and institutional constraints. It is assumed that pedestrian agents are in different motivational states. They may at every point during the trip have general interests in conducting particular activities, without having decided on the specific store to visit, but they may also be in a more goal-directed motivational state in which case they have already decided which store to visit. The motivational states are of influence on the impulse and non-impulse store choice processes and therefore on the planned and unplanned visits to a store. All these aspects affect pedestrian agents' time duration in visiting stores. Pedestrian agents move over a street network and are part of a pedestrian flow in this street network. However pedestrian agents can be temporarily removed from the pedestrian flow by visiting a store and participating again in the pedestrian flow after visiting that store. In that case, the time spent by a pedestrian agent in a store is relevant. For the simulation run this time duration is determined by a Monte Carlo simulation. The findings from the collected data of the duration of a visit to a store indicate that this time duration meets the Weibull distribution, and that this duration also depends of the store category as well as the priority of the store.

This paper gives in Sect. 2 a brief description of the pedestrian movement simulation. Section 3 presents the data collection efforts for the experimental design. Section 4 reports findings of time spent in a store. A discussion about the conclusions and future directions will conclude this paper.

2 Pedestrian Movement Simulation

Pedestrian movement simulation consists of pedestrian agents and a simulation environment, which consists of a street network and a set of stores. Polygons are used to indicate borders and functional areas such as walkways. Each cell in the network has information about which agents and polygons occupy it. Also, it contains information about other features such as appearance of stores that are observable from that cell. A pedestrian agent moves with his own behavior and personal characteristics. Every time step, there is an update about agent's positions. The cellular network provides percepts to the pedestrian agent and the pedestrian agent performs actions based on their percepts. Behavioral principles drive the pedestrian movement. Details of the equations representing these behavioral principles are beyond the scope of this paper and are presented in [2].

In the case of the test ground of the city center, each store consists of a cell containing store information. A street network consists of cells with cell information. Pedestrian agents are situated in the cells of the network, namely a street cell or a store cell. The network is irregular because a clear border between a store and adjacent cell is desired. Additionally, each cell in this network is identified by its node and these nodes are linked together.

For populating pedestrian agents in the environment and for attaching activity agendas to pedestrian agents, a Monte Carlo simulation is used which implies that the behavior of each pedestrian agent is simulated by a series of draws of random numbers from successive probability distributions [3]. These probability distributions are based on real data collections, such as time spent in a store, attaching inner lane or outer lane as an entry point, speed, and pedestrian characteristics (gender, age, etc.).

NetLogo is used for the simulation because it easily allows the empirical testing of the principles of the simulation approach. An attractive feature is its ability to integrate GIS data directly into the simulation. With the integration of GIS, pedestrian agents can move around 'real space'. In the simulation, MapInfo data will be integrated with NetLogo. On the basis of this GIS, a network structure with nodes and links will be generated. The nodes are related to polygons in the original drawing, and the links will be determined by the topology of the polygons. The information of the polygons is available for pedestrian agents moving in the network. This information could be store-related information, but also information about the area and perimeter of the polygon.

Figure 1 shows the activity diagram of the simulation setup. The simulation process starts with loading the environment involving GIS information and databases

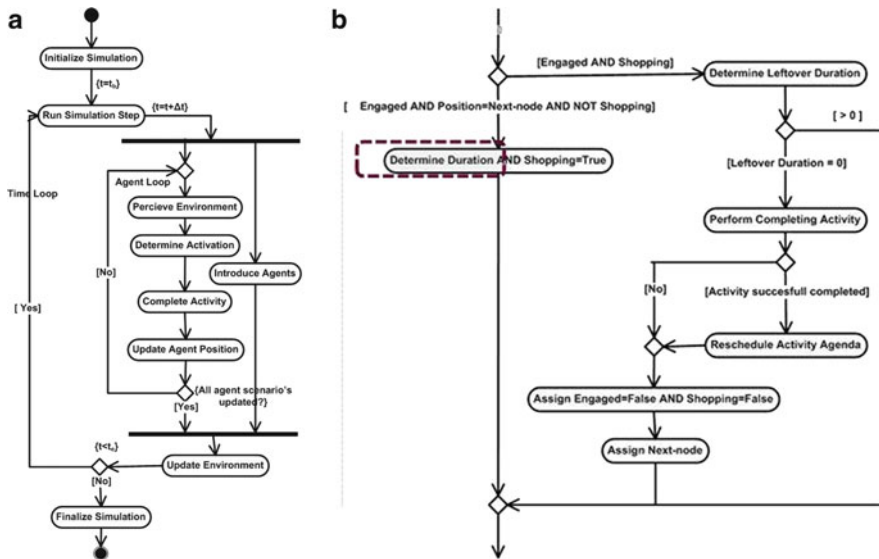


Fig. 1 Activity diagram of (a) the simulation setup and (b) completing an activity

for instance activity agendas and personal characteristics for creating pedestrian agents. The creation of an initial situation at time t_b (beginning time) means that the environment will be populated with pedestrian agents. The simulation run starts at time t_b . The simulation *time step* includes the creation of zero or more pedestrian agents using the Monte Carlo method: a pedestrian agent would need to be assigned an initial scenario. Also, there is an update of pedestrian agent scenario's that results in pedestrian agent actions and a schedule of the next step. The consequence is the movement to a new position. Then, an update of the environment will be realized. The simulation run stops at time t_e (ending time).

3 Simulation Process

This section provides some understanding in the engineering basis of the simulation process using NetLogo [4]. The model structure is based on *contexts* and *projections* [5]. The core data structure is called a context that represents from a modeling perspective an abstract population; the objects in these populations are referred as agents. The context provides the basic infrastructure to define a population and the interactions of that population; it creates an abstract environment in which agents exist at a given point in the simulation. The context also holds its own internal state for maintaining the collection of agents. This state can consists of multiple types of data. These provide agents with information about the world in which they interact. In addition, data fields can be maintained by the context. A data field is an

n-dimensional field of values with which the agents in a context can interact. These data fields can be directly associated with a physical space. The field is generic, which means each value is derived from a set of coordinates.

Projections take the population as defined in a context and impose a new structure on it. This structure defines and imposes relationships on the population by using semantics defined in the projection; therefore an agent population is realized once a projection is applied to it. This means that projections are added to a context to allow agents to interact with each other. Each context can have an arbitrary number of projections associated with it (1-n relationship); in our case it concerns about two projections.

A feature of NetLogo is the ability to integrate GIS data directly to the simulation; it provides a set of classes that allow shape-files to be displayed. For example, shape-files can be provided by MapInfo and ArcGIS. A GIS contains multiple layers of data; each layer is made up of a number of elements. Each feature in the layer in the layer has two aspects to it, its geographical coordinates (but it could be also a polygon, polyline or polypoint) and the data associated with it [5]. GIS store data about layers in database files, with each record in the file referring to a feature in GIS. Actually, NetLogo integration with GIS means shapefile integration while they use the same shape-file; NetLogo is used to read the shape-file data. Agents are created using these data and the simulation process. This means that the context creator provides the population. Agents can be created, re-created and destroyed at every simulation step. The interaction with the environment is provided by the shape-file containing GIS data; multiple GIS layers are the projections within NetLogo. Two projections are assumed, one for the GIS data and the other one for the generated network from this GIS data. The context needs these GIS data for the data fields which provides the information from the environment.

In this approach, the environment consists of polygons representing the network of stores and streets. The presence of adjacent cells means that connections are possible, for instance pedestrian agents can move from a “street” cell to an adjacent “store” cell. If cells are not strictly adjacent, no movement from each other is possible. Cells containing store information are not always strictly adjacent, for example. In MapInfo, feature data will be connected to cells of the network and layers will be created. After that, MapInfo provides the shape-file that will be loaded in NetLogo. This shapefile provides the environmental information. The simulation run can be performed.

Each cell in the network has a node. An agent is located in a node on the underlying representation and can move on the implicit generated network to other nodes. Strictly speaking, it does not follow a cellular automata approach because an agent moves from node to node and is situated randomly in the cell related to that node.

The test ground is the inner-city center of Eindhoven. The simulation will be performed on a part of this city center, particularly on a section of the city center.

Table 1 shows a number of features as part of the provided MapInfo GIS database; each cell in the network includes these features such as an identification number, type indicating store cell or street cell, and category indicates store category

Table 1 Polygon features of the network

Identification	Type	Category	Description	Priority
12,002	0	5	McDonalds	1.00
12,004	0	3	Etos	1.05
11,001	0	1	C&A	2.30
13,001	1	0	C&A	0.00

(for example category number 3 represents a health and body store). This database is used by the data fields that are used in NetLogo for environmental information for pedestrian agents perceiving this environment. Priority means the proportion of visits; for example a priority of 2.3 means that 2.3 % of the visits are intended to visit that store.

The pedestrian agent model system simulates which shopping activities are conducted by pedestrians, where (destination choice), when (choice of timing), for how long (duration), and which route is used for implementing the activity agenda (route choice). All these activities influence pedestrian's positions in the simulation run. Data collecting efforts are needed to calibrate the agent model system for the test ground: a survey that is a sample of respondents who are asked about their activity agenda. This survey includes questions for pedestrians who have completed their visit to the city center and ask them about the nature of their completed activity patterns (which store, for how long, sequence, and route). Also, a survey was conducted about pedestrian's awareness of stores and signaling intensity of stores as well as the visit of a store and the completion of activities.

4 Time Duration

Time duration is the time spent by a pedestrian in a store. For the simulation run the time duration is determined by a Monte Carlo simulation.

The findings from the collected data of the duration of a visit to a store indicate that this duration meets the Weibull distribution, and that this duration is dependent of the store category as well as the priority of the store. Figure 1 shows the activity diagram of completing an activity in which time duration will be determined.

The Weibull probability function is given by:

$$f(x; k; \lambda; \theta) = \frac{k}{\lambda} \left(\frac{x - \theta}{\lambda} \right)^{k-1} e^{-\left(\frac{x - \theta}{\lambda} \right)^k} \quad (1)$$

where, k is the shape parameter ($k > 0$), λ is the scale parameter, and θ is the location of the distribution.

Table 2 shows the values of the parameters of the Weibull distribution for different store categories. The specific store category includes among others jewelry, bell companies, candy shop, etc. Striking is the distinction in clothing stores on

Table 2 Weibull parameters at different store categories

Category	Description	Priority (%)	K	λ	θ
1	Clothes	≥ 1	1	1	0.46
1	Clothes	≥ 0.5 and < 1	1.22	.99	0
1	Clothes		1.80	.80	0
2	Shoes		1.10	.62	0
3	Body and health		1.65	.75	0
4	Department store		1.47	.83	0
5	Specific	< 0.7	1.22	.88	0
5	Specific	≥ 0.7	1.32	.48	0

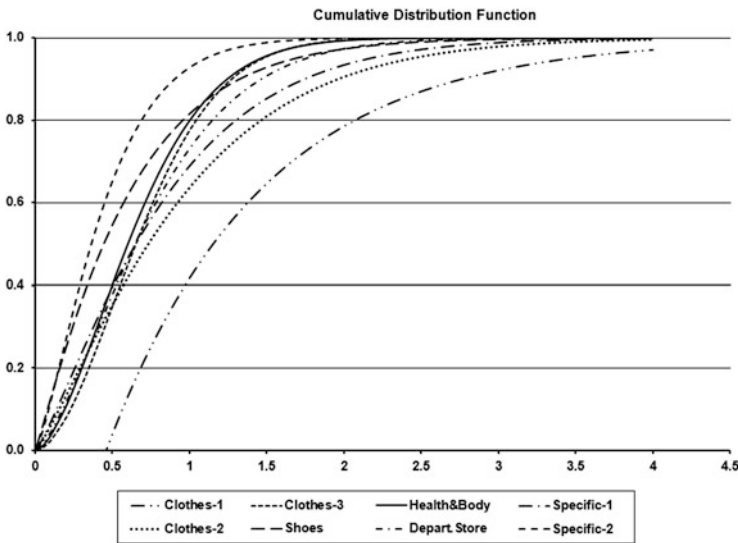


Fig. 2 Weibull probability density function at different k, λ, θ

the prioritization. Figure 2 shows the corresponding distribution functions. The percent point function $G(p)$, which is the inverse cumulative distribution function, is given by:

$$f(x; k; \lambda; \theta) = \frac{k}{\lambda} \left(\frac{(x - \theta)}{\lambda} \right)^{k-1} e^{-\left(\frac{(x - \theta)}{\lambda} \right)^k} \tag{2}$$

Given a random number p from a uniform distribution in the interval $(0, 1)$, the value of $G(p)$ has a Weibull distribution with parameters k, λ , and θ . That means, given a random number p on the x-axis provides the time duration on the y-axis. Figure 3 shows the percent point function.

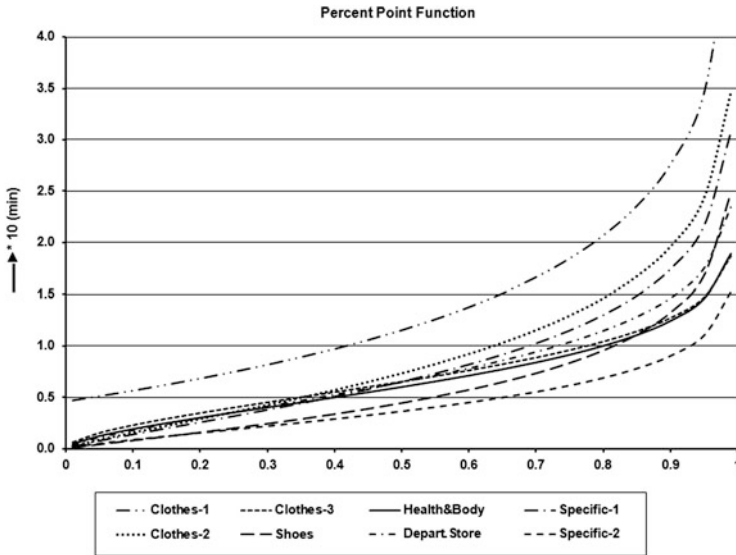


Fig. 3 Percent point function at different k, λ, θ

5 Discussion and Future Directions

In this paper, we presented a simulation platform for performing the pedestrian movement simulation principles were discussed as well as the simulation process. In the current state of the pedestrian agent model system, which is the simulation, all data for the pedestrian movement simulation were collected. The findings about the determination of time duration of visiting a store when completing an activity were presented. The framework for processing agent-based pedestrian activity simulations will be implemented and all the data will be integrated in the agent model system. This is a step by step process. At this moment, the signaling intensity of a store is represented by a priority of visiting the selected regarding store. At this moment, the store visits are not split up in planned and unplanned visits.

The pedestrian model system will be tested in a 2D environment, because we want to validate the basic principles. Also, pedestrian agents move from node to node and are situated into the cells related to those nodes. They are situated randomly in those cells, but if the area is occupied they cannot move to that cell. This reduces the complexity of the simulation by ignoring collisions and with that collision detection. These certain characteristics of the system make the simulation feasible because computer power is less binding. If all the parts are implemented, validation of the pedestrian model system will be performed. The data collection will be split up into two parts and the results of the separate simulation experiments will be compared.

Future developments should make the pedestrian agent model suitable for a 3D environment with lifelike virtual persons. In that case, the pedestrian agent movement will be realized from cell point to cell point considering collision detection. Finally, this will result in a virtual environment of a real situation, populated with virtual persons and a real person (user) moving amongst these virtual persons. A user can assess an environment that has high reality content. Preferences of users can be collected and the utility of a proposed situation can be estimated where appropriate. With this approach, it is possible to gain a deeper insight into the activity behavior of city center visitors and thus in the pedestrian flows in city center environments, even for those that do not exist yet.

References

1. W. Ali and B. Moulin, "How artificial intelligence agents do shopping in a virtual mall: a 'believable' and 'usable' multi-agent based simulation of customers' shopping behavior in a mall", in *Canadian AI, LNAI 4013*, L. Lamontagne and M. Marchand, Eds. Berlin: Springer-Verlag, 2006, pp. 73–85.
2. J. Dijkstra, H. J. P. Timmermans, and B. de Vries, "Activation of shopping pedestrian agents – empirical estimation results," *Proc. Of the 11th Conference on Computers on Urban Planning and Urban Management CUPUM'09*, Hong Kong, June 2009 (CD-ROM).
3. M. Bierlaire, G. Antonioni, and M. Weber, "Behavioral dynamics for pedestrians," in *Moving through Nets: the Physical and Social Dimensions of Travel*, K.W. Axhausen, Ed. Elsevier Science Ltd., 2005, pp. 81–105.
4. W. Zhu and H. J. P. Timmermans, "Cut-off models for the 'go-home' decision pedestrians in shopping streets," *Environment and Planning B: Planning and Design*, vol. 35, no. 2, 2008, pp. 248–260.
5. R. Najlis, and M. J. North, "Repast for GIS," in *Proc. Of the Agent 2004 Conference on Social Dynamics: Interaction, Reflexivity and Emergence*, C. M. Macal, D. Sallach, and M. J. North, Eds. Chicago, Illinois, 2004, pp. 225–260

Motions Effect for Crowd Modeling Aboard Ships

K.V. Kostas, A.-A.I. Ginnis, C.G. Politis, and P.D. Kaklis

Abstract Pre-computed ship-motion history has been used in the multi-user Virtual Reality (VR) system VELOS in conjunction with a kinematically-oriented *inclination* steering behavior as simple means for considering the effects of ship motion on simulated passengers' movement. This first approach does not account for the dynamic nature of the phenomenon, thus ignoring motion accelerations. Ship-motion accelerations, however, are critical to the assessment of a person's balancing and/or sliding aboard ships and consequently to its capability of performing an assigned task. In this work, we are focusing on the exploitation of pre-computed ship motions and accelerations and we investigate the usage of the concepts of Motion-Induced Interruptions (MIIs) and tipping coefficients in modeling the effects of ship-motion accelerations on passengers.

Keywords Evacuation simulation • Ship motions • Motion-induced interruptions

1 Introduction

Virtual Environment for Life On Ships: V.E.L.O.S [1] is a multi-user Virtual Reality (VR) system that aims to support designers to assess (early in the design process) passenger and crew activities aboard a ship for both normal and hectic conditions of operations and to improve the ship design accordingly. The crowd

K.V. Kostas (✉) • C.G. Politis
Department of Naval Architecture (NA), Technological Educational Institute of Athens (TEI-A), Athens, Greece
e-mail: kvkostas@teiath.gr; cpolitis@teiath.gr

A.-A.I. Ginnis • P.D. Kaklis
School of Naval Architecture and Marine Engineering (NAME), National Technical University of Athens (NTUA), Athens, Greece
e-mail: ginnis@naval.ntua.grdeslab.ntua.gr; kaklis@deslab.ntua.gr

modeling component of VELOS is build upon the steering behaviors technology and related enhancements that allow for consideration of passenger grouping and crew assistance behavior effects in ship-evacuation simulations [2].

Furthermore, VELOS provides communication interfaces enabling data import from computational packages, including *sea-keeping* and fire events modeling software. Pre-computed ship-motion history has been used in VELOS in conjunction with a kinematically-oriented *inclination* steering behavior as a first simple step for considering the effects of ship motion on simulated passengers' movement. Inclination behavior resembles in definition and effect the influence of a gravity field that would hinder agent motion accordingly. The aforementioned approach is a simple kinematic model that does not account for the dynamic nature of the phenomenon thus ignoring motion accelerations. Ship-motion accelerations, however, are critical to the assessment of a person's balancing and/or sliding aboard ships and consequently to its capability of performing an assigned task. In this work, we are focusing on the exploitation of pre-computed ship motion accelerations, readily available by the connected sea-keeping computational packages. Based on the works by Graham et al. [3, 4] and Crossland et al. [5] we investigate the usage of the therein introduced concepts of *Motion-Induced Interruptions (MIIs)* and *tipping coefficients* towards modeling the effect of ship-motion accelerations on passengers aboard.

Specifically, in accordance to the calculated *tipping coefficients* and *MII*, we modify steering behaviors' weighting and/or behavior parameters to address the corresponding possibility of a motion interruption and degradation of assigned tasks' effectiveness. The assumption employed here is that a ship-motion-interrupted simple task, such as walking from point A to point B with MII incidents, could equivalently be modeled by appropriately modifying the steering-behavior blending leading to an analogous deduction of task effectiveness.

The rest of the paper is structured in three sections. Section 2 presents VELOS along with its major components and functionalities. Section 3 describes the ship-motion module of VELOS for both the simplified (kinematic) and dynamic approach. Finally, in Sect. 4, example involving typical passenger and crew movements aboard ship is presented. The simulated passengers' movement is examined with and without consideration of the ship motions effect.

2 The VELOS Environment

VELOS is based on *VRsystem* [6], a generic multi-user environment with a broad range of functionalities including geometric- and VR-modeling, as well as crowd microscopic modeling through a library of steering behaviors. Additionally, *VRsystem* can communicate with computational packages, e.g., sea-keeping software for improving the environment realism and taking into account ship-motion effect on passengers' movements. VELOS evacuation-specific functionality is greatly enhanced by the VR nature and client-server architecture provided by *VRsystem*,

namely, the participation and real time interaction of remote multiple users in the form of avatars. These VRsystem-inherited features entail a very distinctive approach to evacuation analysis in VELOS, when compared with evacuation tools in pertinent literature [7, 10]. The major key-points of the evacuation-specific functionality of VELOS are:

1. An integrated framework for both the *International-Maritime-Organization (IMO) simplified* and the *IMO-advanced* method of evacuation analysis.¹ Especially for the advanced method, we enhance IMO's approach by eliminating some important model omissions (e.g., ship motion, fire) and restrictive assumptions (e.g., simplistic crowd behaviors, full availability of escape arrangements).
2. Enrichment of the geometrical model of the ship with topological information for the improvement and better support of the path-planning procedure.
3. Efficient communication through a number of interfaces that enable dynamic specification and handling of the required input data. These data comprise passenger/crew demographics and allocation, behavioral parameters, environmental conditions (fire, flooding) as well as ship motions.
4. Post-processing of the fundamental output (agent trajectories) for extracting evacuation-specific information, e.g., travel-time distribution, cumulative arrival time, passenger densities at specified areas.

2.1 Crowd Modeling

Steering behaviors technology is the basis of VELOS crowd modeling module. Individual agents are powered by an artificial intelligence structure, referred to in the pertinent literature as mind; see [14, 15]. The mind utilizes a collection of simple kinematic behaviors, called steering behaviors, to ultimately compose agents' motion. Specifically, for each time frame, agents' velocity vector is computed by adding the previous velocity vector to the mind-calculated steering vector. This vector, in a simple approach, is a weighted average combination of the individual steering vectors provided by each associated steering behavior in agent's mind. The resulting steering vector is clipped to max_force parameter value and the resulting velocity vector is also clipped to another parameter value: max_velocity. This last parameter is generally different for each agent and follows the distributions of maximum speeds suggested by IMO for passenger and crew demographics (see [1, 2] for additional details).

Nearly 20 steering behaviors have been so far implemented within VELOS. These behaviors, based on the works of C.W. Reynolds [14] and R. Green [15], include: *Seek, Arrive, Wander, Separation, Cohere, Leader Follow, Obstacle Avoidance & Containment, Path-following, Pursuit, Flee, Evade, offset-{Seek, Flee, Pursuit, Evade, Arrive}*.

¹IMO, MSC. Circular 1,238.

2.2 Ship Motions and Accelerations

VELOS provides several interfaces for the consideration of ship motions and accelerations. Specifically, there are modules that allow importing of pre-computed ship responses either in the frequency or time domain. Furthermore, there is also functionality for importing time histories of linear velocities and accelerations for selected points aboard a ship that are recorded with the aid of accelerometers. Thus, ship accelerations can be either estimated via numerical differentiation of ship motions or acquired from the experimental measurements.

Generally, ship motions comprise time histories of the displacements of a specific point P of ship (usually ship's center of flotation) as well as time histories of ship rotational motions (pitch, roll and yaw). Using numerical differentiation we can calculate linear velocity \mathbf{v}_p and acceleration $\dot{\mathbf{v}}_p$ of point P and angular velocity $\boldsymbol{\omega}_B$ and acceleration $\dot{\boldsymbol{\omega}}_B$ of the ship. Then, using the following well-known relations from rigid-body kinematics we can calculate velocity and acceleration at every point Q on ship:

$$\mathbf{v}_q = \mathbf{v}_p + \boldsymbol{\omega}_B \times \mathbf{r}_{pq}, \quad (1)$$

$$\dot{\mathbf{v}}_q = \dot{\mathbf{v}}_p + \boldsymbol{\omega}_B \times (\boldsymbol{\omega}_B \times \mathbf{r}_{pq}) + \dot{\boldsymbol{\omega}}_B \times \mathbf{r}_{pq} \quad (2)$$

where, \mathbf{r}_{pq} the vector formed by P and Q.

3 Motion Effects Modeling

The effects of ship motions on passengers and crew aboard are modeled in two ways as it is presented in detail in the sequel. The first simplified approach is based on a kinematic modeling that utilizes the ship motions while the second approach takes into account the dynamic nature of the phenomenon and relies on the availability of ship accelerations

3.1 Inclination Behavior

Advanced evacuation analysis in VELOS is combining the availability of ship motion data with the so-called *Inclination* behavior that has been introduced, as a first layer, for considering the effect of ship motion on agent's movement. Pre-computed ship-motion history is imported in VELOS through a suitable series of interfaces. Inclination behavior resembles in definition and effect the influence of a gravity field that would hinder agent motion accordingly. Specifically, we consider a static global force-vector \mathbf{g} normal to deck's plane in the upright position of the ship.

If the deck deviates from its upright position (i.e., non zero heel, and/or trim, angles), the projection of \mathbf{g} on it will obviously acquire a non-zero value \mathbf{g}_p , which forms *Inclination's steering vector* as follows: $\mathbf{f}_i = \lambda(\phi)\mathbf{g}_p$, where $\lambda(\phi)$ is an appropriate weight function depending on the angle ϕ formed between \mathbf{g} and the normal to the deck plane. Inclination behavior is active when ϕ lies between two threshold angles: the lower threshold is used to discard plane motions with negligible effect on agent's motion, while values above the upper threshold lead to movement inability, as the limit of agent's balancing capabilities is surpassed. Threshold angles and the weight function $\lambda(\phi)$ are defined via experimental data; see, e.g., [11, 12].

3.2 Motion Induced Interruptions (MII)

During certain weather conditions, i.e., rough weather, walking and even more working in the ship becomes difficult and even the most experienced sailors will experience events where they must stop their activity, be it a specific task or merely standing, and take suitable measures to minimize the risk of injury, or more generally change their stance so that balance can be retained; these events are called, in pertinent literature, Motion-Induced Interruptions (MIIs). MIIs can be identified by considering the dynamic equations of motions of the person due to ship motion leading to the onset of loss-of-balance due to tipping or sliding.

Baitis et al. [13] and Graham et al. [3, 4] have proposed the following relations for the consideration of tips to port or starboard. Specifically, a tip to port will occur if:

$$T_{LATp} = \frac{1}{g} \left(\frac{1}{3}h\ddot{\eta}_4 - \ddot{D}_2 - g\eta_4 - \frac{l}{h}\ddot{D}_3 \right) > \frac{l}{h}, \tag{3}$$

and a tip to starboard if:

$$T_{LATs} = -\frac{1}{g} \left(\frac{1}{3}h\ddot{\eta}_4 - \ddot{D}_2 - g\eta_4 + \frac{l}{h}\ddot{D}_3 \right) > \frac{l}{h} \tag{4}$$

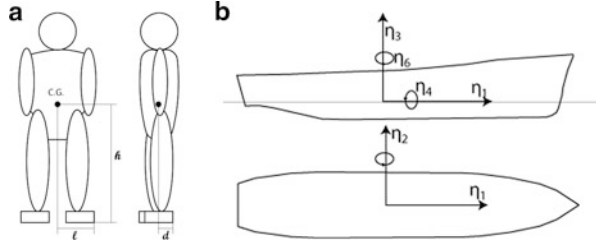
Similarly, the following tipping coefficients can be derived when considering tips to the aft or fore part of the ship:

$$T_{LONa} = \frac{1}{g} \left(\ddot{D}_1 + \frac{1}{3}h\ddot{\eta}_5 - \frac{d}{h}\ddot{D}_3 \right) > \frac{d}{h} \tag{5}$$

$$T_{LONf} = \frac{1}{g} \left(\ddot{D}_1 - \frac{1}{3}h\ddot{\eta}_5 - \frac{d}{h}\ddot{D}_3 \right) > \frac{d}{h}$$

In the above equations, η_1 (surge), η_2 (sway), and η_3 (heave) stand for the translational while η_4 (roll), η_5 (pitch) and η_6 (yaw) stand for the rotational components of ship motion along the x-, y- and z- axis of the ship-coordinate system, respectively; see Fig. 1b. Furthermore, $\mathbf{D} = (D_{-1}, D_2, D_3) = (\eta_1, \eta_2, \eta_3) + (\eta_4, \eta_5, \eta_6) \times (x, y, z)$ denotes the displacement of point P (x, y, z). Finally, symbols l , h and d denote the

Fig. 1 (a) Person half-stance, C.G. and half-shoe width (b) Ship coordinate system



half-stance length, the vertical distance to person’s center of gravity and half-shoe width respectively as shown in Fig. 1a. Typical values for $\frac{l}{h}$ lie in the interval (0.20, 0.25) while for $\frac{d}{h}$ lie in (0.15, 0.17).

In the context of steering behaviors technology agent’s velocity at each time frame is calculated as follows:

1. Compute steering vector $f = \sum w_i f_i$ where w_i are weights and f_i are the individual steering vectors from each simple behavior included in agent’s mind.
2. New velocity is computed as:

$$v_{new} = \begin{cases} (v_{prev} + f) \frac{\max_velocity}{\|v_{prev} + f\|} & \text{if } \|v_{prev} + f\| > \max_velocity \\ (v_{prev} + f) & \text{otherwise} \end{cases} \quad (6)$$

Taking into account the above discussion concerning tipping coefficients, the effect of ship motions on passenger movement is implemented in the following way:

1. Adjustment of max_velocity according to the following rule:

$$\max_velocity = \begin{cases} as\ is, & \text{if } T_{LAT} < 0.20 \\ \max_velocity (-20T_{LAT} + 5), & \text{if } 0.20 < T_{LAT} < 0.25 \\ 0, & \text{if } T_{LAT} > 0.25 \end{cases} \quad (7)$$

That is, we have a linear reduction of max_velocity when $T_{LAT} > 0.20$ leading to a zero max_velocity when $T_{LAT} > 0.25$ (Motion Induced Interruption).

2. Adjustment of w_i weight values in computation of the steering vector. A typical scenario would include an increase of the wander behavior contribution and a decrease in Obstacle Avoidance and Separation contribution.
3. Adjustment of the parameters of each individual steering behavior. Such adjustments include (a) the increase of the radius and position of the *wandering circle* for the wander behavior, which essentially leads to a wider range of possible turning angles and (b) the reduction of the neighborhood radius of Separation behavior allowing passenger agents to come closer to each other. (For a description of Separation and Wander behaviors see [2, 15]).

Fig. 2 Points A, B and C on deck 5

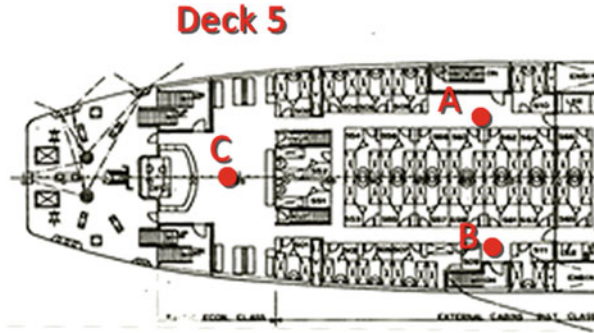
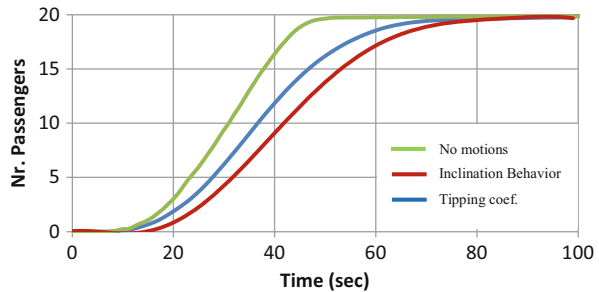


Fig. 3 Average cumulative arrival time for test cases 1, 2 and 3



4 Ship Motion Example

In this section, we examine passengers’ movement on Deck 5 of a RO-RO passenger ship with and without ship motions’ effect consideration. Specifically, we simulate the movement of two groups of passengers (20 persons) from points A and B respectively, to point C (see Fig. 2) in still water, and at a sea state described by a wave spectrum with 4 m significant wave height, 11 s peak period and 90° ship heading (beam seas). Ship responses were pre-computed and imported into VELOS using the SWAN seakeeping software package [16]. The cases examined have as follows:

- Test Case 1 (No waves): Still water
- Test Case 2 (Sea state as described above): Kinematic modeling of motion effects through inclination behavior
- Test Case 3 (Same sea state): Dynamic modeling using tipping coefficients implementation.

Figure 3 depicts the average cumulative arrival time to point C for each of the three example cases. Each of the test cases has been simulated 500 times and the average travel times and arrival rates at point C have been collected. As it can easily be seen from this figure the time required for the prescribed passengers’ movement is the least when we are in still water. The effect of the wavy sea state which induces ship motions and hinders passengers’ movement is illustrated with the right-shifting of the remaining two curves. The total travel time needed for both

inclination behavior and tipping coefficient modeling is about the same (~ 70 s) and considerably higher than the still water case (~ 50 s), where, obviously, no motion effect is considered. However the arrival rate (slope) for the tipping coefficient modeling is steeper than the slope of the curve corresponding to the kinematical approach.

5 Conclusions

We have demonstrated the usage of the two (kinematic and dynamic) ship motions' effect modeling approaches in a simple simulation example aboard a ship. The example results provide some first evidence that the followed modeling approaches are capable of capturing, at least qualitatively, the effect of ship motions on passengers and/or crew movements. A next step in our work will obviously involve the usage of the approaches in a full passenger ship evacuation scenario and the comparison of the simulation output with experimental results.

References

1. A.I. Ginnis, K.V. Kostas, C.G. Politis, & P.D. Kaklis, 2010, "VELOS: A VR Platform for Ship-Evacuation Analysis", *JCAD special issue on Computer Aided Ship Design*, volume 42, issue 11, p.1045–1058.
2. K.V. Kostas, A.A-I Ginnis, C.G. Politis & P.D. Kaklis, 2011, "Use of VELOS platform for modeling and accessing crew assistance and passenger grouping in ship-evacuation analysis" in *IMAM 2011 Genoa proceedings : "Sustainable Maritime Transportation and Exploitation of Sea Resources"*, Eds E. Rizzuto, C. Guedes Soares, vol. 2, pp. 729–736.
3. R. Graham, 1990, "Motion-Induced Interruptions as Ship Operability Criteria", *Journal of Naval Engineers*, vol. 102, issue 2, pp. 65–71.
4. R. Graham, A. Erich Baitis & W.G. Meyers, 1992, "On the Development of Seakeeping Criteria", *Journal of Naval Engineers*, vol. 104, issue 3, pp. 259–275
5. P. Crossland, M.J. Evans, D. Girst, M. Lowten, H. Jones and R.S. Bridger, 2007, "Motion-induced interruptions aboard ship: Model development and application to ship design", *Journal of Occupational Ergonomics*, vol. 7, pp. 183–199.
6. K.V. Kostas, "Virtual Reality Kernel with Support for Ship Life-cycle Modeling", PhD Thesis, National Technical Univ. Athens (NTUA), School Naval Archi-ecture & Marine Engineering, 255 pages, 2006.
7. Galea ER, Lawrence P, Gwynne S, Sharp G, Hurst N, Wang Z, et al. Inte-grated fire and evacuation in maritime environments. In: *Proceedings of the 2nd International Maritime Conference on Design for Safety*, Sakai, Japan; 2004, p. 161–170.
8. Vassalos D, Kim H, Christiansen G, Majumder J. A mesoscopic model for passenger evacuation in a virtual ship-sea environment and performance-based evaluation. In: *Proceedings of Conference on Pedestrian and Evacuation Dynamics*, Duisburg; 2001.
9. Vassalos D, Guarin L, Vassalos GC, Bole M, Kim H, Majumder J. Advanced evacuation analysis - testing the ground on ships. In: *Proceedings of Conference on Pedestrian and Evacuation Dynamics*, Greenwich; 2003.

10. Drager KH, Orset S. EVAC – the mustering and evacuation computer model resulting from the BriteEuram project MEPdesign. In: Proceedings of Conference on Pedestrian and Evacuation Dynamics, Duisburg; 2001, p. 355–368.
11. W. Bles, S. Nooy, and L.C. Boer. Influence of ship listing and ship motion on walking speed. In Proceedings of Conference on Pedestrian and Evacuation Dynamics, 2001.
12. P. Crossland. The influence of ship motion induced lateral acceleration on walking speed. In Proceedings of the 2nd International Conference on Pedestrian and Evacuation Dynamics, Greenwich, 2003.
13. Baitis, A. E., Holcombe, F. D., Conwell, S. L., Crossland, P., Colwell, J., and Pattison, J. H., 1995, 1991–1992 Motion Induced Interruptions (MII) and Motion Induced Fatigue (MIF) experiments at the Naval Biodynamics Laboratory. Technical Report CRDKNSWC-HD-1423-01. Bethesda, MD: Naval Surface Warfare Center, Carderock Division.
14. Robin Green, Steering behaviors. In SIGGRAPH 2000 Conference Proceedings, 2000.
15. C. W. Reynolds. Steering behaviors for autonomous characters. In GDC'99 (Game Developers Conference), 1999.
16. PD Sclavounos, Computation of wave ship interaction, Ch. 4, in Advances in Marine Hydrodynamics, Ed. M. Okhusu, p. 177–232, 1996.

On Modeling Groups in Crowds: Empirical Evidence and Simulation Results Including Large Groups

Verena Reuter, Benjamin S. Bergner, Gerta Köster, Michael Seitz, Franz Tremel, and Dirk Hartmann

Abstract Research on pedestrian movement strives to mitigate risks at large events or public infrastructures by better understanding the flow of a crowd. Thus, for evacuation planning it is essential to understand what constitutes a crowd. This includes the crowd's composition of various groups of people and its influence on the evacuation process. This paper is a joint effort by social scientists and mathematical modelers cooperating in the research project REPKA to shed more light on this aspect. REPKA (Regional Evacuation: Planning, (K)Control, and Adaptation) focuses on open space evacuation of big events, especially the regional evacuation of national soccer matches. Here, larger groups of fans with a spirit of togetherness are eminently present. Social scientists and mathematical modelers work on this task from different perspectives relying on the tools of their trade: Empirical surveys – interviews and observations – have been conducted by social scientists to gather information on the occurrence and relevance of large groups. They are the basic input for mathematical modelers together with first suggestions on consistent distributions for the group composition. The mathematical modelers integrate these results into a pedestrian stream model that includes larger groups composed of subgroups. They demonstrate how the occurrence of larger crowds affects the flow of a crowd at a road crossing.

Keywords Pedestrian movement • Crowds • Pedestrian flows • Large events • Social groups • Observations • Simulation

V. Reuter (✉) • B.S. Bergner
University of Technology Kaiserslautern, Kaiserslautern, Germany
e-mail: verena.reuter@ru.uni-kl.de; bergner.benjamin@t-online.de

G. Köster • M. Seitz • F. Tremel
University of Applied Sciences Munich, Munich, Germany
e-mail: gerta.koester@hm.edu; m.seitz@hm.edu; franz.tremel@hm.edu

D. Hartmann
Siemens AG Munich, Munich, Germany
e-mail: hartmann.dirk@siemens.com

U. Weidmann et al. (eds.), *Pedestrian and Evacuation Dynamics 2012*,
DOI 10.1007/978-3-319-02447-9_70,
© Springer International Publishing Switzerland 2014

1 Introduction

In the course of the REPKA research project (www.repka-evakuierung.de), attention has been drawn to the potential impact of social groups within crowds. In general, investigating and modeling groups has become a new focus of crowd research. This new direction is triggered by the knowledge that mass pedestrian dynamics cannot solely be explained by the rational behavior of single members of the crowd nor by outdated ‘panic’ models where each individual acts egoistically and is driven by barbaric impulses [2, 14]. In a first attempt to go beyond purely physical models, Helbing et al. [4] assume “a mixture of socio-psychological and physical forces influencing the behavior in a crowd”. Furthermore, Singh et al. [18], Yang et al. [19], Qiu and Hu [13] have introduced first group models.

Modern socio-psychological research about fear and ‘panic’ behavior in flight situations shows that groups of people, especially families and friends with strong ties, stay together if possible [11]. This is even true in an emergency situation. In fact, making contact with affiliated persons takes precedence over individual flight [17]. The loss of companions and uncertainty about their well-being has a destabilizing effect on people affected by disaster, whereas the presence of companions reduces fear [11].

Considering pedestrian crowds composed of groups, evacuation times will certainly increase if people seek each other before following instructions of security staff and moving to safety. Not only do they lose time to save themselves, but they hinder a fast flow when turning against the stream of fleeing people. Today, there is also evidence, both empirical and from computer simulations, that the mere fact that groups want to stay together impacts the pedestrian flow and thus critical parameters such as evacuation times [9, 12]. The physical part of this effect is easily explained by the fact that persons who stick together form bigger particles in a granular type of flow thus hindering the progress of evacuation. However, there are also some indications that social groups can speed up the movement of a crowd in certain scenarios by the additional organizing structure imposed by groups [9].

So far modeling research has concentrated on small groups of 2–4 persons neglecting larger groups. However, soccer fans, our group of interest, often visit soccer games in groups of 5 and more people, e.g. friends, relatives, colleagues, or fan club members. The modelers’ task is to take the empirical observations and mold them into a mathematical model that can be implemented on a computer. This is an intricate task: Firstly, the model must be closed in the sense that there are no unsolved issues within the model that lead to open ends in the computational simulation model. Secondly, the complexity of real life must be reduced to a level that can be handled on a computer. Both restrictions lead to drastic simplifications. Hence, the true challenge is to identify and capture the essential characteristics of the observed phenomenon – but not more.

For empirical operationalization in the sociological studies and for implementation of groups in the mathematical models, a joint definition of the term *social group* is needed. A social group in our definition consists of two or more persons, who visit

the event together. That means they arrive at and leave the venue together or have arranged to meet at the venue to spend time together during the event. Especially if they travel together, they have strong ties in case of evacuation, because they depend on each other. Furthermore, for social scientists and modelers social groups are characterized by a common goal: In spatial terms, to move in the same direction and, in general sense, to stay together as a group. They interact in a relatively continuously communication process and have a sense of a common bond. Group members make great efforts to stay together because of their strong ties, which has a clear impact in evacuation situations.

This paper is structured as follows: First the results of the empirical investigations are presented. Then the mathematical model is sketched. This part is kept short since it is treated in more detail in other contributions to these conference proceedings [10, 16]. Finally the conclusions drawn from this joint effort of sociologists and mathematical modelers are discussed and an outlook is given on desirable next steps.

2 Empirical Studies

In a first step we take a systematic inventory of large groups at big events, like a soccer match. Within this approach we show the relevance of large groups in context of flight situations. We conducted a survey of 328 standardized interviews in the run-up to two home matches of the local soccer club ‘1st FC Kaiserslautern’ in the Fritz Walter Stadium in Kaiserslautern. To identify the group size of people visiting the event, standardized questionnaires are the most suitable empirical method. This provides more valid data than observations, because questionnaires obtain the greatest possible approximation to the factual size of a social group. Results revealed by observation would be falsely or too imprecisely. It is quite difficult for an outsider to define the correct number of people belonging to a social group. For this, those persons belonging to a group would have to be identified and uninvolved bystanders must be excluded. During the observation a certain group may not be complete yet, because they meet further members later. Therefore, in our survey attendants were asked with how many companions they visit the event.

As only one person per group was interviewed, this provides information about the group size of 1,287 attendees (see Table 1). Additionally, we conducted 1,135 interviews on 4 days at the traditional Nürnberg Christkindlesmarkt (Christmas market), for the purpose of comparison. This includes information about the group size of 3,791 attendees.

All interviews were short face to face interviews (5–10 min), using standardized questionnaires. Interview participation was voluntary and the analysis was made anonymous. Evaluation of the interviews revealed similar results showing that there were large groups at both events. Table 1 shows the quantity of persons visiting the soccer match (results of these interviews are integrated into the pedestrian stream model). It becomes evident that only very few people were visiting the event alone (3 %).

Table 1 Group sizes (collected data and extrapolation) at the soccer stadium in Kaiserslautern (Germany), 2010

Soccer stadium		Derived relative frequency of affiliation to a group size (corresponds to the probability with which a randomly selected person belongs to a group of size n) (N = 1,287)	
Group sizes n	Percentage of interviewees that belong to a group of size n (N = 328)		
Individuals	11 %	3 %	Individuals
Small groups	63 %	42 %	Small groups
Large groups	20 %	34 %	Large groups
11-15 persons	6 %	21 %	
Total	100 %	100 %	100 %

The percentage of interviewees belonging to a certain group size in the table refers to the absolute number of interviewees at the event ($N = 328$). Only one person per group was interviewed. Example 63 % of the interviewees were in a group of 2–4 persons, what we define as a small group. With a sample of 328 among more than 40,000 soccer fans present at a game, double counts are extremely unlikely. Example one interviewed person which is a member of a 4-person-group, represents 4 persons absolutely. It is therefore permissible to estimate the relative frequencies of the group sizes from the sample (see Table 1). In the computer model, we use the relative frequencies as probability distribution to create group sizes. Interviews at the Christmas market show similar results to those at the soccer matches. Statistically aggregating the extrapolation of both events we observe that roughly 52 % of the visitors came in small groups and roughly 45 % in large groups. Only 3 % of the visitors were alone. Summing up, we confirm that large groups play a very important role in the structure of crowds. But what may be the impact of their presence in an evacuation scenario?

To further understand the crowd behavior and its consequences for pedestrian flows, we have conducted first observations on the behavior within large groups. We want to know, how large groups behave passing different obstacles. Do large groups split up or stay together walking around the hindrance? In the following, we differ between moving obstacles, like people walking in the opposite direction, and static obstacles, like a parking car or people standing in the way. Therefore, several observations were conducted: First, we trailed a large group of 9 people in the pedestrian zone over 2 h in order to examine the process of splitting up and rejoining more detailed. Second, about 1,800 observations (filming and on-site observations) around the soccer stadium were conducted. Whether groups stay together or split up when they are faced with obstacles has to be observed in ‘real life’. People’s behavior in such everyday situations is unconscious for the most part and cannot be queried by interviews. Thus, observation is the most suitable method here. Interest here is in getting information about splitting up or staying together of people actually walking in a group, not about the exact number of group members. Conducted observations are open and non-participating with structured evaluation protocol. People knew about being observed or filmed (‘open’ and not ‘covert’ observation), but soon forgot this fact. The observers did not intervene in the situation they observed, thus it is a non-participating observation. The observers watched the groups for some time to ensure that people are part of the group. Each situation, in which a group splits up, stays together or reunites, is listed in a structured observation sheet. By this, we got information about the frequencies of small or large groups splitting up or staying together, faced with static or moving obstacles.

Observations show, that large groups split up into subgroups with a loose coherence. The large group of nine in the pedestrian zone splits up into subgroups of changing sizes, mainly into groups of two and three people, then rejoining into groups of four and five people. This process repeats many times during the observation. The interspaces between the different subgroups are also varying. This fact depends on external conditions, like the physical density of space around, and

Table 2 Observations (n = 1,813) at the soccer stadium in Kaiserslautern: behavior of large and small groups passing moving and static obstacles

Observations					
Total		Split up		Stay together	
Large groups	614	276	45 %	338	55 %
Small groups	1,199	196	16 %	1,003	84 %
Moving obstacle		Split up		Stay together	
Large groups	349	163	47 %	186	53 %
Small groups	396	71	18 %	325	82 %
Static obstacle		Split up		Stay together	
Large groups	265	113	43 %	152	57 %
Small groups	803	125	16 %	678	84 %

the subjective perception of the individual subgroup members. The splitting up was also observed at moving and static obstacles in different characteristics. This first case study has given reason to observe group behavior and movement in a higher number of cases at the stadium. Observations of social groups, actually visiting the event together, revealed further insights into the behavior of social groups passing different obstacles (see Table 2). Large groups clearly split up more often at obstacles (45 %) than small groups (16 %). Small groups have a high coherence; they stay together in 84 % of all cases. Results also show, that there is only little difference whether an obstacle is a moving or a static one (see Table 2).

Summing up, all in all large groups have a strong presence in the build-up of crowds and therefore are highly relevant in case of evacuation. First it has been revealed that crowds at the soccer stadium consist of a high percentage of large groups. After that, in a first case study, we have described that large groups split up into subgroups with a loose coherence. Depending on the actual surroundings, a recurring splitting up and rejoining was observed. Especially obstacles, static and moving alike, have an impact on the movement of large groups. That has given reason to examine this behavior in a high number of cases at the stadium. The different behavior at obstacles will clearly have relevance for design of escape routes and the event’s surrounding area. Example if groups stay together while passing a narrow point, the evacuation time increases, because people slow down. In case of accidental break up they will stop or even turn back to reunite with lost companions. By this, they become hindrances for pedestrian flow. In further research steps it is important to review these effects on evacuation scenarios with the help of simulation models.

3 Modeling and Simulation

The impact of small groups in a crowd on evacuation times has been investigated empirically and by simulation by several scientists [9, 12]). No empirical evidence on the impact of larger groups is known to the authors. Measurements with statistical

significance are difficult to obtain, because very large amounts of data have to be gathered and analyzed, often by hand. The presence of large groups, especially at big events, is apparent, e.g. as shown by our empirical study. It is thus a logical step to get first insights by means of simulation studies.

The results of the empirical survey lead to a list of requirements for a group model. Above all, both small groups of two to four persons (so-called *communication groups*) and larger groups of five and more persons must be represented. Based on first observations in the project by the social scientists, made when trailing a large group for a couple of hours, it is assumed that the larger groups frequently split up in subgroups that again form communication groups.

With *communication group* we denote a number of persons, who do not only stay together, but display a group formation that favors easy communication among the members. This requirement for small group models is based on the empirical work in Moussaïd et al. [12]. Our own implementation of the model, based on a combination of attractive forces expressed by potentials, and a need to catch up or slow down, if communication gets uncomfortable, is described in Köster et al. [9] and in Seitz et al. [16]. In Köster et al. [10] it is described how the model is validated, that is, how it is compared to experimental observations. Essentially the virtual persons in our small groups walk abreast when the path is free but have a tendency to switch to a line formation when encountering bottlenecks. Each of the communication groups has a leader, a role that is passed along among group members and filled by the person closest to the groups' shared destination.

In a large group, as defined in our model, the leaders of the communication groups want to stay together with the other group leaders. They are attracted to each other, thus, ensuring that the large group stays together. However, they do not attempt a communication formation of the larger structure. In fact the correct formation of larger groups in different situations is an open research problem.

The distribution of group sizes in a crowd depends on the event. A Poisson type distribution as suggested in Coleman and James [1] and James [7] is convenient for implementation but it certainly does not hold for all realistic events. Here we use the detailed distribution as found at the soccer stadium in Kaiserslautern that gives relative frequencies for groups sizes from 1 (individuals) to 15. A second distribution is necessary to define how large groups split up into subgroups. This is again an open question. Here, for consistency's sake, we assume that the distribution follows the pattern of the distribution of small groups in the whole sample. In other words we look at all observed groups of size less or equal to 4 and among these at the relative frequencies of individuals. The resulting values are 0.167 for individuals, 0.467 for pairs, 0.227 for groups of three and 0.139 for groups of four.

The group model is realized within a cellular automaton model of pedestrian movement described in Hartmann [3], Köster et al. [8, 9].

In a first step, we are interested in observing visually the difference between a crowd composed solely of small groups and a crowd with larger groups that in turn are composed of subgroups. In Figs. 1 and 2 a crowd moves from left to right. In Fig. 1 the crowd consists solely of communication subgroups that have a clear tendency to walk abreast. In Fig. 2 the crowd is composed of large groups that split

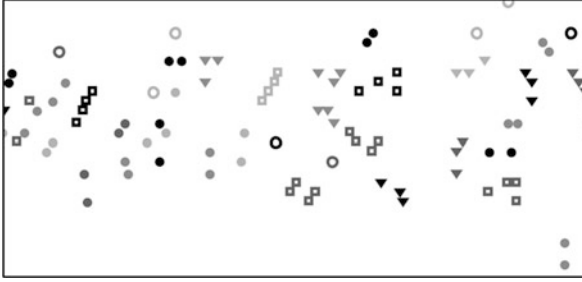


Fig. 1 Crowd moving from *left to right* composed of individuals and communication groups of sizes 2–4. Different symbols mark different groups. The groups walk abreast whenever the path is free. The size of the groups is encoded using different geometrical forms

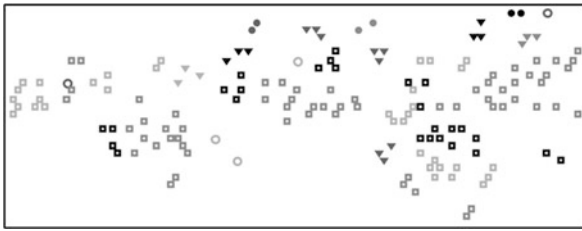


Fig. 2 Crowd moving from *left to right* composed of small and large groups that split up in subgroups. Different symbols indicate different group sizes. All large groups are denoted by *squares*. The subgroups become visible through the communication formation they display when the path is relatively clear

up in subgroups. We observe that the large groups look like larger particles in a granular flow. From this we would expect an influence on the flow of the crowd whenever a bottleneck or another pedestrian stream is encountered.

To further investigate this hypothesis, we consider a computer simulation where two pedestrian streams cross at a right angle (see Fig. 3). The first experiment is with crowds that consist solely of individuals. At the intersection no impact is visible. The two streams interweave smoothly, which contradicts empirical evidence [6]. The second picture shows large groups of 15 that split up into subgroups according to the empirical distribution observed at Kaiserslautern. The third picture shows the same with groups of 25. Here, we clearly observe congestions. Moreover we get the impression that the two streams drag each other along, which is consistent with empirical studies at crossings where a band pattern is seen [5, 6]. This leads us to the hypothesis that the typical band pattern at pedestrian crossings is brought forward, at least partially, by the presence of groups. Overall the streams are much less homogeneous than in the aggregated crowd. This is most pronounced right after the crossing. The last picture in Fig. 3 shows pedestrian streams with large groups

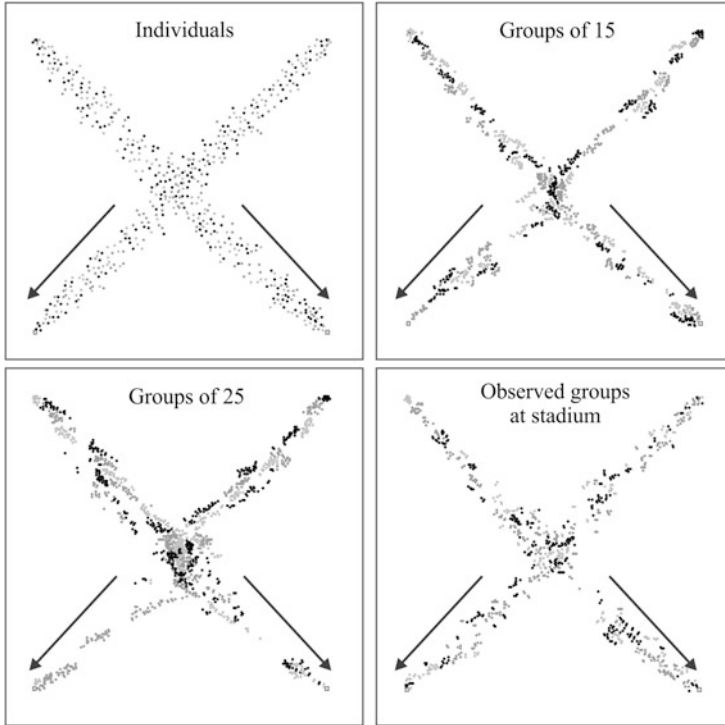


Fig. 3 Two streams of pedestrians at a crossroad. Each upper corner is the source of a pedestrian stream that moves in the direction of the opposite lower corner (indicated by *arrows*). The two streams intersect at a right angle in the middle

distributed according to the empirical study in Kaiserslautern. The congestion is still visible, however much less apparent. This is no surprise, since the average group size is only 4.1 persons.

4 Conclusion

We have presented a combination of empirical studies and computer simulations to investigate how the presence of large groups impacts the flow of a crowd. The empirical results are the basis of a group model (within a microscopic pedestrian simulation) that assembles large groups from small communication groups. The distribution of the virtual crowd composition in the simulation is based on empirical data.

The computer simulations suggest that large groups behave as moving obstacles especially at crossroads where pedestrian streams drag each other along instead of smoothly interweaving as aggregated crowds consisting of single individuals would.

We conclude from this that the typical band pattern observed at crossings may be best explained by the presence of groups. When larger groups are present, the disturbed flow also suggests that large groups would further hinder a fast evacuation, if they keep staying together.

Many questions regarding crowd composition and group behavior remain open. Among them are wider and more detailed investigations of suitable distributions, especially within large groups. Socio-psychological research findings about fear and ‘panic’ behavior in flight situations show, that people try to stay together. Our observations of group behavior faced with obstacles in ‘normal’ situations show varying results for large and small groups: Small groups predominantly stay together, but large groups split up in about half of the cases. How members of a large group would behave in a true emergency, is still unknown.

Acknowledgements This work was partially funded by the German Federal Ministry of Education and Research through the priority program “Schutz und Rettung von Menschen” within the project REPKA—Regional Evacuation: Planning, (K)Control and Adaptation.

References

1. Coleman, J. S.; James, J. (1961): The Equilibrium Size Distribution of Freely-Forming Groups. In: *Sociometry*, Vol. 24, Issue 1, pp. 36–45.
2. Drury, J.; Stott, C. (2011): Contextualising the crowd in contemporary science. In: *Journal of Contemporary Social Science* 6 (3), pp. 275–288.
3. Hartmann, D. (2010): Adaptive Pedestrian Dynamics Based on Geodesics. In: *New Journal of Physics* 12 (4), pp. 1367–2630.
4. Helbing, D.; Farkas, I. J.; Vicsek, T. (2000): Simulating dynamical features of escape panic. In: *Nature*, Vol. 407, pp. 487–490.
5. Helbing, Dirk (2001): Traffic and related self-driven many-particle systems. In: *Reviews of Modern Physics*, Vol. 73 (4), pp. 1067–1141.
6. Helbing, D.; Molnár, P.; Farkas, I.; Bolay, K. (2001): Self-organizing pedestrian movement. In: *Environment and Planning B* 28, pp. 361–383.
7. James, J. (1953): The Distribution of Freely-Forming Small Group Size. In: *American Sociological Review*, Vol. 18, pp. 569–570.
8. Köster, G.; Hartmann, D.; Klein, W. (2011a): Microscopic Pedestrian Simulations: From Passenger Exchange Times to Regional Evacuation. In: Hu, B.; Morasch, K.; Pickl, S.; Siegle, M. (eds): *Operations Research Proceedings 2010: Selected Papers of the Annual International Conference of the German Operations Research Society*, pp. 571–576.
9. Köster, G.; Seitz, M.; Treml, F.; Hartmann, D.; Klein, W. (2011b): On modeling the influence of group formations in a crowd. In: *Journal of Contemporary Social Science* 6 (3), pp. 397–414.
10. Köster, G.; Treml, F.; Seitz, M.; Klein, W. (2012): Validation of crowd models including social groups, PED 2012.
11. Mawson, A. R. (2005): Understanding Mass Panic and Other Collective Responses to Threat and Disaster. In: *Psychiatry: Interpersonal and biological processes*, Vol. 68, Issue 2, pp. 95–113.
12. Moussaïd, M.; Perozo, N.; Garnier, S.; Helbing, D.; Theraulaz, G. (2010): The Walking Behaviour of Pedestrian Social Groups and Its Impact on Crowd Dynamics. In: *PLoS ONE*, Vol. 5, Issue 4.

13. Qiu, F., Hu, X. (2009): Modeling group structures in pedestrian crowd simulation. In: *Simulation Modelling Practice and Theory*, 18, pp. 190–205.
14. Reichert, S. (2011): Mass action and mundane reality: an argument for putting crowd analysis at the centre of the social sciences. In: *Journal of Contemporary Social Science* 6 (3), pp. 433–449.
15. REPKA-project website: repka-evakuierung.de: [<http://www.repka-evakuierung.de>]
16. Seitz, M., Köster, G., Pfaffinger, A. (2012): Pedestrian group behavior in a cellular automaton, PED 2012.
17. Sime, J. D. (1983): Affiliative Behaviour during escape to building exits. In: *Journal of Environmental Psychology*, Vol. 3, Issue 1, pp. 21–41.
18. Singh, H., Arter, R., Dodd, L., Langston, P., Lester, E., Drury, J. (2009): Modelling Subgroup Behaviour in Crowd Dynamics DEM Simulation. In: *Applied Mathematical Modelling* 33, pp. 4408–4423.
19. Yang, L. Z., Zhao, D. L., Li, J., Fang, T. Y. (2005): Simulation of the kin behavior in building occupant evacuation based on Cellular Automaton. In: *Building and Environment*, 40 (3), pp. 411–415.

Pedestrian Agent Based Model Suited to Heterogeneous Interactions Overseen by Perception

L. Bourgois and J.-M. Auberlet

Abstract Most of the work about pedestrian simulations concern situations of homogeneous interactions between them as for planning and for designing in transportation studies. These studies assume that pedestrians broadly share common behavior and goal (reaching out of a building, crossing a street, following target . . .). They do not take into account the many inter-pedestrian interactions induced by a dynamical environment requiring a contextual adaptation, for instance a situation with a danger perceived. In order to model different interactions between pedestrians in complex and dynamic context/situation such as urban area, we propose an exploratory work which concerns different types of interaction between pedestrians and other actors. Thus the model will be able to take simultaneously different kind of interaction. Technically, to deviate from a dangerous pedestrian, one will accept to get closer to other “normal” pedestrians whereas in panic situation, pedestrians may forget their initial destination. Thus, one alters for a while his interactions or his destination based on his perception of the environment and of the context. Our framework is the Multi-Agent Systems, within which the pedestrian travels can be seen as an agent coordination problem, coordination which is often competitive, occasionally cooperative. Thus, we propose an Agent-based model with a hierarchical architecture driven by perception, articulated with some controllers suited for various situations. The model is generic since it use for different task as road crossing, collision avoidance, danger avoidance and group interaction. First scenarios were tested to check our model.

Keywords Pedestrian • Simulation • Perception • Context • Dynamical interaction

L. Bourgois (✉) • J.-M. Auberlet
Université Paris-Est, IFSTTAR-IM-LEPSIS, 58 boulevard Lefebvre, 75732 Paris/CEDEX 15,
France
e-mail: laure.bourgois@ifsttar.fr; jean-michel.auberlet@ifsttar.fr

1 Introduction

Heterogeneous crowd models are needed in some applications including education, entertainment, training (for the military and police) and human factors analysis for building evacuation, for sport events [18] and for military simulation (especially in case of urban warfare [15]).

Moreover, most of the work about pedestrian simulations concerns situations of homogeneous interactions. These studies assume that pedestrians broadly share common behavior and goal (reaching out of a building, crossing a street ...). Excepted in military simulation and game, there is only few research where actors do not share identical goals. However those researches do not focus specially on elaborating a pedestrian moving model, but they rather treat of patrol optimization (where to send efficiently the police ...) [19].

In order to model different interactions between pedestrians in complex and dynamic context/situation, we propose an exploratory work about a flow of pedestrians in the presence of an immediate and shifting danger (a pacific demonstration with a military assault). We propose here an Agent based model with a hierarchical architecture driven by perception, articulated with a controller suited for various situations. The model is generic since it is used for pacific demonstrators and for control force. We experiment two scenarios: one where some policemen try to catch some leaders in a crowd, another where a control force squad charges a pacific crowd.

In this paper, we discuss related work in Sect. 2. Our proposed general pedestrian hierarchical structure and the initial moving model are related in Sect. 3. We present the identification of various situations of danger in Sect. 4. First results of simulation in different scenarios are detailed in Sect. 5. Section 6, we talk over our contribution and perspectives.

2 State of the Art

Concerning pedestrian modelling, we only list microscopic approaches that represent pedestrians as individual entity/particles or model that can fit with this level of details. These models include two major approaches: pedestrian subjected to forces [7] or to behavioral rules [20].

The most widely used among those models is the Social Force Model (SFM) [7] for crowd simulation. It describes a pedestrian as a particle subjected to attractive forces (its destination, some pedestrians) and to repulsive forces (fixed obstacles as wall and mobile obstacles as other pedestrians). It tries to trail straight ahead in order to reach its destination following a shortest path route, and to avoid obstacles. Helbing interprets the private sphere notion as a “repulsive sustained field”, sum computed in function of environment obstacles and an attractive force function of a desired walking speed and a given destination (and possible “attractive” pedestrians to form groups. This model can be seen as a reusable component for moving

pedestrian for its nice extensibility and may be calibrated differently according to various situations to modeled [21]. However, SFM has major shortcoming: the simulated pedestrians hold a behavior totally reactive (ones avoid obstacle at last sight with no anticipation) and there is no simultaneous handling of heterogeneous interactions between pedestrians.

Teknomo in his work [22] uses social force notion for determining pedestrians' next positions. The main difference with SFM lies in complex formulation with the mean of second order differential equation of the movement. Moreover, Teknomo adds a term to handle collisions but do not considers heterogeneous characteristic of pedestrians' interactions.

For pedestrian modeling, Hoogendoorn goes over concepts of control theory [9]. A pedestrian optimizes a utility function endowed with a set of various costs relative to acceleration, nearness obstacles (mobiles as some pedestrians or static as walls), and deviation from the initial computed optimum trajectory. As Allen does for a driver [2], Hoogendoorn provides a conceptual architecture for a pedestrian carrying three levels [9]:

- A strategical level, which deals with the long-term decisions (task or route planner . . .),
- A tactical level, which deals with the mid-term decisions (section route choice, street decision crossing, types of interactions relative to some pedestrians or some different kinds of danger . . .),
- An operational level, which deals with the instantaneous moving model depending on the agent dynamic environment.

Hoogendoorn recommends collaboration between the three levels. However, he does not give any formalization or precise description.

Work of McKenzie aim to develop a tool with a set of models of military simulation with a credible crowd psychological [15]. Crowd-MAGS project [16] shares the same objectives. With a Multi Agent System approach, each pedestrian is modeled by an agent endowed with a set of complex behaviors (set of hierarchical rules). McKenzie aims to extend existing crowd models with explicit social concepts. A pedestrian agent is able to identify its belonging to a group and to deduce thereby a set of action to perform.

Recent work [17] tackle the attractive forces between pedestrians in order reproduce the observed recurring patterns in groups. These researches assume that pedestrians are conscious of the group relationship. We point out that it does not address the problem of a crowd of anonymous without collective motivation.

3 A Hierarchical Architecture

Our model takes place within the framework of perception-interpretation-selection-decision [23]. We note that the interpretation and selection process can be disconnected and the importance of decision feedback on those process. We also follow

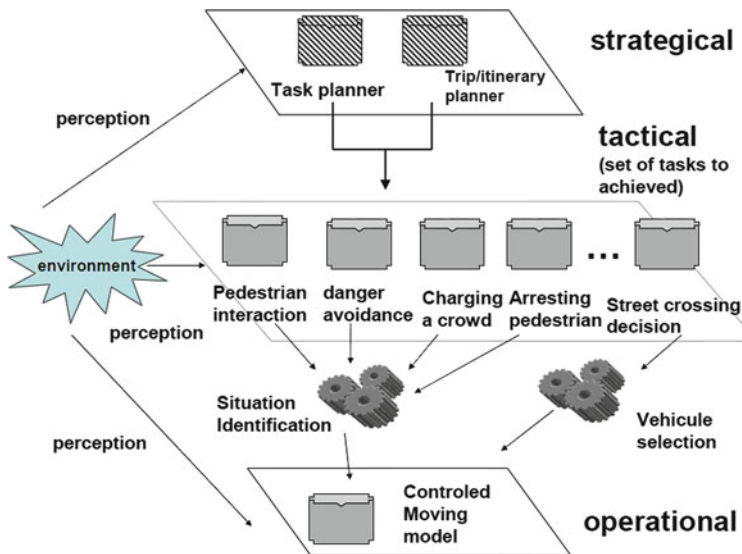


Fig. 1 A perception-driven hierarchical architecture with heterogeneous tasks

Hoogendoorn’s concept [9] introduced in Sect. 2, that distinguishes three decision levels: strategic, (planning ...) tactical (section route choice ...), operational (instantaneous motions ...).

In [5] we have presented a hierarchical structure linked with an automata which intends to describe junction between tactical and operational level to undertake heterogeneous interactions between pedestrians when some particular situations are identified. Up today, we extend this architecture in order to provide issues for:

- Identifying different type of danger (military assault versus police arresting some pedestrian)
- Modeling different tasks as charging a crowd and intercepting some pedestrian and there consequences on the controlled moving model.

The operational level may be controlled in different ways depending on the nature task to perform (crossing the street, escape, charging, arresting some pedestrian ...).

Figure 1 presents a perception-driven hierarchical architecture for modeling a pedestrian agent moving in an urban context. If as expected, percepts do influence pedestrians’ actions, the main originality of our works lies in the use of the interpretation of the percepts. This architecture can be seen as a hybrid one [13]. It is set task-driven (strategical level) and subtask-driven to achieve (tactical level). The various tasks involve different interactions between the three levels. We focus on interactions between tactical and operational level especially for the following tasks: interacting normally with others pedestrians, avoiding danger, charging a crowd, intercepting some pedestrian.

Basically, we employ the widely used Social Force Model of Helbing for moving agents [7]. We enhanced this model with sensitivity measures and by introducing additional features [3].

We provide pedestrian agents with different features in order to influence their perceived interaction and the way to manage them. In our examples, a pacific demonstrator has to perceive other pacific pedestrians and obstacles and to differentiate them from some danger. They must distinguish a charging squad from a policeman intercepting someone. Moreover our model provides a mean for police force to identify the pedestrian “target” among other non-combatant pedestrians.

3.1 Pedestrian Agent Characteristics

A pedestrian is represented by a circle, which has a variable radius. We extend our previous representation of a pedestrian [3–5], each pedestrian agent has:

- A set of parameters P_α dedicated to controlled moving model that mainly are:
 - A_α , its obstacle reaction intensity (pedestrians, walls),
 - B_α , a reactivity threshold, over which the pedestrian agent does not react anymore to environmental elements.
- A set of tasks T_i to achieve which is a subset of Beh , all the possible behavior of a pedestrian $Beh = \{normal\ pedestrian\ interaction, danger\ avoidance, charging\ a\ crowd, arresting\ some\ pedestrian, street\ crossing\ decision\}$
- A state q_α of perception with $q_\alpha \in \wp(\{neutral, normal, charge, arrest\})$

In order to mathematically conveniently describe these characteristics, we introduce in the following equation, let α be an agent, it is defined by:

$$\alpha = (c_\alpha, df_\alpha, v_\alpha^0, P_\alpha, T_{1_\alpha}, \dots, T_{n_\alpha}, q_\alpha) \quad (1)$$

with c_α its geometrical co-ordinates, df_α it's final/local destination, v_α^0 its walking desired speed, P_α its instantiated parameters for controlling the moving model, $T_{1_\alpha}, \dots, T_{n_\alpha}$ the current task(s) it has to perform, q_α its current perception of danger.

The next subsections go into details of the description of the pedestrian's perception and for the moving model in a general framework (i.e. without danger or charging/following behavior).

3.2 Perception Model (Operational Level)

In the initial approach of Helbing [7, 10], a pedestrian may influence another pedestrian depending both on their respective distance between them and on their azimuth. Agents or obstacles behind a pedestrian have a variable influence on its

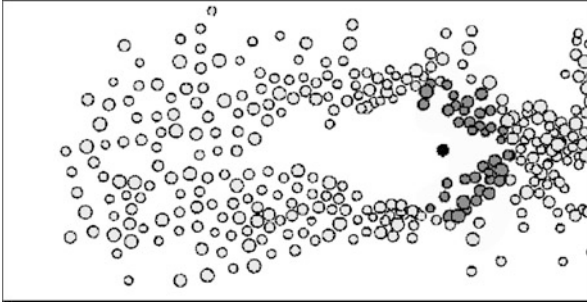


Fig. 2 Example of a snapshot of a crowd avoiding a dangerous pedestrian

trajectory and speed. We remark here that perception does take into account neither the speed nor the walking direction of the agents, but only their respective locations. Helbing did not mention the depth of the field of vision [7, 10], thus we added a variable in order to perceive only the neighbors [3] and only the pertinent ones [4]. To sum up, perception is based on the depth of the field of vision and the sensibility parameter (that determines the anisotropy of the agent). To overcome the drawback of the uniform reaction to stimuli, in [5] we enhanced the pedestrian representation with an internal state for danger perception. Thereby, our approach allows modeling some particular situation of danger (for instance a policeman arresting a pedestrian or a crowd avoiding a dangerous pedestrian). Figure 2 shows an example of a snapshot of one of our simulation. Each pedestrian is represented in 2D by a circle. Pedestrians in light grey are those who doesn't perceive any danger and dark grey pedestrians locally perceive the dangerous pedestrian (figured in the center in black).

3.3 Initial Moving Model (SFM)

Each agent has a desired speed v_α^0 and tries to walk in a (desired) direction \vec{e}_α , which depends on its current position c_α and on its destination, df_α (final or local). It also tries to maintain its speed actual v_α to its desired speed $\vec{v}_\alpha^0 = v_\alpha^0 \vec{e}_\alpha$, which is therefore the target for the agent to reach. Agent acceleration $\vec{\gamma}_\alpha$ is then defined in [10] by the following equation:

$$\vec{\gamma}_\alpha = \frac{1}{\tau_\alpha} \left(v_\alpha^0 \vec{e}_\alpha - \vec{v}_\alpha \right) + \sum_{\beta (\neq \alpha)} \vec{f}_{\alpha\beta} + \sum_{obst} \vec{f}_{obst} \quad (2)$$

with:

- τ_α a parameter representing the impatience of the agent to reach its desired speed,
- $\vec{f}_{\alpha\beta}$ and \vec{f}_{obst} , respectively the repulsive forces to avoid obstacles (mainly pedestrians, and walls) and to keep its private sphere.

A repulsive force exerted on agent α by a pedestrian or an obstacle β is defined in abbreviated form as follow:

$$\vec{f}_{\alpha\beta} = wA_{\alpha}e^{f(B_{\alpha},d_{\alpha\beta})}\widehat{d}_{\alpha\beta} \quad (3)$$

with:

- w a function representing the vision field sensibility,
- $f(B_{\alpha},d_{\alpha\beta})$ a function of B_{α} and $d_{\alpha\beta}$, the distance between α and β ,
- $\widehat{d}_{\alpha\beta}$ the normal vector pointing from β to α (see [10] for more details).

In a non dangerous situation, we used A_{α} and B_{α} with the same value as in [10] (see [3, 4] for more details). As mentioned before, the original SFM [10] does not limit the field of vision. In [4] we introduced a contextual goal-oriented perception filtering, i.e. we claim that, the depth of the field of vision depends on the agent dynamic context.

4 Identification of Various Situations of Danger

For monitoring the moving model, we propose a perception and task driven automata. This tool allows the identification of various situations of danger. Indeed, Lamarche [12], notes that automata allow to take into account the immediate changes in the environment (operational level) while providing a mechanism for making decisions in the medium term (tactical). Moreover, an automata can handle the temporal coherence of the sequence of actions, on the contrary to a simple set of rules [12–14]. Finally, this formalism has useful properties for the treatment of “deadlocks” (model checking).

4.1 Context and Task Driven Automata for Controlling the Moving Model

For the interaction between the tactical and the operational levels, we use the formalism of a finite automata (Fig. 3). This automata enables to identify the situation of interaction with other surrounding pedestrian. It makes it possible to control the moving model according to the current context and to the tasks to execute.

Each state of the automata represents an internal state of the pedestrian agent which can be modeled by constraints. These are constraints combinations displayed in Table 1. Transitions are labeled with the name of the actions presented in Table 2. Formally, let (Q, V, P, T) be an automata with: $Q = \{q_0, q_1, q_2, q_3\}$ the set of states,

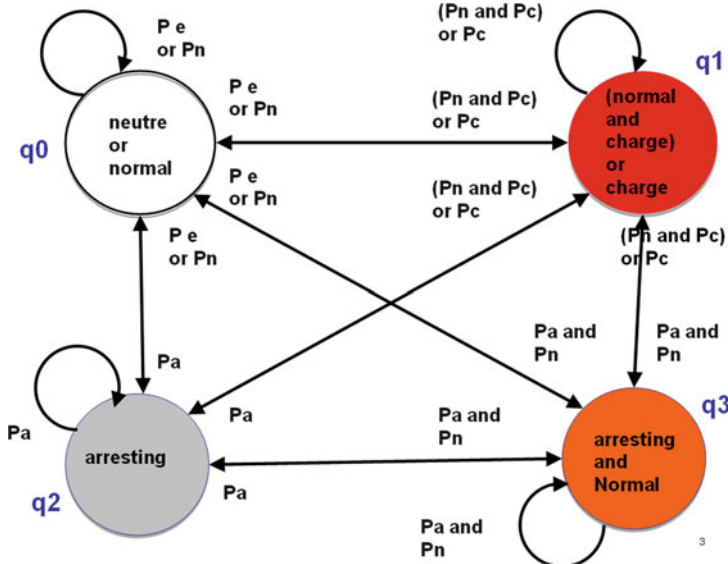


Fig. 3 The perception-driven automata

Table 1 Constraints and semantic

Boolean	Semantic
Neutral	SFM without any interactions
Normal	SFM with interaction with pacific pedestrians
Arrest	SFM with intense reaction to avoid the arrestation
Charge	SFM with intense reaction to avoid the controle forces and relaxation of the initial destination

Table 2 Perception and semantic

Perception	Semantic
P_e	The pedestrian doesn't perceives any pedestrian
P_n	The pedestrian perceives only pacific pedestrians (at least one)
P_a	The pedestrian perceives an arrestation of another pedestrian by a policeman
P_c	The pedestrian perceives that controle forces are charging

$V = \{normal, charge, arrestation\}$ the set of Boolean variables, $P: Q \rightarrow \wp(V)$ the function labelling the states with variables, $E = \{P_e, P_n, P_a, P_c\}$ the set of possible transitions between states, $T: Q \times E \rightarrow Q$ the function assigning Boolean variables to the states. According to its internal state, the pedestrian alters one or several parameters of the moving model and modifies its interactions (i.e. adds or removes some forces). Tables 1 and 2 show the way for undertaking the modifications.

4.2 Task of Danger Avoidance

The reaction of pedestrians to a danger differs depending on the nature of the perceived danger. We propose two models of response for each scenario (arresting, charging).

Arresting Situation When one perceives “dangerous” pedestrian or a situation of arrest, one should be willing to keep a larger distance between him rather than the usual distance for his usual comfort. To express this willingness of moving away, we assumed that the intensity of the reaction of pedestrians to stimuli (parameter A) must increase. Besides, one should reduce his distance of comfort between him and other pedestrians in order to reproduce realistic trajectories (thus enhance the parameter A). This particular task of danger avoidance has been tackled in [5].

Charging Situation Pedestrian agents shall momentarily forget their initial destination and only avoid the danger and other pacific pedestrians. As in the precedent scenario, one should reduce his distance of comfort with other pacific pedestrians. For that aim, the reaction A to charging policemen is enhanced whereas the reaction to pacific demonstrator is reduced as in [5]. In that way, we hold different kinds of interactions between pedestrians.

5 First Results

In order to validate and verify the consistency of our model, we executed several series of simulations.

Arrest Situation For these simulations, we have simulated a corridor of 60 m long by 10 m wide. On this corridor, the flow of pedestrians is congested: 6,000 pedestrians per hour (see [6] for pedestrians flow calibration). On Fig. 3, we can see for the same simulation step, two screenshots of a flow with policemen (figured in black square) and without. During the simulation, each pacific pedestrian become tinged with the colour corresponding to the current number of perceived pedestrians as follow:

```

let n be the number of perceived pedestrians:
if (n>=15) color = BLACK;
if (n>=10 && n<15) color = PATTERN;
if (n>=5 && n<10) color = LIGHT GREY;
if (n<5) color = WHITE;

```

On Fig. 4, we see that the crowd has been dispersed due to the presence of policemen. By consequence, there is an emergence of groups of pedestrians (see the top left and the bottom center of the figure).

Charging Situation We simulated a city square of 100 m long by 40 m wide, with no street furniture. At one corner of the square there is a narrow street that can be

Fig. 4 Emergence of groups of pedestrians in case of several arrests

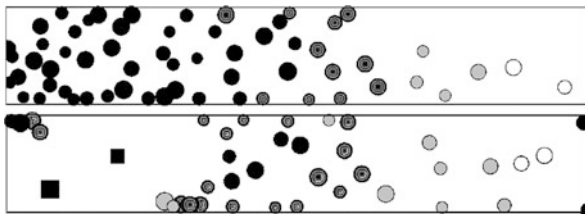
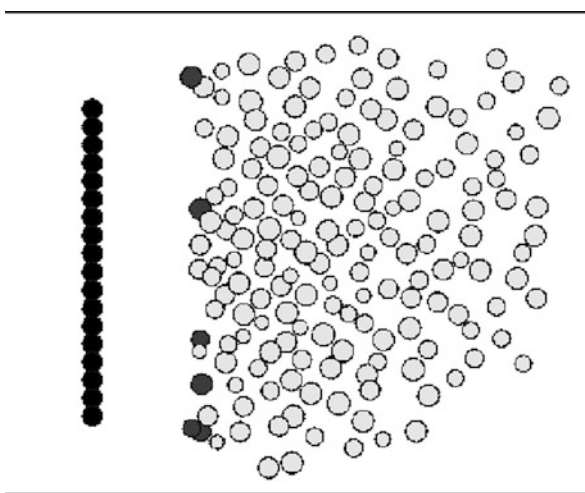


Fig. 5 Screen-shot of a charging scenario



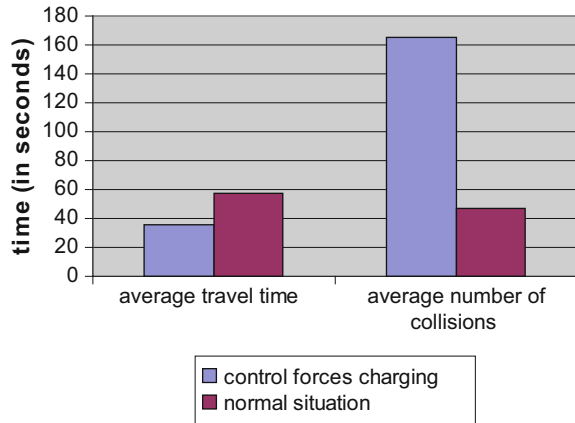
seen as a bottleneck where the demonstrators may withdraw into. We simulated 20 policemen in a line and in front of them 200 pacific demonstrators. Figure 5 presents the policemen (figured in black) charging the pacific demonstrators that doesn't yet perceive the danger (figured in light grey) and the first demonstrators that try to escape (figured in dark grey).

We recorded, for each pedestrian agent, two macroscopic indicators to evaluate our model:

- The average travel time (indicator of performance of the model),
- The average number of collision (indicator of quality of the model).

We can see (Fig. 6) that in a charging situation the average number of collisions is four times higher than in a normal situation (in a high density crowd). The average travel times decreases of a third with control forces charging. The reactive feature of our model accounts for the contradiction between these two indicators (average time, average number of collisions). Indeed, when one pedestrian begin to escape from the charging squad, it collides with others pedestrians since they do not perceive the danger continue to apply the initial SFM model. However, in real situation, if one sees someone running, he will probably start to run in the same

Fig. 6 Macroscopic indicators for the evaluation of our perception model



direction (as he may infer a charging situation). We must therefore refine our model by means of spreading information of perceived danger. This future amelioration will decrease the number of collisions.

6 Discussion and Perspectives

We have presented a pedestrian agent model encompassing both normal avoidance and different kind of danger avoidance. Those tasks are highly dependent on the perception of the situation, we hence focus on a hierarchical architecture linked with a process for identifying the pertinent task to achieve. Our simulations take place in a corridor and a place endowed with a street seen as a bottleneck for demonstrators. We exhibit the emergence of group phenomenon in case of an arresting situation and a high number of collision coupled with a low average travel time that show up a situation of panic induced by the charging scenario.

In order to enhance the quality of our model, one perspective is to associate our proposed model to computational modelling of emotion. Indeed adding an emotion propagation module for agents' interactions should give promising results to get accurate and realistic pedestrian trajectories and to compare them with real data [9].

Now we would like to compare our results with works like the ones of M. Hoogendoorn [9]. However, even if there are some references for collective behavior, we point out the lack of data about pedestrians.

More research is needed to better understand and to reproduce global behavior for a group of pedestrians on particular in the case of crowd dispersion in an urban warfare or in an emergency evacuation. Several problems arise like group identification or group formation.

At last, another perspective of this work is to propose an approach for agent goal automatic-determination in function of the context like in a BDI (Belief Desire Intention) architecture [1].

Acknowledgements This research has been funded by the project Terra Dynamica supported by *fond unique interministeriel* (FUI 8).

References

1. Adel, S., Ramdane, M., Sahnoun, Z.: Towards more flexible BDI Agents, In: International Conference on Agents and Artificial Intelligence (2012)
2. Allen, T. M., Lunenfeld, H., Alexander, G.J.: Driver information Needs, In: Highway Research Board, vol. 36, pp. 102–115 (1971)
3. Bourgois, L., Oulhaci, A., Auberlet, J.-M.: Simulation de déplacement: Vers un modèle de perception et de prédiction du comportement d'autrui, In: Journées Francophones des Systèmes Multi-Agents (2010)
4. Bourgois, L., Saunier, J., Auberlet, J.-M.: Towards contextual goal-oriented perception for pedestrian simulation, In: International Conference on Agent and Artificial Intelligence (2012)
5. Bourgois, L., Rabai, H., Auberlet, J.-M.: Adaptation dynamique du comportement: vers un modèle guidé par la perception, In: Reconnaissance de Formes et Intelligence Artificielle (2012)
6. Fruin, J.: **Pedestrian planning and design**, In: Metropolitan Association of Urban Designers and Environmental Planners (1971)
7. Helbing, D., Molnar, P.: Social force model for pedestrian dynamics, In: Physical Review E, vol. 51, pp. 4282–4286 (1995)
8. Hoogendoorn, M., Treur, J., van der Wal, C., Van Wissen, A.: Agent-based modelling of the emergence of collective states based on contagion of individual states in groups, In: Transactions on computational collective intelligence, pp. 152–179 (2011)
9. Hoogendoorn, S. P., Daamen, W.: Pedestrian Behavior at Bottlenecks, In: Journal Transportation Science (2005)
10. Johansson, A., Helbing, D., Shukla, P.K.: Specification of the Social Force Pedestrian Model by Evolutionary Adjustment to Video Tracking Data, In: Advances in Complex Systems, 2007.
11. Lamarche, F.: Humanoïdes virtuels, réaction et cognition: une architecture pour leur autonomie, Thèse de doctorat, IRISA Rennes (2003).
12. Lamarche, F., Donikian, S.: La sélection d'action. Le traité de la réalité virtuelle, In: Presses de l'Ecole de Mines de Paris, vol. 5, chap. 12 (2009)
13. Malenfant, J., Denier, S.: ARM: un modèle réflexif asynchrone pour les objets répartis et réactifs, Actes de LMO 2003, In: Revue L'Objet, Hermès/Lavoisier, vol. 9, n° 1–2, pp. 91–103 (2003)
14. Mandiau, R., Hanon, D., Grislin-le Strugeon, E.: Modèles comportementaux appliqués à la navigation de piétons, Granié, M.-A., Auberlet, J.-M. (eds.), In: Le piéton et son environnement - Quelles interactions ? Quelles adaptations ?, Actes du 1er colloque francophone de la plateforme intégrative COPIE – Comportement du Piéton dans son Environnement, pp. 49–60, Les Collections de l'INRETS, Paris (2007)
15. McKenzie, F., Petty, M., Kruszewski, P., Gaskins, R., Nguyen, Q.-A., Seevinck, J., Weisel, E.: Integrating crowd-behavior modeling into military simulation using game technology, In: Journal Simulation and Gaming (2008)
16. Moulin, B., Larochelle, B.: Crowdmags, Multi-agent Geo-Simulation of the interactions of a crowd and control forces, In: Modelling, Simulation and Identification (2010)

17. Moussaïd, M., Perozo, N., Garnier, S., Helbing, D., Theraulaz, G.: The walking behaviour of pedestrian social groups and its impact on crowd dynamics, In: PLoS ONE (2010)
18. Pelechano, N., O'Brien, K., Silverman, B., Badler, N.: Crowd Simulation Incorporating Agent Psychological Models, Roles and Communication, In: 1st Int'l Workshop on Crowd Simulation (2005)
19. Poulet, C., Corruble, V., El Fallah-Seghrouchni, A., Ramalho, G.: The Open System Setting in Timed Multiagent Patrolling, In: IAT, pp. 373–376 (2011)
20. Reynolds, C.W.: Flocks, Herds, and Schools: A Distributed Behavioral Model, Computer Graphics, In: SIGGRAPH (1987)
21. Simonin, O., Ferber, J.: Un modèle multi-agent de résolution collective de problèmes situés multi-échelles, In: Journées Francophones des Systèmes Multi-Agents (2003)
22. Teknomo, K.: Application of microscopic pedestrian simulation model, In: Transportation Research Part F, vol. 9, pp. 15–27 (2006)
23. Weyns, D., Steegmans, E., Holvoet, T.: Towards active perception in situated multi-agent systems, In: Applied Artificial Intelligence (2004)

Pedestrian Gap Acceptance in Micro-Simulation Modelling

Paul Simon Townsend

Abstract Recent development in pedestrian modelling has seen vehicle based micro-simulation interacting with pedestrian models to allow the simulation of a greater variety of urban spaces. This provides a more holistic picture of how junctions and streets function from a multi-modal perspective that incorporates the effect that vehicular movement has on pedestrians and vice versa by quantifying simulation results in a measurable way. These models are still in their infancy and require further functionality and research to improve the quality of output and ease of modelling. This paper develops a pedestrian gap-acceptance based algorithm for modelling a variety of opportunistic pedestrian behaviours.

Keywords Agent • Behaviour • Gap • Pedestrian • Shared space

1 Introduction

In recent years, there has been an increase in the popularity of ‘Less Managed’¹ schemes, especially across Europe and the United Kingdom. Such schemes are categorised by their informal approach to traffic control and the ability to balance the priorities of different modes in a space by the design of that space, rather than the need for formal control methods such as traffic signals, road markings and policing measures, such as speed cameras. One such design type is shared space that has become popular in the UK after success in Europe, though there are a

¹A term coined by the author to describe a space in which drivers and pedestrians must make their own decisions as to when it is safe to proceed, rather than following formal indications.

P.S. Townsend (✉)

Crowd Dynamics International Limited, Knutsford, UK

e-mail: paul.townsend@crowddynamics.com

variety of different possible designs as noted in the Appraisal of Shared Space by the Department for Transport, UK [1].

This led to a market requirement for micro-simulation models to be able to cope with such pedestrian-vehicular interactions [2] and furthermore be able to quantify the effect that an urban space has on all users, whether by mechanical mode or on foot. Recent developments have seen a variety of models now capable of performing this type of analysis to varying degrees of sophistication.²

This paper focuses on one pedestrian and vehicular micro-simulation model, the Urban Analytics Framework (UAF). Background information on the software can be found at [3]. It describes the user- and observation- driven requirements to be able to provide more flexible modelling and, in particular, a feature that would allow pedestrian gap-taking behaviour³ to be modelled in any urban environment.

The author has carried out some experimental research to discover the potential needs for a gap acceptance model. The research methods are explained and conclusions drawn from the data collected. The basic requirements for a pedestrian gap-acceptance algorithm are then outlined. The concepts of 'scan area' and 'space type' are introduced alongside other techniques. The basic algorithm is then developed to cope with different scenarios and behaviours as observed in reality.

2 Gap Acceptance Experiment

2.1 *Experimental Methods*

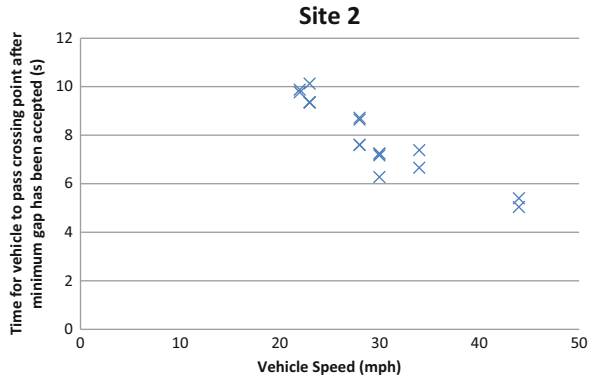
Experiments were undertaken at four sites in an urban area. These four sites were chosen as they have different road widths and different average vehicle speeds. Both one and two way traffic operations were studied. Four different observers were used to provide variation in age and mobility. The experiments were performed at off-peak times. Each set of site observations included cars, vans and heavy goods vehicles.

At each site, the observer was asked to watch a particular vehicle coming towards them and indicate when they considered it unsafe to cross. The location of the vehicle at this time was determined from video and its speed assessed using a radar gun. In essence, this determined the minimum gap that a pedestrian would accept for various vehicle speeds along different roads. Twenty results were gathered at each location over a period of 1 h.

²Examples of commercially available packages include Urban Analytics Framework, Vissim and Legion for Aimsun.

³Pedestrian gap-taking behaviour is where a pedestrian will decide to cross the road in between two vehicles travelling along that section of road, providing the separation of vehicles (gap) is perceived by the pedestrian to be large enough to cross safely.

Fig. 1 Graph showing the variation in time of a gap accepted by pedestrians against vehicle speed



2.2 Results

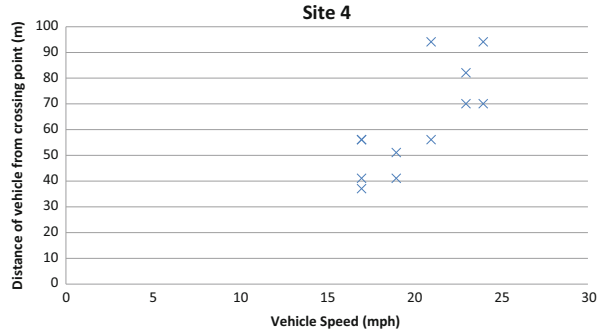
The results shown in this section are not considered statistically significant; the sample set available cannot be considered large enough to draw strong conclusions. The purpose of the research was to discover the potential range of behaviours that may need to be modelled and hopefully to inspire future research into exactly how models should be calibrated. It was not possible during the experimentation period to gather enough results to be able to suggest any trends that exist across sites, nor to gather any data on how behaviour varies as road width or average speed varies etc.

Therefore, any results that arise from the data collected are potential trends in crossing behaviour – waiting to be confirmed by future research. However, these potential trends must be included to cover all potential behaviours required.

Figure 1 shows the variation in gap time accepted by pedestrians at site 2, an 8 m wide road with speed limit 30 mph (48 km/h). There is a potential trend in crossing behaviour at this location. As speed increases, the gap taken in terms of time is shorter. In fact, this is because the distance at which the vehicles were located from the crossing point at the time the pedestrians took a gap was very similar regardless of speed. Therefore, there is a modelling requirement for a fixed distance on a particular road that does not depend on vehicle or pedestrian speed.

Figure 2 shows results from Site 4, a 6 m wide road with a 30 mph speed limit, although due to various local factors, the average speed is around 20 mph. There is a potential trend shown whereby the pedestrians at this location took larger gaps as the speed increased. Therefore, there is a requirement to model different gaps that are based on the speed of the vehicle, with a fixed time between the vehicle and the crossing point.

Fig. 2 Graph showing the variation in distance of a vehicle from crossing point against the speed of the vehicle at the minimum gap accepted by the pedestrian



2.3 Further Research

The experiments were conducted to get an idea of the range of behaviour that is seen when pedestrians cross the road. It is clear that these experiments need expanding to gain statistically significant results, with a much wider range of road widths, vehicle speeds and with more test subjects.

There were numerous difficulties in performing these experiments in uncontrolled environments. The analysis of the data was difficult due to experimental error. This has led the author to conclude that a controlled experiment where constant vehicle speeds are maintained, for example on a test track or even an entirely simulated environment would best suit further collection of data.

3 Functional Requirements

This section outlines the functional requirements for the algorithm. These are based on current research, best practice guidance, and experimental data as described in the previous section. Experience from project work by the author and requests from software users have led to the following scenarios that the algorithm should be able to model being identified:

- Pedestrian gap taking behaviour on multiple lane roads
- Pedestrian gap taking behaviour, accounting for a median strip
- Site specific behaviour; i.e. all pedestrians have the same behaviour in one location
- Pedestrian variable behaviour; i.e. different groups of pedestrians will exhibit different crossing behaviours at the same location
- Ability to model any size, direction or location of crossing
- Vehicle types can differ in their ability to react to a pedestrian
- Shared Space mixed priority behaviour

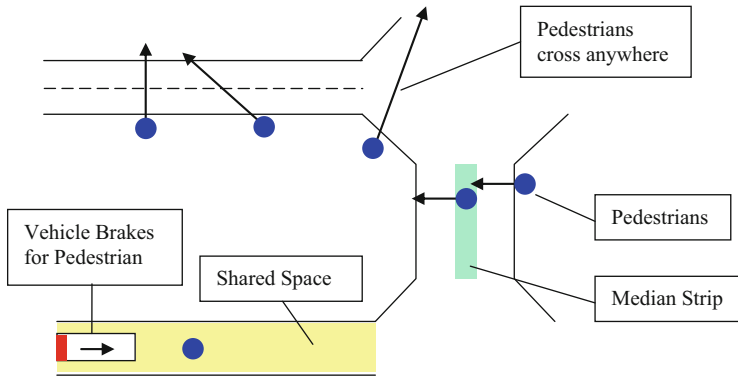


Fig. 3 Diagrammatic explanation of required functionality

These scenarios are a subset of the potential variety of behaviours and situations that could exist in reality. Therefore, a key requirement of the algorithm is that it can cover the above scenarios, but remain flexible enough for a model to be created of any space or behaviour. This is shown diagrammatically in Fig. 3.

4 Development of Algorithms

This section discusses the chosen methods, required variables, user input and formulation of the basic algorithms required for the chosen solution.

4.1 Choice of Method

A number of possible methods have been identified which cover part of the requirements. However, to cover all requirements as previously stated, as well as making the algorithm efficient, it is not possible to use one of these methods alone.

The solution chosen was to base the algorithm on ‘scan areas’⁴ and add in decision based logic to enable pedestrians to differ in their perception of gaps depending on their walking speed and risk perception.

Whilst the most natural approach would be that each vehicle and each agent⁵ has a scan area that represents the area they would both check for each other, the

⁴‘Scan areas’ are polygons that represent the areas where a vehicle or pedestrian will make a decision to slow down or cross the road when the other is inside the area.

⁵An agent represents a pedestrian in the simulation. The two terms are used interchangeably.

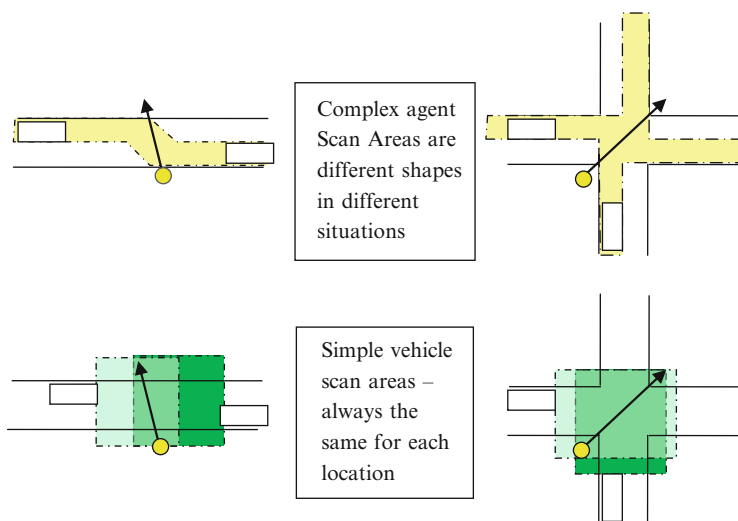


Fig. 4 Simplifying the scan area principle by using vehicular scan areas rather than pedestrian scan areas

intricacies of providing such a method are overly complex. This implies that the input required to build a model based on this would also be very complex.

Micro-simulation vehicles move more simplistically than agents. They follow the centre of a lane on a road and can only speed up or slow down along that path.⁶ An agent can move in any direction and will regularly change direction, avoiding other pedestrians. It is the vehicle's relatively simplistic movement that means attaching a scan area to a vehicle, which will enable an agent to make a gap acceptance decision, makes modelling simpler. This may seem counter-intuitive at first. However, if an agent bases their decision to accept a gap on the basis of vehicular distance then having an area in front of the vehicle at the same distance provides the same result and does not rely on computational methods to determine where the road space is relative to the agent. This concept is illustrated in Fig. 4.

However, as the above method does not allow for a difference in crossing behaviour of different groups of pedestrians, a layer of decision logic can be added to compensate for this. i.e. if an agent is inside a vehicle scan area, perform some calculation to determine whether to cross based on the individual agent's attributes.

The benefit of this combination is that for an agent to determine whether they are inside a vehicle scan area and if so to perform a more computationally intensive check is more efficient than performing computational checks on every vehicle.

Considering the situations that need to be modelled and the insight gained from the experiments, there are a number of variables required within the model that can

⁶This is a simplification – for example, vehicles can also change lane. However, the resultant paths of vehicles remain relatively simple.

be user defined to enable the calibration of the behaviour at a specific site or to model a variety of behaviours at the same site. These are as follows:

1. Ability to control how big a gap must be for an agent to cross based on the variable speed of a vehicle in any location
2. Ability to set a fixed distance at which an agent will cross, regardless of vehicle speed
3. Ability to allow different pedestrian groups to take different gaps based on their walking speed
4. Ability to control the distance or time in front of a vehicle in which a vehicle will slow down for an agent.

4.2 Definition of Pedestrian Space in UAF

The UAF user interface allows the user to draw areas of space over a road network. These spaces represent pedestrian only areas and shared areas where vehicles and agents interact when an agent is approaching or inside these areas. In addition to this, a new space, called shared priority space, has been created in order to implement the functionality of the chosen method. The relevant space types are shown below:

- Pedestrian Only – vehicles do not react to agents in this space
- Shared Courtesy – vehicles will slow down for an agent in pedestrian only space when they are approaching shared courtesy space and when inside shared courtesy space
- Shared Priority – agents will enter this space based on finding an acceptable gap, vehicles will slow down for agents already in this space.

4.3 Agent Detection Area

The ‘agent detection area’ is one of two scan areas associated with a vehicle. If an agent is inside this area and about to enter shared priority space, they will make a decision as to whether to cross or not. Increasingly complicated scenarios are considered to develop the algorithm.

Single Lane Road On a single lane road, only a pedestrian crossing on one side of the road needs consideration as the scenario is symmetric along the path of the vehicle, implying that the shape of the scan area must also be symmetrical in this case.

Site observation has suggested that a pedestrian does not step into the road until the rear of a vehicle has passed them. There is an equilibrium distance where behaviour changes from willing to cross the road to not doing so. The pedestrian would not cross at any point in between these two distances, which implies that the

Fig. 5 Agent detection area around a vehicle on a single lane carriageway

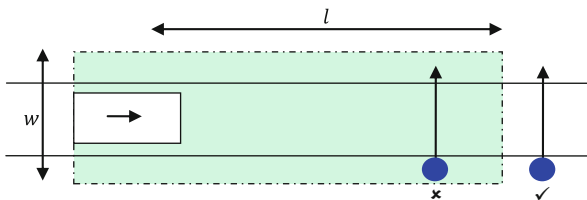
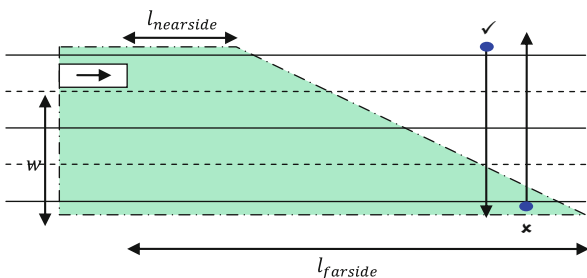


Fig. 6 Multi-lane carriageway dimensions of agent detection area



agent detection area of a vehicle should be a rectangular shape starting at the rear of the vehicle at a distance l from the front of the vehicle. This is shown in Fig. 5.

It is necessary to allow this distance to be a specified distance, x , or variable due to vehicle speed v_{veh} based on a time, t . To provide a flexible model, these values can be combined so that distance l is as per Eq. 1.

$$l = x + v_{veh} \times t \tag{1}$$

The width of the pedestrian detection area, w , is also made variable so that the model is completely flexible, allowing the user to apply a percentage, p , to the width of the road the vehicle is currently traversing, r_{veh} , and an additional arbitrary distance, y . This allows for different road widths and configurations of road widths and junctions to be modelled. This is shown in Eq. 2.

$$w = y + r_{veh} \times p \tag{2}$$

Multi-Lane Carriageway The first case considered is for a vehicle travelling in the nearside lane of a multi-lane carriageway. This case is non-symmetric, i.e. a pedestrian on the far side of the road to a vehicle will potentially require a longer gap than a pedestrian on the near side. Hence, additional area is required on the far side. This is illustrated in Fig. 6.

As the single lane carriageway scenario essentially represents the near side crossing of a pedestrian against a vehicle in the nearside lane, distance $l_{nearside} = l$ from Eq. 1. $l_{farside}$ is then required to be a percentage increase, p , of the nearside

lane value. To maintain flexibility, an arbitrary distance, d is added on per lane. The number of lanes is denoted by n . Equation 3 shows this.

$$l_{farside} = l_{nearside} + n \times ((l_{nearside} \times p) + d) \quad (3)$$

In the second case on a multi-lane carriageway, a vehicle may be travelling in a lane that is more than one other lane away from both sides of the carriageway. Equation 3 is easily modified to ensure this case is included. The number of lanes between the vehicle and each side of the road is denoted by n_1 and n_2 , respectively. These are shown in Eqs. 4 and 5.

$$l_1 = l_{nearside} + n_1 \times ((l_{nearside} \times p) + d) \quad (4)$$

$$l_2 = l_{nearside} + n_2 \times ((l_{nearside} \times p) + d) \quad (5)$$

Algorithm The c++ pseudo code below illustrates the algorithm when an agent is making a decision based solely on whether they are inside a vehicle's scan area or not.

```
//if agent a is about to cross a road and needs to make
//a decision
if(a.approachingRoad())
{
    //check each vehicle in local area
    for (each Vehicle v)
    {
        //check whether inside agent detection area
        if (v.inAgentDetectionArea(a))
        {
            //agent prevented from crossing
            a.setCross(false);

            //exit loop as no need to check other
            //vehicles
            break;
        }
    }
}
}
```

Adding Variability for Different Pedestrians Different pedestrian groups essentially have different speeds and different perceptions of risk and acceptable gaps.

This can be modelled by allowing the individual agent walking speed to be taken into account. This is further enhanced by adding a ‘buffer time’⁷ into the calculation. The algorithm above is adapted to this effect, and is shown below.

```
//if agent a is about to cross a road and needs to make
//a decision
if(a.approachingRoad())
{
    //check each vehicle in local area
    for (each Vehicle v)
    {
        //check whether inside agent detection area
        if (v.inAgentDetectionArea(a))
        {
            //check time it will take until
            //vehicle would
            //theoretically collide with agent in road
            int time = v.checkTimeToCollision(a);
            //N is buffer time of an agent
            //if vehicle will hit agent before it can get
            //across the road

            if (time < a.getMinimumTime() + a.getN())
            {
                //agent prevented from crossing
                a.setCross(false);
                //exit loop as no need to check other
                //vehicles
                break;
            }
        }
    }
}
//...
//snippet of time to collision check
```

⁷The ‘buffer time’ is an additional time by which a pedestrian wants to be safely across the road before a vehicle passes. Larger buffer times can therefore be used to model more cautious group pedestrian behaviours.

```

int Vehicle::checkTimeToCollision(agent a)
{
    //calculate a line in front of agent
    line L = a.line();

    //intersect(point,path,line) determines
    //distance from a
    //point along a path to a line
    //returns a large integer if path doesn't
    //cross line

    //use vehicle location and future path of
    //vehicle
int dist = intersect(v.location(),v.getPath(), L);

    //at current speed of vehicle, how long until
    //the vehicle crosses the line in front of
    //agent
int time = dist / v.speed();

    //if path doesn't cross line, the return value
    //will be a large integer so will not prevent
    //agent from
    //crossing
return time;
}

```

Median Strip The function that returns a line in front of an agent (denoted in the code as `a.line()`) can be constructed so that it returns a line which represents the path an agent will take whilst in the road space directly in front of it. This uses the definition of space in UAF, illustrated in Fig. 7.

This means that median strip behaviour, where a pedestrian will only initially consider vehicles on the side of the road before the median strip, can be modelled. The user can draw the space so that a vehicle on the other side of the road will be ignored. This is shown in Fig. 8.

4.4 Vehicle Scan Area

The agent detection area controls how agents react to vehicles, which models the gap acceptance behaviour well. At site locations with low vehicle speeds and shared

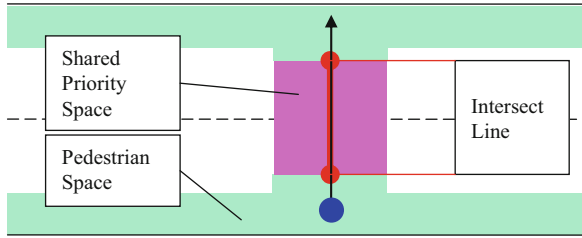


Fig. 7 Using the UAF space definition to determine where the intersect line should be taken from

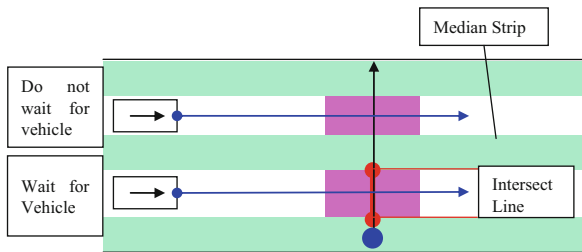


Fig. 8 Using the UAF space definition to determine where the intersect line should be taken from

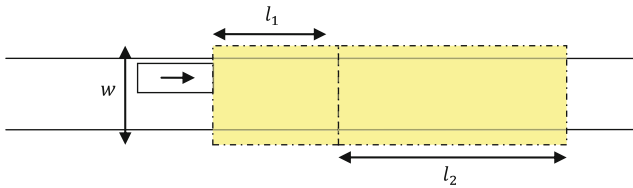


Fig. 9 Vehicle scan area dimensions

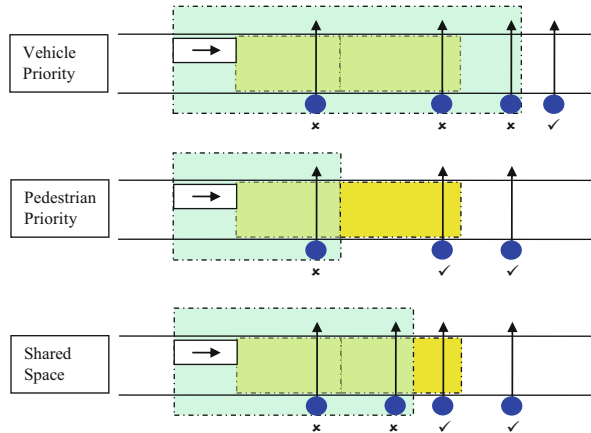
space, regular pedestrian behaviour is such that a pedestrian may take a gap that requires a vehicle to slow down or even stop for the pedestrian. Therefore, there is a requirement for the vehicle to react to pedestrians in a crossing space.

The ‘vehicle scan area’ is a polygon attached to a vehicle such that the vehicle will slow down or stop for a pedestrian who is inside the area and crossing a road. The definition of when an agent is classed as crossing the road can be found in 5.1.

The vehicle scan area is defined similarly to the agent detection area. The area is defined in two parts. Figure 9 shows the lengths and widths that make up the scan area definition.

The width of the scan area is defined identically to the agent detection area. l_1 is made up of the Stopping Sight Distance, as defined by Manual for Streets 2, CIHT [4]. l_2 is defined using a fixed distance or time, similarly to the agent

Fig. 10 Showing when an agent will cross or not in different positions relative to a moving vehicle for different types of space behaviour



detection area, though there is no need to employ different lengths for different types of carriageway.

The vehicle scan area works in unison with the agent detection area to provide a variable behaviour where a pedestrian may choose to step in front of a car, forcing the car to slow down; or may allow the vehicle to pass. It is also used to model pedestrian priority crossings, where no pedestrian gap acceptance is in place. This is shown in Fig. 10.

It is important to note that the exact combinations of length of each scan area are likely to change with road speed, road width etc. This is especially true of the shared space example, where vehicle speeds are usually low with different volumes of flow of vehicles and pedestrians. The variance in priority and gap taking behaviour is highlighted by a study recently commissioned by The Department For Transport, UK [5]. The models will require calibration based on a variety of these factors. However, modelling such variation in behaviour requires a variety of different scenarios to be modelled to obtain a range of results from which to compare different design options.

5 Conclusions

The requirement to be able to model pedestrian gap acceptance is clear – certain less managed designs of streets and junctions rely on pedestrians and vehicles making decisions as to when to proceed or not. To be able to compare junction and street design options and to output quantitative metrics for pedestrians and vehicles, these types of space need to be considered in the modelling process.

This paper has outlined some basic experimental research carried out in order to gain an insight into the most appropriate methods for modelling less managed spaces. The results from the experiments provided clues as to the type of modelling

that should be available. However, it is clear that this research can be greatly improved upon in order that pedestrian models can be better calibrated and so that the decision processes made when crossing a road and accepting a gap can be better understood.

From this research and in discussion with user groups of the UAF micro-simulation software, a set of algorithms have been developed to encapsulate the requirements for pedestrian gap acceptance modelling. The methods chosen have purposefully remained flexible as research has shown that there are a variety of different behaviours at various sites.

It remains the case in modelling these types of pedestrian and vehicular interactive behaviour that various scenarios must be tested in order to capture a range of results, which are useful to analyse a junction and compare design options.

Further research is required as more and more less managed schemes are implemented. If there is consistency in the variety of behaviours which are dependent on a number of factors, the model calibration can be improved. This may reduce the need to model a range of scenarios in one location and make the modelling process more efficient. However, it is clear that these behaviours can now be modelled in micro-simulation and that a wider variety of options for any urban location can be analysed to provide a better indication of how these complicated spaces operate.

References

1. DfT Shared Space Project, Stage 1: Appraisal of Shared Space, Report for Department for Transport, MVA Consultancy (2009)
2. Economic Impact of Traffic Signals, Greater London Authority, p. 46 (2009)
3. UAF Simulation Information, <http://www.pedestrian-simulation.com>
4. CIHT, Manual for Streets 2, Wider Application of the Principles p. 073 (2010)
5. Designing the Future, Shared Space Operational Assessment, Report for Department for Transport, MVA Consultancy (2010)

Pedestrian Simulation Using Geometric Reasoning in Velocity Space

Sean Curtis and Dinesh Manocha

Abstract We present a novel pedestrian representation based on a new model of pedestrian motion coupled with a geometric optimization method. The model of pedestrian motion seeks to capture the underlying physiological and psychological factors which give rise to the *fundamental diagram*—the phenomenon that pedestrian speed reduces as density increases. The optimization method computes collision-free velocities directly in velocity space. The resultant method exhibits the same types of self-organizing behaviors shown by previous models, is both computationally efficient and numerically stable, can be intuitively tuned to model cross-cultural variation, and is sufficiently robust that a single set of simulation parameters produces viable results in multiple scenarios.

Keywords Pedestrian model • Geometric • Constraint-based optimization • Fundamental diagram • Density sensitivity

1 Introduction

The ultimate goal of pedestrian dynamics is to be able to evaluate pedestrian responses to various environments and conditions in vitro. Given the specification of a novel space, we seek to apply a simulation to predict how real humans will act in that space. As with all simulation domains, the challenge of simulating human pedestrians is one of balancing the need for a model which is comprehensible and computationally tractable against the requirement that the simulation results

S. Curtis (✉) • D. Manocha
University of North Carolina at Chapel Hill, Chapel Hill, NC, USA
e-mail: seanc@cs.unc.edu; dm@cs.unc.edu; <http://gamma.cs.unc.edu/PEDS>

sufficiently reproduce real-world phenomena; the credibility of predictions based on simulations depend on the belief that the model accurately extrapolates behavior into new spaces. Unlike other simulation domains (e.g. fluid simulation), pedestrian dynamics possesses no governing equations against which pedestrian models can be compared. As such, it is impossible to definitively assert if a single “correct” model exists or what it may look like. Scientists actively search for models which exhibit human-like behaviors while simultaneously possessing desirable computational characteristics.

To that end, we present a novel microscopic model for simulating pedestrians. Like other pedestrian models, our model computes a collision-free velocity for each virtual pedestrian based on a *preferred* velocity and its local neighborhood of static and dynamic obstacles (e.g. other pedestrians). Our model uses a geometric optimization technique, called ORCA[1], to directly compute, in velocity space, the collision-free velocity that most closely matches the preferred velocity.

The ORCA model has been shown to exhibit self-organizing behavior [2] and can reproduce small-scale pedestrian-pedestrian interactions [3]. It has also been shown to be efficient [4] and stable [5]. Together, efficiency and stability dictate how practical the approach is. Efficiency describes the model’s computation cost per simulation time step. The stability indicates how large a time step can be taken. High stability and efficiency means simulations can run very quickly, allowing multiple iterations to be taken.

Despite its computational strengths, pedestrians simulated with ORCA do not adhere to the fundamental diagram; their speed does not decrease as density increases (see Fig. 2). We provide a unique model of pedestrian motion which seeks to capture the underlying factors which cause groups of pedestrians to exhibit the fundamental diagram. Pedestrian models typically function by adapting a preferred velocity to local dynamic conditions. Usually, the preferred velocity represents the speed and direction the pedestrian would take if he were alone in the space. We apply our motion model directly to the preferred velocity, adapting it to density conditions, and then pass the result to the pedestrian model. This density-dependent behavior model introduces behaviors consistent with the fundamental diagram into ORCA while preserving ORCA’s computational benefits. Finally, for the experiments given, the model is robust; a single set of simulation parameters produces good results across different scenarios.

The remainder of the paper is organized as follows: We give a brief overview of related work in Sect. 2. In Sect. 3 we present the basis of our geometric optimization algorithm, *velocity obstacles* and ORCA. Section 4 gives the motivation, details and impact of the density-dependent pedestrian behavior model. In Sect. 5 we generalize the model for two dimensions and show the results. Finally, in Sect. 6 we analyze the model’s strengths and weaknesses.

2 Related Work

There has been a great deal of work in the pedestrian dynamics community in devising models for pedestrian motion and interaction. The research has largely focused on two approaches: cellular automata (CA) and social forces (SF). Recently, motion-planning techniques in velocity space have been applied to pedestrian simulation with promising results.

Cellular automata approaches work by discretizing the simulation domain into a grid of “cells”. An agent may occupy at most one cell and a cell may contain no more than a single agent. Pedestrians move from cell to cell based on various techniques. These approaches were quite common in simulating vehicular traffic. Blue and Adler first applied these techniques to pedestrians using a set of crafted rules for determining pedestrian movement and showed that they were able to reproduce observable pedestrian phenomena in both uni-directional and bi-directional flows [6, 7]. Other approaches applied probabilistic techniques to determine agent movement and augmented the functionality with scalar and vector fields to reproduce emergent phenomena [8]. CA-based approaches tend to exhibit some artifacts due to the discretization of the space. There has been extensive research to understand and mitigate these effects. Kirchner et al. examined the impact of the size of the cells [9]. Maniccam investigated the impact of exchanging square cells for hexagonal cells [10]. Yamamoto et al. introduced the “real-coded cellular automata” to minimize the aliasing artifacts which arise from traversing a rectilinear grid [11]. CA-based approaches remain an active branch of research; these methods have been used as a basis to simulate complex scenarios with more elaborate pedestrian behaviors. [12, 13].

Social-force-based models treat pedestrians like mass-particles and applies Newtonian-like physics to evolve the simulation. The first such model was introduced by Hirai and Tarui [14]. The agent would interact with obstacles and agents in the environment through the superpositioning of repulsive forces. Later SF-based models explored alternate formulations of the repulsive forces or novel forces including, compression and friction forces for evacuation [15], relative-velocity-dependent forces [16, 17], and group formations [18]. A more complete overview can be found in [19]. SF-based models have been shown to exhibit self-organizing behaviors [20].

Recently, techniques from robotics have been applied to pedestrian simulation with promising results. Agent interactions are based on *velocity obstacles* (VO). One agent defines a set of velocities for another agent which would lead to an inevitable collision. Agents then select a velocity outside of this set for a collision-free path. Originally, each agent assumed that all other agents were non-responsive [21]. Later VO-based models introduced alternative VO formulations which assumed that agents were aware that those around them would also respond [1, 22, 23]. Pedestrian simulation using VO-based models has been shown to exhibit self-organizing behaviors and varying flow through a bottleneck [2] as well as accurate microscopic interactions between individual pedestrians [3].

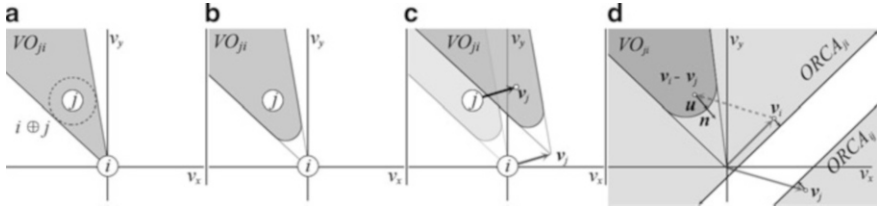


Fig. 1 Velocity obstacles. (a) The velocity obstacle formed by agent j on i . (b) The truncated velocity obstacle for time window τ . (c) Agent i assumes j takes constant velocity \mathbf{v}_j ; VO_{ji} is displaced by \mathbf{v}_j . (d) The formulation of the half plane $ORCA_{ji}$, including the minimum change in relative velocity, \mathbf{u} , the direction of minimum change, $\hat{\mathbf{n}}$. We also show the symmetric half plane $ORCA_{ij}$

3 Velocity Obstacles

Before we discuss the details, we'll define some notation and terminology. In discussing real and virtual humans, we need to be able to make a clear distinction between the two. To that end, we make the arbitrary choice to use the term “pedestrian” or “subject” to refer to real humans and “agents” for virtual humans. Each agent is modeled as a two-dimensional circle modeled with the state vector: $[r, \mathbf{p}, \mathbf{v}, \mathbf{v}^0]^T \in \mathbb{R}^7$, where r is the radius of the disk, \mathbf{p} , \mathbf{v} , and \mathbf{v}^0 are two-dimensional vectors representing the current position, current velocity and preferred velocity, respectively. By convention v^0 and v are the preferred speed and current speed (i.e. the magnitudes of the corresponding vectors). When properties of agent i are discussed, the elements of the state will be subscripted with the agent's index (e.g. r_i and \mathbf{v}_i^0).

Velocity obstacles exploit an intuitive principle. As two agents move through a shared space, each agent observes the position *and* velocity of the other agents and predicts whether a conflict will happen in the future. For example, agent i may occupy a position on agent j 's intended path of travel, but if i is gone before j arrives, there is no conflict. This principle is formalized with the *velocity obstacle* [21].

The velocity obstacle is, as the name implies, an obstacle, but rather than lying in workspace or configuration space, it lies in velocity space. Velocity space, for pedestrians, is a two-dimensional space in which each point represents a velocity. In Cartesian space, a position is a point and a velocity is a vector. Each velocity vector in Cartesian space maps to a point in velocity space. So, a workspace obstacle represents a set of positions which the agent cannot occupy; a velocity obstacle represents a set of velocities an agent cannot assume.

For agents i and j , agent j induces a velocity obstacle on i , VO_{ji} , and i induces a symmetric velocity obstacle on j , VO_{ij} . The velocity obstacle VO_{ji} is a cone, originating at \mathbf{p}_i , which tightly bounds the Minkowski sum of agent i 's geometry with j 's (Fig. 1a). If the *relative* velocity between agents i and j remains within this cone, there will be an inevitable collision. In practice, we are typically concerned

with collisions that can occur within the next τ s. Including this term truncates the cone (Fig. 1b); very small relative velocities will not lead to collisions within τ s, so these velocities are not included in the obstacle.

This velocity obstacle consists of the set of *relative* velocities that lead to collision. A single agent cannot exert unilateral control over the relative velocity. If agent i assumes that j will not change velocity, i must take full responsibility for avoiding the collision. This behavior is modeled by translating VO_{ji} by j 's velocity (Fig. 1c). Given this assumption, agent i can avoid collision with agent j by selecting a *feasible* velocity—a velocity that lies outside the velocity obstacle. This is the original velocity obstacle formulation, in which each agent assumes that every other agent is a non-responsive, dynamic obstacle [21].

However, this model is a poor representation of pedestrians because pedestrians do, in fact, react to each other. This leads to two significant issues for agents. First, if agent i predicts agent j 's velocity incorrectly, the velocity obstacle will have error (the amount of error depends on how bad the prediction is). The error may be sufficiently large, that even if both agents select velocities lying outside the velocity obstacle, they may still collide within τ s. Second, both agents overreact to their neighbors (because they falsely assume that the other will make no effort to avoid collision). This can easily lead to oscillatory motion as the agents overreact in successive steps.

Van den Berg et al. proposed an alternate formulation to VO which addresses these issues: Optimal Reciprocal Collision Avoidance (ORCA) [1]. The truncated cone, VO_{ji} , is replaced with a half plane, $ORCA_{ji}$. The half plane can be considered a union of many truncated cones. In effect, rather than assuming the agent j will take a particular velocity, agent i assumes that it will take one velocity from a large set and plans to avoid all of the velocities in that set. Agent j does the same with respect to i . These two sets are defined so that there is no pair of feasible velocities which can lead to collision within τ s. This solves the first problem. The second problem—oscillatory motion due to individual overreaction—is solved by defining the planes such that the amount of change to the relative velocity required to avoid collision is evenly distributed between the two agents. Each agent assumes the other agent will make an equal effort to avoid collision. The effort is evenly apportioned and no agent overreacts.

The ORCA half-plane can be constructed geometrically in the following manner. Assume agents i and j have velocities \mathbf{v}_i and \mathbf{v}_j , respectively, and that these velocities place them on a collision course (i.e. $\mathbf{v}_i - \mathbf{v}_j \in VO_{ji}$). Let \mathbf{u} be the vector from $\mathbf{v}_i - \mathbf{v}_j$ to the closest point on the boundary of the velocity obstacle (Fig. 1d). More formally,

$$\mathbf{u} = \left(\underset{\mathbf{v} \in \delta VO_{ji}}{\operatorname{argmin}} \|\mathbf{v} - (\mathbf{v}_i - \mathbf{v}_j)\| \right) - (\mathbf{v}_i - \mathbf{v}_j) \quad (1)$$

is the minimum change in relative velocity between i and j necessary to guarantee no collision within τ s. To model the reciprocity, half of the minimum change is applied to each agent. So, we can define the ORCA velocity obstacle induced by agent j on agent i as:

$$\text{ORCA}_{ji} = \{\mathbf{v} | (\mathbf{v} - (\mathbf{v}_i + \frac{1}{2}\mathbf{u})) \cdot \hat{\mathbf{n}} < 0\}, \quad (2)$$

where $\hat{\mathbf{n}}$ is the normalized direction of \mathbf{u} . Proof of the guarantees can be seen in the original paper [1].

The ORCA algorithm has several desirable properties:

- It is very computationally efficient. For example, it has been used to simulate 35,000 agents in better than real time (2.6 s of simulation for 1 s of computation) [4].
- It has been shown to produce consistent and stable results for time steps as large as 0.2 s [5].
- Pedestrian simulations with this model have exhibited self-organizing behaviors (e.g. lane formation, arching, jamming, etc.) and reduced flow through a bottleneck [2].
- Microscopic interactions between individual agents have also been reproduced using these approaches [3].

However, there is an important phenomenon, which pedestrians exhibit, that ORCA agents do not: the fundamental diagram (see Fig. 2). To be considered a viable pedestrian model, ORCA agents must reproduce the fundamental diagram. Our goal is to introduce this property while preserving ORCA's desirable properties.

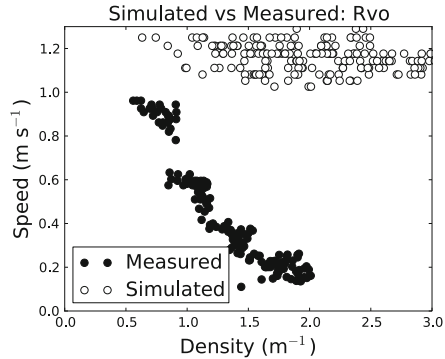
4 Adherence to the Fundamental Diagram

The fundamental diagram is the observed relationship between pedestrian density and speed [24]; as density increases, speed decreases. However, ORCA agents do not adhere to this pattern; the agents can move at arbitrarily high speeds even at extreme density. This is because the ORCA algorithm is only concerned with collisions. If the relative velocity between two agents is zero, no collision is possible, regardless of their relative positions. We illustrate this phenomenon by reproducing a real-world experiment with ORCA.

Seyfried et al. performed a simple experiment to examine the fundamental diagram [25]. They approximated a one-dimensional scenario with periodic boundary conditions by creating a narrow elliptical path, in which pedestrians were forced to walk single file. They performed a series of tests. In each test, they increased the number of subjects in the ring, implicitly increasing the density, and measured the speed of the subjects. We reproduced their experiment in a virtual context.¹ The results of the simulation are shown in Fig. 2. The black dots show the experimental data; as density increases, speed decreases. The white dots show the simulated

¹We refer the reader to the original paper [25] for the full experimental parameters.

Fig. 2 Comparison of ORCA with experimental data in a simple one-dimensional experiment [25]. The experimental data (*black dots*) show decreasing speed as density increases. The simulated data (*white dots*) show consistent speed, regardless of density



results; agent speeds remain consistent, regardless of the density.² Human beings clearly exhibit a response to density which leads to changes in their walking speed which is not captured by the ORCA formulation.

To use ORCA as a pedestrian model, ORCA agents must, in addition to self-organizing behaviors, also show behavior consistent with the fundamental diagram. We propose a density-dependent behavior model, which models underlying physiological and psychological factors which lead to the fundamental diagram. In this section, we will discuss the evidence for what these factors may be, define a model based on those observations, and show the results of applying that model.

4.1 Model of Density-Dependent Behavior

Biomechanists have performed extensive analysis on the human walking gait and have deduced the following [26]:

1. Humans choose a gait that minimizes the energy expenditure per unit distance traveled.
2. For any given speed, there is a “natural” stride length which minimizes the energy expenditure. Imposition of other stride lengths leads to a greater than optimal energy expenditure.
3. The “natural” stride length grows as walking speed increases.

In other words, to walk a particular speed, there is a natural stride length. But the converse is also true; for a particular stride length, there is a natural walking speed. We believe that this physiological property is a significant factor which leads to the fundamental diagram. As density increases, the space available to a pedestrian decreases. If it decreases sufficiently to limit stride length, speed must likewise

²The variation in simulation speed arises from normally distributed preferred speeds for the agents.

decrease. To walk a certain speed with a “natural” gait, a minimum amount of space is required.

However, this physiological cause is not the sole contributing factor to the fundamental diagram. Researches have shown that sensitivity is also dependent on cultural factors [27]. In this experiment, the previous one-dimensional experiment was re-created with Indian subjects in place of German subjects. The Indian subjects proved to be less sensitive to density than their German counterparts. From this we deduce that there is a psychological/sociological component. This component serves to increase the amount of space required to walk at a particular speed beyond the strictly physical requirements.³ In addition to this cultural factor, we assert that a pedestrian’s ability to accurately estimate required and available space is imprecise and possibly even instinctual; the fact that pedestrians rarely collide suggests that this estimation is conservative.

We combine the biomechanical data with the social observations to create a model which accounts for the human factors which lead to the fundamental diagram. Specifically, we propose a linear model of a physiological constraint and a psychological constraint.

Physiological constraint: Biomechanists have researched the relationship between the dominant modes of human walking. Although the pedestrian dynamics community largely subscribes to the idea that the relationship between stride length (L) and walking speed (v) is linear [24], more recent research suggests the relationship is actually quadratic [26, 28]:

$$L(v) = \frac{H}{\alpha} \sqrt{v}, \quad (3)$$

where $\alpha = 1.57$ is a “stride factor”, as determined by Dean from experimental data [28] and H is the normalized height of the agent ($height/1.72$ m).⁴

Psychological constraint: Psychologists and biomechanists have shown that humans have a strong sense of personal space—a “buffer” that extends beyond mere physical requirements [27, 29]. We are unaware of any mathematical models which relate changes in personal space to speed or cultural factors, but we recognize the fact that they do play a role and must be accounted for. In the absence of more specific data, we assume the extra buffer space (B) is a simple linear function of the physiological space requirement:

$$B(v) = \beta L(v). \quad (4)$$

³In ordered marching, as seen with soldiers, the fundamental diagram can be completely eliminated as walking can be coordinated to maintain speed at high density.

⁴Dean originally presented the relationship between stride frequency (f) and speed (v) [28]. We have used the relationship $v = fL$ to reformulate Dean’s work as the relationship between stride length and speed.

When walking slowly and taking small steps, the buffer space is small. When walking quickly, and taking large steps, the buffer space grows. It is controlled by the stride buffer parameter, β . We will show that varying the buffer value is sufficient to reproduce differences observed across different cultures (Sect. 4.2).

From these constraints, we can define our novel models of both: the space required (S) to move at a particular speed and its inverse, the natural speed for a given available space:

$$S(v) = B(v) + L(v) = (1 + \beta)L(v) = (1 + \beta)\frac{H}{\alpha}\sqrt{v}, \quad (5)$$

$$v(S) = \max\left(v^0, \left(\frac{S\alpha}{H(1 + \beta)}\right)^2\right). \quad (6)$$

We use the equations to modify the *preferred speed* of the agent. The pedestrian models we've discussed in this paper (SF, CA and VO) all share a common paradigm. Each agent has a strategic intent which is adapted to local dynamic conditions by the pedestrian model. The strategic intent is typically the trajectory the agent would walk in the absence of other agents. Derived from a global navigation strategy, this might be the shortest path through a building to its goal traversed at some preferred speed. This strategy is communicated to the pedestrian model as a preferred velocity toward an immediate goal. The pedestrian model adapts the preferred velocity to account for nearby agents and obstacles such that the agent makes progress towards its goal without collisions. Most research has focused on this local adaptation (probabilities and floor fields in CA [8], repulsive forces in SF [15–17], and velocity obstacles in VO [1, 21]). However, we suggest that models may be improved if we consider the idea that the intent itself adapts to local conditions. At the very least, by allowing for this possibility, we have access to more degrees of freedom in simulating pedestrians.

By modifying the preferred velocity, we are hypothesizing that pedestrians do adapt their intentions. The data supports this hypothesis. Chattaraj et al. reported that the freespace walking speeds of the subjects in the one-dimensional experiment had a mean speed of 1.24 m/s with a standard deviation of 0.15 m/s [27]. However, in Fig. 3, the experimental subjects show an interesting behavior. At the lowest densities (0.5–1.0 people/m²), the speeds saturate to less than 1 m/s. At the sparsest, the agents should be able to walk faster than 1 m/s, but they choose not to. This is evidence that their intent has adapted to their circumstances.

4.2 Density-Dependent Behavior in One Dimension

With this new model for preferred speed, we can repeat the one-dimensional experiment. We give each of the agents a default preferred speed according to the distributions reported above. We've introduced two new parameters: the physiological stride factor (α) and the psychological stride buffer (β). We use normally

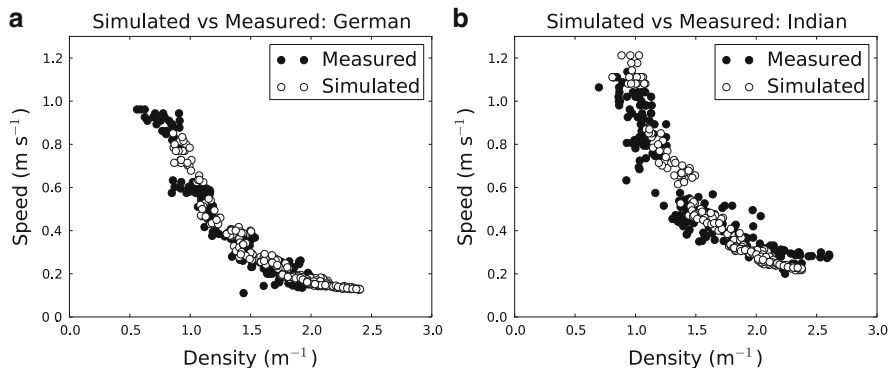


Fig. 3 Comparisons between measured and simulated data in the one-dimensional experiment described in [25, 27]. (a) shows the results with German subjects and (b) shows the same for Indian subjects

distributed values for these parameters. The mean for stride factor, $\mu_\alpha = 1.57$, is the value provided by Dean in his work. By varying the value with the standard deviation, $\sigma_\alpha = 0.15$, we simulate normally distributed heights. We selected the mean stride buffer value that fit the data well, which gave us a mean and standard deviation for β of $\mu_\beta = 0.9$ and $\sigma_\beta = 0.2$. All other simulation parameters were the same as the simulation that produced the data in Fig. 2. Figure 3a shows the results using our density-dependent speed model. Unlike the results shown in Fig. 2, the simulated agents closely follow the fundamental diagram displayed by the German subjects.

To illustrate the full effect of the speed buffer parameter, we also reproduced the Indian experiment. The authors reported that the Indian subjects exhibited essentially the same freespace speeds as the German subjects. We make the reasonable assumption that the physiology is the same across cultures, so we should be able to reproduce the Indian subjects' behavior by changing *only* the psychological constraint. Reducing the stride buffer value should decrease the agents' sensitivity to density. Changing β to the distribution, $\mu_\beta = 0.45$, $\sigma_\beta = 0.125$, captured the Indian behavior, supporting the hypothesis (all other parameters were identical). The results can be seen in Fig. 3b.

5 Estimating Available Space

To apply (6) to two dimensional scenarios, we need to determine the scalar “space” available to the agent. We propose a method for computing the space available for an agent, based on the relative positions and velocities of its neighbors. Our method is based on the following principles:

- As personal space has been observed to be biased forwards in the pedestrian’s direction of travel [29], the space that matters most lies in the agent’s preferred direction of travel ($\hat{\mathbf{v}}^0 = \mathbf{v}^0 / \|\mathbf{v}^0\|$).
- The presence of other agents reduces the amount of available space. The degree to which they limit it depends on their walking speed, their orientation and their position, relative to the preferred direction of travel.
- The total reduction of available space imposed by neighboring agents can be approximated by the single agent that reduces the available space the most.

The method relies on a metric called the “effective” distance. Effective distance (E_{ji}) represents the overall impact of agent j on agent i ’s perception of available space, based on the principles listed above. The perceived space available for agent i (S_i) is the smallest effective distance of all of agent i ’s neighbors. The effective distance of a neighbor, j , depends on its position relative to i , its orientation, and its speed. We define effective distance of agent j with respect to agent i (E_{ji}) as the combination of the Euclidian distance between agents i and j (d_{ji}), a directional penalty (Δ_{ji}), and an orientation penalty (O_{ji}), as follows:

$$S_i = \min \left(\sum_{j \in N_i} E_{ji} \right), \quad (7)$$

$$E_{ji} = d_{ji} + \Delta_{ji} - O_{ji}, \quad (8)$$

$$\delta_i = \frac{(1 + \beta)H}{2\alpha} \sqrt{v_{\max}}, \quad (9)$$

$$\Delta_{ji} = 0.15\delta(1 - (\hat{\mathbf{v}}_i^0 \cdot \hat{\mathbf{d}}_{ji})), \quad (10)$$

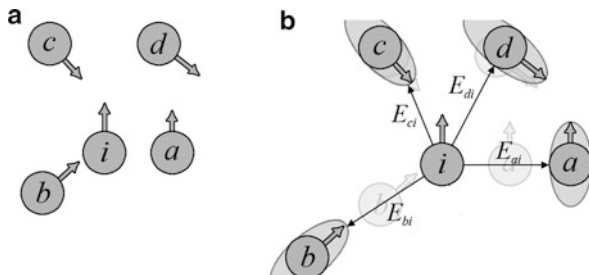
$$O_{ji} = \max \left(r_j, \frac{H\sqrt{v_j}(1 + \beta)|\hat{\mathbf{v}}_j \cdot \hat{\mathbf{d}}_{ji}|}{2\alpha} \right), \quad (11)$$

where N_i is the set of i ’s neighboring agents, $\hat{\mathbf{d}}_{ji}$ is the unit-vector pointing from agent i to agent j , and δ_i is the maximum Euclidian distance at which another agent can cause agent i to slow down. Figure 4 illustrates effective distance.

The *directional penalty*, Δ_{ji} , increases the effective distance of an agent based on agent j ’s angular displacement from agent i ’s preferred direction of travel. If agent j lies directly in the direction of travel, the directional penalty is zero and the effective distance remains the same as the Euclidian distance. As the direction to j moves away from the preferred direction, the effective distance increases. This term represents an approximation of the elliptical personal space observed in experiments [29]. Neighbors to the side of the agent must be closer than those in front to have the same constraining influence.

The orientation penalty computes how much of the distance between agent and neighbor is consumed by the neighbor’s stride. The space the agent consumes is predominantly in the direction of its travel. If the agent is moving perpendicularly

Fig. 4 An illustration of effective distance. (a) shows the position of agents i , a , b , c and d in Cartesian space. (b) shows the effective distance between agents a , b , c , and d with i based on their direction and orientation



to the displacement vector ($\mathbf{d}_{ij} \cdot \mathbf{v}_j = 0$), then the closest point on the agent is its side and it consumes a distance equal to its radius. However, if it is walking in the direction of the displacement, it is occupying a portion of the space between i and j equal to half its stride length.

Figure 4a shows the configuration of agent i and its four neighbors in Cartesian space. Agents a and b are closest based on simple Euclidian distance. However, Fig. 4b shows the impact of effective distance. The ellipses represent the space consumed by each agent’s stride. Because the angle between preferred direction and direction towards agents a and b is large, agents a and b receive a large directional penalty. Agents c and d are physically the same distance from agent i and receive the same directional penalty. But because agent c ’s velocity is nearly parallel to the displacement direction, its stride consumes more of the available space than d . Thus, the space available for agent i is E_{ci} .

5.1 Density-Dependent Behavior in Two Dimensions

We evaluate the efficacy of the density-dependent behavior in two dimensions by comparing real world experiments with comparable simulated scenarios. Zhang et al. performed experiments on the flow of groups of pedestrians in a corridor. They examined both uni-directional [30] and bi-directional flow [31]. We refer the reader to the papers for exact details on the spatial configuration of the experiment environment.

Simulation Parameters: It has been observed that humans can be bounded by an ellipse with major and minor axes of 0.24 and 0.15 m, respectively [24]. The area of this ellipse is 0.11 m^2 . We model the agents as circles with the same area as that ellipse: a circle with a radius of 0.19 m. This represents a statistical model of the human more than a physical one.

As with the one-dimensional experiment, we use normally distributed values for three key parameters: preferred speed (v^0), stride factor (α), and stride buffer (β). Because one of our goals is to create a pedestrian model that doesn’t require scenario-specific tuning, we applied the same values for the uni- and bi-directional

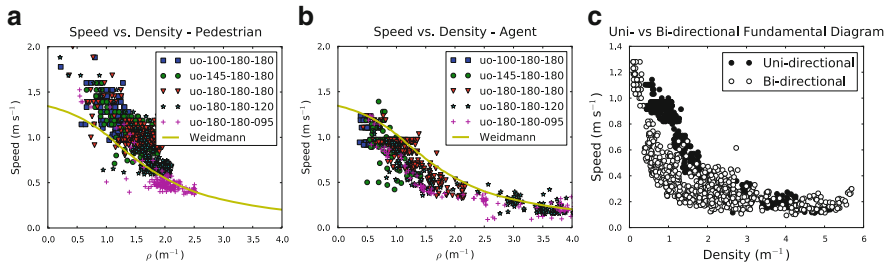


Fig. 5 Comparisons of the fundamental diagram for real-world and simulated data for the uni-directional flow experiment [30]. (a) The real-world pedestrian data. (b) The simulated agent data. Weidmann’s model [24] is plotted for reference. (c) Comparison of the fundamental diagram exhibited by simulated agents in uni-directional and bi-directional flow. In the range of density between 1.0 and 2.0 m⁻², the bi-directional flow speed falls off more quickly. This same phenomenon was observed in real crowds [31]

flow experiments as we did for the one-dimensional experiment. All other simulation parameters (e.g. initial density, number of agents, etc.) are as specified in the experiment documentation.

5.2 Two-Dimensional, Uni-Directional Flow

In the uni-directional flow experiments, Zhang et al. controlled the flow of pedestrians into a corridor of uniform width [30]. They recorded the trajectories of the subjects over multiple iterations, each with an increased level of flow into the corridor (and a corresponding increase in density). Once the maximum in-flow was achieved, they began constricting the exit width in subsequent iterations to further increase density. We reproduced this scenario. Please, refer to the original paper for the details [30]. The results can be seen in Fig. 5.

There are several points we would emphasize with respect to Fig. 5. First, although the agents don’t exactly reproduce the behaviors observed in the subjects of the experiment, they do produce a behavior consistent with Weidmann’s model of the fundamental diagram. Second, the subjects themselves exhibit speeds far above what Weidmann’s model would predict. It may be a property of the set of subjects (mostly students [30]). It may also be something unique to the experiment. This requires further study. Third, the agents achieve much higher density than do the experiment subjects. Nothing physical prevents the subjects from drawing closer together and achieving comparable density. We must assume that there is some psychological/cultural factor which keeps them sparsely distributed for which our model doesn’t account.⁵

⁵In the experiment, the subjects began in a space with a density of 3 people/m². If the initial density were higher, would it affect the observed density?

5.3 *Two-Dimensional, Bi-directional Flow*

In a later paper, Zhang et al. performed similar experiments as those in the previous section, but this time included bi-directional flow [31]. One of the interesting phenomena observed in this experimental data is that, in the band of density between 1.0 and 2.0m^{-2} the bi-directional flow is more sensitive to density and the speed decreases more quickly. We observed this same phenomenon in our simulated data, as shown in Fig. 5c.⁶ At the same time, the previously noted density issues also arose in the simulation of bi-directional flow.

6 Analysis and Conclusion

We have presented a new model for pedestrian dynamics based on ideas from robotics. The velocity obstacle formulation provides an intuitive basis for simulating human pedestrians. Originally devised for robots, we have shown that it can be easily extended to conform to human behavior based on biomechanical models and empirical observations. We have further shown that the model's parameter space is well-behaved; it does not require per-scenario tuning. We performed all experiments with the same settings. Previous research has shown that this formulation leads to a wide range of self-organizing behaviors (e.g. lane formation, arching, vortices, etc.) [2] and it has also been shown to be a very stable approach, admitting time steps as large as 0.2 s [5].

There are still aspects of this formulation which can be improved. First, while there is very strong agreement between simulation and real-world data in the one-dimensional experiments, the agreement in two dimensions isn't as strong. While the agents exhibit behavior consistent with the fundamental diagram, it's not quite the same as the measured data. One possible source for this disagreement may be the effective distance function (7). More analysis of the pedestrian data may suggest a better mapping from local agent configurations to "effective distance", yielding better agent behaviors. More importantly, RVO agents exhibit a tendency to reach maximum density with little effort. While pedestrians are known to reach very high densities, it would seem that it requires significant systemic pressures to do so [4]. This requires greater understanding so that it can be incorporated into our model.

Acknowledgements This research is supported in part by ARO Contract W911NF-10-1-0506, NSF awards 0904990, 1000579, 1117129, and 1142382, and Intel. The experimental data was made possible by DFG-Grant Nos. KL 1873/1-1 and SE 1789/1-1 and the "Research for Civil Security" program funded by German Federal Ministry of Education and Research.

⁶For visual clarity, we follow the example of the experiment authors in presenting those samples which lie within one standard deviation of the mean.

References

1. Van den Berg, J., Guy, S.J., Lin, M., Manocha, D.: Reciprocal n-body collision avoidance. In: Inter. Symp. on Robotics Research. (2009)
2. Guy, S.J., Curtis, S., Lin, M.C., Manocha, D.: Least-effort trajectories lead to emergent crowd behaviors. *Phys. Rev. E* **85**(1) (2012) 016110
3. Guy, S.J., Lin, M.C., Manocha, D.: Modeling collision avoidance behavior for virtual humans. In: Proceedings of the 9th International Conference on Autonomous Agents and Multiagent Systems: volume 2 – Volume 2. (2010) 575–582
4. Curtis, S., Guy, S.J., Zafar, B., Manocha, D.: Virtual tawaf: A case study in simulating the behavior of dense, heterogeneous crowds. In: 1st IEEE Workshop on Modeling, Simulation and Visual Analysis of Large Crowds. (2011) 128–135
5. Curtis, S., Snape, J., Manocha, D.: Way portals: Efficient multi-agent navigation with line-segment goals. *I3D '12* (2012) 15–22
6. Blue, V.J., Adler, J.L.: Emergent fundamental pedestrian flows from cellular automata microsimulation. *Transportation Research Record: Journal of the Transportation Research Board* **1644** (1998) 29–36
7. Blue, V.J., Adler, J.L.: Cellular automata microsimulation of bidirectional pedestrian flows. *Transportation Research Record: Journal of the Transportation Research Board* **1678** (1999) 135–141
8. Burstedde, C., Klauck, K., Schadschneider, A., Zittartz, J.: Simulation of pedestrian dynamics using a two-dimensional cellular automaton. *Physica A: Statistical Mechanics and its Applications* **295** (2001) 507–525
9. Kirchner, A., Klupfel, H., Nishinari, K., Schadschneider, A., Schreckenberg, M.: Discretization effects and the influence of walking speed in cellular automata models for pedestrian dynamics. *J. Stat. Mech.* **2004** (October 2004)
10. Maniccam, S.: Traffic jamming on hexagonal lattice. *Physica A: Statistical Mechanics and its Applications* **321** (2003) 653–664
11. Yamamoto, K., Kokubo, S., Nishinari, K.: Simulation for pedestrian dynamics by real-coded cellular automata (rca). *Physica A: Statistical Mechanics and its Applications* **379** (2007) 654–660
12. Bandini, S., Federici, M., Manzoni, S., Vizzari, G.: Towards a methodology for situated cellular agent based crowd simulations. *Engineering societies in the agents world VI* (2006) 203–220
13. Sarmady, S., Haron, F., Talib, A.: A cellular automata model for circular movements of pedestrians during tawaf. *Simulation Modelling Practice and Theory* (2010)
14. Hirai, K., Tarui, K.: A simulation of the behavior of a crowd in panic. In: Proc. of the 1975 International Conference on Cybernetics and Society. (1975) 409–411
15. Helbing, D., Farkas, I., Vicsek, T.: Simulating dynamical features of escape panic. *Nature* **407** (2000) 487–490
16. Yu, W.J., Chen, R., Dong, L.Y., Dai, S.Q.: Centrifugal force model for pedestrian dynamics. *Phys. Rev. E* **72** (Aug 2005) 026112
17. Chraïbi, M., Seyfried, A., Schadschneider, A.: Generalized centrifugal-force model for pedestrian dynamics. *Phys. Rev. E* **82**(4) (2010) 046111
18. Moussaïd, M., Perozo, N., Garnier, S., Helbing, D., Theraulaz, G.: The walking behaviour of pedestrian social groups and its impact on crowd dynamics. *PLoS ONE* **5**(4) (2010)
19. Seyfried, A., Schadschneider, A., Kemloh, U., Chraïbi, M.: Force-based models of pedestrian dynamics. *Networks and Heterogeneous Media* **6**(3) (2011) 425–442
20. Helbing, D., Molnár, P., Farkas, I., Bolay, K.: Self-organizing pedestrian movement. *Environment and Planning B: Planning and Design* **28**(3) (2001) 361–383
21. Fiorini, P., Shiller, Z.: Motion planning in dynamic environments using velocity obstacles. *IJRR* **17**(7) (July 1998) 760–762
22. van den Berg, J., Lin, M., Manocha, D.: Reciprocal velocity obstacles for real-time multi-agent navigation. *ICRA* (2008) 1928–1935

23. Van den Berg, J., Patil, S., Sewall, J., Manocha, D., Lin, M.: Interactive navigation of multiple agents in crowded environments. In: I3D '08, New York, NY, USA, ACM (2008) 139–147
24. Weidmann, U.: *Transporttechnik der Fussgaenger*. Schriftenreihe des IVT (1993)
25. Seyfried, A., Steffen, B., Klingsch, W., Boltes, M.: The fundamental diagram of pedestrian movement revisited. *J. Stat. Mech.* (10) (October 2005)
26. Inman, V.T., Ralston, H.J., Todd, F., Lieberman, J.C.: *Human Walking*. Williams & Wilkins (1981)
27. Chattaraj, U., Seyfried, A., Chakroborty, P.: Comparison of pedestrian fundamental diagram across cultures. *Advances in Complex Systems* **12**(3) (2009) 393–405
28. Dean, G.A.: An analysis of the energy expenditure in level and grade walking. *Ergonomics* **8**(1) (1965) 31–47
29. Gérin-Lajoie, M., Richards, C.L., McFadyen, B.J.: The negotiation of stationary and moving obstructions during walking: Anticipatory locomotor adaptations and preservation of personal space. *Motor Control* **9** (2005) 242–269
30. Zhang, J., Klingsch, W., Schadschneider, A., Seyfried, A.: Transitions in pedestrian fundamental diagrams of straight corridors and t-junctions. *J. Stat. Mech.* **2011**(06) (2011) P06004
31. Zhang, J., Klingsch, W., Schadschneider, A., Seyfried, A.: Ordering in bidirectional pedestrian flows and its influence on the fundamental diagram. *J. Stat. Mech.* (02) (2012) P02002

Quantitative and Qualitative Validation Procedure for General Use of Pedestrian Models

Mario Campanella, Serge Hoogendoorn, and Winnie Daamen

Abstract This paper proposes a simple validation procedure that combines qualitative and quantitative assessments. The aim is to simplify the task of validation and still produce reliable results. By applying the procedure to the Nomad microscopic model it was revealed that parameter sets calibrated with flows that expose pedestrians to different situations and optimized with several calibration assessments (multi-objectives) are more accurate and present more realistic pedestrian behaviour. It also showed that for some parameter sets the model performed significantly better when simulating unidirectional flows than bidirectional flows or than a congested flow through a bottleneck. This result implies that validations using only one type of flow (especially if it is a unidirectional) are not reliable in respect of the general use of the parameter set.

Keywords Validation • Pedestrian models

1 Introduction

Typically the application of a model includes a description of the population characteristics, the walking infrastructure and the traffic demand. The population is usually represented internally in the model and determined via the model parameters that were obtained in an optimization procedure during the calibration process. The infrastructure and inflows determine the type of situations pedestrian walk.

The fundamental premise for the use of pedestrian models is the confidence that their results are within an accepted deviation of reality. However, pedestrian behaviors vary according to local conditions such as densities, direction of interaction between pedestrians (walking towards each other, crossing, overtaking) and internal

M. Campanella (✉) • S. Hoogendoorn • W. Daamen
Department of Transport & Planning, Delft University of Technology, Delft, The Netherlands
e-mail: m.c.campanella@tudelft.nl; s.p.hoogendoorn@tudelft.nl; w.daamen@tudelft.nl

states determined by age, culture, purpose of the trip. The process of determining the adequacy of a model (and its parameter set) is called validation [1].

In general, authors distinguish two types of validation, qualitative and quantitative [2–5]. Some of these authors refer to these respectively as verification and validation and both terminologies are used in this paper.

The common approach of verification is to show that the walker model is able to reproduce some basic movement characteristics of pedestrians. For instance pedestrians should not get trapped in corners and avoid collisions. A more elaborate verification process shows that the model is capable of reproducing self-organized phenomena such as the formation of lanes or that the fundamental diagram relations are consistent (e.g. speeds decrease with increase of densities).

A typical validation will compare some empirically obtained data about pedestrians with the outcomes of the model. Ideally the comparison (assessment) is performed reproducing similar population characteristics, walking infrastructure and inflows.

Galea [2] reports two extra model check's that must be performed before the validation, component testing and functional validation. The first deal with the implementation of the simulation model and is not the subject of this paper. Functional validation is the necessary inspection that the model displays the capability to perform the desired simulations in the same level of detail required. This paper proposes a validation procedure and applies it to the operational level of the Nomad model. Therefore, it is implicit that the Nomad model presents the capability to replicate the situation the originated in the empirical data.

A literature research on validation of pedestrian models showed that usually authors perform a limited amount of validation assessments and very few considerations are given regarding the applicability of the model in different walking situations and population characteristics.

This paper argues that if no parameter set is calibrated for the specific task, the set to be used for predictions must have shown to perform well in various validation assessments utilizing several walking situations giving a measure of general usability. To support that, we performed a series of validations using eight different parameter sets, three types of flow representing different walking situations. A validation procedure is proposed combining three quantitative and several qualitative assessments to determine the accuracy of the sets. The results of the assessments are presented with the implications for the use of microscopic models and conclusions are made regarding the factors influencing the general usability of the parameter sets.

2 Validation Procedure

High density situations are often present during evacuations and are usually more difficult to be accurately reproduced by models. Therefore high density situations are included in the procedure. The validation procedure is composed

by a quantitative and a qualitative component. Four aspects were considered in the set-up of the procedure, the inclusion of quantitative assessments commonly used in pedestrian simulations, the inclusion of quantitative assessments influenced by high densities, a larger influence of the quantitative assessments in the final outcomes, the qualitative assessments should show how well the different parameter sets are reproducing pedestrian behaviours in a microscopic and macroscopic scale.

To diminish the complexities of implementation and allow an easy interpretation of results the procedure was made as simple as possible. The procedure is based in the combination of the different assessments in a simple score. The assessments must represent significantly different situations, aspects of pedestrian traffic and pedestrian behaviours.

The procedure presented in this paper combines all qualitative assessments into one verification score. This score is combined with all scores of the quantitative assessments to obtain the final validation score. This was done to increase the importance of the quantitative assessments in the final score. Alternatively, weights could have been used to the same purpose. Using weights for the different assessments makes it easier to increase the importance of certain assessments in the final score but also increase the complexity of the procedure.

2.1 Validation Score

The validation ends with a general score obtained after combining the results of all the each quantitative and qualitative assessment. Each assessment resulted in a score that ranged between, bad, medium and good. The quantitative assessments were graded according to the size of the relative errors of the simulated results:

$$\text{bad} := \text{error} > 10\% \quad \text{medium} := 5\% < \text{error} < 10\% \quad \text{good} := \text{error} < 5\% \quad (1)$$

Each qualitative assessment was assigned one of the scores according to their resemblance to the empirical data. Each qualitative assessment could be assigned three values between good, medium and bad. A visual inspection was enough to assign one of these values for each assessment.

The combination of the assessment scores is done using a simple averaging procedure performed after grading the scores. The bad score gets a grade 0, the medium gets 1 and the good gets 2. An average of the grades is then tabulated between three intervals of equal length to calculate the final score:

$$\text{bad} := 0 < \text{score} \leq 2/3 \quad \text{medium} := 2/3 < \text{score} \leq 4/3 \quad \text{good} := 4/3 < \text{score} \leq 2 \quad (2)$$

Table 1 Overview of the average travel times (TT^{exp}) for the experiments

Experiment	Mean of travel times (s)	Std dev of travel times (s)
Bidirectional	7.8	0.9
Unidirectional	7.2	0.7
Bottleneck	15.8	6.6

2.2 Quantitative Assessments

Three quantitative assessments were chosen: average travel times, the speed x density fundamental relation and bottleneck capacity C. The first two are commonly [2, 4, 5] used as outcomes from simulations and the capacity must be measured in congested traffic.

2.2.1 Travel Times

The travel time assessment $error_{TT}$ is the average of the travel time errors of each pedestrians resulted from each simulation (Table 1):

$$error_{TT} = \frac{\sum_{s \in \text{simulations}} error_{TT}^s}{\#simulations} \times 100 \text{ (in \%)} \tag{3}$$

with :

$$error_{TT}^s = \frac{TT^s - TT^{exp}}{TT^{exp}} \text{ and } TT = \text{average travel time}$$

Additionally to the average travel times the Kolmogorov-Smirnov (KS) statistics for the cumulative curve of travel times are calculated. The smaller the KS statistics the better is the goodness-of-fit of the simulated distributions. Figure 1 shows the experimental cumulative curves that are used in the determination of the KS statistics.

2.2.2 Fundamental Diagrams

The assessment using the fundamental diagram (FD) utilizes the speed-density relation because it is the one that presents the least scatter from all three relations allowing for a simple way of comparing the outcomes of the simulations. Three characteristics of the $u \times k$ relations will be used in the FD assessment, the slope, the scatter and the maximum density achieved in the flows. These

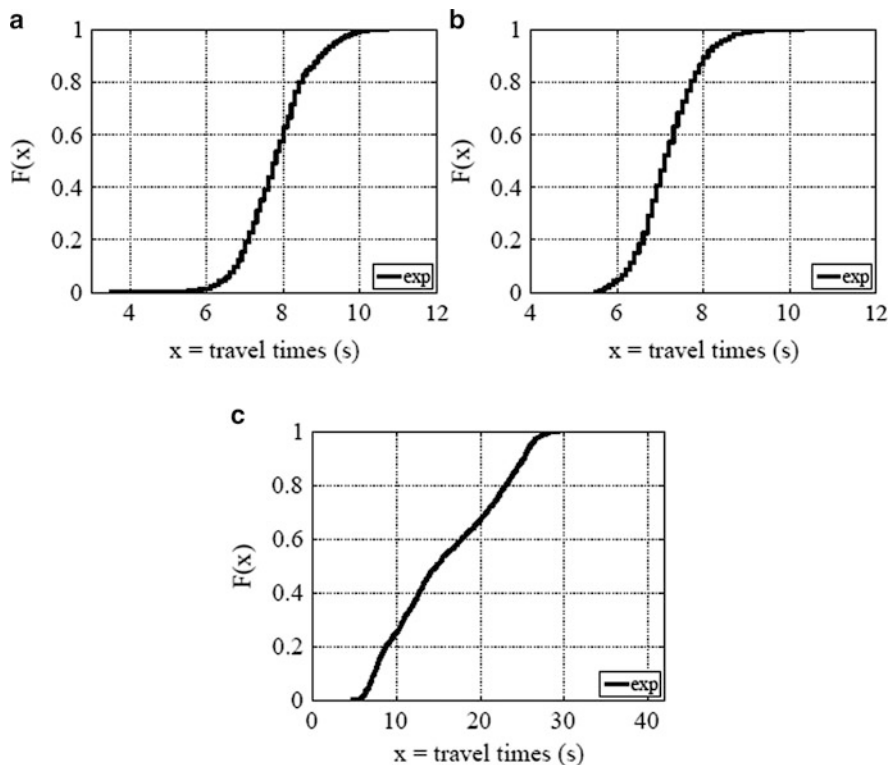


Fig. 1 Travel times cumulative distributions for the experiments

three characteristics are compared along the experimental density range. The u_{xk} diagrams were obtained according to the definition in [4] using the whole area to compute the densities and a time aggregation interval of 1 s to compute the speeds. The experimental u_{xk} points are divided over bins of density intervals of 0.1 peds/m². All points in a bin are used to calculate the mean and standard deviation values of the walking speeds. The means account for the slope and the deviations for the scatter. The mean curve and the two shifted curves above and below the mean by the standard deviation can be seen in the u_{xk} plot in Fig. 2.

The slope errors are the differences of the mean speeds in each bin for the simulated and experimental trajectories. If the amount of bins is not the same, only the bins present in both flows are used (the $error_{\max(k)}$ described below accounts for the difference in the number of bins). The average error for all bins is computed for each set of trajectories and then the trajectories errors are averaged to obtain the slope error ϵ_u :

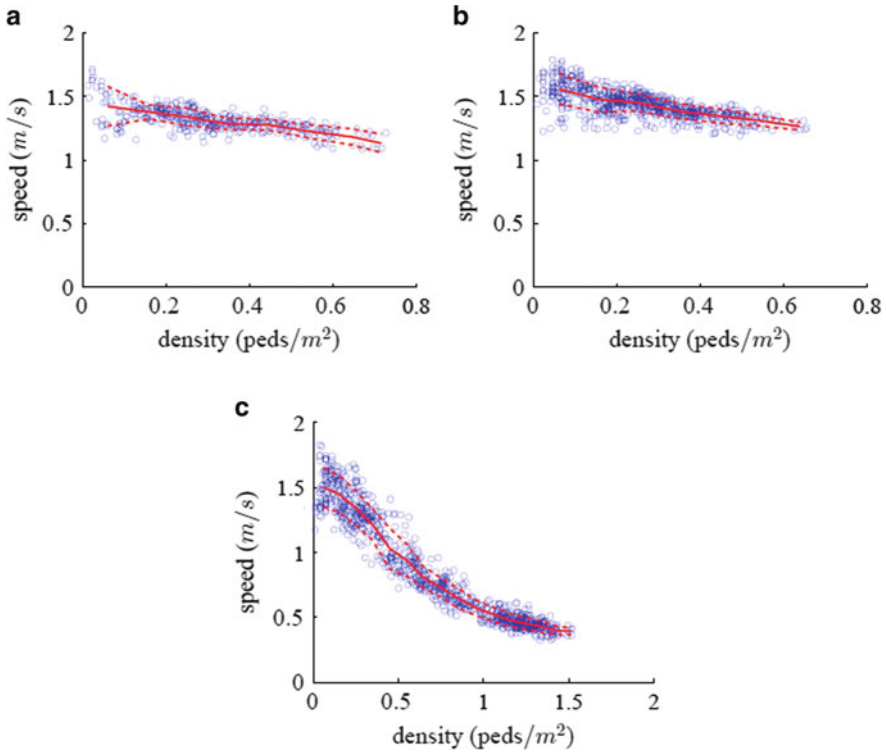


Fig. 2 Speed-density plots for the experimental trajectories with the fitted exponential curves

$$\begin{aligned}
 & \sum \text{error}_u^s \\
 \text{error}_u &= \frac{s \in \text{simulations}}{\# \text{simulations}} \times 100 \text{ (in \%)} \\
 & \text{with :} \\
 & \sum \text{error}_u^b \\
 \text{error}_u^s &= \frac{\hat{b} \text{bins}}{\# \text{bins}} ; \\
 \text{error}_u^b &= \frac{u^b - u^{\text{exp}}}{u^{\text{exp}}} \text{ and } u = \text{average speed}
 \end{aligned}
 \tag{4}$$

The scatter of the $u \times k$ relation is measured similarly by the errors of the standard deviations of the speeds $\text{error}_{\sigma(u)}$ in each bin:

$$\begin{aligned}
 & \sum \text{error}_{\sigma(u)}^s \\
 \text{error}_{\sigma(u)} &= \frac{s \in \text{simulations}}{\# \text{simulations}} \times 100 \text{ (in \%)} \\
 & \text{with :} \\
 & \sum \text{error}_{\sigma(u)}^b \\
 \text{error}_{\sigma(u)}^s &= \frac{\hat{b} \text{bins}}{\# \text{bins}} ; \\
 \text{error}_{\sigma(u)}^b &= \frac{\sigma(u)^b - \sigma(u)^{\text{exp}}}{\sigma(u)^{\text{exp}}} \text{ and } \sigma(u) = \text{stdev of speed}
 \end{aligned}
 \tag{5}$$

The maximum density error_{max(k)} are the differences of the maximum densities achieved by the simulated and the experimental flows:

$$\text{error}_{\max(k)}^s = \frac{\sum_{s \in \text{simulations}} \text{error}_{\max(k)}^s}{\#\text{simulations}} \times 100 \text{ (in \%)} \tag{6}$$

with :

$$\text{error}_{\max(k)}^s = \frac{\max(k)^s - \max(k)^{\text{exp}}}{\max(k)^{\text{exp}}} \text{ and } \max(k) = \text{max density}$$

The uxk assessment is calculated as the average of the three errors using Eq. 2 after they are translated according to Eq. 1. With this we prevent the final validation to be too affected by one (or more) very large percentage errors as it would if we would simply average the values.

$$\text{error}_{\text{uxk}} = \text{mean} (\text{error}_u, \text{error}_{\sigma(u)}, \text{error}_{\max(k)}) \tag{7}$$

2.2.3 Bottleneck Capacity

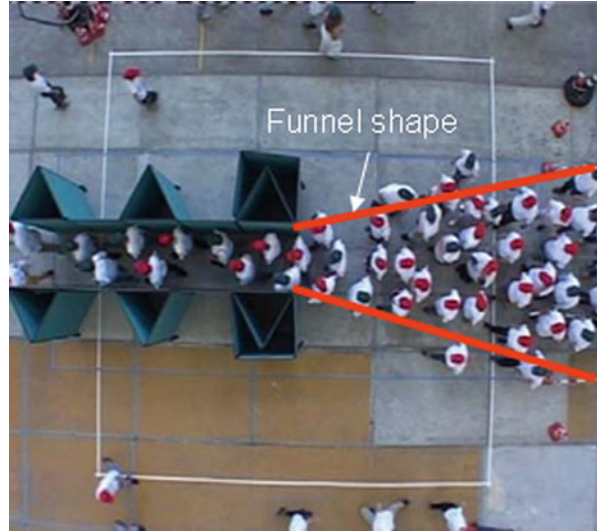
The bottleneck capacity assessment is calculated as the maximum flow obtained in the entrance of the corridor (bottleneck). The flows were calculated by counting a fixed amount of pedestrians and measuring the time needed for the first and the last pedestrians to pass the cross section. This procedure has the advantage of being very simple but it does require some adjustment to find out the correct amounts of pedestrians to be counted. If the amount is too small then natural fluctuations and tracking errors will create non realist high capacities. The contrary will create too small capacities due to gaps in the congested flow. The proposed solution was to increase the amount of pedestrians in steps of 10 until the maximum difference between two consecutive flows during the congested period was not larger than 5 % of the maximum flow. The smallest amount that fulfilled this criteria using the empiric data from the experiments [7] was 50 pedestrians and the capacity obtained was $q_c = 1.63(\text{peds/s})$. The interval of time needed for 50 pedestrians to pass the bottleneck with maximum flow is $t = 50(\text{peds})/1.63(\text{peds/s}) = 30.7 \text{ s}$. The validation assessment is the relative error of the capacities:

$$\text{error}_{q_c}^s = \frac{\sum_{s \in \text{simulations}} \text{error}_{q_c}^s}{\#\text{simulations}} \times 100 \text{ (in \%)}$$

with :

$$\text{error}_{q_c}^s = \frac{q_c^s - q_c^{\text{exp}}}{q_c^{\text{exp}}} \text{ and } q_c = \text{flow capacity}$$

Fig. 3 The funnel shape upstream the bottleneck



2.3 Qualitative Assessments

The qualitative assessments judged the avoidance behaviours and explored some specific characteristics of the different types of flow used in the validations. The formation and stability of lane formation in the bidirectional flows, the zipper-effect in a narrow corridor and funnel shape (see Fig. 3) in front of the bottleneck in a congested flow through a bottleneck. For more details refer to [2].

2.3.1 Bidirectional Flows

The experimental data was analyzed and showed that lanes were present in the trajectories and almost always when pedestrians were walking in both directions distinct lanes could be observed [3]. These lanes were usually very stable lasting for long periods. During the experiments no frontal and lateral collisions between pedestrians could be observed. The walking area had no solid wall but pedestrians always stayed inside the delimited area. Using these observation points and noticing some undesired side effects of the simulations permitted the following five qualitative assessments of bidirectional flows:

1. The formation of self-organized lanes and their stability. (Good – lanes are formed and are stable, Medium – lanes are formed but are unstable, Bad – lanes are not formed).
2. The avoidance behaviour (a). How pedestrians behave when walking straight on. (Good – never collide, Medium – few collisions, Bad – many collisions).

3. The avoidance behaviour (b). How often they collide with nearby pedestrians. (Good – never collide, Medium – few collisions, Bad – many collisions)
4. The avoidance behaviour (c). Are pedestrians being pushed backwards in straight on collisions? (Good – never pushed, Medium – few pedestrians, Bad – many pedestrians.)
5. Staying in the simulated area (Good – always stay, Medium – few pedestrians walk outside, Bad – many pedestrians walk outside).

2.3.2 Unidirectional Flows

Also in the unidirectional flows no frontal and lateral collisions between pedestrians could be observed in the experiments. The walking area did not have solid walls and pedestrians always stayed inside the delimited area. Using these observation points and noticing some undesired side effects of the simulations permitted the following three qualitative assessments of unidirectional flows:

1. The avoidance behaviour (a). Average distances that pedestrians keep from each other. (Good – similar distances, Medium – larger distances, Bad – very large distances).
2. The avoidance behaviour (b). How often they collide with nearby pedestrians. (Good – never collide, Medium – few collisions, Bad – many collisions)
3. Staying in the simulated area (Good – always stay, Medium – few pedestrians walk outside, Bad – many pedestrians walk outside).

2.3.3 Narrow Corridor Bottleneck Flows

The narrow bottleneck experiment presents the most diverse conditions of flow by presenting free and congested flow. The model must therefore be able to correctly predict the behaviours in these two situations. The free-flow condition is usually well simulated by microscopic models and therefore did have a minor role in the proposal of the assessments. However, these flows should be well predicted by any model, always. The most difficult challenges appeared in the congested flow up and downstream of the bottleneck and most of the six verification criteria are expressing behaviours during congestion:

1. The formation of the self-organized zipper-effect inside the corridor (Good – Pedestrians are displaced laterally and stay stable at this position, Medium – positions are not fixed, Bad – pedestrians follow each other).
2. A funnel shape is formed upstream of the bottleneck in congested flow (Fig. 3). (Good – funnel is formed, Medium – funnel is not stable, Bad – never formed)
3. The avoidance behaviour (a). How often they collide with nearby pedestrians. (Good – never collide, Medium – few collisions, Bad – many collisions)
4. The avoidance behaviour (b). Slow pedestrians get trapped outside the corridor. (Good – never get trapped, Medium – few get trapped, Bad – many get trapped)

Table 2 Overview of the experiments used in each validation assessment

Assessment	Experiments		
	Bidirectional (bidir)	Unidirectional (unidir)	Narrow bottleneck (bneck)
Travel Times	X	X	X
Capacity			X
Speed Density	X	X	X

5. The avoidance behaviour (c). Are pedestrians being pushed towards the obstacles? (Good – never pushed, Medium – few pedestrians, Bad – many pedestrians.)
6. Staying in the simulated area (Good – always stay, Medium – few pedestrians walk outside, Bad – many pedestrians walk outside).

3 Validation Set-ups

The validations performed in this paper used three trajectories data sets presented in [2], the bidirectional experiment (bidir), the unidirectional experiment (unidir) and the narrow corridor bottleneck experiment (bneck). The data was applied to three different mappings, average travel times, bottleneck capacity q_c and $u \times k$ fundamental relation. Table 2 shows that in total seven different validations are performed.

The simulations are run by assigning the same parameter sets to all pedestrians and are finished when the last pedestrian has left the walking area. In all calibrations the whole set of trajectories were used and the same was done in the validations. The use of all trajectories was necessary because the three quantitative validation assessments represent aggregated behaviours and could not have been applied to a part of the population. This potential over-fitting problem is addressed by performing 30 runs of simulations for each parameter set. Each simulation run has a slightly different initial state by means of variations of the pedestrian free speeds, their initial positions and entry times. These different initial states cause significant variation of the validation results along the runs showing that they are effectively generating different situations for the simulated pedestrians.

The free-speeds of pedestrians were assigned using a normal distribution with mean $\mu = 1.5$ m/s and $\sigma = 0.2$ accounting for the heterogeneity encountered in the population.

3.1 Parameter Sets

In total eight parameter sets were used in this paper and they can be separated in two groups. The first constituted of six sets that were obtained via a calibration using one

objective function and one type of flow. These sets are named in this paper as the specialized sets. The second group here called general is composed of two sets that combined the errors of objective functions using three types of flow.

The specialized group has three sets estimated by minimizing the Kolmogorov-Smirnov statistics using cumulative curves of travel times for three different types of flow. These are named *bidirTT*, *unidirTT* and *bneckTT*. The other three sets were estimated using the same experimental data but used a trajectory based calibration procedure [5]. These calibrations result in parameters for each pedestrian in the experiment. The average of these individually estimated parameters are named *bidirAC*, *unidirAC* and *bneckAC*. One general set named *multiTT* was estimated by minimizing a multiple-objective that added the Kolmogorov-Smirnov statistics of the three experiments. The other general set was estimated in [6].

This set called *multi* was estimated via a manual calibration effort that used the trajectories of the three experiments and three different mappings: *uxk* relations of the *bidir* and *unidir*, capacity *qc* of the *bneck* and the distribution of self-organized lanes of the *bidir*.

4 Results

The first important result was that the stochastic variation of the assessments using the *general* parameter sets was significantly smaller. The reason for this was found in the significantly better behaviour of the pedestrians expressed by the better qualitative scores that measured the interactions, the *multi* set obtaining the maximum score in all three flows.

Table 3 clearly shows that for all validation criteria and in almost all experiments the individually estimated sets *bidirAc*, *unidirAc* and *bneckAc* performed badly. This clearly indicates that the average of optimal individual behaviours does not correspond to good collective behaviours. The other parameter sets had much better validation results and these results varied between the criteria and experiments.

4.1 Travel Times

In general travel times were well predicted. This was expected given that most of the parameters were estimated with a objective using travel times. With the exception for the *bneck* experiment that produced bad results for almost all sets.

The travel times for the *bneck* flow are very sensitive to the initial condition. The reason for this large sensitivity in this flow is due to the congested regime that is present for the most part of the experiment. The initial position, entry time and free-speeds affect decisively the manner that individual pedestrians will maneuver until passing the bottleneck. The 5 m distance between the sections where pedestrians enter the area and the bottleneck entrance is of the same order of magnitude of

Table 3 Overview of all verification and validation results and the overall validation score

Exp.	Parameter sets	Verification	Travel times	Fundamental diagrams	Capacity	Validation score
Bidir	BidiTT	Bad	Good	Bad		Bad
	BidiAc	Medium	Bad	Bad		Bad
	MultiTT	Medium	Good	Bad		Medium
	Multi	Good	Good	Bad		Medium
Unidir	UniTT	Medium	Good	Medium		Medium
	UniAc	Medium	Medium	Medium		Medium
	MultiTT	Good	Good	Medium		Good
	Multi	Good	Good	Medium		Good
Bneck	BneckTT	Medium	Bad	Medium	Good	Medium
	BneckAc	Bad	Bad	Bad	Bad	Bad
	MultiTT	Medium	Medium	Medium	Medium	Medium
	Multi	Good	Bad	Bad	Good	Medium

Fig. 4 Two faster pedestrians overtaking on the outside of the congested bneck simulation using the bneckTT parameter set



the 4 m of the width of the entrance section. Therefore, the initial position will be determinant for the total walking distances and will also influence the type of maneuvers pedestrians will apply. Visually inspecting the experiments and the simulations it was observed that pedestrians created in the middle of the entrance cross section have a tendency to walk straight towards the bottleneck area. However, when created in the outward parts of the cross section, faster pedestrians will have a larger probability to reach the bottleneck area by overtaking on the outside of the congestion and squeezing themselves along the obstacles to reach the corridor entrance (Fig. 4).

4.2 Fundamental Diagrams

For all experiments the slope errors were small indicating that all sets were able to produce a good agreement in the uxk behaviour. However, the scatter assessment was not well predicted indicating the importance of this very often neglected aspect of the fundamental diagrams. The worst results were found in the maximum densities ($error_{max(k)}$) when all sets, apart of one, had errors above 15 %. This indicates that the sets are not representing accurately the traffic conditions in large

densities. The explanation is that in the experimental data pedestrians were less active and waited in a queue like manner producing a funnel (Fig. 3). In the simulations they tended to spread more around the bottleneck entrance creating a wider or no funnel at all, reducing the densities upstream of the bottleneck. A similar effect occurred in the bidirectional and unidirectional flows when pedestrians veered to the edges and sometimes outside the designated corridor. This was possible because there were no containing walls in the corridors.

4.3 Capacity

All sets apart of the *bneckAc* produced good values for capacities. This result contradicts the bad performance of the *uxk* in the higher densities. The explanation is that although pedestrians spread around the bottleneck, their behaviour in the entrance of the bottleneck was closer to reality.

4.4 Verification

The multi set produced a good verification for 13 of the 14 assessments. Only the zipper effect in the *bneck* was bad. The multiTT had slightly worse results but still quite satisfactory but better than the *specialized* sets.

5 Discussion and Implication on the Application of Walker Models

The two assessments that are of large interest in simulations (travel time and capacity) produced good results showing the good applicability of the Nomad model. As expected the *general* parameter sets obtained better general validation results. The last column of Table 3 shows the validation scores. One unforeseen advantage of the *general* parameter sets was the lesser sensitivity against the initial conditions. This is evidently a desired characteristic since walker models are to be applied in several situations and should not require too many runs to get statistically valid results.

5.1 The Problem of Using Unidirectional Flows in Validations

All the assessments produced the best results for the unidirectional flow. The lower densities achieved in this experiment is one of the reasons. But since the

bidirectional experiment reaches similar densities, the simulation of leaders-followers must be less difficult than ongoing collision avoidance. Therefore, validations should not use only unidirectional flows when the sets are not going to be used solely in unidirectional simulations.

5.2 *The Need to Simulate Realistic Walking Behaviour*

Given that pedestrian models are used mostly to estimate aggregate traffic data it is not evident that the individual behaviour must be precisely simulated. In fact inter and intra pedestrian heterogeneity (behaviour differences in the population and in the same pedestrian given the same conditions) makes it impossible to predict exact individual behaviour. However, on average this paper shows that the general sets gave almost as good quantitative results as the specialized sets and much better verification results. Good verification results are desired because they indicate that the model behaves less stochastic diminishing the sensitivity of simulation results. Therefore, the simulated pedestrians must present heterogeneity, however under limiting bounds, such as real pedestrians.

The necessity of more homogeneity in the behaviour is larger with the increase of density. In these situations there is a larger probability of interactions between pedestrians potentially causing large accelerations that may disturb too much the simulated flow. But in reality pedestrians are able to keep walking in laminar flows to very high densities [12]. This reasoning is supported by the results of this paper when the *general* sets usually performed better in the high density assessments.

6 Conclusion and Future Work

This paper proposed a new and very simple validation procedure that combines qualitative and quantitative assessments. Spite its simplicity it was able to show that several assessments effectively reveal the differences in accuracy between parameter sets. The good results for the validation of the unidirectional flow when the same did not happen for the others show that this type of flow should not be relied solely for validation purposes. It should always be accompanied by other types of flow that are more challenging for pedestrian models. Sets optimized with multiple-objectives simulate better behaviours diminishing the variability of the results. The smaller variability and the better accuracy make them more suited to be used in simulations and should accompany all pedestrian models. These results strongly encourage the pursuing of accuracy in a wide range of situations (generality).

Both *general* sets were validated using the same experimental data used in their estimations. Therefore, the next step is to apply the validation procedure to different trajectory sets and investigate further the over-fitting effects. Also, the good results

for the *general* sets indicate that there is a good incentive to investigate other objective functions for the calibration and to introduce modifications to the Nomad model.

References

1. Lint, H. V., editor Innovations in Dynamic Traffic Management - lectures of the Course: Intelligent Transport Systems & Services for Road Transport. Delft University of Technology (2009).
2. Galea, E. A general approach to validating evacuation models with an application to exodus. *Journal of Fire Sciences*, 16(6), pp 414 -436 (1998).
3. Klügl, F. A validation methodology for agent-based simulations. In Proceedings of the 2008 ACM symposium on Applied computing, SAC'08, ACM, New York, NY, USA. pp. 39–43. (2008).
4. Klüpfel, H. Crowd Dynamics Phenomena, Methodology and Simulation, chapter 10. Emerald Group Publishing Limited, pp. 215-244 (2009).
5. Schadschneider, A. and Seyfried, A. Validation of ca models of pedestrian dynamics with fundamental diagrams. *Cybernetics and Systems: An International Journal*, 40, pp. 367–389 (2009).
6. Hoogendoorn, S.P., Bovy, P.H.L.: Normative Pedestrian Behavior Theory and Modeling, In Taylor, M.A.P. (ed.), *Transportation and traffic theory in the 21st century*, Oxford: Pergamon, Elsevier science, pp. 219–245 (2002)
7. Daamen, W. and Hoogendoorn, S. Controlled experiments to derive walking behaviour. *European Journal of Transport and Infrastructure Research*, 3(1), pp 39–59 (2003).
8. Hoogendoorn, S.P. and Daamen, W.: Pedestrian behavior in bottlenecks. *Transportation Science*, (39), pp 147–159 (2005)
9. Hoogendoorn, S. and Daamen, W. Self-organization in pedestrian flow. In *Traffic and Granular Flow 03*, pp 373–382 (2005).
10. Campanella, M., Hoogendoorn, S.P and Daamen, W. Macroscopic relations in pedestrian traffic flows. In the Proceedings of the Eighth International Conference on Traffic and Granular Flow (TGF'09) (2009).
11. Daamen, W, Campanella M. and Hoogendoorn, S.P. Calibration of Nomad parameters using empirical data. In the Proceedings of the Ninth International Conference on Traffic and Granular Flow (TGF'11) (2011).
12. Campanella, M., Hoogendoorn, S.P., and Daamen, W. Improving the nomad microscopic walker model. In 12th IFAC Symposium on Control in Transportation Systems (CTS09) (2009).
13. Helbing, D.; Johansson, A. & Al-Abideen, H. Z. The Dynamics of crowd disasters: an empirical study. *Physical Review E*, 75, 046109 (2007).

Shared Space Modeling Based on Social Forces and Distance Potential Field

Bani Anvari, Winnie Daamen, Victor L. Knoop, Serge P. Hoogendoorn, and Michael G.H. Bell

Abstract Urban design is moving towards space sharing in order to increase the community texture and safety of street surroundings. However, there is a need for a simulation tool capable of representing future shared space schemes to help judging the designs under which shared space design is a suitable alternative to traditional street designs. This paper presents a microscopic mathematical model that is used as a traffic simulation tool capable to represent main behaviors of pedestrians and cars in any shared space layout. This is achieved by generating a route map which helps agents to find the shortest path towards their target destinations on the strategic level. On the operational level, the Social Force Model (SFM) is used and extended for a mixed traffic to produce feasible trajectories. The trajectory results are presented to give a face-validation of the functionality of the shared space simulation model.

Keywords Shared space • Social force model • Flood fill algorithm

1 Introduction

Shared space is about changing the way streets function through reducing the dominance of vehicles. This is often obtained through the use of a shared surface street, which itself aims at integrated space use [3]. Shared space allocates more degrees of freedom to its traffic participants. As a result of this increased freedom, traffic engineers became concerned about ensuring safe and efficient movement of

B. Anvari (✉) • M.G.H. Bell

Department of Civil and Environmental Engineering, Centre for Transport Studies, Imperial College London, London SW7 2BU, UK
e-mail: b.anvari09@imperial.ac.uk

W. Daamen • V.L. Knoop • S.P. Hoogendoorn

Transport & Planning, Delft University of Technology, Delft, The Netherlands

pedestrians and drivers in these shared schemes. Computer modeling does permit an approach towards an operational field evaluation for future shared space designs while describing the behavior of traffic participants. A combination of two traffic systems requires way of finding the path to a destination between different traffic modes, handling social interactions through the shared area and also the propulsion typical for each mode. Many theoretical models have been proposed so as to uncover the laws which govern both vehicle traffic as well as pedestrian dynamics [2, 5, 17]. In regards to the analysis of pedestrian behavior using methods from physics, the Social Force Model (SFM) is one of the most discussed models on the microscopic level [13, 15, 16]. The SFM has the potential to describe gap acceptance behaviour emergently. It offers the possibility of a unified theory that can explain both vehicle and pedestrian movement, both separately and in interaction with each other.

A literature review on mixed traffic is given in Sect. 2. The main behavior of shared space users is explained based on social forces in Sect. 3. The shortest path to the destination is generated based on the flood fill algorithm for each shared space user here (Sect. 4). Finally, Sect. 5 illustrates the ability of the mathematical model through qualitative examination of the performed simulations.

2 Background

Concerning mixed pedestrian-vehicle flows over a network, limited numbers of studies have been reported in the literature. Among pedestrian and vehicle interaction models, Helbing et al. [8] formulated and analyzed the interaction of pedestrians with vehicles on the crossing sections and Jiang and Wu [11] explored a lattice gas model in order to study the vehicle and pedestrian flows in a narrow channel. The pedestrian traffic is studied in [1, 10] using VISSIM and vehicle and pedestrian modes are operated independently and controlled by the traffic signals at potential conflicting areas. Apart from shared space scenarios, the interaction of pedestrians and vehicles was modeled on the microscopic level by using the SFM for pedestrian behavior, the single track model for car dynamics and a game theoretic force for solving conflicts in [14].

This paper addresses modeling mixed traffic environments with the use of the SFM. Social forces are used for both pedestrian and car dynamics. The SFM is formulated in such a way that shared space users avoid collisions and interruptions within their personal space. Simulations of the SFM show that it is essential to integrate a shortest path algorithm in order to model a human-like behavior. Potential field methods [12] and related path modification methods [4] have been a popular choice, due to their relative ease and effectiveness at coordinating motion. A distance map based on a combination of Manhattan Metric and Chessboard Metric is used in this paper to navigate shared space users into the direction of the shortest path to their goal according to the infrastructure of the environment.

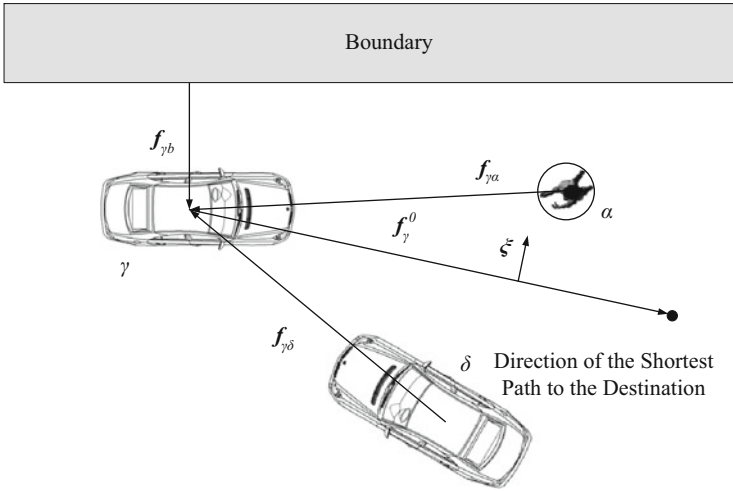


Fig. 1 Force terms exerted to a car from a pedestrian/car/boundary

3 A Microscopic Model for Shared Space Users

The microscopic model presented in this section is based on Helbing’s SFM [7]. The new arrangement of a shared space environment integrating vehicles is shown in Fig. 1. The sum of the force terms exerted to a car γ from a pedestrian α , a boundary b and another vehicle δ can be seen in Eq. 1. The last term is a random fluctuation force exerted to the sum of the forces to show the velocity fluctuation due to diverse behaviors. Each summand will be explained in the following sections.

$$\frac{d\mathbf{v}_{\gamma}(t)}{dt} = \mathbf{f}_{\gamma}^0 + \sum_{\delta(\delta \neq \gamma)} \mathbf{f}_{\gamma \delta} + \sum_{\alpha} \mathbf{f}_{\gamma \alpha} + \sum_b \mathbf{f}_{\gamma b} + \xi \tag{1}$$

3.1 Driving Force

The driving force of a car is similar to the one applied for pedestrians as this force term describes the motivation to move towards a certain destination. The driver γ is assumed to move in a desired direction \mathbf{e}_{γ}^0 with a desired speed v_{γ}^0 that is adapted to the actual velocity \mathbf{v}_{γ} within a certain relaxation time τ_{γ} .

$$\mathbf{f}_{\gamma}^0 = \frac{v_{\gamma}^0 \cdot \mathbf{e}_{\gamma}^0(t) - \mathbf{v}_{\gamma}}{\tau_{\gamma}} \tag{2}$$

The desired direction \mathbf{e}_γ^0 above points into the direction of the shortest path to the destination. This is achieved by calculating a distance map that is explained in Sect. 4.

3.2 Interaction Forces Considering the Geometric Model of Cars

Shared space layouts are aiming to make a smooth traffic flow through reducing the stop and go behavior. Drivers try adapting to the behavior of other shared space users. Any deviation from their path to their destination is mainly due to collision avoiding interactions. The interaction between a car γ , either with another car ($U = \delta$) or with a pedestrian ($U = \alpha$) is described in Eq. 3. The socio-psychological force $\mathbf{f}_{\gamma U}^{\text{soc}}$ is to keep a certain distance from nearby users. The deceleration force $\mathbf{f}_{\gamma \delta}^{\text{dec}}$ is to cover the follow-the-leader behavior of drivers if a car is faster than a leading car within a close distance. Assuming no physical contact, vehicles do not get closer than a certain distance to another agent. Hence, no physical force is included.

$$\mathbf{f}_{\gamma \delta}(t) = \mathbf{f}_{\gamma \delta}^{\text{soc}}(t) + \mathbf{f}_{\gamma \delta}^{\text{dec}}(t) \quad (3)$$

To describe the socio-psychological force $\mathbf{f}_{\gamma U}^{\text{soc}}$, an exponential function is applied to reflect the role of distance. The repulsive force increases when agents get closer and it will almost vanish when they move far away from each other.

$$\mathbf{f}_{\gamma U}^{\text{soc}} = A_{\gamma U} e^{\frac{r_{\gamma U} - d_{\gamma U}}{B_{\gamma U}}} \mathbf{n}_{\gamma U} F_{\gamma U} \quad (4)$$

The $\mathbf{n}_{\gamma U}$ is the normalized vector pointing from another user (car or pedestrian) to the car γ . $A_{\gamma U}$ and $B_{\gamma U}$ are constant parameters that indicate interaction strength and interaction range of the repulsive force $\mathbf{f}_{\gamma U}^{\text{soc}}$. $d_{\gamma U}$ is the distance between the center of agents, and $r_{\gamma U}$ is the sum of their radii. Since the form factor and the radii are different from the one for pedestrians, these factors are redefined.

3.2.1 Determination of the Sum of Radii

Contrary to a circular specification for a pedestrian in the SFM, an ellipse with radius r_γ is modeled for a car (Fig. 2). The radius r_γ depends on the angle $\varphi_{\gamma U}$ between the desired direction of a car and the direction of the close-by pedestrian or car who is exerting a force. The radius of the ellipse $r_\gamma(\varphi_{\gamma U})$ in polar coordinates is as follows:

$$r_\gamma(\varphi_{\gamma U}) = \frac{w}{\sqrt{1 - \epsilon^2 \cos^2(\varphi_{\gamma U})}}, \text{ where } \epsilon = \frac{\sqrt{l^2 - w^2}}{l} \quad (5)$$

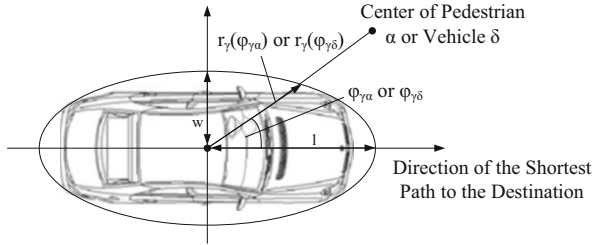


Fig. 2 Vehicle modeling using a geometrical approximation of an ellipse

In Eq. 5, $2l$ and $2w$ are assumed to be the average length and width of a modeled car. The sum of the radii is $r_{\gamma U} = r_{\gamma} + r_U$ and $d_{\gamma U}$ is the distance between the center of a car γ and another shared space user (car or pedestrian). The form factor $F_{\gamma U}$ (Eq. 6) is used only to consider the anisotropic behavior of human beings. Considering that a car movement is restricted to change of direction, and lateral movement is not possible, an effective field of view is included in this form factor. In addition, there is a difference between a pedestrian and a car following another car since the leading car driver will not only react on the cars in front but also to the cars behind it.

$$F_{\gamma U} = \left(\lambda_{\gamma} + (1 - \lambda_{\gamma}) \frac{1 + \cos(\varphi_{\gamma U})}{2} \right) \cdot q \tag{6}$$

q is the ‘effective factor’ that will distinguish between a car-pedestrian or a car-car interaction. The driver’s view angle is compared to the effective field of view in Fig. 3.

3.2.2 Car-Following Feature

The deceleration force $\mathbf{f}_{\gamma\delta}^{\text{dec}}$ in Eq. 3 is considered for drivers in the same direction of movement within a certain distance to adopt the behavior of the leading car. The social force $\mathbf{f}_{\gamma\delta}^{\text{soc}}$ is assigned zero in this case.

The deceleration force $\mathbf{f}_{\gamma-1,\gamma}^{\text{dec}}$ is defined in Eq. 7 [9] and its magnitude depends on the distance between cars $d_{\gamma\delta}$ considering the velocity dependence safe distance $d(v_{\gamma\delta})$, velocity differences $\Delta v_{\gamma\delta}$ and braking time τ'_{γ} .

$$\mathbf{f}_{\gamma\delta}^{\text{dec}} = \frac{\Delta v_{\gamma\delta} \Theta(\Delta v_{\gamma\delta})}{\tau'_{\gamma}} e^{-[\frac{d_{\gamma\delta} - d(v_{\gamma\delta})}{B_{\gamma\delta}}]} \cdot p, \text{ where } \begin{cases} \Theta(\Delta v_{\gamma\delta}) = 1, & \text{if } (v_{\gamma} > v_{\delta}) \\ \Theta(\Delta v_{\gamma\delta}) = 0, & \text{otherwise} \end{cases} \tag{7}$$

The angle between the desired direction of a driver γ and the desired direction of the driver in front of him δ determines whether their movements are confluent or opposed. Therefore, the deceleration force is only included ($p = 1$) in the sum of the forces when $|\varphi_{\gamma\delta}| > 10^\circ$ or $|\varphi_{\gamma\delta} + \varphi_{\delta\gamma} - 180| < 10^\circ$. Otherwise, $p = 0$ and the social force will result in collision avoidance behavior.

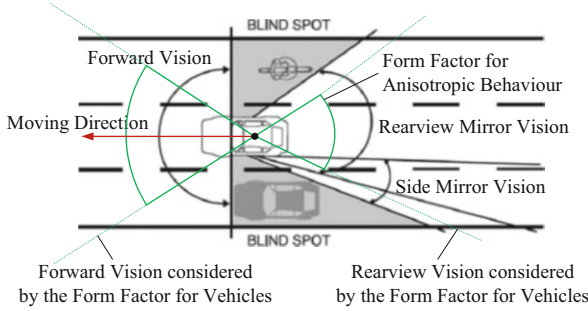


Fig. 3 Effective field of view compared to driver’s vision

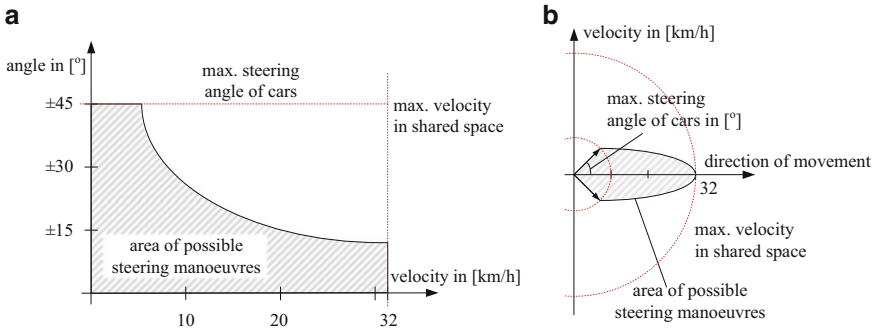


Fig. 4 Vehicle velocity versus steering angle. (a) Velocity versus steering angle. (b) Steering manoeuvres in polar coordinates

The interaction between cars and boundaries/obstacles is described by considering that cars are not expected to have any physical contact with boundaries or obstacles. An expression similar to Eq. 4 is defined to avoid car accidents.

3.3 Relation Between Steering Angle and Moving Velocity

As mentioned in Sect. 3.2, vehicles have restricted lateral movement. These limitations are included within the model. Regarding pedestrians, the angle of movement can be within $[0, 2\pi]$, whereas the desired velocity should be $v_\alpha(t) = 5.4 \frac{\text{km}}{\text{h}}$. In respect of cars, not only the velocity is restricted to $20 \frac{\text{miles}}{\text{h}}$ ($32 \frac{\text{km}}{\text{h}}$), but also the angle of steering is limited. As shown in Fig. 4a, the limitation function can be described as $v_{\gamma\text{empirical}}(\psi_{car})$, where $\psi = \arctan\left(\frac{v_{y2}}{v_{y1}}\right)$ is called the steering angle. This function is assumed based on observed behaviors. Figure 4b illustrates the same concept in polar coordinates and Eq. 1 gives the resulting angle of movement and the velocity by computing $\mathbf{v}_\gamma(t)$. So, it is necessary to constrain Eq. 1. The steering

angle ψ is considered to be within the interval $[0, \pm 30^\circ]$, while $v_\gamma(t)$ is considered not to exceed $32 \frac{\text{km}}{\text{h}}$.

3.4 SFM Adjustment and Extension for Pedestrians

Since the original SFM [6] only considers forces exerted by pedestrians and obstacles onto other pedestrians, forces exerted by vehicles onto pedestrians need to be included as well. The existence of cars in a shared space environment is expressed by a new socio-repulsive force $\mathbf{f}_{\alpha\gamma}$ term from cars to a pedestrian (Eq. 8). This new force explains the most important interaction behavior of a pedestrian keeping a certain distance to the nearby car since no physical interaction should occur.

$$\frac{d\mathbf{v}_\alpha(t)}{dt} = \mathbf{f}_\alpha^0 + \sum_{\beta(\beta \neq \alpha)} \mathbf{f}_{\alpha\beta} + \sum_b \mathbf{f}_{\alpha b} + \sum_\gamma \mathbf{f}_{\alpha\gamma} + \xi \quad (8)$$

Similar to the interaction force between pedestrians in the Social Force Model, an exponential function is applied to pedestrian α to represent the influence of distance between the pedestrian and the close-by car γ as

$$\mathbf{f}_{\alpha\gamma}^{soc} = A_{\alpha\gamma} e^{\frac{r_{\alpha\gamma} - d_{\alpha\gamma}}{B_{\alpha\gamma}}} \mathbf{n}_{\alpha\gamma} F_{\alpha\gamma}, \quad (9)$$

where $r_{\alpha\gamma} = r_\alpha + r_\gamma$; $d_{\alpha\gamma}$ is the distance between the center of pedestrian α and car γ ; $\mathbf{n}_{\alpha\gamma}$ is the normalized vector from car γ to pedestrian α . The form factor $F_{\alpha\gamma}$ is also set similar to Eq. 6 to explain the anisotropic behavior of pedestrian α when facing car γ .

4 Desired Direction of Movement by Distance Map

The direction of the desired velocity is meant to be equivalent to the direction of the shortest path to the destination avoiding obstacles. A distance potential field is calculated by the flood fill algorithm for agents' navigation. The floor area is divided into cells of size $15 \times 15 \text{ cm}^2$. Agents move to one of the eight neighboring cells with the closest distance to the target in each time step. This is achieved by calculating the flood fills based on a combination of Manhattan metric D^M and Chessboard metric D^C [12]:

$$D^{V2} = (\sqrt{2} - 1)D^m + D^C, \text{ where } \begin{cases} D^M = \sum_i |\delta x_i| + \sum_i |\delta y_i| \\ D^C = \sum_i \max(|\delta x_i|, |\delta y_i|) \\ D^m = D^M - D^C \end{cases} \quad (10)$$

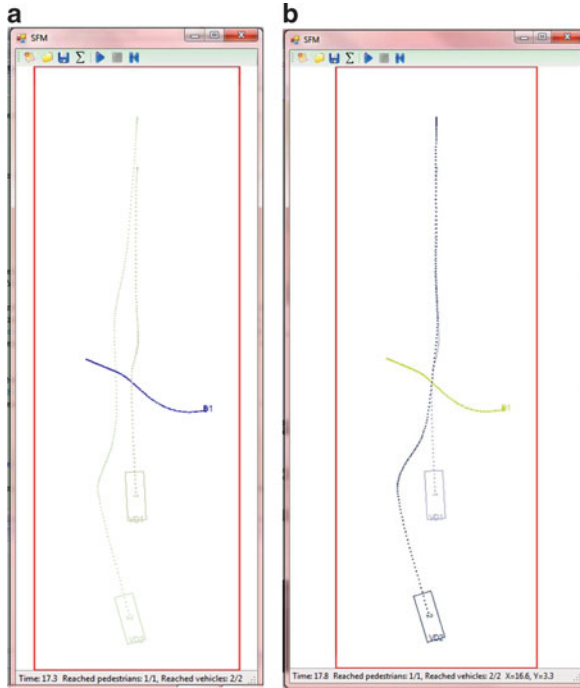


Fig. 5 Snapshot of a driver’s path with the influence of (a) social force (SF) and (b) deceleration force (DC): the moving direction of the cars is from *top* to *bottom* whereas a pedestrian crosses from *left* to *right*

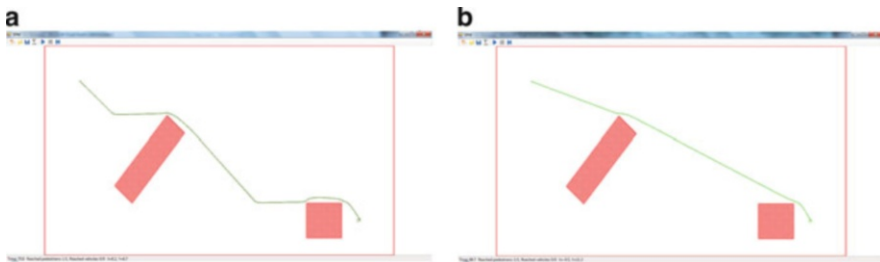


Fig. 6 Obstacle avoidance and way-finding simulation. (a) Without route map. (b) With route map

5 Simulation and Results

This section simulates the presented model to show the behavior of drivers and pedestrians with the car-following feature and the applied distance map. The scenario in Fig. 5 show the influence of the deceleration force $f_{\gamma\delta}^{dec}$ explained in Sect. 3.2. The interaction force improves the driver behavior in regards to the leading car. Figure 6 illustrates the influence of the distance map on pedestrian route choice

behavior based on the flood fill algorithm. The pedestrian therefore chooses a more human-like route after generating a distance map.

6 Conclusions and Future Work

The main contribution of this paper is the integration of the car-following model and a shortest path algorithm into the SFM. By merging these models, shared space dynamics can be modeled and simulated. The experimental results show that the flood fill algorithm is effective and a feasible option for improving the path planning of the SFM as it provides a more human-like route-choice behavior. The mathematical model is flexible and includes the main interaction factors between drivers and pedestrians in mixed traffic environments. For future applications, this model should be calibrated based on real data comparison.

Acknowledgements The authors would like to thank NEARCTIS for the financial support of this study under grant number 224272.

References

1. C. Boenisch and T. Kretz. Simulation of Pedestrians Crossing a Street. In *Traffic and Granular Flow '09*, 2009.
2. M. Chraïbi and A. Seyfried. Generalized Centrifugal-Force Model for Pedestrian Dynamics. *Physical Review E*, 82:046111, 2010.
3. DfT. Shared Space. Technical report, TSO, October 2011.
4. E.W. Dijkstra. A Note on Two Problems in Connexion with Graphs. *Numerische Mathematik*, 1:269–271, 1959.
5. R.S. Franca, M.G.B. Marietto, W.R. Santana, and G. Kobayashi. An Agent-Based Simulation Model for Pedestrian Unidirectional Movement. In *Second International Conference on the Applications of Digital Information and Web Technologies*, 2009.
6. D. Helbing. A Mathematical Model for the Behaviour of Pedestrians. *Behavioral Science*, 36:298–310, 1991.
7. D. Helbing, I. Farkas, and T. Vicsek. Simulating Dynamical Features of Escape Panic. *Nature*, 407:487–490, 2000.
8. D. Helbing, R. Jiang, and M. Treiber. Analytical Investigation of Oscillations in Intersecting Flows of Pedestrian and Vehicle Traffic. *Physical Review E*, 72:0461301–04613010, 2005.
9. D. Helbing and B. Tilch. Generalized Force Model of Traffic Dynamics. *Physical Review E*, 58:133–138, 1999.
10. M.M. Ishaque and R.B. Noland. Trade-offs between Vehicular and Pedestrian Traffic using Micro-Simulation Methods. *Transport Policy* 14, 124:124–138, 2007.
11. R. Jiang and Q.S. Wu. Interaction between Vehicle and Pedestrians in a Narrow Channel. *Physica A*, 364:239–246, 2006.
12. T. Kretz, C. Boenisch, and P. Vortisch. Comparison of Various Methods for the Calculation of the Distance Potential Field. *Pedestrian and Evacuation Dynamics*, 2008.
13. M. Moussaid, D. Helbing, S. Garnier, A. Johansson, M. Combe, and G. Theraulaz. Experimental Study of the Behavioural Mechanisms Underlying Self-Organization in Human Crowds. *Proceedings of the Royal Society B*, 276:2755–2762, 2009.

14. R. Schönauer, M. Stubenschrott, W. Huang, C. Rudloff, and M. Fellendorf. Modeling Concepts for Mixed Traffic: Steps towards a Microscopic Simulation Tool for Shared Space Zones. In *TRB 2012 Annual Meeting*, 2012.
15. A. Seyfried, B. Steffen, W. Klingsch, and M. Boltes. The Fundamental Diagram of Pedestrian Movement Revisited. *Statistical Mechanics: Theory and Experiment*, 10:P10002, 2005.
16. Z. Zainuddin and M. Shuaib. Incorporating Decision Making Capability into the Social Force Model in Unidirectional Flow. *Research Journal of Applied Science* 5, 6:388–393, 2010.
17. H.M. Zhang and T. Kim. A Car-following Theory for Multiphase Vehicular Traffic Flow. *Transport Research Part B*, 39:385–399, 2005.

Simulation Model for Vehicle and Pedestrian Interaction Considering Road Crossing Activities

Bruno R. Werberich, Carlos O. Pretto, and Helena B.B. Cybis

Abstract This paper addresses the pedestrian road-crossing modeling problem. The model presented in this paper has been devised to provide a sound representation of interaction among pedestrians and a more realistic approach for interaction between pedestrians and vehicles. The present research proposes the analysis of two different pedestrian crossing behaviors. One crossing behavior considers a fixed area for pedestrians cross a road. The second one considers pedestrians searching for a gap while walking on the sidewalk. This paper presents the analysis of 180 simulations, considering 18 different parameters settings. From the results of the present research, the analysis of variance (ANOVA) shows that both variables, average headway of vehicles and pedestrian behavior, were statistically significant.

Keywords Pedestrian crossings • Pedestrian behavior • Agent simulation

1 Introduction

The emulation of pedestrians in the traffic environment is a complex problem. In order to represent the real movements of pedestrians, models should be able to simulate several processes, including path planning, sense and avoidance of obstacles, and interaction with other pedestrians.

The road-crossing is a situation where users interact with others, evaluate visual signs and estimate speeds and directions. These aspects have a strong influence on safety and travel times [1, 2]. Pedestrians have several choices before crossing a road. The decision about where and when to cross is influenced by the conditions of the road environment as a whole. From the point of view of traffic engineering,

B.R. Werberich (✉) • C.O. Pretto • H.B.B. Cybis
Production Engineering Department, Federal University of Rio Grande do Sul – UFRGS,
Porto Alegre, Brazil
e-mail: [Bruno.rwe@gmail.com](mailto: Bruno.rwe@gmail.com); [cpretto@gmail.com](mailto: cpretto@gmail.com); [helenabc@producao.ufrgs.br](mailto: helenabc@producao.ufrgs.br)

the main factors influencing operational and user safety perspectives involve the pedestrians' preferred crossing location; the conditions under which they decide to cross the road, and the characteristics of traffic flow.

Recent researches about pedestrians crossing behavior in urban areas are mainly concerned on gap acceptance models, in which pedestrians are associated with an acceptance of a critical gap for road crossing [3, 4]. Part of pedestrian research on crossing behavior regards the analyses of psychological and motivational factors [5, 6, 7].

The pedestrian's choice of a place to cross may be related to three main factors: the pedestrian's wish to walk shorter distances; the wish to cross the road as quickly as possible, and the need to reduce exposure to risk. Literature suggests that the pedestrian's behavior when crossing a road characterizes crossing compliance [8].

The emulation of a more realistic pedestrian behavior pattern provides the basis for the identification of the influence of operational attributes, such as signal timing and project characteristics and the dynamics of the pedestrians' road-crossing process.

Based on these considerations, this paper addresses the problem of modeling the pedestrian road-crossing task. The proposed model considers the behavior patterns at road crossings, considering the pedestrian's decision process about where and when to start crossing the road.

This paper provides a study where two different pedestrians behavior scenarios were modeled and compared. The first one consists on pedestrians trying to cross a road waiting for a gap in the traffic flow at a fixed area on the sidewalk. On the second one, pedestrians walk along the sidewalk to reduce the distance from their destination while observe the traffic flow for a valid gap. If a valid gap is found, pedestrians cross the road.

2 Pedestrian Model

This model can be described as an agent-based micro-simulation, where the decision process is based on a combination of force and rule based approaches [9]. This model was structured as a combination of different modeling approaches in order to express the inherent flexibility of pedestrian behavior. The model was divided into strategic, tactical and operational layers, based on [10] and [11].

2.1 *Space Negotiation*

Based on the Newtonian force models, we developed a space negotiation strategy among pedestrians, defined by a mathematical process inspired on the potential force field concept [12].

To choose the next step, the pedestrian verifies the intensity of the resultant potential force field $Ffr_{(x,y)}$ Eq. 1. $Ffr_{(x,y)}$ represents the value of the resultant force field at any position (x, y) . It is a function of the potential force field at x,y ($Fr_{(x,y)}$) and the Euclidian distance from the candidate's next step point to a pedestrian's destination $d_{(x,y)}$.

$$Ffr_{(x,y)} = Fr_{(x,y)}\beta + \gamma d_{(x,y)} \quad (1)$$

The β and γ coefficients are used to regulate the influence of the force field or the distance value on the choice of the next step. For instance, if the β is too high, the pedestrian will keep a relative high distance from other pedestrians. If the γ is too high, the pedestrian will try to choose the nearest point to the destination, and will not be so sensitive to the proximity to others pedestrians. It is important to notice that terms like "potential field" and "force field" are used as nomenclature only, without a hard analogy with the physical concept.

$Fr_{(x,y)}$ at any point is a function of vector S and U , where S is the pedestrian speed vector and U is a unit vector at the direction of the position (x, y) .

The intensity of the force Fr of a pedestrian p_j is proportional to α . The coefficient α is related to the angle between the unit vector U and the speed vector S and inversely proportional to the square distance between the position (x,y) and the pedestrian's position Eq. 2.

$$\alpha_{pj} = 0,5 + \frac{\cos \theta}{2} \quad (2)$$

And θ is defined by Eq. 3.

$$\theta = \arccos \frac{S_{pj} \cdot U_{pj}}{|S_{pj}| |U_{pj}|} \quad (3)$$

The resultant force of one pedestrian is defined by Eq. 4.

$$Fr_{pj} = \frac{|S_{pj}| \alpha_j}{d_{(pj,Fr_{pj})}^2} \quad (4)$$

The resultant force Fr at any given point is described by the sum of the Fr_{pj} from each pedestrians present at the simulation, as follows Eq. 5:

The force field intensity at any given coordinate (x, y) at the space will be the resulted value of a sum of pedestrians' forces.

The pedestrians use a discrete choice approach for selecting the next step point. In this model, the greatest utility is represented by the alternative that contains the smallest value of the balance between the force field perceived by the pedestrian and the distance to their goal.

2.2 Gap Evaluation

The pedestrian cross the road only if is possible to cross all of the road lanes at once. The gap evaluation model assumes a parallel lane to the x axis of coordinates of the simulation environment. The origin of the coordinate system is in the lower left corner. The flow of vehicles lane takes place from the left to right with constant speed.

For each lane the pedestrian computes T_r and T_c , representing respectively the time required to reach the beginning of the lane and the time required to cross it, regarding their speed and the distances involved. The gap acceptance is defined by following in equations:

$$V_{px} < P_{px} - (V_s \cdot T_r) + V_l \quad (5)$$

$$V_{px} > P_{px} - (V_s \cdot (T_r + T_c + P_{sg})) \quad (6)$$

Where:

V_{px} , is the x coordinate of the vehicle;

P_{px} , is the y coordinate of the vehicle;

V_s , is the vehicle speed;

V_l , is the vehicle length;

P_{sg} , is the time safety margin.

Vehicles that satisfy the in Eq. 5 are the vehicles in the pedestrian's direction. Among these vehicles, some of them will collide with the pedestrian before he can cross the lane in Eq. 6.

2.3 Active Pedestrians' Crossing Behavior: Search for a Gap While Walking

The interaction between vehicles and pedestrians may present different levels of complexity. The simpler and more frequently observed environment consists of situations where pedestrians use sidewalks and cross the road only at traffic lights or pre-defined crossing points. It is possible to stratify the flow of pedestrians and vehicles, and the interaction between them can be defined by straightforward rules. However, in some circumstances, interaction can achieve an increased level of complexity.

Considering the scenario shown in Fig. 1. Pedestrians have their origin at point 1 and their destination at point 3. In real life, some pedestrians can reduce their trip time walking to point 2, while searching for a gap to cross to the opposite sidewalk and reach their destination.



Fig. 1 Search for a gap while walking behavior

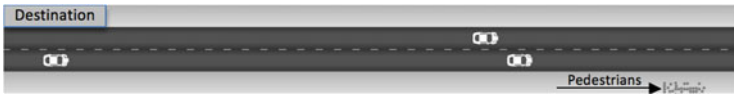


Fig. 2 Simulation scenarios

In the next section, the simulation results of two scenarios were compared. The scenario 1 represents a fixed pedestrians' crossing area. The scenario 2 simulates pedestrians searching for a gap while walking.

3 Simulation Scenarios

The first simulation scenario consists on pedestrians waiting for a gap in the traffic flow at a fixed area on the sidewalk. On the second scenario pedestrians walk along the sidewalk to reduce the distance from their destination while searching for a gap in traffic flow. If a valid gap is found, pedestrians cross the road.

For each scenario, the simulations are performed as shown in Fig. 2, where 40 pedestrians begin their trip in the lower right corner of the picture, represented by circles, and have their destination located in the upper left corner. To reach their destination, pedestrians must cross two lanes of vehicles, with vehicle traffic from the left to the right; the track length is 100 m.

Pedestrians are distinguished from each other by their travel speed and time safety margin for gap acceptance, P_{sg} . However, these pedestrians' parameters are exactly the same for all execution of the simulation. All vehicles have constant speed of 50 km/h. The average headway of vehicles is different for each simulation.

In the simulations, the average speed of pedestrians is 1.2 m/s with a standard deviation of 0.2 m/s, 1 s was used for P_{sg} as the average value with a standard deviation of 0.2 s. The headway standard deviation was 0.72 s. All parameters were generated by a normal distribution.

4 Results

Table 1 shows the result of 180 simulations considering 18 different parameters settings. The response variable of each of the simulations is the average travel time of the 40 simulated pedestrians expressed in seconds. The simulation parameters settings vary according to the following controllable factors:

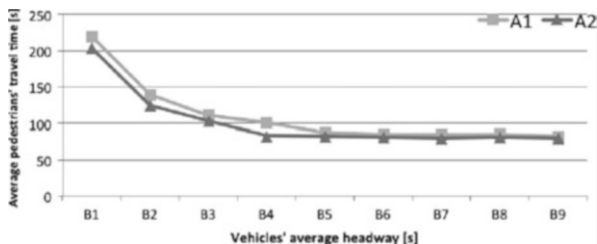
Table 1 Simulation results

		B										Average
A	B1	B2	B3	B4	B5	B6	B7	B8	B9	Average		
A1	189,44	135,59	130,81	102,64	80,21	81,38	82,84	86,81	81,26			
	151,44	130,35	106,86	127,53	95,08	82,85	83,66	84,03	79,84			
	274,02	180,73	120,21	103,63	91,35	89,27	81,33	88,56	80,54			
	226,84	129,12	96,16	95,00	90,78	93,10	80,63	84,39	81,24			
	210,90	105,21	92,30	96,96	83,26	86,00	84,72	80,78	85,67	110,71		
	193,13	139,31	81,99	93,35	89,45	85,09	81,96	86,90	82,69			
	271,66	159,77	110,00	115,27	81,31	80,35	84,18	84,44	81,41			
	231,92	123,13	169,54	92,37	86,21	79,94	86,98	81,53	80,75			
	196,56	128,75	106,09	88,85	85,36	90,91	82,70	96,30	79,92			
	256,79	164,18	102,62	93,63	88,31	79,83	95,41	81,05	86,92			
	220,27	139,61	111,66	100,92	87,13	84,87	84,44	85,48	82,02			
Average	39,60	22,33	24,55	12,04	4,74	4,85	4,26	4,62	2,41			
s.d	207,81	150,31	132,53	83,07	78,62	80,19	80,56	81,28	80,68			
A2	200,39	130,03	87,18	80,94	80,14	81,06	79,92	80,98	79,43			
	80,18	97,97	82,23	84,64	81,38	80,49	78,49	81,08	81,29			
	217,49	134,31	81,21	79,93	85,93	80,69	81,84	81,13	79,78			
	271,06	96,46	106,31	83,96	81,42	81,87	79,87	80,84	79,24			
	224,88	116,82	118,58	80,17	84,42	80,53	79,43	80,61	79,74	101,82		
	226,17	141,96	102,82	81,94	80,65	79,04	79,17	80,16	79,49			
	247,53	142,58	82,71	81,32	80,40	80,05	78,89	79,69	80,24			
	209,60	118,26	83,88	90,02	80,71	80,39	81,26	80,69	80,38			
	150,49	114,50	149,53	80,66	86,42	80,43	81,20	79,54	79,58			
Average	203,56	124,32	102,70	82,66	82,01	80,47	80,06	80,60	79,98			
s.d	53,49	18,59	24,09	3,03	2,63	0,72	1,12	0,61	0,65			

Table 2 Analysis of variance (ANOVA)

	Sum of squares	Degrees of freedom	Mean square	F	P-value	
A	3558,7229	1	3558,7229	9,5437	3,899502435	Significant
B	296287,0914	8	37035,8864	99,3222	1,995962468	Significant
AB	1538,3688	8	192,2961	0,5156	1,995962468	Not significant
Error	60407,5563	162	372,8861			
Total	361791,7396	179				

Fig. 3 Pedestrians’ travel time



Factor A: behavior of pedestrians, defined by two scenarios: A1 (pedestrians wait for gaps in vehicles flow) and A2 (pedestrians walk while searching for gap)
 Factor B: average headway between vehicles distributed in 9 levels: B1 (2.88s), B2 (3.24s), B3 (3.60s), B4 (3.96s), B5 (4.32s), B6 (4.68s); B7 (5.04s), B8 (5.40s) and B9 (5.75s).

Any other factors involved were kept constant in all simulations, including the characteristics of pedestrians as starting location, destination, desired speed and P_{sg} .

A statistical analysis was conducted to evaluate the different between pedestrians behavior. The Table 2 shows the analysis of variance (ANOVA). The P-Value was chosen for a significance level of 95 %.

Factors A and B are significant for a significance level of 95 %. The interaction between factors A and B was not significant. Figure 3 graphically displays the analyzed data.

5 Conclusion

The present research proposes the analysis of two different pedestrian crossing behaviors. One crossing behavior considers a fixed area for pedestrians cross a road. The second one considers pedestrians searching for a gap while walking on the sidewalk. This paper presents the analysis of 180 simulations, considering 18 different parameters settings. The response variable of each of the simulations is the average travel time of the 40 simulated pedestrians, expressed in seconds.

From the results of the present research, the analysis of variance (ANOVA) shows that both variables, average headway of vehicles and pedestrian behavior, were statistically significant on response variable with a significance level of 95 %. The average results of the simulations scenario 1 was 110.71 s, and for the scenario 2 was 101.82 s.

The representation of active pedestrians' crossing behavior (scenario 2) let to reduce of 8.03 % on average travel times. This behavior is consistent with the actual behavior of pedestrians in many urban environments.

It is possible to conclude that the representation of new pedestrians' behavior models, especially regarding crossing activities, is important to soundly represent pedestrians' simulation on urban environment and also has a significant impact on the numerical results.

References

1. Chae, K.. Simulation of pedestrian-vehicle interactions at roundabouts. *PhD Thesis*, North Carolina State University, Raleigh, NC, United States of America, 2005.
2. Chu, X., M. Guttenplan and M. Baltes. Why people cross where they do: The role of the street environment. *Transportation Research Record*, v. 1878, 2004, p. 3–10.
3. Himanen, V., & Kulmala, R. (1988). An application of logit models in analysing the behaviour of pedestrians and car drivers on pedestrian crossings. *Accident Analysis & Prevention*, 20(3), 187–197.
4. Sun, D., Ukkusuri, S. V. S. K., Benekohal, R. F., Waller, S. T. (2003). Modeling of motorist-pedestrian interaction at uncontrolled mid-block crosswalks. In *Proceedings of the 82nd TRB annual meeting*, transportation research board, Washington, 2003.
5. Diaz, E. M. (2002). Theory of planned behaviour and pedestrians' intentions to violate traffic regulations. *Transportation Research Part F*, 5, 169–175. Evans, D., & Norman, P. (1998). Understanding pedestrians' road crossing decisions: An application of the theory of planned behaviour. *Health Education Research*, 13(4), 481–489.
6. Bernhoft, I. M., & Carstensen, G. (2008). Preferences and behaviour of pedestrians and cyclists by age and gender. *Transportation Research Part F*, 11, 83–95.
7. Papadimitriou, E., Yannis, G., & Golias, J. (2009). A critical assessment of pedestrian behaviour models. *Transportation Research Part F*, 12(3), 242–255. Sarkar, S. (1995). Evaluation of safety for pedestrians at macro- and microlevels in urban areas. *Transportation Research Record No 1502*.
8. Roupail, N. M. 1984. "Midblock crosswalks: a user compliance and preference study". *Transportation Research Record*, No. 959, p.41–47.
9. Pretto, C. O.; Cybis, H. B. B. . Modeling Pedestrian movement on road-crossing environment. 12th World Conference on Transport Research, Lisboa, 2010.
10. Pretto, C. O.; Jacobsen, A. C.; Cybis, H. B. B. . A multi-layer simulation model for vehicle and pedestrian. 90th Annual Meeting Transportation Research Board, v. 1. p. 1–15, Washington, 2011.
11. Hoogendoorn, S., Bovy, P., Daamen, W. Microscopic pedestrian wayfinding and dynamics modelling. In: Schreckenberg, M., Sharma, S. (Eds.), *Pedestrian and Evacuation Dynamics*. Springer, pp. 123–155, 2002.
12. Löhner, R. On the modeling of pedestrian motion. *Applied Mathematical Modelling*, n.34, p.366–382, 2010.

Simulation Models of Merging Priorities in Staircases

Henri Hakonen and Marja-Liisa Siikonen

Abstract When evacuating a high-rise building, two streams of evacuees meet at the landings: those who are already descending the stairs and those who are about to enter the staircase through the landing door. In this article, merging of these streams is studied with calculations and with queuing and agent-based simulation models. The agent model considers in detail the interactions between the agents and between the agents and the building. The queuing model has two queues which merge together for each floor of the building. The process is defined by a merge ratio. The merge ratio or priority of one queue does not have an effect on the total egress time, but it affects floor-wise waiting times and journey times. The results show that evacuation of the highest floors of a tall building is not accelerated substantially, because possibilities of adjusting the merge ration are limited.

Keywords Evacuation • Simulation • Stairs • Merge • Behavior

1 Introduction

In evacuation situations streams of occupants merge together. Important points of merging are at staircase landing doors where occupants descending the stairs meet occupants trying to enter the staircase from floor level. The limiting factor in an evacuation situation is usually the capacity of the staircase. During congestion the occupants must interact to find their place in the staircase stream. If the number of occupants is relatively small compared to the stair capacity then the limiting factor is the walking speed of the occupants. The occupants are able to enter the staircase freely and merging is not an issue.

H. Hakonen (✉) • M.-L. Siikonen
KONE Corporation, P.O. Box 7, FI-02151 Espoo, Finland
e-mail: henri.hakonen@kone.com; marja-liisa.siikonen@kone.com

The merging affects the evacuation procedure. The usual phenomenon is that the upper floors of a tall building have a longer evacuation time than the lower floors mainly because of the congestion. To be able to rescue the highest floors fast, the flow inside the staircase should be fluent. One way to achieve this is to make the merging process to prefer the streams inside the staircase instead of the streams coming from the floors. It is assumed that physical factors such as the width of the staircase and doorway, and the location of the landing door affect the merging. Also psychological factors like motivation probably affect the merging procedure. The factors that are quite easy to alter are the location and width of doorway, but reducing the width of doorways to improve the flow inside the staircase is not wise.

The evacuation case study studied two buildings using stairways. Firstly, the egress times and passenger waiting and journey times were calculated manually. Secondly, they were simulated with the KONE Building Traffic Simulator (KONE BTS, [1]) and thirdly with the FDS simulator [2]. Merging procedure was studied for three merge ratios. BTS simulation was also used to study an experimental evacuation case.

2 Staircase Flow Merging Model

Occupant flow in the staircase was modeled as a macroscopic model, which can be easily implemented using discrete event simulation. The queuing model has one staircase section for each floor. Each section has two queues which merge together: one for occupants who are about to enter the staircase section from the floor and one for occupants that are descending from the upper staircase section. The merging is represented by a merge ratio of floor and staircase streams. In principle the merge ratio could be different in each junction, but usually a staircase consists of identical sections, so a single constant is assumed for all floors. Let us denote the merged flow as F which has unit persons per second. Let us denote the merge coefficient from a floor as x , where $x \in [0, 1]$. If the flow from a floor is xF and the flow from an upper staircase is $(1-x)F$. The stair:floor merge ratio is $(1-x):x$. For example if $x = 0.25$ then the merge ratio is 75:25 and the merged stream shall have three persons from the upper staircase for every person per floor.

The staircase simulation model implements the following rules:

1. The density shall not exceed maximum density ($2 \text{ persons}/\text{m}^2$, [3]), otherwise the merging is blocked.
2. The merging of one person takes $1/fW$ seconds, where f is nominal flow (about $1 \text{ person}/\text{m}/\text{s}$) and W is staircase width in meters.
3. After the merging, walking through the staircase section lasts L/s , where L is the length of the staircase section and s is the free walking speed ($0.6 \text{ m}/\text{s}$).
4. After walking, the person either queues for merging to the lower staircase section, or exits the staircase at rescue level.

Table 1 Passenger flows when all floors are emptying simultaneously

Floor	Flow from floor	Flow in staircase
N	$(1-x)^{N-1} * F$	0
N-1	$x * (1-x)^{N-2} * F$	$(1-x)^{N-1} * F$
...
3	$x * (1-x) * (1-x)*F$	$(1-x) * (1-x)*F$
2	$x * (1-x)*F$	$(1-x)*F$
1	$x * F$	F

Rule 1 limits density. Rule 2 limits flow. Rule 3 limits walking speed. Rule 4 directs a person through the staircase. A macroscopic model cannot simulate the movements of the occupants in detail, so it is necessary to assume maximum density corresponding to maximum flow. In reality the walking speed and also the occupant flow decrease significantly in the case of heavy congestion: If the occupant density is more than 3.8 persons per square meter, the walking speed approaches zero [4].

3 Stair Queue Merging in Tall Buildings

The flows per floor in the staircase of an N -floor building are shown in Table 1. Let us assume that the maximum flow out from the staircase is F . The merge coefficient is x . Realistic values of x are around 0.5. In the case where $N = 20$ and $x = 0.5$, the flow from the top floor is $(1-0.5)^{19} = 0.000002 * F \approx 0$. Thus, the flow from the highest floors is about zero, if the occupants enter the stairway from many floors simultaneously. The conclusion is that in a tall building the evacuation of the upper floors is stuck until the lower floors have been emptied. Only in theory, with $x \approx 0$, will the highest floors of a tall building be evacuated first.

4 Evacuation Case Studies

Two evacuation studies are considered in total evacuation of building: A three –level test building, and Jordanstown Campus [5, 6].

4.1 Manual Evacuation Calculations for the Three-Floor Building

In the three-floor building studied, the floor height is 3 m, and the population is 300 persons on each floor. The building and people flow parameters are given in Table 2.

Table 2 Building and people flow parameters

Parameter	Value
Door widths	1.0 m
Staircase width	1.2 m
Staircase section area (effective)	10.4 m ²
Flow rate through door	1.3 persons/m/s
Flow rate in staircase	1.0 persons/m/s
Full flow occupant density	2 persons/m ²

Table 3 Passenger flows (persons/s) in different phases of evacuation in case 3

Floor	3 floors emptying simultaneously		2 floors emptying simultaneously		1 floor emptying simultaneously	
	Flow from floor	Flow in staircase	Flow from floor	Flow in staircase	Flow from floor	Flow in staircase
3	0.225	0.225				
2	0.225	0.45	0.45	0.45		
1	0.45	0.9	0.45	0.9	0.9	0.9

The model does not take account of the pre-movement time or walking time to the staircase door. Three approaches in merging the floor queues to the occupant stream in the stairways are applied:

Case 1: $x = 0$ and occupants in the staircase have priority (100:0)

Case 2: $x = 1$ and occupants waiting on floors have priority (0:100)

Case 3: $x = 0.5$ and every other person joins the stream from a floor queue and every other from the upper staircase stream (50:50)

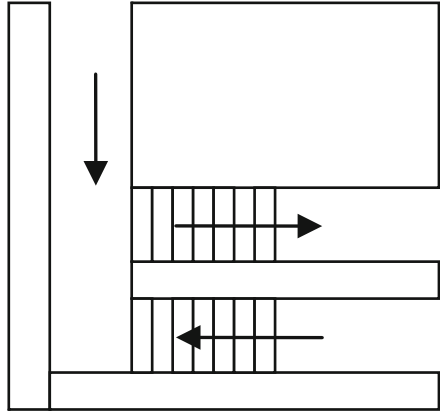
The progress of evacuation can be calculated manually without computer simulations. The idea is to keep track of the current state of evacuation until the evacuation is complete. At each calculation step the next event is found and the duration of the event is calculated. Case 3 is calculated as an example.

The total area of the staircase section consists of slope areas and landing areas. The effective area is calculated by omitting 0.15 m from the edges, which gives 10.4 m². With the maximum occupant density the maximum number of persons in the staircase section is $2 * 10.4 = 20.8$ persons. A maximum of 20 persons in the staircase section is used in the calculations. The effective widths of the door and slope are calculated by subtracting 0.15 m from the sides, which gives 0.7 m for the door and 0.9 m for the slope. The maximum flow in the staircase is limited by the full flow through the ground floor door ($0.7 m * 1.3 persons/m/s = 0.91 persons/s$) and the full flow in the staircase section ($0.9 m * 1.0 persons/m/s = 0.9 persons/s$). Thus, the maximum flow is 0.9 persons/s. The occupants arrive instantly in the floor queue. Therefore the flow through a door is always the maximum flow, 0.9 persons/s, as long as there are people in the floor queue. This also means that full flow conditions hold. Table 3 shows how flows are divided where 1–3 floors are evacuating simultaneously. Table 4 shows the progress of the evacuation.

Table 4 Progress of evacuation in case 3

Time(s)	Description of the evacuation procedure	Event at rescue level
0	Staircase begins to fill with people. Flow into staircase is 0.9 persons/s. Staircase is full in $20/0.9 = 22$ s	
22	Staircase section is full with 20 persons per floor and 280 persons wait on each of floors 1–3. Flow from floor 1 is 0.45/s, because all three floors are emptying simultaneously. It takes $280/0.45 = 622$ s to empty floor 1 (less than floor 2 or 3)	20 persons from floor 1 start to exit
44		20 persons from floor 2 start to exit. Merged with 20 persons from floor 1. This takes $40/0.9 = 44$ s
88		300 persons from floor 3 start to exit. Merged with 280 persons from floor 2 and 260 persons from floor 1. It takes $260/0.45 = 578$ s to evacuate floor 1
644	Floor 1 is empty. Floors 2 and 3 have been emptied with flow 0.225/s. Thus the decrease is $622 * 0.225 = 140$ persons and there are 140 persons left on floors 2 and 3. Flow from floors 2 and 3 is 0.45/s, because two floors are emptying simultaneously. It takes $140/0.45 = 311$ s to empty floors 2 and 3	
666		Floor 1 is evacuated. There are $280 - 578 * 0.225 = 150$ non-evacuated persons from floor 2 and $300 - 578 * 0.225 = 170$ non-evacuated persons from floor 3. It takes $150/0.45 = 333$ s to evacuate floor 2
955	Floors 2 and 3 are empty. It takes $60/0.9 = 67$ to empty staircase between floors 0 and 3	
999		Floor 2 is evacuated. There are 20 non-evacuated persons from floor 3. It takes $20/0.9 = 22$ s to evacuate floor 3
1022	Staircase between floors 0 and 3 is empty	Evacuation is finished

Fig. 1 Stair model with landing door opposite to the stream



4.2 KONE BTS Simulation

The KONE BTS stair model uses the merge ratio 50:50 as a default [7]. According to experimental studies this is a fair assumption [5]. The simulation of congested people flow largely follows the process described in Chapter 2. In addition, KONE BTS simulates passenger behavior such as transfer, direction and history [8].

4.3 FDS + Evac Simulation for the Three-Floor Building

FDS + Evac uses an agent-based model which simulates the physical and social interactions of occupants. It simulates the movements of the agents in a 2D plane. Stair slopes are similar to horizontal planes, except that the agents have slower speeds in slope planes. The speed down the slope was 70 % of normal walking speed. The default parameters of Evac 2.2.1 were used otherwise.

Galea et al. [9] suggested to place the landing door adjacent to the incoming stair to enhance the flow from the floor levels. This prefers emptying the queues from lower building floors first. On the other hand, a landing door opposite to incoming flow might favour the stream from the stairways [5]. In this study, the landing doors opposite the incoming stair were selected to give priority to the flow from the upper floors (Fig. 1).

4.4 Comparison of Results for the Three-Floor Building

The following definitions for statistical parameters are used as below

- Egress time of floor/building: Time from the moment people start to egress from the floors until the population of floor/building has exited the staircase.

Table 5 Waiting times per floor

Floor	Manual calculation			KONE BTS	FDS + Evac
	Case 1	Case 2	Case 3		
1	788	167	312	308	277
2	477	457	529	532	526
3	167	747	529	528	569
Average	477	457	457	457	457
Maximum	999	955	955	958	1,039

Table 6 Average journey times per floor

Floor	Manual calculation			KONE BTS	FDS + Evac
	Case 1	Case 2	Case 3		
1	888	189	333	329	299
2	519	522	584	586	616
3	233	855	647	648	764
Average	520	522	521	523	560

Table 7 Egress times per floor

Floor	Manual calculation			KONE BTS	FDS + Evac
	Case1	Case 2	Case 3		
1	1,021	355	666	656	608
2	706	688	999	1,000	1,020
3	399	1,022	1,022	1,020	1,114
Total	1,021	1,022	1,022	1,020	1,114

- Waiting time of occupant: Time from the beginning of egress until the occupant has entered the staircase.
- Journey time of occupant: Time from the beginning of egress until the occupant has exited the staircase.

The results of calculation Case 3 and result of *KONE BTS* in Tables 5, 6 and 7 match well. The results of *FDS + Evac* differ slightly from the manual calculations and results of *BTS*. It can be analyzed that the flow in the staircase is only 0.87 persons/s in *FDS + Evac*, while it is 0.9 persons/s in calculations and simulations, which is one but not the only reason. *FDS + Evac* has a shorter egress time on floor 1 than *BTS*, but a longer egress time on floor 3. This means that the merging is not 50:50 as in *BTS*, but favors the floor stream. With a 50:50 merge ratio waiting, journey and egress times per floor are the most equal.

4.5 *KONE BTS Simulation for Jordanstown Campus*

An evacuation drill was performed in Jordanstown campus [5, 6]. The building has 6 levels with a total of 581 occupants who exit through one staircase. The staircase

width is 1,160 mm. The BTS simulation uses 860 mm as effective width. The simulated egress time was 11 min 37 s, where it is assumed that occupants arrive at the staircase doors at time 0. The evacuation time of the drill was 13 min 12 s, where it took about 2 min to reach full flow. The results match quite well.

5 Conclusions

In this paper, two studies were made to find out the effect of merging of the people coming from stairways and landing floors. Stair evacuation with congestion is a realistic assumption since the space available for staircases in tall buildings is restricted. The egress times from the highest floors are the longest since the lower floors cause congestion in the staircase. The merging procedure does not affect the total egress time or average journey time. On the other hand, it has a significant effect on the egress times of individual persons and the waiting and journey times per floor. KONE BTS gave about the same egress times that were obtained by manual calculations for a three-floor building. KONE BTS and FDS Evac results were in line. In comparison with an experimental test the egress time with KONE BTS was 11 min while in the evacuation drill it took about 13 min to empty the building.

The merging can be affected in a subtle way by changing the positions of doors. The evacuation of upper floors, however, becomes more fluent if the doors are placed opposite to the incoming staircase stream. The flow from the floors cannot be restricted simply by reducing door widths, because it is important that occupants can exit a fire floor quickly. During congestion the merge ratio balances to 50:50 which gives quite equal service times per floor and is a good approximation for calculations and simulations.

References

1. Siikonen, M.-L., Susi T. and Hakonen H.: Passenger Traffic Flow Simulation in Tall Buildings. *Elevator World* 49(8), 117–123 (2001)
2. Korhonen T. and Hostikka S.: Fire Dynamics Simulator with Evacuation: FDS + Evac, Technical Reference and User's Guide (FDS 5.5.0, Evac 2.2.1). VTT Technical Research Centre of Finland (2010)
3. Barney, G., Cooper, D.A, English, J.: *Elevator & Escalator Micropedia*. IAEE Publications, England, ISBN 0 9525696 1 2, 32–22 (1997)
4. Pauls J.: Calculating Evacuation Times for Tall Buildings. *Fire Safety Journal*, 12(3), 237–245 (1987)
5. Boyce, K., Purser D. and Shields J.: Experimental Studies to Investigate Merging Behaviour in a Staircase. In: *Proceedings 4th International Human Behaviour in Fire Symposium*, Robinson College, Cambridge, 13–15 July 2009. Interscience Communications, pp. 111–122. ISBN 978-0-9556548-3-1 (2009)
6. Purser D. and Boyce K.: Implications of Modelling and Experimental Studies of Evacuation Behaviour on Stairs for Multistorey Building Design. In: *Proceedings 4th International Human*

- Behaviour in Fire Symposium, Robinson College Cambridge, 13–15 July 2009. Interscience Communications, pp. 147–160. ISBN 978-0-9556548-3-1 (2009)
7. Siikonen M-L. and Hakonen H.: Efficient Evacuation Methods in Tall Buildings. *Elevator World* 51(7), 78–83 (2003)
 8. Sorsa J. and Siikonen M-L.: Occupant Wayfinding in Multi-storey Buildings. In: Peacock R.D., Kuligowski E.D., Averill J.D. (eds.) *Pedestrian and Evacuation Dynamics, PED 2010*, Gaithersburg, MD, USA, pp. 881–884. Springer, New York. ISBN 978-1-4419-9725-8 (2011)
 9. Galea E.R., Sharp G. and Lawrence P.J.: Investigating the Representation of Merging Behavior at the Floor—Stair Interface in Computer Simulations of Multi-Floor Building Evacuations. *Journal of Fire Protection Engineering*. 18(4), 291–316 (2008)

Simulation of Handicapped People Finding Their Way Through Transport Infrastructures

Helmut Schrom-Feiertag, Thomas Matyus, and Martin Brunnhuber

Abstract This paper presents a research effort put into enhancing existing simulation models by including models for the motion and orientation behavior of handicapped people being unfamiliar with a transport infrastructure. On the tactical level the perception of guidance systems is modeled and makes it possible to simulate agent navigation through an unknown infrastructure using the present signage. The guidance information is determined against relevant influencing factors in a simulated virtual 3D environment. For the proof of concept the applicability of the wayfinding algorithm is demonstrated in three different scenarios. Results show that the proposed simulation model facilitates an agent to find its way autonomously through a transport infrastructure based on signage information only. This makes it possible to evaluate the visibility of the guidance system and can reveal areas lacking guidance information for people unfamiliar with the infrastructure especially for elderly and handicapped people with reduced reception capabilities.

Keywords Pedestrian simulation • Wayfinding • Handicapped people • Sensory impairment • Visibility • Virtual 3D environment

H. Schrom-Feiertag (✉) • T. Matyus
AIT Austrian Institute of Technology, Vienna, Austria
e-mail: helmut.schrom-feiertag@ait.ac.at; thomas.matyus@ait.ac.at

M. Brunnhuber
VRVis Zentrum für Virtual reality und Visualisierung Forschungs-GmbH, Vienna, Austria
e-mail: brunn@vrvis.at

1 Introduction

Public transport infrastructures must accommodate a large number of passengers while taking into account specific needs of certain groups such as elderly or hand-capped people. Their design needs to facilitate wayfinding for people unfamiliar with the infrastructure.

However, different groups have different needs for their routes and their orientation depending on their sensory and mobility impairments. At the first visit of an infrastructure depending on the signage already finding the elevator can become a challenging task, especially for people having reduced reception capabilities. These individuals need much longer for their orientation, and potentially temporarily block passages for the others, if the design of the infrastructure does not support their needs sufficiently.

Thus the design process is a nontrivial task which nowadays is supported by pedestrian simulations to predict passenger flows already in the planning stage. Current models do not integrate a detailed en-route route-choice model that implements orientation or navigation behavior but rather use the shortest-path or stochastic rules to get a route which is mainly applicable for people familiar with the infrastructure.

Therefore the main contribution of this paper is to propose a simulation model that represents handicapped people and their different behavior in orientation and navigation. On the tactical level the visual perception of guidance systems is modeled and makes it possible to simulate agent navigation through an unknown infrastructure using the present signage. No routing graph has to be defined in advance, only the information obtained from the signage modeled in a virtual 3D environment is used. The visibility depends on the agent's vision capabilities or the level of crowdedness respectively, especially for wheelchair drivers with a lower point of view. A virtual 3D environment including 3D human models representing the simulated agents gives the opportunity to calculate possibly occluded sections from one viewpoint realistically.

In the following Chap. 2 a review of the state of the art is given. Chapter 3 provides a system overview and detailed descriptions about the visible object identification and the agent based simulation allowing the characteristics of individual pedestrians to be assigned and varied as required. To parameterize the agent based simulation field experiments and data collections were made and the results are presented in this chapter. For the proof of concept in Chap. 4 three different scenarios are described to demonstrate the applicability of the wayfinding algorithm. The results are discussed in Chap. 5 and finally in Chap. 6 the conclusions are made and an outlook for future research issues is given.

2 Related Work

Agent based microscopic modeling is an approach for simulating pedestrians as single autonomous individuals by supplying a detailed representation of their behavior, including decisions on various levels (e.g. related to orientation and navigation) and interactions with other pedestrians in the crowd. The goal is to reproduce realistic single autonomous and emergent collective crowd behavior.

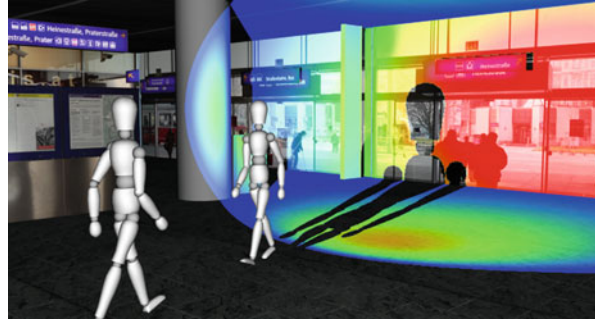
Compared to other models social force-based models has been found to describe pedestrian behavior in more detail concerning the spatial resolution (see e.g. [1]). The most prominent social force model is the model from Helbing [2] which is also used in the presented approach. This model has been calibrated and accordingly adapted using real world data by Johansson et al. [3]. The social force model was also extended by Braun et al. to include individualism [4]. Pelechano et al. [5] merged rule-based and social-force based models and incorporated psychological state into the pedestrian simulation model. Shao and Terzopoulos [6] used a complex cognitive and a behavior model for planning, but did not attempt realistic small-scale motion behavior like the social force model.

Many currently available simulation models are based on the assumption that all pedestrians know the infrastructure and consequently all pedestrians choose one of the known paths to reach their goal. Not every pedestrian is familiar with the infrastructure and for realistic simulation the wayfinding has to be represented in the model. Wayfinding abilities are influenced by a number of physical, psychological, and physiological factors that will influence the ability of people to detect and correctly interpret the information conveyed by the signs. Xie et al. [7] have theoretically and through experimental trials demonstrated that the maximum viewing distance is dependent on the viewing angle and that as the viewing angle increases, the maximum viewing distance decreases in a non-linear manner. These findings have been implemented in a comprehensive evacuation model. They have been shown to be sensitive to the complexity of the geometry and the scenario modeled. While the overall differences in the key evacuation indicators like average total evacuation time and average personal evacuation time resulting from the introduction of the new developments showed to be small, it is nevertheless essential to correctly represent these subtleties, if the model is to correctly represent reality.

3 Simulation of Handicapped People

The presented approach combines a pedestrian simulation with real-time rendering techniques to identify visible objects in a virtual 3D environment. The visible object identification determines the visible objects in the infrastructure from a point of view, especially the visible elements of the guidance system. The returned information is feed to the tactical level of the simulation to support the wayfinding decisions.

Fig. 1 Concept of visibility calculation



3.1 Visible Object Identification

Visible object identification uses a 3D model of the environment to provide visibility information about objects to the simulation. The 3D model gives the opportunity to calculate possibly seen sections from a viewpoint accurately. In the first cycle position information of the simulated persons, so called agents are passed to the visible object identification which does the rendering of the 3D human models in the virtual environment.

In the second cycle the calculation takes place. A single agent is selected to determine the visible objects in his field of view under consideration of occlusions by other agents what possibly occur in dense crowds. A result set containing all visible objects for that agent is returned to the simulation.

The presented technique uses current graphics hardware to calculate visible objects from a viewpoint using the basic concept of shadow maps as shown in Fig. 1. A light source is placed at the point of view and shadowed parts are not visible to the viewer, details can be found in [8].

The effect of occlusions due to other agents in dense crowds can be seen in Fig. 2. In the left image the empty main hall of the train station in Vienna, the “Praterstern” can be seen. For comparison in the right image the effect of dense crowds is shown where most signs are obscured. Especially for wheelchair drivers with lower point of view occlusions hinder information gathering and cannot be neglected for realistic behavior.

Information Coding In addition to visibility, it is important to know the type of signage, like monitor or sign and the information provided. Therefore the 3D model is enhanced with Meta information in advance. The necessary information is annotated for each relevant object, like guidance elements, ticket machines or supermarkets. These data contain a semantic description of information related to the object. The agent’s goal is also specified in a semantic way and it can be examined if the information is relevant.

Agent Perception Each agent has a perception of the environment and a reaction to static and dynamic objects and agents. The guidance information is determined



Fig. 2 Perspective for a wheelchair driver in the empty (left) and crowded train station (right), from the same point of view

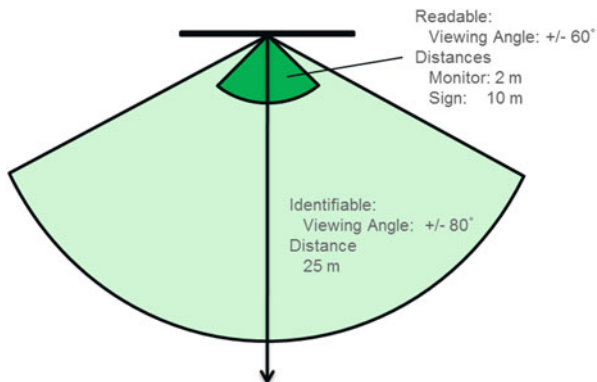


Fig. 3 Classification scheme between identifiable and readable

against relevant influencing factors such as line of sight, occlusion due to other pedestrians and the distances in three-dimensional space. At regular intervals of 1 s the visibility of the guiding system inside the infrastructure is calculated for the agent representing a person unfamiliar with the environment.

The visible object identification returns a list of visible objects and parameters for each object like unique identifier, distance to the viewer, position of the object, surface normal, angle between viewing direction and surface normal in 3D space and finally a visibility value indicating how much of the object surface is visible.

Xie et al. [7] have demonstrated that the maximum viewing distance depends on the viewing angle and that as the viewing angle increases, the maximum viewing distance decreases in a non-linear manner. For the proof of concept a much simpler classification scheme based on hard limits for distance and angle shown in Fig. 3 was used to distinguish between the information interpretations.

An agent with full vision can recognize the type of the signage object within 25 m and an angle $\pm 80^\circ$ and within 10 m and $\pm 60^\circ$ for large signs or 2 m for monitors the complete information can be obtained. The values for distance and angle in this classification scheme can be varied according to the visual impairment.

3.2 *Pedestrian Simulation Model*

Pedestrian motion behavior is often described in three different levels as specified in [9]. The *strategic level* determines the arrival time of the pedestrian at the transport infrastructure, the entry and the pedestrian's goal (e.g. train to Paris). In our case this level is not modeled separately and the origin and the destination at the transport infrastructure are predefined.

The *tactical level* describes the route a pedestrian will choose to move through the continuous physical space of the infrastructure.

The *operational level* calculates the actual movements towards the next intermediate goal performing collision avoidance with obstacles and other agents. Here an agent based approach is used allowing the characteristics of individual pedestrians to be assigned and varied as required.

Operational Level The human motion on an operational level is modeled based on a social force model [2]. Here the resulting force is separated into three parts: First, the attractive force which is directed towards the pedestrian's next goal. Secondly, the sum of the repulsive forces which are directed away from other pedestrians and finally, the boundary forces which are directed away from the surrounding walls or obstacles. As a first approximation the basic social force equations are used for modeling both the pedestrian and the wheelchair movements varying two parameters: (1) The desired speed of the agent on which the attractive force and (2) the horizontal body size on which the repulsive forces are depending.

Tactical Level – Wayfinding for people being unfamiliar with the infrastructure

The tactical level describes the knowledge and the wayfinding process which is defined as the process identifying, determining and following a path or route from an origin to the destination [10, 11]. Wayfinding will be performed to navigate through the transport infrastructure allowing different types of behavior and navigation abilities and requires an interactive behavior between agents and their environments [12].

On the tactical level the perception of guidance systems as described before is applied and makes it possible to simulate agent navigation through an unknown infrastructure using the present signage. No routing graph has to be defined in advance, only the information obtained from the signage modeled in 3D is required.

The main wayfinding strategy, as shown in Fig. 4 is searching randomly in the absence of any information. Information is obtained from signage elements (signs, monitors) in a certain area in front of the signage element.

The process of searching for information consists of two phases, first the visible signage element is identified and walked towards, subsequently at a smaller distance and a suitable angle the information provided is absorbed. In the second phase the semantic information is interpreted and if it is useful to achieve the agent's goal the instructions are utilized to identify the next goal at which the agent walks towards (operational level). Reaching the next goal the tactical level starts again by the first phase.

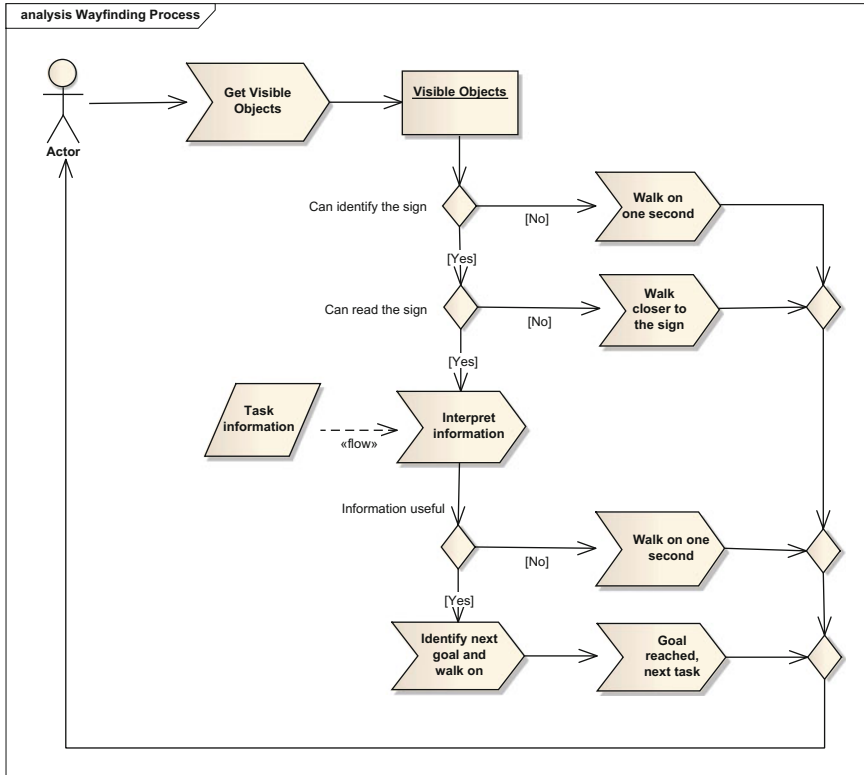


Fig. 4 Wayfinding strategy using guidance information only

3.3 Field Experiments and Data Acquisition

To gather information on group specific behavior comprehensive field experiments were made with 47 people. Eight groups of people were identified who may demonstrate mobility patterns clearly distinguishable from the general population: 70+ age, people with pram, visually impaired, blind, wheelchair users, mobility impaired, hearing impaired and deaf. The main research focus was to investigate differences in walking speed, patterns in gaining information from the environment, orientation and navigation.

The experiment took place at a major transit hub in Vienna, the train station “Praterstern”. For each person in the experiment one out of two different scenarios with typical usage patterns and different levels of complexity was selected. The scenarios contain specific tasks such as buying a ticket and drink for the journey, locating timetable information, or using the restrooms in the station. Empirical methods were combined in order to gain relevant qualitative and quantitative data on pedestrian behavior. A detailed description can be found in [13].

The analysis of the collected data have revealed on the one hand surprising similarities between very different groups, on the other hand extreme deviations within a single group, indicating that the design and organization of the environment and the information have a greater influence on navigation and orientation behavior than disability. The spatial analysis of trajectory data revealed the main routes, deviations from these routes and clusters where people mainly stop. The analysis of the thinking aloud data related to the trajectory helped to identify elements of the guidance system that respondents used to navigate and pointed out typical areas for orientation in the infrastructure.

In the example of the Viennese train station “Praterstern” the monitors are the primarily signage to gain information. After knowing the departure information looking for the way to the train platform is the next step. The train platforms are indicated using a sign conveying the platform number. The visibility depends on the agent’s vision capabilities or the crowdedness respectively, especially for wheelchair drivers with a lower point of view.

For the evaluation of the pedestrian simulation model in addition to the knowledge of group specific motion and orientation behavior, information on the traffic volumes were required. Therefore the traffic volumes from 6 to 10 o’clock and 14 to 20 o’clock on 1 day were counted on all cross sections in both directions and aggregated in 15 min intervals. Additionally randomly selected individuals were followed by observers unobtrusively from an entry until they have left the area to obtain the origin–destination relations.

4 Proof of Concept

In order to demonstrate the functionality of the wayfinding algorithm three different scenarios in the main hall on the ground level at the train station “Praterstern” in Vienna were defined.

4.1 Scenarios

All simulation scenarios are based on the same tasks as shown in Fig. 5: Starting at the elevator exit into the main hall of the “Praterstern” station (1) a wheel chair driver has to get the train to “Stockerau”. The main hall of the train station is on the ground level and the platforms are on the upper level which can be reached by wheelchair drivers by an elevator.

Apart from getting the departure information and buying a ticket, the next tasks are to go to the toilet and afterwards to get some snack for the journey. The order of activities is predefined: First go to the toilet (2), then buy the ticket, look for a monitor to get the departure information (3), go to the supermarket (4) and finally, use the elevator (5) to get up to the platform where the train is departing.



Fig. 5 Locations and shortest route for the scenarios in 2D (left) and in 3D (right)

Table 1 Simulation scenarios

Scenario	Crowd	Agent vision
1	No other agents	Full and reduced vision to half the distance
2	Still standing groups of agents	Full vision
3	Crowd according to the morning peak (07:15 – 08:15)	Full vision

The three scenarios differ in the level of crowdedness and the agent’s vision. In each scenario only one agent is considered unfamiliar with the infrastructure while all others get a route assigned at start up (Table 1).

Scenario 1. This scenario should reveal the differences for pedestrians having different visual impairments. Therefore in the first simulation run one agent with no visual impairments and in the second run an agent with vision reduced to the half range was simulated. To focus on differences caused by the reduced vision only one single agent unfamiliar with the infrastructure was simulated. Consequently, interactions with other agents which can cause side effects were eliminated and allowed a better comparison.

Scenario 2. Is intended to demonstrate how occlusions of elements of the guidance system lead to changes in the agent’s navigation. Here one agent with full vision is simulated in the hall where groups of agents are placed intentional in line of sight along the agent’s route from scenario 1 in order to ensure occlusions.

Scenario 3. In contrast to the very theoretical scenario 2, scenario 3 demonstrates the agent’s movement in a real world situation: A wheelchair driver with full vision moving during peak hour with about 7.000 passengers per hour. For the

simulation of the crowd the agents are initialized with predefined routes based on the origin–destination observations described in Sect. 3.3. In order to compute the routes for each origin–destination pair the visibility graph method of Overmars and Welzl published in [14] is used.

Simulation runs with slightly different start times for the wayfinding agent have been made in order to establish different conditions for the agent, providing situations where navigation is hindered by occlusions through other agents and where it is not.

5 Results

The proposed approach is capable to simulate realistic behavior of pedestrians in public infrastructures considering no knowledge of the infrastructure, route requirements, the orientation and the visual performance.

The combination of simulation and visual object identification in 3D space makes it possible to evaluate the visibility of the guidance system and to show the areas lacking guidance information for people unfamiliar with the infrastructure, especially for elderly and handicapped people with reduced reception capabilities.

A 3D environment including 3D human models for the simulated agents gives the opportunity to calculate possibly occluded sections from one viewpoint realistically.

5.1 Scenario 1

Figure 6a Shows the results from the simulations of the first scenario, an empty train station and an agent having full and half vision. In both cases the agents start at the elevator exit at position 0 and move on to position 1 where they can get an overview of the hall. The overhead sign which indicates the direction to the toilet at position 2 is readable for both of them. Having walked through under the sign they both stop and search for the toilet in the given direction. The agent with full vision can read the sign at the entrance of the toilet (3) already from here and moves directly to position 3. The agent with reduced vision moves on in the given direction searching five times for the toilet until position 2a where he can read the toilet sign at position 3. Leaving the toilet both agents cannot find any helpful information. Therefore they move back to the last visited sign. At position 4a the agent with full vision can already read the sign at position 5 which indicates the direction to the ticket machine. The second agent needs to move to position 4b where he is near enough to read the sign at position 5. Having reached position 5 both can see the ticket machine at position 6 where they buy their tickets. Since a monitor is mounted above the ticket machine they get the departure information there as well. The train to “Stockerau” is leaving at platform 2. From position 6, the entrance of the supermarket at position

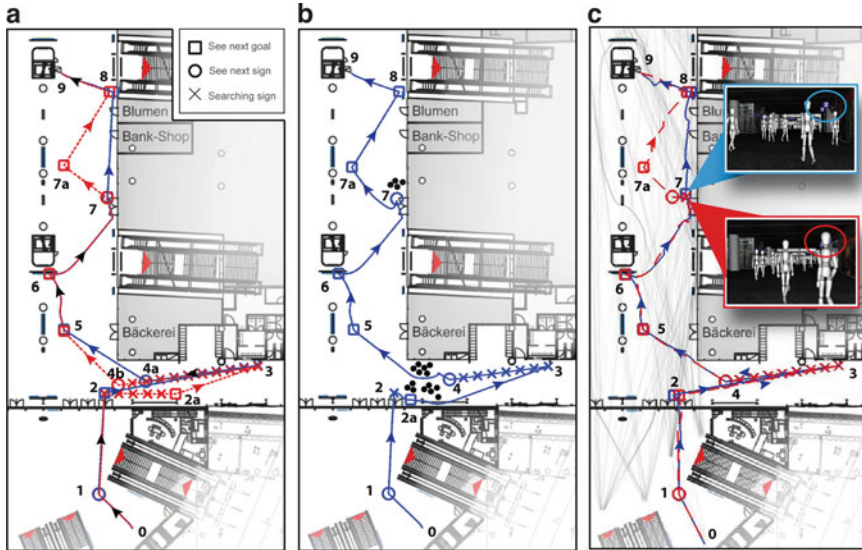


Fig. 6 Simulation results for the three scenarios, (a) Empty hall, (b) Groups blocking vision and (c) Crowd according to the morning peak

7 is visible for both and they move directly over there. Leaving the supermarket the agent with full vision can read the sign at the staircase to platform 2 (position 8), the second agent can only read the sign at position 7a which indicates the direction to platform 2. At position 7a he can read the sign at position 8 as well. Having realized that at position 8 there are only stairs and escalators they look around and find the elevator to platform 2 at position 9.

Once a valid intermediate goal is identified it remains valid until the goal is reached. During this phase no information is gathered and validated if it provides better information. For example the platform 2 sign indicates the right platform, but it cannot be seen if there is an elevator, so the platform sign remains the next goal and if it is reached and there is no possibility to change the levels, an elevator to the platform at the upper level is searched by the agent.

5.2 Scenario 2

Figure 6b Shows the results of the second scenario with still standing groups occluding signage information and an agent with full vision. Three points are worth mentioning. At position 2 the agent is not able to see the toilet sign at position 3 due to the pedestrian group in front of him. So he moves on in the direction the previous sign has indicated until he can see his goal at position 2a. At position 4 the agent is able to read the sign at position 5 although a pedestrian group is standing in front

of him. But in this situation the sign is mounted high enough so he could see it over their heads. Having left the supermarket at position 7 the other agents are very close and he is not able to see the platform sign at position 8 and therefore he takes the same route to 7a as the agent with the reduced vision in the first scenario.

5.3 Scenario 3

Figure 6c Shows the results of the third scenario where the agent with full vision is moving through the hall during the morning peak hour (7:15–8:15). Two runs with slightly different start times were selected to show the differences in dense crowds. In both runs the trajectories till the supermarket (position 7) are identical among each other and also with the trajectory of the agent with full vision in Scenario 1. But after leaving the supermarket the agents are following different paths. One of the agent has free sight to the “platform 2” sign at position 8 (see blue circle in the upper screenshot) and moves on like in scenario 1 (blue path). Whereas, for the other agent the sign is hidden behind a pedestrian (see the red circle in the lower screenshot) and therefore the agent makes a detour via the sign at position 7a (red dashed line) which indicates the direction to platform 2.

5.4 Summary

Each scenario showed different routes compared to the shortest route due to the differences in the range of vision and crowdedness. Especially for wheelchair users crowdedness has a significant impact. Crowds often occlude the signage or form obstacles leading to a higher rate of maneuvers, longer routes and travel discomfort. The approach has shown to be capable of simulating handicapped people finding their way through a transport infrastructure using signage information only.

6 Conclusions and Outlook

The proposed multi-agent based simulation model facilitates an agent to find its way autonomously through a building based on signage information only. This makes it possible to evaluate the visibility of the guidance system for different handicapped groups. It can reveal areas lacking guidance information for people unfamiliar with the infrastructure, especially for elderly and handicapped people with reduced reception capabilities. Especially by the integration of real-time rendering techniques dynamic occlusions through other pedestrians in dense crowds can be taken into account realistically.

Nevertheless the simulation has to be refined in some aspects. The wheelchair model has to be improved since physics of wheel chair movement is limited in the degree of freedom compared to pedestrian movement and in particular does not allow side steps. An interesting aspect if an object is in focus long enough to identify and recognize it.

Cognitive elements like readability, clarity of content, recognizing and understanding information and functional features are also not modeled in the current approach and are currently investigated in the project IMITATE. In this project a controlled test environment which lets the test persons immerse into a near-realistic interactive experience and at the same time measures her reactions to the environment is developed. Due to its increased realism the environment will greatly extend the possibilities to optimize the design of guidance systems in comparison to existing systems. Additionally, these data can be used to calibrate both the operational and the tactical model. This will enhance the standing in the areas of visualization, pedestrian simulation and design of guidance systems.

Acknowledgements This work is part of the project MASIMO and has been funded by the research program line ways2go within the framework of the Austrian strategic initiative IV2Splus “Intelligent Transport Systems and Services plus” under the project number 819192. We thank our partner the Austrian Federal Railway Company (ÖBB) for the access to the railway station “Praterstern” in Vienna for our field experiments and to the plans of the building.

References

1. Bauer, D.: Comparing Pedestrian Movement Simulation Models for a Crossing Area Based on Real World Data. In: Peacock, R.D., Kuligowski, E.D., and Averill, J.D. (eds.) *Pedestrian and Evacuation Dynamics*. pp. 547–556. Springer US, Boston, MA (2011).
2. Helbing, D., Molnar, P.: Social Force Model for Pedestrian Dynamics. *Physical Review E*. 51, 4282–4286 (1995).
3. Johansson, A., Helbing, D.: Analysis of Empirical Trajectory Data of Pedestrians. In: Klingsch, W.W.F., Rogsch, C., Schadschneider, A., and Schreckenberg, M. (eds.) *Pedestrian and Evacuation Dynamics 2008*. pp. 203–214. Springer Berlin Heidelberg, Berlin, Heidelberg (2010).
4. Braun, A., Musse, S.R., Oliveira, L.P.L. de, Bodmann, B.E.J.: Modeling Individual Behaviors in Crowd Simulation. 16th International Conference on Computer Animation and Social Agents (CASA 2003). p. 143. IEEE Computer Society, Los Alamitos, CA, USA (2003).
5. Pelechano, N., Allbeck, J.M., Badler, N.I.: Controlling individual agents in high-density crowd simulation. *Proceedings of the 2007 ACM SIGGRAPH/Eurographics symposium on Computer animation*. pp. 99–108. Eurographics Association, San Diego, California (2007).
6. Shao, W., Terzopoulos, D.: Autonomous pedestrians. *Graph. Models*. 69, 246–274 (2007).
7. Xie, H., Filippidis, L., Gwynne, S., Galea, E.R., Blackshields, D., Lawrence, P.J.: Signage Legibility Distances as a Function of Observation Angle. *Journal of Fire Protection Engineering*. 17, 41–64 (2007).
8. Brunnhuber, M., Schrom-Feiertag, H., Hesina, G., Bauer, D., Purgathofer, W.: Simulation and Visualization of the Behavior of Handicapped People in Virtually Reconstructed Public Buildings. 15th International Conference on Urban Planning and Regional Development in the Information Society, Vienna (2010).

9. Hoogendoorn, S.P., Bovy, P.H.: Pedestrian Route-Choice and Activity Scheduling Theory and Models. *Transportation Research, Part B: Methodological*. 38, 169–190 (2004).
10. Bovy, P.H.L., Stern, E.: *Route choice: wayfinding in transport networks*. Kluwer Academic Publishers (1990).
11. Golledge, R.G., Stimson, R.J. (Robert J.: *Spatial behavior: a geographic perspective / Reginald G. Golledge, Robert J. Stimson*. Guilford Press, New York: (New York: Guilford Press, c1997.).
12. Li, Y., Brimicombe, A.J., Li, C.: Agent-based services for the validation and calibration of multi-agent models. *Computers, Environment and Urban Systems*. 32, 464–473 (2008).
13. Egger, V., Schrom-Feiertag, H., Ehrenstrasser, L., Telepak, G.: Creating a richer data source for 3D pedestrian flow simulations in public transport. *Proceedings of the 7th International Conference on Methods and Techniques in Behavioral Research*. pp. 20:1–20:4. ACM, New York, NY, USA (2010).
14. Bauer, D., Brändle, N., Seer, S., Ray, M., Kitazawa, K.: Measurement of pedestrian movements - a comparative study on various existing systems. *Pedestrian behaviour: Models, data collection and applications*, ed. H. Timmermans. pp. 301–319. Emerald Group Publishing (2009).
15. Overmars, M.H., Welzl, E.: New methods for computing visibility graphs. *Proceedings of the fourth annual symposium on Computational geometry*. pp. 164–171. ACM, New York, NY, USA (1988).

Simulation of Pedestrian Dynamics with Density Control on a Regular Grid

Minjie Chen, Günter Bärwolff, and Hartmut Schwandt

Abstract Discrete modelling of pedestrian dynamics often defines the system geometry on a two-dimensional regular grid. In a simulation system of this category, the individual pedestrians are associated with a fixed exclusive personal space, since they are to be positioned in the corresponding grid cells. However, empirical data show that in low density range, the size of this personal space varies significantly. The purpose of this paper is to present a new method for the density control in pedestrian dynamics on a regular grid while offering a step calculation mechanism for the simulated pedestrians free of local conflict.

Keywords Cellular automaton • Pedestrian flow • Simulation • Variable cell size

1 Introduction

The necessity of crowd control, in outdoor public events of large scales and more generally in indoor facilities, has drawn increasing attention in the recent years. Indoor crowd control is to serve the purpose of an optimal utilization of architectural capacity whereas in emergency cases, of an efficient evacuation strategy. This inevitably involves the study of human behaviours from an engineering perspective, termed as pedestrian dynamics. Due to the peculiar nature of the problem, any experiment of real participants at a sufficiently large scale will be characterized by its high costs. Computer simulation has therefore become alternative tool in this field.

M. Chen (✉) • G. Bärwolff • H. Schwandt
Institut für Mathematik, Technische Universität Berlin, Straße des 17. Juni 136, 10623 Berlin, Germany
e-mail: minjie.chen@math.tu-berlin.de; baerwolf@math.tu-berlin.de; schwandt@math.tu-berlin.de
Project home page: <http://www.math.tu-berlin.de/Projekte/SMDPC>

Macroscopic and microscopic methods build up two basic categories for the modelling of pedestrian dynamics, see [4] for an overview. Unlike those in the macroscopic category, in the microscopic methods the pedestrians will be considered separately, and very often the pedestrians are modelled as agents independent of each other but bound by additional behavioural rules, see e.g. [10]. The social force (SF) model [5] and the cellular automaton (CA) model [1, 13] are the two most important and well-known examples. The SF model considers the interaction amongst pedestrians as the sum of certain fictitious “social forces” which yields similar results by but is not compactible with the basic laws in Newtonian mechanics (see again [10] for a defending opinion). In the CA model and its various extensions (see [1, 6–9, 11, 13]), the state change in the underlying geometry of the simulation is employed for the description of the system dynamics. Obviously in this case, the real-world geometric settings have to be discretized into a grid of cell elements first. To our limited knowledge, the existing CA models are all based on two-dimensional homogeneous grids of rectangles (in most cases, square) and hexagons. An often neglected fact is, in our opinion, since the primary concern of the CA model is the state change of the grid cells on the trajectories of the pedestrians, the cell state transition rules—the number of which is generally of explosively huge magnitude—need not to be dictated clearly in the traditional formal notation, as long as the state evolution of the relevant grid cell elements to describe the pedestrian trajectories is unambiguous. In this sense, we prefer the term grid-based method for our approach, see also the footnote to follow.

1.1 *Grid-Based Approach*

In a grid-based simulation, we must give the thought that the individual pedestrians are associated with an exclusive personal space. In the aforementioned traditional cellular automaton models this personal space is implicitly defined by the cell size of the underlying regular grid, which has typically assumed to be $0.4 \cdot 0.4$ m (see [1, 6]). This leads inevitably to a fixed personal space of the pedestrians. However, empirical data (e.g. [12]) show that in low density range, the size of this personal space varies significantly. In high density range, naturally, this size is clearly restricted by the physical size of the pedestrians. This means that pedestrians in the reality appear to be “compressible” to a certain extent in a way similar to gas particles. This aspect offers a valid argument for the macroscopic models at the same time. Another important issue is the update strategy. A proper update strategy is essential in the cases of either high pedestrian densities or when multiple pedestrians are directed to enter into a same target position on the grid. A straightforward answer to these phenomena would be a sequential procedure or some random arrangement amongst the simulation objects. Keßel et al. [6] introduced a (pseudo-)parallel update and a random sequential update, the latter of which involved further the static and dynamic floor field information induced by the environment and pedestrians [1, 11, 13].

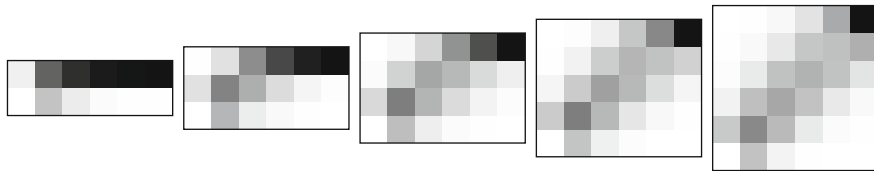


Fig. 1 Explanation of substeps in the cases $\Delta x = 5, \Delta y = 2, \dots, 6$. The relative occurrence of a grid cell position as a dissembled substep is displayed in a *gray* scale. The start position $(0, 0)$ and the end position $(\Delta x, \Delta y)$ are by definition in *white* (no occurrence when start position is not counted in a step) and *black* (definite occurrence, when end position is to be achieved in a step) respectively

Our approach goes in a completely different direction. In our previous work [3] a new solution for the step calculation in the general case—in which the pedestrian step length is larger than one grid cell size (in either or both directions)—has been suggested.¹ This method dissembles a step of $(\Delta x, \Delta y)$ (with Δx and Δy being integers of a proper magnitude) into a series of substeps which can be one grid cell in either direction or a diagonal step (i.e. one grid cell in both directions), see Fig. 1. With consideration of this, deviations on route within a local step (i.e. within a simulation cycle which could take a times pan of one to a few seconds) would become possible and strictly speaking, unavoidable. On the other hand, these local deviations are all under the restriction that the mathematical expectation of the sum of the substeps (i.e. a step in the normal sense) should be equal to the position evolution in geometric sense. Therefore, this is exactly what we need in the modelling. In addition, the notion of substep enables the representation of heterogeneous pedestrians.

Next, we introduce a balancing mechanism in the simulation cycle to decide the update (or execution) sequence of the simulation participants. This improvement, along with the substep calculation, solves the so-called “dead-lock” problem amongst the participants on the local level of simulation. Conflict solution on higher simulation levels is a topic concerns navigation, routing and simulation of social behaviours of pedestrians and is beyond the scope of the current paper.

1.1.1 Balancing Mechanism of the Step Execution of Collected Particles

In the step execution of the particles as a collection in the simulation cycle, the heterogenous particles require different numbers of disintegrated substeps, since

¹We are therefore of the opinion that it is suitable to categorize our approach as a graph-based method rather than a CA extension, since unlike in the case of discrete step length 1, now the state dynamics of the simulation system, in the theoretical context of CA, become only of secondary significance. Our primary focus is the position evolution of the pedestrians in the simulation, by which their trajectories are defined.

according to the substep construction, this number should reflect the actual step length of the particle, which is further related to its velocity.

Let v_{\max} denote the highest reachable velocity of the particles. This is also to be understood as the largest possible step length in a simulation cycle. Let n be an integer with $n \geq v_{\max}$. We divide the simulation cycle into n equal intervals. As a matter of fact, for a particle with velocity v the substeps should be executed exactly in v of the total n intervals. In the rest $n - v$ intervals, the particle makes no movement and can be understood as in a temporarily stopped (or pausing) state.

One possibility is to choose one of the $\frac{n!}{v!(n-v)!}$ combinations from the set $\{1, \dots, n\}$ to decide when a substep is to be carried out. Another option would be the selection of v numbers from the set $\{1, \dots, n\}$ at equal (or similar) distances as a time signal for the substep execution. These variants are less satisfactory since the possible conflicts amongst particles are left untouched.

The situation in which no possible substep is available should not be neglected. To this end, we calculate in each of the n intervals a probability number to decide whether a local substep should be performed at this moment. This number depends on how successful the substeps in the current simulation step have been carried out. See the following code fragment.

```

procedure operational_execution_single begin
  input parameter:  $i$ 
  if destination reached
    mark as "processed";
  else
    count successful substeps in the current simulation
cycle
    and save this number as  $a$ ;
     $p \leftarrow \min\left(\frac{v-a}{i}, 1\right)$ ;
    calculate and execute a substep with probability  $p$ ;
  fi
end.

```

Here the parameter i serves as a time stamp. In the above program block, unsuccessful substeps in the current simulation cycle contribute to a higher probability that a new substep should be attempted (since v and a stay unchanged but i is decremented, cf. the next code fragment). This rules out the possible occurrence of conflicts within the simulation cycle on the local level. The next code fragment describes the execution of the configured steps for all the particles in the simulation cycle.

```

procedure operational_execution begin
  input parameter: a collection of pedestrians
  mark all pedestrians as "unprocessed";
   $i \leftarrow n$ ;
  while  $i \geq 1$ 
  do

```



Fig. 2 A crowd example shows that density can exceed six pedestrians per square metre locally

```

    process all pedestrians marked "unprocessed" by
calling
    procedure operational_execution_single sequentially
        with parameter  $i$ ;
         $i \leftarrow i - 1$ ;
    enddo
end.
```

Our model is completely different from the CA model and its extensions (cf. the extended model for $v_{\max} > 1$ suggested in [8]). The main concern in our model is the execution of the substeps on the lowest simulation level, whereas conflict solution is a problem to be addressed on higher levels of the simulation. The possible local conflict in the substep execution helps us to decide how the substeps are to be performed with the purpose in mind that the step choice should be faithfully carried out according to the configuration in every simulation cycle.

1.1.2 Density Control

We recall that a fixed grid cell size of $0.4 \cdot 0.4$ m (suggested in [1, 6] etc.) implies a maximum density of $2.5^2 = 6.25$ persons per square metre. Empirical data (e.g. those collected in [12]) show that this maximum could still be slightly higher under certain special circumstances. An example is given in Fig. 2. Taking into consideration the real pedestrians' average physical size, an extreme value of roughly nine persons per square metre would be possible. Under such circumstances, pedestrians could be understood as incompressible particles. Owing to this observation, we configure the one-dimensional grid size to be $l_0 = \frac{1}{3}$ m. We proposed in [2] an extension to allow a modifiable personal space for the pedestrian, composed of from one ($1 \cdot 1$) to nine ($3 \cdot 3$) grid cells on a regular grid. Equipped with this, it is now

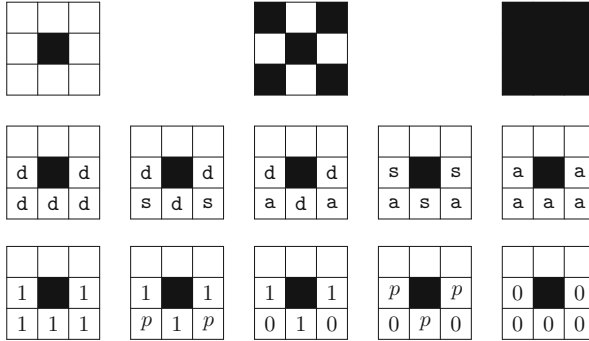


Fig. 3 Schematic presentation of the deactivation and activation of grid cells in the 3 · 3-Moore-neighbourhood. The first row refers to the cases of different pedestrian densities. The second row refers to the deactivation and activation of the relevant grid cells. The third row refers to the deactivation possibilities at those grid positions. The current pedestrian is assumed to be moving in the positive *y*-direction. The five columns will be denoted as **a**, **b**, **c**, **d** and **e**

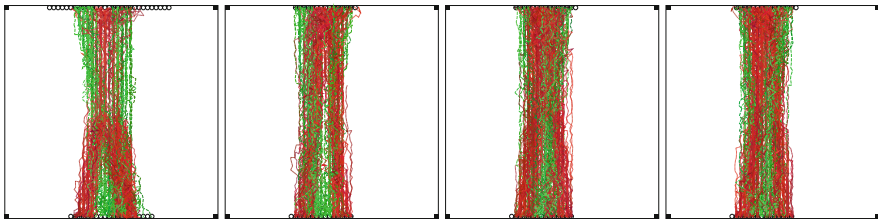


Fig. 4 Overall trajectories of two intersecting pedestrian groups without and with obstacles

possible to simulate the local density up to nine persons per square metre. A higher density should not be necessary to simulate.

A pedestrian’s personal space will then be considered as a multiple (being integer or not) of l_0^2 . Thus, we can modify the personal space by denying the access of some of the grid cell positions in the 3 · 3-Moore-neighbourhood to the other simulation participants. We call this denial of access of cell position “deactivation” (abbr.: *d*). A grid cell definitely not to be deactivated is “activated” (abbr.: *a*). Any state other than these two will be written as *s* and is associated with a probability number *p* for its deactivation. *p* is now to be understood as the “likelihood” that the corresponding cell position is inaccessible to others.

In the context of pedestrian dynamics we observe the phenomenon that a pedestrian tends to “deactivate” certain neighbouring positions for those pedestrians behind him or her. A low density is achieved by means of deactivation of such grid positions. See Fig. 3.

We assume the grid cell states at relative positions $(-1, 1)$, $(0, 1)$ and $(1, 1)$ are known and in total there are *a* particles present which can potentially enter into these positions. Then the highest possible numbers of total particles *n* in

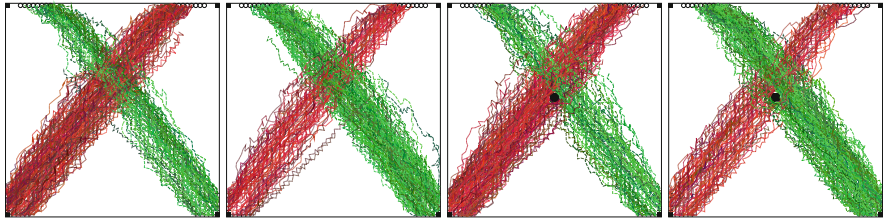


Fig. 5 Overall trajectories of two intersecting pedestrian groups without and with obstacles

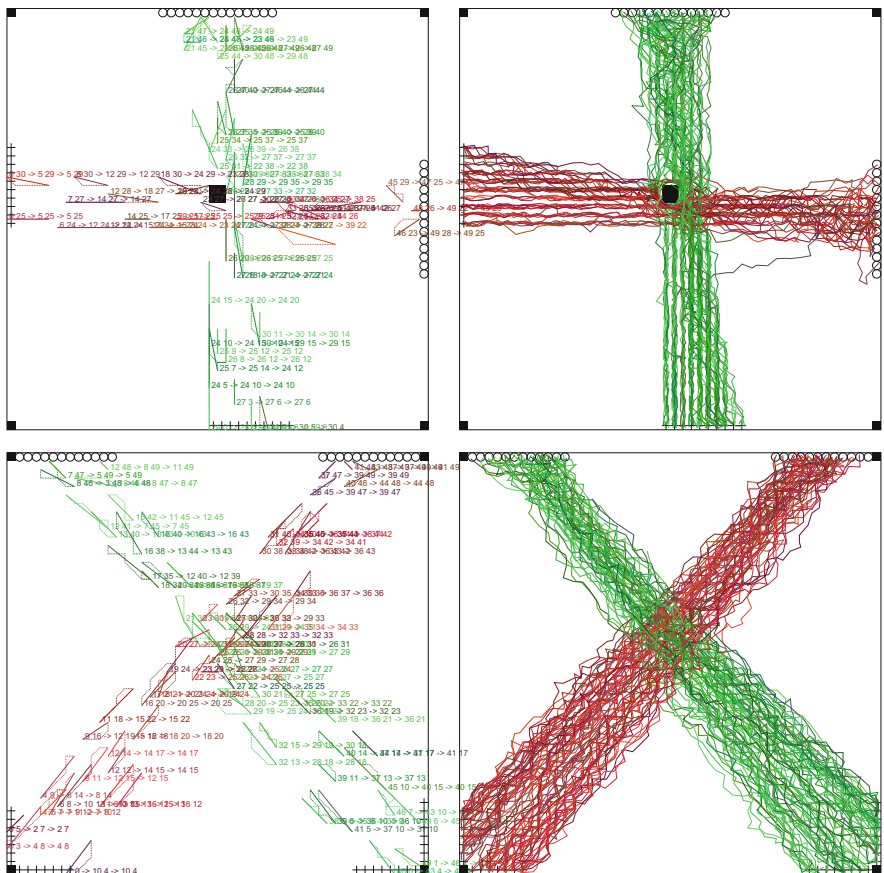


Fig. 6 Snapshots and overall trajectories of a perpendicular intersection of two pedestrian groups (axis-parallel and diagonal)

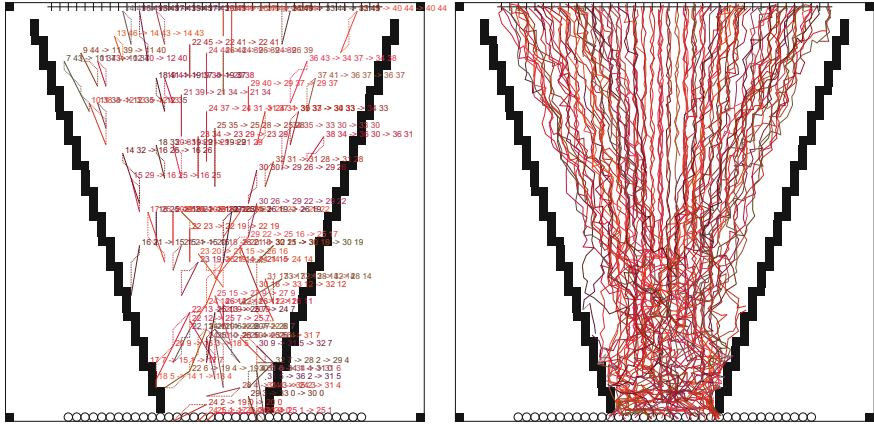


Fig. 7 A single group of pedestrians walking through a bottle-neck

the neighbourhood for the five cases in Fig. 3 can be established as

$$\begin{aligned}
 n_a &= a + 1, & n_b &= a + 2(1 - p), & n_c &= a + 2, \\
 n_d &= a + 2 + 3(1 - p), & n_e &= a + 6.
 \end{aligned}$$

Given a targeted local density ρ , we can estimate n in dependence of $\frac{1}{\rho}$. Further with the knowledge of the actual grid cell position allocation resulted in the last simulation cycle and therefore the number a , the probability p to deactivate the relevant grid cells under the current circumstances can be derived and applied in the next planned simulation cycle. Generally speaking, and taking into consideration empirical data collected by various experiments, only the first three cases will be of interest, the cases **d** and **e** are rare and they are listed here for a formal presentation of our method.

2 Application and Experimental Results

We applied our model to describe the intersection of two pedestrian groups, see Figs. 4 and 5. The figures exhibit both global patterns and some local details (e.g. small deviations for the sake of collision-avoidance). The simulated groups intersected with angles of approximately 180° and 90° . The latter case can still be demonstrated by re-organizing the configuration in that the main moving direction can defined to be either axis-parallel or diagonal. The statistics of these two variants exhibit no substantial difference in the substep calculation, see Fig. 6.

In Fig. 7, the walking through a bottle-neck with density control is presented. In this experiment, insufficient spacial conditions induce a reduced personal space and grid cell accessibility in the neighbourhood has been adjusted thus accordingly.

To achieve a better visual effect, we will re-organize these simulation results and re-compile them into video animation to publish on our project home page.

Acknowledgements The authors gratefully acknowledge the support of Deutsche Forschungsgemeinschaft (German Research Foundation) for the project SCHW548/5-1+BA1189/4-1.

References

1. C. Burstedde, K. Klauck, A. Schadschneider, and J. Zittartz. Simulation of pedestrian dynamics using a two-dimensional cellular automaton. *Physica A*, 295:507–525, 2001.
2. M.-J. Chen, G. Bärwolff, and H. Schwandt. Automaton model with variable cell size for the simulation of pedestrian flow, 2008. An electronic version can be retrieved at: <http://page.math.tu-berlin.de/~chenmin/pub/cbs080331.pdf> (accessed February 24, 2014).
3. M.-J. Chen, G. Bärwolff, and H. Schwandt. A study of step calculations in traffic cellular automaton models. In *13th International IEEE Conference on Intelligent Transportation Systems*, pages 747–752, 2010. An electronic version can be retrieved at: <http://page.math.tu-berlin.de/~chenmin/pub/cbs100709.pdf> (accessed February 24, 2014).
4. W. Daamen, P. H. L. Bovy, and S. P. Hoogendoorn. *Modelling pedestrians in transfer stations*, pages 59–73. In [14], 2002. ISBN 978-3-540-42690-5.
5. D. Helbing, I. Farkas, and T. Vicsek. Simulating dynamical features of escape panic. *Nature*, 407:487–490, 2000.
6. A. Keßel, H. Klüpfel, J. Wahle, and M. Schreckenberg. *Microscopic simulation of pedestrian crowd motion*, pages 193–200. In [14], 2002. ISBN 978-3-540-42690-5.
7. A. Kirchner, K. Nishinari, and A. Schadschneider. Friction effects and clogging in a cellular automaton model for pedestrian dynamics. *Physical Review E*, 67(5):056122, 2003.
8. A. Kirchner, H. Klüpfel, K. Nishinari, A. Schadschneider, and M. Schreckenberg. Discretization effects and the influence of walking speed in cellular automata models for pedestrians dynamics. *Journal of Statistical Mechanics: Theory and Experiment*, 2004(10):P10011, 2004.
9. H. L. Klüpfel. *A cellular automaton model for crowd movement and egress simulation*. PhD thesis, Universität Duisburg-Essen, 2003.
10. M. Moussaïd, D. Helbing, and G. Theraulaz. How simple rules determine pedestrian behavior and crowd disasters. *Proceedings of the National Academy of Sciences of the United States of America*, 108(17):6884–6888, 2011.
11. K. Nishinari, A. Kirchner, A. Namazi, and A. Schadschneider. Extended floor field CA model for evacuation dynamics. *IEICE Trans. Inf. & Syst.*, E87-D(3):726–732, 2004.
12. M. Plaue, M.-J. Chen, G. Bärwolff, and H. Schwandt. Trajectory extraction and density analysis of intersecting pedestrian flows from video recordings. In [15], pages 285–296. ISBN 978-3-642-24392-9.
13. A. Schadschneider. *Cellular automaton approach to pedestrian dynamics - theory*, pages 75–85. In [14], 2002. ISBN 978-3-540-42690-5.
14. M. Schreckenberg and S. D. Sharma, editors. *Pedestrian and Evacuation Dynamics*. Springer-Verlag Berlin Heidelberg, 2002. ISBN 978-3-540-42690-5.
15. U. Stilla, F. Rottensteiner, H. Mayer, B. Jutzi, and M. Butenuth, editors. *Photogrammetric Image Analysis, ISPRS Conference, PIA 2011*, volume 6952 of *Lecture Notes in Computer Science*, 2011. Springer-Verlag Berlin Heidelberg. ISBN 978-3-642-24392-9.

Evacuation of Day Care Centres for Children 0–6 Years: Simulations Using Simulex

L. Ulriksen and A.S. Dederichs

Abstract Children are neglected in today's fire safety design and fire safety modeling. The purpose of this study is to validate the common evacuation model Simulex with respect to children. The model was set up using the standard settings for children available in Simulex. Results on travel speed, horizontal and on stairs as well as the flow through doors for 9 day care centers are compared to data from full scale evacuation experiments for children in the age of 0–2 and 3–6 years. It was found that the walking speed found in the simulations in Simulex overestimates the walking speed found in the exercises for both age groups, except for a few older children running. Furthermore, the simulations overestimate the travel speed on stairs, except for the initial escape in the familiar staircase. Also the prediction of the total evacuation times was shorter than in the experiments. In general Simulex did not give conservative predictions when applied on children population.

1 Introduction

Every fifth human being is a child [1, 2]. Only if there is accounted for this population in the same thorough way as for able-bodied people, during the design process, the same safety level can be guaranteed. The children population has to be considered when prescriptive fire codes or performance-based codes are applied. In Danish Building regulations, [3] employment categories are used to define building sections for people, who are not expected to evacuate but are to be rescued by the fire service. Day care centres are placed in this specific employment category. In many cases occupant safety in the case of evacuation cannot fully be covered by the prescriptive building codes when it comes to new and complex

L. Ulriksen • A.S. Dederichs (✉)

Department of Civil Engineering, Technical University of Denmark, 2800 Kgs. Lyngby, Denmark
e-mail: And@byg.dtu.dk

building design [4] or the conversion of existing buildings into day care centres. In these cases the possibilities of evacuation must be considered using fire safety engineering methods. Furthermore, children are part of heterogeneous populations visiting buildings designed using performance based codes. Computer models are often used in performance-based design to achieve a more detailed calculation of evacuations. Several models, each with certain specialities, are used in building design [5, 6]. Evacuation models range from movement models over simple particle models to agent based models, where behavioural characteristics are addressed [7]. Simulex, which is used in the present study, is a particle model applying implicit behaviour characteristics by introducing features that affect movement only. Many models offer the possibility to model heterogeneous populations and account for people with impairments and children [9]. As most applied models, Simulex is based on and mainly validated against evacuation exercises conducted with adults [9]. There is little data on children in literature available for validation, which makes a proper validation of models for this group impossible.

Data is needed for validation of the models. Literature provides studies on real fire incidents as well as experiments concerning fire and evacuations [1, 6, 10]. The majority of data deal with the evacuation behavior of able-bodied people, which are able to bring themselves to safety in case of an emergency [10–18]. In recent years the focus has raised on a broader population for experiments and models. People with disabilities and other groups that might require assistance during an evacuation or who might be able to equally participate in the evacuation process, if only considered in the building design, are increasingly considered in studies [19–23]. In 1985 a study was made in Kobe, Japan concerning evacuation of day care centres [24]. It was seen that walking speed during evacuation depends on the age of the child and the familiarity with the evacuation path. Larusdottir et al. [1] presented data on the evacuation of children at the age of 0–6 years divided into two groups; “younger children” at the age of 6 months to 2 years and “older children” at the age of 3–6 years. It was found that travel speeds differ between the two age groups just as travel speeds when walking or running. Only in the case of older children running the movement speed is higher than the walking speed of adults as given in literature [18, 25]. Furthermore, it is observed that young children in most cases need assistance to evacuate. The data of this experiment is used as validation in the current paper.

The purpose of the current work is to investigate whether the movement of children in the age 0–6 years during an evacuation can be predicted when using a building evacuation computer model, Simulex, most often used when simulating adults. Computer simulations of different day care centres are carried out. It is investigated how the movement of children is defined and simulated in the model. The results on total egress times, velocities and flow on stairs and through doors from the simulations are compared with results from evacuation exercises at the same day care centres. It shall be seen whether the results achieved by using the model are conservative, when applied to keep children safe in buildings.

In the following section the method and the setup in Simulex are described. The way children are set in the model and the design of the 9 day care centers are

also described. Afterwards results on total evacuation times, velocities in horizontal plane as well as on three stairs are presented and discussed. All results are compared to the data from [1]. Finally, the findings are summarized in the conclusion.

2 Method: Simulations

Simulex version 1.2 is used for the simulations of the day care centres in the current work [7, 26, 27]. Simulex is designed to simulate building evacuation of a large amount of people.

Models of the 9 day care centres are set up in Simulex following the manual. The occupants are defined as children only. The number of children in each simulation is the same as the number of children participating in the evacuation exercises. The children in the simulations are placed in the same rooms as in the evacuation exercises. All children were defined to be walking. It is not possible to specifically define running children.

Generally, persons are assumed to move towards the nearest exit and during a simulation the distance maps are used to lead occupants to the nearest exit [26, 27]. However, it is possible to assign preferred exits in the model. This is done in the simulations leading to the results presented in the current paper. The model is set up, so that occupants use the same exits as in the exercises. In this way occupants are lead to a certain exit instead of the closest, following the experiment.

Warning time and recognition and response times are generally set to zero when running the simulations and added afterwards. However, for 3 day care centres the warning times vary relatively much from room to room in the given centre because of the warning method and misunderstanding of warning from the smoke detector. This is the case for day care centre B, C and D, where the warning times are added to the travel times in the simulations by delaying the start of moving in individual rooms.

Three of the buildings have spiral stairs. In Simulex stairs are defined with the length measured as the slope of the stair. All stairs are modelled as straight stairs. This induces an error, since the stairs in the buildings are spiral stairs. The error may be assumed to lead to shorter travel times for the model predictions. This is however somewhat accounted for as the width of each spiral stair is defined so narrow that it is not possible for occupants to overtake each other.

In the simulated day care centres the door width ranges from 0.70 to 1.05 m.

Simulex does not allow distinguishing between children and adults during simulations, as in the evacuation exercise and data collection. Therefore, it would not be possible in the analysis of the modelling results, to know, whether the walking speed or flow is measured for an adult or a child. Since the goal was to model the movement of children, no adults were added in the simulations. Also the teachers participating in the exercises often just guided the children in the right direction and had no direct influence on the children's movement. Furthermore, it was not

possible to simulate the situation where the teacher had to carry a child, as often the case for younger children in the age group 0–2 years.

Horizontal walking speed was found by registering the time it took occupants in the model to travel over a distance with known length. On stairs the travel speed was found by registering the time from occupants enter the stair till they exit the stair with a known length. Flow through doors was found as a function of person density in front of the door. The person density was found by counting the number of occupants in a square metre in front of the given door in given time steps. The flow is found by registering the number of occupants going out the door in the time steps where the density is the same as mentioned above. These methods are taken from the method applied in the experiment. The simulations are used to find the egress time for each day care centre.

3 Results and Discussion

From the results of the simulations, the egress time, horizontal walking speed, walking speed on stairs and flow through doors are found. In the following subsections the results of the simulations in Simulex are presented and discussed. Furthermore, the results are compared to real data [1] and the theory from Nelson and Mowrer [11].

3.1 Evacuation Time

Figure 1 shows the total evacuation times found in the simulations compared with the exercises. The results show that the times found in Simulex generally are higher than the times found in the evacuation exercises. This applies both to the times for the first person exiting the building (triangle) and the last person leaving the building (square). However, there is a better compliance between the times for the first person out. The fact that the recognition and response times were excluded improved that time. It has to be pointed out that the first person out is the same in the two cases for day care centre K, and for day care centre C the time for the first person out is found to be longer in the simulations than found by the exercises. One explanation is the distribution of the children in the different rooms in respectively the exercises and the simulations.

The difference between the times for the first person out in the exercises respectively Simulex varies between -7 and 56 s. The difference on 56 s is for a day care centre where the children put on outerwear before leaving the building. This process was not accounted for in the simulations. If this number is not considered the times vary between -7 and 24 s.

For the times for the last person to be out the difference in results from the exercises and the simulations varies between 13 and 174 s. The largest difference is seen for the day care centre where the children put on outerwear. In 7 of the 9 cases

Fig. 1 Exit times for first and last person for the 9 day care centres – a comparison of Simulex and real data

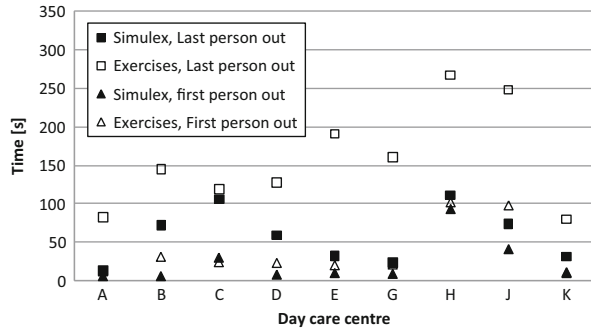


Table 1 Travel speed – horizontal, found in exercises respectively Simulex [m/s]

Age group	Average walking speed, horizontal		
	Walking data	Running data	Simulex
0–2 years	0.60	1.14	–
3–6 years	0.84	2.23	–
All children	–	–	1.13

the difference is more than a minute, which is a rather long time seeing that there are only a relatively small number of occupants and the escape routes are simple and the familiarity of the building and the route was high.

3.2 Travel Speed: Horizontal

The average walking speed on 1.13 m/s found for these simulations (Table 1) is lower than the normal walking speed on 1.4 m/s given in Simulex. This can be explained by the fact that a queue is formed exiting the rooms in the day care centres causing a short distance between occupants. If a queue is not directly formed, occupants in most cases still walk closer to each other due to the flow through doors, which slow people down. I.e. it is seen that almost all occupants in the simulations walk closer to each other than the 1.5 m where the walking speed starts to decrease. From the simulations in Simulex the walking speed is found to vary between 0.21 and 2.20 m/s with an average speed of 1.13 m/s. For comparison, in the Danish code for performance based design a walking speed of 1.30 m/s is suggested for persons able to bring themselves to safety. This is even higher than the data from experiments and is only topped by running children of the older age group.

3.3 Travel Speed: Stairs

Three spiral stairs are part of the evacuation route of the day care centres and included in the simulations. Two of these are traditional spiral stairs and one is a

Table 2 Walking speed on three different spiral stairs [m/s]. Sim is Simulex

Walking speed	Stair 1		Stair 2		Stair 3	
	Sim	Data	Sim	Data	Sim	Data
Mean	0.69	0.58	0.60	0.38	0.69	0.13
Min.	0.49	0.25	0.54	0.26	0.35	0.08
Max.	0.95	1.40	0.69	0.48	0.99	0.33

spiral stair in a square staircase. Stair 1 has a width of 0,8 m and a length of 7,50 m, stair 2 has a width of 0,87 m and a length of 5,50 m, while stair 3 has a width of 0,91 m and a length of 7,50 m. Stair 1 and 2 are known stairs while the children in the exercises have never used stair 3 before. The results are shown in Table 2. The walking speeds in the three cases are relatively close to the data. First persons on the stairs have the fastest walking speed on the given stair. This can be due to the observation that the first persons reaching the staircase were generally the ones assigned the highest horizontal walking speeds, which also means a high walking speed on stairs. The following persons on the stairs generally have a lower walking speed on the stairs. This would also be expected during a real evacuation. Generally no queues were formed on the stairs in the simulations and exercises. The queues were formed in front of the stairs as a result of the change in flow when occupants enter the stair.

It is not possible to simulate occupant's knowledge and familiarity to a given stair when using Simulex. Furthermore, in a design phase of a building the assumptions about the evacuation should be conservative. It should therefore be assumed that the children have no knowledge about stairs in the given building as for stair 3 where the results from Simulex are seen to be much faster than the results from the exercises.

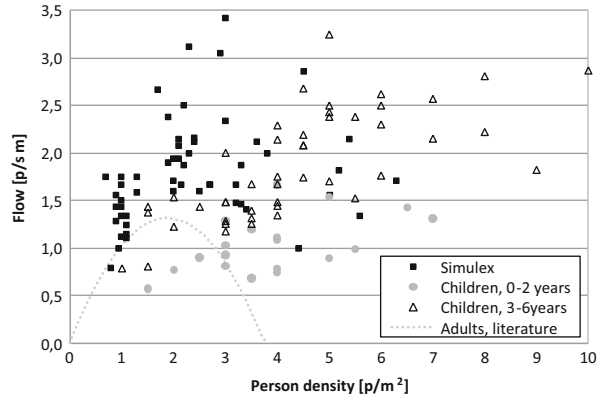
3.4 Flow Through Doors

The flow is found as the individual mean, i.e. with respect to the person density in front of the given door. Figure 2 shows the flow through doors retrieved from the evacuation exercises respectively the simulations in Simulex. For comparison the flow for adults as described in literature [11] is also shown.

In Simulex the flow through doors is detected in varying time intervals where the person density in front of the door is approximately the same. Seeing that occupants are moving, the person density can vary but only time intervals where the density does not vary by more than 1 person in every time step (0.5 s) is used. The time intervals vary from 2.0 to 18.5 s. Person density in front of the door is found by counting the number of occupants in a square meter in front of the door.

The results found from the simulations in Simulex have a large spread. The largest flow is found to be 3.43 p/m·s at a person density of 3.0 p/m² while the smallest flow is seen to be 0.76 p/m·s at a density of 0.80 p/m². Generally the results show that the flow is lower than 3.43 p/m·s at person densities below and over

Fig. 2 Flow through doors as found in the evacuation exercises respectively Simulex. For comparison the flow for adults [11] are also shown



3.0 p/m². Thus the trend is seen to be the same as for the curve for adults found in literature but the flows found in the simulations are outside the ‘adult’ curve except for one measurement at low a person density.

However, some density dependent data accumulations in the results can be seen. This is the case at a person density of about 1.0, 2.0 and 3.5 p/m².

In Simulex the flow through exits should range between 1.1 and 1.4 p/m·s, which should represent adults under normal circumstances. Most of the results found from the simulations are seen to be higher than this range.

A reason for the differences is the body dimensions assigned the occupants in Simulex. The only difference between adults and children in standard settings of Simulex is the body size. This leads to a larger flow for children than adults.

The results from the evacuation exercises are seen to have a large variance like the results from the simulations. But opposed to the results found in the simulations with a peak value, the flow found in the exercises doesn’t drop with higher person densities. In Simulex the walking speed lowers as occupants gets closer to each other. Where the person density is high the distance between occupants is small and the walking speed is therefore low. This could also influence the flow, as the evacuees move slower compared to the exercises.

In the evacuation exercises the maximum person density is 7.0 p/m² for children between 0–2 years and 10.0 p/m² for children aged 3–6 years. In Simulex the maximum person density registered at a given time in the simulations is 6.5 p/m² while the highest density at which a flow is measured is 6.3 p/m². These maximum person densities are higher than the normal maximum density for adults on approximately 4.0 p/m² given in the literature. This difference can be explained by the difference in the general distribution of the person densities and the homogeneous size of the people in the simulations. The person densities found in the evacuation exercises distributed almost evenly between 0.6 and 7.0 p/m² while the largest part of the densities in Simulex is found around 1.0–4.0 p/m².

The highest flow found for the younger children in the exercises is 1.67 p/m·s while it is 3.25 p/m·s for the older children. In the simulations the highest

flow 3.43 p/m·s. These flows are found at different person densities but exceed the maximum flow on 1.9 p/s·m for adults. The older children move faster than the younger children and therefore the flow is higher for this age group.

It is generally seen that the flow found in Simulex is higher than found in the exercises at densities between 1.0 and 4.0 p/m². However, large person densities at which the highest flows for the children are seen, cannot be described applying Simulex. Thus if there are many children in a room the person density at the door is large which in Simulex will give a lower flow than seen in the exercises. Opposite if there are only a few children in a room or if the person density of other reasons is low, Simulex will give a higher flow through the door than found in the exercises.

4 Conclusion

The focus of the present paper is the simulation of the movement of children using an existing building evacuation computer model. Most models are developed for the simulation of primarily adults. However, in several models it is possible to define occupants as children. The simulations undertaken in this work are performed with the model Simulex v. 1.2 where the only difference between children and adults is a difference in body size, i.e. children are simulated as ‘small’ adults.

Evacuation simulations of a total of 9 different day care centres have been carried out. One simulation was performed for each centre. The simulations are carried out with focus on movement of children. Hence, only children are defined in the models.

The work has the following findings: The egress times found in the simulations are seen to be the shortest for the day care centres with doors directly to the open and increasing as the length and complexity of the escape route grows, together with an increased number of children in each room. The average horizontal walking speed found by the simulations is comparable to children running in the experiments, but not walking. The walking speed for persons able to help themselves to safety suggested in the Danish guideline for performance based design, is even more overestimated and is only reached and exceeded by older children running. Applying the guideline is even less conservative than using the simulations in scenarios involving children.

For the walking speed on the three stairs as found by the simulations, Simulex overestimates in all three cases. Not being able to account for affiliation with the surrounding the overestimation is largest for staircase where the children are unfamiliar with the escape route. The lower the children’s familiarity with the stair is, the slower they walk and the greater the overestimation is seen in the simulations in Simulex. However, the exercises provide results from three stairs only and the children’s knowledge of the stairs is very different in the three cases. This affects the generality of the results when comparing Simulex and the real walking speed on stairs for children. Also in this case, the suggested values, given in the Danish code, lay above the other values and are even less conservative in describing the travel speed for ascending children.

Concerning flow through doors, a great variance is also seen in the results from the exercises. At person densities between 1.0 and 4.0 p/m² it is seen that the flow found from the simulations in Simulex is generally higher than found in the evacuation exercises. However, Simulex is not able to simulate the large person densities, at which the highest flows for the children are seen. Thus, if there are many children in a room, the person density at the door is large, which in Simulex will give a lower flow than seen in the exercises. A higher accumulation in datapoints can be seen for densities over 4 p/ms in the experiments. On the other hand, if there are only a few children in a room or if the person density of other reasons is low, Simulex will overestimate the flow through the door when compared to the exercises. Opposed to the results found in the simulation, which show a peak value, the flow found in the exercises doesn't drop with higher person densities.

For the last person out the times found in Simulex are in all cases lower than found in the exercises. It is though not possible to see a trend in the differences as they vary from 13 to 174 s.

In general, Simulex 1.2 does not give conservative results for the egress of children, when setup for children, applied the way it was implemented. It may be concluded that it is not possible to simulate children as 'small' adults. Other features such as velocities, age and behaviour, hereunder densities, should be accounted for.

The results are limited by the design of the stairs, where the model does not enable the design of spiral stair cases, which were part of the evacuation routes in three cases. Furthermore, parts of the evacuation procedure, such as putting on clothes and shoes before exiting the building was not accounted for in the model. Not accounting for these procedures affects the egress times. However, an analysis of the procedures and the discussion whether certain measures within the procedure should be part of the model or changed is not the scope of this paper.

In order to improve the model a differentiation in age groups would be needed. The velocities gained from data should be incorporated into the model, as they are age dependent. The data for children needs to be extended in order to secure validity. It is problematic when evacuation models offer the application of predicting egress times for subgroups of the population without proper validation of these groups. This is not only the case concerning age and gender but also concerning impairments. It is problematic, when the population preferably used for model validation and development, able-bodied people, may be assumed to be the fastest in many cases.

If a computer model should be used to simulate the movement of children during an evacuation, it is necessary to know how the given population is defined in the model, and whether the model has been validated to the group.

Acknowledgement The project was funded by INTERREG IVA and the European Union.

References

1. Larusdottir, A.R. and Dederichs, A.S., Evacuation of Children: Movement on Stairs and on Horizontal Plane, Fire Technology special issue (2010) <http://dx.doi.org/10.1007/s10694-010-0177-6>
2. *Nordic statistical Yearbook*, Nordic Council of Ministers, Nordic Council, (2009)
3. Erhvervs- og Byggestyrelsen: Bygningsreglement, Denmark (2010)
4. Erhvervs- og Byggestyrelsen: Eksempelsamling om brandsikring af byggeri, Byggecentrum, Denmark (2006)
5. British Standards Institution, PD 7974-6:2004: The application of fire safety engineering principles to fire safety design of buildings - Part 6: Human factors: Life safety strategies - Occupant evacuation, behaviour and condition (Sub-system 6), London (2004)
6. Sørensen, L. S.: Brandfysik og brandteknisk design af bygninger, Polyteknisk Forlag, Denmark (2004)
7. Frantzich, H.: Utrymningsvägars fysiska kapacitet, sammanställning och utvärdering av kunskapsläget, Technical Report 3069, Department of Fire Safety Engineering, Lund University (1993)
8. Watts, J. M.: Computer Models for Evacuation Analysis, Fire Safety Institute, in Fire Safety Journal, 12, pp. 237–245, USA (1987)
9. Kuligowski, E. D. and Peacock, R. D.: Review of Building Evacuation Models, Technical Note 1471, Natl. Inst. Stand. Technol., Gaithersburg, MD (2005)
10. Proulx, G.: Evacuation time and movement in apartment buildings, Fire Safety Journal 24, 229–246 (1995) [http://dx.doi.org/10.1016/0379-7112\(95\)00023-M](http://dx.doi.org/10.1016/0379-7112(95)00023-M)
11. Nelson, H. E and Mowrer, F.W.: Emergency Movement, The SFPE Handbook of Fire Protection Engineering (3rd ed), DiNenno, P.J. and Walton, W.D. (ed), Society of Fire Protection Engineers, Bethesda, MD pp. 3-367-3-380 (2002)
12. Proulx, G. Movement of People: The Evacuation Timing, The SFPE Handbook of Fire Protection Engineering (3rd ed), DiNenno, P.J. and Walton, W.D. (ed), Society of Fire Protection Engineers, Bethesda, MD pp. 3-341-3-366 (2002)
13. Nilsson, D.: Exit choice in fire emergencies, Ph.D. thesis, Department of Fire Safety Engineering and Systems Safety, Lund, Sweden (2009)
14. Frantzich, H.: En modell för dimensionering av förbindelser för utrymning utifrån funktionsbaserade krav, Technical report 1011, Department of Fire Safety Engineering, Lund University (1994)
15. Proulx, G. and Reid, I.M.A.: Occupant behavior and evacuation during the Chicago cook county administration building fire, Fire Protection Engineering 16: 283–309 (2006) <http://dx.doi.org/10.1177/1042391506065951>
16. Steffensen, F. B.: Brand og brandsikkerhed i forsamlingslokaler et fælles ansvar, Technical report, Københavns Brandvæsen (2000)
17. Ravn, K.: Undersøgelse af Reaktions- og Beslutningstid, Master thesis, Technical University of Denmark (2008)
18. Bryan, J. L.: Behavioral Response to Fire and Smoke, The SFPE Handbook of Fire Protection Engineering (3rd ed), DiNenno, P.J. and Walton, W.D. (ed), Society of Fire Protection Engineers, Bethesda, MD, pp. 3-315-3-341 (2002)
19. Shields, T.J., Smyth, B., Boyce, K.E. and Silcock, W.H.: Towards the prediction of evacuation behaviours for people with learning difficulties, Facilities 17 (9/10): 336–344 (1999) <http://dx.doi.org/10.1108/02632779910278746>
20. Nisser, M.: Utrymningsssäkerhet för rörelsehindrade, Technical Report, Räddningsverket, Sverige (2001)
21. Gwynne, S.M.V., Boswell, D.L. and Proulx, G.: Understanding the Effectiveness of Notification Technologies in Assisting Vulnerable Populations, Journal of Fire Protection Engineering 19: 31–48 (2009) <http://dx.doi.org/10.1177/1042391508095094>

22. Bruck, D. and Thomas, I.: Comparison of the Effectiveness of Different Fire Notification Signals in Sleeping Older Adults, *Fire Technology* 44: 15-38 (2008) <http://dx.doi.org/10.1007/s10694-007-0017-5>
23. Bruck, D.: Non-awakening in children in response to a smoke detector alarm, *Fire Safety Journal* 32 (4):369–376 (1999) [http://dx.doi.org/10.1016/S0379-7112\(98\)00035-6](http://dx.doi.org/10.1016/S0379-7112(98)00035-6)
24. Murozaki, Y. and Ohnishi, K.: A study of fire safety and evacuation planning for pre-schools and day care centers, *Memoirs of the Faculty of Engineering Kobe University* 32: 99–109 (1985)
25. Nelson, H. E. and Mowrer, F. W.: Emergency Movement. In: P.J.Denno & W. D. Walton (Eds.), *The SFPE Handbook of Fire Protection Engineering* (Third ed., pp. 3-367-3-380). Society of Fire Protection Engineers, Bethesda, MD (2002)
26. Thompson, Peter A., Marchant, Eric W.: A Computer Model for the Evacuation of Large Building Populations, *Fire Safety Engineering Group, University of Edinburg, Fire Safety Journal* 24, pp. 131–148 (1995)
27. Thompson, Peter A., Marchant, Eric W.: Testing and Application of the Computer Model 'Simulex', *Fire Safety Engineering Group, University of Edinburg, Fire Safety Journal* 24, pp. 149–166 (1995)

Stochastic Transition Model for Pedestrian Dynamics

Michael Schultz

Abstract The proposed stochastic model for pedestrian dynamics is based on existing approaches using cellular automata, combined with substantial extensions, to compensate the deficiencies resulting of the discrete grid structure. This agent motion model is extended by both a grid-based path planning and mid-range agent interaction component. The stochastic model proves its capabilities for a quantitative reproduction of the characteristic shape of the common fundamental diagram of pedestrian dynamics. Moreover, effects of self-organizing behavior are successfully reproduced. The stochastic cellular automata approach is found to be adequate with respect to uncertainties in human motion patterns, a feature previously held by artificial noise terms alone.

Keywords Pedestrian dynamics • Cellular automaton • Stochastic transition • Navigation • Dynamic motion field

1 Introduction

Models for pedestrian dynamics cope with different aspects of behavior of human motion patterns. Generally, such models refer to (one or more of) three levels of motion planning: operational (short range), tactical (medium scale), and strategic behavior (large scale). The basic microscopic models (e.g. social force, cellular automaton, or discrete choice) particularly focus on the operational level of motion planning and execution. Especially, the often favored social force approach [1], which defines attraction and repulsion forces between humans, turns out as a good analogy to reproduce substantial effects of self-organization. In contrast to the

M. Schultz (✉)

Department of Air Transport Technology and Logistics, Faculty of Transport and Traffic Sciences “Friedrich List”, Technische Universität Dresden, Dresden, Germany
e-mail: schultz@ifl.tu-dresden.de

social force model (cf. [2, 3]), the incrementally developed motion model [4, 5] is based on a stochastic cellular automata approach [6] to handle the unpredictable behavior of individual path deviations. This paper starts out with an overview of the existing model and then focuses on the identified deficiencies in detail to introduce compensation methods that are needed to overcome grid-based influences on the model behavior. Further on, a calibration against the fundamental diagram and a navigational algorithm are presented. The effects of agent-to-agent interactions are finally taken into account by a dynamic motion field.

2 Basic Stochastic Model

The developed microscopic model of pedestrian motion is based on a square grid structure (cellular automata) and represents a stochastic approach using a 3×3 transition matrix (Moore neighborhood) for agent movements [6]. In contrast to the common understanding of cellular automata, a paradigm change takes place: instead of changing the cell status depending on the status of the surrounding cells (pull concept), the agent moves over the regular grid and enters cells, which have to be free of other agents or obstacles (push concept). To model the undisturbed agent motion, the velocity vector is divided into independent Cartesian components (longitudinal and lateral), which yields three discrete motion events: forward, center, backward and left, center, right respectively. Each motion component is characterized by a specific motion probability μ with a corresponding motion variance σ^2 , which result in a generalized transition probability p as defined in Eqs. 1, 2, and 3.

$$p_{\text{forward or left}} = \frac{1}{2} (\sigma^2 + \mu^2 + \mu) \quad (1)$$

$$p_{\text{center}} = 1 - (\sigma^2 + \mu^2) \quad (2)$$

$$p_{\text{backward or right}} = \frac{1}{2} (\sigma^2 + \mu^2 - \mu) \quad (3)$$

The symmetry of the lateral motion component ($p_{\text{right}} = p_{\text{left}}$) and the assumption that agents do not move backwards ($p_{\text{backward}} = 0$) are simplifying, but reasonable constraints. The motion components are combined to a 3×3 matrix M_{ij} and determine the transition from the center cell to the right adjacent cell (see Fig. 1 (left), forward motion to $M_{1,0}$).

Although the transition matrix apparently possesses a two-dimensional characteristic, only a one-dimensional transition with a lateral deviation (1.5-dimensional) is achieved at this stage. A true two-dimensional transition is ensured by blending two matrices: one matrix represents the horizontal transition M^{0° (Fig. 1, left) and one matrix the diagonal transition M^{45° (Fig. 1, right), which is created by a counterclockwise rotation, whereas the indexes are shifted by one position. In contrast to Burstedde et al. [6], the specific weights in Eq. 4 consider both the motion

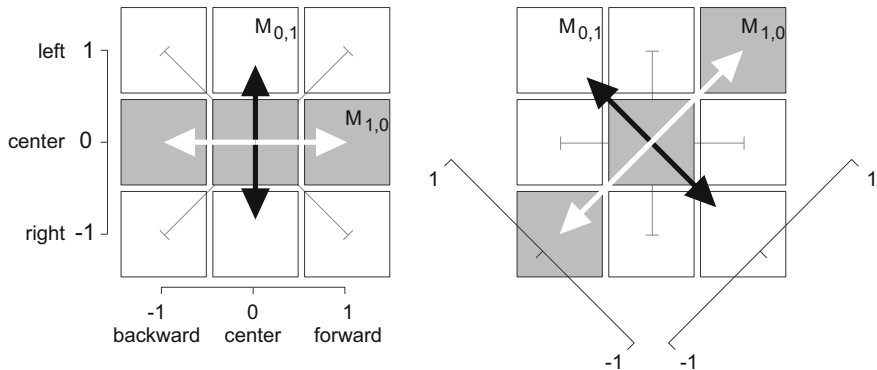


Fig. 1 Individual transition to all connected cells with a probability of M_{ij} for the horizontal (*left*) and diagonal transition (*right*)

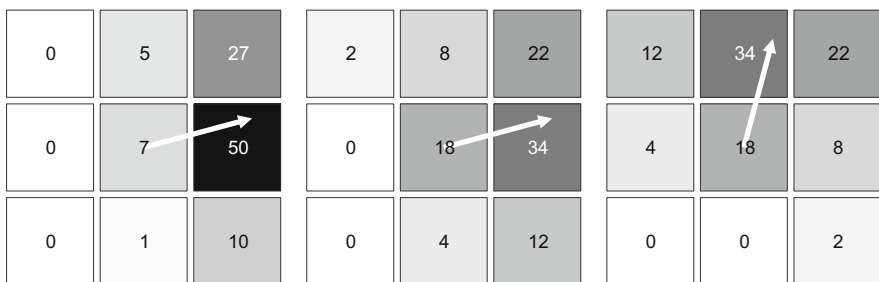


Fig. 2 Sample states of transition matrix M (transition probability in %) using the blending function of Eq. 4 with specific parameter sets for μ, σ^2, α : $\{0.9, 0.3, 15^\circ\}$, $\{0.7, 0.4, 15^\circ\}$, and $\{0.7, 0.4, 75^\circ\}$ (from *left* to *right*)

angle α and the deviating distance of diagonal cells, which additionally results in a normalization of the final transition matrix M .

$$M = (1 - \tan \alpha) M^{0^\circ} + \tan \alpha \sqrt{2} M^{45^\circ} \tag{4}$$

The consideration of the rotational symmetry allows a mapping of all motion directions $\alpha \in [0, 360^\circ]$ [5, 6]. Three examples of final transition matrices are presented at the following Fig. 2, whereas the longitudinal variance ($\sigma_{\text{long}}^2 = \mu_{\text{long}} - \mu_{\text{long}}^2$) and the lateral transition probability ($\mu_{\text{lateral}} = 0$) consequently result from the simplifying constraints. Finally, the parameter set is reduced to $\mu = \mu_{\text{long}}, \sigma^2 = \sigma_{\text{lateral}}^2$, and motion angle α .

Detailed analysis of this stochastic model points out significant directional dependencies which are caused by the underlying regular grid structure. As an example, entering diagonal cells implies a longer path (similar to a higher speed) in comparison to entering horizontal/vertical located cells. Consequently, the next section focuses on these model deficiencies and introduces reliable compensation strategies.

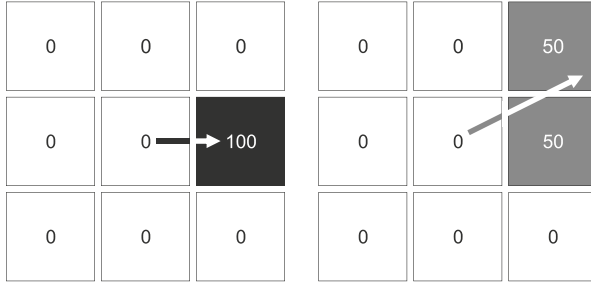


Fig. 3 Unique transition to exact one cell with $\mu_{\text{forward}} = 1$ and $\sigma_{\text{left/right}}^2 = 0$ (left), which is only feasible for transitions at the axes of symmetry, otherwise a cell selection is inevitable (right)

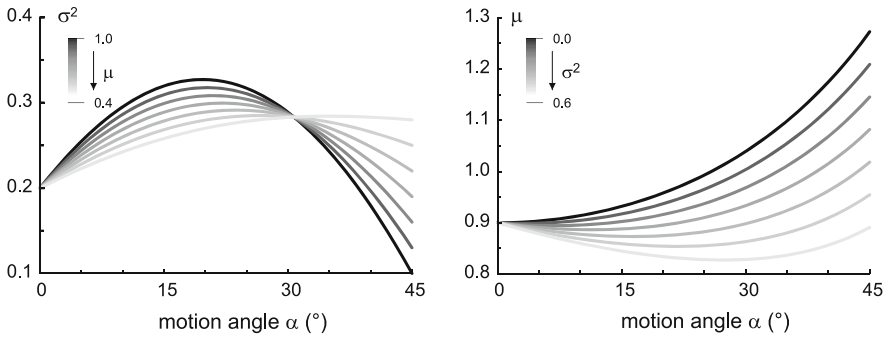


Fig. 4 Error characteristics of motion deviation (left) and motion speed (right) depending on the cross correlation regarding to the motion speed ($1 < \mu < 0.4$ at constant $\sigma^2 = 0.2$) and the motion deviation ($0 > \sigma^2 > 0.6$ at constant $\mu = 0.9$) respectively

3 Deficiencies and Compensations

Besides the obvious distance discrepancy the blending of the horizontal and diagonal matrices results in additional model deficiencies, which affects the operational motion behavior of the agents. A direct transition to the adjacent cells is only possible with rotation angles in multiples of 45° . All other angles immanently result in a stochastic selection process (Fig. 3). This implies both an additional motion variance and a different transition/avoidance behavior. In the case of a horizontal transition (Fig. 3, left) an occupied cell (black) leaves no alternatives and will effectively stop the agent while the motion angle of 22.5° yields equal probabilities (using blending function of Eq. 4) and two optional transitions exist (Fig. 3, right).

The effect of different distance and variance characteristics is shown in Fig. 4; the distance error increases and reaches a maximum at $\alpha = 45^\circ$ and the movement deviation increases and decreases in the range between 0° and 45° . Furthermore, these characteristics are directly coupled and impose a damping effect on each other: increasing lateral variance leads to decreased distance differences and a decreasing

probability of forward motion leads to a more adjusted behavior with a smaller variance difference (Fig. 4). To harmonize the different transition behavior caused by the motion angle dependencies, specific compensation settings for the transition matrix are numerically calculated. The compensation settings qualitatively points out an inverse characteristics to the identified error, whereas both the cross correlation of μ and σ^2 as well as the less smaller influence of additional angle deviations are taken into account [5].

4 Calibration

To complete the stochastic movement model, additional boundary conditions have to be defined regarding both model and agent behavior:

- The update procedure of simulation environment (agent scheduling),
- The behavior in the case of intersecting movement paths (common collision avoidance strategy),
- The amount of motion per simulation turn (number of steps),
- Behavioral implications of blocked cells (obstacles, other agents), and
- Temporarily blocking occupied cells during the movement phase (motion trace).

The sequential update procedure is used in the model, since its points out no significant drawbacks, if the sequence is shuffled at each simulation step [5, 26, 27]. Thus, the constellation of parallel access to one free cell will be avoided (Fig. 5, left). The influences of crossing paths (Fig. 5, center and right) are directly related to the last condition of considering traces and since this trace condition possesses a significant influence to the model, the crossings are not permitted. To evaluate the relevance of the amount of motion per simulation turn, the fundamental diagram is used as a commonly excepted reference for the speed-density relation of pedestrian dynamics [7]. To allow a reliable scenario evaluation an infinite environment was set up with:

- Varying amount of motion per simulation turn (from one to five motion steps),
- Always-move versus waiting procedure at blocked cells, and finally
- The ability of agents to leave a trace of blocked cells during a simulation turn.

The always-move procedure is implemented by the condition that each blocked cell relatively increases the transition probability of the free cells in equal measure to their specific transition probability (only free cells could be selected). The waiting procedure implies that agents immediately stop their motion at the current simulation turn if a blocked cell is stochastically selected for the transition.

The determined movement rules in connection with the ability of motion traces (temporally blocked cells) results in the associated speed characteristics as shown in Fig. 6. The left diagram of Fig. 6 (waiting rule) points out no clear tendency to consider a specific amount of steps per simulation turn. But the always-move rule

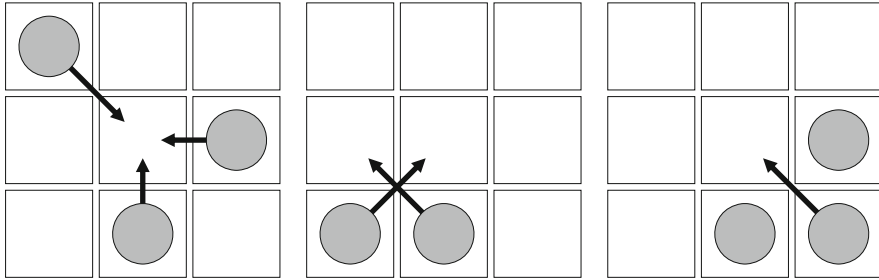


Fig. 5 Demand for determination of movement rules to cope with parallel transition to one free cell (*left*) and crossing paths (*center* and *right*)

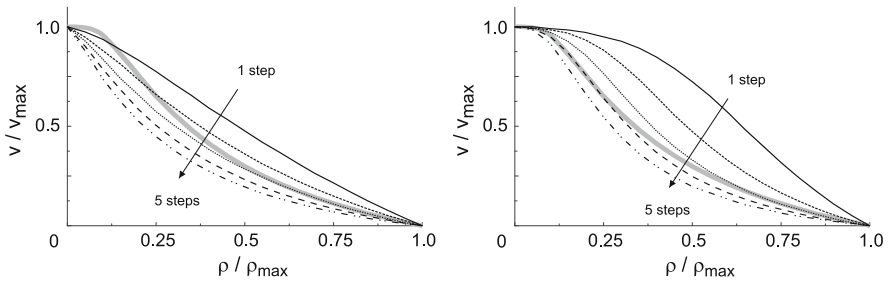


Fig. 6 Normalized speed-density characteristics considering one to five motion steps per simulation turn as well as motion trace for both waiting rule (*left*) and always-move rule (*right*) against the common characteristic of pedestrian dynamics (*bold gray line*, according to Weidmann [7])

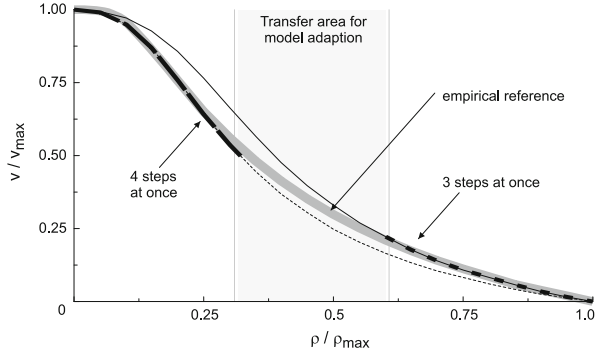
successfully matches the speed-density relation of pedestrian dynamics assuming 3–4 steps at one simulation turn (Fig. 6, right).

Up to this point, the stochastic motion approach only considers the surrounding neighbors, which are directly connected to the local cell position. In comparison to the fundamental diagram of pedestrian dynamics (correlation of individual motion speed and agent density), the developed model reproduces the expected shape if the agent:

- Will not wait if other agents block his way (occupied cells increase the transition probability of surrounding cells),
- Moves three/four steps at one simulation turn (depending on agent density), and
- Leaves a motion trace (temporally block all cells entered at the current simulation turn).

With increasing agent density ($\rho/\rho_{\max} > 0.6$) the number of steps per simulation turn should be reduced from four to three. At Fig. 7 the adequate characteristics of the stochastic movement model is represented in detail. It needs to be emphasized, that low density scenario ($\rho/\rho_{\max} < 0.3$) significantly benefits from a four step implementation whereas the three step implementation leads to slight overestimations compared to the common speed-density relation of the pedestrian dynamics.

Fig. 7 Detailed view to the characteristic of the developed modal against the fundamental diagram of pedestrian dynamics [7]



A normalized notation of this relation is given by Eq. 5, with $v_{\max} = 1.34$ m/s, $\rho_{\max} = 6.25$ pedestrian/m², and $\rho \in (0, \rho_{\max})$.

$$\frac{v}{v_{\max}} = 1 - e^{0.3061 \left(1 - \frac{\rho}{\rho_{\max}}\right)} \tag{5}$$

5 Navigation

For modeling the motion of pedestrians, two main approaches have been evaluated during the least three decades: one uses a set of navigation points to navigate agents around obstacles [10], the other one relies on a discretized grid structure which holds guidance information (walking distance to destination, the direction of shortest/ quickest path) and efficiently takes obstacles into consideration as well. The most prominent and most widely used method that calculates Euclidean distances is a numerical solution of the Eikonal equation [8, 9]. The Fast Marching Method (FMM) is a comparatively fast method and possesses a comparatively small deviation regarding to the Euclidean distance [11–15]. The FMM shows an optimal worst-case behavior (concerning the computation time) and the relative distance error in general decreases with the increasing distance from the destination, implying that a finer grid reduces the distance error. Apart from optimizing the numerical Eikonal equation solver algorithmically, simplified methods could trade calculation exactness for computation speed. The most noticeable example for this is a simple flood fill algorithm over common edges/corners, resulting in p-norm metrics for the vector x (see Eq. 6), with $p = \{1, 2, \infty\}$ for the Manhattan, Euclidean, and Chebychev metric respectively.

$$\|x_p\| := \left(\sum |x_i|^p\right)^{1/p} \tag{6}$$

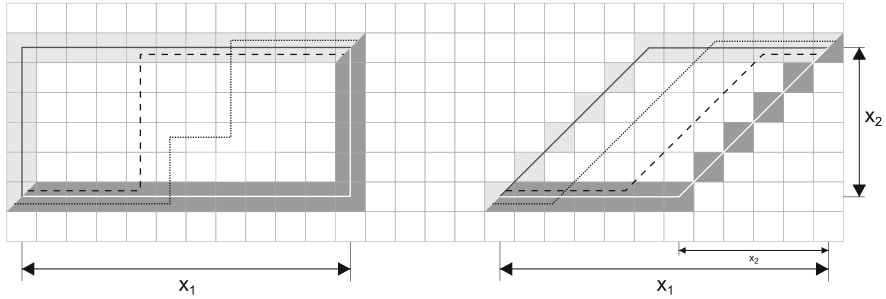


Fig. 8 Manhattan metric (von Neumann neighborhood, *left*) and distance metric grid considering a square grid and a connection over common corners (Moore neighborhood, *right*); *dotted lines* represent equivalent motion paths (same length) and the *colored cells* are the boundaries of these valid paths

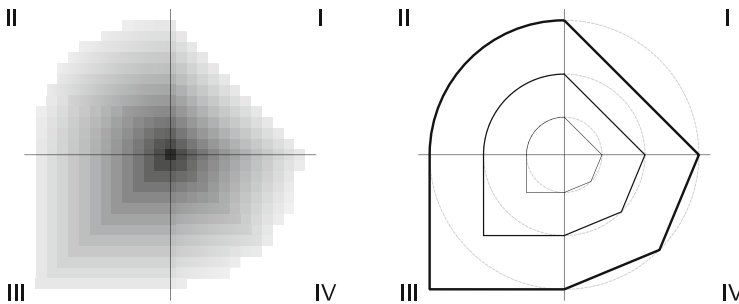


Fig. 9 Comparison of Manhattan (*I*), Euclidean (*II*), Chebychev (*III*) metrics against the derived Moore metric using a color-coded distance field (*left*) and equidistance lines (*right*)

The flood fill algorithm (breadth-first search) for the creation of the potential field was introduced by Lee [17] for the von Neumann neighborhood and is consequently applied for the Moore neighborhood [5, 18] (Fig. 8).

With the Euclidean metric as correct solution, these methods lead to relative errors which remain constant over distance or even increase, which means that a finer grid size does not necessarily improve the precision arbitrarily (Fig. 9). However, it is possible to reduce the error by making some slight modifications upon the simple flood fill methods [16]. In comparison to the Manhattan (quadrant I, see Fig. 9), Euclidean (quadrant II) and Chebychev (quadrant III) metrics, the used flood fill approach for the Moore neighborhood possess a distance metric (quadrant IV) as determined in Eq. 7.

$$\|x\| := |\Delta x| + \sqrt{2} \min(|x_i|) \tag{7}$$

Although the flood fill algorithm obviously features a closer approximation of the Euclidean distance it tends to overestimate the distances.

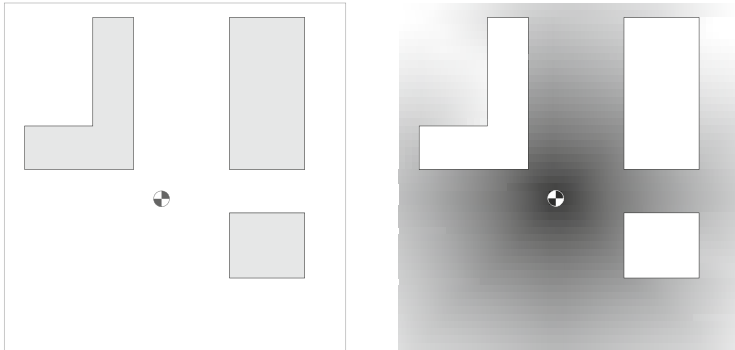


Fig. 10 Sample environment with centered destination (*circle*) and obstacles (*rectangles*) (*left*) and the calculated, color-coded distance field using the Moore metric (*right*)

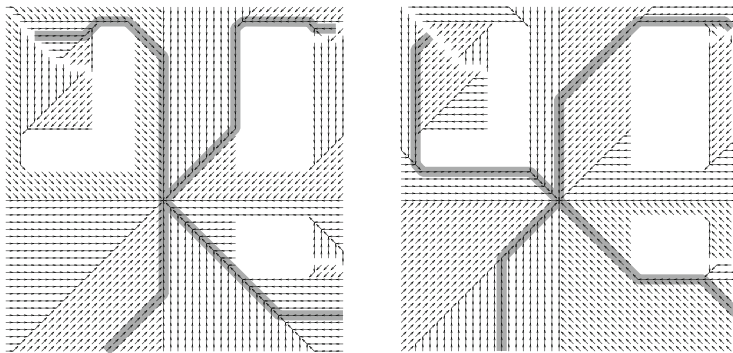


Fig. 11 Contrary heading vector fields based on a distance field calculated clockwise (*left*) and counter-clockwise (*right*)

Regardless of the non-conforming approximation of distance, the Moore metric possesses a significant characteristic which may be used to determine the correct walking direction with respect to the shortest way [5, 18]. This method does neither rely on a computation time expensive sorting of distances of currently *active* cells as the FMM does, nor does it even have the need of the calculation of square roots or similar rather computation-time expensive functions.

As an elementary example an obstacle configuration is set up to calculate the direction from each position of the environment to the highlighted circle (Fig. 10, left). The calculated distance is outlined as a color-coded distance image (black: distance = 0, white: distance $\rightarrow \infty$; Fig. 10, right). A closer view on this image highlights the exposed characteristics of the axis of symmetry (cf. Fig. 11). If agents would use this distance field according to the rule to enter only adjacent cells with the smallest distance value, finally their movements will end up at these axes which results in unnatural crowded areas (jam from nowhere).

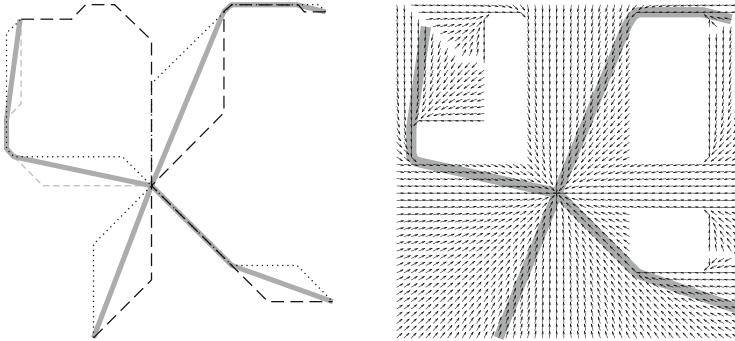


Fig. 12 Combination of clock- and counterclockwise vector fields to a valid directional grid equivalent to the Euclidean distance metric (shortest distance)

In contrast to common smoothed gradient procedures to derive the local motion vectors, the developed algorithm creates the motion vector field already during the flood fill process by storing the direction of the downstream position (originating cell position). The flood fill algorithm starts at the target cell and stores the distance at each surrounding cell, if the already stored distance value is greater than the current distance value. If all adjacent cells filled with the distance information, these cells are used as the next source of distance information. So each cell possesses an originating cell, which was the base for the own distance information. The location of this downstream cell depends on the processing sequence of the algorithm. The idea of distance sorted cells to ensure short computation times by preventing multiple calculations of cell was tested without any indication of potential improvements. But a detailed verification of both clockwise and counterclockwise handling of the cell calculation points out significant directional patterns. Due to the fact that each cell has two possible downstream cells, one diagonal cell and one horizontal/vertical cell (neglecting obstacles), the handling sequence of the flood fill algorithm determines which cell is selected first. As a result, the counter-clockwise cell handling leads to an opposite selection as the clockwise cell handling sequence (Fig. 11). Each cell handling sequence promotes one specific pattern depending on the direction angle to the destination. Figure 11 clearly shows the both directional patterns (cf. lower left quadrant with opposed upper and lower triangles) and a counter-/clockwise behavior.

The combination of both cell handling procedures leads to a valid solution of the movement vector field once they are combined to one aggregated field. Figure 12 shows the aggregation process using four generic starting positions at the outer corners of the quadrants. The common rhombus shape of each single distance segment is emphasized (cf. Fig. 8, right). Addressing the geometric definition of the rhombus, two vector components are used (derived from diagonal and horizontal/vertical connections). The complete directional grid is shown in Fig. 12 (right) and indicates no directional artifacts and the declared paths are fully equivalent to the Euclidean distance metric.

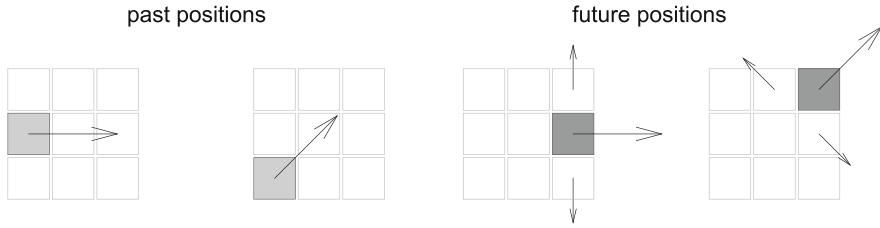


Fig. 13 Past positions and future positions are stored in a dynamic motion field, whereas future positions (path extrapolation) features both an additional lateral component and a slight different characteristics (cell position) for diagonal transitions

6 Interactions

The calculation of directional fields for motion destinations is an essential part of each pedestrian motion model and have to consider several environmental conditions. The proven quality of the algorithm underlines the relevance of the achieved results to the navigational tasks of the agents, even considering static obstacles [5, 18]. In contrast to the static obstacles, dynamic objects are not taken into account on the path planning process (tactical movement level). Although the introduced stochastic motion model considers individual traces during the movement updates, these effects are only confined to a small area (three/four steps, as defined in Sect. 4). Against the background of game design, the interactions of agents are an essential strategic behavioral component and basically considering spheres of influence [20] which is one basic technique (influence maps) for tactical movement decisions of agents [21–25]. A commonly accepted approach to include tactical movement decisions in cellular automata models for pedestrian dynamics is the calculation of a dynamic floor field [6, 19].

Using the idea of the repulsive impact of the walking path of other agents to the individual movement decision a dynamic motion field will be introduced. This grid combines both future position based on the current motion direction and past positions (walking paths). In contrast to the potential field, the cells store movement vectors, where the different characteristic of possible future and past position are considered. Each entered cell stores the local motion direction of the corresponding agent (Fig. 13, left).

Further on, the current local motion direction is used to mark potential future cells in advance (cells are derived from the extrapolation of the prior simulation turn), whereas the adjacent lateral cells store the orthogonal motion vector (Fig. 13, right). This procedure reflects the observed motion behavior of pedestrians to avoid crossed movement paths and to follow preceding pedestrians. Finally, one simulation turn consists of four sub-steps:

1. Randomly sequenced agents update their position using the direction to their individual destinations superposed by the local vector of the dynamic motion field.

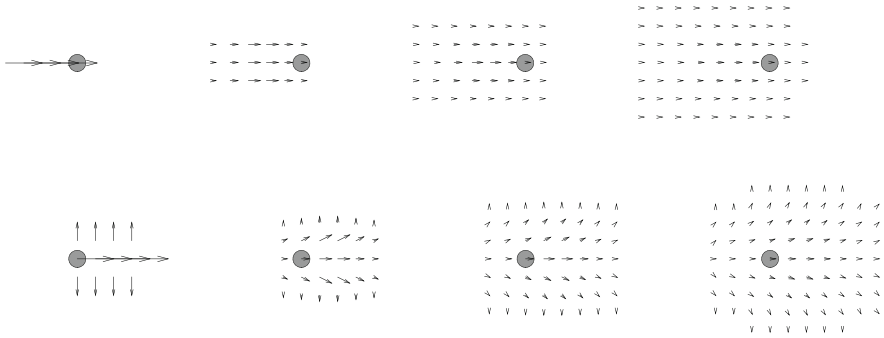


Fig. 14 Dynamic motion field to mark past positions (*top*) and future positions (*bottom*), starting with the initial field on the right considering an isotropic expansion associated with a temporally decay caused by a Gaussian filtering process

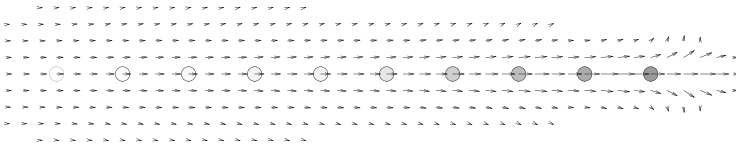


Fig. 15 Combined dynamic field of agent motion to cover individual movements of a certain period of time

2. The local motion direction is added to the dynamic motion field for each entered cell.
3. Considering the current position, the motion steps during the simulation turn are used to extrapolate the motion path.
4. Finally, the entire dynamic motion field is smoothed by a convolution filter using the one-dimensional kernel $(dc/3, dc/3, dc/3)$ with dc $[0, 1]$ as the decay coefficient.

The two step application of the kernel in horizontal and vertical grid direction leads to an isotropic Gaussian filter behavior (see Fig. 14 from left to right).

In Fig. 15 the result of a complete walking path is shown, considering past/future positions, isotropic spatial diffusion, and temporally decay behavior.

The proposed method of a dynamic motion field can also be applied for semi-static obstacles, such as waiting agents, small objects (e.g. baggage, signs, park bench), or temporally blockings of the infrastructure. In contrast to moving agents, the initial vector field of the semi-static obstacles possesses a symmetric characteristic (Fig. 16, left). The repulsive effect of non-moving objects increases if these objects are closely located to each other. In Fig. 16 (right) the superposition of the destination-directed motion field (one-sided walkway from left to right) with the dynamic motion field of the semi-static obstacles evidently points out a collision avoiding behavior. It may be noticed, that the presented example is only a proof of concept and a detailed parameterization has to be done at the field.

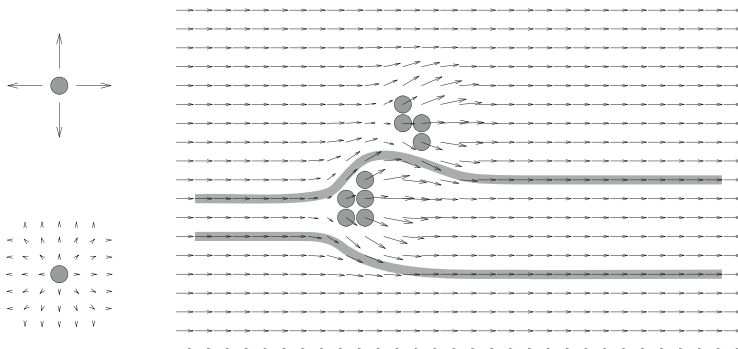


Fig. 16 Dynamic motion field for static objects (*upper left*), isotropic expanded with a temporally decay (*lower left*), and a convincing example of the combination of movement direction field and individual vector fields (*right*)

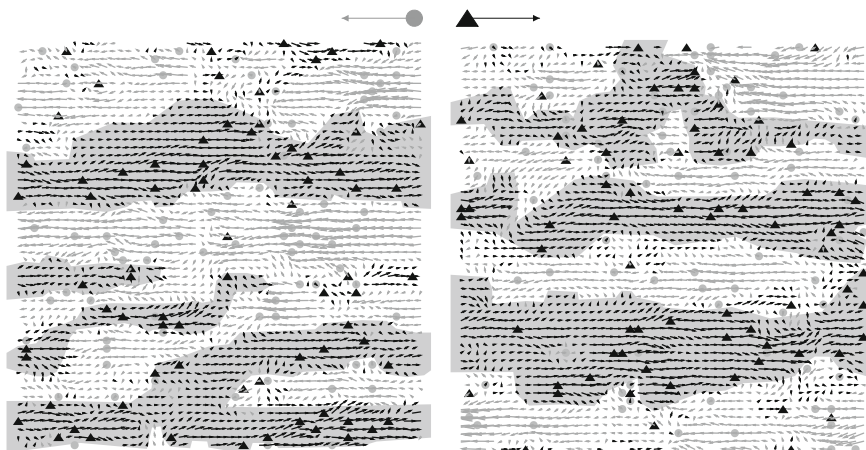


Fig. 17 Result of the complete stochastic model for pedestrian dynamics using a counter flow scenario: sample lane formations with locally aligned agents

The simulation result of a counter-flow scenario is shown in Fig. 17, whereas the separation of agents regarding their movement direction is clearly indicated. Agents with opposite headings avoid collisions considering the dynamic motion field and downstream agents use the trace information to follow agents with the similar heading.

Over the course of time lane formations occur, characterized by areas with agents possessing a comparable motion direction. Due to the fact, that the proposed motion model is based on an immanent stochastic approach, these lanes are not stable in time and space.

7 Summary

The developed model is a substantial extension of a stochastic cellular automata approach. The model development is completed by adding agent-oriented environment analysis, route planning, and mid-range agent interaction. The stochastic motion model proves its capabilities for a quantitative reproduction of the characteristic shape of the common fundamental diagram of pedestrian dynamics. The proposed model possesses a $v_{\max} = 4(3)$ speed characteristic, a simple exclusion statistic and a shuffled sequential update procedure. The underlying regular grid structure of the cellular automata results in a direction-dependent behavior of motion speed and variance. The identified model deficiencies are compensated on a fundamental level to ensure valid local transition matrices for the stochastic motion behavior.

The motion direction is derived from a destination-oriented motion field. This field is calculated by a flood fill algorithm using the underlying regular grid considering a Moore neighborhood, where obstacles are represented by occupied cells. The applied algorithm exactly reproduces the shortest path equivalent to the Euclidean distance. The developed algorithm efficiently prevents distance errors and directional artifacts by combining two complementary directional fields, which are based on a Moore distance metric calculation. Due to the fact, that flood fill algorithms are often used in agent-based simulations to create distance potentials for navigational purposes, this enhanced algorithm provides a fundamental contribution to existing and future simulation environments.

References

1. D. Helbing and P. Molnár (1995), Social force model for pedestrian dynamics, *Phys. Rev. E* 51, pp 4282–4286
2. A. Johansson, D. Helbing, and P. Shukla (2007), Specification of the social force pedestrian model by evolutionary adjustment to video tracking data, *Advances in Complex Systems* 10 (4), pp 271–288
3. M. Moussaïd, N. Perozo, S. Garnier, D. Helbing, and G. Theraulaz (2010). The walking behaviour of pedestrian social groups and its impact on crowd dynamics, *PLoS One* 5 (4)
4. M Schultz, S Lehmann, and H Fricke (2005). A discrete microscopic model for pedestrian dynamics to manage emergency situations in airport terminals, *Pedestrian and Evacuation Dynamics*, pp 369–375, Springer
5. M. Schultz (2010). An individual-based model for passenger movement behavior in airport terminals (in German), PhD thesis, Technische Universität Dresden, <http://nbnresolving.de/urn:nbn:de:bsz:14-qucosa-85592>
6. C. Burstedde, K. Klauck, A. Schadschneider, and J. Zittartz (2001), Simulation of pedestrian dynamics using a 2-dimensional cellular automaton, *Physica A* 295, pp 507–525
7. U. Weidmann (1992). *Transporttechnik der Fußgänger*. Schriftenreihe des Instituts für Verkehrsplanung, Transporttechnik, Strassen- und Eisenbahnbau, 90
8. H. Bruns (1895). *Das Eikonale*. S. Hirzel
9. P. Frank (1927). Über die Eikonalgleichung in allgemein anisotropen Medien, *Annalen der Physik* 389 (23)

10. M. de Berg, M van Kreveld, M Overmars, and O. Schwarzkopf (1997). *Computational Geometry*. Springer, Berlin Heidelberg New York
11. D. Hartmann (2010). Adaptive pedestrian dynamics based on geodesics. *New Journal of Physics*, 12(4)
12. S. Osher and J. Sethian (1988). Fronts propagating with curvature-dependent speed: algorithms based on Hamilton-Jacobi formulations, *Journal of computational physics* 79 (1), pp. 12–49.
13. J. Sethian (1996). A fast marching level set method for monotonically advancing fronts, *Proceedings of the National Academy of Sciences of the United States of America*, 93 (4)
14. R. Kimmel and J. Sethian, (1998). Computing geodesic paths on manifolds, in *Proc. Natl. Acad. Sci. USA*, pp. 8431–8435
15. J. Sethian (1999). *Level Set Methods and Fast Marching Methods*. Cambridge University Press Cambridge
16. T. Kretz, C. Bönisch, and P. Vortisch (2008). Comparison of Various Methods for the Calculation of the Distance Potential Field, in *PED 2008*, pp. 335–346. Springer, Berlin
17. C. Lee (1961). An algorithm for path connection and its application, *IRE Transactions on Electronic Computers EC-10*, no. 3, pp. 346–365.
18. M. Schultz, T. Kretz, and H. Fricke (2010). Solving the Direction Field for Discrete Agent Motion, in S. Bandini et al. (ed.) *Cellular Automata - ACRI 2010, Proceedings*. Volume 6350, *Lecture Notes in Computer Science*, pp. 489–495, Springer
19. A. Schadschneider (2002). Cellular Automaton Approach to Pedestrian Dynamics - Theory. In *Pedestrian and Evacuation Dynamics*, pp. 75–86, Springer
20. A.L. Zobrist (1969), A model of visual organization for the game of GO, *AFIPS Conference Proceedings*, 34, pp. 103–112
21. P. Tozour (2001). *Influence Mapping, Game Programming Gems 2*, Charles River Media
22. P. Tozour (2004). *Using a Spatial Database for Runtime Spatial Analysis, AI Programming Wisdom 2*, Charles River Media
23. P. Sweetser (2004). *Strategic Decision-Making with Neural Networks and Influence Maps, AI Programming Wisdom 2*, Charles River Media
24. S. Woodcock (2002). *Recognizing Strategic Dispositions: Engaging the Enemy, AI Programming Wisdom*, Charles River Media
25. D.C. Pottinger (2000). *Terrain Analysis for Realtime Strategy Games, Game Developer Conference*
26. M. Wölki, A. Schadschneider, and M. Schreckenberg (2006). Asymmetric exclusion processes with shuffled dynamics. *Journal of Physics A: Mathematical and General*, 39, pp. 33–44
27. H. Klüpfel (2003). *A cellular automaton model for crowd movement and egress simulation*, PhD thesis, Universität Duisburg-Essen.

Toward Simulation-Based Egress Optimization in Smart Buildings Using Symbiotic Simulation

Heiko Aydt, Michael H. Lees, Stephen J. Turner, and Wentong Cai

Abstract Buildings have to satisfy certain safety standards by design, for example by featuring well-displayed emergency exits and well-located fire extinguishers. However, the large number of occupants may cause significant congestion in case of a necessary evacuation due to events such as fire. Technology can help to make operations more efficient and egress is no exception. In fact, as we will show in this paper, egress is a good example where technology can make a positive difference. In this paper we analyze the effectiveness of dynamic guidance systems that are able to use real-time sensor data for the decision making process. Furthermore, we show the serious drawbacks of systems that cannot anticipate how an emergency situation will unfold. Due to the complexity of crowd behavior, an agent-based simulation is required in order to simulate the likely course of an egress. We argue how symbiotic simulation can be used to realize a dynamic guidance system that can leverage on the advantages of agent-based egress simulation.

1 Introduction

Increasing population numbers and urbanization has led to densely populated cities. Managing the increasing number of people in cities efficiently has become priority for many city governments. While urbanization has many advantages it comes with its own problems. Most (if not all) large cities have to deal with problems that are typical for their size and density such as traffic jams, for example. Smart traffic systems can help to alleviate the problems to some extent. Another consequence of increasing population density in cities are high-floor buildings (e.g., office towers, mega shopping malls, high-rise residential buildings) that provide shelter, office

H. Aydt (✉) • M.H. Lees • S.J. Turner • W. Cai
School of Computer Engineering, Nanyang Technological University, Singapore
e-mail: aydt@ntu.edu.sg; mhlees@ntu.edu.sg; assjturner@ntu.edu.sg; aswtcai@ntu.edu.sg

space, entertainment, and recreation for thousands of people. Although buildings have to satisfy certain safety standards by design, for example by featuring well-displayed emergency exits and well-located fire extinguishers, the large number of occupants may cause significant congestion in case of a necessary evacuation due to events such as fire.

Technology can help to make operations more efficient and egress is no exception. In fact, as we will show in this paper, egress is a good example where technology can make a positive difference. Buildings are typically equipped with floor plans that show emergency exits and evacuation routes to the nearest exit. While such a static guidance system can give people a general idea where they are currently located and where the nearest exit is, it cannot provide guidance that adapts dynamically to the current situation. In case of an emergency, a situation may become very dynamic for various reasons such as rapid spread of fire and smoke, congested evacuation routes, blocked exits, or even panic. The ability to capture information about a situation in real-time is an important advantage that can help to make egress more efficient. Smart buildings can be equipped with various forms of sensors (e.g., smoke detectors, heat detectors, motion detectors) and actuators (e.g., electronic sign-boards) that can be utilized by a guidance system. This guidance system can use real-time sensor data to dynamically adapt to the current situation and provide useful information (e.g., direction to the nearest/safest exit) to the evacuees by means of various actuators.

Given information about the current situation in the building, the guidance system can compute the preferred route to an exit from any location in the building. There are a number of challenges that need to be considered and adequately addressed. One important issue that we will address in our work is concerned with the dynamics of an emergency situation. We are concerned with dynamics that arise from the rapid spread of fire and smoke as well as human crowd behavior. In particular, crowd dynamics may lead to congestions and bottle-necks in certain parts of the building. Although, a reactive zero look-ahead guidance system can probably take into consideration the number of people in the various parts of the building as well as the current location of the fire(s) in order to determine an ideal route in order to avoid congestion, it lacks predictive capabilities. This can be a serious disadvantage and may even exacerbate certain problems.

In this paper, we present our agent-based egress simulation and introduce a guidance system which makes decisions based on real-time sensor data about the fire situation in a building. We show that a data-driven guidance system can dynamically change the evacuation route and thus improve the effectiveness of the evacuation. However, without the use of simulation a guidance system cannot anticipate (a) how the crowd is likely to behave (e.g., where they move and where bottlenecks will form) and (b) how the fire will spread within the building. Due to the lack of foresight, zero look-ahead guidance systems can make fatal decisions regarding the evacuation route. We illustrate such a case and explain how a symbiotic simulation-based guidance system would be able to overcome the problems of a zero look-ahead guidance.



Fig. 1 Illustration of the floor plans of the ground floor (*left*) and the first floor (*right*). The only exit (*E*) of the building is located on the ground floor. Two staircases (*1*) and (*2*) connect the first floor with the ground floor

2 Simulation Model

2.1 Environment and Fire Model

For simulation purposes, we consider a typical multi-story office building. More specifically, we use publicly available floor plans of the World Trade Center in Long Beach to model the environment. Although the actual building has more floors, the model used for the experiments described in this paper has been limited to two floors: the ground floor and the first floor. Figure 1 (*left*) illustrates a typical floor plan of the building, which has been used to model the ground floor. A modified version of the original floor plan, illustrated in Fig. 1 (*right*), is used to model non-ground floors.

The fire is modeled using a cellular automata, similar to the one described in [1] (except that we do not consider the effects of air flow). The fire model represents every floor of the building as a single layer. Each layer consists of 172×144 cells with a cell resolution of approximately 36×26 cm. To simplify things, each cell can be in one of three states: ‘empty’, ‘unburned’, or ‘burning’. Generally, a floor is made of empty cells, except for rooms and corridors which are represented initially as unburned cells. Fire spreads according to a probability p_f , causing cells to change their state from ‘unburned’ to ‘burning’. In order to enable fire to spread from one floor to another, we use an intermediate layer between two floors which consists mostly of empty cells, except for the areas covered by the staircases. Figure 2 illustrates the various layers of the cellular automaton.



Fig. 2 Illustration of the cellular automaton layers of a two-story building model: the ground floor (*left*) and the first floor (*right*) are connected by a middle layer (*center*) which connects the areas of the staircases in both floors. Empty cells are *light gray*, unburned cells are *dark grey*, and burned cells are shown in *red*

2.2 Knowledge and Communication

Agents are considered to have full knowledge about the building layout, i.e., they know which way will lead them to the exit. This assumption is reasonable, as the building that we consider is an office building and the people in the building are assumed to work there and thus familiar with the location and the layout of the building. Knowledge about the building is modeled by using a graph representation of the building layout. In this graph, vertices represent rooms, corridors, and staircases that are connected to each other by doors. A door is represented by an edge, connecting two vertices with another. A special vertex in this graph is used to represent the ‘outside’ of the building. This special vertex is connected to the network of rooms and corridors by a special type of door, i.e., an exit.

From a routing perspective, the objective of an agent is to find the shortest path that leads out of the building (i.e., shortest path from current vertex to the ‘outside’ vertex). If an agent realizes that a particular path is blocked (i.e., by spotting fire), it updates its own knowledge about the building: doors which are not accessible any longer will be marked. This is done by setting the weight of the corresponding edge to a very large value. Notice that the edge is not removed if a door becomes inaccessible. This would lead to a disconnected graph and agents may not be able to find an exit path any longer. Instead, a large weight is used to indicate that a certain door should be avoided at all costs. However, if there is no other way, agents will ultimately choose to use a path that is burning. In our simulation, such a desperate decision will most likely result in the death of the agent.

Agents can communicate with each other and propagate information regarding the inaccessibility of doors. For this purpose, agents will notify all other agents that are within their social space [2] (i.e., within a distance of approximately 3.6 m) about their knowledge about inaccessible doors. Technically, this is done by sending messages from one agent to another with information about all inaccessible doors. This will cause knowledge about accessibility to converge among agents that are within reach. Agents who are not within reach will not be informed. This avoids

unrealistic spread of information among the agent population. However, if the agent population is uniformly distributed across the building, then information can propagate quickly across the entire population.

3 Guidance System

In this paper we assume a building that is equipped with a dynamic guidance system, i.e., the guidance system can change the evacuation route at any time. The exact implementation of such a guidance system is not subject of discussion in this paper. However, various possible ways can be envisioned how such a system could be implemented. For example, one implementation could involve electronic signs indicating the right direction by displaying arrows. These signs could be placed at the walls of the various rooms and hallways of a building. Another possible implementation could involve LED indicators that are embedded in the floor, similar to the way how LEDs indicate the direction to the nearest emergency exit in airplanes. Such solutions are commercially available (e.g., Pathfinder by Lightstep Technologies¹).

Regardless how the actual guidance system is realized (e.g., by LEDs or displays), there has to be a control system that decides which direction to indicate in which part of the building. In addition, the indicated direction needs to be updated as the emergency situation evolves. We thus assume that the building is equipped with suitable sensors and a data-driven guidance system. By that we mean, that the various sensors in the building provide real-time information about possible fires to the guidance system. This information may include temperature measurement and smoke detector measurements. The control system of the guidance can then use this information to devise the most appropriate evacuation path.

Although the guidance system can react dynamically to new sensor data it cannot anticipate how a situation will unfold in the near future. In other words, the guidance system that we are considering here is a zero look-ahead guidance system. In the simulation model, we realize this guidance system by considering a network of guidance lines (these could be represented by actual LEDs embedded in the floor, for instance). Based on this network of guidance lines, the system can determine the shortest path to the exit on the ground floor from any location within the building. The network is updated dynamically as the situation advances. For example, if a particular doorway becomes inaccessible (due to fire spread), the guidance will update the evacuation routes (i.e., the direction indicated by the guidance lines). Evacuees that follow the guidance system are thus dynamically steered to the exit. Figure 3 illustrates the network of guidance lines used in our simulation model.

¹<http://www.lightsteptechnologies.com/pathfinder.asp>

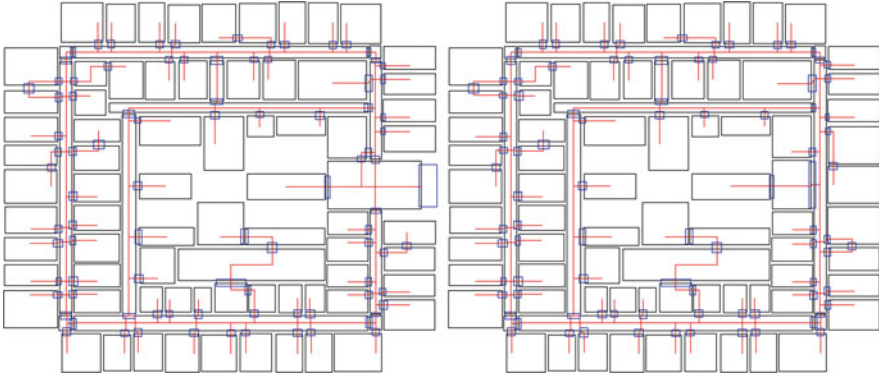


Fig. 3 Illustration of the guidance lines on the ground floor (*left*) and the first floor (*right*) as used by the guidance system. The *red lines* indicate the guidance lines. The *blue rectangles* represent the links between the various areas (e.g., room, corridor)

4 Experiments

4.1 Scenario 1: Base Scenario

The base scenario evaluates the general performance of the guidance system. For this purpose, we compare the survival rates when using the guidance system with the survival rates when the guidance system is not used. A random agent population is distributed uniformly across the building: at the beginning of the simulation there are exactly 2 agents in each room. The setup for a simulation run is concerned with (1) the initial location of the fire at the beginning of the simulation run and (2) whether or not the guidance system is used. The fire spreads with a probability of $p_f = 0.04$. A total of 10 simulation replications are performed for every setup. For evaluation, we consider the average survival rates when using/not using the guidance for all setups. In total, there are 167 different starting locations (i.e., rooms and corridors). In 63.7 % of cases, the survival rate has been significantly higher when using the guidance system with a confidence level of 95 %. There has been no case where the guidance system performed worse. These results are summarized in Figs. 4 and 5 that show a heat-map of the differences in survival rates (if significant) when using the guidance system for the ground floor and the first floor, respectively.

4.2 Scenario 2: Guidance Is Better

In the second scenario, we highlight the advantage of the guidance system, i.e., the ability to incorporate real-time sensor data in the routing process. For example, if a staircase becomes inaccessible due to the fire spread, the guidance can immediately



Fig. 4 Heat map indicating the difference in survival rates (if significant) on the ground floor, depending on the initial location of the fire. The numbers indicate how much better the guidance system performed (in %). Grey indicates that there has been no significant difference

react and change the evacuation route, saving valuable time. For this scenario, we assume that a fire breaks out near to Staircase 2 on the first floor and spreads with $p_f = 0.03$. This case is illustrated in Fig. 6: First, the evacuees will instinctively try to reach the closest staircase to reach the ground floor (see Fig. 6, top left). Initially, they do not know about the location of the fire. Second, by the time they reach the proximity of the staircase it becomes apparent that the staircase is not accessible. The evacuees thus decide to go back and try to reach Staircase 1 (see Fig. 6, top right). However, due to the time lost by trying to reach Staircase 2, the alternative staircase becomes inaccessible, too (see Fig. 6, bottom left and right).

The problem in this scenario is the fact that evacuees have no way of gathering information about the location of the fire in order to determine which evacuation route would be the most appropriate one. In contrast, the guidance system has the advantage of being able to use real-time sensor data to update the evacuation route any time. Figure 7 illustrates the same scenario when using the guidance system. Initially, the guidance system chooses the same route as illustrated in Fig. 6 (top left). However, once the fire spreads, the guidance system realizes that evacuation route becomes infeasible. As a consequence the guidance system chooses the alternative evacuation route (see Fig. 7, left). By the time the fire reaches the proximity of the



Fig. 5 Heat map indicating the difference in survival rates (if significant) on the first floor, depending on the initial location of the fire. The numbers indicate how much better the guidance system performed (in %). Grey indicates that there has been no significant difference

alternative staircase, the evacuees have already reached the staircase (see Fig. 7, right).

Although the guidance system initially choses the same evacuation route (guiding the evacuees towards the closest staircase), it realizes soon that this route is infeasible and updates the evacuation route accordingly. As a consequence, the evacuees can reach Staircase 1 in time before it would also become inaccessible. The better performance of the guidance is clearly due to the information advantage. Based on 10 simulation runs of this scenario, the average survival rate is 94.5 % when using the guidance. This is in stark contrast to an average survival rate of 7.6 % if the guidance is not used.

4.3 Scenario 3: Guidance Is Worse

In the third scenario, we highlight the problem with a reactive guidance system. Although the guidance system can incorporate real-time sensor data into the routing process it does not have any look ahead (as this would require simulation). As a consequence, the guidance system cannot anticipate how the fire is likely to spread within the near future. It is therefore possible, that the guidance system suggests



Fig. 6 Illustration of scenario 2 (without using the guidance system)

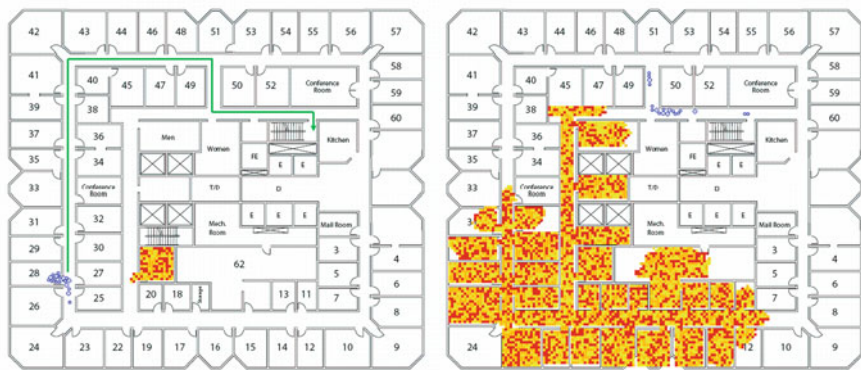


Fig. 7 Illustration of scenario 2 (when using the guidance system)

an evacuation route which, at some time, turns out to be inaccessible. Once this happens, the guidance system needs to recalculate the evacuation route. As a result, the agents lost valuable time due to the lack of foresight of the guidance system.



Fig. 8 Illustration of scenario 3 (when using the guidance system)

Such a case is illustrated in Fig. 8. For this scenario, the fire spread with a probability of $p_f = 0.01$. First, the guidance system will chose an evacuation route towards the staircase that is closer to the exit (see Fig. 8, top left). As the fire develops, this staircase becomes inaccessible and the guidance system directs the evacuees towards the other staircase (see Fig. 8, top right). The evacuees reach the staircase and use to reach the ground floor (see Fig. 8, bottom left). However, by the time the evacuees reach the proximity of the exit, they get trapped because the fire has spread via the other staircase to the ground floor and reaches the exit before the evacuees do (see Fig. 8, bottom right).

The problem in this scenario is the lack of foresight by the guidance system. Initially the guidance system is directing the evacuees towards Staircase 1. By the time the evacuees reach the proximity of this staircase, the fire has almost blocked the access to the staircase. Once this happens, the guidance system will devise an alternative evacuation route. However, due to the time lost, the evacuees will not be able to make it to the exit in time. Based on 10 simulation runs of this scenario, the average survival rate is 45.5 % when using the guidance. However, if the guidance is not used, the evacuees attempt to reach Staircase 2 from the start (thus saving time) which results in an average survival rate of 97.5 %.

5 Related Work

Various works have addressed the issue of smart building evacuation. These works typically aim at optimizing the route to the exit. For example, the fuzzy-based approach, described in [5], aims at optimizing directional indicators (i.e., arrows) in a simple two-dimensional environment. However, this approach considers an oversimplified scenario which does not consider the effects of crowds. In addition, a single scenario is considered only. In contrast, other works that use ant colony optimization [6] and particle swarm optimization [7] have also been applied to building evacuation problems and explicitly consider the behaviour of crowds by using agent-based simulation. In general, agent-based simulation has been used in many works concerned with building evacuation.

However, all these approaches do not use simulation as part of the routing algorithm and thus suffer from the same problem that the zero look-ahead guidance system, described in this paper, is suffering from: the lack of foresight. While ant colony optimization and particle swarm optimization (among many other heuristics that can be found in the literature) are certainly valid and effective in optimizing the evacuation path, they cannot anticipate what is going to happen next. Simulation is required in order to anticipate how the fire will likely spread across the building. Based on this knowledge, a truly smart guidance system would be able to plan a better evacuation route which will be more robust.

The system concept, described in this paper, is similar to the Regal Evacuation Guidance System used in the Pentagon for planning evacuation [11]. However, while the system concept is similar in its objectives, the methods and tools used to construct the system differ significantly. The simulation software describe here, for example, uses advanced agent models capable of replicating human reasoning, emotion and non-optimal (human-like) behaviour. This is extremely critical; researchers have long argued that evacuation models must consider the non-physical as well as the physical aspects. For example, crowd dynamics in the context of emergencies [8] has been extensively studied in [9]. Furthermore, a motivation of the need for a physical and non-physical approach can be found in [10].

6 Conclusions and Future Work

In this paper we have shown how guidance systems, that use real-time sensor data, can make a significant difference during a building evacuation. However, we have also highlighted the limitations of a purely reactive guidance system and the danger that lies within the limited abilities of such a system. Although using a guidance system will generally result in a higher average survival rate, there can be situations in which a guidance system that lacks foresight will make wrong decisions. The ability to anticipate the development of the fire in the near future is a crucial

capability that a smart guidance system needs to support in order to avoid making fatal decisions.

The most suitable way of forecasting the fire spread in the near future is by means of simulations. Once a simulation is available, a symbiotic simulation system can be used to devise a better evacuation route. Symbiotic simulation [3, 4] is a paradigm in which a physical system and a simulation system are closely coupled by sensors and actuators. This relationship is often mutually beneficial. The simulation system benefits from real-time sensor data which makes it possible to perform high-fidelity simulations of the physical system. The physical system, on the other hand, benefits from the outcome of what-if analyses conducted by the simulation system. The purpose of such a what-if analysis depends on the application.

Our future work will be concerned with a smart building application where the guidance system is based on a symbiotic simulation system. The symbiotic simulation system in this application will be concerned with a decision making problem: which is the best evacuation path at a particular time in a specific part of the building? The symbiotic simulation system is capable of evaluating alternative routes (e.g., what-if scenarios) by means of simulation as the egress event progresses. The ability of a symbiotic simulation system to simulate many possible what-if scenarios, enable the guidance system to analyze various possible solutions and select the one which provides the best performance (in terms of evacuation time or safety, for example).

Having a symbiotic simulation-based guidance system would avoid the problems with zero look-ahead guidance systems such as the one described in Sect. 4.3. The guidance system could perform simulations in real-time and thus anticipate how the situation in the building may develop. The guidance system would still have to take into account the various sources of uncertainty. For example, this includes uncertainty in sensor data, uncertainty about how fire/smoke spreads across the building, and uncertainty due to unpredictable behavior of crowds. Nevertheless, a symbiotic simulation-based guidance system can optimize the evacuation route within the limitations posed by these uncertainties. Such a solution can be expected to produce more robust results than any purely reactive guidance system.

Acknowledgements This research has been funded by the NTU SU Grant M58020019 and (AcRF) Tier1 Grant RG10/10(M52020103)

References

1. D.I. Curiac, O. Baniias, C. Volosencu, and D. Pescaru, "Cellular Automata Based Simulation for Smoke and Fire Spreading in Large Buildings". In Proceedings of the International Conference on Development, Energy, Environment, Economics, pages 89–94, 2010.
2. E.T. Hall, "The Hidden Dimension". Bantam Doubleday Dell Publishing Group, 1966.
3. R. Fujimoto, D. Lunceford, E. Page, and A. M. Uhrmacher, "Grand challenges for modeling and simulation: Dagstuhl report". Technical Report 350, Schloss Dagstuhl. Seminar No 02351, August 2002.

4. H. Aydt, S.J. Turner, W. Cai, and M.Y.H. Low, "Symbiotic simulation systems: An extended definition motivated by symbiosis in biology". In Proceedings of the 22nd Workshop on Principles of Advanced and Distributed Simulation, pages 109–116, 2008.
5. C.Y. Chen, "A Fuzzy-based Approach for Smart Building Evacuation Modeling". In Proceedings of the Fourth Conference on Innovative Computing, Information, and Control, pages 1200–1203, 2009.
6. A. Rahman and A. K. Mahmood, "Feasible Route Determination Using Ant Colony Optimization in Evacuation Planning". In Proceedings of the 5th Student Conference on Research and Development, pages 1–6, 2007.
7. B. Yang, C. Wang, H. Huang and L. Li, "A Multi-Agent and PSO Based Simulation for Human Behavior in Emergency Evacuation". In Proceedings of the International Conference on Computational Intelligence and Security, pages 296–300, 2007.
8. A.U.K. Wagouma, A. Seyfrieda, and S. Holl, "Modelling dynamic route choice of pedestrians to assess the criticality of building evacuation". Submitted to the Safety Science Journal. Preprint available online: <http://arxiv.org/abs/1103.4080> (last accessed: 2012-05-07).
9. Pedestrian Dynamics, Juelich Supercomputing Centre (JSC). URL: <http://www2.fz-juelich.de/jsc/appliedmath/ped/> (last accessed: 2012-05-07)
10. Jonathan Sime, "Crowd psychology and engineering". Safety Science, vol. 21 (1), pages 1–14, 1995.
11. Regal Decision Systems, Inc. URL: <http://www.regaldecision.com/EGS.php> (last accessed: 2012-05-07)

The Development and Calibration of an Agent-Based Microsimulation Model for Vehicle-Pedestrian Interaction

Rahul Jobanputra and Marianne Vanderschuren

Abstract With the increases in computer processing power and advances in programming skills, an array of transportation and urban planning computer models are now available to the profession. They are extensively used in developed nations to model complex transport scenarios and interactions. Models vary from a macroscopic level, which focus on the system as a whole and a higher aggregation level, to more complex microscopic tools, which allow the simulation of individual road users and behaviour to obtain more realistic representations at a local/street level.

Microsimulation models, to varying degrees, give researchers and practitioners the ability to analyse the effectiveness of interventions on a disaggregated level, as individual vehicles and/or pedestrians are simulated in detail as they move through the road network with the goal of reaching their destination by the most cost effective or shortest route. The interaction of road users in microsimulation models is refined via parameter settings of, for instance, compliance levels (i.e. attitude to risk), walking speeds, aggression and awareness levels, etc. Default values of these parameters are incorporated in the software at levels set by the vendors. These values affect outcomes of modelled scenarios and may not replicate actual road user behaviour. Calibration of the model is, therefore, vital to match observed conditions and to produce realistic outputs.

However, the complexity of microsimulation models and the large number of parameters that require specification means that calibration is a complex and iterative process. Furthermore, direct measurement of parameter values is very difficult because many of them represent subtle features that are hard to isolate and, because of the extensive amount of data collection required at a disaggregate level.

R. Jobanputra (✉) • M. Vanderschuren
Centre for Transport Studies, Department of Civil Engineering, University of Cape Town,
Private Bag X3, Rondebosch 7701, South Africa
e-mail: rahul.jobanputra@uct.ac.za

This paper describes the development of a simulation model and the evaluation of parameters for a study of road user interaction for a local arterial road in Cape Town, South Africa, using a commercially available package, Paramics. Results are compared to values obtained using default settings, which are drawn from developed world contexts. Visual reviews of the calibrated network reveal that, although the software allows flexible modelling of shared vehicles and pedestrian space, it does not replicate observed local road user behaviour of some vehicles and pedestrians at crossings. Given this finding, an investigation into the possibility of modifying appropriate parameters is also presented.

Keywords Microscopic simulation • Model calibration • Model development • Vehicle-pedestrian interaction

1 Introduction

With the increases in computer processing power and advances in programming skills, an array of transportation and urban planning computer models from a macroscopic to a microscopic scale of evaluation are now available to the profession. They are extensively used in developed nations to model complex transport scenarios and interactions.

The advances have led to the development of many commercial microscopic models, which provide the ability to analyse the effectiveness of interventions on a disaggregated level, as individual vehicles and/or pedestrians are simulated in detail as they move through the road network with the goal of reaching their destination by the most cost effective or shortest route for varying infrastructure settings [6]. These types of models are gaining recognition as methods for assessing urban planning strategies, as well as, measuring and predicting safety and, offer the potential for proactive safety analysis for all road users rather than just the analysis of transportation efficiency.

The majority of models are based on the principles of either: Cellular Automata, Social Force or are Agent-based models [6]. In addition, models based on the use of Geographical Information Systems and regression techniques such as: Space Syntax, are also commercially used for urban space design. However, most researchers agree that multi-agent simulations are the appropriate technique for pedestrian modelling [2, 4]. Apart from the microscopic and dynamic modelling they offer, the fact that pedestrians (agents), may be given a variety of vision, cognition and learning capabilities, renders these systems far more advantageous than ordinary simulation environments. Moreover, the systems may accept complex and very detailed rules and their properties are in full accordance with those of discrete choice models [8].

The interaction between road users in agent-based microsimulation models is refined via parameter settings of, for instance, compliance levels (i.e. attitude to risk), walking speeds, and aggression and awareness levels. Default values of these

parameters are incorporated in the software at levels set by the developers. They affect outcomes of modelled scenarios for key criteria such as volumes and speeds, and may not replicate actual road user behaviour. Calibration of the model is, therefore, vital to match observed conditions and to produce realistic outputs.

However, the complexity of microsimulation models and the large number of parameters that require specification means that the calibration exercise is a complex and iterative process. Furthermore, direct measurement of parameter values is very difficult because many of them represent subtle features that are hard to isolate and, because of the extensive amount of data collection required at a disaggregate level.

The literature cites several studies with the primary goal of providing a robust calibration method. Early research work focussed on search algorithms for calibration based on a single criterion. Multi-criteria calibration has been proposed as an improvement to this by a number of researchers (for example [1, 7, 11]) but, it depends on relative weighting of factors. Research is on-going into methods of removing any biasing of factors using this method. Because of this, and the complexities identified above, many researchers and practitioners reduce the number of parameters to a more manageable level, based on heuristics and on a trial and error basis and calibrate for acceptable values of either speed and volume.

This paper describes the development of a simulation model and the evaluation of parameters for a study of road user interaction for a local arterial road in Cape Town, South Africa, using a commercially available package, Paramics. Results are compared to values obtained using default settings, which are drawn from developed world contexts. Visual reviews of the calibrated network reveal that, although the software allows flexible modelling of shared vehicles and pedestrian space, it does not replicate observed local road user behaviour of some vehicles and pedestrians at crossings. Given this finding, an investigation into the possibility of modifying appropriate parameters is also presented.

2 Study Area/Base Model Development

The basic principle of transport simulation models is to create a model of the road network in which drivers move with a single-minded goal of reaching their destination as efficiently as possible, whilst obeying the rules of the road (as set by the model) and interacting safely with other vehicles in the network. Agent-based transport models extend this principle further by applying similar goals via different rules for pedestrians.

Building a model begins with the scope of the study and its area followed by the collection of fundamental data either from the field or from available databases. This includes a number of key inputs, such as geometry, demand data, road user control data etc. In addition accurate (and normal) calibration and validation data is usually necessary to populate the adjustable parameters which help the model to replicate observed conditions.

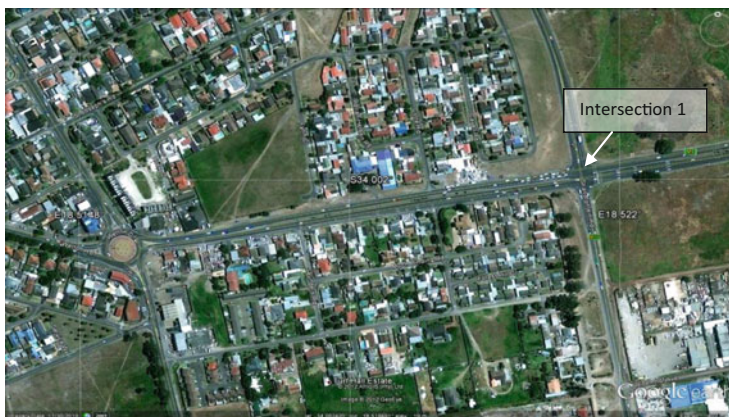


Fig. 1 Study area (Source: Google Earth)

A Google Earth view of the local arterial in Cape Town used for the study is shown in Fig. 1. The main corridor is approximately 600 m in length and consists of dual and three lane carriageways. A free-flow roundabout and a signalised intersection (Intersection 1) frame the corridor. There are no posted speed limit signs in the vicinity and, as can be seen, the area borders the fringes of two separate settlements. Pedestrian footpaths are reasonably well provided at Intersection 1 and the roundabout and haphazardly elsewhere.

Statistics collected and published by the City of Cape Town over the last few years indicate that this particular stretch of road has been the scene of many crashes, with a large proportion of pedestrian fatalities and injuries. An investigation of this area during the peak hours indicates that there are large volumes of pedestrians present, mainly accessing public transportation at formal stops located along the sides of the main road, or via randomly stopping para-transit operations. There is clearly a significant amount of vehicle –pedestrian interaction, both at Intersection 1 (on the eastern side) and at many mid-block crossing points which is germane to this study. However, the reasons for this crash statistic are not immediately apparent as the provision of facilities is not dissimilar to adjacent areas.

Apart from the normal/key data required for model building, as stated, calibration data, for example, vehicle and pedestrian speeds, travel times and, where applicable, queue lengths were also collected. Vehicle speeds were collected from a combination of a GPS enabled smart phone application and in-vehicle video based GPS vehicle tracking systems. Pedestrian data were captured manually and by use of manual video recordings.

An essential step in the development of the working model is to carry out an error correction step so that the calibration process does not result in parameters that are distorted by network coding errors.

Table 1 Model calibration criteria

Criteria and measures	Calibration acceptance targets
Hourly flows, model versus observed	
Individual link flows	
Within 15 %, for 700 vph < flow < 2700 vph	>85 % of cases
Within 100 vph, for flow < 700 vph	>85 % of cases
Within 400 vph, for flow > 2,700 vph	>85 % of cases
Sum of all link flows	Within 5 % of sum of all link counts
GEH ^a statistic < 5 for individual link flows	>85 % of cases
GEH statistic for sum of all link flows	GEH < 4 for all link counts
Travel times, model versus observed	
Journey times network within 15 %	>85 % of cases
Visual audits	
Individual Link speeds	
Acceptable speed-flow relationship	To analyst’s satisfaction
Bottlenecks	
Acceptable queuing	

Source: [12]

^aThe GEH statistic is computed as follows: $GEH = \sqrt{\frac{2(V-E)^2}{(V+E)}}$ where E is the model estimated volume and V is the count

3 Calibration Approach

Because no single model can be expected to contain all the necessary variables that affect real-world road user conditions and, the fact that models can only approximate possible road user scenarios, it is important to set initial acceptability criteria as there is a point where time and effort spent on improvements only results in small changes in accuracy. Generally for vehicles, calibration targets are limited to the consideration of delay, travel time and volume. Fairly typically accepted target results are indicated in Table 1 [12]. By extension, similar values can be accepted for pedestrian flows.

Every simulation model provides a set of user-adjustable, un-calibrated parameters inherent to the model, for the purpose of calibrating the model to local conditions. For the convenience of the analyst, software developers provide suggested default values for these parameters. Values are usually derived from field measurements from the place of origin of the software or reference data. As already indicated, because of onerous data collection requirements (as traffic conditions and user behaviours can vary significantly over a period of time), difficult to measure parameters (e.g. behavioural), as well as the potential adjustment of hundreds of combinations of parameters, it could be tempting to use this default set of values as an approximation. However, the sources of default data are normally from developed nations and thus their application to any areas with different user characteristics should result in problematic simulations. Under some circumstances the default

values may be able to produce reasonable results for the test case. The question is: will they for this study and, if not, just how much of a difference would there be in the outputs using a calibrated and default set of parameters and, if the result is that, which parameters need adjustment, how and by how much. This question is addressed in the sections following.

4 Trial with Default Parameter Set

The default set of parameters within software packages consists of those which affect the main categories to be calibrated: capacity, route choice or overall system performance. Actual definitions of parameters, their values and effects obviously vary between packages (see for example [3]) but they all contribute in some way to the outcome.

The feasibility test to establish whether using the default set of parameters will produce an acceptable result consists of two steps: multiple runs of the model with default values and subsequent comparison to collected field data.

As is common in other simulation packages, Paramics uses a random number generator to provide a stochastically generated simulation pattern in terms of vehicle and pedestrian loading and path. Aggregated output from many runs will, therefore, have a certain distribution of minimum and maximum values. Statistically, the number of repetitions required to ensure that all possible cases are simulated can be determined by the following equation:

$$c = 2 * t_{(1-\alpha/2), N-1} \frac{s}{\sqrt{N}}$$

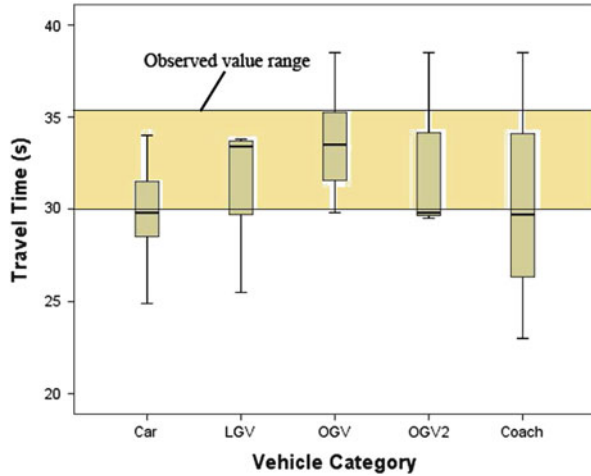
Where: $C = 1 - \text{Confidence Level}$ (for example, for a 90 % confidence level, $C = 0.1$); $t_{(1-\alpha/2), N-1}$ is a t-statistic value for the probability of a two-sided error summing to alpha with $N-1$ ° of freedom; S is the standard deviation and N is the number of repetitions required [5].

In this case, where travel time or speed is pertinent, a relatively high confidence limit can be used. For a 95 % confidence limit and confidence interval of 2, eight repetitions are calculated to be the minimum number required.

Outputs from the software that could be used for comparison with relatively easy to collect field results include: queues, speeds, travel times and volumes.

Acceptability criteria performed by using a box plot of outputs for travel time and comparison of link volumes using the GEH statistic showed that: in comparison to the range of observed travel times obtained for a car, there is a good fit between these and simulated values for all vehicle types (See Fig. 2), but the GEH statistic for two out of three volume cases proved to be unacceptable (i.e. greater than a value of 5).

Fig. 2 Comparison of simulated travel time and field values for the default parameter set



5 Calibration by Adjusting Default Values

Given the number of potential parameters that could be adjusted, and to use a practical approach, available parameters need to be divided into two categories: parameters about which the analyst is reasonably certain about and does not wish to adjust and parameters which the analyst is less certain about and wishes to adjust. Observed data serves as non-adjustable parameters leaving the adjustable parameters to a minimum – usually those that are related to road user behaviour and vehicle characteristics which are difficult to collect from the field. The latter can then be sub-divided into a set that impacts capacity and those that impact route choice.

From the range of parameters for vehicles and pedestrians requiring specification, key parameters were determined by plotting output values in histogram or X-Y format. The ranges of parameter values used for this exercise were determined from available literature or heuristics (see Figs. 3 and 4).

For vehicles, the key parameters were found to be Mean Target Headway (defined in time units as the gap between a leading and following vehicle; related to ‘aggression’ of drivers), Mean Driver Reaction Time (also measured in time units and defines the ‘awareness’ of drivers) and the assignment matrix type. Whereas, for pedestrians, blocking compliance levels (i.e. levels of jaywalking), the area they are deemed to scan prior to crossing (termed the scan area angle in Paramics) and the allowable base speed deviation were found to be the most significant parameters.

It is apparent from the Figs. 3 and 4 that possible combinations of key parameter sets and the ranges of their values can be significant. Acceptable values and combinations can be obtained by comparison of multiple runs to calibration field data through heuristics, trial and error or, via a systematic elimination process

Fig. 3 Effect of mean target headway (MTH) on vehicle travel time

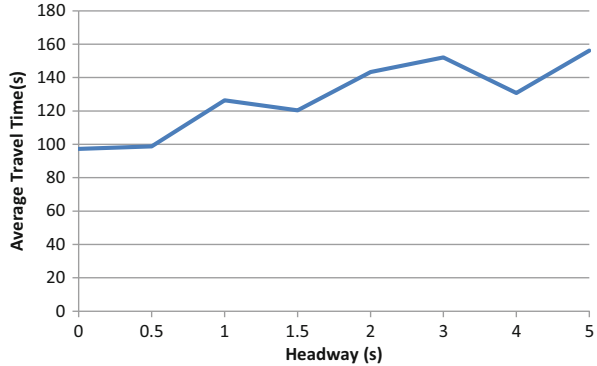
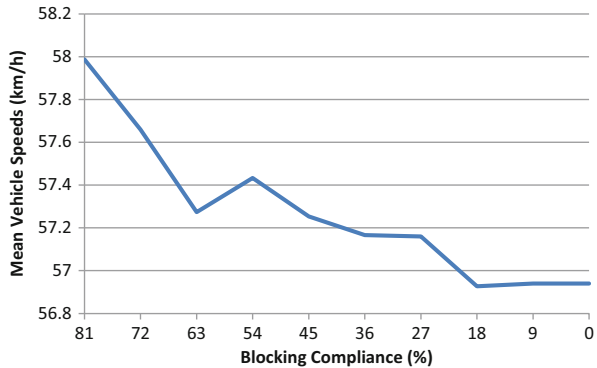


Fig. 4 Effect of pedestrian blocking compliance on mean vehicle speed



of individual and combinations of parameters followed by established statistical optimisation methods means, such as genetic algorithms.

For this calibration process, it was found that a small combination of parameters – Mean Target Headway, Matrix Turning Level, Familiarity for vehicles and Base Speed Deviations for pedestrians – provided outputs that in travel times that were within the band of observed values and GEH values of less than 5 for all link and pedestrian volumes.

It is suggested by Bonsall et al. [3], that ‘... the values of several key parameter values with implicit speed, volume and safety relevance have been based on informed guesswork rather than observation’. Furthermore, it is stated that some empirically grounded parameter values might be generalised to situations other than those from which they were originally determined thereby making them contextually irrelevant. The results of this exercise indicate that the transferability of some default values of parameters is, indeed, questionable but that some results for a network of this complexity may be acceptable.

Fig. 5 Example of mid-block crossing



6 Simulation Software Issues and Possible Modifications

The final step of the calibration procedure is to carry out a visual check of the simulations to ensure that there are no unrealistic vehicle or pedestrian movements. For all simulations with the calibrated set of parameters, despite the fact that the outputs produced performances that reasonably matched field observations for travel time and volumes, it was found that pedestrian and driver behaviour did not match observed behaviour. Critically, this discrepancy occurred at points where pedestrians and vehicles interacted. Jaywalking is prevalent in South Africa (despite regulations against it, see for example Fig. 5) and therefore, the model allowed mid-block crossing, shared spaces at intersections and a level of non-compliant crossing at the signalised intersection. A visual inspection of the animations indicated that a proportion of pedestrians were crossing randomly without observing ‘normal’ gap criteria and that for these pedestrians, the software forced vehicles to give way to pedestrians provided they fulfil defined visibility criteria and they were already on shared space (there are also anti-collision constraints which specify that two entities cannot occupy the same position at the same time [9]). Clearly, in reality this is what actually happens in some instances. However, usually, on roads such as the one presented in Fig. 1 pedestrians may stray onto the road and then stop between lanes or carriageways to make their manoeuvre.

The developers of Paramics have made it possible to specify shared road user space (i.e. where the space is used by both vehicles and pedestrians) – ‘*shared aggressive*’ and ‘*shared courtesy*’. In aggressive shared space agents and vehicles will try with equal effort to move forward avoiding each other, similar to an opposed right turn with traffic sneaking through crossing pedestrians. In courtesy shared space vehicles will avoid entering the shared space until all agents are outside their field of view, similar to a mid-block un-signalised pedestrian crossing [9]. Furthermore, at signalised intersections, modellers can set up a ‘*blocking region*’ which forces compliant pedestrians to cross at the appropriate signal phases.

For this study, specifically at the exits to signalised legs in Intersection 1, a 'shared aggressive' space was found to be the best approximation of field observation of behaviour (and it is actually how exits are used). Despite this, as stated, pedestrian and vehicle behaviour was not consistent with observed behaviour, especially pedestrian crossing behaviour.

The developers have also provided the possibility to modify many of the programs variables by user modification of some algorithms via their Programmer module. A detailed examination of this possibility and subsequent liaison with the developers revealed that, although it is possible to modify the majority of vehicular variables, it is not possible to modify the agent side of the program. Due to this interaction, the developers were made aware of this behavioural discrepancy. They have subsequently begun to modify their software to incorporate a gap-acceptance criterion for pedestrians (similar to the vehicular gap-acceptance criteria). This modification has been demonstrated via their on-line webinars but has yet to be released commercially.

7 Study Synthesis and Conclusion

A review of the literature on the current state and practices in transportation modelling revealed that of the array of transportation models available to the profession, an agent-based model would be the most suitable tool to carry out an investigation of vehicle-pedestrian interaction in a mixed use situation. To varying degrees and through the use of different techniques, commercially available software can simulate this interaction. This study was undertaken using the Paramics suite of programs.

The software was used to develop a network in Cape Town which has a dismal safety record particularly concerning the number of pedestrians affected. It, therefore, represents an area where there is significant road user interaction and where this interaction could be investigated to possibly provide clues as to why there is a safety issue there and whether the software is capable of realistically simulating a particular developing world situation.

In the development of the model, it was recognised that the default set of parameters provided, which affect outcomes, may not be suitable for the network being studied. The calibration process undertaken identified that this was the case. This outcome was not unpredictable, as the network studied is relatively short, unconstrained, has a homogenous pattern of travel (which is normally not the case for many developing nations) and has few interconnections (i.e. is more of a corridor).

Visual reviews of the output animations revealed that, despite adequate calibration, the behaviour of some pedestrians and vehicles did not match observed/known behaviour. Possible modifications to the shared surface specifications and to the program's algorithms were investigated to no avail. From this it is concluded that determining criteria like the 'gap acceptance' criteria usually applied to vehicles

needs to be provided for pedestrians and with this their behaviour may be more in keeping with the realities here. The developers of the software have undertaken to revise their pedestrian module to modify pedestrian behaviour. A trial version was launched earlier this year but, at the time of writing, it has yet to be fully developed.

It is quite apparent from this study that despite undertaking reasonable numerical calibration, it is vital that a visual check of the simulation output is also performed. Given the many uses of microsimulation models, for instance in the design of urban spaces and for safety analysis (which is becoming prevalent), the consequences of not carrying out adequate visual checks could be far reaching.

References

1. Balakrishna, R., Antoniou, C., Ben-Akiva, M., Koutsopoulos, H.N., and Wen, Y. 2007. Calibration of microscopic traffic simulation models. *Transportation Research Record: No.1999*, pp. 198–207.
2. Bierlaire, M., Antonini, G. & Weber, M., 2003. Behavioural Dynamics for pedestrians. In K. Axhausen, ed. *Moving through nets: The physical and social dimensions of travel*. Elsevier.
3. Bonsall, P., Lui, R. & Young, W., 2005. Modelling Safety-Related driving behaviour – impact of parameter values. *Transportation Research Part A*, (39), pp.425–44.
4. Dijkstra, J. & Timmermans, H., 2002. Towards a multi-agent model for visualizing simulated user behaviour to support the assessment of design performance. *Automation in Construction*, pp.135–45.
5. FHWA, 2004. *Traffic Analysis Toolbox Volume III: Guidelines for Applying Traffic Microsimulation Modelling Software*. McLean, VA: Turner-Fairbank Highway Research Centre US Department of Transportation Federal Highway Administration.
6. Harney, D., 2002. *Pedestrian Modelling: Current Methods and Future Directions*. Road and Transport Research.
7. Ma, J., Dong, H. & Zhang, H.M., 2007. Calibration of Microsimulation with heuristic optimisation methods. *Transportation Research Record*, pp.208–17.
8. Papadimitriou, E., Yannis, G. & Golias, J., 2009. A critical assessment of pedestrian behaviour models. *Transportation Research Part F*, (12), pp.242–55.
9. Quadstone, 2011. Paramics UAF version 1.3.1 On-line active help file. [Online] [Accessed April 2012].
10. Sykes, P., 2010. *Traffic Simulation with Paramics*. In J. Barcelo, ed. *Fundamentals of Traffic Simulation*. Barcelona: Springer. pp.131–72.
11. Toledo, T., Ben-Akiva, M., Darda, D., Jha, M., Koutsopoulos, H. 2004. Calibration of Microscopic Simulation Models with Aggregate Data. *Transportation Research Record*, No. 1876, pp.10–19.
12. Wisconsin Department of Transport, 2002. *Freeway System Operational Assessment. Technical Report I-33 Paramics Calibration & Validation Guidelines (Draft)*. Milwaukee: Wisconsin Department of Transport.

The Effect of Integrating Travel Time

Tobias Kretz

Abstract This contribution demonstrates the potential gain for the quality of results in a simulation of pedestrians when estimated remaining travel time is considered as a determining factor for the movement of simulated pedestrians. This is done twice: once for a force-based model and once for a cellular automata-based model. The results show that for the (degree of realism of) simulation results it is more relevant if estimated remaining travel time is considered or not than which modeling technique is chosen – here force-based vs. cellular automata – which normally is considered to be the most basic choice of modeling approach.

Keywords Wayfinding • Navigation • Quickest path • Earliest arrival • Dynamic potential • Dynamic assignment

1 Introduction

Users of crowd simulation software tools have noted that these tools mostly produce a too high pedestrian density close to a corner when a large group of pedestrians has to walk around this corner compared to real people in the same situation [1]. This leads to considerably increased travel times of simulated pedestrians compared to real people as well as compared to travel times of simulated pedestrians on a straight path of the same length. The same authors express their conviction that real people on contrast organize smarter in such a situation. Real people do not insist to walk a short path, but rather accept a longer walking path in exchange for a moderate local density and therefore can maintain their walking speed and in final consequence achieve a smaller travel time, respectively a travel time which is only

T. Kretz (✉)
PTV Group, Haid-und-Neu-Straße 15, D-76131 Karlsruhe, Germany
e-mail: Tobias.Kretz@ptv.de

slightly increased compared to them walking a straight path with the same length. Concerning a first, qualitative empirical evidence, someone reading this article in an office in a busy CBD area can witness this behavior by looking out the window. For everyone with a less busy window view, YouTube can help [2].

Even if one had no empirical indications of human walking behavior in such a situation, it would be a good guess that people desire mostly to minimize their travel time and not their travel distance. After all traffic planning for road networks rests on the assumption that one of the most important factors – if not *the* most important one – for route choice of vehicle drivers is travel time and not route length. The same people who steer vehicles make up for a large share of pedestrians in most situations where pedestrians occur. They may move in different circumstances with different implications of their route and speed choices for their personal effort, but they are the same people.

2 Integrating Travel Time in(to) Models of Pedestrian Dynamics

As real people, when we are in a hurry and desire most to minimize time to arrival, we are faced with the problem that we do not know which direction will be the one that allows earliest arrival – imagine for example to walk through a busy train station while being late in time for the train. Even in retrospective when having arrived it is not always possible to tell if the arrival actually was the earliest possible or if along the path one of the many decisions for a movement direction was wrong with regard to minimizing travel time. This is not only a consequence of the complexity of the problem, but also simply of incomplete information.

Simulating pedestrians we are in a similar situation. If with given constraints for every point in time, every position, and every destination the exact remaining travel time was known for every type of pedestrian, it would in fact not be necessary to simulate anymore. For what would be the additional information one could gain from such a simulation? The simulation would be more or less a discrete representation or instance of the multi-dimensional field of remaining travel times. Furthermore such a simulation would show an optimal solution which most probably would not be a realistic one.

Therefore what is possible is to *estimate* a map of remaining travel times in each time step and make pedestrians choose their desired or preferred walking direction according to this map respectively field. The estimation process at first should model realistically the travel time estimation real people do about the direction options they have and second it should be self-consistent with the actual model of pedestrian dynamics in which the travel time estimation module is used.

This is not a simple task and as a consequence models of pedestrian dynamics usually set the direction of the shortest path as the main or preferred walking direction [3, 4]. However, in the last few years at least two such combined systems

of a remaining travel time estimation and its usage in a pedestrian simulation have been introduced. Both have in common that the travel time estimation (or delay time estimation) is first done for small areas and then numerically integrated to receive the field of remaining travel time from a spot to the destination, which then is used in the pedestrian model where it amends or replaces (the impact of) the field of remaining distance to destination (aka “static potential”).

The first model is the F.A.S.T. model [5–8]. The F.A.S.T. model has developed out of a cellular automata approach. It is arguable if it still is a cellular automata [9], however, the important property that the pedestrians move like chess figures on a regular grid is preserved, making the model both: very fast for execution [10] and rather coarse-grained in the results. A second property is that it is attractiveness of spots which are used in the computation for the next movement step. This distinguishes it from the Social Force Model, where the property which is directly calculated is acceleration (and locations follow via integration over time). The method to estimate travel times considers only the spatial distribution of pedestrians and not their dynamic movement properties¹ [11]. The method for numerical integration is the so called *variant 2* as introduced in [12]. Compared to the Euclidean metric – if a field of constant local distances or travel times is integrated – it includes some artifacts, but the way it is used in the pedestrian model reduces them largely and the computation time of *variant 2* is below the exact methods mentioned in the next paragraph. In this way a main intention of the F.A.S.T. model – having a very fast pedestrian simulation – is preserved, even when the travel time estimation module is active.

The second model is the Social Force Model [13, 14] respectively its implementation in PTV Viswalk [15, 16]. In this approach of a combination of a pedestrian dynamics model with a travel time estimation the velocity of a pedestrian is considered when it is estimated which delay time he will impose to another pedestrian in his surrounding [17].² For the numerical integration the Fast Iterative or Fast Marching Method is used. Either method – in case of distance computation – yields the nearly correct Euclidean distances [18–21]. In the Social Force Model the negative gradients of the resulting field of estimated remaining travel time are used as direction of the desired velocity of a pedestrian being located at the field’s corresponding position. Apart from that PTV Viswalk’s Social Force Model remains unchanged.

Both models have been used with their travel time estimation module in different use cases [22–27]. However, in this contribution it is not intended to solely demonstrate the effect of the usage of the field of remaining travel times, but to argue

¹Of course obstacles are also considered. Considering only them would be no big deal, as they are static. The field of remaining travel times would then be identical or at least very similar to the field of remaining distances. And it would only be necessary to compute it once in advance of the simulation. One of the difficulties of considering travel time is that the field has to be recalculated in every time step or at least frequently.

²Also see that paper for an extensive discussion of related work.

that the decision to use it or not is more important (i.e. has a greater effect) than the decision which basic modelling approach – force-based or cellular automata-based – is applied.

2.1 *Implications and Interpretation*

Normally this would be the place to define the math of the travel time estimation module(s). However, this has been done extensively before [11, 17]. Instead of a repetition this subsection discusses some implications of the method, i.e. it takes some interpretative steps.

It has been observed [28, 29] and sometimes criticized [30] that the Social Force Model (and most if not all of its variants) strictly superpose the repulsive forces of pedestrians. Superposition means that the effect of any pedestrian A on pedestrian B is absolutely independent of any other pedestrian in a scenario.

Superposition is easiest noticed for the Social Force Model due to the similarities with Newtonian Mechanics, however, if one thinks of superposition of *effects* not only forces, then many models with a different modeling approach are just as well superposing effects of pedestrians.

In physics superposition is so common that one might even wonder, how else a model should be constructed. One approach to the answer is to formulate the extreme opposite: “the effect of any pedestrian A_i onto a specific pedestrian B is depends on all other pedestrians A_j and their states”. This phrase is a concretion for (the simulation of) pedestrians of Sherif’s general statement on social systems: “the properties of any part are determined by its membership in the total functional system” [31] and it is a *holistic* position. Figure 1 shows a simple situation, where a superposition of effects does not yield a fully realistic effect and where therefore applying a holistic approach improves the results.

The module of travel time estimation by construction is a holistic approach. One single pedestrian either can have a negligible effect in one setting and a very large one in a different setting, depending on the distribution and dynamic properties of all other pedestrians (and obstacles) in the system, even if his position and dynamic properties are the same in both settings. Therefore the holistic travel time estimation module is an ideal supplement to the superposing force approach.

This line of argumentation shall not mislead to the conclusion that a holistic (concrete: travel time estimating) approach alone is sufficient or superior to a superposing (concrete: force-based) approach. There are situations which are better addressed with forces. Imagine for example in Fig. 1 that there are walls to the left and the right of the group of three pedestrians. Then the observer would be *forced* to slow down, even be *forced* to stop. This is better modeled with *forces*. The travel time estimation module then is not of much help, as it is there to compute a good walking direction. Confined between two walls there would be no more really good direction, but just the task to slow down and resolve the situation without collisions.

A different example which fits better for force-based modeling is when the density is high enough that each pedestrian is *forced* to go with the flow.

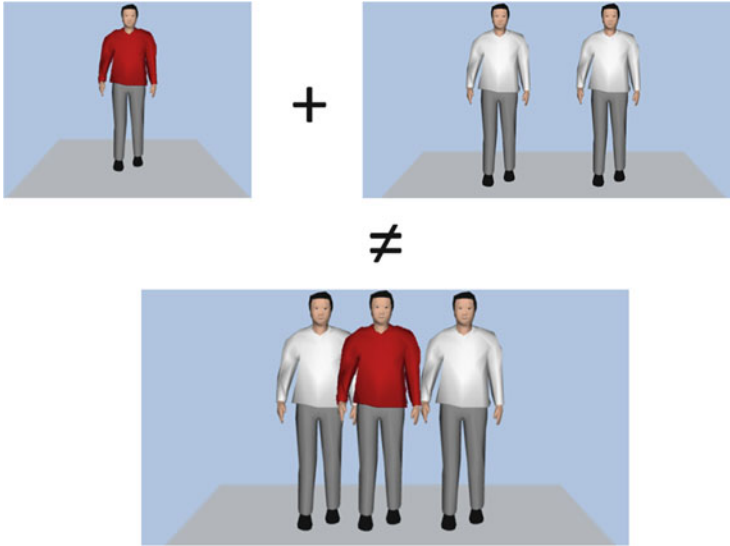


Fig. 1 An inequality with regard to the *effects* of the displayed situations. The idea is that the observer here basically wants to move straight on, but is faced with pedestrians walking the opposite direction. The two *white* pedestrians alone would eventually “channel” the observer to pass between them. In a force-based model their deviation triggering effects – at least for this very moment – would largely cancel. The *red* pedestrian alone would make the observer do a small detour to the left or to the right. However, together the three trigger the observer to do a larger detour to the left or to the right. The effect of all three – especially the red one – on the observer is determined by their membership in the total functional system

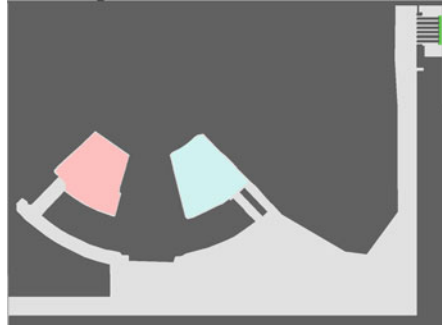
On the contrary scenarios which are only sparsely populated with individual pedestrians can be addressed with both approaches alike.

It is possible to some extent to use only one of the two approaches to model effects which are better modeled with the other approach (only forces and a simple determination of the desired walking direction as has been done usually or only a holistic approach and only a basic treatment of forces and accelerations [32]), but it makes life easier if both are applied, each for its own “natural” purpose.

With the emphasis in the previous lines it has already been insinuated: in a nutshell it appears that it is more natural and therefore easier to use *forces* to model behavior which is experienced to be *forced*.³ A main reason for this experience often is the small time available to react on a stimulus which does not allow for decent planning. On the contrary the holistic approach with its potentially unlimited range for strong interactions is better suited to model conscious planning, intentions or desires.

³Note that not in every language the same word is used for physical force and an (en)forced action. In German it is for example “Kraft” and “Zwang”.

Fig. 2 Scenario. Pedestrians can move on *light grey areas*, while *dark grey areas* denote obstacles. Pedestrians are set on the *light red* and *light blue areas* into the scenario and have to move to the *green area* at the *upper right*



3 The Effect of Integrating Travel Time into Models of Pedestrian Dynamics

3.1 Example 1

The scenario as shown in Fig. 2 is simulated both with the F.A.S.T. model and the Social Force Model of PTV Viswalk *without* applying their modules of estimated remaining travel time. The geometry mimics a simplified part of a stadium and its exterior. In the beginning two groups with each 5,000 pedestrians start their movement in the interior of the stadium.

The first observation is that it is possible to find parameters for both models with which the simulation results become very similar first for the total evacuation times, second for the average individual egress time and third for the spatial en gros distribution of pedestrians all throughout the simulation. If one has a detailed look at the trajectories, these look differently for both models. However, the idea here is demonstrating equivalence for someone interested in an overview, i.e. envisioned as “looking from high above on the whole scenario”.

These are the parameters that were used with the F.A.S.T. model: $k_S = 1.0$, $k_D = 0.0$, $k_I = k_W = 0.6$, $\mu = 0.0$; and these with PTV Viswalk: $\tau = 0.41$, $A_{soc,iso} = 1.0$, $B_{soc,iso} = 0.2$, $\lambda = 0.0$, $A_{soc,mean} = 0.4$, $B_{soc,mean} = 2.8$, $VD = 1.7$, $noise = 1.2$. The latter parameters are identical or close to the default values except for $A_{soc,iso}$, whose value has been clearly reduced to achieve the relatively high densities which occur in the F.A.S.T model with a comparable regularity.

In both cases the free (or desired or preferred) speeds have been (nearly) equally distributed between 1.2 and 2.0 m/s. As they are defined with different methods in both models, the distribution of free speeds is not exactly identical, however very similar. Note that it has been found to be crucial for the equivalence of the results of both approaches to have a very similar distribution of free speeds.

Someone familiar with one of the models will immediately see that neither the chosen parameters nor the free speeds are extreme in any way.

Table 1 Results statistics from 1,000 simulation runs with each of the models. “Av. Individual Egress Time” means the average of egress times of all pedestrians of one simulation run. Over 1,000 runs there are 1,000 averages of which the minimum, average, and maximum are displayed

	Av. individual egress time			Total evacuation time		
	Min.	Average \pm STD	Max.	Min.	Average \pm STD	Max.
F.A.S.T.	1,317.1	1,332.2 \pm 4.9	1,347.9	2,529.0	2,558.9 \pm 9.3	2,590.0
Viswalk	1,324.0	1,337.4 \pm 4.6	1,350.6	2,528.2	2,555.9 \pm 9.1	2,584.3

With these settings the individual egress and the total evacuation times result as shown in Table 1.

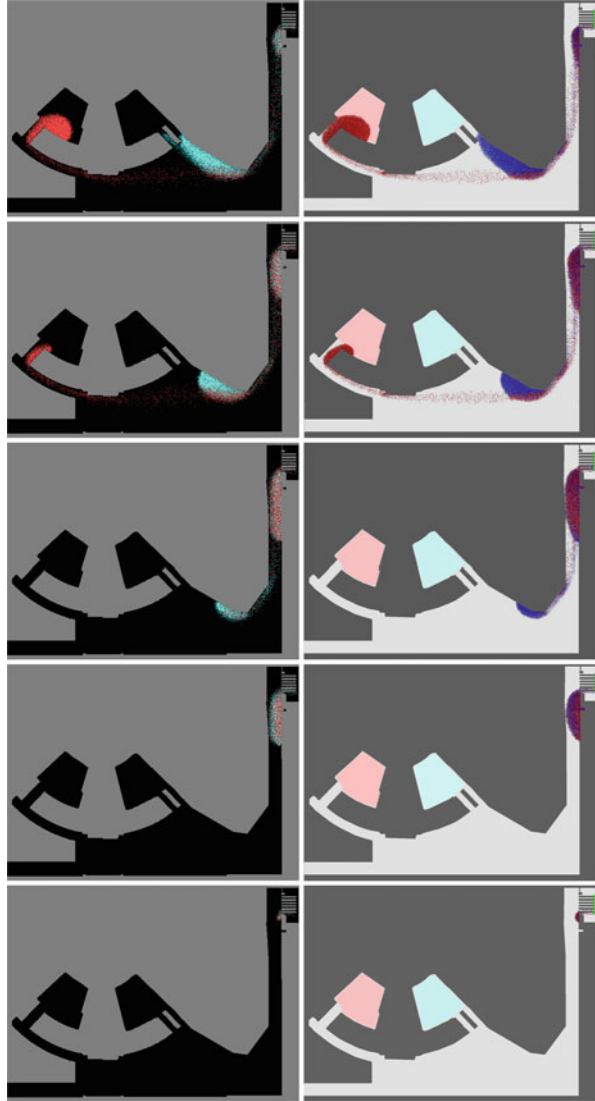
Selecting for both models the simulation run which has the least sum of mean square deviations from the averages for total evacuation and individual egress times Fig. 3 in this way compares the average simulation runs of both models and shows that the results are very similar all through time and space.

While these snapshots show how similar the results are, a second look reveals that the pedestrians move unrealistically close around the corners. As a consequence they ignore all but two or three of the exit gates shortly before the destination area. One may therefore expect that the times as shown in Table 1 are much larger than would be realistic. Someone familiar with one or both of the models (better: model classes) will know that this cannot be fixed by just modifying the parameters. Of course simulated egress and evacuation times can be reduced to some degree with different parameters, but only at the cost of having the models yield unrealistic results somewhere else in this geometry and even more so in different geometries. A reader not familiar with these models here needs to trust the author that this is in fact the case as demonstrating this would by far exceed the available space of this contribution and a strict formal prove is simply not possible.

Using the module of remaining travel time estimation on contrast greatly reduces egress and evacuation times and strongly influences the walking behavior in both models. For these simulations the same parameters as above have been used and in addition for the travel time estimation module used with the F.A.S.T. model it has been set $k_{s_{dyn}} = 1.0$ and $s_{add} = 10$ (see [11, 22]) and for the one of PTV Viswalk $g = 1.5$, $h = 0.7$ and the impact strength has been set to 100 % (see [17]). For this second stage of simulations it has not been attempted actively to find parameters with which the results of the two approaches match, i.e. these values are something like the defaults of the methods judged by previous experience.

Figure 4 shows snapshots from both simulations. By comparing with Fig. 3 it can be seen that the travel time estimation module modifies the simulation dynamics of both models into the same direction: pedestrians utilize the available space at corners better, they utilize the full width of the long corridor to the right better and they utilize the exit gates better compared to the simulations without travel time estimation method as shown in Fig. 3 and the red pedestrians – respectively a center

Fig. 3 Snapshots from the simulations without dynamic potential: *left*: F.A.S.T., *right*: Viswalk, at times 500, 1,000, 1,500, 2,000, and 2,500



line through the stream of red pedestrians – in the open area do not head for the corner of the obstacle but (about) for the edge of the group of blue pedestrians. Last but not least: for both models the evacuation and egress times are about halved as a comparison of Tables 1 and 2 shows.

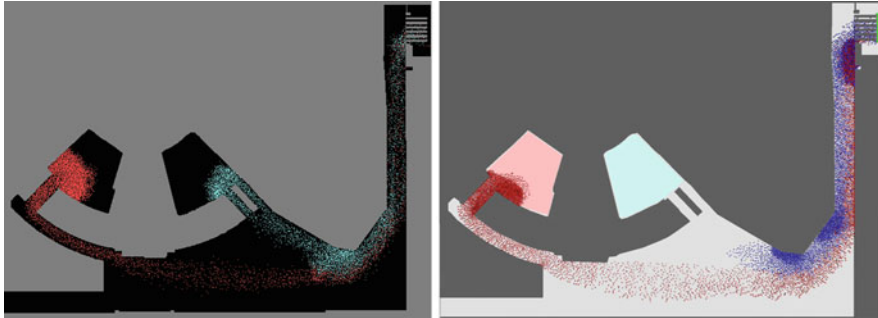


Fig. 4 Snapshots from the simulations with dynamic potential: *left*: F.A.S.T., *right*: Viswalk, each at time 350 s

Table 2 Results statistics from 15 simulation runs with each of the models when the travel time estimation module is used

	Av. individual egress time			Total evacuation time		
	Min.	Average \pm STD	Max.	Min.	Average \pm STD	Max.
F.A.S.T.	784.6	787.6 \pm 1.8	789.9	1,345.0	1,352.7 \pm 4.9	1,363.0
Viswalk	666.5	672.0 \pm 2.4	676.2	1,227.4	1,234.9 \pm 4.6	1,244.2

3.2 Example 2

The first example was composed of a number of basic elements: corridors, corners, gates. To clarify the effect of the travel time modules this is now to be amended by a most simple example: a group of pedestrians walks around a corner and this is compared with examples where the same number of pedestrians walks comparable distances straight on. Details of the geometry are shown in Fig. 5

The corner situation is simulated once without and once with activated travel time estimation module. For the straight examples the travel time estimation is not used it would not have much effect there anyway. So why simulate it at all? The straight geometries are only there to set a reference frame which makes the results less dependent on specific parameter settings. The value of the simulations in the straight geometries will become apparent with the results.

The results for the F.A.S.T. model are given in Table 3 and for PTV Viswalk in Table 4. In this second example it was not intended to achieve agreement between both models. Instead PTV Viswalk was run with default parameters and for the desired speed a population composition was chosen as in the RiMEA [33] test cases (50% male, 50% female; 4% mobility impaired and beyond that the age groups (<30, 30–50, and >50) with equal ratios) with their desired walking speeds according to [34]. In this way much smaller desired speeds were involved than for the F.A.S.T. model where preferred speeds between 1.2 and 2.0 m/s were used. The other parameters were set as in Example 1 (Sect. 3.1).

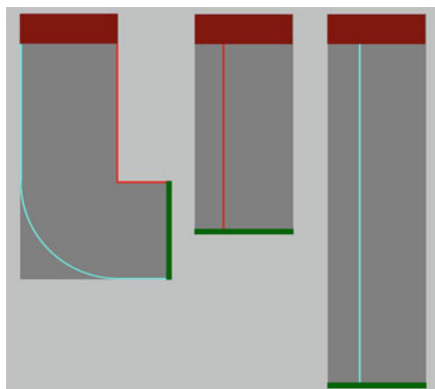


Fig. 5 The corner and the two straight geometries for comparison. 500 pedestrians have to walk from the *dark red* to the *dark green* area. The *red* line is 38 m ($28 + 10$) long, the *cyan* one 69.4 m ($28 + 10 \pi + 10$) long. The width of the areas is 20 m. The dark red insertion area has a length of 6 m

Table 3 Results statistics from 3,000 simulation runs with the F.A.S.T. model. The first line gives the times when no travel time estimation module is used, the second when it is

	Individual egress time			Total evacuation time		
	Min.	Average \pm STD	Max.	Min.	Average \pm STD	Max.
Corner w/o	79.3	84.0 ± 1.2	88.6	142.0	154.2 ± 3.4	171.0
Corner w	66.2	69.4 ± 0.8	72.6	109.0	114.8 ± 2.3	127.0
Straight short	41.8	43.4 ± 0.5	45.0	65.0	70.1 ± 1.9	80.0
Straight long	67.2	69.8 ± 0.8	72.5	102.0	107.4 ± 2.2	118.0

Table 4 Results statistics from 3,000 simulation runs with PTV Viswalk. The first line gives the times when no travel time estimation module is used, the second when it is

	Individual egress time			Total evacuation time		
	Min.	Average \pm STD	Max.	Min.	Average \pm STD	Max.
Corner w/o	104.2	110.5 ± 1.9	117.0	229.4	248.1 ± 6.6	274.4
Corner w	78.2	82.5 ± 1.4	88.3	157.9	174.2 ± 5.0	191.9
Straight short	52.0	55.1 ± 0.9	58.3	96.6	111.1 ± 3.4	123.2
Straight long	81.9	86.6 ± 1.4	90.9	150.4	176.2 ± 5.4	188.8

Although two different models, two different methods for travel time estimation, and different distributions of the desired speed were used, and although for this reason the total evacuation time and the individual average egress time differ in their absolute value for F.A.S.T. and PTV Viswalk, the results shown in Tables 3 and 4 are similar with regard to a number of properties (numbers with regard to average values):

- The individual average egress time in the corner geometry is 120 % (F.A.S.T) respectively 128 % (PTV Viswalk) compared to the case of the straight long corridor if no travel time estimation is made. However, it drops to 99 % respectively 95 %, if the travel time estimation module is active. Simpler spoken: they are clearly longer without and similar with travel time estimation.
- For the total evacuation time about the same relation holds: there the time drops from 144 % (F.A.S.T) respectively 141 % (PTV Viswalk) to 107 % respectively 99 %, if the travel time estimation module is active. Again the summary is that the time is clearly longer in the corner geometry compared to the straight long corridor if the travel time estimation module is not used, but it is about the same with both models if it is used.
- With the corner geometry the average individual egress time is 83 % (F.A.S.T.) respectively 75 % (PTV Viswalk) when the travel time estimation module is used compared to if it is not used.
- With the corner geometry the average total evacuation time is 74 % respectively 70 % when the travel time estimation module is used compared to if it is not used.
- If the travel time estimation module is active the individual average egress time in the corner geometry is 160 % (F.A.S.T.) respectively 150 % (PTV Viswalk) of the one in the straight short corridor.
- If the travel time estimation module is active the total egress time in the corner geometry is 164 % (F.A.S.T.) respectively 157 % (PTV Viswalk) of the one in the straight short corridor.

As the properties for F.A.S.T. and PTV Viswalk in all cases are separate by a maximum of 10 % points, while the effect of the travel time estimation module is much larger, these relations show that the details of the pedestrian model, its parameters (especially walking speeds) and the details of the travel time estimation module method and its parameters are of minor relevance. The effect is clear and distinguishes the case when it is used from the case when it is not used. This implies that with empirical data it should be clearly possible to decide if real people move in such a situation rather based on a shortest or a quickest path paradigm, i.e. if it enhances the degree of realism when the travel time estimation module is used. In addition it should be possible to compute those relations above where times at the corner geometry are related with times in one of the straight corridors with any pedestrian simulation model available. If then for example total evacuation time at the corner is about 150 % of the one in the straight long corridor it can be concluded that pedestrians in the model navigate according to a shortest path paradigm, while if the times are about equal or the time in the corner geometry is even shorter than the one in the long straight corridor it can be conclude that they follow a quickest path paradigm.

For completeness Figs. 6 and 7 show snapshots from the simulations.

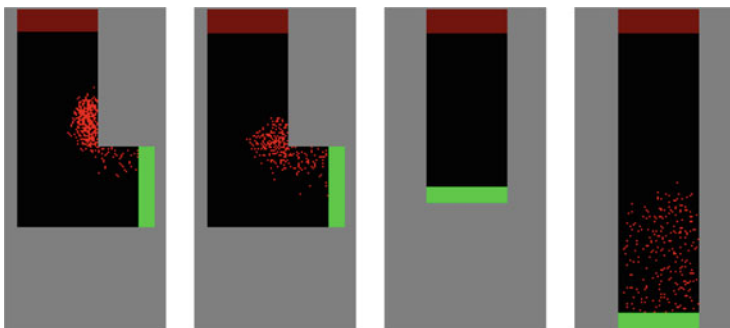


Fig. 6 Snapshots from the simulations with the F.A.S.T. model at 70 s

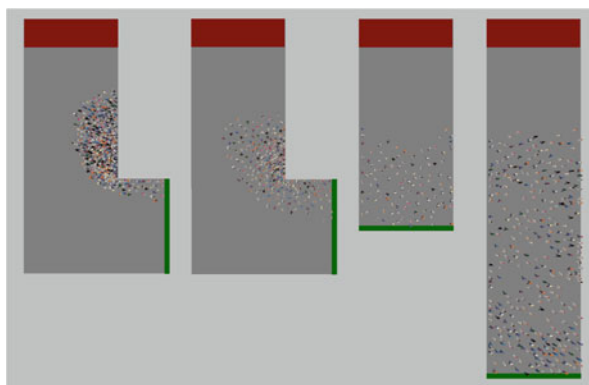


Fig. 7 Snapshots from the simulations with Viswalk at 70 s

4 Summary

In this contribution it was argued that it is of greater relevance for the degree of simulation results of a pedestrian simulation model that pedestrians walk into the direction of estimated earliest arrival instead of the direction of the shortest path than the details of (a) the model of pedestrian dynamics and (b) the details of the travel time estimation module. For this it was first shown that in a non-trivial example two different approaches to modeling pedestrian dynamics can yield very similar results on a moderate level of aggregation if one sets the model parameters appropriately. It was then shown that for both approaches the degree of realism is increased, if one changes from a shortest path direction to a quickest path direction paradigm.

The examination of a simple example scenario confirmed this. With two different models and different desired walking speed distributions and different travel time estimation modules it was found that the effect of using a travel time estimation

module (or using it not) had about the same impact on certain relative properties. This implies a comfortable situation for comparison with empirical data.

A first obvious conclusion is that it would be very interesting to have empirical data for situations as the ones in Example 2 (Sect. 3.2): where between the results for the two straight corridors do the results of the corner geometry lie for real people?

The second conclusion is that because it is (a) possible to have some cellular automata-based model yield such similar results and (b) not possible for both modeling approaches to enhance the degree of realism in certain situations, variants of the Social Force Model which modify exclusively or mainly the forces and do not include a travel time estimation module [29, 35, 36] most probably cannot help to improve the realism of results to the same degree as the travel time estimation module can.

Finally one can summarize that in the formulation of a pedestrian simulation model we can let guide ourselves by a quote which is ascribed to Blaise Pascal: “*Desire and⁴ Force are responsible for all our actions.*” A general way to interpret it in this context is that one equally has to take care for desired (planned or conscious) and for enforced (reactive, unplanned) determinants of motion. A more concrete way to interpret it for a force-based approach to pedestrian dynamics is that one has to put equally much effort in modeling the desired velocity as in modeling the forces.

References

1. Rogsch, C., Klingsch, W.: Basics of Software-Tools for Pedestrian Movement – Identification and Results. Fire Technology (2010) 1–21
2. Various YouTube Contributors: Various Titles. published via YouTube (2007–2010) <http://youtu.be/49HIZbFLPhg>, <http://youtu.be/jtKkHJXUVQY>, <http://youtu.be/LodYbDco0jY>, and <http://youtu.be/IWqnQjwAAac> (accessed March 2012).
3. Schadschneider, A., Klingsch, W., Klüpfel, H., Kretz, T., Rogsch, C., Seyfried, A.: Evacuation Dynamics: Empirical Results, Modeling and Applications. [37] 3142 ISBN:978-0-387-75888-6.
4. Schadschneider, A., Klüpfel, H., Kretz, T., Rogsch, C., Seyfried, A.: Fundamentals of Pedestrian and Evacuation Dynamics. In Bazzan, A., Klügl, F., eds.: Multi-Agent Systems for Traffic and Transportation Engineering. Information Science Reference, Hershey, PA, USA (2009) 124–154 ISBN:978-1-60566-226-8.
5. Kretz, T., Schreckenberg, M.: The F.A.S.T.-Model. In El Yacoubi, S., Chopard, B., Bandini, S., eds.: Cellular Automata – 7th International Conference on Cellular Automata for Research and Industry, ACRI 2006, Perpignan, France, Springer-Verlag Berlin Heidelberg (September 2006) 712–715 ISBN:3-540-40929-7.
6. Kretz, T.: Pedestrian Traffic – Simulation and Experiments. PhD thesis, Universität Duisburg-Essen (2007)
7. Kretz, T., Schreckenberg, M.: F.A.S.T. – Floor field- and Agent-based Simulation Tool. In Chung, E., Dumont, A., eds.: Transport simulation: Beyond traditional approaches. EPFL

⁴Emphasize added by the author of the facing work.

- press, Lausanne, CH (April 2009) 125–135 ISBN:978-1420095098.
8. Kretz, T., Schreckenberg, M.: Moore and more and symmetry. In Waldau, N., Gattermann, P., Knoflacher, H., Schreckenberg, M., eds.: *Pedestrian and Evacuation Dynamics 2005*, Springer Berlin Heidelberg (2007) 297–308 ISBN:978-3-540-47062-5.
 9. Kretz, T.: CA and MAS – with the NaSch as Example. [38] 589–592 ISBN:978-3-642-15978-7.
 10. Kretz, T.: Computation Speed of the F.A.S.T. Model. In S. Dai et al., ed.: *Traffic and Granular Flow '09*. (2010) (accepted for publication).
 11. Kretz, T.: Pedestrian Traffic: on the Quickest Path. *Journal of Statistical Mechanics: Theory and Experiment* **P03012** (2009)
 12. Kretz, T., Bönisch, C., Vortisch, P.: Comparison of Various Methods for the Calculation of the Distance Potential Field. In Klingsch, W., Rogsch, C., Schadschneider, A., Schreckenberg, M., eds.: *Pedestrian and Evacuation Dynamics 2008*, Berlin Heidelberg, Springer-Verlag (2010) 335–346 ISBN: 978-3-642-04503-5.
 13. Johansson, A., Helbing, D., Shukla, P.: Specification of the Social Force Pedestrian Model by Evolutionary Adjustment to Video Tracking Data. *Advances in Complex Systems* **10**(4) (2007) 271–288
 14. Helbing, D., Johansson, A.: *Pedestrian, Crowd and Evacuation Dynamics*. [37] 6476 ISBN:978-0-387-75888-6.
 15. PTV: VISSIM 5.40 User Manual, PTV Planung Transport Verkehr AG, Stumpfstraße 1, D-76131 Karlsruhe. (2010)
 16. Kretz, T., Hengst, S., Vortisch, P.: Pedestrian Flow at Bottlenecks – Validation and Calibration of VISSIM's Social Force Model of Pedestrian Traffic and its Empirical Foundations. In Sarvi, M., ed.: *International Symposium of Transport Simulation 2008 (ISTS08)*, Gold Coast, Australia, Monash University (2008) electronic publication
 17. Kretz, T., Große, A., Hengst, S., Kautzsch, L., Pohlmann, A., Vortisch, P.: Quickest Paths in Simulations of Pedestrians. *Advances in Complex Systems* **14** (2011) 733
 18. Kimmel, R., Sethian, J.: Computing geodesic paths on manifolds. In: *Proc. Natl. Acad. Sci. USA*. (1998) 8431–8435
 19. Jeong, W.K., Whitaker, R.: A fast eikonal equation solver for parallel systems. In: *SIAM conference on Computational Science and Engineering*. (February 2007)
 20. Jeong, W.K., Whitaker, R.: A Fast Iterative Method for a Class of Hamilton-Jacobi Equations on Parallel Systems. Technical Report UUCS-07-010, University of Utah, School of Computing (April 2007)
 21. Jeong, W.K., Whitaker, R.: A Fast Iterative Method for Eikonal Equations. *SIAM Journal on Scientific Computing* **30**(5) (July 2008) 2512–2534
 22. Kretz, T.: The use of dynamic distance potential fields for pedestrian flow around corners. In: *First International Conference on Evacuation Modeling and Management*, TU Delft (2009)
 23. Kretz, T.: Applications of the Dynamic Distance Potential Field Method. In S. Dai et al., ed.: *Traffic and Granular Flow '09*. (2010) (accepted for publication).
 24. Kretz, T.: The Dynamic Distance Potential Field in a Situation with Asymmetric Bottleneck Capacities. In Bandini, S., Manzoni, S., Umeo, H., Vizzari, G., eds.: *Cellular Automata – 9th International Conference on Cellular Automata for Research and Industry, ACRI 2010*. Volume 6350 of *Lecture Notes in Computer Science*, Heidelberg, Springer (2010) 480–488
 25. Kretz, T., Hengst, S., Roca, V., Pérez Arias, A., Friedberger, S., Hanebeck, U.: Calibrating Dynamic Pedestrian Route Choice with an Extended Range Telepresence System. In: *2011 IEEE International Conference on Computer Vision Workshops*. (2011) 166–172 *First IEEE Workshop on Modeling, Simulation and Visual Analysis of Large Crowds*, 6–13 November 2011, Barcelona, Spain.
 26. Kretz, T., Hengst, S., Pérez Arias, A., Friedberger, S., Hanebeck, U.: Using Extended-Range Telepresence to Collect Data on Pedestrian Dynamics. In: *Annual Meeting of the Transportation Research Board 2012*. (2012) (on CD).
 27. PTV Vision: Quickest vs. Shortest Path in a Simulation of Pedestrians . published via YouTube (2011) <http://youtu.be/8SmRBtJ-jeU> (accessed March 2012).

28. Moussaïd, M., Helbing, D., Garnier, S., Johansson, A., Combe, M., Theraulaz, G.: Experimental study of the behavioural mechanisms underlying self-organization in human crowds. *Proceedings of the Royal Society B: Biological Sciences* **276**(1668) (2009) 2755–2762
29. Chraïbi, M., Seyfried, A., Schadschneider, A.: Generalized centrifugal-force model for pedestrian dynamics. *Physical Review E* **82**(4) (2010) 046111
30. Steffen, B., Seyfried, A.: The repulsive force in continuous space models of pedestrian movement. Arxiv preprint arXiv:0803.1319 (2008)
31. Sherif, M.: *The psychology of social norms*. Harper & Brothers, New York (1936)
32. Rascle, M., Nkonga, B., Decoupigny, F., Maignant, G.: Geodesics and Shortest Paths in Pedestrian Motions: A Mathematical Approach. In V.V. Kozlov, A.S. Bugaev, A.S. et al., ed.: *Traffic and Granular Flow '11*, Moscow, Springer-Verlag Berlin Heidelberg (2012) in print.
33. Brunner, U., Kirchberger, H., Lebeda, C., Oswald, M., Könnecke, R., Kraft, M., Thoss, A., Mülli, L., Seyfried, A., Hartnack, C., Wader, S., Spennes, G., Kretz, T.: RiMEA – Richtlinie für Mikroskopische Entfluchtungs-Analysen. 2.2.1 edn. Initiatoren des RiMEA-Projekts: M. Schwendimann, N. Waldau, P. Gattermann, C. Moroge, T. Meyer-König, and M. Schreckenber (2009) (eprint from <http://www.rimea.de/>). (in German).
34. Weidmann, U.: *Transporttechnik der Fußgänger – Transporttechnische Eigenschaften des Fußgängerverkehrs*. Schriftenreihe des IVT 90, ETH Zürich (3 1993) Zweite, ergänzte Auflage. (in German).
35. Lakoba, T., Kaup, D., Finkelstein, N.: Modifications of the helbing-molnar-farkas-vicek social force model for pedestrian evolution. *Simulation* **81**(5) (2005) 339–352
36. Yu, W., Chen, R., Dong, L., Dai, S.: Centrifugal force model for pedestrian dynamics. *Physical Review E* **72**(2) (2005) 026112
37. Meyers, R., ed.: *Encyclopedia of Complexity and Systems Science*. Springer-Science+BusinessMedia, New York (2009) ISBN:978-0-387-75888-6.
38. Bandini, S., Manzoni, S., Umeo, H., Vizzari, G., eds.: *Cellular Automata – 9th International Conference on Cellular Automata for Research and Industry, ACRI 2010*. Volume 6350 of *Lecture Notes in Computer Science*., Heidelberg, Springer (2010) ISBN:978-3-642-15978-7.

Using a Multi-Scale Model for Simulating Pedestrian Behavior

Angelika Kneidl, Dirk Hartmann, and André Borrmann

Abstract In order to model realistic pedestrian crowds, different aspects on different scales have to be taken into account. Besides behavioral aspects, locomotion on short-scale and human navigation on large-scale have to be modeled appropriately. In the simulation models existing to date, these two aspects are modeled separately. To overcome the limitations of currently available models, this paper presents a new hybrid multi-scale model, which closely links information between the short-scale and the large-scale layer to improve the navigational behavior.

In the presented hybrid navigation model, graph-based methods using visibility graphs are used to model large-scale way-finding decisions. The pedestrians' movements between two nodes of the navigation graph (the short-scale) are modeled by means of a dynamic navigation floor field. The floor field is updated dynamically during the runtime of the simulation, explicitly considering other pedestrians for determining the fastest path.

Keywords Wayfinding • Navigation • Dynamic navigation fields • Dynamic floor fields • Cellular automata • Visibility graphs • Locomotion • Route choice • Multi-scale model • Microscopic pedestrian simulation

A. Kneidl (✉) • A. Borrmann
Technische Universität München, Munich, Germany
e-mail: kneidl@tum.de; andre.borrmann@tum.de

D. Hartmann
Siemens AG, Corporate Technology, Munich, Germany
e-mail: Hartmann.dirk@siemens.com

1 Introduction

Simulation of crowd dynamics has become an important field of research in the last years. A variety of different approaches have been developed, focusing on different objectives. Microscopic multi-scale models form one type of models (e.g. [1–3]). These approaches model crowd behavior on different scales: on the small scale, locomotion is modeled, i.e. how do pedestrians move (stroll, walk, run) towards a visible destination while trying to avoid other pedestrians. These aspects are mostly modeled either by cellular automata combined with force models or with continuous floor fields. Each individual's step is calculated according to given potentials (i.e. gradients of the potentials) or forces, until all individuals have reached a designated destination. On the large-scale, navigational aspects are addressed. These include the route choice towards a (not visible) destination via intermediate destinations. The decision of which way to take at each intermediate destination might depend on environmental conditions, e.g. choosing illuminated paths in the evening, and can vary from pedestrian to pedestrian, e.g. take the shortest path, take the fastest path, avoid congestions, follow signage, follow friends, etc. To model these aspects, graphs such as Voronoi diagrams (e.g. [4]), visibility graphs (e.g. [5]), or corridor maps [6] are used and different routing algorithms are applied on those.

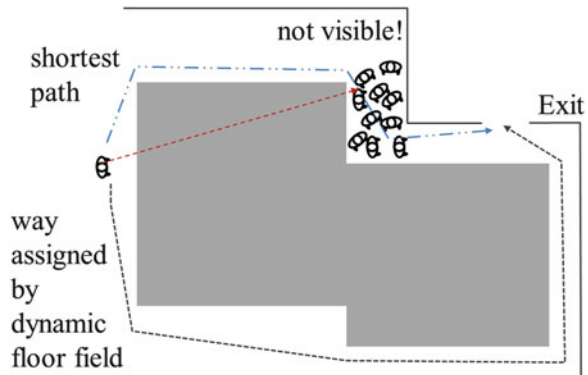
Various models combine these scales into so-called multi-scale models, combining graph-based approaches either with force models (e.g. [3], [7], [8]) or with agent type models (e.g. [9–13], [31]). However, these multi-scale models typically combine the small-scale and large-scale layer in a very simplistic fashion. Thus the limitations of small scale (e.g. being short-sighted) and large scale (e.g. not considering other moving pedestrians for route choice decisions) are usually not resolved. Typically, the large-scale layer provides the next intermediate destination to pedestrians steering in the small-scale layer and no information sharing between the small-scale and the large-scale layer takes place.

In this work, a new hybrid multi-scale approach is proposed, in which a combination of the small-scale and the large-scale layer is driven further: we share information between both layers to improve the accuracy of the model resolving the above mentioned issues.

2 State of the Art

To date, the small-scale and the large-scale layer are combined as follows to form a multi-scale model: The navigation graph is used to generate pedestrians' paths based on a specific navigation strategy. Paths themselves consist of a list of intermediate destinations. The navigation field is then used to navigate pedestrians between these intermediate destinations until the final destination is reached. Although the combination of the layers already improves the realism of simulations, since small scale aspects (e.g. avoiding other moving pedestrians in close vicinity) and

Fig. 1 Example for not distinguishing visible and invisible edges: the pedestrian on the left would walk around the south-west corner navigating according to a dynamic floor field, although he cannot see the congested area from his position



large-scale aspects (e.g. navigation strategy) are addressed, there are still several open issues to be solved:

Current models are limited by the lack of information exchange between the layers resulting in unrealistic effects. On the small scale, static floor fields are often used [14–19], since dynamic floor fields, i.e. fields, which take pedestrians into account, are computationally too expensive. However using static floor fields results in artificial movement patterns. Nevertheless, some approaches use these dynamic fields ([20–22]). On the large-scale, graph-based algorithms assign edge weights without distinction between visible and invisible edges, which we believe is provides more information than actually available for human individuals and thus does not correctly reflect human perception (c.f. Fig. 1).

3 Setup of the New Hybrid Multi-Scale Model

The proposed hybrid multi-scale model consists of two layers; a schematic setup of the model is shown in Fig. 2.

The small-scale layer consists of a cellular automaton. This automaton is composed of hexagonal cells, each of them having the size of an average European male. Pedestrians move on these cells following simple rules that depend on different cell values. In the simplest case these are given as a sum of a navigation field and a repulsive pedestrian field. The navigation fields are derived from dynamic floor fields, which are calculated based on the Fast Marching Method (FMM) [23]. Summing up local repulsions of all other pedestrians, the repulsion field is obtained. The large-scale layer is formed by a navigation graph [5], which is derived automatically from the scenario's geometry. Based on this graph, different routing algorithms are implemented to reflect different navigational behavior.

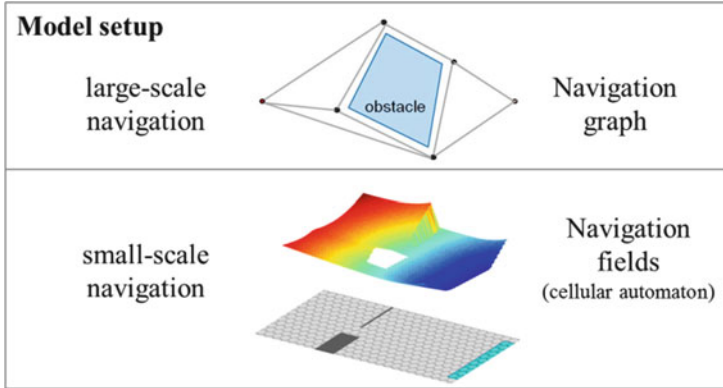


Fig. 2 Setup of the two-layered simulation model

3.1 Information Exchange from Navigation Layer to Locomotion Layer

Instead of calculating one dynamic floor field for each destination, which covers the whole area of the scenario, vertices from the navigation graph serve as intermediate destinations. This enables the division of the scenario area into many small floor fields. The advantage of having many small fields is that only those fields have to be updated where pedestrians are located on. This results in lower computational time, since only small areas have to be updated. A second advantage comes into play, if the directions of the edges of the graph are considered: Since navigation graphs are directed graphs towards the destination, directed floor fields can be created by sorting the cell values x_i according to a key $\kappa(x_i)$, which combines travel times and distance to origin [24]:

$$\kappa(x_i) = \alpha T(x_i) + (1 - \alpha) \beta d(x_i, V^O), \quad (1)$$

where $\kappa(x_i)$ denotes key the values are sorted by, $T(x_i)$ is the time to reach cell x_i ; V^O stands for the origin vertex and $0 \leq \alpha \leq 1$ and $\beta > 0$ are appropriate constants. The difference between an undirected and a directed floor field is depicted in Fig. 3 for different values of α and β . One can see that the choice of α has to be made carefully in order to still obtain a sufficient number of cells being covered by the field.

3.2 Information Exchange from the Small-Scale Layer to the Large-Scale Layer

In current multi-scale models, edge weights for the graph layer are simple distances or travel times, the latter being derived from densities on the edges. Local densities

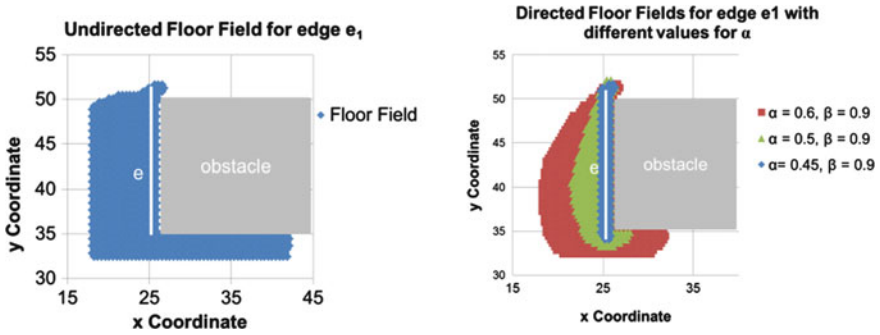


Fig. 3 Comparison between undirected floor field for edge e and directed floor fields for different values of α

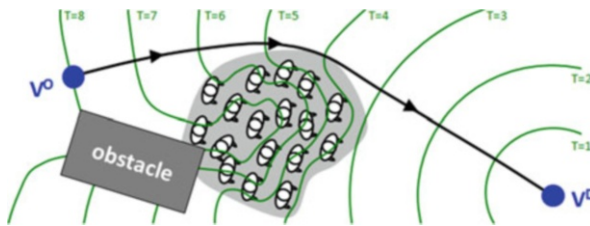


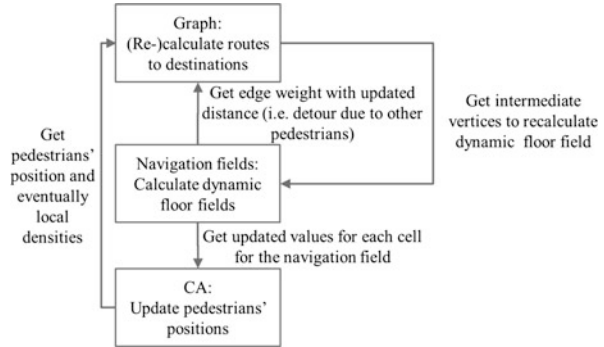
Fig. 4 Schematic sketch of a dynamic floor field estimating travelling times of pedestrians travelling from the origin V^O to the destination V^D

can be accessed easily in cellular automata, since the neighborhood of each pedestrian is known and the occupied cells can be counted. From the determined density, the pedestrians’ velocity on the particular edge is derived by means of a fundamental diagram, and the corresponding travel time is used as edge weight. However due to the local nature of densities, resulting travel times may be inaccurate. This becomes apparent, if only a small part of the edge is congested, i.e. due to a bottleneck. Using mean velocity values may be too optimistic, while taking the minimum velocity results in too pessimistic estimates. Additionally, pedestrians taking a detour in order to avoid congestions cannot be captured.

Taking values from the dynamic floor field improves the estimates significantly. Instead of using velocities and distances to derive travel times, the floor field values from the vertex cells reflect the travel time explicitly. An example that illustrates this improvement in realism of the simulations is given in Fig. 4.

Nevertheless, applying these floor field values as edge weights for all edges of the entire navigation graph would result in unrealistic behavior, since this implies that individuals have global knowledge of the current situation in the entire scene. However, as pedestrians are only able to take congestions into account, which are visible from their current position, a distinction has to be made between visible and invisible edges. This can be achieved easily in a pre-computational step, since a visibility graph is applied. Taking the Euclidean distance for invisible edges and the

Fig. 5 Interaction between the layers of the hybrid simulation model



floor field values for visible edges improves the realism of the calculated routes, when implementing a fastest path strategy.

An overview of the overall information exchange flow within the hybrid multi-scale model is given in Fig. 5.

4 Tests

To illustrate the improvements resulting from the proposed hybrid model, two test cases are presented. All presented simulations rely on the microscopic pedestrian simulator introduced in [16]. For further references we refer also to [25–30].

The first scenario consists of a corridor around a corner; three different simulations have been considered. First, static floor fields have been used, not taking into account other moving pedestrians. The second simulation has been based on dynamic floor fields without using the vertices from the navigation graph as intermediate destinations. The third simulation has combined the graph with floor fields. Results for the different simulations are shown in Fig. 6.

One can see that using static floor fields results in unrealistic patterns. Pedestrians are jamming in front of the corner, while they could walk around the other pedestrians in order to steer around the congestion. The second and third simulation produce more realistic results: The whole width of the corridor is used and no artificial congestion occurs at the left side of the obstacle. Furthermore, one can also observe that the quality of the results is not reduced when using intermediate destinations, although significantly less computational time is required for updating the floor fields.

The second test case we have considered illustrates the importance of distinguishing between visible and invisible edges and thus assigning different edge weights to both sets. The scenario consists of several obstacles and a bottleneck, which is not visible from the origin (c.f. Fig. 7).

If visible and invisible edges are not distinguished, pedestrians detect a new fastest path leading around the south corner of the obstacle when the congestion

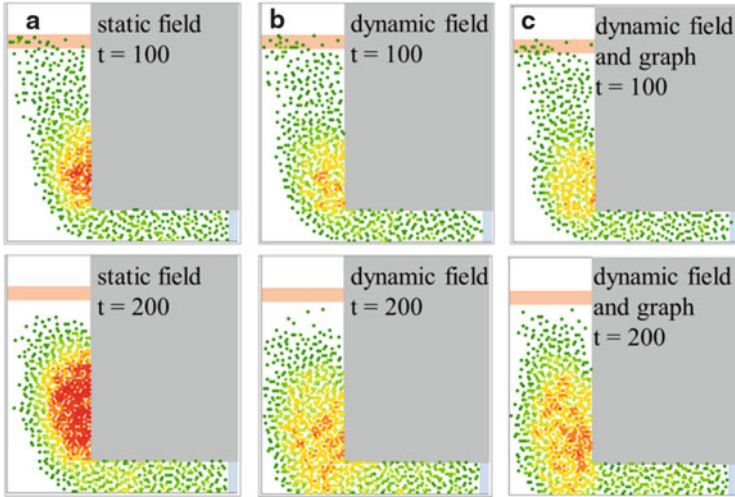


Fig. 6 Simulation screenshots after 100 and 200 s: (a) snapshot with static navigation field; (b) snapshot with an undirected dynamic navigation fields; (c) snapshot with directed dynamic navigation field in combination with a navigation graph

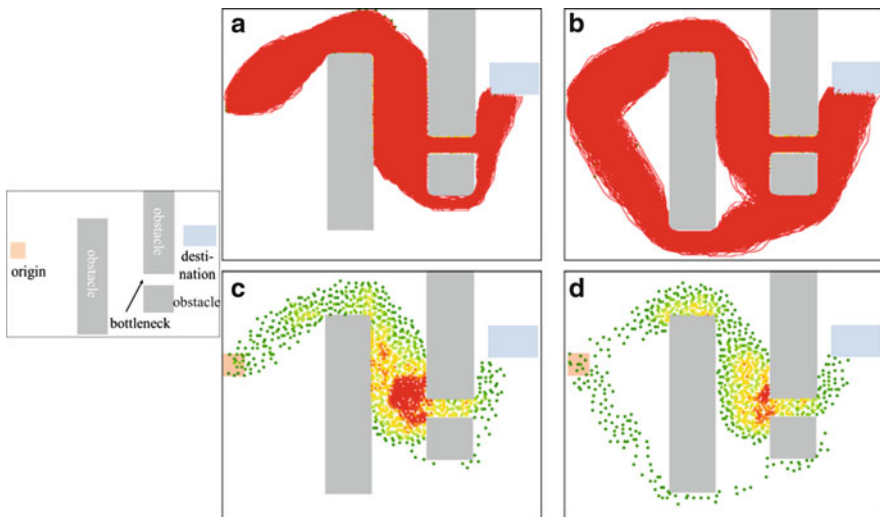


Fig. 7 *Left*: scenario of the test case: there are several obstacles and a bottleneck which is not visible from the origin. *Right*: simulation results: (a) traces of all pedestrians for the simulation with distinguishing between visible and invisible edges; (b) traces of all pedestrians for the simulation without distinction; (c) simulation screenshot of the simulation with distinction between visible and invisible edges; (d) simulation screenshot for the simulation without distinction

in front of the bottleneck forms. This does not seem to be realistic, since pedestrians at the origin typically would not know about the congestion at the bottleneck. If

the distinction between visible and invisible edges is introduced, pedestrians are walking around the north corner of the first obstacle, realizing the congestion and then decide to walk around the south corner of the second obstacle. This seems to be a more natural behavior. All simulation results are visualized in Fig. 7.

5 Conclusions

In this work a new hybrid multi-scale model has been proposed, which combines a small-scale locomotion layer with a large-scale navigation layer in order to overcome the limitations of existing multi-scale models: Using static floor fields for modeling small-scale aspects leads to artificial movement patterns. Calculating dynamic floor fields – i.e. taking into account moving pedestrians – results in a high computational time, since these fields have to be updated every time step in order to reflect the correct values. Introducing intermediate destinations from the navigation graph and dividing the scenario into many small floor fields results in significantly reduced computational effort, since only a few fields have to be updated, namely only those where (many) pedestrians are located on. At the same time, a significant improvement for estimating travel times on individual edges is achieved when compared with static floor fields or density-based approaches. On the large-scale, most simulation tools simply take the fastest path to calculate the routes for the pedestrians. Imprecise estimates lead to routes, which can be misleading. Taking values from the dynamic floor fields for visible edges instead, leads to a more precise estimate for edge weights and thus to more accurate routes.

The presented examples show that this close coupling between the small-scale and large-scale navigation decisions leads to significantly more realistic simulation results than achievable with conventional multi-scale approaches.

References

1. Höcker M, Berkhahn V, Kneidl A, Borrmann A, Klein W. Graph-based approaches for simulating pedestrian dynamics in building models. In: University College Cork, editor. 8th European Conference on Product & Process Modelling (ECPPM). Cork, Ireland; 2010.
2. Wagoum UK, Seyfried A, Holl S. Modelling dynamic route choice of pedestrians to assess the criticality of building evacuation; 2011.
3. Galea ER, Owen M, Lawrence PJ. The EXODUS Model. *Fire Engineers Journal* 1996(July):26–30.
4. Sud A, Andersen E, Curtis S, Lin MC, Manocha D. Real-Time Path Planning in Dynamic Virtual Environments Using Multiagent Navigation Graphs. *IEEE Transactions on Visualization and Computer Graphics* 2008;14:526–538.
5. Kneidl A, Borrmann A, Hartmann D. Generating sparse navigation graphs for microscopic pedestrian simulation models. In: Hartmann T, de Wilde P, Rafiq Y, editors. Proceedings of the 2011 eg-ice Workshop; 2011.

6. Geraerts BR, Overmars MH. The corridor map method: a general framework for real-time high-quality path planning. *Computer Animation and Virtual Worlds* 2007;18(2):107.
7. Kretz T, Hengst S, Rocea V, Perez Arias A, Friedberger S, Hanebeck UD. Calibrating Dynamic Pedestrian Route Choice with an Extended Range Telepresence System. In: 1st IEEE Workshop on Modeling, Simulation and Visual Analysis of Large Crowds; 2011.
8. Chraïbi M, Wagoum UK, Schadschneider A, Seyfried A. Force-based models of pedestrian dynamics. *Networks and Heterogeneous Media* 2011;6:425–42.
9. Funge J, Tu X, Terzopoulos D. Cognitive modeling: knowledge, reasoning and planning for intelligent characters. In: *Proceedings of the 26th annual conference on computer graphics and interactive techniques*. New York, NY, USA: ACM Press/Addison-Wesley Publishing Co; 1999, p. 29–38.
10. Reynolds C. Steering Behaviors for Autonomous Characters. In: *Game Developers Conference*; 1999.
11. Rindsfuser G, Klügl F. Agent-Based Pedestrian Simulation: A Case Study of the Bern Railway Station. In: Nagel K, Koll-Schretzenmayr M, editors. *disP*. Zurich, Switzerland: ETH Zürich; 2007, p. 9–18.
12. Lerner A, Chrysanthou Y, Lischinski D. Crowds by Example. *Computer Graphics Forum* 2007;26(3):655–64.
13. Teknomo K. Modeling mobile traffic agents on network simulation. In: *Transportation Science Society of the Phillippines 2008 – Proceedings of the 16th Annual of Transportation Science*; 2008.
14. Burstedde C, Klauck K, Schadschneider A, Zittartz J. Simulation of pedestrian dynamics using a two-dimensional cellular automaton. *Physica A: Statistical Mechanics and its Applications* 2001;295(3–4):507–525.
15. Klüpfel H. A Cellular Automaton Model for Crowd Movement and Egress Simulation. *Dissertation*. Duisburg; 2003.
16. Köster G, Hartmann D, Klein W. Microscopic pedestrian simulations: From passenger exchange times to regional evacuation. In: *Operations Research - Mastering complexity*; 2010.
17. Nishinari K, Kirchner A, Namazi A, Schadschneider A. Extended floor field CA model for evacuation dynamics. *IEICE Trans. Inf. Syst* 2004;E87D:726–32.
18. Varas A, Cornejo MD, Mainemer D, Toledo B, Rogan J, Munoz V et al. Cellular automaton model for evacuation process with obstacles. *Physica A: Statistical Mechanics and its Applications* 2007;382(2):631–42.
19. Yamamoto K, Kokubo S, Nishinari K. Simulation for pedestrian dynamics by real-coded cellular automata. *Physica A: Statistical Mechanics and its Applications* 2007;379(2):654.
20. Hartmann D. Adaptive pedestrian dynamics based on geodesics. *New Journal of Physics* 2010;12(4):43032.
21. Hartmann D, Mille J, Pfaffinger A, Royer C. Dynamic medium scale navigation using dynamic floor fields. In: *Pedestrian Evacuation Dynamics*; 2012.
22. Kretz T. Pedestrian traffic: on the quickest path. *Journal of Statistical Mechanics: Theory and Experiment* 2009;2009(03):P03012.
23. Sethian JA. *Level Set Methods and Fast Marching Methods*: Cambridge University Press; 1999.
24. Petres C, Pailhas Y, Patron P, Petillot Y, Evans J, Lane D. Path Planning for Autonomous Underwater Vehicles. *IEEE Transactions on Robotics* 2007;23:331–41.
25. Köster G, Treml F, Seitz M, Klein W. Validation of crowd models including social groups. In: *Pedestrian Evacuation Dynamics*; 2012.
26. Seitz M, Köster G, Pfaffinger A. Modeling pedestrian group behavior in a cellular automaton. In: *Pedestrian Evacuation Dynamics*; 2012.
27. Reuter V, Bergner BS, Köster G, Seitz M, Treml F, Hartmann D. On Modeling Groups in Crowds: Empirical Evidence and Simulation Results. In: *Pedestrian Evacuation Dynamics*; 2012.
28. Davidich M, Mayer H, Royer C, Pfaffinger A. Modelling of Waiting Zones. In: *Pedestrian Evacuation Dynamics*; 2012.

29. Davidich M, Köster G. Verification of Pedestrian Stream Models Based on Video Analysis. In: Pedestrian Evacuation Dynamics; 2012.
30. Mayer H, Hartmann D, Klein W, Zechlin O. Influence of emissions on pedestrian evacuation. In: Pedestrian Evacuation Dynamics; 2012.
31. Wagoum UK, Seyfried A, Holl S. Modelling dynamic route choice of pedestrians to assess the criticality of building evacuation; Advances in Complex Systems, 2012, available online.

Using the Social Force Model to Represent the Behavior of Pedestrians at Chaotic Intersections of Developing Countries: The Case of Peru

Felix Cabrera Vega and Juan Carlos Dextre

Abstract In Peru, due to mismanagement, aggressive driving style and pedestrian behavior several conflicts appear among pedestrians, cyclists and vehicles that could not be represented by traditional traffic modeling tools. Studies in some cities of Peru (Cabrera (2010) ¿Pueden los modelos macro-determinísticos y microsimulación analizar adecuadamente las intersecciones semaforizadas en Lima?. XVI Congreso Panamericano de Transporte, Tráfico y Logística – PANAM 2010. Lisboa, Portugal) indicate that analytical models would not be adequate to analyze chaotic traffic situations. Therefore, to assess accurately the benefits of mitigation actions it would be necessary to use traffic and pedestrian micro simulation models that can be capable of representing the behavior of Peruvian pedestrians and its interaction with other transport modes. The software VISSIM and the social force model are used in this study. Both models were calibrated and validated and the pedestrian speed would increase by 25 % and contrary to what Peruvian politicians were thinking, benefits to vulnerable users would not reduce the benefits for vehicles. There would be a 35 % reduction in delays and an increment of 65 % on vehicular speed.

Keywords Social force model • VISSIM • Micro simulation

1 Introduction

In Peruvian cities, an important set of intersections present problems of congestion, pollution and mainly accidents. The study by [1] indicates that among 178 countries, Peru is the first in pedestrian deaths from road accidents (78 %), which are generated because of the traditional management system which gives priority to traffic instead

F.C. Vega (✉) • J.C. Dextre
Pontificia Universidad Católica del Perú, Lima, Peru
e-mail: Cabrera.fi@pucp.edu.pe; jdextre@pucp.edu.pe

of vulnerable users (pedestrians, the disabled, cyclists, etc.). Peruvian politicians privilege to motor vehicles and think that any improvement for vulnerable users would imply less capacity as well as more travel time and delays for vehicles.

Also, due to aggressive driving style and pedestrian behavior, several conflicts appear among pedestrians, cyclists and vehicles that could not be represented by traditional traffic modeling tools. Studies in some cities of Peru [2] indicate that analytical models would not be adequate to analyze traffic situations close to congestion or where there are multiple conflict points among different modes.

Therefore, in order to assess accurately the benefits of applying mitigation actions (to improve road safety) it would be necessary to use traffic and pedestrian micro simulation models that can be capable of representing the behavior of Peruvian pedestrians and its interaction with other transport modes.

2 Traffic and Pedestrian Modeling

2.1 *Microscopic Traffic Simulation*

The microscopic traffic models allow detailed analysis of traffic by considering each vehicle as a unit. Besides, it consider aspects of individual behavior including diversity from the choice of route and departure time [3, 4], as well as sub models related to driving behavior (car following, lane change and gap acceptance) [5, 6]. Typically, the process starts with vehicles entering the network, using statistical distributions of arrivals, then it is specified a destination, a type of vehicle and driver, according to a “starting number” chosen randomly. Subsequently, the vehicles are tracked every second or fraction of a second (e.g. 0.1 s) to register its position, speed and acceleration [7].

Micro-simulation models have a random nature, so they should be tested repeatedly to find answers to a specified level of reliability [8]. Also, in order to accept a model as a good representation of the reality this needs to be calibrated y validated. The model calibration is the stage in which various parameters of the simulation are adjusted in order to replicate the current conditions. If a model is poorly calibrated, it could not adequately represent the current scenario and then could not be used as the basis for modeling scenarios with modifications. When using a poorly calibrated model, the results of all scenarios would be far from the real situation. For example, [9] states that differences of 13 % in the calibration of speed on motorways, could lead to differences of up to 69 % for future conditions, and other studies indicate that differences in the calibration of 20 % could lead to differences of up to 50 % in future situations [10].

According to [11] there are more than 20 calibration methodologies depending on the systems analyzed and the degree of accuracy required, unfortunately there is no consensus on the best methodology, but according to [11] is recommended to apply the Dowling methodology [7].

The heart of the microscopic model are the car following and lane change sub models, which determine the possibility of representing properly the different driving styles. According to [12] car following models can be classified into five groups: Gazis–Herman–Rothery (GHR) model, collision avoidance model, linear model, psychophysical or action-point model and fuzzy logic-based model. Any of these car following models has advantages and disadvantages, however according to previous studies [2] the psychophysical models would be adequate for representing the Peruvian reality.

Among the different micro simulation programs based on the psychophysical theory, VISSIM is the one that have been used recently in Peru, with adequate results [2]. This program uses the model of Wiedemann [13] and considers that drivers have different thresholds of perception and decision mainly represented through the perception of distance and speed differences. It is a stochastic model that works with distribution and functions. Therefore, one of the first steps is to define, through field studies, the variables used in the functions of maximum acceleration and deceleration, desired speed and vehicle types. In VISSIM the parameters used to represent vehicle interactions are grouped in sub models: vehicle following, lane-changing and control traffic light side [14].

2.2 Pedestrian Simulation

Traditionally, the behavior of pedestrians has been modeled from the macroscopic point of view as if they were gases [15, 16] and fluid [17–19] (considering to the flow, speed and density as the main parameters). However, how it is indicated by [20] this could be only partially confirmed, because to get a realistic gas-kinetic or fluid-dynamic theory, corrections should be made to obtain avoidance and deceleration maneuvers, which do not obey momentum and energy conservation. Also, pedestrian areas have been analyzed in normal traffic conditions and evacuation.

In this study, pedestrians move governed mainly looking for the safest and fastest route, which is not necessarily through the crosswalk. Therefore we analyze a situation in normal traffic conditions (without panic), including random routes and where within the space of the junction are conflicts between pedestrians and vehicles. For these reasons a microscopic pedestrian model could be necessary to model this chaotic behavior considering that every pedestrian would be modeled as an individual agent with his own behavior.

According to [21] the main pedestrian micro simulation models could be classified into three groups: cellular automata model, social force models and discrete choice models. In this project the social force model is analyzed.

2.2.1 Social Force Model

It describes the pedestrian behavior through social forces, of attraction and repulsion, which result from the interaction of pedestrians with the environment and with other people. The conception of this theory is due to Lewin [22] and later its mathematical formulation was presented by Helbing [23]. This model uses Newton's equation to calculate the forces and according to [24] the basic ideas of this model consider that pedestrians want to reach a certain destination as comfortable as possible, the motion of a pedestrian is influenced by other pedestrians and finally pedestrians are sometimes attracted by other persons and also keeps a certain distance from borders of buildings, walls, streets or obstacles.

Also, the model considers that all the previously mentioned effects influence the pedestrian's decision at the same time. Additionally, to represent changes on human behavior it adds a fluctuation term.

3 Methodology

A signalized intersection was analyzed in the city of Chiclayo (north of Peru) with an important percentage of vulnerable road users who move in any direction and walk among vehicles in movement. To represent the multiple conflicts and interaction among all users, the traffic micro simulation software VISSIM and its pedestrian module (based on the social force model) were used.

The data for model construction, and manual calibration and validation were collected during two working days (2011), from 11:00 a.m. to 2:00 p.m., by manual counting's and films. The peak hour of each day was modeled. The Fig. 1 shows the conflicts produced inside the junction (mainly vehicles turning right in conflict with pedestrians) and the Fig. 2 shows the pedestrian and vehicle flows used for modeling. From video, pedestrian speeds and three main pedestrian paths were found (only one of them followed the pedestrian crossings).

During the model construction, the default distributions of desired speeds, acceleration and deceleration were used for vehicles. The traffic calibration and validation were performed with traffic volumes and average queue lengths at the two junction arms. The traffic volumes on VISSIM matched the volumes observed on field due to it was used the exact percentage of turning volumes in VISSIM (stochastic volumes could be used too). In the case of queue length calibration, the parameters of Wiedemann car following model were adjusted as well as the critical gap value, which is lower than American or European values which indicates a more aggressive driving style.

In the case of Peru, it was found, in some previous studies [2], that the parameters governing the calibration process are the Wiedemann car following ones; besides, it was established they would be very different from the default values. For urban areas, the Wiedemann model has three main parameters [14]: average desired distance between vehicles stopped (ax), the additive part of the desired



Fig. 1 Junction analyzed in Chiclayo City, Peru

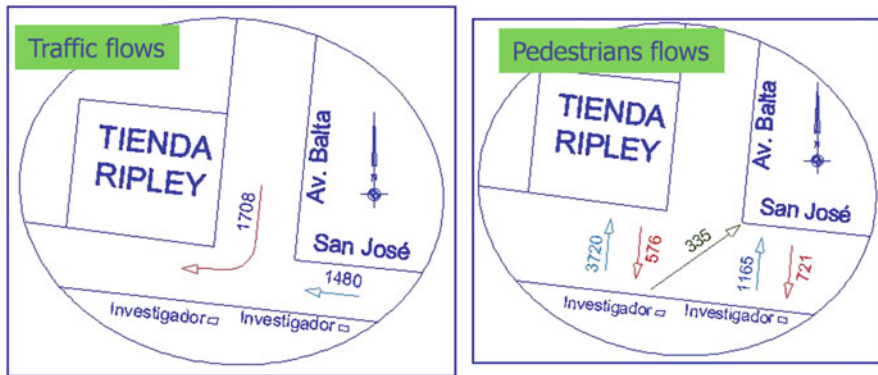


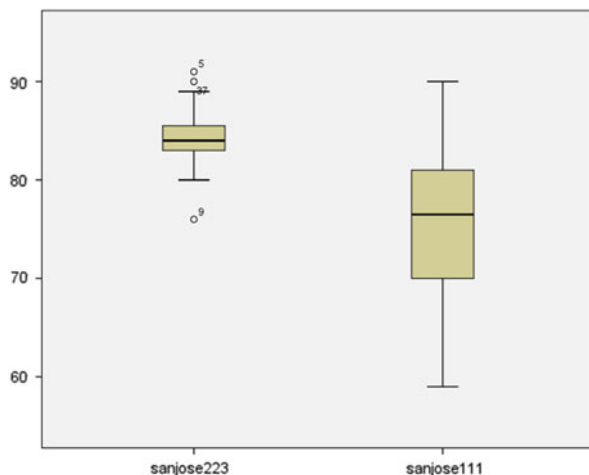
Fig. 2 Traffic and pedestrian flows used for modeling in peak hour

safety distance (bx_add) and the multiplicative part of the desired safety distance (bx_mult) with default values of 2, 2 and 3 respectively.

In order to calibrate the pedestrian model, the parameters affecting the driving force were selected due to the conflicts generated inside the junction and because the calibration was based on speeds and relaxation time. Parameters affecting other forces such as the repulsive forces from other pedestrians and obstacles and the attractive forces had a minor effect on the modeling.

By default, the desired speed distribution (which represents the speed that pedestrians are willing to reach) is defined as a linear function between 0.97 and 1.6 m/s for men and between 0.72 and 1.2 m/s for women [21]. From video was observed that 18 % of people were constituted by children and elderly pedestrians. For this reason, the desire speeds were adjusted considering the study of [25] in which the average speed of elderly pedestrians could vary between 0.62 and

Fig. 3 Distributions of queue lengths obtained with default and calibrated parameters



0.92 m/s. Therefore, it was considered a desired speed between 0.8 and 1.3 m/s for men and between 0.7 and 1.2 m/s for women, as starting points.

The default relaxation time (which can be interpreted as reaction or inertia time) is 0.4 [21]. To represent the Peruvian pedestrian behavior a relaxation time of 0.30 was considered as a starting point.

Furthermore, it was considered during the simulation 10 time steps for simulation seconds, and the results were recorded without including the warm up period. In this project, all the parameters mentioned above were modified manually and 12 runs, with different seed numbers, were made in every case until the final group of parameter produced acceptable results (Table 2). The final group of calibration parameter is as follows: Wiedemann values (1, 1, 1), critical gap of 1.9 s, desire speeds between 0.85 and 1.2 m/s, and relaxation time of 0.35. To highlight the importance of the calibration process the Fig. 3 shows the different distributions of average queue lengths, in one access, obtained with default Wiedemann car following values (2, 2, 3) and the final values of calibration (1, 1, 1).

The calibration methodology suggested by [7] uses parametric test to evaluate if there is evidence of equal means between the sample fields measurements and the sample simulation results. However, there are two aspects that previously would need to be evaluated. Firstly, the distributions from both samples of data need to follow a normal distribution and secondly, it is not sufficient to compare means, it is necessary to analyze whether both distributions are similar. Therefore, to know if the results from field data and VISSIM followed a normal distribution, a Kolmogorov Smirnov test was developed (Table 1). After that, a non-parametric test (U of Mann Whitney) was developed to compare distributions (Table 2). These evaluation were developed at 95 % level of confidence and the p values obtained (majors to 0.05) indicate that there is no evidence to reject the null hypothesis.

Once, the previous conditions were checked, parametric tests were developed to know if the number of runs was sufficient at 95 % level of confidence and if there

Table 1 Test of normality for the collected data and VISSIM results

Null hypothesis	Test	P value
Queue distribution from field follows a normal distribution	Kolmogorov Smirnov for one sample	0.457
Queue distribution from VISSIM follows a normal distribution	Kolmogorov Smirnov for one sample	0.304
Pedestrian speed from field follows a normal distribution	Kolmogorov Smirnov for one sample	0.651
Pedestrian speed from VISSIM follows a normal distribution	Kolmogorov Smirnov for one sample	0.573

Table 2 Comparison of distributions

Null hypothesis	Test	P value
Distributions of queue length are similar	U of Mann Whitney for independent samples	0.117
Distributions of pedestrian speeds are similar	U of Mann Whitney for independent samples	0.363

Table 3 Comparison of average queue lengths from field and VISSIM final adjusted parameters

Average length queue (m)	Standard deviation	P value
72.3 (field)	7.98	
74.97 (Vissim result)	7.65	0.586

Null hypothesis: queue field = queue simulation

Alternative hypothesis: queue field \neq queue simulation

Table 4 Comparison of average pedestrian speed from field and VISSIM final adjusted parameters

Average pedestrian speed, (m/s)	Standard deviation	P value
1.05 (field)	1.2	
0.98 (Vissim result)	0.56	>0.05

Null hypothesis: speed field = speed simulation

Alternative hypothesis: speed field \neq speed simulation

is evidence that the means from two samples (length queues from field data and VISSIM as well as pedestrian speed from field data and the pedestrian model) were similar (Tables 3 and 4). Figure 4 shows the current scenario modeled with VISSIM and its pedestrian module.

After the current scenario was calibrated, traffic and pedestrians volumes from another day were inserted on the model for validation. Parametric evaluation of means for queue lengths and pedestrians speed found a p value major to 0.05 in both cases (Tables 5 and 6), by which the model was considered validated.



Fig. 4 Current scenario modeled with VISSIM and its pedestrian module

Table 5 Comparison of average queue lengths from field data and VISSIM (validation stage)

Average queue length (m)	Standard deviation	P value
42.6	2.28	
45.1	3.92	0.069

Null hypothesis: queue field data = queue simulation

Alternative hypothesis: queue field data \neq queue simulation

Table 6 Comparison of average pedestrian speed from field data and VISSIM (validation stage)

Average pedestrian speed, (m/s)	Standard deviation	P value
1.21 (field)	0.8	
1.13 (Vissim result)	1.29	>0.05

Null hypothesis: speed field data = speed simulation

Alternative hypothesis: speed field data \neq speed simulation

4 Results

After the current scenario was calibrated and validated, a new scenario was constructed considering the same junction geometry and volumes, but with mitigation measures. Among the mitigation measures we can find changes in the number of traffic light phases (one phase exclusive for pedestrian movements), sidewalks and wider crosswalks. In general terms, the proposals focused on providing further facilities for vulnerable road users and improve their safety. Figure 5 shows the modeled scenario with improvements (Tables 7 and 8).

The results indicate that mitigation measures would improve the circulation of all users. Pedestrian speed would increase by 25 % and contrary to what Peruvian politicians were thinking, benefits to vulnerable users would not reduce the benefits for traffic circulation. There is a 35 % reduction in delays and an increment of 65 % on vehicular speed.



Fig. 5 Scenario with improvements to protect vulnerable users

Table 7 Comparison of average queue lengths (current scenario and with improvements)

Average queue length (m)	Standard deviation	P value
74.97 (current)	7.98	
55.58 (with improvements)	7.26	0.00

Null hypothesis: queue current scenario = queue scenario with improvements

Alternative hypothesis: queue current scenario > queue scenario with improvements

Table 8 Comparison of efficiency parameters (current scenario and with improvements)

Efficiency parameters	Current situation X-S	With improvements X-S	P -value
Average delay (seg/veh)	49-7.38	31.63-1.53	0.000
Average delay (seg/pedestrian)	20.39-4.65	14.25-0.437	0.000
Average vehicle speed (km/h)	10.85-1.92	17.26-0.205	0.000
Average pedestrian speed (m/s)	0.98-0.56	1.22-0.89	0.000

Null hypothesis: equal means

Alternative hypothesis of delays: current means > means with improvements

Alternative hypothesis of speed: current means < means with improvements

X mean

S standard deviation

5 Conclusions

The social force model could be used to replicate the behavior of pedestrians and traffic interaction at intersections in Peru, where an aggressive driving style and chaotic behavior is present.

The possibility of combining traffic and pedestrian micro simulation models opens a great opportunity to evaluate in all projects the benefits for all users and not only for private vehicles. For instance, current projects in Peru consider facilities for public transport (Bus Rapid Transit systems) and the possible problems generated such as insufficient pedestrian capacity in terminals, narrow footpaths, conflicts with

vehicles at junctions and design of inadequate infrastructure could be analysed and improved through traffic and pedestrians micro simulation models.

The results would indicate to authorities that the management measures implemented to improve chaotic environments favor to all users and reduce the possibility of pedestrian accidents, highlighting that this would not reduce the benefits for traffic circulation.

The defaults values of the Wiedemann car following model and critical gap are very different with respect to the calibrated values. This could be due to the aggressive driving style observed in Peru and mainly in the junction analysed. By the contrary, on the driving force model (pedestrian model) the differences were smaller which would indicate that in this specific case the behaviour is similar.

References

1. OMS: Informe sobre la situación mundial de la seguridad vial. Es hora de pasar a la acción. Organización Mundial de la Salud. Ginebra (2009).
2. Cabrera, F.: ¿Pueden los modelos macro-determinísticos y microsimulación analizar adecuadamente las intersecciones semaforizadas en Lima?. XVI Congreso Panamericano de Transporte, Tráfico y Logística – PANAM 2010. Lisboa, Portugal (2010).
3. Liu, R., Van Vliet, D., Watling, D.: Microsimulation models incorporating both demand and supply dynamics. *Transp. Res.* 40A, 125–150 (2006).
4. Zhang, M.H., Ma, J., Dong, H. Calibration of departure time and route choice parameters in microsimulation with macro measurements and genetic algorithm. In: *Proceeding of the 85 th TRB Annual Meeting*, Washington , D.C., U.S.A. (2006).
5. Laval, J.A., Daganzo, C.F.: Lane changing in traffic streams. *Transp. Res.* 40B, 251–264, (2006).
6. Ossen, S., Hoogendoorn, S.P., Gorte, B.G.H.: Interdriver differences in car following : a vehicle trajectory-based study. *Transp. Res. Rec.* 1965, 121–129, (2006).
7. Dowling, R., Skabardonis, A., Halkias, J., McHale, G., Zammit, G.: Guidelines for calibration of microsimulation models: framework and application. In: *Proceedings of the 83rd TRB Annual Meeting*, Washington, D.C., U.S.A. (2004).
8. May, A.: *Traffic flow fundamentals*. Prentice Hall, New Jersey, (1990).
9. Bloomberg, L., Swenson, M., Haldors, B.: *Comparison of Simulation Models and the Highway Capacity Manual*, Preprint, Annual Meeting, TRB, Washington, DC, (2003).
10. Algiers, S., Bernauer, E., Boero, M., Breheret, L., Di Taranto, C., Dougherty, M., Fox, K., Francois, G.: *Smartest- Review of micro-simulation models*. Road Transport European Scheme (1997).
11. Hollander y Liu, R.: The principles of calibrating traffic microsimulation models. *Springer Science. Transportation* 35: 347–362, (2008).
12. Brackstone, M., McDonald, M.: "Car-following: A historical review, " *Transp. Res., Part F: Traffic Psychol. Behav.*, vol. 2, no. 4, pp. 181–196, (1999).
13. Wiedeman, R.: *Simulation des Straßenverkehrsflusses*. Schriftenreihe des IfV, 8, Institut für Verkehrswesen. Universität Karlsruhe. (1974).
14. PTV: *VISSIM User Manuel*. Karlsruhe, (2009).
15. Helbing, D.: *Complex Systems* 6, 391 (1992).
16. Helbing, D.: *Stochastische Methoden, nichtlineare Dynamik und quantitative Modelle sozialer Prozesse* (Shaker, Aachen, Germany, 1993).
17. Helbing, D.: *Physikalische Modellierung des dynamischen Verhaltens von Fußgängern* (Diplom thesis, Georg-August University, Göttingen, Germany, 1990).

18. Henderson, L. F.: *Nature* 229, 381 (1971).
19. Henderson, L. F.: *Transp. Res.* 8, 509 (1974).
20. Helbing, D., Buzna, L., Johansson, A., and Werner, T.: Self-organized pedestrian crowd dynamics: Experiments, simulations, and design solutions, *Transportation Science* 39, 1–24 (2005).
21. Sohrad, A., Bierlaire, M., Farooq, B., Danalet, A., Silvan, F.: Scenario Analysis of Pedestrian Flow in Public Spaces. *Transp-or and Ecole Polytechnique Federale De Lausanne*. (2012).
22. Lewin, K., *Field Theory in Social Science*, Harper & Brothers, New York, (1951).
23. Helbing, D., A mathematical model for the behavior of pedestrians, *Behavioral Science* 36, 298–310 (1991).
24. Helbing, D., Molnàr, P.: Social force model for pedestrian dynamics. *Physical review E*, 1995.
25. Teknomo, K.: Application of microscopic pedestrian simulation model. *Transportation Research Part F*, 2006.

Validation of Crowd Models Including Social Groups

Gerta Köster, Franz Treml, Michael Seitz, and Wolfram Klein

Abstract The development of group models within models of pedestrian motion has recently become a new focus of research. This interest was triggered by insight from the social sciences: Small groups often dominate the crowd at large events and the need to associate with family and friends may dominate over flight instincts. It is therefore desirable that crowd simulators adopt the new group models to better mitigate risks for example at large events or at public infrastructures. However, to make this feasible reliable validation tests must be made available. Developers and users alike should be able to check whether the adopted model indeed captures the essential characteristics of a crowd composed of subgroups. As a desirable side effect, common validation tests would make simulation tools easier to compare and their range of application easier to assess. This can help to ensure a minimum quality standard and thus to further mitigate risks. In this paper we suggest basic visual tests and some quantitative test were data is available.

Keywords Validation • Verification • Modeling • Simulation • Crowd • Pedestrian stream • Groups • Social group • Cellular automaton

1 Introduction

Ideally models for physical or social phenomena are developed on the basis of observations. These may be field studies or controlled experiments. Mathematical formulations are derived that match the observed phenomena. Discrete models or

G. Köster (✉) • F. Treml • M. Seitz
University of Applied Sciences, Lothstraße 64, Munich 80335, Germany
e-mail: gerta.koester@hm.edu; franz.treml@hm.edu; m.seitz@hm.edu

W. Klein
Siemens AG Corporate Technology, Munich 81739, Germany
e-mail: wolfram.klein@siemens.com

discretization in time and space of continuous models allow converting the model into a computer program that forms a simulation tool. With help of the simulation tool, a trained user can run through multiple scenarios. In the case of pedestrian stream simulations this puts him or her in the position to gain virtual experience for situations where it is impossible, uneconomical or even unethical to gather real experience. Buildings and events can be planned with a focus on safety making use of that virtual experience. At some point even short term predictions may become possible. However, simulations remain useless, even potentially harmful, if the simulation tool does not reliably reproduce the true phenomena. Hence, one of the biggest challenges in the applied research field of crowd motion is the validation of the proposed models.

The development of group models within models of pedestrian motion has recently become a new focus of research. This interest was triggered by insights from the social sciences: Small groups often dominate the crowd at large events [2] and the need to associate with family and friends may dominate over flight instincts [1, 11, 18]. So far models of small subgroups have been suggested that well capture the movement towards a supposed common goal and ensure a certain spatial structure of the groups for easy communication [8, 12]. It has been shown by both, simulations and measurements that the existence of subgroups in a crowd significantly impacts the behavior crucial for the safety of the crowd such as the flow at a given density or egress times when facing a bottleneck [9, 12]. It is therefore desirable that crowd simulators adopt the new group models to better mitigate risks.

To make this feasible reliable validation tests must be made available. Developers and users alike should be able to check whether the adopted model indeed captures the essential characteristics of a crowd composed of subgroups. As a desirable side effect, common validation tests would make simulation tools easier to compare and their range of application easier to assess. This can help to ensure a minimum quality standard and thus to further mitigate risks. In this paper we build on some basic tests for small subgroups and complement them by tests suitable for larger groups that split into subgroups.

The paper is structured as follows: In the following section we describe essential characteristics of group behaviour that a model should reproduce. We then suggest a number of tests, both qualitative and quantitative. We also demonstrate the feasibility of all suggested tests with our own simulation model that is based on a cellular automaton. In the conclusion we discuss desirable next steps.

2 What Is a Social Group?

The first step towards our objective is to agree on what a social group in a crowd is. In this paper we describe group characteristics that impact the flow of a crowd and hence quantities, such as the egress time at a bottleneck, which may be critical for crowd safety [8]. We present this very basic model of subgroups in a crowd for both small subgroups and larger groups in the form of a list of requirements so that the

choice of implementation remains free. Hence the tests can be used for social force models, cellular automata and other model choices alike.

3 Small Subgroups

We need to identify the relevant characteristics of subgroups that must be captured by the mathematical model to correctly reproduce the geometric cohesion within groups. We need to define typical, if still rather abstract, behavior of groups.

We consider a group as an aggregation of persons who stay together while moving. They move at approximately the same speed towards the same goal. Additionally, we assume that small groups exhibit certain formations [4, 12, 19]. We think that one of the main challenges is to ensure the right type of cohesion: groups, as a whole, must remain very stable, while deformations of groups in time and space must be possible to the extent that, very occasionally, a group member may be lost. This leads to a list of requirements. With the diversity of group patterns in real life, the requirements are not necessarily fulfilled simultaneously by a real group. Nor is the list complete. However, we think, at least for small groups of at most four or five persons, that group formation and group progress may be captured by all the behavioral patterns described in detail below. A more complete rationale of our model and how it ties in with findings from psychology and sociology is given in [8, 9, 17].

- All individuals in the group move towards the same goal.
- Members of a group stay together. Permanent separation of a member from the rest of the group may occur but only in extreme situations.
- All individuals in the group move with the same speed, except for temporal variations caused, for example, by avoiding obstacles and collisions with others.
- The (cooperative) group slows down when a member stays behind.
- Small groups have a basic spatial structure that stays relatively unchanged if walking across a free space, but can be temporarily deformed by external influences such as the presence of a crowd, oncoming traffic or obstacles: They walk abreast.

3.1 *Larger Groups Composed of Subgroups*

A common assumption, yet without extensive empirical evidence, is that large groups break up into smaller subgroups of size two to four that we call communication groups [12]. This was first suggested by social scientists [5]. We additionally assume that large groups also stay together as a whole in a less strict formation. No communication between members of two different subgroups is assumed. For first empirical results to support this we refer to [14].

- Large groups divide into smaller communication groups of up to four pedestrians that are formed in a way to facilitate communication within the subgroups.
- The whole group stays loosely together, but – due to lack of substantial evidence – no formation among the subgroups is assumed at this point.

4 Validation Tests

We suggest a number of basic tests. Typical questions are: Do groups stay together? Do groups keep their velocity when walking along a free path? Do group members walk abreast as suggested by social communication models? Are they capable of splitting and reuniting while navigating around an obstacle like a column? Do larger groups split up into subgroups as suggested by social scientists? Do they still stay together as a whole? Most of our tests are qualitative in their nature and can be conducted by producing snapshots or short videos from the simulation output. In a number of cases it is also possible to introduce heuristic measurement parameters that would allow running the tests in the manner of automatic unit tests that are either passed or failed. This greatly simplifies consistent development and testing.

Qualitative tests that are usually visual are very important as a starting point: a simulation tool, for example, that fails to ensure group cohesion, cannot be considered reliable. However it is very difficult to compare different models and assess their range of application on visual observations only. This is what makes quantitative tests so valuable. In such tests important output parameters are measured and compared against measurements from field or laboratory experiments. For aggregate crowds the perhaps most important quantitative test is based on the density-velocity or equivalently density-flow relationship in a moving crowd. So-called fundamental diagrams express how the crowd slows down with increasing density. A suitable test implementation has been described by the RiMEA initiative [15, 16]. Oberhagemann (2010) presented graphs of fundamental diagrams for small groups in crowds extracted from field studies. We propose tests based on these findings. The authors finally conducted a controlled experiment where students are observed leaving a classroom as individuals, in pairs and in groups [9]. We demonstrate the feasibility of all suggested tests with our own simulation model that is based on a cellular automaton.

The test proposals are structured as followed. First we describe the behavior that we wish the simulation to reproduce through a list of requirements that must be met to pass the test. Then we demonstrate a possible test outcome produced with our own pedestrian motion simulator. Our simulation tool is a cellular automaton model complemented with a model for groups. Information on the basic model can be found in [6, 7]. The group model is described in [8, 17].

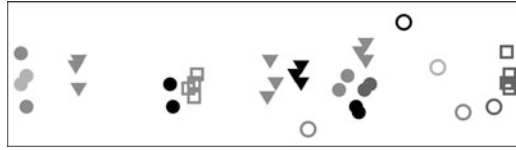


Fig. 1 Groups of different sizes, indicated by the shape of the symbol, walk abreast along a wide corridor. Matching shades of gray further identify the members of a group

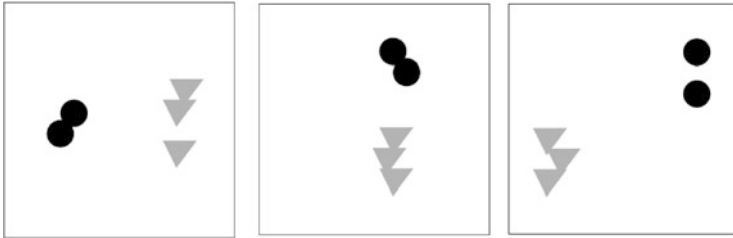


Fig. 2 Two groups walk from left to right. One is faster than the other and is observed just before, while and after passing

4.1 Visual Observation of Small Groups

As a first test for a computer model we suggest to visually check whether group cohesion is adequately captured. We propose to let groups of sizes from 1 to 5 walk along a wide corridor and to visually observe the group progress. We demand, that

- Each group stays together. No group member is lost.
- Group members walk abreast as long as the path is free.
- Faster groups pass slower groups.

Figure 1 shows a snapshot from a simulation output where several groups walk from left to right. Clearly group members walk abreast. Groups do not separate. The series of snapshots in Fig. 2 shows a faster group passing a slower group.

When a group faces an obstacle that is limited in size, say a column, we expect the group to either circumnavigate the column as a whole or to shortly split up and then reunite. We expect the latter especially when the space is narrow. In this test we let groups walk down a corridor with a column placed in the middle. We request that

- Each group either circumvents the column in a whole or splits up in front of the obstacle.
- Group members reunite after passing the obstacle. In our example in Fig. 3 the group briefly splits up.

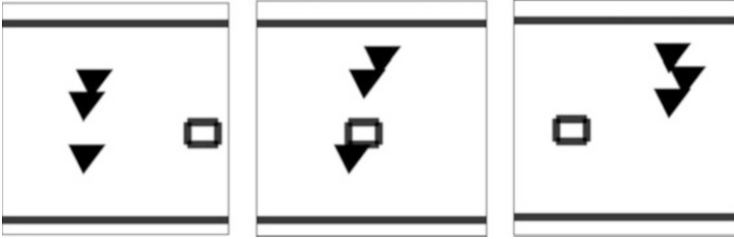


Fig. 3 A group walking from left to right approaches a column placed in the middle of a corridor. The group briefly splits up and then reunites

4.2 *Density-Flow Dependency for Groups*

The denser a crowd the slower progress becomes for everybody. This phenomenon is captured in density-velocity and density-flow diagrams called fundamental diagrams. The best known diagram by Weidmann [20] is widely used to validate pedestrian motion models [3]. It does not, however, include the impact of groups. Oberhagemann [13] has compiled density-velocity diagrams for different group sizes, ranging from 1 to 5, from measurements obtained from video footage at German fairs. With that, there are five fundamental diagrams instead of one. In the test, we restrict ourselves mostly to qualitative comparisons. We suggest producing pedestrian flow with different group sizes and densities and compare the results to Oberhagemann's diagrams. For simplicity we use one group size per experiment. At this point, we enforce high densities by inserting groups at the wide end of a corridor of length 200 m that gently narrows from 20 m at one end to 4 m at the other end. We measure the density when a quasi-stationary flow establishes itself for at least 100 s during a simulated time of 1,000 to 4,000 s. With low densities the quasi-stationary state can be observed for 1,000 s or more. We request the following:

- The velocities match in the sense that they are of the same order of magnitude.
- For each group size, that is for each diagram, the velocity decreases with density in a way that roughly matches the measurements (order of magnitude).
- The bigger the group size the slower the progress. The diagrams form a family of curves one lying above the other.
- The difference between the diagrams disappears with very dense crowds.

Visual comparison of the results in Fig. 4 with the measurement in [13] shows that all requirements above are fulfilled, but that the groups in the computer experiment slow down later than in the field study. Also differences between the velocities for the different group sizes disappear at a higher speeds where they seem to converge asymptotically. The differences may be due to measurement error in both, the real and the virtual setting, or the simplified experiment or the cone geometry.

Fig. 4 Fundamental diagrams obtained from computer experiments. There is a good visual match with published data from field studies [13]

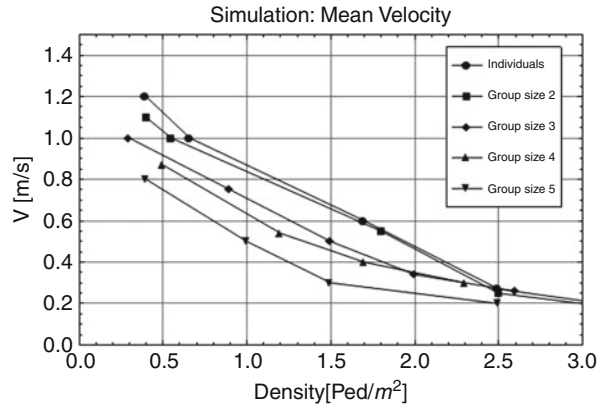
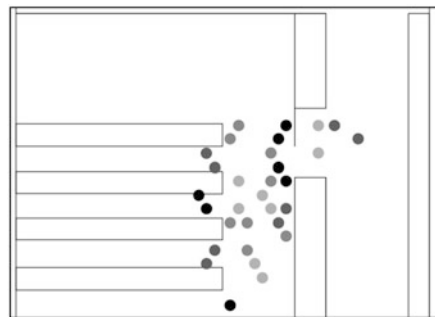


Fig. 5 Visualization of classroom egress



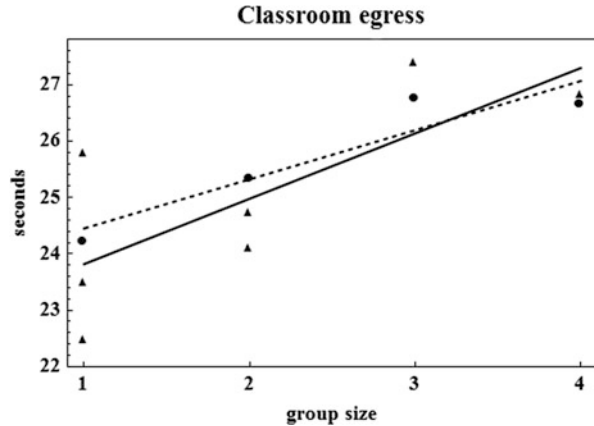
4.3 A Quantitative Test for a Classroom Egress

Quantitative tests are very difficult to come by. No test involving groups is known to the authors. Therefore, in November 2010, the authors conducted a small experiment with a class of 30 computer science students in their first semester. We asked the students to stand at their desks and, at a signal, leave the classroom through a door as only bottleneck. Outside the classroom, in the hallway, they were asked to turn left and walk across a line between the hallway and the larger entrance hall.

The time was measured from the signal to the moment when the last student crossed the line. In a second round, the students were paired with their desk neighbors. In a third and fourth round triplets and quadruples were formed. To quantify the effect of the group size on the egress time, a linear regression model with the group size as explanatory variable and the egress time as response variable was used. A more detailed description and statistical analysis of the experiment can be found in (Köster et al. 2011a).

Not surprisingly the egress time increases with the group size. All three requirements stated below are fulfilled in a matching simulation experiment where the desire to communicate within a group was calibrated. It is depicted in Fig. 5.

Fig. 6 Empirical measurement of a life experiment, a classroom egress, compared to simulation results. *Triangles* denote the measured values. The *solid line* is the result of the corresponding linear regression. *Circles* indicate the means of 500 simulation runs. The *dashed line* is the corresponding linear regression



- The simulated egress times match the measurements in their order of magnitude.
- The egress time increases with the group size.
- A more refined model should allow calibration to a quantitative fit within a certain margin.

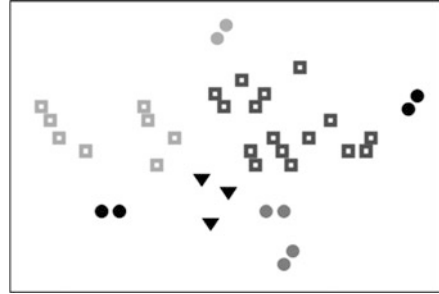
Results of the empirical measurements and the calibration are given in Fig. 6. We want to point out that this calibration differs from the one reported in a previous publication [8]. Since then we further simplified our group model for small groups which made calibration simpler and led to a very close fit to the experimental data [17]. One should, however, beware of overfitting with such a close calibration to a single life experiment.

4.4 Visual Observation of Large Groups Walking Across an Open Field

So far we have only presented tests for small communication groups. However, we often observe large groups in crowds, such as football fans enjoying a game together [14] or flocks of tourists following their guides. Therefore we want to encourage models that can deal with large structured groups as described in [14, 17] and hence we need to validate them.

Unfortunately, no measurements experiments on large groups in crowds are known to the authors. The challenge is to devise tests that are trustworthy in the sense that they show plausible behavior and that they give us directions as far as measurable quantities are concerned, that can later be checked experimentally by independent researchers. We start with simple qualitative tests that are extrapolated from tests for smaller groups. We suggest that

Fig. 7 A large group of 16 persons (*dark gray*) walks across an open space from left to right. It is composed of 8 subgroups. It forms an agglomeration among small groups



- The members of each large group stay together. No group member is lost.
- Each large group divides into small subgroups for which the rules of the small communication groups apply.
- Faster groups pass slower groups. They may split up temporarily, but reunite when the path is free (Fig. 7).

The visual test for small groups we described earlier also make sense for large groups with only slight modifications. E.g. when a large group passes another group we no longer expect the whole group to stay together, but to split up into its subgroups and then reunite. Compare to Fig. 2. The navigation tests for small groups (Fig. 3) where a group has to skirt an obstacle in a corridor can also be carried over to large groups. Again we expect the large group to rather split up in its subgroups than to squeeze by the obstacle as a whole.

4.5 Egress of a Large Room: Extrapolation of a Laboratory Experiment for Individuals

The lack of experimental evidence for large groups makes it impossible to validate a model for large groups quantitatively at this point. Nonetheless we devise a quantitative test with the express intention to make it open to falsification, that is, to allow comparison to experiments that can be conducted by independent scientists at a later stage. We therefore decided to base our test proposal on very carefully conducted laboratory experiments by Liddle et al. [10] where the data is publicly accessible.

In this controlled life experiment, 180 soldiers were gathered in a room connected to a corridor with varying width and length. See Fig. 9. The egress times and densities were measured. For simplicity, we select only one sample width (140 cm) and length (400 cm) for the corridor. The egress time in the experiment is 80s. Our goal is to reenact the experiment with the simulator and then conduct simulation experiments where we have groups of increasing size among the virtual subjects (Fig. 8).

In the virtual world of our simulator we need to complement the input data by individual desired velocities. We assume the free-flow velocities to be normally

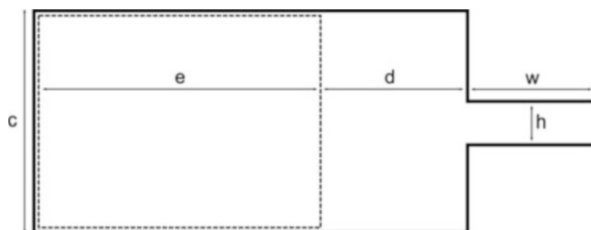


Fig. 8 Geometry of the test scenario: Egress of a large room. The *dashed lines* indicated the area where the (virtual) subjects wait before heading for the door ($h = 1.4$ m, $w = 4$ m, $d = 3.76$ m, $e = 10$ m, $c = 7.1$ m). The size of the waiting area is chosen so that the density with 180 virtual pedestrians corresponds to the density in the controlled experiment

Table 1 Egress of a large room: simulation results. 180 virtual subjects leave the room as individuals, pairs and in groups of increasing size

Simulation experiment	Mean egress time	Variance	10 % quantile	90 % quantile
Individuals	73.63	2.84	71.06	75.65
Groups of 2	86.93	5.91	83.81	89.76
Groups of 4	90.59	4.60	87.55	93.16
Groups of 15	119.32	17.61	113.56	124.10
Groups of 25	127.54	44.65	120.87	135.49

distributed about 1.34 m/s with a standard deviation of 0.26 m/s as suggested by Weidmann [20]. This aggregated model for individual pedestrians is also calibrated according to the fundamental diagram given in [20]. We measure the density in a small area positioned in front of the exit door.

The egress time for individuals in our simulation experiment is a little lower than in the true experiment: 74 s on average in 50 simulation runs compared to 80 s in the experiment, but we think the difference is acceptable. A closer match could only be expected if the distribution of the subjects' velocities were known. In addition, the laboratory experiment was conducted only once, so that we have no information about variances in a bigger sample. We repeat the simulation experiment for pairs and groups of increasing size. The number of virtual subjects stays 180 in every group experiment. As one would expect intuitively, as well as from the classroom egress earlier, the egress time increases with the group sizes. There is a considerable increase in egress times when large groups are introduced (Table 1).

To pass the test successfully we demand that:

- The average egress time for individuals lies within a 10 % margin of the measured time (80 s).
- The average egress time increases with the group size for small and for large groups.
- The introduction of large groups leads to a marked increase in the average egress time (Figs. 9, 10, 11, and 12).

Fig. 9 Egress of a large room: 180 individual virtual subjects leave the room. The simulation results are averaged over 50 runs. The graph denotes the mean spatial density measured in a small area situated in front of the opening to the corridor

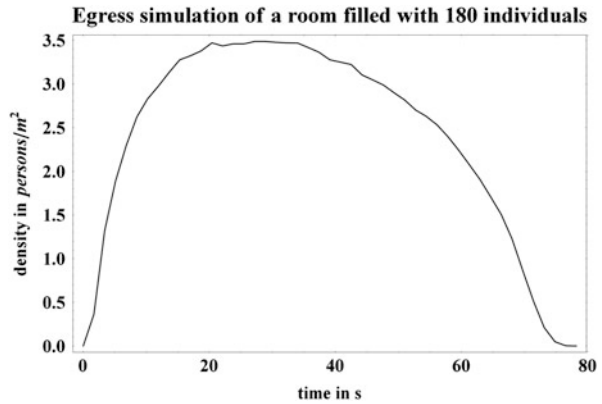


Fig. 10 Egress of a large room: 180 virtual subjects leave the room in pairs. The simulation results are averaged over 50 runs. The graph denotes the mean spatial density measured in a small area situated in front of the opening to the corridor

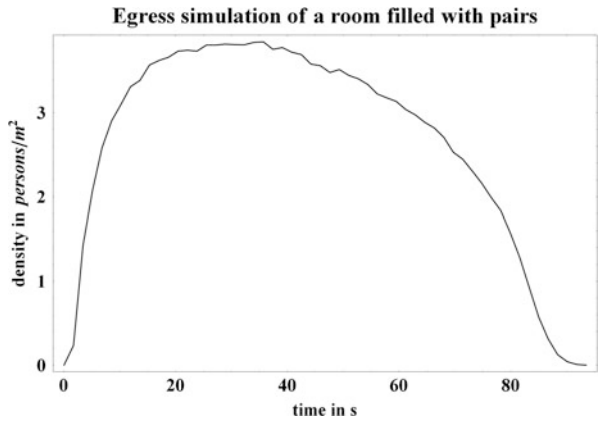


Fig. 11 Egress of a large room: 180 virtual subjects leave the room in quadruples. The simulation results are averaged over 50 runs. The graph denotes the mean spatial density measured in a small area situated in front of the opening to the corridor

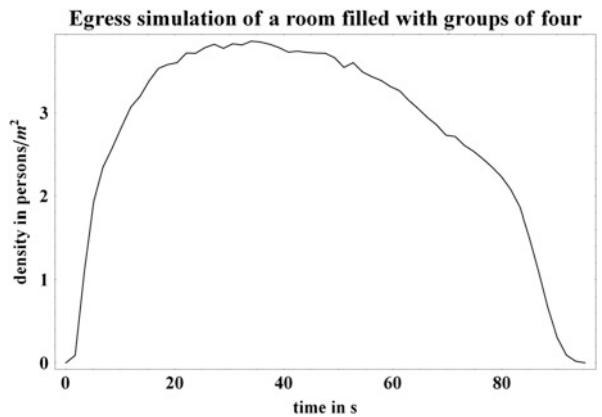
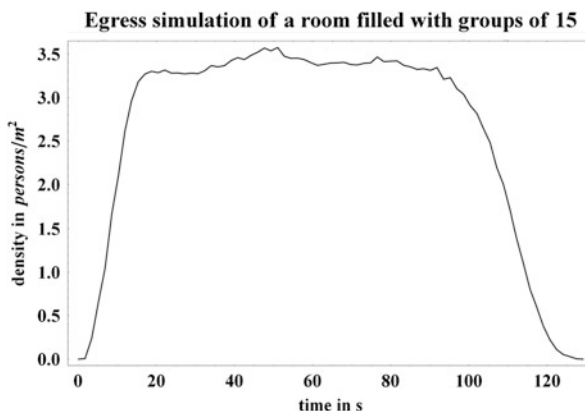


Fig. 12 Egress of a large room: 180 virtual subjects leave the room in groups of 15. The simulation results are averaged over 50 runs. The graph denotes the mean spatial density measured in an area situated in front of the door



5 Conclusion

We presented tests for group models within a pedestrian stream simulator with the objective to give users and developers a guideline for validation: What must we and what can we expect from a state-of-the-art group model? Most of the tests are qualitative, that is, they suggest that known or plausible behaviors be reproduced by the simulation tool in a way that can be viewed through snapshots or short videos. These tests are very valuable as a starting point, but they leave a lot of room for individual interpretation which makes them difficult to standardize.

We also suggested quantitative tests based on published data from field trials and laboratory experiments. Quantitative tests are superior in many ways: Once they are accepted, they can easily be standardized and thus make an unbiased assessment of tools possible. Also they are a good basis for automated unit tests to build a test environment when developing a tool. However, quantitative tests need reliable measurement data as a basis, which requires not only acceptable sample sizes, but also that measurement data be made accessible, including error margins and statistical information such as standard deviations. This is extremely difficult to achieve, especially with large uncontrolled surveys so that the research in this field is still in a pioneering stage. Nonetheless, we believe that a shared suite of quantitative tests should be desirable for serious modelers and experimental crowd researchers alike. The authors would therefore like to encourage both groups to continue to cooperate to achieve this ambitious common goal.

Acknowledgements This work was partially funded by the German Federal Ministry of Education and Research through the priority program Schutz und Rettung von Menschen (Protection and Rescue of People) within the projects REPKA (Regional Evacuation: Planning, Control and Adaptation) and MEPKA (Investigation of Mathematical Properties of Pedestrian Stream Models).

References

1. Aguirre, B. E., Wenger, D., and Vigo, G., (1998). A test of the emergent normtheory of collective behaviour. *Sociological Forum*, 13(2), 301–320.
2. Aveni, A. F. (1977), The not-so-lonely crowd: friendship groups in collective behavior. *Sociometry*, 40(1), 96–99.
3. Davidich, M. and Köster, G., (2012). Towards automatic and robust adjustment of human behavioral parameters in a pedestrian stream model to measured data, *Safety Science* 50, pp. 1253–1260.
4. Fasheng Qiu and Xiaolin Hu., (2009). Modeling group structures in pedestrian crowd simulation. *Simulation Modelling Practice and Theory*. 18:190–205, October 2009.
5. James, J., (1951). A preliminary study of the size seterminant in small group interaction. *American Sociological Review*, 16(4), pp. 474–477.
6. Klein, W., Köster, G., and Andreas M., (2010). Towards the calibration of pedestrian stream models. In: Roman Wyrzykowski, Jack Dongarra, Konrad Karczewski, and Jerzy Wasniewski, editors, *Parallel Processing and Applied Mathematics*, volume 6068, pages 521–528.
7. Köster, G., Hartmann, D., and Klein, W. (2010). Microscopic pedestrian simulations: From passenger exchange times to regional evacuation. *Proceedings international conference on operations research: mastering complexity*, Munich.
8. Köster, G., Seitz, M., Treml, F., Hartmann, D., and Klein, W., (2011a). On modelling the influence of group formations in a crowd, *Contemporary Social Science*, 6:3, 397–414.
9. Köster, G., Seitz, M., Treml, F., and Pfaffinger A., (2011b). How to validate group models in pedestrian stream simulators: a proposal for basic tests. *International Conference on Operations Research*, Zürich, September 2011.
10. Liddle, J., Seyfried, A., Steffen, B., Klingsch, W., Rupprecht, T., Winkens, A., and Boltes M., 2011. Microscopic insights into pedestrian motion through a bottleneck, resolving spatial and temporal variations. arXiv:1105.1532v1.
11. Mawson, A.R., 2005. Understanding mass panic and other collective responses to threat and disaster. *Psychiatry* 68(2), 2005.
12. Moussaïd M, Perozo N, Garnier S, Helbing D, and Theraulaz G., 2010. The Walking Behaviour of Pedestrian Social Groups and Its Impact on Crowd Dynamics. *PLoS ONE* 5(4): e10047. doi:[10.1371/journal.pone.0010047](https://doi.org/10.1371/journal.pone.0010047).
13. Oberhagemann, D., Statische und dynamische Personendichten bei Großveranstaltungen, vfdb Technischer Bericht 13–01, March 2011.
14. Reuter, V., Bergner, B. S., Köster, G., Seitz, M., Treml, F., and Hartmann, D. On Modeling Groups in Crowds: Empirical Evidence and Simulation Results Including Large Groups. In Weidmann U, Kirsch U, Schreckenberg M (eds), *Pedestrian and Evacuation Dynamics 2012*, pp. 835–846. Springer, Cham, 2014.
15. RiMEA e. V., 2009. Richtlinie für Mikroskopische Entfluchtungsanalysen (guideline for microscopic evacuation analysis), 2009. <http://www.rimea.de>
16. Rogsch, C., Klüpfel H., Könnicke, R., Winkens, A., (2009). RiMEA: A Way to Define a Standard for Evacuation Calculations. In Weidmann U, Kirsch U, Schreckenberg M (eds), *Pedestrian and Evacuation Dynamics 2012*, pp. 455–468. Springer, Cham, 2014.
17. Seitz, M., Köster, G., and Pfaffinger, A. 2012. Pedestrian Group Behavior in a Cellular Automaton. In Weidmann U, Kirsch U, Schreckenberg M (eds), *Pedestrian and Evacuation Dynamics 2012*, pp. 807–814. Springer, Cham, 2014.
18. Sime, J. D., (1983). Affiliative behaviour during escape to building exits, *Journal of Environmental Psychology*, 3(1), 21–41.
19. Singh, H., Arter, R. Dodd, L., Langston, P., Lester, L., and Drury, J, (2009). Modeling subgroup behaviour in crowd dynamics DEM simulation. *Applied Mathematical Modelling*, 33:4408–4423.
20. Weidmann, U., (1992). *Transporttechnik für Fussgänger*. Schriftenreihe des IVT, 90.

Velocity-Based Models for Crowd Simulation

Julien Pettré, David Wolinski, and Anne-Hélène Olivier

Abstract Velocity-based models belong to the category of microscopic crowd simulation models. They recently appeared in the crowd simulation literature. They mathematically formulate microscopic interactions as a function of agents' states and their derivatives. In the case of collision avoidance, this property provides agents with the ability to produce anticipated smooth reactions, with great impact on simulation results. This paper is made of five sections. We first describe the main principles of velocity-based models. We then describe an experiment that tends to prove that velocity-based models are founded, at least in the basic case of collision avoidance between two walkers. Next, we describe three models, the Paris model, the Tangent model and the Vision model that were successively proposed by our INRIA group for crowd simulation. We emphasize their differences to allow comparison. We finally discuss the benefit of velocity-based approaches, and what are the problems raised by these approaches and to be addressed in future work.

Keywords Crowd simulation • Microscopic models • Velocity-based models

1 Introduction

The main objective of microscopic crowd simulation is to compute the macroscopic behavior of a crowd by simulating the interactions people have together at a local scale. Pedestrian simulation is a typical example. We expect to predict global traffic conditions from numerical models of the physical interactions people have during their navigation. Basically, they avoid all the static and moving obstacles in their neighborhood: collision avoidance is generally considered to be the most crucial

J. Pettré (✉) • D. Wolinski • A.-H. Olivier
INRIA-Rennes, Rennes, France
e-mail: julien.pettre@inria.fr

interaction for pedestrian crowd simulation, and the absence of interpenetration between simulated bodies to be a hard constraint.

Velocity-based models correspond to a new type of numerical models of microscopic interactions for crowd simulation. They recently appeared in the literature, in 2007, and various solutions were developed from various fields: computer graphics, computational geometry, computer vision and cognitive science. These fields took interest in velocity-based models for various reasons, but a common one is the need for realistic simulation results, or at least believable ones, at all scales of the crowd, even at the smallest one. Too many artifacts were produced by previous techniques, especially because of their lack of anticipation: agents were often trapped in deadlock situations or producing strange oscillating motions. Avoiding a collision with anticipation means that avoidance maneuvers are over before agents get close to each other. Anticipation cannot result from microscopic models that formulate interaction as a function of distance between agents (which is the case of most simulators based on particle systems and physically inspired models).

To allow anticipation, a velocity-based model formulates interactions not only as a function of agents' states (positions), but also as a function of their derivatives (velocities). The basic principle of velocity-based models is to decompose, for each agent, the reachable velocity domain (all the global motions an agent can perform) into two components: the admissible, and the inadmissible velocity domains. The admissible velocity space is the set of velocities at which an agent can move without risk of future collision. At the opposite, a risk of collision appears when the agent moves at a velocity belonging to the inadmissible domain. Obviously, the notion of collision risk is considered with notion of time. Time-to-collision (TTC) is a classically used variable to describe the risk with respect to the time dimension.

How to compute the admissible and inadmissible velocity domains in the case of a crowd, when all obstacles are constantly moving and each agent is performing adaptations independently? By working with short time-windows and by constantly updating agents' states and decisions, we show that velocity-based models provide convincing and smooth simulation results. Some recent efforts in model evaluation on real data showed that this category of models is promising for realistic crowd simulation. The objective of this paper is to provide an overview of some existing solutions. The paper is organized as follows: Sect. 2 situates velocity-based models among other simulation techniques, and gives a list of existing velocity-based models, as exhaustive as possible. Based on experimental observations of collision avoidance behaviors, Sect. 3 shows that velocity-based models are grounded in reality. Section 4 describes three existing velocity models in the objective to provide a pedagogical description and to emphasize their singularities. Finally Sect. 5 further discusses differences between models and proposes future development paths for this new category of models.

2 Background

Crowd simulation can be approached from two opposing perspectives. One is to consider it as a coherent body, which is the macroscopic approach. The other is to build the crowd from local inter-agent interactions, which is the microscopic approach.

From the macroscopic point of view [8, 15], a crowd is modeled to behave like a fluid, thus allowing to use fluid dynamics inspired concepts such as velocity potential fields. The focus of this type of approach is to obtain a coherent behavior from the crowd, leaving aside individual agents' goals and constraints and enforcing non-interpenetration (the primary constraint for crowd simulation) at the last moment. Since these approaches have been designed with only global patterns in mind, many artifacts appear at the local scale. It is for example possible to see agents moving sideways, collisions or even residual interpenetrations.

On the contrary, from the microscopic point of view, individual constraints and goals are most important. A global behavior is then expected to emerge as a result of these complex, local interactions. Various methods exist to simulate these interactions.

A possibility is to discretize the space into cells as in cellular automata and model agents as occupied cells [6, 14]. In this case, interactions are modeled using (often probabilistic) transition rules and their complexity varies with the discretization. Different behaviors can be modeled this way such as the formation of lanes when two groups cross ways for example. However, due to the necessary levels of discretization, it becomes impractical to model complex collision avoidance strategies; this is usually handled by forbidding agents to move to an already occupied cell.

Non discrete models, on the other hand, let agents make decisions based on several different inputs and criteria. The first such model (Boids model) has been proposed in [13] where agents made decisions based on three rules: separation (agents avoid overcrowding), alignment (agents steer towards a common goal) and cohesion (agents keep close to the group).

Another model has been proposed in [4, 5] as an analogy to physics where agents were subject to forces, hence the name Social Forces model. This was a position-based model, all forces which affected the agents were obtained based on their positions. This allowed to model more complex collision avoidance behaviors as well as other phenomena such as friends and store fronts where the forces would be attractive instead of repulsive as is the case for obstacles.

In the recent years, velocity-based models emerged as an evolution of the position-based Social Forces model. These models, also called predictive models, process more information than the position-based ones. They are essentially able to predict the trajectory of the agents and make decisions accordingly. The most popular way of doing so is to establish an admissible velocity domain which contains all velocities that will not lead to a collision. All that remains is then to choose the velocity that is closest to a preferred velocity (for example one that leads

to the goal) thus necessitating the smallest acceleration. These models offer the most advanced local behaviors and are listed (in chronological order) in the following paragraphs.

The Dynamic Window Approach, proposed in [3], aimed to allow robots to avoid collisions. The method is essentially a greedy exploration algorithm of possible velocities weighted by a cost based on the robots' dynamics (the cost is very high if the velocity leads to a collision). This model later inspired the first collision avoidance approaches in the field of crowd simulation.

The first predictive model in crowd simulation was introduced in [10]. It divides the space in front of a given agent into sectors and for each of these, it establishes a minimum and maximum speed which form the interval of speeds that lead to a collision. The agent is then free to choose the velocity outside these intervals that is closest to his preferred speed.

The next velocity-based model is the Reciprocal Velocity Obstacle (RVO) model which was introduced in [2]. In this approach, pairs of agents are represented in the relative velocity space and each velocity (a point in velocity space) that leads to a collision in a certain time window is made unavailable, thus forming a velocity obstacle. The chosen velocity is then the closest one to the preferred velocity and outside the obstacle. This model has since been updated with the ability to divide the avoidance effort between agents as well as the ability to use acceleration information (leading to the newer Acceleration-Velocity Obstacle model).

Proposed in [11], the Linear Trajectory Avoidance (LTA) model explores a set of possible moves and associates a cost to each of them. The cost is a function of future crossing distance, which is estimated by extrapolating trajectories given the current positions and velocities. The model was used in the framework of video tracking of real pedestrians. It acts as a predictor for the tracker, and was proved to significantly increase tracking quality, especially when occlusions occur.

The Tangent model proposed in [12] functions in a similar way where agents (as well as their personal area) are represented in the relative velocity space. However, here the goal is to compute the interaction area (where both agents are the closest) and, based on its position relative to the walkers' personal areas, a decision is made on which agent goes first and which gives way. The resulting adaptation efforts are shared and asymmetrical as observed in real-life scenarios.

Ondrej's et al. [9] Vision model aims to solve interactions based on information accessible from the visual flow, thus simulating a perception-reaction loop. The agents rely on the bearing angle and the approximate time-to-collision to make their decisions. They are also capable of interacting with any kind of static or dynamic obstacle as long as they "see" it.

Finally, [7] introduced a cognitive heuristics model where agents seek a trajectory based on unobstructed space. In very dense scenarios, however, physical forces – a second heuristic – become predominant and lead to unintentional movements and "crowd turbulence". The Tangent and Vision models as well as Paris' model will be further detailed in Sect. 4.

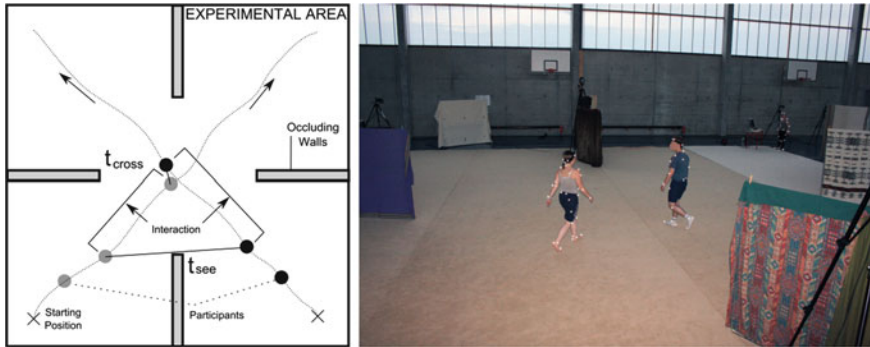


Fig. 1 *Left*: illustration of the experimental setup to observe collision avoidance between two participants. The *square* experimental area is represented from *top* (25 m wide). *Right*: picture taken during experiments. One can see the two participants who received a start signal following orthogonal trajectories and avoiding each other

3 Experimental Validation of Velocity Based Models

The basic principle of velocity-based models is to compute the *admissible velocity domain*, i.e., the velocities at which an agent can move without provoking collisions in the near future. Each model proposes specific methods to compute this domain and to select a specific solution velocity. However, all of them are based on a linear extrapolation of the current situation to check for future collisions. Do humans perform such a prediction? Do they anticipate the future conditions of an interaction and do they react accordingly? To a certain extent, this hypothesis made by velocity-based models is validated by the following experiment.

We designed the experiment illustrated in Fig. 1. The results of this experiment are completely detailed in [1]. We asked some participants to stand at the corners of a square area (25 m. large) and asked them to walk to the opposite corner. We controlled their task with networked computers at each corner. We synchronized participants starting to provoke situations of probable collision between two participants following orthogonal paths. We randomized passage orders and put occluding walls to prevent participants from reacting before they reached their comfort speed and saw each other. We recorded their trajectories using an optoelectronic motion capture system. We observed more than 400 pairwise interactions. The experimental setup is illustrated in Fig. 1.

The variation of individual behavior, reaction delay and comfort speed actually changed the accurate conditions of the crossing. Then, we could analyze the correlation between initial conditions of interactions with the existence and the nature of avoidance maneuvers.

We defined MPD, the minimum distance at which participants would meet if they did not perform any avoidance maneuvers, i.e., if they continued walking straight in their direction at constant speed. In other words, we compute an estimate of the

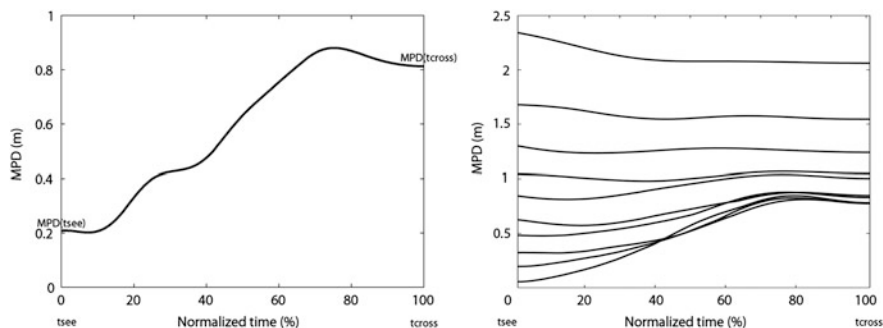


Fig. 2 *Left*: MPD evolution in time during the whole interaction phase. *Right*: mean evolution of MPD during the whole interaction phase for groups of 40 experiments, ranked and grouped by order of initial MPD value

closest approach by linearly extrapolating the participants' trajectories from current position and velocity. The MPD can be computed at any time: Fig. 2, left plot, displays an example of evolution of MPD in time, for the whole interaction phase (the interaction phase starts as soon as participants are able to see each other and ends when they pass at minimal distance). Time was normalized for each experiment and grew from 0 (beginning of interaction) to 100 (end of interaction).

In the example of Fig. 2, left plot, one can observe a typical situation and its evolution in time. At time $t = 0$, $MPD = 0.2$ m, which means that if participants continue walking like this, a collision is predicted (distance is between body centers). Rapidly, MPD starts progressively growing up to 0.8 m. This distance is no more critical and allows participants the avoid collisions. The MPD value is regulated to this value during the last quarter of interaction. How can we interpret this evolution? We here show the clear sign of the ability of humans to predict the situation of future collisions and to react with anticipation. Indeed, by definition, the variation of MPD can only be explained by some maneuvers performed by walkers. We observe (i) that MPD control by participants starts rapidly after they are able to see each other, (ii) that the contribution of maneuvers is positive: MPD is monotonically increasing, (iii) MPD is not exaggeratedly increased, (iv) that maneuvers are over long before interaction is over (interaction duration is 4 s on average).

We described a specific example. We ordered our 400 experiments by the initial MPD value, and formed 10 groups of 40 experiments each. We computed the average evolution of MPD for each group. Results are reported in Fig. 2, right plot. We show that, when MPD is initially low (groups 1, 2, 3, 4, 5, and 6 with $MPD < 1$ m at the beginning of the interaction phase), MPD is controlled by avoidance maneuvers and increased to an average of 0.8 m. For other groups, no avoidance is observed and MPD remains constant on average (still, with some fluctuations, report to [1] for details).

The conclusions of our experiment are the following. First, humans are able to predict the future conditions of interactions with accuracy: avoidance maneuvers (i.e., variations of MPD) were observed only when required. Second, humans are able to react accordingly, in advance, to the benefit of the situation: the fact that avoidance maneuvers are over before people reach their closest approach proves anticipation. These two conclusions partially validate the foundations of velocity-based models and prove them to be closer to real human behavior in comparison with distance based models such as social forces models or other particle models.

4 A Comparative Description of 3 Velocity-Based Models

The fundamental objective of velocity based models is to compute the admissible velocity domain, i.e., the set of walking velocities that prevent agents from colliding with static and moving obstacles in the near future, and to select a specific solution among this set. Various techniques were proposed to compute this domain. Following, we describe and compare 3 solutions that were developed at INRIA in the past 5 years. These models are denoted: the Paris model [10], the Tangent model [12] and the Vision model [9]. The following sections provide a pedagogical description of these solutions, nevertheless, readers should refer to the original papers for more detailed technical descriptions.

4.1 The Paris Model

The Paris model proposes a discrete approach to estimate the admissible velocity domain. Each agent's motion is controlled by the direction of walking θ and its walking speed s . Let us consider an example of interaction between two agents, A and B. We describe below how the motion of A is controlled by the model with respect to the motion of neighbor agent B.

The future positions of B are predicted from the linear extrapolation of the current position and velocity vector (current time is time t_0). In Fig. 3, left image, the current position and velocity of A and B are shown, as well as the future positions of B at times t_1 , t_2 and t_3 .

Several time intervals are considered. For each time interval $[t_i, t_{i+1}]$, the angular sector covered by the predicted motion of B and relative to the position of agent A is computed. In Fig. 3, the left image displays the angular sector covered by B between t_1 and t_2 . The angular sector is delimited by θ_1 and θ_2 . Agent A may enter into collision with B in the time interval $[t_i, t_{i+1}]$ if, and only if, A moves in a direction belonging to this angular sector.

For each time interval and corresponding angular sector, we additionally compute s_{\min} and s_{\max} , which are respectively the minimum speed at which A should move to pass in front of B, and the maximum speed at which A should move to give way

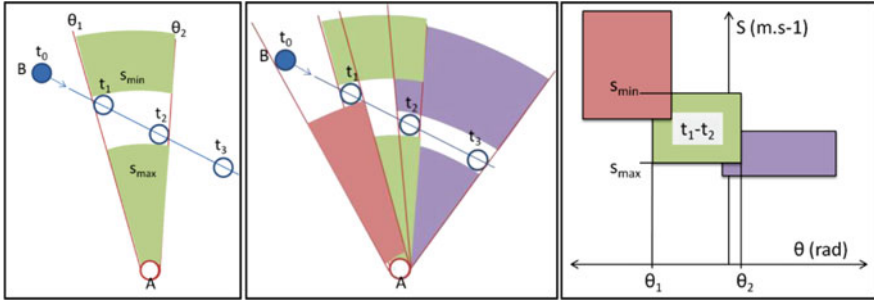


Fig. 3 Illustration of the Paris model: interaction between two agents A and B. *Left*: illustration of the time interval $[t_1-t_2]$, of the angular sector $[\theta_1, \theta_2]$ and of the speed interval $[s_{min}, s_{max}]$. *Middle*: repetition of computations for successive time intervals. *Right*: representation of the deduced admissible velocity space in the control space

to B. In the example of Fig. 3, if A moves in a direction $\theta \in [\theta_1, \theta_2]$ at a speed $s \in [s_{max}, s_{min}]$, there is a high risk of future collision. Figure 3 illustrates these bounds (colored parts of angular sectors are safe speeds).

Steps 1–3 are repeated for each neighbor agent and for each time interval. Portions of inadmissible velocities (belonging to intervals $[s_{max}, s_{min}]$ and $[\theta_i$ and $\theta_{i+1}]$) are successively reported into the control space (Fig. 3, right image: the space left blank corresponds to the admissible velocity domain). By construction, the admissible velocity domain is deduced. The model uses a cost function to deduce the best solution belonging to this domain (that minimizes deviations as well as distance to comfort speed).

As a conclusion, the Paris model iteratively computes the inadmissible velocity domain with some approximation. Indeed, s_{min} and s_{max} should be functions of time, but only the worst cases values are retained for one given time interval and one considered neighbor agent. The shorter the time intervals, the more accurate the model. But this approximation allows the model to be efficient in terms of computation time. In the original paper, to find a trade-off between accuracy and performance, Paris suggests to sample future time in an irregular manner: the first time intervals, which correspond to the imminent future, are shorter than the following ones (the paper suggests: $t_1 = 1$ s., $t_2 = 2$ s., $t_3 = 4$ s., $t_4 = 8$ s.).

The model easily takes into account multiple interactions by looping steps 1–3 of the method for several agents. Each time, a new set of constraints is added to the control space. The model is also able to consider static obstacles: they are sampled and considered as sets of static agents. They are processed the same way as moving agents, with the exception of speed constraints. Only s_{max} is computed, s_{min} has no sense here.

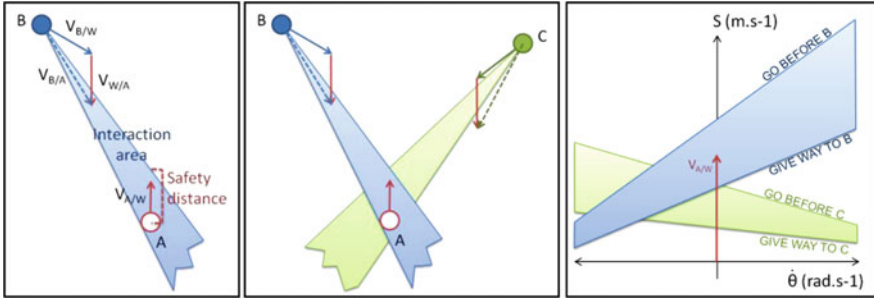


Fig. 4 Principles of the Tangent model. *Left*: interaction between agents A and B. *Middle*: interactions between agent A and (B + C). *Right*: illustration of the resulting constraint in the control space

4.2 The Tangent Model

The Tangent model was designed to reproduce some experimentally observed interactions between two walkers with a very high level of realism, higher than with the Paris model. In particular, the Tangent model considers the human perception of others’ velocity, and introduces some error terms: their role is to delay avoidance maneuvers when accurate perception is not yet obtained. Doing so, the timing of interactions is reproduced. To our knowledge, the Tangent model is still the only one attempting to correctly model interactions in time. The following paragraphs explain the basic principles of the Tangent model. A detailed description is to be found in [12].

The model is described from the example of motion control for agent A during interaction with agent B (see Fig. 4). The velocity vector of B relative to A, $V_{B/A}$, is first computed. By linear extrapolation, $V_{B/A}$ allows to estimate the distance at which B will pass A. When the crossing distance is too low, A has to perform an avoidance maneuver. To this end, we define a safety distance in front of A: we consider that the crossing distance is too low when $V_{B/A}$ belongs to the interaction area represented in Fig. 4, left image. To model when A should react, we consider in addition a perception error ϵ that decreases over time. A actually reacts when $V_{B/A} + \epsilon$ belongs to the interaction area.

To avoid a future collision, the relative velocity vector $V_{B/A}$ must lie out of the interaction area. Agent A can adapt this relative velocity by playing on its own velocity vector $V_{A/W}$ (we cannot assume that A controls B’s motion), we remind that:

$$V_{B/A} = V_{B/W} - V_{A/W} \tag{1}$$

where W refers to the World coordinate system. Figure 4, illustrates these two components of the relative velocity vectors. In the example Fig. 4, one can see that A can for example decelerate: the $V_{A/W}$ component of $V_{B/A}$ would then be shorter and collision avoided. Equally, A could turn to the right.

These adaptations can be better appreciated from the control space point of view. Indeed, the interaction area is similar to two linear inequality constraints that can be projected onto the velocity space. Multiple interactions can then be solved as by solving a system of linear inequalities. Figure 4, middle image, illustrates an interaction between agent A and two other agents (B + C). In the right image, we project the constraints imposed by interaction in the velocity space. This representation enables an easy description of the situation and how to adapt the motion to avoid collisions. One can observe that the current velocity of A will provoke a future collision with B. A could decelerate to give way to B, but will then start interacting with C. In this specific example, one valid solution could be to turn to the right and slightly decelerate: A would give way to B but go before C.

The tangent model can consider static obstacles with geometries described by sets of line segments, as explained in [16]. In comparison with the Paris model, we can see some differences. The time dimension is taken into account: the model describes risks of future collisions, but does not explicitly estimate when said collisions will occur. Instead, by introducing an error term, a reaction time is simulated. To solve interactions with respect to the imminence of collision risk, we actually order interaction with respect to time-to-collision. The system of linear equalities that captures multiple interactions is progressively built in this way until a limit number of interactions is reached or when the solution space becomes null. Doing so, agents react to interactions having a higher risk of collision.

4.3 *The Vision Model*

The two previous models assume that agents, i.e., simulated human walkers, are able to integrate a large quantity of information about neighbors' motions. This information is progressively projected into the control space to deduce the admissible velocity domain. Even though the Tangent model also models motion perception error to better simulate the timing of an interaction, real humans do not process information this way to control their locomotion. They control their walk mainly according to their visual perception of their environment. The objective of the Vision model, in comparison with the two previously proposed models, is to better simulate this perception-action loop.

The neuroscience field stated that humans, during avoidance of static or moving obstacles, successively answer two questions: will a collision with the obstacle occur? When will this collision occur? They react accordingly. The manner in which humans process their optical flow to answer these questions is still under debate but some theories state that two variables are directly exploited by humans for motion control: first, $\dot{\alpha}$, the derivative of the bearing angle, and second, ttc, the time-to-collision. When an obstacle is always visually perceived under the same angle (i.e., $\dot{\alpha} = 0$), and is growing in the image formed on the retina ($\text{ttc} > 0$), a risk of future collision is detected. The imminence of the collision risk is determined by ttc as well.

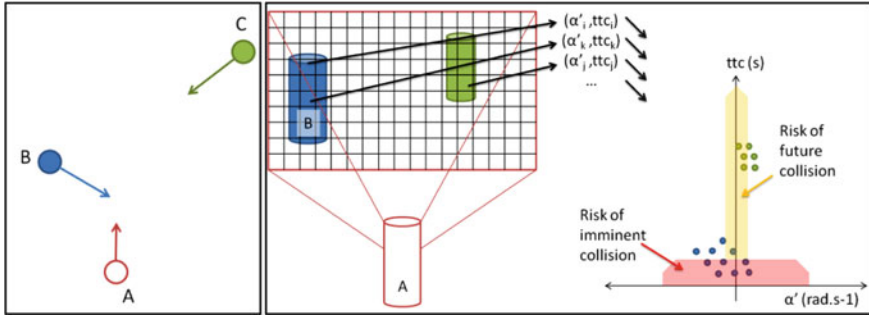


Fig. 5 Principles of the Vision model. *Left*: situation of an interaction between agent A and two other agents (B + C). *Right*: visual representation from the agent A’s point of view is computed and projected into the (α', ttc) -space

The Vision model reproduces this perception action loop. The principle of the model is illustrated in Fig. 5, from the example of an interaction between an agent A and two other agents (B + C), as shown in the left image of the figure. To start, we compute a digital representation of the environment from the perspective of agent A (right image). This representation is computed similarly to classical graphical rendering techniques. A matrix represents the perceived image, each pixel is computed based on rastering techniques. The comparison stops here, we do not compute the pixels’ graphical properties (color, intensity). Instead, for each pixel p_i , two values are computed: $(\dot{\alpha}_i, ttc_i)$, the time-derivative of the bearing angle and the time-to-collision. These values are deduced from the relative position and velocity of the corresponding obstacle the pixel belongs to. It should be noted that an obstacle is possibly represented by several pixels (especially when close or big), and that each value may change for each pixel, because relative positions and velocities slightly change.

At the end of the rendering process, the notion of obstacles disappears, the agent A now interacts with a pixel cloud with various $(\dot{\alpha}_i, ttc_i)$ values. All this visual information is projected into the $(\dot{\alpha}, ttc)$ -space. Agent motion control is performed according to a simple perception-action simulation loop:

1. Pixels with low $\dot{\alpha}$ values correspond to a risk of future collision. When such pixels are perceived, the agent turns to change this situation. The goal of the agent is taken into account when computing this anticipated reaction to avoid large deviations.
2. Pixels with low ttc values correspond to an imminent risk of collision (even with large $\dot{\alpha}$ values because of the body envelope). When pixels with such low values are perceived, the agent decelerates. He adapts his tangential speed to the lowest perceived ttc value.

In the example of Fig. 5, we explain how agent A’s motion control is performed during an interaction with two other agents (B + C). Agent B is perceived with low ttc pixels values whereas agent C is perceived with low $\dot{\alpha}$ pixels values. Both a risk

of imminent and future collision. As a result, agent A will both decelerate and turn to solve this interaction. Pixel detection thresholds as well as motion control laws, which constitute the core of the vision model, are detailed in the original paper.

This model has interesting properties. It is able to consider any type of obstacle, static or moving and with any geometry, with undifferentiated processing because they are all reduced to a set of pixels. Also, the visibility of obstacles as well as their importance relatively to the place they occupy in the perception image is implicitly taken into account. Finally, the model was proven to be capable of simulating the emergence of well known pedestrian patterns under some traffic conditions.

5 Discussion and Conclusion

In this paper, we successively described three different velocity-based models. They propose three different methods to compute the admissible velocity domain and to finally control the agents' motion. They can be compared with respect to various criteria.

First, they were designed with different objectives in mind (see Fig. 6). The Paris model was, chronologically, the first velocity-based model: the objective was to enable anticipated adaptation for crowd simulation. But when a reaction should start? The tangent model answers this question by introducing a "motion perception error" term in the formulation of the model. But both of these solutions remain far from the real perception-action loop that humans use to control their locomotion, which is modeled in the vision approach with yet unparalleled fidelity.

Second, they are based on different control spaces. The Paris model works in the orientation-speed space (we call speed the norm of the velocity vector). The Tangent model works in the angular-tangential-velocity space. Finally, the Vision model independently controls turning motions and speed (respectively from the existence of a risk of collision and its imminence).

Next, all these models take into account obstacles with various geometries, which is a very important property and often neglected in other approaches. The Paris model samples obstacles as set of "static agents". The Tangent model is able to simulate interactions between agents and line segments, which is very practical when considering building-like environments. Finally, the vision model considers indistinguishably any kind of obstacle (other agents or static obstacles) with any geometry, because motion control is performed from their graphical representation.

Also, they consider time-scale in various ways. The Paris model provides both risks of collisions and their situation in time: several time windows are successively explored. At the opposite, the Tangent model computes risks of collision, with one single TTC value (based on current velocities), but unlimitedly explores future time, as for the vision model.

Finally, both the Paris and the Tangent model need additional techniques to filter, order and select interactions (from the visibility of agents, their relative positions in space, the imminence of risk of collision, etc.). Indeed, one agent should not

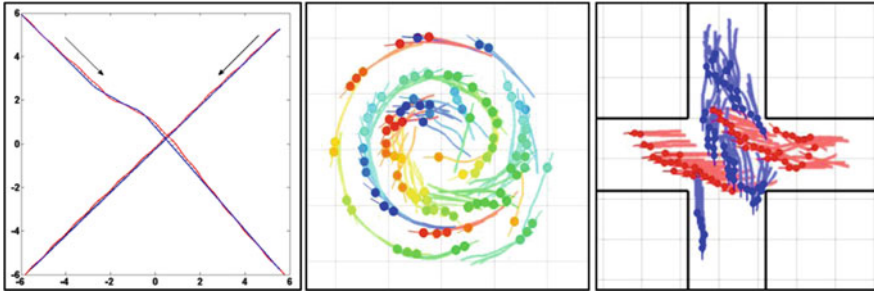


Fig. 6 Simulation results. *Left*: collision avoidance between two agents simulated by the Tangent model, output trajectories (*in color*) are superimposed with experimental data (*black*): situation can be accurately reproduced. *Middle and Right*: simulation results for the Vision model. Emergent formation of pedestrians are observed, conform to real observations

interact with all other agents if numerous (as real humans who only consider a neighborhood). The effect of the used notion of neighborhood on simulation was proven to be important in terms of emergent behaviors. The vision model is here more satisfying, as this selection process is implicitly based on obstacle visibility and relative importance (by their size in the perceived image). The vision model was proven to simulate the emergence of patterns of pedestrians with phenomena similar to reality. Is this property responsible for this interesting behavior?

Other questions still need addressing concerning velocity models. New types of interactions should be addressed. Recently, a new model for the following behavior was proposed, with a high level of realism as evaluated from experimental data. How to combine, for example, following and avoidance behaviors to simulate complex group behaviors, which is crucial in the aim of simulating natural looking crowds?

The fundamental basis of velocity models should also be put again into question. A simple linear extrapolation of trajectories based on current position and velocity is sometimes a bad prediction, especially during maneuvers (a small deviation may completely change the trajectory prediction between two time steps): in crowded places where people constantly adapt their motion, is using a velocity model useless? Probably not, because computations are constantly re-evaluated. But smarter predictions, at the level of real human abilities, would probably make this new type of model even more realistic and useful.

References

1. Anne-Hélène Olivier, Antoine Marin, A. C. J. P. (2012), ‘Minimal predicted distance: A common metric for collision avoidance during pairwise interactions between walkers’, *Gait & posture in press*, 2012.
2. van den Berg, J.; Patil, S.; Sewall, J.; Manocha, D. & Lin, M. (2008), Interactive navigation of multiple agents in crowded environments, *in* ‘Proceedings of the 2008 symposium on Interactive 3D graphics and games’, ACM, New York, NY, USA, pp. 139–147.

3. Fox, D.; Burgard, W. & Thrun, S. (1997), 'The Dynamic Window Approach to Collision Avoidance', *IEEE Robotics & Automation Magazine* **4**(1).
4. Helbing, D. & Molnar, P. (1995), 'Social Force Model for Pedestrian Dynamics', *PHYSICAL REVIEW E* **51**, 4282.
5. Johansson, A.; Helbing, D. & Shukla, P. K. (2007), 'Specification of the Social Force Pedestrian Model by Evolutionary Adjustment to Video Tracking Data', *Advances in Complex Systems* **10**(supp02), 271–288.
6. Kretz, T. & Schreckenberg, M. (2008), 'The F.A.S.T.-Model', *CoRR* **abs/0804.1893**.
7. Moussaid, M.; Helbing, D. & Theraulaz, G. (2011), 'How simple rules determine pedestrian behavior and crowd disasters', *PNAS* **108**, 6884.
8. Narain, R.; Golas, A.; Curtis, S. & Lin, M. C. (2009), Aggregate dynamics for dense crowd simulation, in 'ACM SIGGRAPH Asia 2009 papers', ACM, New York, NY, USA, pp. 122:1–122:8.
9. Ondrej, J.; Pettré, J.; Olivier, A.-H. & Donikian, S. (2010), 'A synthetic-vision based steering approach for crowd simulation', *ACM Trans. Graph.* **29**, 123:1–123:9.
10. Paris, S.; Pettré, J. & Donikian, S. (2007), 'Pedestrian Reactive Navigation for Crowd Simulation: a Predictive Approach', *Computer Graphics Forum, Eurographics'07* **26**(3), 665–674.
11. Pellegrini, S.; Ess, A.; Schindler, K. & van Gool, L. (2009), You'll Never Walk Alone: Modeling Social Behavior for Multi-target Tracking, in 'ICCV'.
12. Pettré, J.; Ondrej, J.; Olivier, A.-H.; Cretual, A. & Donikian, S. (2009), Experiment-based modeling, simulation and validation of interactions between virtual walkers, in 'Proceedings of the 2009 ACM SIGGRAPH/Eurographics Symposium on Computer Animation', ACM, New York, NY, USA, pp. 189–198.
13. Reynolds, C. W. (1987), Flocks, herds and schools: A distributed behavioral model, in 'Proceedings of the 14th annual conference on Computer graphics and interactive techniques', ACM, New York, NY, USA, pp. 25–34.
14. Schadschneider, A. (2001), 'Cellular Automaton Approach to Pedestrian Dynamics - Theory', in M Schreckenberg & S DEditors Shrama, ed., , Technical report, Institut fur Theoretische Physik, Universitat zu Koln, Springer, 11.
15. Treuille, A.; Cooper, S. & Popović, Z. (2006), 'Continuum crowds', *ACM Trans. Graph.* **25**, 1160–1168.
16. Zhang, Y.; Pettré, J.; Ondrej, J.; Qin, X.; Peng, Q. & Donikian, S. (2011), 'Online inserting virtual characters into dynamic video scenes', *Computer Animation and Virtual Worlds* **22**(6), 499–510.

Part IV
Psychology

Fuzzy Prediction of Pedestrian Steering Behavior with Local Environmental Effects

Mojdeh Nasir, Matthew Glenn Watson, Vu Le, Saeid Nahavandi,
and Douglas Creighton

Abstract This research focuses on prediction of pedestrian walking paths in indoor public environments during normal and non-panic situations. The aim is to incorporate uncertain and non-precise aspects of pedestrian interaction with the environment to enhance steering behavior modeling. The proposed model introduces a fuzzy logic framework to predict the impact of environmental stimuli within a pedestrian's field of view on movement direction. The environment is treated as a set of discrete attractions and repulsions. Attractive and repulsive effects of the surrounding environment, which drive the pedestrian to select next step position, are quantified by social force method. A high flow corridor in an office is considered for the case study. Stochastic simulation is used to generate walking trajectories and calculate a dynamic contour map of environmental stimuli in each step. To verify the simulation results and gain a better insight into the problem, a dataset defining walking trajectories of 25 participants passing through that hallway was collected using motion tracking system. Results demonstrate a strong correlation between real data and simulated results.

Keywords Pedestrian steering behavior • Fuzzy logic • Environmental effects • Walking trajectory prediction

1 Introduction

Accurate pedestrian walking path prediction is a fundamental requirement to facilitate urban public area design and has recently attracted attention from researchers across multiple disciplines. During past decades, researchers have

M. Nasir (✉) • M.G. Watson • V. Le • S. Nahavandi • D. Creighton
Centre for Intelligent Systems Research, Deakin University, Victoria, Australia
e-mail: mnas@deakin.edu.au; mgwa@deakin.edu.au; vu.le@deakin.edu.au;
saeid.nahavandi@deakin.edu.au; douglas.creighton@deakin.edu.au

shown an increased interest in crowd dynamics and evacuation behavior in panic conditions under stress and danger situations, but steering behavior under normal and stable conditions and its measurements have seldom been considered. In existing publications, individual and group level wayfinding behavior under normal circumstances has been studied relatively less than others. Also, pedestrian-environment interactions with regards to environmental cognition, spatial behavior, and navigation performance need to be addressed.

Therefore, there is a vivid and essential need to study pedestrian behavior under normal conditions. This study aims the development of future conceptual models to predict pedestrian behavior, and their utilization for design, planning, optimization, and decision-making.

A specific gap in pedestrian steering behavior research is the deficiency in predicting how people choose their next step direction and speed when exposed to specific environmental conditions in normal situations. This behavior mainly relates to implicit environmental cognition. There is an absence of a comprehensive theory on how people behave during normal movement. This study is an investigation into pedestrian steering behavior in normal situation, inclusive of environmental effects in walking path prediction. Our aim is to develop a conceptual model of pedestrian steering behavior for indoor environments under normal conditions.

Human wayfinding is based on “a consistent use and organization of definite sensory cues from the external environment” [1]. Wayfinding is a spatial behavior that reflects the cognitive process of choosing a route from an origin to a target. An individual carries the immediate sensation and perceived information from the surrounding environment to implement this action [1]. It is a behavior that starts with imperfect space observations and leads to imprecise and incomplete knowledge of the environment that results in an action [2]. Lynch, a pioneer in wayfinding research, described pedestrian imprecise knowledge of the surrounding environment by fuzzy elements in the mental image of environment [1]. The demonstrated success of this study is the motivation behind this research.

Golledge et al. [3] believed that movement direction and orientation are fuzzy and have interrelation with a wide range of elements like environmental stimulations. Environmental stimulation changes constantly while a pedestrian move through the area and influences the observer’s perception from environment. Wineman and Peponis [4] showed that to estimate pedestrian movement, understanding the relation between the pedestrian’s perception of environmental stimuli and pedestrian displacement is essential. According to Fajen and Warren [5], human locomotion tasks are controlled by information exchange with the surrounding environment. In Li’s study [6] of urban pedestrian wayfinding, a dynamic interaction model of pedestrian-environment and mobile devices was proposed. Similar to pedestrian behavior modeling, driver route choice behavior was modeled in a fuzzy preference relation approach [7]. In the field of robot navigation and path planning, fuzzy rule-based system have also been successfully applied. Seraji and Howard [8] proposed fuzzy logic rules to model a robot navigation strategy. They have proposed linguistic

fuzzy sets to define two motion control variables. A set of fuzzy logic rules are defined to model the robot with three navigation behaviors including seek-goal, obstacle avoidance, and traverse terrain. Weighting factors and a centroid defuzzification approach was applied to integrate all of the aforementioned navigation behaviors.

These studies suggest that fuzzy logic has the ability to model the diverse and varied nature of pedestrian perceptions and spatial reactions towards the environmental stimulations.

This paper addresses two inspiring issues. Firstly, quantification of environmental stimulations, and secondly, effects of the surrounding environment on walking trajectory. Recent research in the field of pedestrian wayfinding puts emphasis on trajectory prediction to provide rich context information [9] and location-based information services to complete path finding activities for mobile devices including personal digital assistants (PDA) and mobile phones [6].

In this paper, the framework adopted to map the pedestrian displacement is a perception-based fuzzy logic approach. We have considered pedestrian-environment interaction as a non-precise aspect of steering behavior and devise a fuzzy logic model of those features to obtain a reliable prediction of pedestrian walking path. To measure the effect of the information perceived from the surrounding environment, we propose a fuzzy controller. It receives the perception of immediate areas from three points in the field of view as the inputs of the system. These inputs are defined by six membership functions and are categorized as low, medium, and high in attraction or repulsion. The fuzzy controller makes a decision based on 216 rules and provides the output in degrees to represent the turning angle to the left or right in the next step. The proposed model is applied for a case study and represents the trajectory of people walking through the area while having attractive or repulsive interactions with the surroundings.

2 Conceptual Framework of Local Environmental Stimuli

Environmental stimuli are an important part of spatial information that is being captured through the interaction with surroundings. Interaction between pairs of dissimilar objects in the environment is an important and considerable feature that causes the pedestrian to modify walking path. Two different objects can provide enhancement or destruction effects on each other. In fact, two-way interaction may resonate each other's influences or may conflict. For instance, a landmark can dwarf the area around or can strengthen the surrounding region.

To quantify the environmental effects, it is required to define indexes that succinctly define the level of stimuli at each point of the environment. Zacharias, Stathopoulos and Wu [10] studied the effects of microclimate change, social factors and environmental design on spatial behavior. Observation of seven open-space areas in San Francisco's and Montreal plazas reveal that microclimate factors such

as temperature and sunlight are effective elements in spatial behavior of pedestrians in open-space areas of San Fransico's and Montreal plazas.

In this context, we propose to apply social force model as an approach for quantifying environmental stimuli. The following section describes our approach to environmental discretization and how to quantify psycho-sociological forces within the environment.

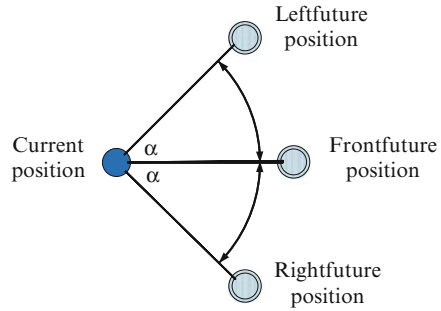
2.1 Spatial Representation of the Environment Within Field of View

Environment discretization is an initial issue in any wayfinding problem. In the majority of studies, static representation is applied by dividing the terrain to grids of 40 by 40 cm cells. Contrary to static representation, dynamic spatial arrangement has been introduced [11]. This is a field of view based concept that captures the dynamic and individual-based features of visually directed walking tasks. The role of field of view in spatial tasks such as navigation and steering activities has been described in many publications such as [12, 13]. In the present work, the traversable terrain that is located in vision field is divided into two sectors. Three points of interest are located in 5 steps ahead approximately in 2 m radius, which is the threshold of pedestrian environmental perception [14]. Points of interests are considered as three possible future positions collected in a set as $A = \{\text{Front Position (FP), Right Position (RP), Left Position (LP)}\}$. Figure 1 shows the traversable area in front of the walking agent that is represented with three feasible future positions. As it is depicted, next step would be taken in one of the left, front or right positions.

2.2 Attractive and Repulsive Environmental Stimulation

An environment induces attractive and repulsive interactions on the pedestrians. These contradictory psycho-sociological stimuli dynamically change in each step of the movement and persistently update the observer information from their surroundings [15]. Obtaining information from the environment provides local awareness that motivates a pedestrian to choose a direction by performing approach or avoidance behavior to achieve a desired goal. In this work, to quantify the level of environmental effects the Helbing social force model is adopted. It is one of the reliable and practical methods to describe pedestrian behavior by defining attractive and repulsive forces in both normal and panic situations [16]. Helbing, Farkas, and Vicsek [17] in their major research, measured socio-psychological forces that influence crowd behavior in panic situations. They deduced the interaction force between two pedestrians or a pedestrian and an object that leads a pedestrian to

Fig. 1 Radial representation of traversable terrain in the next step



a desired destination with ideal speed. Also, self-organization phenomena, which are the outcome of collective interaction amongst pedestrians, are reproducible through this method [18]. Therefore, we have applied the social force method for this investigation. In fact, the total amounts of attractive and repulsive forces in three future positions act as a stimulation to choose a next step direction. The following equation represents social interaction force between pedestrian *i* and *j* at time *t*.

$$F_{ij}^I(t) = A_i \exp[(r_{ij} - d_{ij}) / B_i] n_{ij} \tag{1}$$

Where, *A_i* stands for strength of interaction and *B_i* reflects range of interaction. *r_{ij}* = *r_i* + *r_j*, represents sum of two objects radii and *d_{ij}* = ||*x_i* + *x_j*|| is the distance between two objects' center.

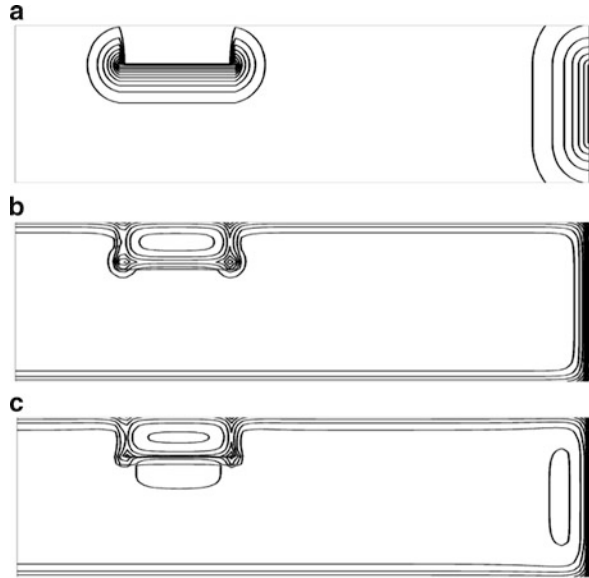
$$n_{ij} = (n_{ij}^1, n_{ij}^2) = (r_i - r_j) / d_{ij}, \tag{2}$$

n_{ij} is the normalized vector from pedestrian *j* to pedestrian *i*.

Warren and Fajen [19] in their major study demonstrated the exponential decay of attractive or repulsive effects from the surrounding environment by object distance. It has been suggested that both the repulsive influence of obstacle and attractive effect of goal decrease with distance. Repulsive force is symmetric and pedestrian do not react to the passed objects [18]. It has been reported that attractive force is similar to repulsive force but in opposite sign and longer interaction range [18].

To represent the extent of interaction within the environment, contour maps of environmental stimuli affecting the surrounding objects are depicted. In Fig. 2, absolute values of attractive, repulsive and total force are depicted in a simple example of a hallway with a printer, and exit door. Attractive interactions are provided by the printer and exit door and have a negative value while repulsive effects are produced by the walls and printer, represented by positive sign. Of course, during steering activity through the corridor, contour map of environmental effects is changing dynamically and will be shown in dynamic figures.

Fig. 2 (a) Contour map of attractive stimulations, (b) contour map of repulsive stimulations, (c) contour map of total environmental effects after summation of attractive and repulsive stimulations



3 Fuzzy Logic-Based Pedestrian Steering Behavior Model

Steering behavior is subject to three fundamental elements known as environmental effects, pedestrian perception from environmental stimulation and the displacement of the pedestrian. The first element is defined by the total psycho-sociological interactions with the objects located in a pedestrian's field of view. Two indicators show the level of interaction with the environment, denoting attractive interactions and repulsive interactions. We assume three levels to each of the indicators namely high, medium, and low.

Each pedestrian perceives and gives meaning to the surrounding environment uniquely. This variability is represented by the perception from dynamic environmental information, which is an input to the fuzzy system. The third element, known as displacement, is the model's output provided by the rules of the fuzzy controller. All of these elements play a significant role in steering behavior, while there is no specific mathematical relationship between them. The foundation of our model is built upon the framework discussed in the next section.

3.1 Structure of Proposed Fuzzy Steering Model

Two illustrative variables in steering activity are pedestrian speed and direction of movement. As a matter of simplification, we have considered constant speed and variable movement direction. Therefore, the angle of direction is the output of

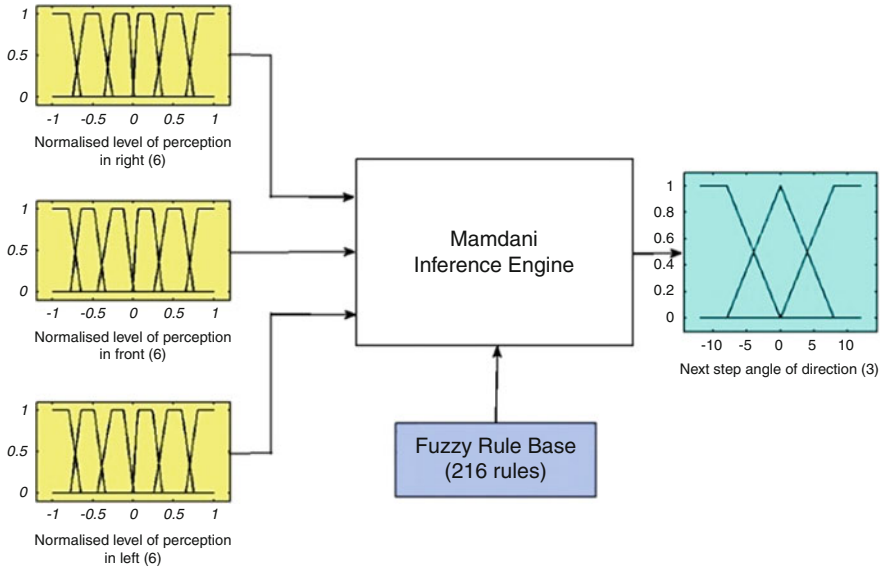


Fig. 3 Architecture of developed fuzzy steering prediction model, with 3 inputs, 1 output and 216 rules

proposed fuzzy approach that is inferred from perceived information of environmental effects.

The fuzzy logic-based model encompasses three inputs, one output and 216 rules as depicted in Fig. 3. The pedestrian’s perceived environmental motivation inputs originate from the level of attractive or repulsive interaction in three possible future positions for the next step. Points of interest are collected in a set, which are described as {Front Position (FP), Right Position (RP), Left Position (LP)}. Total attractive and repulsive forces are calculated in each future position and categorised as {High attractive, Medium attractive, Low attractive, Low repulsive, Medium repulsive, High repulsive}. This linguistic fuzzy input set represents a pedestrian’s level of motivation. As a result, there are six membership functions for each input to the inference engine and the amount of displacement degree in the next step can be inferred in the output.

3.2 Model Assumptions

We have limited this work to indoor public environments and considered a typical office hallway as the case study. We have made the following assumptions to succinctly define the problem. (a) A pedestrian’s foot step is shown by a point in a two-dimensional simulated environment. (b) A pedestrian’s speed in normal

movement is $5 \text{ km/h} = 1.39 \text{ m/s}$ [20]. (c) An itinerary plan is defined by the user to specify the way points. (d) To choose the next step position, three alternatives exist which are move forward, change the direction to the right or to the left. (e) In any current point, the level of total attractive and repulsive interactions induce by all the objects within field of view is calculated. (f) A pedestrian can change the movement direction in the next step in a continuous range of -12° to $+12^\circ$. (g) The output of the fuzzy system is the turning angle degree for the next step. (h) The tendency to move forward is stronger than to move to the right or left. In the case of equal attractive or repulsive levels of motivation in both left and right future points, rules instruct the agent to move forward to avoid angular displacement [14].

3.3 Global Perception

Pedestrians have a priori perception about the space from their place memory. This cognitive spatial perception leads to develop a navigation plan, which comprises of an itinerary list of subsequent intermediate waypoints for steering task. Bearing the itinerary list in mind and exposing with local stimuli lead to a variety of spatial behaviors by pedestrians. In this case study, spatial knowledge from place memory provides individuals with a global view of the area. A pedestrian's steering behavior influenced by this place memory is modified by local variables in the present environment.

In the current work, an itinerary plan is developed by employing dynamic programming. The shortest path from origin to destination is the criteria of dynamic programming to generate the itinerary plan.

3.4 Pedestrian Perception as the Input Sets of Fuzzy System

Obtaining the attractive or repulsive effects of immediate objects located in field of view enable the pedestrian to be aware of their surroundings and feel the level of stimulation in the environment. This local awareness enables the pedestrian to choose a direction and navigate through the area. According to this explanation and referring to discussion in Sect. 3.1, the level of perception in three future travel positions distinguished as {High attractive, Medium attractive, Low attractive, Low repulsive, Medium repulsive, High repulsive} are the linguistic fuzzy input sets. To sum up, there are three inputs each consists of six membership functions. Membership functions imply the degree that a feeling belongs to a set.

Figure 4 shows six membership functions in an input set depicting the perception in one of the future points that is in the front location. The same input set is applied for the other two positions, which are in the right and left hand side.

Fig. 4 The input fuzzy set consist of six membership function describes level of perception in front

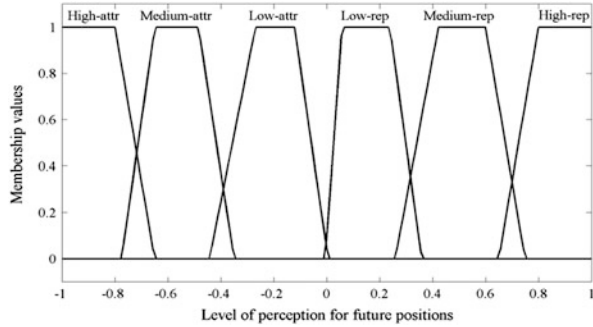
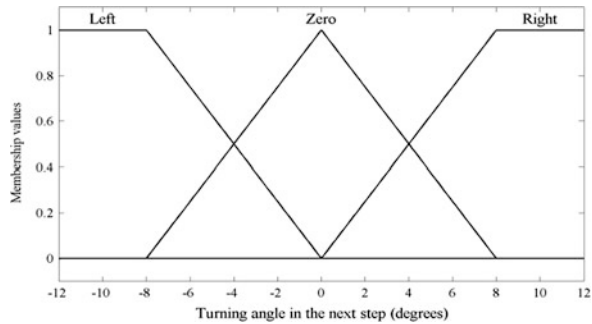


Fig. 5 Fuzzy sets left, zero, and right that describe next step angular change of direction



3.5 Establishing Output Fuzzy Sets for Angular Change of Direction

Antonini, Bierlaire, and Weber pointed out that pedestrians tend to change their movement direction gradually rather than with sudden turning in subsequent steps during a walking task [21]. They have also defined a continuous range of -12° to $+12^\circ$ as the amount of turning angle in the next step.

The aim of this model, which is the output of proposed fuzzy system, is to provide the turning angle of a pedestrian considering attractive and repulsive influences of the surrounding environment contained within their field of view. In this regard, a fuzzy inference engine is developed to receive the pedestrian perceived information from three future points as the inputs and deduce the angular change of direction for the next step as the output of the fuzzy system. Figure 5 represents fuzzy sets for change of direction degrees in the subsequent steps. As the following figure shows, a pedestrian is able to have angular displacement from 0° to -12° , denoting a left turn or from 0° to $+12^\circ$, denoting a right turn.

3.6 *Fuzzy Inference Rules for Angular Change of Movement Direction*

Dealing with two kinds of interactions known as attractive and repulsive in three linguistic descriptions, which are {low, medium, and high} lead to six membership functions. Consequently, involving three input sets result in $6 \times 6 \times 6 = 216$ rules in the form of IF-THEN description. Rules based on the heuristic knowledge of the user have been established and are shown in Table 1. In this table, RP reflects perception in right position, FP stands for perception in front position, and LP represents perception in left position. According to IF-THEN statements, a pedestrian will tend to change direction towards the attractive motivation. In the case of having equal perception in three alternatives, a pedestrian would rather not to change his direction and continue walking forward.

4 Simulation Results

The proposed fuzzy-based approach is a microscopic pedestrian steering behavior model that calculates the movement direction of pedestrians exposed to environmental stimulations. The model uses the perceived level of pedestrian motivation during a walking task to predict the path a pedestrian will take. In order to verify this aim, a hallway area in a public environment is selected and an identical two dimensions environment is simulated. The simulated environment similar to the real hallway includes walls, a printer, entrance, and exit door.

To investigate environmental effects on walking path, attractive and repulsive forces located in a pedestrian's field of view, exerted by the walls, printer and exit are calculated in each step of walking. Dynamic environmental stimulations are provided in the simulated environment and a pedestrian makes the decision for movement direction using fuzzy inference rules. Figure 6 provides the results obtained from simulation in different steps of movement. Subfigures in the left column depict footprints of pedestrian walking through the corridor. Corresponding subfigures in the right column represent contour maps of total attractive and repulsive stimulations induced by walls, printer, and exit.

The printer and exit door are sources of attractive stimuli, whilst the walls and printer obstructions produce repulsive effects. These figures show the trend of alteration in environmental stimuli that provides dynamic information for the pedestrian to choose the movement direction in the next step. Employing the concept of visual field helps the simulation to capture the dynamic property of environmental information that is required to show local awareness of a pedestrian. Moreover, the proposed simulation model employs an exponential decay of environmental influences to produce a smooth and realistic feature in the simulation results.

Table 1 216 fuzzy logic inference rules for next step turning angle of pedestrian steering behavior

Rule	IF-THEN statements															
No.1	IF	RP	is	High-attr	AND	FP	is	High-attr	AND	LP	is	Medium-attr	THEN	Turn angle	is	Not left
No.10	IF	RP	is	High-attr	AND	FP	is	Medium-attr	AND	LP	is	Low-repul	THEN	Turn angle	is	Right
No.55	IF	RP	is	Medium-attr	AND	FP	is	Low-repul	AND	LP	is	High-attr	THEN	Turn angle	is	Left
No.110	IF	RP	is	Low-repul	AND	FP	is	High-attr	AND	LP	is	Medium-attr	THEN	Turn angle	is	Forward
No.200	IF	RP	is	High-repul	AND	FP	is	Low-repul	AND	LP	is	Medium-attr	THEN	Turn angle	is	Left
No.216	IF	RP	is	High-repul	AND	FP	is	High-repul	AND	LP	is	High-repul	THEN	Turn angle	is	Forward

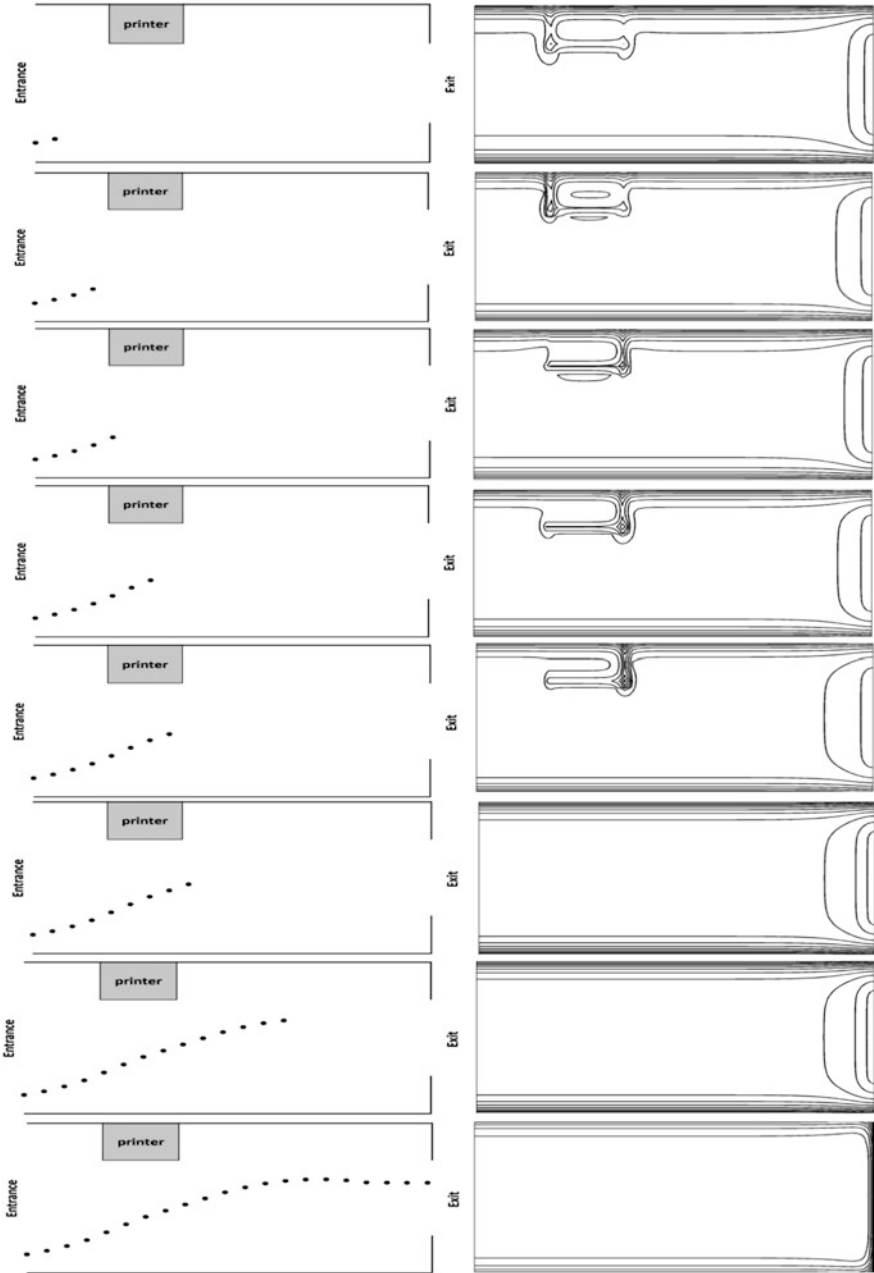


Fig. 6 Trace of walking path by the agent indicating number of steps (*left column*), corresponding total environmental stimuli in each position (*right column*)

Fig. 7 Simulation result shows walking trajectories of 25 pedestrians in the corridor

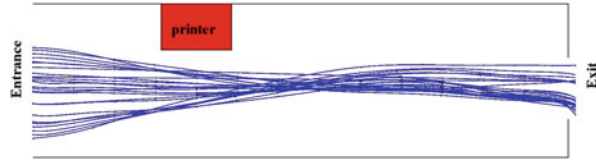


Figure 7 represents stochastic introduction of pedestrians to the simulation environment with different start and end points. It depicts a corridor populated with 25 pedestrians walking through the hallway with different walking paths.

The simulation results imply that fuzzy-based inference system is an appropriate approach for microscopic pedestrian simulation modeling under normal conditions. To achieve a better understanding of the proposed algorithm performance, further investigation has been conducted through an observation and data collection experiment. The precise walking trajectory of participants involved in the experiment is extracted with a motion capture system.

5 Data Collection and Extracting Trajectory Data Set

Collecting suitable datasets to calibrate pedestrian behavior models is a challenging task. Pedestrian flow data is often more complicated and difficult to collect when compared to, for example, traffic data. More so, this type of information is rarely collected due to the lack of demand for such data.

To verify the proposed simulation model of pedestrian steering behavior, we captured the real-time motion of 25 participants in a real scenario using motion capture technology. Motion capture allows the precise trajectory of entities traversing the capture volume to be calculated with sub-millimetre accuracy. Motion capture proved to be a simple, reliable and efficient way of determining the path a pedestrian will take in a real environment. The experiment was conducted in the motion capture laboratory of CISR, Deakin University.

The large volume capture stage used for these experiments utilizes a 35-camera OptiTrack system from Natural Point. The OptiTrack system triangulates highly reflective markers from three or more camera streams in a stage flooded by infrared light. The system is calibrated with a wandering routine to establish the arrangement of cameras in relation to a ground plane. The wand and the ground plane have a defined structure that the system can easily interpret. We can class a unique arrangement of reflective markers as a rigid body. Multiple rigid bodies can be combined to produce a skeleton of a participant wearing a suit strategically populated with reflective markers. To streamline the capture procedure for this experiment, the system was trained to recognize a simple rigid body structure that a participant could wear on their head.

A corridor identical to the two-dimension simulated environment was masked out on the floor of the stage. An origin was set in the capture environment that

Fig. 8 Motion capture data shows walking trajectories of 25 pedestrians in the corridor

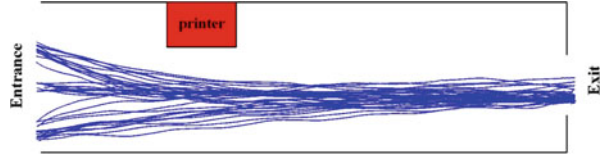
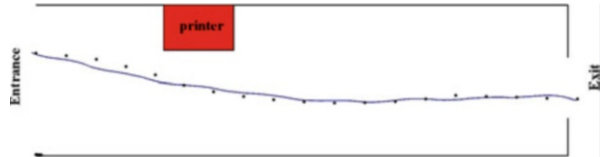


Fig. 9 Comparison between real data with algorithm results for one pedestrian



aligned to the bottom left corner of the corridor. Within the environment, we placed an attractive item of interest that participants could interact with. As a participant traversed the stage, each marker on the rigid body was triangulated at a rate of 120 frames per second. This data represents the positions of each marker visible in the capture stage relative to the origin. For each frame, a trajectory estimate reports the x , y , z position and roll, pitch and yaw of the rigid body. The steering behavior for each participant was calculated from the x and z elements from this trajectory data. Figure 8 shows walking trajectories of participants that were captured by motion capture system.

To compare this real data with the algorithm result, statistical analysis was performed. Mean square error was used to calculate the difference between values of simulation results and real data, which is equal to 0.00249 (m). Also, correlation coefficient between two datasets is 0.9998. Figure 9 compares both real walking trajectory and simulation result for only one participant. The straight line plots the trajectory data set from real experiment and black points depict the algorithm results for subsequent step positions of pedestrian walking through the hallway. The statistical analysis and following figure reveal a significant correlation among real data and simulation results.

6 Conclusions

Pedestrian steering behavior comprises of two-directional interaction task with the surrounding environment that is based on personal perception and reaction. To study the perception-action behaviors, the heterogeneity between different pedestrian's perception and reaction is required. In this regard, we have proposed a fuzzy-based simulation approach to model pedestrian walking direction when influenced by surrounding environment.

A two dimension simulated environment identical to a hallway area of an office building was studied. Different parts of the hallway including walls, entrance, exit, and a printer exert both attractive and repulsive effects on pedestrians. Attractive or

repulsive effects change dynamically during each step of the simulation depending on whether those parts are located in pedestrian field of view or not.

The perceived levels of these two indicators are the inputs of fuzzy logic system. Pedestrians inferred the angle of direction based on fuzzy logic rules according to perceived information in three different future positions within the threshold of pedestrian-environment perception. Simulation results revealed that our proposed framework is a promising approach in developing pedestrian walking trace according to environmental stimuli within a pedestrian's field of view.

The motivation for this paper is to explain pedestrian steering by fuzzy logic rules and extract pedestrian walking paths in indoor environments. Fuzzy logic technique is a justified approach to model problems involved with human behavior and is able to estimate a thought process similar to a real person. We conclude that fuzzy logic can be applied to perception-based decision making process.

The key advantage is that in modeling diverse opinions from different individuals, fuzzy logic systems provide an indication to the way different people decide on a subject. This approach is an effective and practical tool in different applications such as urban planning, environmental designing, traffic planning and transportation, routing and navigation, and spatial cognition.

References

1. LYNCH, K.: *THE IMAGE OF THE CITY*. CAMBRIDGE TECHNOLOGY PRESS, MA, USA (1960)
2. RAUBAL, M., WORBOYS, M.: A FORMAL MODEL OF THE PROCESS OF WAYFINDING IN BUILT ENVIRONMENTS. IN: *SPATIAL INFORMATION THEORY. COGNITIVE AND COMPUTATIONAL FOUNDATIONS OF GEOGRAPHIC INFORMATION SCIENCE*. FREKSA, C., MARK, D. M. (EDS.) LNCS, VOL. 1661, PP. 381–399. SPRINGER, HEIDELBERG (1999)
3. GOLLEGE, R. G., RUGGLES, A. J., PELLEGRINO, J. W., GALE, N. D.: INTEGRATING ROUTE KNOWLEDGE IN AN UNFAMILIAR NEIGHBORHOOD: ALONG AND ACROSS ROUTE EXPERIMENTS. *JOURNAL OF ENVIRONMENTAL PSYCHOLOGY*, 13(4), 293–307 (1993)
4. WINEMAN, J. D., PEONIS, J.: CONSTRUCTING SPATIAL MEANING: SPATIAL AFFORDANCES IN MUSEUM DESIGN. *ENVIRONMENT AND BEHAVIOR*, 42(1), 86–109 (2010)
5. FAJEN, B. R., WARREN, W. H.: BEHAVIORAL DYNAMICS OF STEERING, OBSTACLE AVOIDANCE, AND ROUTE SELECTION. *JOURNAL OF EXPERIMENTAL PSYCHOLOGY: HUMAN PERCEPTION AND PERFORMANCE*, 29(2), 343–362 (2003)
6. LI, C.: USER PREFERENCES, INFORMATION TRANSACTIONS AND LOCATION-BASED SERVICES: A STUDY OF URBAN PEDESTRIAN WAYFINDING. *COMPUTERS, ENVIRONMENT AND URBAN SYSTEMS*, 30(6), 726–740 (2006)
7. RIDWAN, M.: FUZZY PREFERENCE BASED TRAFFIC ASSIGNMENT PROBLEM. *TRANSPORTATION RESEARCH PART C: EMERGING TECHNOLOGIES*, 12(3–4), 209–233 (2004)
8. SERAJI, H., HOWARD, A.: BEHAVIOR-BASED ROBOT NAVIGATION ON CHALLENGING TERRAIN: A FUZZY LOGIC APPROACH. *IEEE TRANSACTIONS ON ROBOTICS AND AUTOMATION*, 18(3), 308–321 (2002)
9. LIU, X., KARIMI, H. A.: LOCATION AWARENESS THROUGH TRAJECTORY PREDICTION. *COMPUTERS, ENVIRONMENT AND URBAN SYSTEMS*, 30(6), 741–756 (2006)

10. ZACHARIAS, J., STATHOPOULOS, T., WU, H.: SPATIAL BEHAVIOR IN SAN FRANCISCO'S PLAZAS. *ENVIRONMENT AND BEHAVIOR*, 36(5), 638–658 (2004)
11. BIERLAIRE, M., ANTONINI, G., WEBER, M.: BEHAVIORAL DYNAMICS FOR PEDESTRIANS. IN: *10TH INTERNATIONAL CONFERENCE ON TRAVEL BEHAVIOR RESEARCH*, PP. 1–22. LUCERNE (2003)
12. CREEM-REGEHR, S. H., WILLEMSSEN, P., GOOCH, A. A., THOMPSON, W. B.: THE INFLUENCE OF RESTRICTED VIEWING CONDITIONS ON EGOCENTRIC DISTANCE PERCEPTION: IMPLICATIONS FOR REAL AND VIRTUAL INDOOR ENVIRONMENTS. *PERCEPTION*, 34(2), 191–204 (2005)
13. ALGADHI, S. A. H., MAHMASSANI, H. S.: SIMULATION OF CROWD BEHAVIOR AND MOVEMENT: FUNDAMENTAL RELATIONS AND APPLICATION. *TRANSPORTATION RESEARCH RECORD*, 1320(1320), 260–268 (1991)
14. ROBIN, T., ANTONINI, G., BIERLAIRE, M., CRUZ, J.: SPECIFICATION, ESTIMATION AND VALIDATION OF A PEDESTRIAN WALKING BEHAVIOR MODEL. *TRANSPORTATION RESEARCH PART B-METHODOLOGICAL*, 43(1), 36–56 (2009)
15. GOLLEDGE, R. G.: HUMAN WAYFINDING AND COGNITIVE MAPS. IN: *WAYFINDING BEHAVIOR, COGNITIVE MAPPING AND OTHER SPATIAL PROCESSES*. GOLLEDGE, R. (ED.), PP. 5–45. THE JOHNS HOPKINS UNIVERSITY PRESS, BALTIMORE AND LONDON (1999)
16. HELBING, D.: A MATHEMATICAL MODEL FOR THE BEHAVIOR OF PEDESTRIANS. *BEHAVIORAL SCIENCE*, 36(4), 298–310 (1991)
17. HELBING, D., FARKAS, I., VICSEK, T.: SIMULATING DYNAMICAL FEATURES OF ESCAPE PANIC. *NATURE*, 407(6803), 487–490 (2000)
18. HELBING, D., MOLNAR, P., FARKAS, I. J., BOLAY, K.: SELF-ORGANIZING PEDESTRIAN MOVEMENT. *ENVIRONMENT AND PLANNING B: PLANNING AND DESIGN*, 28(3), 361–383 (2001)
19. WARREN, W. H., FAJEN, B. R.: BEHAVIORAL DYNAMICS OF HUMAN LOCOMOTION. *ECOLOGICAL PSYCHOLOGY*, 16(1), 61–66 (2004)
20. WEIDMANN, U.: TRANSPORTTECHNIK DER FUSSGAENGER. SERIES SCHRIFTENREIHE DES INSTITUTS FUR VERKEHRSPANUNG, STRASSEN-UND EISENBahnBAU, TECHNICAL REPORT 90, ETH ZURICH, SWITZERLAND (1993)
21. ANTONINI, G., BIERLAIRE, M., WEBER, M.: DISCRETE CHOICE MODELS OF PEDESTRIAN WALKING BEHAVIOR. *TRANSPORTATION RESEARCH PART B: METHODOLOGICAL*, 40(8), 667–687 (2006)

Group Dynamic Behavior and Psychometric Profiles as Substantial Driver for Pedestrian Dynamics

Michael Schultz, Lars Rößger, Hartmut Fricke, and Bernhard Schlag

Abstract Our current research lays emphasis on the extended pedestrian perception and copes with both the dynamic group behavior and the individual evaluation of situations, and hence, rather focuses on the tactical level of movement behavior. Whereas common movement models primary consider operational aspects (spatial exclusion or distance and direction related repulsion), the consideration of psychophysical concepts and intra-group coordination overcomes the idea of directed repulsion forces and derives specific movement decision with respect to the individual evaluation of situations. To provide a solid basis we analyze both data recorded at a mass event and data from a double-staged evacuation test to derive essential group dynamic behaviors and psychological related decision principles, respectively.

Keywords Group behavior • Psychophysics • Pedestrian dynamics

1 Introduction

Models for pedestrian dynamics cope with different aspects of behavior related to human movements. Generally, such models can be assigned to three different levels of movement characteristics: operational, tactical and strategic behavior. The basic microscopic models (e.g. social force, cellular automat, or discrete choice) particularly focus on the operational movement level. Especially, the favorable

M. Schultz (✉) • H. Fricke

Department of Air Transport Technology and Logistics, Faculty of Transport and Traffic Sciences
“Friedrich List”, Technische Universität Dresden, Dresden, Germany
e-mail: schultz@ifl.tu-dresden.de

L. Rößger • B. Schlag

Department of Traffic and Transportation Psychology, Faculty of Transport and Traffic Sciences
“Friedrich List”, Technische Universität Dresden, Dresden, Germany

social force approach [1], which states attraction and repulsion forces between the human beings, turns out as a good analogy to reproduce substantial self-organization effects. Several model modifications and extensions of the social force model have been recently developed by the scientific community. One can notice that sustainable concepts (e.g. discretization, floor fields) will be transferred between the different model approaches, and that the models will converge as an evolutionary consequence. The definition of individual movements as destination driven processes allows for investigations of the superior self-organization effects but it neglects significant group dynamic effects (e.g. intra-group coordination) and psychological influences on (movement) decision processes. The idea of considering the individual human perception to cope with enhanced patterns of movement behavior is from our point of view the next challenge for the upcoming research tasks. An interdisciplinary research approach including the research areas of traffic sciences, sociology, mathematics, physics and psychology will ensure that the proposed methods follows a common agreement of all parties involved. In this paper we present first findings regarding the group related behavior and psychometric profiles of pedestrian and their influence to the movement dynamics.

2 Group Dynamics

For the data acquisition in the field, we recorded the movement behavior of the participants of the German Protestant Kirchentag at Dresden (1.-5. June 2011 with 120,000 fulltime participants and approx. 50,000 guests) and use this data as a solid base for the group constellation and behavior. As our data points out, there are significant differences in the density-speed-relation (fundamental diagram) regarding the constellation of groups. Heterogeneous crowds consists of independent pedestrians possess a homogenous density and each pedestrian has a high flexibility to change the speed and the direction of motion. The effect of *clustered density* (alternating local density clusters and open space) increases with the amount of groups, their mobility, and with the group size (Fig. 1). These density spots significantly change the individual speed characteristic and the corresponding movement behavior (e.g. distance keeping, collision avoidance).

Highly agile groups are benefit from the density clusters by efficiently use of the corresponding free accessible space. So it seemed that a mixture of two different flows exits inside the pedestrian stream. These structures are stable in an environment with lower density. With increasing density the tactical movements are barely manageable and the two separated flows are combined to one (Fig. 2).

Each group member plans his individual path through the crowd and anticipates the group movements respecting the overall group constellation. Our observations suggest the assumption of an altruistically behavior as a common group movement agreement, where the group members tend to optimize the group benefit by means of trouble-free walking paths. In the course of this behavior, group members yield precedence to other members if they expect an advantage for the group.



Fig. 1 Simple heading change of one pedestrian without the need of speed corrections in a region of intermediate density



Fig. 2 Pedestrian movement with restricted freedom to maneuver within the crowd and starting transition from individual to coupled movement behavior

This planning procedure often based on non-verbal communication and fails with increasing density when the direct connectivity between the group members disrupts. Groups with a clear leader and follower structure as well as experienced groups contain of members with a comparable hierarchy status will efficiently solve this synchronized movement task even under crowded situations, which is confirmed by our comprehensive observations at the Kirchentag. The specific solutions to ensure an individual non-conflictive walking path results in a higher variance of speed inside the pedestrian flow compared to the expected standard distributions considering a homogenous flow.

In the following section we will provide the first results of our analyses. We strongly suppose that the ongoing data evaluation will provide further facts to validate our findings about the group behavior.



Fig. 3 Event area for the main mass event at German Protestant Kirchentag

2.1 Environment for Identification of Groups

The main events of the German Protestant Kirchentag took place at an open space near the Elbe River framed by two bridges (Augustusbrücke and Carolabrücke, see Fig. 3). Due to the fact, that the participants have to underpass these bridges to get access to the events, we could conveniently record the movement behavior of the pedestrians from a top view perspective. As agreed upon with the organizer we got access to the operational control center and could efficiently coordinate our data records with the event schedule.

For the data evaluation we developed an adequate software environment with the capability of both automatic and user defined tracking support. In particular the identification of groups the experience of human pattern recognition are not captured by common algorithms. Groups are often consisting of pedestrians in close vicinity to each other, and comparable behaviors regarding to heading, speed and acceleration. We will define this constellation as an aggregation not a group. Our approach for group detection focus on observable social behaviors as holding hands, waiting for members, or communications processes and appearance (e.g. outfit). So, the manual recognition of groups is inevitable. The process of extract pedestrian trajectories consists of five steps:

1. Determine the environmental characteristics (position of record device, distance to area of interest, reference point measurements) and technical specifications of the record device (field of view, distortion, zoom)
2. Calibrate the record device using reference scenarios and an independent measuring system (manual position determination in marked walking area)
3. Identification of the pedestrians and their position changes at each video frame
4. Assignment of group members (in order to distinguish individuals and groups from pedestrian aggregations)
5. Manual cross check of the pedestrian trajectories and the group assignment



Fig. 4 Common group constellation, the horizontal stripe formation is a standard motion behavior at lower densities

2.2 Results

In low density environments the analysis steps for extracting the movement trajectories and the group assignment could be automatically done without user interaction, because the group members possess a clear detectable behavior: (a) close distance to other members and (b) prolonged separation from other groups (Fig. 4). The different intra- and inter-group behavior results in a horizontal stripe formation where groups members move side by side in close distance.

If the separation between the groups is granted during the observation period an algorithm-based tracking provide reliable results. But aggregations of pedestrians caused by local congestions limits the quality of the group assessment. In these instances aggregations could consists of several groups which are not easily detectable by algorithms (Fig. 5).

The empirical knowledge of a human being allows for a significant higher assignment precision and a manual validation has to be performed to ensure valid group assignments. Nonetheless, in some situation even a manual assignment fails, so these pedestrians are not taken into account for the following statistic evaluations.

The population points out a significant emphasis on groups, only 14 % of the population are single individuals. The highest proportion exhibits the group with two members followed by the group with three members. In contrast to the common population recorded by Moussaïd et al. [2], a significant difference in the group structure can be observed (e.g. single individuals possess a rate higher than 45 %) (Fig. 6).

The population of the German Protestant Kirchentag at Dresden (participants of a mass event) naturally differs from the populations of popular commercial walkways. But, in line with expectations the average speed is decreasing with the increasing amount of groups. As we already point out, groups tend to stay together but if the groups reached a size greater than four members, they intend to split up in subgroups



Fig. 5 Formations of groups and aggregation of groups/individuals demands for a combined approach of automatic algorithms and precise user intervention

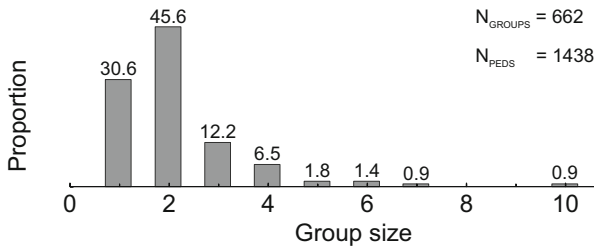


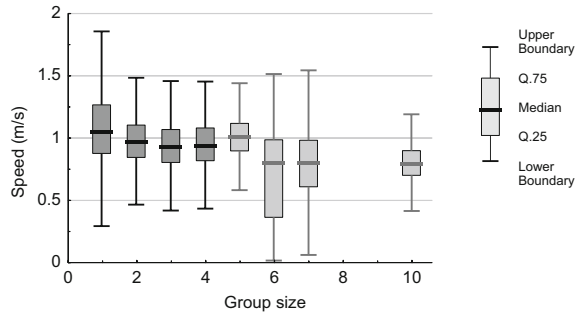
Fig. 6 Proportion in the observed population

to solve complex movement tasks [3, 4]. This behavior can be verified by analyzing the speed characteristic of the identified groups. To characterize the speed behavior a five-number summary descriptive statistics is used (boxplot), defined by lower and upper boundaries as well as the 25 %, 75 % quartile (Q.25, Q.75) and the median (50 % Quartile) (Fig. 7).

The lower and upper boundaries are calculated using the 1.5 multiple of the interquartile range ($IQR = Q.75 - Q.25$), whereas the lower and upper values are within this range. While the median and the standard deviation of the walking speed of the groups continuously decrease with the group size, this trend interrupts at a group size of 5 with an increase of the median speed value. In addition to this interrupt, the standard deviation of the speed increases as well at groups with more than five members (attention should be paid to the small number of occurrences within these group categories: five members (12), six members (9), seven members (6) and a group with ten members occurs six times). To derive statistically valid results this first analysis has to be continued.

The speed characteristics are a common procedure to determine the group behavior. To analyze the nature of the prior identified horizontal stripe formation in detail, the groups are scanned for appropriate candidates, demanding that all group

Fig. 7 Five-number summary descriptive statistics of speed distribution



members move free of external interference. For the analysis of groups with 2, 3, and 4 members 87, 19 and 10 candidates are identified, respectively. The position of each candidate at each recorded video frame (25 Hz) is plotted and a probability density function (PDF) is calculated for the longitudinal (x-position) and transversal (y-position) component referring to the group center (for members: $\text{center}_x = 1/n \sum x_i$, $\text{center}_y = 1/n \sum y_i$). The following Fig. 8 represents standardized pictures of the relative positions of group members considering the mentioned constellations. In the center of the figures a 2×2 m grid shows the position and the PDF of the transversal component, surrounded by the PDF's for the longitudinal positions. The PDF's are smoothed by a centered average covering ± 5 values (spatial discretization 0.01 m) and they allow for a clear separation of the group members.

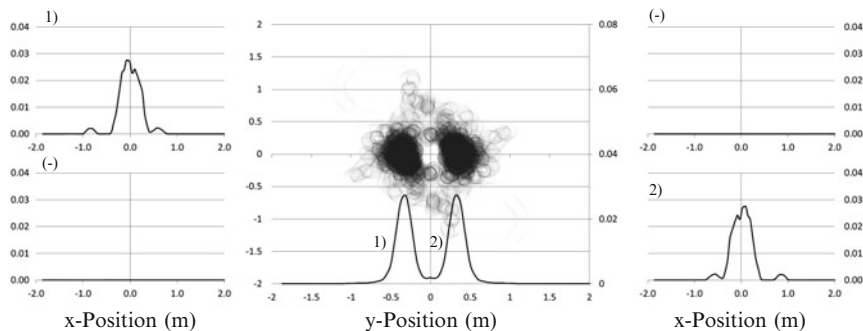
The group with two members points out a symmetric behavior in x and y direction, where the peaks of the lateral positions have distance of 0.66 m. The group with three members shows a pattern where the pedestrian in center take slightly downstream position and the outside surrounding pedestrian take slightly upstream position. The lateral distances of the y-position peak regarding to the center pedestrian are 0.61 m to the left and 0.65 m the right. The up-/downstream pattern also occurs at the group with four members, where the outer members repeatedly take the upstream position. The lateral distance of the inner members is 0.66 m and the distance to their associated outside attendant is 0.54 m in both cases.

These first encouraging results of the group dynamic behavior points out the stringent necessity to focus this research area, to continue the data analysis, and to develop a model which is able to cover these important group effects.

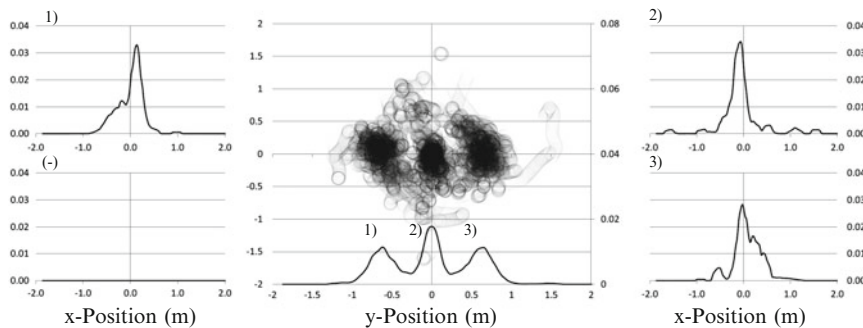
3 Psychometric Profile

Our results reported above clearly indicate the existence of a *clustered density*, i.e. density spots within pedestrian crowds with effects on both individual speed characteristics and collision avoidance behavior. When focusing on the group dynamics and/or on the heterogeneity of movement pattern in pedestrian crowds

Group with 2 members:



Group with 3 members:



Group with 4 members:

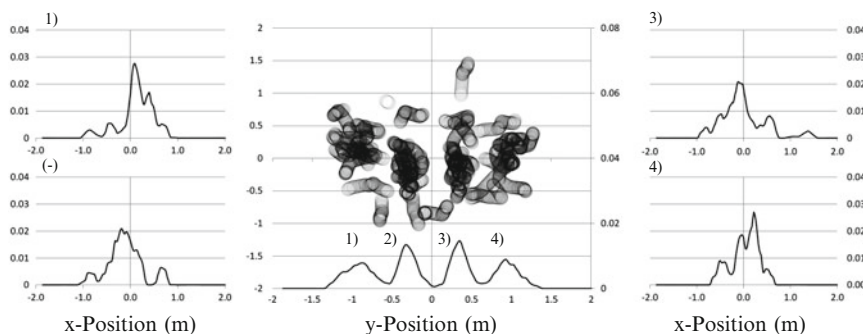


Fig. 8 Position of group members with ID 1, 2, 3, and 4 regarding their local distance to the group center and PDF of the respective distance component

the question arises of how groups emerge according to what characteristics on individual level and which influencing factors on individual level determine the heterogeneity in movement parameters? We initially proposed three different levels in order to describe movement characteristics of pedestrians: the operational level, the tactical level and the strategic level. The consideration of movement related

decisions on the tactical level depending on individual factors seem to be crucial to address this question. Human beings' decision-making processes are described as bounded-rational (e.g. [5]), that is, decisions are subjected to constraints e.g. referring to the information intake, mental workload and cognitive processing. Thus, the usage of heuristics within decision-making provide valuable strategies in order to cope with cognitive boundaries and many authors (e.g. [9, 10]) claimed that decision outcomes are rather satisfying than optimizing. In that course, decision strategies are considerably affected by individual states such as (psycho-) physiological activation (e.g. [13]), affective load (for review see [12]), respectively, moods (e.g. [14]). Individuals' states as responses to certain situational characteristics are in turn linked to personality traits of the subjects. In the context of this paper, we focus on the role of personality traits for movement related decisions and movement parameters in an evacuation situation which is characterized by uncertainty and time pressure. Such scenarios particularly represent demands on decision making processes due to: (a) the fact that often decision rules are not available caused by the uniqueness of the situation (no familiarity), (b) threatening nature and its implications on affective work load and physiological activation, and (c) the time pressure which requires a fast decision.

When should I start to go for the exit: immediately or do I have at least enough time in order to collect my belongings and leave then for exit? Which exit should I take: the nearest one or maybe the one which is afterwards closer to the bus station? In the event of an evacuation, decisions on such questions have to be made and one might assume that they will be made without in-depth consideration about pros and cons for each alternative. The use of heuristic strategies enables us to react also in situations when deliberated thinking and/or thoughtful reasoning about alternatives becomes critical. One strategy might be to look what are doing the others around me. The *herding* effect represents the outcome of such a strategy. E.g., Baddeley et al. [6] considered herding as a time-saving decision-making heuristic and hypothesized that certain personality types will be more likely to use herding heuristic as a decision-making shortcut. In their research on decisions in the financial context the authors found that herding is less likely amongst extraverted and emphatic individuals. The construct extraversion is one of three dimensions of personality according to the personality type model [8] proposed. Extraverted individuals are described as highly interested in social activities and social contacts, as acting spontaneous, are impulsive and tending to risky behavior. Furthermore, it is claimed that extraverts tend to show fast and frequent motor reactions whereas introverts stronger persist in perceptual activities and the analysis of sensory information. In the context of movement pattern in evacuation scenarios, one might assume that extraversion is negatively associated with decision time (start time) for evacuation because of their tendency to fast reactions and positively associated with the movement time because parts of the information processing is shifted into the phase of movement execution. So, for extraverts we hypothesize a more reactive movement pattern characterized by stronger variances in walking speed whereas introverts should exhibit a more anticipative movement pattern with less variance in walking speed. With respect to the question about who will be the leader of group,

we assume that extraverts will start earlier than others, and thus, might provide the social cue for others to follow.

Neuroticism as further personality factor in Eysenck's model refers to the emotional stability of individuals. Individuals scoring high on neuroticism are described as emotionally labile and as tending to show difficulties to recover after emotional experiences. Moreover, neuroticism is associated with a general pattern of faster response times when detecting a threat stimulus or identifying a target cued by a threat stimulus. Decision-making processes can be interfered by dysfunctional thoughts about threatening issues, and therefore, might become suboptimal with respect to the best achievable options. It is difficult to formulate assumption about the effect of neuroticism on movement related decision and movement pattern. One might assume that neurotic individuals show stronger reactions than other to the signal for evacuation, corresponding with being faster prepared to evacuate or faster walking speed toward the exit. On the other hand, it might be plausible that neurotic individuals exhibit more likely than others uncertainty and less self-confidence about what ought to be done, resulting in delays for own decisions and a stronger orientation to the behavior of others. Thus, one might also hypothesize that neurotic individuals are more prone to herding behavior than others. In order to answer the questions and/or to examine our hypotheses we conducted an explorative study on the effects of personality traits on movement related decisions and movement pattern in evacuation scenarios. To our knowledge, it is the first approach to address these issues.

3.1 Experimental Environment

To determine the effect of psychometric profiles data from an evacuation experiment at Technische Universität Dresden are used. One week in advance to this evacuation practice, we conducted a questionnaire survey with students in the same lecture hall and the same student course (lesson 1). The questionnaires contained an ID for the student filled in. The same student course was again asked for participating in a questionnaire survey 1 week later (lesson 2). The same ID was used, and additionally, the questionnaire contained an ID for the seat number within the lecture hall. Both surveys took no longer than 20 min at beginning of a lesson. After two third of total time of the second lesson, the building has been evacuated. Announcement was given by loud speakers (via speech and auditive warning signals), and the whole building was evacuated. No specific reason about the evacuation background was told to students. Location of seats and students movements were recorded by 360° video camera mounted at the ceiling of the lecture hall (Fig. 9).

At the beginning of lesson 1, we used the German version of the EPQ-RK [11] in order to obtain the relevant personality traits. During lesson 2, we used a questionnaire focusing on anxiety and stress. Results presented here exclusively base on the data originated from the EPQ-RK. The EPQ-RK is a standardized instrument measuring extraversion, neuroticism and psychoticism with 50 items

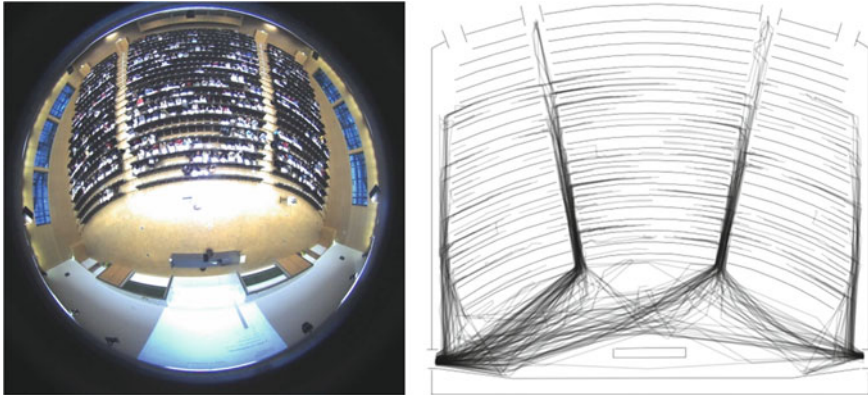


Fig. 9 Data acquisition with a 360° video camera taken at lecture hall and extraction of movement trajectories mapped to a virtual environment



Fig. 10 Virtual environment for display egress progress and psychometric profiles

in total. Movement parameters of students were analyzed with video tracking and visualization software (Fig. 10).

Data on movements and data on personality traits have been matched by linking the IDs from both questionnaires (lesson 1 and 2) and the seat numbers contained in the questionnaire for the second lesson. A number of $N = 301$ students took part in lesson 2 (which was evacuated in the end) and 86 % ($N = 259$) of the students in this lesson filled in the questionnaire. 54.4 % ($N = 141$) were male, and 45.6 % were female students. The mean age was 21.8 years ($SD = 1.96$) and ranged between 19 and 31 years. Participants were absolutely naive about the focus of the questionnaire survey and were told the purpose was to consider personality and stress during the stadium. From this sample we could assign 188 questionnaires (72 %) to the movement data set. From this sample of $N = 188$ students from lesson 2 we could

identify $N = 88$ students also in lesson 1 (46 %), and thus, complete their dataset with the personality data.

3.2 Results

For the pre-movement phase we considered the time point individuals were ready to evacuate the lecture hall (t_{ready}) and the time point individuals actually left their initial locations for the exit (t_{start}). The difference between these two parameters to the group mean values (t_{DEVready} , t_{DEVstart}) was computed for each individual and served as dependent variables. The group mean value was defined as the mean value per seat row and lecture hall sector, whereby a group consisted at least of three individuals. All values were z-standardized (Fig. 11). That is, individuals with a value $t_{\text{DEVready}} < 0$ were faster prepared to start for the exit than the others seated in same row whereas $t_{\text{DEVready}} > 0$ indicated that the individual needed longer time compared to the other group members. Likewise, for t_{DEVstart} less than zero the individual started earlier for the exit than the others and vice versa. According to their extraversion scores and their neuroticism scores individuals were assigned to low score (E^- , N^-) and high score groups (E^+ , N^+) per median split. Pre-movement parameters were subjected to t-test analysis for independent samples to compare group norm deviations for E^- and E^+ , and respectively, for N^- and N^+ .

We considered walking speed, speed deviation and a detour index as variables within the movement phase. In addition to the personality factors neuroticism and extraversion, the walk distance was examined as a further factor. We assumed that speed deviation, mean speed as well as detour were considerably affected by the distance to walk, and were interested in potential interaction effects between distance and personality factors on the movement variables. Results indicated a significant difference for t_{DEVready} between individuals with E^- ($M = -0.28$, $SD = 0.92$) and individuals with E^+ ($M = 0.23$, $SD = 0.89$); $t(61) = -2.127$, $p = 0.037$. Furthermore, the analysis revealed a significant difference for t_{DEVstart} between the E^- sample ($M = -0.42$, $SD = 0.90$) and the E^+ sample ($M = 0.21$, $SD = 0.87$); $t(61) = -2.728$, $p = 0.008$. Contrary to our hypothesis, these findings suggest that introvert more likely belong to the persons who started earlier within a given group whereas extravert were more likely reluctant and started with delay to the group norm. Spearman rho analysis confirmed a moderate positive correlation, corresponding with $r_s(61) = 0.40$, $p = 0.001$ between the absolute extraversion scores and t_{DEVstart} . Concerning neuroticism, t-tests did neither show significant differences between N^- and N^+ for t_{DEVready} ; $t(63) = 1.574$, $p = 0.121$, nor did for t_{DEVstart} ; $t(63) = 1.556$, $p = 0.125$. Spearman rho analysis indicated a weak, negative correlation of $r_s(63) = -0.232$; $p = 0.063$ between neuroticism scores and t_{DEVstart} which was marginally significant ($p = 0.063$). According to the latter, individuals who are more emotionally unstable tend to go for the exit earlier than others within a group.

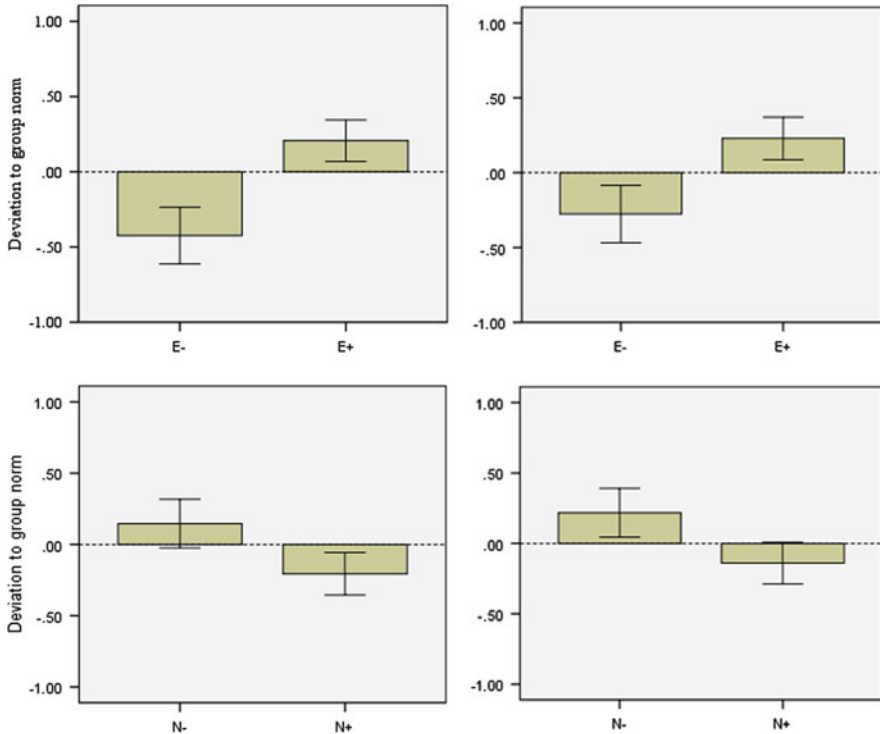


Fig. 11 Mean deviations to the group mean (and standard error) in time: *Ready to start* (a) and *Time to start* (b) depending on Extraversion (above) (z-standardized); Mean deviations to the group mean (and standard error) in time *Ready to start* (a) and *Time to start* (b) depending on Neuroticism (below) (z-standardized)

Thus, walking speed, speed deviation and detour index were subjected to three-factorial ANOVAs with distance, extraversion and neuroticism as factors. Individuals were therefore assigned to two groups according to their walking distance per median split (Distance low D⁻, Distance high D⁺). The ANOVA revealed neither significant effects of distance for personality factors nor for distance on mean walking speed. For speed deviation, ANOVA identified a significant main effect for walk distance on speed deviation; $F(2.75) = 4.591, p = 0.035$. Moreover, we found that speed deviation tend to be higher in the N⁻ group than in the N⁺ group; $F(1.75) = 3.653, p = 0.060$, indicating that individuals with lower scores on neuroticism tend to show more variance in their walking speed than individuals who are more emotionally unstable. The same picture emerged when considering effects on detour index. Both walking distance, $F(1.75) = 24.464, p \leq 0.001, \eta^2 = 0.24$, and neuroticism, $F(1.75) = 6.556, p = 0.012, \eta^2 = 0.08$, showed significant effects on the detour index, corresponding with higher detour values with greater distances, and respectively, higher detour values for individuals who score low on neuroticism. Beyond we identified an interaction effect between walking

distance and neuroticism, $F(1.75) = 6.935$, $p = 0.01$, $\eta^2 = 0.085$, indicating that the differences between N^- and N^+ in the detour index was particularly strong for long distances.

4 Discussion and Outlook

The present study focused on both group dynamic behavior and effects of personality traits on movement related decisions and movement pattern during an evacuation scenario. We initially assumed that extraversion has an effect on decision time in advance to actual movement to the exit, corresponding with faster decision times for extraverted individuals compared to introverted individuals. Moreover, we hypothesized that extraverted individuals would show stronger variances in their walking speed because partly the information processing will shifted from the pre-movement phase to the movement phase resulting in a more reactive movement pattern contrary to an more anticipative movement pattern (and less variance in walking speed) for introverted individuals.

Contrary to our assumptions, the results suggested that extraverted started later for the exit than introverted within a given group. One possible explanation for this effect is that social information and social evaluation by others is more important for extraverted individuals and provides the necessary feedback for the appropriateness of own behavioral pattern. In that context, social cues provided by the immediate surrounding might play a greater role for extraverted individuals, and might lead in turn, to stronger delays for reactions in social situations characterized by high degrees of uncertainty. Neuroticism was considered as a second personality factor assumed to have impacts on evacuation dynamics on individual level. Results showed that individuals high scoring on neuroticism tended to start earlier than other group members for the exit but the most striking result was that they walked for the exit in a more direct manner (less likely detour). This pattern was particularly true for long walking distances. These finding might reflect the stronger perception of urgency induced by the threat stimuli for neurotic individuals.

We are fully aware about potential caveats of our study. So, it was only feasible to examine movement pattern in relation to personality for part of the sample. There is clearly the need for further investigations considering complete samples of individuals within walking under critical circumstances. One might assume that effect reported above become even stronger. However, the results emphasize the importance of personality traits on movement behavior, even in situations of uncertainty and time pressure. Therefore, the examination presented here can be seen as first attempt in order to gain deeper insights into the relation of personality and movement decisions on tactical level and on overt movement behavior on operational level. We are furthermore fully aware that further research is needed to replicate findings presented here and also to uncover mechanism beyond.

References

1. Helbing D, P Molnar (1995). *Social force model for pedestrian dynamics*. Physical Review E 51, pp. 4282–4286
2. Moussaïd M, N Perozo, S Garnier, D Helbing, and G Theraulaz (2010). *The Walking Behaviour of Pedestrian Social Groups and Its Impact on Crowd Dynamics*. PLoS ONE 5(4) : e10047. doi:[10.1371/journal.pone.0010047](https://doi.org/10.1371/journal.pone.0010047)
3. Schultz M, C Schulz, and H Fricke (2008). *Passenger Dynamics at Airport Terminal Environment*, Pedestrian and Evacuation Dynamics 2008, pp. 381–396, Springer
4. Schultz M (2010), *An individual-based model for passenger movement behavior in airport terminals* (in German), PhD thesis, Technische Universität Dresden, <http://nbn-resolving.de/urn:nbn:de:bsz:14-qucosa-85592>
5. Simon H (1959). *Theories of decision making in economics and behavioural science*. American Economic Review, Vol. 49(3), pp. 253–283
6. Baddeley M, C Burke, W Schultz, and P Tobler (2010). *Impacts of Personality on Herding in Financial Decision-Making* Paper provided by Faculty of Economics, Cambridge Working Papers in Economics No. 1006, University of Cambridge
7. Eysenck H J (1953). *The structure of personality*. London: Methuen
8. Eysenck H J (1967). *The biological basis of personality*. Springfield: Ch. Thomas
9. Carvalho P V R., I dos Santos, and M C R Vidal (2005). *Nuclear power plant shift supervisor's decision making during microincidents*. International Journal of Industrial Ergonomics, Vol. 35 (7), pp. 619–644
10. Kobus D A, S Proctor, and S Holste (2001). *Effects of experience and uncertainty during dynamic decision making*, International Journal of Industrial Ergonomics, Vol. 28 (5), pp. 275–290
11. Ruch W (1999). *Die revidierte Fassung des Eysenck Personality Questionnaire und die Konstruktion des deutschen EPQ-R bzw. EPQ-RK*. Zeitschrift für Differentielle und Diagnostische Psychologie, Vol. 20(1), pp. 1–24
12. Loewenstein G and J S Lerner (2002). *The role of affect in decision making*. In R Davidson, K Scherer, H Goldsmith (Eds.), *Handbook of affective science*, pp.619–642, New York: Oxford University Press
13. Harrison Y and J A Horne (2000). *The impact of sleep deprivation on decision making: A review*. Journal of Experimental Psychology: Applied, Vol. 6 (3), pp. 236–249
14. Kuvaas B and G Kaufmann (2004). *Impact of mood, framing, and need for cognition on decision makers' recall and confidence*. Journal of Behavioral Decision Making, Vol. 17 (1), pp. 59–74

Investigating Human Factors in Fire Evacuation: A Serious-Gaming Approach

K. Schatz, J. Schlittenlacher, D. Ullrich, U. Rüppel, and W. Ellermeier

Abstract Applying a performance-based approach to fire protection design emphasizes the safe performance of a building as a whole rather than meeting detailed code requirements. To this effect, fire safety engineers make use of computer models and simulations to describe the expected spread of fire and smoke, and the safety evacuation. Since the protection of human life is the primary aim of the performance-based approach, predicting the behavior of people in danger is an essential purpose of such modeling. Particularly, the relevant human factors (individual decisions and parameters to describe human behavior) have to be taken into account. There is some controversy in the Fire Safety Engineering community on how to model human behavior, because appropriate methods for data collection and validation are not available. The aim of the present research is thus to achieve a better understanding of what actually happens during an extreme situation and how people come to decisions by using a serious gaming approach. The research hypothesis to be examined is: Can human evacuation behavior be explored using a computer game?

Keywords Serious gaming • Evacuation • Human behavior model • Building information modeling

K. Schatz (✉) • U. Rüppel
Institute for Numerical Methods and Informatics in Civil Engineering, Technische Universität Darmstadt, Darmstadt, Germany
e-mail: schatz@iib.tu-darmstadt.de; rueppel@iib.tu-darmstadt.de

J. Schlittenlacher • D. Ullrich • W. Ellermeier
Institute for Psychology, Technische Universität Darmstadt, Darmstadt, Germany
e-mail: ellermeier@psychologie.tu-darmstadt.de

1 Introduction

A new way to reach fire safety design decisions is presently being established as an alternative to the use of prescriptive codes: the performance-based approach. This process started a few years ago driven by the ISO [1]. Applying the performance-based approach to fire protection design emphasizes the safe performance of a building as a whole rather than meeting detailed code requirements. To this effect, fire safety engineers make use of computer models and simulations to describe the expected spread of fire and smoke, and the safety evacuation itself [2]. Since the protection of human life is the primary aim of the performance-based approach, the predicting the behavior of people in danger is an essential purpose of such modeling. Particularly, the relevant human factors (individual decisions and parameters to describe human behavior) have to be taken into account. According to Santos and Aguirre [3], for an evacuation simulation, three analytical dimensions need to be considered: the built environment (physical location), the management of this environment (signage, escape routes), and psychological and social-organizational characteristics of the occupants. Tavares [4] pointed out that an evacuation simulation model must consider four interactions: occupants-structure; occupants-occupants; occupants-fire (in case of fire events) and fire-structure (for this purpose, a fire model should be used).

To examine these human factors, different data-collection techniques like interviews with survivors, online questionnaires, map exercises or simulation experiments are used. These methods often cover only singular aspects of human behavior or studies are carried out independently from each other. Another point is that interviewees typically know that they are not in a dangerous situation and therefore feel no cognitive emergency stress. However, in the Fire-safety Engineering (FSE) community there is some controversy about this point. Santos and Aguirre [3] argue that appropriate methods for validation of the human behavior model are not available. So they state that proper validation tools have to be developed and that multidisciplinary collaboration is needed. However, according to them, the ability to accurately and comprehensively simulate human behavior is lacking in current computer evacuation models [3]. According to Kuligowski and Gwynne [5] these models often have the problem that the behavior simulated in the scenario is actually prescribed by the user (with probabilistic assumptions based on collected data) rather than predicted by the model and that the current models are only simulating separated behavioral facts. This shows there is need for a new methods to validate existing human behavior models and for analyzing human behavior in extreme building evacuation situations.

The aim of the presented research is thus to achieve a better understanding of what actually happens during an extreme situation and how people come to decisions within a serious gaming approach.

2 Serious Games for Fire Safety

The “Serious Gaming” approach combines concepts and methods borrowed from gaming technology with other information technologies for the benefit of “serious” applications. Serious games are naturally designed to achieve additional value beyond pure entertainment, in this case for the analysis of human behavior during the evacuation process.

Trenholme and Smith examined and compared different computer game engines regarding their ability for developing first-person virtual environments. Based on this idea, they explored the rapid prototyping of virtual environments with computer game technology [6, 7]. A study conducted in this research context documented that a single developer needed around 3 weeks for building a realistic model of a real world building. In such a virtual building fire drill evacuation scenarios could be simulated. One result of a user study conducted in this context was that participants judged the simulated environment to be quite realistic so that it can be assumed that virtual environments can support the training and observation of fire evacuee behavior in 3D virtual buildings.

Furthermore, training simulations for fire safety applications have been developed, mainly to train the tactic and strategic skills of firefighters. With these games emergency response teams can prepare themselves for incidents in a virtual environment. Many incidents can be virtually simulated in dynamic training sessions. Examples for virtual training systems are RescueSim [8], Tactical Command Trainer [9] or Emergency 2012 [10]. The focus of these games is on the training and teaching aspect. Nevertheless, no serious game fulfilling the following two requirements could be identified: Firstly, to provide interfaces for rapid development of scenarios based on the digital building model, and secondly, to collect human behavior data in a satisfying manner. Therefore, a new serious game needs to be developed.

3 The Serious Human Rescue Game (SHRG) Approach

The research hypothesis to be examined is: Can human evacuation behavior be explored using a computer game? While playing a game, “real” people rather than software agents will have to slip into the role of the evacuees. To implement this approach, the challenge is to develop a realistic and valid serious game for a new kind of immersive, dynamic and interactive simulation of building disasters. To address the present hypothesis, scientists of the Institute for Numerical Methods and Informatics in Civil Engineering (IIB) and the Institute of Psychology at Technische Universität Darmstadt are working together in a multidisciplinary project team.

The design approach of the SHRG follows the approach of Triadic Game Design (TGD) introduced by Harteveld [11]. This approach specifically focuses on the development of computer games with serious purpose. According to Harteveld,

the approach involves a triad consisting of the interdependent worlds of reality, meaning, and play that has to be balanced during the design process.

The **world of reality** deals with the question how the game is connected to the physical world. Therefore, domain-specific knowledge from the thematic background of the game is required. The challenges are (1) to model the building parametrically (e.g. geometry, structure and further technical semantics based on the actual building design), (2) to enhance the model with an authentic simulation of the emergency scenario (e.g., fire, smoke, explosion, structural damage) and (3) to consider the interactions occupants-structure, occupants-fire and fire-structure. To make sure that the model is valid – underscoring the “serious” in “serious games” – it is essential that the simulations are comparable to state of the art fire safety engineering simulations. One possibility is to retrieve this knowledge from the Building Information Modeling (BIM) process. BIM “*is defined as the creation and use of coordinated, consistent, computable information about a building project in design – parametric information used for design decision making, production of high-quality construction documents, prediction of building performance, cost estimating, and construction planning*” [12, p. 27]. The BIM model created by this process can be used as a “knowledge repository”.

The **world of meaning** focuses on the type of value that is to be gained. The SHRG can be seen as a method or tool to acquire knowledge about emergency scenarios and to provide possibilities for assessment, data-collection, exploration, and theory-testing in a safe environment. To achieve these values, a valid model (see world of reality) for emergency scenarios is required. One aspect that has to be considered in this world is a person’s predisposition to respond in situations of the emergency scenario. These responses are often based on feelings, emotions and individual experience. Especially in emergency scenarios these feelings (e.g., fear, panic) have to be taken into account. If the structural damage and the spread of fire and smoke could be properly simulated in the game scenario, it might be possible to assess the player’s reaction when the chosen egress route is blocked by debris or locked doors. This is an important prerequisite to analyze the interactions occupants-structure and occupants-fire. While playing such a game, data could be collected (1) about the viewing direction, (2) at which virtual objects the player looks, and (3) in which directions he or she decides to move. It is also possible to record biometrical data on the player like heart rate or brain activity at the same time. Immediately after the game session, additional data could be collected by questionnaires. These data could be useful for achieving a better understanding of how the structural status quo influences the decision making process.

The **world of play** refers to type of game and in which genre it can be classified. The concept of the SHRG is a mix of an action and a simulation game. According to Hartveld, the characteristics of an action game, for example, are that they do not have a long learning curve, they are fast-paced and the amount of the avatars life-energy is limited. A simulation game needs to stay close to reality and no predefined story exists (the online simulation results define the story). For the game concept the question what objectives players have to achieve, and by what kind of gameplay a player can reach these objectives needs to be considered. The following

will take up a fire scenario as one possible scenario of a building disaster. In this virtual fire scenario the gamer controls an avatar with a given amount of vitality. The main objective for the gamer is to guide this avatar through the virtual world to a secure area before its vitality reaches zero. Optional objectives could be, that the player/avatar saves as much vitality as possible or that he or she has to find the quickest way to a secure area. So, one requirement is that the information which influences the life-energy and the sense of orientation of a person in case of fire (e.g., heat, smoke, toxic gas), could be provided in the fire scenario (interaction occupant-fire). Another requirement is that it should be possible for the avatar to move through the virtual building and handle objects in the same way as in a real building (e.g., pass doors if they are not locked or handle virtual equipment; interaction occupant-structure).

3.1 BIM-Based Game Scenarios

For this research, the interactions occupant-structure and occupant-fire are of particular interest because they cannot really be investigated by real world experimentation. But creating realistic game scenarios is still time-consuming, because of the large amount of modeling work that has to be performed twice (e.g. 3D-modeling), first by the architect for the parametric building model as part of traditional building planning, and once more by the game artist generating the 3D-game content.

Researchers at IIB are developing new methods for bringing BIM and serious gaming together with the goal of automatically generating the game scenario out of the BIM. Figure 1 shows the logic of combining common BIM and fire safety engineering tools for game content creation.

As described in the previous section, the core part of the SHRG game engine is a simulation model which will include fire, smoke, explosions and structural damage. Therefore, it needs comprehensive information about a building. Requirements here are firstly, to support an international accepted data format, secondly, to have the semantic building information available, and finally, to have access to facility management data and simulation results. As discussed in the previous section, this information should be provided via BIM. BIM nowadays is the standard modeling method for building design, so that with the SHRG a large number of real buildings could be used for the gaming environment with relatively low modeling overhead. The information coming from BIM needs to be in a format, which can be used for (1) generating the objects used by the graphic-engine for visualization, (2) by the physics engine, and (3) to setup fire and smoke simulations. More detailed information about the integration of BIM can be found in [13–15].

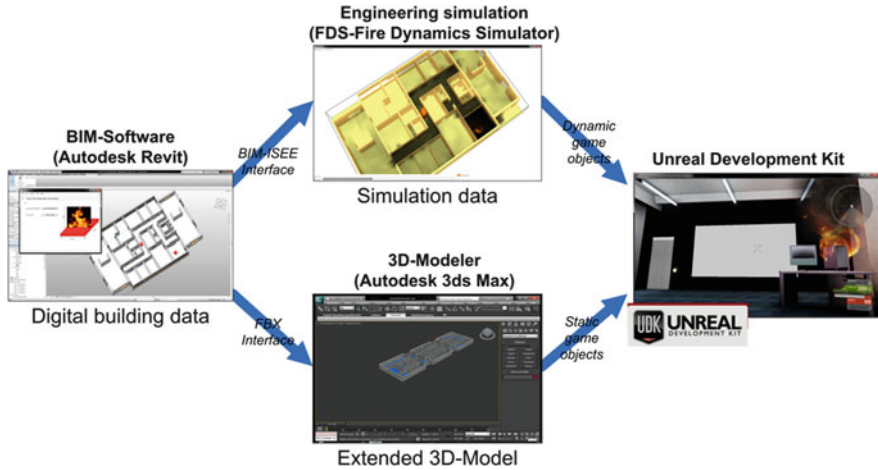


Fig. 1 BIM-based game scenarios

3.2 Presence Inside the Game Scenario

Another challenge is to stimulate an immersive experience in the gamer. This is important to improve the presence of the gamer inside the computer game. Generally, virtual environments vary greatly in the quality of representing the real world. It is plausible to assume that the more accurate and richly detailed the real world is mapped onto the virtual world, and the more the senses can be adequately stimulated, the more the immersive effect of a virtual environment will increase. To test these assumptions, scientists from the Institute of Psychology are currently conducting initial experiments regarding the stereo image capabilities, sound effects and human interface devices (HID) to determine the optimal hardware settings. The senses to be considered in principle are hearing, touch, smell, taste, and sight. In order to minimize unrealistic behavior in the virtual world, the gamer should have the feeling to actually be physically inside the virtual world. Playing computer games, gamers often tend to make unrealistic decisions due to lack of physical pain and injury responses from the virtual world. This is known in military training as the “super-soldier syndrome” [16, 17]. Therefore strategies have to be developed to avoid this effect and to ensure that gamers do not consider themselves to be invulnerable “super-evacuees”.

One aspect that influences presence is the quality of visual 3D rendering. People can see depth because they look at a scene from two different point of views (one from each eye). Based on these two images, the brain can then figure out how close (or far) things are. 3D stereo visualization makes use of this effect and a 3D scene is rendered twice (one for each eye). Subsequently, the two images are displayed overlaid using a 3D display and separated again for the left/right eye via special



Fig. 2 Left4Dead scenario: escape through a burning hotel

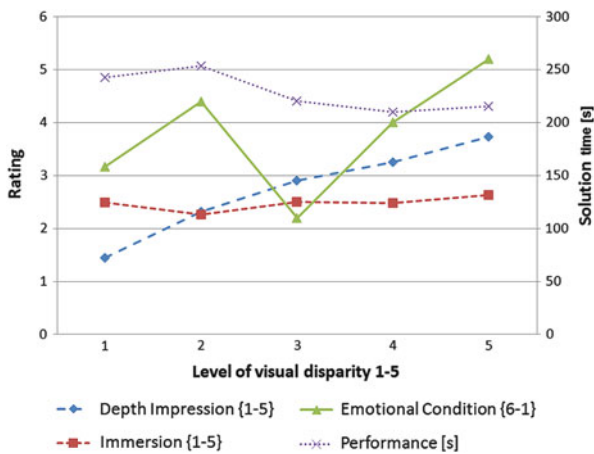


Fig. 3 Experiment results

glasses (e.g. shutter, polarization). The level of disparity influences the distance and the focal length of the two virtual cameras for rendering the 3D scene.

In the context of the SHRG project a small-scale exploratory study was conducted. For this study a customized version of the commercial first-person game Left4Dead was chosen. The main objective for the Participants was to guide an avatar through a burning hotel to a secure area (see Fig. 2).

This experiment was repeated 5 times with different levels of visual disparity presented in a random order. After every run the time taken to escape was measured and the participants had to fill out a questionnaire. The variables depth impression, immersion, emotional condition and performance were measured (see Fig. 3).

It appears that the optical disparity rendered has a strong influence on the depth impression perceived: The larger the optical disparity, the stronger the impression of depth (regardless of game/graphics engine). The present version, however, does not seem to be truly immersive: Ratings of immersion are at low to medium levels, no

matter what the disparity setting. Ratings of perceived stress (emotional condition) seem to indicate that a moderate level of disparity (setting 3, see Fig. 3) works best. Furthermore, there is a weak effect of 3D rendering on performance: The larger disparities appear to facilitate escape from the building (better depth perception slightly reduces solution times).

4 Conclusion and Future Work

In the project “Serious Human Rescue Game” the Institute of Numerical Methods and Informatics in Civil Engineering (IIB) and the Institute of Psychology are working together to research for “human factors” in the evacuation process. This paper introduces the concept of a new kind of a BIM-based serious game for an interactive and real-time simulation of emergency scenarios using a serious gaming approach. According to the concept, BIM-models serve as a basis of the game scenario. This allows a quick setup of scenarios by improving the interoperability to pass the data between the BIM application and the serious game. This feature provides a close relation to the world of reality and has the potential to allow the generation of game scenarios to analyze the interactions occupant-fire and occupant-structure. To find an optimal hardware settings initial experiments regarding the stereo image capabilities, sound effects and human interface devices (HID) are being conducted in the context of this project. This helps to figure out how to adjust the virtual environment to stimulate the desired effect. Eventually, the system developed according to the approach described in this article, should enable new analysis methods for studying the human behavior in extreme situations and it is assumed that particularly, the human factors regarding the interaction occupant-structure and occupant-fire could be explored in a new way. This could help to improve existing or develop new evacuation models.

References

1. ISO TC 92 (2002). Res.244 TG N6 Framework for the long term standardization of fire safety in support of performance-based design.
2. Friedman, Raymond, (1992) An International Survey of Computer Models for Fire and Smoke SFPE Journal of Fire Protection Engineering, 4 (3), 1992, p. 81–92 Available online: <http://www.firemodelsurvey.com>. last accessed May 2012
3. Santos G. Aguirre, B.E. (2004). A Critical Review of Emergency Evacuation Simulation Models. In NIST Workshop on Building Occupant Movement during Fire Emergencies
4. Tavares, R.M. (2008). Evacuation Processes Versus Evacuation Models: “Quo Vadimus”?, Fire Technology 2008, ISSN-1572-8099
5. Kuligowski, E.D.; Gwynne, S., (2010) The Need for Behavioral Theory in Evacuation Modeling, in Pedestrian and Evacuation Dynamics 2008 Isbn: 978-3-642-04504-2, Springer Berlin Heidelberg

6. Trenholme, D.; Smith, S. P. (2008). Computer game engines for developing first-person virtual environments. *Virtual Reality* (2008). Springer London Ltd. pp. 181–187.
7. Smith, S. P.; Trenholme, D. (2009). Rapid prototyping a virtual fire drill environment using computer game technology, *Fire safety journal.*, 44 (4). pp. 559–569.
8. VStep, (2011). RescueSim-Virtual Emergency Response Training, Product Information available online: www.rescuesim.com, Last accessed: May 2012.
9. Vectorcommand Ltd., (2011). Tactical Command Trainer, Product Information available online: www.emergencycommandsystem.com/products/tactical-command-trainer/, Last accessed: May 2012.
10. Koch Media, (2012). Emergency 2012, Product Information available online: <http://e2012.deepsilver.com/emergency-2012/index.html>
11. Harteveld, C. (2011). *Triadic Game Design - Balancing Reality, Meaning and Play*, Springer London, February 2011, ISBN 978-1-84996-157-8
12. Krygiel, E.; Nies, B. (2008). *Green BIM: Successful Sustainable Design with Building Information Modeling*, Wiley Indianapolis, ISBN 978-0-470-23960-5
13. Ruppel, U.; Schatz, K. 2011, Scenario Builder for generating realistic serious game scenarios for fire safety applications, Proceedings of the EG-ICE Workshop 2011, 6–8, July 2011 Twente University.
14. Ruppel, U.; Schatz, K. 2011, Designing a BIM-based serious game for fire safety evacuation simulations, *Advanced Engineering Informatics*, Volume 25, Issue 4, October 2011, Pages 600–611, ISSN 1474-0346
15. Schatz, K.; Ruppel, U. (2012). Ontology-based approach for integrating building information modeling into serious gaming environments. In Proceedings of ICCCBE 2012, Moscow (accepted Paper)
16. Barlow M. And Morrison, P., (2005). Challenging the Super Soldier Syndrome in 1st Person Simulations, Available online: www.siaa.asn.au/get/2411856229.pdf, Last accessed: May 2011
17. Morrison, P., Barlow, M., Bethel, G. And Clothier, S., (2005). Proficient soldier to skilled gamer: training for COTS Available online: http://seal.tst.adfa.edu.au/research/vesl/Papers/Training4COTSSuccess_simtect05.pdf. Last accessed: May 2011.

Occupants Emergency Behaviour in Turkey

Nese Çakici Alp and Gülen Çağdaş

Abstract The design of a building should protect occupants against attacks and other threats such as fires and earthquakes. In order to develop more effective designs, environmental factors and occupant characteristics should be examined thoroughly. Human populations have many differences in respect of physiologic, anatomic, behavioral and anthropometric factors, meaning that every society has its own characteristics. Those differences occur due to the interaction of genetic and environmental factors, and the cultural living standards of the society. A survey was conducted of the occupants of two different office buildings to determine the behavioural characteristics behavior and dispersion of Turkish occupants under emergency conditions. Survey responses were analyzed using SPSS statistical software. The dispersion behaviour of Turkish participants was compared with data from the USA and UK, to understand cultural behavioral differences. This is significant as the first study of emergency human behavior in Turkey. However, many more building designs and occupant groups need to be analyzed to provide comprehensive guidelines.

Keywords Fire safety • Emergency behavior • Behavioral character analysis

N. Çakici Alp (✉)
Kocaeli University, Kocaeli, Turkey
e-mail: nescakici@hotmail.com

G. Çağdaş
Istanbul Technical University, Istanbul, Turkey
e-mail: glcagdas@gmail.com

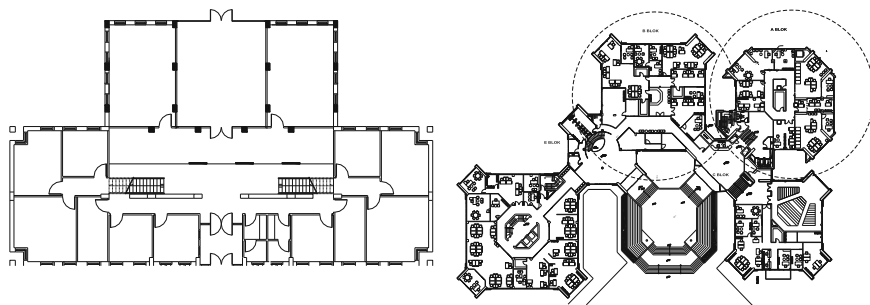


Fig. 1 Ground floor plans of GIT faculty of architecture and KMM buildings

1 Building Occupant and Study Descriptions

Two observations and surveys were conducted in two different building to understand occupants' emergency behavior and psychology in Turkey. The literature on behavior in emergency situations [1–4] was examined and evaluated prior to developing the survey used in the present study. The main purpose of analyzing these surveys was to investigate occupants' emergency behavior and to understand the distribution of changes in emergency behavior in different occupant groups [5].

The first of these surveys was administered on 01.04.2010, following a fire that broke out on the ground floor of the Faculty of Architecture of the GIT (Gebze Institute of Technology), the architectural plan of which is shown in Fig. 1a. The survey included occupants of the building at the time of the fire. A total of 27 people work at the faculty of architecture, which consists of a ground floor and a first floor; in addition, graduate courses are given in the building at some hours of the week. At the time of the fire, there were 17 people in the building. The survey questions were posed to these 17 people who were in the building during the fire. The second survey was administered with the employees of the Kocaeli Metropolitan Municipality (KMM) Building, the ground floor plan of which is shown in Fig. 1b. The building consists of two towers, one with five and the other with six floors, merged with a two-storey main building. The building hosts 600 employees, of which the questionnaire was administered with 123 occupants of the ground floor, first and second floors.

The purpose of the survey was to statistically identify the emergency behavior and psychology of the occupants, and the statistical breakdown of the 'during fire' behavior as per the occupants' age, gender, their knowledge about the building, and their position in the building. The variables used in the analysis of the survey are given in Table 1. As independent variables are not metric, the Kruskal–Wallis test was employed, which conducts a one-way analysis of variance between groups.

Table 1 Dependent and independent variables

Dependent variable	Independent variables
Occupant's age	Response to fire alarm Cue for fire perception
Occupant's sex	First reaction after fire perception.
Occupant's working floor	Evacuation speed
Occupant's duration time	Reaction after facing smoke First exit route in fire

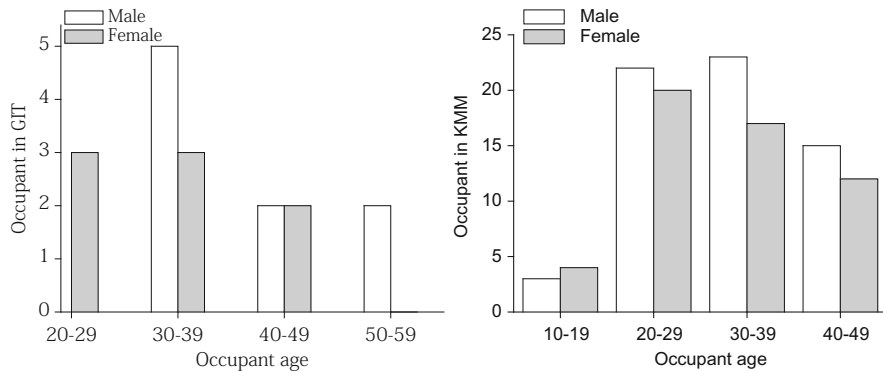


Fig. 2 Occupants age distribution

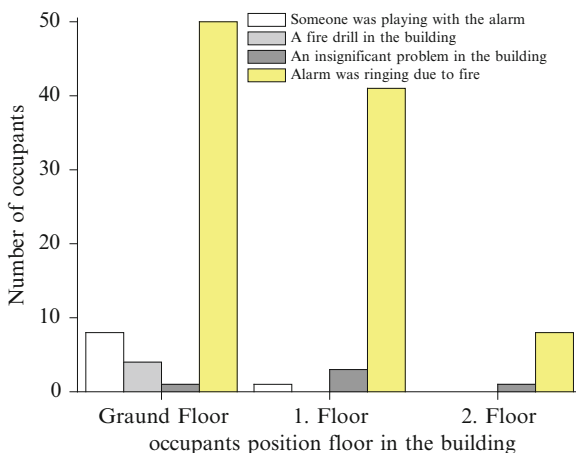
Of the 17 people in the building at the time of the fire, three were from the Faculty of Architecture (17.6 %) in the age group 20–29.8 (47.1 %) were aged 30–39.4 (23.5 %) were aged 40–49, and two people (11.8 %) were aged 50–59. The gender distribution of the occupants is given in Fig. 2. When the ages of the occupants of the KMM building, who participated in the second survey, are examined categorically, the age distribution is seen as follows: age 10–19 (6 %), age 20–29 (36.2 %), age 30–39 (34.5 %) and age 40–49 (23.3 %). The gender breakdown of the occupants is shown in Fig. 2.

The occupants' duration of employment in the buildings varies, with occupants of the GIT (Gebze Institute of Technology) Faculty of Architecture having worked in the building for 1–10 years, and occupants of the KMM (Kocaeli Metropolitan Municipality) building, which was opened only 2.5 years prior to the fire, having worked in the building for 0–2 years. At the GIT Faculty of Architecture, 13 of the 17 participants were on the ground floor and four were on the first floor at the time of the fire. The floor distribution of the occupants of the KMM building during the fire was identified as follows; 54.2 % were on the ground floor, 37.5 % were on the first floor, and 8.3 % were on the second floor. Following analyses examine the emergency behaviours of the occupants of the behavioral two buildings.

Table 2 Kruskal–Wallis analysis of occupants’ responses to emergency alarm

Test	Age	Sex	Duration	Oc. floor
Chi-square	4.514	0.507	2.869	9.781
df	3	3	3	3
Asymp. Sig.	0.211	0.917	0.412	0.021

Fig. 3 Alarm response of occupants according to their position in the building



2 Analyses Results

2.1 Response to Fire Alarm

There are no alarm systems in the GIT Faculty of Architecture building; hence, the effectiveness of the alarm could not be measured for this building. However, the occupants of the KMM building were asked how much importance they give to the alarm system. Occupant responses demonstrate that the alarm was a very important warning element during emergencies. Of the occupants of the KMM building, 85 % agreed that the alarm was ringing due to the fire, while 8 % thought someone was tampering with the alarm, 4.2 % thought there was an insignificant problem in the building, and 3.5 % reported they had thought there was a fire drill in the building. This distribution tells us that 85 % of the occupants will perceive an emergency when the alarm sounds in the building, and start the evacuation process. The Kruskal–Wallis test was used to analyze whether the occupant reaction to the alarm was related to gender, age, duration of employment in the building, the floor where the occupant worked, or the occupants’ knowledge of the building. The results showed that the floor where the occupant worked (Asymp. Sig = P) was a significant factor in their response to the alarm ($P = 0.021$, see Table 2).

As shown in Fig. 3, when the occupants’ thoughts regarding the reason for the alarm’s sounding are examined by floors, it is seen that occupants on the ground

Table 3 Awareness factors of occupants

Factor	GIT (%)	KMM (%)
Heart fire alarm	No alarm	60.2
Noises in the building	41	14.8
Informed by others	24	12
Power cut		4.6
Saw flames or smelt smoke	35	5.6
Sound of explosion		1.9
Fire engineers or fire truck being around		0.9

floor attributed 10 % more significance to the alarm, while also showing 10 % greater perception that someone was tampering with the alarm compared to the thoughts of occupants on other floors.

2.2 How Did You Become Aware That There Was a Fire and You Had to Evacuate the Building?

Another question examined how the occupants' emergency thoughts emerged. The answers given by KMM occupants are ranked by percentage in Table 3. A large majority of the occupants (60.2 %) report having formed the opinion that there was an emergency in the building upon hearing the alarm. Since this result supports the previous survey results, it shows that occupants regard the alarm seriously, and that it is very important to inform building occupants of emergencies using an alarm system.

When the occupants of the GIT Faculty of Architecture building, which has no alarm system, were asked how they became aware the fire, a large proportion (41 %) said they suspected it from the noise in the building, while 24 % reported they had been informed by others in the building. The remaining 35 % reported directly seeing the indications (flames and smoke) or smelling the smoke.

2.3 What Was Your First Action When You Realized There Was a Fire?

Participants were asked what should be their first action before starting to escape. Of the occupants of the KMM building, 55 % said they would warn other occupants by pressing the fire alarm, 31 % said they would notify the fire fighting services, and only 5 % reported they would escape without doing anything. The GIT occupants responded as follows: 25 % would press the fire alarm (although there is no alarm system in the building) and 25 % would go to the point where the fire had started. In

Table 4 Occupants' first actions

Behaviour	KMM (%)	GIT (%)
Pulled fire alarm	55	25
Called fire department	31	12.5
Left the building	5	12.5
Turned off computer	3	6.2
Got personal belongings	2	12.5
Had others call fire department	1	0
Notified other people in the building	1	0
Helped the elderly and the disabled will not escape from the building	1	0
Went to the fire point	1	25
Got valuable office documents and other things with me	0	6.2

Table 5 Occupants' leaving speed

Leaving speed	KMM (%)	GIT (%)
As running	52	29.4
As faster than normal walking speed	42	47.1
As not even stop for any obstacle that may be on their way	4	0
As in their usual walking speed	2	17.6
Did not- do not leave the building	0	5.9

addition, 12.5 % of the occupants reported they had called the fire fighting services, 12.5 % said they had gathered their personal belongings, and 12.5 % said they had immediately left the building (see Table 4).

The Kruskal–Wallis test was used to analyze whether the pre-escape behavior distributions of the occupants of both buildings would vary according to age, gender, height, and weight, duration of employment, job, knowledge of exit points and knowledge of the escape route. The results showed no significant differences in the pre-escape behaviors of the two groups (Asymp. Sig. $p > 0.05$).

2.4 How Quickly Did You Leave the Building?

Occupants were asked how quickly they left the building. Of the occupants of the KMM building, 52 % said they would leave running, 42 % that they would walk faster than their normal walking speed, 4 % said they would not even stop for any obstacle that may be on their way, while 2 % said they would leave the building at their usual walking speed. Of the occupants of the GIT Faculty of Architecture building, 47 % reported they would walk faster than their usual walking speed, 29.4 % reported they would leave running, 17.6 % said they would walk at their usual walking speed, while 5.9 % reported they did not leave the building (see Table 5).

Table 6 Kruskal–Wallis analysis of leaving speed of different occupant groups (GIT)

Test	Age	Sex	Duration	Oc. floor
Chi-square	7.311	4.732	2.411	11.815
df	3	3	3	3
Asymp. Sig.	0.063	0.192	0.492	0.08

Table 7 Kruskal–Wallis analysis of leaving speed of different occupant groups (KMM)

Test	Age	Sex	Duration	Oc. floor
Chi-square	2.832	3.155	5.580	8.711
df	3	3	3	3
Asymp. Sig.	0.418	0.368	0.134	0.033

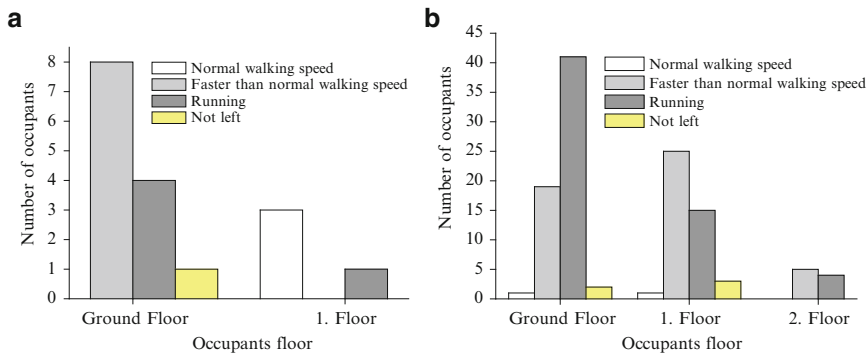


Fig. 4 Speed of emergency evacuation behaviour according to building storey

As seen in Tables 6 and 7, the Kruskal–Wallis analysis showed a significant difference between the behaviours expressed by occupants of the two buildings ($p = 0.033$), and the speed at which occupants left the building would vary according to the floor on which they were located behavior

The breakdown of occupant speed per occupant floor is shown in Fig. 4a for GIT and Fig. 4b for KMM. As can be seen from the figures, occupants on the ground floor report they would act faster compared to occupants on higher floors. Most probably, the fact that the fire broke out on the ground floor and was directly observed by the ground-floor occupants played an important role in this finding.

2.5 What Would You Do if Smoke Occupies Your Exit Route?

Participants were asked how they reacted when faced with smoke on their exit route. Of the GIT occupants, 46 % reported passing through the smoke, 31 % reported looking for another escape route, and 23 % reported having left the building without

Table 8 Emergency evacuation behaviour when faced with smoke

Behaviour	KMM (%)	GIT (%)
Look for another escape route	64.9	30.8
Wait at a safe spot for an officer to rescue	24.3	0
Passing through the smoke	9	46.2
Jump from the window	0.9	0
Shock	0.9	0
Not faced with smoke	0	23.1

Table 9 KMM occupant's directions

Directions	Number of occupant	%
From the emergency exit stairs	71	62.3
Towards the window	34	29.8
From the general used stairs	9	7.9

encountering any smoke. Of the 110 respondents who were occupants of the KMM building, 65 % said they would turn towards another escape route if faced with smoke, 24 % said they would wait at a safe location for an officer to rescue them, and 9 % said they would leave the building via a known exit even if it meant passing through smoke (see Table 8). The Kruskal–Wallis test showed there was no significant difference between the “in-smoke” behaviour of the different occupant groups.

2.6 Preferred Direction for Evacuating the Building?

Participants were asked where they would initially head to when they first realized there was a fire. Of the occupants of the GIT building, which has two exits, 94.1 % said they would leave the building using the exit they always use, while 5.9 % said they would leave from the window. The occupants' ages, genders, duration of employment in the building, knowledge of exits and floor of location were evaluated using the Kruskal–Wallis test. The test did not reveal any significant influence for any of the examined variables ($p > 0.05$).

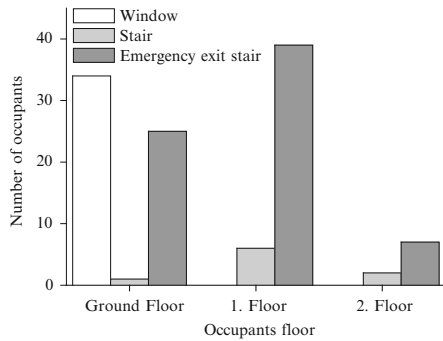
The breakdown of the exit preferences of the KMM occupants are given in Table 9. According to the table, 62.3 % of the occupants would head towards the emergency exit stairs, while 29.8 % would head towards windows and 7.9 % towards their usual daily exit point. The table shows that 7.9 % of the occupants will be exposed to, and likely affected by, smoke during a fire, as they do not head towards the emergency exit stairs.

The Kruskal–Wallis test was used to analyze whether there were any differences between the behaviours of the relevant occupant groups. The results show that the breakdown varies according to the floor where the occupant is located, since Asymp. Sig. $p = 0.00$ (see Table 10).

Table 10 Kruskal–Wallis analysis of exit direction among groups of KMM occupants

Test	Age	Sex	Duration	Oc. floor
Chi-square	4.669	1.157	3.361	43.166
Df	2	2	2	2
Asymp. Sig.	0.097	0.561	0.186	0.000

Fig. 5 Escape directions of KMM occupants according to their floors



Based on this result, the distribution of the escape directions of KMM occupants according to their floors is shown in Fig. 5. This distribution shows that occupants on the ground floor are more likely to exit through the window, while occupants on the first and second floors tend to head towards the emergency stairs.

From the survey results, it is understood that the most important factor affecting occupant behavior is the floor where they are located. The walking speed decreases with every new floor. In addition, the ground floor occupants also have the option of exiting via a window. On the other hand, it is understood that most of the occupants become aware of the emergency through the alarm system. And that is the reason why most occupants report that their first action in an emergency would be to press the alarm button (Table 4).

The first action before escape, after becoming aware of a fire, was compared between occupants from the UK, the USA and Turkey [6]. It is understood that the first actions of the occupants differed significantly between these three countries. This finding reaffirms the assumption that different geographies and structural conditions are likely to produce different behaviours among people (Table 11).

3 Conclusion

From the survey findings, it is understood that occupants demonstrate a tendency to use the emergency exit doors, yet fail to adequately visualize the building in their minds. Among ground floor occupants, equal proportions would use the emergency exit doors and the windows. Unlike the occupants of upper floors, it is statistically demonstrated that ground floor occupants are more likely to use the windows for exit

Table 11 Comparison of the first actions of occupants from the UK, USA and Turkey

Behaviour	UK (%)	USA (%)	TR (%)
Search for fire, went to fire area and fought fire	32.7	22.6	24
Left building	11.4	13.5	38
Called fire department	10.1	9	15
Notified others	8.1	15	3
Got family	5.4	7.6	0.5
Got personal property	1.2	2.1	8
Got dressed	2.2	8.1	0
Turned off appliances	4.1	0.9	3
Pulled fire alarm	2.7	0.9	2
Had others call fire department	2.8	2.2	0.5
Nothing	2.1	2.7	0
Closed door to fire area	3.1	1	0
Removed fuel	1.2	1.7	0
Entered building	0.1	1.6	0

purposes. Among the current Turkish group, it is seen that emergency behavior is not related to occupant age, but related to gender and the floor where the occupant is located. The floor where the occupant is located affects the occupant's escape performance. It is understood that the escape tendency of upper floor occupants is lower compared to those occupants based on lower floor. When compared to other countries, the emergency behavior of Anatolian people appears to differ in terms of priorities and breakdowns. In the present study, the emergency profiles of occupants were drawn through analysis of a limited sample. Expanding these emergency profiles countrywide would increase the consistency of the profiles. Occupant behavior trends and distributions also vary constantly and in the course of time, with developments and changes in building structures and in lifestyles. Hence, it would be appropriate to conduct similar surveys across the country and on an ongoing basis.

References

1. Wood G. P., 1972: The Behavior of People in Fires, Fire research note 953, Building Research Establishment, United Kingdom.
2. Fahy, R.F., Proulx G., 1995: A Study of Human Behaviour during the World Trade Center Evacuation, NFA Journal, 59–67.
3. Sekizawa A., Ebihara M., Nakote H., Kubota K., Nakano M., Ohmiya Y. and Kaneko H., 1999: Occupant's Behaviour in Response to the High-rise Apartments Fire in Hiroshima City, Fire and Materials, 23, 297–303.
4. Proulx G., Reid I. M. A., 2006: Occupant Behaviour and Evacuation during the Chicago Cook County Administration Building Fire, Journal of Fire Protection Engineering, 16, 283–309.

5. Çakıcı N., 2011: Simulation And Representation Of Human Emergency Behaviour And Movement In Buildings Using An Agent Based Model, PhD Thesis, Istanbul Technical University, Istanbul, Turkey.
6. Bryan J., 1995: Behavioural Response to Fire and Smoke, the SFPE, Handbook of Fire Protection Engineering 2nd Edition, National Fire Protection Association, Quincy, MA, 3, 241–262.

Psychological Aspects of German Signal Words in Evacuation Warnings

Laura Künzer, Gesine Hofinger, and Tina Zink

Abstract Signal words in evacuation warnings have an alerting and informing function related to the degree of danger. The psycho-acoustic urgency of the signal word used should match the contextual urgency (urgency mapping). In two experiments, characteristics of five German signal words were tested in the context of underground transportation systems. Participants rated the dimensions semantic field, urgency and explicitness for the German signal words. The German signal words were presented individually (exp. 1) or embedded in different loud speaker announcements with varying voice styles (exp. 2). As expected the ranking order for urgency was the same as for explicitness. Data showed that “Gefahr” is perceived as most urgent and most explicit. “Hinweis” is least urgent and least explicit. For the other three signal words used (“Vorsicht”, “Warnung”, “Achtung”) no clear order was found. “Achtung” is familiar in German announcements and warnings which influenced the ratings. Conclusions for the design of evacuation announcements are drawn.

Keywords Spoken warning • Signal word • Urgency • Explicitness • Semantic field • Evacuation

L. Künzer (✉) • G. Hofinger
Department of Intercultural Business Communication, Friedrich-Schiller-Universität Jena, Jena, Germany
e-mail: laura.kuenzer@uni-jena.de; gesine.hofinger@uni-jena.de

T. Zink
Department of Psychology, University of Regensburg, Regensburg, Germany
e-mail: zink_tina@yahoo.de

1 Introduction and Motivation of the Study

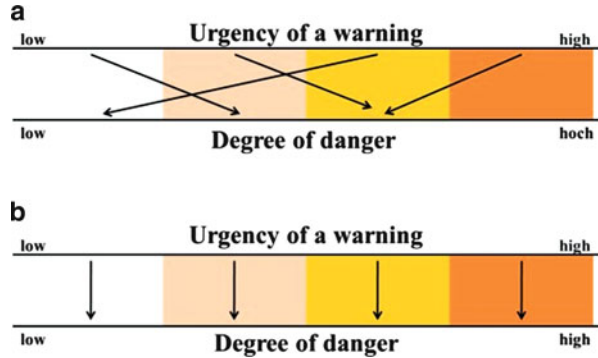
Warnings play an important role in evacuation. In general, warnings carry four functions: They provide safety information, they are created to influence human behavior in a certain way, and they aim at avoiding or reducing injury and loss of life, and are also reminders for widely known dangers [16, 18]. The recipients must be able to act according to the warning which implies understanding of its meaning, reflect the importance of the warnings to the recipient (personalizing), knowing what to do (leave the site) and doing it which is usually named compliance behavior [6]. However, the meaning of a warning is often not clear or cannot be understood properly. Habituation, due to frequent use of a warning without actual danger, can influence the effectiveness of a warning, too (e.g. cry-wolf syndrome; [1, 15]). The issue of poorly designed warnings has been addressed for the last two decades. For instance, Sime [14] reports one example: During an unannounced evacuation exercise in a subway station in Great Britain, the warning given was very imprecise and did not contain specific instructions. Hence, passengers started to gather information instead of leaving the station immediately. If warnings lack information or contain unclear meaning, people will spend valuable time on information retrieval instead of leaving the site [15]. Thus, the time until an evacuation can start could be reduced significantly by warnings that include precise instructions.

It is essential for safe egress to provide adequate information about the danger at hand. Hence, warnings have – apart from an alerting function – an informing function regarding the source and consequences of danger as well as the necessary action [18]. The informing aspect is mainly related to information that is processed consciously whereas the figurative aspect (“iconic aspect”) is perceived more or less subconsciously and gives implicit information about underlying meanings of a warning. In general, recipients react automatically to iconic aspects of a warning [3].

An important iconic part of visual and verbal evacuation warnings are signal words such as “ATTENTION”, “WARNING”, “NOTICE” [3, 5, 8]. Leonard et al. [11] describe signal words as “specific words intended to alert people to the presence of a hazard and the level of danger involved”(S. 176), and Rogers et al. [12] define signal words as “word denoting level of hazard” (S. 107). Consequently, not every signal word used in natural language is appropriate for every safety message. The response to a signal word will partly depend on the connotations or semantic field of the signal word. For English signal words, the semantic field has been researched for at least two decades (e.g., [5, 8, 18]). Relevant dimensions are perceived hazard, arousal strength, intended carefulness, and perceived urgency. For example, “NOTE”, “NOTICE”, “ATTENTION” seem to convey less danger and urgency than “DANGER” or “WARNING” [5].

Another important iconic aspect of warnings is urgency. The concept of urgency mapping emphasizes that the urgency of a warning must be related systematically to the actual context or the degree of danger (e.g. [3, 5]). In that way, recipients can

Fig. 1 (a) Inappropriate urgency mapping; (b) appropriate urgency mapping (according to Ref. [3], p. 7; modified by Ref. [20], S. 27)



understand intuitively the danger at hand, react faster and compliant with a warning [10]. In many cases, warnings are designed by the company’s marketing department; sometimes the department only defines few words for spoken warnings. As a result, the perceived urgency of a warning might be inappropriate as the wording of the warning does not match the actual degree of danger (Fig. 1a shows inappropriate urgency mapping). Urgency mapping not only stresses the need to design warnings carefully, but also highlights the difficulty of designing to provide appropriate urgency (Fig. 1b). Urgency mapping can be applied to different modalities and aspects of warnings. In this paper the focus is on German signal words and spoken evacuation warnings.

Explicitness of the signal word, the semantic field, and the level of perceived urgency are important for spoken warnings. Explicitness should emphasize “the specificity or detail with which potential injury consequences are described. [...] More explicit warnings present information about consequences in greater detail [...]” (S. 598; [10]). Explicitness is an important factor (in the process) of urgency mapping because the more explicit the warning is the more information about an actual danger, consequences or even behavioral directive are conveyed [8]. Therefore, when designing a warning the psycho-acoustic urgency of the signal word used should match the contextual urgency and the content of the warning (congruity).

English signal words have been investigated in numerous studies (e.g. [8]) whereas research on German signal words is still missing [20]. To our knowledge, no studies on urgency mapping or application of German signal words in spoken evacuation warnings have been conducted. Therefore we conducted two experiments to investigate the design of effective evacuation warnings (loudspeaker announcements) using German signal words. The first part of this study dealt with the mapping of German signal words on the dimensions of semantic field, explicitness and perceived urgency. The second part of the study investigated the influence of signal words in complete spoken evacuation warnings that should initiate evacuation behavior.

Five German signal words were analyzed in two consecutive experiments. As described earlier, signal words in the context of danger can be operationalized

according to several dimensions, e.g. hazardousness, intended carefulness. Especially the dimensions urgency, explicitness and semantic field were examined. However, the results also emphasized the impact of context and content, especially in spoken evacuation warnings.

In both experiments the same set of German signal words was selected: ACHTUNG – GEFAHR – HINWEIS – VORSICHT – WARNUNG. Some of these signal words have been suggested by standards (e.g. [9]) to be used as translations for English signal words (GEFAHR = DANGER; VORSICHT = CAUTION; WARNUNG = WARNING). Furthermore, ACHTUNG (literally translated: ATTENTION) was chosen because it is one of the most commonly used signal words in German warnings and it is often suggested as translation for CAUTION or IMPORTANT. The signal words ACHTUNG, GEFAHR, VORSICHT and WARNUNG were expected to represent a moderate to high level of urgency. The German signal word HINWEIS (= NOTICE) was included as a low level counterpart. In both experiments, participants rated several aspects of the signal words on a six point rating scale ranging from “extremely strong/urgent/explicit” to “not strong/urgent/explicit at all” [2, 8, 19]. In this paper, only selected results will be discussed. For a detailed description of method, material and discussion see Zink [20].

The results of this study are to be used in a research project on human factors in evacuation from underground transportation systems (OrGaMIR^{Plus}, see acknowledgements). Thus, the specific context of loud speaker announcement in subway stations was chosen.

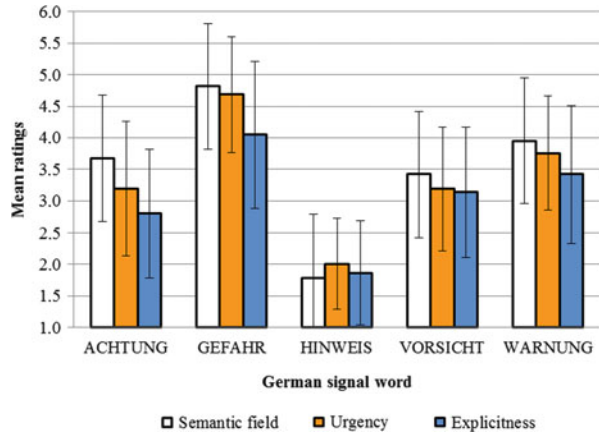
2 Experiment 1: Influence of Semantics on Perceived Urgency in the Context of Subway Systems

2.1 Design and Sample

Experiment 1 analyzed the five German signal words according to the three dimensions: semantic field (= Bedeutungsfeld), urgency (= Dringlichkeit), and explicitness (= Deutlichkeit). The key hypothesis of this study suggested a clear ranking order of the signal words for all three dimensions (GEFAHR – WARNUNG – VORSICHT – ACHTUNG – HINWEIS), while the ranking order for urgency was expected to be the same as for explicitness. The signal words were presented visually, black letters on white background, on a computer screen to offer the most neutral form of presentation.

Fifty-one native German speakers (male = 13) participated in experiment 1. Personal information recorded included e.g. amblyopia, and frequency of use of subway systems. Participants had to be native German speakers.

Fig. 2 Mean ratings and standard deviation of signal words for each dimension (semantic field, urgency and explicitness)



In experiment 1, questions (Q1–Q8) had to be answered for all five signal words. In a first step all five signal words were presented in a random order. After each signal word, participants had to indicate to what extent they perceived each word as a warning in general. Afterwards participants were instructed to imagine they were waiting for the subway train on a platform when hearing an announcement which included one of the signal words; the context was emphasized by two pictures of subway stations. Then, the five signal words were presented in random order. After each signal word participants answered seven questions concerning the dimensions “semantic field” (Q2), “urgency” (Q3–Q6) and “explicitness” (Q7; Q8).

2.2 Results

The mean ratings of the signal words for the three dimension semantic field, urgency and explicitness are presented in Fig. 2.

As expected, GEFAHR was rated highest for every dimension; HINWEIS was rated lowest for every dimension.

The frequency distributions of the dimension urgency was further analyzed (Fig. 3).

The distribution of HINWEIS showed the most prominent peak at “not urgent at all” and was the only signal word that was never rated “extremely urgent”. The distribution of GEFAHR showed a left-skewed distribution, GEFAHR was rated more often “extremely urgent” and “quite urgent” than all other signal words, and GEFAHR was never rated as “not urgent at all”.

Three signal words (ACHTUNG, VORSICHT, WARNUNG) revealed mediate levels of urgency. To further analyze these words, a one-way ANOVA was conducted which showed a significant main effect for the factor signal word ($F(1, 4) = 90.21$,

Fig. 3 Frequency distributions of dimension urgency with respect to the six point rating scale

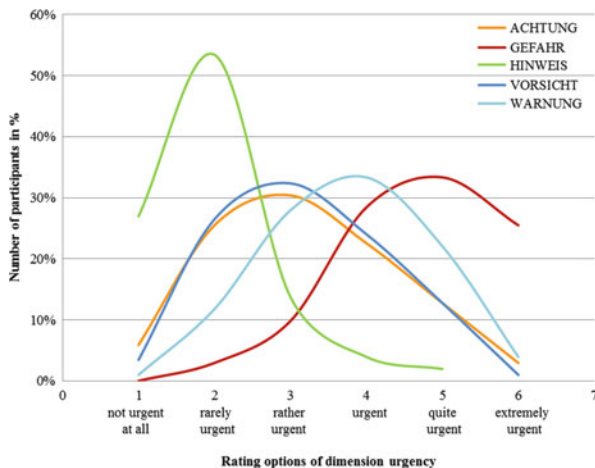


Table 1 Ranking order of signal words separated by the three dimensions urgency, explicitness and semantic field

Dimension	Rank 1	Rank 2	Rank 3	Rank 4
Urgency	GEFAHR	WARNUNG	ACHTUNG VORSICHT	HINWEIS
Explicitness	GEFAHR	WARNUNG	VORSICHT ACHTUNG	HINWEIS
Semantic field	GEFAHR	WARNUNG ACHTUNG	VORSICHT	HINWEIS

$p < 0.001$). Additionally, paired comparisons with repeated measures ANOVAs were conducted for all dimensions. Simple correlations between all three dimensions showed positive correlations for all paired comparisons. The dimensions urgency and explicitness revealed a strong positive correlation ($r = 0.73, p < 0.001$)

Table 1 shows the ranking order for all three dimensions.

A clear ranking order of the five signal words, the ranking order for urgency being expected the same as for explicitness. Table 1 shows that the expected ranking order was found for the extreme levels (GEFAHR and HINWEIS). For the mediate level no clear ranking order for the signal words WARNUNG, VORSICHT, ACHTUNG within all three dimensions was found, but ranking orders for explicitness and urgency were the same. The mapping of five German signal words seems to be ambiguous. More signal words should be taken into consideration in order to get clearer ranking orders. Furthermore, we suggest that further research is necessary, mere translation of signal word as often suggested in norms seem not appropriate, especially with respect to international use of signal words, e.g. English into German.

Table 2 Overview of the four fundamental elements of warnings

Element 1	Element 2	Element 3	Element 4
Signal word	Information about situation/existing hazard	Explanation of consequences of situation/hazard	Behavioral directives for avoiding the hazard

3 Experiment 2: Effects of German Signal Words in Spoken Evacuation Announcements in the Context of Subway Systems

3.1 Design and Sample

The design of experiment 2 used the four fundamental elements of warnings. The focus was on the dimension urgency of German signal words. We expected that perceived urgency of a spoken evacuation warning might not only be influenced by the signal word itself. Hence, we seek to further examine the effect of the semantics of the four warning elements on perceived urgency (see Table 2). Different levels of urgency were implemented using voice style, information about the source of danger and consequences of the situation.

In experiment 2, the signal words were integrated in spoken warnings consisting of the four fundamental elements [13, 17]:

All of the four elements were applied in the spoken evacuation warnings (“complete warnings”) and the sequential arrangement (1–4) of the four elements was retained through the whole experiment. The signal words were the same as in experiment 1. The information about the situation/existing hazard conveyed information about two emotionally neutral situations (“current information”; “technical malfunction”) and two situations which were expected to be considered as dangerous (“fire development¹” and “dispersion of gas”). The explanation of consequences of the situation/hazard named one neutral consequence (“Train operations will be stopped!”) and one consequence that was supposed to convey risk for the physical well-being of the recipient (“Your health may be at risk!”). At the end of the evacuation warning there was only one behavioral directive offered (“Leave the subway station!”) as in a subway system this would be the appropriate action following an evacuation warning. The announcements resulting from the combination of these factors are presented in Table 3.

The spoken evacuation warnings were recorded by a professional female announcer in an urgent and non-urgent voice. Before recording, specific instructions were given to the announcer for each voice style. One instruction was designed to focus on a neutral situation and aimed at recording a voice with a neutral pitch. The

¹The word we used, “Brand”, is not a signal word itself in contrast to “Feuer” (= fire) in English.

Table 3 Overview of variables and values of variables of experiment 2. Codes were used to specify different versions of spoken evacuation warnings, e.g. drH3GS

Variable	Values of variable	Code
0 Voice style	Non-urgent	nd
	Urgent	dr
1 Signal word	ACHTUNG	A
	GEFAHR	G
	HINWEIS	H
	VORSICHT	V
	WARNUNG	N
2 Information about situation/existing hazard	Current information (Aktuelle Informationen)	1
	Technical malfunction (Technische Störung)	2
	Fire development (Brandentwicklung)	3
	Dispersion of gas (Gasausbreitung)	4
3 Explanation of consequences of situation/hazard	Train operations will be stopped! (Der Bahnbetrieb wird eingestellt!)	BB
	Your health may be at risk! (Ihre Gesundheit könnte beeinträchtigt werden!)	GS
4 Behavioral directives for avoiding situation/hazard	Leave the subway station! (Verlassen Sie den U-Bahnhof!)	No code

Combination “drH3GS” = (urgent voice style) HINWEIS! Fire development: your health may be at risk! Leave the subway station!

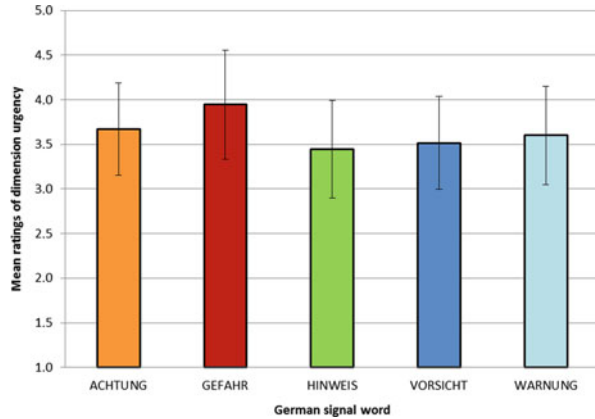
other instruction aimed at producing an urgent voice style by asking the speaker to imagine a situation where a beloved person was in danger.

Table 3 shows all warning variables and related values of variables used in experiment 2. Due to the large number of variables only 28 combinations (14 urgent and 14 non-urgent combinations) were selected to permit comparative testing of the spoken evacuation warnings.

Forty-one participants (male = 10) unknown to the first experiment participated took part in experiment 2. Personal information was recorded including e.g. hearing problems and frequency of use of subway systems; all participants were native German speakers.

Participants were instructed to imagine they were waiting for the subway train on a platform when hearing an announcement. The context was illustrated by two pictures of subway stations. All 28 spoken evacuation warnings were presented to the participants via headphones. Participants had to answer four questions regarding the dimension urgency (Q3–Q6 of experiment 1) after each warning. The questions were slightly customized in experiment 2. At the end, participants were asked to answer five reflective questions concerning experiment 2.

Fig. 4 Mean ratings and standard deviation of five German signal words arranged by the dimension urgency (obtained from data of all spoken evacuation warnings)

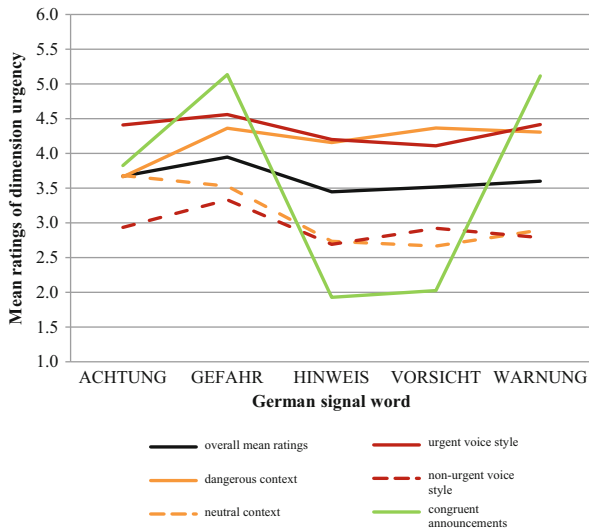


3.2 Results

Some important results are (for a detailed description see [20]):

- As intended (expected), participants perceive an urgent voice style as more urgent than the indifferent/neutral voice style.
- As expected, GEFÄHR received the highest urgency ratings; HINWEIS the lowest ratings. Surprisingly, ACHTUNG achieved second highest urgency ratings, followed by WARNUNG and VORSICHT. Similar to experiment 1, no clear ranking order was found in experiment 2. Mean ratings of variable signal words on dimension urgency are presented in Fig. 4.
- **Importance of context:** An interaction of the variable “Information about situation/existing hazard” and “Explanation of consequences of situation/hazard” was found. Therefore, a new combined variable “context” was composed for further analysis. The variable “context”, has three values: *neutral context* (“Current information”/“Technical malfunction” combined with “Train/Rail operations will be stopped”), *dangerous context* (“Fire development”/“Dispersion of gas” combined with “Your health may be at risk!”) and *mixed context* (“Current information”/“Technical malfunction” combined with “Your health may be at risk!”, or “Fire development”/“Dispersion of gas” combined with “Train operations will be stopped”). The results showed that the dangerous context conveys a higher degree of urgency than neutral context and thus emphasizes the importance of context in spoken evacuation warnings.
- **Influence of voice style:** Interactions between signal word, context and voice style were found in a repeated measure three-way ANOVA ($F(1,4) = 54.02$; $p < 0.001$, $\eta_p^2 = 0.58$): Voice style and context seem to increase a signal word’s urgency. But with respect to ACHTUNG, further analysis showed that rankings in urgency for ACHTUNG showed different interaction effects for the variables context and voice style. Hence we concluded the high ratings of ACHTUNG in perceived urgency to be influenced by other variables, e.g. congruity (see Fig. 5).

Fig. 5 Overall mean urgency ratings for the German signal words and mean ratings for the variables context, voice style and congruity



- Congruity within spoken evacuation warning:** congruity of the four elements of a warning seems to play an important role with respect to perceived urgency of a warning. Congruity represented the “compatibility” of variables within a complete warning: For instance, ndH1BB² and drG3GS³ were considered to be congruent because the composition of these warnings showed no internal contradiction whereas ndH3GS⁴ for example was considered as incongruent. Results revealed more extreme ratings (“extremely urgent” or rather “not urgent at all”) for congruent warnings. Consequentially, congruity should be considered as important factor in urgency mapping of spoken warnings. These results are in accordance with the literature suggesting congruity to increase the credibility of a spoken warning [4, 5].

At the end of experiment 2, participants were asked to answer reflective questions:

The participants were asked if they had detected different signal words in the beginning of the warnings and if they were able to recall the signal words used (without having been instructed to remember the signal words at the beginning

²Combination “ndH1BB” = (non-urgent voice style) HINWEIS! Current information: Train operation will be stopped! Leave the subway station!

³Combination “drG3GS” = (urgent voice style) GEFAHR! Fire development: Your health may be at risk! Leave the subway station!

⁴Combination “ndH3GS” = (non-urgent voice style) HINWEIS! Fire development: Your health may be at risk! Leave the subway station!

of the experiment). Forty-one percentage of participants remembered at least one signal word. ACHTUNG was remembered most often (88 %), followed by GEFAHR (59 %), HINWEIS (54 %), WARNUNG (39 %) and VORSICHT (34 %). ACHTUNG has been suggested to be one of the most often used German signal words, so the high ratings of ACHTUNG on dimension urgency in spoken evacuation might arouse from the frequent use and awareness of participants for this signal word. Even though ACHTUNG seems to imply a moderate level of urgency (for the participants). It is unclear how the frequent use of ACHTUNG influences the ratings identification.

Another question concerned the credibility of the spoken warnings. Credibility was defined as colloquial expression [7]. Over a quarter of the participants (27 %) stated that the urgent voice style was not credible, because the voice style sounded hysterical and exaggerated and they wouldn't expect a voice style like that in a subway announcement. Twenty-two percentage participants stated the non-urgent voice style to be incredible because the spoken warnings sounded too monotone, bored and indifferent. Some participants reported that a non-urgent voice style increased (personal) importance of the spoken warnings whereas other participants reported that the voice style did not draw attention to the contents of the warning. Other participants (22 %) stated both voice styles to be credible. Thirty-seven percentage of participants stated that a spoken warning had little credibility when voice style and contents of the spoken warning did not fit ("lack of congruity"). So, the influence of congruity was reconfirmed by the participants.

4 Discussion and Conclusions

Our research indicates the variables "German signal words", "context" and "voice style" to have differentiated effects on the perceived level of urgency of spoken evacuation warnings. The effects and interactions of these variables seem to have more impact than expected. The results extended our initial expectations, the following aspects were concluded:

- Urgency mapping needs closer consideration and application in standards for evacuation warnings. Our findings suggest varying degrees of urgency depending on variables (German signal word; context; voice style) and warning combinations. By standardizing the use of signal words in warnings and announcements, a determined level of urgency might implicitly be conveyed to the listener and thus increase effectiveness of the presented warning. The signal words GEFAHR or WARNUNG or VORSICHT should not be combined with advisories or passenger information. HINWEIS on the other hand should not be used for spoken evacuation warnings or emergency warnings in general.

- In general, using a signal word in a warning is better than not using a signal word. But our results raise questions concerning the use of ACHTUNG. ACHTUNG, as expected, was mentioned by the participants to be the most frequent used German signal word and was remembered best by participants. Memory effects of urgency are still unknown. However this might offer valuable approaches to warning design in the future. Due to the frequent use of the German signal word ACHTUNG in other (written and spoken) warnings, ACHTUNG should be used with care in evacuation warnings.
- Voice style was found to be effective in arousing attention but also showed problems concerning credibility, especially if the voice style was considered to be too monotone or too hysterical for a publicly spoken announcement. Finding the right balance, especially for avoiding emotions of fear and attitudes of complacency, will be a challenge for warning design in specific contexts. In subway systems, the use of an alarm signal to announce a following spoken warning in a normal vocal range (non-urgent voice style in experiment 2) should be used. The latest developments of synthesized speech might make the use of artificial voices more appropriate.
- A spoken evacuation warning should be presented completely, containing all four fundamental elements of a warning, but also has to be kept as short as possible. “Information on the current situation”, “Explanation of consequences” and “behavioral directives” will help the receiver of a spoken warning to adopt the personal involvement. Therefore, the receiver will start the evacuation without hesitation. However, time to listen, if necessary, the presentation in different languages which prolong presentation times and restricted attention span, might have negative effects on the perception of a spoken warning. Therefore, words like “please”, “Dear passengers” were avoided in the experiment and should be avoided in spoken evacuation warnings, too.

Warnings are not supposed to substitute safety precautions, rather proper warnings must be designed in a safety system in addition to other safety precautions. The presented experiments highlight the complexity of and challenge to designing spoken evacuation warnings adequately. Hence, research on German signal words and warnings has to be extended.

The results presented in this paper suggested semantic differences concerning the different elements of warnings and its/their context dependency. A next step in our research will include a comparison of these findings with US data.

Acknowledgements The paper uses data from the diploma thesis “Deutsche Signalwörter in Warnungen” by Tina Zink [20] which was written as part of the joint research project OrGaMIRPLUS, funded by the German Federal Ministry for Education and Research. One of the aims of the project is to investigate aspects of human factors in evacuations of underground transportation systems, especially warnings and alarms and emergency route design. Special thanks go to Prof. Dr. A. Zimmer, Department of Applied Psychology, University of Regensburg.

References

1. Breznitz, S. (1984). *Cry wolf: The psychology of false alarms*. Hillsdale, NJ: Erlbaum.
2. Drake, K. L., Conzola, V. C. & Wogalter, M. S. (1998). Discrimination among sign and label warning signal words. *Human Factors and Ergonomics in Manufacturing*, 8 (4), 289–301.
3. Edworthy, J. & Adams, A. (1996). *Warning design: A research prospective*. London/Bristol, PA: Taylor & Francis.
4. Edworthy, J., Clift-Matthews, W. & Crowther, M. (1998). Listeners' understanding of warning signal words. In M. A. Hanson (Hrsg.), *Contemporary Ergonomics* (S. 316–320). London: CRC Press.
5. Edworthy, J., Hellier, E., Walters, K., Clift-Matthews, W. & Crowther, M. (2003). Acoustic, semantic and phonetic influences in spoken warning signal words. *Applied Cognitive Psychology*, 17, 915–933.
6. Fitzpatrick, C. & Mileti, D. S. (1994). Public risk communication. In R. R. Dynes & K. J. Tierney (Hrsg.), *Disasters, collective behaviour, and social organisation* (S. 71–84). Newark: University of Delaware press.
7. Greuel, L. (2001). *Wirklichkeit - Erinnerung - Aussage* (1. Aufl.). Weinheim: Beltz.
8. Hellier, E., Aldrich, K., Wright, D. B., Daunt, D. & Edworthy, J. (2007). A Multi Dimensional Analysis of Warning Signal Words. *Journal of Risk Research*, 10 (3), 323–338.
9. itl. (2009). *Warnhinweise - Übersetzung der Signalwörter (EU)* Verfügbar unter: http://www.itl.eu/en/site-services/search.html?tx_indexedsearch%5Bsword%5D=signalw%C3%B6rter&tx_indexedsearch%5B_sections%5D=0&tx_indexedsearch%5Bpointer%5D=0&tx_indexedsearch%5Bext%5D=0&tx_indexedsearch%5Blang%5D=0 [30.03. 2011].
10. Laughery, K. R., Vaubel, K. P., Young, S. L., Brelsford Jr., J. W. & Rowe, A. L. (1993). Explicitness of consequence information in warnings. *Safety science* (16), 597–613.
11. Leonard, S. D., Otani, H. & Wogalter, M. S. (1999). Comprehension and memory. In M. S. Wogalter, D. M. DeJoy & K. R. Laughery (Hrsg.), *Warnings and risk communication* (S. 149–187). Philadelphia: Taylor & Francis.
12. Rogers, W. A., Lamson, N. & Rousseau, G. K. (2000). Warning Research: An Integrative Perspective. *Human Factors*, 42 (1), 102–139.
13. Sanders, M. S. & McCormick, E. J. (1993). *Human Factors in Engineering and Design* (7.). New York, NY [u.a.]: McGraw-Hill.
14. Sime, J. D. (1995). Crowd psychology and engineering. *Safety Science*, 21, 1–14.
15. Tubbs, J. S. & Meacham, B. J. (2007). *Egress design solutions: A guide to evacuation and crowd management planning*. Hoboken, NJ: John Wiley & Sons.
16. Wogalter, M. S. (Hrsg.) (2006). *Handbook of warnings*. Mahwah, NJ: Lawrence Erlbaum Associates.
17. Wogalter, M. S., Conzola, V. C. & Smith-Jackson, T. L. (2002). Research-based guidelines for warning design and evaluation. *Applied Ergonomics*, 33 (3), 219–230.
18. Wogalter, M. S. & Laughery, K. R. (2006). Warnings and hazard communications. In G. Salvendy (Hrsg.), *Handbook of human factors and ergonomics* (3rd ed., S. 889–911). Hoboken: John Wiley & Sons.
19. Wogalter, M. S. & Silver, N. C. (1990). Arousal strength of signal words. *Forensic Reports*, 3, 407–420.
20. Zink, T. (2012). *Deutsche Signalwörter in Warnungen [German signal words in warnings]*. Unveröffentlichte Diplomarbeit [unpublished diploma thesis]. Regensburg: Universität Regensburg.

Psychological Aspects of Human Dynamics in Underground Evacuation: Field Experiments

Robert Zinke, Gesine Hofinger, and Laura Künzer

Abstract The relevance of individual and social human factors in evacuation generally has been accepted, but only few studies aim at determining their specific influence on evacuation behavior. Data come from accident analysis, laboratory experiments, and field studies. A series of studies including passenger counts, passenger interviews and field experiments is reported. Data show that many passengers would need help in an evacuation, that passengers lack knowledge about evacuation signs and behavior, and that they expect their own behavior to be non-compliant with some evacuation orders. Field experiments show instances of helping participants with simulated impairments, and of altruistic as well as egoistic behavior. Results concerning group behavior include staying together and even building “human lumps”.

Keywords Field experiments • Human factors • Passenger evacuation • Social behavior • Subway station • Underground transportation

1 Introduction

Underground transportation systems are a part of everyday life in cities around the world. In the rare event of a major fire or a terrorist attack, the health and lives of passengers depend on fast and safe evacuations.

The research project OrGaMIR^{PLUS}, funded by the German Ministry of Education and Research, deals with human factors in evacuations from underground transportation systems. By specifically addressing human factors such as human social behavior, OrGaMIR^{PLUS} aims to further improve evacuation guidance in

R. Zinke (✉) • G. Hofinger • L. Künzer
Department of Intercultural Business Communication, Friedrich-Schiller-Universität Jena, Jena, Germany
e-mail: robert.zinke@uni-jena.de; gesine.hofinger@uni-jena.de; laura.kuenzer@uni-jena.de

subway systems, e.g. escape routes, and evacuation simulation models. In this paper, we describe results from passenger counts, passenger interviews and results of evacuation field experiments in progress.

2 Human Factors in Evacuation Research

As branch of science and technology, human factors are concerned with human characteristics and technical components to improve human well-being and overall system performance, e.g. safety in underground transportation systems. Human factors focus on human-artifact interactions in a systematic approach (e.g. Refs. [14, 22]).

When considering human factors in evacuation, pedestrian dynamics are relevant behavioral human factors, e.g. keeping distance between pedestrians [9] or orientation behavior [1]. For evacuations as exceptional and dangerous situations, further behavioral and physical human factors should be taken into account, such as decision making, motivation, attitudes and emotions as well as group related characteristics, e.g. social behavior and leadership, but also physical characteristics like size or impairment. The relevance of human factors in evacuation generally has been accepted, but only few studies aim at determining their specific influence on evacuation behavior. Studies rely on different types of data and analysis, as the following examples illustrate.

2.1 Analysis of Real Accidents

The behavior of humans in evacuation, especially from fires, has long been in the focus of research. Researchers often have addressed behavior that may seem irrational or not understandable, like “freezing” or sudden panic (e.g. Ref. [24]). But when the situation and perspective of the persons is taken into account, it turns out that human behavior in evacuation is usually neither irrational nor egoistic [8, 26]. Most researchers today agree that “irrational behavior” is seldom found in real events ([3, 21, 25, 27], contrary to the popular belief that mass panic is the normal thing to happen). Not only rational, also pro-social behavior in evacuation is often found: Dynes [7] reports altruistic behavior in several evacuation scenarios, so does Drury et al. [5]. Fridolf [11] summarizes accidents analysis and field research on fire evacuation in underground transportation systems. According to Fridolf, factors explaining the unwillingness to evacuate a subway train or subway station seem to be information processing (e.g. when dealing with incoherent or unclear information or ambiguous cues from the source of danger) and social influence.

After more than 20 years of research a lot is known about human behavior in real events. But collection and analysis of individual data from real events is difficult and

seldom tried (e.g. Ref. [5], researched behavior in subway trains after the London bombings of 2005). In closing, results concerning human behavior in evacuation do not easily yield clear input factors for design of escape routes or evacuation simulation models.

2.2 Laboratory Experiments

While simulation models have started to embrace a broad access to human factors, empirical data from laboratory experiments still seem to concentrate on external aspects that influence evacuation behavior. These aspects include the relevance of the number of individuals, consequences of escape route dimensions and obstacles for the evacuation time (e.g. Refs. [23, 25]). Individual human factors, e.g. motivation and behavior, are being considered as relevant for the improvement of simulations, yet only few studies investigate these phenomena empirically. Usually, laboratory settings are used for experiments, designed to observe single aspects of individual or group behavior like walking speed, route choice and lane formation, or avoidance behavior (e.g. overview in Fridolf [11]) Human factors in evacuation from underground tunnel systems have only recently been addressed in laboratory experiments. Frantzych and Nilsson [10] intended to assess realistic way finding behavior of passengers, using a 37 m tunnel filled with irritant smoke.

Other evacuation experiments are done to investigate more general characteristics of pedestrian movement such as: evolving patterns and paths of movements in crowds (e.g. Helbing et al. [13]) and underlying social forces (e.g. Refs. [12, 15]). Typical laboratory settings for these experiments are hallways. Sometimes 3D virtual reproductions of an environment are created, e.g. of public buildings to investigate spatial cognition and orientation behavior [4], or even of a subway station to detect social human factors like cooperating or competing behavior in evacuation [6]. A recent example for a subway-related laboratory study is from the METRO project in Sweden [16]: In the laboratory-setting of a prepared and smoke filled road tunnel (vs. a real subway tunnel), passengers' way finding behavior in smoke – resulting from a “burning” subway train – was the human factor investigated, inspected in order to calibrate existing computer simulations.

With settings designed for specific experiments, laboratory experiments offer little room for an explorative approach. Also, they have only limited ecological validity with respect to the complexity of reality, e.g. of underground transportation systems.

2.3 Field Experiments

As laboratory experimental settings lack ecological validity, field studies have been conducted to assess pedestrian dynamics and evacuation behavior in actual circumstances. Of course, also field studies do not represent real evacuation situations,

so results are limited to behavior without fear. Predtetschenski and Milinski [20] considered non-psychological characteristics of passengers in underground transportation systems, such as carrying baggage or wearing different types of clothing. A study by Oswald et al. [19] deals with passenger behavior in evacuation from a train taking place at the surface.

Only few empirical studies have collected data from underground transportation systems (e.g. Kang et al. [2], for the choice between escalators and stairs in underground transportation systems). Within the current GETAWAY project, a research group around Ed Galea from the University of Greenwich investigates way finding-behavior in over-ground and underground terminals. Frantzich (2000, after [11], p. 39) found discussions among participants and habit to be decisive for the choice of path. In the field studies by Norén and Winér [18] and Nilsson [17] analyzing evacuation from street tunnels, participants preferred the closest exit.

Usually, participants in field studies are given questionnaires concerning their experiences and knowledge. Results from field studies on evacuation behavior are limited as participants are never in real danger. So the results are not easily transferable to evacuation in actual dangerous situations. Yet, field studies can get closer to real-life phenomena with respect to human behavior than experiments in a laboratory can.

In the following, we describe a series of studies in a German underground transportation system that were conducted to identify human factors relevant for underground evacuation. A first study with passenger counts aimed at getting to know characteristics of those that could have to evacuate from a specific subway station. In the second study, passengers in the same subway station were interviewed concentrating on their knowledge and attitudes. The third study focusing on evacuation behavior included a series of field experiments in several subway stations.

3 Study 1: Passenger Counts: Who and How Many Are They?

3.1 Objectives

Study 1 in an underground subway station included counts of passengers in order to determine the average number of passengers in a subway station per hour and to identify their composition. Furthermore, the actual occurrences of specific physical aspects of the passengers in a subway infrastructure were to be identified.

Physical characteristics are important aspect of human factors that are likely to be relevant for evacuation. Therefore we wanted to determine the percentage of passengers with impairments in walking and seeing. We were also interested in the way out that passengers and especially passengers with impairments use in order to leave the station. A last interest was in the number of passengers in company, e.g. groups or families.

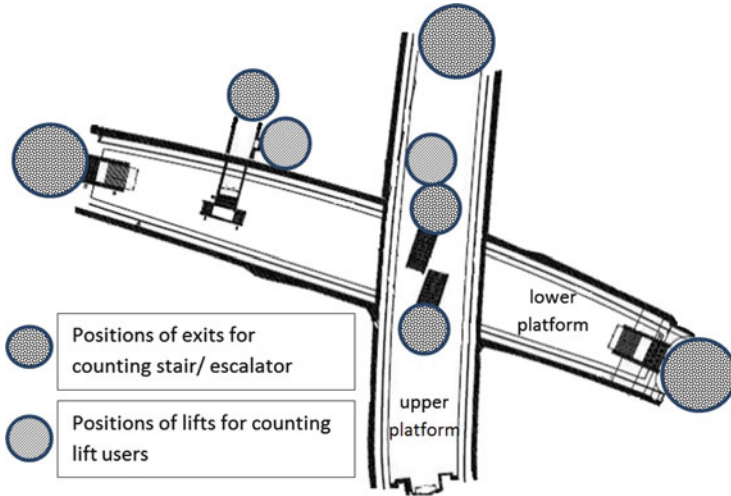


Fig. 1 Simplified model of two-level subway station, indicating all exits observed

3.2 *Design and Participants*

The specific subway station was chosen because it has relevance for commuters in the subway system and it is moderately complex with two platform levels of crossing subway lines (see Fig. 1). Three times, for the duration of 1 h, the total number of passengers was counted. Passenger counts were conducted in the morning (10:15–11:15 a.m.) on 1 day, and at noon (02:30–03:30 p.m.) and in the evening (05:00–06:00 p.m.) of another day during 1 week in summer, in order to compare for possible “rush-hour” effects. Passengers were counted at all entrances and exits, stairs, the escalators and lifts inside the subway station. At the central staircases, the passengers moving up and down were counted by separate persons while every other counting position was taken by only one person. Counts included the total numbers of passengers and the number of passengers with impairments, with bulky luggage, and of passengers traveling in company.

3.3 *Results*

Overall counts at a single subway station summed up for an average of 8,400 passengers per hour at a regular two-level subway station. Roughly 4 % of them had either an observable seeing or walking impairment and 7 % were carrying luggage or were clearly detectable to be in company. A further finding was that a high number of persons using one of the lifts on either platform level (lower level/upper level) was impaired in walking (22 %) or seeing (9 %), carried heavy luggage (26 %) or

were in company (40 %). For the lift users several attributes could hold true for the same passenger, and percentages are relative frequencies compared to the overall number of lift users.

The stairs and escalators in the middle of the subway station were most frequently used. Almost one third of the passengers chose this way to enter or exit either level of the subway station. This is relevant, because passengers will likely choose an exit they already know from previous use [27]. The number of passengers counted at noon (9,245) and in the evening (9,814) were almost equal, compared to the number of passengers in the morning (6,063) which was considerably lower. The number of passengers moving into and coming out of the subway station was near balance for each counting interval.

3.4 Discussion

The 1-h counts only allow for first impressions about the average numbers of passengers. Yet, although the number of passengers in the morning hour was roughly one third less than at other counting intervals, there are always many passengers present in the subway station. The largest proportion of passengers was using the exits in the middle of the subway station. Thus, passenger will likely not use all available exits evenly, unless instructed to do so during evacuation.

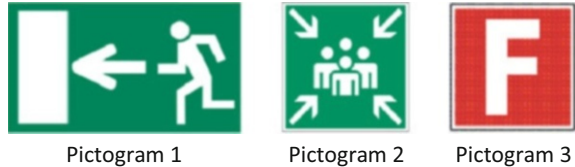
Our study has limitations regarding the counts of passengers with impairments. It is not easy to determine impairments and passengers travelling in company. The actual numbers of passenger with these attributes might therefore be even higher. This study underlines the importance of the special needs of passengers with impairments in evacuation. While lifts are usually turned off in case of fire, they are highly frequented by impaired passengers that will have to walk alternative escape routes.

4 Study 2: Passenger Interviews: What Do They Know and Think?

4.1 Objectives

The aim of study 2 was to determine passengers' knowledge about evacuation, safety pictograms and the infrastructure subway station. Interviews also included questions about passengers' attitudes and estimations of their own behavior in the case of an evacuation from subway stations.

Fig. 2 Three selected pictograms from the questionnaire in study 2



4.2 Design and Participants

213 passengers took part in the structured interviews within a subway station. Passengers were selected by coincidence from the number of passengers waiting for a subway; only German-speaking persons took part (female: 122, male: 88, missing value: 3). Interviewees were of different ages. They were asked to answer 14 questions. Additionally, 39 passengers (female: 25, male: 15) commented on seven pictograms relevant for evacuation.

The pictograms presented included the one for the escape route leading towards the emergency exits (see Fig. 2, pictogram 1). A second pictogram (Fig. 2, pictogram 2) indicates the meeting point after evacuation, where e.g. passengers are being taken care of. Both of these pictograms were chosen from a norm (BGV A8 DIN 4844-2), defining the standard use of pictograms for escape routes in Germany. A third pictogram presented indicates the location of a fire extinguisher (Fig. 2, pictogram 3).

4.3 Results

4.3.1 Pictograms

Three results for the pictograms ($n = 39$) are to be highlighted here. Only three participants did not recognize the pictogram for the escape route leading towards the emergency exits. This indicates that participants would at least recognize the escape route pictograms if looking for a way out. Furthermore recognition of escape route pictograms could be interpreted as a necessary precondition for fast escape from the infrastructure.

On the other hand, 12 participants did not know the pictogram for the meeting point. The pictogram for fire extinguisher was not recognized by 11 participants. Since the meeting point is usually a safe area where users of an infrastructure are to gather after an evacuation in order to do a “role call” or a medical check-up, not finding or recognizing a meeting point would make it difficult for first responders to ensure individual well-being after an incident.

The pictogram for the fire-extinguisher is still in use in the respective public transportation system although a novel and self-explaining pictogram exists. Passengers used to the novel fire extinguisher pictogram could get confused and as a result might not find the fire-extinguisher.

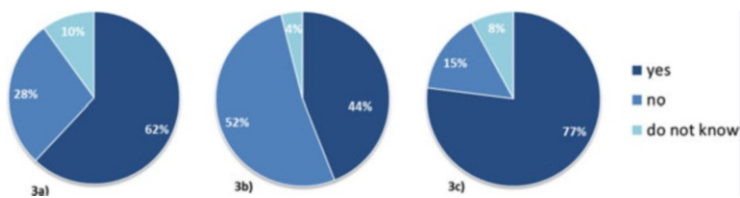


Fig. 3 Passengers' attitudes towards their own evacuation behavior. Explanation in the text

4.3.2 Interviews

Some relevant results from the interviews can be stated for the context of emergencies. The participants that were asked: "Would you stay with your partner/child, even if you could only move on if you separated from one another?" 62 % answered that they would not leave without their partner or child (see Fig. 3a). For the question: "In case of a fire at the (intermediate level of a subway station), would you wait for rescue at the platform level if told to do so?" 52 % of the interviewees replied that they would not wait for rescue at platform level (see Fig. 3b). More than three quarters (77 %) of the participants that were asked: "Would you leave your luggage behind, if this would enable you to move on faster?" stated that they would leave their luggage behind (see Fig. 3c). In consequence, left behind luggage would block the way out for others. Each of these aspects would lead to a less homogenous and predictable escape of passengers from the infrastructure.

5 A Series of Field Experiments: How Do They Act?

5.1 Objectives

Based on results from studies 1 and 2 regarding passengers' knowledge and attitudes and on human factors found in the literature, a series of four field experiments were carried out. Observable evacuation behavior was of interest, especially the influence of social groups. Some preliminary results are presented here.

5.2 Design and Participants

For each trial, participant groups varied between 25 and 90 participants. Most participants were students (of geography or psychology). The age ranged from 19 to 62. All of the participants were native or fluent German speakers, vision and hearing was normal. The trials took place in three underground subway stations in Germany and one in Great Britain (participants were German students).

Each participant received a safety-vest with clearly visible numbers. Pre-existing groups (e.g. fellow students) received safety vests in specific colors. Because of numbers and colors, safety vests facilitated observations and the collection of data from individual participants. Furthermore, different colors of vests were to highlight group membership for participants inside and outside these groups.

In two equal sized groups impairments were simulated by vision-impairing goggles and by bandaging a knee of some participants. Even a person sitting in a wheelchair voluntarily participated in one group. Our goal was to receive additional insights from these participants and to artificially disrupt the flow of evacuation-movement in order to assess help-seeking requests and supporting social behavior of the groups.

In the beginning of the field experiments, participants were confronted with a potentially life-threatening scenario. They were asked to imagine effects of a volatile toxic agent detected within the subway station. Before each trial, they were instructed to leave the subway station into a safe area. Trials started with a spoken announcement including the order to leave the subway station.

Within each trial, participants were asked to walk “as fast as possible” along defined distances in the subway station on either the platform, the track-bed, escalators (either turned on or turned off), and stairs (upwards and downwards). In two subway stations, an additional “tunnel trial” was carried out: Starting from the tracks, participants were asked to go through the tunnel of the subway station and use the emergency exit within the tunnel.

Structured interviews were conducted after each trial. Participants were asked to comment on their own behavior, the group, and how they experienced infrastructural specificities. At the end of each trial, participants answered questionnaires. Questions aimed at their knowledge about underground transportation systems, escape routes, emergency behavior, and at decision making while finding a safe area. Furthermore, participants were asked to assess their integration into the group assigned by color of the safety vests. Social human factors were analyzed on video recordings from different perspectives and standardized observer protocols.

5.3 First Results

Analysis of field experiments is still in progress. But first results reveal, as expected, the importance of different human factors: infrastructural elements, group size and individual characteristics (physical impairments, preliminary experience with similar situations or infrastructure) influenced the speed of evacuation, speeding it up or slowing it down. Other findings include an influence of social human factors. In the following, a few results from the video analysis are presented, focusing on social behavior and group phenomena. Explanatory notes are added in the light of interviews and questionnaire analysis.

Fig. 4 Person in wheelchair being assisted on his escape



5.3.1 Helping Persons with Impairments

The participants moved inside a subway station which offers in general limited space. If participants did not keep up with the pace of the participant group they slow down the overall evacuation and are endangered to be run over by other participants. Especially at bottlenecks or “obstacles” like turned-off escalators, participants tended to offer help to others (not necessary altruistically) to move faster or to avoid falling.

Helping participants with impairments or slower participants to move safely and faster was observed almost in all trials. Helping behavior was always found when the participant with impairment asked actively for help. While help was needed for the stairs, the escalator and the tracks, participants hardly asked for help on the platform.

The seemingly smaller person in Fig. 4 (vest nr 9, yellow), is actually sitting in a wheelchair. At the bottom of the stairs this participant had originally asked a participant of his own group to assist him on the turned-on escalator. That participant pushed the wheelchair while members of other groups joined in to assist spontaneously. Some of them are holding the wheelchair; others are giving room for this participant.

Passengers with impairments have special needs. If these are not met by the infrastructure (e.g. no lift available in fires), they rely on social strategies. This was confirmed by video analysis and also stated in the questionnaires by the participant with simulated impairments.

5.3.2 Push and Shove? Egoistic and Altruistic Behavior

The passenger counts (see study 1) and the answers in the passenger interviews showed that passengers often travel in company, e.g., groups of friends, families, school classes. The intention to help others on their escape depended on the

Fig. 5 Pushing away group members trying to get onto the escalator



membership in a group and on the individual sense of integration into that group. The level of perceived integration (“group cohesion”, see below) is higher in small groups; the level of perceived integration in the group corresponds with altruistic behavior within the group. Helping behavior and groups of people sticking together may not only lead to smoother evacuation but may have contrary effects by creating “human lumps”, as the following episodes illustrate.

In Fig. 5, a major part of members of a large group (wearing orange safety vests) is trying to move up an escalator in order to leave the platform. One participant (contours are highlighted) at the bottom of the escalator is being pushed aside by other participants trying to get past. The participant is forced to bend backwards moving her left leg back in order not to fall over. The participant’s left arm is holding onto the banister while she is trying to get the right arm in front. The participant would hardly have been strong enough to reenter the stream of participants moving up the escalator. Another participant later slowed down and pulled her back onto the escalator. Helping behavior did not depend on group size and was observed in and across all groups, e.g. in the wheelchair example (see Fig. 4).

5.3.3 Group Cohesion and Staying Together

In the tunnel trials, participants separated into smaller groups, staying together in pairs or quadruples. Within these groups, participants mostly relied on guidance of other participants who were familiar with the infrastructural specificities from former trials. When information about the escape route came from a member of another group it was inconsistently assessed as trustworthy or it was ignored. Then, small groups even moved past the nearest emergency exit and continued following the tracks into the tunnel, leading into the direction of the next subway station.

However, in the tunnel trials spontaneous “human lumps” were found as a result of individual factors or social adhesion of groups. Individual factors included waiting for others to support their movement, to give them information, or originated from the waiting participants’ search for information and advice to the right choice of exit.

With respect to the participants wearing vests of the same color, a connection between helping behavior and asking for support was identified. Individually sensed integration in the group differ among participants groups according to their group sizes, with a tendency for a higher level of perceived social integration for smaller groups.

5.4 Discussion

Some of the limitations of the study concerning participants are that in order to meet ethic guidelines of the universities involved, all of the participants had to be informed about the general setting and aim of the field studies. Knowing they were going to evacuate, participants were ready to start leaving. At the same time they were hardly affected emotionally by the scenario announced to them. Yet, a moderate level of stress was experienced, as questionnaires showed.

Furthermore, with an average age of 27 years, the participants were physically in good shape; they also were able to resign from the experiments at any time, and some did do so when tired.

Although we have to rely on individual cases for the analysis of social phenomena at the moment, the (individual) social human factors phenomena presented could be found in several episodes of the trials. With respect to the single phenomena e.g. effects of group membership on staying together and on egoistic or altruistic behavior, the representativeness for evacuation from subway infrastructures is still to be determined.

6 Conclusion

The first findings from our passenger counts, passenger interviews and field experiments emphasize the importance of passengers’ characteristics and the need to understand more distinctly human (social) behavior in emergency situations and their respective influence on the speed and form of the evacuation movement. These aspects need to be included in models of passenger behavior in evacuations. Results are relevant for underground evacuation because passengers can be slowed down not only by architectural bottlenecks but also by individual and social human factors. In further field experiments phenomena will be investigated with larger numbers of passengers, for possible cultural variation and different types of infrastructures.

Acknowledgements This research was funded by the German Federal Ministry of Education and Research (program “Research for civil protection”, project: OrGaMIRPLUS, project number: 13N11525). The studies were conducted in cooperation with Prof. Andreas Pflichtsch from Ruhr-University Bochum and his students.

References

1. Carlson, L.A., Hölscher, C., Shipley T.F. and Conroy-Dalton, R C (2010). Getting lost in buildings. *Current Directions in Psychological Science*, 19, 284–289.
2. Kang, K., Han, K. & Kim, J. (2010). A Study on Passenger Level Change Mode Choice in a Public Transport Transfer System: -Gwangmyeong station case-. *Journal of the Eastern Asia Society for Transportation Studies*, Vol.8, 2010.
3. Cocking, C., Drury, J. & Reicher, S. (2009). The psychology of crowd behaviour in emergency evacuations: Results from two interview studies and implications for the Fire and Rescue Services. *The Irish Journal of Psychology*, 30 (1–4), 59–73.
4. Conroy-Dalton, R. (2005). Space syntax and spatial cognition. *World Architecture: Space Syntax Monograph* 11(185), 41–45.
5. Drury, J., Cocking, C. & Reicher, S. (2009). Everyone for themselves? A comparative study of crowd solidarity among emergency survivors. *British Journal of Social Psychology*, 48 (3), 487–506.
6. Drury, J., Cocking, C., Reicher, S., Burton, A., Schofield, D., Hardwick, A., Graham, D., & Langston, P. (2009). Co-operation versus competition in a mass emergency evacuation: A new laboratory simulation and a new theoretical model. *Behavior Research Methods*, 41, 957–970.
7. Dynes, R.R. (2006). Panic and the vision of collective incompetence. *Natural hazard observer*, Vol. XXXI (2).
8. Fahy, R. F. & Proulx, G. (2009). ‘Panic’ and human behaviour in fire. Paper presented at the 4th International Symposium on Human Behaviour in Fire, Robinson College, Cambridge.
9. Forell, B. (2004). Bewertung der Anforderungen der Musterversammlungsstättenverordnung (Mai 2002) hinsichtlich realistischer Evakuierungsszenarien in Diskotheken und ähnlichen Vergnügungsstätten. Braunschweig: TU Braunschweig.
10. Frantzi, H., & Nilsson, D. (2004). Evacuation Experiments in a Smoke Filled Tunnel. Paper presented at the third International Symposium on Human Behaviour in Fire, Belfast, UK.
11. Fridolf, K. (2010). Fire evacuation in underground transportation systems: a review of accidents and empirical research. Report 3151. Lund: Lunds universitet.
12. Helbing, D., Farkas, I., & Vicsek, T., Freezing by heating in a driven mesoscopic system, *Physical Review Letters* 84, 1240–1243 (2000).
13. Helbing, D., Molnár, P., Farkas, I. J. & Bolay, K. (2001). Self-organizing pedestrian movement. *Environment and Planning B: Planning and Design*, 28, 361–383.
14. Karwowski, W. (2012). The discipline of human factors and ergonomics. In Salvendy, G. *Handbook of human factors and ergonomics* (4th ed.) (3–37). Hoboken, NJ: Wiley.
15. Moussaïd, M., Helbing, D. & Theraulaz, G. (2011) How simple rules determine pedestrian behavior and crowd disasters. *PNAS* 108 (17) 6884–6888.
16. Nilsson, D. (2010) METRO - A research project about fires and explosions in metro systems (underground). Presentation at the International Rail Accident Investigation Conference, 25 November 2010.
17. Nilsson, D. (2009). Exit Choice in Fire Emergencies - Influencing Choice of Exit With Flashing Lights. Lund University, Lund.
18. Norén, A., & Winér, J. (2003). Modelling Crowd Evacuation from Road and Train Tunnels – Data and design for faster evacuations (No. 5127). Lund: Department of Fire Safety Engineering, Lund University, Sweden

19. Oswald, M., Lebeda, C., Schneider, U., & Kirchberger, H. (2005). Full-Scale Evacuation. Experiments in a smoke filled Rail Carriage - a detailed study of passenger behaviour under reduced visibility. Paper presented at the third International Conference on Pedestrian and Evacuation Dynamics, Vienna, Italy.
20. Predtetschenski, W. M. & Milinski, A. I. (1971). Personenströme in Gebäuden - Berechnungsmethoden für die Projektierung. Köln-Braunsfeld: Verlagsgesellschaft Rudolf Müller.
21. Quarantelli, E. (2008). The Nature and Conditions of Panic. In A. Boin (Hrsg.), *Crisis Management* (Vol. 2, S. 309–319). London: Sage Publications.
22. Sanders, M. S. & McCormick, E. J. (1993). *Human Factors in Engineering and Design* (7th ed.). New York, NY
23. Schadschneider, A., Klingsch, W., Klüpfel, H., Kretz, T., Rogsch, C. & Seyfried, A. (2009). Evacuation dynamics: Empirical results, modeling and applications. In B. Meyers (editor.), *Encyclopedia of Complexity and System Science* (S. 517–550). Berlin: Springer.
24. Schneider, U. & Kirchberger, H. (2007). Evakuierungsberechnungen bei Brandereignissen mittel Ingenieurmethoden. *Brandschutz*, 62–76.
25. Schreckenber, M. (2010). Dynamik von Menschenmassen, AKNZ Seminar, 22.06.2010. Deutsche Hochschule der Polizei, Brühl.
26. Sime, J. D. (1995). Crowd psychology and engineering. *Safety Science*, 21(1), 1–14.
27. Tubbs, J. S. & Meacham, B. J. (2007). *Egress design solutions: A guide to evacuation and crowd management planning*. Hoboken, NJ: John Wiley & Sons.

The Effects of the Design Factors of the Train-Platform Interface on Pedestrian Flow Rates

Taku Fujiyama, Roselle Thoreau, and Nick Tyler

Abstract The main purpose of this research was to empirically investigate the effects of the design factors of the train-platform interface on dwell time. We chose the doorway width, the step height and the vestibule setback as design factors, and investigated their effects on the two types of pedestrian flows: boarding-dominant and alighting-dominant flows. We found that (1) a wider doorway increased the pedestrian flow rate, (2) a greater step height led to a lower flow rate, and (3) the flow rates increased as the vestibule setback increased. These results would be useful not only for designers and planners of rolling stock and station platforms, but also for developers of pedestrian simulation models.

Keywords Design factors • Door width • Passenger flow • Train platform interface • Vertical gap

1 Introduction

As pedestrian simulation models are used not only in the simulation of evacuation but also in the planning and design of pedestrian infrastructure, it is necessary to obtain data about how pedestrians interact with external environments (e.g. how pedestrians interact with a step on the pavement) [1]. In transport engineering, pedestrian simulation models are used to assess new designs for station platforms and rolling stock. One major application area is train dwelling at stations on busy commuter lines because even a tiny change in the dwell time can significantly affect

T. Fujiyama (✉) • R. Thoreau • N. Tyler
Department of Civil, Environmental and Geomatic Engineering, University College London,
London, UK
e-mail: taku.fujiyama@ucl.ac.uk; r.thoreau@ucl.ac.uk; n.tyler@ucl.ac.uk

Table 1 The results of existing observational studies

Research	Results	Note
Harris [2]	0.69 (alighting), 0.87 (boarding) passengers per second per metre of door width	
Wiggenraad [3]	Around one passenger per second	Value converted
Arup [4]	0.82 passengers per second	Door width: 1,200 mm

the line capacity at peak times and therefore it is essential to assess various designs in the planning stage and choose the best possible option. A key issue which needs to be considered is the design of the train-platform interface (e.g. door width and size of the gap between the train and the platform).

Some observational studies have been carried out in the past [2–9]. Table 1 summarises the observed flow rates from some existing studies. The table suggests that the flow rates are between 0.69 and 1.00 passengers per second, but the detailed conditions, such as the doorway width, varied between the research studies. Indeed, a review study [10] revealed a large variance in flow rates. Although these existing studies help us understand the boarding and alighting speed at the train-platform interface in general, from the viewpoint of planners and designers of rolling stock and platforms it is important to know what design factors would affect the flow rate and what their effects are. In fact, because many observational studies have investigated the dwell time and/or boarding/alighting flow of one particular rail system, where there is usually little variance in the design factors, a lack of detail regarding the effects of design factors could be regarded as a limitation of the observational studies. An experimental study would be useful in order to systematically investigate how each design factor (e.g. door width) affects pedestrian movements. Therefore, we conducted a series of laboratory experiments to examine the effects of each design factor of the train-platform interface on pedestrian movements, particularly on the pedestrian flow rate.

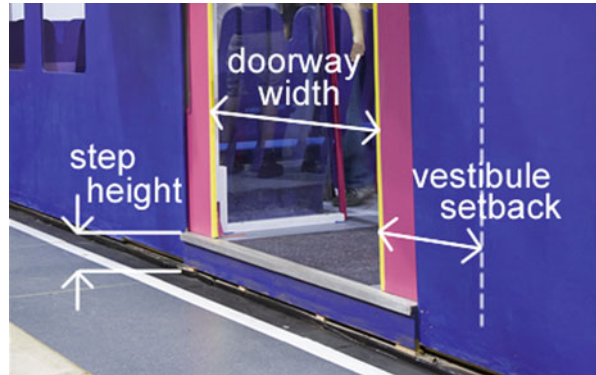
2 Methodology

2.1 Experiment Objectives

The aim of this research is to empirically examine the effects of the design factors of the train-platform interface on dwell time. For the experiment variables, we chose the following design factors and values because these factors can be considered when designing new rolling stock or/and improving the platform infrastructure. Figure 1 shows the definition of each factor.

- *Doorway width*: 1,300, 1,500, 1,800 mm
- *Step height*: 50, 165, 250 mm
- *Vestibule setback*: 0, 400, 800 mm

Fig. 1 Definition of each design factor



The values for each factor were selected based on the common values of existing rolling stock as well as reasonable increments by which the experiment covers the range that is potentially achievable. There were three values for each factor, which means that there were $3 \times 3 \times 3 = 27$ combinations of design factors/values.

The experiment was a part of the Thameslink upgrade project and the results were used to inform its train and infrastructure designers. The experiment was funded by the Department for Transport (of the UK) but there was no influence from the funder on the analysis or on the interpretation of its results. The experiment plan had been approved by the Research Ethics Committee of University College London (UCL).

2.2 Experiment Settings

The experiments were carried out at UCL’s Pedestrian Accessibility Movement and Environment Laboratory (PAMELA), where a mock-up train and a platform were set up. There are several elements of the laboratory, perhaps the most obvious being a computer-controlled paved platform which can be varied in terms of layout and topography. Using the PAMELA platform, it was possible to manage the vertical difference between the train and platform with various gap sizes. Figure 2 shows the plan view of the basic set up of the mock-up train and the platform.

The mock-up train represented a half of a carriage of a typical rolling stock type for suburban metro lines in the UK. The width of the carriage was 2,500 mm, and the seat layout was 2×2 in a row, with the gangway width at 520 mm. Figure 3 shows the standard seating layout of the mock-up train. The distance between the last seats from the vestibule (the one closest to the end of the gangway) and the end of the gangway varied as we changed the doorway width and vestibule setback in the experiment. Figure 4 shows the plan of the A-A’ Section in Fig. 3. The horizontal gap was set as 75 mm in the experiment. The value of 75 mm was chosen because if a train-platform gap is larger than this, there needs to be a boarding device for

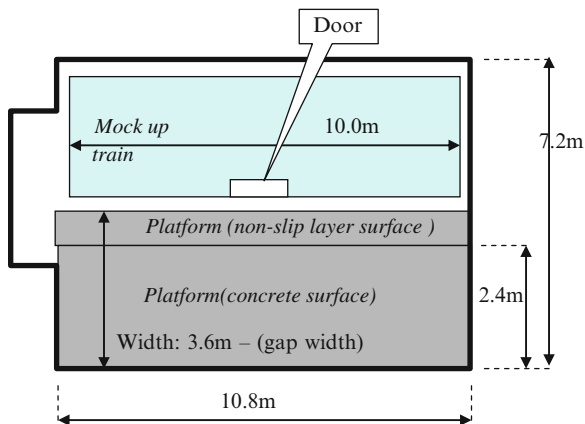


Fig. 2 Train and platform setup

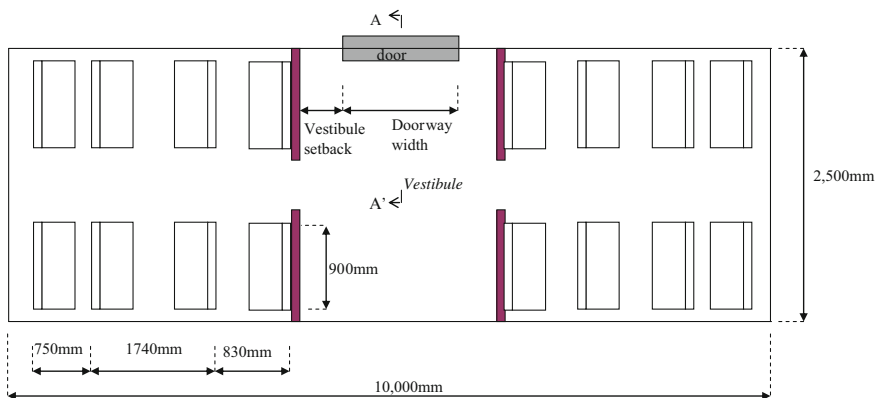


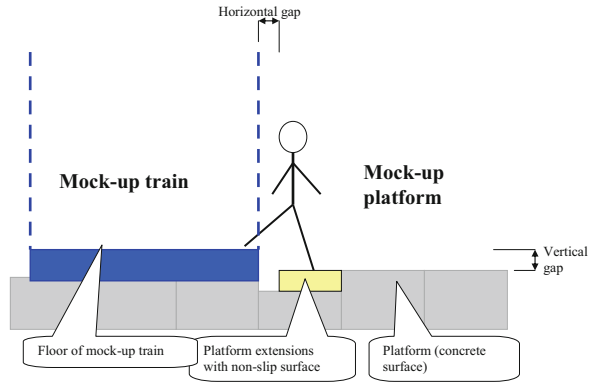
Fig. 3 Standard layout of the mock up train

any wheelchair-compatible doorway [11], and therefore this value is a threshold for designer and planners in the UK.

2.3 Experiment Procedure

There were 27 combinations of design factors/values to be tested (see Sect. 2.1). For each combination of design factors/values, we tested two types of passenger movements: Alighting-dominated flow where 45 participants tried to alight whereas 5 participants tried to board, and Boarding-dominated flow where 45 participants tried to board whereas 5 participants tried to alight. As our purpose is to simulate busy commuter trains, when we test an alighting-dominated flow, the mock-up train was full (70 participants were in the mock-up) before we opened the door.

Fig. 4 The plan of A-A' section (in Fig. 3) of the mock-up platform and the mock-up train



The rest of the participants were on the platform so that they can simulate a crowded platform. When we test a boarding-dominated flow, the number of the participants on the train was 30, which means that if the movement was successfully completed, there would be 70 participants on the train. Again, the rest of the participants were on the platform.

As we included two types of passenger flows, the number of combinations to be tested was $27 \times 2 = 54$ combinations. For each combination, we had two to three runs and in total 132 runs. The experiment lasted 3 days.

During the experiment, the door was opened and closed by a door operator standing behind the mock-up train and operating the door by the ropes connected to the door. In addition, using PAMELA’s sound system, we reproduced background noises and the door opening/closing alerts. Figure 5 shows the timings of the sound effects and door opening/closing alerts in each run. These opening/closing timings were the requirement for the proposed 2-min headway operation of the Thameslink route. The boarding/alighting flow rates, which will be detailed in the Sect. 3, were calculated based on the number of passengers who completed boarding/alighting.

2.4 Participants

On average 117 participants participated in the experiment each day. They were recruited through public advertisements. Fifty-five percentage of the participants were male. Figure 6 shows the average age distribution. Because the Thameslink service connects Central London and London Gatwick and Luton airports, some passengers carry a suitcase. Based on the observed percentage of passengers with a suitcase at St Pancras station, which is one of the main stations of the Thameslink route [12], we asked 12 randomly selected participants to carry a suitcase during the experiment.

Fig. 5 Timings of the sound effects and door opening/closing alerts in each run

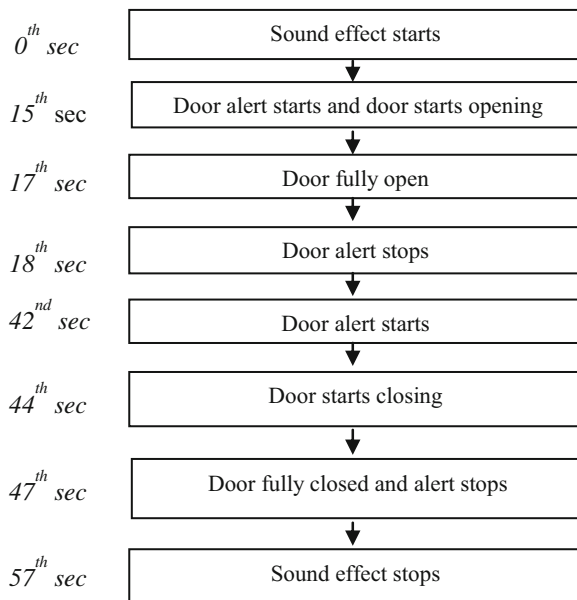
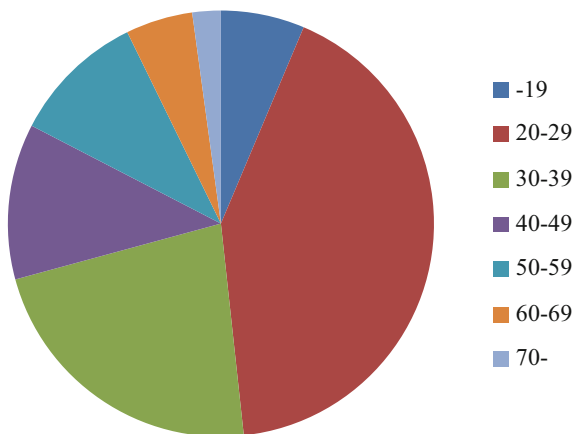


Fig. 6 Age distribution of the participants



3 Result and Discussion

3.1 The Effects of the Doorway Width

Figure 7 shows the relationship between the doorway width and the flow rate for the two types of passenger movements tested: boarding-dominant and alighting-dominant. Table 2 shows the percentage difference of the flow rates of the doorway

Fig. 7 Flow rate by doorway width

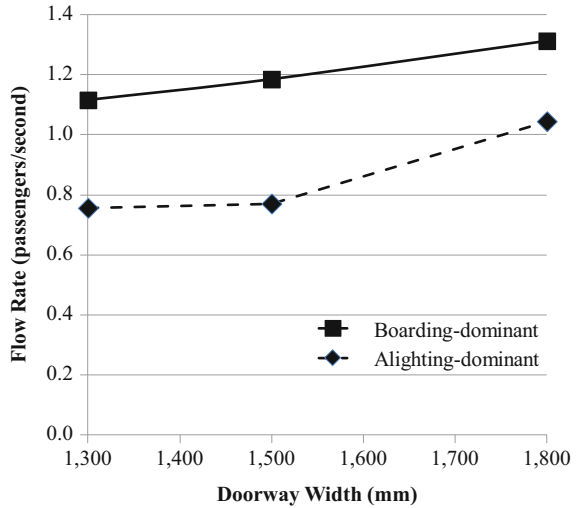


Table 2 Percentage difference in flow rate (from 1,300 doorway width) (%)

Doorway width (mm)	Boarding/alighting movements	Percentage difference in flow rate (from 1,300 doorway width) (%)
1,500	45A/5B	2
	45B/5A	6
1,800	45A/5B	38
	45B/5A	18

widths of 1,500 and 1,800 mm in relation to that of 1,300 mm. It can be seen that a larger doorway increased the pedestrian flow rates. Performance of the alighting-dominant runs especially improved when the doorway was increased from 1,500 to 1,800 mm. One reason for this could be the human body size. The shoulder breadth can be assumed to be 600 mm [13], but it may be necessary to have a doorway of more than 1,500 mm in order to achieve two streams at the door because some non-alighting passengers in the train stood still next to the door and this reduced the effective doorway width for alighting. A doorway of 1,800 mm may make this possible. Because alighting essentially requires two streams of passengers from the seating spaces on both sides of the door, having two streams at the door would improve the alighting flow rate.

For all the doorway widths tested, the boarding-dominant flow showed a better flow rate than that of the alighting-dominant flow. This may be because in the boarding-dominant flow the density of passengers in the train when the door was opened was low, and this could have made it easy for participants to board and could have led to a better flow rate.

Fig. 8 Flow rate by step height

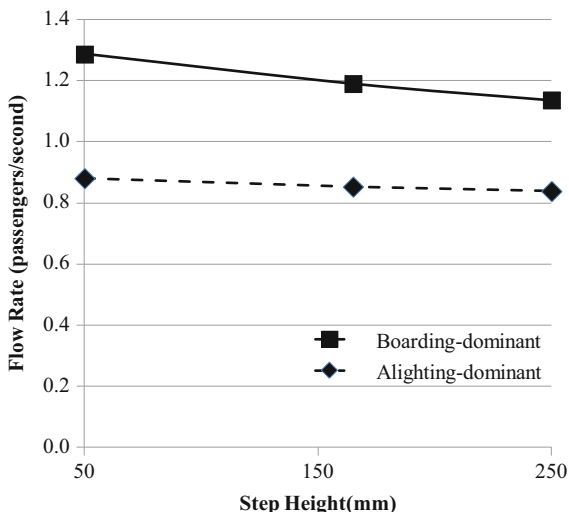


Table 3 Percentage difference in flow rate (from 50 step height) (%)

Step height (mm)	Boarding/alighting movements	Percentage difference in flow rate (from 50 step height) (%)
165	45A/5B	-3
	45B/5A	-7
250	45A/5B	-5
	45B/5A	-12

3.2 The Effects of the Step Height

Figure 8 shows the relationship between the step height and the flow rate. Table 3 shows the percentage difference of the flow rates of the step height of 165 and 250 mm in relation to that of 50 mm. A greater size of step height between the train and the platform led to a lower flow rate. Reducing the vertical difference from 250 to 50 mm would improve the flow rate by around 10 % when boarding is dominant, whereas the alighting-dominant runs showed only a slight improvement. A possible reason for this could be that, as the train floor was at a higher level than that of the platform, the boarding movement required each pedestrian to lift his/her body to a higher level and this body movement could have slowed down the flow rate. In addition, some participants might have reduced the speed because they had to step onto the crowded train carriage and the higher the step the more psychological hesitation they may have had.

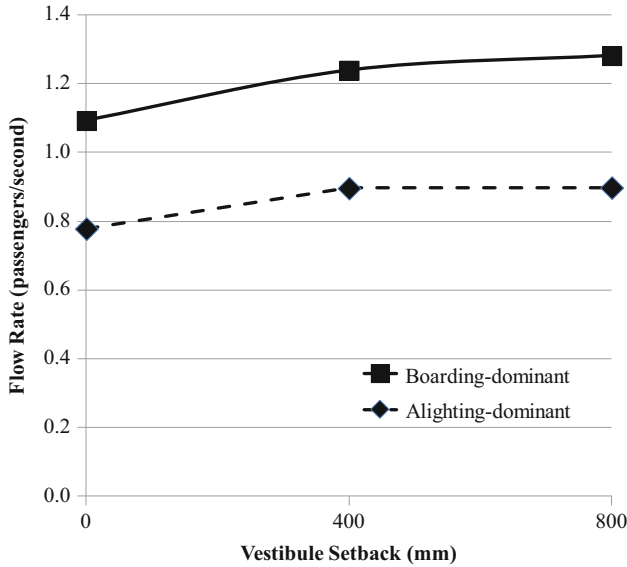


Fig. 9 Flow rate by vestibule setback

Table 4 Percentage difference in flow rate (from 0 vestibule setback) (%)

Vestibule setback (mm)	Boarding/alighting movements	Percentage difference in flow rate (from 0 vestibule setback) (%)
400	45A/5B	15
	45B/5A	13
800	45A/5B	15
	45B/5A	17

3.3 The Effects of the Vestibule Setback

Figure 9 shows the relationship between the vestibule setback and the flow rate. Table 4 shows the percentage difference of the flow rates of the vestibule setback of 400 and 800 mm in relation to that of 0 mm. The flow rate increased as the vestibule setback increased from 0 to 400 mm, but there was no substantial increase from 400 to 800 mm. Why was there no improvement from 400 to 800 mm? One reason could be that the 400 mm vestibule setback allowed “Lean on the screen” people to stand back from the doorway, but in the case of the 800 mm setback, other people stood in front of the people leaning on the door, which resulted in a similar effective width to that of 400 mm.

4 Conclusion

The experiment investigated the effect of the three design factors of the train platform interface, namely the doorway width, the step height and the vestibule setback, on the flow rate of boarding and alighting passengers. It has been found that

- A larger doorway increased the pedestrian flow rate. Performance of the alighting-dominant runs was much improved when the doorway was increased from 1,500 to 1,800 mm in comparison with an increase from 1,300 to 1,500 mm.
- A greater step height between the train and the platform led to a smaller flow rate. Reducing the step height from 250 to 50 mm would improve the flow rate by around 10 % when boarding is dominant, whereas the alighting-dominant runs showed a slight improvement only.
- The flow rate increased as the vestibule setback increased from 0 to 400 mm, but there was no substantial increase from 400 to 800 mm.

These results would be useful not only for designers and planners of rolling stock and station platforms, but also for developers of pedestrian simulation models as the results provide them with empirical evidence for the calibration and validation of their models.

References

1. Fujiyama, T.: Predicting the walking speed of pedestrians on stairs, *Transportation Planning and Technology*, 33 (2), 177–202 (2010)
2. Harris, N.G.: Train boarding and alighting rates at higher passenger loads, *J. of Advanced Transportation*, 40(3), 249–263 (2006)
3. Wiggenraad, P.B.L.: Alighting and boarding times of passengers at Dutch railway stations, TRAIL Research School, Delft University of Technology (2001) available at www.citg.tudelft.nl
4. Arup: Farringdon observation and analysis of passenger movements (and flow rates) across the train/platform interface. Final report – Results and analysis, internal report submitted to Department for Transport (2008)
5. Lee YC, Daamen W, Wiggenraad P, 2007, Boarding and alighting behavior of public transport passengers, presented in the annual conference of Transportation Research Board in Washington
6. Lin, T., Wilson, N. H. M: Dwell time relationships for light rail systems, *Transportation Research Record* 1361, 287–295 (1992)
7. Morlok, E. K., Nitzberg, B. F.: Speeding up commuter rail service: comparative actual performance of different train and station platform designs, *Transportation Research Record* 1872, 37–45 (2004)
8. Weston, J.G., McKenna, J.P: London Underground Train Service Model: A description of the model and its uses, in *computer applications in railway planning and management Comrail 90*, Rome (1990),
9. Zhang, Q., Han, B., Li, D.: Modeling and simulation of passenger alighting and boarding movement in Beijing metro stations, *Transportation Research Part C* 16 635–649 (2008)

10. Harris, N.G., Anderson, R.J.: An International Comparison of Urban Rail Boarding and Alighting Rates, Proceedings of the IMECH E Part F Journal of Rail and Rapid Transit, **221**(4), 521–526 (2007)
11. The Rail Vehicle Accessibility (Non-Interoperable Rail System) Regulations 2010
12. Arup: Report: Observation on luggage of passengers conducted on Friday 4th July 2008 at St Pancras Station (2008).
13. Transportation Research Board: Highway Capacity Manual 2010

Understanding Crowd Panic at Turning and Intersection Through Model Organisms

Nirajan Shiwakoti, Majid Sarvi, Charitha Dias, and Martin Burd

Abstract Previous studies on crowd disasters have highlighted the importance of considering turning and intersecting movement patterns in an escape area. Given the scarcity of data on human panic, there may be merit to use insights from non-human organisms to understand crowd panic as collective behaviour patterns also occur in non-human biological systems. We use model organisms approach by examining empirical data collected from panicking Argentine ants to study crowd panic at turning and intersection. The empirical data showed that the outflow of ants do not decrease proportionately with the increase in turning angles. Likewise, at intersection it was observed that one stream of ants is blocked by another stream of ants for considerable duration resulting in disproportionate flow at the intersection. Although the results are preliminary for statistical significance, these can have implications in testing the models of pedestrian crowds and in development of design solutions that enhances crowd safety.

Keywords Pedestrians • Ants • Evacuation • Collective dynamics • Egress

1 Introduction

The collective movement of pedestrians pose a great challenge to managers of emergency response in many situations, such as the evacuation of public buildings or public assemblies. A chronological list of crowd disasters updated as recent as

N. Shiwakoti (✉) • M. Sarvi • C. Dias
Institute of Transport Studies, Department of Civil Engineering, Monash University,
Melbourne, Australia
e-mail: nirajan.shiwakoti@monash.edu; majid.sarvi@monash.edu; charitha.dias@monash.edu

M. Burd
School of Biological Sciences, Monash University, Melbourne, Australia
e-mail: martin.burd@monash.edu

in 2012 can be found in Still's website [1]. As most of these incidents suggest, the problem of enhancing safety at mass gathering places under panic/emergency condition still exists. We refer panic or emergency as situations in which individuals have limited information and vision (due to high crowd density and short time for egress), and which result in physical competition and pushing behaviour. Proper investigation and understanding complex pedestrian movements are very important for guaranteeing the safety of pedestrians, particularly under panic or emergency conditions.

Turning and crossing maneuvers can be frequently expected in major public infrastructures and have been reported as crucial factors to be considered in crowd disaster management [2]. Several previous researchers have theoretically as well as empirically or experimentally studied these movement patterns, under normal conditions. For example, the interactions between individual pedestrian in crossing streams have been investigated under normal condition [3–6]. Likewise, various self-organized phenomena related with crossing flows have also been verified through empirical data as well as with simulation models. Formation of temporary patterns such as unstable, temporary roundabout traffic has been described in [7]. These temporary roundabouts reduce necessary deceleration, stopping, and avoidance manoeuvres considerably and therefore make pedestrian motion more efficient when two pedestrian streams cross [7]. Formation of diagonal stripes is another phenomena associated with crossing pedestrian flows as described in [8, 9]. Pedestrians move forward with the stripes and sideward within the stripes and therefore they can proceed their walking continuously without stopping thereby increasing the efficiency of the flow.

Several previous studies that aimed at understanding the effects of turning movements on human walking under normal and orderly evacuation conditions can be found in the literature. In a study [10], it was experimentally verified that when the angle of deviation from the former direction increases, mean body velocity decreases. It was found that on average the velocity was significantly lower (around 10 %) when walking along curved rather than straight paths under normal conditions [10]. In another study with cellular automata model [11] it was observed that sharp bends tend to move pedestrians to innermost lanes thereby reducing the capacity of angled corridors. Furthermore, it was verified that right angled corners in wide corridors could become bottlenecks, because the inner pedestrian lanes are substantially blocked by outer pedestrian lanes at corners.

Although considerable efforts have been spent in understanding crossing and turning movement in the past under normal conditions, comprehensive studies to address these phenomena under panic situations are scarce. One reason for this might be the lack of empirical data to validate the predictions from explanatory models [12, 13]. Given that collective patterns of crowd behaviour also occur in non-human biological systems [14–16], the generality of such explanatory models can be tested across wide variations in body size and locomotion patterns.

In this paper, we examine the potentiality of using non-human organisms in providing insight into the complex moving patterns such as turning and crossing under panic condition. First we review the experiences of using non-human organisms to

understand pedestrian crowd panic. This is followed by recent experiments with ants under panic condition to have an insight into turning and crossing movements. Finally, conclusions and recommendations for further studies are presented.

2 Previous Studies on Model Organisms

Use of animal models to explore crowd panic dates back to the early 1970s when rats were used to the study emergency evacuation [17]. In the experiments performed with 10 panicking rats under emergency conditions, it was observed that those rats who were familiar with the exits took less time, in general, to get out of the exit than those rats that were unfamiliar with the exits [17]. Similar behavior could be observed in simulated pedestrian crowd [17]. However, significant gap in the use of model organisms to study human collective dynamics could be observed since then until recently when few researcher attempted to use non-human biological entities to understand pedestrian crowd dynamics [13, 16, 18, 19].

In an experiment performed with a group of 60 mice escaping from a water pool onto a dry platform through doors of various widths and separation, it was observed that the mice displayed the competitive behavior at the exit [18]. The competitiveness resulted in blockage and inefficient escape similar to human. In another study with Cuban leaf-cutting ants under panic conditions, occurrence of symmetry breaking (phenomenon in which some available exits from enclosed spaces are jammed while others go under-utilized) was observed [19]. Differences in the use of the two exits averaged 10.4 % (± 0.1 %) in a normal situation, but increased to 50 % (± 4 %) for a panic situation. This phenomenon is known to occur in human crowd disasters and has been demonstrated using a mathematical model [12].

In a recent study, experiments with Argentine ants were conducted under panic condition to study the effect of with and without a partial obstruction near the exit in a circular chamber [13, 20]. Panic was induced by injecting citronella oil (insect repellent) into the chamber (that contained ants) which created rapid evacuation with dramatic increase in fleeing speed of the ants. It was reported that the presence of a partial obstruction (via a column) at the exit generally enhanced (by around 44 %) the flow of panicking ants as compared to absence of the obstruction [13]. Another series of experiments with Argentine ants were conducted to study the effect of location of the exit on the collective movement patterns of non-human entities during rapid egress [13]. Two scenarios were considered: ants escaping from a square chamber with exit at the middle of the side walls versus exit at the corner. It was reported that corner exit was effective (by around 58 %) in increasing the outflow of ants compared to exit at the middle [13]. With these empirical results a model *EmSim* was developed that could capture the fundamentals of crowd panic between ants and human [13, 20]. The model parameters were scaled up from ants experiment to human situation through the scaling concept used in Biology and were

validated for normal and panic situation using the empirical data from humans and ants [13].

Given these indications that there is potential to use non-human biological organisms to study crowd panic, we recently conducted experiments with Argentine ants to have an insight on turning and crossing movement patterns under panic condition and is presented in next section.

3 Recent Experiments with Ants

Several experiments that use panicking Argentine ants were designed and conducted in order to understand crowd behaviors associated with turning and crossing phenomena under panic conditions. This section describes details of those experiments and some initial observations.

3.1 Turning Experiments

In this experiment, three turning angles (45° , 60° , 90°) along with one straight corridor (i.e. 0° turning) were considered. Snapshot of experiment chamber used for 45° experiment is shown in Fig. 1 for illustration purpose. Each chamber was 25 mm by 25 mm and consisted of an exit corridor of 3.5 mm width. The length of the corridor for the straight and other angled path (45° , 60° , 90°) was 10 mm. For the angled case, the straight corridor continued for 5 mm and then a connecting corridor was placed at the respective angle (i.e. 45° , 60° , 90°). Around 250 ants were allowed to nest naturally inside moisturized chambers. Each chamber was covered with a transparent plastic lid with a small hole of approximately 1 mm diameter, which was used to inject $10 \mu\text{l}$ of citronella to create panic; similar process followed in [13]. A digital video camera was used to record the experiments. The flow of the ants at the fixed downstream point of the corridor was measured for each case. Ten replications were conducted for each angled corridor. Escape times for 100 ants (neglecting first 10 ants to account for initial delays) were extracted from playback of digital video recordings.

The average escape rates based on the first 100 escapes (ignoring the first 10 escapes for initialization) for different angled corridor are shown in Fig. 2. It can be observed that right angled corridor is the most ineffective in terms of the outflow of the ants. For example, when the corridor is changed from straight to a 90° turn, the straight corridor is 28 % more efficient than the 90° turn. The lower performance of other angled corridor (i.e. 45° , 60°) compared to the straight one could be observed in Fig. 2 as well. Importantly, it is very interesting to observe in Fig. 2 that there is a decrease in evacuation time at 60° turn compared to 45° and 90° turns. The decrease in evacuation time with a 60° turn highlights that perhaps the flow of ants do not always decrease proportionately with the increase in turning angles. This certainly

Fig. 1 Experiment setup for 45° angled experiment

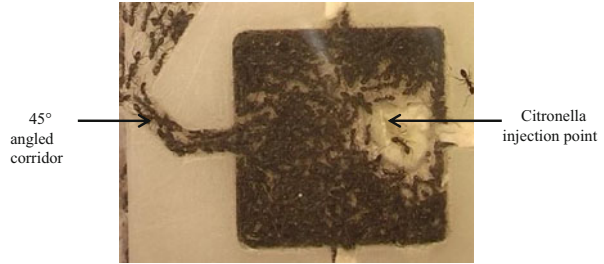
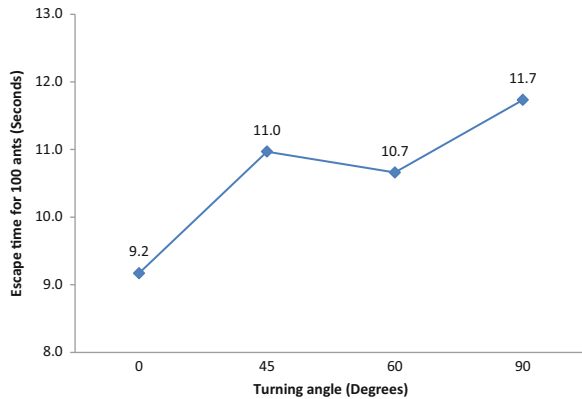


Fig. 2 Comparison of escape time for different angled corridor



appears to be the case for traffic on ant trails. In one study with bifurcating trail networks in foraging ants (under normal condition), it has been reported that the ants adaptively reoriented their direction of motion most successfully along paths with around 60° bifurcation angles [21]. These preferences for particular trail angles have not yet been related to flow rates on the trails, but it seems likely that there may be optimal angles for maximizing flow.

Reduction of velocity when walking on curved paths has been experimentally verified for humans under normal situations [10]. However, no explanations are available to date regarding special phenomena like we witnessed in Fig. 2 which might be very important in planning and designing public gathering places for emergencies. Although the experiments are still in progress and it may be early to draw definite conclusions with statistical significance, it may be of merit testing the above observations in case of human crowds. Recently in one study it was observed that 60° angled corridor displayed better performance in terms of outflow of pedestrians compared to 45° angled corridor based on some simulation trials for pedestrian crowds under panic condition [22]. However, it will be interesting to examine if other models on pedestrian also confirm this sort of behavior in human crowds.

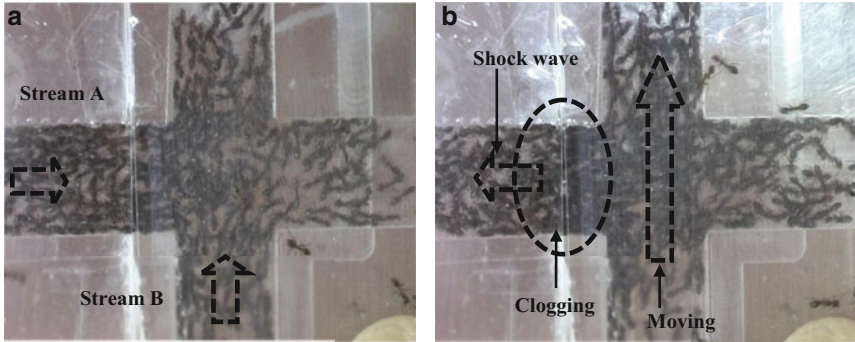


Fig. 4 Occurrence of clogging: (a) approximately 3 s after starting the experiment, (b) formation of clogging starting at approximately 5 s after starting the experiment

It is to be noted here that the clogging period is not symmetric in two streams and substantial variations in clogging duration could be observed among two streams during the experiment. These results are preliminary and more detailed analysis are underway. Nevertheless, the occurrence of these patterns could be of relevance in human crowds. Aggressive pedestrians try to squeeze through preceding pedestrians and therefore, it is quite difficult for pedestrians in the intersecting stream to find a gap. Thus, for a while one stream may be clogged and the other could be moving which can create dangerous situations in case of emergency/panic situation.

4 Conclusion

Angled or circuitous routes and intersecting corridors are unavoidable features of mass gathering places such as public transport facilities, sport stadiums, theatres, and shopping malls. These physical features could have substantial effects on collective egress of human, especially in emergencies. Understanding collective pedestrian movements related with complex movements such as turning and crossing under panic condition is important to assure safety and efficiency of pedestrian movements at mass gathering places. However, our understanding on crowd panic is limited by the scarcity of complementary data to develop and validate explanatory models. Under this study, several preliminary experiments were conducted utilizing ants to understand turning and crossing phenomena under panic conditions. This paper described some initial results and more experiment replications and detailed analysis are in progress.

One of the interesting findings from the turning experiments with ants was that the flow did not decreased proportionately with the increase in turning angles. In case of human crowds, the flexibility on the choice of turning angles can have implications in situations when it is not possible to have straight corridor due

to design and/or space restrictions. More research on those aspects is necessary, however. Nonetheless, the general trend from the experiment shows that the flow of ants is reduced with turning movements compared to straight movements due to strong interactions around the corner.

The main observation of intersecting or crossing experiments was the transition of clogging between two streams i.e. one stream of flow of individuals is blocked by another stream of individuals for considerable time resulting in disproportionate flow at the intersection. This can create dangerous situations in human crowds especially in emergency situations. Longer the duration of clogging of one stream, the more chance of occurrence of trampling and crushing can be expected in a crowd.

The study demonstrate that the animal models might allow empirical testing of human pedestrian models when human subjects cannot easily or ethically be employed, providing the model can be scaled appropriately. Successful prediction of collective movement in organisms of vastly different body sizes would suggest that common underlying dynamics govern the behavior of self-driven particles across a wide size range.

References

1. Still, G. K.: International Crowd Disasters. <http://www.safercrowds.com/CrowdDisasters.html>, Accessed 2 May, 2012 (2012)
2. Chertkoff, M.J., Kushigian, H.R.: Don't Panic: The Psychology of Emergency Egress and Ingress. Praeger Publishers, USA (1999)
3. Daamen, W., Hoogendoorn, S. P.: Experimental Research on Pedestrian Walking Behaviour. Transportation Research Board annual meeting, Washington DC, 1–16 (2003)
4. Helbing, D., Buzna, L., Johansson, A., Werner, T.: Self-organized Pedestrian Crowd Dynamics: Experiments, Simulations, and Design Solutions. *Transportation Science* 39, 1–24 (2005)
5. Guo, R.-Y., Wong, S. C., Huanga, H.-J., Zhang, P., Lam, W. H. K.: A microscopic pedestrian-simulation model and its application to intersecting flows. *Physica A* 389, 515526 (2010)
6. Asano, M., T. Iryo, T., M. Kuwahara.: Microscopic Pedestrian Simulation Model Combined with a Tactical Model for Route Choice Behaviour. *Transportation Research Part C* 18(6), 842–855 (2010)
7. Helbing, D., Molnár, P.: Self-Organization Phenomena in Pedestrian Crowds. In: Schweitzer, F. (ed.) *Self-Organization of Complex Structures: From Individual to Collective Dynamics* London, pp. 569–577 (1997)
8. Ando, K., Oto, H., Aoki, T.: Forecasting the flow of People [in Japanese]. *Railway Research Review* 45 (8), 8–13 (1988)
9. Hughes, L. R.: The Flow of Human Crowds. *Annual Review of Fluid Mechanics* 35, 169–182 (2003)
10. Courtine, G., Schieppati, M.: Human Walking along a Curved Path. I. Body Trajectory, Segment Orientation and the Effect of Vision. *European Journal of Neuroscience* 18 (1), 177–190 (2003)
11. Steffen, B., Seyfried, A. : Modelling of Pedestrian Movement Around 90° and 180° Bends. In: . Capote, A., Alvear, D. (eds.) *Proceedings of the Advanced Research Workshop -Fire Protection and Life Safety in Buildings and Transportation Systems*, pp. 243–253 (2009)

12. Helbing, D., Farkas, I., Vicsek, T. : Simulating Dynamical Features of Escape Panic. *Nature* 407, 487–490 (2000)
13. Shiwakoti, N., Sarvi, M., Rose, G., Burd, M.: Animal Dynamics Based Approach for Modelling Pedestrian Crowd Egress Under Panic Conditions. *Transportation Research Part B* 45, 1433–1449 (2011)
14. Couzin, I., Krause, J. : Self-organization and Collective Behavior in Vertebrates. *Advances in the Study of Behavior* 32, 1–75 (2003)
15. Burd, M., Shiwakoti, N., Sarvi, M., Rose, G.: Nest Architecture and Traffic Flow: Large Potential Effects from Small Structural Features. *Ecological Entomology* 35(4), 464–468.
16. Shiwakoti, N., Sarvi, M., Rose, G., Burd, M.: Enhancing the Safety of Pedestrians During Emergency Egress: Can We Learn from Biological Entities? *Transportation Research Record: Journal of the Transportation Research Board* 2137, 31–37 (2009)
17. Hirai, K., Tarui, K.: A Simulation of the Behaviour of a Crowd in Panic. *Proceedings of the International Conference on Cybernetics and Society*, 409–411 (1975).
18. Saloma, C., Perez, G. J., Tapang, G., Lim, M., Saloma, C. P.: Self-organized Queuing and Scale-free Behaviour in Real Escape Panic. *Proceedings of the National Academy of Sciences* 100, 11947–11952 (2003)
19. Altshuler, E., Ramos, O., Núñez, Y., Fernández, J., Batista-Leyva, A.J., Noda, C.: Symmetry breaking in escaping ants. *The American Naturalist* 166, 643–649 (2005)
20. Shiwakoti N., Sarvi, M., Rose, G., Burd, M.: Biologically Inspired Modeling Approach for Collective Pedestrian Dynamics under Emergency Conditions. *Transportation Research Record: Journal of the Transportation Research Board* 2196, 176–184 (2010)
21. Jackson, E.D., Holcombe, M., Ratnieks, L. W. F.: Trail Geometry Gives Polarity to Ant Foraging Networks. *Nature* 432, 907–909 (2004)
22. Shiwakoti N., Sarvi, M., Rose, G., Burd, M. : Consequence of turning movements during emergency crowd egress. *Transportation Research Record: Journal of the Transportation Research Board* 2234, 97–104 (2011)

Part V
Miscellaneous

A Study for Estimation of Ventilation Capacity of Large Enclosure Considering Real Fire Load

Chan-sol Ahn and Jung-yup Kim

Abstract In this study, we reviewed the performance of smoke control system by national fire safety code to secure evacuation time of occupants in case of a fire in large enclosure structures. Towards this end, we performed numerical analysis modeling of the existing large underground shopping mall and investigated types of business and combustibles loaded inside the stores situated at the shopping mall to fulfill the same configuration requirements with actual fire load conditions. To compare effects of smoke control system by national fire safety code, we created 11 smoke control scenarios of large enclosure shopping malls according to the ventilation capacity and conducted numerical analysis of evacuation behavior of occupants and the spread of fire against each scenario. In addition, to compare the results of the numerical analysis, we analyzed total heat release amount, flash-over occurrence time, residual amount of soot indoors and the number of evacuation failures and the dead, thereby deducing the optimal ventilation capacity.

Keywords Ventilation capacity • Large enclosure • Fire load

1 Introduction

Since recent large enclosure structures have characteristics of poor exchange of outside air and inside air due to high tightness, it is necessary to examine the adequacy of the performance by current fire safety standards to ensure safe evacuation time of occupants in case of a fire in these structures.

For this study, we investigated the overall structure of the target buildings, locations of stores, types of business, areas and ceiling height and examined the

C.-s. Ahn (✉) • J.-y. Kim

Fire research center, Korea Institute of Construction Technology, Gyeonggi 445-861,
Republic of Korea

e-mail: chansole@kict.re.kr; jykim1@kict.re.kr

kinds of fixed combustibles and movable combustibles that make up the inside of the large enclosures through field survey. In addition, to calculate the heat release of the entire large enclosures, we investigated kinds of raw materials, weights, numbers and types of the products, the movable combustibles and office supplies, cabinets and interior decorations categorized as the fixed combustibles and estimated the total heat release amount by stores collected from the field survey using heat release per unit weight of raw materials. To verify the unique heat release of the estimated combustibles, we conducted numerical analysis by developing standard fire models of the stores and based on this, carried out real fire experiment to compare the results.

Through application of the standard fire models of the stores standardized by advance research to commercial models, the fire models of large enclosure structures were completed, and numerical analysis on the fire and evacuation was carried out through application of ventilation capacity presented in the National Fire Safety Code.

In case of a fire in building, the smoke control by forced exhaust method has its advantage of rapid removal of smoke from a fire, but it poses disadvantage in that mass flow of air from the outside can cause the rapid expansion of the fire. Accordingly, it is important to figure out the ventilation capacity that maximize emission of the smoke so that occupants can be evacuated safely, suppressing the rapid spread of fire. In this study, to calculate optimal capacity of a smoke control system, we conducted numerical analysis by setting several smoke control scenarios and compared each scenario based on the number of the dead and safe evacuation time of occupants to determine the adequacy of the results.

2 Experimental Apparatus and Methods

2.1 Selection of Large Enclosures and Investigation of Combustibles

As a target building for numerical analysis on the fire in large enclosures, a large underground shopping mall located in Seoul was selected. The overall appearance of the building is characterized by the size of $107.8 \times 35.8 \times 2.7$ m and area of 3,141 m² occupied by 64 stores inside the building and it has a total of six exits located on the wall in the horizontal direction (Fig. 1).

Sixty-four stores are composed of 13 clothing stores, 18 opticians, 8 bag shops, 5 jewelry store, 5 shoe stores and 15 others. For this study, we investigated a total of 953 kinds of combustibles after obtaining a total of 15 samples, targeting 1–3 stores selected by types of business.



Fig. 1 Large underground shopping mall

2.2 Measurement of Heat Release Per Weight of Raw Material

For measurement of the heat release of raw materials, 49 kinds of raw materials were determined through reclassification of 953 kinds of combustibles surveyed through the field survey by main raw materials, and the heat release per unit weight of raw materials were measured in accordance with ISO 5660-1, targeting 8 kinds of wood, 3 kinds of paper, 9 kinds of textiles, 12 kinds of synthetic resins, 13 kinds of minerals and 4 kinds of composite materials.

2.3 Estimation of Total Heat Release of Combustibles

To estimate the unique heat release of each combustible investigated through the field survey, we utilized raw material heat release measurement values and estimated the unique heat release of the combustible by multiplying heat release corresponding to main materials of the combustibles and total weight together.

2.4 Estimation of the Fire Load by Types of Business

For estimation of the fire load by types of business, 64 stores located in the large enclosure shopping mall was classified into six types of business, 1–3 stores were selected within the same types of business through a random sampling method, and a total of 15 sample stores were finally selected. Based on the fixed combustibles and movable combustibles surveyed in each store, the average fire load by type of business was estimated as follows: Clothing stores 679.1 kg/m^2 , opticians 18.0 kg/m^2 , bag shops 388.1 kg/m^2 , jewelry store 9.8 kg/m^2 , shoe stores 97.5 kg/m^2 , book store 324.3 kg/m^2 and cell phone store 87.0 kg/m^2 , etc. When the estimated fire load by types of business was placed in the same location of 64 shops situated

at the large enclosure shopping mall, total fire load of the large enclosure calculated turned out to be 1,544 GJ.

2.5 Performance Standards for Smoke Control System

Since smoke control system performance standards for underground structures are not presented separately in the National Fire Safety Code, emission performance and performance of the air inflow was determined in accordance with smoke control performance criteria for general structures. As an air inflow method, natural inflow system was selected, and as an air emission method, forced exhaust system. In accordance with smoke control standards by the Fire Services Act, fire control districts were divided into two areas, where indoor air of 100,000 m³ per hour was discharged through a forced exhaust system.

2.6 Calculation of Fire Scenarios

To observe fires phenomenon caused by forced exhaust against large enclosure shopping mall and interactions of occupant's evacuation behaviors, we created 11 smoke control scenarios.

For calculation of evacuation time against shopping mall, FDS + Evac, a general-purpose program for evacuation analysis was used. 0.35 (person/m²) was set into occupant density through conversion of capacity factor 2.8 (m²/person) according to NFPA 101, and 1,100 occupants were distributed and deployed. The starting time of evacuation was calculated in accordance with DD240 published by British Standards Institute in 1997.

The ventilation capacity by force exhaust was set after being divided into 10 equal intervals within the range of $\pm 10,000$ m³/h based on 10,000 m³/h presented in the National Fire Safety Code, and a total of 11 scenarios including reference point were deduced.

In 11 scenarios, it was assumed that the initial ignition occurred in the clothing store located in the center of the shopping mall, and combustion expansion was started from the combustibles displayed in the clothing store exposed to fire source of 700 kW.

2.7 Numerical Analysis of Scenarios

The numerical analysis was conducted, targeting one case in which a smoke control system was not operated, and 11 cases of operating the smoke control system, when all conditions except for ventilation capacity were set all the same in all cases.

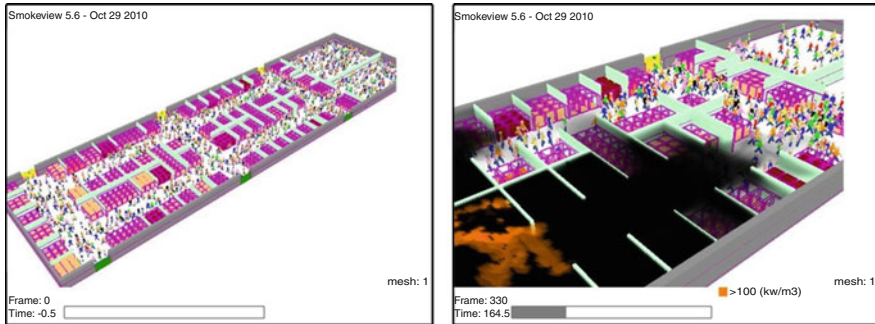


Fig. 2 FDS & evacuation model

To carry out numerical analysis of 11 smoke control scenarios, we used Fire Dynamics Simulator (FDS), which is 3-dimensional field model software for fire analysis developed by BFRL Group of NIST in the US (Fig. 2).

Navier-Stokes equation at low speeds was used as a hydrodynamic inertia model, Large Eddy simulation (LES) for analysis of turbulence, and a mixture fraction combustion model for analysis of combustion phenomenon. In addition, a non-dispersed gray gas radiative transfer model was used for analysis of radiative heat transfer, a main heat transfer phenomenon of a fire.

For analysis on the evacuation behavior of occupants deployed in the large enclosure, FDS + Evac was used. Basic values were used as all constants required to analyze evacuation behavior, and they were set through full reflections of personal property values of Simulex.

For modeling of large enclosures, multi-block grids composed of 27 rectangle grids of $1,078 \times 358$ were used. Toward each fire scenarios, fire phenomena for 600 s and evacuation behavior of occupants were analyzed, and to analyze a single scenario, parallel operation was performed for about 36 h using 32 processors.

3 Results and Discussion

3.1 Changes in Total Heat Release

When standard ventilation capacity by the National Fire Safety Code was discharged, the total heat release was 22,577 MJ and it decreased to 15,000 MJ when smoke control system was not operated. When the ventilation capacity increased by 2 times, the total heat release also increased to 27,000 MJ, which shows the disadvantage of the smoke control system by forced exhaust method since the increase in ventilation capacity leads to increased supply of air from the outside, thereby accelerating the spread of a fire (Fig. 3).

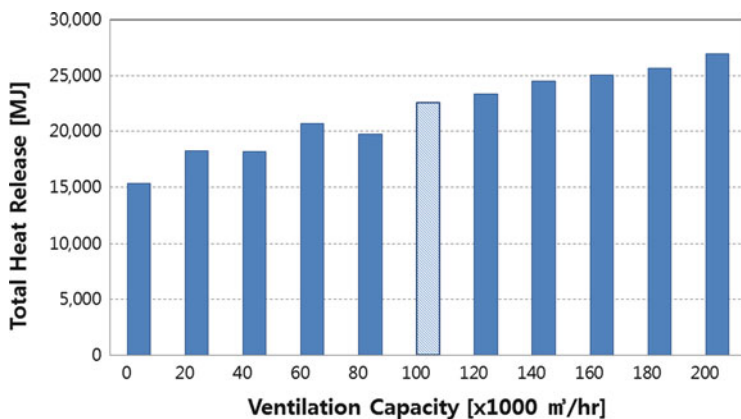


Fig. 3 Variation of total heat release

3.2 Changes in Flash-Over Phenomenon

When controlled by the National Fire Safety Code, flash-over phenomenon occurred in 104 s after the initial ignition, and it occurred in 151 s after the initial ignition due to delay of the supply of fresh air from the outside in case smoke control system was not operated. It was found that as ventilation capacity increased, the time when flash-over phenomenon occurs gradually slackened, and the it came to be faster from 152 s in scenario of ventilation capacity of 80,000 m³/h. From these findings, it can be wrongly concluded that the less the ventilation capacity, the better its result since delay of the occurrence of flash-over phenomenon leads to lengthy evacuation time of occupants, but the fact that should be remembered is that the less the ventilation capacity, the more the amount of combustion gases accumulated, which have an adverse effect on the evacuation behavior of occupants (Fig. 4).

3.3 Changes in the Amount of Residual Soot Inside the Large Enclosures

To estimate the amount of combustion gases accumulated inside the large enclosures, we calculated the amount of residual soot. It was analyzed that when controlled by the National Fire Safety Code, residual soot of 28 kg was found inside the large enclosures, and it increased to 30 kg when smoke control system was not operated. In addition, as ventilation capacity increased, the amount of residual soot gradually decreased, and it decreased to 24 kg in case of smoke control of 200,000 m³/h. However, it was also found that when conducting smoke control of less amount than the standard ventilation capacity, the amount of residual soot

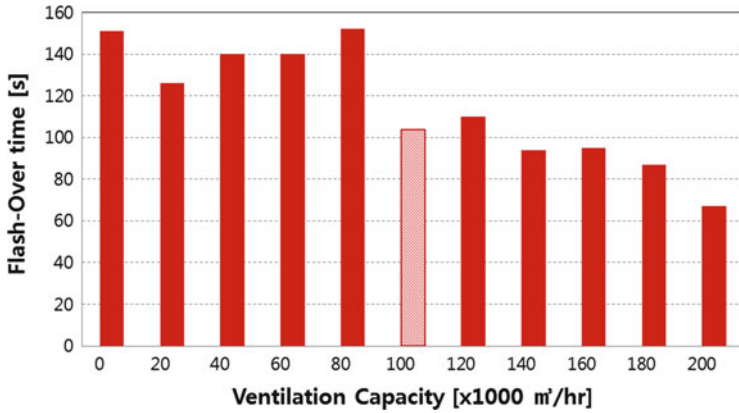


Fig. 4 Variation of flash-over time

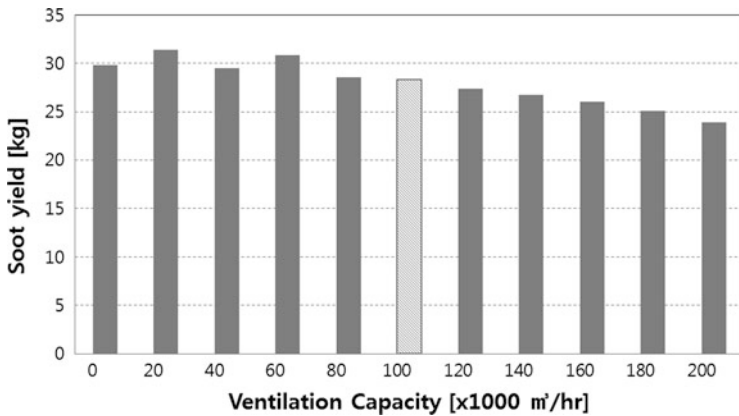


Fig. 5 Variation of soot yield

increased as identified in the above results, and more residual soot existed, compared with case in which smoke control system was not operated in case of some scenarios (Fig. 5).

3.4 Changes in Evacuation Failure and Deaths

As a result of analyzing 11 smoke control scenarios, it turned out that the cases where occupants succeeded in evacuation without failure was found in the case in which ventilation capacity was 80,000 m³/h and the case 200,000 m³/h, and even in case the ventilation capacity by the National Fire Safety Code was selected, the possibility of evacuation failure and deaths existed.

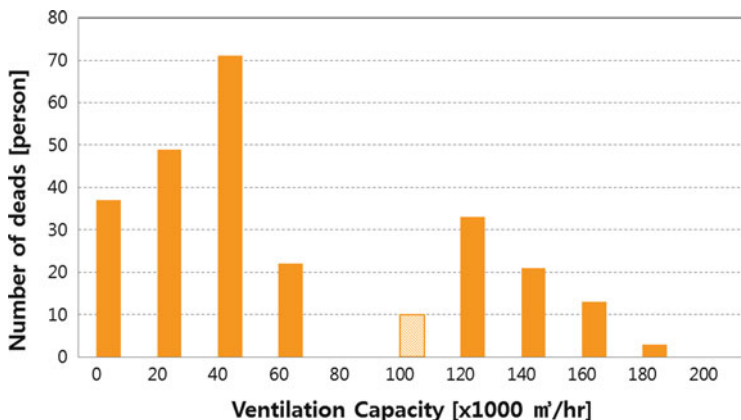


Fig. 6 Variation of people dead

In case ventilation capacity is doubled, smoke from a fire is discharged in large quantities, which can lead to a positive effect on the evacuation behavior and visible range of occupants. However, the fact that mass flow of air from the outside allows fire to reach flash-over phenomenon in a short time, causing the rapid spread of fire should be taken into account.

In case ventilation capacity decreases to 80,000 m³/h, the amount of residual soot increases by 1 kg compared with the case in which standard ventilation capacity is applied, but as the time of flash-over occurrence are delayed by 48 s, and the total heat release decreases to more than 3,000 MJ, which contributes to allowing occupants to secure the evacuation time to the maximum and minimizing the accumulation of smoke from a fire indoors to the minimum (Fig. 6).

4 Conclusion

In this study, we reviewed the performance of smoke control system by the National Fire Safety Code to secure evacuation time of occupants in case of a fire in large enclosure structures.

Towards this end, we performed numerical analysis modeling of the existing large underground shopping mall and investigated types of business and combustibles loaded inside the stores situated at the shopping mall to fulfill the same configuration requirements with actual fire load conditions.

To compare effects of smoke control system by national fire safety code, we created 11 smoke control scenarios of large enclosure shopping malls according to the ventilation capacity and conducted numerical analysis of evacuation behavior of occupants and the spread of fire against each scenario.

In addition, to compare the results of the numerical analysis, we analyzed total heat release amount, flash-over occurrence time, residual amount of soot indoors and the number of evacuation failures and deaths, thereby deducing the following conclusions.

1. Since ventilation capacity of large enclosures by the National Fire Safety Code is the value in which fire load of the combustibles placed on the actual site is not taken into account, it cannot be considered to be suitable for securing safe evacuation time of occupants.
2. The lower ventilation capacity than that specified in the National Fire Safety Code helps to suppress flash-over phenomenon of fire room, but it can worsen the evacuation conditions of occupants due to accumulation of smoke from a fire indoors.
3. The higher ventilation capacity than that of the National Fire Safety Code contributes to rapid removal of smoke from a fire, improving the evacuation conditions of occupants, but it can serve as a risk factor in the evacuation of occupants due to sudden spread of a fire, which leads to a doubling of investment costs for equipment.
4. The optimal ventilation capacity of large enclosure shopping mall selected in this study is 80,000 m³/h, which serves as the most efficient operating point to delay the occurrence time of flash-over phenomenon and minimize the indoor residual smoke from a fire.

Acknowledgement This study was carried out as a part of the project, titled “(12 main) A study on the advancement of fire safety based on performances” performed by Korea Institute of Construction Technology under the support of Ministry of Knowledge Economy.

References

1. Chae H.S., Suk C.M., Kim I.S., Lee J.H., Kim W.J., Prediction of the Fire Behavior According to the Fire Load in an underground Life Space, KIESE, Vol. 21, No. 1, p. 51 (2007)
2. Cooper L.Y., Smoke Movement in Rooms of Fire Involvement and Adjacent Spaces, Fire Safety Journal, Vol. 7, No. 11, p. 33 (1984)
3. Hwang E.K., Kim D.H., Cho J.H., Hwang K.S., A Suggestions for Building Regulation through the Analysis of Problems among the Building Evacuation Laws, KIESE, Vol. 21, No. 4, p. 105 (2007)
4. Kwark J.H., Standardization of the Performance Test Procedure for Smoke Control System, KIESE, Vol. 20, No. 3, p. 21 (2006)
5. Lee E.P., Analysis in the Actual Conditions of Death due to Fires based on Annual Report on the cause of Death Statistics in Korea, KIESE, Vol. 20, No. 1, p. 83 (2006)
6. McCaffery B.J., Quintiere J.C., Harkleroad, Estimating Room Temperatures and the Likelihood of Flashover Using Fire Test Data Correlations, Fire Technology, Vol. 17, No. 2, p. 98 (1981)
7. NIST, FDS (Fire Dynamics Simulator) User's Guide (2010)
8. VTI, Fire Dynamics Simulator with Evacuation Technical Reference and User's Guide (2010)

Multi-agent Transport Simulation for Regional Evacuation Processes

Mohamed Bakillah, Hubert Klüpfel, Gregor Lämmel, and Georg Walenciak

Abstract As periodic wildfires in the southern California, USA, or the Fukushima Daiichi nuclear disaster have shown, man-made and natural disasters might make human areas or regions (temporarily) inhabitable or the safety of inhabitants might be threatened severely, and the evacuation of this area required. One major decision in facing disasters is whether to evacuate or not. Criteria for making that decision on a civil defence level are: the time available for evacuation, the socio-economic situation, the warning systems available, the severity and time evolution of the threat, and so on, and so forth. One major question is whether the available safe evacuation time (ASET) is larger than the required safe evacuation time (RSET). Another one is the feasibility traffic patterns that will result from an evacuation warning. The method presented in this paper is able to determine the RSET.

Keywords Evacuation • Multi-agent simulation • Pedestrians • Risk analysis

1 The GRIPS Research Project

The GRIPS-Project (GIS-Based-Risk-analysis-Information and Planning System) (http://www.geog.uni-heidelberg.de/forschung/gis_grips.html) aims at providing useful and objective information for the decision makers facing questions like

M. Bakillah (✉) • G. Walenciak

Institute for GI-Science, Ruprecht-Karls-Universität, Heidelberg, Germany

e-mail: bakilah@uni-heidelberg.de

H. Klüpfel

TraffGo HT GmbH, Duisburg, Germany

e-mail: kluepfel@traffgo.de

G. Lämmel

Institute for Traffic Systems Planning, Technical University of Berlin, Berlin, Germany

e-mail: laemmel@vsp.tu-berlin.de

whether to evacuate or not. Within GRIPS, the multi-agent transport simulation toolkit MATSim (<http://www.matsim.org>) is used to simulate the evacuation regarding two use-cases [3, 4]. The first use case is simulation of the evacuation of the district Wilhelmsburg in Hamburg, Germany, in consideration of an upcoming flooding (details are described by Durst. et. al. in these proceedings). The second use-case examines the simulation of the evacuation of an area affected by an industrial accident in the city of Essen, Germany. In neither case, the disaster is modelled directly, but handled as an external parameter “threat” that affects a certain region. This is the region potentially to be evacuated.

One of the main goals of the project is the development of a computer tool that can be used by disaster managers as a decision support system. For that matter, both uses-cases are specified in cooperation with local authorities. In this context, two central aspects are of interest: on the one hand the tool might be used shortly after a disaster occurred. Then, civil defence authorities have to decide whether a district should be evacuated or not [16]. On the other hand, the tool might be used in pre-disaster planning, i.e. adapting the traffic and civil defence infrastructure (like shelters).

From the scientific perspective, there are two central issues: extending the existing agent based queue model for transport simulation by a 2D simulation for simulating pedestrians on the small spatial scale (see Laemmel et al. in these proceedings) [2] and the development of a generic data model which describes a wide variety of evacuation simulations [2, 14].

2 Model Components and Behavioural Categories

We will only briefly summarize the state of the art here. Pel et al. provide a comprehensive and current review of the state of the art in dynamic evacuation traffic simulation [12, 15]. They describe three model components:

1. Dynamic travel demand model,
2. Dynamic trip distribution model, and
3. Dynamic traffic assignment model

and three behavioural categories described by these three model components:

4. Evacuation participation and departure time choice,
5. Destination choice, and
6. Route choice.

The parts 2 and 3 are part of the MATSim traffic simulation. The travel demand is currently assumed to be a certain percentage of the overall population. Demand can be assigned to buildings or blocks. The challenge is the fine-grained estimation. The participation and departure time choice can be modelled by statistical distributions. Further details can be found in [13].

3 Multi-Agent Transport Simulation for Regional Evacuation

Existing models are either focusing on the simulation of large areas but simplifying geometric details or they are focusing on small-scale scenarios (like single buildings) with high geometric resolutions. The latter are usually not suited for large areas because of their computational complexity. In the GRIPS project, multimodal traffic is simulated. Currently, the modes are pedestrians, busses, and cars. For vehicular traffic it seems to be reasonable to use a simulation model with a coarse resolution like the queue model in MATSim. However, for more complex situations the queue model is too coarse. This is usually the case when it comes to pedestrians who are navigating through complex environments like train stations [6, 7]. This is a particular problem in Hamburg, since the city railway is part of the authorities' evacuation plan.

When doing multimodal simulations there is also a need to have mode change options. For example a pedestrian might start at home and walk to the next bus stop. After she has reached the bus stop, she has to wait for the bus. When the bus arrives she has to get on the bus. Now let's assume the bus takes her to the next train station, where she leaves the bus and walks to the platform to get on a city railway. The city railway then finally takes her out of the evacuation area.

4 Focus of Application: Flooding and Industrial Accident

The development of the tool includes two basic use-cases, the flooding scenario for Hamburg-Wilhelmsburg and the industrial accident scenario for Essen. Nevertheless, GRIPS is intended to be applicable to a variety of possible cases. Therefore, an extensible data model is developed containing the types of scenarios and their scope. One important aspect regarding the scope may be the scale. For that, the evacuation of a plane or a single building is considered to be out of scope for GRIPS because the tool addresses regional evacuation. For other tools the scope might be building evacuation.

Within the data model, the input required to specify a scenario is analyzed. For now, the minimum information for performing an evacuation simulation in GRIPS is the infrastructure (e.g., road network), the population characteristics and the evacuation area.

In MATSim, the road network is represented as directed graph. In any case, the network must be suitable for routing. However, different information is required for pedestrian routing, vehicular routing or public transport routing. Different scenarios require different input [17]. The data will therefore distinguish between mandatory input and optional input data. Further the data model will have to define important scenario types like pedestrian evacuation [5, 15].

5 The GIS and ABM Based Simulation Tool

The simulation module is based on MATSim, which represents the street and road network as a queuing network. The agents are located initially on a link close to their initial position, i.e. “on the street”. The time it takes for the agents to get onto the street could be calculated by heuristics based on the respective values from the literature [2, 6, 14]. This time will then be part of the reaction time. The reaction time distribution has a strong influence on the formation of congestion. If all persons react immediately, i.e. start evacuating just after the alarm is triggered, this will result in more congestion. In summary, the pre-movement time can be divided into

$$t_{\text{pre-movement}} = t_{\text{detection}} + t_{\text{alarm}} + t_{\text{decision}} + t_{\text{preparation}} \quad (1)$$

The times for detection and for alarm are global, the time for decision and preparation are individual parameters. It is sufficient to impose a statistical distribution for the pre-movement time. The results presented below have been obtained using the prototype version of GRIPS. The workflow comprises three steps

1. Creating the scenario
 - (a) Road network from OSM + network change events (XML)
 - (b) Population from GIS layers (e.g. land use, buildings, currently shape-file)
 - (c) Evacuation area as a polygon (e.g. from hazard calculations, currently shape-file, i.e. static)
2. Running the simulation
3. Analysis of the results

An example for the network is shown in Fig. 2. This network can be dynamically changed when the simulation is running. There is currently no on-trip re-routing of the agents, i.e. the agents do not change their direction when the network changes. This is only taken into account when the agents re-plan their route in the next iteration (for details on network change events for the case of inundation after a Tsunami, please refer to [13]).

6 Simulation Results

In this section we present simple simulation results as a proof of concept. The focus is on the workflow suitable for the application at the civil defense center of command and control and for planning purposes (cf. Fig. 1). The road network shown in Fig. 2 was created from open street map (www.openstreetmap.org). First, the map.osm file is imported into QuantumGIS (an open source program). The evacuation area and the population polygons are drawn on separate GIS layers and saved as shape-files.

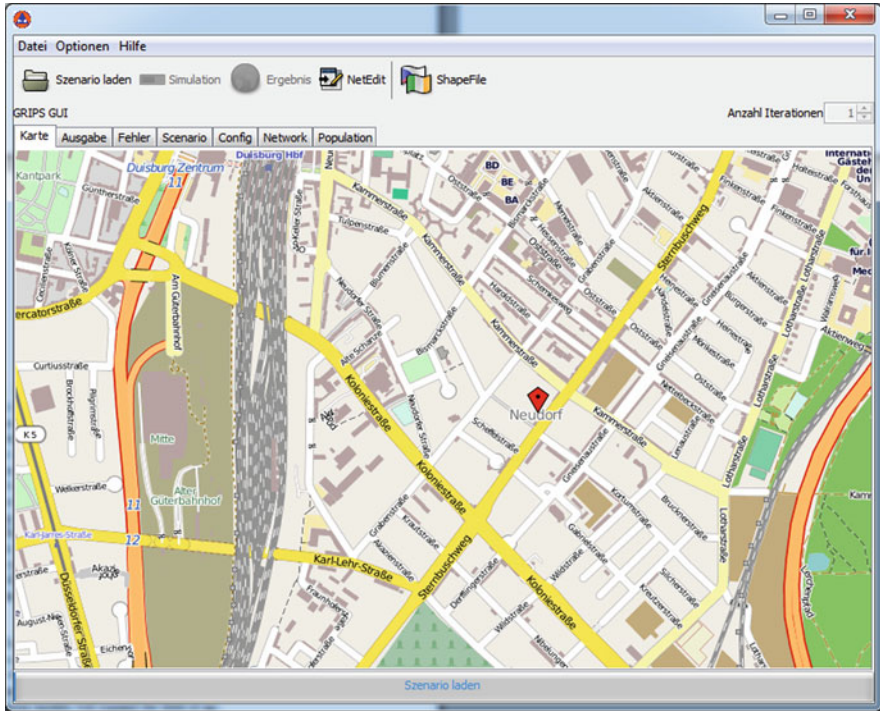


Fig. 1 Screenshot of the GRIPS user interface



Fig. 2 Screenshot of the network (visualized with SenozonVia, www.senozon.com)

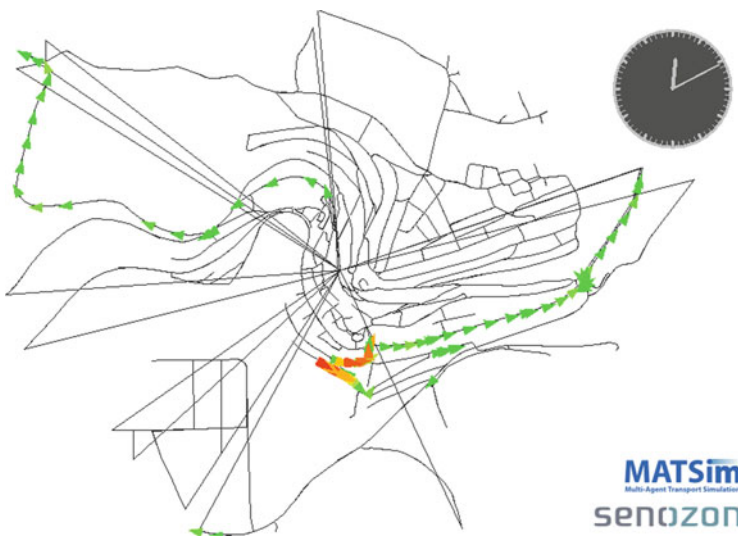


Fig. 3 Screenshot after 10 min (visualized with SenozonVia, www.senozon.com)

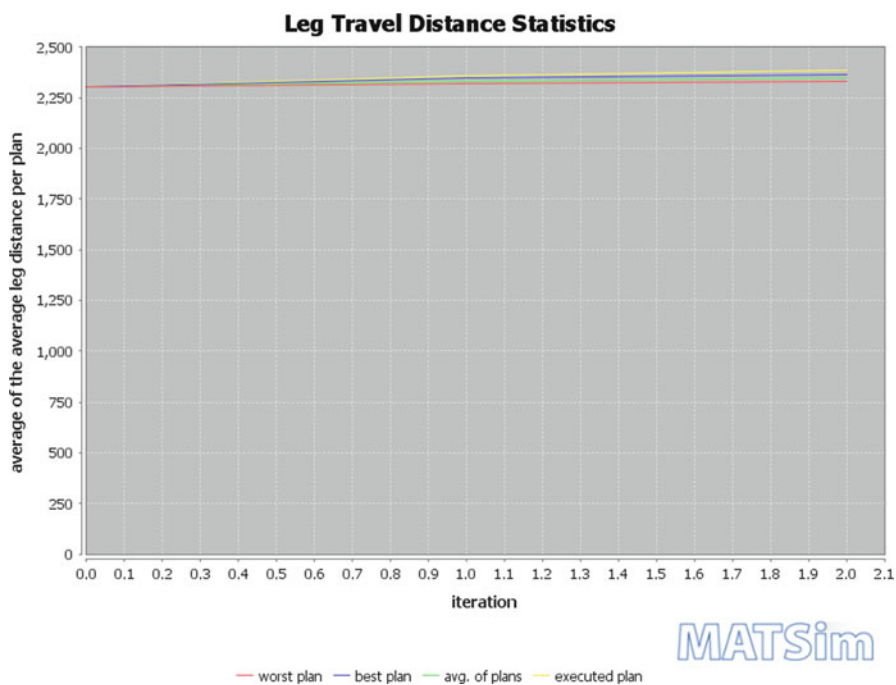


Fig. 4 Travel distances increase with the iteration

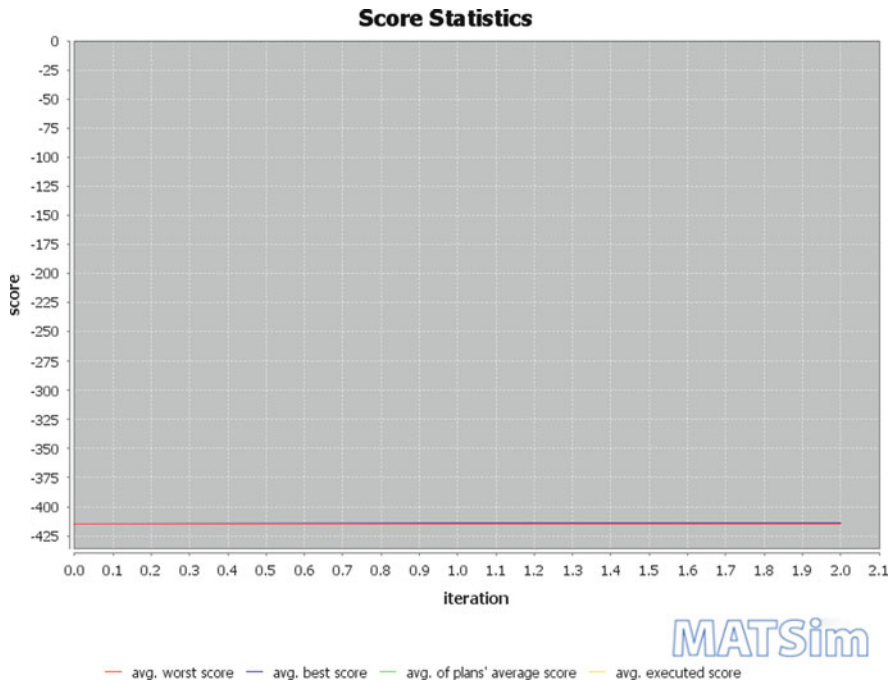


Fig. 5 The scores increase with the iteration

All three files, map.osm, population.shp, and the evacuationarea.shp are processed by the MATSim scenario generator (code and jar-file available at www.matsim.org). The scenario generator creates network.xml and population.xml, i.e. standard MATSim input files. These can be processed by the MATSim evacuation simulation module. The evacuees are located on links close to their initial position. In the first iteration, they are routed to the evacuation node (currently visible in the center of the network, cf. Figs. 2 and 3). Figure 3 shows a snapshot of the simulation, i.e. the situation 10 min after all the agents have started to evacuate.

The simulation is performed iteratively [13]. The agents are searching for a route which leads to shorter travel times (based on the cost function, e.g. the travel time). This process is illustrated in Fig. 4: the length of the paths increases with each iteration. Commuters analyze their decisions and try alternative routes to save time. These alternative routes might be longer (in distance) but faster (in time).

This of course poses the question, whether this iteration process produces realistic results. There are basically two answers to this question:

1. Iteration is interpreted as anticipation
2. No iteration, i.e. all agents use the geometrically shortest path.

Additionally, an iteration in between can be used. The first iteration leads to the longest overall evacuation time. The agents are just taking the shortest path.

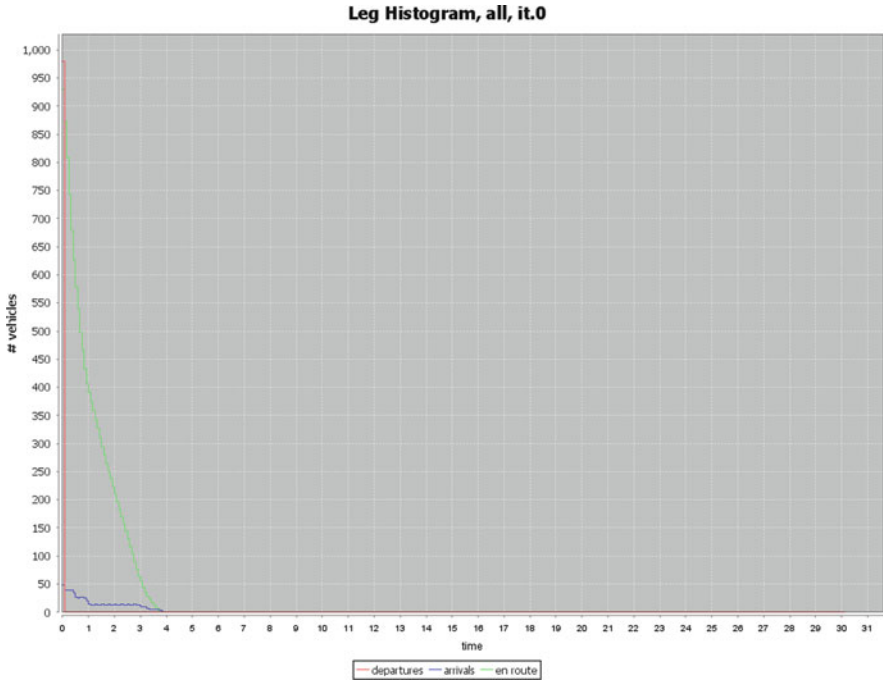


Fig. 6 The vehicles “en route” decrease with time

There might be considerable congestion and no anticipation or reasoning is used concerning the influence of traffic on the agents’ route choice decision. If the agents don’t have any knowledge or experience concerning the evacuation. On the other hand, the final iteration – after relaxation into the Nash equilibrium or user optimum – shows a situation where the agents take into account the traffic situation and search iteratively (or by clever anticipation) for an optimal route. Optimal here means that unilateral changes do not increase the individual performance, e.g. do not decrease the travel time (if the cost function just takes into account the travel time) (Fig. 5).

Other strategies might also be suitable. For example, the risk of being hit by the incoming wave after a Tsunami might be part of the cost function [13]. In this case, no part of the route should go downhill, if risk aversion is very high [2, 12]. A longer route is then accepted because it does decrease the risk in a situation where the warning time is not known (see [8] for details) [8, 10].

The parameters for the road network in our simulation are the standard ones. The capacities depend on the road category [8]. The results shown in Fig. 6 are for iteration 0, i.e. for the shortest path. The curves depend on each other, via

$$N_{\text{en route}} + N_{\text{arrivals}} = \text{const.} = N_{\text{total}} \quad (2)$$

In this example, the total number (cf. Eq. 1) is 1,000 agents. They all depart immediately, which is of course an artificial assumption and used for the purpose of illustration, i.e. to produce a high demand. For iteration 0 (Fig. 6, the overall time is 4 h) which is due to the severe congestion (Fig. 2). Basically all agents use the same road.

7 Summary, Conclusion, and Outlook

We have presented an approach to the traffic simulation for regional evacuation. The scope and aim of the GRIPS research project are described. The paper focused on the work flow and presented some simple results. The reader is invited to reproduce the results. All components used in the workflow are freely available, i.e. open source software (MATSim and QGIS) and open access data (www.openstreetmap.org).

References

1. Freie und Hansestadt Hamburg, Behörde für Inneres und Sport (2008): Sturmflutbroschüre, <http://www.hamburg.de/contentblob/569738/data/sturmflutbroschuere.pdf>. (05.032010)
2. G. Lämmel, H. Klüpfel, and K. Nagel: Risk minimizing evacuation strategies under uncertainty. 5th International Conference on Pedestrian and Evacuation Dynamics, Washington, DC, Mar 8–10, 2010.
3. Nagel, K. et. al. (2010): MATSim - Multi-Agent Transport Simulation Toolkit, TU Berlin und ETH Zurich, URL: <http://www.MATSim.org/> [Stand: 03.03.2010]
4. Gattermann, P. et. al.: *Handbuch für die Sicherheit von Großveranstaltungen*. Österreichisches Institut für Schul- und Sportstättenbau (ÖISS), Wien, 2005.
5. H. Klüpfel: Models for Crowd Movement and Egress Simulation. In: S. Hoogendoorn et. al.: *Traffic and Granular Flow 2003*. Springer, Berlin, 2004.
6. W.M. Predtetschenski and A.I. Milinski (1971): *Pedestrian Flow in Buildings*. Müller, Köln-Braunsfeld, 1971.
7. S. Buchmüller and U. Weidmann: Parameters of pedestrians, pedestrian facilities, and walking facilities. IVT, Technical report 132, ETH Zurich, 2007.
8. D. Purser and M. Bensilium: Quantification of Behaviour for Engineering Design Standards and Escape Time Calculations, *Safety Science* 38(2), 158–182, 2001.
9. RiMEA-Projekt: Richtlinie für Mikroskopische Entfluchtungsanalysen, www.rimea.de
10. A. Schadschneider, W. Klingsch, H. Klüpfel, T. Kretz, C. Rogsch, and A. Seyfried. Evacuation dynamics: Empirical results, modeling and applications. In: *Encyclopedia of Complexity and System Science*. Springer, Berlin and Heidelberg, 2009.
11. J.S. Tubbs and B.J. Meacham: *Egress Design Solutions*. Wiley, New York, 2007.
12. Pel, Adam J.; Bliemer, Michiel C. J.; Hoogendoorn, Serge P. (2012): A review on travel behaviour modelling in dynamic traffic simulation models for evacuations. In: *Transportation* 39 (1), S. 97–123.
13. Gregor Lämmel: *Escaping the Tsunami: Evacuation Strategies for Large Urban Areas Concepts and Implementation of a Multi-Agent Based Approach*. Dissertation, Technical University of Berlin, Fakultät V, Verkehrs- und Maschinensysteme, Berlin, 2011.

14. W. Daamen, S. Hoogendorn, and P.H.L. Bovy: First-order Pedestrian Traffic Flow Theory. In: Transportation Research Board Annual Meeting 2005, Washington DC: National Academy Press, 2005.
15. J.J. Fruin: Pedestrian Planning and Design. New York: Metropolitan Association of Urban Designers and Environmental Planners, 1971.
16. U. Weidmann, Transporttechnik der Fußgänger, Transporttechnische Eigenschaften des Fußgängerverkehrs, Literaturoberprüfung, Schriftenreihe des IVT 90, ETH Zürich, Jan. 1992.
17. M. Bakillah, J. A. Domínguez, A. Zipf, S. Liang, M. A. Mostafavi: Multi-agent Evacuation Simulation Data Model with Social Considerations for Disaster Management Context. Intelligent Systems for Crisis Management Lecture Notes in Geoinformation and Cartography 2013, pp. 3–16.

Agent-Based Simulations of Pedestrian Movement for Site Security: U. S. Secret Service's Current Capabilities and Next Steps

Douglas A. Samuelson

Abstract The U. S. Secret Service (USSS) is responsible for protecting dignitaries, most notably the President of the U.S. This encompasses the Inauguration, the two national nominating conventions, and some other large public events. In recent years, USSS has been directed to expand its functions to include crowd safety at such events. Consequently, USSS continues to develop substantial modeling and simulation capabilities for event planning and personnel training. Recent projects are a stadium/arena Evacuation Planning Tool (EPT), now being marketed by its developer to a number of private stadium management organizations, and Site Security Planning Tool (SSPT), a smaller-scale, video game based simulator for planning and training. Next steps include the incorporation of more realistic crowd behaviors, responses to ongoing events such as toxic plumes or secondary attacks, and continuing movement toward combining large-scale planning, smaller-scale training, and real-time situation monitoring into a single integrated model and interface.

Keywords Agent-based simulation • Pedestrian movement • Pedestrian dynamics • Mass egress • Site security • Law enforcement • Crowd safety • Simulator-based training

1 Introduction

The U. S. Secret Service (USSS), a component of the Department of Homeland Security, is responsible for, among other duties, protecting key dignitaries: the President, the Vice-President, major Presidential candidates during the campaigns,

D.A. Samuelson (✉)
InfoLogix, Inc., Annandale, VA, USA
e-mail: infologix1@aol.com

and their families. Consequently, USSS led the planning and preparation for the national nominating conventions in 2004 and 2008. In the past decade, with increasing concern about possible attacks on large public events, USSS has been directed to take on an expanding role in protecting not only the dignitaries, but also the crowds at some of these large events. By 2008, building from lessons learned in 2004, USSS had acquired substantial modeling and simulation tools to help with planning and training for mass egress [1].

Looking ahead to 2012, USSS undertook a new effort to expand and update its capabilities. A commissioned assessment of the state of the technology [9] indicated that the ideal goal, a single, integrated model and interfaces that could be used for large-scale planning, more local event simulations for training, and real-time situation reporting, is not computationally feasible. Hence USSS elected to follow, in parallel, two development tracks: a model of arena-sized movements, and a training and planning tool at the scale a single USSS agent would see during an event.

2 Evacuation Planning Tool

The planning for 2008 utilized the Evacuation Planning Tool (EPT), an agent-based simulation model of the venues in which the national nominating conventions were to be held [1]. EPT was developed by Regal Decision Systems, which now markets a commercial version, SportEvac, that has been adopted by a number of professional sports franchises and stadium operators.

EPT is a noteworthy improvement in depiction over the pioneering Homeland Security Institute/Redfish Group model [7, 8] that demonstrated the feasibility of modeling large-scale crowd movements in real time. The people are represented as stylized figures rather than as colored dots, and three-dimensional depictions are included (albeit at considerable loss of speed of execution.) People can be tagged with different colors to show whether or not they got out of the venue in a specified time interval. (The animation display can, at the user's choice, be delayed until the computation is complete.)

EPT has provisions for adding more variety in human behaviors. The assessment [9] done to guide the recent effort had identified this task as a priority, as clearly the tendencies of people to try to remain in groups, to go back for straggling members of the group, to become fatigued, and to vary in how they comply with directions are all important factors in how a mass egress will occur. However, Regal made limited progress with this aspect of the model in the course of this project.

Another high-priority step forward was building in more detail of specific venues. How easily a couple of big staircases could be blocked matters quite a bit in assessing how well a mass egress plan would work if such a blockage unexpectedly and suddenly happened. At national nominating conventions, seemingly minor decisions about where to place television cameras, cables and control booths can have major consequences. EPT does have improved capabilities to take in CAD

plans of a venue, where available, and to accept more detailed input by other means, also where available. Still, however, some questions require considerable human effort and judgment to produce a sufficiently accurate and detailed representation.

Yet another desired step was the ability to interface with other models, especially some very good and well-tested models of toxic plume spread [3]. Validation against real events, which are admittedly and fortunately rare but do exist, was another desired step that remains for future research.

A lingering question also is the limit of capability of EPT's current inference engine. The performance-depiction tradeoffs that were best at one point may not be nearly best a few years later, as technology improves, but starting over with a new approach entails large development costs. Starting over completely may be more cost-effective than starting over with a new inference engine within existing data and depiction architectures. These are promising areas for additional research that is not, at this point, contemplated within USSS's budget constraints.

3 Site Security Planning Tool

Much of what USSS considered most urgent and important concerns the training and preparation of individual USSS agents, rather than plans for the venue as a whole. For example, effective crowd direction relies critically on the placement of some key people directing movement, and on their effectiveness and persuasiveness in providing such direction. Also, the individual is key to identifying major changes in the event: for example, detection of a colorless, odorless toxic plume, as in a nerve gas attack, would depend on someone recognizing the unexpected behavior (such as coughing and then falling down) of other people in his field of view.

The Security and Incident Modeling Lab (SIMLAB), a component of the primary training venue for USSS, has relied for many years on hands-on "around the table" exercises in "Tiny Town," an HO-scale reproduction of a number of typical event venues, and on live human "game" exercises. The widespread availability of video games, and the large proportion of younger staff now familiar with such games, suggested a better approach. When USSS learned that the Royal Canadian Defence Force (RCDF) had, in fact, already developed a training simulation, CAMX [4], that could work within a video game engine such as JCATS (Joint Conflict And Tactical Simulation) or VBS2 (Virtual Battle Space 2), pursuing this technology for the current purpose looked very attractive. Accordingly, with the appropriate international and inter-agency agreements, USSS and its contractors worked with RCDF to develop the Site Security Planning Tool (SSPT).

SSPT uses large (55-in.) touch-screen kiosks mounted diagonally in a cabinet to support both third-person top-down (isometric) and first-person perspectives (for virtual walk-throughs of sites). to give trainees a very realistic "look, sound and feel" experience in a very realistic depiction of the venue of interest. Presenting and altering a scenario such as the nerve gas attack is fairly easy in SSPT. This enables USSS to replace other training methods, increasing effectiveness while reducing cost.

As with EPT, SSPT presents a number of opportunities for improvements. The incorporation of more human behaviors is a high priority here, as well, along with the perennial concern for adding realism without unacceptably impairing speed of execution. In fact, for this kind of training, real-time responsiveness is even more required, and departures from it less tolerated, than in the larger-scale tool. Another desired feature is the development of real-time situation displays that closely resemble the SSPT displays used in training. (This appears to be an easier course of action than changing the SSPT displays to resemble some real-time situational display that may be developed.)

USSS and RCDF will continue to assess the effectiveness of training, learn what approaches are most effective, and modify SSPT accordingly. As with EPT, the long-term goal is to dock SSPT with other models, to incorporate additional effects, facilitate detailed input of additional venues, and more readily explore new training ideas.

4 Next Steps

The past decade has seen a proliferation of modeling efforts in pedestrian dynamics, mass egress, and related areas [2, 3]. Just listing them all, much less characterizing strengths and weaknesses, is a daunting challenge. Integrating these modeling efforts, working toward standardization and compatibility, and recognizing what works and what doesn't, both in the modeling and in the depicted practices and policies, remains a rich area for future research – that is, no one is close to figuring it all out. Some priorities emerge, however, from what is now known.

More accurately depicting the variety of human behaviors and what influences them in these situation remains a critical need and a challenge. RCDF is conducting ongoing research to extract human behavior and its effects from a variety of real situations; the 2011 publication summarizing work to date in this area is marked for limited release. The results promise to be of great interest to researchers and incident managers when they are made generally available. Inquiries to the authors of the earlier RCDF report [4] might prove fruitful for the respectably and respectfully persistent.

The effect of different kinds of signage is a subject in its relative infancy, with interesting results already [10, 11]. Medical effects are, in general, insufficiently understood and quite important. For example, medical experts disagree strongly about whether it is more effective to stabilize victims of smoke inhalation and transport them as soon as possible to a hospital to begin treatment, or to treat them on the spot with anti-inflammatory steroids [5]. This decision in turn, affects the placement and movement of medical treatment personnel and victims at the scene, which in turn affects preferred egress routes.

Interactions at different scales, and with different modeling focus, remains another challenge. There are excellent models of the spread of toxic plumes, e.g. [12], but little success so far in docking plume models with movement models.

Good models of egress from a stadium rarely dock with models of pedestrian and vehicle movement in the surrounding community.

Studies and plans regarding movement, in turn, too rarely interact with analyses of site design and resource placement. Stadium egress models indicate that inflow of emergency responders and equipment substantially affects egress. This fact and its implications are routinely taken into account in some building designs: it is quite common, for example, for hotels and large office buildings to have built-in standpipes and, in many cases, pumps and sprinkler systems, greatly improving the speed and effectiveness of response to a fire in comparison to having to bring in hose lines. Sports arenas, however, tend to have less emergency equipment for the number of people at risk. More system-level studies are called for, even before the modeling software reaches the capability to simulate these questions well.

A recent Homeland Security Institute study, based on extensive input from first responders, [6] identified readily accessible, high-fidelity training tools as a top priority need for first responders at this time. Not far behind were real-time identification of new risks, real-time tracking of where responders are and whether they are at risk from developing hazards, real-time monitoring of availability and functionality of resources, and the ability to identify trends, patterns and important content from multiple sources, including non-traditional sources, to support incident decision-making. In short, there is an increasingly widespread perception of growing need for the kinds of tools and methods USSS has been developing.

5 Conclusions

Recent efforts by the U. S. Secret Service have produced interesting improvements in modeling overall planning of mass egress for large venues and for high-fidelity real-time training tools for incident managers and responders. The Evacuation Planning Tool (EPT) is now being commercially marketed to professional sports teams and venue operators. Many such private-sector and local public-sector operators are now interested in better incident planning, and opportunities in this area appear likely to remain promising. EPT/SportEvac may be nearing some limits in its ability to increase fidelity while maintaining fast response, however, so additional research and development opportunities appear likely, as well. The Site Security Planning Tool (SSPT), based on a video game and implemented via touch-screen kiosks, appears to represent a very promising approach which others will want to emulate or implement directly. Much remains to be done.

USSS is using these tools, with effect, in its current efforts to protect the national nominating conventions, the Inauguration, and other large events. Simulation tools have already demonstrated excellent results in providing better site security planning and training at reduced cost.

References

1. Harmon, M., and Joseph, J (2010) Evacuation Planning Tool (EPT) for Emergency Event and Space Planning, in Schreckenberg et. al., eds. *Pedestrian Dynamics and Evacuation (PED2010)*, Springer, New York, NY.
2. Kuligowski, E., and Peacock, R. (2005) Review of building evacuation models, NIST TN 1471, National Institute of Standards and Technology, Gaithersburg, Md.
3. Kuligowski, E., Peacock, R., and Hoskins, B. (2010) Review of building evacuation models, NIST TN 1471, 2nd Ed., National Institute of Standards and Technology, Gaithersburg, Md.
4. Levesque, J, Cazzolato, F, Martonosi, J. (2009) CAMX: Civilian Activity Modelling for eXercises and eXperimentation: Development and trial of a software prototype, Defence R&D Canada, Technical Memorandum, DRDC CORA TM 2009-XXX, Kingston, Canada.
5. Loellgen, H. (2010) Injury of Lung and Heart After Inhalation of Toxic Substances, in Klingsch et. al., *Pedestrian Dynamics and Evacuation 2008*, Springer, New York, NY.
6. Royal, M., Goldstein, E, et. al. (2012) Project Responder 3: Toward the First Responder of the Future, U. S. Department of Homeland Security, HSSAI Document Number RP10-68-94, Homeland Security Studies and Analysis Institute, Arlington, Va.
7. Samuelson, D., Parker, M., Miller, L., Zimmerman, A, Blacksten, H. R., Pommerenck, S. (2007a) Agent-Based Simulation of Mass Egress After an Improvised Explosive Device Attack, Homeland Security Institute Final Report to the Science and Technology Directorate, U. S. Department of Homeland Security, HSI Document Number RP06-IOA-31-03, Homeland Security Institute, Arlington, Va.
8. Samuelson, D., Parker, M., Zimmerman, A, Guerin, S, Thorp, J, and Densmore, O., (2007b) Agent-Based Simulations of Mass Egress After an Improvised Explosive Device Attack, Proceedings of the European Conference on Complex Systems, October 2007, Dresden, Germany.
9. Samuelson, D. (2011) Agent-Based Simulations of Mass Egress: Summary of Current Capabilities and Recommended Next Steps, Technical Report to the U. S. Secret Service, Lionheart Publishing, Atlanta, Ga.
10. Veeraswamy, A., Galea, E.R., and Lawrence, P, Implementation of Cognitive Mapping, Spatial Representation and Wayfinding Behaviours of People within Evacuation Modelling Tools, Proceedings of the 4th International Symposium on Human Behaviour in Fire, Robinson College, Cambridge, UK, pp. 501–512, July 2009
11. Xie, H, Filippidis, L, Galea, E., Blackshields, D., Lawrence, P.J., Experimental Study of the Effectiveness of Emergency Signage, Proceedings of the 4th International Symposium on Human Behaviour in Fire, Robinson College, Cambridge, UK, pp. 289–300, July 2009
12. Young, T., Jr., Boris, J., Hooper, S., Lind, C., Obenschain, K. and Patnaik, G. (2004) Emergency Assessment with Sensors and Buildings: Advances in CT-Analyst Technology. (Presented at CBIS 2004, Williamsburg VA, October 2004) Laboratory for Computational Physics and Fluid Dynamics U.S. Naval Research Laboratory, Code 6400, Washington, DC.

Ant Colony Based Evacuation Route Optimization Model for Mixed Pedestrian-Vehicle Flows

Qiuping Li, Zhixiang Fang, and Qingquan Li

Abstract Evacuation for large-scale activities usually involves a great number of pedestrians and vehicles. By applying ant colony optimization algorithm, an evacuation route optimization model for mixed pedestrian-vehicles flows is proposed in this paper. In this model, we construct a two-tier network structure in which the upper tier network is for path finding and evacuation route guidance, and the lower tier subnetwork which depicts the move directions of pedestrians and vehicles respectively is for the simulation of the movements as well as the conflicts between them. The experiment results show that the proposed model has the merit of modeling the interaction dynamics of pedestrians and vehicles and improving evacuation efficiency in an evacuation case of large-scale activities.

Keywords Ant colony optimization • Mixed vehicle-pedestrian flows • Pedestrian-vehicle conflicts

1 Introduction

Large-scale activities, such as the pop concerts or sport events held in a large stadium usually generate great traffic pressure to the road networks. In the evacuation process, the massive pedestrians and vehicles may cause serious congestion in the parking areas or unsignalized intersections, which could not be ignored in evacuation route planning.

Q. Li (✉) • Z. Fang • Q. Li

State Key Laboratory of Information Engineering in Surveying, Mapping and Remote Sensing,
Wuhan University, Wuhan 430079, China

Engineering Research Center for Spatio-temporal Data Smart Acquisition and Application,
Wuhan University, Wuhan 430079, China

e-mail: leeqiuping@whu.edu.cn; zxfang@whu.edu.cn; qqli@whu.edu.cn

Current evacuation model researches are usually focus on the pedestrian movement in the building environment [1–3] or the vehicle traffic on road networks [4–6], effective mechanisms to optimize the mixed pedestrian-vehicle flows under congested evacuation situations are still worth researching.

Most researches on mixed pedestrian and vehicle flows are mainly for simulation purpose [7–9]. This is because the interactions between pedestrians and vehicles are very complex. Especially, pedestrians are individuals and do not follow strict rules. They spontaneously stop, change directions or make sudden turns. Cellular automaton model (CA) is proved to be an efficient simulation method due to its ability of considering the interactions between vehicles and pedestrians by dividing the time and space into discrete units and updating the flow movements with a set of local rules [7, 8]. In addition, continuous simulation model with a conflict-point detection method can also model the complex traffic system consisting of heterogeneous mixed flows in urban intersections [9]. Some software packages, such as Viswalk, can be integrated with Vissim to simulate the interactions between pedestrians and vehicles [10]. However, these researches provide no solution to optimization of overall evacuation process.

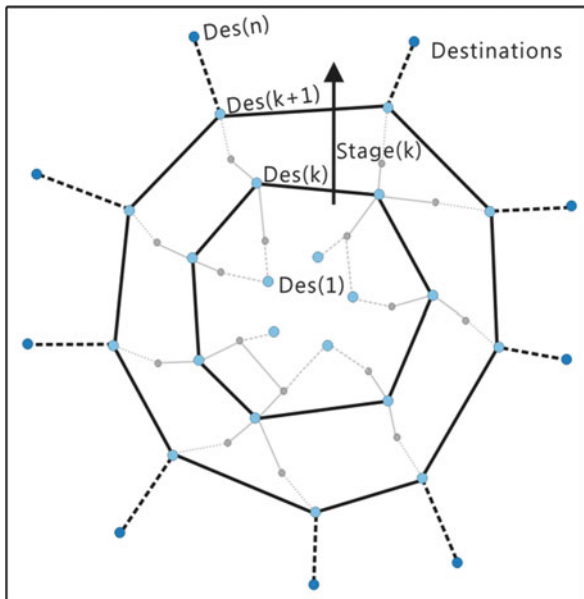
Due to the discrete and heterogeneous characteristics, classic traffic assignment models (e.g. static traffic assignment and dynamic traffic assignment) have some difficulties in dealing with the mixed traffic flows. In this paper, an ant colony based model is presented to optimize the routes for pedestrian-vehicle flows in the case of large-scale activity evacuation. In this model, a two-tier network structure is proposed, in which the upper tier is link-node based network for the path finding and route guidance, and the lower tier network which depicts the move directions of pedestrians and vehicles at intersections respectively, is for the simulation of movements of vehicles and pedestrians and the conflicts between them.

2 Ant Colony Based Evacuation Route Optimization Model

2.1 Definition of Stage-Guided Upper Tier Evacuation Network

An evacuation network is defined as a directed graph $G(N,A)$, where $N = \{1,2, \dots, i, \dots, n\}$ is the set of nodes and $A \subseteq (N*N)$ is the set of links. The path finding process in evacuation usually deals with the issue of guiding evacuees going from one place to another. Therefore, a stage-guided upper tier evacuation network is constructed firstly according to the network structure. Take the stadium evacuation scenario as an example, of which the network structure is usually in a radioactive pattern. All spectator stands can be viewed as the first evacuation stage, the exits of stands are the second stage, and the stadium exits are the third evacuation stage, and so on. Figure 1 is a schematic drawing of a radioactive pattern network, where $Des(k)$ is the set of exits of the k th stage.

Fig. 1 Evacuation network in a radioactive pattern



2.2 Description of Ant Colony Based Algorithm

The basic ant colony algorithm proposed by Dorigo in 1996 [11], imitating ants’ path finding behavior in food searching process, is a kind of artificial or swarm intelligence. In our proposed algorithm, every pedestrian or vehicle is viewed as an ant. A probability selection and a positive feedback strategy are implemented to find the optimal paths for each pedestrian and vehicle in evacuation. At each time step, all the possible paths for each vehicle and pedestrian are found and assigned to them according to a roulette wheel selection method. The paths found in the last time step will guide ants to move along in the dynamic simulation process for the next step. The flow of ACA is described as follows:

Step 1: Initialization

The parameters of the ant colony algorithm, including the maximum number of iterations (NC_max), the current iteration number (NC) and the number of ants (Num_ant) are initialized [12]. The start time of each ant starting to move follows a normal distribution with average value of 60 s [13].

Step 2: Generate an evacuation route for each ant

For any time step, each ant passes one or several nodes, corresponding to its travel speed. In time step t , the transition probability of an ant m located at node $\tau_{ij}(it + 1) = (1 - \phi)\tau_{ij}(it) + \Delta\tau_{ij}$ choosing its adjacent node j is defined as:

$$p_j^m(t) = \begin{cases} \frac{\tau_{ij}^\alpha(t)\eta_{ij}^\beta(t)}{\sum_{w \in V(i)} \tau_{iw}^\alpha(t)\eta_{iw}^\beta(t)} & , (i, w) \in A, \text{ stage}_j \geq \text{stage}_i \\ 0 & , \text{ else} \end{cases} \quad (1)$$

Where $P_j^m(t)$ is the probability of choosing node j , $\tau_{ij}^\alpha(t)$ is the intensity of pheromone trail on link ij , $\eta_{ij}^\beta(t)$ is the heuristic information of link ij , which can be defines as Eq. 2. V_i is the set of nodes adjacent to i . α and β are the parameters representing the relevance of the pheromone and heuristic information in ant's decision-making process respectively. Heuristic information $\eta_{ij}^\beta(t)$ is calculated as:

$$\eta_{ij}^\beta(t) = \frac{1}{dis_{jd}^{\min}} \quad (2)$$

Where dis_{jd}^{\min} is the minimum distance of node j to the exits of current evacuation stage.

Repeat the path finding process until ant m arrives at the final destination. If the ant represents a person who drives to attend the large-scale activities, it has to get to the parking lot by walking first, and then drive to the final destination. After all ants reach the destinations, go to Step 3.

Step 3: Evaluate the objective value

Evacuation time is usually the most significant index to be considered in evacuation planning. The time required for 95 % of all evacuees to flee the evacuation zone which is considered as a practical and meaningful MOE by some studies [14, 15], is taken as the objective value to be optimized in this study.

Step 4: Update global pheromone

Pheromone trail is updated as Eq. 3:

$$\tau_{ij}(it + 1) = (1 - \varphi) \tau_{ij}(it) + \Delta \tau_{ij} \quad (3)$$

$$\Delta \tau_{ij} = \frac{Q}{\frac{\sum_{it=1}^n \sum_{(i,j) \in N} (V/c)_{ij}}{n}} \quad (4)$$

Where it is the current iteration, and $\frac{\sum_{it=1}^n \sum_{(i,j) \in N} (V/c)_{ij}}{n}$ is the average volume-to-capacity ratio of link ij during total n time steps to evaluate the utilization of link ij , if link ij is over used during evacuation process, pheromone increment $\Delta \tau_{ij}$ on link ij would be small.

This pheromone-updating strategy could balance the selection of links with shorter distance to the exits and the links with lower volume-to-capacity ratio.

Step 5: Stopping criterion

If the current iteration NC equals to the maximum iterations NC_max, the algorithm will stop. Then the paths found by the ants for pedestrians and vehicles can be viewed as optimal paths in the multi-modal evacuation situations.

3 Pedestrian-Vehicle Mixed Flow Simulation

3.1 Definition of Lower Tier Subnetwork

To model the details of the interaction between pedestrians and vehicles at the intersections, each intersection and roadway which contains both driving and walking modes is depicted by the lower tier evacuation network. The lower tier evacuation network includes an intersection subnetwork and a road subnetwork, which is for the dynamics simulation of pedestrians and vehicles. An example of an intersection subnetwork is illustrated as Fig. 2. Vehicles and pedestrians follow their move directions calculated by ant colony algorithm, respectively (Fig. 2a, b), and the conflicts between pedestrians and vehicles mostly occur at crosswalks (see Fig. 2c).

3.2 Traffic Flow Simulation

This study simulated movements according to the basic assumption that vehicles move on lanes and pedestrians move only on walkways or crosswalks. Thus, under this assumption, we omit the potential interference between pedestrians and vehicles on roads during the process of evacuation, and only focus on the conflicts happening at the crossroads. Pedestrian and vehicle flows on the road are simulated by queue model proposed by Gawron [16], respectively. The travel speed of pedestrians and vehicles on link *ij* during the simulation time interval Δt is defined as follows:

$$v(t + \Delta t) = \begin{cases} \min(V_{\max}, 1/D_{ij}^t), & \text{if } \text{mod } e = 0 \\ V_{\max} (C_{ij} + 1 - N_{ij}) / C_{ij}, & \text{if } \text{mod } e = 1 \end{cases} \quad (5)$$

Where mode = 0 means it is pedestrian flow, and mode = 1 means it is vehicle flow. D_{ij}^t is the pedestrian density on the sidewalk of link *ij* in Δt . The speed of pedestrians is calculated according to the relationship between density and velocity [17]. C_{ij} is the capacity of vehicles on the lanes of link *ij*, and N_{ij} is the current number of vehicles on it. The formula for speed calculation of vehicles is from literature [5]. In addition, the pedestrians and vehicles are constrained to be in FIFO (First In, First Out) queues [16, 18].

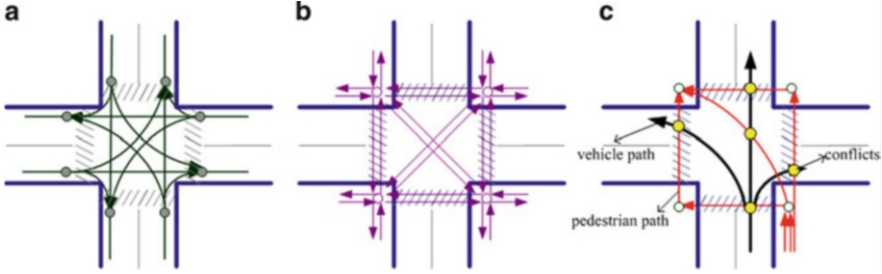


Fig. 2 Lower tier network representation. (a) Vehicle move direction. (b) Pedestrian move direction. (c) Mixed traffic at an intersection

The travel time of ant m passing link ij is defined as:

$$T_{ij}^m = \begin{cases} \frac{l_{ij}}{v_{ij}^t}, & \text{if } \frac{l_{ij}}{v_{ij}^t} \leq \Delta t \\ n\Delta t + \frac{l_{ij}^{n+1}}{v_{ij}(t+(n+1)\Delta t)}, & \text{else} \end{cases} \quad (6)$$

Where $l_{ij}^{n+1} = l_{ij} - \sum_{k=1}^n \Delta t * v_{ij}(t + k\Delta t)$, which means the remaining distance after n time steps' move on link ij .

A conflict matrix is proposed to illustrate the conflicts between pedestrian and vehicle flows at intersections. The conflict matrix of an intersection i is described as below:

$$CM_i = \begin{matrix} & a1 & a2 & \dots & am \\ b1 & \left[\begin{matrix} \lambda_{11} & \lambda_{12} & \dots & \lambda_{1m} \end{matrix} \right] \\ b2 & \left[\begin{matrix} \lambda_{21} & \lambda_{22} & \dots & \lambda_{2m} \end{matrix} \right] \\ \vdots & \left[\begin{matrix} \vdots & \vdots & \vdots & \vdots \end{matrix} \right] \\ bn & \left[\begin{matrix} \lambda_{n1} & \lambda_{n2} & \dots & \lambda_{nm} \end{matrix} \right] \end{matrix} \quad (7)$$

Where $\{a1, a2, \dots, am\}$, $\{b1, b2, \dots, bn\}$ are the move directions of pedestrians and vehicles at intersection i , respectively. λ_{jj} is a boolean value representing whether two move directions (a_j, b_j) could conflict or not.

At any simulation step t , the travel time of ant m crossing the intersection i is defined as follows:

$$T_i^m = \frac{l_i^k}{v_i^m} + t_{delay}^i \quad (8)$$

If ant m is a pedestrian, l_i^k is the length of k th direction branch of the set $\{a1, a2, \dots, am\}$; otherwise, l_i^k is the length of k th direction branch of set

$\{b_1, b_2, \dots, b_n\}$. v_i^m is the speed of ant m at the time of when it enters the intersection.

If the move direction of ant m conflicts with that of other ants which pass intersection i at the same time, the crossing delay t_{delay}^i is set as a constant value by referring to level of service (LOS) of unsignalized intersections in China [19, 20]. Otherwise, the crossing delay is zero. Compared to cellular automaton based micro-simulation approach for mixed pedestrian-vehicle flows, this kind of simplification can increase the computational efficiency, although loses some accuracy to some extent.

4 Case Study Application

In this study, we selected the stadium and adjacent road network at the Wuhan Sports Centre in China as our experiment area. There are 272 nodes and 644 links in the evacuation network (see Fig. 3), which consists of a stadium network and a road network outside the stadium. The detail view of an intersection with all possible move directions of pedestrians and vehicles is also included in Fig. 3.

A hypothetical event like a fire happened on a pop concert held in the stadium was chosen as a scenario. People who drive to attend the pop concert need to walk to the parking lot first and then drive to escape, and others need to walk to the final destinations. Therefore, pedestrian traffic generates from the stadium and vehicle traffic generates from the parking lot.

The proposed ACA has been implemented in C++ language and runs on a PC with 3.06 GHz, 3GB RAM. In this study, we consider the scenario in which more than 20,000 pedestrians and 1,000 cars have to leave. The ACA stopped when the iteration times reached the predefined maximum iteration step (NC_max = 200). The parameter of ACA is set as Table 1.

Since there are some oscillations in the convergence process of the proposed ACA, we described the convergence trend by plotting the current best objective value (Time for 95 % population evacuated named T_{95}) and its corresponding iteration number. From iteration 0 to iteration 40, T_{95} drops very fast, and from iteration 40 on, it remains relatively stable (see Fig. 4). The best value $T_{95} = 3960s$ appears at iteration 165.

Some other indexes besides T_{95} were evaluated for further analysis (see Table 2). Where AET is the average evacuation time, T is evacuation clearance time, AEL is average evacuation path length, and ACT is average pedestrian-vehicle conflict time. The statistical results of iteration 0 which was the initial plan and iteration 165 which got the best objective value, as well as iteration 87 which got the most serious conflicts were listed in the table.

From the table, we can see that iteration 165 almost got the best performance on these four indexes. Besides, there existed some trade-offs among these indexes. Initially, ants searched paths randomly, thus AEL value was the largest. Then by the

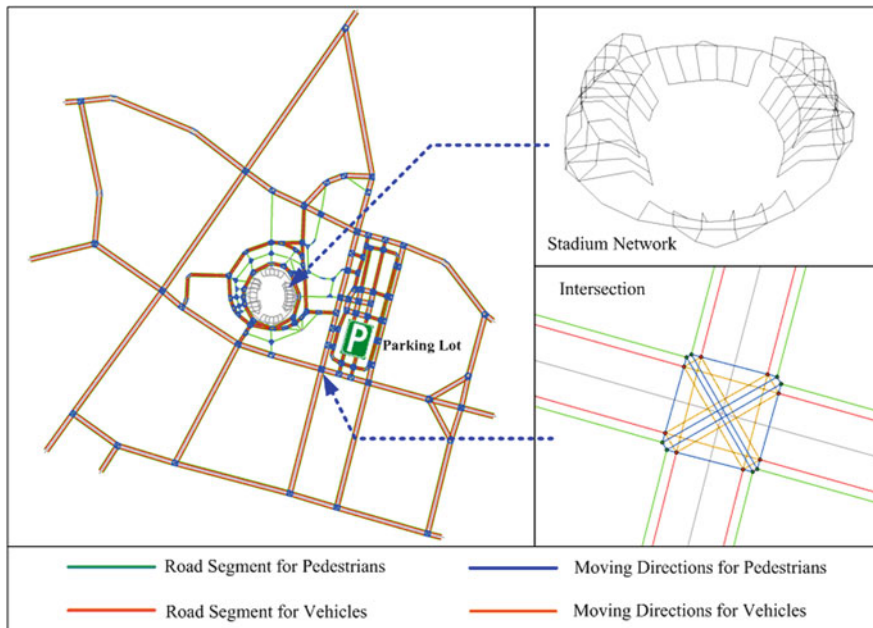


Fig. 3 Evacuation network of experiment area

Table 1 Parameters in ACA

NC_max	Num_ant	Vmax_veh	Vmax_ped	α	β	ρ	Q
200	23,362	15 m/s	2 m/s	2	1	0.3	1

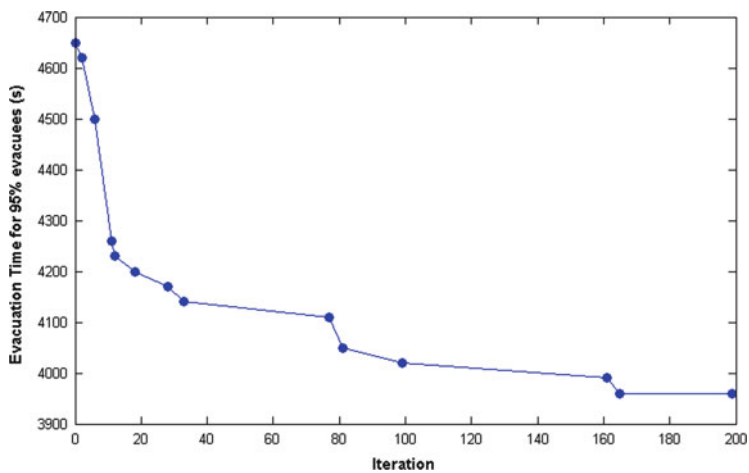


Fig. 4 Evacuation time for 95 % evacuees over the iteration

Table 2 Statistical results of iteration 0, iteration 87 and iteration 165

Iteration	AET(s)	T(s)	AEL(m)	ACT(s)
0	3,095.08	5,460.53	1,382.55	12.59
87	3,412.86	6,240.23	1,216.47	75.55
165	3,183.42	4,170.76	1,175.54	6.40

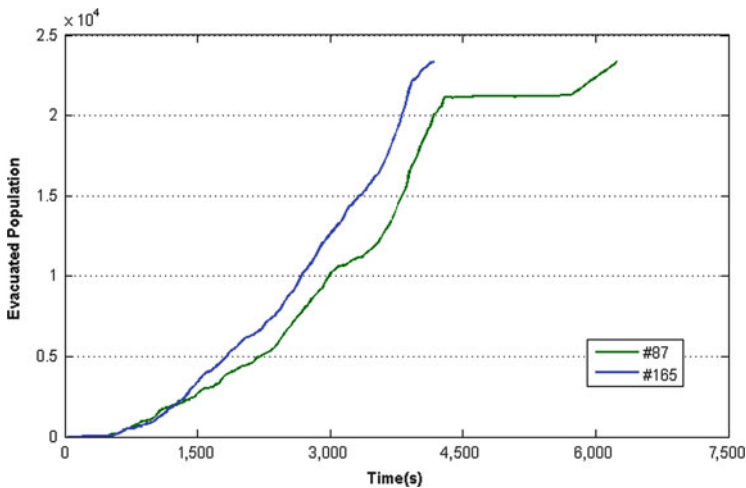


Fig. 5 Evacuation curves

role of pheromone, the shorter and less congested paths attracted more and more ants, so AEL value decreased owing to paths' aggregation.

The evacuation curves of the plan at iteration 87 and iteration 165 were compared in Fig. 5 to analyze the reason why iteration 87 got a much longer evacuation clearance time than that of iteration 165. As we can see from the figure, the curve of iteration 165 was steeper than that of iteration 87, which implied higher evacuation efficiency. There was an even segment in the curve of iteration 87 after 4,500 s, which was probably caused by the detour in the route planning by ant colony algorithm.

Then the space distribution and the degree of pedestrian-vehicle conflicts of the evacuation route plan of iteration 87 and iteration 165 on the evacuation network were compared. As shown in Fig. 6, the places that conflicts occur were mainly the parking lot area and the connection nodes of stadium area and outside road networks. The degree of conflicts of an intersection was represented by the average delay of for pedestrian-vehicle conflicts there, which was expressed by the different colors from green to red of the nodes. The number of conflicted intersections as well as the conflict degree of intersections at the same place at iteration 165 was smaller than that of iteration 87. Take the intersection No. 251 circled by the black dotted line in Fig. 6 as an example, the average delay there was 16 s at iteration 87 but no delay at iteration 165.

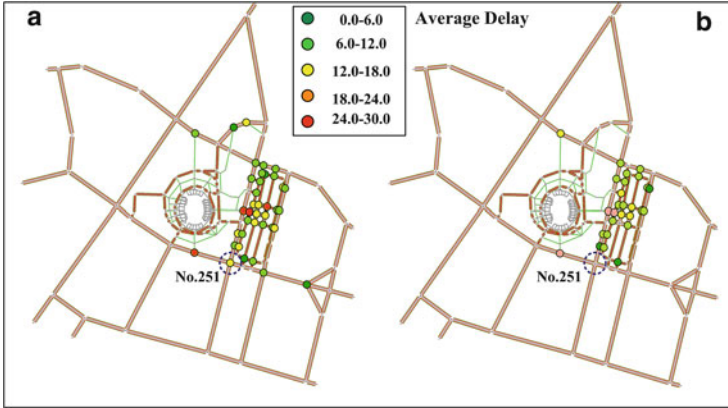


Fig. 6 The pedestrian-vehicle conflict interactions on evacuation network. (a) #87. (b) #165

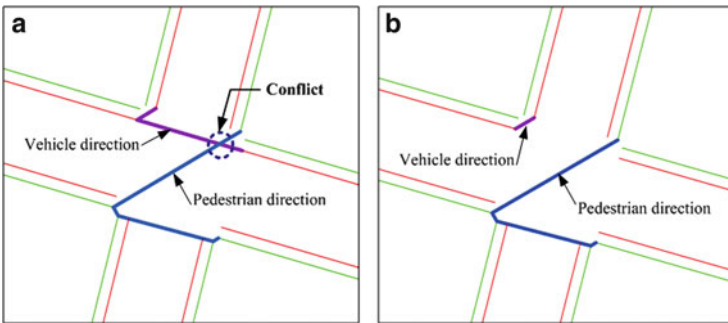


Fig. 7 The detail of move directions of pedestrians and vehicles at intersection No. 251. (a) #87. (b) #165

Figure 7 shows the detail of move directions of pedestrians and vehicles at intersection No. 251. In Fig. 7a, vehicles moving along east–west direction conflicted with pedestrians crossing this intersection from northeast to southwest. The conflict point was pointed out by a circle. However, in Fig. 7b, vehicles passing this intersection moved along right turn lane only, thus the pedestrian-vehicle conflicts disappeared at the 165th iteration.

5 Conclusions

An ant colony based evacuation optimization model for mixed pedestrian-vehicle flows was proposed by making full use of a two-tier network structure. The upper tier network was organized for the optimization of path finding and route guidance,

and the lower tier subnetwork was designed for simulating the movement and interactions of pedestrians and vehicles. This model tries to support the traditional transportation simulation models by modeling the interactions dynamics of both pedestrians and vehicles. The experiment results show that this proposed approach is useful to optimize the evacuation plan involving pedestrian-vehicle mixed flows in evacuation networks. However, it must be noted that the proposed simulation model for dynamics of pedestrians and vehicles is simplified and needs to be further improved in the future work.

Acknowledgements This research was supported by the National Science Foundation of China (grants #40701153, #40971233, #40830530, #60872132).

References

1. Fang, Z. M., Song, W. G., Zhang, J.: A Multi-Grid Model for Evacuation Coupling With the Effects of Fire Products. *Fire Technology*, pp. 91–104 (2012)
2. Siikonen, M. L., Sorsa, J. S.: Evacuation Simulation and Human Behavior Models in Tall Buildings. In: Klingsch, W. W. F. et al. (eds.), *Pedestrian and Evacuation Dynamics 2008*, pp. 653–658. Springer (2010)
3. Chen, P. H., Feng, F.: A Fast Flow Control Algorithm for Real-Time Emergency Evacuation in Large Indoor Areas. *Fire Safety Journal*, pp. 732–740 (2009)
4. Cova, T. J., Johnson, J. P.: A network flow model for lane-based evacuation routing. *Transportation Research Part A*, pp. 579–604 (2003)
5. Stepanov, A., Smith J. M.: Multi-objective evacuation routing in transportation networks. *European Journal of Operational Research*, pp. 435–446 (2010)
6. Xie, C., Turnquist, M. A.: Lane-based evacuation network optimization: An integrated Lagrangian relaxation and tabu search approach. *Transportation Research Part C: Emerging Technologies*, pp. 40–63 (2011)
7. Zhang, X., Chang, G L.: A CA-based Model for Simulating Vehicular-Pedestrian Mixed Flows in a Congested Network. In: 90th Annual Meeting of the Transportation Research Board .*Transportation Research Record*, pp. 116–124 (2011)
8. Wu, H. X.: Microscopic Dynamic Simulation Model for Pedestrian-Vehicle Mixed Traffic.: In International Conference on E-Health Networking, Digital Ecosystems and Technologies (EDT), pp. 153–156. IEEE Press, New York (2010)
9. Wang, L.: Continuous Simulation-based Conflict-point Detection Model for Heterogeneous Mixed Traffic Flows in an Urban Intersection. In: 88th Annual Meeting of the Transportation Research Board. (2009)
10. Viswalk. <http://www.vissim.de/software/transportation-planning-trafficengineering/software-system-solutions/viswalk/> (2011)
11. Dorigo, M., Maniezzo, V., Colormi, A.: The ant system: optimization by a colony of cooperating agents. *IEEE Transactions on Systems, Man, and Cybernetics-Part B*. 26, 1–13. (1996)
12. Fang, Z.X., Zong, X.L., Li, Q. Q., Li, Q. P., Xiong, S. W.: Hierarchical multi-objective evacuation routing in stadium using ant colony optimization approach. *Journal of Transport Geography*. 19,443–451 (2011)
13. Fang, Z. X., Li, Q. Q., Li, Q. P., Han, L. D., Wang, D.: A Proposed Pedestrian Waiting-Time Model for Improving Space-Time Use Efficiency in Stadium Evacuation Scenarios, *Building and Environment*. 46, 1774–1784 (2011)
14. Han, L. D., Yuan, F, Urbanik, T.: What is an effective evacuation operation? *Journal of Urban Planning and Development*. 133, 3–8 (2007)

15. Yuan, F., Han, L. D. : Improving evacuation planning with sensible measure of effectiveness choice: case study. *Transportation Research Record: Journal of the Transportation Research Board.* 2137, 54–62 (2009)
16. Gawron, C.: An Iterative Algorithm to Determine the Dynamic User Equilibrium in a traffic Simulation Model. *International Journal of Modern Physics C.* 9, 393–407 (1998)
17. Lämmel, G., Rieser, M., Nagel, K.: Bottlenecks and congestion in evacuation scenarios : A microscopic evacuation simulation for large-scale disasters, In: Bazzan, A.L., Klügl, F., Ossowski, S. (eds). *Proc. of 5th workshop on Agents in traffic and transportation*, at International Conference on Autonomous Agents and Multiagent Systems, pp. 54–61 (2008)
18. Lämmel, G., Grether, D., Nagel, K.: The representation and implementation of time-dependent inundation in large-scale microscopic evacuation simulations, *Transportation research part C.* 18, 84–98 (2010)
19. Dai, T. Y, Du, R. B, Pei, Y. L.: Simulation of pedestrian Crossing Delay at intersections of urban road. *Computer and Communications.* 4, 75–78 (2008)
20. Zhang, Y. P.: *The Theory of Highway Capacity.* Harbing: Harbing Institute of Technology Press (2007)

Collecte of Data Stemming from the Fine Trajectory of the Pedestrians

Adiaviakoye Ladji, Plainchault Patrick, Bourcerie Marc, and Auberlet Jean Michel

Abstract Walking, the oldest means of transport and practiced used by everyone, represents the “heart of life itself” around which any other means of transport should be subordinately organized. It is necessary to detect, locate, identity, and eventually track pedestrians to understand how they interact with each other.

This article concerns the detection of pedestrians to using a laser sensor. This sensor is located approximately 18 cm above the ground and collects information about in-motion feet distances of pedestrians and the presence of objects within 20 m radius.

A walking model based on the typical foot movements is defined in order to exclusively extract data with the in-motion foot hallmarks. Each laser sensor is controlled by a client computer that sends the information to a server computer, where they are spatially and temporarily integrated in a global database. A tracking method is developed using the MCMCDA (Markov Chain Monte Carlo Data Association) to monitor pedestrians’ trajectories. The system is evaluated by computer simulation and a full-scale experiment is being developed. The simulation is conducted in a school entrance hall where eight laser sensors cover an area of about 1,500 m². The position and direction changes of students during the break where the rush hour, are analyzed. Computer simulation is carried out to examine quantitatively the system performance with respect to the density of the crowd.

Keywords Laser scanning • People detection • Acquisition • Multiple people tracking

A. Ladji (✉) • P. Patrick • B. Marc • A.J. Michel
CER-ESEO / LISA, 4 rue Merlet de la Boulaye, BP 30926, 49000 Angers cedex 01, France
e-mail: ladji.adiaviakoye@eseo.fr; patrick.plainchault@eseo.fr; marc.bourcerie@univ-angers.fr;
jean-michel.auberlet@inrets.fr; <http://www.eseo.fr>

1 Introduction

Over the past decade, human behavior has been studied in various fields such as architectural conception, disaster prevention, traffic engineering, etc.

Pedestrians' trajectory, walking speed and direction changes are basic data for such analysis. Therefore, many tracking systems were developed and several tracking methods were suggested. A broad review of the various sensors used to detect pedestrians as: the piezoelectric, radar, ultrasound, laser and of course camera operating in the visible or infrared are listed in [5].

Due to some constraints, only a few methods have been applied to real scenarios. The vast majority of work focuses on the detection of motion analysis by video image [4], knowing that it has the ability to capture the shape and texture of a pedestrian. From this observation, many detection methods have been developed in the field of vision from monocular or stereoscopic camera [3].

However, the high sensibility to atmospheric conditions, the limited opening angle of the cameras and the impossibility to get direct and accurate information about depth make it crucial to update these tracking methods [6, 7]. Despite the robustness of these methods, it was necessary to develop a monitoring system capable of: to follow a crowd of people in a relatively large area because of frequent occlusions of objects and people moving. Indeed several cameras are necessary to cover a large area to reduce occlusion. However, it is difficult to digitally merge data from multiple cameras, which requires an accurate calibration, a high cost to load and a complicated calibration [2].

Consequently, few systems are capable of measuring a high density of people in large and crowded areas. The laser scanner is one tool that has received increasing attention to the problems of tracking. It measures the distances of nearby objects by emitting eye-safe laser beams in controlled directions. To analyze this information on the distance a wide variety of technical procedures are possible (e.g. flight time, etc.) and depend on the magnitude of the distances to be measured. This type of sensor is often used in many practical applications of robotics [10, 17, 18].

In this research, we study the trajectories of walking that are measured using a laser scanner system. We apply this system to a relatively large and crowded area such as a school entrance hall.

Initially a literature review related work on pedestrian detection using laser scanner data is presented. We recall the operating principle of the laser scanner. In the next section the device is operated as part of our simulations. A method of detecting and monitoring of pedestrians in a hall from a laser scanner system is proposed. The detection algorithm is based on our walk model, keeping only objects with a signature "pedestrian". The data will be used in a database to simulate and validate some of pedestrian behaviors.

2 Overview

2.1 Previous Works

Thanks to improved scanning speed (from 3 frames per second [9] at 30 frames per second [8]), scope (up about 80 m), its angular resolution and also its cost purchase became more accessible. The laser sensor are highlighted in many applications such as: navigation, detection and tracking of moving objects, etc. The items offered here explicitly address the problem of detection, identification, tracking of mobile entities from laser sensor only. In the context of navigation with a mobile platform, the laser scanner has been the cornerstone for the detection and distinction of persons in an environment of static objects. The sensor on the mobile robot is successive laser scans [12, 13] to detect and track people moving around him. Only a few studies designed to monitor a large number of people with fixed laser scanners.

A SICK laser type PLS 200, was used to ensure a robot's navigation in pedestrians areas [10] and the researchers used a *grid-map* representation for mobile cells spotting, a group of close cells being considered a person. The trajectory of moving targets is obtained by the criterion of nearest neighbor between groups of cells that move in consecutive scans.

In the case of the obstruction detection by a robot, the method consists in segmenting the image of the laser scanning each time step and collected sets of points representing objects [12]. Initially the scan is segmented into several parts densely sampled. In the second step these parts are divided into sequences describing objects *almost convex*. With the hypothesis of gaps between the distance of distinct objects, a threshold value is set to find the separate objects. For monitoring, the authors use the network optimization techniques from graph theory.

To track individuals, the team [17] used a mobile platform equipped with two laser scanners mounted at a height of 40 cm. Each minimum local extract a distance profile is considered as an object. Moving objects such as people are different from static objects by calculating the local occupancy grid maps. The data association and tracking operate particulate filters and a sampled form of filters JPDA (Joint Probabilistic Data Association).

In another context, such as monitoring, metering or monitoring of a crowd person from points lasers [14, 15] several laser sensors are deployed to cover a large area [8]. The *clustering* technique is most commonly used, and virtually the only strategy to enable the extraction of people in the laser data.

The authors of [16] seek to detect and track mobile entities. The goal is to find the positions occupied in the laser without previously free. *Violation points* are the positions corresponding to moving objects in each scan. The violations are considered Gauss impulses on the two-dimensions map. New hypotheses are created at points of violations that have value beyond a threshold. Indeed, it is a continuous version of the clustering process instead of the discrete version. The assumptions of moving objects are created from the resulting cumulative Gaussian functions (amplitude beyond a threshold) and are propagated using a gradient technique.

Important thing to remember is that it is a local search method, similar to searching the nearest neighbor.

In order to track multiple people with laser sensors SICK fixed placed 80 cm above ground [14], the method of subtraction of a background model is applied to assemble the impacts to the foreground.

They define a *drop* as a gathering of readings foreground elements adjacent that seem to be on a continuous surface, this assumes that the measures that are spatially separated by less than 10 cm belong to the same *drop*. A technique of mapping is used to link information from the old to new drops with each new scan. A issue we have to consider is the fact that placing sensors 80 cm above the ground negatively impacts the detection process because of occlusions caused by:

- People very close,
- Arm swing pedestrian,
- Accessories (handbags, coats, etc.).

Which makes modeling difficult for accurate monitoring. For monitoring, the authors of [14] combine a Kalman filter to each object.

In [15] the lasers SICK LMS 200 are placed 20 cm from the ground to track people. The author compares two variants of discrete JPDA filter type (paired or independent) integrated within a particle filter. J. Cui & all [21] have done the same for sensors lasers locations, but they has extracted the footprints of legs in the laser planes by using a nonparametric technique of Parzen windows. Particle filtering is the method used to monitor the crowd of pedestrians.

Compared to other studies, the system described in [7] leads to what seems to be the best option to track a large number of people simultaneously. To count visitors, the authors has placed several sensors IBEO LD-A networks to 20 cm of soil. At this height, the occlusions are lower than waist level. Using the periodic movement of the feet in his walk model, it tracks pedestrians through laser data.

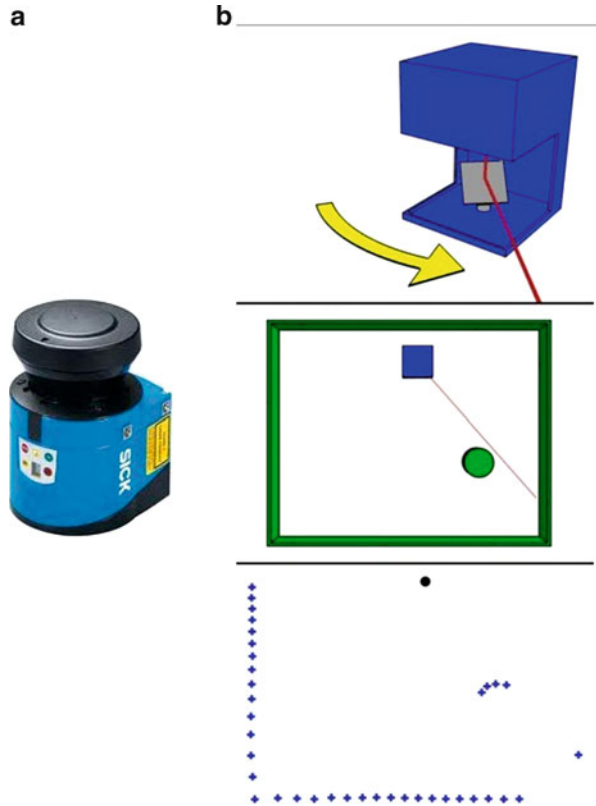
We have to acknowledge the fact that none of the techniques using sensor association (between laser data and video data for instance) were mentioned here. We are fully aware that a single laser solution is not quite enough and therefore, a solution involving several sensors is an option that needs to be considered. However, we would like to first study the laser sensor in depth in order to test its limits and develop a better combination with sensors that will make up for its defects.

The laser sensors used in the studies mentioned above often have the same reference (IBEO LD-A, SICK LMS 200). However, data is processed differently, which makes it difficult to compare the different methods suggested.

3 System Architecture

In our monitoring system, we used a network of laser scanner LMS 111 SICK society. It is possible to retrieve information on the distance through a wide variety of technical processes that depend on the magnitude of the distances to be measured.

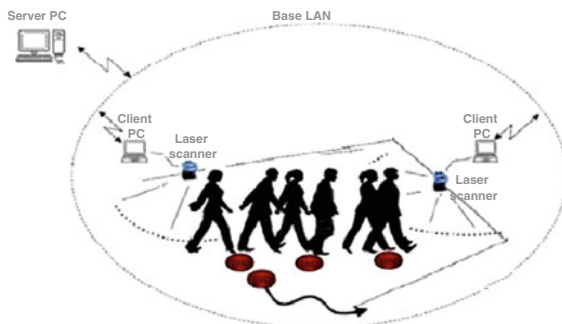
Fig. 1 (a) The laser scanner SICK LMS 111 sensor. (b) 2D scanning laser sensor



Given the application context that motivates us in this article, it is a technique by pulse telemetry also called *measure time of flight* which is a round trip of light between the laser source and the photoreceptor through the target illuminated which is widely exploited. The technique of “time of flight” is one of the most suitable for the distance measurement in a wide range of relative values. Furthermore, this technique offers the advantage of responding to surfaces such as *scattering* or *uncooperative*. Thus, a fraction of the received optical energy is backscattered by the target surface in the direction of incident laser beam. The laser sensor scans the horizontal plane of 270° by rotating a mirror inside (Fig. 1b). It has a high angular resolution of 0.5° and a scan rate of 37.5 Hz. The distance data collected can be expressed as (ρ_i, θ_i) , $\theta_i = 0^\circ$ to 270° in steps of 0.5° , where ρ_i represents the measured distance and θ_i the corresponding angle. By combining the position and direction of the laser scanner range, data can be easily converted into Cartesian coordinates. The laser beam covers a maximum range of 20 m and an average error of 4 cm distance.

In our experiments, the laser scanners were strategically set up to avoid disturbances between scanners nearby and to cover a large area in order to decrease

Fig. 2 System architecture



occlusions. Each laser scanner is controlled by a client computer. All client computers are connected by a LAN cable to a computer server, which collects data (position of the tracks) objects moving of all client computers (Fig. 2). We have chosen to set the laser scan in the horizontal to the ground at ankle height (about 18 cm). This is justified by the fact that:

- There are more occlusions by the waist area than around the ankles
- Our walking model is based on the foot's trajectory

As opposed to video cameras, the laser scanner does not provide information regarding colors. However, it is easy to get data about the depth, which is difficult with a regular video camera. Laser scanners are independent of factors such as lighting, color and texture, so that the system is more accurate and stable. Its effectiveness in monitoring a compact crowd in an environment such as a railway station has been demonstrated by actual experiments [23].

3.1 Our Approach

In order to have a method of detection, identification and tracking of pedestrians inside an entrance hall with a laser sensor SICK LMS 111, we were inspired by the work of [8].

Indeed the simple clustering will fail in detecting person due to other moving objects such as people with luggage, strollers, or when two people walk close to each other. We modeled the pedestrian walk, based on experimental data from different laboratories (scientific and technical support from IRISA Rennes, Laboratory of Physiology and Biomechanics of Muscular Exercise Marseille) [19, 20].

Our kinematic data come from a motion capture system called VICON and composed of six video cameras able to reconstitute the positions of detectors (located on the walker's articulations) in 3D.

The measurement of the trajectory of these points allows then reconstruct the segmented body movement of the walker and even to find the trajectory of its center of mass.

Without a priori knowledge of the number of obstacles in the observed scene, we chose as in [8] to retain only objects with a signature “pedestrian”.

The monitoring process is based on the MCMCDA (Markov Chain Monte Carlo Data Association) method suggested by [22] to portray the complex pedestrian’s trajectory as best as possible. Thus our method is original not only concerning the sensor’s point of view but also the suggested algorithm.

4 Modeling Pedestrian Walking

Walking is represented as a cyclical pattern of movement in biomechanics. The gait cycle is divided into two main phases for each leg (Fig. 3a):

- The **stance phase** during which the foot is in contact with the ground. It represents 62 % of the full cycle of walking.
- The **swing phase** means the phase during which the same foot leaves the ground and advance to its next phase of support. It represents 38 % of the full cycle of walking.

The stance phase is divided into five periods and the swing phase into three periods. These eight periods represent the invariant factors of walking. By convention, the cycle begins when the foot reference (the right foot for us) makes contact with the ground. Human walking locomotion is a process during which there is always one foot in contact with the ground.

The two essential elements to any form of bipedal walking are:

- The periodicity of the movement of each leg of a support position to another in the direction towards progression.
- The continuity of the ground reaction forces that support the body.

We built our walk model based on the periodicity and continuity of the forces of the feet (Fig. 4).

When we report the duration of each period to the total length of stride, we find that the ratio values are almost unchanged, regardless of walking speed. This reveals an important fact: ***regardless of frequency and step length which will vary depending on the morphology of individuals, walking retains almost the same temporal structure.***

When a pedestrian begins to move the right foot, the muscles act to produce the desired movement which will give the initial acceleration of the right foot. While the right foot continues to move, the force decreases and becomes negative in order to stop it. Here we assume that the force decreases linearly and we obtain the acceleration of the right foot on a cycle. Then, the pedestrian begins to move the left foot while maintaining the fixed right foot. By assuming that the cycles are all the same. It is clear that the force exerted on the left foot will change in the same manner as the right foot, while the force on the right foot is zero. We therefore acceleration of both feet over a full cycle.

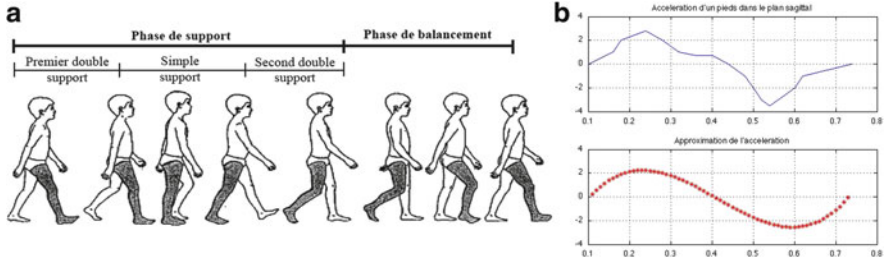


Fig. 3 (a) Normal gait cycle. (b) The acceleration of a foot in the sagittal plane

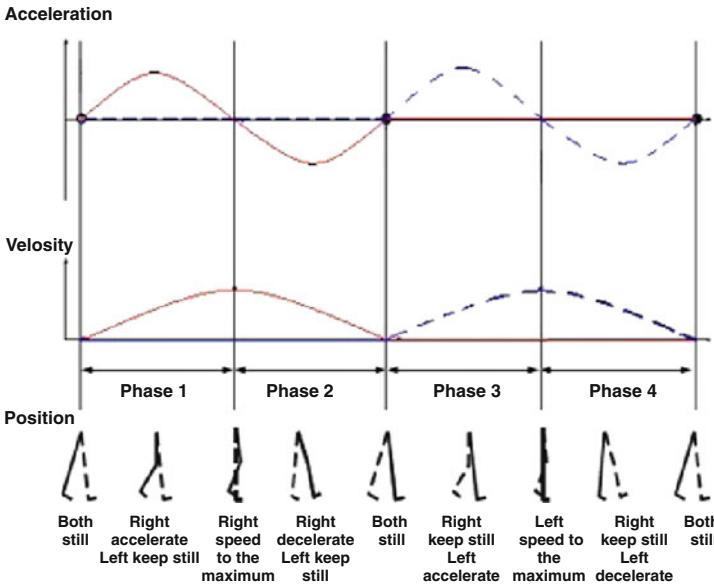


Fig. 4 Walk model

We made a third order polynomial approximation of the acceleration (Fig. 3b) in contrast to [23] which is of order one. We obtained the speed and distance traveled by using an integration with null constants.

Assuming that the cycles are all the same although this assumption is not entirely correct, it is a reasonable approximation. Thus the same way, the distance traveled by the left foot is deducted. Therefore, the distance between both feet is calculated by using the difference in the distance traveled by both feet (Fig. 5). As shown in Fig. 5, the distance between the two feet named x_{dg} varies as a cosine. This is exactly the cubic spline interpolation function of a cosine function. Our results coincide with those of [23] although we have not addressed the problem the same way. **Thus our walk model was considered valid and the third order approximation does not provide more precision than that provided by order one.**

Fig. 5 Walking distance between the two feet

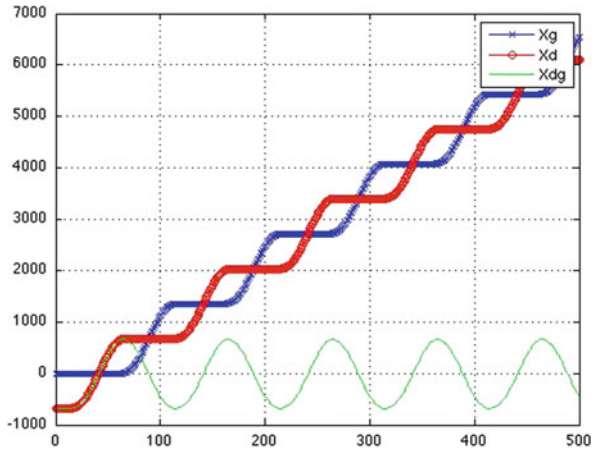


Fig. 6 A digital map of the entrance hall



5 System Evaluation

The system is evaluated on two levels, computer simulations and real experiments. Through simulated experiments, the feasibility of the system in tracking pedestrians in a closed environment is examined. The evaluation by simulation is to quantify system performance, for example, how many sensors are needed to cover a relatively large area, what percentage of pedestrians extracted depending by the crowd density, and so on. Indeed, the system is examined by tracking a large number of pedestrians. The simulation is performed on the environment C++ (Qt Creator) with GUI libraries, bullet physics and Blender. A digital map of the entrance hall is displayed (Fig. 6) in order to define the physical settings. In reality most students inside the hall remains motionless for a long time looking at the information table and talk.

In this simulation, we assume that there is nothing to watch in the lobby in order to simulate the pedestrians who walk in the hallways. Eight laser scanners with the

same specification as the LMS 111 are deployed and their positions are indicated by blue dots. They cover an area of approximately $1,500\text{m}^2$ with five inputs and outputs. The algorithm is designed with the assumption that the pedestrian will do nothing to mask his feet. This will allow us to know the percentage of persons detected and tracked. Any pedestrian leaves the area covered by the laser and reappears later is then considered as a new person. The high resolution sensor allows us to see multiple points but increases the computational cost. In the simulation we reduced the range of laser for gain in computational cost. Concerning walking pedestrian, it's simulated exactly as we have defined in the previous section. Methods are being developed to determine the position and direction changes of pedestrians.

The full-scale experiments will be conducted under the same condition as the simulation. We try to develop a robust algorithm that considers the different possibilities.

6 Conclusion et Perspectives

We suggested a system that follows pedestrians with several laser scanners. First, we did a bibliographic research describing the history of different studies conducted exclusively with laser scanned data.

In a second step, a walk model was designed to write to specific models generated by the feet of pedestrians in the space-time domain that is operating in the tracking step. Pedestrians are detected and tracked using the method MCMCDA. The system we suggest will allow us to follow a large number of pedestrians in a crowded environment. The system will be validated after a two-phase evaluation: computer simulation and real life experiment. For the full-scale experiment, three laser scanners will be set in a school entrance hall. Around 150m^2 will be covered and approximately 100 students will be tracked simultaneously at peak time. We will also consider the variations in visitors flux by using the observed trajectories. Moreover, a simulation will be used to quantify the system's performance. However, the monitoring algorithm is not yet sufficiently robust and specific enough to follow each individual.

By comparing our system with a normal video camera, we can already conclude the following:

First, the extraction of moving objects in the coordinate system of the real world is not as complex as with a normal video camera. Moreover, one can easily convert data in Cartesian coordinates, it is fairly easy to calibrate laser scanners to cover a relatively large area. Finally, we will avoid the "confidentiality issue associated with image rights" pretty sensitive in public places, etc.

Future work will focus on the robustness of tracking by tackling the issue of objects concealment but also accessories such as: shopping carts, strollers, bikes, cars, etc. We will equip students with RFID chips (Radio-Frequency Identification) in association with the laser scanner network to get a more accurate identification.

References

1. K.C. Fuerstenberg and U. Lages, "Pedestrian Detection and Classification by laserscanners", in Proc. of 9th EAEC International Congress, 2003.
2. Marcel Brückner, Ferid Bajramovic, and Joachim Denzler. Self-calibration of camera networks: Active and passive methods. In Chi Hau Chen, editor, *Emerging Topics in Computer Vision and its Applications*, pages 447–469. World Scientific Publishing, December 2011.
3. T. Gandhi and M. Trivedi, "Pedestrian Collision Avoidance Systems: a Survey of Computer Vision Based Recent Studies", in Proc. of the IEEE Int. Transportation Systems Conference, Sept. 2006.
4. Danny B. Yang, Héctor H. Gonzalez-banos, and Leonidas J. Guibas. Counting people in crowds with a real-time network of simple image sensors. In Proc. IEEE International Conference on Computer Vision, pages 122–129, 2003.
5. F. Bu and C-Y. Chan, "Pedestrian Detection in Transit Bus Application: Sensing Technologies and Safety Solutions", in IEEE Intelligent Vehicles Symposium (IV), Las Vegas, June 2005.
6. Chia-Jung Pai and Hsiao-Rong Tyan and Yu-Ming Liang and Hong-Yuan Mark Liao and Sei-Wang Chen, 2004, Pedestrian detection and tracking at crossroads, *Pattern Recognition*, 37, pp.1025–1034.
7. Naoya Ohta, Masanobu Kiyama and Kenichi Yoshikawa, 2003, Pedestrian Detection and Identification Using Two Cameras(in Japanese), *IPSJ Journal*, 44(10), pp.2459–2468.
8. H. Zhao, R. Shibasaki, A Novel system for tracking pedestrians using multiple single-row laser range scanners, *IEEE Trans. SMC. Part A: Systems and Humans* 35 (2) (2005) 283–291.
9. E. Prassler, J. Scholz, M. Schuster, D. Schwammkrug, Tracking a large number of moving objects in a crowded environment, in: *IEEE Workshop on Perception for Mobile Agents*, Santa Barbara, June 1998.
10. E. Prassler, J. Scholz, and P. Fiorini. "Navigating a Robotic Wheelchair in a Railway Station during Rush Hour", *Int. Journal on Robotics Research (IJRR)*, 18(7), pp. 760–772, 1999.
11. L. Trassoudaine, L. Marcellin, P. Checchin, J. Alizon, and J. Gallice. "Smart Servoing of a Controllable Range Sensor for Target Tracking: application to Pedestrians", in *IFAC Conference on Intelligent Autonomous Vehicles*, pages 343–348, Espoo, Finland, June 1995.
12. B. Kluge, C. Koehler, E. Prassler, Fast and robust tracking of multiple moving objects with a laser range finder, in: Proc. of the IEEE International Conference on Robotics & Automation (ICRA), 2001, pp. 1683–1688.
13. M. Montemerlo, S. Thun, W. Whittaker, Conditional particle filters for simultaneous mobile robot localization and people-tracking, in: Proc. of the IEEE International Conference on Robotics & Automation (ICRA), 2002.
14. A. Fod, A. Howard, and M. Mataric, "Laser-based People Tracking", in Proc. of the IEEE International Conference on Robotics and Automation (ICRA), Washington D.C, 2002.
15. O. Frank, J. Nieto, J. Guivant, and S. Scheduling. "Multiple target tracking using sequential Monte Carlo methods and statistical data association", in Proc. IEEE/RSJ Int. Conf. on Intelligent Robots and Systems (IROS), 2003.
16. M. Lindström, J.-O. Eklundh, Detecting and tracking moving objects from a mobile platform using a laser range scanner, in: Proc. IEEE/ RSJ Int. Conf. on Intelligent Robots and Systems (IROS), 2001, pp. 1364–1369.
17. D. Schulz, W. Burgard, D. Fox, A. Cremers, Tracking multiple moving targets with a mobile robot, in: Proc. of the IEEE Computer Society Conference on Computer Vision and Pattern Recognition (CVPR), Kauai, Hawaii, 2001.
18. M. Montemerlo, S. Thun, W. Whittaker, Conditional particle filters for simultaneous mobile robot localization and people-tracking, in: Proc. of the IEEE International Conference on Robotics & Automation (ICRA), 2002.
19. A. Heloir, S. Gibet, F. Multon & N. Courty. Captured Motion Data Processing for Real Time Synthesis of Sign Language. *Lecture Notes in Computer Science*, vol. LNCS-LNAI 3881, pages 168–171, 2006.

20. A. Heloir, N. Courty, S. Gibet & F. Multon. Temporal alignment of communicative gesture sequences. *Computer animation and virtual worlds*, vol. 17, no. 3 + 4, pages 347–358, 2006.
21. J. Cui, H. Zha, H. Zhao, R. Shibasaki. “Laser based Detection and Tracking of Multiple People in Crowds”, in *Computer Vision and Image Understanding (CVIU)*, special issue on “Advances in Vision Algorithms and Systems Beyond the Visible Spectrum”, Volume 106, Issue 2–3, pp. 300–312, May 2007.
22. Songhwai Oh, Stuart Russell, and Shankar Sastry, “ Markov Chain Monte Carlo Data Association for Multi-Target Tracking,” *IEEE Transactions on Automatic Control*, vol. 54, no. 3, pp. 481–497, Mar. 2009.
23. Xiaowei Shao, Huijing Zhao, Katsuyuki Nakamura, Kyoichiro Katabira, Ryosuke Shibasaki, and Yuri Nakagawa. Detection and tracking of multiple pedestrians by using laser range scanners. In *IROS*, pages 2174–2179, 2007.
24. C.L. VAUGHAN, B.L. DAVIS & J.C. O’CONNOR. *Dynamics of Human Gait*. Human Kinetics Publishers, Champaign, Illinois, 1992.

Dynamic Medium Scale Navigation Using Dynamic Floor Fields

Dirk Hartmann, Jana Mille, Alexander Pfaffinger, and Christian Royer

Abstract This contribution considers a new method for dynamic medium scale navigation in microscopic pedestrian simulators. The concept of static navigation floor fields is extended to a dynamic interpretation following ideas of (Kretz, T, Journal of Statistical Mechanics: Theory and Experiment, P03012, 2009) and (Hartmann, D, New Journal of Physics 12(4):043032, 2010) within a cellular automaton approach. Every few simulation steps a new floor field for navigation is constructed by solving the Eikonal equation on the dual grid of the underlying cellular automaton discretization. By considering other pedestrians directly in the construction of the floor field, the realism of the simulations is significantly increased. The new contribution of our work is to additionally consider walking directions of pedestrians. This leads to a significant increase in the realism of simulations.

The increased realism of the new concept is underlined by simulations of various example scenarios proposed in the literature. These show that the method is capable of reproducing a number of phenomena, e.g. lane formation.

Keywords Microscopic model • Navigation • Floor field • Dynamic floor field • Eikonal equation • Fast marching method • Pedestrian flows • Pedestrian crowds

1 Introduction

Microscopic pedestrian simulations are an emerging topic in all phases of the design and operation of infrastructures, e.g. airports [23]. Applications range from an optimal design of airports with respect to passenger comfort to evacuation of

D. Hartmann (✉) • J. Mille • A. Pfaffinger • C. Royer
Siemens AG, Corporate Technology, Munich D-80200, Germany
e-mail: Hartmann.Dirk@siemens.com; Alexander.Pfaffinger@siemens.com;
Christian.Royer@siemens.com

buildings in the case of emergency. In all applications, simulations have to yield as realistic results as possible to ensure a maximum of reliability.

The bottleneck of realism in microscopic models is typically the navigation behavior of single pedestrians. Navigation in existing microscopic pedestrian simulators can be distinguished on two different levels. On a large scale level, pedestrians take tactic navigation decisions, e.g. which (intermediate) destination is visited next or which path/corridor to take next. On a small to medium scale level pedestrians choose the “optimal path” (e.g. shortest or fastest path) towards the next intermediate destination. The navigation of pedestrians, i.e. the choice of the “optimal path”, typically takes into account the interaction with other pedestrians in the field of vision, e.g. increasing travel time and comfort by avoiding crowded regions or to sidestep other pedestrians.

For a complete overview of microscopic modeling approaches to pedestrian flows, we refer to Bellomo and Dogbe [1], Pelechani et al. [23] and Schadschneider et al. [26]. Nearly all existing microscopic simulators reflect these two navigation layers. Typically the macroscopic layer is modeled using an approach based on graphs and the microscopic layer is modeled using a field-based approach. Within the graph based approach (intermediate) destinations, e.g. stores or crossings correspond to vertices of the graph and possible ways correspond to edges of the graph. Classical graph routing algorithms are then applied to determine macroscopic navigation strategies for each pedestrian (c.f. Kneidl et al. [16] and references therein). Microscopic navigation decisions are often based on so called floor fields or navigation fields (most prominently used in cellular automate models; [2, 3, 13–15, 21]). These can be considered as potentials. Pedestrians try to minimize the local potential during the course of their movement, i.e. minima of the potentials correspond to (intermediate) destinations. Also force models [4, 5, 12, 22] fit within this framework, since forces guiding pedestrians to their next destination are usually conservative. In this paper, we will focus on small to medium scale navigation, i.e. the navigation from one intermediate destination to the next.

Also the navigation models on the small scale are quite mature and floor field based methods are used in a number of simulators, still several open challenges have not been solved completely yet. The most severe limitation is that other pedestrians are considered only in a very limited manner. Most pedestrian simulators take other pedestrians only on a small scale into account, i.e. only pedestrians within a few meters are considered for navigation decisions. On the medium scale other pedestrians are neglected. Considering low to medium densities typically realistic results are obtained. In the case of high pedestrian densities this is however not always the case. Only very few simulators use dynamic medium-scale navigation taking other pedestrians into account [3, 8, 19]. However, these methods typically require high computational efforts since navigation fields have to be recalculated dynamically during the simulation. Recently effective computational techniques have been proposed for constructing appropriate dynamic floor fields [9, 16], the simulation of large dense crowds has become well in reach.

In this paper, we will outline in detail a new modification of the method proposed in [8]. This navigation concept not only avoids unnatural congestions,

but also realistically captures effects like lane formation in dense crowds. Instead of considering a repulsion of pedestrians on a short and medium scale independent of the walking direction, the method takes walking directions into account. On a short scale our approach agrees with classical approaches, e.g. Helbing and Molnár [12]. However, on a medium scale, directions of other pedestrians are not taken into account by existing microscopic simulation methods (at least up to our knowledge).

The presented approach does not need an additional floor field as required by the approach of Burstedde et al. [3]. Furthermore the approach is as efficient as the methods outlined in Kretz [19] and Hartmann [8], but simultaneously captures typical effects like lane formation. The increased realism of the approach is demonstrated by simulating different scenarios, among them the ones outlined in Helbing et al. [10]. Effects like lane formation are successfully reproduced in different scenarios. Thus the model allows significantly more realistic simulation results and hence a better prediction of pedestrian flows as well as egress times.

It is planned to apply the considered techniques to larger scenarios in the future, namely regional evacuation in the context of the REPKA project [24]. We believe that the navigation algorithms introduced in this contribution will imply a significant improvement, especially in dense crowds with pedestrians moving in multiple directions. Classical navigation concepts typically lead in this case to large unrealistic congestions not showing lane formations as one would expect in reality. For further contributions within this project we refer to (Kneidl et al. 2012; [6, 7, 18, 20, 25, 27]).

The article is structured as follows: In Sect. 2 we introduce the basic cellular automaton approach we are using. The navigation is based on floor fields and is outlined in Sect. 3. The strength of the proposed method is then highlighted in Sect. 4 considering various scenarios followed by a discussion and outlook in Sect. 5.

2 A Cellular Automaton Approach to Pedestrian Dynamics

Although the concept of small to medium navigation is independent of a specific microscopic simulator, we will present the concepts using the cellular automaton model introduced in [17]. For further references we refer also to (Kneidl et al. 2012; [6, 7, 18, 20, 25, 27]). Generalizations to other microscopic models are straight forward.

The approach relies on a two dimensional spatial discretization using hexagons. Each hexagon is either empty or occupied by a single pedestrian or obstacle. The size of a single hexagon is chosen such that it accommodates an average European male person, i.e. has a size of 0.185 m^2 [29]. Similarly, the time is discretized into equidistant time steps. In each time step, a subset of the persons on the cellular automaton is chosen and allowed to move. We rely on a sequential update which ensures that pedestrians with higher free flow velocities are allowed to move more

often according to their speed. Here, we use a Gaussian distribution according to Weidmann [29].

Each pedestrian allowed to move in a time step chooses one of its neighbor cells to move to. This decision is based on potentials borrowing ideas from electrostatics. To each intermediate destination an attractive potential is assigned – in the simplest case given by the shortest Euclidean distance (for more details we refer to Sect. 3). This “long range” potential used for medium scale navigation (i.e. to the next intermediate destination) is often referred to as floor field or navigation field. Furthermore, to each pedestrian and obstacle a short range (1–2 m) repulsive potential is assigned. That is, also short range navigation is modeled via potentials. The pedestrian then moves to the unoccupied neighbor cell with the smallest summed potential value.

This simple field based approach is furthermore extended to keep spatial and temporal discretization artifacts to a minimum. For a detailed treatment of the complete concept we refer to the original work of Köster et al. [17]. Here, we restrict ourselves to outline in more detail the concept of medium floor field based navigation (c.f. Sect. 3).

3 Floor Field Based Navigation

In the microscopic pedestrian simulator introduced above as well as in most other microscopic simulators medium scale navigation is realized via so called floor field methods. For each intermediate destination a corresponding floor field is constructed for navigation. Such floor fields are spatial fields which have a minimum at the corresponding intermediate destination and which are monotonically increasing with increasing distance from the intermediate destination.

In the simplest case such a floor field is given by the Euclidean length of the shortest paths from each position to the corresponding intermediate destination. This can be efficiently evaluated if the shortest path to the intermediate destination is not blocked by an obstacle. If it is blocked, determining lengths of shortest paths can be quite complicated. Many alternative approaches have thus been proposed, e.g. (Kretz [19]; Nishinari [21] and references therein). Here, we rely on the ideas of Hartmann [8] using the so-called Eikonal equation to derive corresponding floor fields.

Usually navigation fields are of a static structure. However, recently Kretz [19] and Hartmann [8] have introduced independently the concept of dynamics floor fields. These rely on a dynamic recalculation of the navigation field taking other pedestrians into account and yield significantly more realistic simulation results. The concept is outlined below (Sect. 3.1) and a new extension further increasing the realism is introduced (Sect. 3.2).

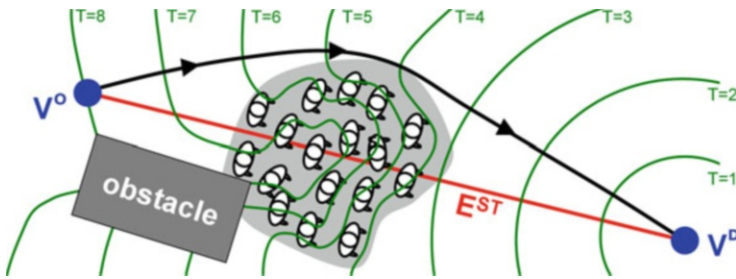


Fig. 1 Schematic illustration of the calculation of a dynamic floor field for navigation from the origin V^O to the destination V^D taking other pedestrians into account

3.1 Concepts

The central idea of Hartmann [8] is to use solutions of the Eikonal equation in two dimensions as floor field values. The Eikonal equation models arrival times $T(x,y)$ of a wave extending with a normal speed $F(x,y) > 0$ from an initial curve $T(x,y) = 0$, the outline of the destination:

$$F^2 \cdot \left[\left(\frac{\partial T}{\partial x} \right)^2 + \left(\frac{\partial T}{\partial y} \right)^2 \right] = 1 \tag{1}$$

where x and y are the spatial coordinates. The Eikonal Eq. 1 can be solved efficiently on the dual grid of the underlying hexagonal cellular automaton using the Fast Marching method [28]. Furthermore, efficient techniques for increasing computational speeds (up to a factor of 10) have been recently introduced [9].

Assuming a constant speed $F(x,y) = 1$ m/s implies that $T(x,y)$ corresponds to Euclidian lengths of the shortest paths. In Hartmann [8] it has been suggested to adapt $F(x,y)$ according to local properties, e.g. different terrains or pedestrian densities (c.f. Fig. 1). Considering a dependence on pedestrian densities, i.e.

$$F(x,y) = \frac{c}{\rho(x,y)} \tag{2}$$

where $\rho(x,y)$ is a measure of the local density of pedestrians, it has been shown that significantly more realistic behavior is obtained (c.f. Figs. 2 or 3). We believe that this consideration of other pedestrians within medium scale navigation mimics significantly better human behavior than approaches with static floor fields. The consideration of other pedestrians on a short scale via local repulsion is still kept in the model.

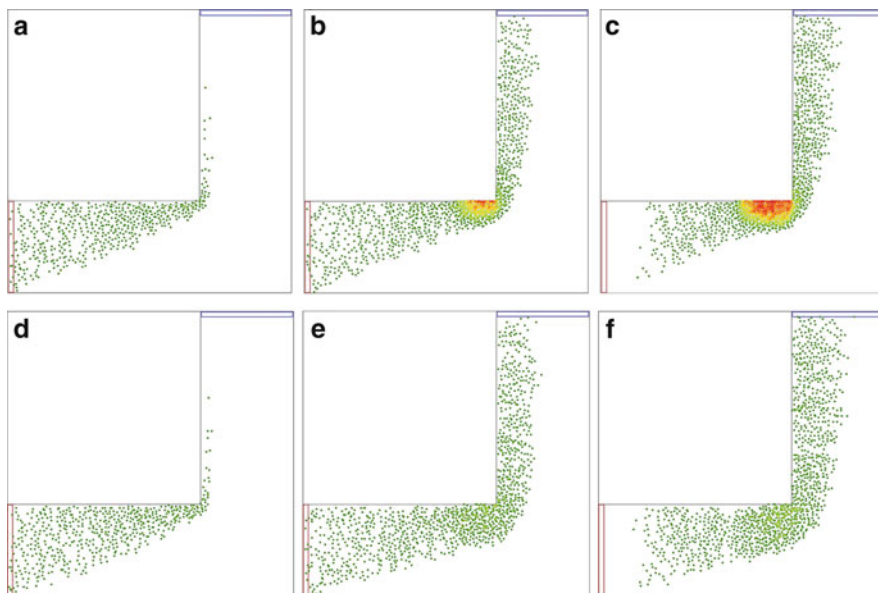


Fig. 2 Navigation around a corner – (a–c) navigation using a constant floor field and (d–f) navigation using a dynamic floor field (snapshots at different time steps are shown, the local density is encoded via colors)

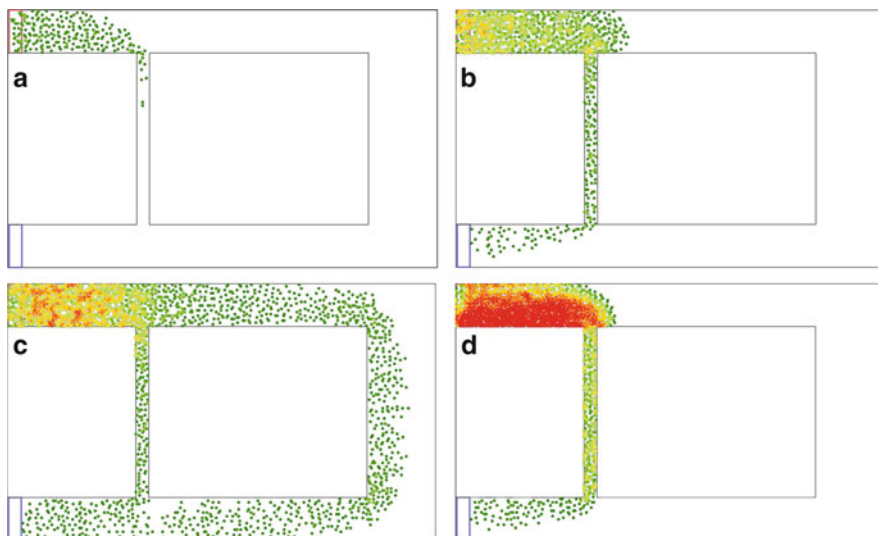


Fig. 3 Alternative routes – adopting a dynamic navigation field pedestrian choose the fastest way, (a–c) screenshots at different time steps are shown. (d) Adopting a constant navigation field pedestrians always choose the shortest way, the overall “egress time” is not optimal compared to (a–c); local density is encoded via color

3.2 *Extended Dynamic Floor Fields*

The concept introduced in Hartmann [8] considers pedestrians independent of their direction of walking. This is a shortcoming considering flows with multiple directions, e.g. pedestrian streams in two directions in a corridor. In general, one would expect that pedestrians walking in the same direction are not as “repellent” as pedestrians walking in the opposite direction. This is typically realized in short scale navigation, e.g. in force based models [12], but not in medium scale navigation. In the following the original concept is extended accordingly to include such effects.

To consider the influence of different walking directions on navigation behavior, we group pedestrians according to their current (intermediate) destinations. Since the directions of walking is by construction of the algorithm (c.f. Sect. 2) always down the gradient of the navigation field, all pedestrians sharing the same navigation field also walk into the same direction.

Following this idea, we propose to use

$$F_D(x, y) = \frac{1}{c_D \rho_D(x, y) + c_{D'} \rho_{D' \neq D}(x, y)} \quad (3)$$

instead of Eq. 2 for determining the navigation floor field for a destination D in the Eikonal Eq. 1. Thus densities of pedestrians $\rho_D(x, y)$ sharing the same destination D are considered differently than densities of pedestrians $\rho_{D' \neq D}(x, y)$ having a different destination $D' \neq D$. We assume that following pedestrians with a different destination is significantly less attractive than following pedestrians with the same destination, i.e. $c_D < c_{D'}$. The short range pedestrian repulsion is adopted accordingly: pedestrians with the same destination have a smaller repulsion than pedestrians with a different destination.

Adopting this extension of the navigation concept, the cellular automaton model of Köster et al. [17] does not only reproduce significantly more realistic navigation behavior but also naturally reproduces lane formation. The increased realism is shown by simulating various example scenarios, among them scenarios involving lane formation as described in Helbing et al. [10].

4 Self-organization Phenomena

In the following we will consider a number of scenarios to underline the increased realism of the proposed approach. These include the navigation around a corner, pedestrians taking detours due to congestions as well as various scenarios involving lane formation.

4.1 Navigation Around a Corner

Most classical microscopic pedestrian simulators suffer from unrealistic navigation behavior around corners in the case of high pedestrian densities: On a medium scale, pedestrians choose the shortest path closely around the corner. Thus pedestrian flows concentrate at the corner. Since interaction with other pedestrians is considered only on a small scale (a few meters) other pedestrians at the corner are realized too late such that congestions occur (c.f. Fig. 2a–c).

Using a dynamic update of the navigation field other pedestrians are included already on a medium scale navigation decision and congestions are avoided. This leads to a significantly more realistic navigation behavior as shown in Fig. 2d–f. Since in this example all pedestrians share the same destination, the advantage of more realistic navigation should at least principally be captured by any dynamic floor field method, e.g. [19].

4.2 Navigation Considering Other Pedestrians

The example considered above included only slight variations of paths due to higher pedestrian densities, i.e. congestions. Taking this concept to the extreme, pedestrians also automatically consider detours if they can optimize their travelling time by doing so. A corresponding simulation for an example scenario is shown in Fig. 3a–c (snapshots at different time steps). In comparison to a static navigation floor field (c.f. Fig. 3d) pedestrians take detours. Since we again consider only a single destination, a similar behavior should be recovered in any microscopic pedestrian simulator using dynamic floor fields.

4.3 Lane Formation in Resting Crowds

The two examples considered above involve only a single destination and thus we expect that all pedestrians move in the same direction. In the following, we will consider scenarios with pedestrians travelling in different directions, i.e. pedestrians having different destinations. One of the most common phenomena observed in this case is lane formation (Helbing et al. [10] and references therein).

As a first example of such a scenario we are considering pedestrians moving through a standing crowd, e.g. during an open air event. The corresponding simulations are shown in Fig. 4 (snapshots at two different time steps). One can clearly observe that paths through the standing crowd are developed. Once a certain path has established it remains relative stable since from a navigation point this path is also preferable for following pedestrians.

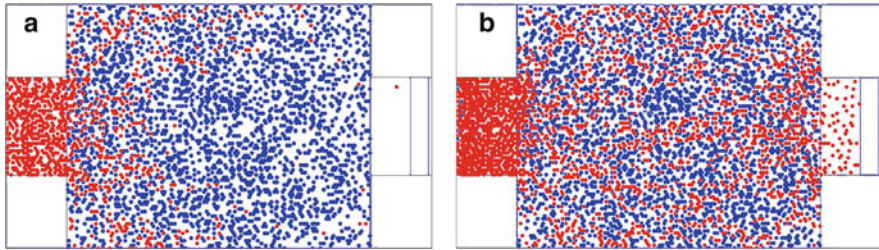


Fig. 4 Lanes forming due to pedestrians moving through a resting crowd (snapshots at two different time steps, destinations are encoded by color)

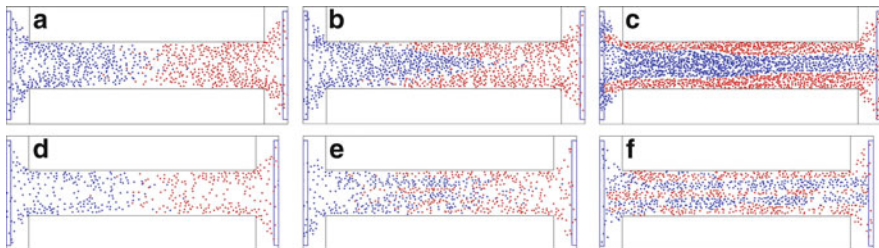


Fig. 5 Lane formation at and different densities – figures (a–c) correspond to a flux of 10 pedestrians/s for each origin and figures (d–f) to a flux of 5 pedestrians/s (screenshots at different time steps, destinations are encoded by color)

4.4 Lane Formation in Corridors

A similar behavior is found in corridors with two pedestrian streams moving in opposite directions. Below we consider a standard scenario as suggested in [10] for two different inflows. The results are shown in Fig. 5. As expected lane formation is observed. The lanes are robust and are persisting for a long time.

Considering inflows of different strength (Fig. 5a–c vs. d–f), we find that the number of lanes developing depends on the inflow of pedestrians. A more detailed investigation on this dependence is a topic of future research. A similar study for a social force model has revealed that for open boundary conditions lanes are dynamically varying. Their number depends on the width of the street, on pedestrian density, and on the noise level (Helbing et al. [10] and references therein).

Summarizing, we conclude that the new approach supports lane formation which cannot be observed in standard cellular automaton approaches to pedestrian flows. Typically, it is required that an additional floor field has to be introduced [3].

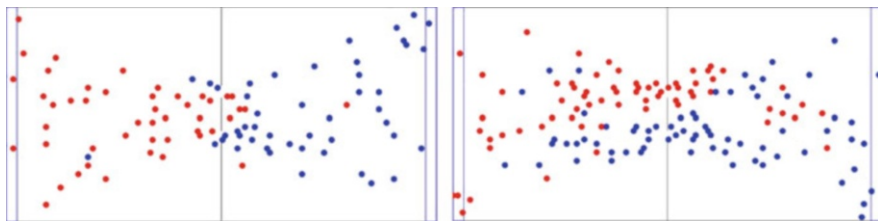


Fig. 6 Lane formation in a narrow passage of two doors (snapshots of two different time steps, destinations is encoded by color)

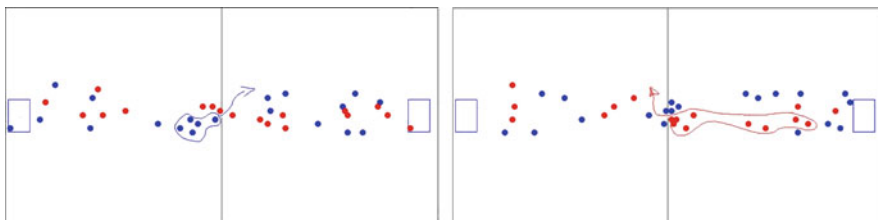


Fig. 7 Oscillations at a narrow passage (snapshots of two different time steps, destinations are encoded by color)

4.5 Lane Formation in Narrow Passages of Two Doors

Similarly lane formation is reproduced in a narrow passage of two doors – a common phenomenon which can be observed in every day live. Snapshots of our simulation at two different time steps are shown in Fig. 6.

4.6 Oscillations at Narrow Passages

In addition to lane formation [10] oscillations at narrow passages are a typical phenomenon in pedestrian crowds. At bottlenecks, like doors, oscillatory changes of the passing direction are typically observed, if people do not panic (Helbing et al. [10] and references therein). Therefore, we also investigate the pedestrian flows at narrow passages within our approach.

The results of a corresponding simulation are shown in Fig. 7. However, oscillations are not profoundly developed and can be only be sensed in an interactive visualization. Thus we conclude that further investigations as well as an extension of the model seem to be necessary.

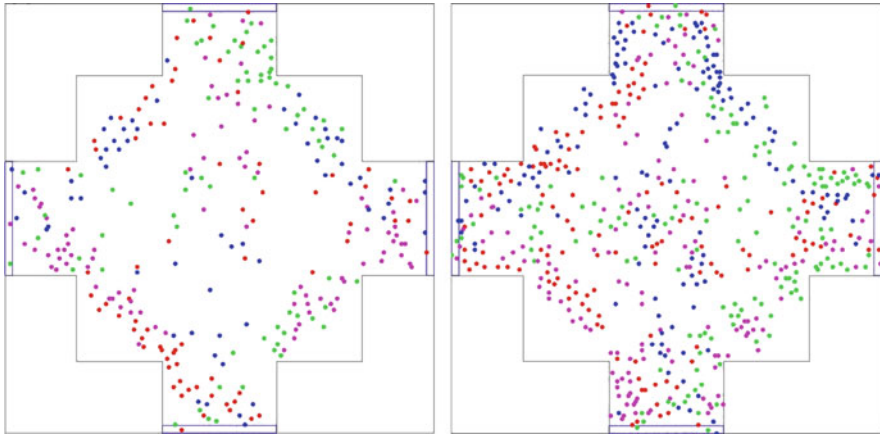


Fig. 8 Interaction of pedestrians at a crossing (snapshots at two different time steps, destinations are encoded by color)

4.7 Intersections

Furthermore, we consider pedestrian streams crossing at intersections, another example suggested by [10]. At intersections one is confronted with various alternating collective patterns of motion which are very short-lived and unstable. For example, phases during which the intersection is crossed in “vertical” or “horizontal” direction alternate with phases of temporary roundabout traffic. Similar behavior could be also seen in our simulations however due to the involved complexity further detailed studies are required (Fig. 8).

5 Discussion and Outlook

Within this work we have introduced a new dynamic medium scale navigation concept based on floor fields. The concept extends the approaches proposed independently by Kretz [8] and Hartmann [19] to explicitly take account of different pedestrian walking directions similar to small scale navigation (e.g. Helbin and Mólнар [12]). Using the cellular automaton model introduced in Köster et al. [17], we have considered several example scenarios to underline the improvement in realism of simulations. On the one hand, considering other pedestrians in a dynamic update of the navigation field, the navigation around corners and in complex domains with multiple corridors is improved (as studied by Hartmann [8]). On the other hand, considering simultaneously the walking directions of pedestrians by means of their destinations, also lane formations could be observed. Whether

the oscillations at doors and typically observed phenomena at intersections can be reproduced is still under active research.

Typically dynamic floor field methods require extensive computational resources (especially for large domains), being a severe disadvantage compared to static floor field methods. However, recently we have shown that the efficiency of dynamic floor field methods can be significantly improved using various strategies, including grid adaptation [9] as well as coupling with macroscopic graphs [16]. Adopting these strategies, dynamic floor field methods now only require little more effort than classical static floor field methods.

Under current research is the application of the outlined methods to much larger scales namely the regional evacuation as investigated in the REPKA project [24]. Especially in emergency situations where dense crowds with multiple directions are expected, we believe that the methods introduced in this article significantly improve the realism of microscopic simulations.

Acknowledgements The authors would like to thank the German Federal Ministry of Education and Research who funded our research through the priority program *Schutz und Rettung von Menschen* within the project REPKA – Regional Evacuation: Planning, Control and Adaptation [24].

References

1. Bellomo, N. & Dogbe, C. (2011): On the modeling of traffic and crowds: A survey of models, speculations, and perspectives. *SIAM Rev.* 53, 409–463.
2. Blue, V., Embrechts, M. & Adler, J. (1997): Cellular automata modeling of pedestrian movements. *IEEE Int. Conf. on Systems, Man and Cybernetics*.
3. Burstedde, C, Klauck, K., Schadschneider, A. & Zittarz, J. (2001): Simulation of pedestrian dynamics using a two-dimensional cellular automaton. *Physica A: Statistical Mechanics and its Applications* 295: 507–525.
4. Chraïbi, M., Seyfried, A. & Schadschneider, A. (2010): Generalized centrifugal force model for pedestrian dynamics. *Phys. Rev. E* 82. 046111.
5. Chraïbi, M., Kemloh, U., Schadschneider, A. & Seyfried, A. (2011): Force-based models of pedestrian dynamics. *Networks and Heterogeneous Media* 6, 425–442.
6. Davidich, M.I. & Köster, G. (2012): Verification of Pedestrian Stream Models Based on Video Analysis. *PED 2012*.
7. Davidich, M.I., Mayer, H., Royer, C. & Pfaffinger, A. (2012): Modelling of Waiting Zones. *PED 2012*.
8. Hartmann, D. (2010): Adaptive pedestrian dynamics based on geodesics. *New Journal of Physics* 12 (4), 043032.
9. Hartmann, D. & Hasel, P. (2011): Efficient floor field methods for microscopic pedestrian crowd simulations. Submitted
10. Helbing, D., Molnár, P., Farkas, I. & Bolay, K. (2001): Self-organizing pedestrian movement. *Environment and Planning B: Planning and Design* 2001 (28), 361–383.
11. Helbing, D. (2001): Traffic and Related Self-Driven Many-Particle Systems.
12. Helbing, D. & Molnár, P. (1998): Social force model for pedestrian dynamics. *Physical Review E* 51: 4282–4286.

13. Huang, H.-J. & Guo, R.-Y (2008): Static floor field and exit choice for pedestrian evacuation in rooms with internal obstacles and multiple exits. *Phys. Rev.* 78, 021131.
14. Kirik, E., Yurgelyan, T. & Krouglov, D. (2009): The shortest time and/or the shortest path strategies in a CA FF pedestrian dynamics model *J. Siberian Fed. Univ. Math. Phys.* 2 271–8.
15. Klüpfel, Hubert (2003): A cellular automaton model for crowd movement and egress simulation. PhD-Thesis Universität Duisburg-Essen.
16. A. Kneidl, D. Hartmann, A. Borrmann : A hybrid multi-scale approach for simulation of pedestrian dynamics, *Transportation Research Part C: Emerging Technologies*, Volume 37, December 2013, Pages 223–237
17. Köster, G., Hartmann, D. & Klein, W. (2010): Microscopic pedestrian simulations: From passenger exchange times to regional evacuation. *Operations Research - Mastering complexity.*
18. Köster, G., Treml, F., Seitz, M. & Klein, W. (2012): Validation of crowd models including social groups. *PED 2012.*
19. Kretz, T. (2009): Pedestrian traffic: on the quickest path. *Journal of Statistical Mechanics: Theory and Experiment 2009*, P03012
20. Mayer, H., Hartmann, D., Klein, W. & Zechlin, O. (2012): Influence of emissions on pedestrian evacuation. *PED 2012.*
21. Nishinari, K., Kirchner, A., Namazi, A. & Schadschneider, A (2004): Extended floor field CA model for evacuation dynamics. *IEICE Trans. Inf. Syst.* E87D, 726–732.
22. Parisi, D. R., Gilman, M. & Moldovan, H. (2009). A modification of the social force model can reproduce experimental data of pedestrian flows in normal conditions. *Physica A* 388: 3600–3608.
23. Pelechano, N., Allbeck, J. M. & Badler, N. (2008): *Virtual crowds: Methods, simulation, and control.* Morgan & Claypool Publishers.
24. REPKA (2012): Regionale Evakuierung: Planung, Kontrolle und Anpassung. <http://www.repka-evakuierung.de>
25. Reuter, V., Bergner, B., Köster, G., Seitz, M., Treml, F. & Hartmann, D. (2012): On Modeling Groups in Crowds: Empirical Evidence and Simulation Results Including Large Groups. *PED 2012.*
26. Schadschneider, A., Klingsch, W., Klüpfel, H. and Kretz, T., Rogsch, C. & Seyfried, A. (2009): Evacuation dynamics: Empirical results, modeling and applications. *Encyclopedia of Complexity and System Science*, 3142–3176.
27. Seitz, M., Köster, G. & Pfaffinger, A. (2012): Modeling pedestrian group behavior in a cellular automaton. *PED 2012.*
28. Sethian, J.A. (1999): *Level Set Methods and Fast Marching Methods.* Cambridge University Press.
29. Weidmann, U. (1993): *Transporttechnik der Fussgänger: Transporttechnische Eigenschaften des Fussgängerverkehrs (Literaturauswertung).* Schriftenreihe des IVT, ETH Zürich.

Effect of Social Groups on Crowd Dynamics: Empirical Findings and Numerical Simulations

Dirk Oberhagemann, Rainer Könnecke, and V. Schneider

Abstract In 2009 a joint research project titled EVA started. It finished in Mai 2012 and covered various research topics related to risk assessment, planning and organization of large scale events. This paper will focus on empirical data collection and analysis and its use for the calibration and validation of the microscopic evacuation and pedestrian dynamics model ASERI. The empirical data presented here was collected at various large festivals and similar events like public viewing or championship celebrations. The focus is on established average and peak population densities. Extensions introduced into the ASERI simulation software as part of the EVA project include effects of group formation and group movement. Social groups in size of up to 6 persons are frequently present during public events. Quite often such groups comprise the majority of visitors. Walking behaviour and crowd flow of social groups differs considerably from those of single pedestrians. A fundamental diagram of walking velocity versus density of people could be derived from the analysis of the empirical data showing a considerable reduction in walking speed with increasing group size. This empirical findings can be reproduced by numerical simulations with the ASERI model.

Keywords Large scale events • Crowd movement • Social groups • Microscopic simulation • Fundamental diagram • Population density

D. Oberhagemann
German Fire Protection Association vfdB e.V., Altenberge, Germany
e-mail: info@vfdb.de

R. Könnecke (✉) • V. Schneider
IST GmbH, Frankfurt, Germany
e-mail: r.koennecke@ist-net.de; v.schneider@ist-net.de

1 Introduction

Major large scale events like public viewing, open air concerts or large festivals make high demands on all responsible parties, especially with respect to human safety. From disasters that occurred in the past it can be concluded that crowd incidents with serious consequences to life and health of people can have a variety of causes. So it is not possible to focus on emergency situations alone, but it is required to analyse a large number of scenarios in the forefront of such large scale events. Usually, such scenarios will comprise high density crowd movement. In order to define and assess scenarios for reliable safety concepts it is necessary to obtain significant information on limiting factors like number of visitors (including timed and peak data), available space (including information of the position of stalls, stages, locked areas, barriers, areas reserved for emergency groups and staff members) and behavioural aspects (including external effects like weather condition and its possible impact on the event). Hence a joint research project titled EVA (Risiko Großveranstaltungen – Planung, Bewertung, EVakuierung und Rettungskonzepte) was established in order to define and analyse relevant design parameters [1, 2]. The EVA project started in March 2009 and will be finish by end of Mai 2012. This paper will focus on empirical data collection and analysis of crowd movement at large scale events and its use for the calibration and validation of the microscopic evacuation and pedestrian dynamics model ASERI, with emphasize on the influence of social groups on crowd dynamics.

A large amount of data – mainly in the form of video recordings – was collected by Dirk Oberhagemann and his vfdb team. Further empirical input was provided by the Disaster Research Agency – Institute for Sociology of the Christian Albrechts University in Kiel and the Institute of Fire and Emergency Technologies (IFR Dortmund). While the data analysis from the vfdb group was essentially manually, the Fraunhofer-Institute for Chemical Technology ICT contributed computerized digitalization, filtering and visualization techniques. IST was responsible for model development and numerical simulations. A summary of empirical findings and related numerical simulations was published as a Technical Report by the German Fire Protection Association vfdb [3].

2 The ASERI Evacuation and Crowd Flow Model

ASERI is a computer model designed to simulate egress movement of people in geometrically complex spaces of arbitrary size, circulation of people (e.g. in large shopping malls or in commuter and passenger systems). The simulation is performed on a microscopic basis. Occupant movement is modelled continuous in space, based on the current individual orientation, unrestricted walking speed and available egress route choice options. Density effects are modelled on a fundamental behavioural basis and not by explicit (empirical) velocity vs. density relations. Exposure to asphyxiates, heat and smoke can be considered if required.



Fig. 1 Fifty-five thousand visitors distributed at the Cranger Kirmes area

Individual decisions and related actions may contribute to a delay in starting the evacuation or cause interrupts, especially in the initial phase of the evacuation process. Furthermore, egress route choice is strongly influenced by individual aspects like knowledge of the building layout or smoke tolerance. Certain features of behavioural response are modelled in a probabilistic manner rather than a deterministic way. This probabilistic approach allows for a more profound evaluation of the evacuation process by performing a number of replicate runs for a given scenario.

Body size is defined by shoulder and chest width, according to the concept of body ellipse modelling the horizontal projection of a human body. A minimum inter-person distance and the maintenance of a boundary layer clearance from walls and stationary obstacles is implemented. Beside its standard mode (“egress”) ASERI supports an additional “danger” mode allowing for smaller and a mode for “comfortable” walk with larger layer clearance and inter-person distances. Shoulder and chest width can be assigned individually, either by explicit input or by specifying a distribution appropriate for the respective population. By introducing effective size parameters, this concept allows for the definition of agents with increased space requirement, including persons with limited mobility or occupants with luggage.

The geometrical scenario (buildings, facilities or urban units) is defined in a hierarchical way, based on interconnected levels. Each level is further subdivided using enclosures, rooms, corridors, stairs, ramps, ladders, tiers and safe areas as basic units. Obstacles, seat rows, recesses or signage and lighting can be specified inside units. It is therefore possible to model very large and geometrically complex buildings or spaces with tens of thousands of occupants (agents) moving simultaneously. Examples for the application of ASERI to large scale events can be found in [4, 5]. Figures 1 and 2 illustrate the simulation of crowd movement with ASERI for a hypothetical egress scenario at the Cranger Kirmes, a festival that has been studied by members of the EVA project.

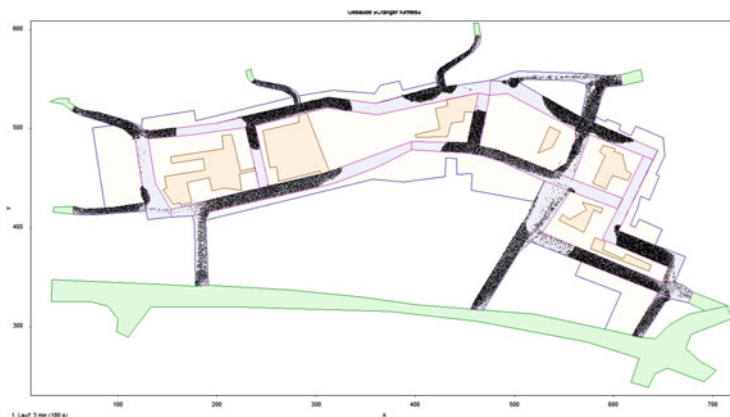


Fig. 2 Congestion at radial streets 5 min after start of egress movement

Within the EVA project, ASERI has been extended to include phenomena like counter-flow, effects of variable barriers and the movement of groups. The increase in population required to model large scale events could be handled by introducing parallelization techniques. The generation of 3D-models of urban spaces is now possible by transferring KLM-data (e.g. from Google Earth or OpenStreetMap) directly into ASERI layouts.

3 Population Densities at Large Scale Events

German codes and standards usually do not provide quantitative prescriptions on acceptable or required population density. The only exceptions are the German Assembly Code (MVStättV) yielding a number of 2 persons/m² for assemblies as a basis for egress analysis and the German Traffic regulations (StVO) allowing an occupant density of 8 standing persons per square meter in buses. While similar numbers for assemblies can be found in international standards, the accepted occupant density for buses lacks any scientific justification. In addition, the German vfdb Guideline “Methods of Fire Safety Engineering” [6] includes recommendations of population densities to be used for egress analyses for a multitude of occupancies, compiled from various international sources. In this Guideline a number of 5 standing persons/m² is recommended for the design of assemblies.

These numbers can now be compared to observations at large scale events. The analysis of videos and photographs from large festivals and similar public events yields maximum population densities of 5–6 persons/m². Usually, the population density does not exceed 4 persons/m² and the average value (related to the total accessible assembly area) is below 2 persons/m². These population densities describe voluntary positioning, not enforced situations. These investigations also



Fig. 3 Public viewing at soccer WM 2006 – marked area with 5 persons/m²

demonstrated the difficulty to estimate population densities from reported visitor numbers, even if the average dwelling time is known with reasonable accuracy. The reported total number of visitors quite often exceeds the actual number by a factor of 2 and more. The observed population densities are consistent with physiological models of projected surface area as a function of size and body-mass-index.

Figures 3 and 4 illustrate static and dynamic population densities close to the observed limits. The critical value for a dynamic population density is located by about 6 persons/m². Values that high were observed in the Dortmund railway station when it had to be closed due to overcrowding during the Dortmund Loveparade in 2008.

4 The Effect of Group Movement on Crowd Dynamics

From observations of large scale events it was possible to obtain empirical data on typical group size distributions (Table 1) and average walking speed of single pedestrians and social groups depending on local population density (Fig. 6).

Within the EVA project a group formation and group movement model was implemented into the ASERI simulation tool. In a typical scenario including social groups the group members are initially located at close vicinity to each other, while the group as a whole is placed at a random position within the simulation area. The group velocity is governed by the minimum unrestricted walking speed of the individual group members. This group velocity limits the unrestricted walking



Fig. 4 Entrance to public viewing area – marked area with 4 persons/m²

Table 1 Typical distribution of group sizes at large festivals (*F* female, *M* male)

Group size	Number	Persons	Total population (%)
Single (1)	133	133	5
Group M/M (2)	114	228	8
Group M/F (2)	406	812	27
Group F/F (2)	202	404	14
Group (3)	199	597	20
Group (4)	129	516	17
Group (≥ 5)	53	265	9
Total	1,236	2,955	100

speed of all group members. In order to model the dynamics of group coherence in a crowded environment, social affiliation is an important factor. ASERI includes four types of interpersonal relations: mutual positive, mutual negative, asymmetric (e.g. parent–child combinations) and neutral (no specific social relation). These relations define the range of mutual interpersonal distances that are tolerated without violating the coherence of the group. If due to the movement of other people in a crowded situation the interpersonal distance exceeds the respective tolerable limit, the group members further ahead will slow down or even wait until group coherence is again established. This leads to a further slowing down of the effective group velocity, defined as the velocity measured with respect to the actual path length covered by the group members and the required time interval.

An important test case for the validation of the dynamic group model of ASERI is the calculation of the fundamental diagram – the walking speed as a function of population density – for various group sizes. Using the relative distribution of group size and solitary pedestrians presented in Table 1 the fundamental diagram

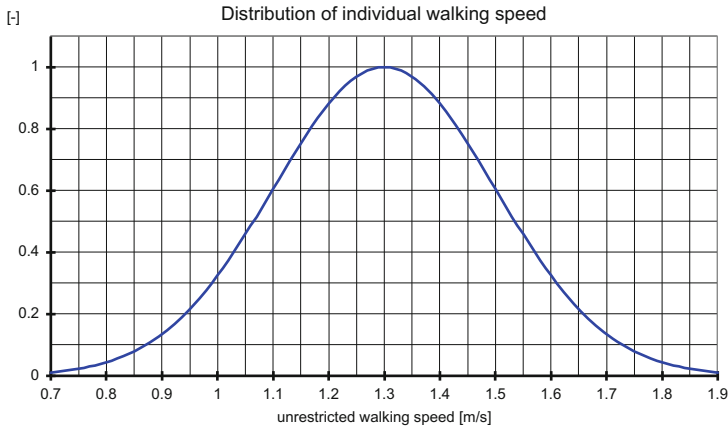


Fig. 5 Distribution function for individual unrestricted walking speed

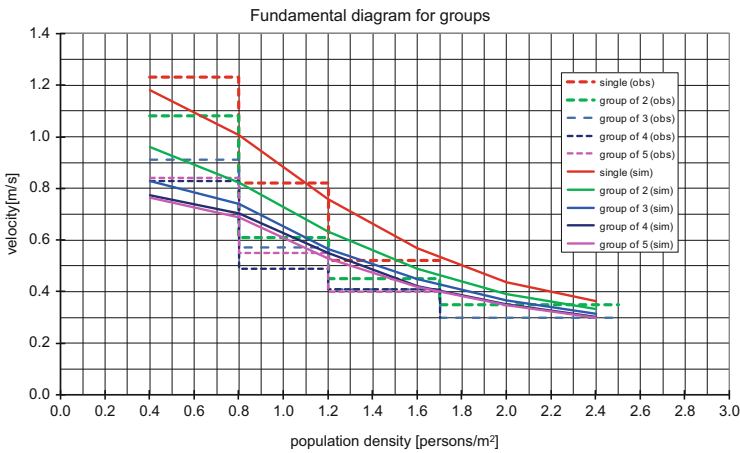


Fig. 6 Fundamental diagram (simulation vs. observation) for various group sizes

is calculated for a section of a promenade (width 11 m, length 120 m). The initial population density varies between 0.4 persons/m² and 2.4 persons/m². People are assumed to walk into one direction (no counter-flow). The average unrestricted walking speed of the population is 1.3 m/s. The individual unrestricted walking speed is determined according to the distribution function shown in Fig. 5. Individual body size is determined according to the standard distribution of ASERI recommended for evacuation simulation for a general population type.

The following interpersonal relations are assumed for the respective groups: 50 % of the relations to other group members are of the type “mutual positive” and 50 % of the “neutral” type. The minimum interpersonal distance to a group member is 1 m for type “mutual positive” and 5 m for “neutral”. With this set of

parameters the fundamental diagram shown in Fig. 6 is derived. The dashed lines in Fig. 6 indicate the observed walking speeds for certain ranges of population density. The straight lines are the corresponding simulation results. There is a very good agreement between observation and numerical simulation.

5 Summary

Within the joint EVA research project, established population densities at large scale events and the effect of group formation on crowd movement were investigated. Observed peak densities of up to 5 persons/m² are consistent with physiological models and typical design parameters found in national and international guidelines.

It was possible to derive a fundamental diagram of walking speed versus population density for various group sizes. The empirical findings could be reproduced by the group dynamic model implemented into the ASERI simulation software.

The research project “Risiko Großveranstaltungen – Planung, Bewertung, EVakuierung und Rettungskonzepte – EVA” is sponsored by the German Bundesministerium für Bildung und Forschung BMBF (Förderkennzeichen 13 N10300).

References

1. Könnecke, R., Schneider, V.: Risk management at major events - Study of behavioral aspects and implementation into the ASERI microscopic evacuation model. In: Proceedings 5th International Conference on Pedestrian and Evacuation Dynamics (PED), Gaithersburg, MD USA, 8.–10. März 2010
2. Schneider, V., Könnecke, R.: Microscopic modelling of crowd movement at major events. In: Proceedings Interflam2010, Fire Science & Engineering Conference, Nottingham, UK, July 2010
3. Oberhagemann, D. (ed.): Statische und dynamische Personendichten bei Großveranstaltungen. vfdB Technischer Bericht TB 13–01, März 2012
4. Schneider, V.: Simulating the Evacuation of Large Assembly Occupancies. In: Proceedings of the 2nd International Conference on Pedestrian and Evacuation Dynamics, University of Greenwich, London (2003), pp. 319–330
5. Hosser, D., Forell, B. and Schneider, V.: Sicherheit in deutschen Stadien und Arenen - eine Nachlese. In: vfdB-Zeitschrift 1 (2007), pp. 33–42
6. Hosser, D. (ed.), Leitfaden “Ingenieurmethoden des Brandschutzes”, vfdB TB 04/01, 2. Auflage Mai 2009

Estimating PCE-Type Factors for Heterogeneous Pedestrian Traffic Using Simulation

Ronald John Galiza, Luis Ferreira, and Phil Charles

Abstract Similar to vehicle traffic, pedestrian flow can also be classified as heterogeneous. This paper introduces the concept of equivalent factors for converting mixed older adults and commuter pedestrian flow into equivalent commuter flow. The methodology employed was derived from vehicle passenger car equivalent (PCE) methodologies. Pedestrian micro-simulation models are utilized to generate data for the pedestrian time-space (TS)-flow relations where flow equivalency is derived. Data for the model input and calibration and validation were collected for commuter-only traffic and older adult and commuter combination. Results from the model were used to create the TS-flow relationship and pedestrian equivalent factors calculated. An application of the equivalent factor illustrates the importance of considering heterogeneity in pedestrian walkway design. This methodology can be adopted to compute other equivalent factors for other pedestrian types considering local pedestrian characteristics.

Keywords Heterogeneous traffic • Older adult • Commuter • Pedestrian equivalent • Micro-simulation • Time-space

R.J. Galiza (✉)

School of Civil Engineering, The University of Queensland, Brisbane, Australia

Institute of Civil Engineering, University of the Philippines, Quezon City, Philippines

e-mail: r.galiza@uq.edu.au; rjsgaliza@gmail.com

L. Ferreira • P. Charles

School of Civil Engineering, The University of Queensland, Brisbane, Australia

e-mail: L.Ferreira@uq.edu.au; P.Charles@uq.edu.au

1 Introduction

Vehicle traffic does not always consist of passenger cars but also recreational vehicles, buses, and trucks. Vehicles taking up more space and have lower performance (especially uphill) result in a reduction in vehicle throughput. This diversity issue is resolved by converting the heterogeneous flow into an equivalent passenger car flow using passenger car equivalent (PCE) factors. This calculation is relevant to capacity and LOS determination, lane requirements, and determining the effect of traffic on highway operations.

Similarly, pedestrians having varied capabilities and body sizes can also be classified as heterogeneous. Most pedestrian facilities design guides suggest some form of adjustment in order to consider the effects of those who occupy larger spaces and those carrying large items and walk slower. This paper introduces the concept of pedestrian equivalent factors using micro-simulation techniques. The aim of which is putting forward a standard methodology for dealing with heterogeneous pedestrian flow like the PCE methodology.

This paper is organized as follows. The next section briefly discusses past work on how pedestrian diversity is tackled in design followed by the PCE methodology adapted in Sect. 3. The succeeding section details the field data collection, the micro-simulation set-up, and the model calibration and validation process. The pedestrian equivalent factors are then calculated utilizing modeling results followed by an illustration of the potential application of the method to the design of pedestrian facilities. The paper ends with a presentation of the relevant findings and recommendations for future investigation.

2 Past Work on Pedestrian Diversity in Design

An attempt in considering the effect of heterogeneity in pedestrian traffic was suggested by the Highway Capacity Manual (HCM) [1] wherein if 0–20 % of pedestrians are elderly, a design walking speed of 1.2 m/s is recommended while 1.0 m/s for percentage more than 20 %. Teknomo [2] in his theoretical experiments found that the average speed of the system decreased logarithmically as the percentage of elderly pedestrian increases. Pauls [3] suggesting considering increasing sidewalk and passageway widths to accommodate enlarged lateral dimensions and sway behavior caused by slow movement speeds of the elderly and obese.

Only a few studies have recognized the importance of pedestrian diversity in facilities' design [1, 4–6]. An attempt to devise similar factors for luggage-laden pedestrians in airports was explored by Davis and Braaksma [5]. Particularly, the Transit Capacity and Quality of Service Manual (TCQSM) which is the transit counterpart to the HCM, contains quantitative techniques for calculating passenger circulation and level-of-service (LOS) in transit stations or terminals [7]. Because the basis for the LOS guides were derived from primarily commuter traffic, an

adjustment factor is recommended to account for pedestrians who use additional space, such as wheelchair users, those transporting large items and pedestrians who use service animals [6]. Generally, no consensus or standard procedure for tackling pedestrian heterogeneity in design has been proposed. Taking the lead from vehicle traffic, a similar methodology is explored in this paper for hypothetical pedestrian traffic scenarios.

3 Adapted PCE Methodology

The approach proposed by Huber [8] for the case of a traffic stream containing passengers cars and only one type of truck was adapted for estimating pedestrian equivalent factors. He quantified the effect of trucks by relating the traffic flows for the same performance measure (e.g. density, speed, delay, etc.). For example, if total travel time is the performance measure employed, a total travel time-flow relationship could be used to relate the traffic flows at equal travel time values with and without trucks. In an initial study by [9], it was found that total travel time measure exhibit little sensitivity to variations in pedestrian spatial characteristics. To address the issue, a time-space (TS) measured was recommended.

The TS concept was first introduced as a method for analyzing sidewalk corners and crosswalks [10]. This method is typically recommended for application in any facility where pedestrian activities (waiting, queuing, walking and processing) occur. Benz [11] expanded the use of the method to examine pedestrian activities in waiting and circulation areas of transportation terminals. Basically, the method was used to compare the total amount of time and space people utilize (demand) for different activities (waiting, queuing, walking or processing) against the total time-space available for a particular pedestrian facility. In addition to being utilized across pedestrian activities, Benz [11] recommends use across different groups of pedestrians within the total population of users wherein characteristics can be included separately. The system demand is the product of the number of pedestrians, space (area) occupied and the time it is occupied, as shown in Eq. 1. This equation was utilized to develop the TS-flow relationships which form the basis for the equivalency factors.

$$TS_{demand} = \sum P_i \times S_i \times T_i \tag{1}$$

where:

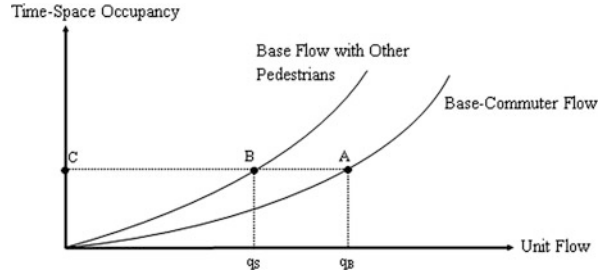
TS_{demand} = time-space required/occupied (m²-s)

P_i = number of pedestrians involved in activity (e.g. walking) in group i

S_i = space (required) occupied per pedestrian in group i

T_i = average time (walking) in analysis area per pedestrian in group i.

Fig. 1 Time-space (*TS*) occupancy as a function of flow (Adapted from Huber [8])



In the context of heterogeneous pedestrian flow, different types of pedestrians demonstrate variations in physical and operational characteristics and therefore use differing amounts of *TS* (in terms of ped-m²-s or ped-m-s) in a walking facility. Temporally, slower pedestrians require more time to pass through a walkway. Slower pedestrians also cause faster pedestrians to slow down and increase total walking time resulting in higher *TS* demands. Similarly, increased body size and the use of walking devices considerably increase the area occupied by pedestrians, amplifying *TS* demands. In estimating the *TS* demand, pedestrian traffic volume, body size distribution or average body size, and average travel time (or speeds through a section) are required.

Since any two points on a horizontal line in Fig. 1 have equal value of the performance measure, the sum of the products of corresponding flows and pedestrian equivalents is constant. The resulting relationship will then produced,

$$E_S = \frac{1}{p} \left(\frac{q_B}{q_S} - 1 \right) + 1 \tag{2}$$

where:

- E_S = pedestrian equivalent factor of the other pedestrian type
- p = proportion of other pedestrian type in mixed pedestrian flow
- q_B = base pedestrian flow rate
- q_S = equivalent flow rate for mixed pedestrian flow

The procedure for the determination of the flow rates q_B and q_S and E_S can be summarized in four steps, as adapted from Demarchi and Setti [12]:

1. Establish the relationship between *TS* occupancy and unit flow rate for the base stream, containing commuters only;
2. Establish a similar relationship (in step 1) for the mixed stream, containing $(1 - p)$ commuters and p other pedestrians;
3. Find equivalent flow rates q_B and q_S for the same *TS* values (at desired points) using linear interpolation; and
4. Calculate the other pedestrian’s equivalent factor E_S using Eq. 2.

4 Data Collection

The purpose of the data collection stage is to obtain the attributes for simulation model development. Independent data sets were collected for the model input and calibration and validation process. It is required that detailed attributes of pedestrian types be collected for the modeling exercise.

4.1 Model Input

Free-flow walking speeds defined in the form of probability distribution functions is one of the primary input variables for the micro-simulation models. The data were collected through a field study of different pedestrian types in walkway facilities in Brisbane, Australia in July 2010. Free-flow walking speeds were computed by recording the travel time of commuters and older adults on a predefined trap length on the walkway. The field study results are broadly in line with those from the literature. It was found that the average free-flow walking speed of commuters was 1.50 and 1.09 m/s for older adults. The values for commuters and older adults agree with Fitzpatrick's field study results [13].

4.2 Validation Data

In order to calibrate and validate micro-simulation models composed of different pedestrian types, field data comprising the same type of pedestrians need to be collected. A video survey of pedestrian traffic stream composed of adults and older adults was conducted on a walkway near the Royal National Agricultural (RNA) Showground in Brisbane, Australia. This was conducted during the Queensland Caravan and Camping Show in June 11–15, 2010. This event was chosen because of the increased number of older adults attending. The pedestrian walkway was located between buildings hosting the event. The digital video recording equipment was located in clear view of a predefined box within the video line of sight. The dimension of the box measured 3.5 m by 3 m (walkway width). Three hours duration of video data was collected.

The recorded videos of pedestrian movements were played back and data manually extracted in the computer. There were four groups of data collected corresponding to four micro-simulation models. These groups were based on the data collected consisting of commuter traffic only and a combination of commuters and older adults. They include flows composed of commuters only, commuters with 10 % proportion (between 5 % and 15 %) of older adults, commuters with 20 % proportion (between 15 % and 25 %), and with 30 % older adults (between 25 % and 35 %).

Table 1 Validation data samples

Data group name	N	Variable	Mean	Std dev	Min	Max
Commuters only	80	Speed, m/min	72.36	9.03	38.40	90.00
		Density, ped/m ²	0.65	0.35	0.11	1.49
		Flow, ped/m-min	44.59	19.79	8.28	81.65
10 % older adults	38	Speed, m/min	60.33	6.08	43.80	70.20
		Density, ped/m ²	1.00	0.21	0.80	1.49
		Flow, ped/m-min	59.50	9.00	43.68	84.04
20 % older adults	41	Speed, m/min	59.80	7.54	44.40	76.20
		Density, ped/m ²	0.88	0.27	0.57	1.49
		Flow, ped/m-min	50.81	10.74	33.17	70.63
30 % older adults	47	Speed, m/min	59.90	5.60	49.80	73.80
		Density, ped/m ²	0.81	0.19	0.34	1.26
		Flow, ped/m-min	48.48	9.44	25.09	65.66

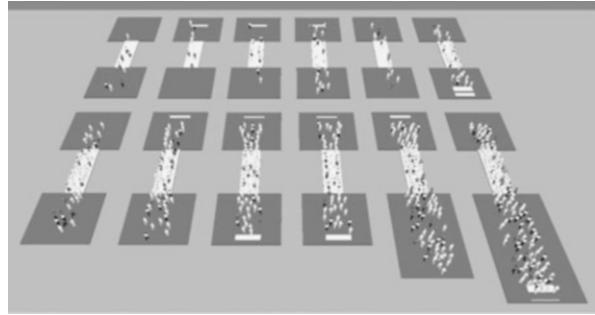
Table 1 describes statistics of the data groups described above for the validation. These statistics illustrate the ranges where the models can be applied across speed, density, and flow measurements. Statistics include mean, standard deviation, and the range for each group. The limited range of the data collected for the validation was handicapped by the limitation of the number of pedestrians that can be accommodated in the data collection set-up described above. A much more extensive data set will result in a bigger observation area (box) for the pedestrian combinations (commuters and older adults) in question.

5 Pedestrian Micro-Simulation

The analysis and design of exclusive pedestrian facilities require a myriad of data, design variables and inputs, computational methods and outputs making desktop analysis difficult. As a solution, computerized methods have been developed to investigate implications of various scenarios on complex transport terminals [14]. The popularity of micro-simulation has continued to grow in the past decade resulting in numerous software being developed. Making use of simulation models is a practical way of undertaking a study without the risk of injury to pedestrians. In addition, a computer-based simulation model allows introduction of a much greater number and variety of influencing microscopic factors across operational, physical, and behavioral characteristics (e.g. desired, speed, body sizes, type of facility, responses, aggressiveness, etc.). Pedestrian micro-simulation being an abstraction of reality must first be calibrated and validated before it can be used for prediction or other purposes.

Ideally PCE factors (as well as the proposed equivalent factors) are derived from flow relationships of field collected data covering various possible scenarios. In recent years, micro-simulation has been widely used in lieu of traditional analytical

Fig. 2 Pedestrian micro-simulation set-ups across flows



procedures [15–19]. If the pedestrian equivalency factors were to be developed using field data, sites with desired traffic flow rates and pedestrian compositions would have to be located. Ultimately, in developing the pedestrian equivalent factors for design purposes, actual field data should be collected.

The widely used micro-simulation model VISSIM [20] was used to test this proof of concept. VISSIM employs the ‘Social Force Model’ published by Helbing and Molnar [21] designed to represent the stochastic behavior of pedestrian movements. This pedestrian behavior model has been validated by researchers [22, 23]. VISSIM was chosen because separate pedestrian groups can be defined with their corresponding characteristics.

5.1 Micro-Simulation Set-Up

The experimental set-up was adapted from Campanella et al. [4] and expanded to three flat walkway test beds in order to consider the effect of walkway width. The first walkway measured 10 m by 1.5 m, the second 10 m by 3 m and the third 10 m by 4.5 m. Shown in Fig. 2 is the 3-m walkway width across 12 flow rates. The type of flow considered for factor estimation was unidirectional.

5.2 Traffic Variables Considered

PCE is believed to vary with prevailing traffic conditions (unit flow and proportion of other vehicles), geometric (width, grades, etc.), and control conditions (unidirectional or two-way). Similarly, pedestrian traffic is hypothesized to vary with respect to volumes, walkway widths, and proportion of other pedestrians. As such, various traffic variables are evaluated as defined in Table 2.

Table 2 Traffic variables considered in the simulation models

Traffic variable	Combinations
Unit flow rate (ped/m-min)	6, 12, 18, 23, 28, 33, 41, 49, 57, 66, 74, 82
Walkway widths (m)	1.5, 3.0, 4.5
Percent other pedestrians (%)	10, 20, 30

Table 3 Simulation scenarios

Model name	Older adults (%)	Body area (m ²)	Free-flow speed (kmh)
Commuter only	0	0.14 all	Commuter pdf
10 % older adults	10	0.14 all	Commuter pdf Older adults pdf
20 % older adults	20	0.14 all	Commuter pdf Older adults pdf
30 % older adults	30	0.14 all	Commuter pdf Older adults pdf

5.3 Model Scenarios

Table 3 details the scenarios replicated by the micro-simulation models corresponding to data collected in the previous section. The first model consists of commuter traffic only with uniform body size input and field-collected free-flow speed probability density functions (pdfs) of commuters. The other three models are combinations of commuters and older adults with older adult proportions of 10 %, 20 % and 30 % referred to as 10 % Older adults, 20 % Older adults, and 30 % Older adults, respectively. Free-flow speed pdfs for both commuters and older adults were used as input to the three latter models. Body size were kept uniform for both commuters and older adults as they are very much similar within the Australian population according to Kothiyal and Tettey [24].

6 Model Calibration and Validation

Before any pedestrian micro-simulation model can be utilized to evaluate situations targeted by the modeler, a comprehensive calibration process must first be implemented. This process involves the collection of real-world data for input and an iterative process to adjust software model parameters to increase model realism. The latter involves collecting data from observations of real pedestrians wherein average values or distributions of values (pdfs) are used as model input. The former, meanwhile, deals with changing pedestrian behavior parameters within the software, such that the micro-simulation results closely replicates real values. To be able to quantify the accuracy of the model in replicating field conditions, visual inspection

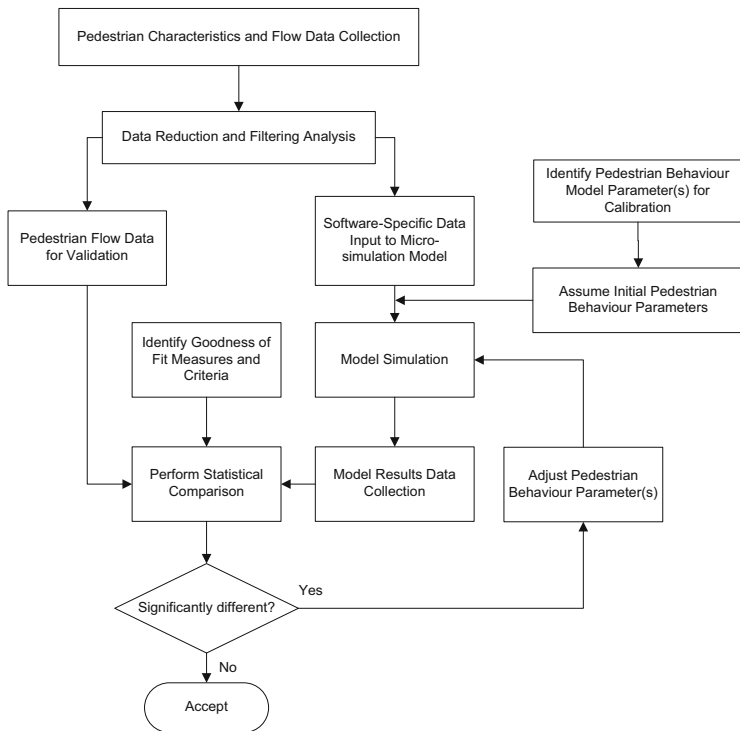


Fig. 3 Pedestrian simulation model calibration and validation framework

or use of statistical analysis can be employed. This process of comparing model results versus observed data is called validation. Visual inspection employs plotting the model results and observed data into a single graph. Model acceptability for this method of validation is very much subjective and can be influenced by scales. Statistical analysis coupled with model acceptability guides is a more acceptable process of quantifying model accuracy.

Figure 3 describes the methodology employed for the calibration and validation of the pedestrian simulation models developed as adapted from Barcelo [25]. The approach utilizes pedestrian characteristics and flow data corresponding to the requirements of the modeled scenarios. The collected data are then reduced and filtered by removing unreliable measurements (outliers). In this process, the pedestrian data set required for direct input to the simulation models are put together. While pedestrian flow data are set aside for the validation phase. After inputting software-specific data into the models, the underlying pedestrian behavior model parameters for adjustment needs to be identified. Choosing calibration parameters is guided by the scenario being modeled. A list of the types of parameters not recommended for calibration are enumerated by Hollander and Liu [26]. This is followed by the initialization of all pertinent behavior model parameters, normally

Table 4 Calibrated VISSIM parameter values

Parameter	Commuter	10 % older adults	20 % older adults	30 % older adults
tau (τ)	Commuter = 0.4	Commuter = 0.4 Older adult = 0.4	Commuter = 0.4 Older adult = 0.3	Commuter = 0.4 Older adult = 0.3

utilizing software default values. The simulation models are then run multiple times based on the developed experimental design.

Relevant model results are extracted corresponding to the validation data set aside. Before any statistical comparison or estimation of goodness of fit measures is undertaken, measures need to be identified along with criteria for acceptability. Hollander and Liu [26] provides comprehensive guide to choosing goodness of fit measures. If the goodness of fit criteria are not met by comparing observed and modeled values, appropriate adjustment(s) of parameters is/are undertaken. With new parameter values, the model is again run and results comparison repeated until fit is satisfactory.

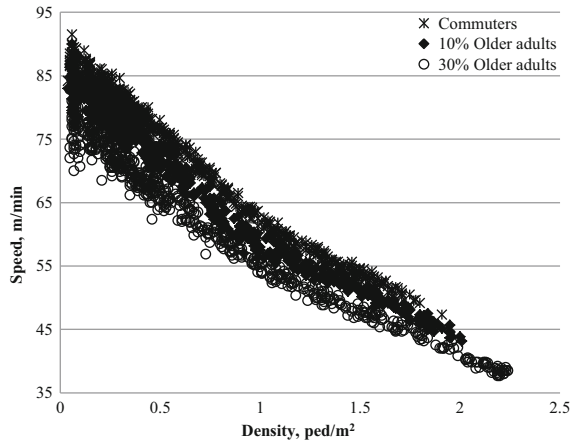
6.1 VISSIM Parameter Estimation

The Social Force Model employed by VISSIM to govern pedestrian behavior movement consists of forces acting on a pedestrian. These forces cause the pedestrian to decelerate or accelerate based on the resultant of all of the forces. Within these forces, numerous parameters can be adjusted for the calibration process. For more details on these parameters, refer to the latest VISSIM manual. As a consequence of the simplicity of the micro-simulation model set-up described above, only one VISSIM pedestrian behavior parameter was identified for adjustment, tau (τ). The other pedestrian behavior parameters were kept at their default values. A manual adjustment process for tau was employed by starting from the default value of 0.4. The value of tau was incremented by 0.1 depending on how modeled values compare to observed values. The increment (decrement) in the value tau was guided by the general trend of speed and flow comparison with the validation data. Paired samples t-tests of modeled versus observed data were employed for this purpose at the 95 % confidence level. When this statistical test result was satisfactory, the model was considered calibrated. The final values of tau are listed in Table 4.

6.2 Repeated Runs and Output Data Collection

Due to stochastic nature of simulation models, multiple runs utilizing different random seed generators should be applied. Results of these models generate different values for every run. The greater the number of runs, the more accurate

Fig. 4 Simulated speed-density relations



the aggregated model result about a stable value but would required more run time and effort in results collection. Another method for increasing the number of model results for steady-state simulation (traffic parameters remain constant throughout the run) is by employing batch means. ‘Batch means are sample means of subsets of consecutive subsamples from a simulation output sequence’ [27, p. 683]. This technique in not new and has been analyzed by various researchers [27–30]. The required number of runs/data points for model results to be accurate is defined by,

$$n = \left(\frac{s \cdot z_{\alpha/2}}{\epsilon} \right)^2 \tag{3}$$

where n is the required number of model runs; s is the standard deviation of the examined model traffic measure; $z_{\alpha/2}$ denotes the critical value of Student’s t-test at confidence level $1 - \alpha$ ($z_{\alpha/2} = 1.96$ for a confidence level of 95 %); and ϵ is the required accuracy in terms of the traffic measure.

In order to have a blanket condition to satisfy Eq. 3, a combination of multiple runs and batch means was employed. There were 5 runs and 10 batch means for each run totaling 50 data points. The 50 points satisfy the above equation with 95 % confidence level and ± 1.0 m/min error for speed data collection. For the simulation set-up described, a warm-up period of 2 min was employed before data collection.

6.3 Simulated Pedestrian Fundamental Diagrams

Figures 4 and 5 show the speed-density and flow-density relations, respectively of simulated commuters and select combinations of older adults (10 % and 30 %). Figure 4 confirms the findings from literature that an increase in the proportion older adults (slower pedestrians) results in lower aggregate walking speeds for similar density values. This also effect lower throughput per unit width as shown in Fig. 5.

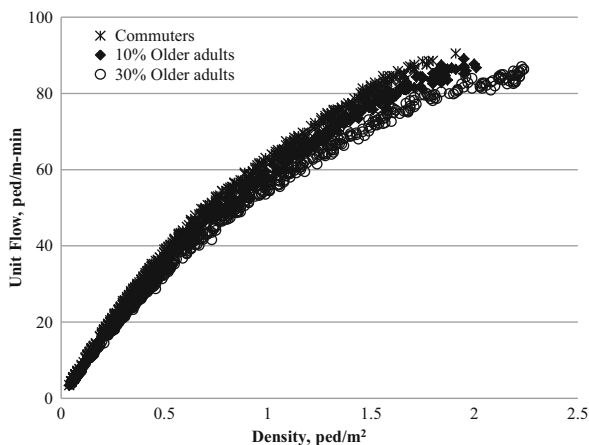


Fig. 5 Simulated flow-density relations

7 Simulation Model Application

7.1 Pedestrian Equivalent Factor Estimation

The pedestrian equivalent factors proposed are used to convert mixed pedestrian traffic into uniform flow. These types of factors are generally utilized for capacity analysis and LOS determination of pedestrian walkway facilities. In this light, computations of the factors at defined LOS criteria are more appropriate, from LOS A to E.

Figure 6 shows the TS-flow relations derived from the commuter-older adult combination. Logically, as the flow rate increases, pedestrian TS occupancy increases. Increased older adults proportion also increases the values for TS for similar flows. Utilizing these TS-flow relations, flow equivalencies at LOS flows were calculated. Pedestrian equivalent factors results are listed in Table 5 for various LOS', older adult proportions, and walkway widths.

7.2 Pedestrian Equivalent Factor in Facilities Design

The procedure to determine the required walkway width for a transit terminal corridor is based on maintaining a desirable pedestrian LOS [6]. For pedestrian capacity analysis, the width of the walkway is estimated based on desired operating LOS and prevailing pedestrian condition. The factors computed in Table 5 can be used to determine the appropriate width of a corridor when traffic is composed of a

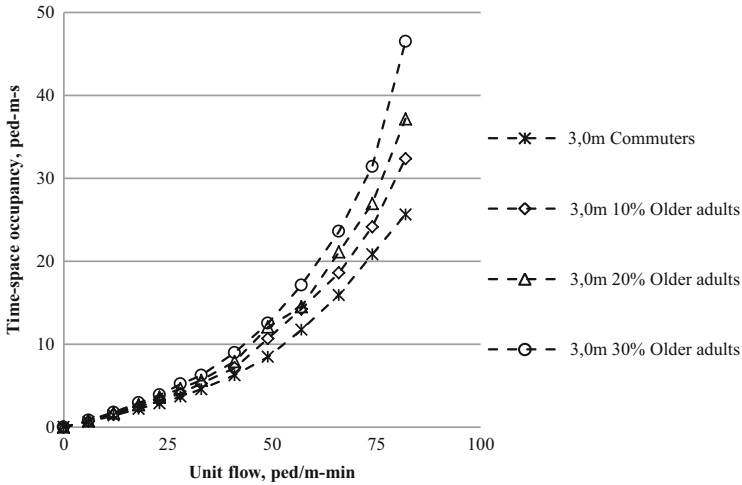


Fig. 6 TS-flow relations for flow equivalency estimation: 3.0 m walkway

Table 5 SPE factors for older adults

Unit flow ped/m-min	LOS equivalent	1.5 m			3.0 m			4.5 m		
		10 %	20 %	30 %	10 %	20 %	30 %	10 %	20 %	30 %
12	A	1.93	1.94	1.88	2.01	1.94	1.87	1.83	1.95	1.88
28	B	2.12	2.03	2.01	1.89	2.01	1.86	2.04	1.94	2.02
41	C	1.90	1.84	1.81	2.02	1.83	1.80	1.67	1.67	1.77
57	D	1.82	1.71	1.69	2.10	1.90	1.66	2.15	2.03	1.87
74	E	2.61	2.05	1.87	1.69	1.64	1.63	2.23	1.94	1.85

mix of commuters and older adults. To illustrate the pedestrian equivalent factors’ possible application, a hypothetical pedestrian scenario is described below.

For the design of a hypothetical walkway located in a transit facility, LOS C is the desired operating condition. A uniform flow arrival of 4,000 pedestrians is expected to utilize the facility consisting of 80 % commuters and 20 % older adults. If flow is unadjusted, the flow rate is 66.7 ped/min which translates to a walkway width of 1.6 m for LOS C (divided by unit flow rate = 41 ped/m-min in Table 5). Conversely, when older adults (SPE factor of 1.84 from Table 5 for unit flow of 41 ped/m-min and 1.5 m width) are considered, a flow of 77.87 ped/min will be computed. A resulting walkway width of 1.90 m will be required for this scenario. A comparison of the two situations is summarized in Table 6. For the given mix and desired LOS, the effective walkway width is 27 cm greater than that for a group consisting entirely of commuters. The 27 cm difference is almost half an additional pedestrian lane width and may be the difference between being able to walk without difficulty or not. With higher proportions of older adults, the gap between the two scenarios may become more significant.

Table 6 Comparison of unadjusted and mixed pedestrian flow scenarios

	Unadjusted flow	With older adults
Equivalent pedestrian flow, ped/h	4,000	4,672
Flow rate, ped/min	66.67	77.87
Estimated effective walkway width, meter	1.63	1.90

8 Conclusion

This paper introduced the concept of pedestrian equivalency factors in order to convert heterogeneous pedestrian flow into a uniform commuter flow. This methodology introduced can be used to develop local pedestrian equivalent factors. The time-space approach utilized in this research is robust in that it considers both the temporal and spatial differences in characteristics of pedestrians. This approach used pedestrian micro-simulation in lieu of field-collected data to develop the pedestrian equivalent factors to illustrate this novel concept. It is suggested that ideally the proposed equivalent factors should be derived from flow relationships from field data covering various possible scenarios. The data required for developing equivalent factors using this methodology include: pedestrian traffic volumes, body size distributions or average body sizes, average travel times, across various proportions of other pedestrians, and across walkway widths. Collection of input data poses as a great challenge when implementing this method but with advances in pedestrian data collection methodologies, data collection can be more straightforward. Regardless, transport engineers, architects, and urban transport planners can apply the methodology to develop localized pedestrian equivalent factors.

Further investigation is recommended to utilize the methodology in developing pedestrian equivalent factors using field collected data. Two major undertakings are also recommended:

1. Investigate the effects of other pedestrian types, e.g. obese travelers, wheelchair users, parents with prams, people in groups, etc.; and
2. Further investigate the effects of facility type (ramps and stairs) and operational characteristics (bi-directional and cross-flows) on the applicability of the methodology.

References

1. TRB: Highway Capacity Manual 2000: Transportation Research Board, National Research Council, Washington, DC (2000)
2. Teknomo, K.: Microscopic Pedestrian Flow Characteristics: Development of an Image Processing Data Collection and Simulation Model, Department of Human Social Information Sciences, Tohoku University. PhD thesis. 141

3. Pauls, J.: Demographic Changes Leading to Deterioration of Pedestrian Capabilities Affecting Falls Safety and Crowd Movement Performance Including Facility Evacuation: TRB Annual Meeting, 87th, 2008, Washington DC (2008)
4. Campanella, M., Hoogendoorn, S.P., Daamen, W.: Effects of Heterogeneity on Self-Organized Pedestrian Flows. Transportation Research Record: Journal of the Transportation Research Board 2124, 148–156 (2009)
5. Davis, D.G., Braaksma, J.P.: Adjusting for Luggage-Laden Pedestrians in Airport Terminals. Transportation Research Part A: General 22, 5, 375–388 (1988)
6. Kittelson and Associates: Transit Capacity and Quality of Service Manual - 2nd Edition: Washington, DC (2003)
7. TRB: Highway Capacity Manual 2010: Transportation Research Board, National Research Council, Washington, DC (2010)
8. Huber, M.: Estimation of Passenger-Car Equivalents of Trucks in Traffic Stream (Discussion and Closure). Transportation Research Record 869, 60–70 (1982)
9. Galiza, R.J., Ferreira, L.: Developing Standard Pedestrian Equivalent (Spe) Factors: A Pce Approach for Dealing with Pedestrian Diversity: Transportation Research Board 91st Annual Meeting Compendium, Washington, DC (2012)
10. Fruin, J., Benz, G.: Pedestrian Time-Space Concept for Analyzing Corners and Crosswalks. Transportation Research Record 959, 18–24 (1984)
11. Benz, G.: Application of the Time-Space Concept to a Transportation Terminal Waiting and Circulation Area. Transportation Research Record 1054, 16–22 (1986)
12. Demarchi, S.H., Setti, J.R.: Limitations of Passenger-Car Equivalent Derivation for Traffic Streams with More Than One Truck Type. Transportation Research Record 1852, 96–104 (2003)
13. Fitzpatrick, K., Brewer, M.A., Turner, S.: Another Look at Pedestrian Walking Speed. Transportation Research Record: Journal of the Transportation Research Board 1982, 21–29 (2006)
14. Schoon, J.: Pedestrian Facilities: Engineering and Geometric Design. Thomas Telford Limited, London (2010)
15. Elefteriadou, L., Torbic, D., Webster, N.: Development of Passenger Car Equivalents for Freeways, Two-Lane Highways, and Arterials. Transportation Research Record 1572, 51–58 (1997)
16. Webster, N., Elefteriadou, L.: A Simulation Study of Truck Passenger Car Equivalents (Pce) on Basic Freeway Sections. Transportation Research Part B: Methodological 33, 5, 323–336 (1999)
17. Ingle, A.: Development of Passenger Car Equivalents for Basic Freeway Segments, Civil Engineering, Virginia Polytechnic Institute and State University. MEng thesis. 130
18. Patrick, S., Taranto, V., Blanksby, C., Luk, J., Ritzinger, A., Fraser, S.: Review of Passenger Car Equivalency Factors for Heavy Vehicles: 23rd Australian Road Research Board Conference, Adelaide, Australia (2008)
19. Arasan, V.T., Arkatkar, S.S.: Micro-Simulation Study of Effect of Volume and Road Width on Pcu of Vehicles under Heterogeneous Traffic. Journal of Transportation Engineering 136, 12, 1110–1119 (2010)
20. PTV-AG, <http://www.ptvag.com/>
21. Helbing, D., Molnar, P.: Social Force Model for Pedestrian Dynamics. Physical review E 51, 5, 4282–4286 (1995)
22. Ishaque, M., Noland, R.: Pedestrian and Vehicle Flow Calibration in Multimodal Traffic Microsimulation. Journal of Transportation Engineering 135, 6, 338–348 (2009)
23. Boenisch, C., Kretz, T.: Simulation of Pedestrians Crossing a Street: Traffic and Granular Flow, Shanghai, China (2009)
24. Kothiyal, K., Tettey, S.: Anthropometric Data of Elderly People in Australia. Applied Ergonomics 31, 3, 329–332 (2000)
25. Barcelo, J.: Fundamentals of Traffic Simulation. Springer Science, (2010)

26. Hollander, Y., Liu, R.: The Principles of Calibrating Traffic Microsimulation Models. *Transportation* 35, 347–362 (2008)
27. Chen, E.J., Kelton, W.D.: A Procedure for Generating Batch-Means Confidence Intervals for Simulation: Checking Independence and Normality. *Simulation* 83, 10, 683–694 (2007)
28. Sherman, M., Goldsman, D.: Large-Sample Normality of the Batch-Means Variance Estimator. *Operations Research Letters* 30, 319–326 (2002)
29. Fishman, G.: Grouping Observations in Digital Simulation. *Management Science* 24, 5, 510–521 (1978)
30. Whitt, W.: The Efficiency of One Long Run Versus Independent Replications in Steady-State Simulation. *Management Science* 37, 6, 645–666 (1991)

Getting Out of the Way: Collision-Avoiding Pedestrian Models Compared to the Real World

Gregor Lämmel and Matthias Plaue

Abstract Numerical simulation of human crowds is a challenging task and a number of models to simulate pedestrian dynamics on a microscopic level have been established. One aim of those models is to reproduce a realistic, and in particular collision-free, movement of crowds in complex environments. This work investigates three approaches on their capability to reproduce a collision-free movement of pedestrian crowds in complex dynamic environments. The baseline model is the well-known social force model. While in the social force model pedestrians do not explicitly avoid each other, the second model extends the social force model to avoid collisions explicitly. The observed collision-avoiding behavior produced by the third model is reached by calculating velocity obstacles. These are obstacles in the velocity space, meaning that if a pedestrian chooses a velocity that lies inside the velocity obstacle, then a collision occur at some time. This work discusses the models and their integration in a multi-agent simulation framework. The models are tested on data from a real-world experiment conducted at Technische Universität Berlin. In this experiment, two pedestrian flows intersected at an angle of 90° . The models' performance with regard to the reproduction of a realistic crowds movement and their computational complexity are discussed in this work.

Keywords Intersecting pedestrian flows • Multi-agent simulation • Human crowd experiments

G. Lämmel (✉)

Transport Systems Planning and Transport Telematics, TU Berlin, Sekr. SG12, Salzufer 17–19, 10587 Berlin, Germany

e-mail: laemmel@vsp.tu-berlin.de

M. Plaue

Department of Mathematics, TU Berlin, Sekr. 6–4, Straße des 17. Juni 136, 10623 Berlin, Germany

e-mail: plaue@math.tu-berlin.de

<http://www.math.tu-berlin.de/projekte/smdpc>

1 Introduction

One possible approach to model the movement of crowds are Cellular Automata (CA) [14]. CA models represent the environment with a grid-like structure, where each cell of the grid may contain at most one pedestrian at a time. CA models have often been used for the simulation of evacuation scenarios. A common problem with existing CA models, however, is that they do not model complex wayfinding, since in most CA models wayfinding is implemented via a globally defined potential field. In theory, it would be possible to assign an individual potential field to each pedestrian. This approach, however, would be too complex in terms of computational costs for large scenarios.

Other simulation concepts use (discretized) differential equations similar to equations known from the description of molecular dynamics [8, 10]. Probably the best known model based on the molecular dynamics analogy is the social force model [11]. In social force model simulations, each pedestrian has a desired velocity towards a desired destination and adapts her current velocity accordingly. A pedestrian's incentive to avoid obstacles such as other pedestrians is modeled by repelling forces. Force-based models are well understood and have reasonable computational costs.

There is another class of models that try to achieve collision-free pedestrian movement in complex environments. These models are based on the so-called configuration space obstacle approach and have their foundation in computational geometry and robotics. In this context the configuration space describes all possible locations a pedestrian can reach. Locations that cannot be reached are the so-called configuration space obstacles. For this approach the pedestrians and the obstacles in the environment (e.g., walls and other pedestrians) are represented as a set of simple polygons. A path through the environment is collision-free if and only if the path does not intersect the Minkowski sum of the polygonal obstacles with the polygonal representation of the pedestrian reflected in her reference point [1].

An extension to the configuration space obstacle approach is the velocity obstacle approach [5]. Similar to the configuration space obstacles the velocity obstacles describe all velocities a pedestrian can choose that will lead to a collision at some point in time assuming straight movement and no acceleration of rest of the pedestrians. In the velocity obstacle approach every pedestrian chooses at each point in time a velocity that avoids collision and is close to the desired velocity.

This work investigates three approaches with regard to their capability of reproducing collision-free realistic pedestrian movement. First, there is the social force model as it is introduced in [11]. While the social force model does not let the pedestrians avoid collisions explicitly the collision-avoiding force-based model proposed by Zanlungo et al. [25] takes potential collisions into account. This means the repelling forces do not only depend on the locations of the obstacles and pedestrians but also on their velocities. When calculating the actual force that affects a given pedestrian the model calculates the minimal time of closest approach to all other pedestrians and obstacles in the environment. All pedestrians are then

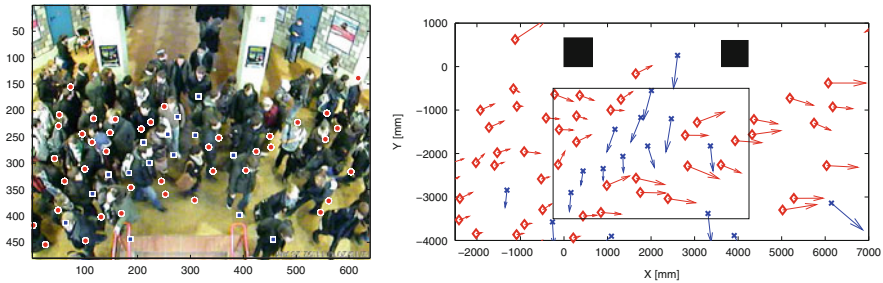


Fig. 1 Experiment with two pedestrian flows intersecting at 90° at time step $t = 88.3$ s. *Red diamonds: group A, blue crosses: group B. Arrows indicate the velocity of the pedestrians*

projected up to this point in time assuming constant movement. The influencing force on the pedestrian in question is calculated based on this projection and weighted by the inverse of the minimal time of closest approach. This leads to a behavior that tries to avoid the next potential collision under the assumption of constant movement. Like in other force-based models, too, each pedestrian has a desired velocity to which she adapts in a given time if free movement is possible. However, most existing force-based models do not address the important problem of complex wayfinding. In our approach, complex wayfinding is implemented via a navigation graph and a least cost path search: a force that lets a pedestrian move along the navigation graph replaces the simple desired velocity vector. Thus, it is possible to simulate pedestrian movements to multiple destinations in a complex environment.

The third approach discussed in this work is based on the reciprocal velocity obstacle approach [24]. But instead of calculating valid velocities during every time step the pedestrians choose valid accelerations preferably close to the desired one. This approach leads to a similar result like choosing a valid velocity directly but lets the model be better integrated with force-based models. This integration is needed since the calculation of the desired velocity and the short-range interaction is still based on forces. Like with the first and the second approach, the desired movement is based on a force that lets each agent move along a navigation graph.

We compare the results of simulations performed by the three models with data obtained from a real-world experiment conducted at Technische Universität Berlin, see Fig. 1.

The remainder of this work is organized as follows. Section 2 gives a discussion of all three simulation models and describes extensions that have been made in order to integrate those models in a multi-agent simulation framework for the simulation of pedestrian crowds in complex dynamic environments. Experimental results are shown in Sect. 3. A discussion on this results is given in Sect. 4. Section 5 concludes this work and gives a short outlook.

2 Simulation Models and Framework

The simulation models investigated are all fully integrated into MATSim. MATSim stands for Multi-Agent Transport Simulation and provides a toolbox for various kinds of transport simulations (see, e.g., [23]). MATSim’s major field of application is the simulation of vehicular traffic in large-scale scenarios.

In recent times MATSim has also been used for the simulation of pedestrians in the evacuation context [4, 16, 17]. The underlying traffic flow simulation relies in all this works on a queue model [6]. The queue model has the advantage of being highly efficient while retaining important physical parameters like free speed travel time or flow capacity of links. However, when it comes to crossing pedestrian streams it seems to be questionable if a queue model can simulate those streams adequately.

This work extends MATSim with the capability of simulating pedestrians in a two-dimensional continuous space. The following sub-sections discuss the agent movement model. We distinguish between two stages in the movement models. The first stage deals with the low level movement of the agents, meaning collision avoidance, velocity adaptation and so on. The second stage deals with the more high level movement of the agents, meaning moving along a given route. While for all three models the second stage is implemented in the same manner, for the first stage two general approaches are investigated. The social force model and the collision-predicting force model are driven by repelling and attracting forces, which are “pushing” the agents through the environment. In contrast to this approach, the reciprocal velocity model calculates velocities that let the pedestrians avoid collisions. Detailed model descriptions are given in the following.

2.1 Social Force Model

Here and in the following the space that a pedestrian occupies in the 2D space is approximated by a circular disk. The true shape of a pedestrian indisputable differs from this simplification. Some authors argue that the space is better approximated by an ellipse [13] and what is more this ellipse should be velocity dependent [3]. While a velocity dependent elliptical representation seems to be a plausible choice, since pedestrians need more space in walking direction when moving faster, it is also more consuming in terms of computational costs. For that reason we stick with the simpler circular representation for the benefit of faster computation.

The general force model is defined according to an analogue of Newton’s law ($F = m \cdot a$).

$$\mathbf{f}_i(t) = \frac{m_i}{\tau} (\mathbf{v}_i^0(t) - \mathbf{v}_i(t)) + \sum_{j \neq i} \mathbf{f}_{ij}(t), \quad (1)$$

where $\mathbf{v}_i^0(t)$ is the desired velocity vector for agent i at time t . The term $\mathbf{v}_i(t)$ denotes the agent's actual velocity at time t . The time constant τ describes the time that is needed to adjust the actual velocity to the desired velocity. The second term of the equation builds the sum over all influential entities j in the environment (i.e., other agents, walls, and obstacles). Each of those entities emit a repelling (or attracting) force to agent i .

Many different force models have been discussed in recent years (see, e.g., [19] for an overview), most of them are build on the so-called social force model introduced by Helbing and Molnár [11]. The basic social force model implicitly reproduces collision-avoiding behavior as it can be observed in real-world situations. It has been shown that the model works particularly well in high density conditions, such as one observes in evacuation situations [9]. The social force model is defined as follows:

$$\mathbf{f}_i(t) = \frac{m_i}{\tau}(\mathbf{v}_i^0(t) - \mathbf{v}_i(t)) + \sum_{j \neq i} \mathbf{f}_{ij}(t) + \sum_W \mathbf{f}_{iW}(t), \quad (2)$$

where \mathbf{f}_{ij} denotes the repelling force emitted by agent j towards agent i and \mathbf{f}_{iW} denotes the repelling force emitted by obstacle W (e.g., walls) towards agent i . Both forces are calculated in the same way. For that reason only the calculation of \mathbf{f}_{ij} is discussed in detail here. The interested reader is referred to [9] for a detailed discussion.

$$\mathbf{f}_{ij}(t) = A_i \exp((r_{ij} - d_{ij})/B_i) \mathbf{n}_{ij} + g(k(r_{ij} - d_{ij}) \mathbf{n}_{ij} + \kappa(r_{ij} - d_{ij}) \Delta v_{ji}^t \mathbf{t}_{ij}). \quad (3)$$

The first term of the equation's right hand side describes the so-called repelling social force between agent i and agent j ; A_i and B_i are constants, $r_{ij} = r_i + r_j$ is the sum of i 's and j 's radius, and d_{ij} is the distance between the disks centers of i and j . The term $\mathbf{n}_{ij} = \mathbf{d}_{ij}/d_{ij}$ describes the unit vector pointing from agent j to agent i . The second term of the equation's right hand side expresses the physical force between agent i and agent j . The physical force only acts if a collision actually occurs. This is guaranteed by the function $g(X)$, which is zero as long as no collision occurs and equal to its argument else. If a collision occurs there are two additional forces. First, there is a strong repelling force given by $k(r_{ij} - d_{ij}) \mathbf{n}_{ij}$, with k a constant. Second, there is a strong tangential force given by $\kappa(r_{ij} - d_{ij}) \Delta v_{ji}^t \mathbf{t}_{ij}$. Again, κ is a constant, \mathbf{t}_{ij} is the tangential unit vector ($= \mathbf{n}_{ij}$ rotated by $\pi/2$), and Δv_{ji}^t is the tangential velocity difference of agent i 's and j 's velocities. The social force model is straightforward to implement and has reasonable computational costs. One disadvantage of the model is that potential collisions are not explicitly considered. A novel approach that relies on the social forces paradigm but considers potential collision explicitly has been proposed by Zanlungo et al. [25].

2.2 Collision-Predicting Force Model

The collision-predicting force model proposed by Zanlungo et al. [25] also calculates repelling forces but it projects the present scene into the future in order to detect potential collisions.

In the model each agent i computes for each other agent j in the environment the angle θ_{ij} between \mathbf{d}_{ij} and \mathbf{v}_{ij} . Where \mathbf{d}_{ij} denotes the vector pointing from agent j 's position to agent i 's position and \mathbf{v}_{ij} denotes the relative velocity between both agents. If $|\theta_{ij}| > \pi/4$ then $t_{ij} = \infty$. Otherwise t_{ij} reflects the time of the closest approach of both agents under the assumption that neither agent i nor agent j changes her velocity or direction of movement. The agent then takes the minimum of these times $t_i = \min_j(t_{ij})$.

Afterwards the agent computes the configuration of the environment for t_i by again assuming that none of the pedestrians change the velocity or direction of movement. Let $\mathbf{d}'_{ij}(t_i)$ denote the predicted vector pointing from agent i to agent j at time t_i . The agent j 's influence on agent i (second term in Eq. (1)) is

$$\mathbf{f}_{ij}(t) = A_i \frac{v_i(t)}{t_i} \exp(-d_{ij}(t)/B_i) \frac{\mathbf{d}'_{ij}(t_i)}{d'_{ij}(t_i)}. \quad (4)$$

The constants A_i and B_i are free parameters in the model. Equation (4) is not only applicable for other agents in the environment but also for any object that is not moving, like walls or obstacles.

2.3 Reciprocal Velocity Obstacle Model

Another approach to model a collision-avoiding behavior in a pedestrian simulation extends a well-known approach to calculate collision-free movement of robots in complex geometries. Consider for now that there is only one agent who wants to navigate through a static environment without colliding with any obstacle (e.g., walls, furniture, etc.). The problem for the agent is to decide for any location in the environment if she would collide with an obstacle if she would be at this location. If the agent would have no dimension (i.e., point shape) then this problem would be straightforward to solve. However, since the agents represent pedestrians in the underlying context, they have a polygonal shape. To decide whether an agent collides with an obstacle at a certain location in the environment one must decide whether the polygon representing the agent intersects with some other polygon (i.e., obstacle). The computation used to determine whether two polygons intersect is a rather complex operation and would lead to long computation times.

Instead of calculating the intersections directly one can determine collision-free locations by a simple approach that relies on so-called configuration space obstacles. For a detailed description of this approach the reader is referred to [1]. The basic

procedure works as follows: First, each agent is assigned to a reference point relative to her shape. If the agent has a circle shape then this could for example be the center of the circle. Second, the shape of the agent has to be reflected in its reference point. In the case of a circle with the reference point locate at the center this operation has no effect. Third, for every obstacle in the environment one has to compute the Minkowski sum of the obstacle and the agent's reflected shape. The Minkowski sum of two polygons A and B in Euclidean space is defined as $A \oplus B = \{\mathbf{a} + \mathbf{b} | \mathbf{a} \in A, \mathbf{b} \in B\}$. The result of this operation is a set of so-called configuration space obstacles. The position of an agent is collision-free or admissible as long as her reference point lies in no configuration space obstacle. With this method it is easy to calculate collision-free paths for a single agent in complex geometric environments. When it comes to a pedestrian simulation with a great number of agents, this approach does not longer work.

An extension of the configuration space approach for dynamic environments is the so-called velocity obstacle approach [5]. A velocity obstacle is a set of velocities that would lead to a collision at some future time under the assumption that none of the moving entities change their velocity. The authors demonstrate that the velocity obstacle approach result in near-optimal collision-free paths with respect to distance or travel time. However, if two agents approach in a simulation and both of them try to avoid a collision using the velocity obstacle approach, the agents' movements start oscillating between moving in the desired direction and dodging each other. The reason is that both of the agents try to avoid each other, which leads to an undesirable feedback.

A method that deals with this issue is the reciprocal velocity obstacle approach [24]. The reciprocal velocity obstacle approach takes the collision-avoiding behavior of the other agents into account by assuming that the other agents use the same method to avoid collisions. In other words if two agents are about to collide, then both of them take a share of responsibility to avoid the collision. Such a behavior seems to be realistic also for real-world situations where pedestrians perform collision avoiding movements. The reciprocal velocity obstacle approach calculates for every agent at every time step a velocity obstacle. If a velocity lies inside the obstacle, then a collision would occur at some future time. Again, under the assumption of constant movement of all agents. The authors note that there may be situations where a collision-free velocity is not possible. Therefore they propose a penalty approach that calculates a penalty based on divergence from the desired velocity and the time to the next collision for a set of candidate velocities. The penalty calculation for an agent i at time t and velocity \mathbf{v}'_i takes the following form:

$$penalty_i(\mathbf{v}'_i(t)) = w_i \frac{1}{tc_i(\mathbf{v}'_i(t))} + \|\mathbf{v}_i^0(t) - \mathbf{v}'_i(t)\|. \quad (5)$$

In the simulation the agents then choose the intended velocity $\mathbf{v}_i(t)$ out of a set of candidate velocities so that \mathbf{v}_i minimizes the penalty.

$$\mathbf{v}_i = \arg \min_{\mathbf{v}'_i} penalty_i(\mathbf{v}'_i) \quad (6)$$

It is obvious that the penalty approach does not guaranty a collision-free movement. This means the simulation model has to deal with collisions somehow. In this work we propose combining the reciprocal velocity approach with a social force like agent interaction model. This yields in a hybrid model that calculates a force based on velocities that are chosen according to the reciprocal velocity approach and deals with collisions by applying agent interaction forces similar to the social force model. The approach ends up with a single force that works on the agent in question.

$$\mathbf{f}_i(t) = \frac{m_i}{\tau}(\mathbf{v}_i^0(t) - \mathbf{v}_i(t)) + \sum_{j \neq i} \mathbf{f}_{ij}(t), \quad (7)$$

where $\mathbf{v}_i(t)$ is chosen according to Eq. 6 and the agent interaction force is $\mathbf{f}_{ij}(t)$:

$$\mathbf{f}_{ij}(t) = g(A_i \exp((r_{ij} - d_{ij})/B_i)\mathbf{n}_{ij}), \quad (8)$$

with all operators, constants, and variables defined in the same way as they are defined in Eq. 3.

2.4 Agent Navigation and Desired Velocity Determination

In the current setup every agent starts at a link in the navigation graph. A simple approach would be to let \mathbf{v}_i^0 point towards the to-node of the start link at the beginning. As soon as the node is reached, \mathbf{v}_i^0 points to the to-node of the next link and so on until the agent reaches her destination. However, in [7] it has been shown that such an approach leads to an unrealistic behavior in situations when agents are moving next to each other. The reason is that those agents are pulled together at close range to a node, and after the node is passed their trajectories diverge again. The authors proposed a force system that follows the route in the navigation graph. The basic idea is that each agent keeps a shadow tag on the navigation graph, which moves along the graph as the agents move forward. Furthermore, the agents are connected by a virtual rubber strap to their corresponding shadow tag. The agents are driven by a driving force that works parallel to the link which has the shadow tag on it. The virtual rubber strap pulls the agents towards the shadow tag if they diverge to much from the link. This leads to the following force:

$$\mathbf{f}_i^{move}(t) = \frac{m_i}{\tau}(\mathbf{v}_i^0(t) - \mathbf{v}_i(t)) + A_{path} e^{d_i^p(t)/B_{path}} \mathbf{d}_i^p(t), \quad (9)$$

where $d_i^p(t)$ is the agent i 's distance to the current link, and $\mathbf{d}_i^p(t)$ is the perpendicular unit vector pointing from the agent to the current link.

For the social force model and the collision-predicting force model this approach is straightforward to implement. One only has to replace the term $\frac{m_i}{\tau}(\mathbf{v}_i^0(t) - \mathbf{v}_i(t))$

in Eq. 2 by \mathbf{f}_i^{move} . However, for the reciprocal velocity obstacle model the integration is more elaborate. We propose to derive the desired velocity $\mathbf{v}_i^0(t)$ for the penalty calculation in Eq. 5 from \mathbf{f}_i^{move} . This is achieved by implementing a “simulated” acceleration of agent i by \mathbf{f}_i^{move}/m_i for one simulation step and taking the resulting velocity as the intended velocity $\mathbf{v}_i^0(t)$ for Eq. 5. Details for the calculation of accelerations and velocity updates are given in the next section.

2.5 Integration into MATSim

The models discussed so far calculate forces or velocities as a function of time in a continuous time model. However, in order to integrate the model into a computer simulation the time has to be discretized. This means that an agent’s velocity will only be updated at discrete time steps. There are different ways how to update velocities at discrete time steps. A commonly used way is the Euler–Cromer method (see, e.g., [2]), which is based on the following equations:

$$\mathbf{a}_i(t) = \frac{\mathbf{f}_i(t)}{m_i}, \quad (10)$$

$$\mathbf{v}_i(t+h) = \mathbf{v}_i(t) + h\mathbf{a}_i(t), \quad (11)$$

$$\mathbf{r}_i(t+h) = \mathbf{r}_i(t) + h\mathbf{v}_i(t+h). \quad (12)$$

Here, $\mathbf{r}_i(t)$ is the agent i ’s position at time t and h is the time step size.

3 Experiments

In 2010, a series of human crowd experiments were conducted at Technische Universität Berlin, with the main goal of evaluating simulation models of intersecting pedestrian flows. In the experiment which we use here, the participants have been divided into two groups (group A , 142 subjects, and group B , 83 subjects), and each of the groups was instructed to walk along a given path. These paths were arranged such that the two pedestrian groups intersected at an angle of about 90° . The scene was recorded with three networked and temporally synchronized video cameras. The individual trajectories captured by each camera have been extracted afterwards from the video data by photogrammetric means. Afterwards, the paths of the pedestrians captured by different cameras were then merged by matching trajectories of minimal spatio-temporal distance. The latter procedure

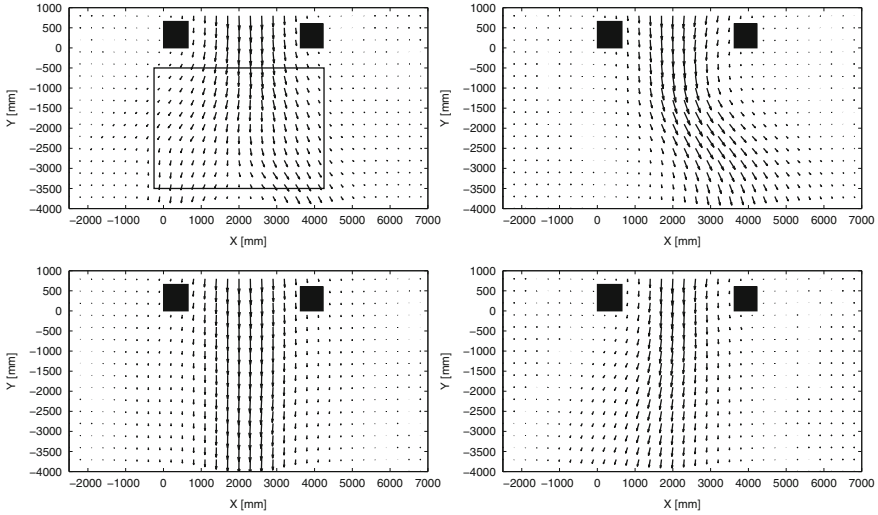


Fig. 2 Temporally averaged pedestrian flow field of group *B*. *Upper left*: experiment, *upper right*: Helbing simulation [9], *lower left*: van den Berg et al. [24], *lower right*: Zanlungo et al. [25]

was facilitated by the Kuhn–Munkres algorithm, also known as the Hungarian method [15, 18]. For details, we refer to [21, 22]. See Fig. 1 for a snapshot of the experiment.

In Sect. 4, we evaluate the performance of the force-based models and the reciprocal velocity obstacle model by comparison with the real-world data in terms of the pedestrian density and flow. In order to compute these data, we first calculate a dynamic local density and flow field from the trajectories via kernel density estimation similar to [12] but with variable kernel bandwidth – for details on the method, see [20] (Fig. 2).

In order to test the simulation models discussed in the previous section. A digital model of the experiment area has been implemented and for each person of group *A* and group *B* an artificial agent is created. The simulations are performed on a laptop computer with a 2.66 GHz dual core CPU. The results of the simulation models compared with experiment or given in Figs. 3–5 respective. A discussion on the results is given in the next section. Another important issue is the runtime performance of the simulation models. Our implementation of the social force model needs about 3 s to simulate the experiment, the collision-predicting force model needs 16 s, and the reciprocal velocity obstacle model needs 5 s. The simulation times are reasonable for the social force model and the reciprocal velocity obstacle model. The collision-predicting force model, however, could become to slow for larger scenarios.

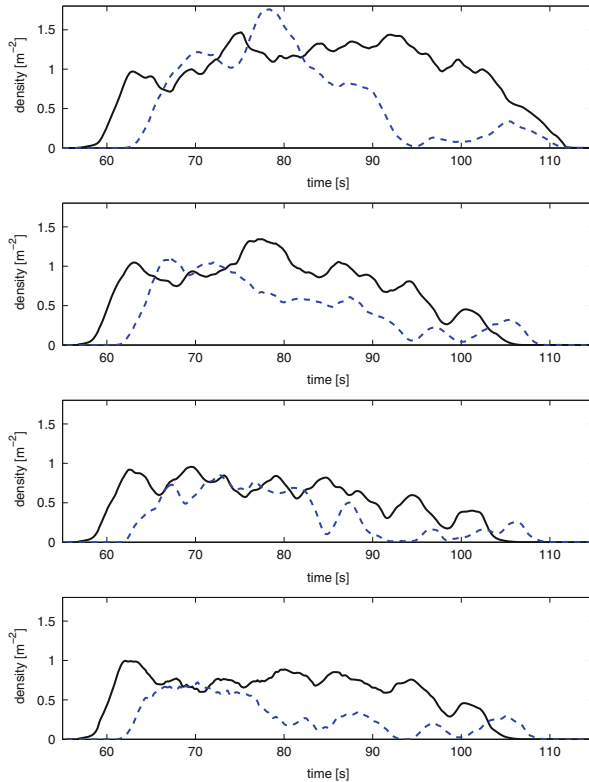
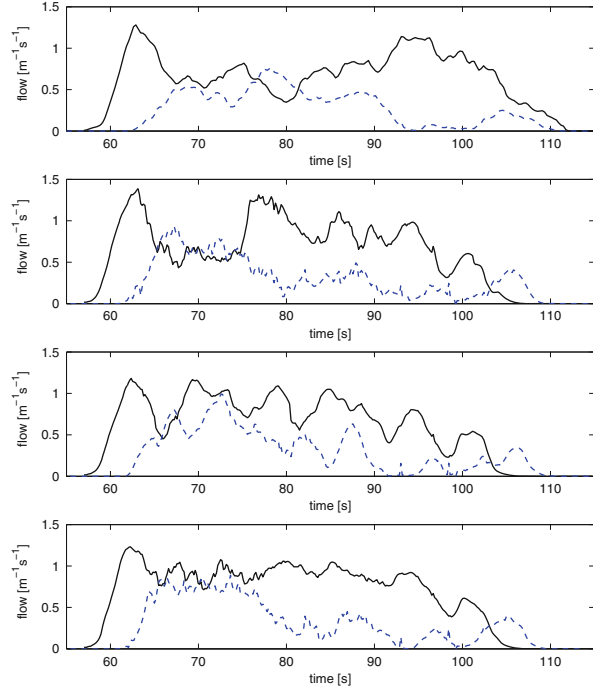


Fig. 3 Pedestrian density vs. time, averaged across the region marked in Figs. 1 and 2. *Black line*: group A, *dashed blue line*: group B. From top to bottom: experiment; simulations: Helbing et al. [9], van den Berg et al. [24], and Zanlungo et al. [25]

4 Discussion

There are two general observations in the results. First, all of the models deliver usable results in terms of travel time. This is best shown in Fig. 3. On average the last pedestrian of either groups leaves the scene after about 110s. The trends of the density curves are also similar even though none of the models reach such high densities as observed in the experiment. The reason for this lies in the nature of the simulation models which leads to the second observation. The simulation models can be divided into two classes. On the one hand there is the social force model, where the pedestrians act like colliding rubber balls. This behavior lead to a strong deviation from the desired movement direction (see Fig. 5). On the other hand there are the collision-predicting force model and the reciprocal velocity obstacle model. In both models the agents' strategy to avoid collisions is more efficient than can be observed in reality. Thus, less congestion is observed. This is indicated by lower densities compared to the experiment and the social force model (see Fig. 3).

Fig. 4 Main flow components vs. time, averaged across the region marked in Figs. 1 and 2. *Black line*: flow of group *A* in *x*-direction, *dashed blue line*: flow of group *B* in $-y$ -direction. From top to bottom: experiment; simulations: Helbing et al. [9], van den Berg et al. [24], and Zanlungo et al. [25]



One reason for the over-optimization could be caused by the fact that the simulation models do not explicitly distinguish between pedestrians who are moving in the same direction and those who are intersecting the desired path. Furthermore, when the movement for a pedestrian is calculated, all other pedestrians are considered as individual obstacles and not as groups of obstacles. The hypothesis would be that humans make this distinction and that they try to avoid penetrating groups of persons that apparently belong together. If this hypothesis is true, then the simulation models should be extended accordingly. However, there are further investigations necessary to make a conclusive statement about this hypothesis.

5 Conclusion and Outlook

This contribution discusses three different approaches for the simulation of crossing pedestrian streams. The probably best-known simulation model in the pedestrian context is the social force model. The social force model does not consider collisions explicitly. The second model is an extension to the social force model, which does consider collision explicitly and calculates social forces accordingly. The third model, the reciprocal velocity obstacle model, lets agents avoid collisions by calculating admissible velocities close to the desired one. While none of the

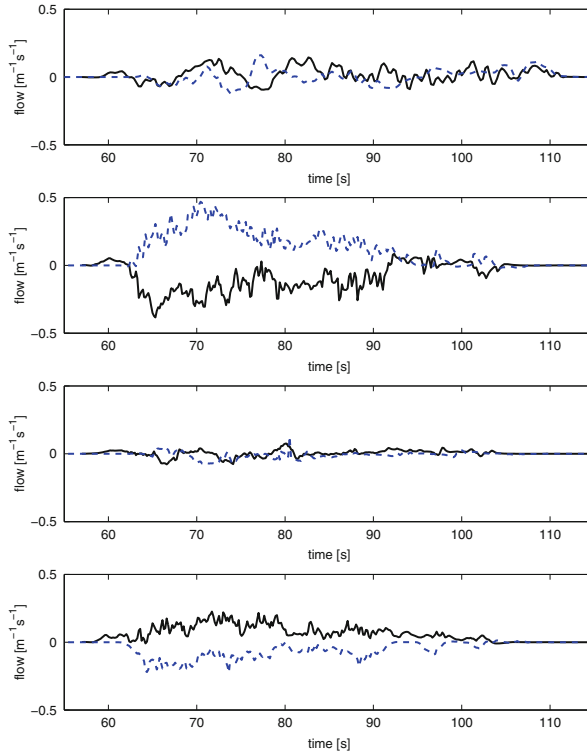


Fig. 5 Secondary flow components vs. time, averaged across the region marked in Figs. 1 and 2. *Black line*: flow of group A in y -direction, *dashed blue line*: flow of group B in x -direction. From top to bottom: experiment; simulations: Helbing et al. [9], van den Berg et al. [24], and Zanlungo et al. [25]

models is novel, several adaptations were necessary to integrate them into a multi-agent simulation, where the agents can choose paths to arbitrary destinations. Furthermore, the reciprocal velocity obstacle model has been extended to deal with collisions similar to the social force model, if those occur. The results are plausible even so improvements are possible. In future work it is planned to test the models on other pedestrian experiments. One focus could be the test of the group hypothesis stated in the previous section. If the hypothesis is true, then the development of a simulation model that takes groups of pedestrians into account when calculating collision-avoiding movements could also be the topic of future research.

Acknowledgements This project was funded in part by the German Ministry for Education and Research (BMBF) under grant 13N11382 (“GRIPS”) and by the German Research Foundation (DFG) under grants NA682/5-1, SCHW548/5-1 and BA1189/4-1.

References

1. de Berg, M., van Kreveld, M., Overmars, M., Schwarzkopf, M.: *Computational Geometry*. Springer (2000)
2. Cheney, W., Kincaid, D.: *Numerical Mathematics and Computing*. Thomson, fifth edn. (2004)
3. Chraïbi, M., Seyfried, A., Schadschneider, A.: Generalized centrifugal-force model for pedestrian dynamics. *Phys. Rev. E* 82, 046111 (Oct 2010), <http://link.aps.org/doi/10.1103/PhysRevE.82.046111>
4. Döbler, C., Kowald, M., Schüssler, N., Axhausen, K.: Within-day replanning of exceptional events. *TRR* (2012)
5. Fiorini, P., Shiller, Z.: Motion planning in dynamic environments using velocity obstacles. *The International Journal of Robotics Research* 17(7), 760–772 (1998)
6. Gawron, C.: An iterative algorithm to determine the dynamic user equilibrium in a traffic simulation model. *International Journal of Modern Physics C* 9(3), 393–407 (1998)
7. Gloor, C., Mauron, L., Nagel, K.: A pedestrian simulation for hiking in the alps. In: *Proceedings of the Swiss Transport Research Conference (STRC)*. Monte Verita, CH (2003), see www.strc.ch
8. Helbing, D., Buzna, L., Johansson, A., Werner, T.: Self-organized pedestrian crowd dynamics: experiments, simulations and design solutions. *Transportation Science* 39, 1–24 (2005)
9. Helbing, D., Farkas, I., Vicsek, T.: Simulating dynamical features of escape panic. *Nature* 407, 487–490 (2000)
10. Helbing, D., Farkas, I., Molnar, P., Vicsek, T.: Simulation of pedestrian crowds in normal and evacuation situations. In: Schreckenberg, M., Sharma, S.D. (eds.) *Pedestrian and Evacuation Dynamics*, pp. 21–58. *Proceedings of the 1st international conference, Duisburg, 2001*, Springer (2002)
11. Helbing, D., Molnár, P.: Social force model for pedestrian dynamics. *Phys. Rev. E* 51(5), 4282–4286 (1995)
12. Helbing, D., Johansson, A., Al-Abideen, H.Z.: Dynamics of crowd disasters: An empirical study. *Phys. Rev. E* 75, 046109 (2007)
13. Johansson, A., Helbing, D., Shukla, P.: Specification of the social force pedestrian model by evolutionary adjustment to video tracking data. *Advances in Complex Systems* 10, 271–288 (2007)
14. Klüpfel, H., Meyer-König, T., Keßel, A., Schreckenberg, M.: Simulating evacuation processes and comparison to empirical results. In: Fukui et al, M. (ed.) *Traffic and granular flow '01*, pp. 449–454. Springer, Berlin Heidelberg New York (2003)
15. Kuhn, H.W.: The Hungarian method for the assignment problem. *Naval Research Logistic Quarterly* 2, 83–97 (1955)
16. Lämmel, G.: *Escaping the Tsunami: Evacuation Strategies for Large Urban Areas. Concepts and Implementation of a Multi-Agent Based Approach*. Ph.D. thesis, TU Berlin (2011), <http://opus.kobv.de/tuberlin/volltexte/2011/3270/>
17. Lämmel, G., Grether, D., Nagel, K.: The representation and implementation of time-dependent inundation in large-scale microscopic evacuation simulations. *Transportation Research Part C: Emerging Technologies* 18(1), 84–98 (2010)
18. Munkres, J.: Algorithms for the assignment and transportation problems. *Journal of the Society for Industrial and Applied Mathematics* 5(1), 32–38 (1957)
19. Oleson, R., Kaup, D., Clark, T., Malone, L., Boloni, L.: Social potential models for traffic and transportation. In: Bazzan, A., Klügl, F. (eds.) *Multi-agent systems for traffic and transportation engineering*, chap. VII, pp. 155–175. *Information Science Reference (IGI Global)* (2008)
20. Plaue, M., Bärwolff, G., Schwandt, H.: On measuring pedestrian density and flow fields in dense as well as sparse crowds (2012), to appear in *Proc. PED2012*
21. Plaue, M., Chen, M., Bärwolff, G., Schwandt, H.: Multi-view extraction of dynamic pedestrian density fields (2012), preprint

22. Plaue, M., Chen, M., Bärwolff, G., Schwandt, H.: Trajectory extraction and density analysis of intersecting pedestrian flows from video recordings. In: Proc. PIA11. LNCS, vol. 6952, pp. 285–296 (2011)
23. Raney, B., Nagel, K.: An improved framework for large-scale multi-agent simulations of travel behaviour. In: Rietveld, P., Jourquin, B., Westin, K. (eds.) Towards better performing European Transportation Systems. Routledge, London (2006)
24. van den Berg, J., Lin, M.C., Manocha, D.: Reciprocal velocity obstacles for real-time multi-agent navigation. In: Proc. IEEE Intl. Conf. on Robotics and Automation. pp. 1928–1935 (2008)
25. Zanlungo, F., Ikeda, T., Kanda, T.: Social force model with explicit collision prediction. EPL (Europhysics Letters) 93(6), 68005 (2011)

Influence of Rhythm and Velocity Variance on Pedestrian Flow

Daichi Yanagisawa, Akiyasu Tomoeda, and Katsuhiro Nishinari

Abstract We have developed a simple model for pedestrians by dividing walking velocity into two parts, which are step size and pace of walking (number of steps per unit time). Theoretical analysis on pace indicates that rhythm that is slower than normal-walking pace in a low-density regime increases flow. We have verified this result by our experiment with real pedestrians.

The experimental result also indicates that the rhythm contribute to synchronize the movement of pedestrians. In order to investigate whether the synchronized movement improves pedestrian flow, we develop a variable transformation method and apply to the total asymmetric simple exclusion process and a simple evacuation model. Our theoretical result implies that pedestrian flow in a circuit increases, while pedestrian outflow decreases by the synchronized movement. We have examined the result of the circuit case by the real experiment again.

D. Yanagisawa (✉)

College of Science, Ibaraki University, 2-1-1, Bunkyo, Mito, Ibaraki 310-8512, Japan

e-mail: daichi@mx.ibaraki.ac.jp

A. Tomoeda

Meiji Institute for Advanced Study of Mathematical Sciences, Meiji University, 1-1-1, Higashi Mita, Tama-ku, Kawasaki, Kanagawa 214-8571, Japan

CREST, Japan Science and Technology Agency, 1-1-1, Higashi Mita, Tama-ku, Kawasaki, Kanagawa 214-8571, Japan

e-mail: atom@isc.meiji.ac.jp

K. Nishinari

Research Center for Advanced Science and Technology, The University of Tokyo, 4-6-1, Komaba, Meguro-ku, Tokyo 153-8904, Japan

Department of Aeronautics and Astronautics, School of Engineering, The University of Tokyo, 7-3-1, Hongo, Bunkyo-ku, Tokyo 113-8656, Japan

e-mail: tknishi@mail.ecc.u-tokyo.ac.jp

Keywords Rhythm • Synchronization • Variance • Pedestrian dynamics • Asymmetric simple exclusion process • Cellular automaton

1 Introduction

Pedestrian dynamics has been vigorously studied by physicists over recent decades [1, 2]. Many interesting phenomena, such as arching and lane formation, are analyzed by pedestrian-dynamics models [3–5]. Flow-density diagrams and velocity-density diagrams, which are often called fundamental diagrams, are also investigated actively by both simulation [6, 7] and experiment [8–12] to reveal the basic characteristics of pedestrian dynamics.

Important goals of pedestrian-dynamics research along with elucidation of collective phenomena are development of solutions to ease congestion and contribution to the safety [13].

Thus, we will develop a method to increase pedestrian flow in the congested situation in this paper. In Ref. [14] the effect of music on individual pedestrians has been studied experimentally. Inspired by this research, we analyze the effect of rhythm on crowded pedestrians theoretically by our simple model and reveal that slow rhythm increases pedestrian flow in congested situations without any danger. The result is also verified by our real experiments. When pedestrians walk with rhythm, their movement synchronized and the variance of the flow becomes small. Therefore, we would also like to study how a synchronization of pedestrians' movement affects pedestrian flow.

2 Stride and Pace Function

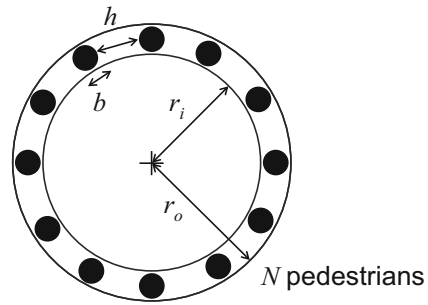
We consider a simple circuit as in Fig. 1. Inner and outer radius of the circuit is r_i and r_o , respectively. There are N pedestrians in the circuit, and the size of each pedestrian is b . If we write the length of the circuit as $L = \pi(r_i + r_o)$, density ρ and headway distance h is described as

$$\rho = \frac{N}{L}, \quad h = \frac{L - bN}{N}.$$

We model the velocity V of an individual pedestrian in detail by dividing it into two parts as $V(\rho) = S(\rho)P(\rho)$, where S (stride function) and P (pace function) represent length of a stride and pace of walking (total number of right and left steps per unit time), respectively.

The explicit expression of the stride function is intuitively determined as follows. It is plausible to assume that there is the maximum length of stride s for pedestrians in the low-density regime ($\rho \in [0, \rho_c]$). ρ_c is the critical density, where the flow

Fig. 1 Schematic view of the circuit considered in this paper



achieves the maximum. In the high-density regime ($\rho \in [\rho_c, \rho_j]$), pedestrians are no more able to walk with their maximum stride, and it decreases linearly as the headway distance decreases. ρ_j is the maximum density, where the flow becomes zero. Thus, the stride function is described as

$$S(\rho) = \begin{cases} s & (0 \leq \rho \leq \rho_c), \\ kh(\rho) & (\rho_c \leq \rho \leq \rho_j), \end{cases}$$

where the parameter $k \in (0,1]$.

The explicit expression of the pace function is determined as follows. If the density is low and a pedestrian does not interact with each other, it is feasible to assume that pedestrians walk with constant pace p . However, contrary to the stride function, it is difficult to obtain the explicit expression of the pace function in the high-density regime with some intuitive assumptions, thus, we consider a simple linear function as follows.

$$P(\rho) = \begin{cases} p & (0 \leq \rho \leq \rho_c), \\ p - a[h_c - h(\rho)] & (\rho_c \leq \rho \leq \rho_j), \end{cases}$$

Where h_c is the critical headway achieved at $\rho = \rho_c$. For more details about the stride and pace function, see Ref. [15].

3 Improvement of Flow by Slow Rhythm

The pedestrian flow is calculated as $Q(\rho) = \rho V(\rho) = \rho S(\rho) P(\rho)$. The second derivative of the flow indicates that convexity of the flow $Q(\rho)$ in the high density regime is dominated by the characteristic of the pace function, i.e., whether the pace increases ($a < 0$), decreases ($a > 0$), or remains constant ($a = 0$) according to the increase of the density. The following figures show the stride function and the pace function in the case $a > 0$ and $a = 0$ (Fig. 2).

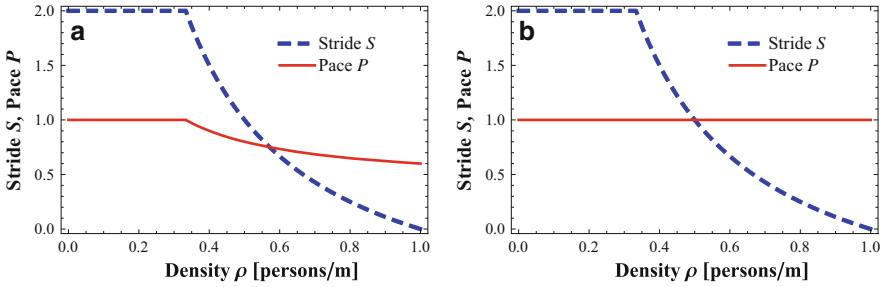


Fig. 2 Plots of the stride function S and the pace function P in the case $b = 1, s = 2, k = 1, p = 1$. (a) $a = 0.2 > 0$. (b) $a = 0$

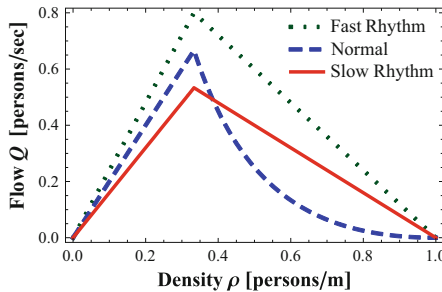


Fig. 3 Theoretical flow-density diagram for the fast-rhythmic walking case ($p = 1.2, a = 0$) the normal walking case ($p = 1.0, a = 0.5$), and slow-rhythmic walking case ($p = 0.8, a = 0$) in the case $b = 1, s = 2, k = 1$

Here we would like to propose a solution to improve flow in the congested situation from our model, in which the velocity of pedestrians is represented by the product of stride S and pace P . If pedestrians walk with a constant rhythm, in other words if we can control the walking pace by rhythm using a device such as a metronome, the rhythm exactly corresponds to the pace. Therefore, fast and slow rhythms increase and decrease the flow, respectively (Fig. 3).

We assume that the pace of pedestrians decreases in the high density regime ($a > 0$), i.e., the flow-density diagram is convex downward in the normal-walking case. The following figure shows the result of the theoretical analysis. It is obvious that fast-rhythmic walking improve the flow in both the low and high density regime. What we surprise is that the flow of the slow-rhythmic walking case becomes larger than the normal walking case. This phenomenon may give a safety solution to ease congestion in the real world since the flow increases without any excessive haste.

4 Experiment 1 and 2

We have performed the two experiments, where pedestrians walk in the one-dimensional circuit as in Fig. 1 ($r_i = 1.8$ [m], $r_o = 2.3$ [m]) (Fig. 4). Two kinds of walking were performed in the experiments. In the first case, we did not give any specific instructions to the participants, so that they walked normally. In the latter case, the participants were instructed to walk with the rhythm. In the experiment 1, approximately 136 [beats per minute (BPM)] rhythm is given by clapping, and in the experiment 2, 70 [BPM] rhythm is given by an electric metronome. Note that we did not uniform which foot to move first.

The experimental results indicate the followings.

1. The flow greatly improves when the participants walk with 136 [BPM] rhythm.
2. We see that the flow is larger in the normal case than the 70 [BPM] rhythmic case in the low-density regime, so that we have verified that 70 [BPM] is slower than the normal-waling pace.
3. The flow increases linearly as the density increases in the low-density regime in the normal and 70 [BPM] cases, so that we have verified that participants walked with constant stride and pace.
4. The flow decreases linearly in the high-density regime in the rhythmic case as expected from our analysis.
5. We observe that the flow in the normal-walking case in the experiment 2 is convex downward in the high-density regime as we have assumed in the theoretical analysis.
6. Since the theoretical assumptions of the convexity are satisfied in the experimental flows, the crossing appears, and the flow of the slow-rhythmic (70 [BPM]) case exceeds that of the normal case in the high-density regime. Therefore, we have succeeded to verify that slow rhythm improves the pedestrian flow (Fig. 5).

The experimental errors are small; however, we observe that they are smaller in the rhythmic-walking case than in the normal-walking case in the high-density regime. This result implies that rhythm removes the heterogeneity of pedestrians' movement, synchronizes it, and contributes to the homogeneous spatial distribution, which may achieve improvement of the flow.

5 Variable Transformation Method

As we have seen in the previous section, it seems that rhythm does not only maintain the pace of walking in the high-density regime but also decreases the variance of pedestrians' walking, i.e., synchronizes the movement of pedestrians. In the following sections, we investigate how the synchronization effect contributes to pedestrian flow.



Fig. 4 Snapshot of the experiment 1

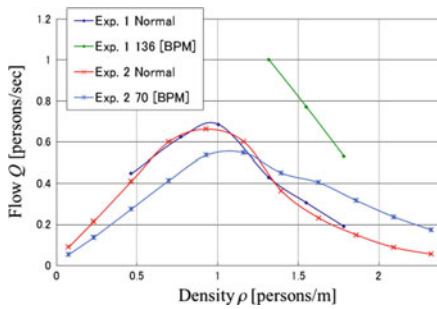


Fig. 5 Flow-density diagram in the experiment 1 and 2. The curves are added to improve visibility

Firstly, we would like to study the synchronization effect theoretically by using cellular-automaton models (CAMs). We consider that synchronization of the movement of pedestrians relates with variance of the movement of each pedestrian in this paper, for example, when the movement of pedestrians synchronized, the variance of the movement among pedestrians becomes zero. Therefore, we need to control variance of the walking velocity; however, mean and variance of velocity are dependent each other in CAMs, for example, if a pedestrian moves one cell with the probability p in one time step, his/her mean and variance of traveling time for one cell are

$$\text{Mean} : \frac{1}{p} \text{ [step]},$$

$$\text{Variance} : \frac{1-p}{p^2} \text{ [step}^2\text{]},$$

respectively. Therefore, we develop a method to determine the mean and variance of velocity independently. Note that a calibration method of the particle density in CAMs is developed in [16].

When we apply CAMs to the real situation, we have to determine the size of a cell and the length of one time step since both space and time are discrete in CAMs. Let us denote them as Δl [m/cell] and Δt [sec/step]. If a pedestrian moves one cell with the probability p in one time step, his/her mean velocity in the real situation is calculated as

$$v(p, \Delta l, \Delta t) = p \frac{\Delta l}{\Delta t} \text{ [m/ sec].}$$

In the equation above, the mean velocity v is a function of the parameters $p, \Delta l$ and Δt . If we transform this equation as follows:

$$\Delta t(v, p, \Delta l) = \frac{p\Delta l}{v} \text{ [sec /step],}$$

then the length of one time step Δt becomes a function of v, p and Δl . Since the mean velocity is determined by v in this equation. The parameter p no longer affects the mean velocity, and can be utilize for controlling the variance. Thus, when we substitute this to an equation which represents a physical quantity, we are able to determine the mean and variance of the velocity independently. Let us examine the validity of this method by the travel time for one cell. By multiplying the equations of mean and variance of traveling time for one cell by Δt and $(\Delta t)^2$ and substituting the equation of Δt , the mean and variance of the velocity are describe as

$$\text{Mean : } \frac{\Delta t}{p} = \frac{\Delta l}{v} \text{ [sec],}$$

$$\text{Variance : } \frac{(1 - p) (\Delta t)^2}{p^2} = \frac{(1 - p) (\Delta l)^2}{v^2} \text{ [sec}^2\text{].}$$

The parameter p disappears from the equation of the mean, so that we are able to change the mean and variance of the velocity independently. Since p is a probability, its domain is $[0,1]$, thus the variance achieves the maximum $(\Delta l/v)^2$ and the minimum 0 at $p = 0$ and $p = 1$, respectively.

6 TASEP

The totally asymmetric simple exclusion process (TASEP) [17] is one of the basic one-dimensional stochastic CAMs. A schematic view of the TASEP with a parallel-update rule and a periodic boundary condition is depicted in Fig. 6. A pedestrian



Fig. 6 Schematic view of the TASEP with a parallel-update rule and a periodic boundary condition

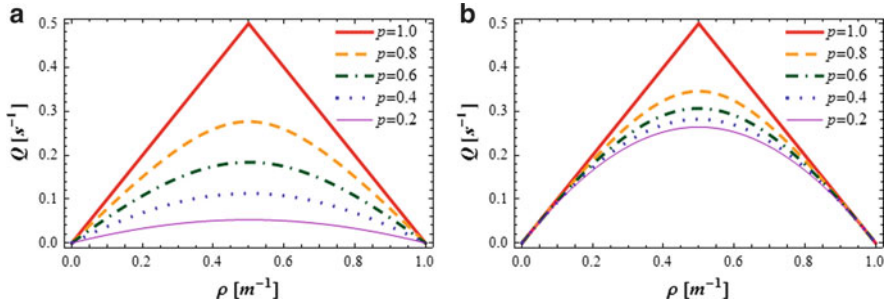


Fig. 7 Flow-density diagram of the TASEP. (a) (TASEP-A) Before applying the variable transformation method. (b) (TASEP-B) After applying the variable transformation method

represented by a black circle proceeds one cell to the right with the probability p in one time step, only if his/her right neighboring cell is empty. Since the effect of excluded-volume effect is implemented by automatically in the TASEP, it can be utilized for considering pedestrian dynamics. The Expression of flow in the TASEP is described as

$$Q(\rho, p) = \frac{1 - \sqrt{1 - 4p\rho(1 - p)}}{2} \text{ [step}^{-1}\text{]}.$$

By dividing the equation above by Δt and substituting the equation of Δt , the expression of the flow is transformed as

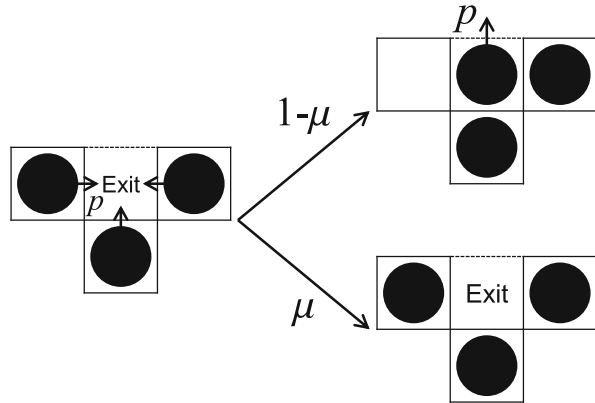
$$\text{(TASEP - A)} \quad Q(\rho, p, \Delta t) = \frac{1 - \sqrt{1 - 4p\rho(1 - p)}}{2\Delta t} \text{ [sec}^{-1}\text{]},$$

$$\text{(TASEP - B)} \quad Q(\rho, v, p, \Delta l) = \frac{v}{\Delta l} \cdot \frac{1 - \sqrt{1 - 4p\rho(1 - p)}}{2p} \text{ [sec}^{-1}\text{]},$$

where $\rho(=N/L)$ is the density of pedestrians. By changing the value of p in the equation (TASEP-B), we are able to analyze the effect of variance on flow in the TASEP.

Figure 7a, b show flow-density diagrams (fundamental diagrams) depicted by using the equation (TASEP-A) with $\Delta t = 1$ and the equation (TASEP-B) with $v = 1$ and $\Delta l = 1$, respectively. The result of Fig. 7a is well known; the flow achieves

Fig. 8 Schematic view of a simple evacuation model in the case $n = 3$



the maximum at $p = 0.5$ and increases as p increases. Since p represents the mean velocity of individual pedestrians, it is obvious that large p attains large flow. Figure 7b is similar to Fig. 7a; however, this result is new and surprising because the values of v and Δl are constant, i.e., mean velocity is same in all the five curves ($p = 0.2, 0.4, 0.6, 0.8, 1.0$). Small p implies large variance, so that the flow becomes large when the variance is small even if the mean velocity of individual pedestrians is same.

7 Simple Evacuation Model

In this section, we would like to apply our transformation method to a simple evacuation model [18] as shown in Fig. 8. The model focuses on an exit cell and its Neumann neighboring cell, and updated in parallel. The number of the neighboring cells is given as n . Since we consider congested situation, we assume that pedestrians enter the n neighboring cell with the probability 1 if they are empty. The pedestrians at the n neighboring cell move to the exit cell with the probability p . When more than one pedestrian move to the exit cell at the exit same time, a conflict occur. We solve this phenomenon by using friction parameter $\mu \in [0,1]$. One of them randomly succeeds to move to the exit cell with the probability $1 - \mu$, while movements of all of them are denied with the probability μ . The pedestrian at the exit cell get out from the room with the probability 1.

Average pedestrian outflow through the exit cell, i.e., the average number of pedestrians go through the exit cell in a unit time step, is calculated as follows:

$$Q(n, p) = \left[\frac{1}{r(n)} + \frac{1}{p} \right]^{-1} [\text{step}^{-1}],$$

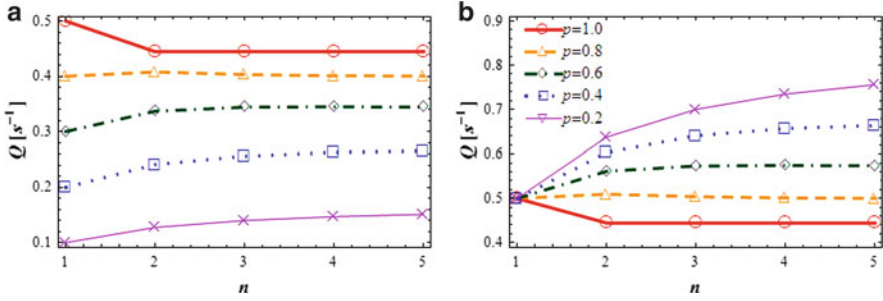


Fig. 9 Average pedestrian outflow Q as a function of the number of neighboring cells n in the case $\mu = 0.2$. **(a)** (Evac.-A) Before applying the variable transformation method. **(b)** (Evac.-B) After applying the variable transformation method

where,

$$b(k) = \binom{n}{k} p^k (1 - p)^{n-k},$$

$$r(n) = \sum_{k=1}^n [(1 - \mu) b(k)].$$

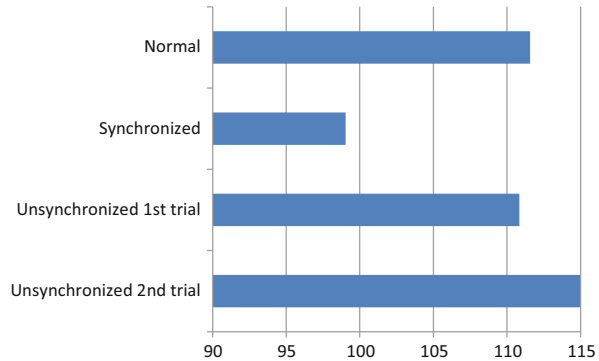
By dividing the equation of flow by Δt and substituting the equation of Δt , the expression of the average pedestrian outflow is transformed as

$$\text{(Evac. - A)} \quad Q(n, p, \Delta t) = \frac{v}{\Delta l} \left[\frac{1}{r(n)} + \frac{1}{p} \right]^{-1} [\text{sec}^{-1}],$$

$$\text{(Evac. - B)} \quad Q(n, v, p, \Delta l) = \frac{v}{\Delta l} \left[1 + \frac{p}{r(n)} \right]^{-1} [\text{sec}^{-1}].$$

Plots of (Evac.-A) with $\Delta t = 1$ and (Evac.-B) with $v = 1$ and $\Delta l = 1$ as a function of the parameter n (number of neighboring cells) in the case $\mu = 0.2$ are shown in Fig. 9a, b, respectively. In Fig. 9a, the outflow in the case $p = 1$ is the largest of the five. Since the parameter p represents the mean velocity before the transformation and the friction parameter is small ($\mu = 0.2$), the large average pedestrian flow achieved by large p . By contrast, in Fig. 9b, the outflow in the case $p = 1$ is the smallest of the five. The small p indicates the movement of pedestrians varies, thus, contrary to the TASEP case; unsynchronized movement improves the pedestrian outflow in our simple evacuation model. Synchronized movement induces increase of conflicts, so that it is not adequate for situations where many pedestrians gather at one place such as evacuation.

Fig. 10 Lap time for three rounds in the experiment 3



8 Experiment 3

We have performed a similar experiment as in Sect. 4 to verify the theoretical result obtained from the TASEP case in Sect. 6. The parameters of the circuit are $r_i = 0.6$ [m] and $r_o = 1.1$ [m], and ten male participants mainly consisted of university students go around the circuit. We performed the following three conditions, which were normal walking (Normal), walking with slow synchronized rhythm (Synchronized), and walking with slow unsynchronized rhythm (Unsynchronized). The first two are as same as the experimental conditions described in Sect. 4. The last one is a new condition. We gave portable music players, which can play 70 [BPM] rhythm of electronic metronome, to the participants. In the experiment, the participants started playing the rhythm independently, so that they heard 70 [BPM] rhythms in unsynchronized timing.

In the both Synchronized and Unsynchronized conditions, the participants heard the 70 [BPM] rhythms, thus, all the participants walk in the same pace. The difference between the two conditions is that whether they heard the rhythm from the same speaker or earphones connected to their portable music players, namely, the timing of beep sounds, whose variance implicitly corresponds to the parameter p in the TASEP. When the participants heard the synchronized rhythm, they walked in the same timing, so that Synchronized condition corresponds to large p . In contrast, when the participants heard the unsynchronized rhythm, they walked in the different timing, so that Unsynchronized condition corresponds to small p .

Lap time for three rounds are shown in Fig. 10. Since the density is $\rho = 1.87$ [persons/m], which is in the high-density regime, and 70 [BPM] rhythmic walking achieves larger flow than normal walking (Fig. 5), the lap time in the Synchronized condition is smaller than that in the Normal condition. When we compare the Synchronized condition and the Unsynchronized condition, we find that the lap time in the Synchronized condition is smaller than that in the Unsynchronized condition. This result qualitatively agrees with our theoretical expectation that large p (Synchronized) attain larger flow than small p (Unsynchronized) even if the mean velocity is same.

9 Conclusion

From our simple theoretical model and experiment with real pedestrians, we have verified that 70 [BPM] rhythm, which is slower than the walking pace in the low-density regime, improve the pedestrian flow in a circuit. The experimental result also indicates that rhythm contribute to synchronize the movement of pedestrians, thus, we apply a variable-transformation method to the TASEP and a simple evacuation model to investigate the effect of synchronization of pedestrians' movement. Our theoretical result implies that synchronization of the movement improves flow in a circuit, while it decreases outflow from an exit. We have performed another experiment with real pedestrians to verify the first result. The experimental result supports our theoretical result, i.e., even if the walking velocity of each participant is same, the flow is larger in the synchronized movement case (walking with the rhythm from a speaker) than the unsynchronized movement case (walking with the rhythm from a portable music player given to each participant).

Acknowledgment We thank Kozo Keikaku Engineering Inc. in Japan for the assistance of the experiment 1 in Sect. 4. This work is financially supported by the Japan Society for the Promotion of Science and the Japan Science and Technology Agency.

References

1. Helbing, D.: Traffic and related self-driven many-particle systems. *Rev. Mod. Phys.*, 73(4), pp. 1067–1141 (2001)
2. Schadschneider, A., Chowdhury, D. and Nishinari, K.: *Stochastic Transport in Complex Systems*. ELSEVIER (2010)
3. Helbing, D. and Molnar, P.: Social force model for pedestrian dynamics. *Phys. Rev. E*, 51(5), pp. 4282–4286 (1995)
4. Muramatsu, M., Irie, T. and Nagatani, T.: Jamming transition in pedestrian counter flow. *Physica A*, 267, pp. 487–498 (1999)
5. Burstedde, C., Klauck, K., Schadschneider, A. and Zittartz, J.: Simulation of pedestrian dynamics using a two-dimensional cellular automaton. *Physica A*, 295, pp. 507–525 (2001)
6. Parisi, D.R., Gilman, M. and Moldovan, H.: A modification of the social force model can reproduce experimental data of pedestrian flows in normal conditions. *Physica A*, 388, pp. 3600–3608 (2009)
7. Chraïbi, M., Seyfried, A. and Schadschneider, A.: Generalized centrifugal-force model for pedestrian dynamics. *Phys. Rev. E*, 82(4), 046111 (2010)
8. Seyfried, A., Steffen, B., Klingsch, W. and Boltes, M.: The fundamental diagram of pedestrian movement revisited. *J. Stat. Mech.*, 2005, P10002 (2005)
9. Online-Database at ped-net.org homepage (<http://www.pednet.org/>) and the references there in (2008)
10. Zhang, J., Klingsch, W., Schadschneider, A. and Seyfried, A.: Transitions in pedestrian fundamental diagrams of straight corridors and T-junctions. *J. Stat. Mech.*, 2011, P06004 (2011)
11. Zhang, J., Klingsch, W., Schadschneider, A. and Seyfried, A.: Ordering in bidirectional pedestrian flows and its influence on the fundamental diagram. *J. Stat. Mech.* 2012, P02002 (2012)

12. Jelic, A. Appert-Rolland, C. Lemerrier, S. and Petre, J.: Properties of pedestrians walking in line: Fundamental diagrams. *Phys. Rev. E*, 85(3), 036111 (2012)
13. Yanagisawa, D., Kimura, A., Tomoeda, A., Nishi, R., Suma, Y., Ohtsuka, K. and Nishinari, K.: Introduction of frictional and turning function for pedestrian outflow with an obstacle. *Phys. Rev. E*, 80(3), 036110 (2009)
14. Styns, F., Noorden, L., Moelants, D. and Leman, M.: Walking on music, *Human Movement Sci.* 26, pp. 769–785 (2007)
15. Yanagisawa, D., Tomoeda, A. and Nishinari, K.: Improvement of pedestrian flow by slow rhythm. *Physical Review E*, 85(1), 016111 (2012)
16. Kanai, M.: Calibration of the Particle Density in Cellular-Automaton Models for Traffic Flow. *J. Phys. Soc. Jpn.*, 79(7), 075002 (2010)
17. Spitzer, F.: Interaction of markov processes. *Adv. Math.*, 5(2), pp. 246–290 (1970)
18. Yanagisawa, D. and Nishinari, K.: Mean-field theory for pedestrian outflow through an exit. *Phys. Rev. E*, 76(6), 061117 (2007)

Interaction Behavior Between Individual Pedestrians

Winnie Daamen, Serge Hoogendoorn, Mario Campanella, and Dirk Versluis

Abstract In this contribution, data on pedestrian interactions are analyzed stemming from newly performed laboratory experiments. It has been found that pedestrians perform interaction movements in 88 % of all occasions they meet another pedestrian. These interaction movements consist of lateral and/or longitudinal evasive maneuvers. For crossing situations the approach direction has no influence on the passing side. However, if the approach angle increases and the situation comes closer to bidirectional, pedestrians prefer passing each other on the right hand side. Walking in a hurry increases the probability of passing in front of another pedestrian. Meeting two pedestrians increases the probability of passing at the back. Pedestrians prefer larger lateral evasion in bidirectional situations and larger longitudinal evasion in crossing situations. Moreover, men laterally evade more than women and hurried pedestrians laterally evade more than normally walking pedestrians. Finally, the extent of evasion is larger when small groups are encountered.

Keywords Pedestrian interaction • Laboratory experiments

1 Introduction

Recently, public places such as shopping malls and public transport terminals have become more and more crowded due to increased population size and mobility. Planners and designers of such public spaces have a large need for accurate

W. Daamen (✉) • S. Hoogendoorn • M. Campanella
Department of Transport & Planning, Delft University of Technology, Delft, The Netherlands
e-mail: w.daamen@tudelft.nl; s.p.hoogendoorn@tudelft.nl; m.c.campanella@tudelft.nl

D. Versluis
HTM, The Hague, The Netherlands
e-mail: versluis.dirk@gmail.com

evaluation tools. Microscopic pedestrian simulation models, such as the social forces model [1], Legion [2], and Nomad [3], can provide an objective assessment of a pedestrian facility and quantitatively predict critical areas and bottlenecks in the facility's design.

An important feature of these microscopic models is the ability to represent individual walking behavior in a realistic way to be able to extrapolate towards unknown and future situations. However, detailed observations of this behavior are missing.

Especially these interactions between individual pedestrians appear to be poorly simulated on the microscopic level [4]. Pedestrian movements in these situations mostly look rather abrupt and jerkily where smooth and fluent paths are expected. The main goal of the research described in this paper is to identify the interaction between individual pedestrians.

Based on a literature study, major aspects that influence pedestrian interaction but are not yet included in theory and models, have been indicated. To check the validity of these presumed (existing and new) influential aspects, new laboratory experiments have been performed. The resulting data have been analyzed and implications for microscopic pedestrian modeling are indicated.

The outline of this paper follows the research approach closely. It starts with the setup of the experiments. Then, analyses of the resulting trajectory data are presented. We end with conclusions and recommendations for future research.

2 Experimental Setup

In order to identify and quantify pedestrian interaction movements we collected detailed data on this process in laboratory experiments. Based on the literature study, we have selected the following experimental variables: age, body size, gender, free speed, travel purpose, maneuverability, number of pedestrians and walking arrangements. In the experiments, the influence of the experimental variables on pedestrian interaction movements will be measured. This requires observations on the intended path, where pedestrians are not hindered by other pedestrians. Walking outside the intended path in unhindered walking implies that interaction movements are performed. Interaction movements can be quantified by measuring lateral and longitudinal evasion from the mean trajectory and mean speed graph in unhindered walking. A simple measure to describe pedestrian interaction behavior is the passing side. The participants may pass each other on the left hand side or on the right hand side (in bidirectional and overtaking situations) or at the front or at the back (in crossing situations).

Table 1 shows an overview of the interaction experiments. Each experiment consists of several repetitions performed by different couples (i.e. sets of participants) to guarantee statistical reliability of the results. Each bi-directional and overtaking experiment consists of (at least) 48 runs in total and each crossing experiment consists of 72 runs in total.

Table 1 Overview of interaction experiments

Experiment number	Motion pace		Walking arrangements					Number of pedestrians		Maneuverability	
	N	H	↕	↑↑	↘	↗	↙	1-on-1	2-on-1	O	R
1 (ref.)	X		X					X		X	
2		X	X					X		X	
3		X		X				X		X	
4	X				X			X		X	
5	X					X		X		X	
6		X				X		X		X	
7	X						X	X		X	
8	X					X			X	X	
9	X		X						X	X	
10	X		X					X			X
11	X					X		X			X

N = Normal, H = Hurry, O = nO reduced maneuverability, R = Reduced maneuverability

The experiments have taken place on a single day and only a limited number of participants (1–3) can be active at once. Furthermore, the total workload (i.e. the total distance to be walked) for each participant has to be acceptable, so about 8 km of walking for a full day. The selection of participants has to meet the requirements on the fixed individual experimental variable gender. Taking all this into account, a group of eight participants (four men and four women) was found most suited for the experiments. A walking length of 20 m has been chosen for the final experimental design. Interaction is expected to happen halfway this length, i.e. at 10 m from the initial starting position.

The experiments have been performed in a hall on Friday January 9th in 2009. An impression of the experimental site can be found in Fig. 1a. A concrete floor of approximately 40 × 16 m is available under a 10 m high ceiling. Video cameras have been attached to the ceiling (see Fig. 1b for an example of the resulting images) and an existing method [5] has been used to derive trajectory data with an accuracy of approximately ±0.02 m for each recorded image (25 per second) in optimal lighting conditions.

3 Analyses on Unhindered Walking

The aim of this section is to derive boundaries for an intended path in unhindered walking, both in lateral and in longitudinal direction. As presented before, walking outside of these boundaries in interaction situations implies that interaction occurs. The boundaries for unhindered walking depend on the effects of swaying and natural deviation. To derive the swaying amplitude a sine function is estimated through this trajectory using a nonlinear least square method, while upper and lower boundaries

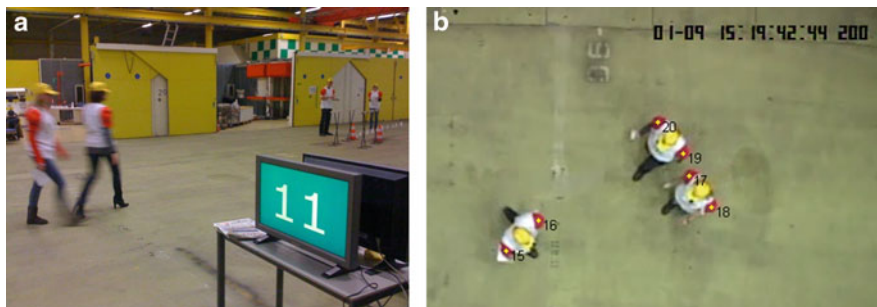


Fig. 1 Overview of the experimental site. (a) Site overview. (b) Top view from camera

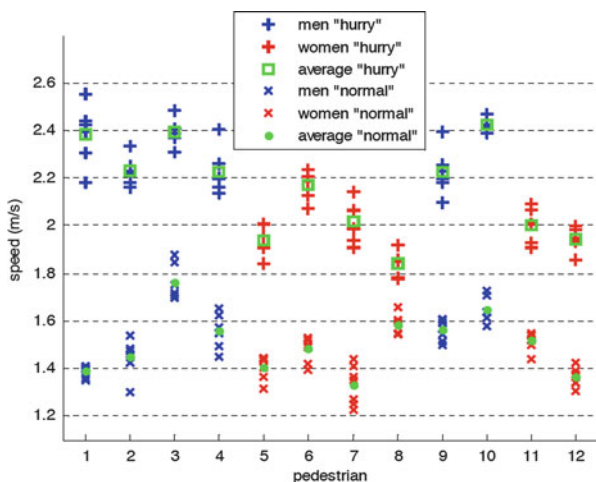


Fig. 2 Walking speed in unhindered conditions

on the amplitude and frequency of the sine function allow for a proper fit. The fitted sine function appears to follow the observed trajectory pretty well, i.e. amplitude, frequency and phase of the sine function resemble the observed trajectory.

Figure 2 shows the observed free speeds calculated over each complete trajectory in unhindered walking. It can be seen that, as expected, almost all hurried runs are performed with a higher free speed than the normal runs. On average, men walk faster than women, especially in hurried conditions. The step length in each run of each participant can be derived from the frequency of the sine function, for it is equal to half the sine period. It follows that the step length (like the swaying amplitude) is individually defined. On average, men have larger step lengths than women, which can be explained by the fact that men on average have longer legs than women have. Moreover, the step length is larger in hurried conditions than in normal conditions. It seems that hurried pedestrians try to maintain their relatively

high walking speed with larger step length than in normal walking conditions. In hurried walking conditions the step frequency is on average larger than in the normal walking condition. Apparently, pedestrians increase their motion pace not only by lengthening their steps but also by increasing their step frequency. Moreover, on average men seem to have a lower step frequency than women, especially at normal motion pace. It seems that mainly the larger step length is accountable for the fact that men walk faster than women and that the influence of step frequency is rather small.

Even in unhindered walking deviations occur in both longitudinal and lateral direction, which are visible in the trajectories. Especially the swaying effect should be accounted for in order to correctly assign a deviation from the path to an interaction instead of to a natural sway. Therefore, the trajectories for the individual pedestrians have been corrected for this individual swaying effect and boundaries have been determined by taking two standard deviations from the mean path.

4 Analyses on Interaction Movements

Although literature research has shown that interaction exists between pedestrians, these interaction movements have not been quantified yet. Since trajectory observations are only available around the interaction location, we choose to quantify interaction movements as the extent of lateral and longitudinal evasion. These are defined as the evasion from the individual mean trajectory and the individual mean speed graph in unhindered walking conditions.

The first step is to verify that interaction movements occur in the dataset. For this, the individual repetitions of an individual pedestrian are compared with his individual interaction boundaries. As an example, Figure 3 shows the interaction movements of a participant in the bidirectional interaction experiment. It can be seen that the lower longitudinal interaction boundary is crossed in three runs, i.e. the walking speed has dropped while interacting. Also, participant 3 shows lateral evasion movement to the right hand side (i.e. negative y-value) in all runs. As expected, the results show that 95 % respectively 96 % of the normal and hurried unhindered walking trajectories are within the interaction boundaries. Only 12 % of all trajectories from the interaction runs are within the interaction boundaries, indicating that no interaction movements are performed here. In these cases, the other participant(s) of the couple perform(s) an interaction movement.

Most interaction movements occur in both lateral and longitudinal direction. Mere lateral interaction movements occur more often than mere longitudinal ones, especially for bidirectional situations. An explanation is that in these situations lateral movement by one of the participants is compulsory in order to pass each other, while in crossing situations only a change of walking speed (i.e. in the longitudinal direction) may avert a collision as well. Hurried participants stay within the interaction boundaries more often than normally walking participants (16 % vs. 12 %). If they evade, they tend to do so in the lateral direction: adjusting their

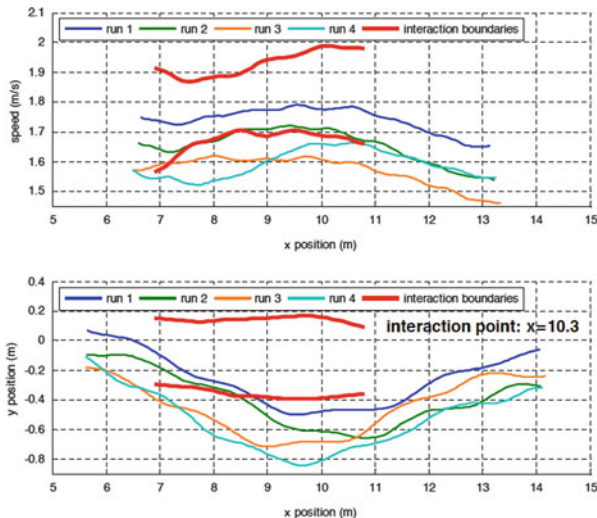


Fig. 3 Bi-directional interaction movements (Participant 3 in couple 13)

walking speed is difficult for hurried participants, since slowing down would annul their hurry and speeding up is laborious for they already walk relatively fast. Also, hurried pedestrians may (enforce and) be granted their intended path more often than normal walking pedestrians.

4.1 Passing Side

Individual pedestrians strongly prefer to pass each other on the right hand side in bidirectional situations (96.6 %). Lateral evasion occurs in line with the passing side. However, a substantial amount (26 %) of the observations shows an increased walking speed during interaction, whereas 22 % shows a decreased walking speed. Most increased walking speed observations are found while a lateral evasion is performed as well. The lateral evasion is likely to be even larger when a small group of two pedestrians has to be passed, explaining why most of the increased walking speeds are found for trajectories from the bidirectional 2-on-1 situation.

For individual overtaking situations the passing side does not seem to be governed by general behavioral or external rules, as is the case in car traffic. The passing side was about equal: in 25 out of 48 runs the person was overtaken on the right hand side. Most participants did have an individual preference: they overtook at the same side during all repetitions. The lateral evasion of the overtaker occurs in line with the passing side (100 % compliance). In nearly half the repetitions the overtaker did not increase his speed to overtake, but walked with a constant speed.

For all crossing experiments combined, in accordance with the expectations, the participants from the right have a slight tendency of passing in front of participants coming from the left (58 %). However, in the 135 ° crossing situation pedestrians from the right hand side tend to pass in front of pedestrians from the left hand side (82 %), which is similar to passing on the right hand side in the bidirectional situation. For crossing situations with an approach angle less than or equal to 90° the passing side is therefore independent of the side of approach.

For all crossing interaction situations 71 % of the observations show an increased walking speed and a lateral evasion towards the destination of the other pedestrian while passing in front or a decreased walking speed and a lateral evasion towards the origin of the other while passing at the back. However, in 67 % of the remaining observations in crossing situations pedestrians may try to solve a collision course by laterally evading to the left hand side. Pedestrian gender has no influence on the passing side in crossing situations (in 52 % of the cases women pass in front of men), but walking in a hurry increases the chance of passing in front (81 %), as does walking in a small group (65 %).

4.2 *Extent of Evasion*

Table 2 gives an overview of the extent of evasion for the different walking configurations. Pedestrians generally prefer larger lateral evasion in the bidirectional situation and larger longitudinal evasion in crossing situations. This can be explained by the necessity for lateral evasion to continue walking in the bidirectional situation, while in crossing situations longitudinal evasions may avert a collision as well.

It appears that men laterally evade more than women do (26 cm vs. 22 cm). Moreover, men make larger changes in walking speed than women do (0.15 m/s vs. 0.10 m/s). This can be seen as gallantry towards others. However, this gallantry should have appeared in more women passing in front of men in the crossing situations, but this is not the case. The gender issue is therefore recommended for further research.

It seems that pedestrians laterally evade as much while meeting a hurried pedestrian as they do when meeting a normally walking pedestrian (23 cm). It appears that hurried pedestrians take the initiative by performing a lateral evasion movement while interacting. This improves their opportunity to maintain their hurried pace. Pedestrians encountering a hurried pedestrian make larger changes in their walking speed than while encountering a normally walking pedestrian (0.13 m/s vs. 0.10 m/s). In addition, individual interaction movements are larger when more other pedestrians are encountered (43 cm vs. 28 cm).

Table 2 Extent of evasion in several walking arrangements

Experiment	Interaction point (m)		Lateral evasion (m)		Longitudinal evasion (m/s)		Observations
	μ	σ	μ	σ	μ	σ	
1 Bidirectional	10.0	0.46	0.26	0.18	0.11	0.06	168
3 Overtaking	8.1	1.66	0.35	0.44	0.13	0.09	96
4 Crossing 45°	9.7	0.74	0.09	0.28	0.17	0.16	144
5 Crossing 90°	10.1	0.70	0.23	0.32	0.14	0.14	144
7 Crossing 135°	10.0	0.51	0.16	0.24	0.11	0.09	142

5 Implications for Theory and Models

As has been shown in literature and underpinned better in this paper, existing theories do not correctly describe interaction behavior of pedestrians in situations where two single pedestrians meet each other or a single pedestrian meets a pair. Not only the heterogeneity in pedestrian behavior, but also the difference in behavior in different situations (bi-directional interactions, crossing interactions) is not covered in these theories. However, since these theories do correctly describe pedestrian flow behavior, the problem is in the ‘summability’ of pedestrian behavior. This means that the behavior of a group of pedestrians is not simply the behavior of the sum of all individuals in the group, which explains the specific research into this group or crowd behavior (see e.g. [5]). Finally, this paper showed that pedestrians in a hurry, or more generally spoken in a different state of mind, demonstrate clearly different behavior from normal walking pedestrians. Current theories do not include these different behaviors. In some facilities (e.g. train stations), this deviating behavior will be more important than in other facilities (e.g. shopping centers). The consequences of this different behavior on the total flow behavior should be investigated in more detail.

6 Conclusions and Recommendations

This paper showed that pedestrians perform interaction movements in 88 % of all occasions when they meet another pedestrian. These interaction movements consist of lateral and/or longitudinal evasive maneuvers.

For crossing situations the approach direction has no influence on the passing side. However, if the approach angle increases and the situation comes closer to bidirectional, pedestrians prefer passing each other on the right hand side. In the bidirectional situation pedestrians strongly prefer passing on the right hand side. Walking in a hurry increases the probability of passing in front of another pedestrian in crossing situations. Meeting a small group of two pedestrians increases the probability of passing at the back. Pedestrians seem to prefer larger lateral evasion in

bidirectional situations and larger longitudinal evasion in crossing situations. Men laterally evade more than women and hurried pedestrians laterally evade more than normally walking pedestrians. Finally, the extent of evasion is larger when small groups are encountered.

Several aspects regarding individual pedestrian interaction need further research. Among these are the initiation moment of interaction movements and the effects of gender, body size and age on pedestrian interaction. Also, the effect of ‘near collision courses’ on interaction movements, the passing side and the extent of evasion is recommended for further research. Including shoulder rotation in pedestrian simulation models may improve the interaction behavior and the visualization of pedestrian movement. These aspects can be investigated with the video data obtained in this study.

References

1. Helbing, D., Molnar, P.: Social Force Model for Pedestrian Dynamics, *Phys. Rev. E*, vol. 51, No. 5, pp. 4282–4286 (1995)
2. www.legion.com. Accessed July 31, 2011
3. Hoogendoorn, S.P., Bovy, P.H.L.: Normative Pedestrian Behavior Theory and Modeling, In Taylor, M.A.P. (ed.), *Transportation and traffic theory in the 21st century*, Oxford: Pergamon, Elsevier science, pp. 219–245 (2002)
4. Moussaïd, M., Helbing, D., Garnier, S., Johansson, A., Combe, M., Theraulaz, G.: Experimental Study of the Behavioural Mechanisms underlying Self-organisation in Human Crowds, *Proceedings of The Royal Society B*, Vol. 276, pp. 2755–2762 (2009)
5. Hoogendoorn, S.P., Bovy, P.H.L., Daamen, W.: Extracting Microscopic Pedestrian Characteristics from Video Data, In: *Transportation Research Board annual meeting 2003*, Washington DC: National Academy Press, pp 1–15 (2003)

New Wayfinding Techniques in Pathfinder and Supporting Research

Charles Thornton, Richard O’Konski, Bryan Klein, Brian Hardeman,
and Daniel Swenson

Abstract This paper presents the wayfinding and door selection algorithm used by the Pathfinder egress simulator. The development of Pathfinder’s Locally Quickest algorithm will be discussed along with unforeseen consequences and one promising, but discarded, initial attempt. Validation of this new model is presented as well as characteristics of the third party research that make simulator validation possible.

Keywords Pathfinder • Evacuation • Simulation

1 Introduction

Pathfinder is a commercial agent-based emergency egress simulator. The software includes a user interface, simulator, and 3D visualization system. The wayfinding method discussed in this paper is an aspect of the simulator.

Simulation agents, or occupants, moving from their starting locations to an exit must choose a route to follow when walking toward their chosen exit. This route selection process (wayfinding) significantly affects the overall simulation results, as time spent waiting in queues and time spent walking control the time it takes all agents to reach their objectives.

Previously, Pathfinder used a simple procedure to perform this wayfinding task. Using the A Star (A*) search algorithm, Pathfinder would calculate, for each agent, the shortest possible path the agent could take to exit the model. Because this approach did not account for queue formation at doorways, bottlenecks along the selected route, and equivalent alternative routes, it was necessary to use a variety

C. Thornton (✉) • R. O’Konski • B. Klein • B. Hardeman • D. Swenson
Thunderhead Engineering, 403 Poyntz Ave STE B, Manhattan, KS 66503, USA
e-mail: thornton@thunderheadeng.com; okonski@thunderheadeng.com;
klein@thunderheadeng.com; swenson@thunderheadeng.com

Fig. 1 Shortest-path-only agents fail to utilize the full width of divided doors



of workarounds to encourage agents to walk a few extra steps to avoid large queue times. An illustration of this problem is shown in Fig. 1.

Figure 1 shows a case where simulated agents attempted to exit a room using a divided door. Initially, the agents were positioned in the lower portion of the room. In this case, only one agent utilized the upper portion of the divided door. This occurred because the shortest path-based wayfinding algorithm relied only on the distance between the agents' initial starting position and the nearest intended exit. The calculation did not take into account the impact congestion would have on total travel time.

A similar problem occurred any time agents needed to pass through a bottleneck on the way to multiple exits (e.g. a hallway that led to an entry area that contained a bank of exit doors). In this situation, the path planning algorithm performed the same calculations for each agent after reaching a common point. This led to situations where all of the agents would pursue only the nearest of many available doors.

2 Locally Quickest

The Locally Quickest algorithm is designed to overcome the problems mentioned in the previous section. Instead of calculating a complete path to the exit at the beginning of the simulation, the Locally Quickest algorithm selects a door leading out of the current room. This process is repeated each time the agent enters a new room, until the agent has exited the simulation.

When evaluating routes leading out of the current room, agents calculate a time estimate for each route (i.e. door). This estimate takes into account the following parameters:

- An estimate for how long it will take to reach and pass through a local door, and
- An estimate for how long it will take to reach a valid exit after arriving at the local door.

When selecting a local door, agents compare the time to traverse the shortest path to the door with the time it would take to move through the queue that has formed at the door. The time required to enter the room beyond the door is assumed to be the larger of these two values.

To calculate the time to reach an exit beyond the local door, Pathfinder performs a distance calculation based on A* path search. Agents use the results of the distance calculation with their maximum velocities to estimate a time. This calculation assumes that agents have no knowledge of queues in other rooms, so the results represent the fastest possible time beyond the agent's current room.

After estimating the local travel time and the time beyond the current room, agents select the door that provides the fastest overall time to their goal. In cases where multiple local doors appear to provide very similar travel times, agents will select a path through the nearest of the equivalent doors.

2.1 Local Movement Time

The local movement time calculation is important in ensuring that agents intelligently utilize all available egress doors within the current room. This element of the algorithm provides agents with a way to decide to use a longer route if the shortest available route is congested.

Calculating local movement time in an empty room is a straightforward process. The distance to the next doorway can be determined using A* search and the agent's velocity can be used to derive movement time from the distance. However, the presence of other agents makes this process much more challenging. It is necessary for the agent to estimate how long it will take to reach the door when waiting in a queue.

An early approach operated on the assumption that congestion would exist primarily around the doors (e.g. in areas where agents were waiting to pass through the door) and that a fine-grained density calculation [1] could indicate areas of congestion. An example of this approach is shown in Figs. 2 and 3.

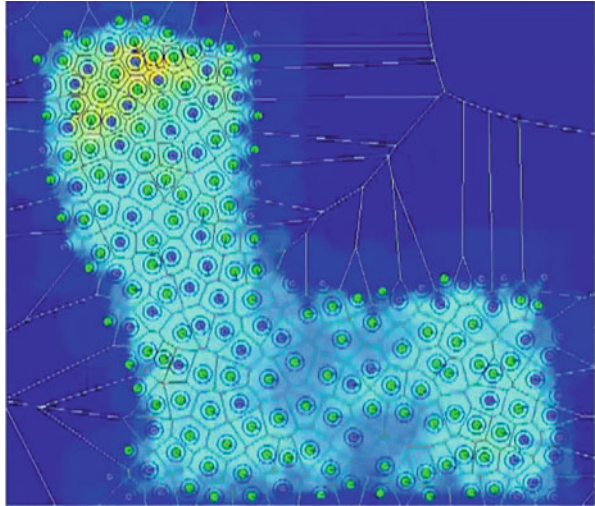
The model shown in Fig. 2 is an L-shaped room with 12 exit doors. The exit doors are structured like turnstiles with 0.5 m deep divisions. All agents were initially packed into the upper-left portion of the model, making the top exit door the closest for most agents. Figure 3 is a visualization of the Voronoi-diagram-based, fine-grained density calculation as the agents began to reach the exit doors.

Using the Locally Quickest approach implemented with the fine-grained density information produced better doorway utilization than the original shortest path algorithm, but it had serious shortcomings. Because the algorithm integrated density over a straight line path, estimates for a door on the far side of another door's

Fig. 2 A Pathfinder simulation where a large group turns a corner, then exits through a series of turnstiles



Fig. 3 A visualization of the fine-grained, Voronoi diagram-based density calculation used to determine density in the simulation shown in Fig. 2



queue would receive time estimates that combined multiple doors. Also, the density calculation was not computationally fast enough to scale up to stadium-sized models.

2.2 Door Queue Approximation

Because of difficulties with a density estimation-based approach, an approach to calculate local travel time based on door queue estimates was developed. To estimate the wait time to travel to a door, agents use the maximum of two values:

- A simple estimate based on minimum travel distance and agent velocity, and

- An estimate of time that will be spent waiting in that door's queue.

To estimate the time spent waiting in a door's queue, Pathfinder needed a way to estimate queue size. This is complicated by the different time at which door selections are made by each agent. It was necessary for agents to select a door before the queues were well-formed (i.e. when other agents were still moving closer to their selected doors).

The selected approach was to store a record of which agents were using each door within each room. Then, when an agent needs to measure queue size for a door, the value can be determined by counting the agents that are waiting on the door and are also closer to the door than the agent.

Once this count is determined, Pathfinder can then calculate the wait time at the door using maximum specific flow estimates from the SFPE Handbook [2]. The greater of this calculation and the pure movement time is then used as the local time estimate for reaching the door.

This calculation is repeated periodically for each agent to account for evolving door decisions made by the other agents.

3 Backtrack Prevention

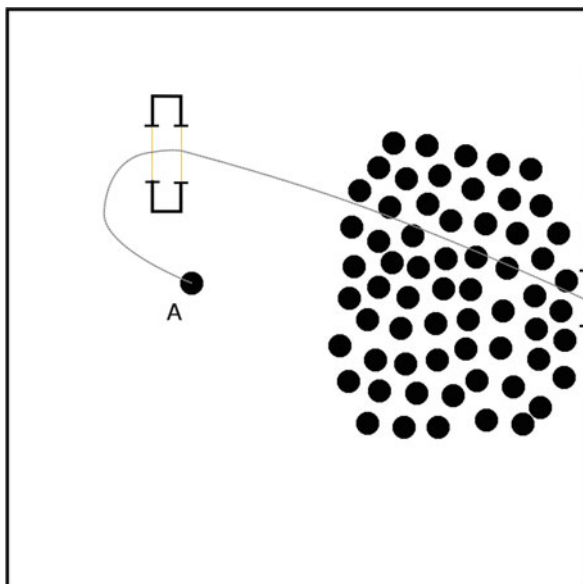
Agents are only aware of queue sizes in their current room. When they enter a new room, knowledge of the last room is replaced by knowledge of the current room. Without any sort of backtrack prevention in place, large queues could lead to agents moving back and forth between two rooms until the queue situation changed. To prevent these oscillations, the Locally Quickest algorithm uses the following rules when selecting the list of doors agents are allowed to evaluate when considering an exit plan:

- Available local doors must have a shorter path to the agent's destination than the door through which the agent entered the current room.
- Local doors may not lead back into the room the agent previously occupied.
- If the previous criteria eliminate all available doors (e.g. the agent has been pushed into a closet) or the agent has been pushed through an unintended door, backtrack prevention is disabled. All local doors are available.

4 Downstream Queues

Another issue that occurs with certain floor plans is failure to apply downstream queue knowledge. Previously, the time from a local door to the destination has been discussed as an optimized value. However, because the algorithm places so much emphasis on the current room, situations where the current room is also a subsequent

Fig. 4 Two floor plans that require downstream queue awareness to function properly



room require that knowledge of the current room be applied to time estimates to any segments of the route after the local door that pass through the current room.

Figure 4 shows a room that contains a smaller room with two doors. The agent denoted by the letter “A” must choose between three available doors. Two doors belong to the small room contained in the upper left quadrant of the larger room. The third door is the goal door at the right.

The current description of the locally quickest algorithm suggests that, when evaluating the time beyond the doors of the small room a minimal, distance-based time calculation be used. However, in this case, that would cause the agent to walk through the tiny room, believing that upon emerging the large queue at the right will have dissipated. If you initialized the simulation in this configuration, many agents would peel off of the back of the queue and instead line up to go through the tiny room before emerging and lining up again behind the “real” door.

Pathfinder solves this problem by storing the optimal route calculated beyond each local door. If the route passes through the agent’s current room, the agent replaces the time estimation for that segment of the route with a more accurate version based on the agent’s knowledge of the current room. The improved estimate is made in exactly the same way as the initial door queue time approximation, by comparing the time it takes to travel the segment distance to the time spent waiting in queues and keeping the maximum value.

Fig. 5 Selected images of a pathfinder simulation of the case study

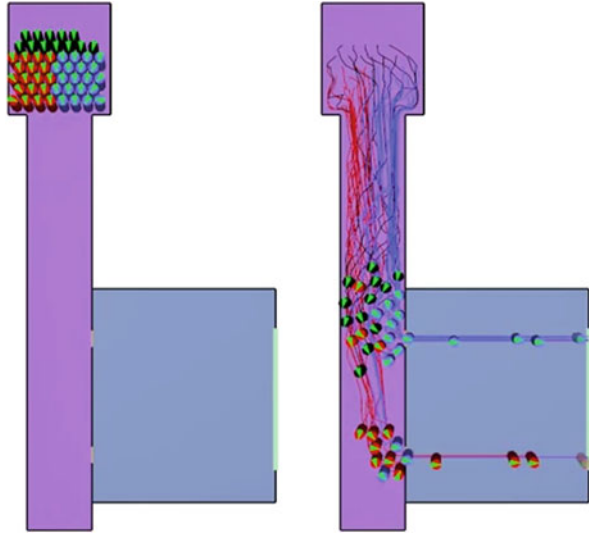


Fig. 6 Results of door selection case study

	Pathfinder Exit Usage	
	Top	Bottom
Left (blue)	16	4
Right (red)	5	13
Back (black)	5	7

5 Door Selection Case Study

To test the impact of the Locally Quickest movement algorithm on agent door selection, a door selection case study from VTT Research Notes 2562 [3] was used. In this study, university students were monitored as they moved from a staging area, through a hallway and into a lecture hall. The lecture hall had two entrance doors arranged consecutively along the same wall.

Pathfinder was compared against a general observation of the researchers who performed the test, "... people on the right (relative to the direction of movement) on the starting grid chose [the second door]. People on the left of the grid or in the center of the front rows chose the first door: door 1. In the back row, there was a tendency to use door 2." Figure 5 shows the floor plan of the case study.

The floor plan in Fig. 5 shows the starting locations and movement paths of a Pathfinder simulation model for this test case. The results of the simulation are shown in Fig. 6.

In Fig. 6 the first door is indicated as "Top" and the second door is indicated as "Bottom". People to the right, left, and back are indicated as "Right (red)", "Left (blue)", and "Back (black)".

These results indicate that the results in Pathfinder agree with the general observations given by Rinne, Tillander, and Grönberg. The success of this case study represents a significant step forward for Pathfinder which previously would have given significant bias to the first door in all cases.

References

1. Steffen, B. and Seyfried, A. (2010) Methods for measuring pedestrian density, flow, speed and direction with minimal scatter. *Physica A* 389 (2010) 9, 1902–1910
2. Nelson, H. E. and Mowrer, F. W.: Emergency Movement. In: P. J. Denno & W. D. Walton (Eds.), *The SFPE Handbook of Fire Protection Engineering* (Third ed., pp. 3–367–3–380). Society of Fire Protection Engineers, Bethesda, MD (2002)
3. Rinne, T., Tillander, K., and Grönberg, P. 2010. Data collection and analysis of evacuation situations (pp A86-A92). VTT Research Notes 2562, Finland.

OpenPedSim: A Framework for Pedestrian Flow Analysis

Armel Ulrich Kemloh Wagoum, Mohcine Chraibi, Christian Eilhardt, Stefan Nowak, Igor Kulkov, Daniel Weber, Kathrin Sauer, Hubert Klüpfel, and Andreas Schadschneider

Abstract There exists a wide range of simulation software for the pedestrian dynamics area. Most of these software are commercial, or do not give an insight in their functionality. While this might be of little importance for some end user, it is very important for researchers to know exactly what the models are performing. This constitutes a significant advantage in the interpretation of the results. In this paper we introduce OpenPedSim (Open Pedestrian Simulation), an open source framework for performing pedestrian simulations. This framework should support researchers by the development of new models by providing a suitable environment with appropriate interfaces.

A.U.K. Wagoum (✉)
Forschungszentrum Jülich GmbH, Jülich Supercomputing Centre, Jülich 52428, Germany
Division Civil Security and Traffic, Institute for Advanced Simulation, Jülich, Germany
e-mail: u.kemloh.wagoum@fz-juelich.de

M. Chraibi
Forschungszentrum Jülich GmbH, Jülich Supercomputing Centre, Jülich 52428, Germany
e-mail: m.chraibi@fz-juelich.de

C. Eilhardt • S. Nowak • A. Schadschneider
Institute for Theoretical Physics, Universität zu Köln, Köln 50937, Germany

I. Kulkov • D. Weber
Physik von Transport und Verkehr, Universität Duisburg-Essen, Duisburg 47048, Germany

H. Klüpfel
TraffGo HT GmbH, Duisburg 47057, Germany
e-mail: kluepfel@traffgo.ht

K. Sauer
IMS Gesellschaft für Informations- und Managementsysteme mbH, Dinslaken 46539, Germany

1 Introduction

In recent years pedestrian dynamics has gained more importance and a lot of attention due to continuously growing urban population and cities combined with an increase of mass events. In this context simulations are already performed and critical decisions are taken based on the simulation results. There are many simulation software packages for this purpose [1–6].

2 Motivation

The motivation for starting OPS was the following: In many universities and thesis projects, a lot of time is spent on setting up a proper environment for the development of the new idea. Although the main objective is, for instance the development of a new pedestrian model, the work on utilities like an editor for the geometry or for the input of data, a tool for visualizing the results is an enormous entry barrier. Another side issue is the definition of file formats. Only after those steps have been successfully taken, the real work starts. And usually this work has to be done as fast as possible. Most of the time, the result is code which is neither reusable, nor maintainable, nor scalable. We are hereby introducing OpenPedSim (Open Pedestrian Simulation), an open source framework for performing pedestrian simulations, to address those issues. The primary goal of OpenPedSim is to provide students and researchers with a toolbox that will let them focus on their main task, i.e. the development, calibration, and validation of new models or model features. OPS is currently focusing on evacuation, but will be extended to cover other areas as well. These include: passengers exchange, commuter traffic in railway stations. Finally, OpenPedSim also provides sample data sets for calibration and validation. We are developing some standards and benchmark scenarios for evaluation pedestrian simulations. This task is closely linked to Rimea [7] and the IMO validation cases [8].

3 Conventions

The modules which are proper parts of OpenPedSim are denoted OPSx, where x stands for the editor (i.e. OPSed), the simulation kernel (i.e. OPSgcfm), etc. Modules which have not yet been implemented are shown in *italic* (e.g. OPScontrol and OPSreport). “Modules” which are not part of OPS, but are freely available and closely linked to OPS do not have the OPS prefix (e.g. PeTrack).

4 Getting Started with OpenPedSim

OpenPedSim is hosted at Sourceforge. The different modules of OpenPedSim can be downloaded from <http://sourceforge.net/projects/openpedsim/files/>. There are also pre-compiled binaries for the common platforms (Windows/Linux/OSX). The latest development code snapshot can be downloaded via the revision system subversion (svn) at the URL: <https://openpedsim.svn.sourceforge.net/svnroot/openpedsim>. The development language is C/C++. Developers and users are highly encouraged to participate.

5 Work Flow in Pedestrian Flow Analyses

As said above, a major aim of OpenPedSim is to make life simple (i.e. as simple as possible) for students, researchers, and programmers. Therefore, OpenPedSim provides well-designed interfaces and file-formats to reflect the steps that have to be carried out when simulating pedestrian flows and analyzing the results. Usually, a pedestrian flow simulation comprises the following steps:

- Importing the geometry (either from CAD or from GIS)
- Specifying the population (synthetic population, including activities)
- Specifying further parameters (e.g., environment, hazards)
- Performing simulation runs (including parameter variation, stochastic variance, etc.)
- Data Analysis and Interpretation

The single modules of OPS are designed to provide the capabilities for performing each of these steps. At the same time, the steps are separated from each other (“divide and conquer” [9]). From a technical point of view, the modules are the focus. The following list shows their application domain:

- Editor ↔ Geometry
- Editor ↔ Population
- Editor ↔ Environment
- Simulation Kernel ↔ Performing simulation runs
- Visualizer, Reporting Tools ↔ Data Analysis

6 The OPS Framework

The OPS framework is described in Fig. 1. It consists of loosely coupled modules. i.e., the modules can be used individually, but then only part of the work flow described above is covered. The editor allows the creation of new scenarios for a simulation. A scenario comprises a geometry, information about the pedestrians

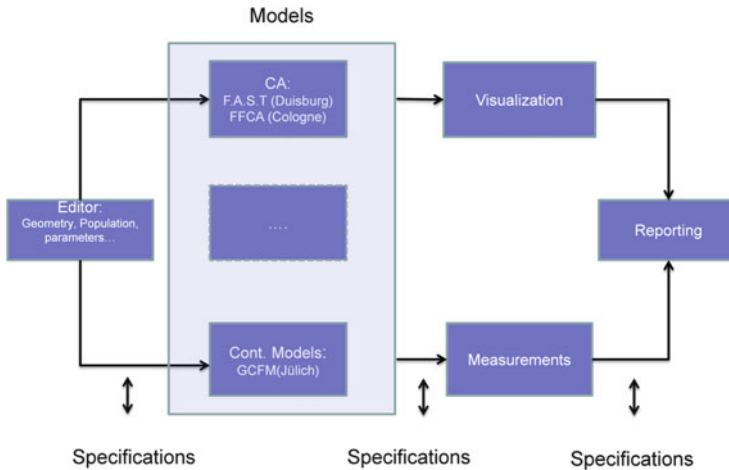


Fig. 1 Structure of the Open Pedestrian Simulation framework. The ellipses denote further simulation modules which can easily be plugged in, since the modules like OPSed or OPStraVisTo are self-contained and the interfaces are well-designed, specified, and documented

and other constraints. Constraints can be the state of rooms or doors, blocked for instance. These are the input to the models. The results of the models are then visualized using the module designed for that purpose. The results are the trajectories of the individual pedestrians in the simulation. But other models can output other type of results as well, density for instance. In addition, a measurement tool analyses the results. Finally a report is generated.

A very important point here is the specification of the different interfaces. A clear and open specification facilitates the integration of new components, in this case of new models. All interfaces are not specified yet.

6.1 OPS-Modules: OPSed, OPSgcfm, OPSfast, and OPSreport

OpenPedSim actually consists of the following modules: OPSed, OPSgcfm, OPSfast and OPStraVisTo. The editor OPSed provides geometries for continuous models as well as for cellular automata.

6.2 OPSfast, OPSgcfm, and OPSFast: Performing Pedestrian Flow Simulations

There are actually three simulation kernels implemented in the framework. OPSgcfm [10] is a space continuous model. OPSfast [11] and OPSffca are cellular automata based models.

6.2.1 OPSgcfm

OPSGcfm is an implementation of the generalized centrifugal force model [10]. The GCFM is a spatially continuous force-based model. The model describes the motion of pedestrian as a superposition of forces. Consequently and according to Newton second law the motion of a pedestrian i can be described as following:

$$m_i \ddot{\vec{R}}_i = \vec{F}_i = \vec{F}_i^{\text{drv}} + \sum_{j \in \mathcal{N}_i} \vec{F}_{ij}^{\text{rep}} + \sum_{w \in \mathcal{W}_i} \vec{F}_{iw}^{\text{rep}} \quad (1)$$

where \vec{F}_i^{drv} is the driving force of pedestrian i to move towards a desired destination, $\vec{F}_{ij}^{\text{rep}}$ the repulsive force emerging from pedestrian j to i and $\vec{F}_{iw}^{\text{rep}}$ the force between the pedestrian i and walls or other stationary obstacles. The set \mathcal{N} resp. \mathcal{W} is the set of all pedestrians resp. walls that influences pedestrian i at a given moment. The basis of force-based models is the simple idea of expressing mathematically the motion of pedestrians by mean of force. It takes advantage from the well-known laws of the Newtonian mechanics. However some care is necessary while implementing those models. A detailed discussion of the some intrinsic problems of this approach, like penetration of particles, unrealistic oscillations and velocities are elaborated in [12].

6.2.2 OPSffca

As a cellular automaton model the OPSffca is discrete in time, space and state variables. It is based on the Floor Field Cellular Automaton (FFCA) [13, 14]. The dynamics is defined by transition probabilities which are determined with the help of two floor fields. The static floor field acts as a potential and represents the desire of the pedestrians to take the shortest path to the exit. The dynamic floor field covers the interaction between pedestrians. It is inspired by the chemotaxis of ants. Pedestrians leave a virtual trace which is attractive to other pedestrians. This translates the long ranged interaction between pedestrians into a local interaction with memory, thereby greatly reducing computation time. The virtual trace has its own dynamics in the form of diffusion and decay. Despite being a simple and computationally fast model, the FFCA model is able to reproduce typical collective phenomena such as lane formation in corridors or clogging at bottlenecks [15]. Additionally, the model is used in the Hermes project [16] to predict traffic jams. Furthermore, the model has been calibrated with empirical data from experiments [17].

6.2.3 OPSfast

OPStfast is an implementation of the F.A.S.T. cellular automaton model described in [11, 18]. Thanks to T. Kretz for donating his source code to OPS. As basically all

CA models for pedestrian flow simulation, OPSfast is a rule-based model. In each time-step (called “round” in [11, 18]) the update of the pedestrians is divided into 3 substeps: (1) Choosing an exit, (2) choosing a destination cell and (3) moving towards the destination cell. The first 2 substeps are probabilistic processes while the last step is deterministic with exception to the order in which pedestrians perform their movements. In every time step pedestrian i chooses an exit E with a probability $p(i,e) = N(1 + \delta_{i,e}/S(i,e))^2$, where $S(i,e)$ is the distance to exit E and $\delta_{i,e}$ is 1, if the pedestrian chose E in the previous time step and 0 otherwise. N is normalization constant. The choice of the exit is done in parallel for all pedestrians. The transition probability calculated to choose a destination cell is composed of partial probabilities representing different influences on the movement of the pedestrian. As in the FFCA model there is a static and a dynamic floor field. Additionally the effects of inertia when walking through curves, the desire to keep a safety distance from walls and the desire to keep a distance to other pedestrians are accounted for. The relative strengths of the various influences are weighted against each other by coupling constants, which have to be carefully calibrated. As in the first sub-step the choice of the destination cell is done in parallel for all pedestrians. In the last part of the update the actual movement of the pedestrians is carried out. The single moves from cell to cell are performed in a random sequential order which is established anew in every time-step. To account for the dynamic space consumption of pedestrians, cells which have been occupied once during this process are blocked for other pedestrians in this time-step.

6.3 *OPStraVisTo: Visualization of Trajectories*

For visualization purposes, we developed the Trajectories Visualization Tool, which is built on top of the Visualization Toolkit (VTK) libraries [19]. VTK is open source and platform independent library for computer graphic and provides many algorithms for visualization and data analysis as well as an interface to the C++, Java, Python and Tcl languages. OPStraVisTo reads a file containing the simulation results (coordinates, velocities, orientations . . .) together with geometry information and allows the user to interact with this information in form of an animation, for instance focusing on an area of interest or masking views. OPStraVisTo can also be used in an online mode, where simulation results are directly streamed to the application. The user interface is designed with QT.

6.4 *OPSreport: Reporting Tool*

The reporting tool is a module specified in the OPS framework and integrated in the overall work flow. Due to limited resources, the implementation of OPSreport has not yet started.

7 Summary and Outlook

At the moment the system is loosely coupled. A further integration of the different modules might be worthwhile. One idea is to provide a tool called OPScontrol. This tool then might run a certain number of simulations based on a valid model created with OPSed. The next step would be to identify the simulation run which should be investigated further and run this simulation with a detailed output, i.e. the trajectories of all persons in detail. Finally OPScontrol would invoke OPSreport to create a PDF containing a summary of the simulation results. Of course, there are many more possibilities. Another idea is to use several simulation kernels for the same scenario and compare the results “automatically” (i.e. by running OPScontrol) with the appropriate (command-line) parameters.

Acknowledgements This work has been partially performed within research projects HERMES and SPIDER in the program “Research for Civil Security”, field “Civil Protection and Rescue” funded by the German Government, Federal Ministry of Education and Research (BMBF). The project grant numbers are 13N9952, 13N10234, 13N10236.

References

1. T. Korhonen, S. Hostikka, S. Heliövaara, and H. Ehtamo. FDS + Evac: An Agent Based Fire Evacuation Model. Proceedings of the 4th International Conference on Pedestrian and Evacuation Dynamics, 2008.
2. I.S.T. Integrierte Sicherheits-Technik GmbH. Benutzerhandbuch Aseri, Version 4.6.
3. B. Raney and K. Nagel. An improved framework for large-scale multi-agent simulations of travel behavior. Towards better performing European Transportation Systems, pages 305–347, 2006.
4. E. R. Galea, S. Gwynne, P.J. Lawrence, L. Filippidis, D. Blackspields, and D. Cooney. Building EXODUS V 4.0 - User Guide and Technical Manual, 2004. www.fseg.gre.ac.uk.
5. Simulex User Guide, Virtual Environment 5.9. www.ies4d.com.
6. TraffGo HT GmbH. Handbuch PedGo 2, PedGo Editor 2, 2005. www.evacuationsimulation.com.
7. RIMEA-Richtlinie für Mikroskopische Entfluchtungsanalysen. www.rimea.de.
8. IMO, London. Interim Guidelines for Evacuation Analyses for New and Existing Passenger Ships, 2002. MSC/Circ. 1033.
9. B. Stroustrup. The C++ Programming Language. Addison-Wesley, Reading, 3 edition, 1997.
10. M. Chraïbi, A. Seyfried, and A. Schadschneider. Generalized centrifugal-force model for pedestrian dynamics. Phys. Rev. E, 82:046111, 2010.
11. T. Kretz and M. Schreckenberg. The F.A.S.T.-Model. In Cellular Automata, volume 4173/2006 of Lecture Notes in Computer Science, pages 712–715. Springer Berlin/Heidelberg, 2006.
12. M. Chraïbi, U. Kemloh, A. Seyfried, and A. Schadschneider. Force-based models of pedestrian dynamics. Networks and Heterogeneous Media, 6(3):425 – 442, 2011.
13. C. Burstedde, K. Klauck, A. Schadschneider, and J. Zittartz. Simulation of pedestrian dynamics using a two-dimensional cellular automaton. Physica A: Statistical Mechanics and its Applications, 295(3–4):507–525, 2001.
14. A. Kirchner and A. Schadschneider. Simulation of evacuation processes using a bionics-inspired cellular automaton model for pedestrian dynamics. Physica A: Statistical Mechanics and its Applications, 312(1–2):260–276, 2002.

15. A. Schadschneider, A. Kirchner, and K. Nishinari. CA Approach to Collective Phenomena in Pedestrian Dynamics, volume 2493 of Lecture Notes in Computer Science, pages 239–248. Springer, 2002.
16. A. U. Kemloh Wagoum, M. Chraibi, J. Mehlich, A. Seyfried, and A. Schadschneider. Efficient and validated simulation of crowds for an evacuation assistant, *Computer Animation and Virtual Worlds*, vol. 23, no. 1, pp. 3–15, 2012.
17. A. Schadschneider, C. Eilhardt, S. Nowak, and R. Will. Towards a calibration of the floor field cellular automaton. In Richard D Peacock et al., editors, *Pedestrian and Evacuation Dynamics*, pages 557–566. Springer, 2011.
18. T. Kretz. *Pedestrian Traffic - Simulation and Experiments*. PhD thesis, Universität Duisburg-Essen, 2007.
19. K. Martin W. Schroeder and B. Loreense. *Visualization Toolkit: An Object-Oriented Approach to 3D Graphics*, volume 4th edition. Kitware Inc., 2006.

Optimizing Pedestrian Environments with Evolutionary Strategies

Marijn Swenne and Thomas Bäck

Abstract The environment of pedestrians has a big influence on their movement efficiency. Poorly designed environments can lead to high pedestrian densities which in turn increases the risk of injury, or in the case of egress, increases tardiness. A common approach is to have an expert design an environment and test it with a simulator. We propose a method to design a pedestrian environment by using pedestrian simulation in combination with optimization by means of evolutionary strategies. The results demonstrate that optimized environment layouts can improve pedestrian throughput in comparison with basic layouts designed by humans.

Keywords Pedestrian • Environment • Optimization • Evolutionary strategy • Simulator

1 Introduction

The goal of this research is two-fold: First, a realistic pedestrian simulator is proposed, which secondly is used as a fitness evaluator for an Evolutionary Strategy (ES) for optimization. It is demonstrated in this paper how an ES can be used to find an environment that maximizes pedestrian efficiency.

For the simulator, the Social Forces Model (SFM) is used. This model represents one of the three main classes of microscopic pedestrian models. The other ones are the Benefit Cost Cellular Model (BCCM), and the Magnetic Force Model (MFM). The BCCM was first proposed by Gipps and Marksjo [3] in 1985. In this model, the space in which agents are placed is represented as a 2D cellular grid. All agents, obstacles and other objects are defined as a cell or collection of cells. This

M. Swenne (✉) • T. Bäck
Leiden University, Niels Bohrweg 1, 2333 CA Leiden, The Netherlands
e-mail: mswenne@liacs.nl; marijn.swenne@gmail.com; baeck@liacs.nl

implies that agent location and movement are discreet while pedestrian location and movement are not. Other well known examples of BCCMs are by Kirchner and Schadschneider [7] and Burstedde et al. [2]. The MFM as proposed by Okazaki [9] is based on each pedestrian, obstacle and goal having a magnetic polarity. The agents and obstacles have a positive pole whereas the agent goals have negative poles. The movement of each agent is the equation of all magnetic fields resulting in agents eventually moving to their goals while avoiding collisions. Finally, the SFM by Helbing and Molnár [6] is very similar to the MFM but assumes that repulsion and attraction are a result of social pressures. SFM is currently one of the most commonly used models.

In the remainder of this paper, the underlying principles of pedestrian behavior are outlined in Sect. 2, and its corresponding simulator implementation is explained in Sect. 3. Section 4 presents the setup of the environment optimization experiments conducted, and Sect. 5 provides a discussion of the results achieved by optimization. Finally, conclusions are given in Sect. 6.

2 Pedestrian Behaviour

To create a realistic simulator we have looked at different empirical studies on various aspects of pedestrian behaviour. Decisions pedestrians make on an individual level are used to model agents. Patterns that occur as a result of these decisions are used to validate the model. Two key components of pedestrian behavior modeling are perception and emergent behavior, as outlined in the following sections.

2.1 Perception

Pedestrians observe their surrounding mainly by sight. Goffman [4] observed pedestrians and developed a model describing how pedestrians take note of the fellow pedestrians. He called this process scanning (see Fig. 1a). In this model only a subset of the other pedestrians are influential. Whether a pedestrian is influential is determined by its proximity, its radial orientation and whether they are separated by other pedestrians.

Pedestrians only take note of what is in front of them and within their influence area. This influence area is shaped like a halved ellipse stretched in front of the pedestrian. Its size is 2 m in radius on the minor axis aligned to the width of the pedestrian and 5 m in radius on the major axis in front of the pedestrian. Also, other pedestrians will only be of influence if they are in direct line of sight.

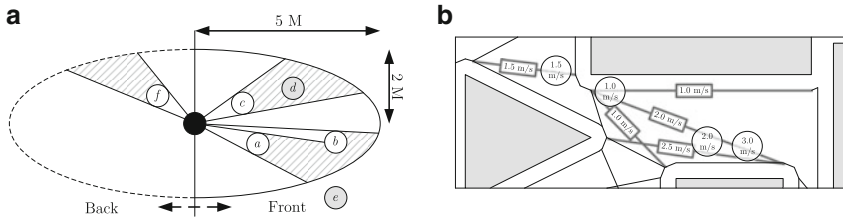


Fig. 1 Agent perception in the social forces model and path selection. **(a)** Goffman scanning. **(b)** Agent speed (*circle*) and average speed on edge (*rectangle*)

2.2 Emergent Behaviour

Emergent behaviour is any behaviour of a system that is not a property of any of the components of that system, but rather results from the interactions of its components. In a pedestrian simulation this would mean any behaviour that is not a property of a pedestrian but the result of inter-pedestrian behaviour. A good example is the pedestrian lanes that emerge at pedestrian stream intersections. Pedestrians do not consciously create them or are even aware of these lanes.

According to Helbing et al. [5] there are three types of emergent behaviour among pedestrians, namely, lane formation, circular flows and the clogging effect. Lane formation happens when two opposing streams of pedestrians interact. This results in pedestrians forming ribbons to avoid collision. Circular flows occur at an intersection where pedestrians enter from multiple directions. Circular flows will occur in the centre of this intersection but have a short lifespan. Finally, the clogging effect occurs at bottlenecks. Groups of pedestrians will form in front of the bottleneck in the shape of half a circle.

3 Pedestrian Simulation Implementation

The simulator developed for this research is based on the social forces model. Functionality for dynamic obstacle avoidance based on the observational studies described in Sect. 2 is implemented in the simulator. The way agents plan their route makes use of a Reduced Visibility Graph (RVG) as described by LaValle [8].

3.1 Pathfinding

Pathfinding ties into the social forces model by influencing the steering force f^γ . It can be separated into three components: Graph construction, path selection and

attractor point selection. For every environment a graph G is constructed. For every agent, one path P is selected from graph G . And for every time step, per agent, one attractor point ap on path P is selected. The following paragraphs give a brief explanation of the implementation of these components.

3.1.1 Graph Construction

First, an Euclidean pathfinding graph G is constructed as follows: Let \mathcal{B} be a collection of obstacle borders, each $b \in \mathcal{B}$ belonging to an obstacle $o \in \mathcal{O}$. b_o is an extension of polygon o by range r , drawing a region of constant width around o .

A common value for r is the radius of an agent. If two obstacle borders are overlapping, the overlapping edges are broken at the point they cut each other. All edges that are enclosed are discarded with the remaining edges forming a new obstacle border, replacing the original two. G is constructed by creating a reduced visibility graph from the polygons contained in \mathcal{B} .

3.1.2 Path Selection

Every edge of G contains congestion data, being the average speed of agents that walk over that edge. An agent is considered to be walking over an edge if the circle representing the agent overlaps with the edge, see Fig. 1b. When calculating a route, it is the expected travel time that determines the shortest path. When congestion increases there is an increased chance of recalculating the route for a possible faster alternative. The result of this path selection is a series of line segments $P = p^n, \dots, p^0$, with p^0 being the agent's goal.

3.1.3 Attractor Point Selection

The attractor point ap is the point that will be used to determine the steering force for agent a . Let T_a be a collection of all tangent lines on obstacles \mathcal{O} that have a 90° angle with agent a and let T'_a be the collection of line segments resulting from breaking each line from T_a where they are overlapping. Attractor region R_a is a polygon constructed from all line segments in T'_a that are in direct line of sight of a and not obstructed by other line segments from T'_a . ap_a is the point where the border of R_a cuts P_a or p_a^0 if no such point exists. See Fig. 2b.

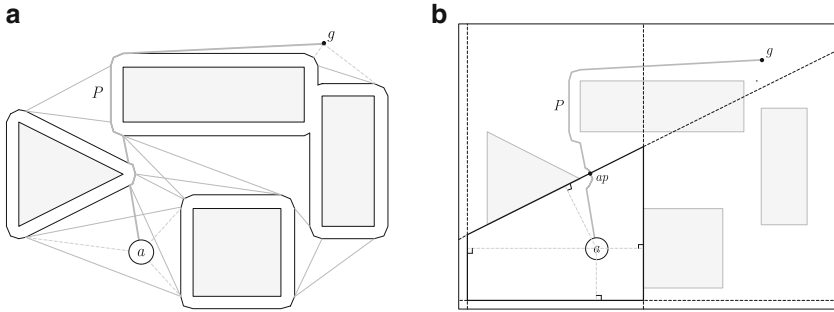


Fig. 2 Pathfinding. (a) Path selection on RVG for agent a to goal g . (b) Attractor box construction and attractor point ap selection

3.2 Social Forces Implementation

In the social forces model \vec{F}_a and \vec{f}_a are the forces resulting from all static obstacles (\vec{F}_a) and all dynamic obstacles (\vec{f}_a) repelling agent a . To determine the magnitude of the repulsion vector for each individual obstacle, force functions $U(|\vec{d}_{ao}|)$ for static obstacles and $V(|\vec{d}_{ab}|)$ are used. $|\vec{d}_{ao}|$ or $|\vec{d}_{ab}|$ is the distance between agents a and obstacle o or agent b . $U(|\vec{d}_{ao}|)$ is implemented as follows: The distance vector $\vec{d}_{ao} = \vec{o} - \vec{a}$, r_a is the radius of a , and m_a is the Goffman ellipse distance of agent a . r_a ensures the distance to the border of agent a is the effective distance and m_a increases the repulsive force on agents.

$$U(|\vec{d}_{ao}|) = \frac{m_a + r_a - |\vec{d}_{ao}|}{(|\vec{d}_{ao}| - r_a)^2} \tag{1}$$

A selection process was added based on Goffman’s research on how pedestrians observe other pedestrians. In Fig. 1 a, a visual representation is given to illustrate which agents exert influence, with the grey agents being excluded. $V(|\vec{d}_{ab}|)$ is implemented such that, as stated by Goffman, the radial orientation determines how influential another pedestrian is, i.e., a pedestrian to the side exerts less social pressure than in front of the agent considered. Let $L(a, b)$ be the distance between a and the ellipse contour at angle \hat{d}_{ab} , and let $L(a, min)$ be the distance between a and the ellipse contour on its minor axis. Then, the scalar function $V(|\vec{d}_{ab}|)$ is given by

$$V(|\vec{d}_{ab}|) = |\vec{d}_{ab}|^{-2} \cdot \frac{L(a, b)}{L(a, min)} \tag{2}$$

4 Experiments

The corridor and intersection experiments aim at producing environments that represent optimized geometric setups. Each setup contains agent starting areas and a collection of static obstacles \mathcal{O} . Each starting area has a corresponding goal area. Agents are spawned in their starting areas and will attempt to find a route to their goal. When an agent reaches its goal area, it is removed from the simulation. In this context, maximizing pedestrian efficiency means minimizing the average time between agents being spawned and removed. Efficiency is measured in percentages where 100 % equals the mean time agents need to complete their route if there are no static or dynamic obstacles.

To test whether an evolutionary strategy can find a better environment than a human designer, we have provided three basic environments for both the corridor and intersection experiment. For both optimization experiments we have used a so-called $(1, \lambda)$ -ES as described by Bäck [1], with $\lambda = 10$.

4.1 Simulator Validation

For the different types of emergent behaviour described in Sect. 2.2, environments were created that should show the emergent behavior if used by real pedestrians. The results are interpreted by looking at a real time representation of a pedestrian simulation and noting the similarities and dissimilarities between the pedestrian and agent behaviour.

4.2 Corridor and Intersection

The corridor setup shown in Fig. 3a (left) has agents starting in areas Z and X with the goal of the agents spawning in area Z to reach area X , and vice versa. Alongside the corridor in between areas Z and X are five static obstacles a, b, c, d, e . These obstacles are square pillars that can be moved along the width of the corridor (denoted by the dotted line) and changed in radius r . Each obstacle is represented for the evolutionary strategy by two real valued dimensions, one representing the position along the width of the corridor and the second one representing the obstacle's radius.

The intersection setup in Fig. 3b (right) consists of two corridors intersecting in a 90° angle with the overlapping, traversable part of the two corridors being area K . The starting areas where the agents spawn are W, X, Y and Z . The goal area for the agents that spawn in W is Y , for Y it is W , for X it is Z and for Z it is X .

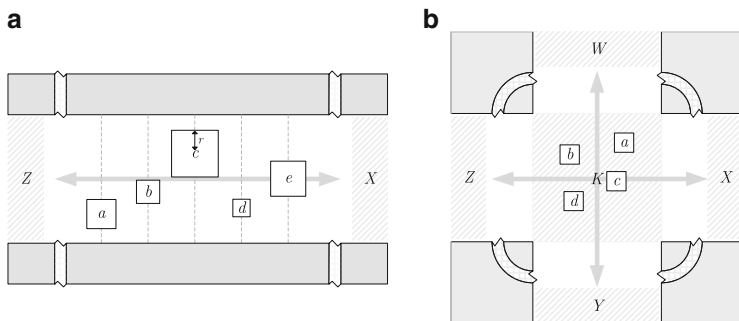


Fig. 3 Range of obstacle movement in experiments. (a) Corridor setup. (b) Intersection setup

In area K , four square static obstacles a, b, c, d of identical size are placed. They can be moved to any place within K while not overlapping the border of K and not overlapping any of the other obstacles. Each obstacle is represented by two real valued dimensions, being the x and y position of the obstacle in the intersection.

5 Results

5.1 Simulator Validation

Overall, the expected emergent behaviour is observed, although some more profound than others. The clogging effect is very much present in the simulator. Lane formation also occurs readily as is seen with pedestrians. The number of agents that make up a lane also concurs with that observed amongst pedestrians. Finally, the time one particular lane survives is also, as with pedestrians, very limited.

5.2 Environment Optimization

Three runs were executed for both the intersection and corridor experiment. The stop condition for optimization runs is based on an internal convergence measure of the solution set maintained by the optimizer. In terms of computational effort, the average completion time per optimization run is about 1–2 days. In the corridor runs convergence of optimization was achieved, although this seemed to be lacking in the intersection runs. An illustration on how these runs develop can be seen in Fig. 4 for the corridor (left) and intersection (right). Note that the fitness values used by the

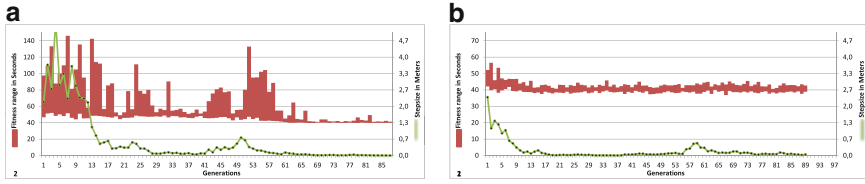


Fig. 4 Progression of the evolutionary strategy over time, measured in generations of the optimizer. Pedestrian performance range is from the child with the best fitness to the child with the worst fitness of that generation. (a) ES C2. (b) ES I2

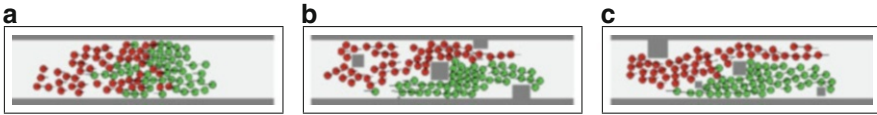


Fig. 5 Visual representation of the empty corridor environment (*left*) and two optimized corridor environments during a fitness evaluation. (a) Empty. (b) ES C1. (c) ES C2

optimizer are the average number of calculation steps needed for an agent between spawning and reaching its goal. The best solution found in each run, i.e., the solution with the best fitness, is used as a representative. They are designated with a C for corridor and I for intersection runs, e.g., the best solution from the second corridor run is labeled C2.

For each environment and spawn frequency,¹ 50 simulations are performed, and the average performance is measured. The results are presented as a percentage of the agent potential. An agent’s potential is the time taken from start to goal if no obstacles are present. In the corridor setup this is 32.35 s, and for the intersection setup this is 19.08 s. All results are summarized in Fig. 6 showing how the fixed and the optimized environment’s geometry efficiency changes with increasing spawn frequency. For large spawn frequency, optimization can clearly increase efficiency on the corridor.

A visual representation of the two optimized environments with the best fitness in the corridor experiment and the typical emerging agent behavior is shown in Fig. 5b, c, in comparison to the empty corridor in (a).

For the evolution strategy runs for the corridor experiment, both stepsizes and fitness ranges decrease over time. This indicates that convergence is taking place. Moreover, at high spawn frequency all optimized solutions show a better mean pedestrian efficiency than an empty corridor. In contrast, the runs for the intersection experiment do not exhibit the same convergence. In the intersection runs the stepsize decreases over time, but the solutions found do not improve significantly. Also, the

¹Spawn frequency, in Hz, refers to how often agents are added to a starting area.

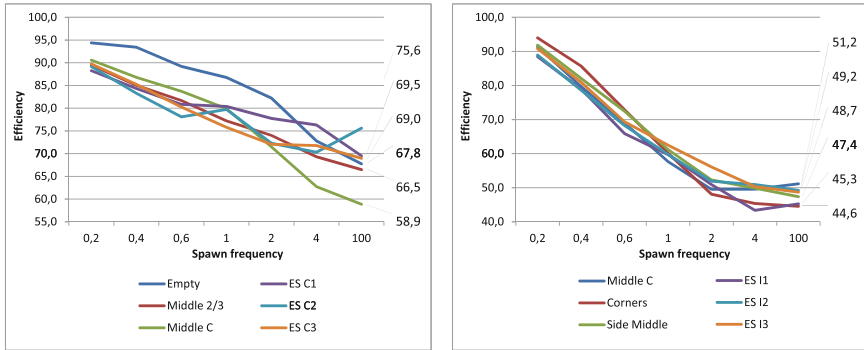


Fig. 6 Mean fitness comparison of the six corridor (*left*) and intersection (*right*) environments

fitness range within one generation, although fluctuating, remains small and does not decrease over time. In case of the intersection, no improved configuration (when compared to the empty intersection) could be found.

6 Conclusions

The simulator has been shown to produce realistic behaviour in environments where circular flows do not occur. Although the stochastic simulation generates a noisy landscape for the optimization, at high density, solutions can be discriminated and convergence takes place.

In the corridor experiment it was found that all optimization runs produced a better solution at high density than the empty corridor (best “hand-designed” solution). This is the most promising result of this research as it not only shows that placing obstacles in pedestrian areas can lead to an increased pedestrian efficiency but also suggests that the location and size of obstacles can be found by an optimizer.

References

1. Th. Bäck. *Evolutionary Algorithms in Theory and Practice*. Oxford University Press, Oxford, UK, 1996.
2. C. Burstedde, K. Klauck, A. Schadschneider, and J. Zittartz. Simulation of pedestrian dynamics using a two-dimensional cellular automaton. *Physica A: Statistical Mechanics and its Applications*, 295(3–4):507–525, 2001.
3. P. G. Gipps and B. Marksjo. *Mathematics and Computers in Simulation*, 27:95–105, 1985.
4. E. Goffman. *Relations In Public: Microstudies In The Public Order*. Basic Books, 1971.
5. D Helbing, A Johansson, and H. Z. Al-Abideen. The dynamics of crowd disasters: An empirical study. *Phys. Rev. E*, 75:046109, 2007.

6. D. Helbing and P. Molnár. Social force model for pedestrian dynamics. *Physical Review E*, 51(5):4282–4286, 1995.
7. A. Kirchner and A. Schadschneider. Simulation of evacuation processes using a bionics-inspired cellular automaton model for pedestrian dynamics. *Physica A*, 312(1–2):260–276, 2002.
8. S. M. LaValle. *Planning Algorithms*. Cambridge University Press, Cambridge, U.K., 2006. Available at <http://planning.cs.uiuc.edu/>.
9. S. Okazaki. *Trans. of A.I.J.*, 283:111–119, 1979.

Estimating Pedestrian Destinations Using Traces from WiFi Infrastructures

Antonin Danalet, Michel Bierlaire, and Bilal Farooq

Abstract Gathering data about pedestrian origin, destination and route is difficult, particularly indoor and on a large scale. These data are important for route choice modeling, description of congestion, and flow estimation. Most data collection techniques are device-centric. In this paper, we focus on the communication network infrastructure and propose to use WiFi traces to generate pedestrian destinations. Due to the poor quality of WiFi localization, a probabilistic method is proposed that infers visited destinations based on WiFi traces and calculates the likelihood of observing these traces in the pedestrian network, taking into account prior knowledge. The output of the method consists in generating several candidate lists of destinations, and assigning the probability of each list being the true one. Results show that it is possible to predict the number of destinations, the time spent at it and the localization of it, discriminating intermediary signals from signals generated at destination.

Keywords WiFi traces • Pedestrian destinations • Pedestrian network • Probabilistic measurement model

1 Introduction

In recent years, interest in crowd dynamics and pedestrian modeling is reviving due to urban growth and its pressure on urban infrastructure. Crowd and pedestrian simulation is emerging as a tool for designing new infrastructures and optimizing the use of current infrastructures. Innovative data collections and experiments are vital in estimating the demand for these infrastructures. In order to predict the total

A. Danalet (✉) • M. Bierlaire • B. Farooq
Transport and Mobility Laboratory, School of Architecture, Civil and Environmental Engineering,
Ecole Polytechnique Fédérale de Lausanne, Lausanne, Switzerland
e-mail: antonin.danalet@epfl.ch; bilal.farooq@epfl.ch; <http://transp-or.epfl.ch>

demand within a given area, a destination choice model needs to be developed. Origin-destination matrices are traditionally used for car trips as an important source of information for strategic planning, management of transportation networks, or optimization of transportation networks. For pedestrians, such data are important for route choice modeling, description of congestion, efficient design of new facilities, and travel guidance and information systems. According to a report by Cisco [1], there will soon be more smartphones and tablets than human beings on Earth: seven billions by the end of 2012 and ten billions in 2016. In this context, research has been done on digital footprints on smartphones for route choice [2] or real-time traffic monitoring [3], but until now not focusing on pedestrians. Smartphones generate information about the user in two ways. First, data is collected directly on the phone, following a device-centric approach. Second, smartphones create traces in the communication infrastructures. A device-centric approach has some major disadvantages. It is difficult to convince enough individuals to participate in such surveys and to have access to their phone. Resulting data are related to an individual and not to a specific area, that could be of interest. Moreover, the transport mode of the individual is difficult to predict, and thus focusing on pedestrian behavior is not straight forward. Finally, the privacy of the users is threatened since data on a smartphone are not just related to mobility. In this paper, we collect digital footprints from the communication network infrastructure composed of WiFi access points (APs). This data collection is transparent for the users and data are already partially collected for network operations purpose. WiFi traces allow for the localization of mobile devices in a given infrastructure, typically at the scale of pedestrians, but they are scarce and fuzzy. We propose a methodology to use these traces to generate lists of destinations visited by pedestrians. We use a campus as a case study. Localization data are collected using a tool developed by Cisco. This technique is unique to our knowledge in studying pedestrians. Moreover, the methodology presented here considers disaggregate destinations in the infrastructure and not the access points. It solves the well-known pingpong effect in literature about mobility from on access point to another. This methodology could be adapted for transportation hubs or in companies, since a big proportion of them are already covered by WiFi.

2 Probabilistic Method for Estimating Pedestrian Destinations

We are proposing a modeling approach to extract the possible destinations visited by pedestrians from digital traces from communication networks. It merges localization from WiFi traces and pedestrian map information to compute the likelihood that a given list of destinations has generated the observed traces. Using this approach for pedestrian behavior modeling is relevant given that the pedestrian networks are traditionally denser than other mobility networks and localization is often sparse. This probabilistic method is presented for the case of WiFi traces, but could be

used with other data collection techniques. The input of this probabilistic method consists in time stamps and localization data coming from the WiFi infrastructure. We define a measurement as $\hat{s} = (\hat{x}, \hat{t})$, where \hat{x} is the position of the measurement (x-y coordinates and floor) and \hat{t} the timestamp of the signal. The measurement \hat{x} can be anywhere, and not only at AP locations. We define a destination as a place where the user is spending time, i.e., $d = (x, t^-, t^+)$, where x is the position of the destination, t^- the time of arrival at the destination, and t^+ the time of departure from the destination. The output of the probabilistic method consists in a set of candidate lists of destinations, with the probability of each list of destinations being the true one. In the next section, we present first how to generate lists of destinations and in Sect. 2.2, we present a probabilistic measurement model associated to a list of destinations.

2.1 Generation of Lists of Destinations

2.1.1 Generating Position of the Destination

Inspired by the methodology developed by Bierlaire et al. [4] for smartphone GPS data, we generate positions for each signal using the concept of *domain of data relevance* originally introduced by Bierlaire and Frejinger [5]. For each signal from an access point, we generate the domain of data relevance for that signal. It corresponds to a physical area in space where a given piece of data is relevant. This simplifies the computation by limiting the area we observe for each signal. The definition of the area can be different depending on the precision of the measurement, i.e., the domain of data relevance depends on the type of data.

Using the domain of data relevance DDR_i for each signal \hat{s}_i , we generate a tree for each individual. Each node represents a possible destination. It is connected with all possible next destinations contained in the domain of data relevance DDR_{i+1} of the following signal in time, \hat{s}_{i+1} . For a list $\hat{s}_1, \hat{s}_2, \dots, \hat{s}_n$ of signals for a given individual, the result of this process is a tree structure with n levels of all combinations of locations of potential destinations. A leaf of this tree would correspond to a list x_1, x_2, \dots, x_m of location of potential destinations, where m is the number of distinct localizations. This tree is built recursively. For each signal $\hat{s}_i, i = 1, \dots, n$ for a particular individual in chronological order, we consider all possible locations of destination in the domain of data relevance DDR_i . At each new signal \hat{s}_j , the tree structure of lists of candidate destinations is extended with all location associated with \hat{s}_j (Figs. 1 and 2).

2.1.2 Generating Time of Arrival and Departure for the Destination

Once a list of potential locations of destinations is defined, the time of arrival and departure at these locations needs to be generated. Given two consecutive signals \hat{s}_i

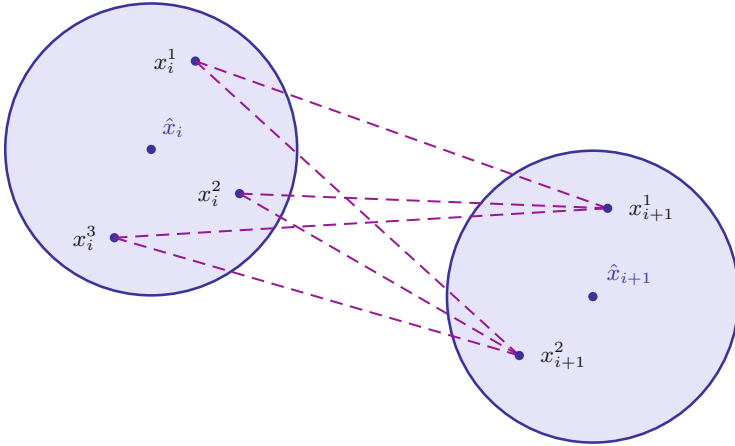


Fig. 1 The symbolic representation of two domains of data relevance DDR_i and DDR_{i+1} corresponding to signals \hat{s}_i and \hat{s}_{i+1} following each other chronologically. We assume DDR_i contains three possible destinations x_i^1, x_i^2, x_i^3 , and DDR_{i+1} contains two possible destinations x_{i+1}^1, x_{i+1}^2

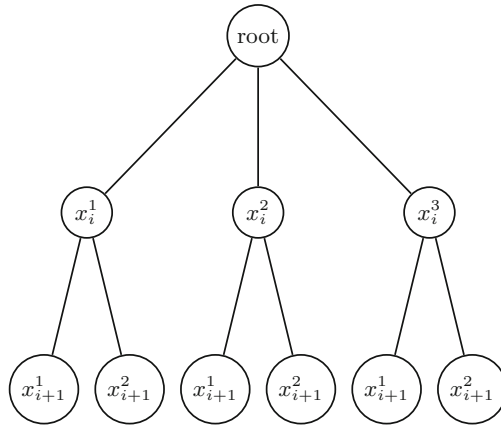


Fig. 2 The tree corresponding to the two signals in Fig. 1. A leaf of the tree represents a possible list of destinations

and \hat{s}_{i+1} and their corresponding timestamps \hat{t}_i and \hat{t}_{i+1} , a trip between the position of the two generated positions x_i and x_{i+1} of the consecutive destinations d_i and d_{i+1} is assumed to take place. This trip defines both the departure time t_i^+ from destination d_i and the arrival time t_{i+1}^- at destination d_{i+1} . The departure of the trip occurs after signal \hat{s}_i and the arrival occurs before the next signal \hat{s}_{i+1} . In order to estimate the travel time $tt_{x_i, x_{i+1}}$ between destinations d_i and d_{i+1} necessary to generate coherent departure and arrival times for the trip, simple assumptions are made. For distance, we assume the pedestrian to follow the shortest path. Similarly,

we use a standard value of 1.34 m/s for speed based on [6]. In this way, the time of departure t_i^+ is taking place between the signal timestamp \hat{t}_i and $\hat{t}_{i+1} - tt_{x_i, x_{i+1}}$. The arrival time t_{i+1}^- is happening between the end of the trip $t_i^+ + tt_{x_i, x_{i+1}}$ and the signal timestamp \hat{t}_{i+1} . The assumptions on the distributions reflects the lack of knowledge of the interval. Between two following signals, no information is generated.

Algorithm 1: Generation of lists of destinations algorithm

```

for each  $ID$  do
    Create a tree structure for lists of destinations  $T$  with a root node;
    for signal  $\hat{s}_i$  with  $i = 1, \dots, n: \hat{x}_i, \hat{t}_i$  do
        Define the corresponding Domain of Data Relevance,  $DDR_i$ ;
        for each  $x_i \in DDR_i$  do
            for each  $d_{i-1} \in DDR_{i-1}$  do
                Draw  $t_{i-1}^+ \sim \text{Uniform}(\hat{t}_{i-1}, \hat{t}_i - tt_{d_{i-1}, d_i})$ ;
                Draw  $t_i^- \sim \text{Uniform}(t_{i-1}^+ + tt_{d_{i-1}, d_i}, \hat{t}_i)$ ;
                Connect  $d_i$  with  $d_{i-1}$  in  $T$ ;
    
```

2.2 Probabilistic Measurement Model

A likelihood is associated with each list of destinations. It takes into account the inaccuracy in the WiFi traces, the activity time at destination and a travel model based on the measurements. The destination probability $P(d_1, \dots, d_m | \hat{s}_1, \dots, \hat{s}_n)$ can be decomposed as:

$$P(d_1, d_2, \dots, d_m | \hat{s}_1, \dots, \hat{s}_n) = \frac{P(\hat{s}_1, \dots, \hat{s}_n | d_1, d_2, \dots, d_m) \cdot P(d_1, d_2, \dots, d_m)}{\sum_{d \in D} P(d_1, d_2, \dots, d_m)} \quad (1)$$

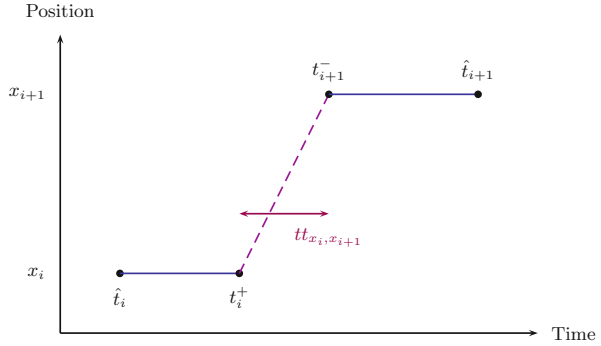
where $P(\hat{s}_1, \hat{s}_2, \dots, \hat{s}_n | d_1, d_2, \dots, d_m)$ is the measurement likelihood, $P(d_1, d_2, \dots, d_m)$ is the prior knowledge we have about the lists of destinations, and D is the set of all candidate lists of destinations.

2.2.1 Measurement Likelihood

For each list of potential destinations, our goal is to compute the probability that the visited destinations generated the observed signals:

$$P(\hat{s}_1, \hat{s}_2, \dots, \hat{s}_n | d_1, d_2, \dots, d_m) \quad (2)$$

Fig. 3 Time-space representation of two consecutive destinations i and $i + 1$



where m is the number of visited destinations in the studied time interval and n the number of signals in the same time interval. With this definition, each signal corresponds to a destination. In practice, locations of consecutive destinations \hat{x}_i, \hat{x}_{i+1} are not necessarily different. A list of destinations is composed of two processes: staying at a destination, and moving to the next one. These processes are defined by the times of arrival t^- and the times of departure t^+ . Staying at a destination d_i happens between t_i^- and t_i^+ , while trips between destinations happens between t_i^+ and t_{i+1}^- . We assume these consecutive and different events to be independent. It is important to notice that there is no signal during the trips by definition. While the device is in a given location, we assume that the chance it will generate a signal depends only on the distance between the location and the signal. Thus we can decompose Eq. 2 as:

$$P(\hat{s}_1, \hat{s}_2, \dots, \hat{s}_n | d_1, d_2, \dots, d_m) = \prod_{j=1}^m P(\hat{s}_{i_{j-1}+1}, \dots, \hat{s}_{i_j} | d_j) \tag{3}$$

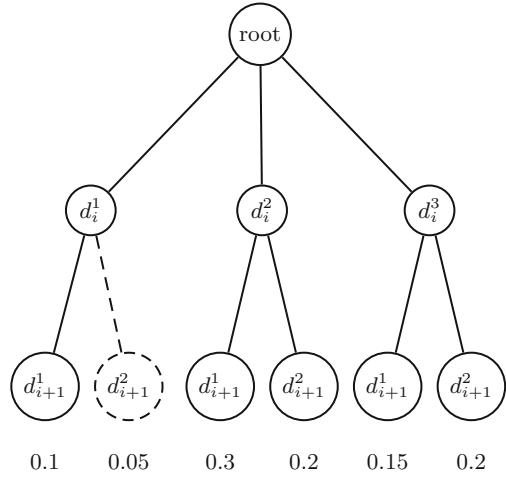
$$= \prod_{j=1}^m \prod_{i=1}^n P(\hat{s}_{i_j} | d_j) = \prod_{j=1}^m \prod_{i=1}^n P(\hat{x}_{i_j} | x_j) \tag{4}$$

where the time $\hat{t}_{i_{j-1}+1}$ to \hat{t}_{i_j} of signals $\hat{s}_{i_{j-1}+1}$ to \hat{s}_{i_j} are in the time interval t_j^-, t_j^+ of destination d_j (Fig. 3).

2.2.2 Prior

The prior knowledge $P(d_1, d_2, \dots, d_m)$ of the state variables can be decomposed in a travel model and an activity model. The location of the consecutive destinations x_{i-1} and x_i are assumed to be independent in order to simplify the model; it could be further extended with models on activity choice (see [7] and [8] about activity chains in general, and [9] for pedestrians in particular). Moreover, the dependencies

Fig. 4 The tree of Fig. 2 with the probability for each leaf to be the correct one. If we fix $L = 5$, we need to eliminate one leaf since we have six leaves in the tree. The leaf with the smallest probability to be the correct one is eliminated (dotted line). It implies the list of destinations d_i^1, d_{i+1}^2 is eliminated



of d_i only depend on the previous destination d_{i-1} but not on the ones before. Thus, the prior knowledge can be decomposed in the following way:

$$P(\dots, d_{i-1}, d_i, \dots) = P(\dots, x_{i-1}, t_{i-1}^-, t_{i-1}^+, x_i, t_i^-, t_i^+, \dots) \tag{5}$$

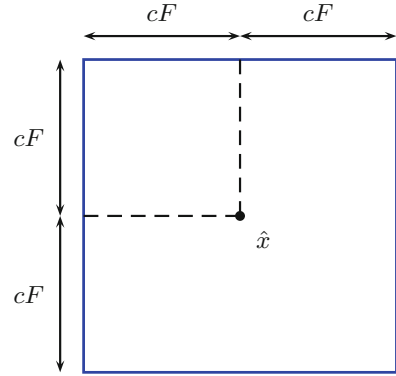
$$= \dots \cdot P(x_i | t_i^-, t_i^+) \cdot P(t_i^- | t_{i-1}^+, x_{i-1}, x_i) \cdot P(t_i^+ | x_i, t_i^-) \cdot \dots \tag{6}$$

where we assume t_i^+ to depend only on t_i^- and x_i , and t_i^- to be independent of t_{i-1}^- . $P(x | t_i^-, t_i^+)$ represents the prior probability of visiting a specific place x during a time window t^-, t^+ , e.g., a restaurant on campus during lunch break. Without any information, we can assume a uniform distribution and this term cancels out of the equation. $P(t_i^- | t_{i-1}^+, x_{i-1}, x_i)$ is a travel model and compute the probability of arriving at destination at a certain time knowing the previous destination and the time of departure from the previous destination. It depends on the distance between the two destinations and a distribution of speed. Finally, $P(t_i^+ | x_i, t_i^-)$ consists in an activity model and represents the prior knowledge of the time spent at destination depending on the type of destination.

2.2.3 List Elimination Procedure

This process is combinatorial and quickly produces a huge number of possible lists of destinations. To avoid this problem, a list elimination procedure limits the size of the set of lists of destination to a certain threshold L . At every new signal, if the set of candidates is larger than L , the least likely lists of destination produced so far are eliminated (Fig. 4).

Fig. 5 Ninety-five percent confidence square for localization tool by Cisco



3 Case Study: EPFL Campus

We conduct an experiment on EPFL campus. EPFL campus hosts 12,500–13,000 people every day. A pedestrian network has been created by Camptocamp, an Open Source GIS software company. It consists of a graph in three dimensions, containing 50,131 vertices and 56,655 edges. The database contains 17,502 points of interest that corresponds to the list on <http://map.epfl.ch>, and 13,783 rooms, all corresponding to vertices in the pedestrian network. We selected 5,387 of them as potential destinations for pedestrians. We use A* algorithm to find a route on campus and we balance between the shortest path and the simplest path by giving each edge of the pedestrian network a weight. It represents the aversion to floor changes and less important walkways.

We collect localization data using Cisco Context Aware Mobility API with the Cisco Mobility Services Engine (MSE) with 12 users who accepted to participate in the experiment. A confidence factor cF provides a 95% confidence square around each x-y coordinates and is unique for both directions (see Fig. 5). cF has a mean of 187 m in this dataset, with a minimum of 16 m and a maximum of 1,240 m.

We assume that the errors in latitude and longitude are independently and normally distributed. We decompose both the measurement \hat{x} and the location of the destination x in latitude and longitude \hat{x}_{lat} , \hat{x}_{long} , x_{lat} and x_{long} . Assuming the errors in latitude and longitude are independent, $P(\hat{x}|x) = P(\hat{x}_{lat}|x_{lat}) \cdot P(\hat{x}_{long}|x_{long})$ with:

$$P(\hat{x}_{lat}|x_{lat}) = \frac{1}{\sigma\sqrt{2\pi}} \exp\left(-\frac{(\hat{x}_{lat} - x_{lat})^2}{2\sigma^2}\right) \quad (7)$$

$$P(\hat{x}_{long}|x_{long}) = \frac{1}{\sigma\sqrt{2\pi}} \exp\left(-\frac{(\hat{x}_{long} - x_{long})^2}{2\sigma^2}\right) \quad (8)$$

where $\sigma = \frac{cF}{2}$, with cF the confidence factor defined in Sect. 2.1.1.

4 Results

We explored the methodology with traces from one of the authors. Seventy-one signals were generated on Wednesday April 11, 2012. The domain of data relevance needs to be computed for each signal. We select this confidence square as our domain of data relevance and all possible locations of destinations in it. The domain of data relevance consists of points of interest, offices and classrooms. For the points of interests, all locations in the 95 % confidence square have been used. For offices and classrooms, the density being large, the number of locations in the 95 % confidence square is too large and make the process non-tractable. A 20-meter-radius circle was used as the domain of data relevance. The methodology used in this example is the probabilistic measurement model presented in Sect. 2.2, in particular Eq. 1. The measurement equations are Eqs. 7 and 8. As a prior, only the travel model is being used, $P(t_i^- | t_{i-1}^+, x_{i-1}, x_i)$. No prior probability of visiting a specific destination knowing the time of the day or activity model representing time spent at destination depending on the type of destination is used. The travel model is analytically developed using the distance and the travel time between the two destinations x_{i-1} and x_i . The weighted shortest path in the pedestrian graph generates the distance of the route between x_{i-1} and x_i . The travel time is simply $t_i^- - t_{i-1}^+$. Finally, the speed s of the pedestrian can be computed: $s = \frac{dist(x_{i-1}, x_i)}{t_i^- - t_{i-1}^+}$. We assume s to be distributed with a mixture of negative exponential and a normal. The first represents when the pedestrian is stopped or traveling at low speed, while the second represents a pedestrian at regular speed:

$$f(v) = \omega \lambda e^{-\lambda v} + (1 - \omega) \frac{1}{\sqrt{2\pi\tau^2}} e^{-\frac{(\ln v - \mu_m)^2}{2\tau_m^2}} \quad (9)$$

Parameters have been estimated in [2] from smartphone data ($\omega = 0.46$, $\lambda = 0.2$, $\mu = 4.41$, $\tau = 1.51$). The list elimination procedure is used with a threshold $L = 20$. It means that at each signals, only the 20 most likely lists of destinations are kept. The result is thus 20 lists of destinations with their corresponding likelihood to be the right one. All destinations where time spent is less than 2 min should be considered as intermediary destinations, i.e., signals generated while moving from one place to another. If all destinations where the time spent at destination is less than 2 min are removed, six destinations remain.

The true list of destinations has been recorded by the tracked author (Table 1). We observe first that the total number of destinations in the day is estimated correctly from the 71 signals. Using a threshold of 2 min spent at destination, we reach the same number of destinations that the truth. The precision of the times of arrival and departure at destination is difficult to estimate since the truth is not very precise, in particular in the afternoon. Still, in the morning, the times of arrival and departure correspond with the reported ones. About localization, one destination is perfectly predicted, and others are predicted in a range of 6–58 m. It is good in comparison with the mean size of the 95 % confidence square of 374×374 m. We can observe

Table 1 Comparison between the most likely output of the model and the truth as reported by one author. Δx represents the distance (in meters) in the same horizontal plane, no vertical coordinate is taken into account

Model			Truth			Δx (in meters)
Time spent	Floor	Location	Time spent	Floor	Location	
8.35–10.38 am	0	Office	8.32–10.30 am	1	Classroom	58
10.39–11.51 am	2	Office	Until 11.47 am	3	Author's office	6
11.56 am–12.53 pm	1	Restaurant	From 11.55 am	1	Restaurant	0
12.58–1.33 pm	3	Office	Around 1 pm	3	Author's office	8
1.39–2.00 pm	1	Office	Around 2 pm	3	Cafeteria	11
2.01–7.40 pm	0	Classroom	Until around 7.45 pm	3	Author's office	13

an important lack in precision in the prediction of the floor. This prediction depends only on the localization tool by Cisco. These results must be seen as a proof-of-concept, that could be further developed in a detailed and comprehensive case study (Fig. 6).

5 Conclusion

A relevant field of research within pedestrian behavior is the estimation of demand for urban infrastructures such as railway stations or airports. The challenge consists in gathering pedestrian destination data at a large scale. In this preliminary research, we develop a methodology detecting the different destinations visited by a device using its traces in the WiFi infrastructure supported by knowledge of the underlying pedestrian map. We present an empirical study on a campus and give first results. The methodology presented here is flexible and tunable. It allows for introducing a priori knowledge on the destinations and information on the pedestrian map structure, in a behaviorally coherent way. In particular, the prior knowledge of schedules (for trains in a railway station, for planes in an airport, or for classes on a campus) can be added in the model. We emphasize here the importance of a good knowledge of the map behind the technical infrastructure. In our experiment, a complete pedestrian network is available. This methodology uses the concept of domain of data relevance and avoids the traditional pingpong effect observed in other studies. Here, if access points are changing very often from one to another while the device is in fact static, the real destination is contained in both domain of data relevance and will not change. This methodology is used here with traces from WiFi infrastructures for pedestrians, but can be used with other types of sensors data.

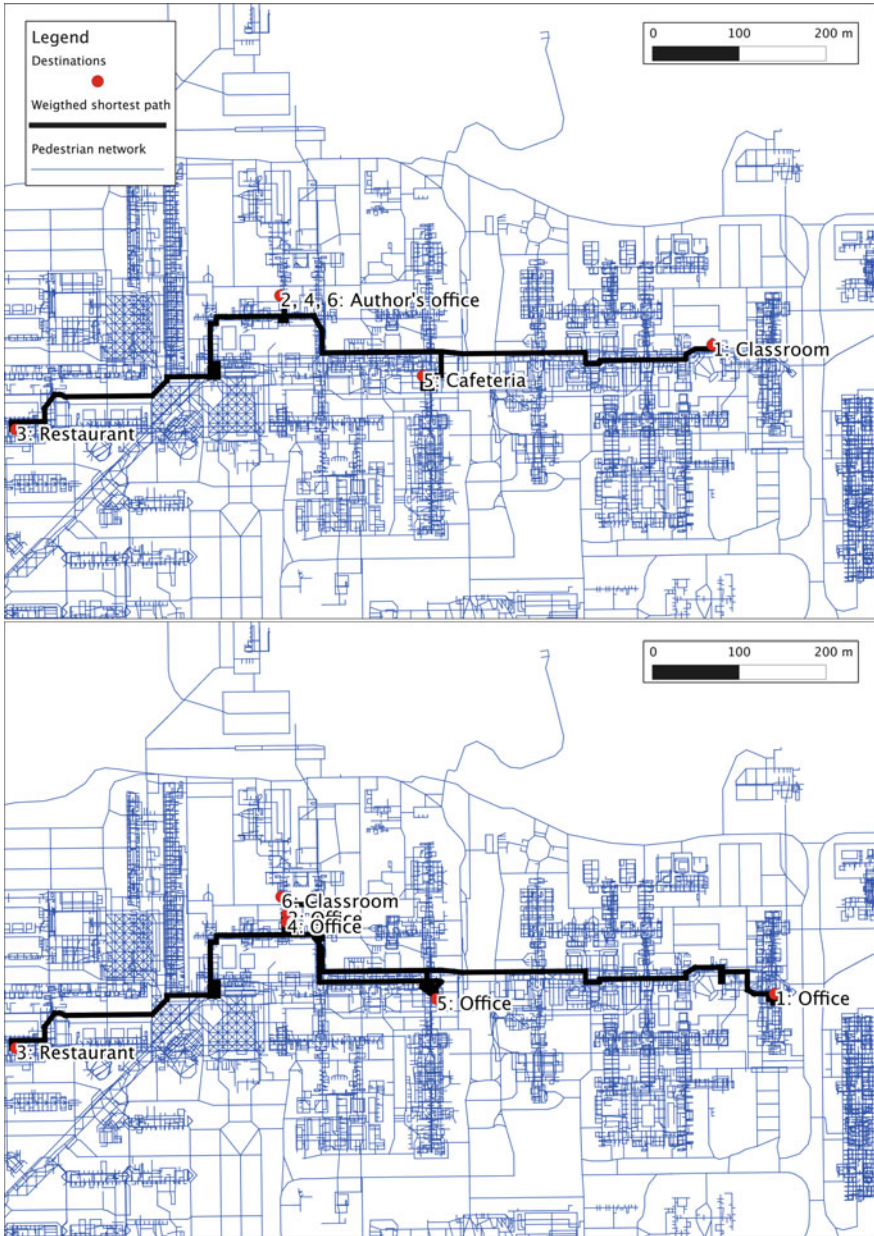


Fig. 6 True destinations as reported by one author (above) and resulting destinations of the most likely output of the model (below) on EPFL campus pedestrian network. Destinations are connected with the weighted shortest path

References

1. Cisco. Cisco Visual Networking Index: Global Mobile Data Traffic Forecast Update, 2011–2016. Tech. Rep. (2012).
2. Bierlaire, M., Chen, J. & Newman, J. P. Using location observations to observe routing for choice models. In *Proceedings of the 89th Transportation Research Board Annual Meeting* (Washington D.C., US, 2010).
3. Herrera, J. C. *et al.* Evaluation of traffic data obtained via GPS-enabled mobile phones: The Mobile Century field experiment. *Transportation Research Part C: Emerging Technologies* **18**, 568–583 (2010).
4. Bierlaire, M., Chen, J. & Newman, J. P. Modeling Route Choice Behavior From Smartphone GPS data. Tech. Rep. TRANSP-OR 101016, Transport and Mobility Laboratory, Ecole Polytechnique Fédérale de Lausanne (2010). URL <http://transp-or.epfl.ch/documents/technicalReports/BierChenNewm10.pdf>.
5. Bierlaire, M. & Frejinger, E. Route choice modeling with network-free data. *Transportation Research Part C: Emerging Technologies* **16**, 187–198 (2008). URL <http://linkinghub.elsevier.com/retrieve/pii/S0968090X07000551>.
6. Buchmüller, S. & Weidmann, U. Parameters of pedestrians, pedestrian traffic and walking facilities. IVT-Report Nr. 132, Institut for Transport Planning and Systems (IVT), ETHZ (2006).
7. Axhausen, K. W. & Herz, R. Simulating Activity Chains: German Approach. *Journal of Transportation Engineering* **115**, 316–325 (1989).
8. Abdelghany, A. F., Mahmassani, H. S. & Chiu, Y. Spatial Microassignment of Travel Demand with Activity Trip Chains. *Transportation Research Record: Journal of the Transportation Research Board* **1777–2001**, 36–46 (2007).
9. Hoogendoorn, S. P. & Bovy, P. H. L. Pedestrian route-choice and activity scheduling theory and models. *Transportation Research Part B* **38**, 169–190 (2004).

Pedestrian Conflicts, Pedestrian Comfort Levels, and Current Pedestrian Levels of Service

Jaisung Choi, Sangyoup Kim, Sunggyu Kim, Minsu Jin, Yongseok Kim, and Jinkug Kim

Abstract The current methodology of analyzing pedestrian levels of service stated in the KHCM (Korean Highway Capacity Manual) excludes pedestrian comfort from its primary measures of effectiveness, resulting in mismatching levels of service calculated with the KHCM and the ones stated by pedestrians on the basis of comfort. This can lead to undesirable designs of pedestrian facilities, and in order to deal with this problem a research was carried out to apply the concept of pedestrian conflict for assessing pedestrian comfort. The approach adopted in this study included recalibrating relationships between pedestrian flow and pedestrian conflict and making adjustments to pedestrian levels of service given in the KHCM. In this effort, characteristics of pedestrian flows and conflicts for five field sites located in Seoul were investigated by using video cameras, and selected pedestrians on the five sites were interviewed to determine their levels of comfort for the given walking conditions. Based on these field survey data, this study then demonstrated that there were close relationships between pedestrian comfort, flow rate, density, and pedestrian conflict. A follow-up adjustment to pedestrian levels of service in the KHCM was proposed by this study and an additional survey of pedestrians discovered that the proposed adjustment would better explain how pedestrian comfort levels change with pedestrian flow for a given facility.

Keywords Sidewalks • Pedestrian comfort levels • Pedestrian conflicts • Pedestrian flow • KHCM (Korean Highway Capacity Manual)

J. Choi (✉) • S. Kim • S. Kim • M. Jin
Department of Transportation Engineering, University of Seoul, Seoul, South Korea
e-mail: traffic@uos.ac.kr; road@uos.ac.kr; ic@uos.ac.kr; latent@uos.ac.kr

Y. Kim • J. Kim
Highway Research Division, SOC Research Department, Korea Institute of Construction Technology, Seoul, South Korea
e-mail: safeys@kict.re.kr; jinkug@kict.re.kr

1 Introduction

1.1 Background and Objectives

Walking is a basic travel mode for human beings and also considered a fundamental element in human activity. Therefore, it is important to provide pedestrians with comfortable and safe pedestrian space in urban streets. Traditionally, studies on pedestrian behaviors in South Korea have not been remarkable, so Korean Highway Capacity Manual (KHCM) uses a procedure that has been adapted from a similar procedure in the USHCM (United States Highway Capacity Manual, HCM in this paper) which is originally developed for analyzing vehicle flow [9]. As a result it is addressed that the pedestrian section in the current KHCM has produced unrealistic results when pedestrian comfort levels are the main issue of analysis [7]. Therefore, the KHCM procedure needs to incorporate pedestrian comfort into measures of effectiveness in order to assess pedestrian levels of service more realistically. A research was carried out to deal with this task and this paper summarizes the result.

1.2 Research Approach

The KHCM provides some guidelines to determine the levels of service for pedestrian facilities that are simply based on the freedom of movement for pedestrians. It is considered in this study that the existing guidelines should be fixed to explain levels of pedestrian comfort for a pedestrian facility. For example, in the KHCM, the pedestrian level of service for pedestrian volume of 20 pedestrians/min is B, and then this study attempts to identify the corresponding pedestrian comfort level for this volume level. Pedestrian satisfaction level for a given facility was also considered in this investigation, and it is conceived that pedestrian comfort will vary depending upon the extent of pedestrian conflicts. In this effort, characteristics of pedestrian flows and conflicts for five field sites located in Seoul were investigated by using video cameras. In addition, some selected pedestrians on the five sites were interviewed to determine their levels of comfort for the given walking conditions. Based on the finding from this investigation, an adjustment to pedestrian levels of service in the KHCM was proposed by this study.

2 Literature Review

2.1 Existing Levels of Service for Pedestrians

As shown in Fig. 1, pedestrian levels of service in the KHCM apply primary measures of effectiveness including pedestrian flow rate, occupying space, density,

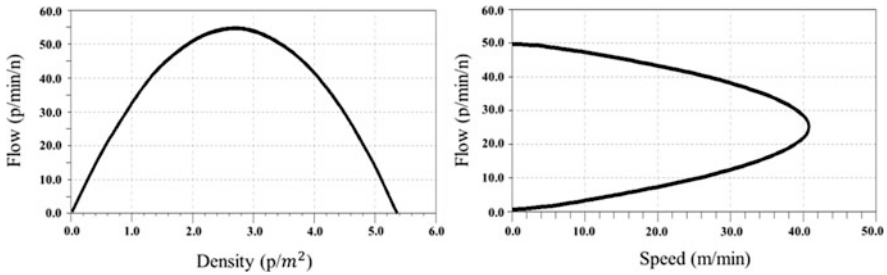


Fig. 1 Pedestrian flow characteristics described in the KHCM

Table 1 Pedestrian levels of service in the KHCM in conjunction with Fruin’s and the HCM

LOS	J Fruin		HCM		KHCM	
	Space (m ² /p)	Flow (p/min/m)	Space (m ² /p)	Flow (p/min/m)	Space (m ² /p)	Flow (p/min/m)
A	>3.5	≤20	>5.6	≤16	≥3.3	≤20
B	3.5–2.5	>20–30	>3.7–5.6	16–23	≥ 2.0	≤32
C	2.5–1.5	>30–45	>2.2–3.7	23–33	≥1.4	≤46
D	1.5–1.0	>45–60	>1.4–2.2	33–49	≥0.9	≤70
E	1.0–0.5	>60–80	>0.75–1.4	49–75	≥0.38	≤106
F	<0.5	>80	<0.75	Variable	<0.38	–

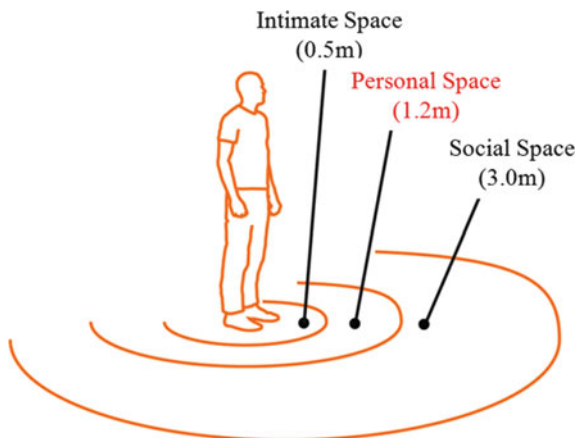
Note: Fruin [2] pedestrian planning and design

and speed [9]. However, these variables are applied mainly because they are applied in the HCM, and the fact that major components of the HCM generally copy the research findings made by J Fruin lead to locality problems in South Korea. Furthermore, pedestrian levels of service by J Fruin was developed in 1971 and in this analysis procedure he attempted to explain pedestrian service levels for a given facility based on the extent of moving freedom perceived by pedestrians. However, his theory ignores that the relationship between vehicle flow and vehicle level of service is quite different from the relationship between pedestrian flow and pedestrian level of service [7]. As a result, although useful when carrying out operational analysis of pedestrian flow for existing sidewalks, this theory is not as useful when engineers wish to determine the pedestrian comfort levels. Table 1 compares pedestrian levels of service in the KHCM [9] with the ones suggested by Fruin [2] or the HCM [12].

2.2 Candidates for Improving the Measures of Effectiveness

Pedestrians want to have a certain amount of space while they are in walking. Such spaces include physical dimensions, personal space, and space zones in locomotion. The physical dimensions of the body determine working widths of doorways and

Fig. 2 Space between others
[Hall 3]



passageways. Although body depth and shoulder breadth are the primary human measurements used by designers of pedestrian spaces, larger dimensions generally allow for pedestrians to ensure natural psychological preferences to avoid bodily contact with others, and body sway [2], and these larger dimensions deserve attention when engineers are concerned with pedestrian comfort levels.

The pedestrian has his/her own personal space preferences which are related to his sense of territory and body image. It was reviewed that if freedom of choice exists, pedestrians would adopt personal spacing which avoids contact with others. These psychological preferences of avoiding bodily contact with others should be determinants of inter-person spacing in queues and other crowded pedestrian environments [2].

It is considered in this study that a comfortable and convenient walking is provided when pedestrian spaces shown in Fig. 2 are sufficiently given to pedestrians. Therefore, pedestrian levels of service on the basis of comfort levels can be determined by assessing the amount of pedestrian spaces that can be obtained for a given facility. This study demonstrates how engineers can carry out this procedure.

3 Methodology

In this study, a pedestrian interview was made to identify major influencing factors for pedestrian comfort levels, and it was discovered that pedestrians perceive pedestrian mobility as the primary component of the comfort levels, followed by the degree of congestion, delay, and conflict. Other factors include the degree of connectivity between sidewalk, aesthetics, and the intervention from adjacent vehicular traffic lanes. Again, pedestrian levels of service in the KHCM lack the capability of directly reflecting the influence of pedestrian comfort into the measures of effectiveness and this study deals with this limitation by applying the concept of

pedestrian conflict, a measure hopefully explains the extent of pedestrian comfort levels for a pedestrian facility.

3.1 Data Collection and Analysis

Two different field data were collected in this study in order to examine how a new measure of effectiveness to describe pedestrian comfort levels compares with the existing variables for pedestrian flow including volume, density and speed. First, conventional data for pedestrian flows including volume, density, and speed were collected (Fig. 3). It was then followed by another data collection of the number of pedestrian conflicts while in walking. Second, some pedestrians were selected and asked to state their perceived levels of service on the basis of comfort levels. The following is the detailed description.

3.1.1 Characteristics of Pedestrian Flow

Five field study sites located in Seoul as given in Table 3 were selected in this study and a beforehand investigation was carried out in order to obtain a relatively wide range in pedestrian levels of service. Data collection was made for 3 months covering September to November of 2011. Data were collected in AM and PM peak hours (Table 2).

This study considered that one pedestrian conflict occurs when: (1) a pedestrian alters walking paths to avoid other pedestrians entering his/her predetermined private space, (2) a pedestrian slows down to avoid walking in the collision course with other pedestrians, (3) pedestrians make weaving maneuvers. It was assumed in this study that pedestrians involve various pedestrian conflicts to avoid making contacts with other pedestrians and that by assessing the extent of these pedestrian conflicts it would be possible to explain how pedestrians perceive different levels of comfort. E.T. Hall [3] addresses that pedestrians generally care to have 1.2 m distance from other pedestrians on sidewalks, and this study adopts this distance as the size of pedestrian distance. Therefore, one conflict occurs when pedestrians are apart less than 1.2 m distance but no conflict with greater than this distance.

3.1.2 Perceived Levels of Pedestrian Comfort

This study carried out a pedestrian interview to examine pedestrian levels of service in the KHCM and test the new pedestrian levels of service developed in this study. In this interview, a total of 500 subjects—100 subject for each field survey site—were asked to state their perceived comfort levels for a sidewalk they had just passed and also major influencing factors for their answers. Five levels of service from A to E were used, and the hourly results of the field survey data were compared with the results of pedestrian flow and conflict.

Table 2 Five field survey sites

Site ID	Location	Description	Average pedestrian volume(ped./h)	Effective width of sidewalk (m)
1	Seocho4-dong Seocho-gu	Kyobotower	8,115	7.5
2	Myeong-dong Jung-gu	CGV(Cinema)	4,760	7.9
3	Myeong-dong Jung-gu	Teenie Weenie	4,162	4.5
4	Sogong-dong Jung-gu	Lotte department store	3,512	6.0
5	Gwanhun-dong Jongno-gu	Dohan temple	3,424	5.5

Table 3 Adjustment of pedestrian levels of service in the KHCM

LOS	Flow (p/min/m)	Space (m ² /p)	Density (p/m ²)	Speed (m/min)	Conflict rate (%)
A	≤17	≥4.0	≤0.25	≥75	–
B	≤30	≥2.27	≤0.44	≥73	≤30
C	≤45	≥1.47	≤0.68	≥69	≤48
D	≤83	≥0.68	≤1.47	≥57	≤78
E	≤97	≥0.52	≤1.94	≥50	>78

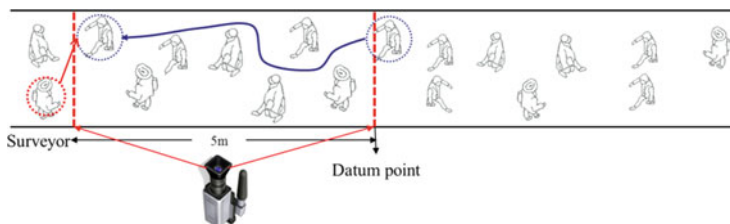


Fig. 3 Data collection method (Pedestrian traffic stream, # of conflict, pedestrian satisfaction)

3.2 Results and Implications

3.2.1 Congruency of Levels of Service in the KHCM

Levels of service in the KHCM were compared with pedestrian levels of service actually perceived by pedestrians. As a result, it was found that pedestrian levels of service based on the KHCM were congruous with pedestrians’ answers only in a range of 43 %. In a follow-up analysis, it was also discovered that both levels of service were congruous at good levels of service (LOS A–B), and not so congruous at poor levels of service (LOS C–E). Summarizing, it can be concluded that pedestrian levels of service in the KHCM fail to produce realistic results when the main issue of the analysis is pedestrian comfort levels.

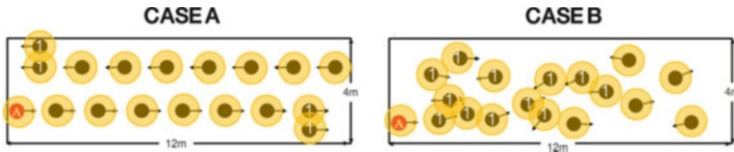


Fig. 4 Different pedestrian levels of service for a same level of pedestrian volume

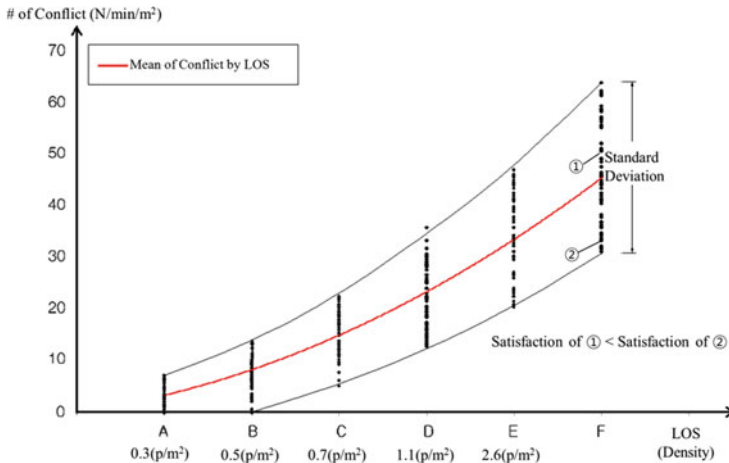


Fig. 5 Relationship between pedestrian conflicts and density

3.2.2 Characteristics of Pedestrian Conflicts

This section explains the essence of this study. In Fig. 4., Case A and Case B have the same level of pedestrian volume, so it is expected in the KHCM that both cases will produce the same level of service. However, in the real world, pedestrians walking in Case B should feel a lower pedestrian level of service than in Case A, since pedestrians in Case B will involve a higher number of pedestrian conflicts, pedestrian discomfort in this study. Therefore, this difference needs to be reflected into pedestrian levels of service when engineers want to assess pedestrian comfort levels.

This finding can also be applicable to pedestrian density. Again, as shown in Fig. 5, different pedestrian levels of service can be obtained in the KHCM for a same level of pedestrian density. It was found that the number of pedestrian conflicts increases at high pedestrian densities and the standard deviation of the pedestrian conflicts increase with density. Theoretically, at each level of service, there generally are two different levels of pedestrian conflicts divided by the center line, so a supplementary measure of effectiveness without showing this problem should be used when engineers want to determine pedestrian comfort levels.

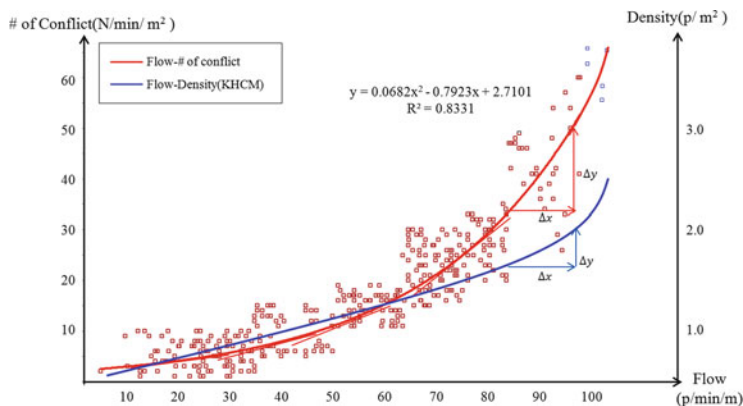


Fig. 6 Relationships between pedestrian conflict, flow rate, and density

In summary, this study attempts to configure pedestrian conflict, flow rate, and density in one graph such as shown in Fig. 6, so that engineers can compare one variable with other two variables. As a result, it was found that both pedestrian conflict and density increase with pedestrian flow rate, but the number of pedestrian conflicts increases more rapidly than pedestrian densities after passing a 60 pedestrians/min/m level, resulting in a close relationship with actual observations ($R^2 = 0.833$). Based on this finding, it was concluded that pedestrian conflict deserves much support in future pedestrian analysis as a primary measure of effectiveness for pedestrian comfort levels.

3.2.3 Adjustment to Pedestrian Levels of Service in the KHCM

It was conceived that the number of pedestrian conflicts needs to be replaced by the rate of pedestrian conflict to account for different volume levels. As expected, the rate of pedestrian conflict increases significantly at high densities, but the rates of increase show an inconsistent pattern for the whole density values. Therefore, there exist many break points of pedestrian conflict rates as given in Fig. 7. In detail, it was shown that LOS A has 0 % pedestrian conflict rate, LOS B 30 %, LOS C 48 %, LOS D 78 %, and LOS E 78 %. Matching points of pedestrian density were LOS A for less than 0.25 (pedestrians/min/m), LOS B 0.44, LOS C 0.68, LOS D 1.48, and LOS E 2.6.

Applying these relationships between pedestrian conflict rates and other pedestrian flow parameters, this study adjusts pedestrian levels of service in the KHCM as proposed in Table 3. Figure 8 demonstrates existing and adjusting levels of service.

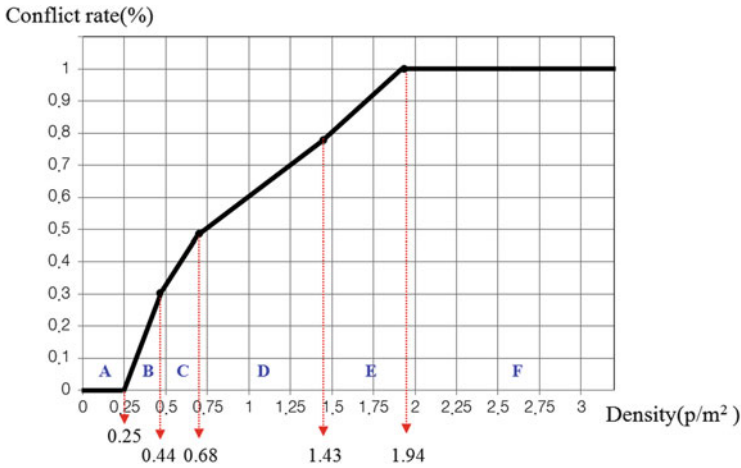


Fig. 7 Relationship between pedestrian conflict rate and density

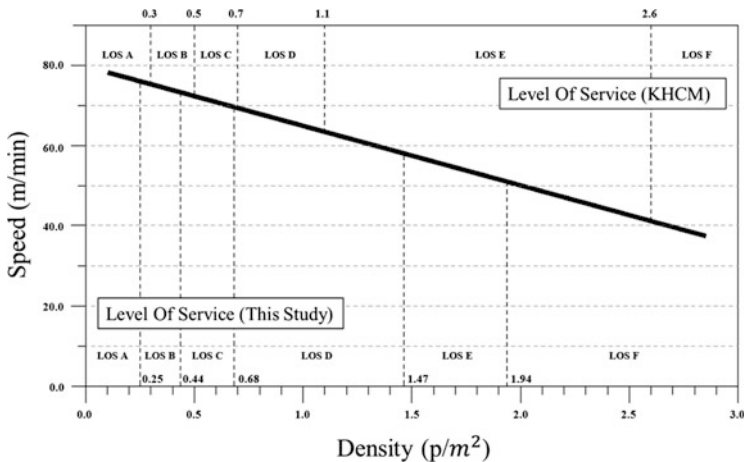


Fig. 8 Adjustment of pedestrian levels of service in the KHCM based on conflict rates

3.2.4 Additional Pedestrian Interview

In order to verify the proposed LOS table, an additional interview was made. The result shows a great increase of congruency as demonstrated in Fig. 9. For example, 15 % improvement was realized at LOS A, 9 % at LOS B, 24 % at LOS C, 48 % at LOS D, and 22 % at LOS E. In total, 29 % improvement was realized by applying the proposed LOS table. It is concluded that the proposed adjustment to the KHCM should be useful when pedestrian comfort levels need to be determined.

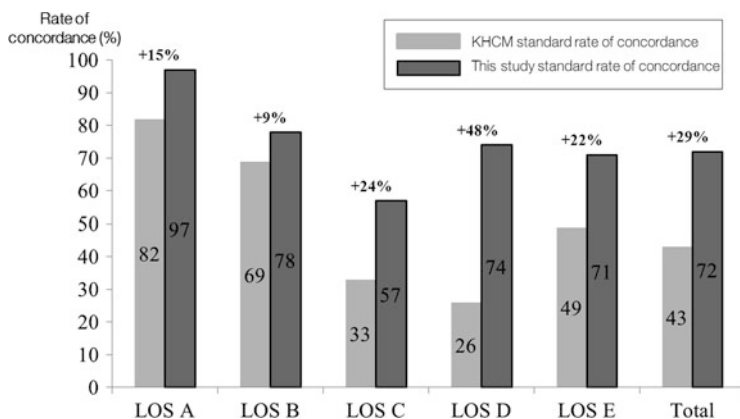


Fig. 9 Congruency of proposed LOS and the KHCM

4 Conclusions

It is important to be able to assess pedestrian comfort levels for pedestrian facilities built for them. Traditionally, pedestrian levels of service have been examined by applying pedestrian flow parameters including flow rate, density, and speed. However, these parameters are not useful when engineers want to determine pedestrian comfort levels. To deal with this limitation, this study carried out following tasks:

1. What are major factors influencing pedestrian comfort levels?
2. Can pedestrian conflicts be observed in the field? And what are their behavioral characteristics?
3. An investigation that relates pedestrian conflicts to existing pedestrian flow parameters, so that the existing pedestrian levels of service in the KHCM can be adjusted to reflect the effect of pedestrian comfort.

It was verified that the proposed LOS table works more realistically than the one in the KHCM. The proposed LOS table should be of service in future analyses of pedestrian comfort levels.

References

1. Choi, J., Kim, S. and Kim, Y. (2011). Determining the sidewalk width by using pedestrian discomfort levels and movement characteristics. *KSCE Journal of Civil Engineering* 15(5): 883–889.
2. Fruin, J. (1971). *Pedestrian Planning and Design*. Metropolitan Association of Urban Designer and Environmental Planners, New York.
3. Hall, E.T. (1990). *The Hidden Dimensions*. Anchor Books.

4. Im, J., Shin, H., Kim, H. (2006). New Pedestrian Level of Service by Trip Purpose and Walkway Function. *KSCE Journal of Civil Engineering* 24(5): 723–728.
5. Jensen, S. U. (2007). Pedestrian and Bicyclist Level of Service on Roadway Segments. *Transportation Research Record* 2031: 43–51.
6. Kim, Y., Choi, J. (2006). A Balanced Approach to the Planning and Design of Urban Streets. *Journal of Korean Society of Transportation* 24(6): 55–64.
7. Kim, S., Choi, J. and Kim, S., Tay. R. (2012). Behavioral Evaluation of Personal Distance for Pedestrians to Improve the Analysis of Levels of Services in Sidewalk Pavement Design. 4th Urban Street Symposium.
8. Landis, B., Vattikuti, V., Ottenberg, R., McLeod, D. and Guttenplan, M. (2001). Modeling the roadside walking environment: pedestrian level of service. *Transportation Research Record* 1773: 82–88.
9. MLTMA (2001). *Korean Highway Capacity Manual*. Ministry of Land & Transportation and Maritime Affairs, Seoul, Korea.
10. Sarkar, S. (2003). Qualitative Evaluation of Comfort Need in Urban Walkways in Major Activity Centers. *Transportation Quarterly* 57(4): 39–59.
11. Pushkarev, B and Zupan, J. (1975). *Urban Space for Pedestrians*. A Report of the Regional Plan Association, MIT Press, Cambridge.
12. TRB (2000). *Highway Capacity Manual*. Transportation Research Board, Washington, US.

Scalable Evacuation Simulation and Visualization Using GPU Computing

Kensuke Yasufuku

Abstract In this paper, we will describe our novel approach to real-time visualization of crowd flow using a scalable agent-based evacuation simulation that is suitable for execution on GPUs. To simulate the crowd behavior, we used the social force model in which each individual is represented by a self-driven particle subject to social and physical forces. The social force calculations were executed using CUDA technology, a parallel-processing architecture for many-core GPUs. As a result, the GPU version was shown to have better scalability than the CPU version. In a case study of an evacuation scenario of a large underground shopping mall, the GPU version is approximately seven times faster than the CPU version and was capable of sustaining an interactive frame rate when visualizing the evacuation.

Keywords Evacuation simulation • GPU computing • Visualization

1 Introduction

Agent-based evacuation simulations are commonly used to assess the safety of buildings and urban environments. Real-time simulation tools are especially effective for interactively analyzing evacuation behaviors. However, computing and visualizing massive crowds in real-time is a computationally intensive task because most algorithms for calculating the interactions among all the individuals have a complexity of $O(n^2)$. In previous work, researchers have reduced this complexity by employing special data structures, such as cellular automata models or network models. Additionally, researchers have significantly increased computational performance by adapting existing CPU-oriented algorithms to parallel processing

K. Yasufuku (✉)
Cybermedia Center, Osaka University, Osaka, Japan
e-mail: yasufuku@cmc.osaka-u.ac.jp

architectures [1]. A promising new parallel architecture uses commodity graphics processing units (GPUs) having many cores, offering the performance benefits of parallel processing at a low cost. This was the advent of the movement called GPU computing. In 2007, NVIDIA released the CUDA (Compute Unified Device Architecture) [2], which is a parallel-processing architecture for their next-generation GPUs; the CUDA allows programmers to use a special version of C to code algorithms for execution on the GPU. Using this technology, it is now easier to design agent-based simulations that can be executed on GPUs in order to enhance scalability. In this paper, we will describe our novel approach to real-time visualization of crowd flow in a large underground shopping mall using a scalable evacuation simulation that is suitable for execution on GPUs.

2 Method

2.1 Scalable Evacuation Simulation

Figure 1 shows the flow chart for the scalable evacuation simulation we developed. The evacuation simulation uses an agent-based system. Namely, an evacuee is modeled as an agent. The modeling of each agent's behavior consists of (1) the macroscopic route choice model: setting a destination and calculating the route; and (2) the microscopic crowd walking model: approaching the destination and avoiding collisions with other agents and obstacles. In our research, we implemented a shortest route choice model and the social force model [3]. The base programming language is C++. The social force model operations were implemented in CUDA in order to enhance scalability.

2.1.1 Macroscopic Route Choice Model

In the macroscopic route choice model, people calculate their migration route and choose their destination. The migration route is the shortest path, assuming that the people have prior knowledge of the positions of destinations. To calculate the shortest path, a search algorithm is used and space model data is created to fit the algorithm.

Specifically, the process of the route choice model is as follows. First, a destination (e.g., an exit or staircase) is selected by applying the Dijkstra method to a coarse network model which divide the floor plan into rooms, corridors, stair sections, etc. Second, the shortest path to the destination is calculated based on the position of the agent by applying the A* search method to a fine network model which divides a floor plan into a number of small grid cells. However, although agents move in a continuous coordinate system, the shortest path determined under the fine network model, which has a discrete coordinate system, is based on

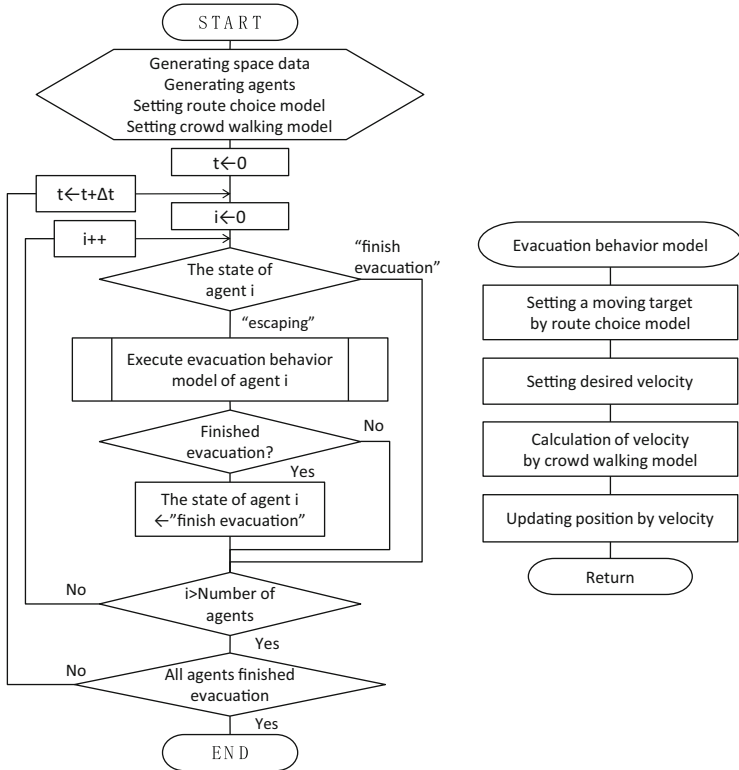


Fig. 1 Scalable evacuation simulation flow

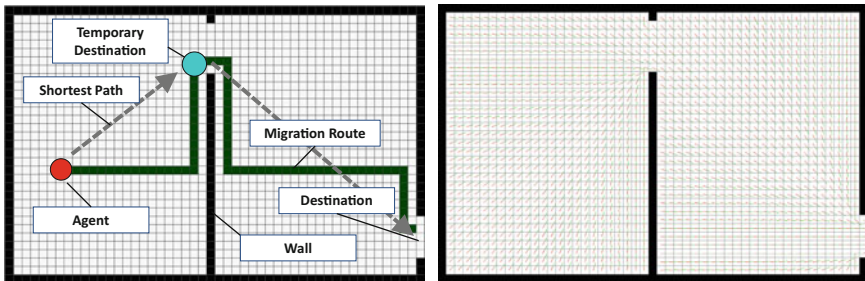
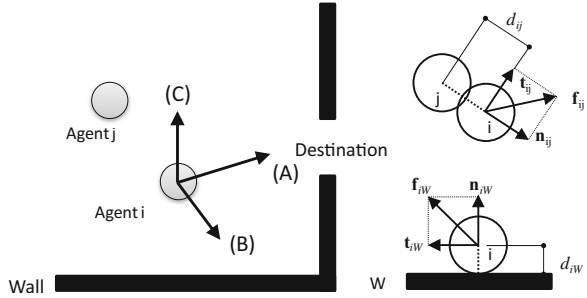


Fig. 2 Route choice model and precomputed floor field for finding a shortest path

Manhattan distance. To resolve this difference, the destination is selected using the Euclidean distance of the migration route determined under the fine network model. The left-hand side of Fig. 2 shows an example of the route choice model.

As the size of the building and number of agents increases, the time it takes to calculate the shortest path grows rapidly. In this paper, we precomputed a floor field [4] covering each cell point to generate the shortest path data so that we could

Fig. 3 Social force model



simulate tens of thousands of agents in a very large space in real time (right-hand side of Fig. 2). Thus, agents are able to use path data from the cell point they are currently.

2.1.2 Microscopic Social Force Model

We used the social force model to approximate microscopic evacuation behavior. In the social force model, each individual is represented by a self-driven particle subject to social and physical forces. Accordingly, individuals with a certain mass like to move in a certain direction at a certain speed, adapting their velocity within a certain time period, while keeping their distance from other individuals and obstacles. Therefore, the social forces consist of (A) an attracting force from the closest destination, (B) repulsive forces from other individuals, and (C) repulsive forces from walls and other obstacles, as shown in Fig. 3. The mathematical representation of these forces is presented in (1) through (3). Each individual calculates the force necessary to prevent it from exceeding a preset speed limit and updates its walking speed once per time step.

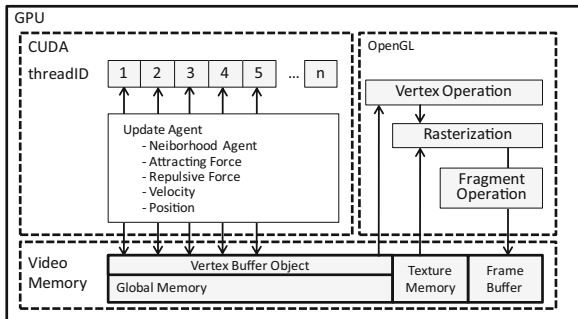
$$m_i \frac{d\mathbf{v}_i}{dt} = m_i \frac{v_i^0(t)\mathbf{e}_i^0(t) - \mathbf{v}_i(t)}{\tau_i} + \sum_{j(\neq i)} \mathbf{f}_{ij} + \sum_W \mathbf{f}_{iW} \tag{1}$$

$$\mathbf{f}_{ij} = \{A_i \exp[(r_{ij} - d_{ij}) / B_i] + kg(r_{ij} - d_{ij})\} + \mathbf{n}_{ij} + \kappa g(r_{ij} - d_{ij}) \Delta v_{ij}^t \mathbf{t}_{ij} \tag{2}$$

$$\begin{aligned} \mathbf{f}_{iW} = \{ & A_i \exp[(r_i - d_{iW}) / B_i] + kg(r_i - d_{iW})\} \mathbf{n}_{iW} \\ & + \kappa g(r_i - d_{iW}) (\mathbf{v}_i \cdot \mathbf{t}_{iW}) \mathbf{t}_{iW} \end{aligned} \tag{3}$$

Conventional methods implement agent-based modeling using CPU-oriented algorithms. However, in recent years, the use of GPUs for general purpose computing has become a new area of research. In our new simulation, the social force model operations were executed on a GPU using CUDA technology, which is a

Fig. 4 Parallel processing using CUDA



parallel-processing architecture for GPUs with many cores. Specifically, one thread was allocated per agent to calculate the social forces on that agent (Fig. 4). Although CPUs can only concurrently execute one thread per core, CUDA can run tens of thousands of threads simultaneously. Thus, the GPU’s computational power is sufficient for updating the behavior of massive crowds in real time.

2.2 Case Study

2.2.1 Evacuation from a Large Underground Shopping Mall

As a case study of scalable evacuation simulation, we created an evacuation scenario for a large underground shopping mall in Osaka, Japan. Figure 5 shows the plan of an actual underground shopping mall. This underground shopping mall has 1,200 retail stores and restaurants, as well as a subway and intercity rail station. Thus, this underground area has a relatively complicated space composition. In our research, we simulated a 25,000-person evacuation from this underground shopping mall.

3 Results and Discussions

3.1 Performance of Scalability

For performance testing, we evaluated two versions of the simulation. The first version was executed on a GPU, and the second was executed on a CPU. The same algorithm and data structures were used in both cases; these tests were performed on an Intel Core i7 930 2.80 GHz CPU and an NVIDIA GeForce GTX 460 GPU. Figure 6 shows the average time required to compute the social force of all agents in the absence of the rendering process. The tests were executed for each

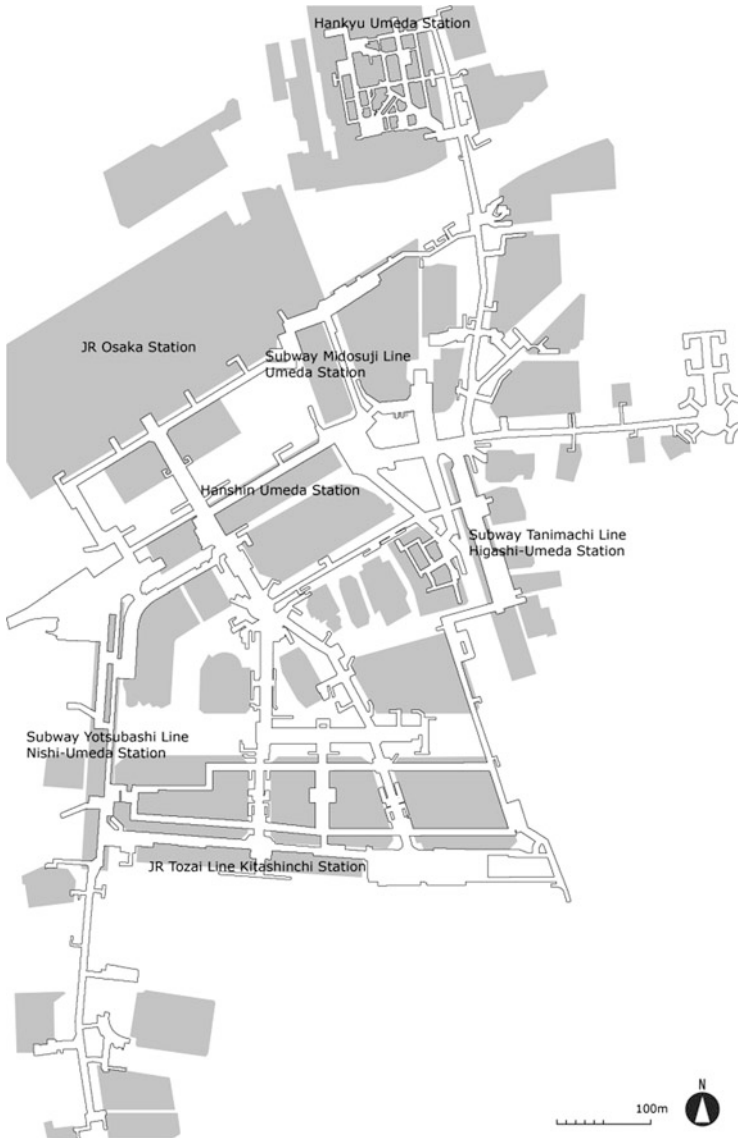


Fig. 5 Case study plan

implementation type by varying only the number of agents, which ranged between 1,000 and 10,000. It was found that the GPU version had better scalability than the CPU version. For example, at 10,000 agents, the GPU version was approximately seven times faster than the CPU version. Moreover, it could be clearly observed that

Fig. 6 Performance comparison between GPU and CPU

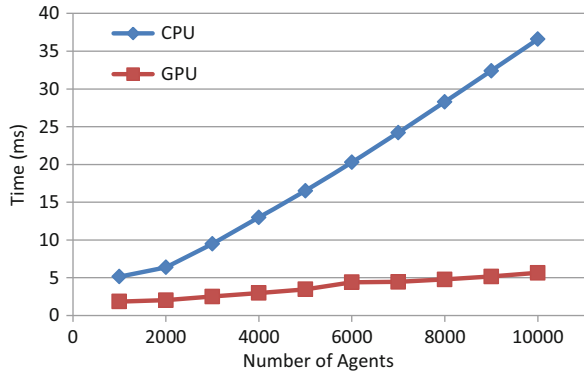
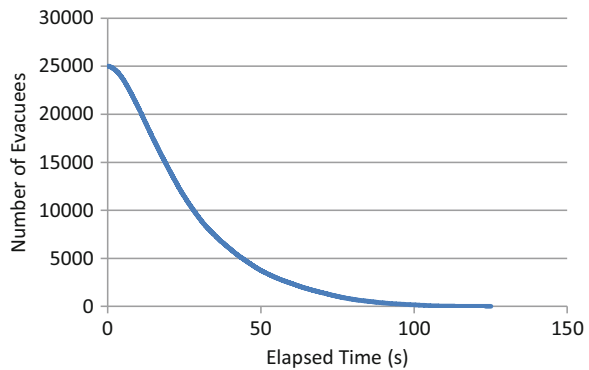


Fig. 7 Sample result to determine evacuation time: number of people not yet evacuated



the performance of the GPU version was sufficient to sustain interactive frame rates for rendering complex models of agents and buildings.

3.2 Result of Case Study

Figure 7 shows the evacuation time result of the case study. It took 2 min to evacuate all the people from the large underground shopping mall according to the evacuation simulation. The time series graph of the number of evacuees shows that the rate of people who have reached the safe area was large from approximately 5–50 s after the start of the evacuation. Then, the rate of evacuation was small gradually. This indicates that the exits are unequally distributed. In order to shorten the evacuation time, evacuation guidance is important. Although some might claim that there is no practical use in simulating a situation in which evacuees are uniformly distributed and all evacuees escape through one of the nearest staircases, we think this simulation can serve as a guide for analyzing the evacuation of this type of area.



Fig. 8 Crowd flow in large underground shopping mall

3.2.1 Interactive Visualization

Figure 8 shows two snapshots of the interactive visualization of evacuation crowd flow in the large underground shopping mall. Such visualization enables the control of viewpoint and also allows a fully zoomable map. These functions are effective for interactively analyzing evacuation behaviors.

Dynamic route choice is also effective for the trial-and-error stage of planning an evacuation interactively. By using multi-floor field data, the evacuation simulation is real time, although the route choice model is based on precomputed floor field data.

4 Conclusion

In this paper, we have described an agent-based scalable evacuation simulation that can be executed on GPUs while visualizing crowd flow in a large underground shopping mall interactively. We demonstrated that the GPU-based implementation was capable of supporting up to 25,000 people at an interactive frame rate using current graphics hardware and CUDA technology. Therefore we have shown that this simulation has potential as an effective tool for assessment of evacuation safety

or use in the trial-and-error stage of creating an evacuation plan in the context of large urban environments.

References

1. Seyfried, A., Chraibi, M., Kemloh, U., Mehlich, J., Schadschneider, A.: Runtime Optimization of Force Based Models within the Hermes Project. *Pedestrian and Evacuation Dynamics*, pp. 363–73, Springer, Maryland (2010)
2. NVIDIA CUDA Parallel Programming and Computing Platform, http://www.nvidia.com/object/cuda_home_new.html
3. Helbing, D., Farkas, I., Vicsek, T.: Simulating Dynamical Features of Escape Panic. *Nature*. 407, 487–490 (2000)
4. Burstedde, C., Klauck, K., Schadschneider, A., Zittartz, J.: Simulation of pedestrian dynamics using a two-dimensional cellular automaton. *Physica A*. 295, 507–525 (2001)

Starting-wave and Optimal Density in a Queue

Akiyasu Tomoeda, Daichi Yanagisawa, Takashi Imamura,
and Katsuhiko Nishinari

Abstract We have investigated the fundamental relation between the density and the propagation speed of *starting-wave*, which is a wave of people's successive reaction in a relaxation process of a queue, by both our mathematical model built on the stochastic cellular automata and experimental measurements. The analysis of our mathematical model implies that the relation is well approximated by power law $a = \alpha \rho^{-\beta}$ ($\beta \neq 1$) and the experimental results verify this feature. Moreover, when the starting-wave is characterized by power law ($\beta \neq 1$), we have revealed the existence of optimal density, where the required time which is sum of the waiting time until the starting-wave reaches and the travel time of last pedestrians in a queue to pass the head position of the initial queue is minimized. This optimal density

A. Tomoeda (✉)

Meiji Institute for Advanced Study of Mathematical Sciences, Meiji University, 1-1-1 Higashi Mita, Tama-ku, Kawasaki, Kanagawa 214-8571, Japan

JST CREST, 1-1-1 Higashi Mita, Tama-ku, Kawasaki, Kanagawa 214-8571, Japan
e-mail: atom@isc.meiji.ac.jp

D. Yanagisawa

College of Science, Ibaraki University, 2-1-1, Bunkyo, Mito, Ibaraki 310-8512, Japan
e-mail: daichi@mx.ibaraki.ac.jp

T. Imamura

Research Center for Advanced Science and Technology, The University of Tokyo, 4-6-1, Komaba, Meguro-ku, Tokyo 153-8904, Japan
e-mail: timamura@iis.u-tokyo.ac.jp

K. Nishinari

Research Center for Advanced Science and Technology, The University of Tokyo, 4-6-1, Komaba, Meguro-ku, Tokyo 153-8904, Japan

Department of Aeronautics and Astronautics, School of Engineering, The University of Tokyo, 7-3-1, Hongo, Bunkyo-ku, Tokyo 113-8656, Japan
e-mail: tknishi@mail.ecc.u-tokyo.ac.jp

inevitably plays a significant role to achieve a smooth movement of crowds and vehicles in a queue.

Keywords Jamology • Stochastic cellular automaton • Queuing system • Starting-wave • Optimization problem

1 Introduction

Various kinds of self-driven particles (SDP) systems, such as evacuation dynamics of pedestrians and vehicular traffic have attracted a great deal of attention in a wide range of fields during the last few decades [1–3]. Especially, the interdisciplinary investigations for the dynamics of jamming phenomena in SDP systems, so-called *Jamology*, have been progressed by developing sophisticated mathematical models considered as a system of interacting particles driven far-from equilibrium.

One of the typical problems is how to realize a smooth and safe movement of crowds and vehicles. We would like to point out that the wave of successive reaction in a relaxation process in a queue, so-called *starting-wave*, plays a significant role for the waiting time in a queuing system of not only pedestrians but also vehicles, since quick-start in walking and driving accomplishes the more smooth movement of crowds and vehicles in a queue. In order to resolve a queue of pedestrians and vehicles, the departure rate from the cluster should become larger than the arrival rate in principle. From this point of view, it is important to investigate the propagation speed of starting-wave, since the fast propagation speed of starting-wave eventually actualize high departure rate. Here we focus on the realization of a smooth movement of teeming number of the athletes at the start in a marathon considered as a long queue, since the athletes located rearward position have some unavoidable delay in a queue and this delay raises the possibility of a traffic disturbance in the surrounding area.

In this paper we have investigated the propagation speed of starting-wave of pedestrians and have found that the fundamental relation between the velocity of starting-wave and the density is characterized by power law $a = \alpha \rho^{-\beta}$ ($\beta \neq 1$) by both our mathematical model and experimental measurements. In our previous study [4], we have found that this fundamental relation is well approximated by the power law by numerical simulations based on our mathematical model. However, here we would like to report new results obtained from the numerical simulations of our new mathematical model, its analytical calculations and new experimental measurements including the high density region. Moreover, we have also revealed the existence of optimal density, where the required time of last pedestrians in a queue, that is, the sum of waiting time until the arrival of the starting-wave and travel time to pass the head position of the initial queue is minimized in the case of high velocity.

This contribution is organized as follows. In Sect. 2, we propose the mathematical model for pedestrians' walking built on the stochastic cellular automaton. The

fundamental relation between the velocity of starting-wave and the density is investigated by both numerical simulations and analytical calculations of our model in Sect. 2. Moreover, the existence of optimal density which minimizes the required time in a queue is also shown in Sect. 2. In Sect. 3, these results obtained from our mathematical model are verified by experimental measurements of pedestrians. Finally, Sect. 4 is devoted to the concluding discussions.

2 Mathematical Model

In this section, we explain our mathematical model built on the stochastic cellular automaton models such as ASEP [5–7] and ZRP [8–10], which can capture fundamental features of jamming phenomena in various collective dynamical system. Particularly, these cellular automaton models are more suitable to describe the queuing system than the mathematical model based on the traditional queuing theory [11], since cellular automaton models can consider the excluded-volume effect and spatial structure explicitly. In fact, an extension of the M/M/1 queuing process with a spatial structure and excluded-volume effect is recently introduced [12, 13] and its dynamical features are analyzed [14], as the ASEP on a semi-infinite chain with open boundary.

Let us imagine that the passage is partitioned into L identical cells that each cell can accommodate at most one particle (pedestrian) at a time, enforcing the excluded-volume effect. The length of each cell corresponds to 0.5 m by considering the reasonable volume exclusion effect of pedestrians. N ($2 \leq N \leq L$) indicates the total number of particles which are initially placed at equal distance h_0 cell. The parameters (N, L, h_0) satisfy the equally-spaced condition as follows:

$$h_0 = \frac{L}{N} - 1. \quad (1)$$

We impose the semi-open boundary condition, where particles walk away from the right boundary. The update rules of our cellular automaton model are applied in parallel to all particles as follows (also see Fig. 1):

First of all $t = 0$, only the particle at the head of a queue t moves forward with hopping probability $p(h)$, which depends on their current headway distance h defined by the vacant cells in front of them. The function form of $p(h)$ is defined by the same one in [4] which is calculated from the experimental data [15]. In order to investigate the propagation speed of successive reactions, all of the following particles cannot move forward before the starting-wave reaches to themselves. Then $t = 1$ the following particle (only second particle in the queue) can move forward with probability $p(h)$. In the case of Fig. 1, this probability $p(h)$ at time $t = 1$ corresponds to $p(3)$. Then, the particle which once has moved can move forward with maximum velocity V_{max} . The usual maximum velocity in the solvable stochastic cellular automaton models, which corresponds to 1 cell per 1 time step,

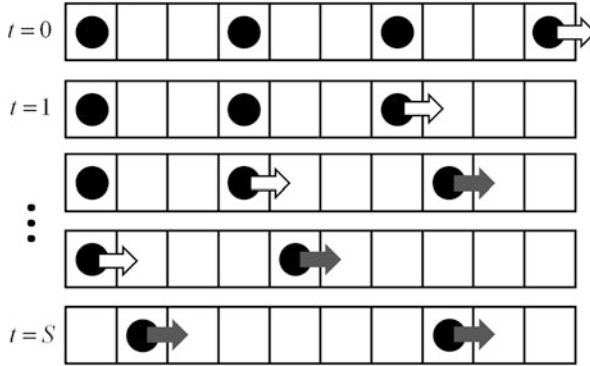


Fig. 1 Schematic view of time development of our mathematical model for the parameters $(N, L, h_0) = (4, 10, 2)$ and $V_{max} = 3$. The *white arrow* indicates the hopping probability $p(h)$ of the particle who moves forward for the first time in this dynamics. Whereas, the *gray arrow* indicates the maximum velocity V_{max} of the particle who moves forward after the particle once has moved. The right boundary corresponds to the open boundary, that is, particles leave from the system via the right boundary

is not enough fast to treat the situation of the start in a marathon. Accordingly, a particle can move forward with probability $p(h)$ for the first time after the starting-wave has reached and then the particle can move forward deterministically with maximum velocity V_{max} . After the second particle moves forward, the next particle can also start to move with probability $p(h)$ in sequence. Finally, the last moves forward at the time $t = S - 1$. As just described, only if the next cell is empty and the predecessor had already started, following particles can start to move forward in our model unlike the usual stochastic cellular automaton models such as ASEP and ZRP with parallel update.

In the numerical simulations and analytical calculations of our model, we have estimated the propagation speed of starting-wave under several densities which are decided by the initial number of particles in a queue. Taking into account the appropriate conversions 1 step = 0.4 s and 1 cell = 0.5 m, the propagation speed a is calculated by

$$a = \frac{0.5(L - 1)}{0.4S}, \tag{2}$$

where S is the required steps for the last particle to start walking (see Fig. 1).

As a significant result of numerical simulations we have found the power law in the relation between propagation speed of starting-wave and the initial density of pedestrians as shown in Fig. 2. Each plot corresponds to the average velocity after 100 iterations of numerical simulations. Assuming this power law, we describe the simple relation between propagation speed and density of pedestrians in analogy with the sonic speed of gas as the form

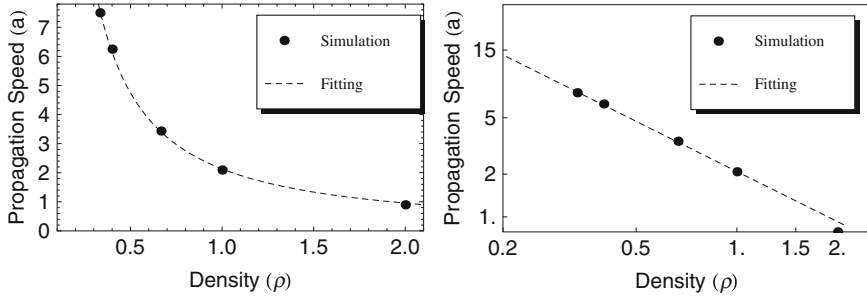


Fig. 2 The simulation results (*dots*) and fitting relation (*dashed curve* or *dashed line*) between propagation speed of starting-wave and density of pedestrians by our mathematical model. *Left figure* shows the normal plot and *right figure* shows double logarithmic plot

$$a = \alpha \rho^{-\beta}, \tag{3}$$

where ρ and a are the density and the propagation speed of starting-wave, respectively. α and β indicate positive parameters. By fitting these simulation results, we have obtained the parameter values $(\alpha, \beta) = (2.13, 1.16)$. Moreover, these parameters (α, β) can be calculated when the maximum velocity is $V_{max} \geq 3$. Under this condition, the expectation value of the required steps S for the last to start walking is given by

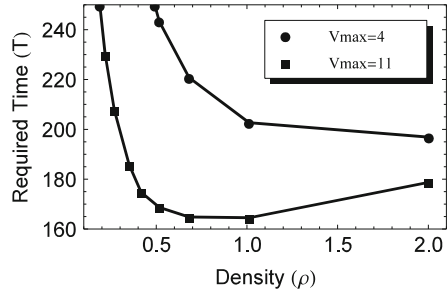
$$S = \sum_{k=0}^{N-1} \binom{N-1}{k} p(h+1)^{N-1-k} (1-p(h+1))^k (N+k), \tag{4}$$

since particles only stop once with probability $1-p(h+1)$ at most. From Eq. 4, we obtain the propagation speed for each given headway distance h_0 . This data set provides the parameters $(\alpha, \beta) = (2.13, 1.15)$ from the fitting form Eq. 3. The parameters have a good agreement in both numerical simulations and analytical calculations. The interesting fact here is that the propagation speed obtained from the mathematical model shows the nonlinearity, i.e., $\beta \neq 1$.

Furthermore, in order to investigate the required time under the nonlinearity of the fundamental relation, our model estimates the required time in the cases of low maximum velocity and high maximum velocity as shown in Fig. 3. In the case of low maximum velocity, the required time decreases as the density increases, since the propagation speed of reaction is enough fast by comparing the walking speed. Whereas, the density $\rho = 0.667$ takes the minimum of the required time in the case of high maximum velocity, since the lost time until the arrival of the starting-wave is large by comparing the time to walk longer distance.

The required time T for given initial density $\rho_0 = N/L$ is calculated as

Fig. 3 Required time in numerical simulations for each maximum velocity



$$T(\rho_0) = \frac{L}{a(\rho_0)} + \frac{L}{V_{max}} \tag{5}$$

First term and second term of right-hand-side in Eq. 5 indicate the required time to start walking and the one to reach the head position of the initial queue after start walking, respectively. Substituting the relation Eq. 3) into Eq. 5, one obtains a condition to exist the extreme value $dT/d\rho_0 = 0$ as

$$\rho_0^\beta = \frac{\alpha}{V_{max}(\beta - 1)} \tag{6}$$

In order to exist the value of ρ_0 , β satisfies $\beta > 1$, since the parameter α , β and V_{max} are all positive value. The value of $\beta \sim 1.16$ as noted before is larger than 1.

Therefore, it is found that an optimal density does exist for given parameter α , β and V_{max} . Note that, if the hopping probability $p(h)$ is always constant and the initial headway distance corresponds to zero, our model is reduced to ASEP with the step initial condition. In this situation, the probability distribution of the required time can be obtained exactly in [16–18].

3 Experiments

In our experiments, we have measured the propagation speed of starting-wave and required time in a queue to pass the head position of the initial queue under the various densities which are decided by the initial number of pedestrians along a line and the length of the queue as well as our mathematical model.

At first, we make a long straight passage (L meters) and put marks with a distance of 0.5 m between them as shown in Fig. 4. As an initial condition of pedestrians, all pedestrians N stand in line with same headway distance. After that, the leader of queue starts to walk by the cue and then we measure the two required time, which are the time until the last pedestrian starts to walk and the time until the last pedestrian passes the head position of the initial queue. Thus, we have obtained the propagation speed of successive reaction which is calculated from the length of initial queue



Fig. 4 A snapshot of our experimental passage

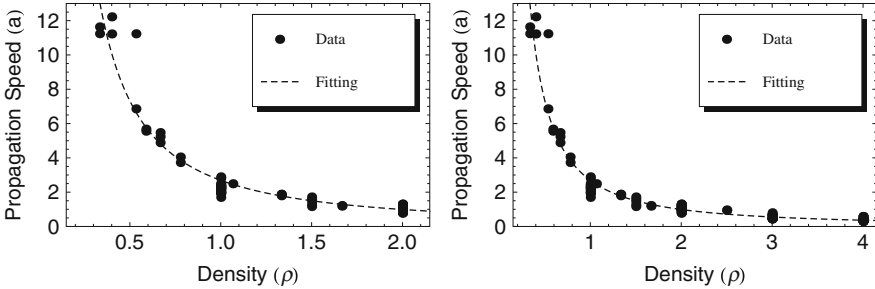


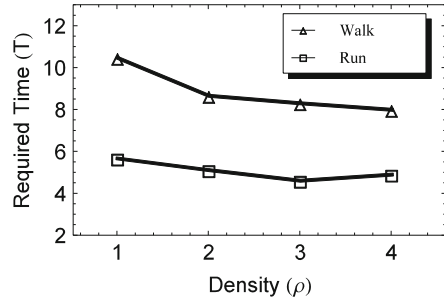
Fig. 5 Experimental results of propagation speed of successive reaction. Even if the results include the higher density region where the model could not mention, the power law can well approximate the relation between propagation speed and density

divided by the former required time under each given density determined by a combination of L and N . Moreover, the latter required time corresponds to the delay time from the cue to pass the head position of the queue. As well as the numerical simulations, we have obtained the set of parameters $(\alpha, \beta) = (2.90, 1.36)$ by fitting our experimental data based on Eq. 3 as shown in Fig. 5.

Comparing the fitting function based on the form Eq. 3 and the data, we have found that the fitting function is quite suitable for describing the relation between the density of pedestrians and propagation speed of starting-wave in pedestrian dynamics even in the results obtained from different pedestrians. What we would emphasize here is our actual experiments have proven that the power law well captures a characteristic feature of starting-wave, that is, the relation between the propagation speed of starting-wave and density, as well as the results from our mathematical model. Moreover, its nonlinearity, i.e. $\beta > 1$, satisfies the requirements for optimizing the initial density of queue.

In the previous section our mathematical model with high walking velocity shows the existence of an optimal density to minimize the required time in a density region. The required time in the cases of high velocity and low velocity are plotted in Fig. 6. From these results, we have observed that the optimal density to minimize the required time does not exist in the case of low velocity, however, in the case of high velocity the optimal density surely exists at the density $\rho = 3.0$ by comparing among four densities. Thus, the validity of numerical simulations and analytical calculations of our mathematical model is supported by substantiative experiments.

Fig. 6 Experimental results of required time in the case of high velocity and low velocity. The experiments with walking and running correspond to the low velocity case and the high velocity case, respectively



4 Conclusions

In this contribution, we have investigated the propagation speed of pedestrians' reaction in relaxation process of a queue so-called starting-wave toward a smooth movement of crowds, since the fast starting-wave achieves high departure rate. We have first proposed our mathematical model which is built on the stochastic cellular automaton models in analogy with the mathematical modeling for the traffic flow, then we have revealed a special relation between the propagation speed of pedestrians' reaction and the density, which is well approximated by power law $a = \alpha \rho^{-\beta}$ ($\beta \neq 1$) by using numerical simulations and analytical calculations. Moreover, we have also found the existence of optimal density, where the travel time of last pedestrians to pass the start line for the initial queue is minimized. The requirement for the existence of optimal density from our mathematical model is $\beta > 1$. These results obtained from our mathematical model are verified by actual experiments. This optimal density inevitably plays a significant role to design not only the initial queue of pedestrians but also the traffic intersections and signals.

Acknowledgments We thank Kozo Keikaku Engineering Inc. in Japan and the members of the Meiji University Global COE Program "Formation and Development of Mathematical Sciences Based on Modeling and Analysis" for the assistance of the experiments, which is described in Sect. 3. We also acknowledge the support of Japan Society for the Promotion of Science and Japan Science and Technology Agency.

References

1. D. Chowdhury, L. Santen and A. Schadschneider, Phys. Rep. 329, 199 (2000).
2. D. Helbing, Rev. Mod. Phys. 73, 1067 (2001).
3. A. Schadschneider, D. Chowdhury and K. Nishinari, *STOCHASTIC TRANSPORT IN COMPLEX SYSTEMS FROM MOLECULES TO VEHICLES*, Elsevier, (2010).
4. A. Tomoeda, D. Yanagisawa and K. Nishinari, fifth International Conference on Pedestrian and Evacuation Dynamics, Springer.
5. B. Derrida, Phys. Rep., 301, 65 (1998).

6. N. Rajewsky, L. Santen, A. Schadschneider and M. Schreckenberg, *J. Stat. Phys.*, 92, 151 (1998).
7. G. M. Schutz, *Phase Transitions and Critical Phenomena*, 19 (Acad. Press, 2001), G. M. Schutz, *J. Phys. A: Math. Gen.*, 36, R339 (2003).
8. F. Spitzer, *Adv. Math.*, 5, 246 (1970).
9. M. R. Evans and T. Hanney, *J. Phys. A: Math. Gen.*, 38, R195 (2005).
10. M. Kanai, *J. Phys. A*, 40, 7127 (2007).
11. G. Bolch, S. Greiner, H. de Meer and K. S. Trivedi, *Queueing Networks and Markov Chains*, Wiley-Interscience, U.S.A., 1998.
12. C. Arita, *Phys. Rev. E*, 80, 051119 (2009).
13. C. Arita and D. Yanagisawa, *J. Stat. Phys.*, 141, 829 (2010).
14. C. Arita and A. Schadschneider, *Phys. Rev. E*, 83, 051128 (2011).
15. A. Seyfried, B. Steffen, W. Klingsch, and M. Boltes. *J. Stat. Mech.*, 10002 (2005).
16. K. Joahnsson, *Commun. Math. Phys.*, 209, 437 (2000).
17. T. Imamura and T. Sasamoto, *J. Stat. Phys.*, 128, 799 (2007).
18. A. Borodin, P.L. Ferrari, and T. Sasamoto, *Commun. Math. Phys.* 283, 417 (2008).

The Love Parade Disaster

Causes and Consequences

Hubert Klüpfel

Abstract On July, 24th 2010 there was a severe incident at the love parade in Duisburg, Germany. At the entrance ramp to the festival area, 21 persons died in a crowd crush and many were injured. In this contribution, the background of the disaster is presented and the causes and consequences that can be identified to date are described. The major finding for the cause of the disaster is the following: it was triggered by a break-down of the inflow from the main ramp to the festival area resulting in congestion and high local density on the ramp. The consequence was an increasing attractiveness of alternative access points to the venue (at the same time ways to escape from the congestion): a frame, a container, and most of all a narrow stair located at the side of the main-ramp. This closed feedback loop of causes and consequences formed a vicious circle and produced densities, pressures, and forces within the crowd that led to severe injuries, asphyxia, crushed rib cages, and the death of 21 people. Understanding the causes of this disaster might hopefully be helpful in preventing future incidents.

1 Background: The History and Character of the Love Parade

The history and background of the Love Parade are described in [3], which provides a thorough introduction to the topic of this contribution. All readers are encouraged to refer to [3] for background information.

H. Klüpfel (✉)
TraffGo HT GmbH, Duisburg, Germany
e-mail: kluepfel@traffgo.de

The Love Parade (German: Loveparade) was a popular electronic dance music festival and parade that originated in 1989 in West Berlin, Germany. It has been held annually in Germany 1989–2003 in Berlin, then again in 2006 in Berlin and from 2007 to 2010 in the Ruhr region. The 2004 and 2005 events in Berlin and the 2009 event in Bochum [1] were cancelled. On 24 July 2010, a crowd crush at the Love Parade caused the death of 21 people, with at least 500 others injured. [2] As a consequence of this, the organiser of the festival announced that no further Love Parades would be held and that the festival was permanently cancelled. [3], Refs. [1] and [2] as in [3]

Recently, a thorough investigation of the topic has been published [24]. This analysis comes conclusions similar to those presented here, especially the complex interplay and interdependence of several factors contributing to the disaster.

2 The Disaster

The disaster happened on July, 24th, 2010 in Duisburg, Germany. The event was not cancelled after the disaster but continued.

Entrance was granted at 12:00 CEST (10:00 UTC). A 240-m tunnel from the east and a series of underpasses from the west met at a ramp that was supposed to be the only entrance and exit point of the festival area. [7] A smaller ramp existed between the underpasses from the west. Because of overcrowding, police at the entrance began announcing over loudspeakers that new arrivals should turn around and head back. [8, 9] The side of the tunnel that was the entry of the parade area was closed, but people continued to enter the tunnel from the rear, despite being told it was closed. A stampede occurred as the ramp between tunnel underpasses and the festival area became overcrowded. [7, 8]

There was some debate as to how the deaths occurred. Some reports suggested they were caused by people falling off a staircase as they tried to escape the tunnel. [8, 9] However, autopsies showed that all of the fatalities were due to crushed rib cages. [10, 11]

(quoted from [3], references [7–11] of the quotation are as in [3]).

3 Causes of the Disaster

The discussion about the causes of the disaster focussed on three groups of actors responsible for planning, organizing, and supervising the event:

- The organizer
- The police
- The city

The events at the love parade are also subject of a legal investigation. In this context, an expert report has been prepared by K. Still. Some of the results of this report are discussed below. The full report is available for download [19].

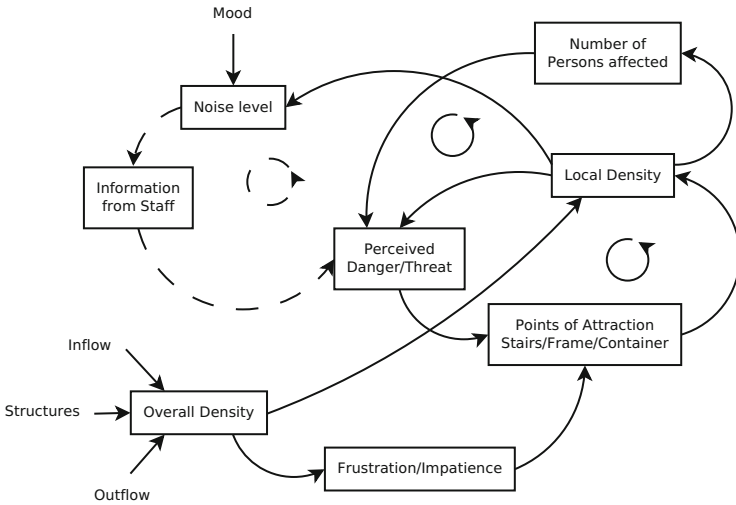


Fig. 1 The event as a system (Adapted from Mamrot [17])

3.1 The Festival Area

At <http://www.openstreetmap.org/?lat=51.42181&lon=6.77458&zoom=15&layers=M> the festival area can be seen online. It was a former freight yard in the city centre next to the main station. For the love parade, the part between the two streets “Koloniestraße” and “Karl-Lehr-Straße” (both directed from West to East) was used. The A59 motorway borders the area in the west and the railway tracks in the east (both in north–south direction). The railway tracks border the area in the east (also in north–south-direction). North of the area is the central station. Between the area and the central station are some parking lots (“P”).

The A59 motorway is beneath surface level (i.e. in a tunnel) in the vicinity of the central station, but at surface level (or nearly at surface level) next to the festival area. The A59 was blocked on the day of the event. It was intended to be used as part of the emergency escape routes, access routes for the emergency services, and potentially assembly space for evacuees. The area has an extension of approximately 900 m in north south and 240 m in east–west-direction. In the north it is bordered by “Koloniestraße”. In the south it extends beyond “Karl-Lehr-Straße” for about 200 m. Both streets, i.e. “Koloniestraße” and “Karl-Lehr-Straße” are below surface level, i.e. tunneled below the festival area. That is the reason, why access to the festival area was via a ramp from “Karl-Lehr-Straße” in the south. Details are described in the next section.

A map showing the routes from the central station to the festival area can be found at <http://www.raveline.de/wp-content/uploads/2010/07/Besucherstrom1.jpeg>.

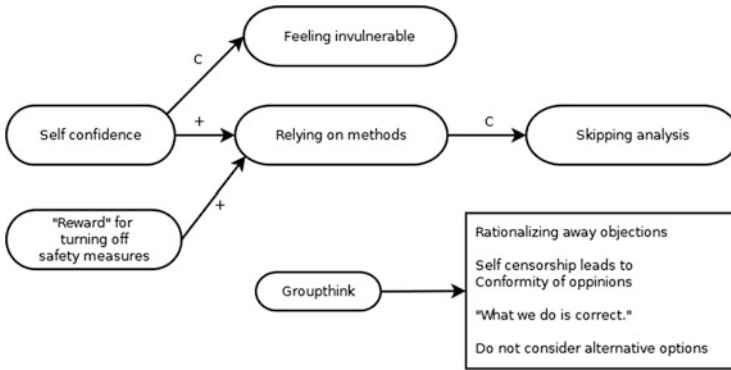


Fig. 2 Psychological explanation (According to Dörner [16])

3.2 The Way from the Station to the Festival Area

The way from the central station (“Duisburg Hbf”) to the festival area is shown in Fig. 2. It is via “Neudorfer Straße” and “Grabenstraße” to “Karl-Lehr-Straße” in the east and via “Friedrich-Wilhelm-Straße” and “Düsseldorfer Straße” to “Karl-Lehr-Straße” in the west. The idea was to separate flows already in the central station (“Hauptbahnhof”), which has four exits and entrances, two in the west and two in the east. The northern entrances (close to “Landfermannstraße”) were assigned to the directions “Oberhausen/Essen” and the southern entrances to the directions “Düsseldorf/Krefeld”.

3.3 The Capacities of the Tunnel and the Ramp

One of the major reasons for the crowd crush on the ramp identified in [19] is the insufficient capacity of the ramp. The ramp is located in the centre of the map in Fig. 1 (“Alter Güterbahnhof”). Its width is 18 m. There is a second ramp in the south of the festival area. It is longer than the main ramp and located west of it. Its width is approximately 7 m. This second ramp is called side ramp in the remaining part of this paper. The crowd crush took place on the main ramp.

In his report, K. Still concludes that the width of the entry ramp to the festival area was too narrow to cover the demand [19]. There, a flow rate of 82 per meter per minute is used. The width of the main ramp was determined from CAD drawings to be 18.28 m (see [19], page 14). The flow per hour is then:

$$F = f \cdot w = 82 \text{ P/m/min} \cdot 18.28 \text{ m} = 89,938 \text{ P/h} \tag{1}$$

(the result in [19], page 14, of this calculation is 89,790 people per hour).

For the day of the event, an effective width of 10.59 m is reported in [19], pages 14 and 15, obtained from photographs. Based on that effective width, a flow capacity of 52,103 is calculated. The comparison of the demand reported in the safety concept (reprinted on page 15 of [19]) and the actual capacity then leads to the two values of 52,103 P/h as capacity and 145,000 P/h as the peak demand between 17.00 and 18.00 h. In this calculation, the estimated demand is taken from the planning documents. The actual number of persons on the site has been estimated to be roughly 180,000 persons [17]. On the other hand, the width of the ramp was not taken from the plans but from the actual situation in [19]. The side ramp was neglected completely. If the calculation is based on the situation as planned (i.e. without hindsight bias), then two factors have to be taken into account

1. The planned effective width of the main-ramp
2. The availability of the side-ramp.

The side-ramp was part of the entry and exit concept the parade character of the festival is visible from the float course. The 16 float-trucks circled around the old freight yard building in the centre. When repeating the calculation with a total width of 25 m for both ramps, the results is the following:

$$F = f \cdot w = 82 \text{ P/m/min} \cdot 25 \text{ m} = 123,000 \text{ P/h} \quad (2)$$

Then, the excess demand would be 22,000 persons in the hour between 5 and 6 pm (17.00 and 18.00 h).

This is the only hour, when the demand exceeds the capacity. Assuming a density of 1.5 P/m², a queue in the tunnels and underpasses of “Karl-Lehr-Straße” approximately 600 m long (in two directions) would form. This estimate is based on a width of 15 m of “Karl-Lehr-Straße”. This queue would then reach beyond “Grabenstraße” in the east and “Düsseldorfer Straße” in the west. The distance between both streets (i.e. the length of “Karl-Lehr-Straße”) is about 820 m.

Those simple considerations show that the actual situation can be described as a capacity problem: the main entry ramp was too narrow because of stands, fences, and cars located there. The “simple math” approach does not cover the major fault of the planning process, though. If the ingress would have been as planned concerning geometry and schedule, then the demand would have been in excess of the capacity only in the time between 5 and 6 pm. This of course would have required strict adherence to the planned processes and their thorough implementation.

The different cordons were implemented by the police are shown (“Polizeiikette”). A detailed analysis of the events with references to the available internet videos can be found in [24]. The police chains were erected after the inflow to the festival area via the main ramp came to a stop. At the upper end of the ramp, the persons stopped. The concept of pushing did not work, i.e. the so called pushers at the upper end of the in-ramp were not able to keep a steady inflow. This might have different reasons: it might not have been possible because of the floats leaving too little room

or there might have been too few pushers. The analysis in [26] concludes that this is one of the major causes of the later crowd crush.

4 The Event as a System

When looking at the event as a system, the different influences on the comfort and safety of the visitors depend on and influence each other. For the case of the crowd crush, the situation is shown in Fig. 1. There are three potentially dangerous feedback loops.

1. Density – Threat – Attraction of Escape – Density (always $\rightarrow (+)$)
2. Density – Number of Victims – Perceived Danger – Attraction of Escape – Density
3. Noise $\rightarrow (-) \rightarrow$ Information $\rightarrow (+) \rightarrow$ Danger – Attraction – Density – Noise

Those are loops, i.e. there is no primary cause. Furthermore, straight lines denote a positive coupling (increase), dashed lines a negative influence (decrease) in Fig. 1. Please note that there are positive feedback loops (1 and 2) and there is a negative feedback loop (3). For (3) the noise level decreases the information flow which again increase (“minus times minus is plus”) the perceived danger.

The width of the ramp itself is therefore part of the problem. The narrower the ramp, the higher the local density. If the local density exceeds a certain level, the feedback loops might be triggered.

There are certain factors that still might prevent the onset of the feedback loop:

- Reducing the stress of the persons (perceived danger and threat) by providing information
- Decreasing the attractiveness of the points of attraction.

The first of those measures is an intervention on the spot, the second is rather a preventive measure to be identified during the planning process and carried out as a precaution. One major problem of the venue and the event was nevertheless the fact that there was effectively only one entry and exit point to the venue. On the other hand, there were two separate ramps. The venue was opened 2 h lat, which already led to frustration and congestion on Grabenstraße and Düsseldorfer Straße, since security checks and entry control were performed when entering Karl-Lehr-Straße. The system love parade was therefore prone to the feedback loops and consequently avalanche effects illustrated in Fig. 1. These feedback loops and avalanche effects were not anticipated during the planning process, which is the second major cause of the disaster. Of course, the detailed causes of the events cannot be foreseen. Precautions were planned to avoid overcrowding in the train station after the event or on the festival area. Less consideration was given to the on-ramp in this regard.

5 The Logic of Failure

The assessment of complex systems has been investigated by Dörner [21]. He identified major factors as the causes of disasters like the one in Chernobyl. His conclusions can be transferred to the love parade disaster.

They are illustrated in Fig. 2. We have kept the original formulations of [21] (translation by HK) in order to show how similar the psychological and sociological mechanism are.

5.1 *Group Think and Disregarding Alternatives*

One major factor is group think and the resulting confirmation bias. Once a decision is made or anticipated, the search for arguments focuses on the support of this decision. For the case of the love parade, this decision is the choice of the entrances and exits. There would have been an option to choose an additional entry and exit via “Am Güterbahnhof” in the north of the festival area (cf. Fig. 1). This was neither considered by the organizer nor demanded by the authorities (city, police, or others). There was experience from previous love parades in Dortmund and Essen. Especially in Dortmund, high densities developed within the central station. Therefore, the idea was to avoid that in Duisburg by stretching the distance between the festival area and the station on the way back and consequently decreasing the inflow into the station after the event.

5.2 *Confirmation Bias and Overconfidence*

The planning process of the love parade was based on assumptions that did not hold true. The question is: was this just accidental or could it have been seen in advance. It seems to be clear that there have been errors in the planning process and during the day, i.e. operational mistakes. One major issue is the width of the ramp towards the festival area and (even more important) that fact that there entry and exit were combined. “Confirmation bias (also called confirmatory bias, my-side bias or verification bias) is a tendency of people to favour information that confirms their beliefs or hypotheses.” [3]

People display this bias when they gather or remember information selectively, or when they interpret it in a biased way. The effect is stronger for emotionally charged issues and for deeply entrenched beliefs. [3]

A series of experiments in the 1960s suggested that people are biased toward confirming their existing beliefs. Later work re-interpreted these results as a tendency to test ideas in a one-sided way, focusing on one possibility and ignoring alternatives. In certain situations, this tendency can bias people’s conclusions.

Explanations for the observed biases include wishful thinking and the limited human capacity to process information. Another explanation is that people show confirmation bias because they are weighing up the costs of being wrong, rather than investigating in a neutral, scientific way.

Confirmation biases contribute to overconfidence in personal beliefs and can maintain or strengthen beliefs in the face of contrary evidence. Poor decisions due to these biases have been found in military, political, and organizational contexts. [3]

6 Consequences of the Disaster

6.1 Political Consequences

The major political consequence of the love parade disaster was the dismissal of the Lord Mayor of Duisburg, Adolf Sauerland in February 2012. In the public, he was blamed for not having reacted properly to the disaster. In the immediate aftermath of the disaster in July and August 2010, the different parties involved blamed each other for being responsible.

6.2 Legal Consequences

There is currently a legal investigation. As of May 2012 it is not clear, if and when this investigation will result in a court procedure. Seventeen persons are currently indicted, 11 of them employees of the city, the head of the legal and former head of the city planning department, one high-ranked police officer and six employees of the organizer [20].

6.3 Consequences for Event Safety

There is currently a discussion going on, whether a special regulation concerning the safety of events should be implemented. The current “Guideline for Venues” (Versammlungsstättenverordnung, resp. Sonderbauverordnung NRW for the state of North-Rhine-Westphalia, where Duisburg is located) has a strong focus on fire safety [24, 25]. This is reflected in the description of the width and length of escape routes, the definition of fire containment zones, and a focus on preventive and technical fire safety measures. The ingress into a venue is not regulated. There is the requirement to provide a safety concept for venues with more than 5,000 visitor spaces. The interpretation is that 5,000 visitors might be at the venue at one

single time. The total number of visitors might of course be larger, especially for an event lasting for a whole day or longer.

6.4 *Ultimate and Proximate Causes*

What has not been discussed in this paper is the police action. The location of two chains formed by the police in order to restrict further inflow from the ramp to the festival area. The reason was that there was congestion at the end of the ramp. Floats were circulating on the festival area. The idea in the safety concept was to pull the audience entering the area away from the head of the ramp by tuning the movement of the floats appropriately. This obviously did not work. Since a major concern was overcrowding of the festival area itself, the ingress was restricted on the ramp by a police chain from 16:01 to 16:40 h. Two chains further upstream did not succeed and broke down at 16:14 h. The most severe crush was during that time. This is a proximate cause, though. The ultimate causes have been described in the previous chapter. Nevertheless will the question, if the fatalities could have been prevented by alternative interventions from the police, be part of the legal investigation.

7 Summary, Conclusion, and Outlook

This paper presented a short summary of the love parade disaster on July, 21st 2010 in Duisburg, Germany. Errors and mistakes during the planning process as well as in the organization and operation of the event were identified. All actors involved have probably contributed to the failures: the municipal authorities, the organizer, and the police. One major distinction is between ultimate and proximate causes. The proximate causes are the overcrowding on the day caused by late opening, counterflow on the ramp, an insufficient management of the inflow, non existing alternative stages, etc. Those causes are proximate in the sense that they are themselves caused by planning mistakes which are the ultimate causes. These ultimate causes might include the choice of the festival location and especially the usage of the tunnel and the two ramps for ingress and egress. The concept chosen required a near to perfect implementation and operation which was obviously not the case. Another ultimate cause might have been the fact that this event took place at this location for the first time. Other events – like street parades or carnivals – that grow over time are based on years of experience and an iterative improvement of concepts and precautions.

References

1. “Loveparade 2009 Fällt Komplette Aus” (in German language). *Westdeutscher Rundfunk (WDR)*. 15 January 2009. Retrieved 16 January 2009.
2. “Love Parade report blames organisers for stampede – ABC News (Australian Broadcasting Corporation)”. *Abc.net.au*. Retrieved 2010-07-28.
3. <http://en.wikipedia.org/wiki/loveparade> (accessed April 4th, 2012).
4. http://en.wikipedia.org/wiki/Confirmation_Bias (accessed April 13th, 2012)
5. http://wikileaks.org/wiki/Loveparade_2010_Duisburg_planning_documents,_2007-2010 (accessed April 13th, 2012).
6. Arbeitsgemeinschaft der Leiter der Berufsfeuerwehren in der Bundesrepublik Deutschland (AGBF): Sicherheitskonzepte für Versammlungsstätten, 28.03.2008.
7. Catastrophe point: 25 metre long mouth of the Karl-Lehr-Strassen Tunnel (German) underpass area with Ostrampe (east-ramp) especially around the small stairs (sight walk - 3 days after, by WDR Fernsehen) (German); see also video at 17:00 o'clock.
8. “Stampede at German Love Parade festival kills 19”. *BBC News*. 24 July 2010. Retrieved 24 July 2010.
9. “19 killed in stampede at Love Parade street party”. *France 24*. 24 July 2010. Retrieved 24 July 2010.
10. Sohn, Michael; Gera, Vanessa (24 July 2010). “18 killed in mass panic at Germany’s Love Parade”. *The Washington Post*. Retrieved 24 July 2010.
11. interview: crowd manager Carsten Walter (German)
12. Erlass des Innenministers NRW vom 11.08.2010, Az. 71/38.05.01. Wortlaut und Erläuterungen unter <http://www.im.nrw.de/sch/819.htm>
13. Landtag NRW, Ausschussprotokoll Apr 15/7 vom 04.08.2010. <http://www.landtag.nrw.de/www/www.landtag.nrw.de/portal/WWW/dokumentenarchiv/Dokument/MMA15-7.pdf>
14. Gattermann, P. et. al.: *Handbuch für die Sicherheit von Großveranstaltungen*. Österreichisches Institut für Schul- und Sportstättenbau (ÖISS), Wien, 2005.
15. Widmer, P. et.al.: *Handbuch Sicherheit bei Veranstaltungen*. Schweizerische Stiftung für Risikoberatung, Zürich, 2005. (PDF).
16. Mamrot D.: Loveparade Duisburg 2010 – *Wi(e)der die normale Katastrophe*. Ingenieurforum 3/2010, Seiten 38 bis 41. www.vfdb.de/downloads
17. Oberhagemann D.: *Analyse der Besucherzahlen und der Ereignisse auf der Rampe zum Veranstaltungsgelände während der Loveparade 2010 in Duisburg*. (30.07.2010). (vfdb), <http://www.vfdb.de/download/AnalyseLoveparade2010.pdf>
18. Dörner, D.: *Die Logik des Mißlingens*. Rororo, Reinbek, 1992.
19. Still, K.: *Duisburg – 24th July 2010. The Love Parade Incident. Expert Report. 9th December 2011*. <http://www.derwesten-recherche.org/wp-content/uploads/2012/02/Still-Gutachten.pdf> (accessed April, 19th, 2012).
20. <http://www.rp-online.de/niederrhein-nord/duisburg/nachrichten/loveparade-jetzt-17-beschuldigte-1.2528178> (accessed, May, 10th, 2012)
21. Nagel, G.: *Die Projektgruppe “Sicherheit von großen Veranstaltungen im Freien” – eine Initiative des MIK NRW*. In [26], pages 19–30.
22. Rübél, J.: *Aktuelles aus dem Bauordnungsrecht*. In [26], pages 1–18.
23. Kirchner, U. (Hrsg.): *Fachtagung Ingenieurkammer Bau NRW*. Düsseldorf, 6. Juni 2011. (in German)
24. Dirk Helbing and Pratik Mukerji: *Crowd Disasters as Systemic Failures: Analysis of the Love Parade Disaster*. *EJOP*, 2012. (open access)
25. Paul, Siegfried et.al.: *Sicherheitskonzepte für Großveranstaltungen*. Beuth, Berlin, 2012.
26. Maria Pretorius, Steve Gwynne and Edwin R. Galea: *The Collection and Analysis of Data from a Fatal Large-Scale Crowd Incident*. Paper to be presented at the Human Behaviour in Fire Conference, Cambridge, UK, Sept 2012.

Utilizing Crowd Insights to Refine Disease-Spreading Models

Anders Johansson and Lara Goscè

Abstract Everyday life gets increasingly crowded, not only in our major cities, with their transport hubs and other points where flows merge, but also during mass gatherings such as religious and sports events. As a result, not only safety and efficiency aspects of overcrowding are of importance, but also health aspects such as the spread of diseases are important to address. Therefore, we illustrate how insights into crowd research can be used to refine models used to forecast likely trajectories of the spread of diseases.

Keywords Epidemics • Crowd safety • Disease spreading • Pedestrians

1 Introduction

As our planet gets increasingly crowded – in particular our cities – high-density crowds are not rare events seen only in mass gatherings such as sports and religious events. Rather, high crowd density is now an everyday feature in many peoples' lives. Cities have been singled out as the engines of wealth generation, innovation and creativity [1, 2]. Therefore, to be able to sustain this development, *crowd science* has to rapidly reinvent itself from being mainly a science of building evacuation to a multi-disciplinary science aimed at concurrently optimizing the safety (e.g. overcrowding), health (e.g. the spread of disease), security, efficiency,

A. Johansson (✉)

The Systems Centre, Faculty of Engineering, University of Bristol, Bristol, UK

Centre for Advanced Spatial Analysis (CASA), University College London (UCL), London, UK

e-mail: a.johansson@bristol.ac.uk

L. Goscè

The Systems Centre, Faculty of Engineering, University of Bristol, Bristol, UK

e-mail: cexlg@bristol.ac.uk

and environmental aspects related to crowded places at various scales. It is clear that all these challenges cannot be solved within one discipline alone. However, medical scientists working on health aspects around mass gatherings recently launched a large-scale interdisciplinary effort to form a new discipline – ‘*Mass Gathering Medicine*’ [6, 7].

In this spirit, the contribution of this paper will be to lay out the first few steps towards bringing the science of crowd modeling and the science of the modeling of infectious diseases together.

2 Macroscopic Modeling of the Spread of Disease

The goal of mathematical epidemiology is to study how an infection can spread between a population and what control measures can be taken to contain it.

The dynamics of infectious diseases is complex, with many interdependent factors that must be considered. In order to model the progress of an epidemic disease in a population comprising many individuals, their diversity must be reduced to a few keys characteristics which are relevant to the infection under consideration. Therefore the population can be divided into compartments and so these models are called compartmental models.

One of the earliest and most commonly used compartmental model is the SIR model, where time t is the independent variable, $S(t)$ denote the number of individuals who are susceptible to a given disease, that is, who are not yet infected at time t , $I(t)$ denotes the number of infected individuals able to spread the disease by contact with susceptible individuals, and $R(t)$ denotes the number of individuals who have recovered from the disease, and cannot be infected again. The total population size is $N = S + I + R$.

In 1927 Kermack and McKendrick [3–5] proposed a model based on three non-linear ordinary differential equations

$$\begin{aligned}\frac{dS}{dt} &= -\beta SI \\ \frac{dI}{dt} &= \beta SI - \alpha I \\ \frac{dR}{dt} &= \alpha I\end{aligned}\tag{1}$$

where β is a constant transmission rate and α is a constant recovery rate, which gives the mean infectious period as $1/\alpha$.

The number of individuals in each compartment must be integer values, but if the host population size N is sufficiently large, then S , I and R can be treated as continuous variables. Since R is determined once S and I are known, then the third equation can be dropped from the model so that it can be reduced to the following system of two equations:

$$\begin{aligned}\frac{dS}{dt} &= -\beta SI \\ \frac{dI}{dt} &= (\beta S - \alpha) I\end{aligned}\tag{2}$$

Although the system is reduced, it is still analytically unsolvable, which means that it is not possible to find the solution as an explicit formula, however it may be studied through a qualitative approach without finding its exact form.

First of all, the model makes sense only if $S(t)$ and $I(t)$ remain non-negative and if one of them reaches zero, the system can be considered terminated. Then,

$$\frac{dS}{dt} < 0 \wedge \frac{dI}{dt} > 0 \iff S > \alpha/\beta \quad (3)$$

thus I increases as long as $S > \alpha/\beta$, but since S decreases for all t , I ultimately decreases and approaches zero. If $S(0) < \alpha/\beta$, I decreases to zero (no epidemic), while if $S(0) > \alpha/\beta$, I first increases to a maximum attained when $S = \alpha/\beta$ and then decreases to zero (epidemic).

Let us now introduce a small number of infected individuals into a population entirely made up by susceptible individuals and investigate whether there will be an epidemic. If everyone is initially susceptible ($S(0) = N$) then a newly introduced infected individual can be expected to infect other people at rate βN during the expected infectious period $1/\alpha$. Thus the first infected individual can be expected to infect,

$$\mathfrak{R}_0 = \frac{\beta N}{\alpha} \quad (4)$$

individuals. The number R_0 is called *basic reproduction number* and is the most important quantity to consider when analysing any epidemic model for an infectious disease. Studies of the basic reproduction number have shown that, usually, when $R_0 > 1$, the disease will spread through the whole population, but when $R_0 < 1$, the disease will die out before reaching the whole population [14]

When trying to forecast likely developments of real-world diseases, it is important to have a good estimate of parameter β , the transmission rate, which is one of the most elusive parameters to obtain information about, in particular if the studied disease is recent and there are not much data available.

3 Microscopic Modeling of the Spread of Disease Coupled with a Crowd Model

As we have seen, models describing the spread of diseases, are typically aggregate. Models describing the movement of pedestrians on the other hand, are typically highly disaggregate, and describe the movement of individuals. Let us therefore try to couple a microscopic pedestrian model – the social-force model [17] with a disease spreading model, which is defined as:

1. Assign an infection-status attribute, S , I , or R to individual pedestrians at the start of the simulation.

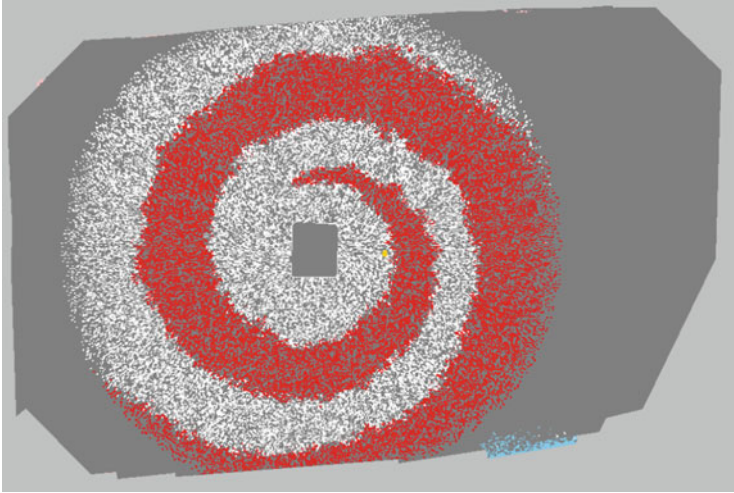


Fig. 1 Result of a disease-spreading model coupled with a crowd model, with the recovery rate $\alpha = 0$, rate of spread $\beta = 100\%$, and critical distance $d = 0$, for the sake of illustration. The crowd moves counter-clockwise and initially only one person in the crowd is infected, which creates a spiral-shaped disease propagation as the simulation progresses. In reality, crowd movement and the spread of infectious disease are of course processes that occur on very different time scales, which make them infeasible to visually couple together in this way

2. Let infected individuals recover with rate α .
3. Let infected individuals spread their disease to other pedestrians within a distance d , with probability per time unit, β .

To illustrate this model, we run it for the crowded Grand Mosque in Mecca (Fig. 1), where a large crowd circulate Kaaba in counter-clockwise direction. At time t , only one person in the crowd is infected (state I), and everyone else are susceptible (S) to an infection. The critical distance at which infections spread is set to $d = 0$, which means that infection only propagates at physical contact. Since the dynamics of crowd movement happens on much shorter time scales than the dynamics of the spread of diseases, we set $\alpha = 0$ and $\beta = 100\%$ for the sake of illustration. The result is a spiral propagation of the disease.

A second example [6, 7], shows a similar SIR model as the one coupled with the social-force model, but this time coupled with empirical movement data obtained by GPS tracking (Fig. 2). The fractions of people in states S , I , and R are plotted in Fig. 3 (left) and compared with the result of a macroscopic Kermack-McKendrick model (Fig. 3 right). Apparently, the population level results are very similar in a microscopic and in a macroscopic model. This means that the microscopic model managed to reproduce similar system dynamics as in the macroscopic model.

However, the advantage of having a microscopic model that can reproduce the systems level dynamics of a more traditional aggregate model, is that one can more easily investigate interventions such as screening, immunization, quarantining, or



Fig. 2 Illustration of a disease-spreading model coupled with an empirical dataset of human movement, obtained by GPS sensors in central London [6]

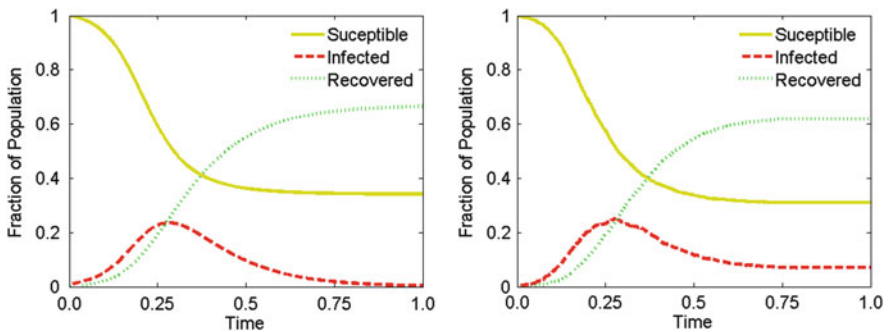


Fig. 3 *Left* S, I, R curves as a function of time, for the Kermack-McKendrick model. *Right*: The evolution of fractions S, I, R , obtained by microscopic simulation with empirical movement data in central London obtained by GPS devices [6]

other mobility restrictions (which are all individual-level interventions), and see what impact they would have on the rate of spread of various types of diseases.

4 Mesoscopic Modeling of the Spread of Disease

Because state-of-the-art disease-spreading models are more aggregate than crowd models, and since they typically do not contain an explicit space, or the usage of that space by pedestrians, they therefore rest on the assumptions that populations are well-mixed and homogeneous.

However, as detailed empirical data of human mobility has become increasingly available, crowd research has shown that these assumptions are not realistic. There are a number of spatial and temporal correlations, patterns and relations in pedestrian crowds, e.g.

- Pedestrians move in groups whose sizes can be approximated by a zero-truncated Poisson distribution [15],
- Pedestrians adapt their walking speed to the surrounding crowd density, with a resulting non-linear and non-monotonic flow profile [12],
- Crowd density on a small scale can be approximated by a Gaussian distribution [13],
- Pedestrians across a range of geographies and cultures, all keep a net-time headway of 0.5 s [13],
- Settlement patterns in cities follow fractal growth where cluster sizes are distributed in a log-normal way [11], and
- Human trajectories exhibit a high degree of regularity both in time and space, which cannot be accurately described by Lévy flight and random walk models [10].

Empirical movement and interaction data behind these studies come from various traditional sources such as surveys, but also from live real-time sources such as GPS tracking, video-based tracking, and mobile phone tracking.

Recent studies of the spreading of disease, have started to bring an explicit structure of human interaction into these models, and have used abstract spaces such as social networks. For example, a study of a sexual-contact network revealed a scale-free structure, which means that the ‘mean field theory’ approach describing average behaviour results in very different spreading dynamics compared to if the strong clustering of the real empirical network is taken into account [16].

Other studies, have looked at the global airline transportation network as a medium for the spreading of disease [9, 18]. However, even in these network-based models, the system dynamics will depend on the dynamics within the nodes of these networks, and these nodes correspond to airports or other physical spaces, and the dynamics within the nodes depend strongly on the crowd dynamics in these.

For pedestrian movement in fine scale physical spaces such as public transport hubs, street networks, and city centres, it is not yet known how the dynamics of disease spreading is affected by the crowd findings listed above. The state-of-the-art of the sciences of crowd dynamics and epidemics modelling has been detailed in two recent review papers [6, 7], which lay out the missing pieces and a way forward to bridge the gap between the latest theory and empirical characteristics of crowd dynamics and disease spreading.

So far, no systematic research programme has been carried out to do the research needed in order to facilitate the design of the next generation of disease-spreading models, by incorporating the empirical crowd features outlined above, and making use of live real-time sensing of pedestrian movement.

Therefore, as a first step, let us go back to the SIR model (Eq. 1) and see how we can start to incorporate some of the empirically obtained features that have been obtained through crowd research.

If in a given space there is a large number of people in contact with each other, a possible disease could spread more easily because the interactions between infected and susceptible individuals will be more frequent. We can therefore modify the so far constant transmission rate β , to become dependent on the crowd density ρ which is defined as $\rho = N/A$, where N is the total population size and A is the corresponding area in which the population is contained.

Starting with the simple assumption that β is proportional to the crowd density, we can write $\beta = k\rho$ were in the simplest case k can be a constant that reflect the type of disease under consideration.

If we go back to the original SIR model and analyse the qualitative considerations we have taken and the definition of the basic reproduction number we have given, our model can now be described with

$$\frac{dS}{dt} < 0 \wedge \frac{dI}{dt} > 0 \iff S > \frac{\alpha A}{kN} \quad (5)$$

and

$$\mathfrak{R}_0 = \frac{kN^2}{\alpha A} \quad (6)$$

which is consistent with the idea that a disease is more likely to spread in a small area more densely populated than in a big area where a small population is better distributed in space.

Thus, it does not seem strange that we are most likely to find the majority of the epidemics that affect the world in the most densely populated areas on the planet.

Take for example the H1N1 Influenza A, also known as the ‘swine flu’ (pandemic in the Spring of 2009) which spreads in the same way as the regular seasonal influenza viruses spread, mainly through people who are infected with the virus and are coughing and sneezing (but also by touching contaminated objects and then touching the nose or mouth and causes a wide range of flu-like symptoms; fever, cough, headaches, chills etc.)

5 Summary and Outlook

It is important, for the control of an epidemic and its eradication from the population, to study how the proximity of people plays a role in its diffusion and what kind of prevention can be done in highly populated cities and mass gatherings. Our aim is to take more detailed empirical crowd characteristics into account, such as the

distribution describing variation of local crowd densities within an area, and to see how they can be incorporated to improve the accuracy of disease-spreading models.

The two adjacent fields of research – crowd modeling and the modeling of the spread of diseases – have traditionally been treated as two separate fields of study without much overlap. However, we have illustrated that it is possible to make rapid progress by combining the state-of-the art in both fields.

The value of being able to sense and model human mobility and thus being able to refine models that can more accurately forecast the spread of disease, will be achieved by enabling more efficient strategies and policies for vaccination, quarantining and other interventions, and would make it possible to make use of existing resources in a more efficient way, and would ultimately improve public health and reduce costs at the same time.

Acknowledgements This work is supported by the EPSRC funded Industrial Doctoral Centre in Systems, Universities of Bristol and Bath (Grant EP/G037353/1).

References

1. Glaeser, E.: *Triumph of the City: How Our Greatest Invention Makes Us Richer, Smarter, Greener, Healthier and Happier*, The Penguin Press, New York (2011)
2. Bettencourt, L., West, G., Lobo, J., Helbing, D., Kühnert, C.: Growth, innovation, scaling, and the pace of life in cities, *PNAS* (2007)
3. Kermack, W.O., McKendrick, A.G.: A Contribution to the Mathematical Theory of Epidemics. *Proc. Roy. Soc. Lond. A.*, 115, 700–721 (1927)
4. Earn, D.J.D.: A light introduction to modelling recurrent epidemics. In: *Mathematical Epidemiology* (edited by Brauer F., van den Driessche P., Wu J.). *Lecture Notes in Mathematics*, 1945. *Mathematical Biosciences Subseries*. Springer-Verlag, Berlin (2008)
5. Breban, R., Vardavas, R., Blower, S.: Theory versus data: how to calculate R_0 , *PLoS ONE*, vol. 2, no. 3, article no. e282 (2007)
6. Johansson, A., Batty, M., Hayashi, K., Albar, O., Memish, Z., and Marozzi, D.: Crowd and environmental management during mass gatherings, *The Lancet Infectious Diseases* 12(2), 150–156 (2012)
7. Khan, K., McNabb, S., Memish, Z., Eckhardt, R., Hu, W., Kossowsky, D., Sears, J., Arino, J., Johansson, A., Barbeschi, M., McCloskey, B., Henry, B., Cetron, M., and Brownstein, J. S.: Infectious disease surveillance and modelling across geographic frontiers and scientific specialties, *The Lancet Infectious Diseases* 12(3), 222–230 (2012)
8. Pastor-Satorras, R. and Vespignani, A.: Epidemic Spreading in Scale-Free Networks. *Phys. Rev. Lett.* 86: 3200–3203 (2001)
9. Colizza, V., Barrat, A., Barthélemy, M., Vespignani, A.: The role of the airline transportation network in the prediction and predictability of global epidemics. *PNAS* 103 (7): 2015–2020 (2006)
10. González, M.C., Hidalgo, C.A., Barabási, A.—L.: Understanding individual human mobility patterns. *Nature* 453, 779–782 (2008)
11. Batty, M.: The size, scale, and shape of cities, *Science* **319**, 769–771 (2008)
12. Helbing, D., Johansson, A., Al-Abideen, H.Z.: Dynamics of crowd disasters: An empirical study, *Physical Review E* **75**, 046109 (2007)
13. Johansson, A.: Constant-net-time headway as a key mechanism behind pedestrian flow dynamics, *Physical Review E* **80**, 026120 (2009)

14. Goscè, L.: R_0 , The basic reproduction number in epidemiology, Master's Thesis, Università Federico II, Naples, Italy (2012)
15. Moussaïd, M., Perozo, N., Garnier, S., Helbing, D., and Theraulaz, G.: The Walking Behaviour of Pedestrian Social Groups and Its Impact on Crowd Dynamics, *PLoS ONE* **5**(4): e10047 (2010)
16. Liljeros, F., Edling, C.R., Amaral, L.A.N., Stanley, H.E., Aberg, Y.: The Web of Human Sexual Contacts, *Nature* **411**, 907–908 (2001)
17. Helbing, D., Farkas, I., and Vicsek, T.: Simulating dynamical features of escape panic, *Nature* **407**, 487–490 (2000)
18. Khan, K., Arino, J., Hu, W., Rappos, P., Sears, J., Calderon, F., Heidebrecht, C., Macdonald, M., Liauw, J., Chan, A., Gardam, M.: Spread of a Novel Influenza A (H1N1) Virus via Global Airline Transportation, *N Engl J Med* **361**, 212–214 (2009)

Venue Suitability for Large-Scale Events from the Viewpoint of Safety Measures

Masatoshi Kaitsuji and Akihiko Hokugo

Abstract This study analyzes recent crowd disasters at mass events by examining event planning and event security planning, analyzing disaster videos, conducting interviews and on-the-spot investigations and reviewing disaster investigation reports. Analysis reveals that these disasters occurred related to three venue-suitability factors: (1) projected visitor number which determines most of venue safety measures; (2) venue space planning including event content types; and (3) access route for crowd flow. Also shown are the influences of venue topographic and structural conditions on access route for crowd flow. At most of those disaster sites, access routes were highly-fenced areas like tunnels and bridges which do not lead to escape routes. Where these venue-suitability factors are not appropriately arranged, preventing the excessive accumulation of high-density crowd is difficult, even if appropriate security measures are taken. To avoid these crowd disasters, it is essential to judge venue suitability during the event planning stage.

Keywords Venue suitability factor • High-density crowd • Crowd flow

1 Akashi Citizens' Summer Festival Disaster (Japan, July 2001)

This disaster was attributed to the crowd flow in access routes and the venue space use planning. The festival was held at Okura Beach, Akashi City, Japan in July 2001. During fireworks display, accumulation of high-density crowd became excessive to

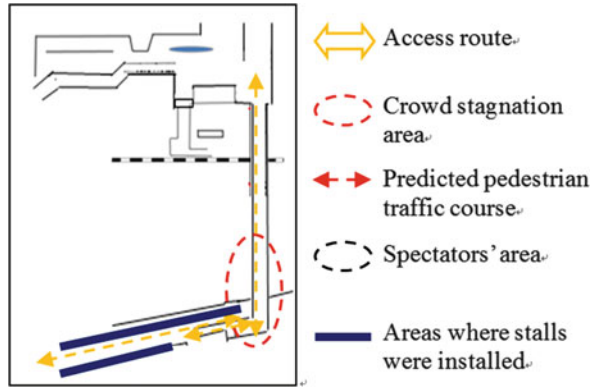
M. Kaitsuji (✉)

Graduate School of Engineering, Kobe University, Kobe, Japan
e-mail: mk01-007@nifty.com

A. Hokugo

Research Center for Urban Safety and Security, Kobe University, Kobe, Japan
e-mail: hokugo@kobe-u.ac.jp

Fig. 2 Map of pedestrian overpass



a viewing space at the southern end. The overpass is 6 m wide but narrows to 3 m at the stairway to the venue, forming a bottleneck for the crowd flow (Fig. 2).

Although the festival was expected to attract some 100,000 people, the one-way pedestrian capacity of the four access routes was 24,000 people/h, that of the pedestrian overpass being 14,000 people/h. The entire venue structure and overpass design provided a double-bottleneck for the crowd flow. In addition, the venue space use planning allowed many vending stalls to be installed near the bottom end of the overpass stairway, also hindered smooth flow of pedestrians.

2 Duisburg Love Parade Disaster (Germany, July 2010)

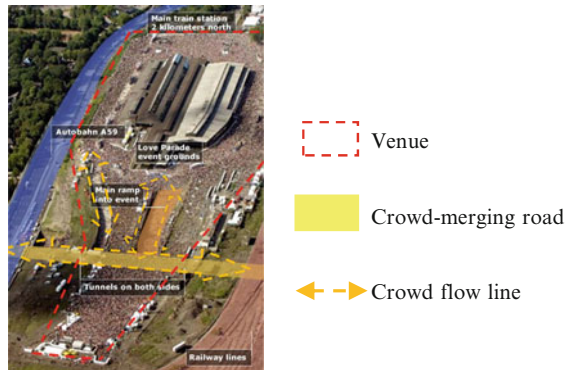
During the Love Parade festival held in Duisburg, Germany, a crowd of people going to the venue met head-on with a crowd returning from the venue on the access route. Under excessive high-density crowd accumulation and a complex crowd surge, people fell and were crushed, resulting in 21 deaths and over 500 injuries. Causes of this disaster were related to all three venue-suitability factors.

Projected Number of Visitors The Love Parade organizer had announced about 1 month prior to the festival that over a million people were expected at the festival. In response to this projection, police requested that the municipality and the organizer reconsider whether or not to hold the festival [2]. This fact implies the possibility that the festival had been planned with no specific projection of the number of visitors. We estimated the numbers of people arriving at the venue, leaving the venue and remaining at the venue. Our estimation was based on the following assumptions: the venue area was approximately 84,000 m²; the maximum venue space capacity for visitors was approximately 250,000 people with a crowd density of 3 people/m²; and the number of visitors was approximately 480,000. Based on these data, we analyzed the venue space use planning and the crowd flow in the access routes.

Fig. 3 Area around the venue [3]



Fig. 4 Accumulating crowd [4]



Venue Space Use Planning The venue was in the rectangular site of a former freight train station (Figs. 3 and 4). The Love Parade festival is an audience-involving, typical exciting music festival featuring stage music by DJs and parade floats targeted mainly to young people.

The parade was performed on wide roads (40–80 m wide) elliptically surrounding the abandoned freight train station buildings. The effective venue area is estimated to be approximately 84,000 m² (Figs. 3 and 4).

The venue was assumed to have a space capacity for accommodating approximately 250,000 people. The crowd control planning was such that people were guided to an event stage which was set up in the north end of the venue so that they were expected to move from the back side of the venue to the venue’s entrance/exit. With the organizer’s space use planning, however, it must have been difficult for people to proceed around the venue, with excessive accumulation of crowd here and there (Fig. 4).

Table 1 Estimated number of ingress, egress and staying people

Time division	Ingress	Egress	Staying
11:00–13:00	106,000	–	106,000
13:00–14:00	70,000	–	166,000
14:00–15:00	60,000	10,000	186,000
15:00–16:00	60,000	40,000	206,000
16:00–17:00	60,000	50,000	226,000
17:00–18:00	60,000	55,000	246,000
18:00–19:00	50,000	65,000	246,000
19:00–20:00	14,000	80,000	180,000
Total	480,000	300,000	480,000

According to our estimation for the present study, there were over 100,000 people at the venue at 13:00 when the event began, with people continuing to arrive at a rate of approximately 60,000–70,000 people/hour (Table 1).

The number of egress people, mainly short-time stayers, began to increase at around 15:00. Since the sum of ingress and egress people is estimated to be approximately 100,000 people/hour, accumulating crowd at the venue should exceed any safety limit unless a crowd of egress people flows smoothly (Fig. 4).

Crowd Flow in Access Routes According to the event plan, two routes (18–30 m wide, each approximately 2.5 km long) were set, one on the east side and the other on the west side of the venue, to guide people from the nearest railroad station to the venue. These routes were traffic-controlled for exclusive use by festival-goers, but were intended for use by both ingress and egress people (Fig. 3).

Two ramps were set up for access to the venue: a main access ramp (115 m long, 30 m wide) and a secondary access ramp (120 m long, 13 m wide). Each ramp originates at the middle of the east–west crowd navigation route (tunnel), forming a T-junction where streams of people entering the tunnel from both ends merge. Both ramps have a concrete wall (approximately 7 m high) on each side (Figs. 5, 6, and 7).

Whereas the total pedestrian capacity of the two access ramps is 240,000 people/h, of which 160,000 people/h is for the main ramp, and 80,000 people/h for the secondary ramp, that of the crowd-merging east–west navigation route (tunnel) is 97,000 people/h.

The crowd flow should therefore be restricted by the east–west tunnel, very likely causing crowd accumulation. Moreover, since the two access ramps and the east–west navigation route are set for two-way pedestrian traffic, streams of ingress and egress people unavoidably meet, aggravating the crowd accumulation.

At around 16:41 when the crowd disaster occurred, approximately 226,000 people were estimated to have been at the venue, about 60,000 people/h entering the venue, and about 50,000 people/h leaving the venue (Table 1). These ingress and egress rates indicate the possibility that crowd stagnation occurred in the venue access ramps and at the T-junction where each access ramp meets the east–west navigation route.



Fig. 5 Access ramps [3], [red dashed box] Venue



Fig. 6 Main access ramp (Photographed by one of the authors)

The main and secondary access ramps are bounded on both sides by concrete walls. The only escape means is a stairway (approximately 7 m high and 76 cm wide) provided on the east-side wall of the main ramp. In addition, the east–west navigation route with which the two access ramps merge is in a highly confined tunnel environment. Under such structural conditions, the crowd density and pressure are sure to build up rapidly from accumulated crowds of people entering the access ramps one after another.

It can be observed from the YouTube video images [4] that individuals and crowd went into a panic with screams and yelps, trying to escape from the rushing crowd.

Fig. 7 Crowd-merging navigation route
(Photographed by one of the authors)



3 Other Crowd Accidents related to Venue-Suitability Factors

Four other similar examples of crowd accidents are outlined below and in Table 2. Besides these six examples, crowd disasters occurred in the past during large-scale outdoor events were in many cases caused by venue-suitability factors.

3.1 Tokyo Imperial Palace Nijubashi Bridge Disaster (Japan, 1954)

Some 380,000 people visited the Imperial Palace to wish the emperor a happy new year and sign their names on the visitor's registers. The entrance and exit routes were set separately to ensure one-way pedestrian traffic at the venue. If the flow of crowds had been smooth, there would have been no problem. However, crowd accumulation occurred around the registry area, making it necessary to restrict access to the venue. To reach the entrance where access to the venue was restricted, people gathering in the Imperial Palace Plaza must pass over the Nijubashi Bridge (20 m wide). Since no crowd control was conducted, a huge crowd of people rushed onto the bridge. When the crowd ingress was then restricted on the bridge, many people fell down, resulting in a crowd disaster.

This disaster was caused by crowd control failure attributable to insufficient preliminary study of the crowd flow in access routes that would affect the crowd flow at the venue.

Table 2 Crowd accidents considered attributable to venue-suitability factors

Tokyo Imperial Palace disaster (Japan, 1954) 16 deaths, 48 injuries

Outline: a huge accumulated crowd at a high density on the bridge, causing many people to fall down

Number of visitors: approx. 380,000 (projected and actual)

Venue space use plan: the entrance and exit were set separately to ensure one-way pedestrian traffic

Crowd flow in access routes: a crowd of people gathering in the Imperial Palace Plaza was allowed to enter the very narrow bridge (20 m wide) under no crowd control



Yahiko Shrine disaster (Japan, 1956) 124 deaths, 177 injuries

Outline: an ingress crowd of 8,000 people ran into an egress crowd of 1,000 people on the staircase outside the main gate to the venue, causing people to fall off the staircase

Number of visitors: approx. 30,000 (projected and actual)

Venue space use planning: possible effect of change made to the venue use planning on the crowd flow had not been studied or forecast sufficiently

Crowd flow in access routes: since the gate connecting the access route to the venue was extremely narrow at 5.1 m, a huge egress crowd met head-on with a huge ingress crowd



Baihe Fireworks Display disaster (China, 2004) 37 deaths, 37 injuries
 Outline: crowds of people began crossing the bridge at the venue simultaneously from both sides, causing crowd accumulation on the bridge. The wooden parapets collapsed, and many spectators fell into the river

Number of visitors: not clear (projected and actual)
 Venue space use plan: preliminary study of the crowd flow at the venue was insufficient. The pedestrian capacity of the bridge connecting both sides of the river was too small relative to the number of visitors

Crowd flow in access routes: due to no projection of the number of visitors and inappropriate venue space use planning, many people entered the 100 m long, 6 m wide bridge simultaneously from both sides



Water Festival disaster (Cambodia, 2010) 348 deaths, over 600 injuries
 Outline: a huge crowd of people rushed to an access bridge, and many people were crushed and fell into the river

Number of visitors: not clear (projected and actual)
 Venue space use planning: the venue was situated in a vast development area but in a highly confined environment

Crowd flow in access routes: due to inaccurate projection of the number of visitors and inappropriate venue space use planning, many people entered the 100 m long, 8 m wide bridge simultaneously from both sides



3.2 *Yahiko Shrine Disaster (Japan, 1956)*

The area of the shrine's grounds where a crowd disaster occurred was approximately 2,000 m². The overall width of the main gate to the grounds was 5.1 m. The approach to the grounds was a confined space bounded on both sides by fences. Outside the main gate was an approximately 2 m high staircase. That is, the venue had a structural problem that hampered the smooth flow of crowds. A crowd of some 8,000 people leaving the shrine's grounds after enjoying the shrine's new-year event met head-on with a crowd of some 1,000 people walking toward the grounds, causing high-density crowd accumulation on the staircase. Staircase parapets collapsed under the crowd pressure, and many people fell off the staircase. This disaster was also caused by crowd control failure attributable to insufficient preliminary study of the crowd flow in access routes that would affect the crowd flow at the venue.

3.3 *Baihe Fireworks Display Disaster (China, 2004)*

A crowd disaster occurred during a fireworks display held in the Baihe area in the suburbs of Beijing. At the venue, a narrow bridge (100 m long, 6 m wide) connects the parks on both sides of the Baihe River. Approximately 3,000 spectators began crossing the bridge simultaneously from both sides and met head-on at the middle of the bridge, resulting in crowd accumulation. Under increased crowd density and pressure, the wooden parapets collapsed, and many spectators fell into the river. The event planning had been developed solely by the event organizer, with no projection of the number of visitors and without sufficient preliminary study of the crowd flow at the venue. It is also reported that the security agency had not been informed about the holding of the event.

3.4 *Water Festival Disaster (Cambodia, 2010)*

This festival was held on a delta island in a river in Phnom Penh, i.e. in a confined area with only three bridges for access to the venue. Since this island was a newly developed commercial zone, a large number of people had been expected to gather at the venue. However, whether the projected or actual number of festival-goers was determined is not clear. In addition, since preliminary study of the relationship between venue accessibility and crowd flow at the venue had been insufficient, crowds of people leaving the island and entering the island simultaneously rushed to cross a narrow bridge from both ends, and collided with each other on the bridge. Presumably, high crowd density and pressure sent people into extreme panic, resulting in a disaster in which many people were crushed and fell into the river.

All of the above-mentioned crowd accidents were caused by venue-suitability factors that have the following points in common.

1. The event venue was situated in a generally closed environment, and the disaster occurred at a no-escape bridge or tunnel connecting two areas of the venue.
2. The event organizer had not performed sufficient comprehensive preliminary study based on a review of factors affecting crowd flow.
3. The event organizer had not performed sufficient comprehensive study regarding crowd flow, including a venue access crowd control planning.
4. Insufficient study of crowd flow at the venue and the access routes, coupled with inaccurate projection of visitors, resulted in an improper crowd control planning.

4 Conclusion

4.1 Projected Number of Visitors

The projected number of visitors is basic numerical data on which the venue space use planning and prediction of the crowd flow in access routes are based. All safety measures to be taken at the venue are based on the projected number of visitors. If the actual number of visitors is far larger than the projection or if unexpectedly huge numbers of people visit the venue when no projection was made, the available security force and equipment will be inadequate. As a result, even if the best possible safety measures are taken, it will be difficult to prevent an occurrence of high-density crowd accumulation that can lead to a crowd disaster. This means that the projected number of visitors is a critical factor in judging venue suitability.

4.2 Venue Space Use Plan

The content of an event determines the characteristics of the event and the demographic of visitors to the event. The type of event determines the required venue capacity and the flow of crowds at the venue. The venue space use planning therefore has a significant influence on the crowd flow, including the possibility of crowd accumulation. The venue space use planning, which is linked with the crowd flow in access routes, is an important factor in judging venue suitability.

4.3 Crowd Flow in Access Routes

The content and type of an event determine the flow of crowds in access routes. Unless the crowd flow is smooth in access routes, high-density crowd accumulation can occur, leading to high probability that a crowd disaster will occur.

Judging from the fact that many of the crowd disasters discussed here took place in a confined access route to the venue as indicated by the above examples, the structural condition of each access route is also an important venue suitability judgment factor.

To prevent crowd accidents at a large-scale event, it is essential during the event planning stage to judge the venue suitability from the viewpoint of safety measures. It is also important that the event organizer and planner, security company, police and fire departments, transportation company, and all other concerned parties hold comprehensive discussions on event-related information and venue suitability judgment factors and share recognition of risks.

References

1. Akashi City Summer Festival Accident Investigation Committee's Report, 2002
2. Municipal Government's Report, 2010 (in German) <http://www.mik.nrw.de/themen-aufgaben/schutz-sicherheit/gefahrenabwehr-feuerwehr-katastrophenschutz/grossveranstaltungen/loveparade-2010.html>
3. Google Maps
4. Love Parade on YouTube <http://www.youtube.com/watch?v=1kXtBaiwwP8>

WALK: A Modular Testbed for Crowd Evacuation Simulation

Stefan Münchow, Ia Enukidze, Stefan Sarstedt, and Thomas Thiel-Clemen

Abstract When large numbers of people gather in public spaces such as stadiums, railway stations, shopping centers and concert halls there is an increased risk of mass emergence and disasters. Critical situations could possibly be prevented with appropriate tools to anticipate them. WALK is a modular designed crowd evacuation simulation system using a multi-agent approach.

One major goal of WALK is to provide a framework for the simulation and comparison of different socio-psychological theories to gain essential insights about the emergence of crowd behavior. Moreover, the framework is supposed to allow the simulation of many diverse scenarios. In order to achieve these goals, the system has to offer a maximum level of flexibility by following software engineering best practices. In this paper, we will explain the customizable architecture of WALK, which enables scientists from different fields, e.g. psychology and computer science, to use it as a testbed for their studies.

Keywords Crowd simulation • Multi-agent system • Pedestrian evacuation

1 Introduction

Latest occurrences like terrorist attacks and accidents at public mass events [e.g. 1] have indicated a demand for efficient evacuation concepts. Due to the fact that field tests of crowd evacuations are not feasible and in most cases plain impossible,

S. Münchow (✉) • S. Sarstedt • T. Thiel-Clemen
Hamburg University of Applied Sciences, Hamburg, Germany
e-mail: stefan.muenchow@haw-hamburg.de; stefan.sarstedt@haw-hamburg.de;
thomas.thiel-clemen@haw-hamburg.de

I. Enukidze
Hamburg University, Hamburg, Germany
e-mail: ia.enukidze@stud.uni-hamburg.de

evacuation concepts are tested using computer simulation systems. There are many different approaches for simulating crowd behavior: Flow-based and gas-kinetic approaches, social force models and cellular automata [e.g. 2, 3]. Although these approaches are adequate to show crowd movement, they do not facilitate the simulation of divergent individual behaviors caused by personality traits or emotions. The currently most promising and most commonly used approach is to simulate human beings as agents within a multi-agent system. It allows the simulation of individuals on a microscopic level, whereas crowd behavior is not explicitly defined but emerges from the sum of the agents' individual decisions. This seems to be the most natural way for modeling persons.

In many simulation systems, there is spent little effort in the system design. As a consequence these systems are inflexible and tightly bound to specific well-defined scenarios. The agents are most often designed to show just one particular aspect of human decision-making in detail. This can produce realistic human-like behavior in a single scenario, but does not work for different ones [4]. There is a lack of a more generic system that can handle diverse scenarios and enables testing of different socio-psychological theories.

The goal of WALK is to fill this gap and to be usable for many areas of application. For that reason, the system is based on a flexible architecture which follows proven software engineering principles. It comprises two levels where flexibility is crucial: First, the overall system should allow the definition and simulation of different scenarios with differing environment complexity and crowd sizes. As we want to simulate small crowds with hundred agents up to large-sized crowds with thousands of agents, the system must be scalable. To achieve this, we will implement a distributed multi-agent simulation system. Second, the agents have to be composed of different components for decision-making, socio-psychological aspects and action. This enables WALK to be applicable in two different ways:

- By its scenario-independent and extensible design, it can serve as a tool for civil protection in governmental institutions. It can be used to prevent or analyze crowd accidents and evacuations in different situations.
- As it is open towards different socio-psychological theories, WALK can serve as a testbed for studies of psychologists, social scientists and computer scientists in fundamental research.

This work shows the WALK architecture on the two levels mentioned above and points out the benefits of our design decisions. In Sect. 2 some essential socio-psychological factors are described. Section 3 explains the architecture on the overall system and the agent level. In Sect. 4 we describe our development methodology, which ensures the system to be as general as possible. In Sect. 5 the current state of the system and open issues for future research are discussed.

2 Psychological Aspects

Crowd behavior occurs in a wide range of situations. Science still tries to understand crowd phenomena and to explain why and how crowd behavior patterns emerge. There is no unified socio-psychological theory about crowd behavior in emergencies. Scientists differ in their opinions regarding typical behavior of individuals, their rationality or emotionality [5], psychosocial vulnerability (e.g. ‘selfishness’, mass panic) or collective resilience (e.g. help, unity) in critical life-threatening situations [6].

One of the main insights of research in the last years is that crowd behavior is affected and generated by the sum of individual decisions. In other words, each individual responds to and is affected by a situation in his or her own way [6]. On the other hand the role of the social context, the surroundings and dynamics are decisive. Specifically, the motives, goals and behavior of a person are influenced by the physical environment (e.g. stairs or a fence), the social surroundings (strangers, friends or family) and the internal state of the person (cognitive and emotional, e.g. being afraid or curious) [7].

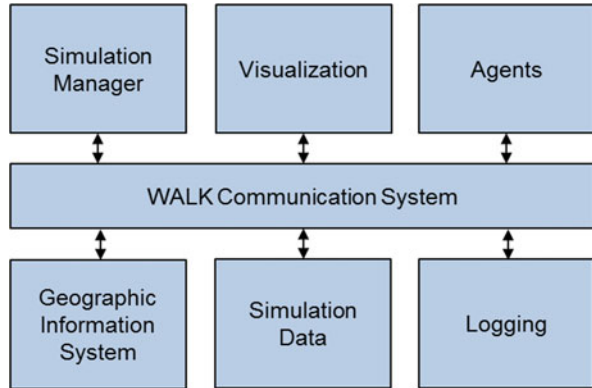
It is hardly possible to study crowd behavior under real circumstances. Systematic studies of human behavior in critical situations and quantitative theories capable of predicting crowd dynamics are rare. Due to the ethical implications of such research, it is not possible to reenact a disaster or mass over-crowding. Thus, the behavior of people panicking under these circumstances is difficult to observe. As a consequence, computer simulations seem to be the most promising approach to validate different theories and to facilitate a confident management of mass evacuations.

Many computer scientists have modeled human factors, e.g. emotions and personality, into their agents. Often they have utilized very mathematical or logical approaches because these fit to our way of thinking. Many systems use the emotion model of Ortony, Clore and Collins [8] due to its clear and structured definition. As it is structured like a tree, it is well-suited for computational models even though it has some drawbacks: It describes what emotions are and under which circumstances they arise but does not explain how behaviors in critical situations emerge from specific emotions, which is crucial for the correct implementation of a crowd simulation.

3 System Design

For enabling WALK to simulate a wide range of different scenarios and for testing and comparing different socio-psychological theories, a carefully considered and flexible system design is required. In this section the WALK architecture is described on the overall system and the agent level.

Fig. 1 WALK overall architecture



3.1 Overall System

In order to provide a customizable and scalable simulation system, we designed a distributed message-oriented architecture. One requirement to WALK is to allow the simulation of large-sized crowds with low communication and management overhead for the agents. Another important requirement is the ability of developing new components for the simulation system in a team in parallel and integrating them into the existing system.

To reach these goals, we propose a service-oriented architecture with independent components communicating over a high speed message bus, the *WALK Communication System*. It distributes all messages among the components of the simulation. By applying this design, a tight coupling between the components is avoided and single modules can be replaced easily without affecting the remaining system. New components can be added without much effort. In addition, the system can be distributed to many physical computers, which results in scalability and enables the simulation of thousands of agents simultaneously. We are currently researching the potentialities of an efficient collocated partitioning. Figure 1 shows the overall system design with the *WALK Communication System* as its central component.

Each module in WALK is responsible for just a single task, whereas complex tasks are accomplished by components communicating with each other. By this design, we reach a high degree of cohesion and ensure a simple maintenance and extension of our system. This aspect is crucial as WALK is still under development and refined permanently.

All simulation data will be stored in a database in a common data format. This will allow the replay and visualization of once computed simulation runs on different devices, e.g. desktop PCs, tablet computers and smartphones. Moreover, stopping and restarting the simulation at an arbitrary point in time will be possible. This will enable users of the system to take a particular situation from a recorded

simulation run, alter agent parameters and the environment, start a new simulation run with these settings and observe the impact on the simulated course of events.

As mentioned before WALK is able to simulate different scenarios that differ in environment complexity, events and agent groups. To ensure this, no scenario-dependent information is stored directly in the system. The simulation is configured by a scenario definition, which includes a complete specification of the environment, occurring events and agent groups or single agents. Moreover, the environment is stored as geographical data in a *Geographical Information System*, which will use data from Google Maps or NASA Maps in the future. It is capable of storing indoor and outdoor areas. Events can be defined to occur once at a specified instant of time in the simulation or repeatedly within a specified time frame. Examples for such events are the start of a fire at a specified position in the environment or a fire alarm. At last, agent groups or single agents together with their positions and basic parameters, e.g. age distribution and personality types, can be added to the scenario definition.

All these factors enforce a maximum of flexibility and scenario-independence on the overall system level. By this, we reach the first goal of WALK to be able to simulate various scenarios and to be applicable as a tool for the prevention and analysis of crowd emergencies in civil protection.

3.2 Agents

While many simulation systems use an agent-based approach, there are few noteworthy approaches for a general agent architecture that follows proven software engineering principles and enables the modeling of human factors [4]. WALK agents are equipped with a simple, component-based design. By considering socio-psychological factors, e.g. emotion, personality traits and social behavior, our agents are supposed to show realistic human-like behavior. The aim is to create a universal agent architecture, which allows the realization and test of different socio-psychological theories in an easy and experimental way. This testbed will be used together with an incremental development method in cooperation with scientists from different research areas, e.g. psychologists and social scientists, to gain insights about the emergence of crowd behavior and its simulation.

Discoveries in behavioral research have shown that every person in an emergency situation runs through a cycle of perception, interpretation, decision-making and action [9]. This cycle is implemented in the WALK agents. In each phase there are different components involved, which contribute to the process of the agents' decision-making. The agent design is also inspired by cognitive agent architectures like ACT-R [10] and C4 [11] and adapts some of their concepts.

All components interact via a memory which stores all currently important information for the agent's reasoning cycle. It also includes a declarative memory for long-term knowledge, e.g. the building structure, and a procedural memory for knowledge about actions, e.g. how to open a door. Due to the fact that all

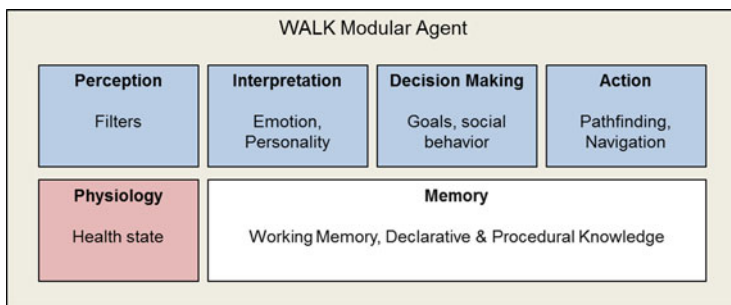


Fig. 2 WALK agent architecture

modules within the agent communicate via the memory, we enforce a loose coupling between them. This structure is similar to the one of the overall system and allows us to develop WALK in an experimental way: As any component can be replaced easily, we are able to implement different socio-psychological theories and compare them with each other. As a consequence, WALK can be used in the second application area mentioned above: As a testbed for fundamental research in the area of psychology, social and computer science. A blueprint of the current agent design is shown in Fig. 2.

This design enables us to evaluate the impact of different human factors on the emergence of typical crowd behavior in the simulation. For instance, we are able to replace the *Interpretation* component or one of its subcomponents and thus change the way a situation is appraised and an emotion arises in the agent. Due to the fact that there is no unified socio-psychological theory about crowd behavior, we are able to approximate realistic agent behavior in an experimental way by trying different theories.

There are few approaches to simulate social factors, like the theory of social comparison [12]. As social factors are vital for the realism of a crowd simulation, there is demand for further research. We will respect these factors in WALK just as emotions and personality to gain insights about their impact on the simulation results.

4 Development Methodology

The development of a generalizable and scenario-independent simulation system is a great challenge and requires a special approach. We propose a development methodology including steady validation and improvement. This will help us to address the most common problems in crowd behavior modeling: Tight coupling to a specific scenario and insufficient validation techniques [4].

In cooperation with the supervisory school authority in Hamburg, Germany, we collect data from real evacuation drills in schools. By defining the exact school

geometry in WALK, we are able to simulate the school evacuation in the system and compare the results to the collected data from the real drill. Data is collected by filming critical areas of the building, e.g. main exits, during the drill and analyzing the video material to identify movement patterns and trajectories of single agents. In addition, anonymized surveys and location systems based on RFID and WLAN are used to track single individuals.

Our development cycle contains prototyping, permanent validation with data from real evacuation drills and gradual improvement. First, psychologists and social scientists form hypotheses about individual and social behavior in a given situation. They serve as “domain experts” and explain relevant theories to computer scientists, who translate these theories into computational models. After that, real evacuation drills are performed and all relevant data is collected. It is then compared to the simulation results. As a consequence, we can use the insights for our next development cycle and refine the system. As there is no “right” way to design the agents and to equip them with socio-psychological factors, this approach ensures a steady reconsideration of our system design, which leads to more generality.

By application of this analysis-implementation-validation-cycle in cooperation with psychologists and social scientists false assumptions become obvious in an early stage of development and can be corrected immediately. It will help to create a simulation system that is not bound to a particular scenario and approximates realistic human-like behavior gradually.

5 Discussion

The Commission on Civil Protection of the German Federal Ministry of Interior has recently published its latest report on current threats to the public [13]. The report covers a broad spectrum of threats starting from CBRN (chemical, biological, radiological, and nuclear) over to terroristic attacks and the impacts of global change. It does not only reflect the scientific opinion of the commission, but also outlines main results of a synopsis of similar reports from an international point of view.

From that it becomes very obvious that high-quality software tools to support all phases of civil protection and homeland security are urgently needed. But it should be noted that every phase requires specific priorities. For instance, in prevention and training scenarios the sensitivity, variability, and the context of state variables are important, whereas in disaster management performance issues come to the fore.

The WALK system was developed and is under development in tight cooperation with the commission and with other stakeholders of disaster management in Germany. Beside interdisciplinary research issues the applicability and scalability of the generic framework is one of the key goals.

The basic simulation framework is realized and provided with simple agents. Socio-psychological factors are not implemented yet. We are currently preparing the first real evacuation drills in schools. Due to the fact that we are performing

the first development cycle at the moment, we have to deal with many questions concerning suitable tracking technologies and data privacy issues. With each cycle performed our system will evolve and also the methodology will get more mature and effective.

Open research issues are the up-scaling of the simulation and an efficient distribution of the system to a cluster of computers. As we want to simulate evacuation scenarios for cities with hundreds of thousands of inhabitants, a partitioning of the system and a dynamic adaption to the necessary level of detail in a simulated scenario will be required. These issues will be considered in detail in further research.

References

1. Staatsanwaltschaft Duisburg 2010. Presseerklärung der Staatsanwaltschaft Duisburg zu den Ermittlungen im Zusammenhang mit den Geschehnissen bei der 'Loveparade' in Duisburg'. http://www.sta-duisburg.nrw.de/presse/Presseerklaeungen/Loveparade_Presseerkl_rung_vom_27_07_2010.pdf
2. Henderson, L. F. 1971. "The Statistics of Crowd Fluids", *Nature*, 229, 381–383.
3. Helbing, D., Farkas, I. and Vicsek, T. 2000. "Simulating dynamical features of escape panic". *Nature*, 407, 487–490.
4. Zhou, S., Chen, D., Cai, W., Luo, L., Low, M. Y. H., Tian, F., Tay, V. S.-H., et al. 2010. "Crowd modeling and simulation technologies". *ACM Transactions on Modeling and Computer Simulation*, 20(4), 1–35.
5. Schneider, B.(2011). *Die Simulation menschlichen Panikverhaltens*. Wiesbaden: Vieweg + Teubner Verlag / Springer Fachmedien.
6. Drury, J., Cocking, C. & Reicher, S. (2009). The Nature of Collective Resilience: Survivor Reactions to the 2005 London Bombings. *International Journal of Mass Emergencies and Disasters*. Vol. 27, No. 1, pp. 66–95.
7. Wijermans, F. E. H. (2011). *Understanding crowd behaviour: Simulating situated individuals*. Groningen: University of Groningen.
8. Ortony, A., Clore, G. L., and Collins, A. 1988. "The cognitive structure of emotions". Cambridge [England]: Cambridge University Press.
9. Kuligowski, E.D. 2009. "The Process of Human Behavior in Fires". National Institute of Standards and Technology, NIST, Technical Note 1632.
10. Anderson, J. R., Bothell, D., Byrne, M. D., Douglass, S., Lebiere, C., & Qin, Y. (2004). An integrated theory of the mind. *Psychological review*, 111(4), 1036–60. doi:10.1037/0033-295X.111.4.1036
11. Burke, R., Isla, D., Downie, M., Ivanov, Y., & Blumberg, B. (2001). *Creature smart: The art and architecture of a virtual brain*. Proceedings of the Computer Game Developers Conference.
12. Kaminka, G. A., & Fridman, N. (2006). A cognitive model of crowd behavior based on social comparison theory. Proceedings of the AAAI-2006 workshop on cognitive modeling. Retrieved from <http://www.aaai.org/Papers/Workshops/2006/WS-06-02/WS06-02-004.pdf>
13. Commission on Civil Protection (2011): *Vierter Gefahrenbericht (4th Report on current threats to the public)*, The Commission on Civil Protection of the German Federal Ministry of Interior (Eds.), in German, 176 pp.